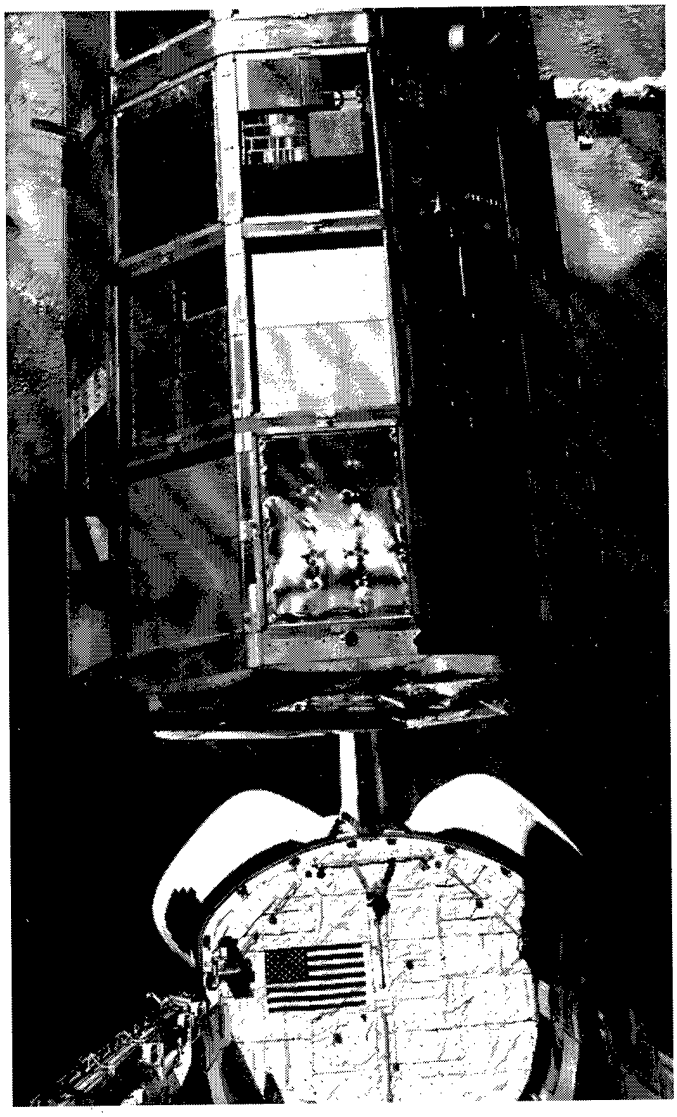
NASA Conference Publication 3134
Part 2

LDEF — 69 Months in Space

First Post-Retrieval Symposium



Proceedings of a symposium held in Kissimmee, Florida June 2-8, 1991

NASA

DTIC QUALITY INSPECTED 4

PLEASE RETURN TO:

BMD TECHNICAL INFORMATION CENTER
BALLISTIC MISSILE DEFENSE ORGANIZATION
7100 DEFENSE PENTAGON
WASHINGTON D.C. 20301-7100

19980309 221

DISTRIBUTION STATEMENT A
Approved for public release;
Distribution Unlimited

13666

Accession Number: 3666

Publication Date: Jan 01, 1992

Title: LDEF - 69 Months in Space: First Post-Retrieval Symposium, Part 2

Personal Author: Levine, A.S. (Editor)

Corporate Author Or Publisher: NASA Langley Research Center, Hampton, VA 23665-5225 Report Number: L-17042

Report Prepared for: NASA, Washington, DC 20546-0001 Report Number Assigned by Contract Monitor: NASA CP-3134, Part 2

Comments on Document: This document is a compilation of papers presented at the First Long Duration Exposure Facility (LDEF) Post-Retrieval Symposium, June 2-8, 1991

Descriptors, Keywords: Space Experiment Data Analysis Material Coating Thermal System Power Propulsion Cosmic Ray Ion Micrometeoroid Electronics Optics Life Science

Pages: 00612

Cataloged Date: Aug 04, 1992

Document Type: HC

Number of Copies In Library: 000001

Record ID: 24430

NASA Conference Publication 3134
Part 2

LDEF — 69 Months in Space

First Post-Retrieval Symposium

Edited by
Arlene S. Levine
NASA Langley Research Center
Hampton, Virginia

Proceedings of a symposium sponsored by the National Aeronautics and Space Administration, Washington, D.C., and held in Kissimmee, Florida June 2-8, 1991

PLEASE RETURN TO:
SDI TECHNICAL INFORMATION CENTER

NASA
National Aeronautics and Space Administration
Office of Management
Scientific and Technical Information Program
1991

Foreword

On July 20, 1989, President George Bush charted a new course for human exploration of space:

> ". . . a long-range continuing commitment. First, for the coming decade -- for the 1990's -- Space Station *Freedom*, our next critical step in all our space endeavors. And for the next century, back to the moon, back to the future, and this time, back to stay; then a journey into tomorrow, a journey to another planet -- a manned mission to Mars. Each mission should and will lay the groundwork for the next."

The Long Duration Exposure Facility (LDEF) is providing critical technology for future spacecraft, including Space Station *Freedom,* and thus plays a major role in the President's vision of human exploration of space.

LDEF was carried into orbit in April 1984 by the Space Shuttle *Challenger.* The 11-ton satellite contained 57 experiments to assess the effects of the space environment, i.e., ionizing radiation, meteoroids, cosmic dust, and high altitude atomic oxygen on materials and mechanical, electronic, optical, and living systems. In January 1990, after 69 months in low Earth orbit, LDEF was retrieved by the Space Shuttle *Columbia* and returned to Earth. The retrieval occurred 57 months after it was originally planned, due in part to the *Challenger* tragedy. The 69 months in space provided experimenters the unique opportunity to sample and measure the space environment over a longer time period than originally planned.

The 57 LDEF experiments were returned to the Principal Investigators and their science teams for analyses and interpretation. In June 1991, over 400 LDEF researchers and data users met in Kissimmee, Florida for the First LDEF Post-Retrieval Symposium. The papers presented contained important new information about space environments and their impact on materials, systems, and biology. This publication contains the material presented at the symposium, categorized by subject:

LDEF Mission and Induced Environments
Space Environments - *Ionizing Radiation*
Space Environments - *Meteoroid and Debris*
Space Environmental Effects - *Materials*
Space Environmental Effects - *Systems*
Space Environmental Effects - *Biology*
Space Environmental Effects - *Microgravity*
The Future

During the symposium Sally A. Little, NASA Headquarters, chaired the **LDEF Mission and Induced Environments** session; William L. Quaide, NASA Heaquarters,

chaired the **Space Environments** - *Meteoroid and Debris* session; Thomas W. Crooker, NASA Headquarters, and Bland A. Stein, NASA Langley Research Center, co-chaired the **Space Environmental Effects** - *Materials* session; Judith H. Ambrus, NASA Headquarters, and P. Rex Miller, W.J. Schaefer and Associates co-chaired the **Space Environmental Effects** - *Systems* session; and James L. Jones, NASA Langley Research Center chaired the session called **Others**.

Some presentations in these documents underwent a title change; others were combined with two or three presentations; two were not presented orally. However, all oral presentations are represented in written form. Where full-length papers were unavailable, the abstracts have been reprinted. All papers were reviewed for technical content as well as form.

We wish to thank the contributors, as well as the reviewers of these papers. We also wish to thank Dr. William H. Kinard, without whose vision and persistence, there would not be an LDEF project or the valuable data it has collected.

The LDEF Science Office plans to organize and conduct two additional symposia, one in San Diego in June 1992 and another in 1993. The proceedings from these two symposia will be published as NASA Conference Publications.

We believe that the LDEF data reported in this three-part document will make important contributions to charting the new course for the exploration of space.

Use of manufacturers' trade names in this publication does not constitute an official endorsement of such products or manufacturers, either expressed or implied, by the National Aeronautics and Space Administration.

Arlene S. Levine
LDEF Science Office
NASA Langley Research Center

CONTENTS

FOREWORD iii

*** PART 1**

LDEF MISSION AND INDUCED ENVIRONMENTS

LONG DURATION EXPOSURE FACILITY--A GENERAL OVERVIEW 3
Robert L. O'Neal and E. Burton Lightner

LONG DURATION EXPOSURE FACILITY (LDEF) SPACE ENVIRONMENTS OVERVIEW 49
William H. Kinard and Glenna D. Martin

PINHOLE CAMERAS AS SENSORS FOR ATOMIC OXYGEN IN ORBIT;
APPLICATION TO ATTITUDE DETERMINATION OF THE LDEF 61
Palmer N. Peters and John C. Gregory

USE OF THE LONG DURATION EXPOSURE FACILITY'S THERMAL MEASUREMENT
SYSTEM FOR THE VERIFICATION OF THERMAL MODELS 69
William M. Berrios

MEASURED SPACE ENVIRONMENTAL EFFECTS TO LDEF DURING RETRIEVAL 85
Carl R. Maag and W. Kelly Linder

PARTICLE TYPES AND SOURCES ASSOCIATED WITH LDEF 101
E. R. Crutcher and W. W. Wascher

MIGRATION AND GENERATION OF CONTAMINANTS FROM LAUNCH THROUGH 121
RECOVERY: LDEF CASE HISTORY
E. R. Crutcher, L. S. Nishimura, K. J. Warner and W. W. Wascher

QUANTIFICATION OF CONTAMINANTS ASSOCIATED WITH LDEF 141
E. R. Crutcher, L. S. Nishimura, K. J. Warner and W. W. Wascher

MOLECULAR FILMS ASSOCIATED WITH LDEF 155
E. R. Crutcher and K. J. Warner

ORGANIC CONTAMINATION OF LDEF 179
Gale A. Harvey

SPACE ENVIRONMENTS - IONIZING RADIATION

SUMMARY OF IONIZING RADIATION ANALYSIS ON THE LONG DURATION
EXPOSURE FACILITY 199
T. A. Parnell

PREDICTION OF LDEF IONIZING RADIATION ENVIRONMENT 213
John W. Watts, T. A. Parnell, James H. Derrickson, T. W. Armstrong
and E. V. Benton,

GAMMA RADIATION SURVEY OF THE LDEF SPACECRAFT 225
G. W. Phillips, S. E. King, R. A. August, J. C. Ritter, J. H. Cutchin, P. S. Haskins,
J. E. McKisson, D. W. Ely, A. G. Weisenberger, R. B. Piercey and T. Dybler

* Part 1 is presented under separate cover.

THE INTERACTIONS OF ATMOSPHERIC COSMOGENIC RADIONUCLIDES WITH SPACECRAFT SURFACES 237
J. C. Gregory, G. J. Fishman, B. A. Harmon and T. A. Parnell

SURFACE ACTIVATION OF CONCORDE BY ^{7}BE 249
P. R. Truscott, C. S. Dyer and J. C. Flatman

CHARGED PARTICLE ACTIVATION STUDIES ON THE SURFACE OF LDEF SPACECRAFT 255
Ilhan Olmez, Forrest Burns and Paul L. Sagalyn

RADIOACTIVITIES OF LONG DURATION EXPOSURE FACILITY (LDEF) MATERIALS: BAGGAGE AND BONANZAS 257
Alan R. Smith and Donna L. Hurley

MEASUREMENTS OF INDUCED RADIOACTIVITY IN SOME LDEF SAMPLES 271
C. E. Moss and R. C. Reedy

GAMMA-RAY SPECTROMETRY OF LDEF SAMPLES AT SRL 287
Willard G. Winn

INDUCED RADIOACTIVITY IN LDEF COMPONENTS 301
B. A. Harmon, G. J. Fishman, T. A. Parnell and C. E. Laird

THERMOLUMINESCENT DOSIMETRY FOR LDEF EXPERIMENT M0006 313
J. Y. Chang, D. Giangano, T. Kantorcik, M. Stauber, and L. Snead

RADIATION EXPOSURE OF LDEF: INITIAL RESULTS 325
E. V. Benton, A. L. Frank, E. R. Benton, I. Csige, T. A. Parnell and J. W. Watts, Jr.

CHARGED PARTICLE LET-SPECTRA MEASUREMENTS ABOARD LDEF 339
I. Csige, E. V. Benton, A. L. Frank, L. A. Frigo, E. R. Benton, T. A. Parnell and J. W. Watts, Jr.

IONIZING RADIATION CALCULATIONS AND COMPARISONS WITH LDEF DATA 347
T. W. Armstrong, B. L. Colborn and J. W. Watts, Jr.

LDEF GEOMETRY/MASS MODEL FOR RADIATION ANALYSES 361
B. L. Colborn and T. W. Armstrong

THE LDEF ULTRA HEAVY COSMIC RAY EXPERIMENT 367
D. O'Sullivan, A. Thompson, J. Bosch, R. Keegan, K.-P. Wenzel, A. Smit and C. Domingo

PRELIMINARY RESULTS FROM THE HEAVY IONS IN SPACE EXPERIMENT 377
James H. Adams, Jr., Lorraine P. Beahm and Allan J. Tylka

HEAVY ION MEASUREMENT ON LDEF 393
R. Beaujean, D. Jonathal and W. Enge

SPACE ENVIRONMENTS - METEOROID AND DEBRIS

LARGE CRATERS ON THE METEOROID AND SPACE DEBRIS IMPACT EXPERIMENT 399
Donald H. Humes

STUDY OF COSMIC DUST PARTICLES ON BOARD LDEF: THE FRECOPA EXPERIMENTS AO138-1 AND AO138-2 419
J. C. Mandeville and Janet Borg

METEOROID/SPACE DEBRIS IMPACTS ON MSFC LDEF EXPERIMENTS 435
Miria Finckenor

HYPERVELOCITY IMPACT MICROFOIL PERFORATIONS IN THE LEO SPACE ENVIRONMENT (LDEF, MAP AO023 EXPERIMENT) 443
J. A. M. McDonnell and T. J. Stevenson

METEOROID AND DEBRIS SPECIAL INVESTIGATION GROUP DATA ACQUISITION PROCEDURES 459
Thomas H. See, Martha K. Allbrooks, Dale R. Atkinson, Clyde A. Sapp, Charles G. Simon, and Mike E. Zolensky

METEOROID AND DEBRIS SPECIAL INVESTIGATION GROUP PRELIMINARY RESULTS: SIZE-FREQUENCY DISTRIBUTION AND SPATIAL DENSITY OF LARGE IMPACT FEATURES ON LDEF 477
Thomas H. See, Friedrich Hörz, Michael E. Zolensky, Martha K. Allbrooks, Dale R. Atkinson and Charles G. Simon

PRELIMINARY ANALYSIS OF LDEF INSTRUMENT AO187-1 "CHEMISTRY OF MICROMETEOROIDS EXPERIMENT" 487
Friedrich Hörz, Ronald P. Bernhard, Jack Warren, Thomas H. See, Donald E. Brownlee, Mark R. Laurance, Scott Messenger and Robert B. Peterson

SIMS CHEMICAL ANALYSIS OF EXTENDED IMPACT FEATURES FROM THE TRAILING EDGE PORTION OF EXPERIMENT AO187-2 503
Sachiko Amari, John Foote, Charles Simon, Pat Swan, Robert M. Walker, Ernst Zinner, Elmar K. Jessberger, Gundolf Lange and Frank Stadermann

IDE SPATIO-TEMPORAL IMPACT FLUXES AND HIGH TIME-RESOLUTION STUDIES OF MULTI-IMPACT EVENTS AND LONG-LIVED DEBRIS CLOUDS 517
J. Derral Mulholland, S. Fred Singer, John P. Oliver, Jerry L. Weinberg, William J. Cooke, Nancy L. Montague, Jim J. Wortman, Philip C. Kassel and William H. Kinard

ION MICROPROBE ELEMENTAL ANALYSES OF IMPACT FEATURES ON INTERPLANETARY DUST EXPERIMENT SENSOR SURFACES 529
Charles G. Simon, Jerry L. Hunter, Jim J. Wortman and Dieter P. Griffis

LDEF IMPACT CRATERS FORMED BY CARBON-RICH IMPACTORS: A PRELIMINARY REPORT 549
T. E. Bunch, F. Radicati di Brozolo, Ronald H. Fleming, David W. Harris, Don Brownlee and Terrence W. Reilly

DYNAMIC (COMPUTER) MODELLING OF THE PARTICULATE ENVIRONMENT: TRANSFORMATIONS FROM THE LDEF REFERENCE FRAME TO DECODE GEOCENTRIC AND INTERPLANETARY POPULATIONS 565
J. A. M. McDonnell and K. Sullivan

LDEF DATA CORRELATION TO EXISTING NASA DEBRIS ENVIRONMENT MODELS 567
Dale R. Atkinson, Martha K. Allbrooks and Alan J. Watts

DERIVING THE VELOCITY DISTRIBUTION OF METEOROIDS FROM THE MEASURED METEOROID IMPACT DIRECTIONALITY ON THE VARIOUS LDEF SURFACES 569
Herbert A. Zook

M AND D SIG PROGRESS REPORT: LABORATORY SIMULATIONS OF LDEF IMPACT FEATURES 581
Friedrich Hörz, R. P. Bernhard, T. H. See, D. Atkinson and M. Allbrooks

PRELIMINARY MICROMETEOROID AND DEBRIS EFFECTS ON LDEF THERMAL CONTROL SURFACES 583
Martha K. Allbrooks, Dale R. Atkinson, Thomas See and Fred Hörz

THE INTERSTELLAR GAS EXPERIMENT 585
D. L. Lind, J. Geiss, F. Bühler and O. Eugster

COLOR PHOTOGRAPHS 595

AUTHOR INDEX 605

PART 2

SPACE ENVIRONMENTAL EFFECTS - MATERIALS

PRELIMINARY FINDINGS OF THE LDEF MATERIALS SPECIAL INVESTIGATION GROUP 617
Bland A. Stein and H. Gary Pippin

ATOMIC OXYGEN AND ULTRAVIOLET RADIATION MISSION TOTAL EXPOSURES FOR LDEF EXPERIMENTS 643
R. J. Bourassa, J. R. Gillis and K. W. Rousslang

EFFECTS OF SPACE ENVIRONMENT ON STRUCTURAL MATERIALS 663
C. Miglionico, C. Stein, R. Roybal, R. Robertson, L.E. Murr, S. Quinones, J. Rivas, B. Marquez, A.H. Advani, W.W. Fisher and R. Arrowood

MEASUREMENT OF THE 0^{18} TO 0^{16} ISOTOPE RATIO FOR CHARACTERIZING OXIDE SURFACE LAYERS ON LDEF SAMPLES 679
Paul L. Sagalyn

CHEMICAL CHARACTERIZATION OF SELECTED LDEF POLYMERIC MATERIALS 687
Philip R. Young and Wayne S. Slemp

CHARACTERIZATION OF POLYMER FILMS RETRIEVED FROM LDEF 705
Alan Letton, Neil I. Rock, Kevin D. Williams, Thomas W. Strganac and Allan Farrow

MEASUREMENTS OF EROSION CHARACTERISTICS FOR METAL AND POLYMER SURFACES USING PROFILOMETRY 723
Ligia C. Christl, John C. Gregory and Palmer N. Peters

LONG DURATION EXPOSURE FACILITY (LDEF) PRELIMINARY FINDINGS: LEO SPACE EFFECTS ON THE SPACE PLASMA - VOLTAGE DRAINAGE EXPERIMENT 737
Brian K. Blakkolb, James Y. Yaung, Kelly A. Henderson, William W. Taylor and Lorraine E. Ryan

INTERACTIONS OF ATOMIC OXYGEN WITH MATERIAL SURFACES IN LOW EARTH ORBIT: PRELIMINARY RESULTS FROM EXPERIMENT AO114 753
J. C. Gregory, L. Christl, G. N. Raikar, J. J. Weimer, R. Wiser and P. N. Peters

EFFECTS ON LDEF EXPOSED COPPER FILM AND BULK 755
Palmer N. Peters, John C. Gregory, Ligia C. Christl and Ganesh N. Raikar

LDEF EXPERIMENT AO034: ATOMIC OXYGEN STIMULATED OUTGASSING 763
Roger C. Linton, Rachel R. Kamenetzky, John M. Reynolds and Charles L. Burris

ATOMIC OXYGEN UNDERCUTTING OF LDEF ALUMINIZED-KAPTON MULTILAYER INSULATION 781
Kim K. deGroh and Bruce A. Banks

PRELIMINARY RESULTS FOR LDEF/HEPP THERMAL CONTROL SAMPLES 797
Lonny Kauder

ATOMIC OXYGEN INTERACTIONS WITH FEP TEFLON AND SILICONES ON LDEF 801
Bruce A. Banks, Joyce A. Dever, Linda Gebauer and Carol M. Hill

VACUUM ULTRAVIOLET (VUV) RADIATION - INDUCED DEGRADATION OF FLUORINATED ETHYLENE PROPYLENE (FEP) TEFLON ABOARD THE LONG DURATION EXPOSURE FACILITY (LDEF) 817
David E. Brinza, A. E. Stiegman, Paul R. Staszak, Eric G. Laue and Ranty H. Liang

SPACE ENVIRONMENTAL EFFECTS ON SILVERED TEFLON THERMAL CONTROL SURFACES 831
C. S. Hemminger, W. K. Stuckey and J. C. Uht

RESULTS OF EXAMINATION OF SILVERED TEFLON FROM THE LONG DURATION EXPOSURE FACILITY 847
Ken Rousslang, Russ Crutcher and Gary Pippin

SILVER TEFLON BLANKET: LDEF TRAY C-08 861
E. R. Crutcher, L. S. Nishimura, K. J. Warner and W. W. Wascher

PRELIMINARY INVESTIGATIONS INTO UHCRE THERMAL CONTROL MATERIALS 875
François Levadou, Mike Froggatt, Martin Rott and Eberhard Schneider

INITIAL MATERIALS EVALUATION OF THE THERMAL CONTROL SURFACES EXPERIMENT (S0069) 899
Donald R. Wilkes, M. John Brown, Leigh L. Hummer and James M. Zwiener

UNUSUAL MATERIALS EFFECTS OBSERVED ON THE THERMAL CONTROL SURFACES EXPERIMENT (S0069) 919
James M. Zwiener, Kenneth A. Herren, Donald R. Wilkes, Leigh Hummer and Edgar R. Miller

EFFECTS OF LOW EARTH ORBIT ENVIRONMENT ON THE LONG DURATION EXPOSURE FACILITY THERMAL CONTROL COATINGS 935
Thomas R. Sampair and William M. Berrios

SPACECRAFT THERMAL CONTROL COATINGS 945
Jean-Claude Guillaumon and Alain Paillous

LONG DURATION EXPOSURE FACILITY EXPERIMENT M0003-5 THERMAL CONTROL MATERIALS 961
Charles J. Hurley

RESULTS OF EXAMINATION OF THE A276 WHITE AND Z306 BLACK THERMAL CONTROL PAINT DISKS FLOWN ON LDEF 975
Johnny L. Golden

ION BEAM TEXTURED AND COATED SURFACES EXPERIMENT (IBEX) 989
Michael J. Mirtich, Sharon K. Rutledge, Nicholas Stevens, Raymond Olle and James Merrow

ELLIPSOMETRIC STUDY OF OXIDE FILMS FORMED ON LDEF METAL SAMPLES 1005
W. Franzen, J. S. Brodkin, L. C. Sengupta and P. L. Sagalyn

SPACE ENVIRONMENTAL EFFECTS ON THE INTEGRITY OF CHROMIC ACID ANODIZED COATINGS 1023
Walter L. Plagemann

M0003-10: LDEF ADVANCED COMPOSITES EXPERIMENT 1041
Gary L. Steckel and Tuyen D. Le

LDEF - SPACE ENVIRONMENTAL EFFECTS ON MATERIALS: COMPOSITES AND SILICONE COATINGS 1055
Brian C. Petrie

PRELIMINARY RESULTS FROM THE LDEF/UTIAS COMPOSITE MATERIALS EXPERIMENT 1057
R. C. Tennyson, G. E. Mabson, W. D. Morison and J. Kleiman

LONG DURATION EXPOSURE FACILITY EXPERIMENT M0003 DEINTEGRATION/ FINDINGS AND IMPACTS 1073
M. J. Meshishnek, S. R. Gyetvay, and C. H. Jaggers

SURVEY OF RESULTS FROM THE BOEING MODULES ON THE M0003 EXPERIMENT ON LDEF 1109
H. G. Pippin, Owen Mulkey, Juris Verzemnieks, Emmett Miller, Sylvester Hill and Harry Dursch

RESULTS FROM ANALYSIS OF BOEING COMPOSITE SPECIMENS FLOWN ON LDEF EXPERIMENT M0003 1115
Pete E. George and Sylvester G. Hill

HIGH-TOUGHNESS GRAPHITE/EPOXY COMPOSITE MATERIAL EXPERIMENT 1143
David K. Felbeck

EFFECTS OF LDEF FLIGHT EXPOSURE ON SELECTED POLYMER MATRIX RESIN COMPOSITE MATERIALS 1149
Wayne S. Slemp, Philip R. Young, William G. Witte, Jr. and James Y. Shen

EFFECT OF SPACE ENVIRONMENT ON COMPOSITE MATERIALS AND THERMAL COATINGS (AO138-9) 1163
Michel Parcelier and Jean Pierre Assié

EFFECT OF SPACE EXPOSURE OF SOME EPOXY MATRIX COMPOSITES ON THEIR THERMAL EXPANSION AND MECHANICAL PROPERTIES (AO138-8) 1175
Heinrich Jabs

MECHANICAL PROPERTIES OF SILICATE GLASSES EXPOSED TO A LOW-EARTH ORBIT 1187
David E. Wiedlocher, Dennis S. Tucker, Ron Nichols and Donald L. Kinser

PATTERNS OF DISCOLORATION AND OXIDATION BY DIRECT AND SCATTERED FLUXES ON LDEF, INCLUDING OXYGEN ON SILICON 1189
A. R. Frederickson, R. C. Filz, F. J. Rich and P. Sagalyn

COLOR PHOTOGRAPHS 1201

AUTHOR INDEX 1205

* PART 3

SPACE ENVIRONMENTAL EFFECTS - SYSTEMS

SYSTEMS SPECIAL INVESTIGATION GROUP OVERVIEW 1217
James B. Mason, Harry Dursch and Joel Edelman

SPACE AGING OF SOLID ROCKET MATERIALS 1225
Dean M. Lester, Leon L. Jones, R. B. Smalley, Jr. and R. Neil Ord

EFFECTS OF THE SPACE ENVIRONMENT ON SPACE-BASED RADAR PHASED-ARRAY ANTENNA; STATUS AND PRELIMINARY OBSERVATIONS (LDEF EXPERIMENT AO133) 1227
J. B. Whiteside, D. Giangano, R. L. Heuer, E. Kamykowski, M. Kesselman, W. D. Rooney, R. Schulte and M. Stauber

AN OVERVIEW OF THE FIRST RESULTS ON THE SOLAR ARRAY MATERIALS PASSIVE LDEF EXPERIMENT (SAMPLE), AO171 1241
Ann F. Whitaker and Leighton E. Young

EXPERIMENT M0003-4 ADVANCED SOLAR CELL AND COVERGLASS ANALYSIS, AN OVERVIEW 1255
Terry M. Trumble

PRELIMINARY ANALYSES OF WL EXPERIMENT # 701, SPACE ENVIRONMENT EFFECTS ON OPERATING FIBER OPTIC SYSTEMS 1257
E. W. Taylor, J. N. Berry, A. D. Sanchez, R. J. Padden and S. P. Chapman

LDEF FIBER OPTIC EXPOSURE EXPERIMENT NO. S-0109 1283
A. R. Johnston, L. A. Bergman and R. Hartmayer

OPTICAL PERFORMANCE OF EXPOSED SOLAR CELL COVERS 1299
Thomas H. Allen, Bryant P. Hichwa, Steven R. Selee, Jerry Dodds and Greg S. Long

RULED AND HOLOGRAPHIC DIFFRACTION GRATINGS EXPERIMENT (AO138-5) 1301
Francis Bonnemason

POST-FLIGHT CHARACTERIZATION OF OPTICAL SYSTEM SAMPLES, THERMAL CONTROL SAMPLES, AND DETECTORS FROM LDEF EXPERIMENT M0003, SUB-EXPERIMENTS 6 AND 13 1315
Randall R. Hodgson, James N. Holsen and Robert A. Drerup, Jr

LDEF ACTIVE OPTICAL SYSTEM COMPONENTS EXPERIMENT 1317
M. D. Blue

EFFECTS OF LONG-DURATION EXPOSURE ON OPTICAL SYSTEM COMPONENTS 1327
Gale A. Harvey

EFFECTS OF LONG TERM EXPOSURE ON OPTICAL SUBSTRATES AND COATINGS (S0050-2) 1341
John Vallimont and Keith Havey

VACUUM DEPOSITED OPTICAL COATINGS EXPERIMENT 1343
Jean Charlier

SPACE ENVIRONMENTAL EFFECTS ON COATED OPTICS 1361
T. M. Donovan, J. M. Bennett, R. Z. Dalbey, D. K. Burge and S. Gyetvay

* Part 3 is presented under separate cover.

CONTAMINATION OF OPTICAL SURFACES IN EARTH ORBIT 1377
Donald L. Kinser, Robert A. Weller, M. H. Mendenhall, D. E. Wiedlocher, R. Nichols, D. Tucker and A. Whitaker

DURABILITY EVALUATION OF PHOTOVOLTAIC BLANKET MATERIALS EXPOSED ON LDEF TRAY (S1003) 1379
Sharon K. Rutledge and Raymond M. Olle

ADVANCED PHOTOVOLTAIC EXPERIMENT, S0014: PRELIMINARY FLIGHT RESULTS AND POST-FLIGHT FINDINGS 1395
David J. Brinker, John R. Hickey and David A. Scheiman

EVALUATION OF LDEF EXPERIMENT S1002 1405
L. Preuss

LDEF SP-HVDE (SPACE PLASMA-HIGH VOLTAGE DRAINAGE EXPERIMENT) POST-FLIGHT RESULTS: LEAKAGE CURRENT AND DISCHARGE 1419
J. Y. Yaung, W. C. Wong, B. K. Blakkolb, L. E. Ryan, J. E. Chedotte and W. W. L. Taylor

LONG DURATION EXPOSURE FACILITY (LDEF) LOW TEMPERATURE HEAT PIPE EXPERIMENT PACKAGE (HEPP) FLIGHT RESULTS 1431
Roy McIntosh, Craig McCreight and Patrick J. Brennan

LONG DURATION EXPOSURE FACILITY LOW-TEMPERATURE HEAT PIPE EXPERIMENT PACKAGE POWER SYSTEM RESULTS 1441
Smith E. Tiller and David Sullivan

RESULTS FROM THE LDEF/AO076 CASCADED VARIABLE CONDUCTANCE HEATPIPE EXPERIMENT 1455
Michael G. Grote

TRANSVERSE FLAT PLATE HEAT PIPE EXPERIMENT 1467
David Shular

EXPOSURE TO SPACE RADIATION OF HIGH-PERFORMANCE INFRARED MULTILAYER FILTERS AND MATERIALS TECHNOLOGY EXPERIMENT (AO056) 1477
Gary J. Hawkins, John S. Seeley and Roger Hunneman

PASSIVE EXPOSURE OF EARTH RADIATION BUDGET EXPERIMENT COMPONENTS LDEF EXPERIMENT AO147: POST-FLIGHT EXAMINATIONS AND TESTS 1493
John R. Hickey

TRANSMITTANCE MEASUREMENTS OF ULTRAVIOLET AND VISIBLE WAVELENGTH FILTERS FLOWN ABOARD LDEF 1511
Thomas A. Mooney and Ali Smajkiewicz

RADIATION SENSITIVITY OF QUARTZ CRYSTAL OSCILLATORS EXPERIMENT FOR THE LONG DURATION EXPOSURE FACILITY (LDEF) 1523
J. S. Ahearn and J. D. Venables

LDEF ELECTRONIC SYSTEMS: SUCCESSES, FAILURES AND LESSONS 1533
E. A. Miller, L. K. Brooks, C. J. Johnson, J. L. Levorsen, O. R. Mulkey, D. C. Porter and D. W. Smith

EFFECT OF SPACE EXPOSURE ON PYROELECTRIC INFRARED DETECTORS 1547
James B. Robertson

LDEF MECHANICAL SYSTEMS 1549
W. Steve Spear and Harry W. Dursch

ON-ORBIT COLDWELDING FACT OR FRICTION? 1565
Harry Dursch and Steve Spear

THERMAL CONTROL SURFACES EXPERIMENT - FLIGHT SYSTEMS PERFORMANCE 1577
Donald R. Wilkes, Leigh L. Hummer and James M. Zwiener

FRENCH COOPERATIVE PASSIVE PAYLOAD (FRECOPA) SYSTEM RESULTS 1593
Christian Durin

EFFECTS OF ULTRA-VACUUM AND SPACE ENVIRONMENT ON CONTACT OHMIC RESISTANCE LDEF EXPERIMENT AO138-11 1607
Jean-Pierre Assié and Alfred Perotto

MICROWELDING (OR COLD-WELDING) OF VARIOUS METALLIC MATERIALS UNDER THE ULTRA-VACUUM LDEF EXPERIMENT AO138-10 1613
Jean Pierre Assié and Eric Condé

SPACE ENVIRONMENTAL EFFECTS - BIOLOGY

SEEDS IN SPACE EXPERIMENT 1625
Jim A. Alston

SPACE EXPOSED EXPERIMENT DEVELOPED FOR STUDENTS (SEEDS) (P0004-2) 1635
Doris K. Grigsby and Nelson J. Ehrlich

SURVIVAL OF EPIPHYTIC BACTERIA FROM SEED STORED ON THE LONG DURATION EXPOSURE FACILITY (LDEF) 1637
Andrew C. Schuerger, Bret L. Norman and Joseph A. Angelo, Jr.

FIRST BIOLOGICAL AND DOSIMETRIC RESULTS OF THE FREE FLYER BIOSTACK EXPERIMENT AO015 ON LDEF 1639
G. Reitz, H. Bücker, R. Facius, G. Horneck, M. Schäfer, J. U. Schott, J. Bayonove, R. Beaujean, E. V. Benton, M. Delpoux, C. Heilmann, W. Heinrich, A. R. Kranz, H. Planel, Y. Gasset, G. Gaubin, G. Portal, E. H. Graul, W. Rüther, E. Schopper, C. A. Tobias and T. C. Yang

PRELIMINARY TOTAL DOSE MEASUREMENTS ON LDEF 1643
G. Reitz

TOTAL DOSE EFFFECTS (TDE) OF HEAVY IONIZING RADIATION IN FUNGUS SPORES AND PLANT SEEDS - PRELIMINARY INVESTIGATIONS - 1651
A. R. Kranz, M. W. Zimmermann, R. Stadler, K. E. Gartenbach and M. Pickert

PRELIMINARY RESULTS OF THE ARTEMIA SALINA EXPERIMENTS IN BIOSTACK ON LDEF 1661
E. H. Graul, W. Rüther and C. O. Hiendl

LONG-TERM EXPOSURE OF BACTERIAL SPORES TO SPACE 1667
G. Horneck, H. Bücker and G. Reitz

SPACE ENVIRONMENTAL EFFECTS - MICROGRAVITY

RESULTS OF THE TTF-TCNQ AND THE CALCIUM CARBONATE CRYSTALLIZATION ON THE LONG DURATION EXPOSURE FACILITY 1675
Kjeld Flemming Nielsen and M. David Lind

THE FUTURE

THE ROLE OF THE LONG DURATION EXPOSURE FACILITY IN THE DEVELOPMENT OF SPACE SYSTEMS 1687
Sally A. Little

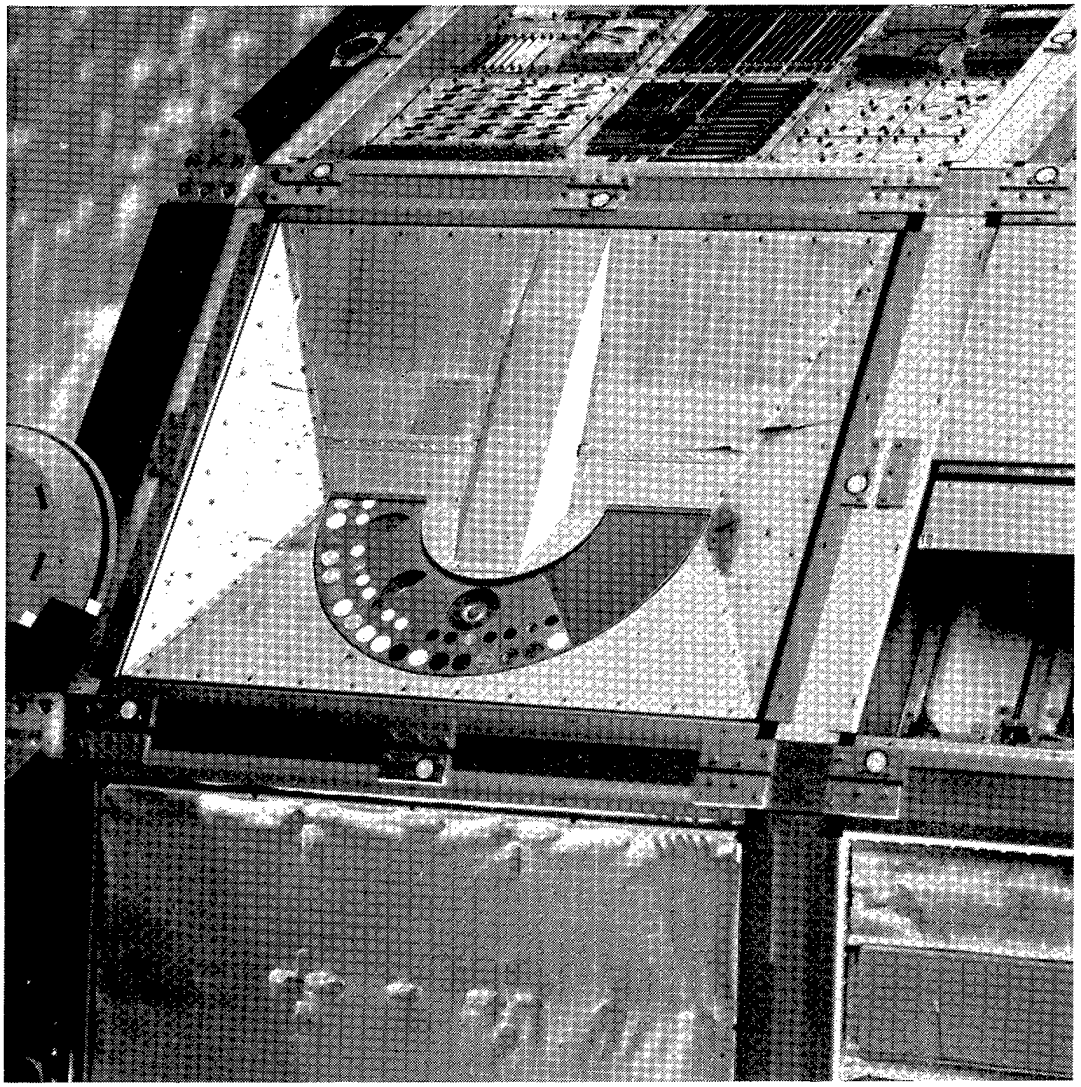
RETRIEVABLE PAYLOAD CARRIER--NEXT GENERATION LONG DURATION EXPOSURE FACILITY 1691
Arthur T. Perry

COLOR PHOTOGRAPHS 1701

AUTHOR INDEX 1703

PART 2

SPACE ENVIRONMENTAL EFFECTS
MATERIALS



PRELIMINARY FINDINGS OF THE LDEF MATERIALS SPECIAL INVESTIGATION GROUP

Bland A. Stein
NASA - Langley Research Center
Hampton, VA 23665-5225
Phone: 804/864-3492, Fax: 804/864-7729

H. Gary Pippin
Boeing Defense and Space Group
Mail Code 8232, P. O. Box 3999
Seattle, WA 98124-2499
Phone: 206/773-2846, Fax: 206/773-4946

SUMMARY

The retrieval of the National Aeronautics and Space Administration's Long Duration Exposure Facility (LDEF) from low-Earth orbit provided an opportunity for the study of long-duration space environmental effects on materials that is unparallelled in the history of the U.S. space program. The 5-year, 9-month flight of LDEF greatly enhanced the potential value of most LDEF materials, compared to that of the original 1-year flight plan. NASA recognized this potential by forming the LDEF Space Environmental Effects on Materials Special Investigation Group (MSIG). Its goal is to explore the expanded materials analysis opportunities available in the LDEF structure and on experiment trays, so that the combined value of all LDEF materials data to current and future space missions would be addressed and documented.

This paper presents the charter and scope of MSIG activities, followed by an overview of the preliminary MSIG observations. These observations of low-Earth orbit environmental effects on materials were made in-space during LDEF retrieval and during LDEF tray deintegration. Also presented are initial findings of laboratory analyses of LDEF materials. Included are effects of individual environmental parameters: atomic oxygen, ultraviolet radiation, meteoroid and debris impacts, thermal cycling, vacuum, and contamination, plus combined effects of these parameters. Materials considered include anodized aluminum, polymer-matrix composites, polymer films, silvered Teflon thermal blankets, and a white thermal control paint. MSIG plans for further evaluations and data basing are addressed.

INTRODUCTION

The National Aeronautics and Space Administration / Strategic Defence Initiative Organization Space Environmental Effects on Materials Workshop, June 1988, identified and prioritized candidate materials spaceflight experiments needed to validate long-term performance of materials on future spacecraft (reference 1). Working groups considered six environmental factors which may have significant effects on spacecraft materials: atomic oxygen, solar radiation, trapped radiation, micrometeoroids and debris, contamination, and spacecraft charging. Although most of the priorities of each group were parochial to its specific discipline, the highest priority identified by all participants of that workshop was virtually unanimous: The return of the NASA Long Duration Exposure Facility safely to earth, followed by a detailed analysis of its materials to compare with data obtained in previous relatively short in-space exposures and to validate or

identify deficiencies in ground testing and simulation facilities and materials durability analytical models. As this LDEF Symposium proved, the expectations of the NASA/SDIO Workshop were well founded. The initial in-space and experiment deintegration observations of LDEF at the end of its remarkable flight are providing the LDEF investigators an unparalleled opportunity to define space environment parameters and their long-term individual and combined effects on critical properties of materials for spacecraft applications.

The National Aeronautics and Space Administration Long Duration Exposure Facility (LDEF), ref. 2, was launched into low-Earth orbit (LEO) from the payload bay of the Space Shuttle Orbiter Challenger in April 1984 (figure 1). It was retrieved from orbit by the Columbia in January 1990 (fig. 2). The 57 LDEF experiments covered the fields of materials, coatings, and thermal systems; space science; power and propulsion; and electronics and optics. LDEF was designed to provide a large number of economical opportunities for science and technology experiments that require modest electrical power and data processing while in space and which benefit from post-flight laboratory investigations of the retrieved experiment hardware on Earth. It was also designed to maintain these experiments in a stable orbital attitude to enable determination of directional effects of the space environment parameters. Most of the materials experiments were completely passive; their data must be obtained in post-flight laboratory tests and analyses.

The 5 year, 9 month flight of LDEF greatly enhanced the potential value of most LDEF materials, compared to that of the original 1-year flight plan. NASA recognized this potential by forming the LDEF Space Environmental Effects on Materials Special Investigation Group (MSIG) to address the expanded opportunities available in studies of the LDEF structure and experiment tray material which were not originally considered to be materials experiments, so that the value of all LDEF materials data to current and future space missions would be assessed and documented. Similar Special Investigation Groups were formed for the disciplines of Systems, Ionizing Radiation, and Meteoroids/Debris.

Individual papers (see, for example, ref. 3) have presented initial post-retrieval observations, but this symposium was the first opportunity for all LDEF investigators to present initial results of their observations and analyses of LDEF data in one forum.

This summary paper presents the preliminary findings of the LDEF MSIG, beginning with its charter and general plans. Visual observations in space and during experiment tray deintegration are surveyed, indicating effects of individual low-Earth orbit environmental parameters and synergistic effects of these parameters. Specific effects on material properties and analysis models are considered for a few examples of metals, polymers, composites, thermal control blankets and paints on LDEF. Initial results of atomic oxygen fluence and mission total solar exposure calculations are presented. Each of these findings has been further detailed in the 11 additional papers presented at this symposium which describe initial MSIG evaluations (refs. 4 through 14). This paper concludes with an outline of planned MSIG evaluations and a brief recapitulation of its current findings.

THE MATERIALS SPECIAL INVESTIGATION GROUP

The MSIG was chartered to investigate the effects of the long-term LEO exposure on structure and experiment materials which were not originally planned to be test specimens, and to integrate the results of these investigations with data generated by the Principal Investigators of the LDEF experiments into the LDEF Materials Data Base. The LDEF Materials Data Analysis Workshop (ref. 15) addressed the plans resulting from that charter. The detailed MSIG Materials Analysis Plan was distributed to the LDEF technical community; additional copies are available from the authors of this paper.

MSIG membership includes 25 technical experts in the fields of atomic oxygen, radiation, contamination and other space environment effects on materials. Researchers with experimental and analytical experience in chemical, mechanical and physical properties of spacecraft materials and data basing are included. Several members provide liaison with the other LDEF Special Investigation Groups. The members represent technical laboratories and organizations throughout the United States, and laboratories in Canada and Europe. A number of MSIG members are also Principal Investigators of LDEF experiments.

Initial considerations of MSIG related to significant issues concerning space environmental effects on materials and the data potentially available from LDEF analyses to address these issues, as outlined in fig. 3. The general plan for MSIG operations is as follows:

- Systematically examine identical materials in multiple locations around LDEF to establish directionality of atomic oxygen erosion, ultraviolet radiation degradation, contamination, etc.

- Analyze selected samples from LDEF "non-materials" experiments and samples contributed from LDEF materials experiments.

- Establish central materials analysis capability:
  - Standardized, non-contaminating procedures for sampling / shipping / archiving
  - Uniform test / analysis procedures and ground simulation tests
  - Basis for assessment of laboratory-to-laboratory variations in materials data

- Focal point for coordination of all LDEF materials analyses:
  - Sponsor LDEF materials workshops / symposia
  - Generate unified LDEF Materials Data Base, including data from principal investigators, supporting data groups, and special investigation groups

The Boeing Defense and Space Group Laboratories in Seattle and Kent, Washington were selected as the MSIG central analysis laboratory by the MSIG, shortly after its formation in 1989.

VISUAL OBSERVATIONS IN SPACE AND DURING LDEF TRAY DEINTEGRATION

LDEF was subjected to extensive photographic and video surveys by the Shuttle Orbiter Columbia astronauts during its retrieval from orbit (fig. 2), prior to insertion into the Columbia Payload Bay. After the Columbia landing at Edwards Air Force Base in California and the ferry flight to the NASA-Kennedy Space Center in Florida, LDEF was again subjected to extensive photographic analysis prior to and during deintegration of the experiment trays. This section describes and illustrates some of the initial observations concerning materials on LDEF, catagorized according to low Earth orbit environmental effects which can degrade material properties.

Atomic Oxygen Effects

Significant degradation of polymer films and polymer-matrix composites was observed on the forward-facing experiment trays of LDEF, particularly those near the LDEF leading edge, 8° of

yaw off row 9 towards row 10. (Experiment trays on row 9 are generally referred to as leading edge trays; row 3 trays are similarly referred to as trailing edge trays. Flat surfaces on rows 6 and 12 thus receive a "grazing incidence" flux of atomic oxygen). Surface recessions of greater than 0.005-inch were observed for Kapton and Mylar films. In the NASA-Langley polymer films and coatings experiment, S0010 on row 9, a number of polymer films up to 0.003-inch-thick were completely eroded (fig. 4) and approximately one ply (~0.005-inch) of graphite/epoxy composite was eroded. This erosion is attributed to atomic oxygen (AO) impingement.

Forward-facing surfaces of silvered Teflon (Ag/FEP) second surface mirror thermal blankets on experiment A0178 from the Dublin Institute of Advanced Studies (which had faced the atomic oxygen flux) appeared non-specular (diffuse) and "milky" in color, as shown in fig. 5 for Ag/FEP on tray C8. The same thermal blanket material on the rear surfaces of LDEF, which experienced low atomic oxygen fluences, remained specular and appeared identical to control specimens, as shown in fig. 5 for identical Ag/FEP material on tray F2 from experiment P0004, Park Seed Co. Scanning electron microscope evaluations of the non-specular Ag/FEP indicated surface erosion of approximately 0.001-inch of FEP Teflon. Based on FEP specimens recovered from previous exposures in space, ref.16, AO erosion of the FEP surface of 0.00012 was predicted for the LDEF exposure. More studies are needed to determine whether a threshold exposure level exists for FEP Teflon erosion in LEO due to AO and UV, as postulated in ref. 17.

It was originally feared that that the diffuse surface appearance of the Ag/FEP might indicate a change in the thermal control properties of this material, which has been widely used in space vehicle thermal protection systems. However, as will be shown subsequently, solar absorptance/thermal emittance ratios of eroded Ag/FEP were not degraded. Significant changes in thermal control properties of the thermal blankets were only noted where heavy surface contamination is present.

Further details of atomic oxygen interactions with LDEF materials, including AO "undercutting" are presented in refs. 7 and 8.

Solar UV Radiation Effects

The ability to determine the effects of specific space environments on materials due to the remarkable stability of LDEF's orbital attitude was repeatedly demonstrated by observation of similar or identical materials at various positions around the LDEF satellite. A good example is shown in fig. 5. At the top of the photograph for tray F2 is a disk of white A276 thermal control paint on a tray clamp. This disk received the full solar ultraviolet (UV) radiation exposure but very little atomic oxygen. It turned a brown color and its thermal control properties (discussed subsequently) were significantly affected. A similar A276 disk on tray C8, which received extensive doses of solar radiation plus atomic oxygen, remained white and (as shown subsequently) retained its thermal control properties. Solar ultraviolet effects on unprotected polymer films were noted on a number of LDEF experiments, resulting in film discoloration and mechanical degradation, as discussed in several presentations at this symposium.

Meteoroid and Debris Effects

Thousands of meteoroid and debris impacts were observed on experiment trays and on the LDEF structure. There were no catastrophic structural effects of these impacts. The largest impact crater was approximately 0.2-inch in diameter. The impact density was much larger on the ram-facing surfaces of LDEF than on the wake-facing surfaces. Presentations by LDEF Principal

Investigators and the Meteoroid and Debris Special Investigation Group at this symposium provided extensive details of initial investigations of these impacts.

Silvered Teflon thermal blankets were easily penetrated by these impacts. An interesting phenomenon was noted: A delaminated area (vapor-deposited silver/Inconel coating delaminated from the FEP Teflon) from a fraction of an inch to more than one inch in diameter surrounded the thousandth-inch diameter craters made by the meteoroid/debris impacts (figs. 6 and 7). Although the thermal control properties of the Ag/FEP were not generally affected by the LDEF exposures, the thermal behavior of delaminated Ag/FEP is not the same as the original material (see subsequent section) and requires further study.

Vacuum, Contamination, and Thermal Cycling Effects

A thin, brownish molecular contamination layer was observed on all LDEF areas exposed to sunlight. Figure 8 shows this contamination on the exposed areas of the LDEF "skeleton" structure after the experiment trays were removed. The lighter regions on the aluminum alloy structural elements are areas which were covered by tray edges or tray clamps; the darker regions have the contamination layer. Significant outgassing in the vacuum of low-Earth orbit and subsequent deposition of contaminants was also evident in several localized areas of the LDEF surface, particularly around some electrical interconnects; this contamination was much heavier than the general contamination layer. Preliminary MSIG contamination studies will be discussed later in this report.

Thin polymer films were observed to be broken on experimental trays on rows 3, 6, 8, and 9 and on the space end of LDEF. Thermal cycling may have been a contributing factor to this polymer film degradation.

Synergistic Effects

As mentioned previously, one of the most important aspects of the LDEF mission was the stability of the vehicle's orbital attitude. Similar materials on different surfaces of LDEF thus received different combinations of space environmental factors. Since combinations of such factors as atomic oxygen, electromagnetic and particulate radiation, thermal cycling, vacuum, and meteoroid and debris impacts are extremely difficult or impossible to correctly simulate in ground test facilities, LDEF offers a unique opportunity to study these synergistic effects on spacecraft materials subjected to long term LEO exposures.

Meteoroid/debris impacts and AO appear to have combined to produce dark "bullseyes" on silvered Teflon thermal blankets (fig. 7). Ag/FEP adhesively bonded films show a similar effect. The darker bands in the bullseyes may be areas of the delamination where silver completely disbonded from the FEP Teflon, and the silver surface was subsequently oxidized by AO. The lighter bands may be areas which delaminated with a thin layer of FEP still attached to the Ag; this thin layer subsequently inhibited oxidation of the silver surface.

The widespread molecular contamination previously discussed appears to be due to combined effects of vacuum, thermal cycling, atomic oxygen, and solar UV radiation. Several theories have been postulated to explain the widespread contamination film on LDEF. One which seems to be supported by most observations to date involves a complex organic/silicone "cloud" which emanated from the inside of LDEF and from some of the experiments when they were heated by the sun in the vacuum of LEO. This cloud surrounded LDEF during its flight (or, at

least, during the initial orbits). Solar UV radiation and/or AO could have polymerized ingredients of this cloud, which then condensed on external surfaces during the cooler parts of their thermal cycles. Close examination of the brown molecular contamination showed that it had been deposited in numerous layers. Subsequent exposure to atomic oxygen appears to have "fixed" this contamination by oxidizing the silicones into silicates.This contamination was generally lighter in color on the surfaces which were exposed to the highest atomic oxygen fluences. That observation may indicate that, later in the LDEF mission, the contamination cloud was less dense or had dissipated completely so that continuing AO exposure eroded the silicate surface of the contamination. This contamination scenario is alluded to in refs. 4 and 6. It remains to be confirmed by future detailed chemical/morphological study of the contaminated surfaces on various parts of the LDEF structure and trays. LDEF may provide some of its most important findings as a large scale "contamination witness plate".

Another example of synergism of low-Earth orbit environmental factors was indicated by the behavior of the A276 thermal control paint disks, as illustrated in fig. 5. The coloration of the disks on the wake-facing surfaces of LDEF, and changes in their thermal control properties discussed later in this report, appears to be caused by vacuum UV effects on the polyurethane binder in the white paint. On the ram-facing LDEF surfaces (exposed to AO), this UV-affected layer was eroded away and the coating remained white, with unchanged thermal control properties. Erosion of the paint binder loosened the outer-surface pigment particles of the paint, some of which may have dislodged from the surface. However, enough pigment was retained to maintain the thermal control property stability throughout the 5.8-year LDEF mission.

MSIG POST-DEINTEGRATION ANALYSES AND OBSERVATIONS

Since the completion of LDEF experiment tray deintegration in May of 1990, the Materials Special Investigation Group has had access to LDEF structural materials, thermal control coatings and films, materials from "non-materials experiments", and a few selected specimens from LDEF materials experiments. Most of the MSIG testing and analysis has been performed at the Boeing Defense and Space Group Laboratories. Significant additional MSIG testing and analysis has also been performed in the laboratories of NASA - Langley Research Center, NASA - Lewis Research Center, Aerospace Corp., and the Jet Propulsion Laboratory. This section describes the initial findings of these post-deintegration analyses on various LDEF materials.

Chromic-Acid Anodized 6061-T6 Aluminum Alloy

The LDEF structure and experiment trays and the tray clamps were fabricated from 6061-T6 aluminum alloy. They were subjected to the LEO environment for 5 years and 9 months. They experienced numerous meteoroid and debris impacts. No significant changes were observed which would affect structural performance.

The aluminum structure, experiment trays, and clamps were chromic-acid anodized to form a thin thermal control layer on its surface with a solar absorptance-to-thermal emittance ratio (α_s/ε) of 2.0. Thermal control properties were measured at Boeing on 228 tray clamps; all LDEF side and end tray locations were extensively sampled (ref. 13). The average solar absorptance and thermal emittance properties and the ratios are shown in fig. 9 for the sides of the clamps facing the space environment (exposed side), the sides facing inward towards the LDEF structure (unexposed side) and 4 control specimens which were maintained in ground storage during the LDEF mission. Thermal control properties were not significantly changed by the LDEF exposure. However, there

was a slight increase in the α_s/ε average for the exposed surfaces (from 2.00 to 2.24). This increase has also been found by other LDEF investigators.

Polymer Films and Polymer-Matrix Composites

As indicated previously, uncoated polymer films and uncoated polymer-matrix composites facing the LDEF atomic oxygen flux were severely degraded by atomic oxygen (see refs. 6 and 18). Non-fluorinated polymer films on LDEF row 9 showed surface recessions of 0.005-inch or greater. This erosion correlated very well with fluence and direction of the AO flux. Figure 10 shows an example of Kapton polyimide film eroded by AO impingement at a grazing angle, studied at NASA - Langley (ref. 6). The eroded morphology results in a diffuse surface appearance; an adjacent area of the Kapton film remained smooth and specular in appearance because it was shadowed from AO by another specimen adjacent to it.

Uncoated graphite fiber reinforced polymer-matrix composites exposed on row 9 lost approximately 1 ply (0.004 to 0.005-inch) of thickness due to atomic oxygen erosion. The graphite fibers eroded somewhat less than the polymer matrices; exposed and loose fibers could be seen on eroded surfaces. Mechanical properties of 4-ply, $[\pm 45°]_s$ thermoset-matrix composites generally degraded in proportion to the erosion of the matrix; elastic moduli of selected specimens showed a reduction of about 25% compared to control specimens (ref. 18). There were some initial indications that thermoplastic-matrix composites may have degraded less than thermoset-matrix composites. The most positive initial finding concerning the polymer-matrix composite materials flown on LDEF is that thin inorganic coatings prevented AO erosion and adhered very well to the composite surfaces during 5.8 years of environmental exposure, including thermal cycling, in low-Earth orbit. One such coating consisted of micron-thick layers of vacuum-deposited SiO_2/Ni.

Polymer film and polymer-matrix composite surfaces eroded by AO were examined to determine effects on polymer chemistry (ref. 6). Figure 11 shows a typical example of the results in a Diffuse-Reflectance FTIR analysis of C6000/P1700 (graphite/polysulfone) composite exposed on LDEF row 9 and an unexposed control specimen. This and auxiliary analyses showed no significant changes in chemistry or molecular weight distribution of the polymer matrix in the regions of LDEF exposed to (and eroded by) atomic oxygen. Studies on the effects of other environmental parameters of the low-Earth orbit on the properties of polymers and polymer-matrix composites which were not exposed to significant fluences of atomic oxygen have been initiated.

Silvered Teflon (Ag/FEP) Second Surface Mirror Thermal Blankets

Properties were measured at Boeing on specimens from all silvered Teflon thermal blankets from LDEF experiment A0178 (Dublin Institute for Space Studies); details are reported in ref. 11. The average FEP Teflon recession rate due to AO exposure was calculated at several locations around the LDEF surface to be $0.35 \pm 0.01 \times 10^{-24}$ cm^3/atom. This erosion yield is considerably higher than previous data generated for Ag/FEP material samples exposed for several days at high AO flux in the Shuttle Orbiter payload bays during Space Shuttle missions STS 5 and STS 8 (ref. 16). This information also implies an induction period prior to the onset of significant mass loss due to AO erosion for Ag/FEP thermal blankets in LEO (ref. 17). Additional MSIG studies on Ag/FEP at NASA-Langley, Aerospace Corp., and Jet Propulsion Laboratory are presented in ref.

6, which has an excellent description of Ag/FEP second surface mirror blanket composition and function, and refs. 9 and 10, respectively.

As noted previously in this paper, silvered Teflon thermal blankets delaminated at meteoroid/debris impact sites. NASA - Lewis Research Center conducted a test in air to qualitatively determine the effects of the delamination on the thermal behavior of the Ag/FEP blanket material. The results are illustrated in fig. 12. An infrared camera was positioned to directly view the 0.5-mm impact site surrounded by the 10-mm wide delamination. A heating lamp behind the Ag/FEP specimen provided a transient heat pulse. The FEP Teflon surface on the unaffected area of the blanket heated immediately, as indicated by the lighter area in the infrared photograph. The delaminated region (darker region surrounding the perforated impact site) showed a definite thermal lag, indicating that the thermal control properties of Ag/FEP are significantly affected by the delamination. Further studies will be required to quantify this behavior.

Thermal control properties, α_s and ε, were measured at Boeing for LDEF-exposed Ag/FEP blanket material from each of the rows utilized for LDEF experiment A0178 (ref. 11). The results are shown in fig. 13. Specimens in rows 6 through 11 had diffuse surfaces due to AO erosion while specimens from rows 1 through 5 were specular, similar in appearance to unexposed (control) material. No significant differences were noted in α_s/ε ratio for these specimens (fig. 13), excepting for a dramatic increase in α/ε for the specimen in row 7 that has a heavy contamination layer on it.

Mechanical property measurements on the Ag/FEP blankets (ref. 11) included tensile strength and elongation and dynamic mechanical analysis. The tensile strengths of the exposed films are shown as a function of LDEF row number in fig. 14. Strengths were measured on samples exposed to the LEO environment and on control specimens on the same blankets which were folded under the sides of the trays and thus not exposed to AO, solar radiation, etc. In the areas of high AO fluence, rows 6 through 11, no significant differences in tensile strength were noted between exposed and unexposed specimens. The blanket specimen cross sectional areas have been measured to include the effects of FEP erosion in the strength calculations. In the areas of low AO fluence (rows 1 through 5), however, the tensile strength of the Ag/FEP was degraded by approximately 30%. This implies that solar UV radiation combined with the other LEO environmental factors, but in the absence of atomic oxygen erosion, has affected at least the surface of the FEP Teflon. Considerations of this phenomenon are presented in ref. 9. Further studies are required to determine the detailed mechanism(s) of this degradation. Surface analyses of the AO-affected Ag/FEP blanket materials were conducted at Boeing using optical microscopy, scanning electron microscopy, scanning ion mass spectrometry, and electron spectroscopy for chemical analysis. The results supported an AO erosion mechanism causing the characteristic "microforest" morphology with no indication of FEP surface chemistry change due to chemical interactions with AO. Analyses at NASA - Langley confirmed these findings.

White Thermal Control Coating Disks

The A276 white thermal control coating disks (see fig. 5 and previous discussion) were subjected to general microscopic examination, surface spectroscopy, thermal control property determinations, and cross-section studies at Boeing (ref. 12). The general findings of the surface analyses were that most anomalies on the disks appear to have been a result of preflight handling damage and contamination. The on-orbit contamination film deposited on some of the disks contained silicon dioxide and fluorine.

Solar absorptance and thermal emittance values were determined for the A276 disks on 100 tray clamps; all LDEF side and end tray locations were sampled. The results are shown in fig. 15. Specimens which faced the atomic oxygen flux (angle of incidence from 0° to slightly more than 90°) showed showed marginal increases in emittance and no significant change in absorptance, so that they remained white with α/ε values of approximately 0.31 to 0.38 at the end of the LDEF mission. Discoloration of the polyurethane resin binder in the A276 paint increased solar absorptance of the wake-facing disks on LDEF from 0.28 (control specimen) to ≤ 0.57, raising the α/ε values from 0.32 (control) to a range of values between 0.61 and 0.66 in the disks at high angles of incidence (fig. 15) at end of mission. Cross-sections of these A276 paint disks showed that the increase in wake-facing disk absorptance was due to UV darkening of the outermost resin layer in the thermal control coating, further supporting the mechanism discussed previously. Erosion measurements on these cross-sectioned A276 paint disks were of questionable value, due to paint thickness variability.

LDEF CONTAMINATION

One of the critical tasks conducted by MSIG for the LDEF Program is the definition of LDEF contamination for supporting data to all LDEF investigators. The major part of this effort is performed by Boeing. Initial results are presented in refs. 4 and 5. A detailed preliminary report on both particulate and molecular aspects of LDEF contamination was distributed. Additional copies are available from the LDEF Science Office at NASA - Langley Research Center.

MSIG examined and photographically documented more than 2000 items of LDEF hardware and collected more than 200 tapelifts from representative LDEF surfaces. Surface morphology and surface chemistry studies of 14 Ag/FEP thermal blankets included optical and electron microscopy, ESCA, SIMS, micro-FTIR, and optical crystallography. The silicon-containing molecular contamination layer (fig.8) found on many LDEF surfaces (discussed previously) was conspicuously absent from AO-exposed Ag/FEP, due to AO erosion of the FEP surface. The particulate contamination population on the Ag/FEP blankets increased with proximity to the edges of the trays. Contamination characteristics of more than 90 anodized aluminum alloy tray clamps have been determined. Impact-penetrated particulate contaminants were found, aiding in the chronology of LDEF contamination. Selected areas of 22 experiment trays and 16 tray clamps were subjected to contamination particle count analysis. The counts for large particles ($>100\mu m$) were higher than expected, based on current contamination models.

Contamination, particularly molecular contamination, undoubtedly increases the difficulty of analysis of effects of LEO environmental parameters on LDEF materials. But, in another sense the opportunities offered by LDEF as a large scale contamination experiment for a satellite in long-term LEO exposure is unique in spaceflight history. In that sense, much more study of the contaminated LDEF surfaces is warranted than the preliminary studies completed to date. As a contamination experiment, LDEF is:

- The ultimate witness plate for the Shuttle Orbiter Payload Bay
- A long-term molecular film deposition experiment in LEO
- A study of orbital effects on both molecular and particulate surface contaminants
- A validation study for current contamination monitoring systems

LDEF ATOMIC OXYGEN AND SOLAR EXPOSURE CALCULATIONS

MSIG studies are being performed by Boeing to determine atomic oxygen fluences and solar exposures for supporting data to all LDEF investigators for the analysis of their experiments (ref. 14). Atomic oxygen fluences were calculated for each tray location, utilizing the model atmosphere from MSIS-86 (ref. 19). The atomic oxygen fluence model was modified by Boeing to include molecular velocity distribution and atmospheric motion. The effects on the model calculations are shown in fig. 16. Previous models which do not include thermal molecular velocity predict very low atomic oxygen fluences for incidence angles greater than 90°. AO fluences for incidence angles up to 80° are not significantly affected by the model corrections but grazing angle (~90° to ~110°) fluences are significantly changed when the corrections are included. The data in fig. 15 support the necessity for these changes in the AO fluence model, showing indications of significant AO effects on the α/ε behavior of A276 white thermal control paint at incidence angles greater than 90°.

Utilizing the revised atomic oxygen fluence model, AO fluence calculations were made for each tray location at the conclusion of the LDEF mission. The detailed report of the preliminary results is available from the LDEF Science Office at NASA - Langley Research Center*. Those results are summarized in fig. 17. The 8° LDEF yaw angle of the ram direction from row 9 is included in these calculations. The ram direction fluence was 8.4×10^{21} atomic oxygen atom impacts per square centimeter; this is approximately 6% of the expected Space Station Freedom ram fluence after 30 years of exposure in LEO. There were significant atomic oxygen fluences on LDEF at angles greater than 90° to the ram direction (as noted above); 4.3% of the AO ram fluence was deposited on LDEF experiment trays at a 90° angle of incidence.

Calculations of solar UV exposures, expressed as equivalent sun hours (ESH), are summarized for each LDEF tray location in fig. 18. Maximum exposures were 14,500 ESH, received on the space end trays. The leading and trailing edge trays (rows 9 and 3) both received 11,100 ESH. The side trays (rows 6 and 12) received 6,500 ESH and 6,900 ESH, respectively. The Earth end trays received the lowest solar UV exposures, 4,500 ESH.

CONTINUING MSIG EVALUATIONS AND ACTIVITIES

As noted in several sections of this report, further studies of LDEF specimens of the classes of materials studied to date will yield definitive data on materials behavior and the complex mechanisms of materials degradation in the LEO environment. MSIG studies of some LDEF materials have barely begun. The tasks remaining in the MSIG plan include evaluations of archived specimens of composite materials, fluorocarbons, polymer films, adhesives, organic and inorganic coatings, fasteners, lubricants, o-rings, and copper grounding straps. In addition, the MSIG central analysis laboratory and other laboratories will be providing analyses of high-priority materials specimens from LDEF Principal Investigators and other Special Investigation Groups.

*These AO fluence data are the results of preliminary calculations. Further refinements in calculations of LDEF orbits will result in small adjustments in these fluences. The new fluence data will be released by the LDEF Science Office to all LDEF Investigators as quickly as possible.

The LDEF materials data will be a unique collection of long-term exposure effects in LEO on a large range of documented materials, with control specimens on LDEF (facing inwards) and in storage in laboratories on earth. The data from the completed analyses, those in progress, and those to be conducted will enable validation of space environmental effects models and foster modification of these models for more accurate prediction of long term materials behavior in space than is currently possible. The LDEF data will also be used by MSIG to evaluate current methods of ground testing of materials durability in individual and combined parameter simulations of space environmental effects on new candidate spacecraft materials, which have been developed since LDEF was launched. This information should be invaluable to developers of new materials concepts to meet the requirements of future long-term space missions. LDEF will certainly provide the benchmark for for planning of future space environmental effects in-space experiments and the reference data for such experiments.

The other remaining MSIG tasks include documentation and archiving of as many LDEF materials specimens as can be preserved to retain their characteristics for future analyses. Degradation of specimen surfaces due to interactions with the atmospheres in ground laboratories is a considerable concern, as pointed out in ref. 6. The final MSIG task is the development of data bases for all LDEF materials data, utilizing the NASA - Marshall Space Flight Center MAPTIS data basing system. Spacecraft designers and their materials analysts from industry and government will be consulted to determine the most useful format(s) for the LDEF materials data for spacecraft design.

MSIG PRELIMINARY FINDINGS

The charter of the LDEF Materials Special Investigation Group, the scope of its activities, initial observations and preliminary findings of its studies to date, and plans for future evaluations of LDEF materials have been presented.

General observations include the following:

- Aluminum structure: No significant changes were observed which would affect structural performance
- Uncoated polymers, composites, films on leading edge were eroded / oxidized
- Molecular contamination of LDEF was extensive
- Atomic oxygen fluence models must be revised to account for thermal velocity distributions to accurately predict grazing angle fluences

Specific findings on materials include:

- Chromic acid anodized aluminum thermal properties were not significantly changed
  - Small increases in absorptance / emittance ratios noted
- Uncoated polymeric matrix composites and polymer films were degraded
  - Carbon fibers, polymer matrices, and films eroded by atomic oxygen
  - Thin inorganic coatings prevented erosion and exhibited good adherence

- Silvered FEP Teflon thermal control blankets were affected by LDEF exposures
  - AO erosion of FEP Teflon significantly greater than predicted; induction period implied
  - Sizeable delaminations of silver from FEP at meteoroid/debris impacts; thermal "lag"
  - No significant degradation of absorptance / emittance
  - Degradation of tensile strength due to UV

- A276 white thermal control paint was affected
  - Absorptance nearly doubled due to UV / contamination effects in LDEF areas where atomic oxygen fluence was low
  - Absorptance not changed in areas of LDEF subjected to high atomic oxygen fluence, which eroded and "cleaned" the surface

MSIG provided enhanced definition of LDEF mission environments to all LDEF investigators:

- Atomic oxygen fluences and total solar exposures

- Contamination exposure history

In conclusion, LDEF not only met, but has already surpassed the expectations of space environmental effects experts (ref. 1) regarding the value of its mission. Preliminary LDEF information on current spacecraft materials is already useful for design of future satellites for long-term LEO missions. Future data and analyses by LDEF Principal Investigators and MSIG will provide guidelines for improved models to define space environmental effects on materials, for methodology to improve ground simulation testing on emerging materials, and for development of new concepts in durable materials for spacecraft.

REFERENCES

1. Teichman, Louis A. and Stein, Bland A. (Compilers): NASA/SDIO Space Environmental Effects on Materials Workshop. NASA Conference Publication 3035, 1989.

2. Clark, Lenwood G.; Kinard, William H.; Carter, David J. Jr.; and Jones, James L. Jr. (Editors): The Long Duration Exposure Facility (LDEF). NASA SP-473, 1984.

3. Kinard, William H.; Martin, Glenna D.; and O'Neal, Robert L.: Initial Results from the Long Duration Exposure Facility Postretrieval Observations. AAS Paper 91-15, 1991.

4. Crutcher, E.R.: Nishimura, L.S.; Warner, K.J.; and Wascher, W.W.: Migration and Generation of Contaminants from Launch through Recovery: LDEF Case History. Presented at the First LDEF Post-Retrieval Symposium, Kissimmee, FL, June 1991.

5. a. Crutcher, E.R. and Wascher, W.W.: Particle Types and Sources Associated with LDEF.
   b. Crutcher, E.R.: Nishimura, L.S.; Warner, K.J.; and Wascher, W.W.: Quantification of Contaminants Associated with LDEF.
   c. Crutcher, E.R. and Warner, K.J.: Molecular Films Associated with LDEF.
All presented at the First LDEF Post-Retrieval Symposium, Kissimmee, FL, June 1991.

6. Young, P.R. and Slemp, W.S.: Chemical Characterization of Selected LDEF Polymeric Materials. Presented at the First LDEF Post-Retrieval Symposium, Kissimmee, FL, June 1991.

7. de Groh, K.K. and Banks, B.A.: Atomic Oxygen Undercutting of LDEF Aluminized Kapton Multilayer Insulation. Presented at the First LDEF Post-Retrieval Symposium, Kissimmee, FL, June 1991.

8. Banks, B.A.: Atomic Oxygen Interactions with FEP Teflon and Silicones on LDEF. Presented at the First LDEF Post-Retrieval Symposium, Kissimmee, FL, June 1991.

9. Brinza, D.E.; Liang, R.H.; and Stiegman, A.E.: VUV-Induced Degradation of FEP Teflon Aboard LDEF. Presented at the First LDEF Post-Retrieval Symposium, Kissimmee, FL, June 1991.

10. Hemminger, C.S.; Stuckey, W.K.; and Uht, J.C.: Space Environmental Effects on Silvered Teflon Thermal Control Surfaces. Presented at the First LDEF Post-Retrieval Symposium, Kissimmee, FL, June 1991.

11. Rousslang, K.; Crutcher, E.R.; and Pippin, H.G.: Results of Examination of Silvered Teflon from the Long Duration Exposure Facility. Presented at the First LDEF Post-Retrieval Symposium, Kissimmee, FL, June 1991.

12. Golden, J.L.: Results of Examination of the A-276 White and Z-306 Black Thermal Control Paint Disks Flown on LDEF. Presented at the First LDEF Post-Retrieval Symposium, Kissimmee, FL, June 1991.

13. Plagemann, W.L.: Space Environmental Effects on the Integrity of Chromic Acid Anodized Coatings. Presented at the First LDEF Post-Retrieval Symposium, Kissimmee, FL, June 1991.

14. Bourassa, R.J.; Gillis, J.R.; and Rousslang, K.W.: Atomic Oxygen and Ultraviolet Radiation Mission Total Exposures for LDEF Experiments. Presented at the First LDEF Post-Retrieval Symposium, Kissimmee, FL, June 1991.

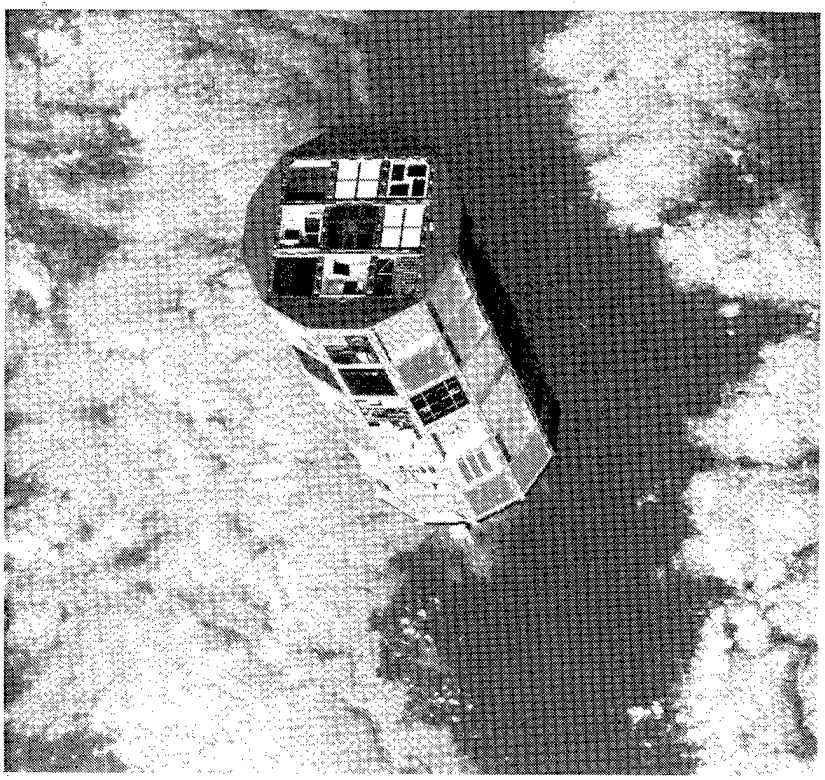
15. Stein, Bland A. and Young, Philip R. (Compilers): LDEF Materials Data Analysis Workshop. NASA Conference Publication 10046, 1990.

16. Visentine, J.T.; Leger, L.J.; Kuminecz, J.F.; and Spiker, I.K.: STS-8 Atomic Oxygen Effects Experiment. AIAA Paper 85-0415, 1985.

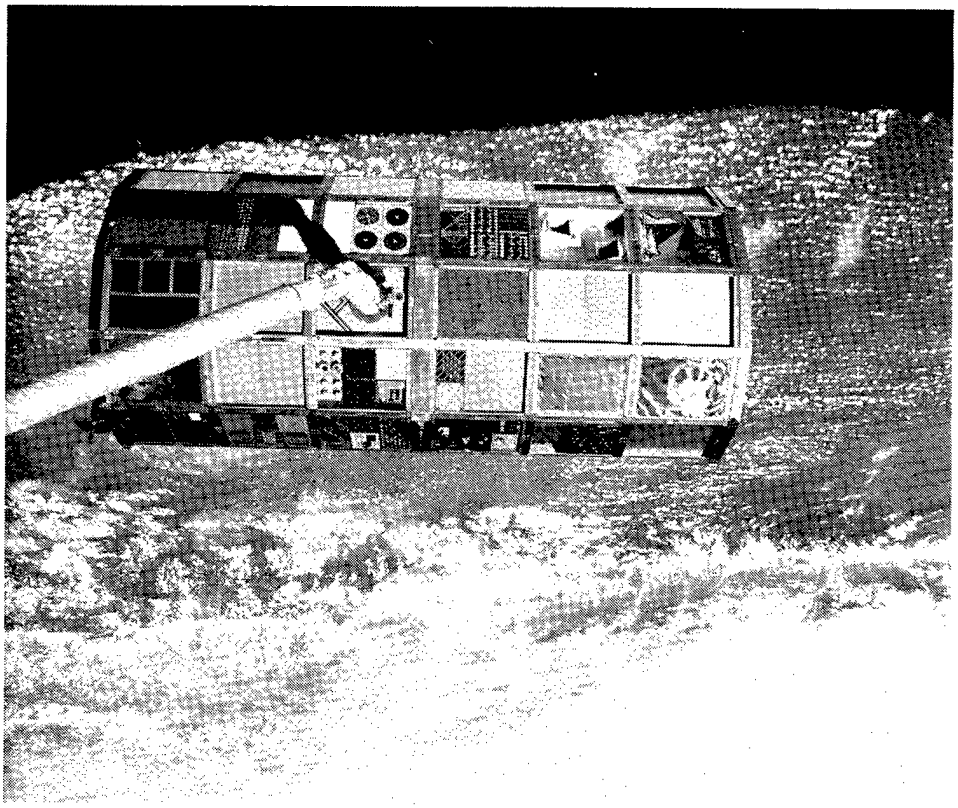
17. Koontz, S; Leger, L.; and Albyn, K.: Vacuum Ultraviolet Radiation/Atomic Oxygen Synergism in Materials Reactivity. Journal of Spacecraft and Rockets, May-June 1990.

18. Slemp, W.S.; Young, P.R.; Witte, W.G., Jr.; and Shen, J.Y.: Effects of LDEF Flight Exposure on Selected Polymer Matrix Resin Composite Materials. Presented at the First LDEF Post-Retrieval Symposium, Kissimmee, FL, June 1991.

19. Hedin, A.E.: MSIS-86 Thermospheric Model. Journal of Geophysical Research, Vol.92, 1987.



1. LDEF in orbit, April 1984.

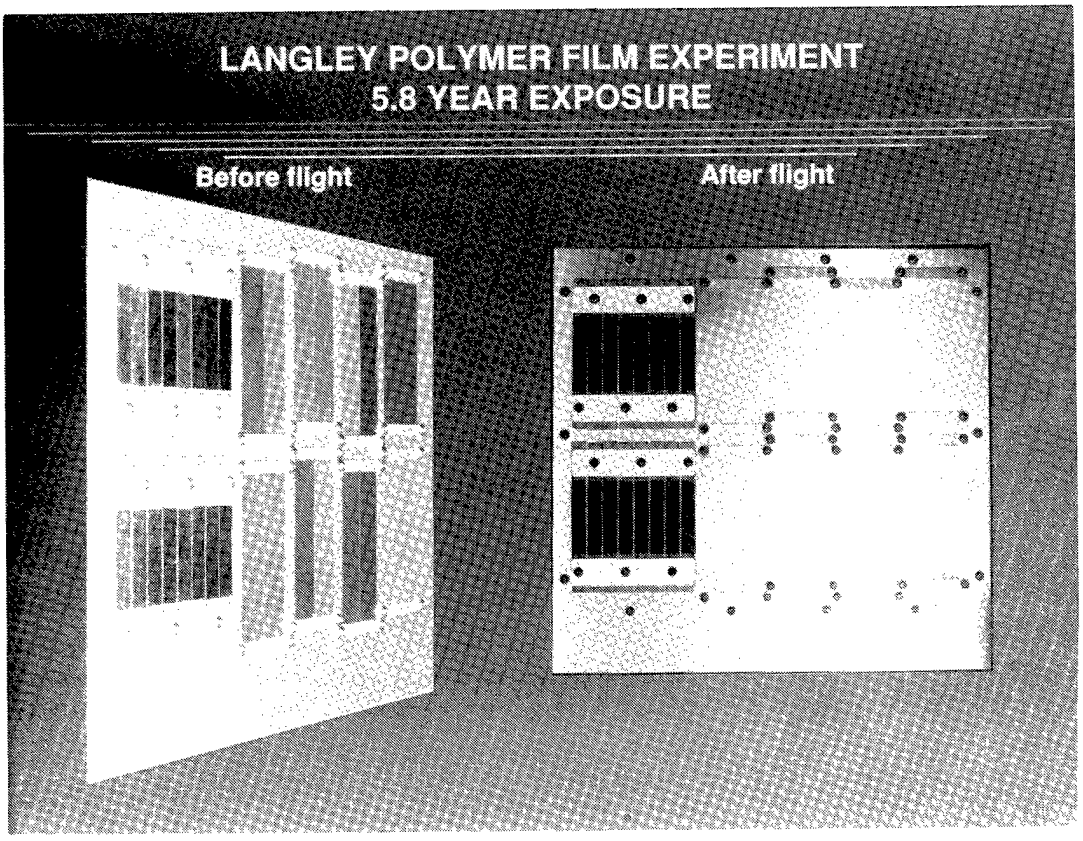


2. LDEF retrieval after 5.8 years in low-Earth orbit, January 1990.

SPACE ENVIRONMENTAL EFFECTS ON MATERIALS

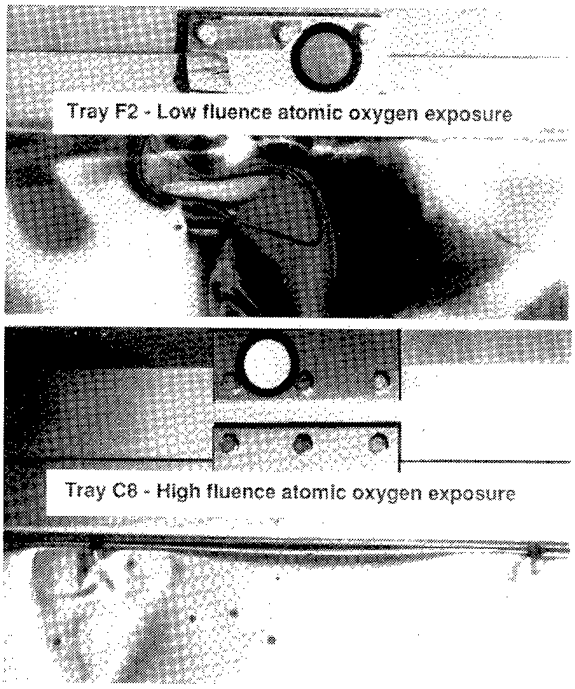
Materials Issue	Data Available from LDEF
• Stability of Material Properties - Optical - Mechanical - Thermal - Physical - Chemical	• Polymers, Metals, Composites, Ceramics, Glasses, Coatings, Films
• Combined Space Environment Effects Models	• AO, Electrons, Protons, UV, ΔT, M & D, Vacuum • Control Specimens on LDEF and in Ground Storage
• Atomic Oxygen Effects	• Erosion Rates and Mechanisms • Modifications to Fluence Models
• Meteoroid/Debris Impact Effects	• Delamination of Blankets, Composites • Crater/Impact Particle Chemistry
• Contamination	• Molecular & Particulate Levels/Chemistry

3. LDEF data available to address current issues in space environmental effects on materials.

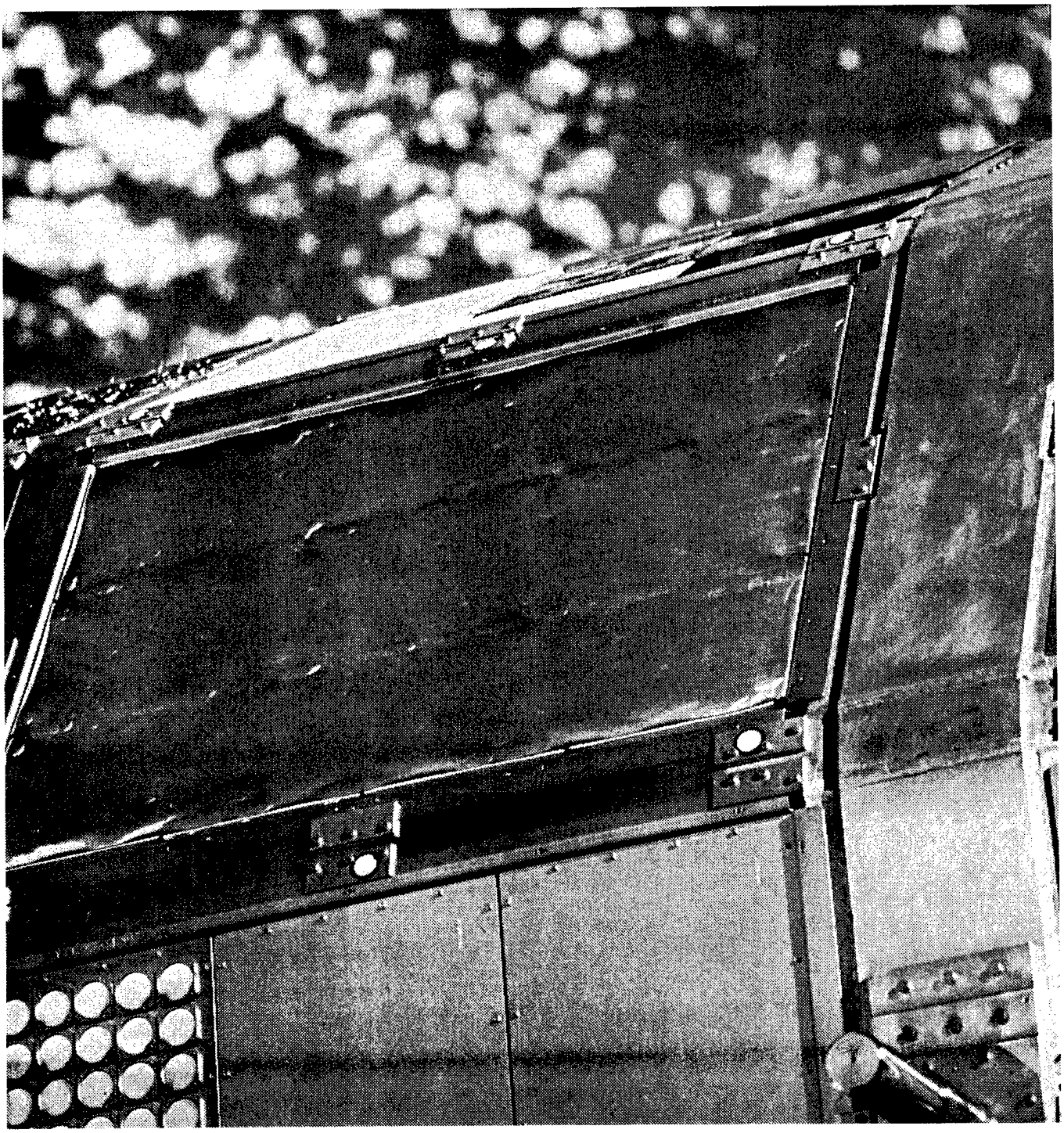


4. NASA-Langley Research Center LDEF polymer film experiment.

LDEF
Silver/Teflon second surface mirror thermal blankets



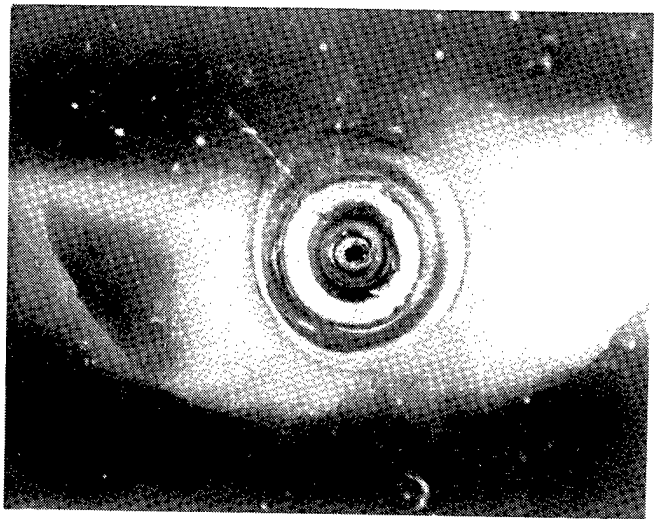
5. Silvered Teflon (Ag/FEP) second surface mirror thermal blankets and A 276 thermal control paint disks after exposures on LDEF trays F2 and C8.



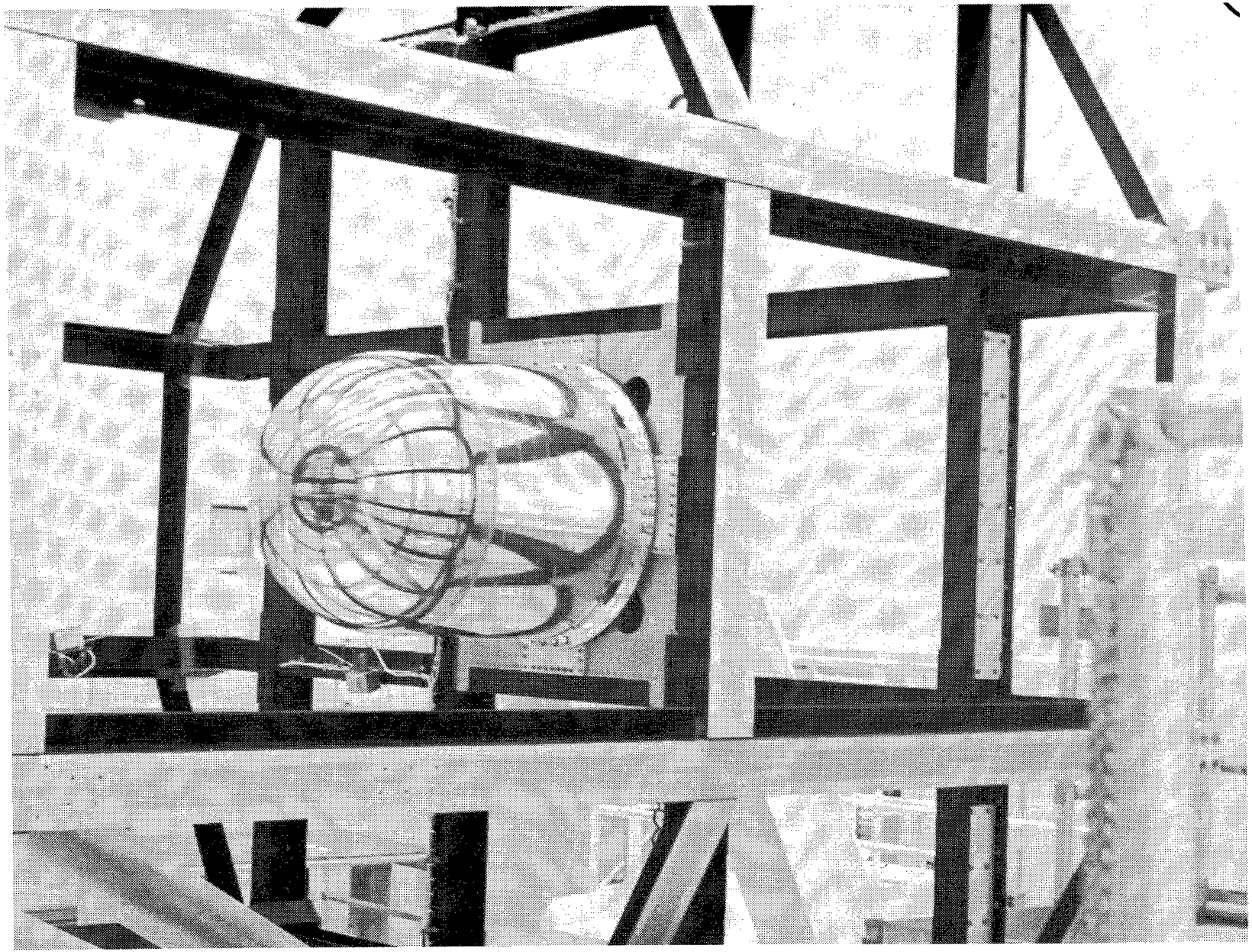
6. Ag/FEP second surface mirror thermal blanket on LDEF tray D7 showing delaminations (light areas) surrounding meteoroid/debris impacts.

PHOTOMICROGRAPH OF MICROMETERIOD IMPACT ON LDEF SILVERED TEFLON THERMAL BLANKET

Low magnification (x16)



7. Micrometeoroid impact on LDEF silvered Teflon thermal blanket material, showing "bullseye" and delamination areas around impact crater.



8. Molecular contamination on LDEF structural elements.

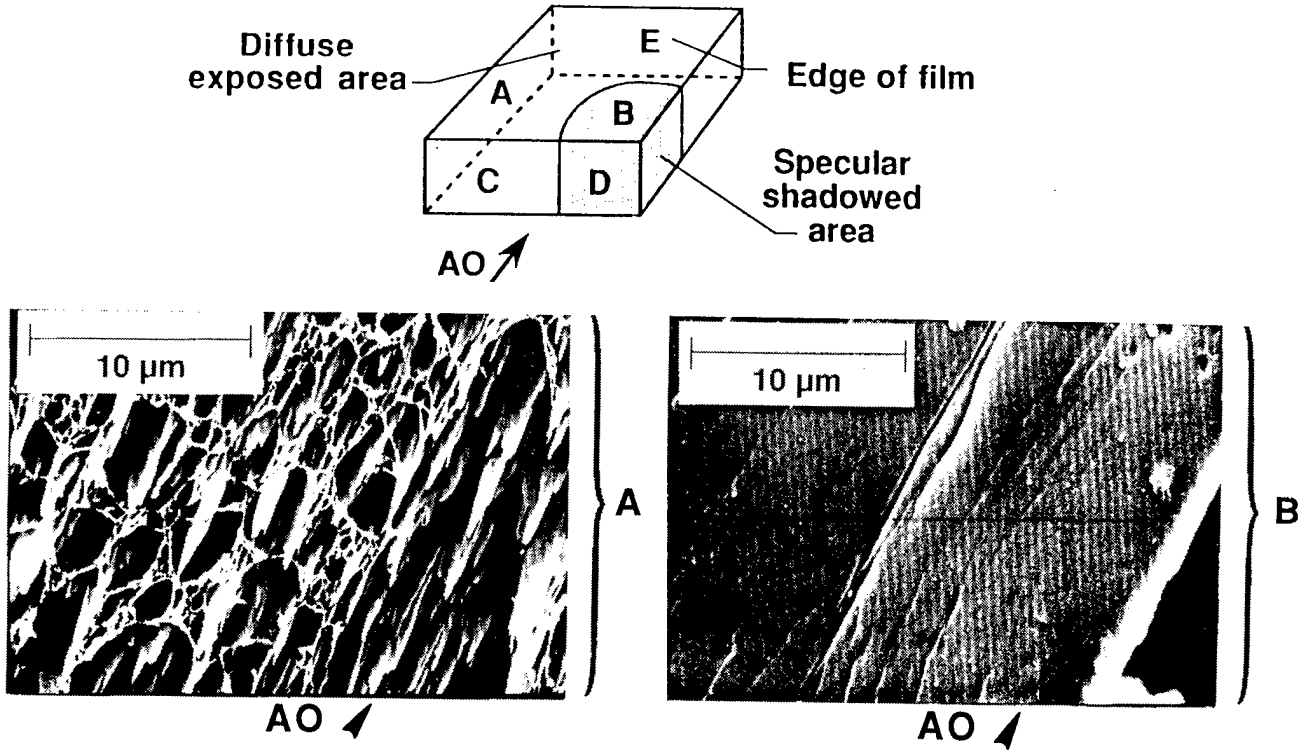
ABSORPTANCE AND EMITTANCE PROPERTIES OF ANODIZED ALUMINUM (6061-T6) CLAMPS ON LDEF

SPECIMENS AND LOCATIONS	α_s	ε	α_s/ε
Exposed Side of Clamps; All Areas of LDEF[1]	0.34	0.15	2.24
Unexposed Side of Clamps; All Areas of LDEF[1]	0.34	0.16	2.12
Control; In Storage on Earth[2]	0.36	0.18	2.00

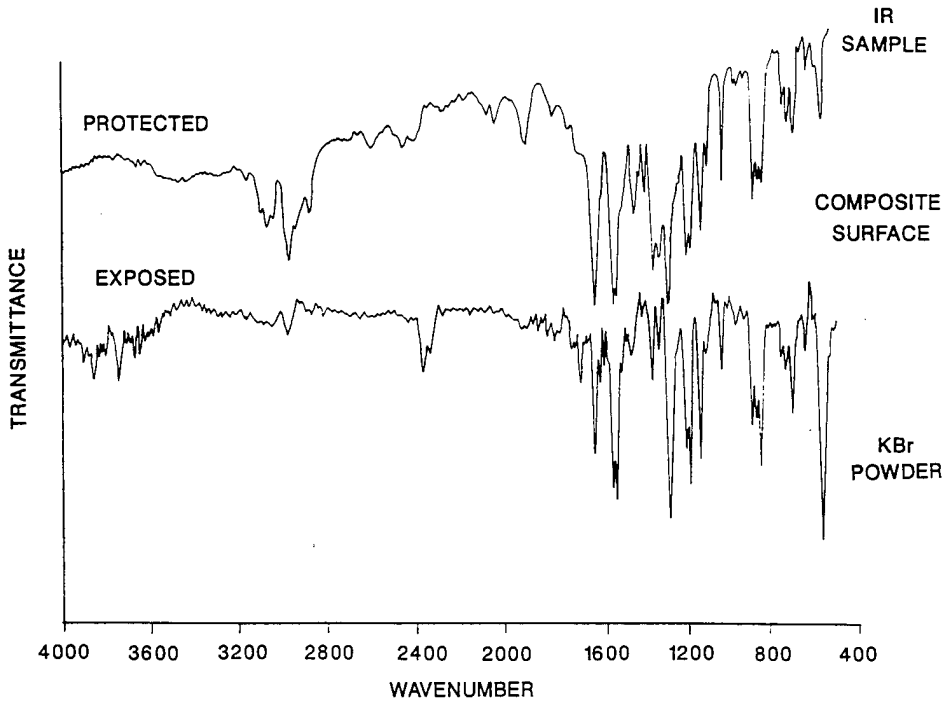
[1]Average of measurements from 228 clamps, 3 data points per clamp
[2]Average of measurements from 4 control specimen clamps, 3 data points per clamp

9. Solar absorptance and thermal emittance of LDEF anodized aluminum tray clamps.

SEM OF LDEF-EXPOSED KAPTON FILM

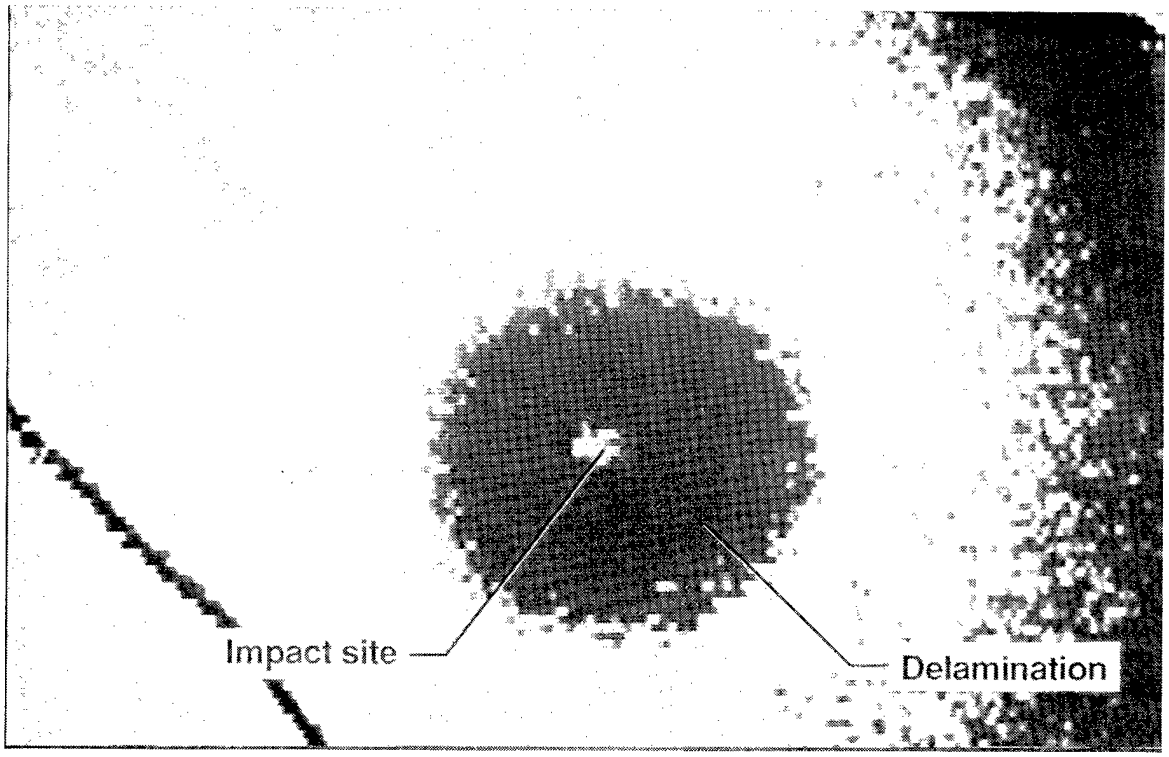


10. Scanning electron photomicrographs of Kapton film showing grazing angle AO-eroded/diffuse surface in exposed area and unaffected smooth/specular surface in area shadowed by another LDEF surface.



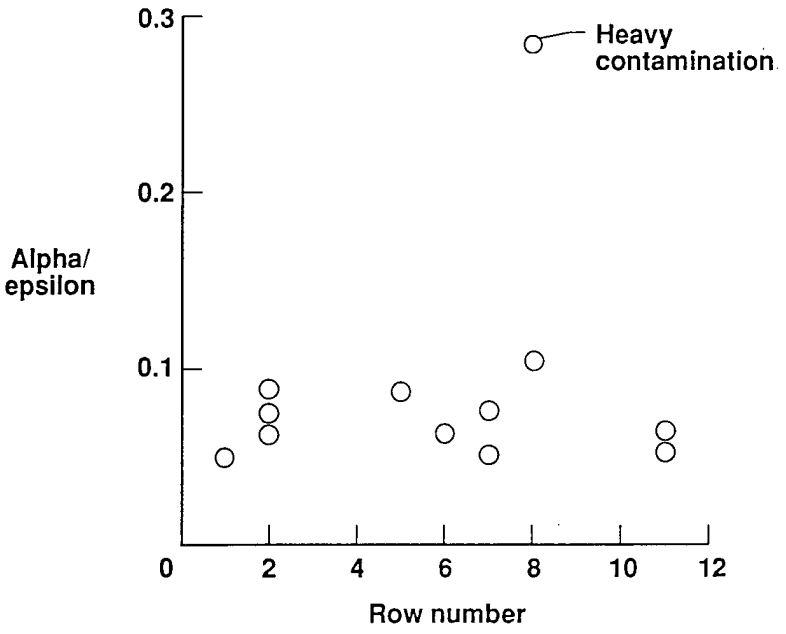
11. DR-FTIR spectra of LDEF C6000/P1700 (graphite/polysulfone) composite specimens.

LDEF A0178 Thermal Blanket

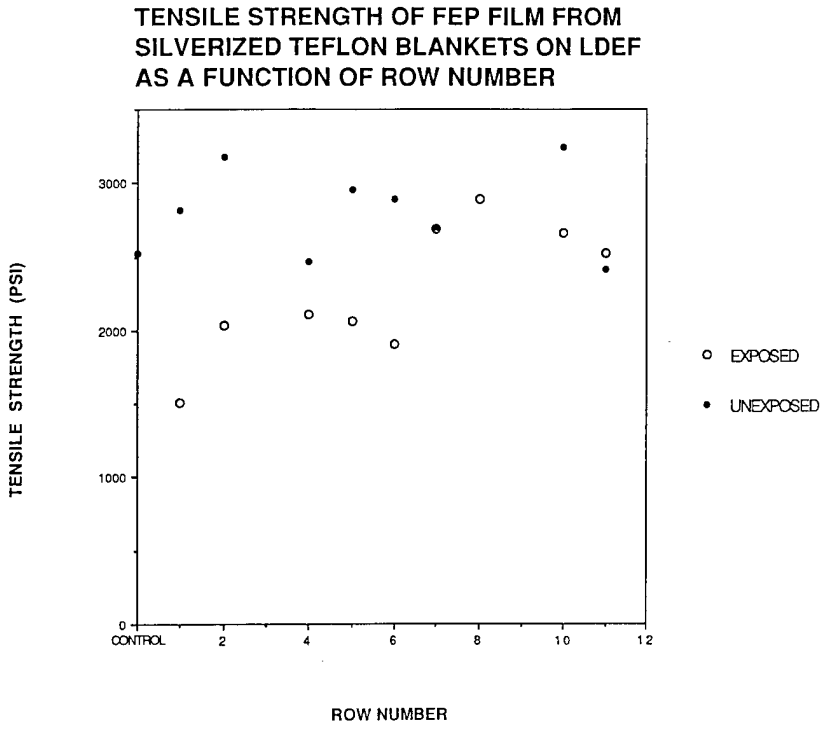


- **Impact diameter ~0.5mm**
- **Delamination diameter ~10mm**
- **Infrared camera photograph**
- **Transient heating in air**

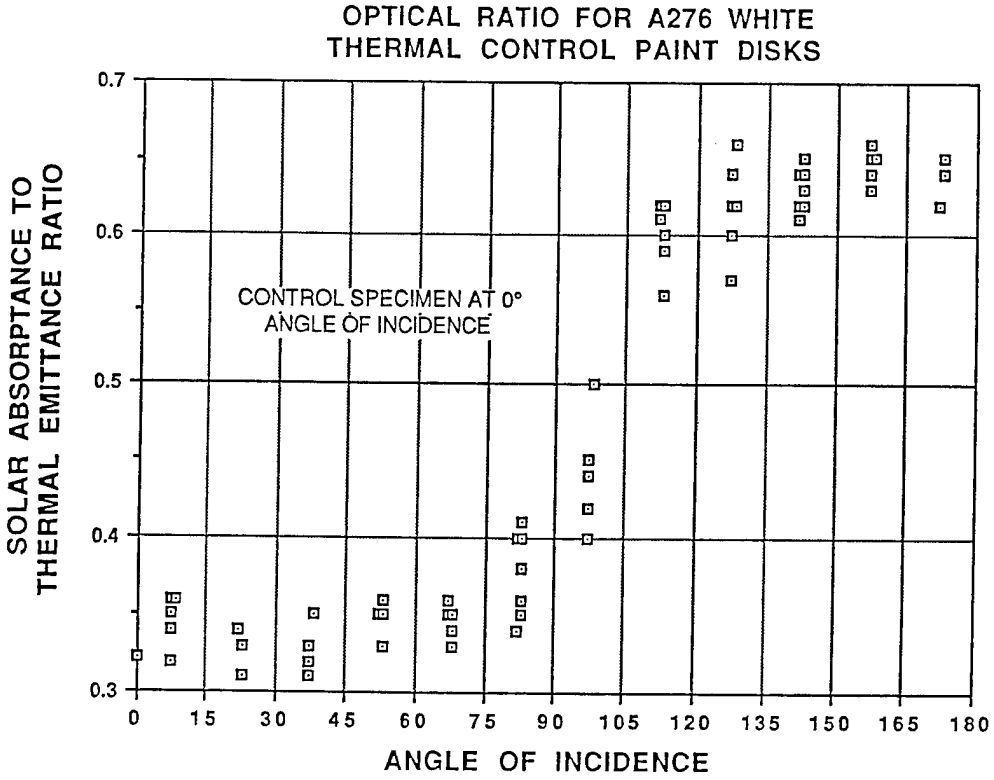
12. Thermal lag in delaminated silvered Teflon second surface mirror thermal control blanket flown on LDEF.



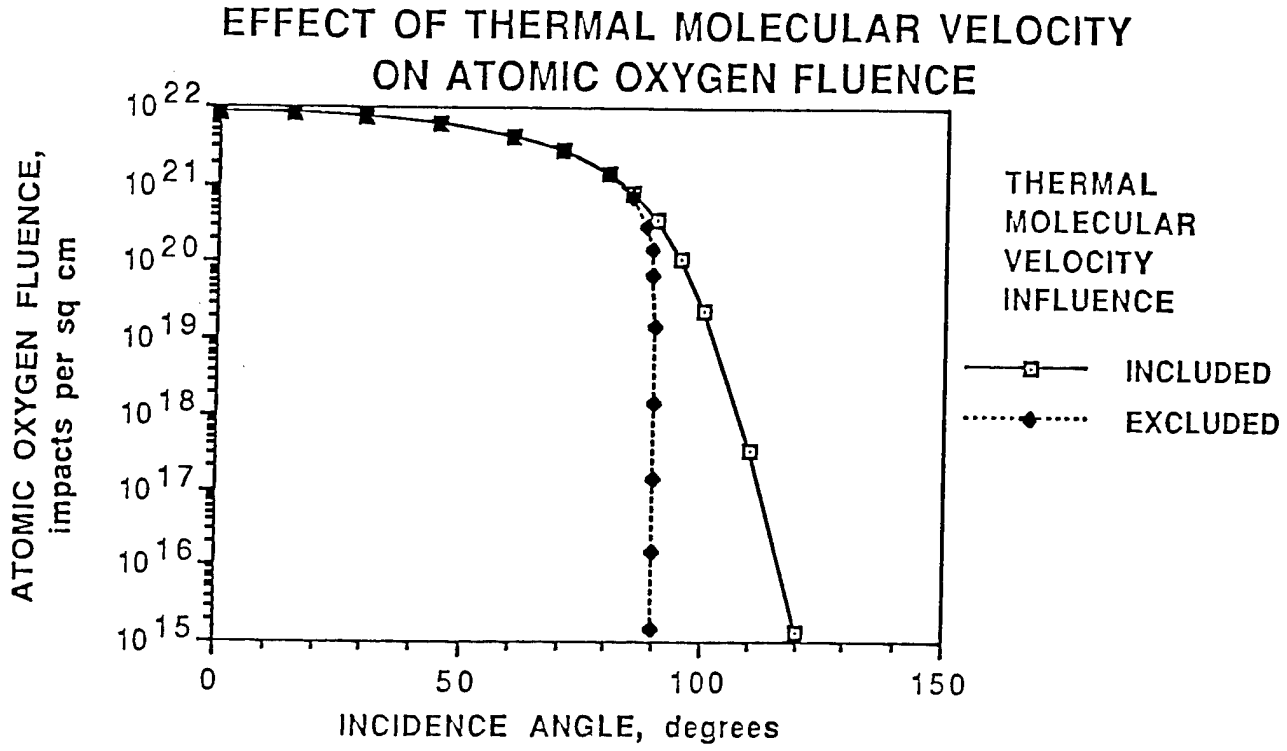
13. Solar absorptance/thermal emittance ratios for silvered Teflon thermal blankets after LDEF exposure.



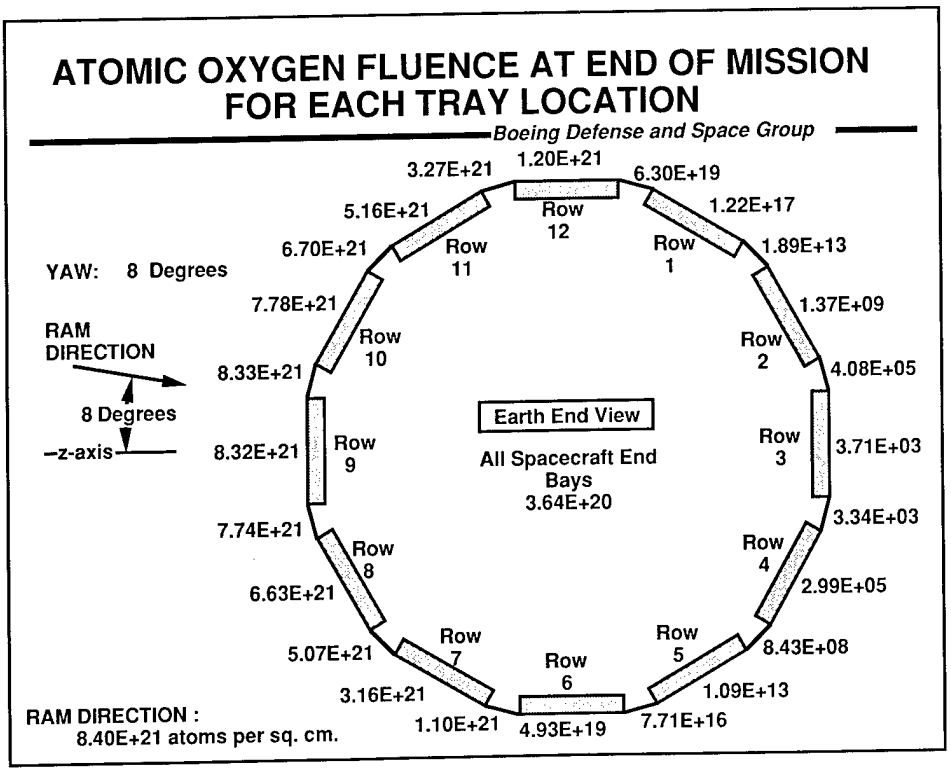
14. Tensile strengths of silvered Teflon thermal blanket specimens exposed to LDEF space environment parameters and specimens on LDEF shielded from the space environment (unexposed).



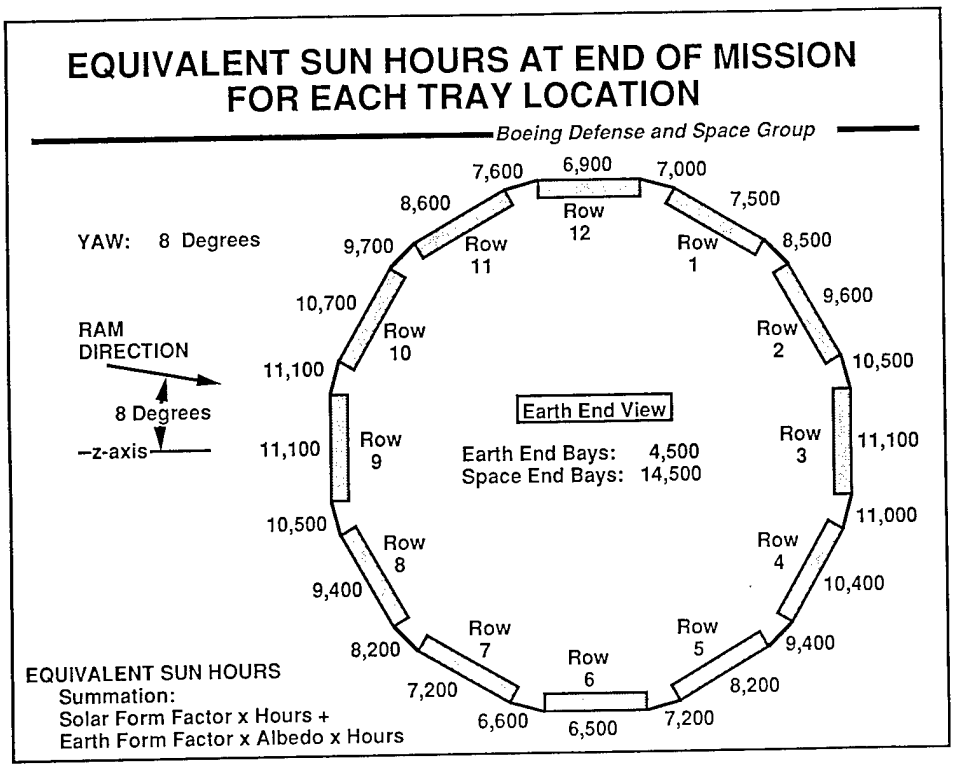
15. Solar absorptance/thermal emittance ratios for A 276 white thermal control paint disks after LDEF exposure.



16. Effect of thermal molecular velocity on atomic oxygen fluence.



17. Atomic oxygen fluence at end of mission on each LDEF tray location.



18. Equivalent sun hours at end of mission for each LDEF tray location.

ATOMIC OXYGEN AND ULTRAVIOLET RADIATION MISSION TOTAL EXPOSURES FOR LDEF EXPERIMENTS*

R. J. Bourassa
Boeing Defense & Space Group
P.O. Box 3999
Seattle, WA 98124-2499
Phone: 206/773-8437, Fax: 206/773-4946

J. R. Gillis
Boeing Defense & Space Group
P.O. Box 3999
Seattle, WA 98124-2499
Phone: 206/773-9956, Fax: 206/773-4946

K. W. Rousslang
Department of Chemistry
University of Puget Sound
Tacoma, WA 98416
Phone: 206/756-3123, Fax: 206/756-3500

SUMMARY

Atomic oxygen and solar radiation exposures were determined analytically for rows, longerons and end bays of the Long Duration Exposure Facility (LDEF). Calculated atomic oxygen exposures are based on an analytical model that accounts for the effects of thermal molecular velocity, atmospheric temperature, number density, spacecraft velocity, incidence angle and atmospheric rotation. Results also incorporate variations in solar activity, geomagnetic index and orbital parameters occurring over the 6-year flight of spacecraft.

Solar radiation exposure calculations are based on the form factors reported in the Solar Illumination Data Package prepared by NASA Langley. The earth albedo value for these calculations was based on the Nimbus 7 earth radiation data set.

Summary charts for both atomic oxygen and solar radiation exposure are presented to facilitate the use of the data by LDEF experimenters.

INTRODUCTION

When atomic oxygen collides with a spacecraft surface traveling at relative velocities of 7-8 km/sec, the collision energy is 4-5 eV. At this energy, atomic oxygen may initiate a number of chemical and physical reactions with the materials of the surfaces with which it collides. These interactions contribute to material degradation, surface erosion, and contamination. Also, recent theories propose that atmospheric atomic oxygen plays a role in the production of shuttle glow.

* Work done under NAS 1-18224, Task 12

For these reasons, atomic oxygen fluence on spacecraft surfaces is an important design consideration. LDEF flew in low earth orbit for nearly six years. Because of its unique 12-sided geometry, atomic oxygen fluence varied from experiment to experiment. Knowing the atomic oxygen fluence on the materials carried by LDEF will give experimenters the ability to correlate degradation effects with exposures.

The ultraviolet component of solar radiation also causes deterioration of materials. The exposure of LDEF experiments to solar radiation varied with their location. Interpretation of the effects of the space environment on exposed material requires quantitative knowledge of both the atomic oxygen and the solar radiation environments. The purpose of this work is to prepare summaries of these environments for use by experimenters.

The geometry and coordinate system of LDEF are shown on Figure 1. The vehicle is a 12-sided structure 30-feet long and 14-feet in diameter. In orbit, the long axis of the vehicle pointed away from the earth. The coordinate system as indicated in the figure is right handed with the x-axis pointed vertical, parallel to the long axis of the vehicle. Experiment locations are designated by row numbers and tray letters. Looking toward the earth end of the vehicle, row numbers increase in a clockwise direction (1 through 12). The tray letters increase upward in the vertical direction (A through F).

The angle of incidence for each experiment tray surface was fixed by the geometry of the LDEF and its constant flight attitude on orbit. The longeron between rows 9 and 10 was the nearest ram-facing surface.

LDEF was deployed in space in a nearly circular orbit on April 7, 1984. The initial mean altitude was 482 km, the orbit was inclined 28.5° to the equator, and the mission duration was 2,106 days.

ATOMIC OXYGEN EXPOSURE

The first of the two objectives of our work was to calculate atomic oxygen exposures for the LDEF experiments. Results for this objective are summarized in Figure 2. The Figure shows the mission total atomic oxygen exposure accumulated on each tray and longeron location of LDEF during its mission. The view is of the earth end of the spacecraft. In this view, the row numbers increase in the clockwise direction. The calculation is based on an 8° yaw angle, zero roll angle and zero pitch angle. The ram direction lies between rows 9 and 10. All trays on a row received the same atomic oxygen fluence. Top and bottom trays received equal fluence.

The values given in Figure 2 are mission total values. More extensive data has been prepared in tabular form for LDEF (ref. 1). Atomic oxygen fluxes and fluences were calculated for each month for the first four and one-half years of the LDEF mission. During the last year of the mission, results were compiled for each week. Fluences for any period of time during the mission can be interpolated from tabulated data.

Derivation of the Equation for Atomic Oxygen Exposure Calculations

Molecules in a gas in thermal equilibrium have a Maxwellian speed distribution characteristic of their temperature. At 1000°K, the average molecular speed of atomic oxygen is 1.15 km/sec compared to an average speed of a spacecraft relative to the atmosphere of 7.24 km/sec at 400 km altitude in an easterly orbit. Because of thermal molecular motion, atomic oxygen flux on a surface at high incidence

angles is not accurately given by the product of number density, spacecraft velocity and projected surface area. An equation to account for the effect of thermal molecular velocity is derived in the following paragraphs.

The velocity of a molecule with respect to the spacecraft is the vector sum of its thermal velocity and the velocity of the spacecraft reversed. This relationship is depicted in Figure 3. The thermal velocity of a molecule is described by two distribution functions. G(c), the Maxwell speed distribution function represents the fraction of molecules with speed in the range c to (c+ dc). The value of the speed distribution function varies with temperature. (A symbol glossary follows the text.)

$$G(c) = (1/N)\,(\partial N/\partial c) = (M/2\pi RT)^{3/2}\,[\exp(-Mc^2/2RT)]\,(4\pi c^2) \tag{1}$$

H, the solid angle distribution function, represents the fraction of molecules with velocity vectors directed in the range of solid angles ω to $(\omega + d\omega)$. Since all directions of the velocity vector are equally probable, the solid angle distribution function is a constant.

$$H = (1/N)(\partial N/\partial \omega) = 1/(4\pi) \tag{2}$$

The population of atomic oxygen molecules in the vicinity of the spacecraft is considered to be divided into infinitesimal velocity classes. For a given velocity class, molecular velocity is added to the ram vector to obtain the velocity of molecules in the class relative to the spacecraft. An equation for the component of relative velocity perpendicular to the spacecraft surface is then derived for the specified molecular velocity class.

$$u = v \cos \alpha + c \cos \beta \tag{3}$$

Using the relative velocity equation and the two distribution functions, an equation is derived for flux at the surface caused by molecules contained in the velocity class. This equation is modified by expressing solid angle in terms of plane angle measured from the surface normal.

$$(\partial^2 F/\partial c \partial \omega) = HGNu \tag{4}$$

$$(\partial \omega/\partial \beta) = 2\pi \sin \beta \tag{5}$$

$$(\partial^2 F/\partial c \partial \beta) = (1/4\pi)GNu(2\pi \sin \beta) \tag{6}$$

The derivation yields a differential equation for molecular flux in terms of two independent variables and four constants. The independent variables are thermal molecular speed and the direction of the molecular velocity vector relative to the surface. The constants are temperature, number density spacecraft velocity and the angle the surface makes with the ram direction of the vehicle.

The differential equation for flux is integrated with respect to the independent variables, molecular speed and angle, to obtain an equation for flux in terms of temperature, number density, spacecraft velocity and incidence angle. Values for the latter items are held constant during the integration process. To arrive at the equation for flux, limits for integration are devised for leading surfaces to include all molecules swept out by the advancing surface.

The gas molecules surrounding the spacecraft are separated into two speed populations. The first population includes those molecules that do not have sufficient velocity to "outrun" the spacecraft even if traveling directly away from the spacecraft surface. The second population includes those molecules

that can "outrun" the advancing surface if traveling in a path directed at a sufficient angle away from the surface. Molecules that "outrun" the spacecraft are not included within the limits.

$$F = \int_0^{v\cos\alpha} \int_0^{\pi} (\partial^2 F/\partial c \partial\beta)\partial\beta\partial c + \int_{v\cos\alpha}^{\infty} \int_0^{\arccos[(-v\cos\alpha)/c]} (\partial^2 F/\partial c \partial\beta)\partial\beta\partial c \qquad (7)$$

Integration limits for trailing surfaces (surfaces on the aft side of the spacecraft) can be devised to include molecules with velocities such that they can catch the spacecraft. However, the resulting integral is identical to that derived for leading surfaces. Hence, the integral shown leads to a valid equation for flux (atoms per unit area per unit time) for both leading and trailing surfaces, as follows:

$$F = 1/4\, N \langle c \rangle \{\exp(-U^2) + U\pi^{1/2}[1 + \mathrm{erf}(U)]\} \qquad (8)$$

Where: $\langle c \rangle = (8RT/\pi M)^{1/2}$

and: $U = (2/\pi^{1/2})(v/\langle c \rangle)\cos\alpha$;

To simplify the equation, terms resulting from the integration process have been gathered into two expressions. The first expression, $\langle c \rangle$, can be recognized as the equation for average molecular speed consistent with kinetic molecular theory. The second expression, U, is a dimensionless statement for the normal component of speed for the advancing surface relative to average molecular speed multiplied by constant factors that appear in the integral.

To illustrate agreement with kinetic theory, two specific limiting cases are considered: (1) zero spacecraft velocity; and, (2) zero average molecular speed (zero temperature).

If, $v = 0$, then: $F = 1/4\, N \langle c \rangle$ (9)

If, $\langle c \rangle = 0$, then: $F = Nv\cos\alpha$ (10)

Otherwise: $F = 1/4\, N \langle c \rangle f(U)$ (11)

In the case of zero spacecraft velocity, $v = 0$, the equation is identical to that for the collisions by perfect gas molecules with a stationary plane surface. In the case of zero temperature, $c = 0$, the equation is identical to that for a stationary gas of known density swept out by a moving surface. In equation (11), the function, f(U), equals the quantity shown in braces in equation (8).

Equation (8) has been derived elsewhere in connection with research on heat transfer and drag in rarefied gases (ref. 2).

Computer Program for Atomic Oxygen Flux Calculations

The need for a computer program to handle the continuously varying inputs to equation (8) can be understood from the information shown in Figure 4. The figure shows atomic oxygen flux plotted as a function of altitude for atmospheric conditions of minimum, standard, and maximum solar activity. Atomic oxygen flux is sensitive to both altitude and solar activity. During periods of increased solar activity, the region of atomic oxygen generation in the earth's atmosphere expands outward because of absorption of extreme ultraviolet (EUV) radiation. This effect causes an increase in the number density of atomic oxygen at a given altitude. At a typical altitude for LDEF, 400 km, the atomic oxygen flux for

maximum solar activity is more than an order of magnitude greater than the atomic oxygen flux for minimum solar activity. It is obvious that characterization of the atmosphere for a single typical condition would not be valid for the entire LDEF mission.

Figure 5 shows the flow chart for the computer program that was developed to calculate atomic oxygen flux. The program accounts for orbit position, co-rotation of the earth's atmosphere, spacecraft attitude (yaw, pitch, and roll), the condition of the atmosphere (altitude, latitude, longitude and time dependent factors), spacecraft velocity and surface inclination, and thermal molecular velocity.

The parameters for the orbit routine include inputs of apogee, perigee, perigee angle, epoch time, epoch longitude, and the orbit inclination. Outputs from the orbit routine are altitude, latitude, longitude, local solar time, and spacecraft velocity. The computer model accounts for co-rotation of the earth and the atmosphere. The atmosphere rotates with the earth while the spacecraft rotates around the earth. The velocity of the atmosphere relative to the spacecraft (ram vector) is equal to its own motion minus the motion of the spacecraft. The relationship between the quantities is shown in Figure 6.

The net effect of atmospheric motion is to decrease ram speed for a spacecraft in an easterly directed orbit and to cause a small displacement of the ram direction from that of the spacecraft heading. For an altitude of 400 km, the ram speed is decreased 0.43 km. The ram direction shifts 1.86° to right and left of the heading during a complete orbit.

Yaw, pitch, and roll, together with horizontal angle and elevation angle determine the angle between the ram vector and surface normal.

The MSIS-86 model atmosphere program uses the output of the orbit routine, including solar activity, indexed by the 10.7 cm radio flux and the geomagnetic activity index, to determine the atomic oxygen density and atmospheric temperature. The MSIS-86 model calculates atomic density variations on the basis of global changes in exospheric temperature.

The kinetics routine uses temperature and density outputs from the MSIS-86 model, the angle of incidence, and the resultant ram speed to predict the atomic oxygen flux using the equation derived from molecular kinetics.

Condition of The Atmosphere

Atomic oxygen density in the atmosphere at orbital altitudes is strongly influenced by changes in the degree of solar activity. The 10.7 cm radio flux is used as a measure of solar activity and of the associated extreme ultraviolet radiation that affects atomic oxygen generation. Atomic oxygen density variations correlate closely with 10.7 cm flux, although the 10.7 cm flux itself has little if any impact on the atmosphere.

Solar activity data used for LDEF atomic oxygen flux calculations were obtained from the National Geophysical Data Center (NGDC/NOAA), Boulder, CO. Figure 7 tracks solar activity as measured by the 10.7 cm flux versus time after the release of LDEF. The average daily flux was determined every month for the first 4 1/2 years, and then, because of increased solar activity, every week until recovery of the LDEF, 5 years and 10 months after launch. The change in plotting interval causes the abrupt change in the appearance of the plotted function.

Another factor affecting the condition of the atmosphere is the geomagnetic index. During increased solar activity, the sun ejects plasma into the earth's magnetosphere, producing geomagnetic storms. These storms dump charged particles from the magnetosphere into the atmosphere, where

through collisions, the particles ionize and heat the atmosphere. This geomagnetic effect augments and parallels effects of extreme ultraviolet radiation caused by increased solar activity. The end result is an increase in the atomic oxygen density at orbital altitudes.

Geomagnetic index data for the time span of the LDEF flight was obtained form NGDC/NOAA through September 1989 and for the balance of the mission from the Air Force Global Weather Center (AFGWC), Omaha, NB. Figure 8 shows the geomagnetic index as a function of time after launch for the LDEF mission. The average index was determined every month for the first 4 1/2 years, and then, because of increased solar activity, every week until recovery of the LDEF, 5 years and 10 months after launch.

Ground tracking station observations of LDEF taken by NORAD were obtained through NASA. These observations provide altitude and other state vector information needed to define the LDEF orbit. Figure 9 shows the decay of the LDEF orbit with time as defined by the NORAD data. During the last year of flight, LDEF lost altitude rapidly, and as a result was exposed to an environment with progressively higher atomic oxygen density.

Figure 10 demonstrates the significance of the combined effects of declining altitude and varying solar activity in terms of atomic oxygen density in the atmosphere. Atomic oxygen flux (atoms/sq cm per sec) is proportional to the number density of monatomic oxygen (atoms/cubic cm). Decreasing solar activity caused density to decrease during the first three years of flight. Thereafter, the combination of increasing solar activity and decreasing altitude caused density to increase rapidly. These variations in the environment are dominant factors controlling atomic oxygen fluxes and fluences calculated for LDEF.

Features of the LDEF Atomic Oxygen Calculation

Figure 11 shows cumulative ram direction atomic oxygen fluence for LDEF expressed as a percent of total fluence for the mission. This plot reflects the combined effect on atomic oxygen fluence caused by varying solar activity and loss of altitude. Roughly 54 percent of the atomic oxygen exposure accumulated during the last six months of the LDEF mission. The last year of the flight accounted for 77 percent of the exposure.

The effect of thermal molecular velocity on atomic oxygen flux is shown in Figure 12. The plot compares atomic oxygen flux corrected for thermal molecular velocity with calculated values ignoring thermal molecular velocity. When thermal molecular velocity is considered, calculations show that surfaces parallel to the ram direction receive approximately four percent of the head-on flux. Surfaces at angles greater than 90° from ram experience a small atomic oxygen flux. Within roughly 87.5° of ram, predicted atomic oxygen fluxes with or without the inclusion of thermal speed are nearly equal.

Improvements in the atmospheric model and the orbit position program will lead directly to improved accuracy in the atomic oxygen calculations. The atomic oxygen calculation is very sensitive to orbit altitude as shown in Figure 4. In the current version of the computer program, a simplified orbit routine was used for determination of altitude for points on orbit.

It should also be noted that the calculation is based on a zero pitch angle. With a zero pitch angle atomic oxygen fluences on the space end and earth end of the vehicle are equal. Experimental evidence bearing on pitch angle is still being evaluated. A small change in pitch angle would significantly alter calculated fluences for space and earth end bays. Thus, recalculation of fluences should be considered if pitch angle is changed.

SOLAR EXPOSURE

A primary objective of the Long Duration Exposure Facility (LDEF) mission was to study the effects of the space environment on various materials over an extended period of time. Solar radiation is an important contributor to materials degradation.

The rate of accumulation of solar exposure in terms of equivalent sun hours depends upon the solar form factor for direct solar radiation and upon the earth albedo form factor combined with an appropriate value of albedo for earth reflected radiation.

Form Factors

The solar form factor for a surface is a function of its orientation with respect to the sun's rays. The earth albedo form factor for a surface on a spacecraft is a function of the position of the spacecraft relative to the earth's illuminated hemisphere and to the orientation of the surface with respect to the local vertical direction. Both form factors when averaged over a complete orbit are defined by the angle that the spacecraft's orbit plane makes with the sun's rays and the orientation of the exposed surface with respect to the spacecraft's heading and vertical coordinates.

The angle between the orbit plane and the sun's rays (Figure 13) is defined as β. The range of β is obtained by adding the inclination of the earth's equator with its orbit plane, 23.5°, to the inclination of the spacecraft's orbit plane with the earth's equator, 28.5° for LDEF. Therefore, β varies from -52° to +52° for LDEF. Berrios and Sampair (ref. 3) have calculated the orbit averaged solar form factors and albedo form factors for each row and both ends of the LDEF vehicle as a function of β over the range -52° to +52°. Further, they have provided a table defining β angle for each day of the LDEF mission. Sampair has made the form factor and β angle functions available in digital format. Thus, the means for determining both solar form factor and earth albedo form factor for LDEF on an orbit average basis are available from their report.

All that is needed to proceed with the determination and summation of solar exposure in equivalent sun hours for LDEF is a value of earth albedo to use when calculating the earth reflected component of solar exposure. For each day of the mission, earth reflected and direct solar exposure may then be added and accumulated to obtain total solar radiation exposure for each LDEF surface as a function of mission time.

The data provided by Berrios and Sampair were based on an estimated yaw angle of 10° for LDEF. Experimental evidence now shows that yaw was 8°. In the work reported herein, results have been corrected to a yaw angle of 8° by way of a four-point Lagrangian interpolation formula.

Earth Albedo

Earth albedo has been determined from Nimbus 7 radiometer measurements and reported by G. Louis Smith, David Rutan and T. Dale Bess (ref. 4) for the period from November 1978 to October 1985. The Nimbus 7 short wave radiometer covered the wavelength band from 0.2 to 3.8 μm; the spectral dependence of albedo within this band was not determined. The albedo values of Smith et al. are available for every 5 degrees of latitude and longitude, except for small regions near the earth's poles

where some monthly data are missing. Rutan revised and extended the data to July 1987 and made it available in digital format for the calculations reported herein.

The LDEF orbit is inclined 28.5 degrees to the equator and sweeps across the region from 28.5° N to 28.5° S latitude. Monthly average albedos for the region from 30° N to 30° S were calculated using Rutan's data. These average albedos for each month are displayed in Figure 14. There are small seasonal albedo variations -- albedo tends to be higher in summer and winter than in spring and fall. However, these seasonal variations are quite small; their standard deviation is only 0.007 from the average of all albedos of 0.246. We, therefore, chose to use a constant average albedo of 0.246 for all dates. The error in earth reflected radiation caused by using this grand average albedo rather than the monthly average albedos should be less than 5 percent in any month and should average to near zero over any six month or longer period.

Calculated Results for Solar Exposure

Cumulative equivalent sun hours of total direct solar and earth reflected radiation have been calculated for each row and longeron and both end bays of LDEF. These data are presented in Figure 15. The user may use the values given to calculate full spectrum solar fluence (joule/cm^2) by multiplying cumulative equivalent sun hours by 492.48 joule/cm^2-hr. This factor is based on a solar irradiance of 0.1368 w/cm^2 (ref. 5). Similarly, the solar fluence in the 0.2 to 0.4 μm band may be obtained by multiplying the cumulative equivalent sun hours by 39.24 joule/cm^2-hr. This factor is based on a solar irradiance of 0.0109 w/cm^2 in this band. Fluences for other spectral bands may be calculated in like manner.

As may be seen from the Figure 15, the highest exposure is to the space end and the lowest to the earth end. Of the 12 rows, the leading and trailing rows (9 and 3, respectively) receive the highest exposure, and those nearly parallel to ram direction (rows 6 and 12) receive the lowest exposure, about 60 percent of the leading edge exposure.

Figure 16 shows the buildup of cumulative equivalent sun hours with time for five typical trays. Build-up is quite linear with time for earth and space ends and rows 3 and 9 (trailing and leading edge rows), but row 12 shows a marked seasonal effect. Row 12 is oriented in a northerly direction and, hence, receives the most intense radiation in the northern hemisphere summer and the least intense radiation in the northern hemisphere winter. The opposite is true for row 6, which is oriented in a southerly direction. Seasonal effects decrease as row orientation becomes perpendicular to ram direction.

Figure 17 shows a comparison of direct and earth reflected radiation for the earth end bay. The LDEF earth end bay received 72 percent of its exposure from earth reflected radiation and 28 percent from direct solar radiation. This is the highest proportion of earth reflected radiation received by any of the experiment locations. Earth reflected radiation accounted for 9 to 15 percent of the total solar radiation received by rows 1 through 12. The space end bays received no earth reflected radiation.

Solar exposures for LDEF rows, longerons, and end bay locations are available in tabular form as functions of time (ref. 6). Using the tabulated information, solar exposure in equivalent sun hours can be determined for any interval of time during the LDEF mission for any experiment.

SYMBOLS

<c>	Average molecular speed, cm/sec
c	Molecular speed, cm/sec
F	Atomic oxygen flux, atoms/cm^2-sec
G	Maxwell's speed distribution function
H	Solid angle distribution function
M	Molecular weight, g/g-mole
N	Number density, molecules/cm^3
R	Universal gas constant, ergs/g-mole-K°
T	Absolute temperature, K°
u	Absolute value of the component of relative velocity of a molecule perpendicular to an exposed surface, cm/sec
v	Spacecraft orbital speed, cm/sec
α	Angle between the normal to an exposed surface and the spacecraft ram vector
β	For the atomic oxygen analysis: angle between the velocity vector of a molecule and the normal to an exposed surface For the solar exposure analysis: angle between the sun's rays and the spacecraft orbit plane
π	Value of pi, 3.14
ω	Solid angle, steradians

REFERENCES

1. R. J. Bourassa, and J. R. Gillis, Atomic Oxygen Flux and Fluence Calculation for Long Duration Exposure Facility (LDEF), NAS1-18224, Task 12, Boeing Defence and Space Group, Seattle, WA (1990).

2. T. S. Tsein, Superaerodynamics, Mechanics of Rarefied Gases, J. Aero. Sci., 13, pp. 653-664 (1946).

3. William M. Berrios and Thomas Sampair, Long Duration Exposure Facility Solar Illumination Data Package, Orbital Environment Data Group, NASA/LaRC (1991).

4. G. Louis Smith, David Rutan and T. Dale Bess, Atlas of Albedo and Absorbed Solar Radiation Derived From Nimbus 7 Earth Radiation Budget Data Set - November 1978 to October 1985 , NASA Reference Publication 1231 (1990).

5. A. S. Jursa, Ed., Handbook of Geophysics and the Space Environment, p. 1-5, Air Force Geophysics Laboratory (1985).

6. R. J. Bourassa, and J. R. Gillis, Solar Exposure of Long Duration Exposure Facility Experiment Trays NAS1-18224, Task 12, Boeing Defence and Space Group, Seattle, WA (1990).

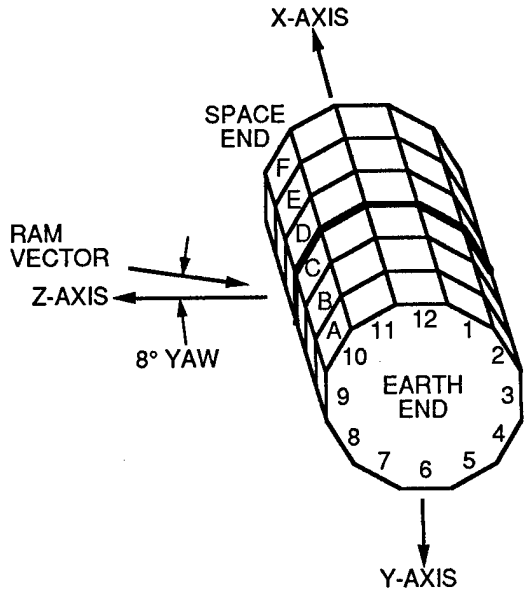


FIGURE 1. Definition of LDEF coordinates.

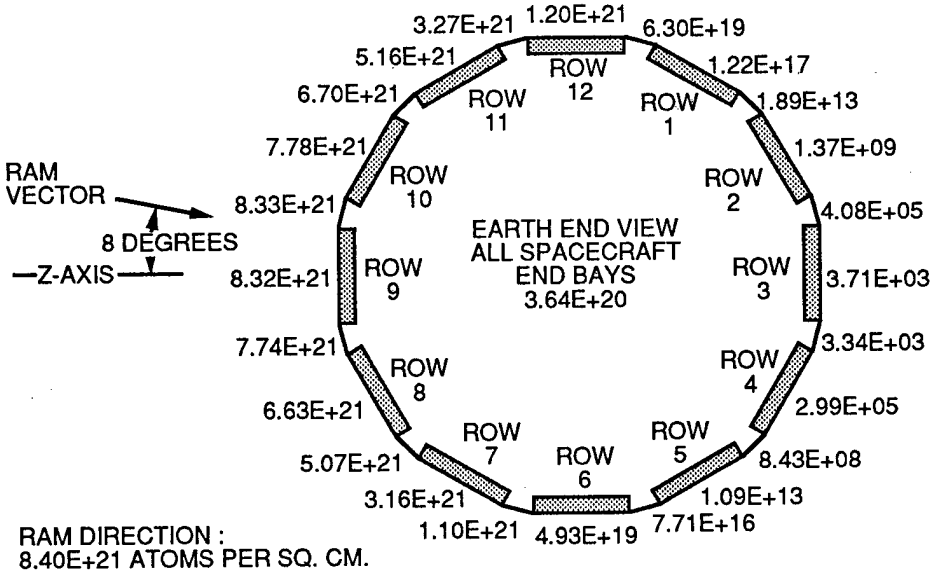


FIGURE 2. Atomic oxygen fluences at end of mission for each tray location.

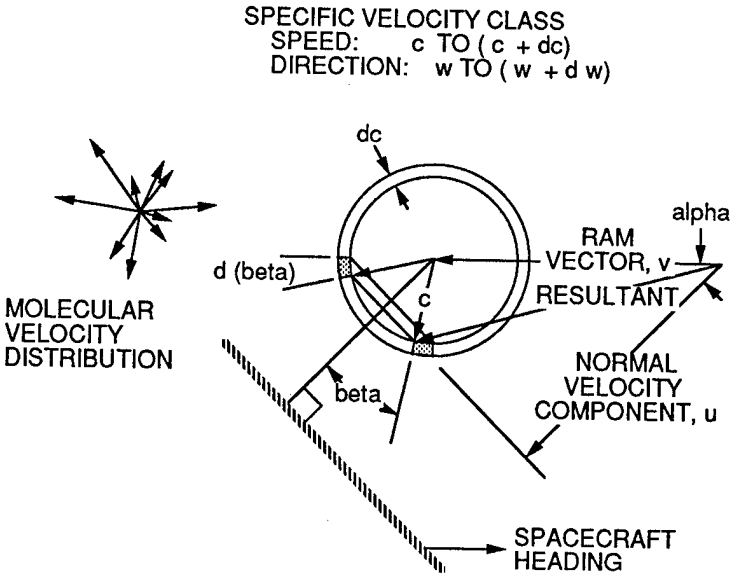


FIGURE 3. Vector addition of molecular and ram velocities.

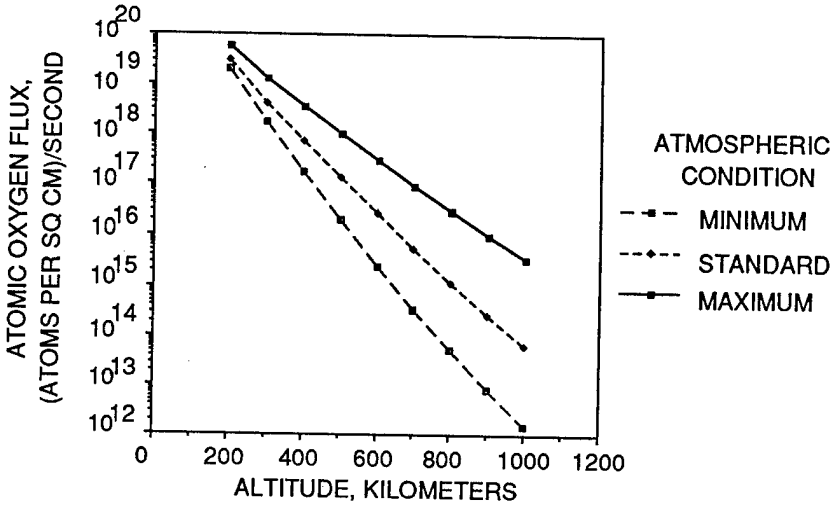


FIGURE 4. Effect of solar activity on atomic oxygen flux.

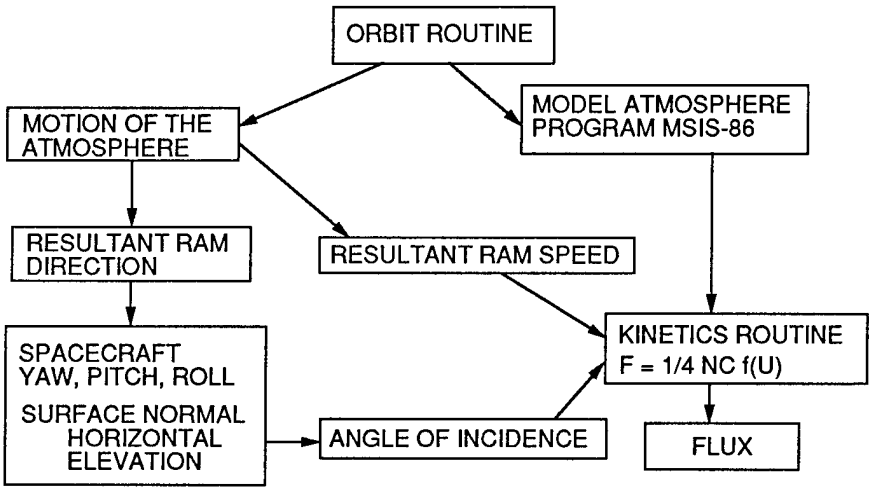


FIGURE 5. Program flow chart.

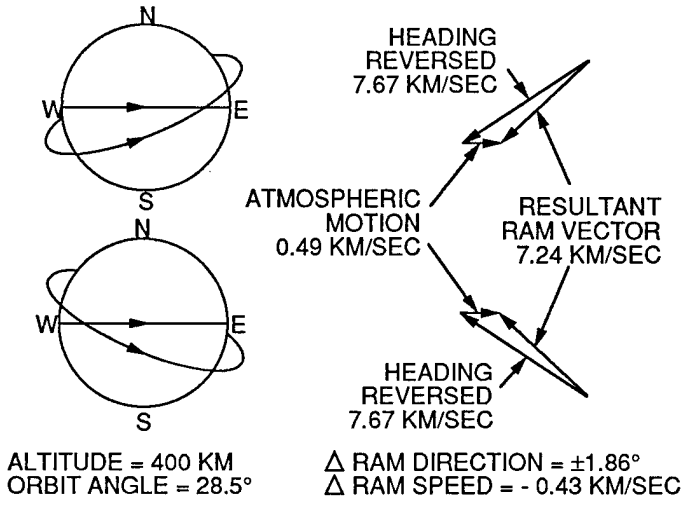


FIGURE 6. Co-rotation of the atmosphere.

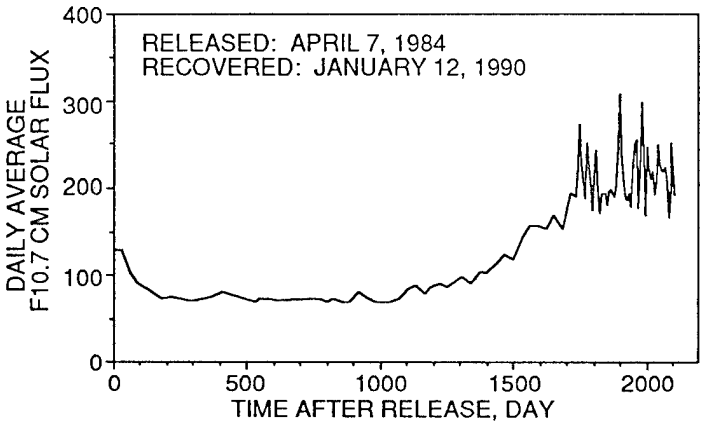


FIGURE 7. Daily average F10.7 cm solar flux for LDEF.

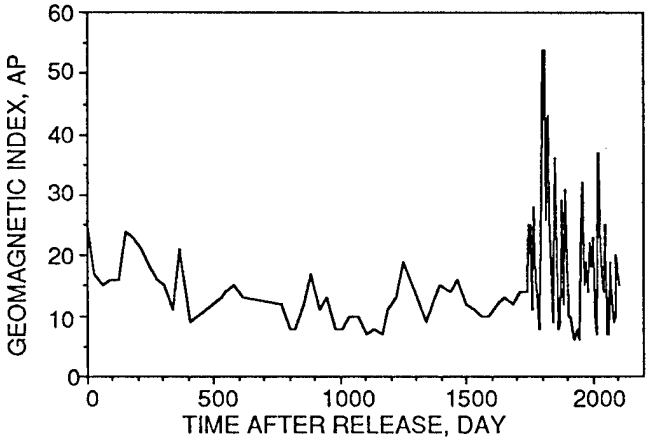


FIGURE 8. Geomagnetic activity index for LDEF.

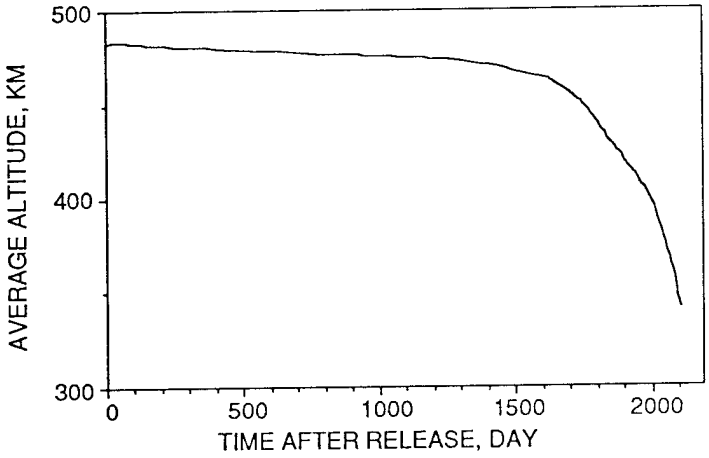


FIGURE 9. Average altitude of LDEF.

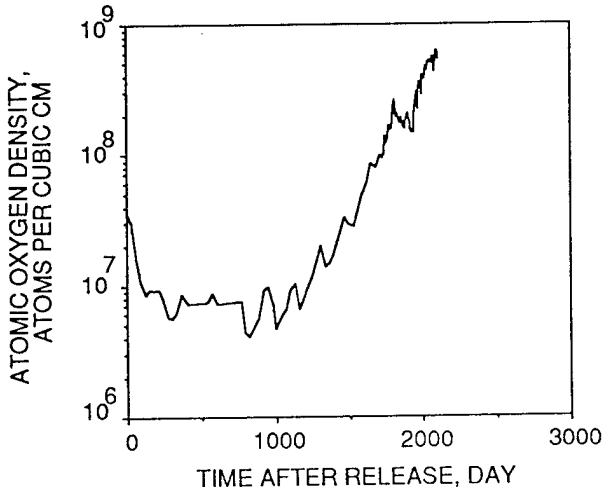


FIGURE 10. Atomic oxygen density.

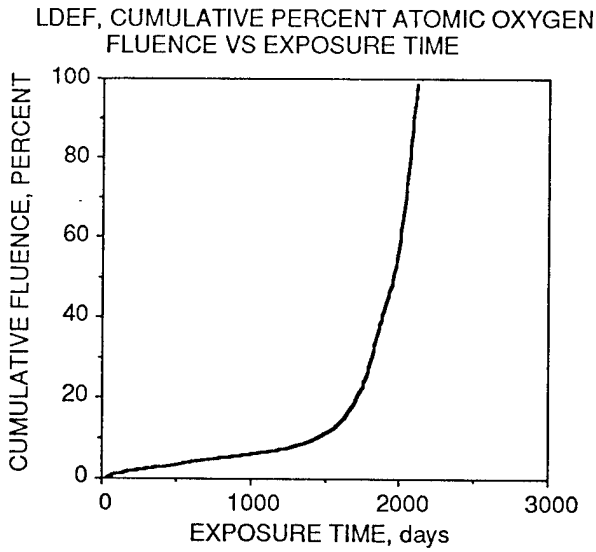


FIGURE 11. Atomic oxygen fluence as a percent of total exposure.

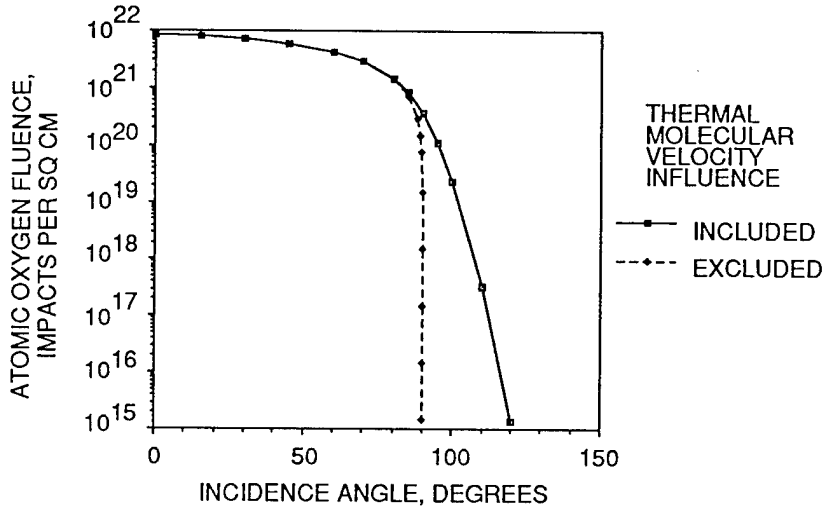


FIGURE 12. Effect of thermal molecular velocity on atomic oxygen fluence.

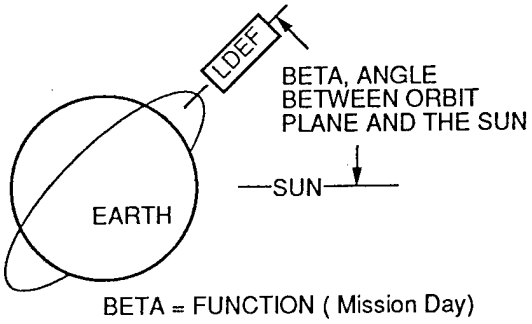


FIGURE 13. Definition of beta angle.

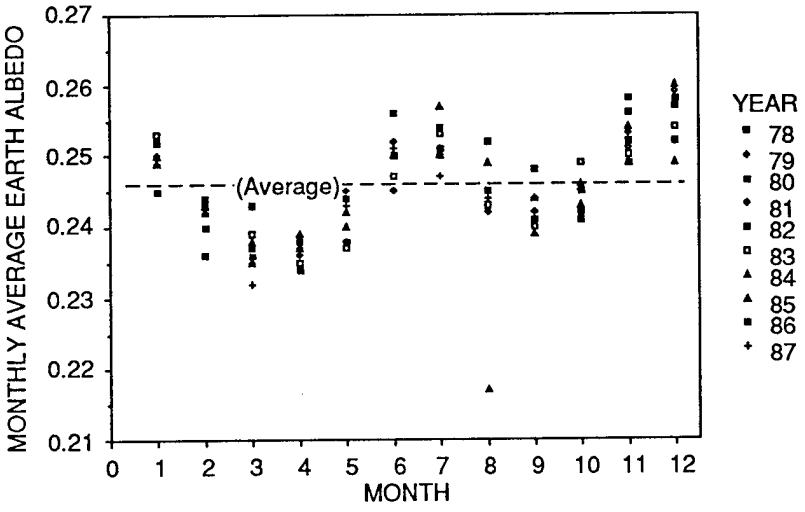


FIGURE 14. Average earth albedo for latitudes 30°N to 30°S calculated from Nimbus 7 measurements, Nov 78 to Jul 87.

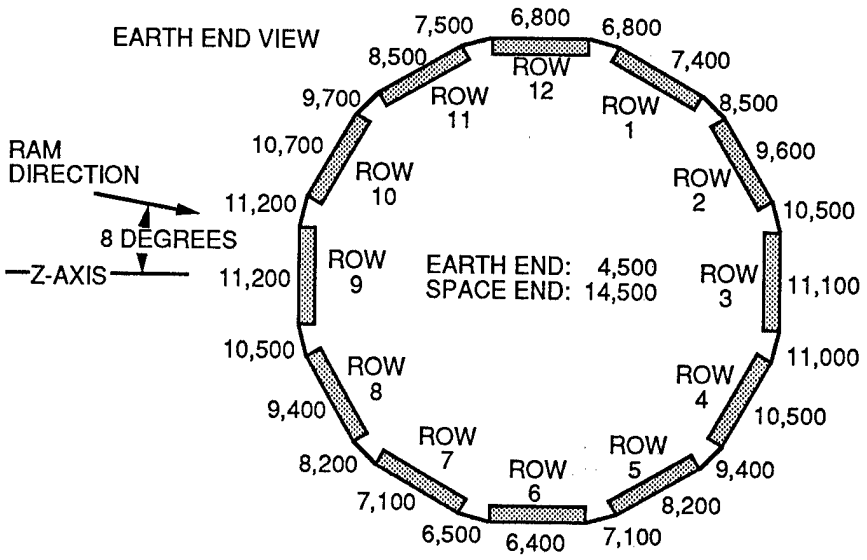


FIGURE 15. Cumulative equivalent sun hours for each tray location.

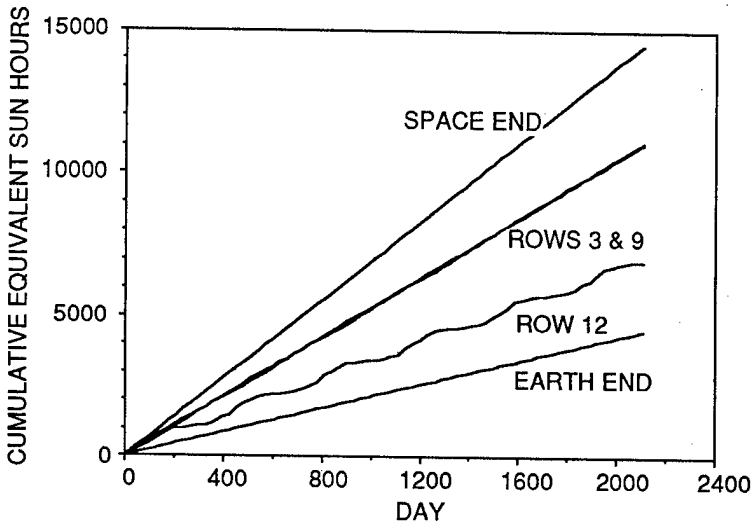


FIGURE 16. Cumulative sun hours for typical experiment trays.

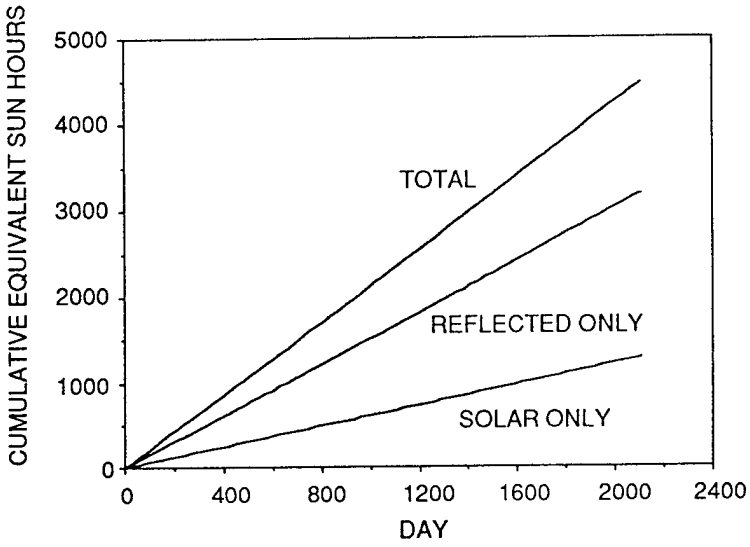


FIGURE 17. Earth reflected and direct solar exposures for earth end bays.

EFFECTS OF SPACE ENVIRONMENT ON STRUCTURAL MATERIALS

C. Miglionico, C. Stein, R. Roybal, and R. Robertson
Phillips Laboratory (WSMD) Kirtland AFB, New Mexico
Phone: 505/846-4798, FAX: 505/844-3888

L. E. Murr, S. Quinones, J. Rivas, B. Marquez,
A. H. Advani, W. W. Fisher, and R. Arrowood
Department of Metallurgical and Materials Engineering
The University of Texas at El Paso, El Paso, Texas
Phone: 915/747-5468, FAX: 915/747-5616

SUMMARY

A preliminary study of materials exposed in space in a low-earth orbit for nearly six years has revealed a wide range of micrometeorite or microparticle impact craters ranging in size from 1 to 1000 μm in diameter, debris particles from adjacent and distant materials systems, reaction products and other growth features on the specimen surfaces, and related phenomena. The exposed - surface features included fine-grained and nearly amorphous materials as well as a large array of single-crystal particles. A replication-type, lift-off technique was developed to remove reaction products and debris from the specimen surfaces in order to isolate them from the background substrate without creating microchemical or microstructural artifacts or alterations. This resulted in surface features resting on a carbon support film which was virtually invisible to observation by electron microscopy and non-dispersive X-ray analysis. Characterization of these surface features involved observations by optical metallography, scanning electron microscopy (SEM), transmission electron microscopy (TEM) and energy-dispersive X-ray spectrometry (EDS) including an analytical transmission electron microscope with a STEM attachment. Some evidence for blisters on leading-edge aluminum alloy surfaces and a high surface region concentration of oxygen determined by Auger electron spectrometry suggests atomic oxygen effects where fluences exceed 10^{21} atoms/cm^2. The results illustrate a wide variety of materials phenomena which must be addressed in the evaluation of materials exposure in space, and the formidable materials characterization effort which will be necessary to understand these features.

INTRODUCTION

Perhaps one of the most exciting materials experiments in this decade involves the characterization of a host of materials - metals, alloys, ceramics, composites, polymers, semiconductors; and coating, laminates, and multicomponent materials systems - exposed in space in low earth orbit (LEO) for nearly 6 years. The NASA - LDEF (Long Duration Exposure Facility) Satellite (containing some 57 multinational experiments in trays composing 12 rows on a 12-sided cylinder the size of a bus) as shown in Fig. 1 was placed on non-geosynchronous orbit by the Space Shuttle Orbiter Challenger in April of 1984. The LDEF was retrieved on-orbit January 12, 1990 by Space Shuttle Orbiter Columbia in the first NASA shuttle mission to follow the Challenger tragedy in January of 1986. The LDEF, mounted in the LDEF Assembly and Transfer System (LATS) located at Kennedy Space Center (Fig. 1(b)) was systematically inspected and photographed in a sequence of partial rotations of LDEF to allow experimenters to see specific rows and trays (Fig. 1) from an optimal viewing position. This deintegration process took several months to complete.

In this paper we report on some preliminary results of observations of several important materials

issues involving characterization using light optical and electron optical tools: optical metallography, scanning electron microscopy (SEM), analytical TEM (TEM fitted with an energy-dispersive X-ray analysis system and SEM and scanning transmission electron microscope (STEM) capability), and Auger electron spectroscopy.

Experimental Procedures and the Development of Materials Characterization Protocols

Although, as illustrated in Figs. 1 and 2, there are an enormous range of materials panels to be examined, this paper will deal with some preliminary observations and the development of some simple and effective techniques for the examination and characterization of surface features and surface-related phenomena. We will limit our discussions to the examination of a few sections ("x") of an aluminum 6061-T6 test panel illustrated in the test array shown in Fig. 2(b).

Initial observations of surface effects and surface-related phenomena involved optical microscopy and metallography followed by observations of uncoated specimens of the test area in a scanning electron microscope (SEM) fitted with an energy-dispersive X-ray spectrometer (EDS) attachment.

Initial observations revealed a high density of impact craters which ranged in size from more than 1000 μm to less than 1 μm in diameter. In addition, the surfaces also exhibited various "debris" particles and what appeared to be growth structures and surface-related reaction products, including "crystals" and non-crystalline-appearing features. These surface features could be examined by EDS in the SEM but the X-ray signals from very small particles were often compromised by X-ray spectra from the supporting aluminum matrix, and it was difficult to elucidate the elemental nature of the particles or to determine anything specific about their internal microstructures or crystal structures.

Unambiguous and detailed examination of surface "debris" and related surfaced features (including reaction products) required the development of a lift-off technique which would allow these features to be selectively removed from the test material surface without creating chemical or microstructural alterations or other artifactual contributions which would compromise or complicate an examination of the isolated products. Utilizing a rather standard surface replication technique illustrated in Fig. 3 (ref. 1), a plastic (polymer) film was placed over a selected area of the surface and a standard (3mm) transmission electron microscope (TEM) copper grid placed on the plastic and allowed to dry. A sticky tape was used to gently pull the plastic and adhering grid from the surface and a carbon support film was then vapor deposited onto the back side of the plastic support system. The grid, with plastic and carbon support encapsulating the "particles" lifted from the surface, were then placed on a wire screen in a petri dish containing acetone. A hot plate was used to gently heat the acetone to create a vapor in the covered petri dish and wash the plastic from the grid-lift-off composite to produce a carbon support on the grid holding the particles removed from the surface.

These grids with carbon support films containing "particles" stripped from the aluminum alloy surface were then examined in an analytical transmission electron microscope or scanning transmission electron microscope (STEM) fitted with an SEM detector and an EDS attachment. This allowed high-resolution and high-definition microanalysis of surface particles and debris to be examined independent of the surface-related matrix. The carbon support film was also essentially "invisible" to the electron probe and contributed only a weak carbon signal to the EDS spectrum (see references 1 and 2).

Auger spectrometry accompanied by systematic surface sputtering was performed on the leading-edge exposed surfaces on the 6061-T6 aluminum shown in Fig. 1. The backside of these samples was also examined for comparison. Microhardness measurements were also performed on exposed and unexposed (reverse) surfaces.

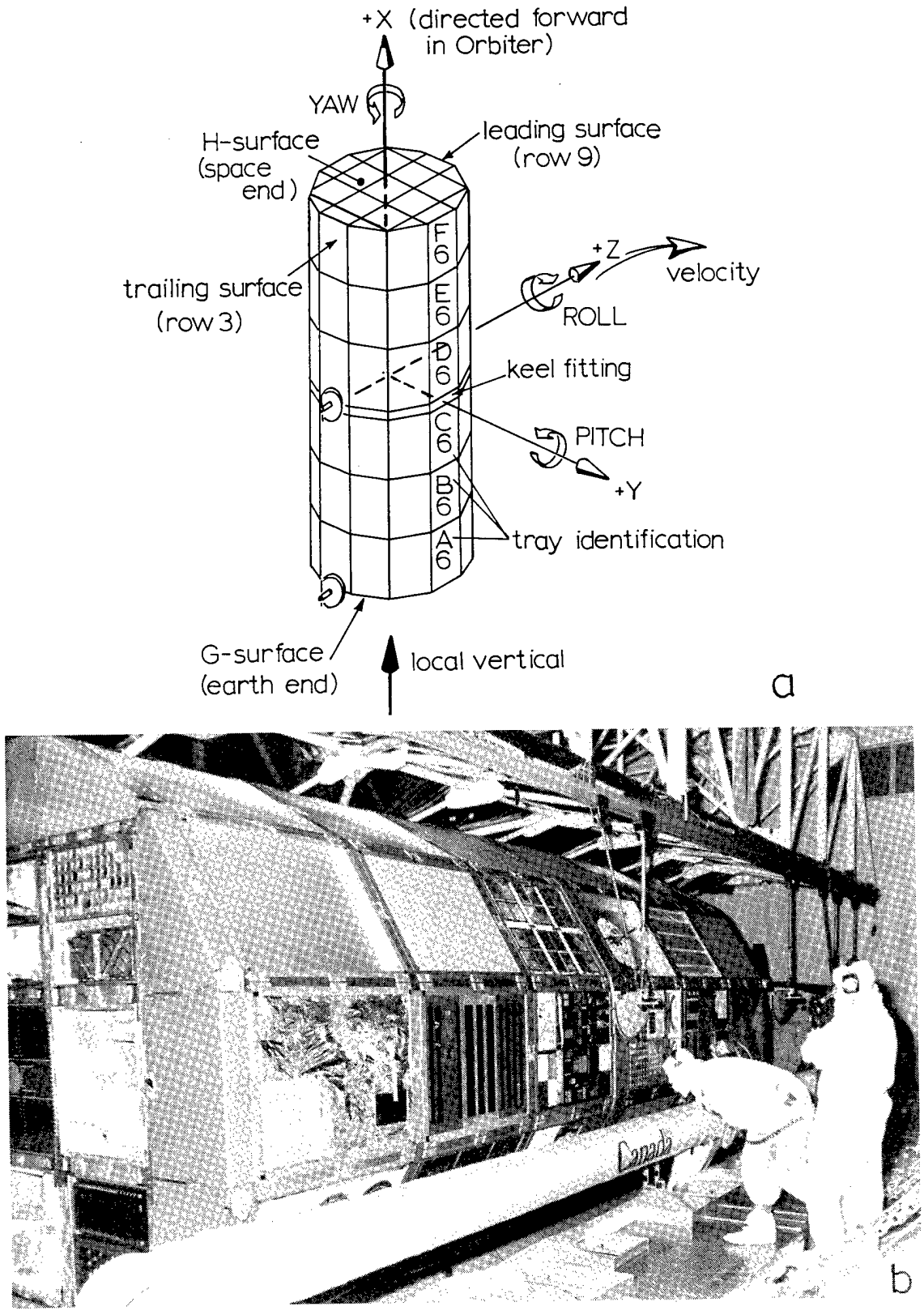


FIG. 1: NASA-LDEF orbital orientation model schematic (a) and NASA photograph of LDEF suspended above the payload bay of the Space Shuttle Orbiter Columbia during its move to a transportation canister and the LATS at Kennedy Space Center (b).

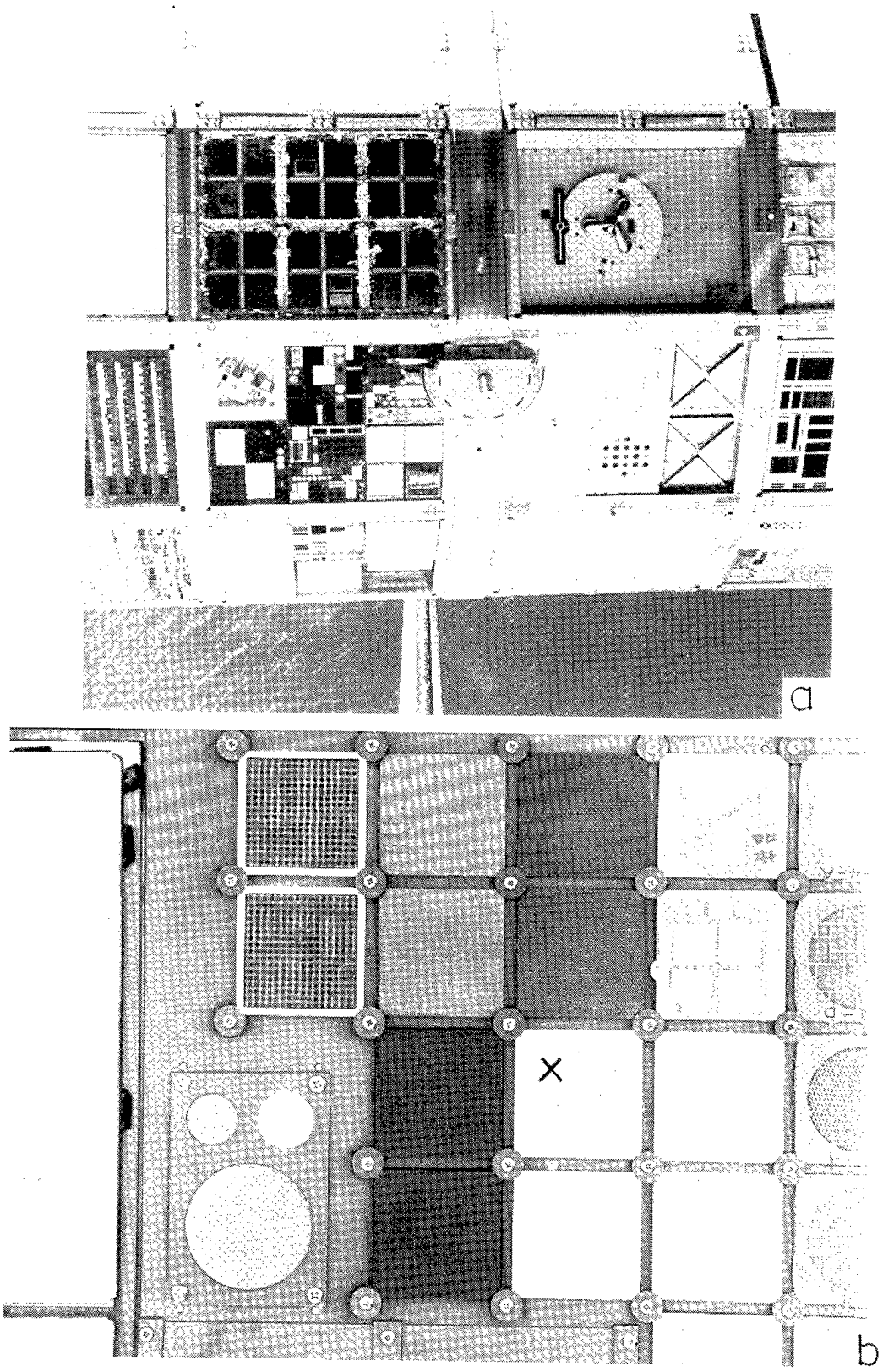


FIG. 2: Orbital view of LDEF during retrieval showing damaged silver-coated teflon thermal blanket and specimen arrays in a bay area including M0003 on the leading edge of the satellite (a). An enlarged view of the specimen area included in this investigation and shown in (a) is illustrated in (b).

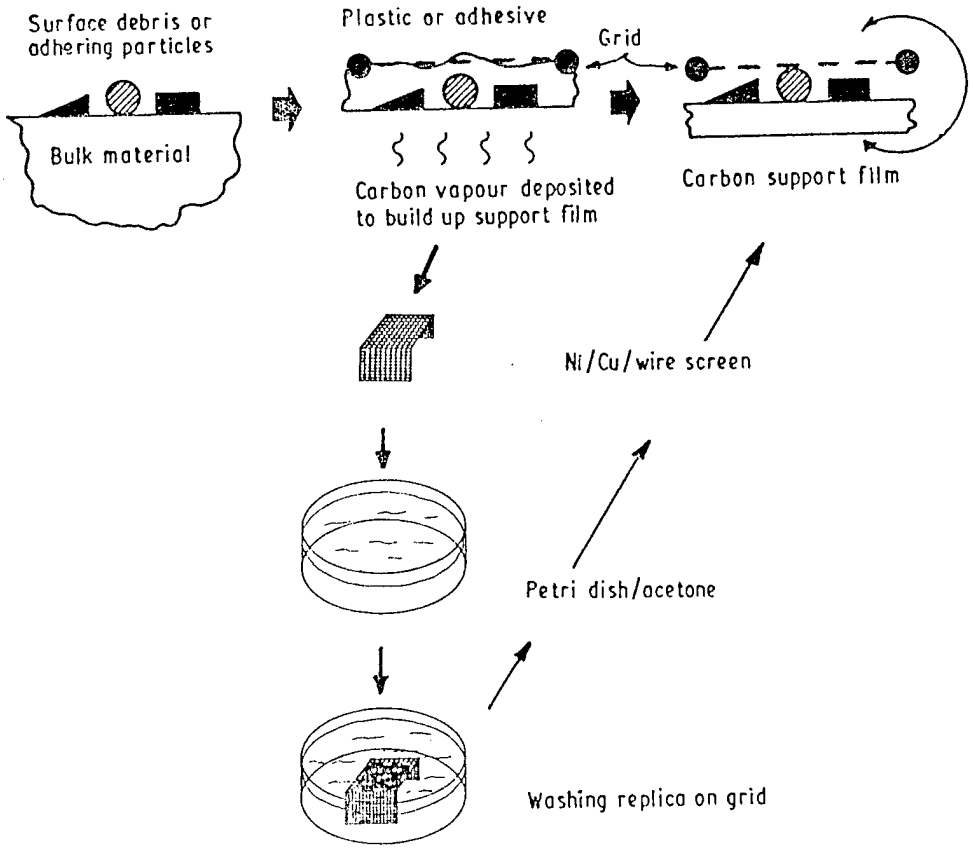


FIG. 3: Schematic representation of replication technique adapted for surface lift-off. From reference 3.

RESULTS AND DISCUSSION

Sample Characterization of Leading Edge Surfaces: 6061-T6 Aluminum alloy (Macroscopic Examination)

Figure 4 shows a composite view of a region of the 6061-T6 aluminum sample surface illustrating a range of surface phenomena, including artifacts which are not space environment related. The artifacts include roll marks, scratches, and micro-gouges. The space effects include debris particles (shown prominently by comparing inserts A and B (representing the reverse side and exposed side portions respectively magnified by a factor 2), micrometeroid impacts, and related features (arrows) which appear to be blisters.

Figure 5 shows for comparison a large micrometeroid impact crater and a ruptured blister. The ejecta pattern around the impact crater and the stretched and ruptured blister cap are clearly distinguishable features. Although the impacting particles are generally thought to vaporize during impact, observations of debris within the impact craters indicate reactions between the impacting particle and the impacted substrate. This is an important feature of the effect of space environments on structural materials because such impact-related reactions could form intermetallic phases or other brittle products. These intermetallic phases could initiate microcracks or cause other deleterious effects especially if impacting particles or

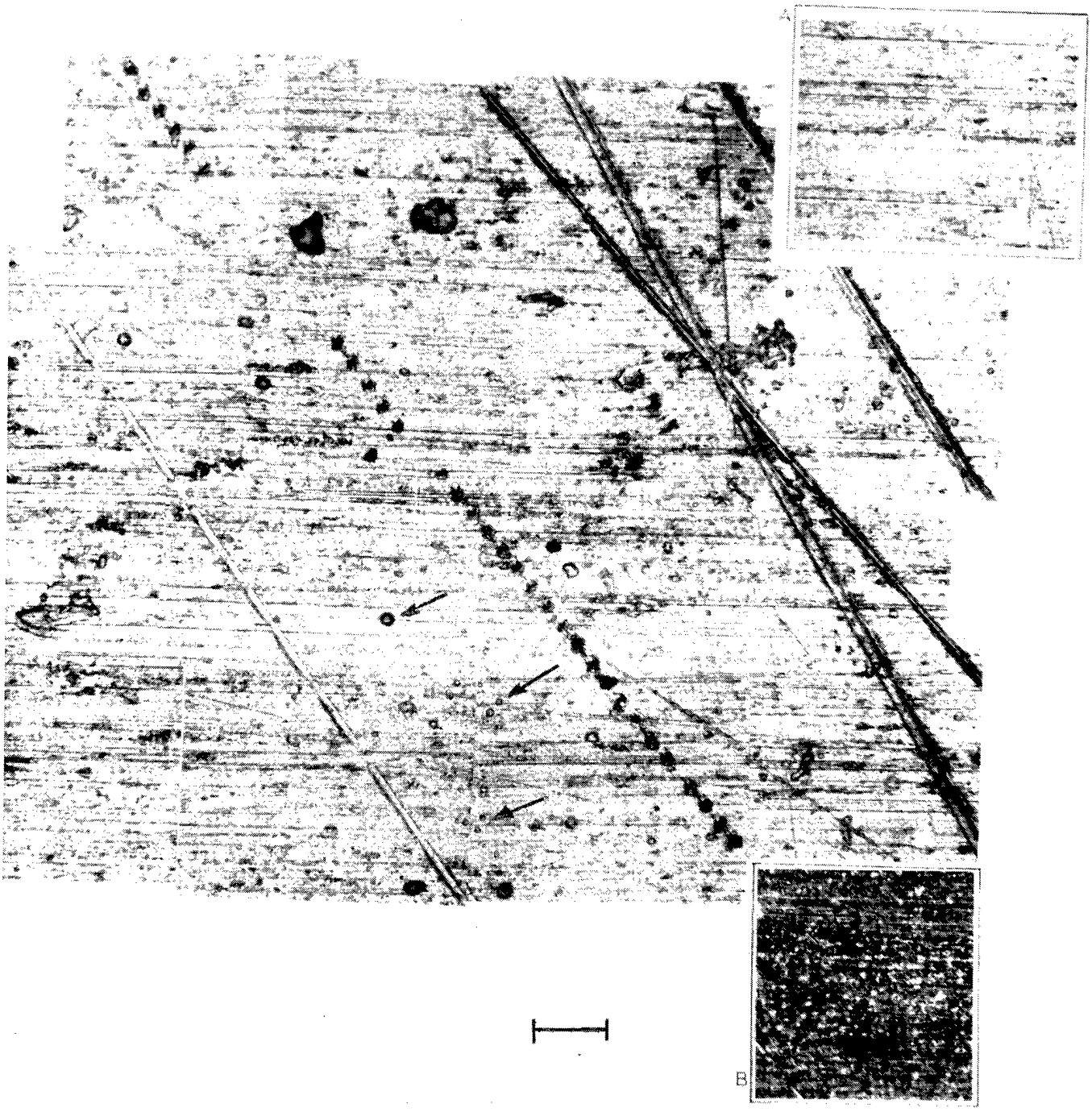


FIG. 4: Optical micrograph composite of surface area on aluminum alloy test plate near the leading edge of LDEF marked X in Fig. 1(c). Insert A shows a typical view from the reverse (unexposed) side of the test plate while insert B shows a 2X view of a region from the exposed side shown in the composite. The arrows illustrate blisters on the surface magnification marker = 10 μm.

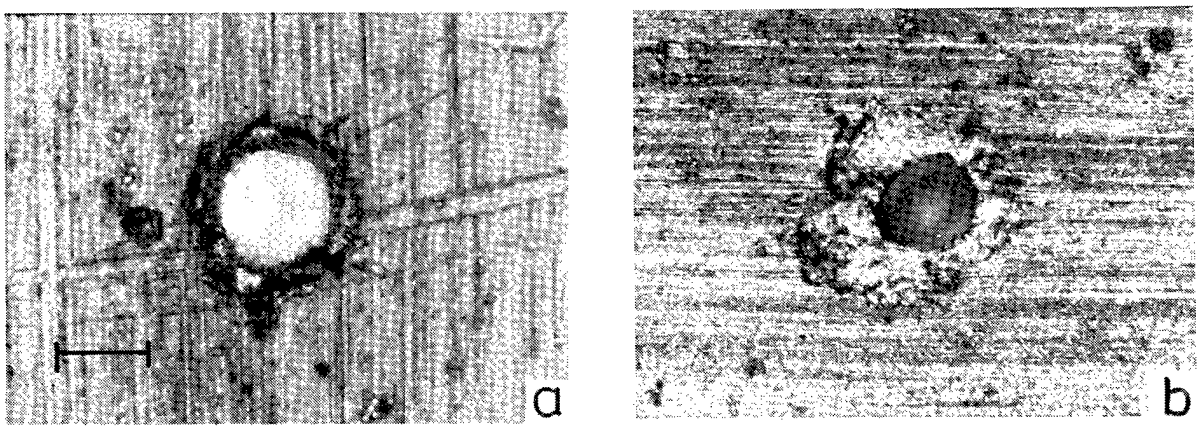


FIG. 5: Optical (light) micrographs comparing a micrometeoroid impact crater (a) and a burst blister (b) on the surface of a 6061-T6 aluminum test panel near the leading edge of LDEF in region marked X in Fig. 1(c). The impact crater (a) shows an ejecta rim while the burst blister (b) shows shear bands in the stretched and fractured surface cap. Magnification marker = 10 μm.

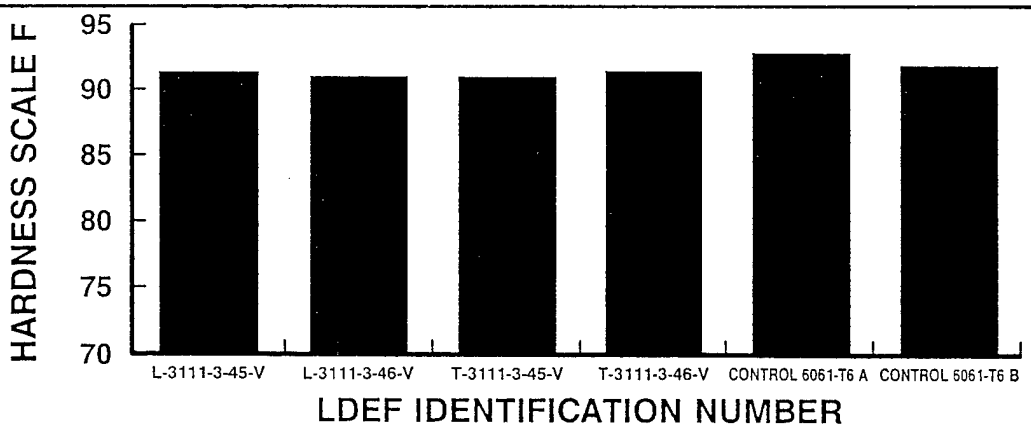
micrometeroites contain iron, nickel, or combinations thereof and impact aluminum or aluminum alloys as illustrated in Fig. 5(a). We are currently developing a technique to section large impact craters to allow detailed observations and analysis of the crater base and any reaction zones or deformation regions which exist in the crater base regions.

From a mechanical perspective, there is some evidence from hardness and mechanical (tensile) testing that leading-edge exposed 6061-T6 aluminum samples are altered. This shows up in hardness data and UTS data as illustrated in Fig. 6. The reasons for this alteration are not clear, but there is evidence from Auger electron spectrometry that significant oxygen is injected into the exposed surfaces. This feature, illustrated in the data reproduced in Fig. 7, also supports the notion that blisters are forming by atomic oxygen bombardment and absorption during exposure in LEO as shown in Figs. 4 and 5. Surface-related oxygen is not observed on the reverse side of the leading-edge exposed 6061-T6 aluminum or on the trailing-edge exposed surfaces. These observations provide rather compelling evidence for atomic oxygen effects on exposed surfaces, especially on the leading edge where fluences exceed 10^{21} atoms/cm^2.

Sample Characterization of Leading Edge Surfaces: 6061-T6 Aluminum Alloy (Microscopic Examination)

Figure 8 is an illustration of one of dozens of observations of growth-like surface debris which contain sulfur and silver as shown in the accompanying EDS spectrum. It is believed that the silver originates from a silver-coated polymer film which was located above the specimen tray in Fig. 2(a). This tray was covered by silver-coated panels which exhibit only remnants of the original film around the edges of individual panels. The experimental tray (Fig. 2(b)) contains test panels of graphite polysulfone, and these were observed to be heavily corroded and eroded by interaction with atomic oxygen as described previously (see reference 4). It is possible, therefore, that the silver available in debris particles from the upper tray reacted with sulfur available through erosion of the graphite-polysulfone by reaction with atomic oxygen, forming AgS_x or even combinations of AgS_x/AgO_x, since oxygen is also present in the EDS spectrum shown in Fig. 8(b).

The availability of sulfur due to reactions of atomic oxygen with the polysulfone and other sulfur -



LDEF No.	HARDNESS SCALE		CROSS SEC	MAX LOAD	UTS
	F	B	(in^2)	(lb)	(psi)
L-3111-3-45-V	91.5	61	0.0113	543.75	48119.47
L-3111-3-46-V	91.0	60	0.0114	556.25	48793.86
T-3111-3-45-V	91.0	60	0.0114	556.25	48793.86
T-3111-3-46-V	91.5	61	0.0112	543.75	48549.11
CONTROL 6061-T6 A	93.0	63	0.0156	765.00	49038.46
CONTROL 6061-T6 B	92.0	62	0.0155	750.00	48387.10

FIG. 6: Hardness and related mechanical property data for exposed 6061-T6 aluminum samples and unexposed samples (controls).

containing panels, and other reactions with atomic oxygen apparently also gave rise to other surface reaction products which are illustrated in Fig. 9. Figure 9(a) shows what appear to be thin crystals of MgO/MgS complexes as suggested from the associated EDS spectra as shown in Fig. 9(b), and selected-area electron diffraction patterns obtained for similar crystals lifted from the surface using the replication technique illustrated in Fig. 3, (reference 3).

Of course the aluminum peak in Fig. 9(b) arises from the aluminum alloy (6061-T6) test sample and some of the magnesium peak may also be background signal. However by lifting these particles from the surface and performing EDS in the analytical transmission electron microscope, these features can be unambiguously demonstrated. Figure 10 shows some examples of MgO/MgS particles lifted from the surface which do not contain aluminum in the EDS spectrum (Fig. 10(b)) and which are also not crystals, at least large crystals as suggested in the SEM images of Fig. 9(a) or Fig. 10(a). The selected-area electron diffraction (SAD) pattern indicated a very fine-grain (nearly amorphous) structure well below the crystal morphologies suggested in the SEM image (Fig. 10(a)) where "crystal" geometries measure 0.5 x 2μm.

We are devoting a significant effort to the development of a matrix of chemical elements associated with the plethora of fine (microscopic) particles present on the test panel surfaces, especially on leading edge units using conventional TEM (bright-and dark-field imaging), analytical TEM (including selected-area electron diffraction (SAD) patterns), EDS, SEM, and STEM mode imaging. This detailed analysis of individual particles is necessary to establish their chemical and structural identity and provide clues about

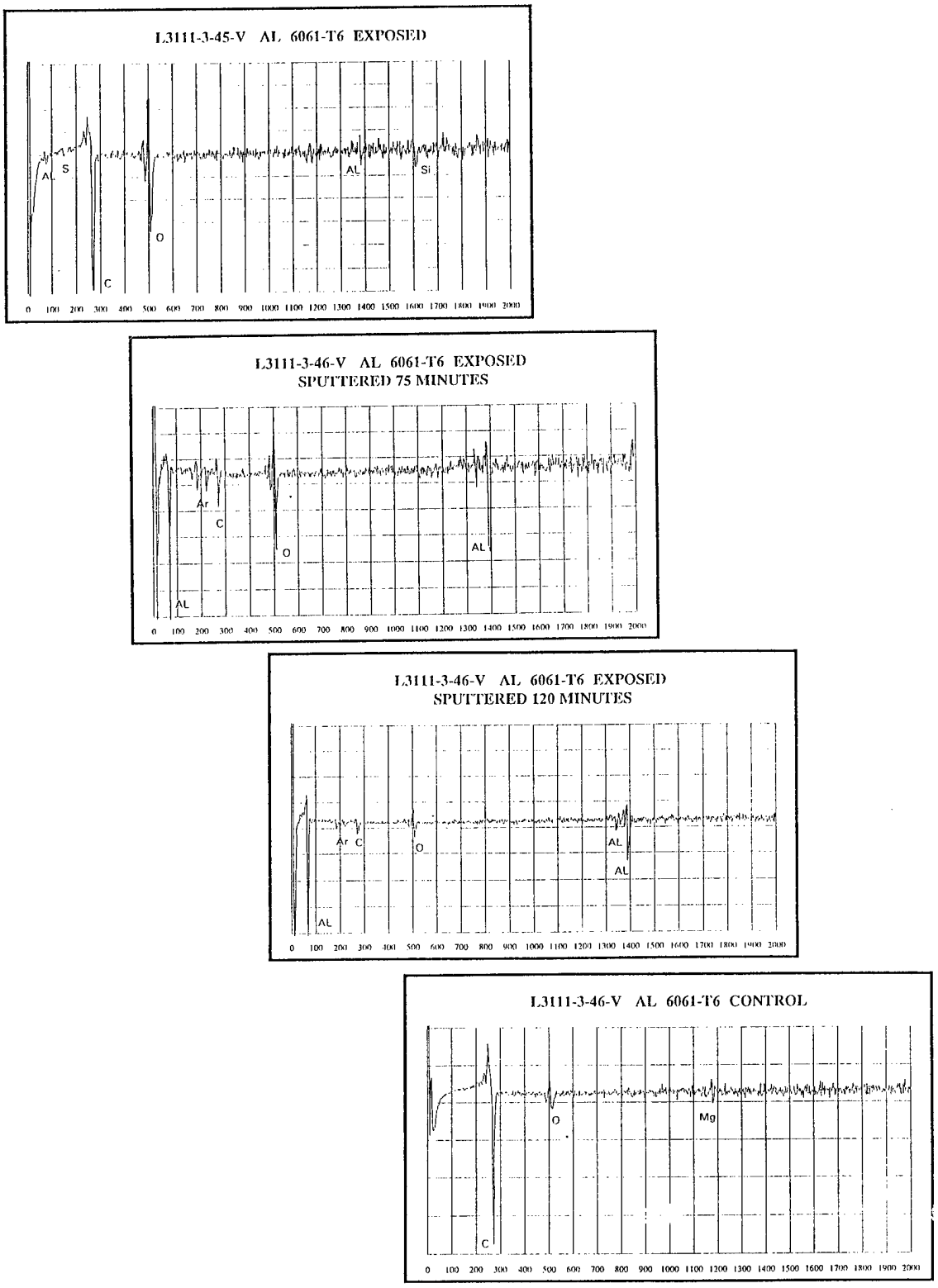


FIG. 7: Auger electron spectra for exposed and control (unexposed) 6061-T6 aluminum alloy surface regions. The sputter depths are proportionate to sputter time. Note the decline of oxygen with sputter time. The prominent carbon peak illustrates a hydrocarbon film covers the surface as a contaminant from LDEF.

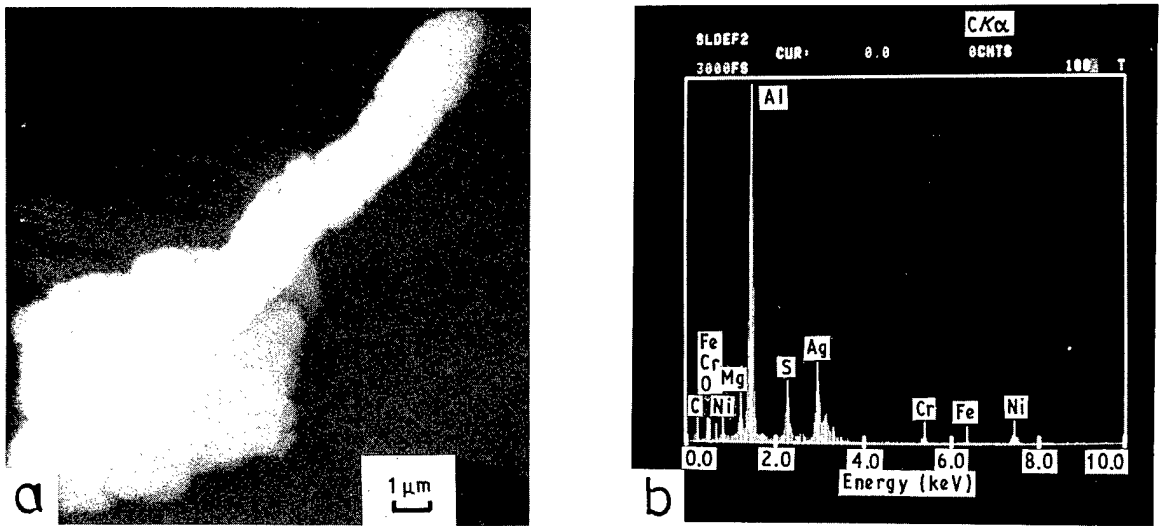


FIG. 8: (a) Silver sulfide growth structure on the aluminum test panel in the SEM. (b) EDS elemental analysis spectrum.

their specific origins. Figures 11 and 12 show some examples of these analyses which illustrate the diversity in particle morphology, crystallinity, chemistry, and microstructure. We have recorded the details of particle morphology, chemistry, and crystallography for more than 100 different particles whose origins are traced to micrometeoroid debris (often from the ejecta (Fig. 3(a)), contamination from other panels (for example gypsum (Ca-S-O) crystals (Fig. 12(a)) were traced to a chalk number printed on a neighboring panel), stratospheric particles (such as salt and other mineral crystals), and related phenomena. Many particles are single crystals, difficult to rationalize as space dust (interplanetary dust particles - IDPs) (reference 5). However, many chondritic alkali-alumina silica compositions and related IDP chemistries occur as shown in Fig. 12(b). A rather crude summary of the elemental distributions in the particle or particle-cluster samples examined (similar to those in Figs. 11 and 12) is reproduced in Fig. 13.

CONCLUSIONS

It must be recognized that the results presented in Figs. 4 to 13 represent only a very small sampling of one of 57 different trays of experimental/test materials and hundreds of panels of the LDEF Satellite. While these results are neither representative nor conclusive, they do illustrate a wide range of materials issues which will have to be addressed in assessing the effects of space environments on structural and other materials and materials systems. We have demonstrated that it will be necessary to isolate surface debris and reaction products from materials exposed in space and that replication techniques originally designed for electron microscopy examination of surfaces (references 1 and 2) can be applied to lift off and isolate such surface features. This technique has allowed debris and reaction products to be examined by a variety of analytical techniques associated with analytical transmission electron microscopy; including the surface morphology by SEM, internal microstructures by STEM and TEM, EDS, and SAD (reference 1).

While the results presented in Figs. 4 to 13 are somewhat preliminary, they illustrate the role that atomic oxygen may play in surface alteration and reaction in low-earth orbit space environments, as well as the role to be played by debris created from other, proximate materials. The prospects for the growth of new and even different phases and materials chemistries from those reported on earth, and the possibilities for impact-related reactions and materials interactions provokes the necessity to address a broad range of space-related materials issues and the development of expedient and carefully planned analytical protocols.

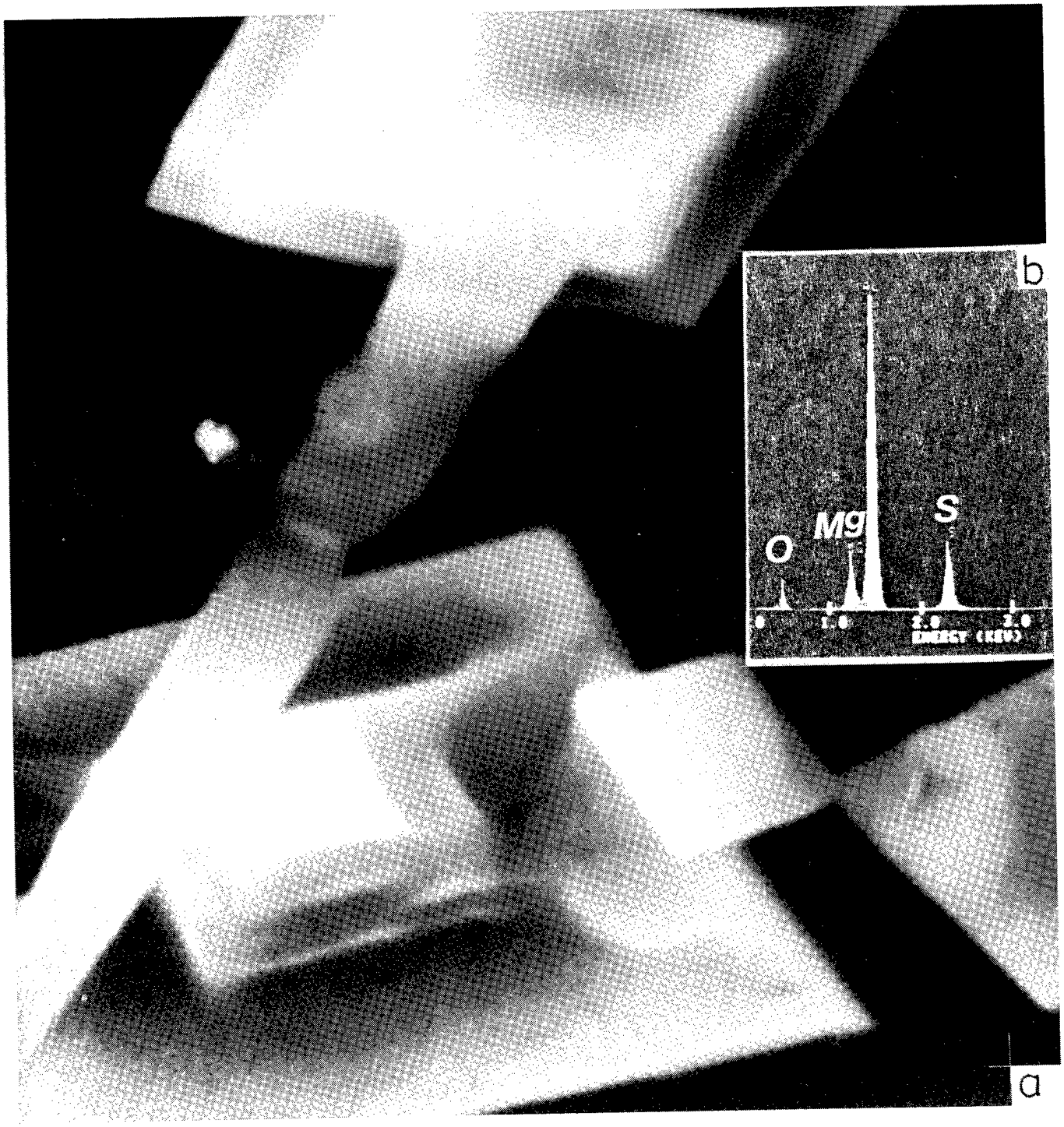


FIG. 9: Mg-S-O crystals observed on the aluminum alloy test panel surface. (a) SEM view showing thin cubic crystal geometry. (b) EDS analysis. The aluminum peak represents the panel background.

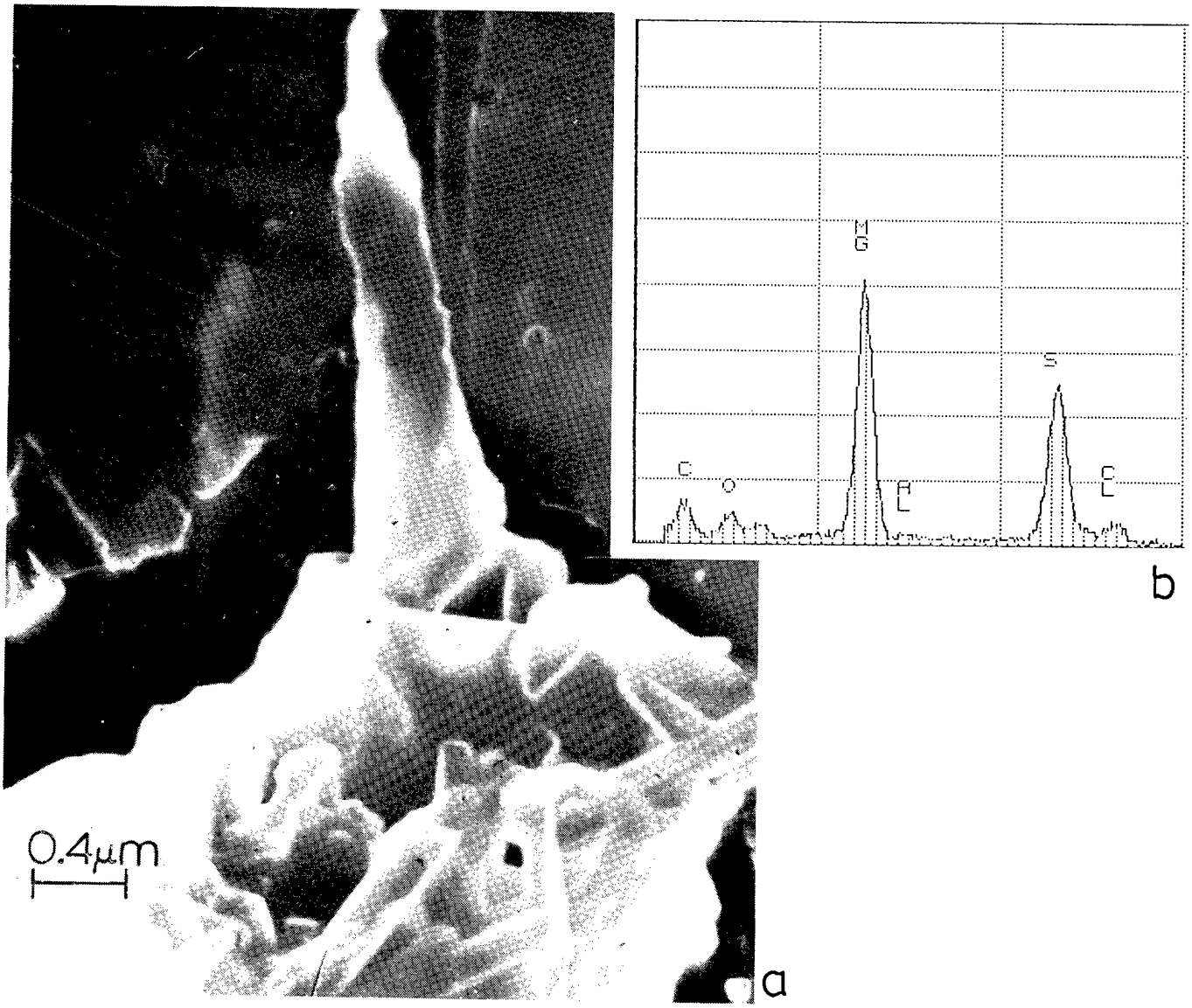


FIG. 10: Mg-S-O particles embedded in a carbon support film which have been lifted from the aluminum alloy test panel surface and examined in the analytical TEM. (a) SEM mode view of particle cluster. (b) EDS spectrum. Note absence of aluminum peak in contrast to Fig. 9(b).

In addition, the interactive role of UV radiation, atomic oxygen, temperature fluctuations, and other phenomena need to be carefully and unambiguously evaluated.

The variety of effects suggested in the analytical results illustrated in Figs. 4 to 13 attest to the new frontiers in space materials research which will be opened up when materials requirements for space structures and space craft become an important component of research in the materials sciences.

Finally, the large number of micro-meteorite impacts coupled with the prospects for surface debris and related reaction products forming on materials surfaces as shown in Figs. 8 to 13 raise a spectre of problems and concerns for optical materials and coatings, optical systems, and space optics. The Hubble

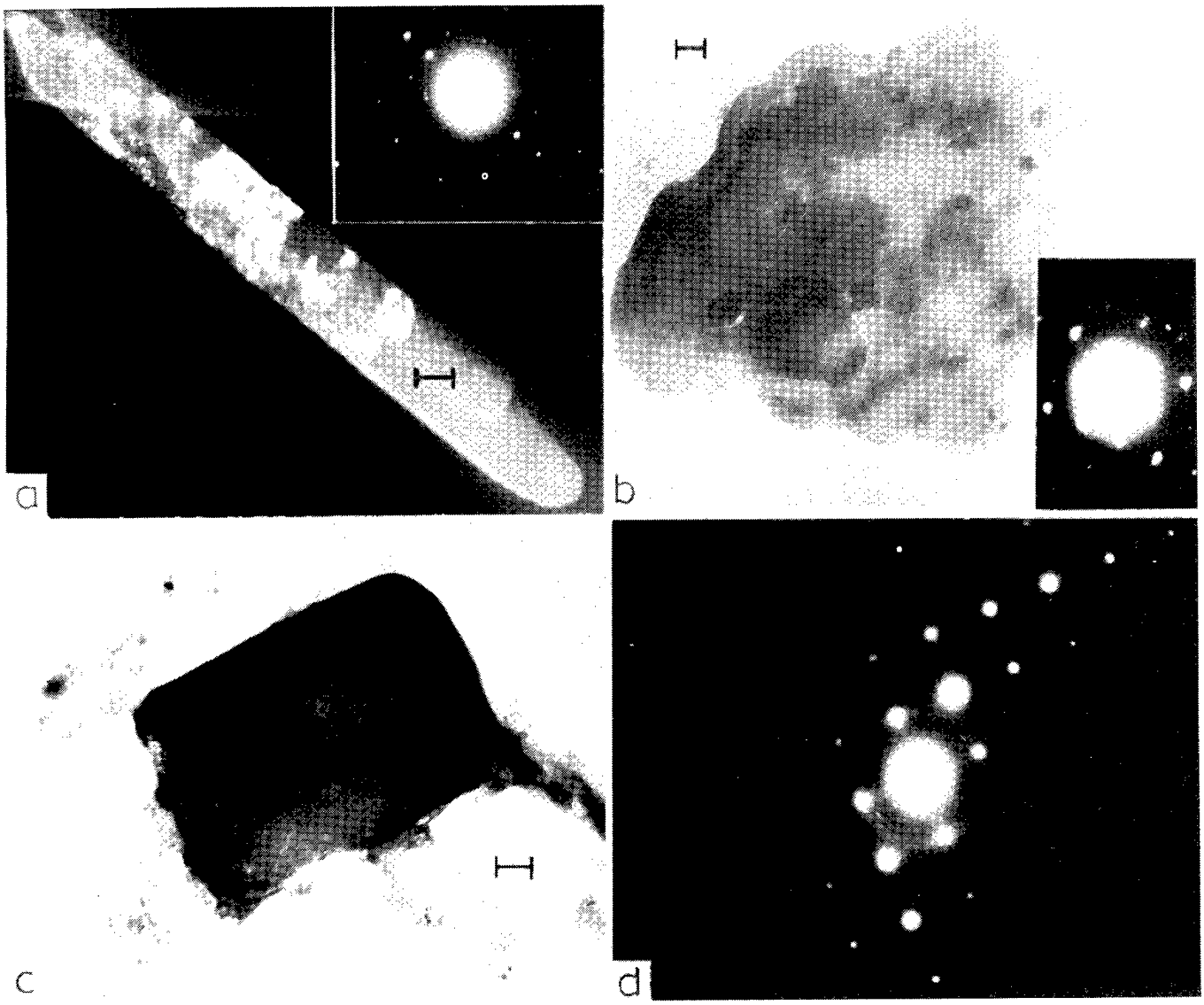


FIG. 11: Examples of isolated particulate analysis in the analytical TEM of LDEF leading-edge aluminum 6061-T6 test panel surfaces. (a) Dark-field TEM image and SAD pattern insert for Al-O crystals containing inclusions. (b) Bright-field TEM image and SAD pattern insert for Mg-S crystal. (c) Bright-field TEM image of NaCl crystal. (d) SAD pattern showing cubic symmetry for (c). Magnification markers are 0.1 μm.

telescope and similar space optics systems will be susceptible to a variety of these materials concerns, and the necessity for a high level of precision in optical materials has already been demonstrated in the NASA Hubble telescope, and similar concerns must be considered for other space optical and guidance systems as well as a host of other related concerns.

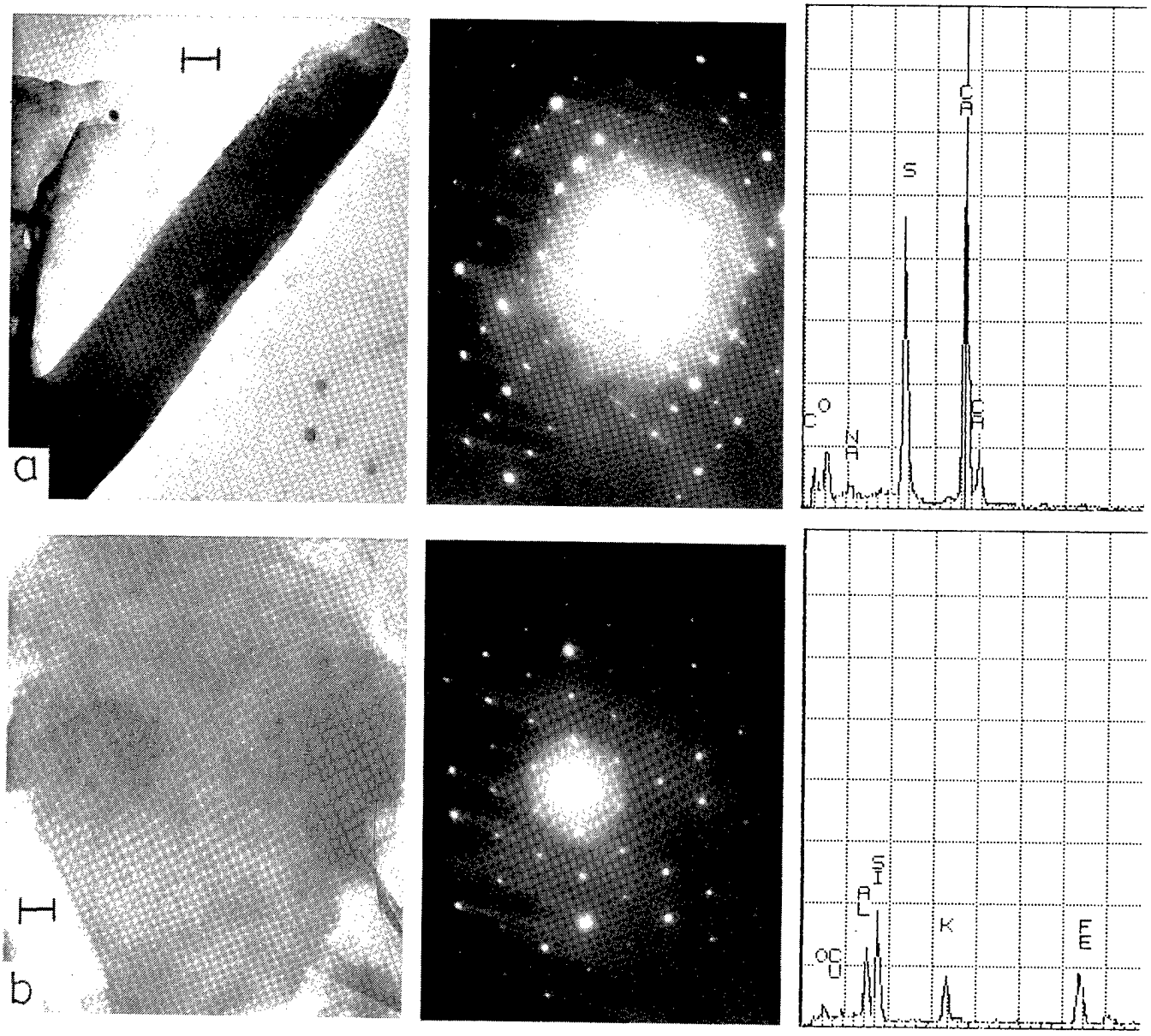


FIG. 12: (a) Example of gypsum (Ca-S) crystals. (Bright-field TEM image. Magnification marker is 0.1 μm.; SAD pattern; EDS spectrum). (b) Example of silicate particle. (Bright-field TEM image. Magnification marker is 0.1 μm.; SAD pattern; EDS spectrum).

ACKNOWLEDGMENTS

This research was supported by the U.S. Air Force Phillips Laboratory LDEF Experiment (with specific support from Wright-Patterson AF Base, Ohio) and in part by a NASA-Johnson Space Center Research Grant (NAG 9-481) to develop space materials characterization protocols at the University of Texas at El Paso.

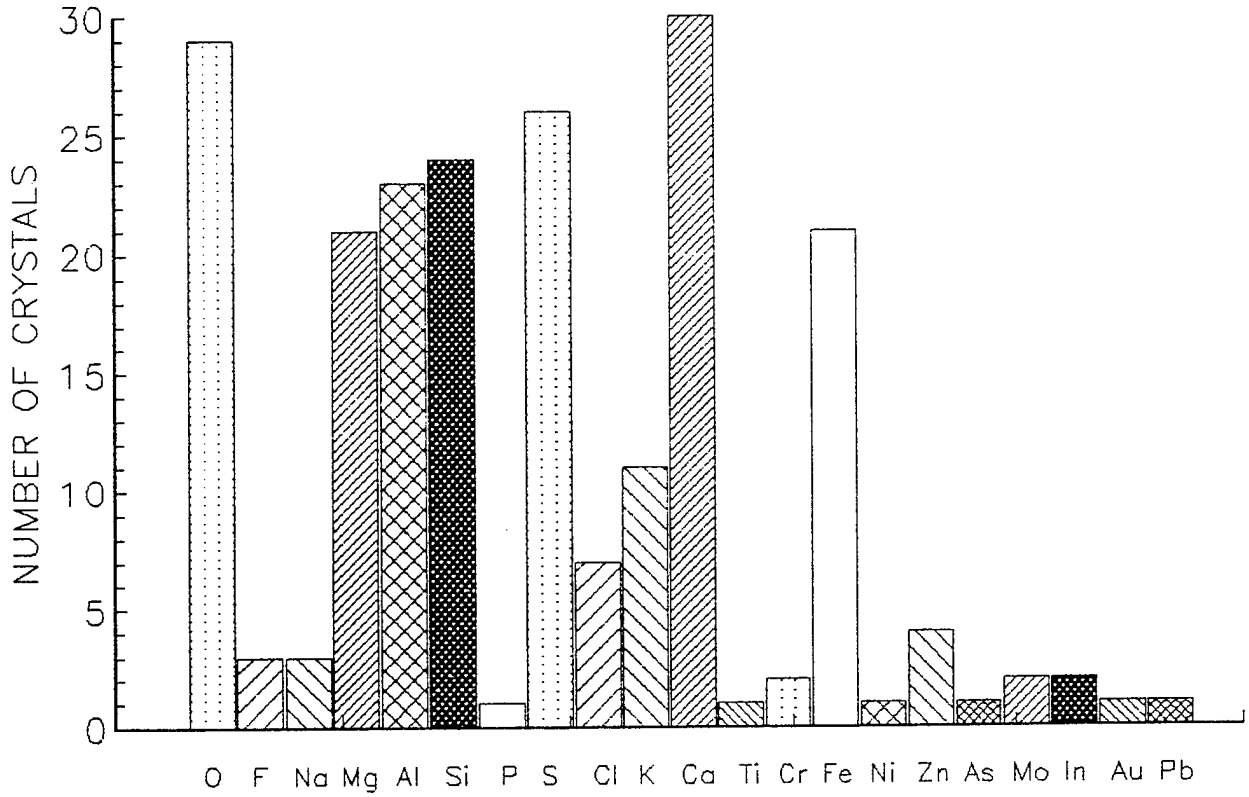


FIG. 13: Histogram of elemental distributions in particles extracted from LDEF aluminum alloy surfaces.

REFERENCES

1. L. E. Murr, *Electron and Ion Microscopy and Microanalysis: Principles and Applications*, 2nd Edition, Marcel Dekker, Inc., New York, 1991.

2. L. E. Murr (ed.), *Industrial Materials Science and Engineering*, Marcel Dekker, Inc., New York, 1984, p. 519.

3. C. Miglionico, C. Stein, and L. E. Murr, "Effects of Space Environment on Structural Materials: A Preliminary Study and Development of Materials Characterization Protocols", *J. Materials Science*, August 1, 1991.

4. Donald E. Hunton, "Shuttle Glow", *Scientific American*, November, 1989, p. 92.

5. M. E. Zolensky, "The Relationship Between Hydrous and Anhydrous Interplanetary Dust Particles", *Microbeam Analysis - 1991*, D. G. Howitt (Ed.), San Francisco Press, Inc., San Francisco, CA, 1991, p. 287.

MEASUREMENT OF THE O^{18} TO O^{16} ISOTOPE RATIO FOR CHARACTERIZING OXIDE SURFACE LAYERS ON LDEF SAMPLES

Paul L. Sagalyn

U.S. Army Materials Technology Laboratory
Watertown, MA
Phone: 617/923-5398, FAX: 617/923-5385

SUMMARY

The ratio of the density of the oxygen 18 isotope (O^{18}) to the density of the oxygen 16 isotope (O^{16}) is a strong function of altitude in the atmosphere because of the stronger gravitational attraction on the heavier isotope. It is proposed that the measurement of this ratio for oxide surface layers on LDEF samples can easily distinguish oxides formed in orbit from contaminative oxides formed during retrieval procedures. Since the satellite altitude is known as a function of time, it may be possible to use the measured ratio to determine the time of formation of oxide layers, the accuracy depending upon the stability of the atmosphere.

INTRODUCTION

The isotopic composition of atmospheric oxygen at sea level is given in table I. For the purposes of this paper we can neglect the small amount of O^{17}. The approximate composition at sea level can then be taken as 99.8% O^{16} and 0.2% O^{18}.

The earth's atmosphere is a dynamic system which is not in thermal equilibrium. Nevertheless, for an approximate calculation, the author will assume thermal equilibrium; and in this case the density of a particular molecular species is given by the "Law of Atmospheres" (reference 1):

$$n(Z,T) = n(O,T) \exp[-MgZ/kT] \quad (1)$$

where Z is the geometric altitude in meters, T is the absolute temperature, M is the mass of the molecule in kg, g the acceleration due to gravity in m/sec^2, and k is Boltzman's constant.

The ratio of the densities of two molecular species, each given by equation (1), will depend on the mass difference of the two molecules. At orbital altitudes, where the oxygen is 99% atomic, it is obvious that the mass difference between molecules carrying O^{18} and O^{16} is two nuclear units. However, in table II it is shown that to

an excellent approximation in the low altitude region where the oxygen is diatomic, the bulk of the O^{16} (99.6%) is carried in molecules with two O^{16}'s and the bulk (99.9%) of the O^{18} is carried in molecules with only one O^{18}. The mass difference is therefore again two units. The transition region between the diatomic and monatomic regimes is more complicated and will be neglected.

Using equation (1) we can then write:

$$R(Z) = \frac{n^{18}(O)}{n^{16}(O)} \exp\left[-\left(M^{18} - M^{16}\right) gZ/kT\right] \tag{2}$$

$$= R(O) \exp[-CZ/T],$$

where $n^{18}(Z)$ is the particle density of O^{18}, $n^{16}(Z)$ the same for O^{16}, R(Z) is the ratio of the isotopic densities as a function of altitude, and M^{18} and M^{16} are the isotopic masses in kg. C is defined as:

$$C = (M^{18} - M^{16})\, g/k = 2.36 \times 10^{-3} \text{ mks units.}$$

The density ratio decreases with altitude because the O^{18} is more tightly bound to the earth. The individual densities are given by:

$$n^{18}(Z) = n^{18}(O) \exp[-0.0212\ Z/T], \quad n^{16}(Z) = n^{16}(O) \exp[-0.0189\ Z/T].$$

The individual densities decay 6-7 orders of magnitude more rapidly than does their ratio.

SYMBOLS

Z	altitude (meters)
T	temperature (Kelvin)
$n^{18}(Z)$	particle density of oxygen 18
$n^{16}(Z)$	particle density of oxygen 16
M^{18}	nuclear mass of O^{18} (kg)
M^{16}	nuclear mass of O^{16} (kg)
g	acceleration due to gravity (meters/sec^2)
k	Boltzman's constant

R(Z)	ratio of the O^{18}/O^{16} densities
C	constant defined as $(M^{18} - M^{16})g/k$
N^{18} N^{16}	particle counts in a hypothetical SIMS experiment
V	satellite linear velocity
P	sticking probability for an oxygen atom hitting the surface
t	time in orbit required to form a desorbed layer
A	area desorbed in a SIMS experiment
e	SIMS efficiency
V_Z	vertical component of the satellite velocity

APPLICATIONS

Contaminative Versus Orbital Oxides

In order to evaluate equation (2) at orbital altitudes we need a value for the temperature. Figure 14-21 of reference 2 gives the kinetic temperature of the atmosphere as a function of altitude. Looking, for example, at the proposed mean CIRA data, there are two regions of roughly approximate temperature, 0 through 200 km and 200 km and above. Temperatures for a two zone model for the atmosphere could be estimated from these plots. As a check we can use the molecular densities given in tables 14-7, 14-8, and 14-9 of reference 2 and use equation (1) to calculate an effective temperature for the atmosphere. It is simpler to use nitrogen for this calculation since, unlike oxygen, nitrogen remains molecular up to orbital altitudes. The nitrogen density data used is listed in table III. The resulting effective temperatures are listed in table IV.

Using just the density data for 0 km and 470 km (initial orbital altitude) yields an overall average effective temperature of 496 K. Using a two zone model gives an effective temperature of 290 K for the altitude range 0 through 200 km and 1055 K for 200 through 470 km. The latter numbers agree well with figure 14-21 of reference 2. Because of the way the numbers were derived, when applied to oxygen, they will make exactly the same prediction for the density at 470 km. Substituting T = 496 in equation (2) yields:

$$R(470)/R(O) = 0.11.$$

The model predicts an order of magnitude change in the isotope ratio between sea level and orbital altitude! Although this effect is 6-7 orders of magnitude smaller than the changes in the individual densities, when considering the accuracy of mass spectrometers it is a very large effect and should be easily measurable.

Resolution

Since the satellite altitude is known accurately as a function of time, in principle a measurement of the oxygen isotope ratio for a given oxide layer on a sample could be used to date the formation of the layer. Of course the particle densities vary widely because of variations in solar heating but it is nevertheless interesting to calculate the ultimate resolution of the method. By resolution is meant the shortest time in orbit or smallest altitude change, which will lead to a detectable change in the isotope ratio *in the sample*. Consider two adjacent layers of oxide of arbitrary thickness, say d. We imagine a SIMS type experiment in which a small region of area A is sputtered off and the number of O^{18} and O^{16} ions are separately counted in a mass spectrometer. In a counting experiment the standard deviation, σ_N, is given by $N^{1/2}$. Let N^{18} and N^{16} represent respectively the number of counts resulting from desorbing one layer of thickness d. By definition:

$$R = \frac{N^{18}}{N^{16}} .$$

Since $N^{16} >> N^{18}$, the standard deviation in R is given approximately by:

$$R = \frac{\left(N^{18}\right)^{1/2}}{N^{16}} .$$

What we are trying to calculate is $\Delta R = R1 - R2$, where R1 and R2 are the measured values of the isotope ratio for two adjacent layers. Since we are interested in small values of the difference, for the calculation of the error in R, a second order effect, we can assume that the counts for the two layers are equal. It then follows easily that the standard deviation in the difference, ΔR, is given by:

$$\sigma_{\Delta R} = \frac{\left[2\,N^{18}\right]^{1/2}}{N^{16}} . \qquad (3)$$

R is given as a function of altitude by equation (2). To obtain equation (4), below, we differentiate equation (2) and set the result equal to equation (3):

$$\Delta R(Z) = R(Z)\left[\frac{-A\ \Delta Z}{T}\right] = \frac{\left[2N^{18}\right]^{1/2}}{N^{16}} \quad . \tag{4}$$

Equation (4) determines the minimum value of ΔZ which will give a change in R equal to the standard deviation in the measurement of ΔR.

The number of counts obtained in the hypothetical SIMS experiment will be proportional to the thickness of the layer desorbed. To any value of the thickness there will be a corresponding time in orbit, t, required to form the layer. Assuming the altitude to be high enough so that the gas is monatomic, the number of atoms counted will be the number imbedded in the sample in time, t, times the efficiency of the SIMS apparatus or:

$$\begin{aligned} N^{18} &= (n^{18})VtPAE \\ N^{16} &= (n^{16})VtPAE \end{aligned} \tag{5}$$

where V is the satellite velocity ($n^{18}V$ is the incident particle flux), P is the sticking probability for an incident atom, A is the area desorbed by the SIMS, and e is the SIMS efficiency, the fraction of the absorbed atoms which actually gets counted.

ΔZ and t are related by:

$$\Delta Z = V_Z\, t \tag{6}$$

where V_Z is the vertical component of the satellite velocity.

We now substitute equations (5) and (6) into equation (4) and solve for ΔZ:

$$\Delta Z = \left[\frac{2T^2 V_Z}{(n^{18})\ VPAEC^2}\right]^{1/3} \quad . \tag{7}$$

As an example, equation (7) has been evaluated using the following numerical parameters, valid at 464 km. This altitude was chosen because of the availability of a NASA orbital data plot which began at 464 km. V_Z was calculated graphically from this plot.

$n^{18} = 9.9 \times 10^9/m^3$

$T = 1055\ K$ $\qquad$ $e = .01$

$C = 2.36 \times 10^{-3}$

V	=	8×10^3 m/sec	Vz	=	2.6×10^{-4} m/sec
A	=	1 cm^2	P	=	0.001

The value chosen for P is just a guess. However, the cube root in equation (7) makes the results relatively insensitive to the choice of parameters. Using these values with equations (6) and (7) gives for the resolution:

ΔZ	=	10 meters at 464 km
t	=	11 hours

CONCLUDING REMARKS

The intrinsic resolution of the method appears to be very high. In a dating experiment the accuracy of the result will probably depend on the atmospheric stability rather than the experimental accuracy. Measurements of the ratio, $R = O^{18}/O^{16}$, as a function of depth on the surface of samples exposed to the space environment should be very interesting.

It would also be very interesting on future missions to fly a dedicated mass spectrometer, with resolution high enough to distinguish between O^{18} and normal water vapor (i.e., containing two O^{16}'s), and continuously monitor the ratio, R, in the atmosphere. This data would be very valuable for correlating with the sample measurements. It would also give interesting information about atmospheric dynamics. The fluctuations in R would not be expected to exactly track the fluctuations in the total pressure (essentially O^{16}). That is, if the pressure at orbital altitude increases due to the expansion of gas from a lower altitude, the deeper the origin of the new gas, the greater the fluctuation of R will be relative to the fluctuation in the total pressure.

TABLE I. SEA LEVEL COMPOSITION OF ATMOSPHERIC OXYGEN		
O^{16}	O^{17}	O^{18}
99.758%	0.00039%	0.204%

TABLE II. MOLECULAR ISOTOPIC COMPOSITION NEGLECTING O^{17}			
Type of O_2 Molecule	16-16	18-16	18-18
% Occurrence	99.517	0.407	4×10^{-4}

TABLE III. NITROGEN DENSITY DATA		
Altitude km	Density no./cubic meter	Reference
0	2.1×10^{25}	Calc. for STP
200	2.6×10^{15}	2, table 14-9
470	5.6×10^{11}	2, table 14-9

TABLE IV. NITROGEN EFFECTIVE TEMPERATURES	
Altitude range km	T effective Kelvin
0 - 470	496
0 - 200	290
200 - 470	1055

REFERENCES

1. Reif, F.: Fundamentals of Statistical and Thermal Physics. McGraw Hill, New York, NY, chapter 6, 1965.

2. Handbook of Geophysics and the Space Environment. Air Force Geophysics Laboratory, A. S. Jursa, Ed., 1985.

CHEMICAL CHARACTERIZATION OF SELECTED LDEF POLYMERIC MATERIALS

Philip R. Young
NASA Langley Research Center
Hampton, VA 23665-5225
Phone: 804/864-4265, Fax: 804/864-8312

Wayne S. Slemp
NASA Langley Research Center
Hampton, VA 23665-5225
Phone: 804/864-1334, Fax: 804/864-7729

SUMMARY

The chemical characterization of selected polymeric materials which received exposure on the Long Duration Exposure Facility is reported. The specimens examined include silvered fluorinated ethylene propylene (FEP) teflon thermal blanket material, polysulfone matrix resin/graphite fiber reinforced composites, and several high performance polymer films. These specimens came from numerous LDEF locations and, thus, received different environmental exposures.

The results of infrared, thermal, x-ray photoelectron, and various solution property analyses have shown no significant change at the molecular level in the polymer that survived exposure. However, scanning electron and scanning tunneling microscopies show resin loss and a texturing of the surface of some specimens which resulted in a change in optical properties. The potential effect of a silicon-containing molecular contamination on these materials is addressed. The possiblity of continued post-exposure degradation of some polymeric films is also proposed.

INTRODUCTION

The NASA Long Duration Exposure Facility (LDEF) provided a unique environmental exposure of a wide variety of materials and experiments (ref. 1,2). The spacecraft traveled approximately 34,000 orbits and three-quarters of a billion miles during its 5-year and 9-month journey. The effects of atomic oxygen, ultraviolet and particulate radiation, meteoroid and debris, vacuum, contamination, and thermal cycling on the LDEF and its contents is providing a data base unparalleled in the history of research on space environmental effects. This paper reports on the chemical characterization of selected polymeric materials which flew onboard the spacecraft.

The objective of the present study is to assess the response of various materials to the long-term low Earth orbital (LEO) exposure obtained on LDEF. The approach has been to characterize the molecular level effects of this exposure as well as more obvious visual, physical, and mechanical effects. The benefit of this approach is intended to be fundamental information for use in developing new and improved materials for long-term LEO missions.

Specimens selected for this study came from Langley experiments and from materials made available to the Materials Special Investigation Group during LDEF deintegration activities

at the Kennedy Space Center in the January-May 1990 time period. They include silvered perfluorinated ethylene propylene (FEP) teflon thermal blanket material, Kapton film, and P1700/Celion 6000 polymer matrix/graphite fiber reinforced composites. The chemical characterization of these materials using infrared spectroscopy, dynamic and thermomechanical analyses, solution property measurements, and x-ray photoelectron spectroscopy are reported. The potential effect of a silicon-containing contaminant on the performance of these materials is discussed. In addition, the possibility of continued post-exposure degradation of some polymeric materials is proposed. This study is intended to add to the body of knowledge on space environmental effects on materials being derived from the LDEF mission.

EXPERIMENTAL

Infrared spectra were recorded on a Nicolet 60SX Fourier Transform Infrared Spectrometer System using a diffuse reflectance technique (DR-FTIR) (ref. 3). UV-VIS spectra were run on a Perkin-Elmer Lamda 4-A spectrophotometer. Dynamic mechanical spectra were obtained on a DuPont Model 982 Dynamic Mechanical Analyzer Model 1090 Thermal Analyzer (DMA). Glass transition temperature (Tg) determinations were made on a Perkin-Elmer Model 943 Thermomechanical Analyzer (TMA). Additional thermal analysis was performed using a DuPont Model 1090/Model 910 Differential Scanning Calorimeter (DSC). The equipment and techniques used to make solution property measurements have been previously reported (ref. 4). Gel permeation chromatography (GPC) was performed on a Waters Associates system in chloroform using a $10^6/10^5/10^4/10^3$ Å Ultrastyragel column bank.

X-ray Photoelectron Spectroscopy (XPS) measurements were conducted at the Virginia Tech Surface Analysis Laboratory, Department of Chemistry, VPI&SU, Blacksburg, VA (ref. 5). Measurements were made on a Perkin-Elmer PHI 5300 spectrometer equipped with a Mg X-ray Kα source (1253.6 eV), operating at 15 kV/120mA. Typical operating pressures were $<10^{-7}$ torr. Analyses were made at take-off angles of 45° or 90°.

Scanning electron microscopy (SEM) and energy dispersive X-ray (EDS) analyses were conducted both at Virginia Tech and at Langley. An ISI SX-40 SEM (ISI, Milpitas, CA) equipped with a Tracor Northern Z-MAX 30 EDS analyzer (Tracor, Madison, WI) was used at Virginia Tech. A Cambridge StereoScan 150 SEM (Cambridge Instruments, Deerfield, IL) equipped with an EDAX S150 detecting unit (EDAX International Inc., Prairie View, IL) was used at the Langley Research Center. The visual appearance of selected specimens was documented using various photographic techniques.

DISCUSSION

During the months preceding the LDEF retrieval, a significant effort went into planning for the chemical characterization of polymeric materials onboard the vehicle. Much of this effort was summarized at the LDEF Materials Data Analysis Workshop which ran concurrent with activities surrounding the successful return of the spacecraft to the Kennedy Space Center in early 1990 (ref. 2). Chemical, physical and mechanical changes were anticipated as the result of environmental exposure. Among the anticipated chemical effects were modification to molecular structure, molecular weight (MW) and molecular weight distribution (MWD) changes, Tg and crystallinity effects, and changes in surface chemistry. Resin loss, changes in transparency and α_s/ε, and contamination were also expected to be observed.

An approach for characterizing these effects was adopted. Where appropriate, solution property measurements including GPC, low angle laser light scattering photometry (LALLS), differential viscometry (DV), GPC-LALLS, and GPC-DV were considered to be invaluable in determining how the MW and MWD responded to exposure. FTIR analyses were expected to play a key role in following molecular level changes in the polymer backbone. Various thermal anlyses including DSC, DMA and TMA would also be employed to examine Tg, Tm, and crystallinity effects. Finally, extensive use was planned for XPS, EDS, SEM, and Scanning Tunneling Microscopy (STM) for examining environmental effects on surface chemistry. Thus, the examination of selected polymeric materials proceeded in a deliberate step-by-step manner as the various specimens became available for analysis. As evidenced by the foregoing discussion, the present effort was, indeed, focused on characterizing the molecular level effects of environmental exposure.

Specimens selected for this study are described in Table I. They were included as part of larger experiments intended to evaluate the LEO environment on a variety of materials and experiments for advanced spacecraft application (ref. 1). Figure 1 depicts the LDEF structure and orbital inclination. The location of specimens on LDEF is included in Table I along with a summary of pertinent exposure conditions.

Ag/FEP Film. The thermal blanket material, also known as flexible second-surface mirror (SSM) thermal control coating, is used in a variety of space applications where thermal control is a consideration (ref. 6). Figure 2 gives a schematic of the SSM describing its composition and function. The outer layer consists of a nominal 5 mil Type A FEP copolymer teflon film. Solar radiation passes through this transparent film and is reflected away by the silver backing. This yields a low absorption of solar radiation, α_s. The thermal emittance, ε, is a function of the polymer bulk infrared absorption and, therefore, is dependent on material thickness. These properties provide for a variable α_s/ε ratio, desirable for certain spacecraft thermal considerations. The material has both thermal blanket and adhesively bonded application.

Visual inspection of the fully integrated LDEF at the Kennedy Space Center revealed that the appearance of all the SSM material was not the same. Thermal blankets located near the Row 3 trailing edge exhibited a highly specular appearance while those located near the Row 9 leading edge exhibited a diffuse or "frosted" appearance. The change from specular to diffuse was essentially graduated as the location changed from trailing to leading edge. Since this observation correlated with the anticipated atomic oxygen fluence at these locations, the two phenomena were assumed to be related.

DR-FTIR analysis of specular and opaque blanket specimens revealed surprisingly similar spectra (ref. 7). Extensive thermal analysis of selected materials also failed to detect significant differences. The FEP film layer was delaminated from the urethane backing and analyzed. The vapor deposited silver remained on the urethane layer. Figure 3 shows the DSC thermogram from -120°C to 340°C for a specular specimen which flew on Row 5. Inflections in the trace around -10°C are likely associated with the Tg of the FEP teflon. The melt endotherm (Tm) around 250°C is also apparent. All analyzed specimens showed essentially the same DSC thermogram. No significant differences were noted in Tg, Tm, or the heat of fusion for any specimen.

XPS analysis also failed to reveal major differences in the surface chemistry of opaque flight specimens as compared to control materials. Table II summarizes XPS results for selected opaque specimens. No appreciable amount of oxygen was incorporated into these specimens nor had the surface concentration of carbon and fluorine changed.

Thus, based on FTIR, DSC, and XPS analyses, we concluded that the opaque appearance of the thermal blankets was not a result of a change in chemical properties. However, subsequent SEM and STM analysis showed that the appearance was likely due to "texturing" or "carpeting" of the FEP surface by atomic oxygen erosion (ref. 8). Figure 4 shows SEM photomicrographs of a Row 5 (specular) and a Row 8 (diffuse) blanket specimen. The texturing noted for the diffuse sample is essentially perpendicular to the plane of the film and in the direction of the atomic oxygen flow. This phenomenon has been observed on previous shuttle flights (ref. 8).

As will be discussed in a later section, the surface of several blanket specimens which remained specular was found by XPS to be contaminated with a silicon-containing species. For example, data for the tray F2 material given in Table II shows about 1.5% atomic concentration of silicon on the film surface. Figure 5 shows DR-FTIR spectra for this specimen and a control. A subtraction of the two spectra revealed the presence of a carbonyl group in the exposed specimen.

The multiple XPS carbon peaks and elevated oxygen concentration associated with the F2 specimen was assumed to be associated with this contamination. Although no silicon was found on the specular C5 specimen, the multiple carbon peaks for that example, shown in Figure 6, were also initially assumed to be associated with contamination. However, emerging research is suggesting that the FEP surface is crosslinked by deep UV exposure (ref. 9). The possibility of UV crosslinking of fluoriniated polymers is currently being investigated (ref. 10). This phenomenon most likely was not observed with opaque blanket specimens because atomic oxygen had eroded the UV-crosslinked layer away.

Kapton Film. Kapton film from the space end of LDEF was also examined. The 5 mil thick 0.5 inch wide strips were included as part of an experiment to evaluate the effect of the space environment on polymers considered for space-based radar phased-array antenna material (ref. 11). The location of these films at position H7 was such that the flow of atomic oxygen was perpendicular to the 5 mil film edge and parallel to the film surface.

Figure 7 shows SEM micrographs of one of the films. The sketch at the top of the figure identifies a portion of the film with the appropriate SEM. For example, 7a shows the leading film edge directly exposed to AO while 7b shows the trailing edge which received only sweeping exposure. 7c and 7d show exposed and protected film surfaces. Texturing is noted on surfaces exposed to atomic oxygen. However, in contrast to the perpendicular projections shown in Figure 4, the texturing in Figure 7c is in the plane of film (and AO flow). The "spider web" feature observed in Figure 7c to be connecting the tips of "christmas trees" has been observed with other film specimens (ref. 12). Chemical analysis suggests that this web effect is due to residual Kapton.

Additional FTIR, UV-VIS, DMA, TGA, and XPS analyses were conducted on exposed and control Kapton films. No interpretable differences were noted between specimens by these techniques except for a substantial decrease in UV-VIS transmission for exposed diffuse-appearing films (ref. 12).

P1700/C6000 Polysulfone Composites. A series of epoxy and polysulfone composites flew on a Row 9 experiment and received 5.8 years of LEO exposure (ref. 13). The physical and mechanical property analysis of these specimens is found elsewhere in this publication. The extensive chemical characterization of the thermoplastic polysulfone matrix resin specimens is discussed herein.

Figure 8 shows a photograph of a P1700/C6000 polysulfone/graphite flight specimen. The dark circular eroded region received direct exposure for the duration of the flight. The

remaining outer surface was protected by an aluminum template which held the specimen in place.

Figure 9 gives DR-FTIR spectra of protected and exposed regions of the composite. A portion of "protected" surface was cut from the specimen and placed at the focal point of the diffuse reflectance optics to obtain that particular spectrum. This technique failed to produce a satisfactory "exposed" spectrum due to the insufficient matrix resin on the specimen surface. However, the spectrum shown was obtained by filing into the exposed surface and mixing the resultant powder with KBr (ref. 3). The two spectra in Figure 9 are essentially identical, suggesting that the molecular structure of the polymer which survived exposure is similar to the original molecular structure.

DMA also indicated a loss of resin due to exposure. Figure 10 shows DMA curves for polysulfone composite samples cut from larger specimens. The magnitude of the damping peak, a function of the amount of matrix resin, decreased significantly after exposure. Subsequent resin/fiber content measurements showed greater than a 10% resin loss in exposed specimens (ref. 14). The fact that DMA damping peaks for protected and exposed composites remained at the same temperature suggests that the Tg for this material had not changed significantly due to exposure.

The possibility that the Tg of the exposed side might be different from the protected side was examined by thermomechanical analysis. The TMA probe was carefully placed in contact with exposed and protected surfaces of several polysulfone specimens. Any movement in the probe as a function of temperature was recorded. Table III summarizes the results of this evaluation. The Tg of a non-flight control specimen was essentially independent of the side examined. The slight variation in reported values can be explained by the discretionary judgment the analyst used in determining the inflection point in the TMA curve indicative of the glass transition. The Tg of flight samples given direct and protected flight exposure is also given in Table III. A careful examination of all data suggests there is no significant difference in Tg for any of these samples.

Solution property data was obtained on selected polysulfone composites. The matrix resin was extracted using chloroform and quantified by a previously reported procedure (ref. 4). Figure 11 shows GPC molecular weight distributions relative to a polystyrene standard for P1700 resin like that used to prepare prepreg, a control composite that remained at Langley, one which flew protected from direct exposure, and a composite which received direct exposure. The distributions are virtually superimposable. There is also no discernable difference in various molecular weight averages for these four materials. Table IV summarizes molecular weight data obtained by GPC relative to polystyrene, and absolute values obtained by GPC-DV and GPC-LALLS. As might be expected, slight differences are noted in values obtained by different techniques. However, these data support the general conclusion that there is no significant difference at the molecular level between polymer which survived exposure and the original polymer.

Contamination. The possibility that molecular contamination may bias some of the observations made in this study must also be addressed. Visual inspection of the LDEF at KSC revealed that a brown "nicotine-like" stain was deposited on selected surfaces. This contaminant may have resulted from outgassing from various experiments as well as from the LDEF structure itself. XPS and EDS analyses confirmed the presence of silicon in this residue. Table V summarizes XPS data on selected specimens discussed in this paper. As much as 20.5% atomic concentration of silicon was detected on specimen surfaces. Additional XPS and FTIR analyses suggested that the silicon is in the form of an organic silicone on surfaces not exposed to AO, and an inorganic silicate on surfaces receiving AO exposure.

KRS-5 infrared optical windows were flown as contamination monitors on a Row 9 experiment. Figure 12 shows how the windows were mounted and summarizes XPS results on a specimen which received 5.8 years of flight time. Note 20.0% silicon on the exposed side, 3.3% on the vented side, and no silicon on the control specimen. Further, the 102.9 eV binding energy of the AO-exposed silicon is the binding energy of a silicate. The 101.9 eV B.E. for the protected side is that of a silicone. The conversion of silicone to the silicate upon exposure to atomic oxygen is an accepted phenomenon. Further, silica/silicate coatings have been shown on LDEF and elsewhere to be effective barriers to atomic oxygen erosion (ref. 14, 15). Thus, surfaces covered with this contamination layer may have responded differently to the LDEF environment than had they not been contaminated.

Post-Exposure Effects. Some polymeric materials which received exposure on LDEF may exhibit post-exposure effects. Environmentally exposed films and coatings have been qualitatively observed in this laboratory to continue to change in appearance with time. An appreciation of this phenonmenon may be necessary in order to analyze LDEF specimens in an efficient manner.

A series of thin films in a Langley experiment received 40 hours of LEO exposure in 1983 onboard STS-8. Those films were photographed and characterized upon their return to Langley. In February 1991, the flight specimens were removed from a desiccator where they had been stored in tin containers. Two of four films had dramatically changed in appearance.

Figure 13 shows photographs of controls and flight specimens taken in 1983 and repeat photographs taken in 1991. PEN-2,6 shown in 13a, is a state-of-the-art polyester designed to exhibit improved radiation stability (ref. 16). The film had cracked and turned opaque during storage. PMDA-DAF, shown in 13b, is an experimental polyimide expected to exhibit unusual environmental stability (ref. 17). That film turned opaque and lost much of its integrity.

Additional post-exposure effects were reported at the First LDEF Post-Retrieval Conference held June 2-8, 1991, in Kissimmee, Florida (ref. 18). Among these were comments by the presenters that some paints were bleaching to a lighter shade, that certain degraded optical fiber bundles were returning to their original color, and that the pastel colors associated with micrometeoroid and debris impacts on AO-exposed silvered teflon thermal blankets had changed to a dull brown. These distressing observations keynote the urgency in analyzing non-metallic materials onboard LDEF in an expedient manner.

CONCLUDING REMARKS

The LDEF is providing a wealth of information on the effects of extended exposure of spacecraft materials to the space environment. The present study examined how selected uncoated polymeric materials responded to almost 6 years of LEO exposure. Dramatic visual effects were observed. However, chemical characterization of these samples suggests that there is no significant change in the molecular structure of the surviving polymer. Any molecular level effects attributable to exposure were probably lost in the layer of material eroded away by atomic oxygen. The quantitative analysis of similar materials which received different LDEF exposures, for example, polysulfone specimens on Row 3, is anxiously awaited.

ACKNOWLEDGEMENT

This report was not possible without the capable assistance of a number of individuals. The authors thank Carol R. Gautreaux, A. C. Chang, Judith R. J. Davis, Karen S. Whitley, Ann C. Van Orden, and Reta R. Barrett. The contribution of Kapton films by James B. Whiteside is gratefully acknowledged.

REFERENCES

1. L. G. Clark, W. H. Kinard, D. J. Carter, and J. L. Jones, ed.; The Long Duration Exposure Facility (LDEF). NASA SP-473, 1984.

2. B. A. Stein and P. R. Young, compilers; LDEF Materials Data Analysis Workshop. NASA CP-10046, 1990.

3. P. R. Young, B. A. Stein, and A. C. Chang; SAMPE Intl. Symp., 28, 824(1983).

4. P. R. Young, J. R. J. Davis, and A. C. Chang; SAMPE Intl. Symp., 34(2), 1450 (1989).

5. NASA Grant NAG-1-1186, Virginia Polytechnic Institute and State University, Blacksburg, VA.

6. W. S. Slemp, NASA Conference Publication 3035, Part 2, 1989, pp. 425-446.

7. P. R. Young and W. S. Slemp, NASA TM 104096, September 1991.

8. S. H. Koontz, NASA Conference Publication 3035, Part 1, 1989, pp. 241-253.

9. A. E. Stiegman, D. E. Brinza, M. S. Anderson, T. K. Minton, E. G. Laue, and R. H. Liang, JPL Publication 91-0, May 1991.

10. NASA Grant NAGW-2495, University of Queensland, Brisbane, Qld, Australia.

11. R. J. DeIasi, M. L. Rossi, J. B. Whiteside, M. Kesselman, R. L. Hever, and F. J. Kuehne, NASA SP-473, 1984, pp. 21-23.

12. P. R. Young and W. S. Slemp, unpublished LDEF results.

13. W. S. Slemp, NASA SP-473, 1984, pp. 24-26.

14. P. R. Young, W. S. Slemp, W. G. Witte, and J. Y. Shen; SAMPE Intl. Symp., 36(1), 403(1991).

15. W. S. Slemp, B. Santos-Mason, G. F. Sykes, Jr., and W. G. Witte; Section 5-1 to 5-15, NASA TM 100459, Vol. 1, 1988.

16. V. L. Bell and G. F. Pezdirtz; J. Polym. Sci. Polym. Chem. Ed., 21, 3083(1983).

17. V. L. Bell; J. Polym. Sci. Polym. Chem. Ed., 14, 225(1976).

18. NASA CP 10072. June 1991.

TABLE I SPECIMENS, LDEF LOCATION AND PRELIMINARY ENVIRONMENTAL EXPOSURE CONDITIONS

SPECIMEN	LOCATION	Exposure[a] AO (atoms/cm^2)	Exposure[a] UV (sun hours)
Silvered FEP Teflon	A[b] 10[c]	7.78 x 10^{21}	10,700
Thermal Blanket	C 8	6.63 x 10^{21}	9,400
	C 5	1.09 x 10^{13}	8,200
	F 2	1.37 x 10^{9}	9,600
KAPTON Film	H 7	3.64 x 10^{20}	14,500
Adhesively Bonded	B 9 (10 month)[d]	2.60 x 10^{20}	--
Silvered FEP Teflon	B 9	8.32 x 10^{21}	11,100
934/T300 Epoxy Composite	B 9		
P1700/C6000 Polysulfone Composite	B 9		
KRS-5 Window	B 9		

[a] Boeing Aerospace supplied MSIG calculations; NAS1-18224, TASK 12.
[b] LDEF tray location (see figure 1).
[c] LDEF row location (see figure 1).
[d] Environmental Exposure Control Cannister.

GENERAL INTEGRATED LDEF ENVIRONMENT

- Particulate Radiation
  e^- and p^+: 2.5 x 10^5 rad
- Vacuum
  10^{-6} - 10^{-7} torr
- Altitude
  255-180 nautical miles
- Micrometeoroid and Debris
  34,336 impacts (0.5mm to 5.25mm)
- Thermal Cycles
  ~34,000 (-40 to 190°F extremes)
- Orbital Inclination
  28.5°

TABLE II XPS RESULTS FOR SELECTED SILVERED FEP TEFLON MATERIALS

	REFERENCE SPECIMENS			OPAQUE SPECIMENS			SPECULAR SPECIMENS		
PHOTO PEAK	STANDARD[a]	CONTROL[b]	STANDARD[c]	A10	C8	B9/5.8 yr[d]	B9/10 mo[e]	F2	C5
C 1s B.E. (eV)[f]	290.9	290.9	290.9	290.9	290.9	290.9	290.9	290.9/289.0/284.2	290.9/289.0/284.5
A.C. (%)[g]	31.6	29.6	31.3	28.5	30.4	31.4	30.8	39.8	37.5
F 1s B.E.	689.0	688.9	688.6	688.5	688.8	688.6	688.4	686.8	686.9
A.C.	65.6	66.4	68.7	69.8	66.2	67.5	68.7	47.8	56.5
O 1s B.E.	--	--	--	530.9	--	532.2	532.5	531.0	531.0
A.C.	NSP[h]	<1.0	NSP	1.3	<0.5	1.1	0.5	7.4	2.8
Si 2p B.E.	--	--	--	--	--	--	--	102.7	--
A.C.	NSP	NSP	NSP	NSP	NSP	NSP	NSP	1.5	NSP

[a] Commercially obtained blanket.
[b] Flight control blanket.
[c] Commercially obtained, adhesively bonded.
[d] Adhesively bonded, full exposure.
[e] Adhesively bonded, enviromental control canister exposed.
[f] Binding energy, electron volts.
[g] Atomic concentration, percent.
[h] No significant peak.

TABLE III THERMOMECHANICAL ANALYSIS OF P1700/C6000 POLYSULFONE COMPOSITES

Sample	Tg (°C)	Contacted side
Langley Control	167°	Random
	167°	
	170°	
	166°	
Flight Control	164°	Side A
	166°	Side B
Flight Exposed	170°	Exposed side
	171°	
	169°	Nonexposed side
	171°	

TABLE IV MOLECULAR WEIGHT OF POLYSULFONE MATRIX RESIN

Sample, Technique	M_N[a]	M_W	M_Z	M_W/M_N	Intrinsic[b] Viscosity
Resin control					
GPC	19,000	70,000	117,000	3.8	
GPC-DV	18,000	50,000	83,000	2.8	0.45
GPC-LALLS	21,000	46,000	74,000	2.2	
Static LALLS		45,900			
Langley control					
GPC	18,000	68,000	113,000	3.9	
GPC-DV	16,000	50,000	81,000	3.1	0.43
GPC-LALLS	18,000	40,000	65,000	2.1	
Flight protected					
GPC	19,000	68,000	114,000	3.7	
GPC-DV	17,000	53,000	87,000	2.9	0.40
GPC-LALLS	21,000	40,000	66,000	1.8	
Flight exposed					
GPC	18,000	68,000	114,000	3.7	
GPC-DV	17,000	48,000	80,000	2.9	0.44
GPC-LALLS	21,000	46,000	71,000	2.2	

[a] Molecular weight in g/mole
[b] Intrinsic viscosity in dL/g

TABLE V XPS RESULTS FOR SELECTED LDEF POLYMER SPECIMENS

PHOTO PEAK	A10 (BLANKET) STAINED[a]	A10 (BLANKET) UNSTAINED[a]	F2 (BLANKET)	H7 (KAPTON) EXPOSED	H7 (KAPTON) PROTECTED[b]	B9 (EPOXY COMPOSITE) EXPOSED	B9 (EPOXY COMPOSITE) PROTECTED[b,c]
C 1s B.E. (eV)[d]	284.6	284.6	290.9/289.0/284.2	284.6/288.0	284.6/288.0	284.6	284.6/288.0
A.C. (%)[e]	31.7	30.8	39.8	31.4	62.9	54.3	62.8
F 1s B.E.	689.3	689.6	686.8	--	--	--	--
A.C.	1.2	2.3	47.8	--	--	--	--
O 1s B.E.	533.0	532.8	531.0	532.5	531.8	532.8/535.0	532.5
A.C.	47.9	46.5	7.4	46.7	25.5	33.0	24.8
N 1s B.E.	--	--	--	400.1	399.9	399.9	399.7
A.C.	--	--	--	3.8	8.7	5.2	3.4
Si 2p B.E.	103.4	103.2	102.7	103.2	102.5	102.9/105.7	102.7
A.C.	19.2	20.5	1.5	17.1	2.2	7.5	3.4

[a] Visual observation.
[b] Protected from direct exposure.
[c] 2.0% F, 2.0% S, 1.7% Na also detected.
[d] Binding energy, electron volts.
[e] Atomic concentration, percent.

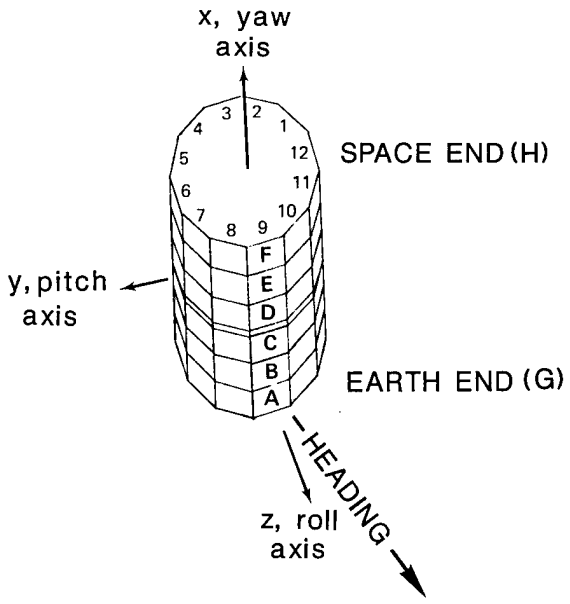


Figure 1. LDEF sketch and orbital inclination.

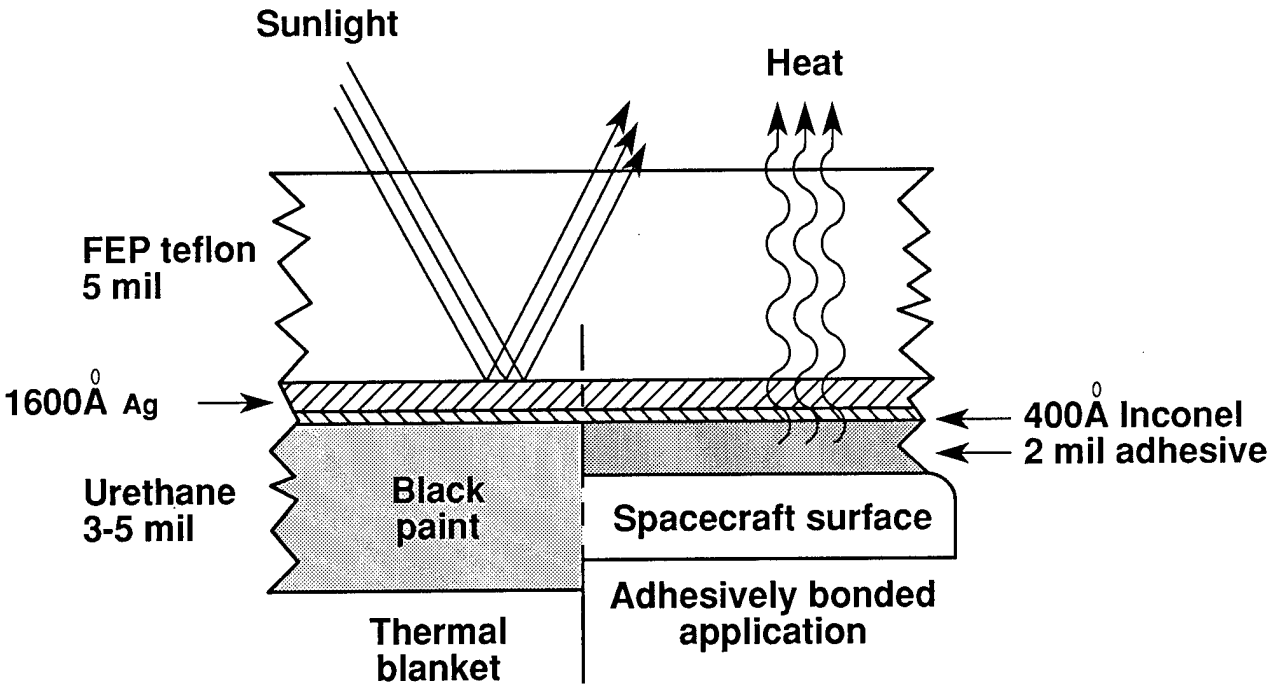


Figure 2. Flexible second-surface mirror thermal control coating in thermal blanket and adhesively bonded applications.

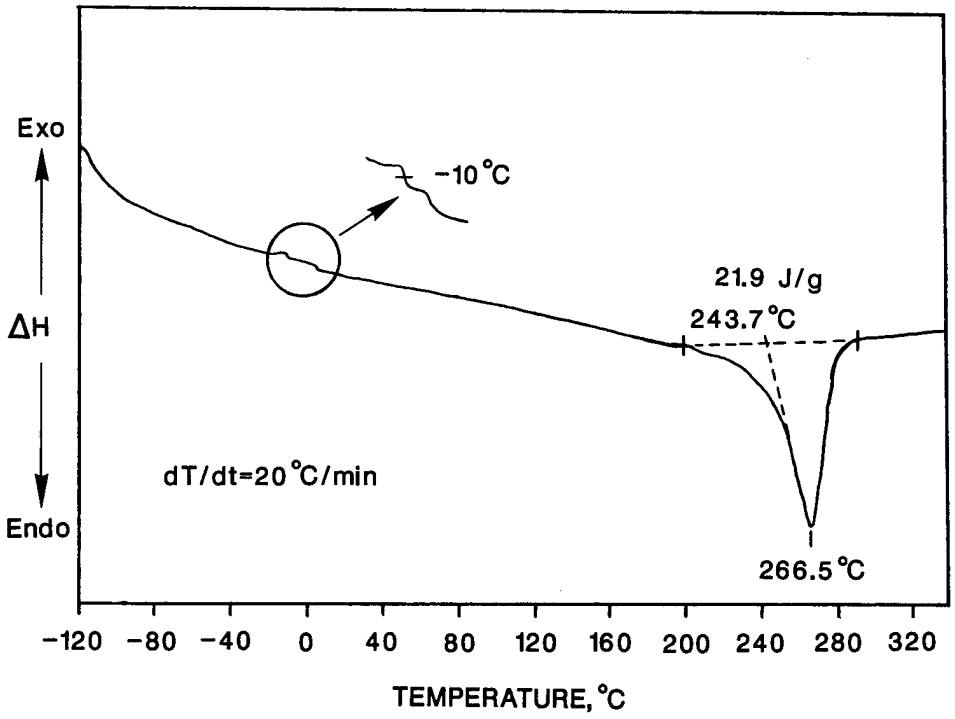


Figure 3. DSC thermogram of C5 thermal blanket specimen.

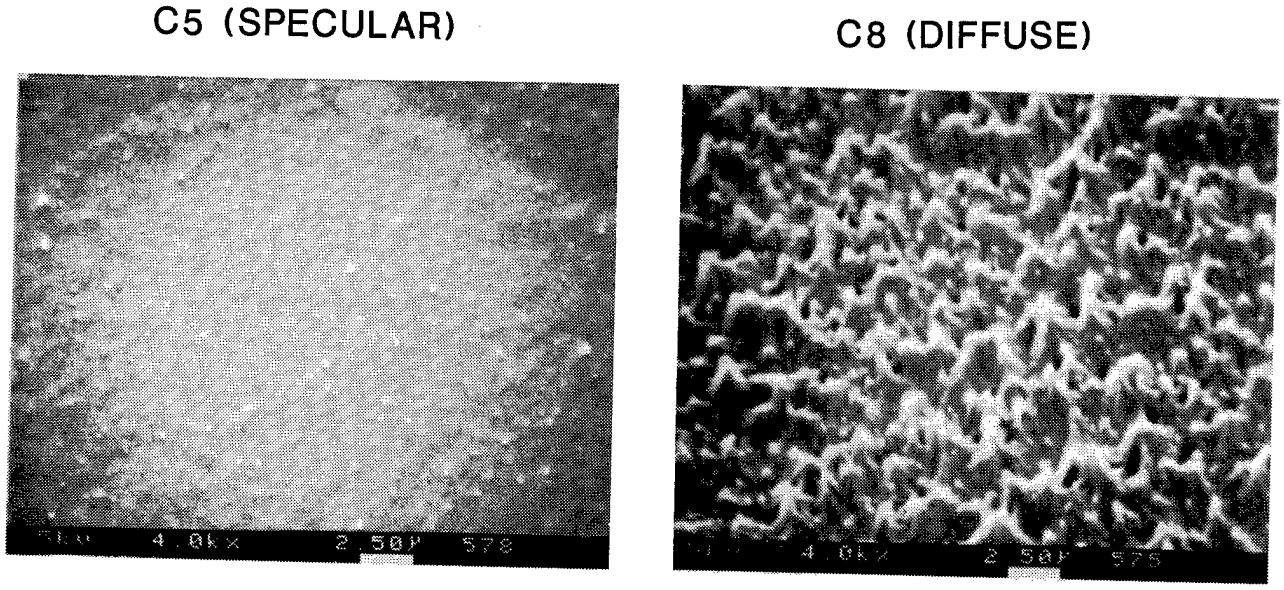


Figure 4. SEM of C5 and C8 silvered FEP teflon thermal blanket specimens (X4000).

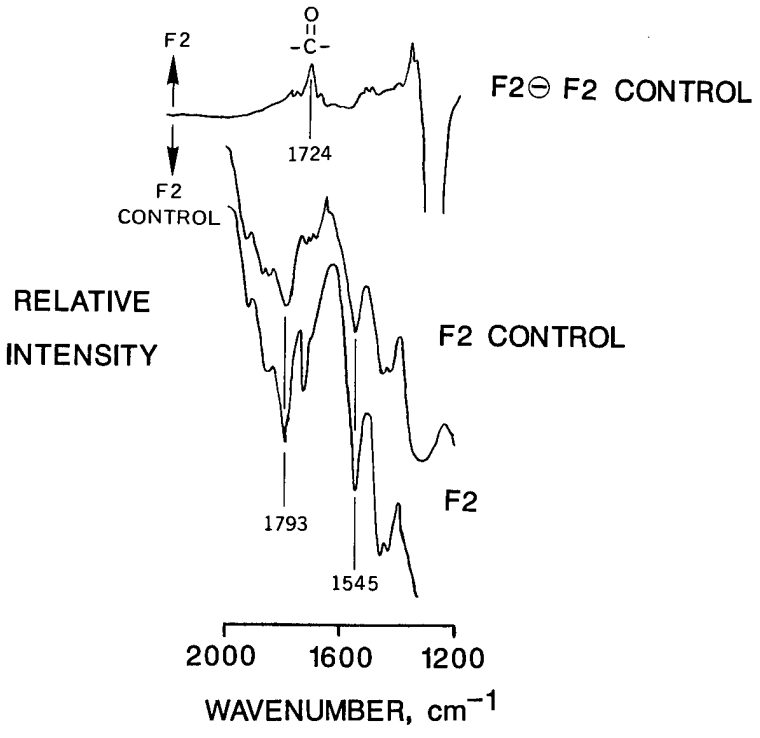


Figure 5. DR-FTIR spectra of F2 flight and control thermal blanket specimens.

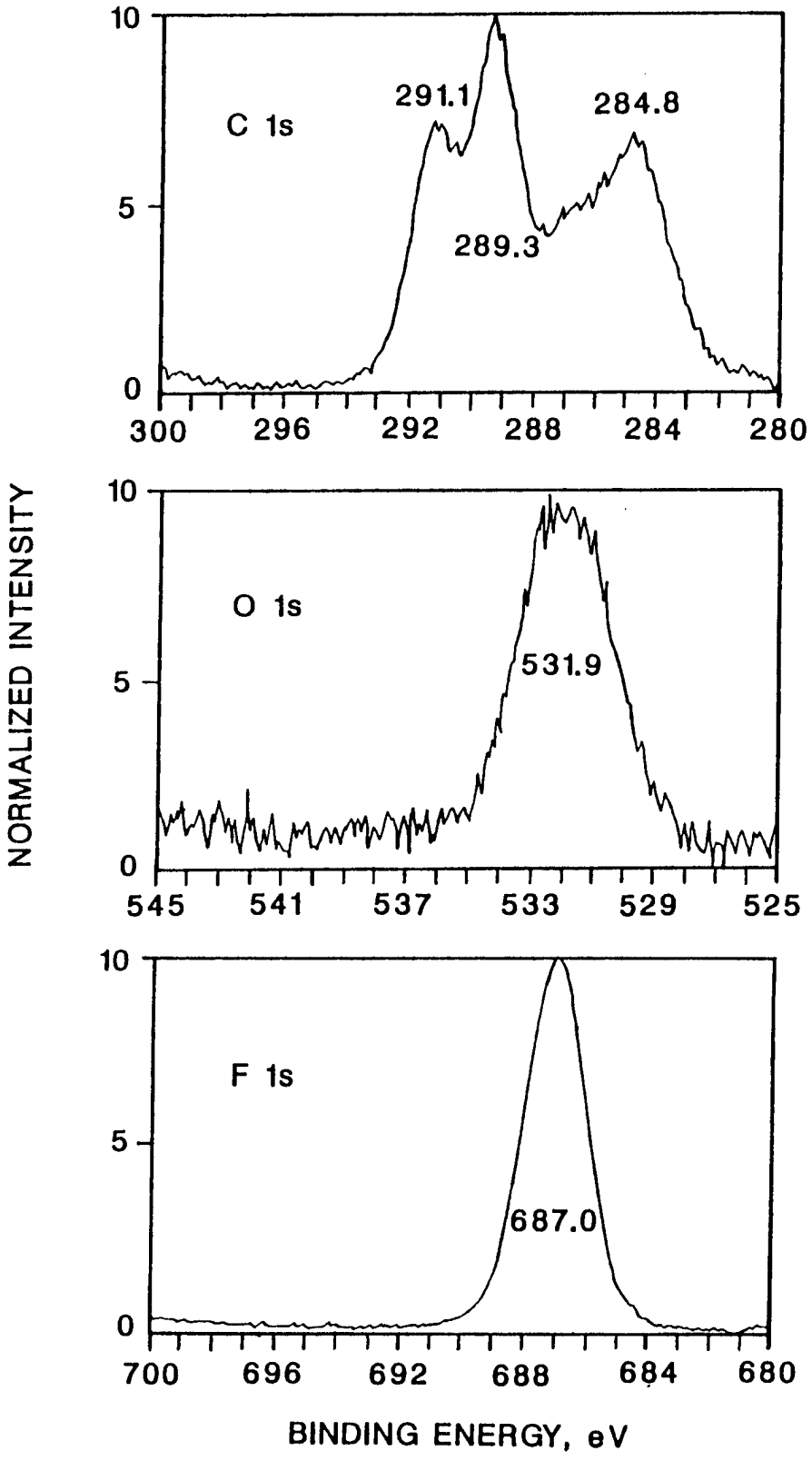


Figure 6. Narrow scan XPS spectra for C5 thermal blanket specimen.

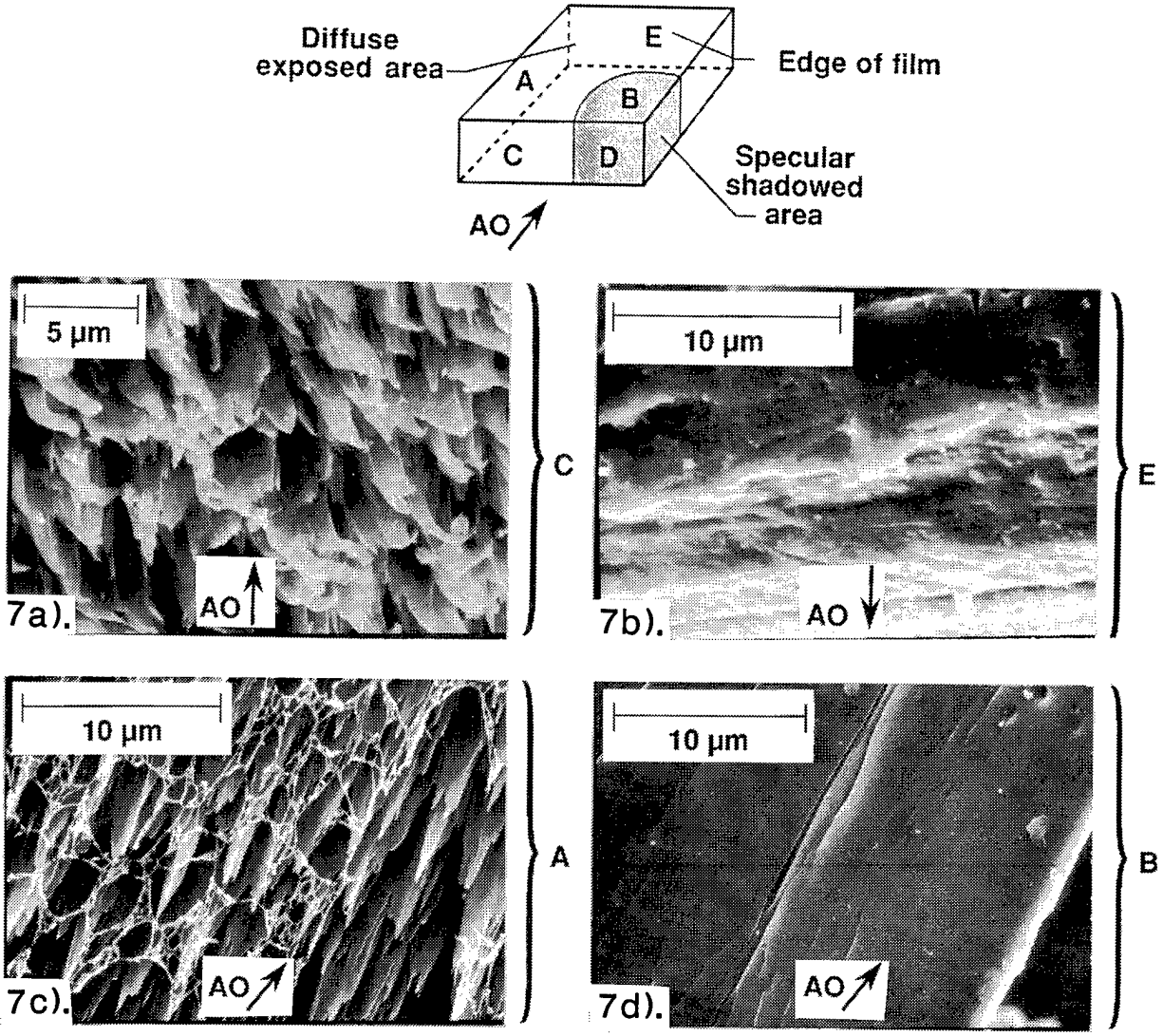


Figure 7. SEM of LDEF-exposed Kapton Film.

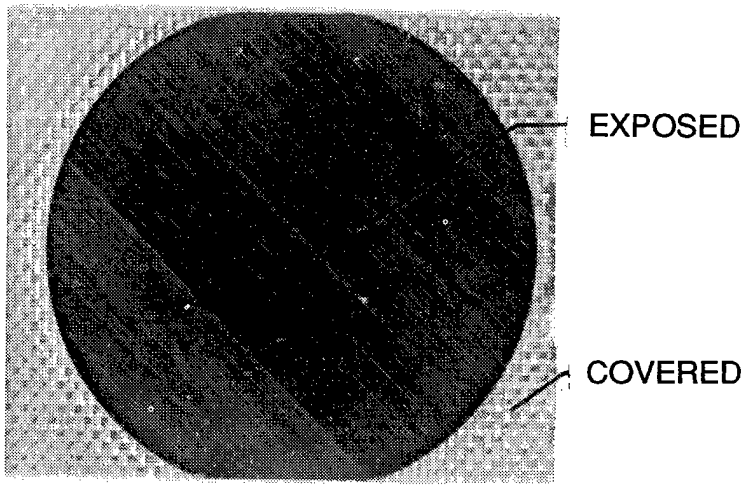


Figure 8. LDEF exposed P1700/C6000 polysulfone (± 45°)s composite.

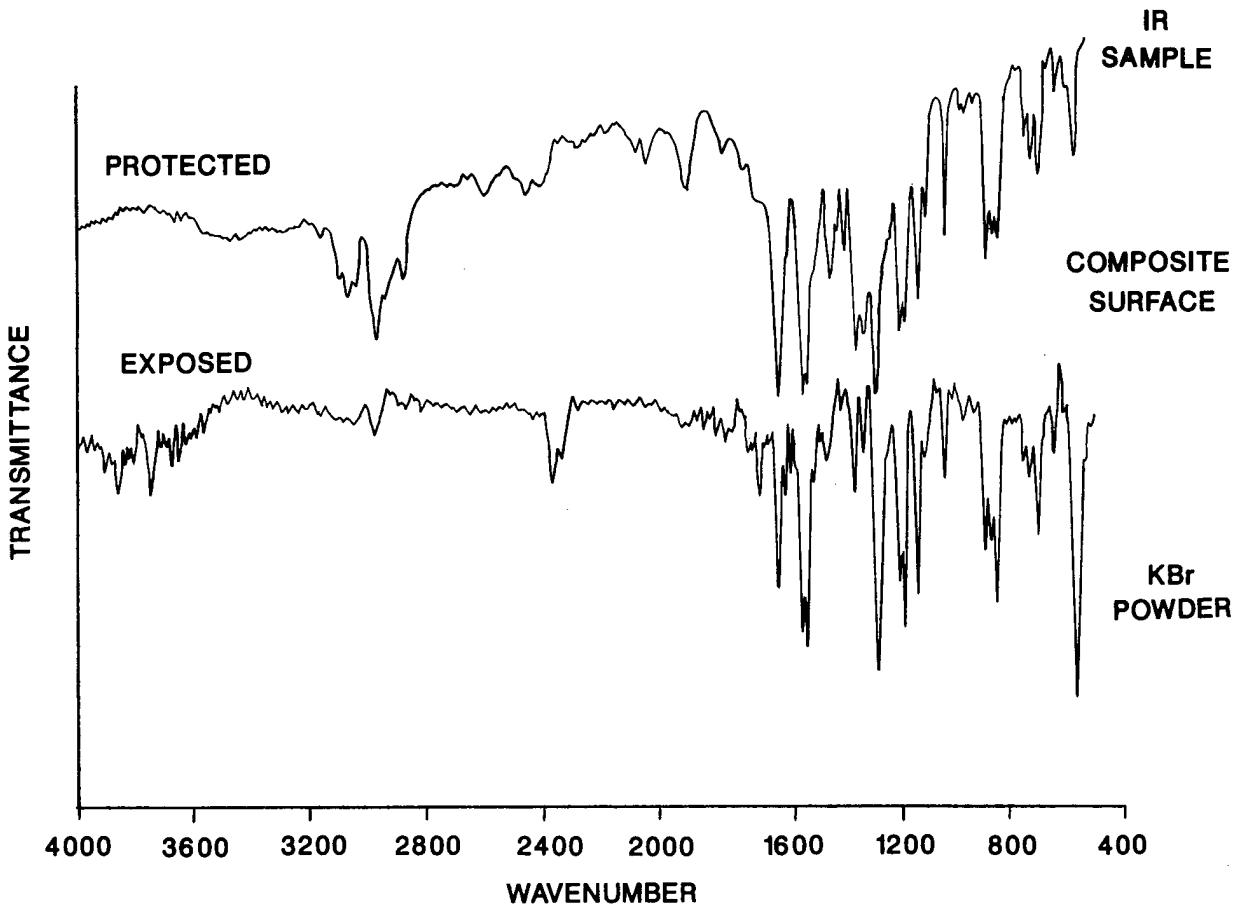


Figure 9. DR-FTIR spectra of LDEF-exposed P1700 polysulfone/C6000 composites.

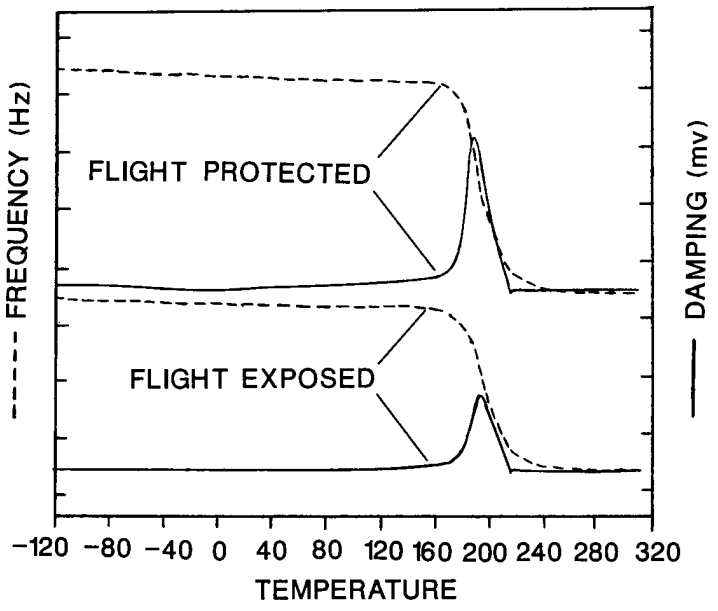


Figure 10. DMA of LDEF-exposed P1700/C6000 polysulfone composites.

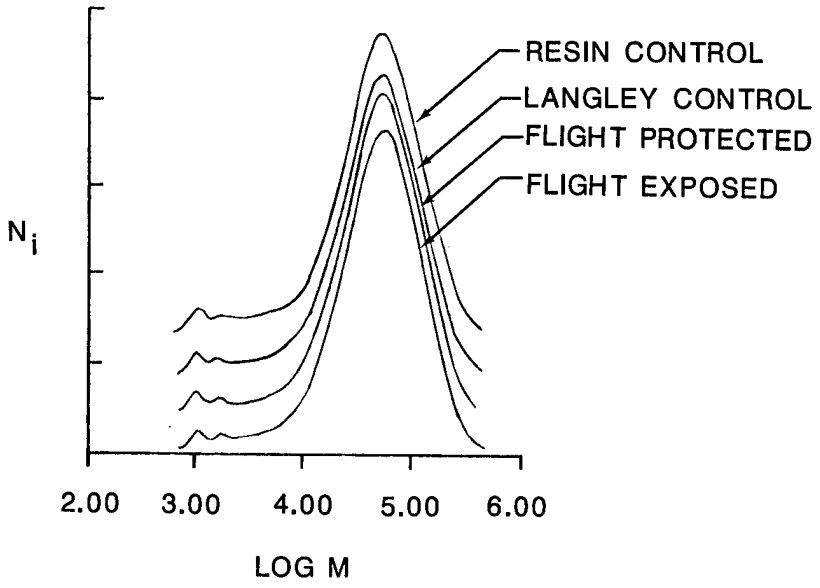
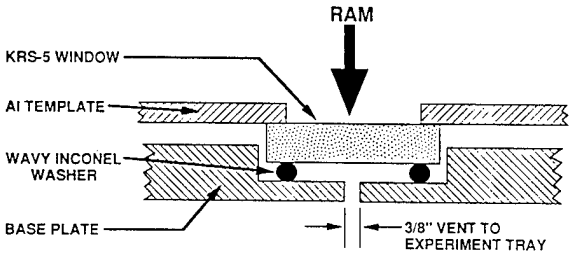


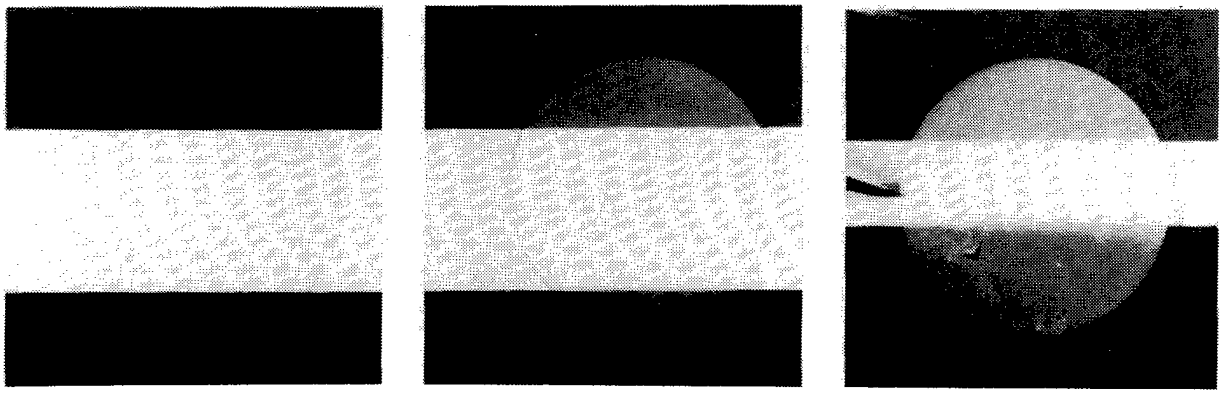
Figure 11. GPC molecular weight distribution of P1700 polysulfone composite matrix resins.



XPS RESULTS

Photo Peak	Binding Energy (eV)	Atomic Conc. (%)
DIRECT EXPOSURE		
C 1s	284.6	15.8
O 1s	529.3/532.5	54.5
Tl 4f 7, 5	118.0/122.3	9.2
I 3d 5, 3	618.7/630.2	0.5
Si 2p	102.9	20.0
NO DIRECT EXPOSURE (VENTED)		
C 1s	284.6	36.1
O 1s	529.5	36.3
Tl 4f 7, 5	118.6/123.1	23.2
I 3d 5, 3	618.7/629.5	1.1
Si 2p	101.9	3.3
CONTROL		
C 1s	284.6/286.5	42.2
O 1s	533.0	21.7
Tl 4f 7, 5	118.3/122.7	25.8
I 3d 5, 3	619.0/630.5	10.1
Si 2p	- - - -	- - -

Figure 12. LDEF-exposed KRS-5 optical window.

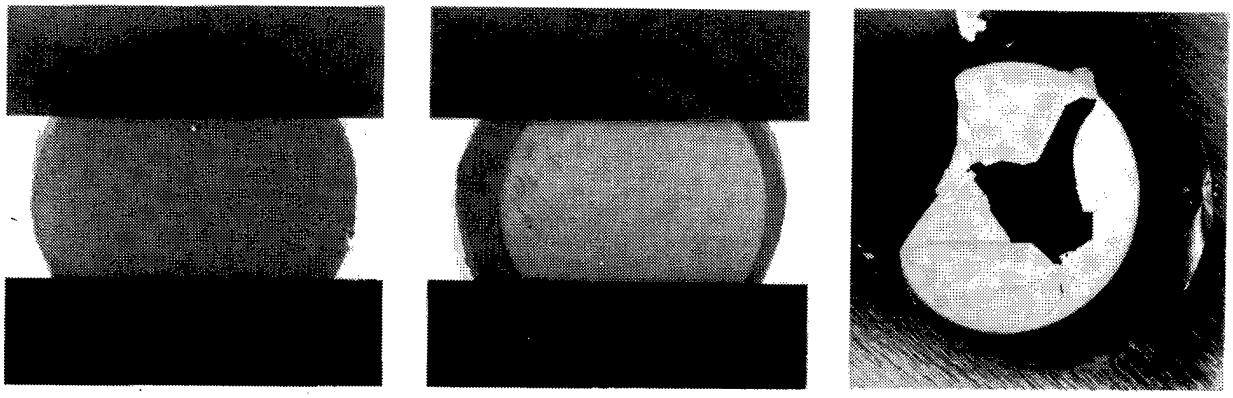


Control
1983

Flight specimen
September 1983

Flight specimen
February 1991

a). STS-8 exposed PEN-2,6 polyester film.



Control
1983

Flight specimen
September 1983

Flight specimen
February 1991

b). STS-8 exposed PMDA-DAF polyimide film.

Figure 13. Post exposure effects in two experimental polymer films.

CHARACTERIZATION OF POLYMER FILMS RETRIEVED FROM LDEF

Alan Letton
Neil I. Rock
Kevin D. Williams
Polymer Science and Engineering Program
Department of Mechanical Engineering
Texas A&M University
College Station, Texas 77843-3123

Thomas W. Strganac
Allan Farrow
Department of Aerospace Engineering
Texas A&M University
College Station, Texas 77843-3141

ABSTRACT

One of the trays aboard LDEF was an experiment having the objective of assessing the effects of long term exposure of candidate balloon films, tapes, and lines to the hostile environment of space. The fortuitous location of these materials on LDEF minimized direct impact by atomic oxygen thus providing an opportunity to study the effects of low earth orbit environments on polymeric materials without the worry of atomic oxygen abrasion. The resulting chemical, morphological and thermomechanical changes for polyethylene specimens are reviewed. In addition, preliminary data for fluorinated ethylene/propylene copolymers used for thermal blankets is presented. Polyethylene is observed to crosslink and branch from exposure to atomic oxygen and/or ultraviolet with a decrease in crystallinity.

INTRODUCTION

It has recently been observed that exposure of polymers to the low earth orbit (LEO) environment can result in significant degradation due primarily to atomic oxygen attack. LEO lies between 200 and 500 km above the earth's surface and has an atmosphere which consists predominantly of atomic oxygen (ref. 1). Spacecraft at this particular orbit travel at a rate of 8 km/s which has the effect of providing the atomic

oxygen with a translational energy of approximately 5 eV as it strikes ram facing (direction of travel) surfaces. Under these conditions many polymers are degraded with resulting mass loss.

With the increasing importance of polymers in orbiting spacecraft it has become imperative to determine how, and to what extent, the properties of polymers are affected by this type of an environment. Knowing this, polymers can subsequently be developed or selected which are suitable for LEO applications. This paper presents the results of analysis performed on thin film polymers retrieved from the Long Duration Exposure Facility (LDEF).

LDEF is essentially a free-flying cylindrical structure which was developed by NASA to accommodate 57 totally self-contained experiments on trays mounted on the exterior of the structure (ref. 2). LDEF was placed in LEO by the shuttle Challenger in April of 1984 and was expected to be retrieved after only 10 months in space for postflight investigation. However, delays resulted in the structure's late return in January of 1990 after nearly 6 years in space (ref. 3 & 4). One of the trays aboard LDEF was a Texas A&M University submittal - experiment S1006. This experiment had the objective of assessing the effects of long term exposure of candidate balloon films, tapes, and lines to the hostile environment of space (ref. 5). Included in this experiment tray were polyethylene, polyester and nylon films in addition to Kevlar fibers.

The location of these samples on the LDEF was fortuitous because they were exposed to the smallest amount of direct sunlight of any other experiment row aboard the satellite (ref. 5 & 6). Photographs of the experiment tray before exposure (Figure 1) and after exposure (Figure 2) are visual records of the effect of exposure on these materials. In addition, the samples were placed such that the normal from the surface of the samples was nearly perpendicular to the ram direction of the atomic oxygen flux, thereby limiting the atomic oxygen fluence of the specimens.

Several mechanical and analytical tests were performed on exposed polymer samples and their controls to discern relative changes in mechanical behavior and morphological and chemical properties. These tests included dynamic mechanical analysis (DMA), differential scanning calorimetry (DSC), size-exclusion chromatography (SEC), Fourier transform infrared spectroscopy (FTIR), and scanning electron microscopy (SEM). Reported here are the results for select materials described below.

EXPERIMENTAL

MATERIALS

The three LDEF materials studied were: (1) Silver-backed Teflon® - fluorinated ethylene propylene copolymer (FEP) taken from a leading edge (ram facing) thermal blanket aboard LDEF. Part of the material was protected from the environment and is used as a control. Thermal blankets for space application are a laminate of 5 mil FEP with a reflective silver coating (approximately 1000 to 2000 Å), which is vapor deposited on one surface (ref. 7). The layer of silver is then coated with a layer of black paint (Chemglaze Z306) (ref. 7). The black paint and most of the silver coating were removed with toluene before testing. The silver backing over most of the unexposed part of the material was difficult to remove and so remained. The presence of this silver was taken into account in our testing. (2) 0.35 mil thick SFX film. This is a blend of

high density polyethylene (HDPE) and linear low density polyethylene (LLDPE). (3) 1.0 mil Stratofilm® - low density polyethylene (LDPE) film. Both the SFX and the Stratofilm® were blown films taken from experiment S1006's tray. These materials are typically used in high altitude scientific balloons.

Exposure Environment, Long Duration Exposure Facility

LDEF was placed in LEO at an altitude of 476 km which, by the time LDEF was recovered, had decayed to a height of 333 km (ref. 8). Experiment S1006 was located along row 6 of LDEF. As a result of this location, the polymer samples contained within the experimental tray were exposed to a minimum level of UV radiation and a moderate atomic oxygen fluence compared to other locations aboard LDEF (ref. 9). Except for the earth-end bays, the row containing these samples was exposed to the lowest equivalent sun hours . These polymer samples received 6500 equivalent sun hours which is just under half of a maximum of 14,500 hours seen by the space end bays (ref. 9). In addition, the specimen surfaces were almost parallel to the ram direction (8° off tangent) and the specimens themselves were recessed within the tray. This limited the atomic oxygen fluence to the polyethylene films which received a total fluence of only 4.93×10^{19} atoms/cm^2 (ref. 9). The maximum atomic oxygen fluence was experienced by the leading edge surface and was 8.40×10^{21} atoms/cm^2. The minimum atomic oxygen fluence was observed on the trailing edge and was 3.34×10^3 atoms/cm^2 (ref. 9). A schematic of the tray's orientation relative to LDEF's orientation is provided in Figure 3.

Variations in temperature have been estimated for the tray containing experiment S1006. However, the temperature variations for the actual samples contained within the experimental tray have not been determined as yet. Tray temperatures varied between -21°C and 51°C for the first year in orbit and are not believed to have exceeded this range over the remaining 5 years of LEO exposure.

Test Procedures

Differential Scanning Calorimetry

Differential scanning calorimetry was performed on both exposed and control samples of LDPE and HDPE/LLDPE films using a DuPont-1090 controller with a DuPont-910 cell. These films were tested according to ASTM D-3418. The samples were heated to 190°C and held at this temperature for 10 minutes before being cooled to 30°C at a rate of 10 degrees per minute. This procedure erased any previous thermal history and provided the initial melt temperature and heat of fusion. The samples were then reheated to 190°C and held for 10 minutes before being cooled to 30°C at 10°C per minute. Crystallization and second melt temperatures were thereby determined in addition to their respective specific heats. Knowing this, differences in percent crystallinity between control and exposed polyethylene samples are found.

Size-Exclusion Chromatography

Size-exclusion chromatography was carried out using a Waters Associates 150C ALC/GPC with a Viscotek 150R differential viscometer retrofit. Orthodichlorobenzene (ODCB) at 135°C and a flow rate of 1.2 mL/min. was employed as the solvent. This particular SEC uses 250 µL injections and has a column set of 10^3, 10^4, 10^5, and 10^6 µm. Both control and exposed LDPE and HDPE/LLDPE were dissolved and tested

as a 0.125% solution (w/v). Calibration was done using NIST reference standard number 1475, which is a linear polyethylene. Apparent molecular weight distribution (MWD) and intrinsic viscosity are obtained; in addition branching frequency and actual MWD is also determined.

Viscoelastic Analysis

Viscoelastic analysis was accomplished through the use of a Rheometrics Solids Analyzer II (RSA II). Stress relaxation tests were conducted at a strain lying within the linear viscoelastic range of the respective polymer film and at a temperature beyond the glassy region in order to obtain a relatively quick and pronounced relaxation. Knowing the dimensions of each sample, the relaxation modulus was determined as a function of time. Stress relaxation tests were performed on the control and exposed films. For measurements at constant frequency, 1.6 Hz, the storage and loss tensile moduli, E' and E" respectively, were recorded at temperatures between -150°C and 100°C. The strain was selected to be in the linear viscoelastic region, determined from previous experiments in which the strain was progressively increased until the non-linear region was identified as the onset of the moduli's dependence on strain.

Scanning Electron Microscopy

A JEOL JSM-T330A was used to produce micrographs of exposed and control surfaces of the FEP, LDPE and HDPE/LLDPE films. All of the samples were coated with 250Å of gold-palladium and scanned with an accelerating voltage of 20 kV.

Fourier Transform Infrared Spectroscopy

FTIR spectra of all the thin film polymer samples were collected using direct transmission and attenuated total reflectance (ATR) configurations. A Nicolet 520 was used for the direct transmission spectra and a Nicolet 60SXB was used for the ATR spectra. Peak deconvolution and reconstruction software (FOCAS) was supplied by Nicolet to determine peak areas and to improve peak resolution.

RESULTS AND DISCUSSION

Low Density Polyethylene

Figure 4 shows a typical DSC heating curve for the control LDPE. Initial and second melt temperatures are close to the second melt occurring at 107.3°C and with an endothermic transition of 106 J/g. On cooling, recrystallization occurs at 94.7°C with an exothermic heat of 111.0 J/g associated with crystallization.

The melting temperatures for the exposed LDPE are considerably depressed when compared to the control LDPE as shown in Figure 5. The initial and second melt temperatures are 99.3°C and 98.1°C, respectively. Since melting temperature is consistent after repeated heatings, this implies that there has been a permanent change in the molecular structure of the polymer after exposure aboard LDEF. The corresponding heats of fusion for the exposed polyethylene have also decreased indicating a reduction in crystallinity and a possible decrease in lamella size. Recrystallization of the exposed LDPE occurred at 86.5°C with a endothermic enthalpy of 58.4 J/g. The enthalpy associated with the second melt was 64.4 J/g.

If the measured heat of fusion ΔH_f^* of a particular polyethylene and the heat of fusion ΔH_f of an equivalent mass of perfectly-crystalline polyethylene are known, the percentage crystallinity χ can be found from the equation:

$$\chi = (\Delta H_f^* / \Delta H_f)\, 100 \qquad (1)$$

The heat of fusion of crystalline dotriacontane has been used as the true specific heat of fusion for a completely-crystalline polyethylene (ref. 10). Using this value for ΔH_f, the percent crystallinity for control LDPE was found to be 39% while that of the exposed was 23.8%. This represents a 39% reduction in crystallinity as a result of exposure to LEO. The depression of the melting point as well as the decrease in crystallinity suggest that branching has occurred. For this reason, SEC measurements were used to determine branching frequency.

The branching frequency, λ is defined as the number of branched units in a molecule divided by the molecular weight, M (ref. 11). Branching frequency was determined by application of the theory of Zimm and Stockmayer (ref. 12). This theory relates a particular branching index *g*, to the product of λ and M. λ is first assumed to be constant and the universal calibration in the SEC is used to convert the chromatogram into an ηM (η is the intrinsic viscosity) distribution. By assuming an initial value for λ, a series of M values are converted into corresponding values of λM from which *g*, η and ηM values are determined. The calculated value of η is compared with that determined experimentally by the in-line viscometer. By an iterative procedure, the originally chosen value of λ is adjusted so that the calculated value of η is equal to that experimentally determined within the margin of accuracy desired. Both λ and the actual molecular weight distribution are then known.

Although not usually very dependent on M, Figure 6 does show an increase in λ with M for the control LDPE. Figure 7 is a presentation of the MWD for both the control LDPE and the soluble portion of the exposed LDPE. Only 8% (by weight) of the exposed LDPE could be dissolved. This in itself, is a clear indication that crosslinking has occurred. The longer, higher molecular weight molecules have crosslinked to form an insoluble gel leaving only the low molecular weight molecules.

Figure 8 is a Mark-Houwink plot of both control and exposed LDPE and HDPE/LLDPE in addition to a linear reference material. This plot is derived from the Mark-Houwink equation given as $\eta = kM^a$ where k and a are constants for a linear polymer. For a given molecular weight M, a polymer is said to be branched if its intrinsic viscosity, η is less than that of the linear reference. From the figure, it is apparent that both the control and the soluble portion of the exposed LDPE exhibit branching. Below a molecular weight of 10^4, the exposed LDPE shows a higher degree of branching than the control. However, above this molecular weight, the intrinsic viscosity becomes independent of the molecular weight and the polyethylene appears to gel. At low molecular weights, some polymers in Figure 8 appear to have a higher intrinsic viscosity for a given molecular weight than the reference material. This may be due to errors associated with short chain branching at the lower molecular weights (ref. 11).

Gel formation and branching resulting from exposure to LEO is further supported by the viscoelastic data and by the FTIR results. FTIR results for two regions of interest are presented in Figures 9 & 10. The data presented are associated with the 1470 cm^{-1} doublet and the 730-720 cm^{-1} doublet. The 730-720 cm^{-1} doublet is associated with two chain structures. The 720 cm^{-1} is accepted as representing vibrations associated

with aliphatic hydrocarbons of the type $(CH_2)_{n>4}$ while the 730 cm^{-1} absorption band is associated with methylene structures. The relative change in peak absorbance suggests the presence of branches and/or crosslinks in the structure. These same results are evident in the 1472/1463 cm^{-1} doublet presented in Figure 10. The change in relative peak heights suggests the presence of branches and/or crosslinks.

The changes reported in structure and crystallinity have a surprisingly small effect on the mechanical properties of the polymer. In Figure 11, the dynamic moduli, E' and E" , are presented for the exposed and control specimens. Below -25°C, the polymer is in its glassy region where localized motions dominate. It is expected that crosslinking and branching would have little effect on properties as is illustrated. Above this temperature one would expect to see an increase in modulus associated with increased crosslinking. Branching would be expected to have little effect on the storage modulus but may increase the loss modulus because of the increased number of relaxations. The data presented in Figure 11 suggests both crosslinking and branching. The crosslinking is evident in the increase in the storage modulus at the high temperatures. Branching is also evident by the slight increase in the loss modulus for the same region. In general however, the changes observed are small, suggesting that the distribution and size of crystalline structures may be more important than molecular properties. This hypothesis will be investigated using light scattering and x-ray scattering analysis. Stress relaxation data further supports this hypothesis (Figure 12). At -120°C and at 50°C the exposed relaxation modulus is higher than for the control suggesting a crosslinking mechanism. The fact that the relaxation curves parallel each other indicates no change in the relaxation mechanisms. At 0°C the modulus of the control is higher than that of the exposed. This is in the glassy transition region and results from the difference in the glass transition profiles.

HDPE / LLDPE BLEND

Initial and second melt temperatures for control HDPE/LLDPE are shown in Figure 13 to be similar; melting occurs at 125°C with an endothermic heat of 117.8 J/g. Recrystallization occurs after cooling at a temperature of 113.6°C with an exothermic heat of crystallization of 133 J/g. The heating thermogram in Figure 14 indicates a significant depression in the melting point temperature of the HDPE/LLDPE blend after exposure aboard LDEF. There is also essentially no change in the melting point temperature of the exposed HDPE/LLDPE after reheating with the second melt occurring at 101.5°C and an endothermic heat of fusion of 44.2 J/g. From equation (1), the percent crystallinity of the control HDPE/LLDPE was found to be 46.2%. After exposure, the crystallinity decreased by 64.7% to 16.3% which is less than the corresponding value for the exposed LDPE.

As with the LDPE, only a portion of the exposed HDPE/LLDPE was soluble in ODCB. This is indicative of crosslinking. The Mark-Houwink plot of the control and soluble portion of the exposed HDPE/LLDPE is illustrated in Figure 8. The intrinsic viscosity of the control polyethylene varies little with molecular weight while that of the exposed appears independent of molecular weight. This suggests a high degree of branching in the unexposed polyethylene blend and even more branching in the exposed as it seems to have gelled.

Micrographs of the films' surface aid in determining the effect of exposure on morphology and physical properties. Figure 15a is a SEM micrograph of the semi-crystalline surface of the control HDPE/LLDPE. Notable is the presence of lamella. Figure 15b is a micrograph of the polyethylene after exposure aboard LDEF. Figures 15b does not show the typically reported 'rug like' surface of a polymer directly exposed to

atomic oxygen but instead shows a number of microscopic spheres on the surface of the sample. These spheres are formed by the solidification of molten polyethylene under microgravity conditions. It is likely that melting occurred on the polyethylene surface as a result of thermal cycling and UV energy dissipated as heat. This hypothesis is being evaluated through thermal models.

The shape of the spheres can be explained by the fact that as gravitational forces are reduced, surface tension is more dominant in driving the element of polymer (in the melt form) to a low energy geometry. As a result, the resolidified polymer is spherical in shape rather than flat and oblong as is the case on earth. These figures provide evidence that atomic oxygen attack was not significant at the polyethylene surface. These spheres would have been quickly removed if direct exposure to atomic oxygen had occurred. FTIR data for the HDPE/LDPE blends is presented in Figures 16 and 17. As before, the 730-720 cm^{-1} doublet and the 1464 cm^{-1} doublet are used to support the existence of crosslinking. The changes observed are interpreted in the same fashion as for the LDPE film.

FEP Copolymer

Figure 18 is a SEM micrograph of the control FEP copolymer taken from a leading edge thermal blanket. Both the control and exposed FEP samples were taken from the same strip of material. The control was taken from that portion of the material protected from direct exposure to UV radiation and atomic oxygen.

The surface of the exposed FEP is shown in Figure 19. The surface appears to have been significantly roughened with sharp peaks angled towards the direction of atomic oxygen flow. These micrographs suggest that atomic oxygen and VUV radiation, acting in concert, degrade FEP and that the atomic oxygen flux is highly directional in its erosion of the surface. This is in agreement with observations made by Stiegman et al. (ref. 7), not only for FEP samples exposed aboard LDEF, but also for FEP samples taken from a hyperthermal atomic oxygen simulator. Preliminary FTIR data (not presented here) suggest little change to the chemistry of the polymer in terms of branching or crosslinking. This does not imply that atomic oxygen induced degradation has not occurred.

CONCLUSION

The fortunate location of the Texas A & M experiment tray provided the rare opportunity to observe well document materials, polyethylene in this case, after long exposure to atomic oxygen in particular and LEO environments in general. The results provide insight into the nature of changes observed for polymeric materials not directly exposed to atomic oxygen. The observed reduction in cyrstallinity and the increased branching and crosslink frequency suggests that the chemical changes took place simultaneous to thermal cycling. This behavior is observed in the SEM micrographs for the exposed and control PE blend. The exposed specimens show crystalline lamella in the process of melting. For the specimen presented, the kinetics of melting seem to be of the same order of magnitude as the crosslinking process. If crosslinking had occurred first, the spherical domains would not form.

Not only did the crystallinity decrease, but the melt temperature decreased as well with a concurrent

increase in crosslinking and branching. The notably insoluble portion of specimens resulting from SEC measurements is an indicator of the large amount of crosslinking present. This could not be surmised from the FTIR or DMA data alone. The mechanical properties measured by dynamic mechanical analysis suggest that for the specimens analyzed, the crystalline nature of the polymer contributes significantly to the overall mechanical properties.

ACKNOWLEDGMENTS

The authors are indebted to Mr. Bruce Foster and colleagues at Texas Eastman Company in Longview, Texas for their invaluable assistance and use of their polymer laboratory. In addition, Rheometrics, Inc. is thanked for their continued support. The use of the JEOL JSM-T330A scanning electron microscope at the Electron Microscopy Center here at Texas A&M University is also cited.

REFERENCES

1. Dauphin, J., in " Looking Ahead for Materials and Processes" , (Eds. de Bossu, J., Briens, G., and Lissac, P.), Elsevier Science Publishers B. V., Amsterdam, 1987, p. 345
2. Clark, L. G., Kinard, W. H., Carter, D. L., and Jones, J. L., Eds., " The Long Duration Exposure Facility (LDEF). Mission 1 Experiments" , NASA SP-473, 1984, p.1
3. Seltzer, R., Chemical Engineering & News, January 8, 1990, p. 5
4. Kolcum, E. H., Aviation Week & Space Technology, February 26, 1990, p. 23
5. Allen, D. H. in " The Long Duration Exposure Facility (LDEF). Mission 1 Experiments" , (Eds. Clark, L. G., Kinard, W. H., Carter, D. L., and Jones, J. L.), NASA SP-473, 1984, p. 49
6. Allen, D. H. in ' The Long Duration Exposure Facility (LDEF). Mission 1 Experiments' (Eds. L.G. Clark, W. H. Kinard, D. L. Carter and J.L. Jones), NASA SP-473, 1984, p.49
7. Stiegman, A. E., Brinza, D. E., Anderson, M. S., Minton, T. K., Laue, E. G., Liang, R. H., " An Investigation of the Degradation of Fluorinated Ethylene Propylene (FEP) Copolymer Thermal Blanketing Materials Aboard LDEF and in the Laboratory" , JPL Publication 91-10, May 15, 1991
8. Kinard, W. H., O'Neal, R. L., " Long Duration Exposure Facility (LDEF) Results" , AIAA 29th Aerospace Sciences Meeting, January, 1991
9. " LDEF Spaceflight Environmental Effects Newsletter" , vol. 2, no. 3, June 15, 1991
10. Bacon, K., " Characterization of Polyolefins by Differential Thermal Analysis" , Journal of Polymer Science, 1960, vol. 42, p. 15
11. Scholte, T.G., in "Developments in Polymer Characterization - 4", Dawkins, J.V., Ed., 1983, Applied Science Publishers, London and New York.
12. Zimm, B.H. and Stockmayer, W.H., Journal of Chemical Physics, 1989, vol. 17, p.1301

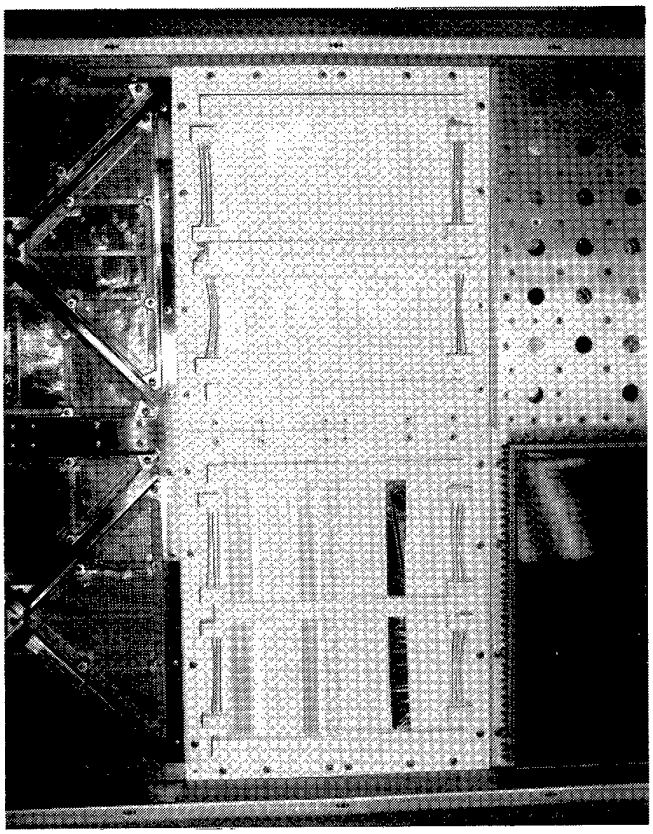


Figure 1, Experiment tray before exposure.

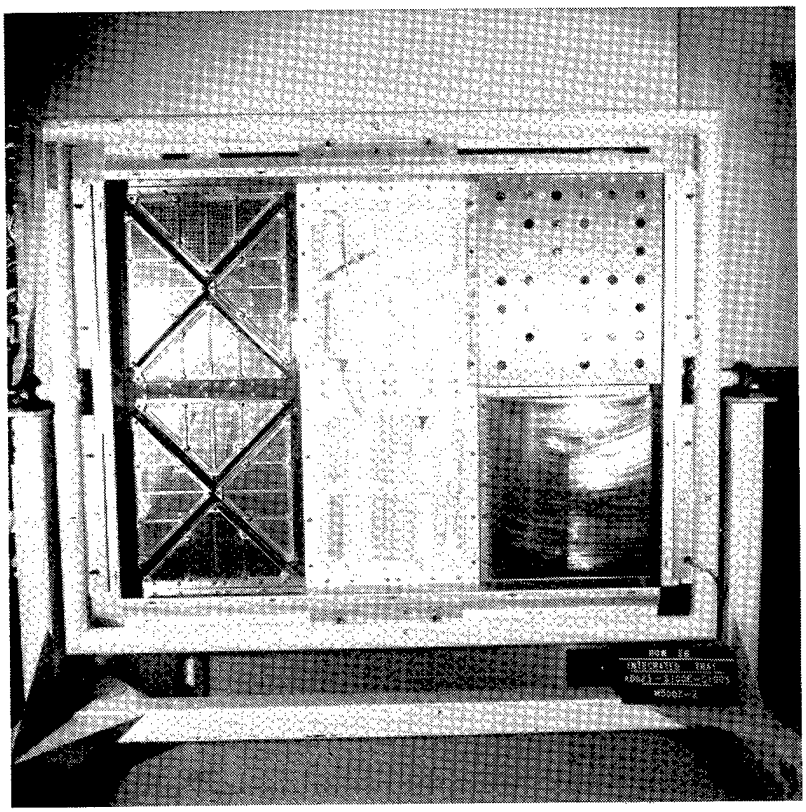


Figure 2, Experiment tray after exposure.

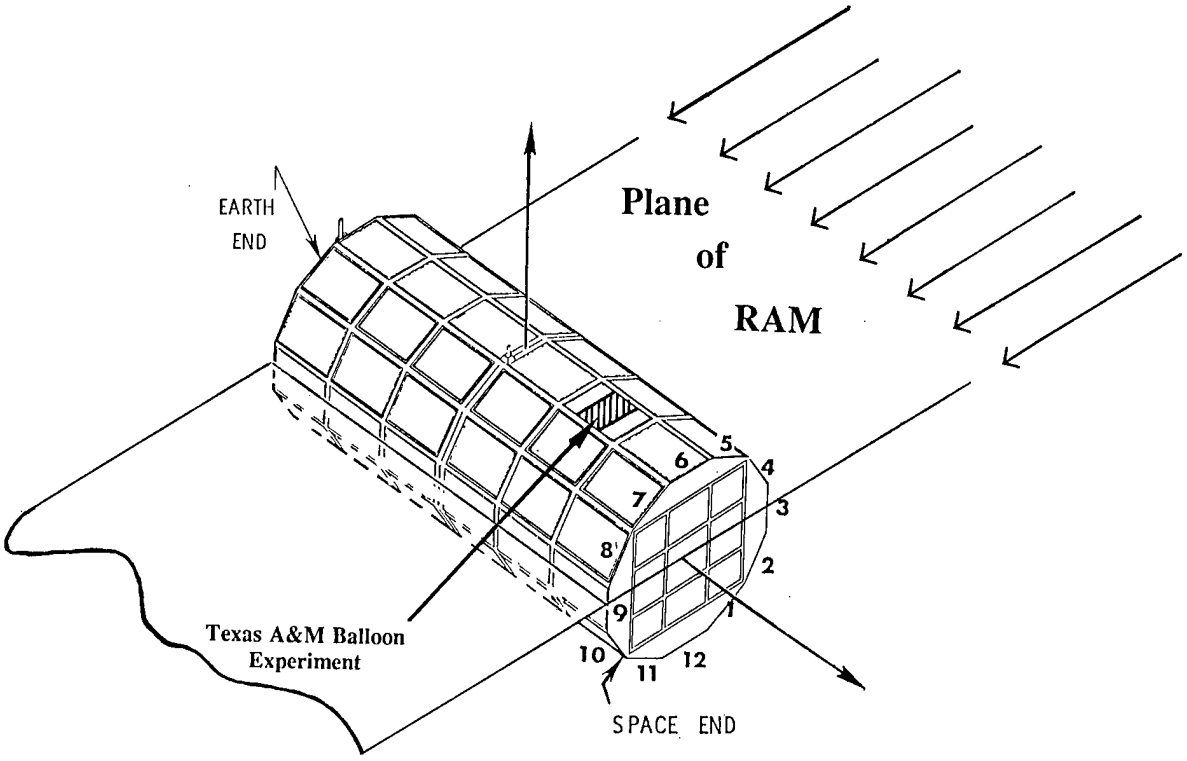


Figure 3, Orientation of the Texas A & M University film experiment.

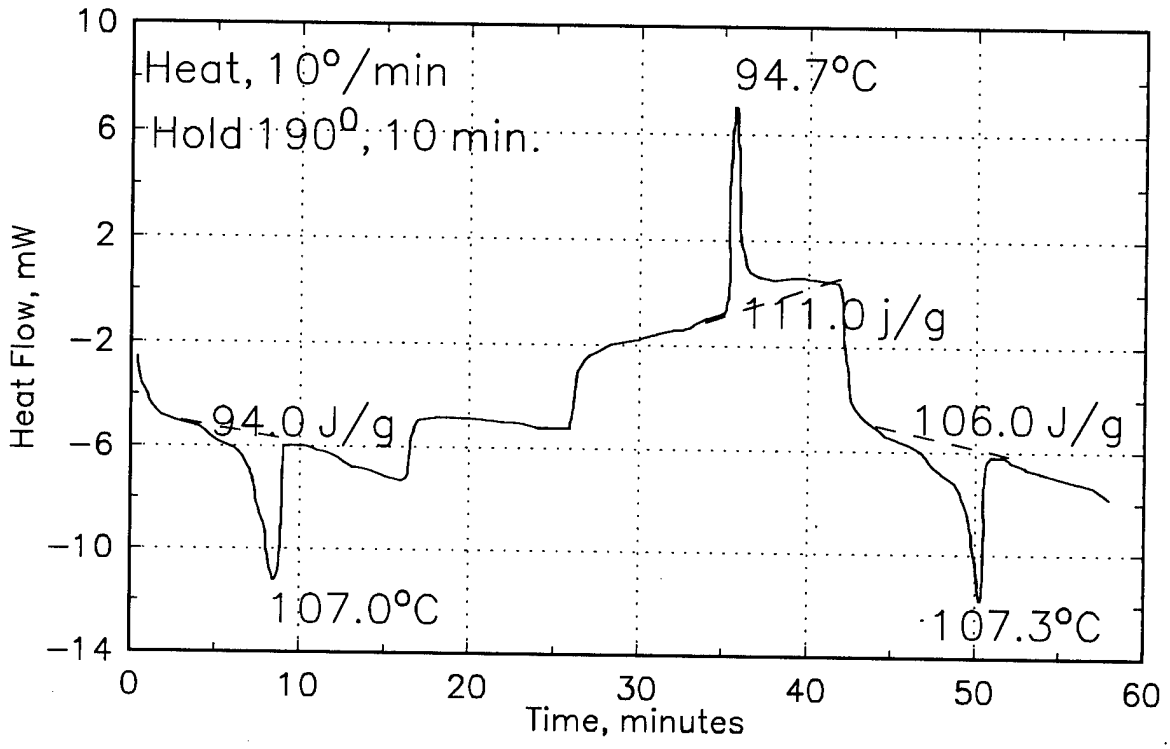


Figure 4, Typical DSC thermogram for the control LDPE. Shown here is a heating, cooling and second heating cycle.

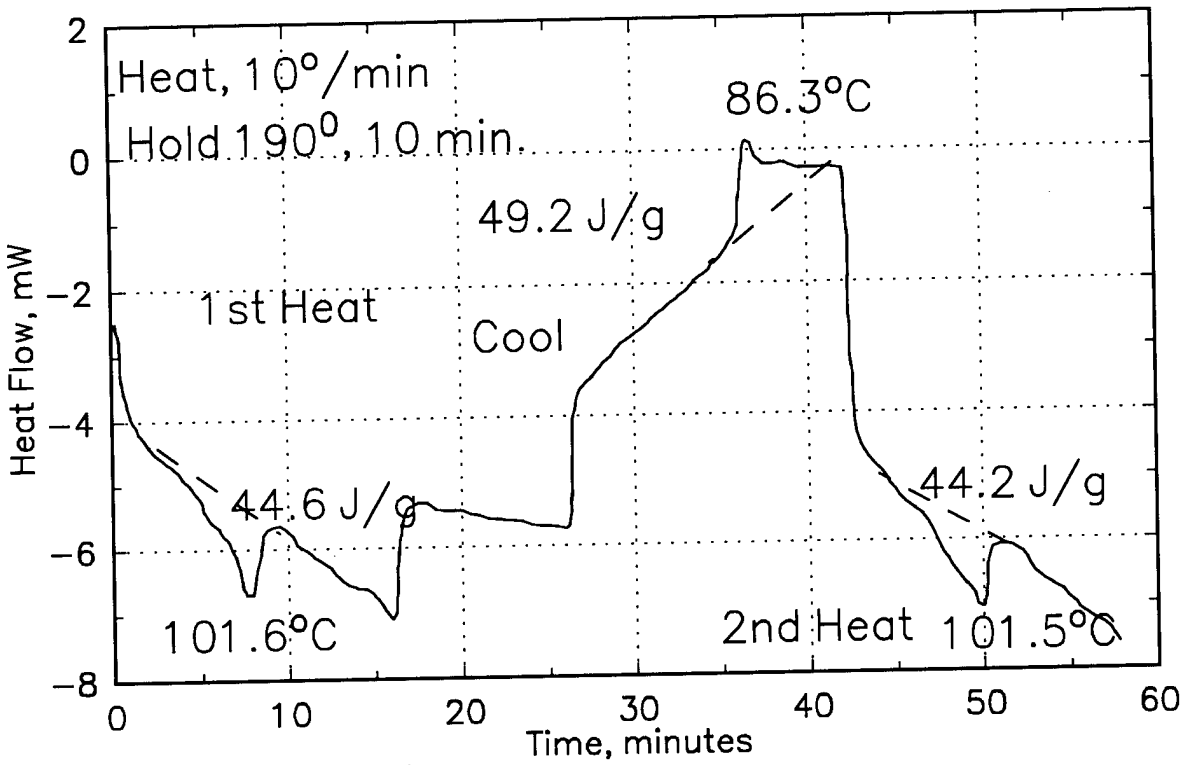


Figure 5, Typical DSC heating profile for an exposed LDPE. Details are provided in the text.

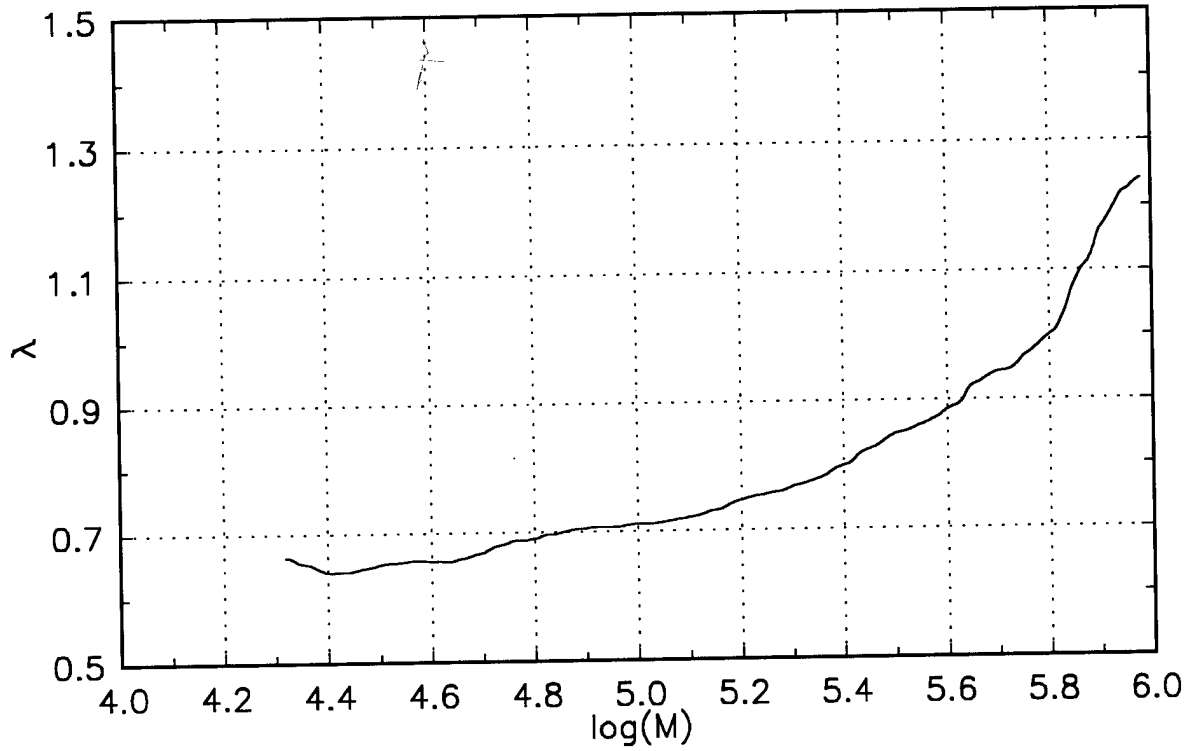


Figure 6, The dependence of branching frequency on molecular weight for the control LDPE.

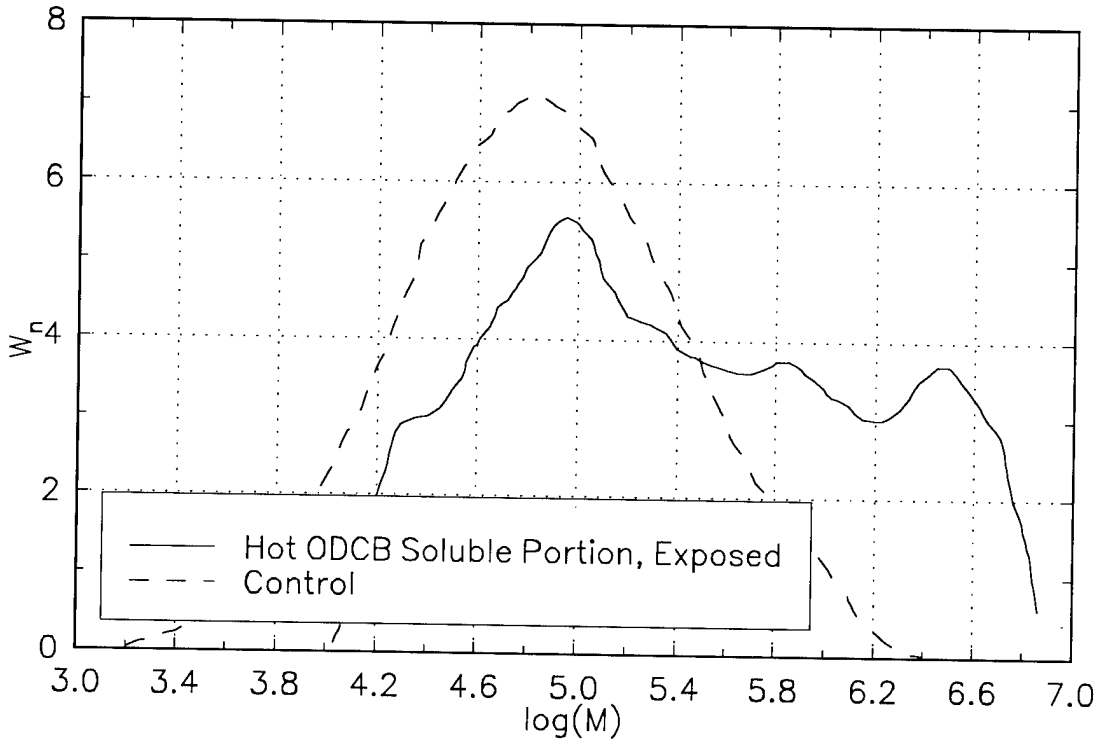


Figure 7, Molecular weight distribution for the control LDPE and the soluble portion of the exposed LDPE.

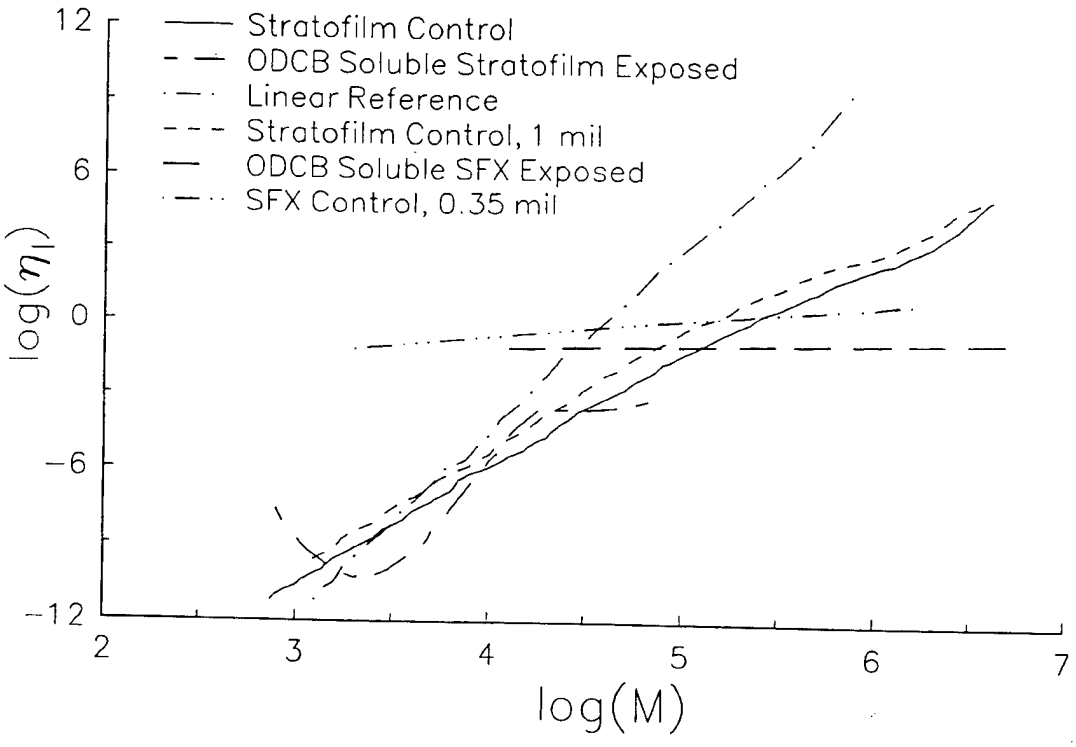


Figure 8, Mark-Houwink plot of both control and exposed LDPE and HDPE/ LLDPE films.



Figure 9, FTIR spectra for exposed (top) and control (bottom) LDPE specimen, 730 & 720 cm^{-1} absorbtion band.

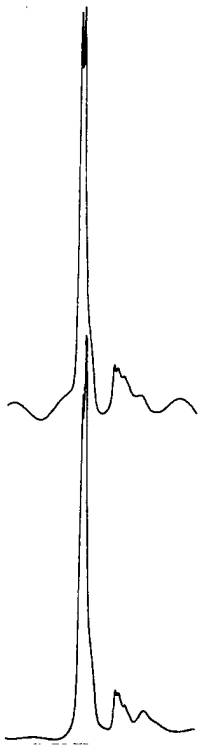


Figure 10, FTIR spectra for exposed (top) and control (bottom) LDPE specimen, 1470 cm^{-1} doublet.

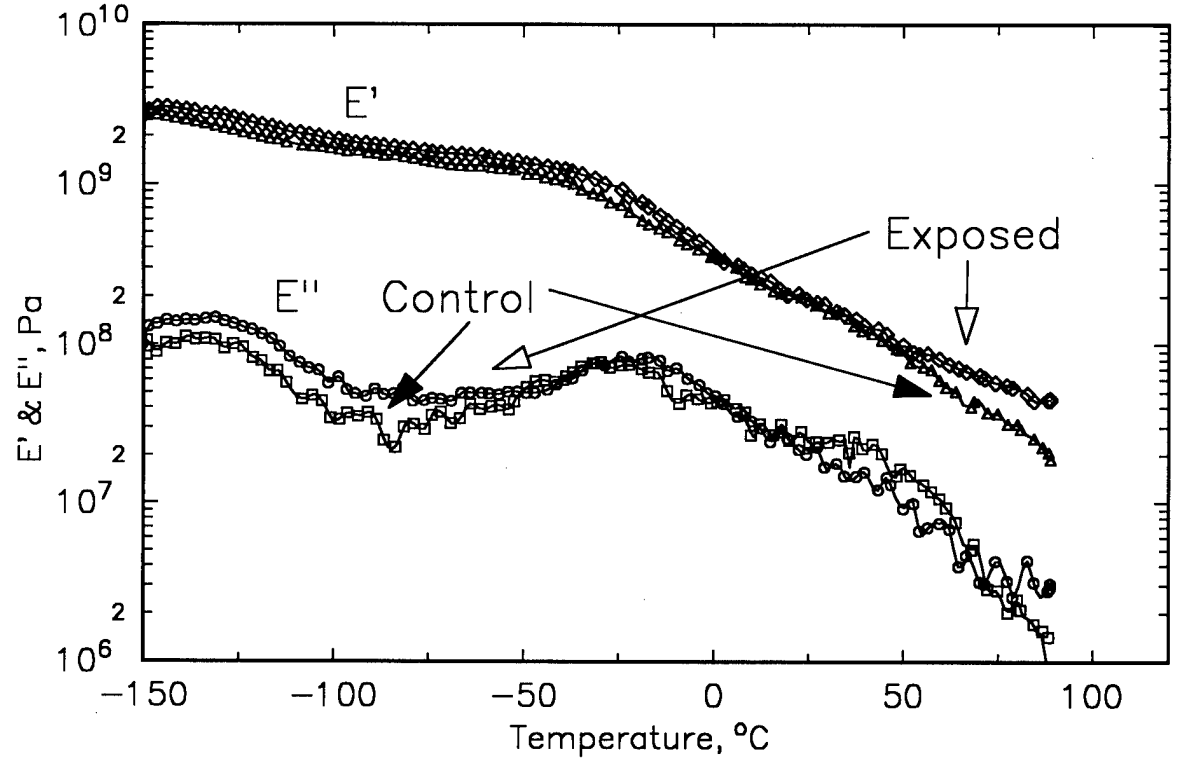


Figure 11, DMA temperature ramp, 1.6Hz frequency, for exposed and control LDPE.

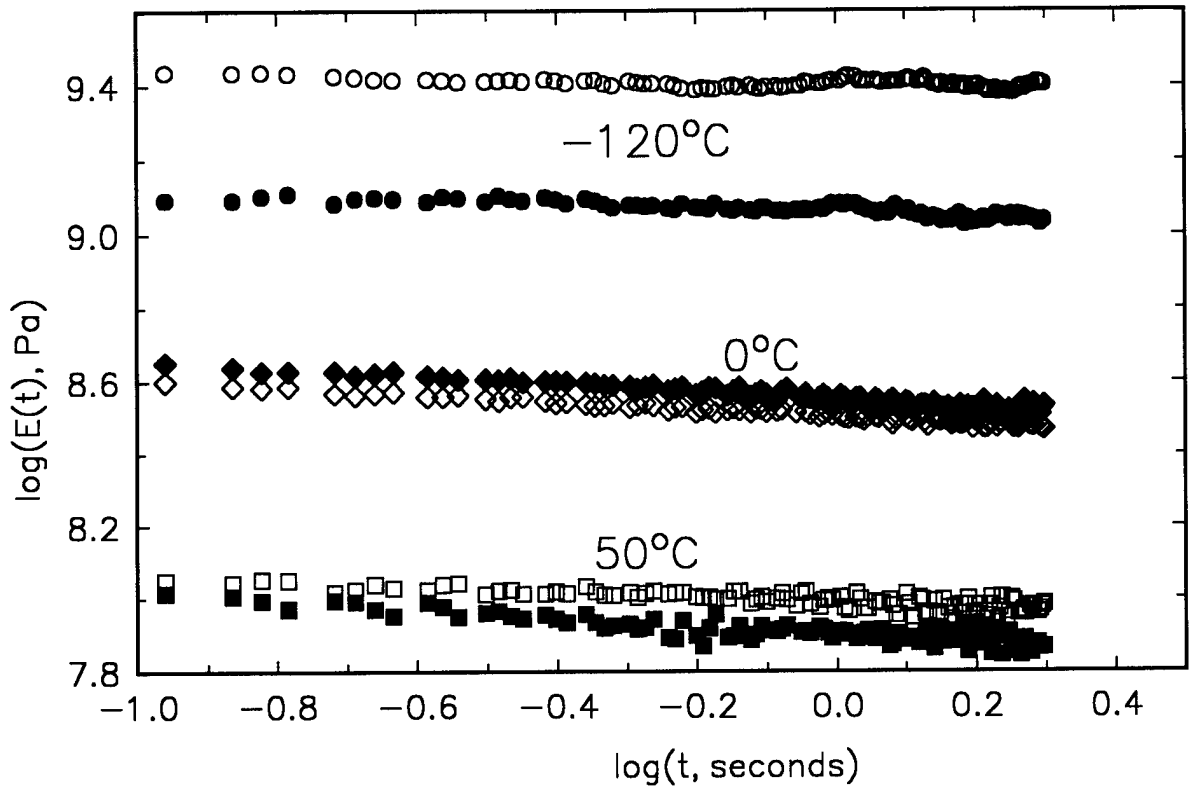


Figure 12, Stress relaxation modulus for LDPE at three temperatures.

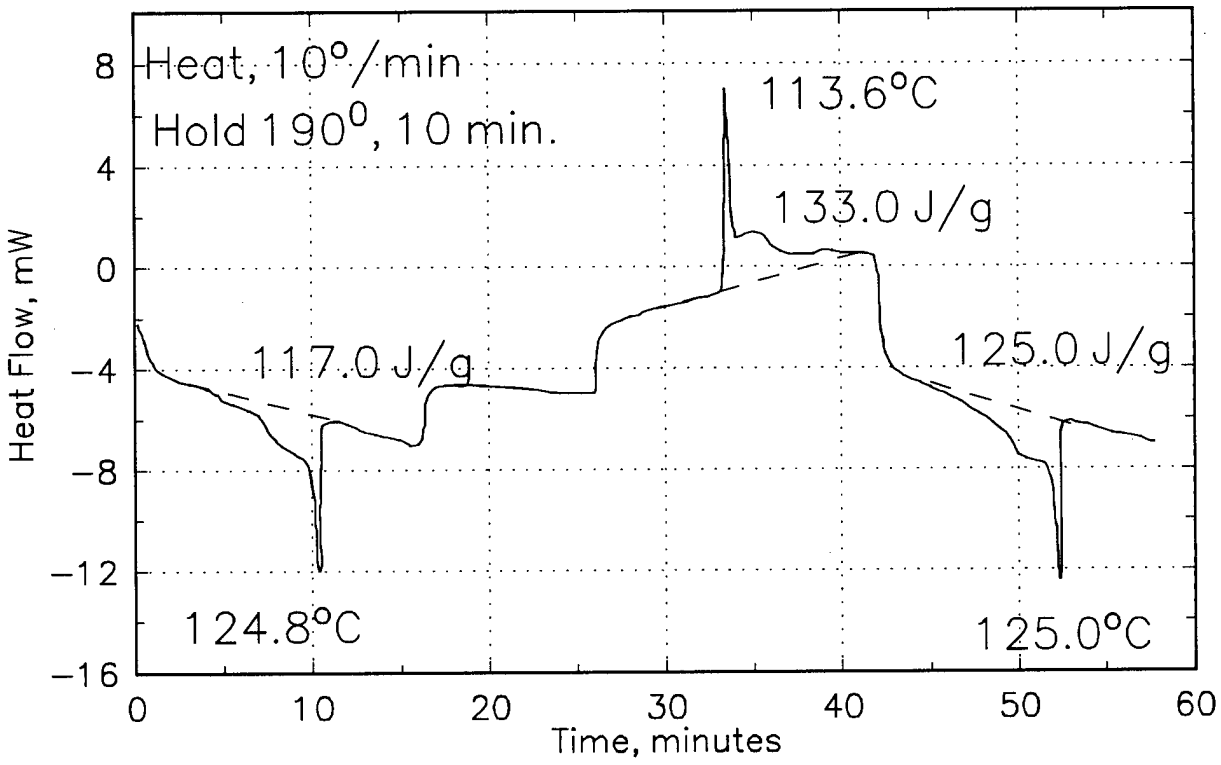


Figure 13, Typical DSC thermogram for control HDPE/LLDPE. Details of heating and cooling cycles are discussed in the text.

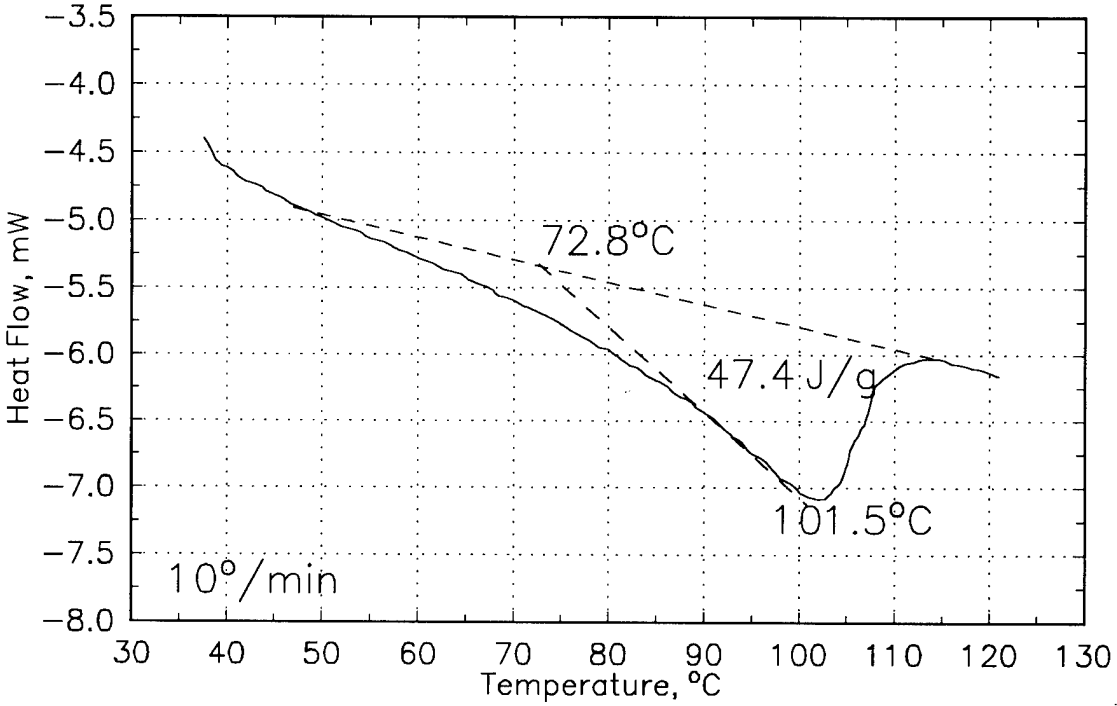


Figure 14, Typical DSC thermogram for exposed HDPE/LLDPE. Data taken from the second heat of the exposed specimen.



Figure 15a, SEM micrograph of the control HDPE/LLDPE surface. Micrograph was recorded with a 10° tilt.

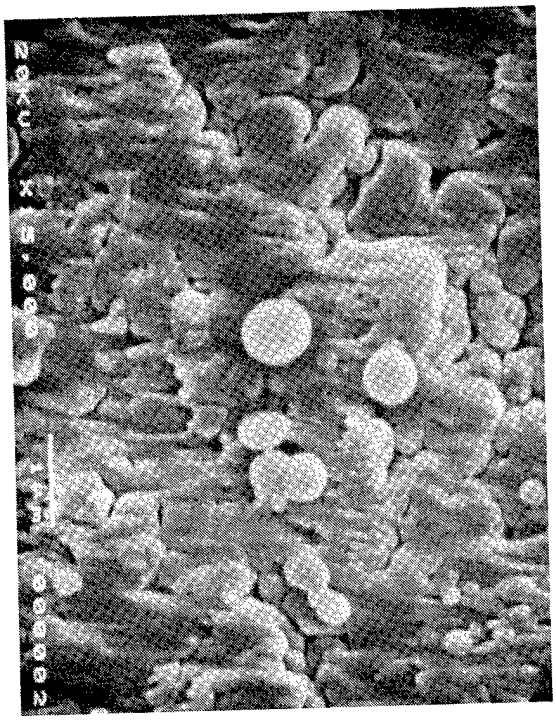


Figure 15b, SEM micrograph of the exposed HDPE/LLDPE surface. Micrograph was recorded with a 10° tilt.



Figure 16, FTIR spectra for the control (bottom) and exposed (top) HDPE/LLDPE. 1464 weave number doublet is presented.



Figure 17, 730/720 cm^{-1} doublet for the exposed (top) and control (bottom) HDPE/ LLDPE blend.

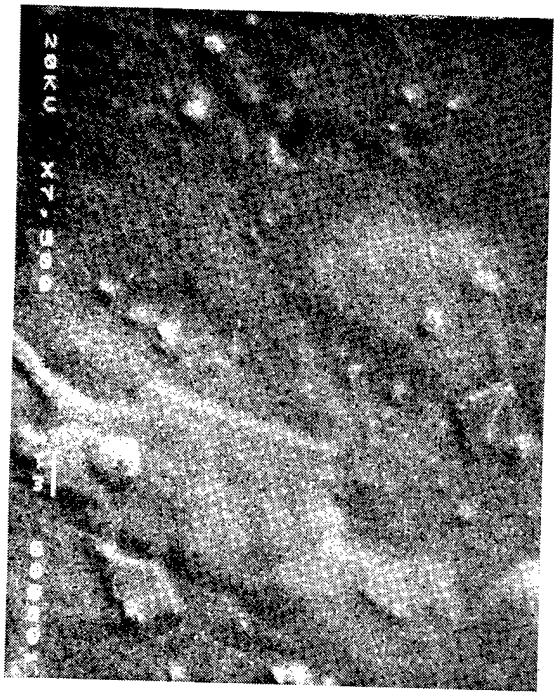


Figure 18, SEM micrograph of control FEP copolymer.

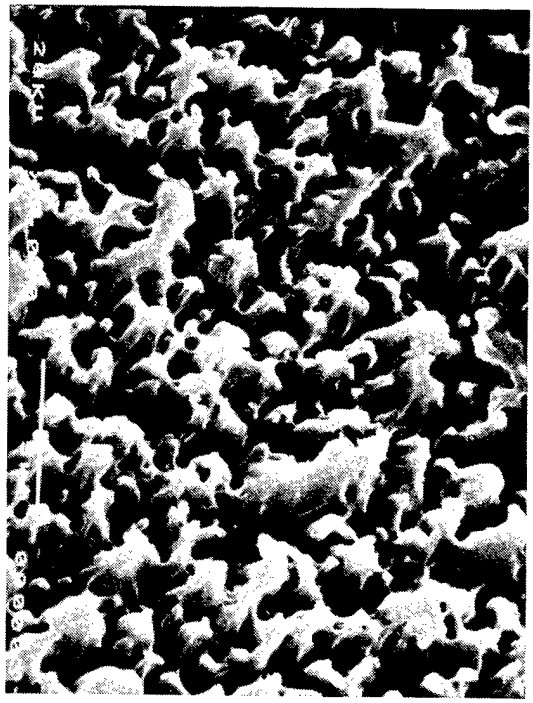


Figure 19, SEM micrograph of exposed FEP copolymer.

MEASUREMENTS OF EROSION CHARACTERISTICS FOR METAL AND POLYMER SURFACES USING PROFILOMETRY

Ligia C. Christl and John C. Gregory
The University of Alabama in Huntsville*
Huntsville, Alabama 35899
Phone: 205/895-6840, Fax: 205/895-6349

Palmer N. Peters
Space Science Laboratory, NASA/MSFC
Huntsville, Alabama 35812
Phone: 205/544-7728, Fax: 205/544-7754

SUMMARY

The surfaces of many materials exposed in low earth orbit are modified due to interaction with atomic oxygen. Chemical changes and surface roughening effects can occur which alter optical and other properties (ref.1). The experiment A0114 contained 128 solid surface samples, half of which were exposed on the front and half on the rear of LDEF. Each sample has been subjected to many analyses, but this paper will only describe the methods and techniques used to measure the changes in roughness, erosion depths and material growth using profilometry.

INTRODUCTION

The effect of atomic oxygen on materials is highly variable. No method of measuring the effects is optimum for all materials. We have developed several techniques found valuable in analyzing a wide range of materials, varying from minute effects on the level of atomic dimensions to heavily etched surfaces. One of the most effective techniques has been to utilize the measurement of etched steps at interfaces between exposed and unexposed, or masked, areas by stylus profilometry. Stylus profilometers typically measure the vertical displacement of a stylus (usually a fine pointed diamond) as it is scanned horizontally across the surface. Highly magnified vertical displacements are plotted against horizontal positions greatly exaggerating surface detail. This technique has the ability to measure a wide range of etch steps, from below 1 nm to 1 mm. For measurements below 1 nm it is essential that optically flat surfaces be used and that the steps be measurable over very short lateral distances. As shown elsewhere (ref.2), to produce etch steps over short lateral distances requires very thin masks, preferably thin film patterns resistant to atomic oxygen that are strongly bonded to the substrate being exposed, or at least knife-edged masks essentially in contact with the surface; these types of mask avoid structures which

* Work supported in part by a grant from UAH Research Institute and NASA grant NAGW-812 and contract NAS8-36645.

shadow the sample from the incident oxygen, preventing etch profiles with wide lateral dimensions. Lack of shadowing is particularly important on surfaces experiencing little effect, since even optical flats have variations or waves on their surfaces which cannot be distinguished from etch steps unless the steps are very sharp or patterned. One of the best patterns is a series of closely spaced lines for the masks, which produce a square wave pattern in the surface, providing multiple steps for comparison. An alternative approach for some thin films is to scratch narrow grooves through the thin film but without damaging the substrate. The depth of the scratches in both exposed and unexposed regions is then measured at a number of locations. This works well for materials softer than glass but hard enough to avoid excessive formation of furrows adjacent to the scratches. When done properly, the scribe will not scratch the substrate and will leave a flat bottom in the scratched area, indicating the full thickness of the film has been removed, as opposed to a v-shaped scratch which offers no assurance of this. Not only can etch steps be measured this way, but contaminant layers or increases in thicknesses in exposed areas due to oxidation or other causes, can be determined accurately, sometimes to a few 0.1 nm. This latter ability is valuable in conjunction with optical measurements on thin films where it is not known whether an increase in light transmission is due to a thinning of pathlength by removal of material or a change in optical properties. Measurement of an increase in the film thickness in the exposed areas helps to establish the latter. Thus, some metals have volatile oxides and are thinned while some form stable, clear oxides and are thickened, but are more transmissive to light. Good reflectance measurements are also desired in conjunction with the transmission measurements to account for any contamination or surface changes.

MEASUREMENTS

A wide variety of material surfaces were exposed to the atomic oxygen fluence, UV degradation and space contamination in the LDEF-A0114 experiment. The atomic fluence for the LDEF was 9.73×10^{21} atom cm^{-2} over its nearly six years exposure.

The surfaces consisted of polished bulk samples and high purity thin optical metal films sputtered or evaporated onto 1 inch flat fused silica disks. Each disk had one half of its surface masked, to be used as a control surface, and the other half was exposed to the environment. The samples were mounted in an aluminium panel, as shown in Figure 1. By masking half of each sample, it was possible to measure changes in roughness, erosion depths, material growth and changes in film thickness. These changes were measured, using a Taylor-Hobson Talystep Profilometer, model number 223-27, and a Taylor-Hobson Form Talysurf, model number 279-17.

The Talystep is a surface-profiling instrument designed to measure micro-thin film deposits, with a height resolution of ~1 Å and a lateral resolution of ~1μ. The one used for our measurements consisted of a conical diamond tip stylus of 1μm radius, with an adjustable force of 1 to 30 mgf. One mgf was used for tracing soft metals like Au, Ag and Sn films, to minimize damage to the surface. The Talystep measures the thickness of a film by moving the stylus at a constant rate across a groove cut in the film or across the step between the film and the substrate at the edge of the sample. To minimize thermal gradients and vibrations that affect the performance of the instrument on the most sensitive scales, the Talystep is enclosed in a plexiglas box and mounted on a vibration isolation table that in turn is placed on a granite slab in an air conditioned room (ref.3)

Calibration of the instrument was done using a standard provided by Taylor-Hobson. It is comprised of a frame and a base on which two glass plates are mounted. For checking the lower magnification ranges the left hand plate has three grooves nominally 2.5 micrometers deep with an

uncertainty of ± 0.05 μm. To check the highest magnification; the right-hand plate has three grooves nominally 0.025 μm deep with an uncertainty of ± 0.005 μm.

The Talysurf instrument is similar to the Talystep but operates over larger ranges with lower resolution. The program supplied with this instrument is able to measure many different shapes. Also, the stylus loading force is much greater, with a range from 75 to 100 mgf. A statistical analysis package, provided with the system, calculates both the mean value and standard deviation of the data values obtained from a series of measurement. Corrections for the accurate movement of the stylus arm and the size and shape of stylus tip are made by the computer. In order for the computer to make these corrections, a series of constants, whose values represent the characteristics of the individual stylus geometry, are required. These constants can be input via the keyboard or determined from a calibration routine automatically.

DISCUSSION

Examples of applications of stylus profilometry to different materials illustrate its ability to measure numerous features of exposed and unexposed surfaces. Nine examples will be discussed here. Figure 2 illustrates the ability to measure the roughness of a typical coated surface (unexposed iridium) on an optical flat of moderate quality. The RMS roughness is strongly influenced here by the longer period wave on the surface compared to the short period roughness. A sharp transition is shown in Figure 3 for an iridium sample scanned from exposed to unexposed areas. Even though the surface has a wave associated with it, a step of ~3.6 nm increase in thickness on the exposed area is apparent. The roughness on the exposed surface is also obviously increased by spikes which so far have not been satisfactorily explained. The increase in thickness could result from contamination or modification of the film itself. Studies are still underway to interpret the cause. Figure 4 represents a stylus trace on the same iridium sample from unexposed to exposed area. Although the roughness of the exposed area varies over the surface, the increase in thickness is comparable (3.5 nm and 3.6 nm), except at the knife edge boundary for Figure 4; although the sloped surface of the knife edge might enhance contamination effects at the boundary, insufficient data exists to positively identify the cause of the feature.

The gold film also shows a similar increase in thickness on the exposed area (~3.5 nm) however the gold surface does not exhibit the spikes on the exposed surface that were observed on the iridium surface. Figure 5 shows a stylus trace across one scratch in the unexposed area. Figure 6 shows a stylus trace across two scratches in the exposed region. Note that the rms roughness includes the depth of the scratches. The actual rms roughness on exposed was ~1.0 nm and the unexposed was ~ 0.7 nm for the gold sample.

Figure 7 shows how multilayer coatings can be resolved by the scratching and profiling, in some cases. In this figure a silver film deposited over a carbon film was investigated. The two scratches gave ~19.4 nm and ~20.1 nm for the unexposed carbon thickness and ~33.3 and ~31.3 nm for the unexposed silver thickness. The exposed portion of the silver over carbon sample could not be resolved into two layers, but only one. The total thickness of this exposed area averaged ~112.2 nm compared to the total of ~52 nm for the unexposed area. See Figure 8.

Figure 9 illustrates etching of polycrystalline carbon of such magnitude that the etch depth exceeds the range of the Talystep used above and required the use of the Talysurf. The very rough nature of exposed combustible materials that erode heavily with formation of volatile products has been documented by SEM and other imaging techniques. The stylus profilometer provides

accurate measurements of the spikes or plateaus that form at locations of slower etch, and provides an estimate of the maximum etch depth.

Polymethylmethacrylate, PMMA, is a plastic which is readily etched by atomic oxygen, forming a large number of small spikes at the bottom of the etch and a large etch step, as shown in Figure 10, and Figure 11. Figure 10, was traced on a sample mounted on the ambient temperature plate and Figure 11 is for a sample mounted on a separate thermally isolated plate of semipolished aluminum. The purpose was to examine the etch rate as a function of temperature. The small increase in etch in Figure 11 may be due to slightly higher temperature of the hot plate sample. The smooth plateau at the right of the etched area in Figure 10 is due to an artefact caused by the stylus catching on the large etch step and dragging the sample a short distance; heavily etched samples need to be secured for this reason.

CONCLUSION

Stylus profilometry is a very effective non destructive or minimal scratching technique to measure roughness, erosion depth and material growth of metals, polymers and carbons exposed to the atomic oxygen.

We have demonstrated that these instruments (Talystep and Talysurf), used in combination with some of the techniques mentioned (scratching, step and transition measurements), have a wide range of resolutions, from ~1Å to a few hundred microns.

Examples, like iridium film, show the reliability of the instrument, giving the same thickness value for the transition in any direction scanned.

Stylus profilometry, by indicating decreases, or increases, in film thicknesses enables interpretations of changes in optical density measurements, i.e. whether thinning of the film or an increase in thickness with optical property changes are responsible for optical density changes.

REFERENCES

1. Peters, P.N., Gregory, J.C., and Swan, J.T., "Effects on Optical Systems from Interactions with Oxygen Atoms in Low Earth Orbits," Applied Optics, 25, 1290-1298 (1986).

2. Peters, P.N., Sisk, R. C., and Gregory, J.C., "Velocity Distributions of Oxygen Atoms Incident on Spacecraft Surfaces," J. Spacecraft and Rockets, 25(1), 53-58 (1988).

3. Bennett, J. M., and Dancy, J. H., "Stylus Profiling Instrument for Measuring Statistical Properties of Smooth Optical Surfaces," Applied Optics, 20, 1785-1802 (1981).

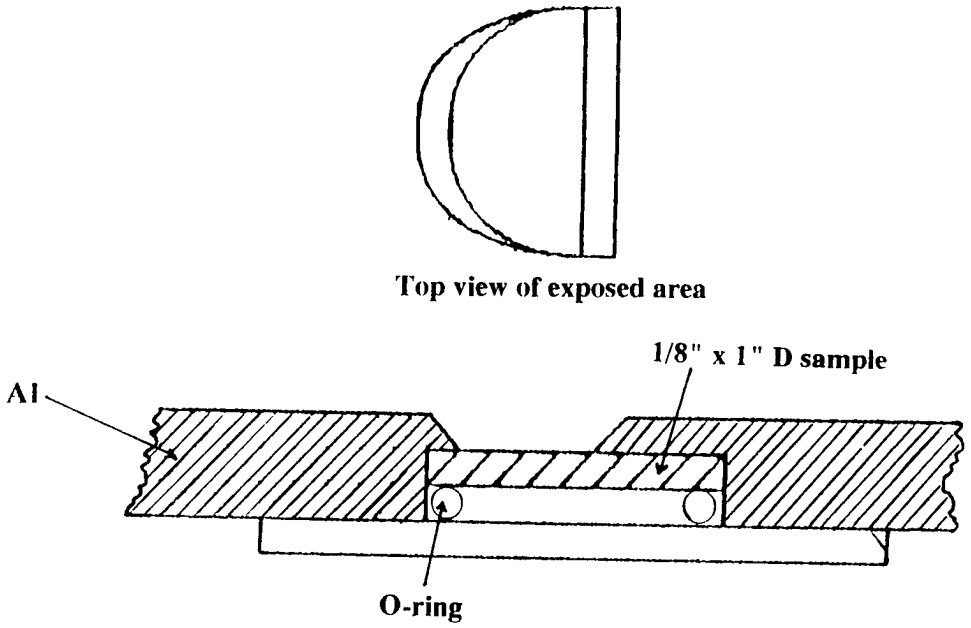


Figure 1. Cross-section of sample holder between exposed and unexposed areas

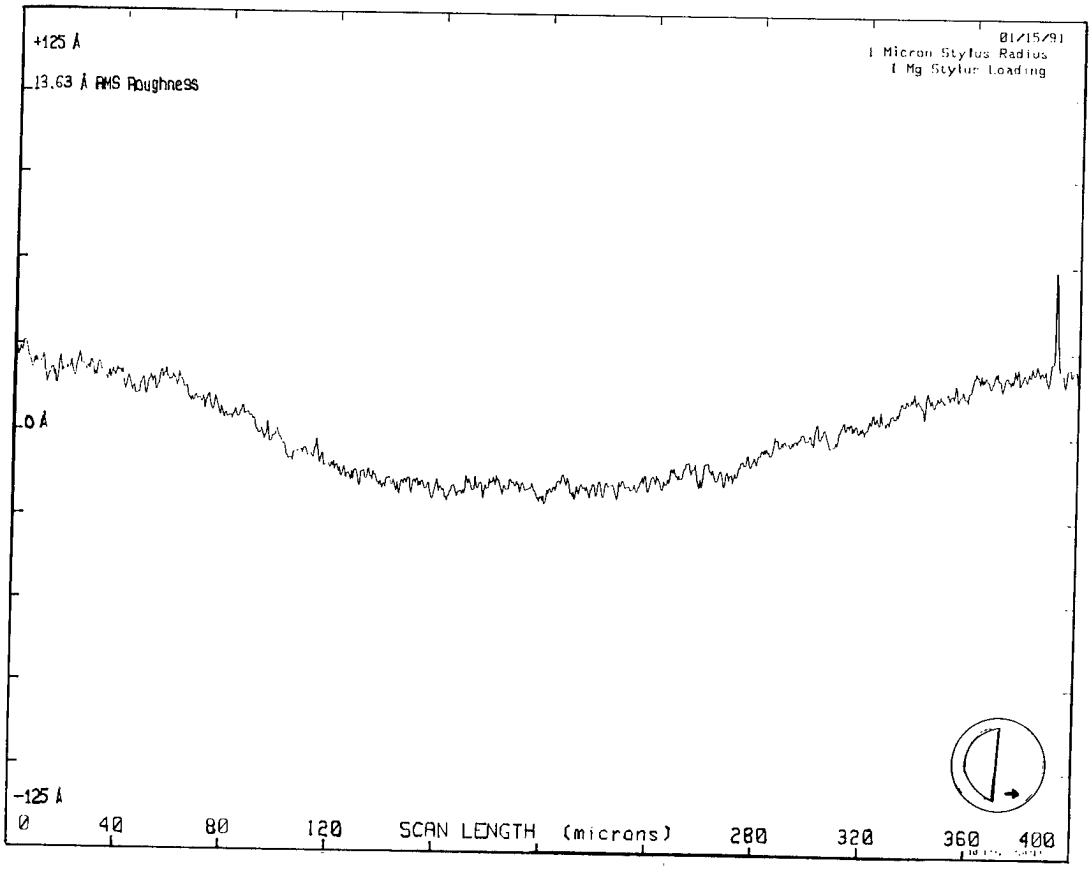


Figure 2. Surface profile of unexposed Iridium film

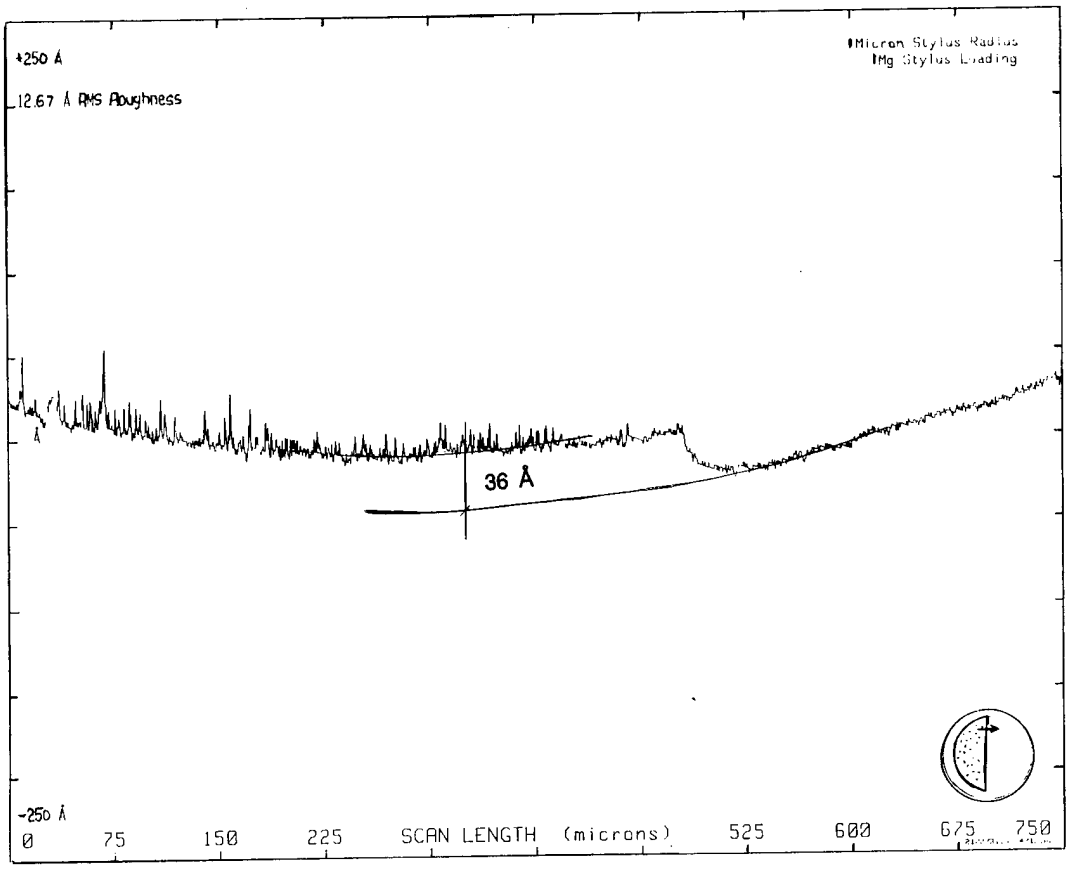


Figure 3. Surface profile of transition from exposed to unexposed of Iridium film

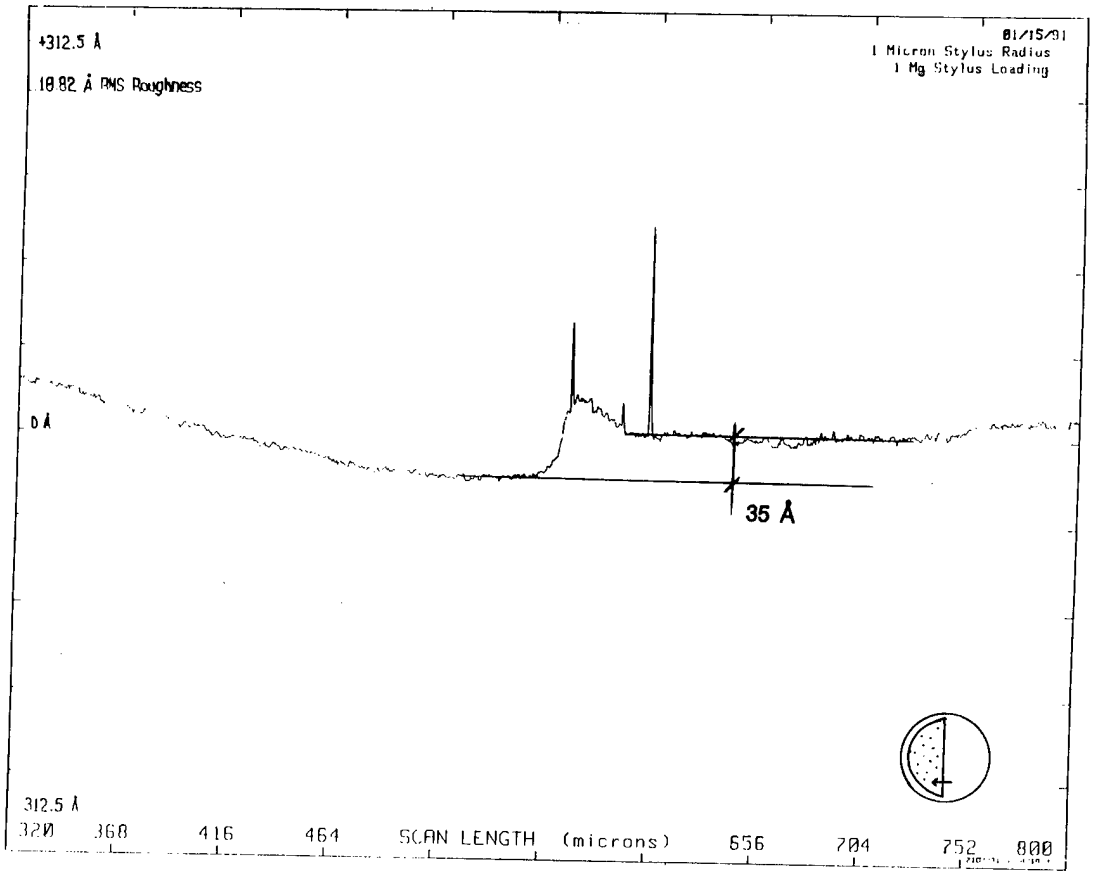


Figure 4. Surface profile of transition from unexposed to exposed of Iridium film

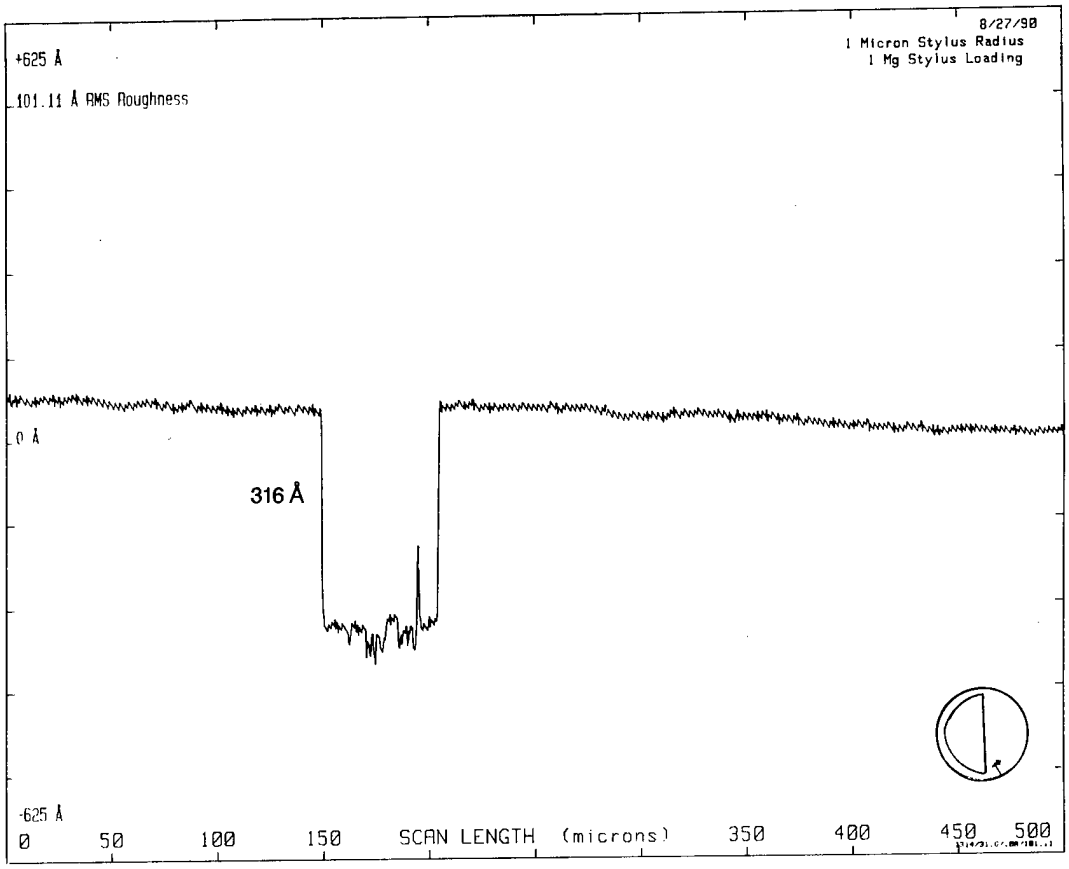


Figure 5. Surface profile of unexposed Gold film

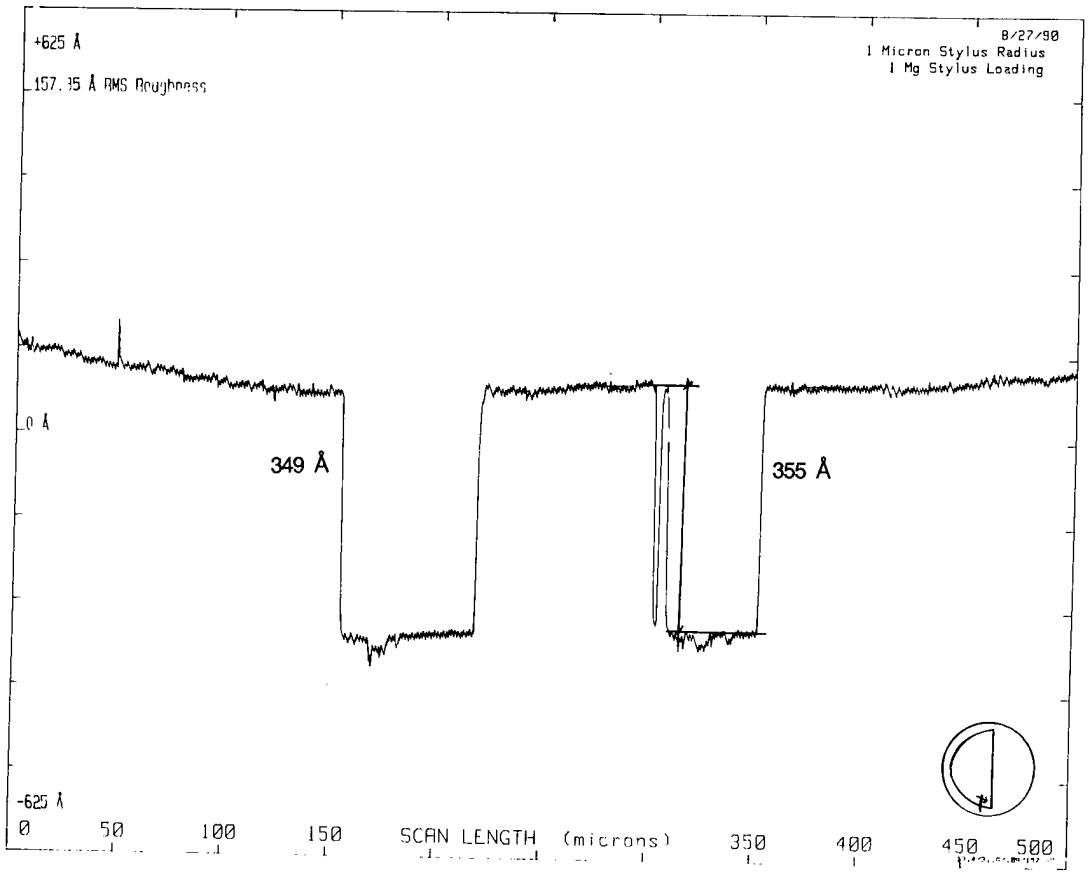


Figure 6. Surface profile of exposed Gold film

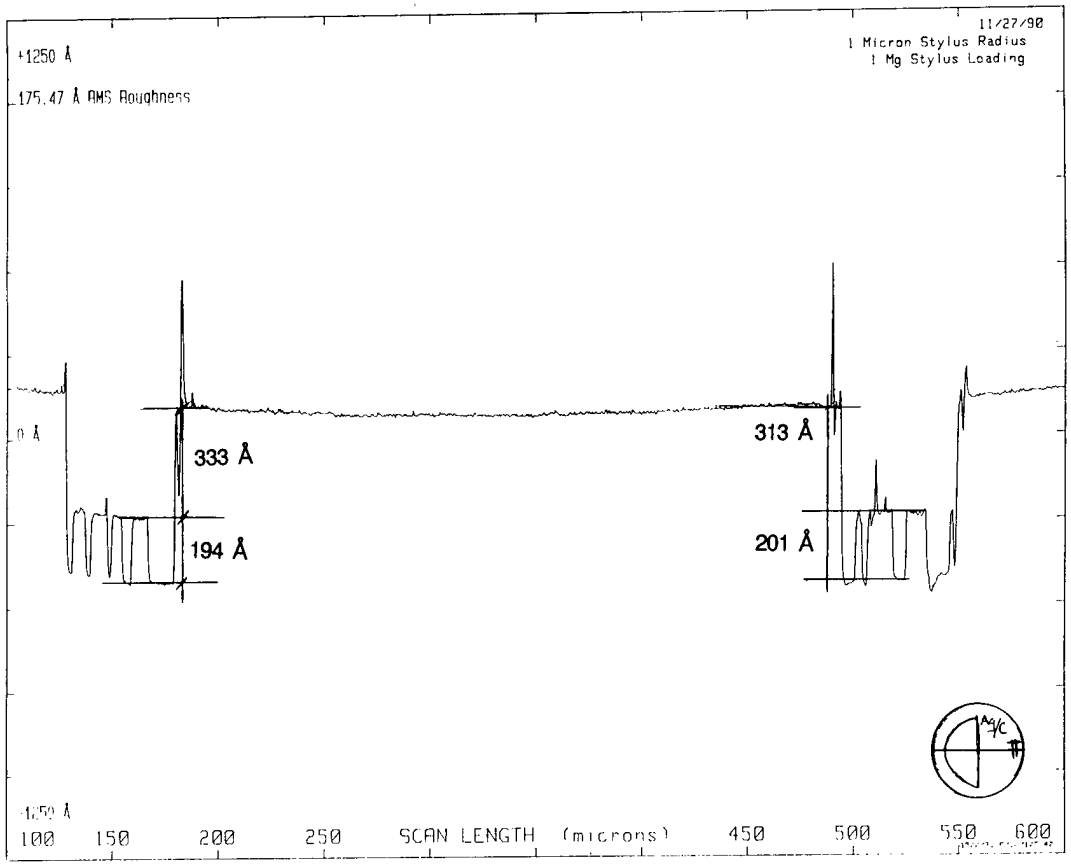


Figure 7. Surface profile of unexposed Silver over Carbon film

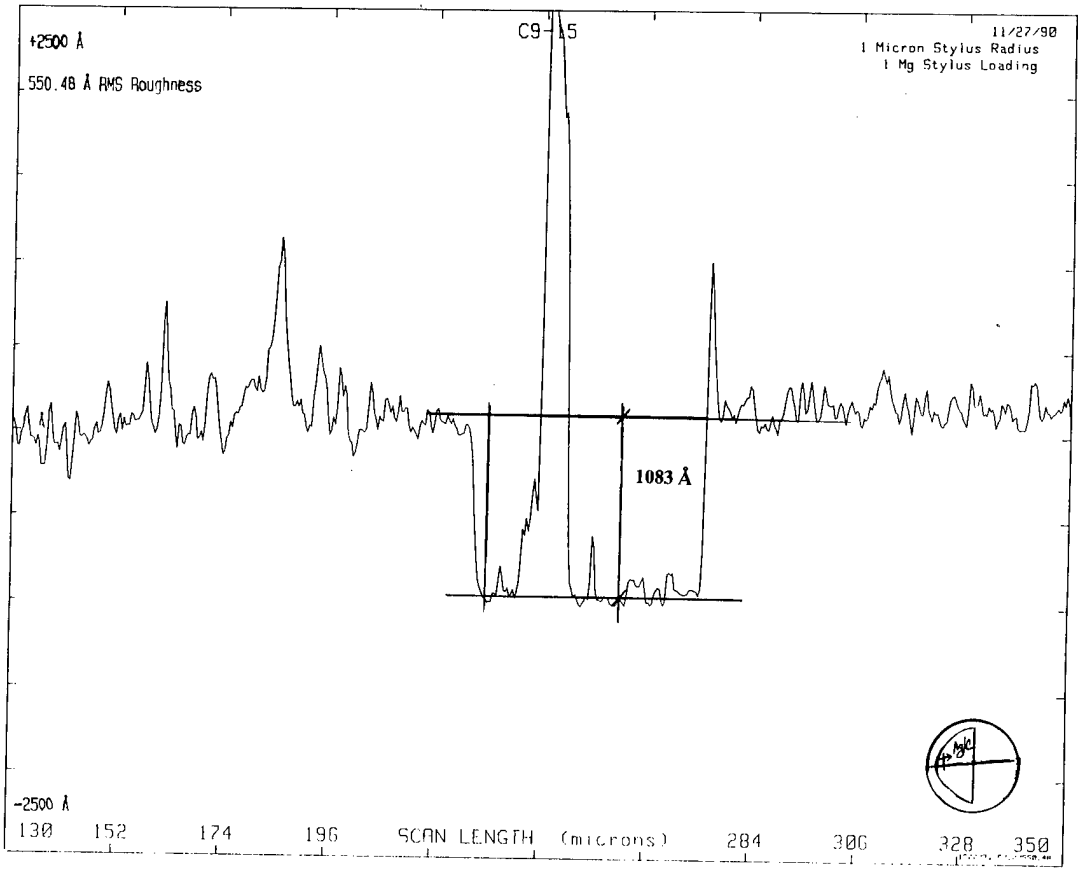


Figure 8. Surface profile of exposed Silver over Carbon film

Polycrystalline Carbon (C9-05)

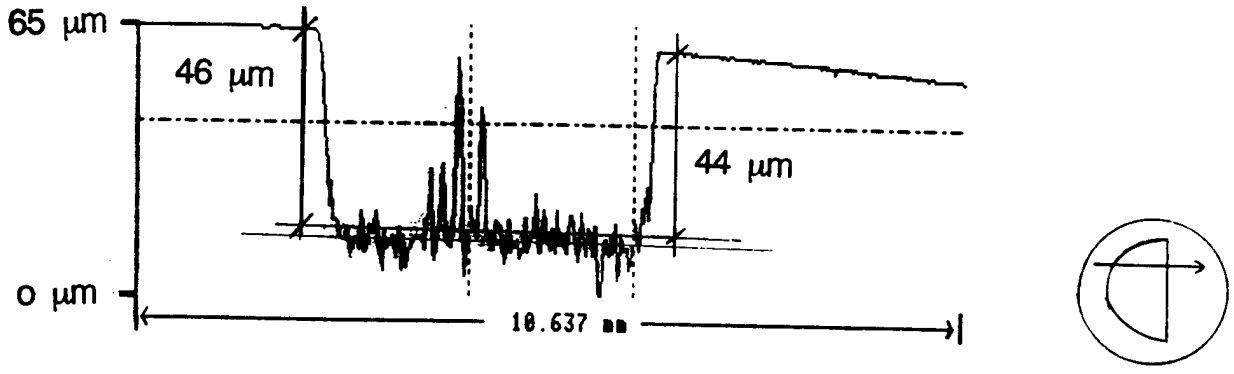


Figure 9. Surface profile of Polycrystalline Carbon

PMMA (C9-31)

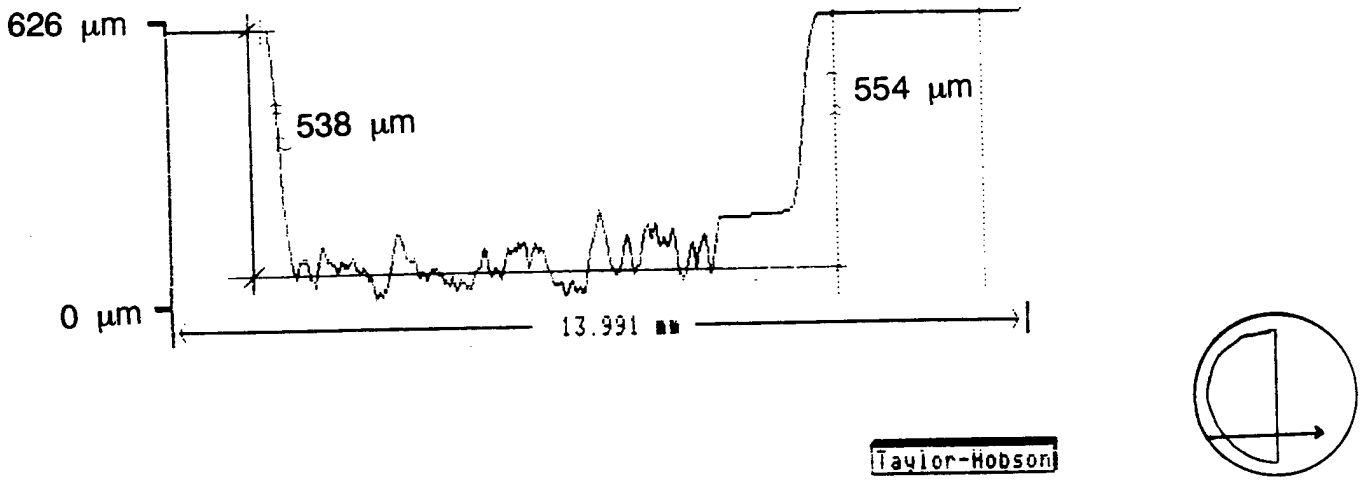


Figure 10. Surface profile of Polymethylmethacrylate at ambient temperature

PMMA (C9H-03)

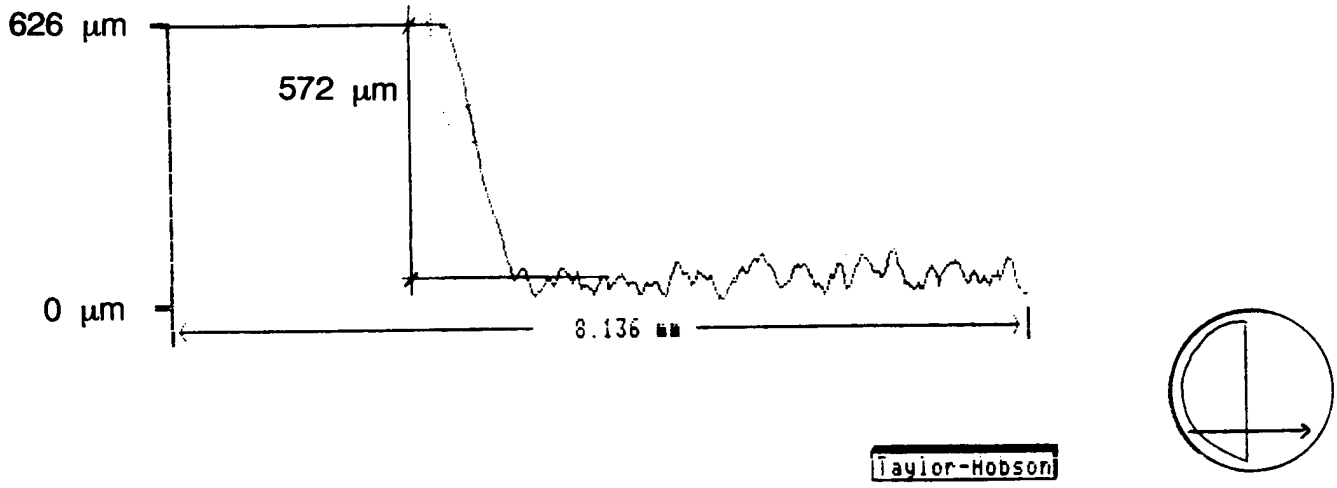


Figure 11. Surface profile of Polymethylmethacrylate at 10^0 C above the ambient temperature

LONG DURATION EXPOSURE FACILITY (LDEF) PRELIMINARY FINDINGS:

LEO SPACE EFFECTS ON THE SPACE PLASMA - VOLTAGE DRAINAGE EXPERIMENT

Brian K. Blakkolb, James Y. Yaung, Kelly A. Henderson,
William W. Taylor and Lorraine E. Ryan
TRW Space & Defense
Redondo Beach, CA 90278
Phone: 213/813-8960, Fax: 213/812-8768

SUMMARY

The Space Plasma - High Voltage Drainage Experiment (SP-HVDE) provided a unique opportunity to study long term space environmental effects on materials because it was comprised of two identical experimental trays; one tray located on the ram-facing side (D-10), and the other on the wake-facing side (B-4) of the Long Duration Exposure Facility (LDEF). This configuration allowed for the comparison of identical materials exposed to two distinctly different environments. The purpose of this work is to document an assessment of the effects of five and three-quarter years of low Earth orbital space exposure on materials comprising the SP-HVDE (experiment no. A0054). The findings of the materials investigation reported here focus on atomic oxygen effects, micrometeor and debris impact site documentation, thermal property measurements, and environmentally induced contamination.

INTRODUCTION

The trays of the SP-HVDE were dedicated to a spacecraft charging and current drainage experiment in which large numbers of dielectric samples were placed under electric stress and exposed to the LEO space environment. The objective of the experiment was to determine the current drainage behavior of positively and negatively charged dielectrics; to recover, inspect, and further test these samples in laboratory facilities; and to specify allowable electric stress levels for these materials as applied to solar-array and thermal control surfaces intended for prolonged use in the space environment.

Each experimental tray consisted of an aluminum structural frame measuring 50 x 34 x 3 inches with six fiberglass reinforced epoxy modules carrying the charged dielectric surface samples above, and housing the associated power supplies and electronics below. The outer surfaces of the modules were coated with white Chemglaze™ A-276 thermal control paint*. The space between the dielectric sample modules was covered by strips of 3 mil thick Kapton™ coated with a layer of vapor deposited aluminum on the reverse side (VDA-Kapton™) and fixed to the structure with acrylic transfer adhesive and Kapton™ tape†. To serve as the dielectric surfaces, various thicknesses of

*Chemglaze is a registered trademark of Hughson Chemicals, Lord Corp., 2000 West Grandview Blvd., P. O. Box 1099, Erie, Pa. 16512.

†Kapton is a registered trademark of E.I.Du Pont De Nemours & Co., Inc, Polymer Products Department, Industrial Films Division, Wilmington, DE. 19898.

VDA-Kapton™ were bonded to the fiberglass modules with silver-filled conductive epoxy to provide continuity to the electronics of the experiment.

Objective and Scope

As outlined above, the experimental intent of the SP-HVDE was quite specific; the results being discussed in detail by Yaung.[1] Even though the trays were not expressly designed to gather data about other aspects of space materials exposure, much can be learned from a more general examination of the experimental hardware. Thus, the objective of this work is to document and assess the effects of long term space exposure on materials comprising the SP-HVDE with the investigation concentrating on the following separate, but interrelated, aspects of the interaction between materials and the space environment: atomic oxygen effects, micrometeors and space debris, environmentally induced thermal property changes, and contamination.

FINDINGS

Atomic Oxygen Effects

According to data furnished by the LDEF Systems Special Investigation Group‡, the SP-HVDE trays were exposed to fluences of 7.88×10^{21} atoms/cm^2 and 1.15×10^{5} atoms/cm^2 for the ram-facing (Row 10) and trailing edge (Row 4) trays, respectively. Since atomic oxygen number density, and hence flux, is inversely proportional to orbital altitude^2, it is estimated that atomic oxygen flux increased on the order of one magnitude over the orbital history of the LDEF, with the spacecraft experiencing fifty percent of the cumulative atomic oxygen fluence during the last one hundred days on orbit.

The Kapton™ polyimide material on the ram-facing tray exhibited substantial degradation due to the impingement of atomic oxygen, as is clearly seen in Figure 1. The 2, 3, and 5 mil thickness VDA-Kapton™ making up the dielectric samples was almost completely eroded leaving the 2000-3000 angstrom vapor deposited aluminum layer bonded, by the conductive epoxy, to the module. These effects are in marked contrast to the trailing edge tray, pictured in Figure 2, which was not exposed to a high flux of energetic atomic oxygen.

The construction of the experimental trays was such that the edges of the VDA-Kapton™ dielectric surfaces were over-taped by a layer of Kapton™ tape with a silicone-based adhesive. While the 0.5 mil Kapton™ tape backing was completely eroded, the silicone adhesive protected the underlying material from atomic oxygen attack. This result was not altogether unexpected because silicones are known to be atomic oxygen resistant.

‡Long Duration Exposure Facility Systems Special Investigation Group, Interim Report, Dec. 1990, pg 10.

The erosion yield of Kapton™ is accepted as approximately $3x(10^{-24})$ cm^3/atom. From this value, the fluence required to erode the various thicknesses of Kapton™ present on the experimental trays was estimated and plotted as Figure 3. The sharply nonlinear erosion rate is associated with the increased atomic oxygen flux which accompanied the orbital decay of the LDEF from 257 nautical miles at deployment to approximately 180 nautical miles at retrieval.

Erosion morphology of the remaining Kapton™ is documented in Figures 4 and 5. The scanning electron micrograph in Figure 4 shows the edge of a specimen of VDA-Kapton™ where erosion has occurred through the entire depth of the material down to the vapor deposited aluminum layer on the reverse side. The micrographs shown in Figure 5 were taken looking normal to the surface of the specimen. The angled erosion features are indicative of, and consistent with, the off-normal impingement angle (approximately 22 degrees, accounting for the 8 to 12 degree yaw misalignment of the LDEF) of the ram flow with respect to the surface orientation.

Micrometeors & Space Debris

A visual survey of all exposed tray surfaces cataloged 187 impact sites on the ram-facing tray and 23 on the wake-facing tray. Sixty-seven percent of the impact sites for both trays fall within a 0.004 to 0.015 inch diameter size range with the number of impacts logged between the two trays matching pre-flight estimates of an 8 to 1 ratio. Estimates of the percent area coverage of particulate impact damage were made from the number and size distribution data and revealed area coverages of $1.3x(10^{-3})$ and $2.0x(10^{-4})$ percent for the ram- and wake-facing SP-HVDE trays, respectively. The impact site survey was conducted without the use of magnification devices, therefore only those sites which were visible to the unaided eye were counted. The diameter of each logged impact site was subsequently measured using a 100x optical microscope with a graduated eyepiece. The smallest and largest impact features logged using this method were 0.001 inches, and 0.046 inches in diameter respectively.

The orbital particle environment is defined in terms of the number of impacts expected per square meter, per year, vs. particle diameter. The impact sites logged on the SP-HVDE trays appeared to be uniformly distributed over the surface with the number flux being consistent with available particle environment models and flight data. Cumulative flux data, based on impact feature diameter, for the two SP-HVDE trays is plotted in Figure 6. Also plotted in the figure are data from a dedicated micro-particle impact experiment located at position B-3, adjacent to the wake-facing SP-HVDE tray, and the predicted flux from the European Space Research and Technology Center (ESTEC) micrometeor and debris flux model.[3] While the SP-HVDE data do not exactly match that of the dedicated experiment or the models, it is significant to note that each of the data sources follow the same non-linear trend with respect to declining flux versus increasing particle size. Some uncertainty is introduced in trying to

directly compare the flight results with model predictions because impact craters may be from 2 to 10 (or more) times the actual diameter of the impacting particle. A lack of knowledge of the composition of the impacting particles also obscures the correlation between impact crater data and flux model predictions, as the latter is given as a function of assumed particle density with higher particle densities being associated with lower fluxes.

Impact Site Documentation

Particle impact sites were documented on four types of surfaces: layered tapes and polymer films, glass fiber reinforced composites, aluminum plate (0.063 inch thickness), and unsupported Kapton™ films; each will be discussed in turn.

Layered Tapes and Films. Impacts on soft materials such as layered tapes and polymer films are typified by concentric openings exhibiting raised edges and decreasing diameter with increasing depth. The progressive decrease in diameter corresponds to the loss of specific energy experienced by the particle as it penetrates each successive layer. The raised edges at each layer of penetration have a melted appearance, indicating the material became hot enough to flow. This morphology is consistent with the thermal effects characteristic of hypervelocity impacts. Delamination, peeling under the influence of shearing forces at the edges, and shock compression in the layers with rebound of surface material are also noted.

Hard Surface Impacts. There were no impacts which completely penetrated the 0.188 inch thick epoxy-fiberglass tray surfaces. Damage was confined to exposed and broken glass fibers and areas of crushed epoxy matrix material. The damage found on these surfaces was typical of reported flight and ground based hypervelocity impact data for the fiber reinforced composites.[4]

The features cataloged on the dielectric surfaces of the wake-facing tray were similar to those on the polymer tapes and films described above. On the ram-facing surfaces, however, virtually all of the polyimide dielectric material had been eroded by atomic oxygen, leaving only the vapor deposited aluminum (VDA) layer bonded to the fiberglass substrate with conductive epoxy. The impact features on these ram-facing surfaces are typified by raised mounded spall zones of loose and flaking VDA material surrounding a relatively smaller central impact site exhibiting varying degrees of substrate damage. This has been classified according to the following scheme: (I) central impact pit crater with definite depth and broken and exposed fibers, (II) damage to surface fibers but incomplete penetration of the fiber layer, (III) little or no damage to the surface fibers with very shallow, if any, penetration. Twenty percent of the impacts on the ram-facing surfaces were class (I), forty percent class (II), and forty percent class (III). Energy dispersive x-ray spectroscopic examination of a limited number of ram-facing impact sites did not detect the presence of any species which could be conclusively identified as residual from either meteors or anthropogenic debris.

Unsupported-Film Impacts. A number of impact sites were logged on the VDA-Kapton™ film covering the areas between the charged dielectric surface modules of the wake-facing tray. Figure 7 shows the result of such an impact as viewed from the front surface. The diameter of the penetration is 0.028 inches. The upward tearing and ejection of molten material are the result of shear stresses and shock heating which are characteristic of hypervelocity particle impacts.

The penetration feature shown in Figure 8 appears to lack the characteristic features described above, even though the impacted material was the same in both cases, 3 mil. VDA-Kapton™. The rear side of the penetration (not shown) has a raged appearance but lacks thermal and shear-induced deformation directed toward the front surface. One possible explanation for such an impact feature may be that the impacting particle was not traveling fast enough for thermal and strain-rate dependent deformations to occur, but did carry sufficient kinetic energy to penetrate the material.

Aluminum Tray Surface Impacts. There were three impacts logged on 63 mil. aluminum tray mounting flanges, the most accessible of which was removed, by excision of a section of the tray flange, for further analysis.

The experimental trays were constructed such that the area where the impact occurred, was covered by one layer each of acrylic transfer adhesive, 3 mil VDA-Kapton™, and 0.5 mil Kapton™ tape with silicone-based adhesive. Photomicrographs of the 0.047 inch diameter crater are shown in Figure 9a. The raised crater edge is the result hypervelocity impact characteristics discussed above. Very high pressures are also characteristic of such impacts and the temperatures generated are high enough to melt or vaporize the substrate and particle materials[4]. Since the crater extends down into the aluminum tray flange, it was expected that a surface analysis would detect aluminum and traces of the impacting particle. SEM/WDS and AUGER/ESCA found silicon and oxygen as the predominant species, with traces of potassium, sodium, iron, copper, and sulfur. The presence of these trace elements is characteristic of salt residue, from sea spray. Figure 9b provides a close-up view of the surface morphology of the "petal-like" structures protruding inward from the edges of the crater. Figure 9c shows the crater floor at 500x magnification. The loop structures appear to have been trapped in a distinctly separate phase which looks as though it were molten and resolidified. At this time, there is no explanation for this unique morphology.

Thermal Properties

Solar absorption (a_s) and normal emittance (e_n) measurements were performed on thermal blanket materials and thermal control paint coated surfaces of both experimental trays.

Thermal Blanket Material

Hemispherical emittance, as calculated from the normal emittance, for wake-facing VDA-Kapton™ surfaces was found to be unchanged versus unflown material, having a nominal value for e_h of 0.80 +/-0.02. The measured solar absorptance for these surfaces was within 3 percent of the values for unflown material (a_s=0.44); the calculated difference being less than the resolution of the measurement.

With virtually all of the Kapton™ eroded from the leading edge thermal blanket material, the measured thermal properties of these surfaces was closer to that of raw VDA than VDA-Kapton™. Absorptivity was 85 percent less than the unflown VDA-Kapton™ (a_s=0.44) and 63 percent less than that of raw VDA (a_s=0.20); making these atomic oxygen degraded surfaces comparatively better mirrors. A similarly large difference was found in the e_h of flight vs. unflown specimens, with flight samples having an emittance 84 percent lower than unflown VDA-Kapton™ (e_h=0.80), but virtually the same value as raw unflown VDA (e_h=0.11). Even though the individual properties of the flown samples differ significantly from unflown material, the a/e ratio is within 10 percent of the unflown VDA-Kapton™ material (a/e=0.66).

Thermal Control Paint

There were also significant differences in thermal properties of the white Chemglaze™ A-276 thermal control paint, between ram- and wake-facing trays. On the wake-facing tray, ultra-violet radiation-induced darkening of the polymeric paint binder increased the measured solar absorptance by a factor of 1.63 over unflown material (a_s=0.26) The emittance (e_n=0.88) of these surfaces remained essentially unchanged. On the ram-facing tray, erosion of the polymeric paint binder by energetic atomic oxygen left the metallic oxide pigment of the paint exposed on the surface and resulted in a 48 percent lower solar absorptance (a_s=0.14 vs. 0.26) but emittance remained unchanged. These thermal property changes account for a 53 percent decrease in the a/e ratio (a/e=0.14 vs.0.30 for unflown material).

Contamination

Evidence of spacecraft self-contamination was found on both ram and wake-facing trays, with outgassing products from paints, coatings, adhesives, and RTV-silicones being the suspected source. Outgassing products from the LDEF, through interactions with UV radiation, and energetic atomic oxygen in the LEO environment, produced the observed contamination phenomenon.

Outgassing Deposits

On both trays, pearlescent SiO_x film deposits were found at vent sites where volatile organic compounds, escaping from the interior of the tray, deposited on nearby surfaces. Figure 10 shows such a deposit on Kapton™. The patterns formed by the contaminant film are

consistent with effusive flow, with the heaviest accumulation being closest to the vent source. The pearlescent appearance is due to the varying degree of light diffraction caused by the gradual thickness change of the film. The film shows resistance to energetic atomic oxygen, as can be deduced from the condition of the Kapton™ underlying the deposit. The fact that the Kapton™ was substantially undergraded, suggests that these deposits were laid down relatively early in the flight.

Nicotine Stain

While the pearlescent film deposits appear to be the result of a direct line of sight contamination at a vent site, a distinctly different contamination phenomenon is also present; the so called "nicotine stain" shown in Figure 11. The deposit is red-brown in color and composed of layers of hydrocarbon contamination (characteristic of the organics found in paints, coatings, adhesives, etc.) and covered by a skin of SiO_x material. The deposition of the material is thought to be the result of the backscattering of outgassed species by the ram-induced flow of ambient species. There is a strong directional dependence to the contamination patterns consistent with the orientation of the ram-facing tray with respect to the ram direction. The shadowing in the wake of the rivets, and the absence of the material on the wake-facing tray also suggest a flow induced deposition mechanism.

Hall, et.al., 1985 and Stewart, et.al., 1990 have demonstrated that surfaces which are illuminated by solar radiation preferentially collect volatile condensable material, even if these surfaces are at a higher temperature than surrounding, unilluminated surfaces.[5&6] The patterns seen here however, do not show a smeared appearance as would be expected with a changing sun angle. Therefore, it is not thought that preferential deposition is the only mechanism operating in the deposition of the "nicotine stain", although, ultra-violet radiation may certainly be responsible for darkening of the material.

CONCLUSIONS

The examination of the SP-HVDE trays (A0054) has improved the existing materials stability and environmental effects data base on long term space effects. This work reinforces the predictive value of particle flux models and serves to validate the phenomena of solar radiation and atomic oxygen induced thermal property degradations. The contamination patterns seen on surfaces reaffirm models used to design spacecraft venting and design of protective measures for contamination sensitive spacecraft surfaces. Finally, these initial findings can contribute to better designed and longer-lived spacecraft through documentation of LEO space environmental effects on spacecraft materials.

REFERENCES

[1] Yaung, J. Y., Wong, W. C., Blakkolb, B. K., Ryan, L. E., Chedotte, J. E., Taylor, W. W., "LDEF SP-HVDE Post-Flight Results," First Long Duration Exposure Facility Post-Retrieval Symposium, NASA CP-3134, 1992.

[2] Visentine, J.T., Whitaker, A.F., "Material Selection Guidelines to Limit Atomic Oxygen Effects on Spacecraft Surfaces," NASA TM 100351, Feb. 1989, pg.11.

[3] FRECOPA experimental tray data reported in the LDEF Spaceflight Environmental Effects Newsletter, V.1, No.5, Oct. 3, 1990, p.9

[4] Cour-Palais, B. G., The Long Term Effects of the Micrometeoroid and Orbital Debris Environments On Materials Used in Space," NASA/SDIO Space Environmental Effects on Materials Workshop, CP-3035, 1989, pp.257-280.

[5] Hall, D. F., Stewart, T. B., Hayes, R. R., "Photo-enhanced Spacecraft Contamination Deposition," AIAA-85-0953, AIAA 20th Thermophysics Conference, June 19-21, 1985.

[6] Stewart, T. B., Arnold, G. S., Hall, D. F., Marvin, D. C., Hwang, W. C., Young, O., Rolaine, C., and Marten, H. D., "Photochemical Spacecraft Self-contamination: Laboratory Results and Systems Impacts," Report No. TOR-0090(5470-01)-3, The Aerospace Corporation Laboratory Operations, July 25, 1990.

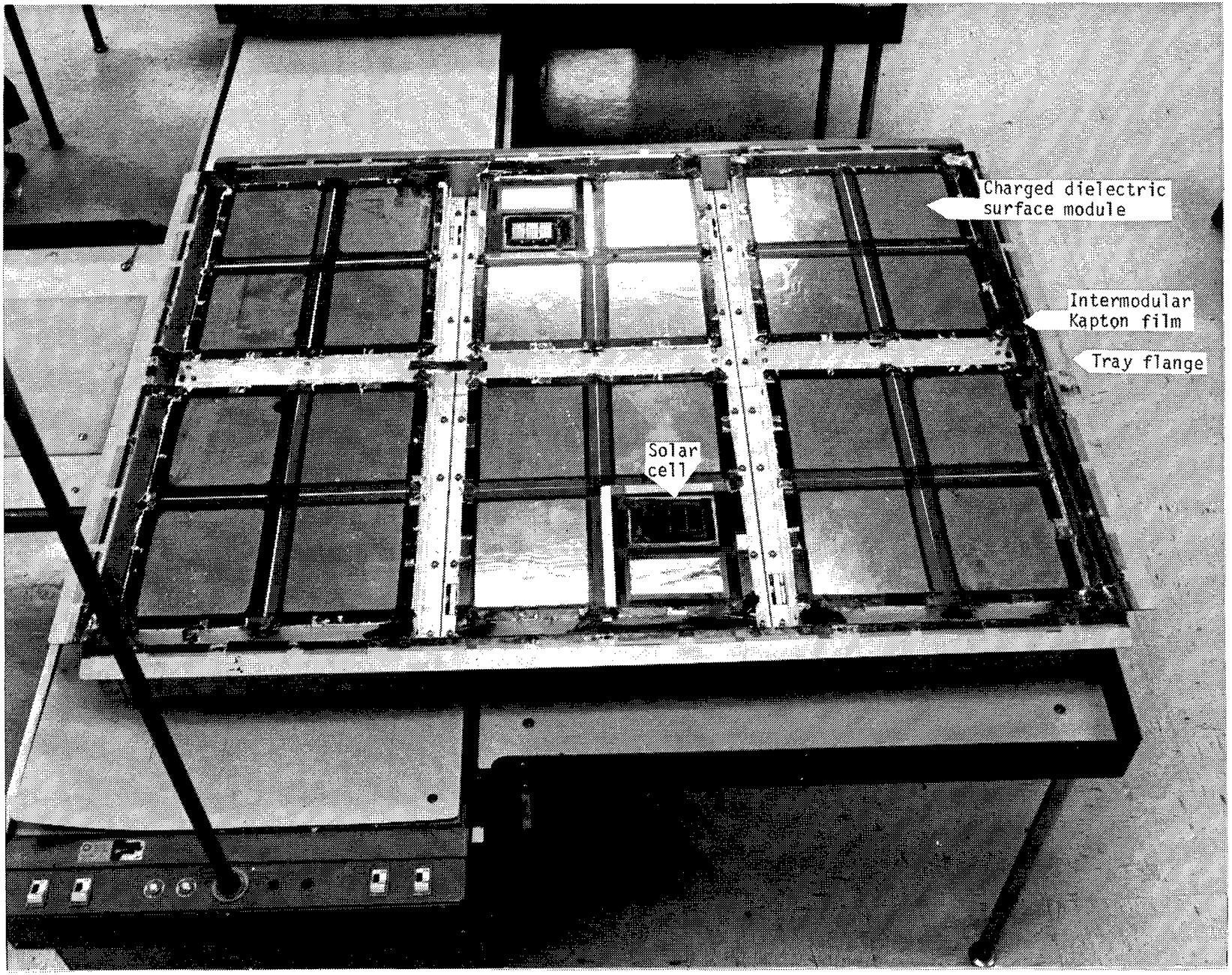


Figure 1. Ram-Facing SP-HVDE Tray (Post Flight)



Figure 2. Wake-Facing Tray (Post Flight)

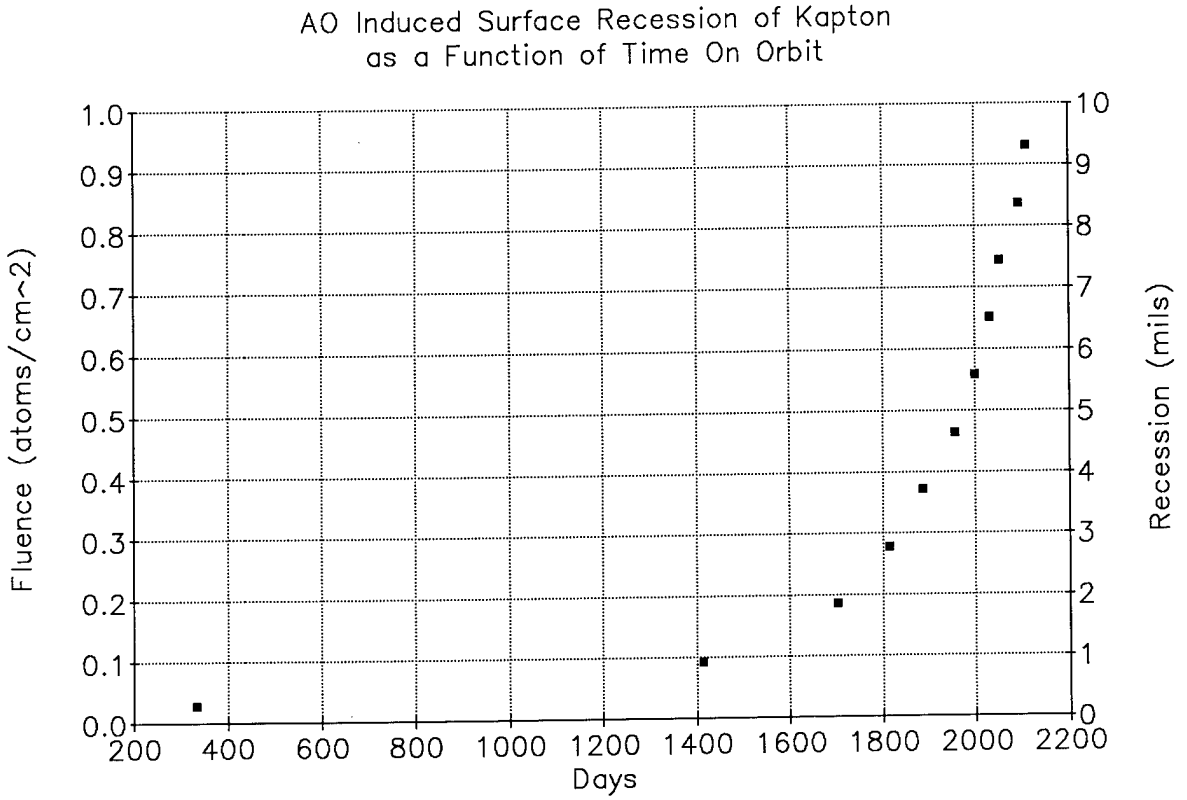


Figure 3

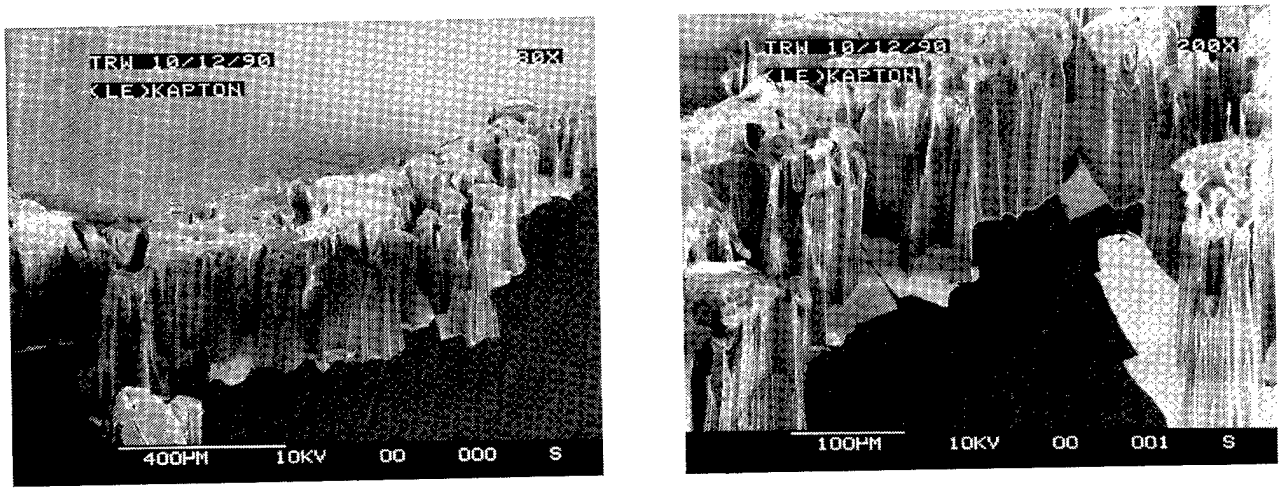


Figure 4.
Edge-on View. Atomic Oxygen Erosion of 3 mil Polyimide Film.

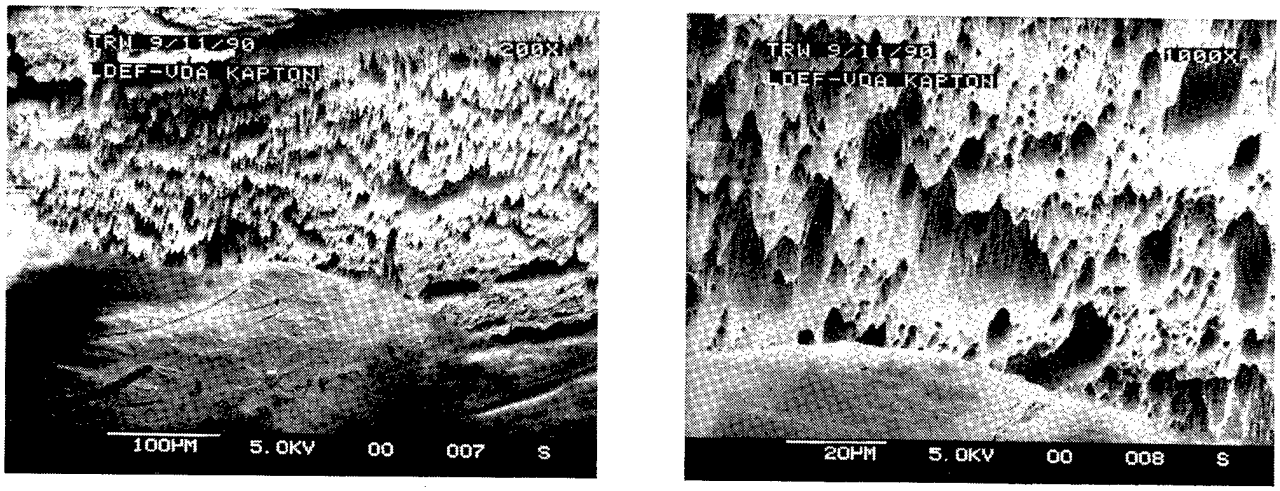


Figure 5.
Angled Erosion Morphology of Polyimide Film.

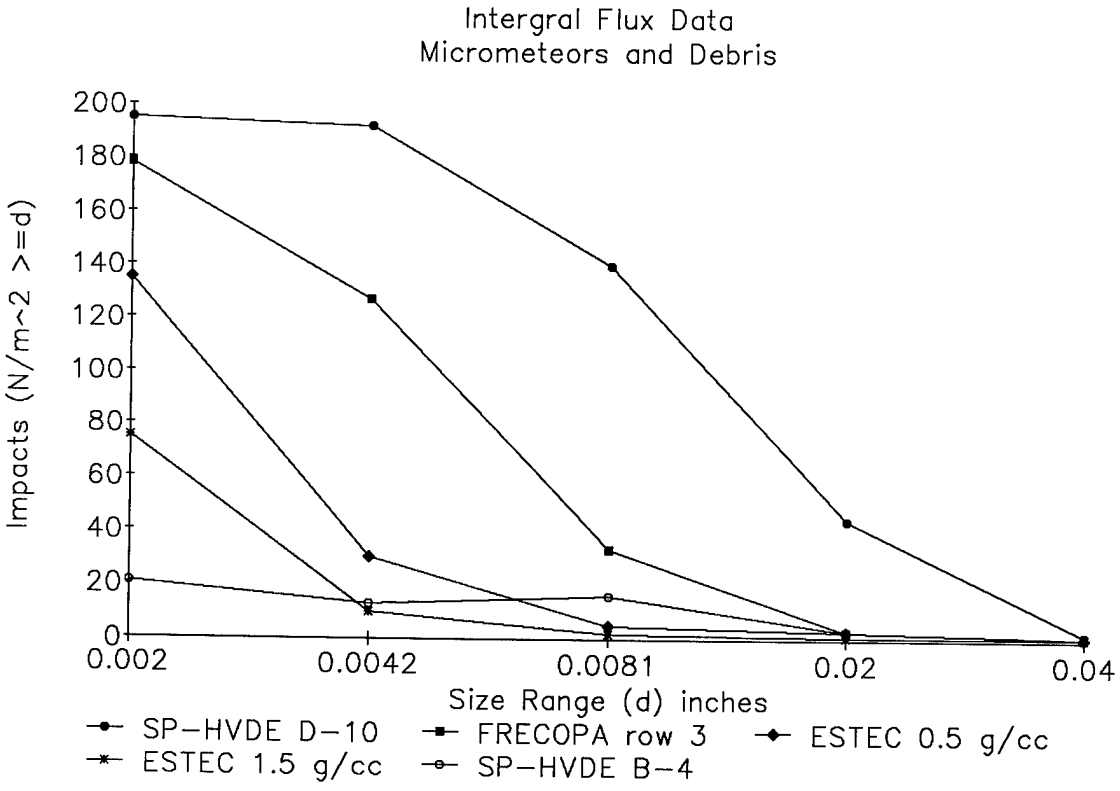


Figure 6.

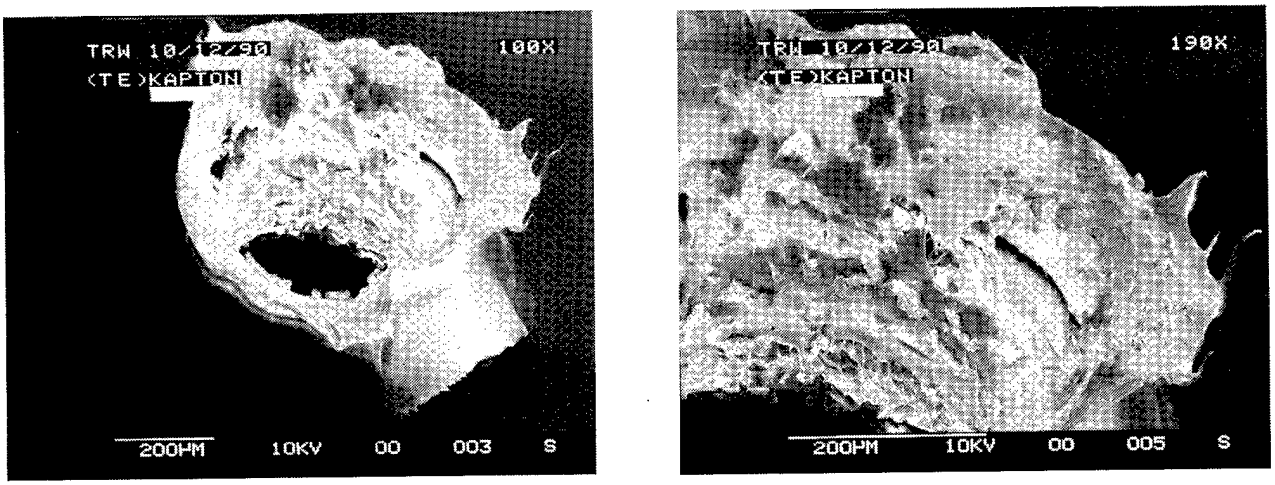


Figure 7.
Hypervelocity Penetration of 3 mil
Polyimide Film. SP-HVDE Wake-facing Tray

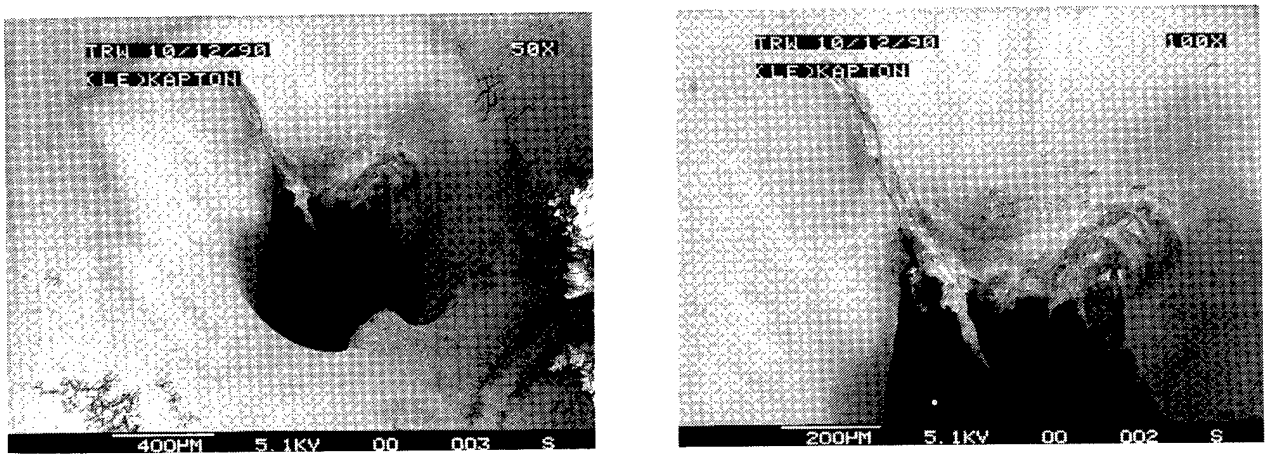


Figure 8.
Particle Penetration of 3 mil Polyimide Film. Lack of
Thermal and Shear Effects Suggests Low Velocity Impact.



Figure 9a.

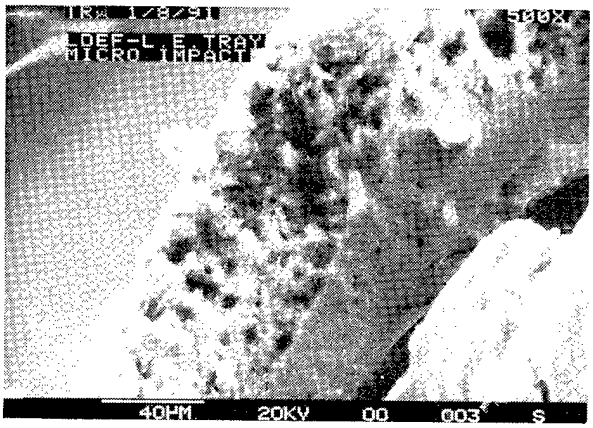


Figure 9b.

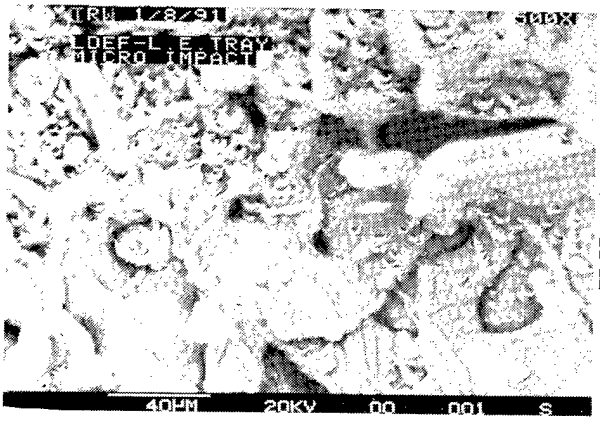


Figure 9c.

Figure 9a. Hypervelocity Impact Crater on Ram-facing Tray Flange.
Figure 9b. Edge-on Close-up of "Petals".
Figure 9c. Crater Floor.

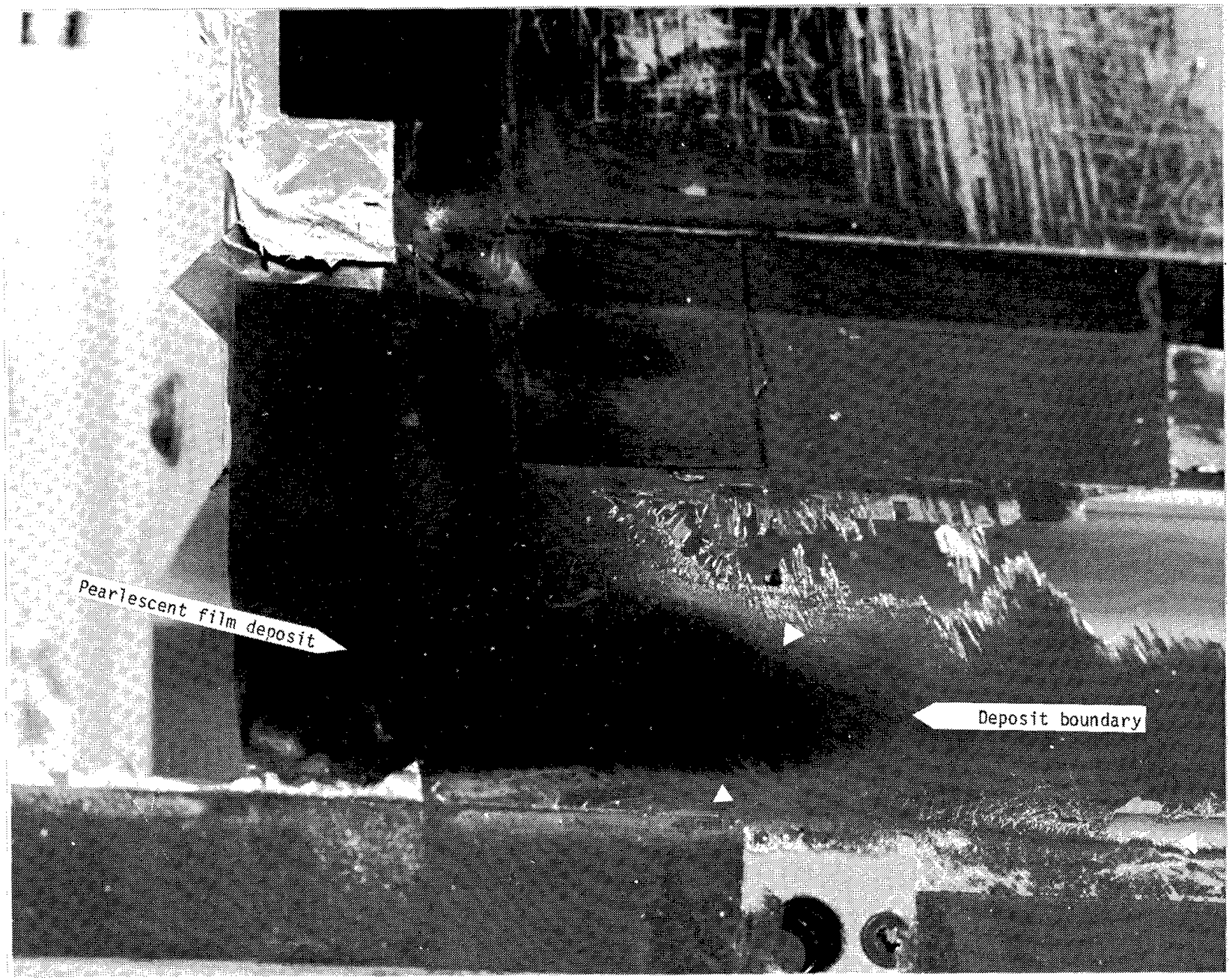


Figure 10. Pearlescent Outgassing Deposit on Kapton

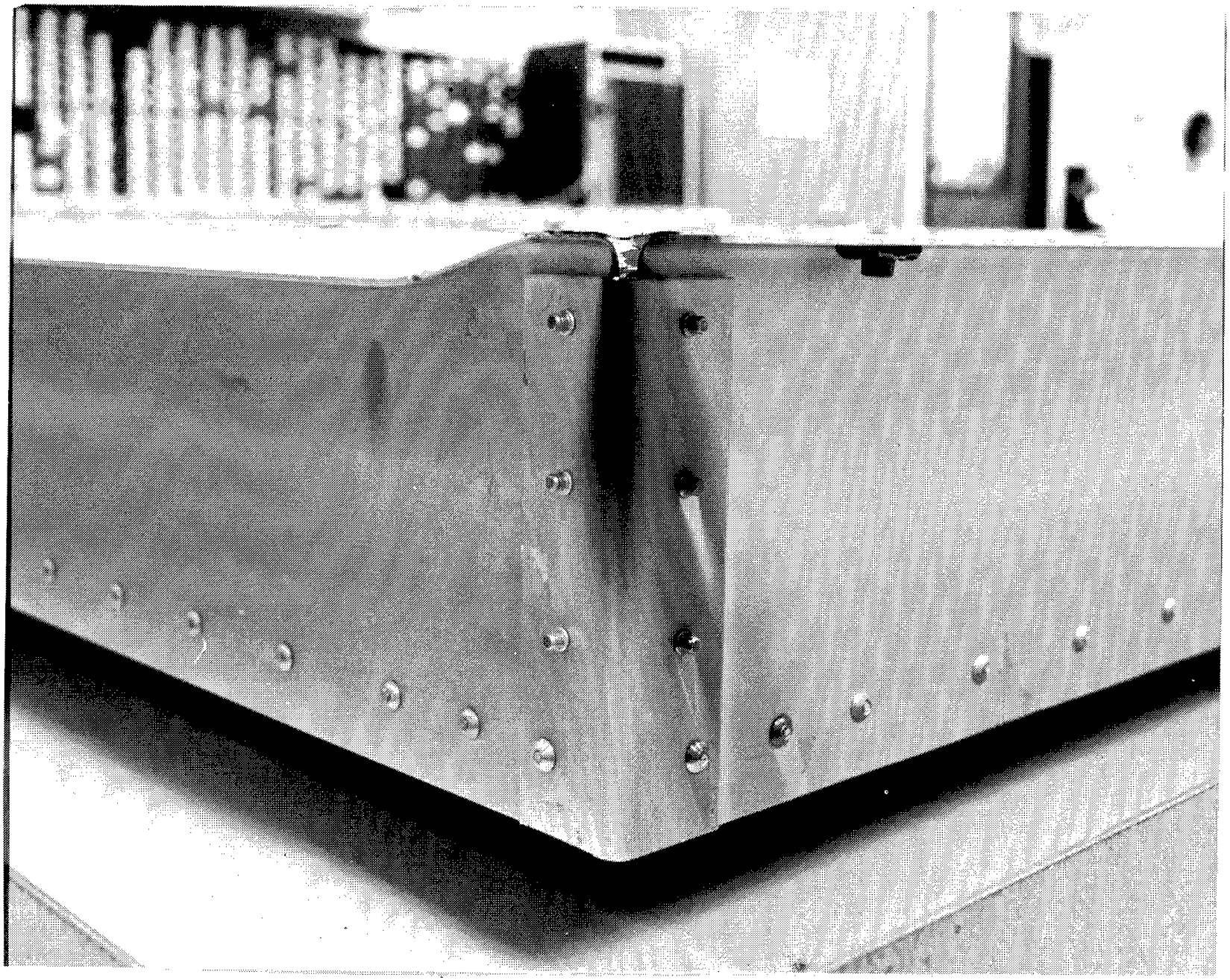


Figure 11. Nicotine Stain

INTERACTIONS OF ATOMIC OXYGEN WITH MATERIAL SURFACES IN LOW EARTH ORBIT: PRELIMINARY RESULTS FROM EXPERIMENT A0114

J. C. Gregory, L. Christl, G. N. Raikar, J.J. Weimer, R. Wiser
Surface Science Laboratory
The University of Alabama in Huntsville
Huntsville, Alabama 35899

P.N. Peters
Space Science Laboratory, NASA, MSFC

ABSTRACT

The UAH atomic oxygen experiment consisted of two trays (one-sixth of an LDEF tray each) of 64 one inch diameter solid samples. One tray was placed on the leading edge C9 and one on the trailing edge C3 of the spacecraft. Half of each sample was covered to provide a control. Thus it was intended that the effects of atomic oxygen and solar UV irradiation on the surface properties of each material could be distinguished from each other and from the effects of aging. Sixteen of the samples were placed on a thermally isolated plate of highly polished aluminum, while the main plate was coated with the thermal control coating S13-GLO. Though the experiment was entirely passive it was hoped that effects of thermal activation might be observed, if present. The plates were expected to stabilize at temperatures differing by 20 - 30°C. The experiment also carried a device to measure the spacecraft altitude (reported elsewhere at this meeting) and several oxygen atom reflectometers which have not been analyzed to date.

The samples included thin films of metals Os, Ir, Pt, Ni, W, Mo, Al, coated onto fused silica optical flats, metal carbides (WC, SiC), solid carbons of various types, eight polymers and some other coatings of various types.

Analysis is essentially complete using stylus profilometry with the high sensitivity Talystep and the lower sensitivity Talysurf machines. Though the integrated fluence of O atoms on LDEF was 30 times that on previous missions, etch depths on polymers such as the polyimide Kapton show excellent agreement with extrapolations from previous flight data . Some new effects are however observed. We have shown in a previous experiment on STS-8 that profilometry of this kind can show steps of 50 Å (for example those due to oxide film growth on metals) and this is now the preferred method for estimating etch depth (or mass loss) of erodible substances. We have also begun surface analysis of the materials using FTIR, SEM, XPS and Auger electron spectroscopies.

Experiment No. A0114

EFFECTS ON LDEF EXPOSED COPPER FILM AND BULK

Palmer N. Peters
Space Science Laboratory, NASA/MSFC
Huntsville, Alabama 35812
Phone: 205/544-7728, Fax: 205/544-7754

John C. Gregory,* Ligia C. Christl,* Ganesh N. Raikar*
The University of Alabama in Huntsville
Huntsville, Alabama 35899
Phone: 205/895-6028, Fax: 205/895-6349

SUMMARY

Two forms of copper were exposed to the LDEF Mission 1 environment: a copper film initially 74.2 ± 1.1 nm thick sputter coated on a fused silica flat and a bulk piece of OFHC copper. The optical density of the copper film changed from 1.33 to 0.70 where exposed and the film thickness increased to 106.7± 0.5 nm where exposed. The exposed area appears purple by reflection and green by transmission for the thin film and maroon color for the bulk copper piece. The exposed areas increased in thickness, but only increase in the thickness of thin film sample could be readily measured. The increase in film thickness is consistent with the density changes occurring during conversion of copper to an oxide, however, we have not been able to confirm appreciable conversion to an oxide by x-ray diffraction studies. We have not yet subjected the sample to e-beams, or more abusive, investigations out of concern that the film might be modified.

*Work supported in part by grant from UAH Research Institute, and NASA grant NAGW-812 and contract NAS8-36645.

INTRODUCTION

The copper samples represent 2 of 64 cylindrical samples of 2.54 cm (1 inch) diameter that were flown on the leading, C9, tray of LDEF Mission 1 for 5 3/4 years of exposure in low Earth orbits. Matching trailing samples, which showed little effect, were located in the C3 tray. Appreciable effects on the copper were not anticipated, since active oxygen discharges on the ground for short periods had not shown the same gross degradation effects that silver had. The samples were mounted on ambient temperature surfaces believed to have had approximately room temperature values.

Copper oxide has a number of forms [1] ; two common forms of oxide are cuprite, Cu_2O, and tenorite, CuO. Cuprite has the properties: Molecular weight of 143.08, color is red, octahedral cubic structure, index of refraction of 2.705, and specific gravity of 6.0. The tenorite is black monoclinic, has a molecular weight of 79.54, index of refraction of 2.63, and specific gravity of 6.3 to 6.49. Copper has a molecular weight of 63.546, a cubic structure and a specific gravity of 8.92.

MEASUREMENTS

The copper samples were investigated by a number of techniques; these included: visual inspection by eye and optical microscope, photography, optical density measurements with visible white light using a scanning microdensitometer, thickness measurements by stylus profilometry, x-ray diffraction (XRD) electrical resistance measurements, ellipsometry, x-ray photoelectron spectroscopy (XPS), and profiling by optical interference techniques. We have not yet utilized scanning electron microscopy (SEM), Auger Electron Spectroscopy (AES), scanning Auger Microscopy (SAM), energy dispersive spectroscopy (EDS), or surface cleaning methods out of concern that we might modify the samples.

DISCUSSION

Visual inspection showed obvious changes to the exposed areas of both copper samples, as shown in Fig. 1. The bulk sample showed a maroon

discoloration, which did not change color with viewing angle, indicating that an interference film was not responsible for the color. The discoloration on the bulk sample was very-uniform in color. The thin film sample appeared basically purple when viewed off-normal and its reflectance and appearance were more poorly defined. By transmission the exposed area appeared green, and, while basically uniform, appeared to have small traces of inhomogenieties.

Optical densitometry measurements showed considerable changes in the optical density in the visible; the unexposed copper film had an optical density of 1.33 and the exposed area had an optical density of 0.70. The changes in optical properties appear to be too great to be attributed to contamination, and the fact that contaminants on the trailing surface produced minor optical changes compared to the ram direction supports a model involving atomic oxygen interaction.

The stylus profilometry measurements were practical only on the thin film sample, because the discoloration changes were relatively thin. Changes on the order of 10's and 100's of nm are difficult to measure at steps on surfaces unless the steps are very sharp and the surface is very flat. Neither of these conditions could be satisfied for the bulk copper sample; attempting to remove fine scratches of discoloration would also scratch the underlying copper; also, steps at the knife edges of the masking cover were not distinct enough to separate them from the uneven surface of the polished, but not flat copper disk. The thin copper film of 74.2 ± 1.1 nm initial thickness, however, was deposited on a fused silica flat and both the unexposed and exposed areas were easily scratched with fine lines near the mask boundary, exposing bare silica. The square negative pulse-like traces gave good indications of the thicknesses of exposed and unexposed regions at several locations around the mask perimeter. The average thickness in the exposed area was 106.7 ± 0.5 nm. Measurements at the mask edges gave a height of the step equal to an average of 34.3 nm, in agreement with the difference in total film thicknesses.

Using literature values [1] for the copper and its oxide and assuming that film expansion occurs normal and not lateral to the surface, we can estimate what should happen to film thickness if copper is converted to an oxide. Taking the reciprocal of the copper density and multiplying this by the molecular weight and dividing by Avogadro's number gives 1.183×10^{-23} cm^3/atom as an estimate for each atom. Since film densities are usually not exactly the same as bulk densities, this is only an

approximation, but taking the cube root of this value gives 2.28×10^{-8} cm, with which we can estimate the number of copper atoms in our 74.2 nm thick film, i.e. over a 1 cm^2 area we should have about 325 atomic layers and about 6.25×10^{17} copper atoms. One-half as many Cu_2O molecules can be formed from these copper atoms; thus, finding the cm^3/molecule for Cu_2O, as before, and multiplying by 3.13×10^{17} molecules gives 1.24×10^{-5} cm^3, or 124 nm thickness over the 1 cm^2 area. Similar calculation for CuO gives 129 nm over a 1 cm^2 area. Comparing these values to the measured value of 106.7 nm, indicates that partial conversion to either oxide would expand the copper sufficiently to give the measured value for the exposed material. X-ray diffraction results so far suggest free copper predominates both exposed and unexposed areas and only hints at the presence of Cu_2O, as shown in Fig. 2; however, these studies are very difficult because of the thinness of the film and further studies designed for thin films may improve the results.

Electrical resistance measurements were performed with two probe contacts at only a couple of locations, since soldering or outer bonding techniques were not allowed, and minimal contact with the surface was desired. Values of less than 100 ohms per square were obtained in the exposed area, which was orders of magnitude higher than in the unexposed area. No temperature dependent measurements to confirm metallic or semiconducting properties have been performed yet. Resistance calculation for a copper film 74.2 nm thick gives 0.23 ohms/square, which is also the order of accuracy of the two contact measurements used.

Ellipsometry measurements were attempted on the exposed surfaces with disappointing results; as with previous attempts to measure the optical properties of silver oxide, no definitive results were obtained. We have not determined the cause of the difficulty, but suspect overlying contamination and perhaps inhomegeniety in the film itself as possible reasons for failing to get good results.

XPS measurements were carried out using Mg Kα X-rays (1253.6 eV) as the excitation source. Three specimens (two thin films, C3-16 and C9-16, and one bulk, C9-30) were analyzed which showed varying degrees of surface contamination and the atomic concentrations of the all the species on these surfaces are shown in Table 1. Cu 2p core level was used to characterize the presence of Cu_2O and CuO in addition to X-ray excited Cu $L_{2,3}M_{4,5}M_{4,5}$ Auger lines. It has been shown previously [2 and references therein] that Cu $2p_{3/2}$ from CuO is relatively broad and is

accompanied by a satellite on the high binding-energy side at about 9 eV and is due to the multiplet splitting in the $2p^5 3d^9$ final state. The Cu $2p_{3/2}$ peak from Cu_2O has a single peak which is considerably narrower and closely resembles the peak from metallic Cu. On the bulk Cu sample we obtained Cu 2p peak resembling CuO in the exposed and metallic Cu in unexposed regions, respectively. However, on the thin film specimens, only single Cu $2p_{3/2}$ peak was obtained in both exposed and unexposed regions which may be construed as indicating the presence of pure copper or Cu_2O species on the surface. This is supported by x-diffraction results discussed above. The Cu $L_{2,3}M_{4,5}M_{4,5}$ Auger spectra of CuO and Cu_2O show distinct diffrerences and their spectral shapes are considerably different. This will be discussed in detail elsewhere [3].

Eventually partial cleaning of small areas of the surfaces may be attempted by low flux argon ion bombardment through apertures, enabling profiling the film thickness, but this partially destructive technique will be delayed until other approaches have been exhausted.

Profiling the surface by optical interference techniques works best when the whole surface has similar optical properties, with preferably high reflectance. The results on the two halves with greatly different optical properties were poor, compared to the mechanical stylus profiles.

Scanning electron microscopy and energy dispersive spectroscopy will eventually be tried on a turbo pumped SEM system and perhaps with limiting apertures again. While these techniques should provide very useful results, especially on an EDS system with thin window capable of analyzing oxygen x-rays, it is important to be cautious, since electron beams can polymerize some materials like pump oil and break some bonds in other materials. We wish to investigate the surfaces further before taking these steps.

While selective modification occurred only in the ram direction, expansion of the exposed film was consistent with partial conversion to an oxide, and other supportive evidence suggests that the copper was modified by heavy oxidation in the areas exposed to the orbital ram. We lack full confirmation that this is the cause at this time.

REFERENCES

1 : "Physical Constants of Inorganic Compounds", Handbook of Chemistry and physics, P. B87-89, 52 Edition (1971), Ed. Robert C. Weast, The Chemical Rubber Co, Cleaveland, Ohio

2 : J. Ghijsen, L.H.Tseng, J. van Elp, H. Eskes, J. Westerink, G.A.Sawatzky, and M. T.Czyzk, Phys. Rev. B38 (1988) 11322

3 : G.N. Raikar, J.C.Gregory and P.Peters

Table 1

Atomic Concentration						
Unexposed Region						
Element	Cu	O	C	Si	Na	Cl
C3-16	6	21	67	5	0	1
C9-16	3	21.5	66	9	0	0.5
C9-30	5.5	25	63	5	0.5	1
Exposed Region						
Element	Cu	O	C	Si	Na	Cl
C3-16	9	23	62.5	4	0.5	1
C9-16	4	37.5	44.5	14	0	0
C9-30	9	55	18.5	17	0	0.5

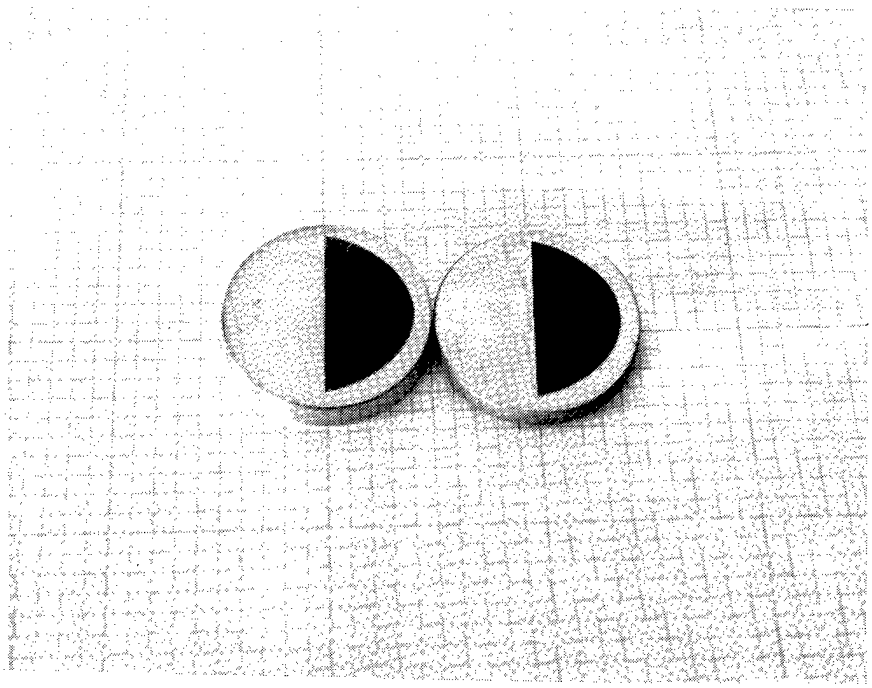


Figure 1: Photograph of the bulk and thin film copper samples from C9 tray

LDEF EXPERIMENT A0034: ATOMIC OXYGEN STIMULATED OUTGASSING

Roger C. Linton, Rachel R. Kamenetzky
and John M. Reynolds
NASA Marshall Space Flight Center
MSFC, AL 35812
Phone: 205/544-2526, Fax: 205/544-0212

Charles L. Burris
Southern University
Baton Rouge, LA 70813
Phone: 504/771-4701, Fax: 504/771-4706

SUMMARY

The passive LDEF Experiment A0034, "Atomic Oxygen Stimulated Outgassing", consisted of two identical one-sixth tray modules, exposing selected thermal control coatings to atomic oxygen and the combined space environment on the Leading Edge and, for reference, to the relative "wake" environment on the Trailing Edge. Optical mirrors were included adjacent to the thermal coatings for deposition of outgassing products. Ultraviolet grade windows and metal covers were provided for additional assessment of the effects of the various environmental factors. Preliminary results indicate that orbital atomic oxygen is both a degrading and optically restorative factor in the thermo-optical properties of selected thermal coatings. There is evidence of more severe optical degradation on collector mirrors adjacent to coatings that were exposed to RAM-impinging atomic oxygen. This evidence of atomic oxygen stimulated outgassing is discussed in relation to alternative factors that could affect degradation. The general effects of the space environment on the experiment hardware as well as the specimens are discussed.

INTRODUCTION

The interaction of atomic oxygen with materials in low earth orbit (LEO) is, for many materials, a degrading factor leading to erosion, surface modification, and emission of gaseous species. While these emitted gaseous products are generally low molecular weight byproducts of oxidation, concerns for the atomic oxygen stimulated emission of optically degrading outgassing products led to the development of the subject LDEF experiment (A0034). These concerns were primarily based on observations of the relative degree of contamination for thermal control coatings exposed to varying degrees of atomic oxygen on Skylab.

LDEF experiment A0034 was designed to provide evidence of atomic oxygen interaction with selected thermal control coatings leading to the stimulation, emission, and deposition of optically degrading outgassing byproducts on adjacent optical collector mirrors. Duplicate experiment modules were fabricated to provide exposure to atomic oxygen and the combined space environment for the module mounted on the Leading Edge (Row 9) and, for comparison, exposure to the relative "wake" environment of the Trailing Edge (Row 3). Duplicate specimens in each module were mounted under windows and opaque covers to provide some measure of effects of individual environmental factors. The experiment was passive in function, relying on comparative post-flight analysis of the exposed specimens for evaluation.

HARDWARE CONFIGURATION

Each of the modules of Experiment A0034 consisted of a top cover and a base plate, sandwiching a framework of divider plates that defined 25 individual compartments for the thermal control coating specimens (figure 1). The coatings were applied to individual substrates and mounted to the rear of the module base plate, exposing the coating by means of apertures machined in the base plate. Mirror mounts on the divider plates ensured that each of the 25 thermal coating compartments would have at least one optical mirror adjacent to each coating. Apertures machined in the top cover plates provided exposure to the space environment for each of the 25 coating compartments; in the final configuration, four top cover apertures in each module were blocked with aluminum plates, and in six others, uv-grade quartz windows were mounted to provide additional levels of environmentally controlled space exposure for the coatings.

Six types of thermal coatings were selected for flight, including five white coatings (S13G, S13G-LO, Z-93, YB-71, and A276) and one black absorber coating (Z306). The two polyurethane-based coatings, A276 and Z306, were flown in only the Leading Edge module. substrates. The polyurethane-based specimens were spray coated at MSFC, while the other specimens were all prepared, on supplied substrates, by the Illinois Institute of Technology Research Institute (IITRI).

The mirrors included in each thermal coating compartment for collection of the outgassing products were silicon monoxide overcoated aluminum on pyrex substrates, with the exception of four other types of optical reflectors included in each of the two flight units. These other reflectors included thin film gold, silver, osmium, and magnesium fluoride overcoated aluminum on glass substrates.

GENERAL POST-FLIGHT OBSERVATIONS

Whether viewed on the ground or in space, as LDEF Retrieval Mission photographs show (Figure 2), the only discernable features of the flight units, in the absence of directed

lighting, are the top covers of the two flight units with the square patterns of 25 apertures each. These covers were machined from stock 2024-T6 aluminum and chromic-acid anodized. The most obvious visible evidence of space exposure effects, excluding at this time discoloration of the thermal coating specimens, was the contrast in appearance of the Leading and Trailing Edge top covers.

Leading Edge exposure to atomic oxygen apparently "cleaned" the top cover of the C3 unit, while the top cover of the Trailing Edge unit was considerably darkened. Table 1 is a summary of the measured pre-flight and post-flight thermophysical properties of the top covers, indicating a significant increase in the solar absorptance of the exposed side of the Trailing Edge top cover. The darkened appearance and increased solar absorptance did not appreciably change following solvent wipes of the top cover of the Trailing Edge unit.

The two flight units occupied one-sixth of the tray located at position C3 on the LDEF Leading Edge and an equal berth at C9 on the Trailing Edge. As a result of the recessed and aperture-limited location of the specimen thermal control coatings, the incident integrated flux of solar radiation was restricted to a level estimated at one fourth of the direct Leading or Trailing Edge total. By contrast, the quartz windows in the top covers were directly exposed, enhancing the likelihood of uv-induced photochemical changes in contaminant layers adhering to the inner window surfaces.

The thermal coatings were exposed to the maximum level of Leading Edge RAM-impinging atomic oxygen, although evidence exists to indicate that a small outer segment of each Leading Edge coating specimen was shielded from atomic oxygen by the systematic eight degree offset in RAM exposure. The most visible evidence of this is a discolored, presumably uv-darkened, outer crescent of the A276 specimen exposed in the "open" position, a feature corresponding in location to that area likely shadowed from atomic oxygen by the RAM offset angle.

There exists considerable evidence, to be discussed later, that the contaminant collector mirrors, mounted orthogonal to each coating specimen, received significant exposure to atomic oxygen, presumably by reflection or scattering from the adjacent coating.

Most of the intrinsically white thermal control coatings of the Leading Edge unit remained relatively white following the flight mission, including specimens located under the uv-grade quartz windows (Figure 3). The exceptions are the A276 specimen located under one of the windows, which is significantly darkened by solar ultraviolet exposure, and one of the S13G specimens open to the space environment, which is lightly darkened with a reddish hue.

All of the thermal coating specimens exposed on the Leading Edge show definitive effects of exposure on closer and microscopic examination (including fluorescence observations), and many of the effects are attributable to atomic oxygen. In contrast, specimens of S13G and S13G-LO exposed directly ("open") on the Trailing Edge unit are significantly darkened. Specimens of Z-93 and YB-71 exposed on the Trailing Edge unit are much less obviously changed in appearance (Figure 4).

FLUORESCENCE OBSERVATIONS

Fluorescent emissions from the thermal control coatings under black-light illumination revealed patterns of material-dependent visible changes as a result of the space environmental exposure. Atomic oxygen and solar ultraviolet radiation are the primary factors influencing modifications in coating fluorescent behavior.

For the included six types of thermal control coatings, the induced changes in fluorescence are similar in pattern for the three zinc oxide-based coatings (Z93, S13G, and S13G-LO) as well as for the two polyurethane-based coatings (A276 and Z306). The zinc orthotitanate (YB-71) coatings provided no detectable evidence of intrinsic or induced fluorescence. The intrinsic yellow glow of the three zinc oxide-based coatings under black-light illumination is suppressed as a result of exposure on the Leading Edge. Fluorescent emission of S13G and S13G-LO directly exposed on the Trailing Edge is shifted in color to longer wavelengths (orange), while the fluorescence of Z93 specimens directly exposed on the Trailing edge is apparently suppressed to the same degree as Z93 specimens on the Leading Edge. The degrees of change induced by the various space exposure can be seen in Figure 5, a photograph taken under black-light illumination of representative A0034 specimens.

Specimens of the two polyurethane-based coatings were included only in the Leading Edge unit. Distinct fluorescent emission under black-light illumination is seen for specimens of these coatings exposed under the UV windows, excluding atomic oxygen. This induced fluorescence is generally lost as a result of exposure to atomic oxygen for specimens of these coatings on the Leading Edge, although the Z306 specimen directly exposed on the Leading Edge is faintly fluorescent when viewed, under black-light, at an angle approximately 10 degrees off-normal.

RESULTS

Window Contamination

Molecular contamination on the inner surface of the uv-grade quartz windows provided one comparable measure of the optical degradation attributable to the various types of coatings. These contaminated films are yellow and red in color and relatively strongly bonded to the inner glass surfaces.

The visible darkening of the flight windows and the measured degradation in ultraviolet transmittance are significantly greater for the windows from the Leading Edge unit compared to the windows exposed to similar coatings on the Trailing Edge. Since the inner surfaces of the sealed (teflon gasket) windows are not exposed to atomic oxygen, one cause for enhanced deposition on Leading Edge windows may be thermal in origin, arising from different susceptibilities to deposition as a result of more rapid cooling during sun/shadow transitions for

the LDEF row receiving more direct sun illumination in the (early) mission phase when outgassing should have been more prevalent.*

The transmission losses of these windows indicate the relative severity of contamination effects resulting from outgassing and solar uv-induced photochemical reaction for the various types of underlying thermal control coatings. In Figures 6 and 7, the results for windows of both flight units are provided in the form of spectral transmittance curves for each window (identified by the type of coating it was sealed with).

Thermal Control Coatings

The spectral diffuse reflectance, as a measure of solar absorptance, and the infrared thermal emittance of coatings exposed on the Leading Edge unit were generally not significantly changed as a result of the mission exposure, with the exceptions, previously mentioned, of one of the S13G specimens ($\Delta\alpha = +0.09$, $\Delta\epsilon = 0$) and the A276 specimen exposed under a uv-grade quartz window ($\Delta\alpha = +0.15$, $\Delta\epsilon = +0.05$). Measurements of thermal emittance were performed with a Gier-Dunkle DB-100 portable reflectometer. To derive the solar absorptance values, the spectral diffuse reflectance of each specimen was measured in the range 200 - 2200 nanometers using a Varian/Cary 2300 spectrometer with integrating sphere attachment and calibrated standards. While the spectral reflectance data for the visibly white coatings of the Leading Edge show little change, the differences for visibly darkened coatings from the Trailing Edge unit are significant, as the typical results for Trailing Edge control ("C") and uncovered ("O") S13G-LO indicate (Figure 8). These effects are summarized in Figure 9.

The increases for the RTV resin-bonded S13G and S13G-LO specimens on the Trailing Edge reflect the effects of space radiation exposure in the relative absence of atomic oxygen, limited by the recessed, aperture-restricted view.

The intended function of the windows on the Leading Edge, as a measure of controlled (uv only) exposure, was severely compromised by the uv-absorbing contaminant layers. Sufficient throughput of solar ultraviolet radiation for significant interaction and degradation of the underlying coating was detected for the "window-exposed" A276 specimen. The less contaminated windows of the Trailing Edge unit can be seen as more efficient, though not full function, transmitters of solar uv radiation for the radiation-sensitive coatings.

Changes in the infrared thermal emittance of most of the exposed coatings were very small, generally within the range of uncertainty for the portable reflectometer.

* Idea from Gary Jongeward, S-Cubed, Inc.

Collector Mirror Contamination

Evidence for atomic oxygen stimulated outgassing was derived from the comparative degradation of the contaminant collector mirrors. Few of these mirrors, mounted adjacent to each coating specimen in both Leading and Trailing Edge units, were visibly contaminated, though reflectance measurements indicate significant degradation for many of the "visibly clean" mirrors. The primary assumption is that measured reflectance degradation of the collector mirrors is attributable to outgassing and deposition from the adjacent coating specimen.

Spectral reflectance measurements of the silicon monoxide overcoated (140 nanometers nominal thickness) aluminum mirrors were made using the Varian/Cary 2300 spectrometer. For all of the exposed mirrors, the measured degradation was basically restricted to uv wavelengths on the order of 300 nanometers or less.

The reflectance degradation of collector mirrors from the Trailing Edge unit is generally less than for mirrors associated with similar coatings on the Leading Edge (Figure 10). The basic evidence for enhanced outgassing, and therefore greater collector mirror deposition and degradation, exists in the levels of systematically decreased reflectance of collector mirrors associated with significantly outgassing coatings exposed uncovered on the Leading Edge, compared to lesser levels of degradation for the same coatings with exposure in the absence of atomic oxygen (Figure 11). Another series of optical measurements sensitive to contaminant layer thickness, using an automated ellipsometer (Gaertner L115B), also indicated a systematic pattern of enhanced degradation for collector mirrors exposed to uncovered (open) thermal control coatings on the Leading Edge.

Ranking the thermal control coatings for relative severity of induced optical effects has been attempted on the basis of both the collector mirror reflectance degradation (@ 300 nm) and the transmission loss of the contaminated uv windows (Figure 12), for specimens exposed on the Leading Edge. The reversal of ranking of the coatings based on collector mirror reflectance degradation compared to window transmission loss is one measure of the potentially significant role of uv-induced photochemical change in determining the optical effects of contamination.

Degradation of the reflectance of the collector mirrors by the natural space environment is an alternative mechanism that was considered. Evaluation of the silver and osmium mirrors in each of the flight units provided direct evidence of the complete oxidation of the silver film and the complete oxidation and evaporative removal of the osmium film on the Leading Edge, and substantial oxidation of the corresponding thin film mirrors on the Trailing Edge. The results indicate substantial atomic oxygen fluence reflected or scattered from the adjacent coating for both the Leading Edge and, to a lesser degree, the Trailing Edge.

The magnesium fluoride (MgF2) filter included in the Leading Edge unit was measurably degraded in transmittance at center bandwidth (220 nm) wavelengths. Another magnesium fluoride filter, included as a guest sample on the adjacent A0114 experiment (Gregory and Peters), and directly exposed to atomic oxygen on the Leading Edge, was significantly degraded

at center bandwidth (140 nm) wavelengths and the transmission shifted to longer wavelengths. Corresponding filters exposed on the Trailing Edge were not measurably degraded.

More direct evidence for atomic oxygen interaction with the (SiO) collector mirrors, from a stylus profilometer ("Talleystep") trace of one of the exposed mirrors from the Leading Edge unit, indicated a decrease in thickness of the silicon monoxide in the exposed area compared to the protected outer edge.

CONCLUDING REMARKS

Material dependent fluorescence changes induced in the coatings as a result of the space exposure were found to be governed primarily by atomic oxygen and solar ultraviolet exposure. Detailed spectral measurements of fluorescent emission are being obtained to correlate with the flight specimen black-light observations. Laboratory atomic oxygen and uv exposure testing of these types of specimens are in progress to investigate the nature of these induced effects.

Evaluation of the optical degradation of the contaminated collector mirrors, including the results of both spectral reflectance and ellipsometer measurements, provides evidence for increased (stimulated) levels of outgassing for coatings exposed to atomic oxygen.

The optical effects of the deposited contamination and the relative rankings of coatings for severity of degradation as a result of deposition were significantly affected by solar radiation. The significance of ultraviolet wavelength irradiance in the degradation of these thermal coatings is revealed in the contrasting degradation of uv-sensitive specimens on the Trailing Edge compared to specimens exposed under the contaminated windows of the Leading Edge.

Some obvious discrepancies in the response to space exposure for a few of the coating specimens, compared to the average response observed for specimens of a type, indicate the existence of batch variations which must be considered in generalized predictions of response to space exposure.

ACKNOWLEDGEMENTS

The authors wish to thank Dr. Robert L. Scott, Jr. for invaluable contributions as the original Principal Investigator. Additionally, appreciation is expressed for the contributions of: James Morgan of Southern University; Marcus Thomas of Sverdrup, Inc.; Yosh Harada and Richard Mell of IITRI; Roger Harwell, John Trenkle, Lou Ann Fikes, Floyd Roberts, Whitney Hubbs, and Joey Norwood of MSFC; James Hathaway of University of Alabama in Huntsville.

TABLE 1. - OPTICAL PROPERTIES OF TOP COVER
(ANODIZED ALUMINUM)

	Leading Edge Exposed Front		**Trailing Edge** Exposed Front	
	α	ϵ	α	ϵ
Mean	0.35 - 0.42 0.38	0.11 - 0.16 0.13	0.46 - 0.49 0.47	0.09 - 0.17 0.13
	Unexposed Back		Unexposed Back	
Mean	0.40 - 0.46 0.42	0.13 - 0.16 0.15	0.40 - 0.50 0.45	0.08 - 0.18 0.14

Summary: $\%\Delta\alpha$ (Mean) = 23.7 RAM/WAKE

TABLE 2. - CONTAMINANT COLLECTOR MIRRORS -
EFFECTS OF THE NATURAL ENVIRONMENT

MIRROR TYPE	LEADING EDGE	TRAILING EDGE
SiO/PYREX	CONTAMINANT COLORATION	
OSMIUM/QUARTZ	TOTAL REMOVAL (60nm) (ESTIM. REFLECTED FLUENCE ≥ 2E20 ATOMS/CM2)	PARTIAL REMOVAL (ESTIM. REFL. F≃ 1E19 ATOMS/CM2)
SILVER/QUARTZ	OXIDIZED/REMOVED (ESTIM. REFL. FLUENCE> 1E19 ATOMS/CM2)	OXIDIZED (ESTIM. REFL. F≃ 9E18 ATOMS/CM2)
GOLD/QUARTZ	SLIGHT VISUAL DIFF.	NO OBVIOUS EFFECT
MgF2/A1	NO VISIBLE EFFECT (UV TRANSMISSION EFF.)	NO VISIBLE EFFECT (UV %T EFFECT)

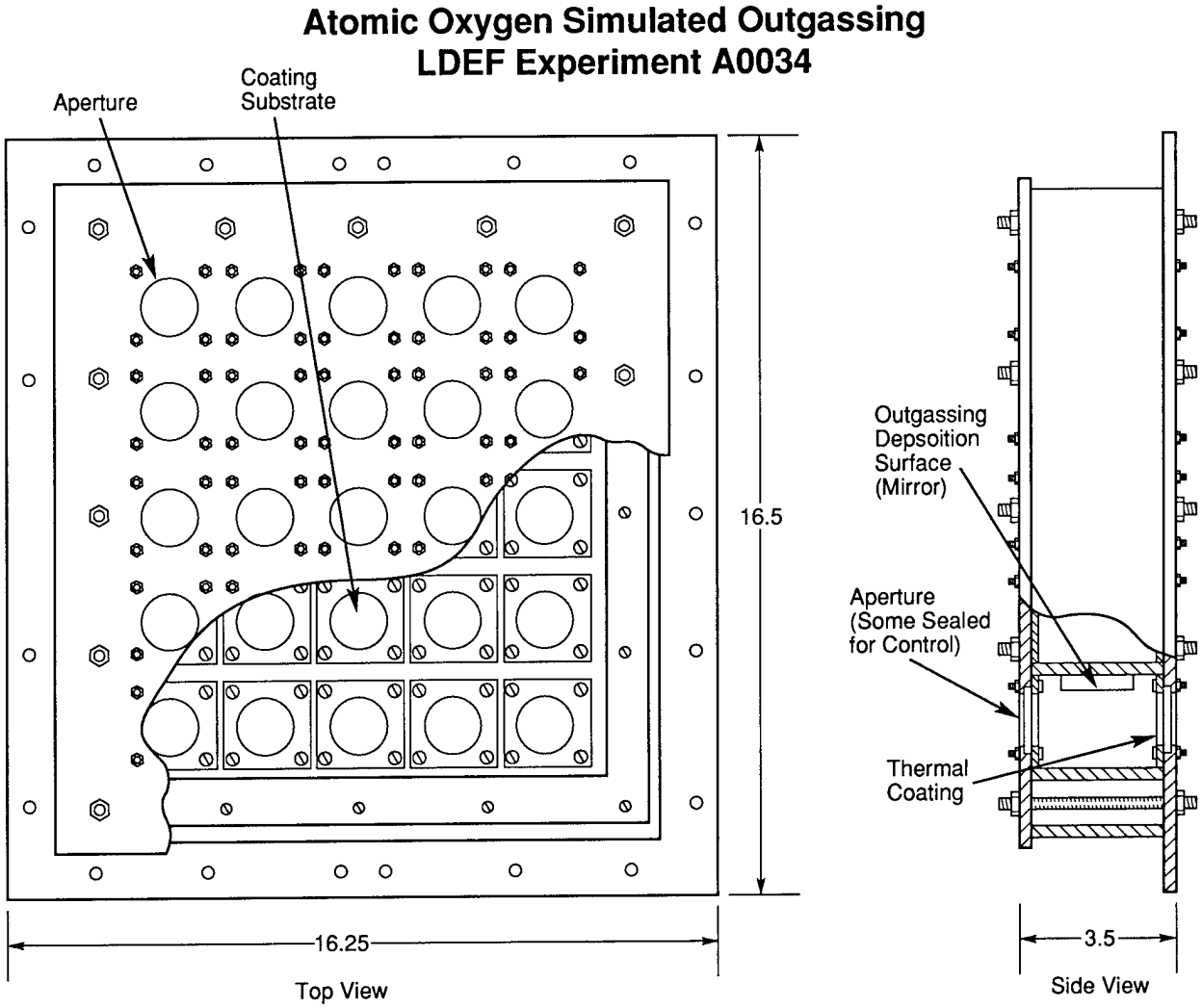


FIGURE 1. SCHEMATIC OF LDEF EXPERIMENT A0034

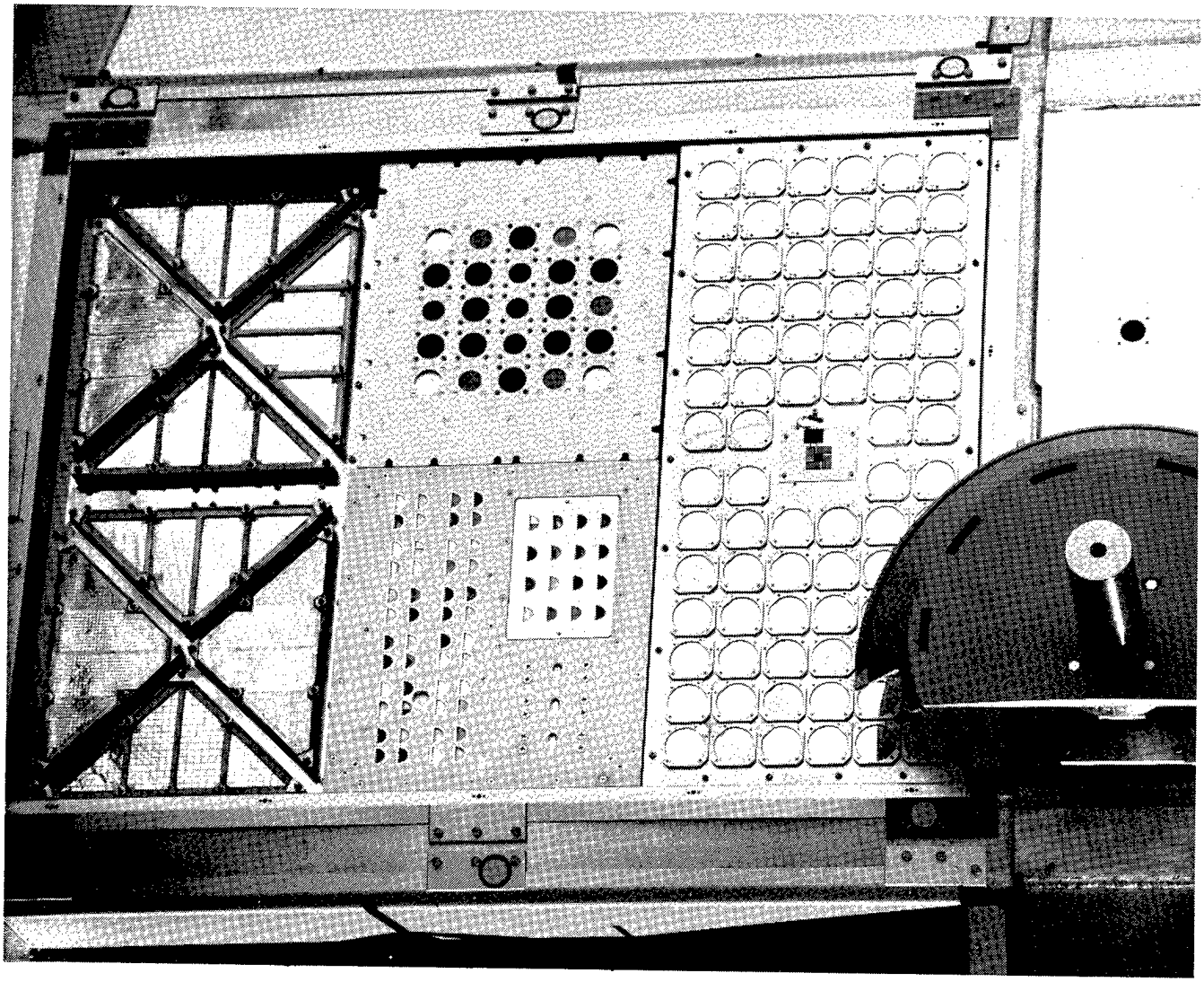


FIGURE 2. STS-32 ONBOARD VIEW - A0034 ON TRAILING EDGE

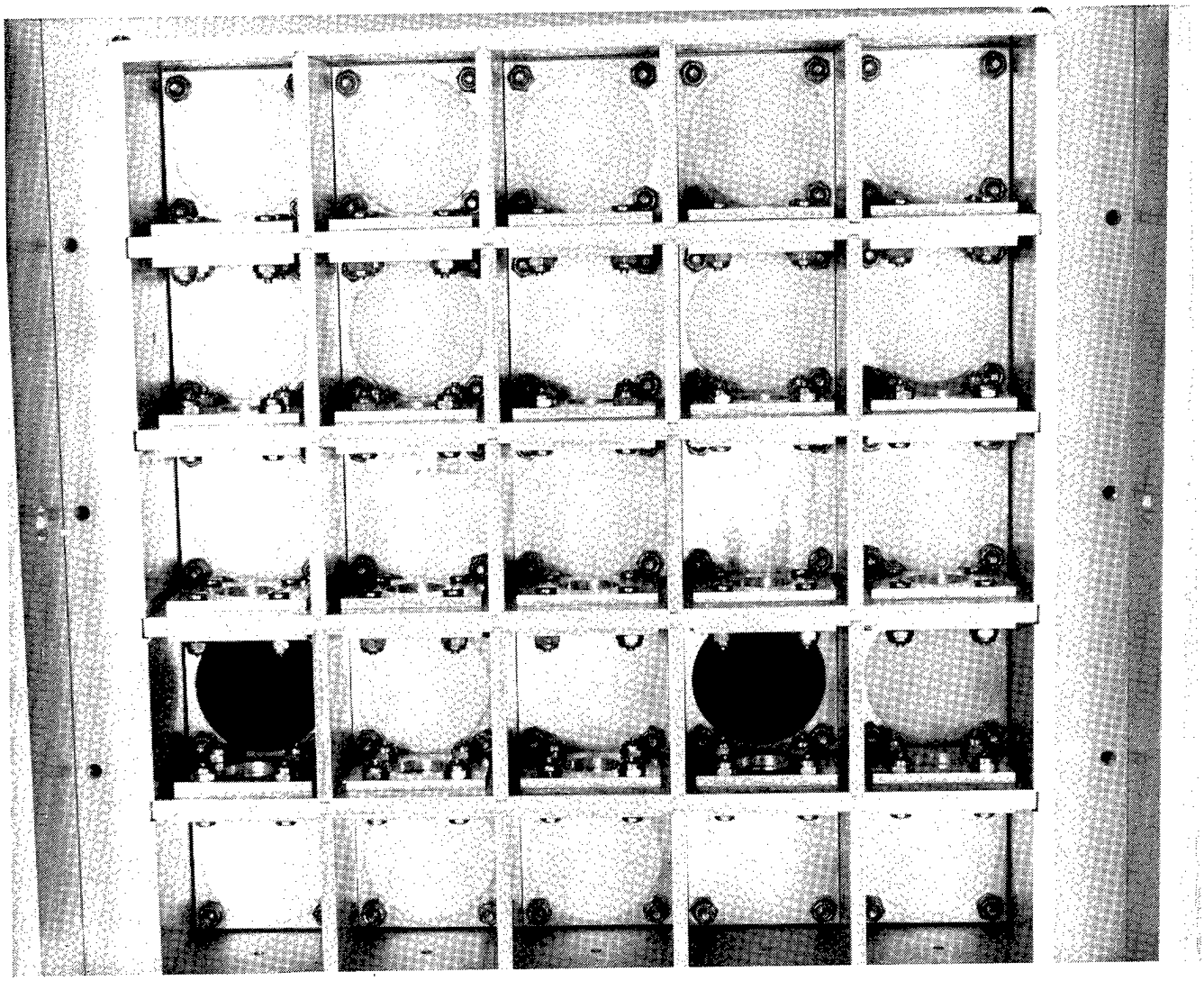


FIGURE 3. LEADING EDGE COATING SPECIMENS - COVER REMOVED

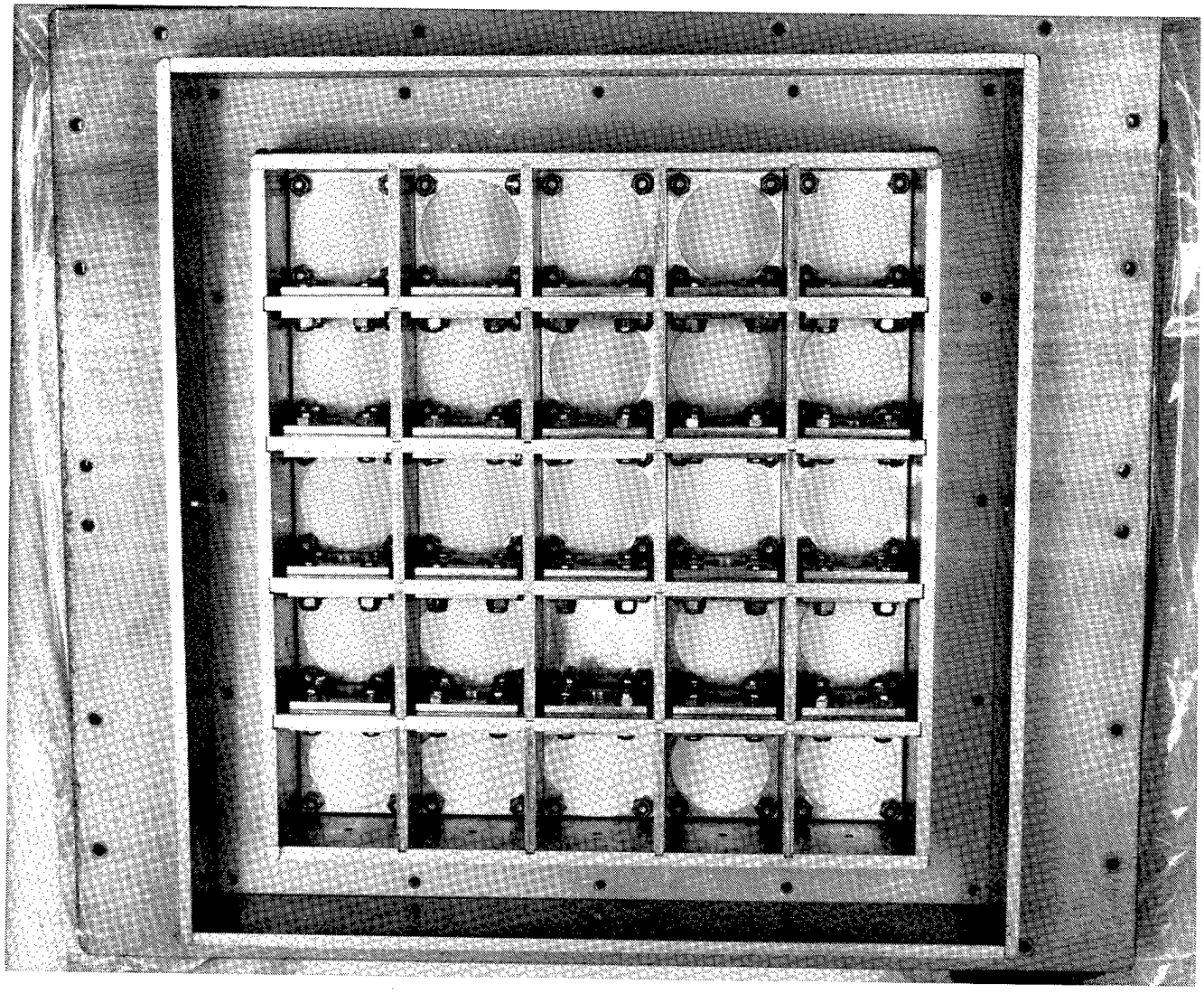


FIGURE 4. TRAILING EDGE COATING SPECIMENS - COVER REMOVED

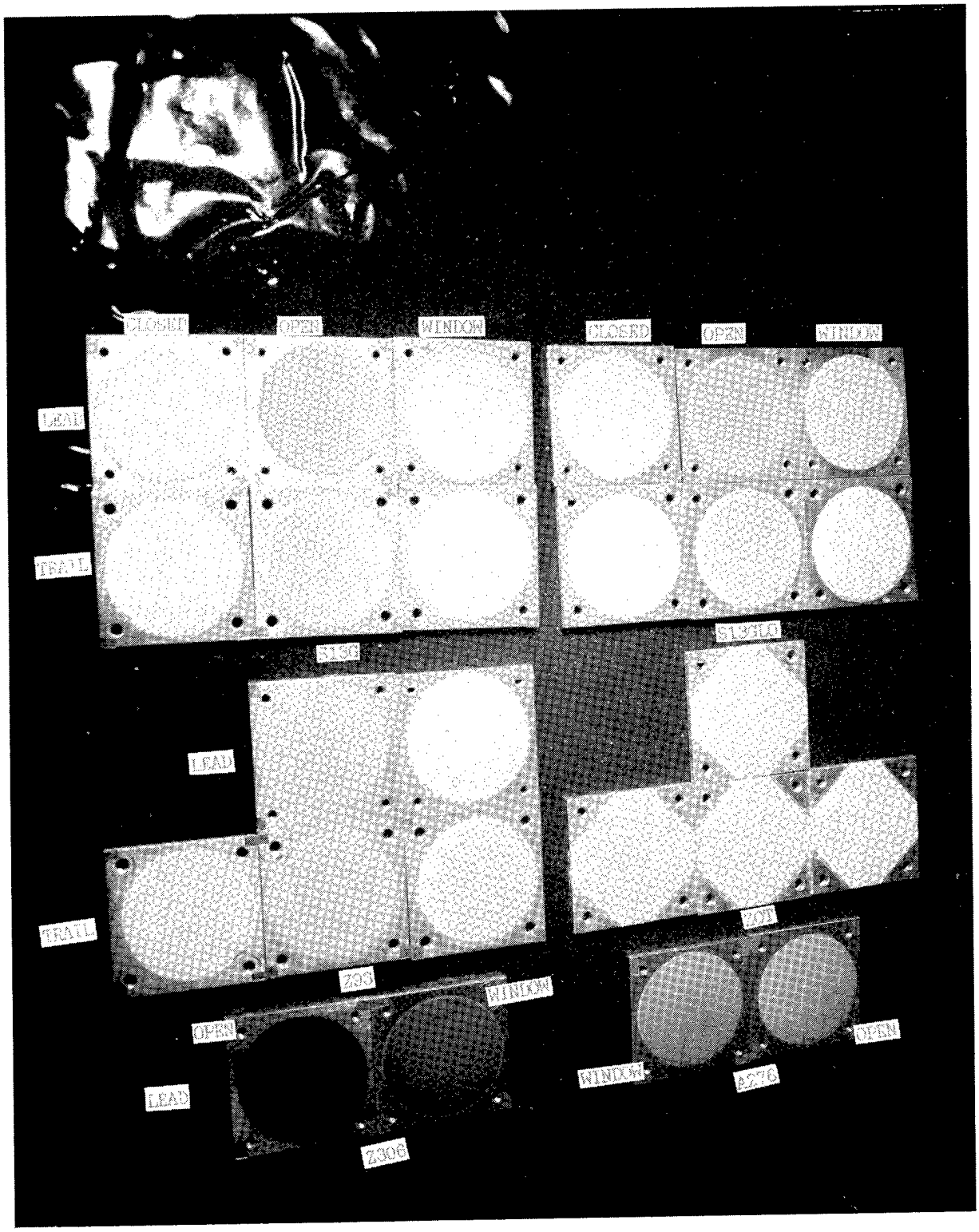


FIGURE 5. BLACK-LIGHT ILLUMINATED FLUORESCENCE OF COATINGS

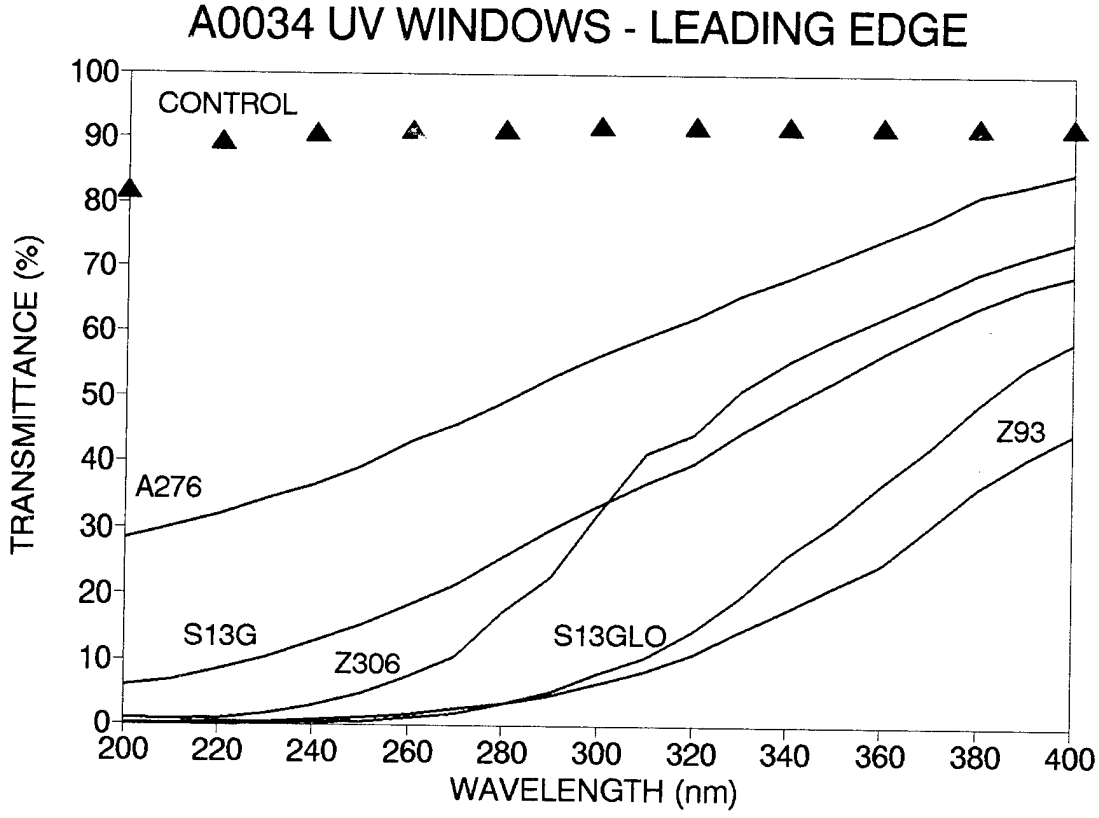


FIGURE 6. UV WINDOW TRANSMISSION LOSS - LEADING EDGE

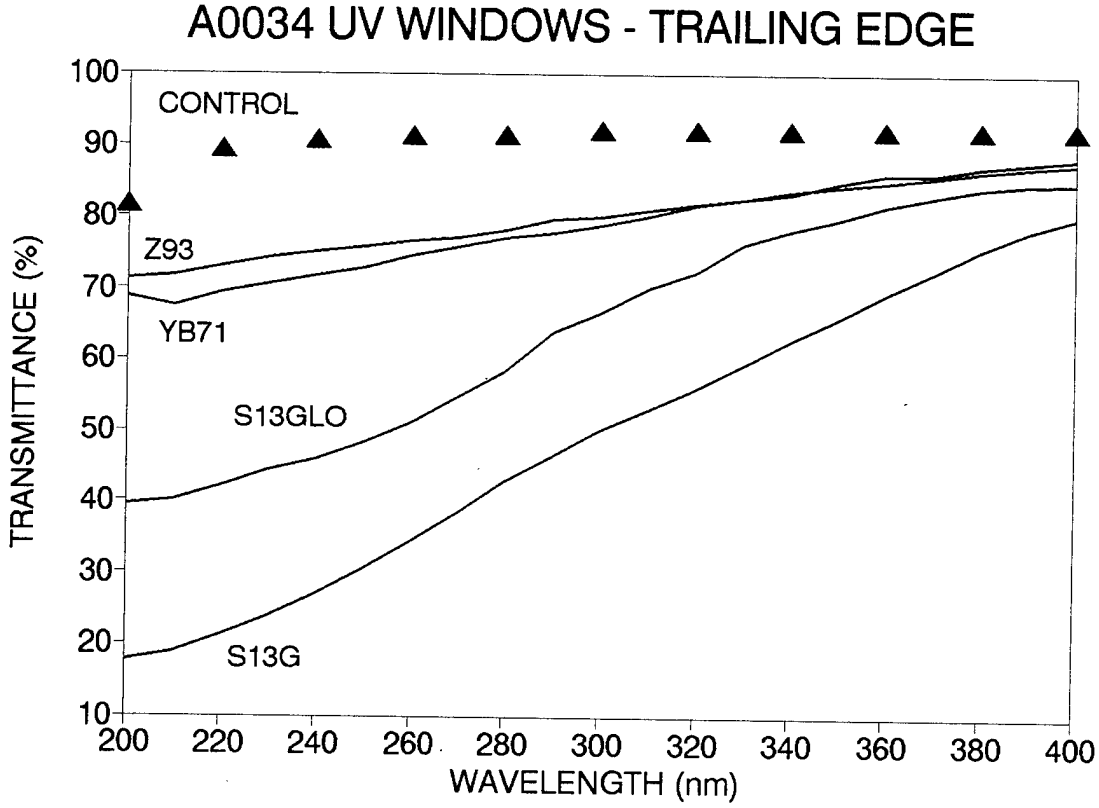


FIGURE 7. UV WINDOW TRANSMISSION LOSS - TRAILING EDGE

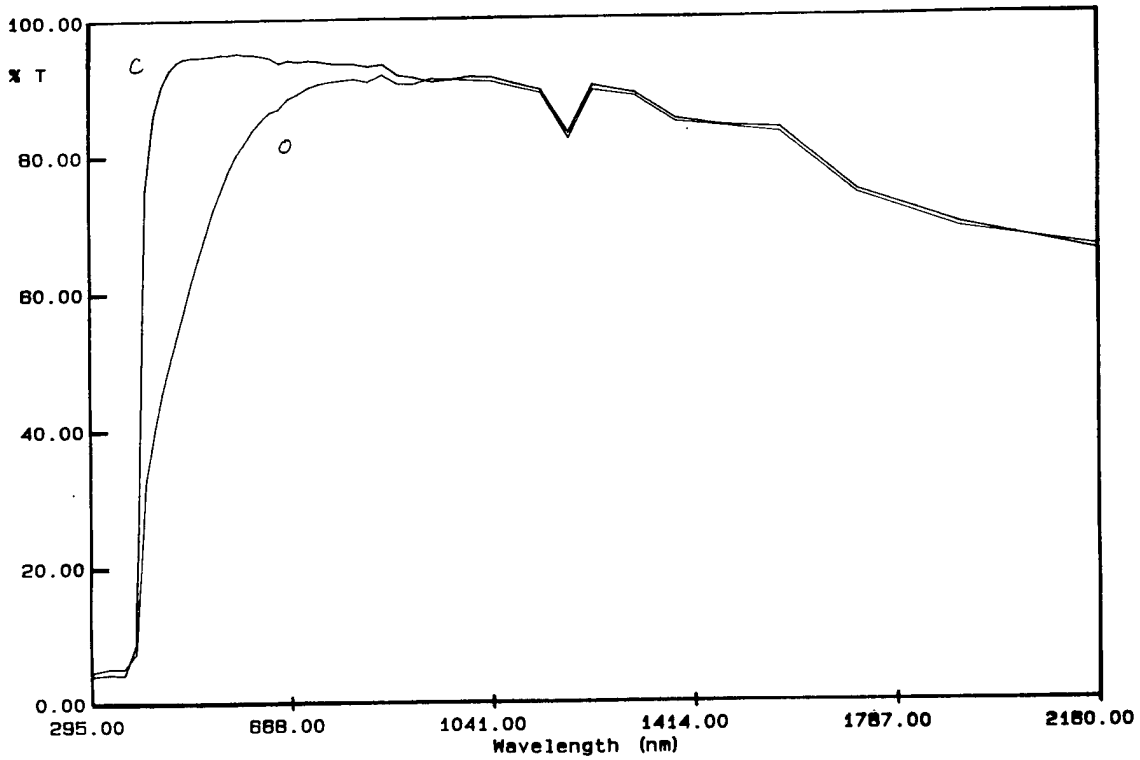


FIGURE 8. OPTICAL DEGRADATION OF S13G-LO (TRAILING EDGE)

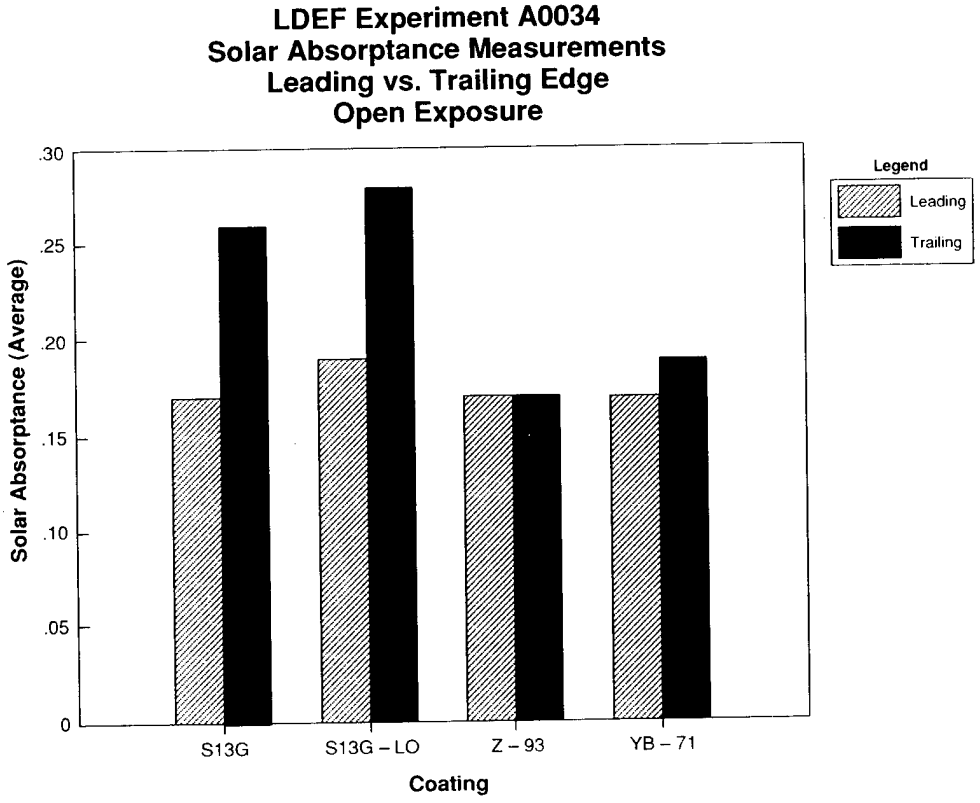


FIGURE 9. SOLAR ABSORBTANCE SUMMARY - LEADING VS. TRAILING

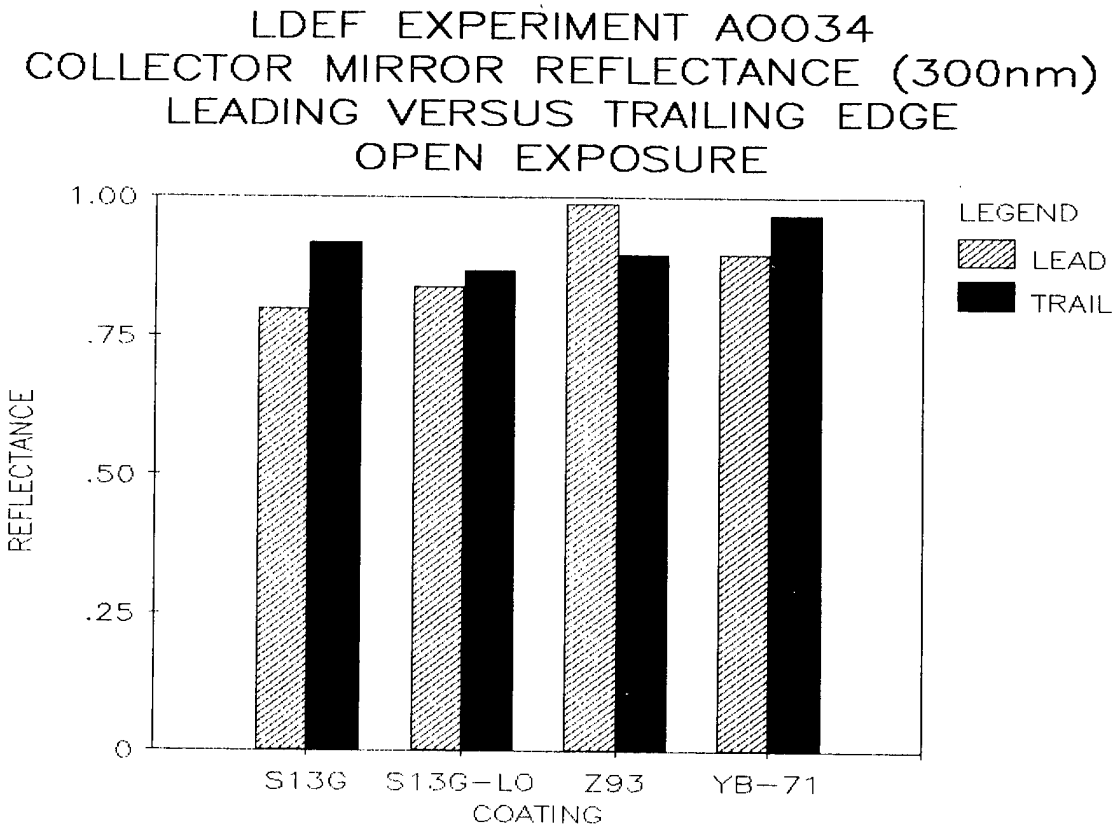


FIGURE 10. COLLECTOR MIRROR REFLECTANCE - LEADING VS. TRAILING

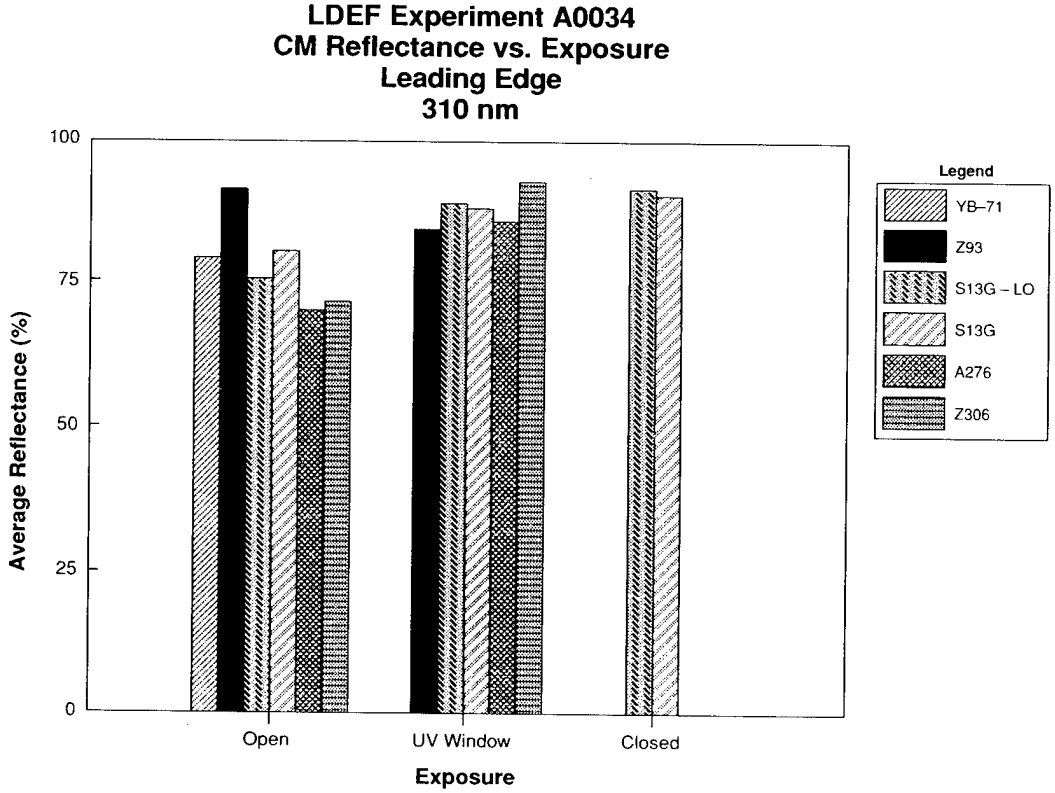


FIGURE 11. COLLECTOR MIRROR REFLECTANCE - LEADING EDGE (OPEN)

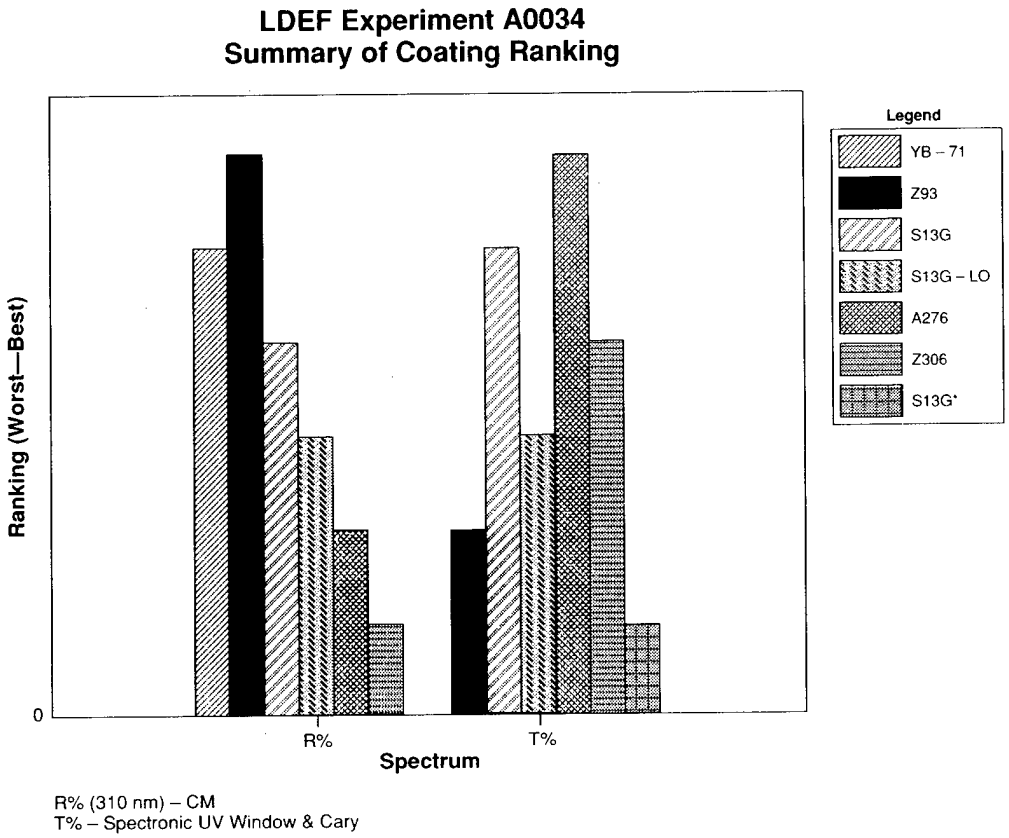


FIGURE 12. SUMMARY OF COATING RANKING - REFLECTANCE/TRANSMITTANCE

ATOMIC OXYGEN UNDERCUTTING OF LDEF ALUMINIZED-KAPTON MULTILAYER INSULATION

Kim K. de Groh
Bruce A. Banks
NASA Lewis Research Center
Cleveland, OH 44135
Phone: 216/433-2297, Fax: 216/433-6106
Phone: 216/433-2308, Fax: 216/433-6106

SUMMARY

Atomic oxygen undercutting is a potential threat to vulnerable spacecraft materials which have atomic oxygen protective coatings. Such undercutting is due to atomic oxygen attack of oxidizable materials at microscopic defects in the protective coatings. These defects occur during fabrication and handling, or from micrometeoroid and debris bombardment in space. An aluminized-polyimide Kapton multilayer insulation sample that was located on the leading edge of the Long Duration Exposure Facility (LDEF) has been used to study low Earth orbit directed ram atomic oxygen undercutting. Cracks in the aluminized coatings located around vent holes provided excellent defect sites for evaluation of atomic oxygen undercutting. The experimentally observed undercutting profiles were compared to predictions from Monte Carlo models for normal incident ram atomic oxygen attack. The shape of the undercut profile was found to vary with crack width, which is proportional to the number of oxygen atoms entering the crack. The resulting profiles of atomic oxygen undercutting which occurred on LDEF indicated wide undercut cavities in spite of the fixed ram orientation. Potential causes of the observed undercutting are presented. Implications of the undercutting profiles relevant to Space Station Freedom are also discussed.

INTRODUCTION

In low Earth orbit (LEO) a harsh environment exists which can cause considerable damage to vulnerable spacecraft materials. The environment experienced by orbiting spacecraft includes atomic oxygen, ultraviolet radiation, thermal cycling, and micrometeoroid and debris bombardment.[1] Atomic oxygen, the predominant species in LEO[2], is extremely reactive, particularly at ram impact energies (≈4.5 eV). Materials that are susceptible to oxidation must be protected when used for long durations in LEO. Atomic oxygen attack of protected oxidizable materials can occur at microscopic pin hole defects (voids) or scratches in the protective coatings which are a result of fabrication and handling, or due to micrometeoroid and debris bombardment. Oxidation of underlying materials at defect sites causes undercutting. Atomic oxygen undercutting can produce cavities in the oxidized material which are larger than original defect in the protective coating. Atomic oxygen undercutting can result in the degradation of several materials properties (i.e. mechanical, optical, etc.), which

may affect system performance. Undercutting may also cause further damage to the protective coating if the protective coating tears or curls when undercut. This damage mechanism of undercutting and tearing will likely propagate and lead to structural failures. Spacecraft materials which have shown a tendency to degrade (based on ground-based atomic oxygen evaluation) through an undercutting-tearing propagation mechanism include early configuration photovoltaic solar array blanket materials[3] and solar concentrator materials[4] for Space Station Freedom (SSF). Other spacecraft materials that have the potential for degradation through undercutting include fiber glass epoxy composite structural members used for photovoltaic array extension or any oxidizable material shielded with a protective coating. As a result of the potential damaging effects of atomic oxygen undercutting, efforts have been made to understand and model the erosion processes that occur in various atomic oxygen environments (normal incident space ram, sweeping (sun tracking) space ram, ground-based directed atomic oxygen, ground-based sweeping atomic oxygen and plasma asher atomic oxygen exposure). Monte Carlo models have been developed for protected Kapton polyimide substrates, based on ground-based undercutting profiles at scratch sites, which predict atomic oxygen undercutting profile responses in various space and ground-based atomic oxygen environments.[5,6] Comparison of the Monte Carlo predicted LEO undercut profiles with actual space flight samples should contribute to the understanding of LEO materials durability as predicted by ground-based testing.

The Long Duration Exposure Facility was in orbit for 5.8 years. This provided an excellent opportunity to study the effects of LEO directed ram atomic oxygen undercutting. Undercutting of protected oxidizable materials at defect sites on ram facing surfaces was expected to occur on LDEF even though LDEF was in a fixed orbital orientation because of atomic oxygen velocity components which are transverse to the ram direction. Three causes of atomic oxygen transverse velocity components have been identified which contribute to directed ram undercutting. The first of these components involves scattering of unreacted atomic oxygen. Upon entering a hole in the protective coating, atomic oxygen has a low probability of reaction on first impact (≈14% for Kapton[6]). The unreacted atomic oxygen is scattered approximately with a cosine distribution. Unreacted atomic oxygen scattered below the protective coating may have multiple opportunities to react with the substrate material causing undercutting (see figure 1). The second transverse velocity component contributing to undercutting involves the thermal velocity of atomic oxygen. Atomic oxygen in LEO during the LDEF mission had an average temperature of 1227 K.[7] Therefore a Maxwellian distribution of speeds of the atomic oxygen existed having random orientation which was vectorially added to the orbital ram velocity. The result is that atomic oxygen impact velocities had a distribution of directions and energies. The thermal velocity of an average energy oxygen atom for LDEF altitudes was ≈1.4 km/sec. The maximum misalignment from ram direction of an average energy oxygen atom is calculated to be ≈10° (see figure 2). Thus, there was a significant angular distribution of atomic oxygen flux impacting LDEF due to thermal velocity contributions. The third transverse velocity component occurred because the orbit of LDEF was at a ≈28.5° inclination with respect to the Earth's atmospheric velocity vector. This caused the ram atomic oxygen direction to sweep sinusoidally in LDEF's horizontal plane. Figure 3 shows schematically how the ram atomic oxygen direction varied by ≈3.7°. An atmospheric velocity of 0.493 km/sec and an orbital velocity of 7.673 km/sec were used to calculate the 1.86° ram velocity sweep from the fixed orbital orientation.

As a result of the thermal and orbital inclination contributions, there was a Gaussian distribution of atomic oxygen flux with respect to angle from ram impacting LDEF. Because of the orbital inclination, the angular flux distribution was wider in LDEF's horizontal plane than in its vertical plane. This is shown schematically in figure 4. To visualize what effect the variation in flux distribution in LDEF's horizontal and vertical planes can have on LDEF materials, one can consider a pin hole camera containing an oxidizable material, located on LDEF's leading edge. It would be expected that an elliptical erosion region would occur with the longest axis in LDEF's horizontal plane (see figure 5). All these contributions (scattering, thermal velocity, orbital inclination) combined with LDEF's 8° yaw off-set[8], result in a more complex interaction and resulting atomic oxygen erosion process than the more simplistic result that one might expect of atomic oxygen arriving from only the fixed orbital orientation.

An aluminized-Kapton multilayer insulation (MLI) sample which was located on the leading edge of LDEF (F-9), was used to study LEO directed atomic oxygen undercutting. Undercutting profiles were compared to Monte Carlo models that predict LEO ram atomic oxygen attack. Variations in the undercut profiles between various crack sizes, and between cracks that were located in the vertical and horizontal planes of LDEF are presented. These results provide evidence of the complex interactions which LEO directed atomic oxygen can have on spacecraft, and the potentially damaging effect undercutting can have on vulnerable materials which have defected protective coatings.

EXPERIMENTAL PROCEDURES

Material

The material evaluated in this study was an aluminized-Kapton multilayer insulation sample from the McDonnell Douglas Cascaded Variable Conductance Heat Pipe Experiment, Experiment A0076[9] (see figure 6). This sample was located on the leading edge of LDEF (row F-9), and was exposed to directed ram atomic oxygen. The Kapton was 0.0076 mm (0.3 mil) thick, with vent holes, and aluminized (1000Å) on both sides. The sample was launched with an exterior layer of 0.0762 mm (3 mil) thick Kapton containing no vent holes, aluminized only on its unexposed side. The exterior layer of Kapton was completely oxidized well before the retrieval of LDEF, causing loss of the unsupported Al, and exposing the underlying protected MLI Kapton to atomic oxygen.

Fluence Exposure

The LDEF ram atomic oxygen fluence for 0° yaw off-set has been determined to be 8.40 x 10^{21} atoms/cm^2.[7] Unfortunately, LDEF orbited slightly misaligned about the yaw axis such that Row 9 was not facing perpendicular into the velocity direction. Row 12 faced slightly into the ram atomic oxygen direction and row 6 was tilted away from the ram atomic oxygen. Misalignment of the surfaces from the velocity direction alters the atomic oxygen fluence. Based on an average of four types of measurements, the LDEF yaw misorientation has been

estimated to be 8°.[8] The current calculated fluence for row 9, at an 8° yaw off-set from ram, has been determined to be 8.32 x 10^{21} atoms/cm^2. [7]

Because the MLI sample was covered with a sheet of 0.0762 mm (3 mil) Kapton, the atomic oxygen fluence of the MLI sample is equal to the LDEF 8° yaw misalignment fluence for Row 9 minus the fluence necessary to erode away the Kapton. The fluence necessary to erode the Kapton cover sheet is equal to the thickness of the Kapton (0.0762 mm) divided by the erosion yield of Kapton. The erosion yield of Kapton at 8° off normal is the erosion yield for normal incidence multiplied by $(\cos 8°)^{1/2}$, because the ram atomic oxygen erosion yield of Kapton has been found to be dependent on $(\cos\theta)^{1/2}$. [5] This fluence is calculated to be 2.55 x 10^{21} atoms/cm^2. An erosion yield of 3 x 10^{-24} cm^3/atom for Kapton was assumed based on space flight data.[10,11] The resulting atomic oxygen fluence for the MLI sample is calculated to be 5.77 x 10^{21} atoms/cm^2.

Atomic Oxygen Undercutting Evaluation

Small sections of the MLI sample were mounted with the atomic oxygen exposed side up, onto aluminum scanning electron microscope (SEM) stubs using carbon paint. These samples were then examined using a JEOL JSM-840A Scanning Microscope. Characteristic micrographs were taken of defect sites, including pin hole defects and microscopic cracks in the aluminization. Crack width measurements were obtained from electron micrographs of the aluminum-coated Kapton. Samples were then soaked in slightly diluted hydrochloric acid to remove the aluminum film. The samples were then remounted, coated with ≈150Å of gold, and re-examined with the SEM. Identical locations were imaged so that defect widths could be directly compared with the undercut width. Undercut profile images of these areas were obtained by tilting samples, with the aluminum removed, at high tilt angles (60-75°).

Monte Carlo Model Comparisons

Predicted Monte Carlo undercut profiles are shown in Figure 7 for normal incident space ram and sweeping space ram atomic oxygen exposure conditions. Because both modeled exposures do not take into account angularly distributed velocity variations associated with the Maxwellian speed distribution and orbital inclination components, it is expected that the observed LDEF undercutting profiles would be shaped somewhere between the normal incident and sweeping space ram predictions. Details of the Monte Carlo model are described in reference 5.

RESULTS AND DISCUSSIONS

Initial examination of the MLI sample revealed wide undercutting at defect sites. Figure 8 shows extensive undercutting at pin hole defects. The degree of undercutting was extensive compared to Monte Carlo models for normal incident space ram. Although this was expected because the model does not take into consideration thermal or orbital inclination contributions

to undercutting, an additional mechanism unique to this space experiment has been identified which may have contributed to undercutting. When the Kapton cover layer was partially oxidized causing holes in the cover layer, atomic oxygen probably entered the holes and scattered around between the bottom of the aluminized cover layer and the first MLI layer. This would cause a more isotropic arrival of atomic oxygen during the period of partial loss of the cover layer than would be experienced during directed ram exposure. This scattering process is shown schematically in figure 9.

The size and shape of undercutting was found to vary with crack size, which is proportional to the number of oxygen atoms entering the defect. Smaller cracks were found to have U-shaped undercut profiles which were wider at the Kapton/aluminum interface than at the base of the profile. Wider cracks had more circular undercut regions and the undercut profile was wider at the base than at the Kapton/aluminum interface (see figure 10). Figure 11 schematically shows the difference in undercut profiles for wide and narrow cracks. Because the ram atomic oxygen swept parallel to horizontal cracks and perpendicular to vertical cracks (see figure 12), it was expected that there would be a difference in the undercut profiles for vertical and horizontal cracks. Because the MLI sample had concentric cracks around the vent holes, a comparison could be made between the undercut profiles of vertical and horizontal cracks on LDEF. Figure 13 shows electron micrographs of wide horizontal cracks with and without the aluminum coating. Figure 14 shows electron micrographs of comparably wide vertical cracks with and without the aluminum coating. By tilting the sample with the aluminum removed, the undercut profiles for these horizontal and vertical cracks can be seen (see figure 15). There are some distinct differences between the undercut profiles for horizontal and vertical cracks. The horizontal crack profiles are rounded at the base and have a shallow pit burrowed in the bottom along the crack length. The vertical crack profiles are wider and smooth at the base. Figure 16 shows similar trends for undercut profiles of narrow horizontal and vertical cracks. The variation in the undercut shapes may be possible because the directed atomic oxygen direction swept parallel to horizontal cracks (causing a deeper undercutting) and swept perpendicular to vertical cracks (causing a widening and smoothing effect) as seen in figure 17. The off-center burrowed pits of the horizontal crack profiles and unsymmetric shape of the vertical crack profiles can be attributed to the 8° yaw offset. In addition to LDEF's aluminized-Kapton MLI cracks having a difference in the undercut profile shape of horizontal and vertical cracks, vertical cracks had wider undercut widths than horizontal cracks of the same size (see figure 18). Undercut widths exceeded crack widths by a factor of 2.5 to 12.5 for horizontal cracks, and 3.1 to 16.6 for vertical cracks. These undercut widths were measured at the Kapton/Al interface; however for wide cracks, the degree of undercutting was more severe because the base of the undercut profile was larger than at the measured interface.

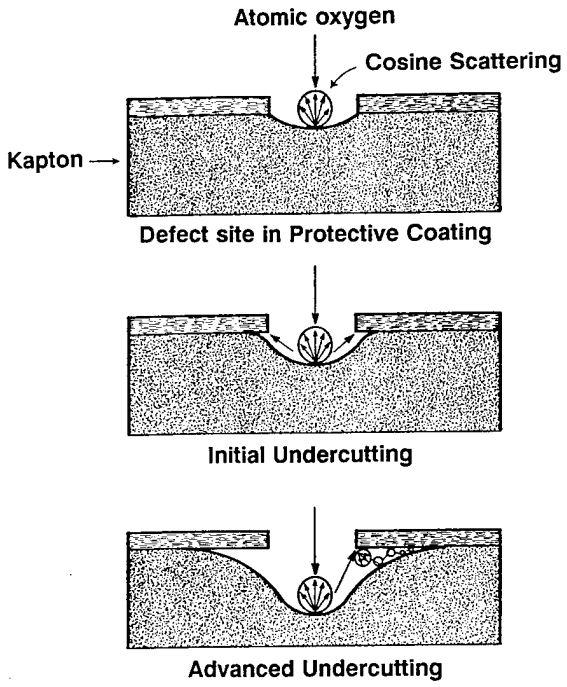
CONCLUSIONS

Cracks in the aluminization of a Kapton MLI sample flown on the leading edge of LDEF allowed characterization of LEO directed ram atomic oxygen undercutting. Atomic oxygen undercut profile shapes and sizes were found to vary with crack width which is proportional to the number of oxygen atoms entering the crack. Narrow cracks had U-shaped profiles which

were wider at the top than the bottom. Wider cracks had more circular undercut profiles which were wider at the bottom than the top. The orbital inclination of LDEF with respect to the Earth's atmospheric velocity vector caused the ram atomic oxygen direction to sweep sinusoidally in LDEF's horizontal plane. The sweeping ram direction caused a variation in the undercut profiles for horizontal and vertical cracks. Horizontal crack undercut profiles were rounded and had shallow pits burrowed along the base. Vertical crack undercut profiles were wider and smooth at the base. In addition to having a variation in the shape of the undercut profiles, vertical cracks had wider undercut profiles than horizontal cracks of the same width. Undercut widths exceeded crack widths by a factor of 2.5 to 12.5 for horizontal cracks, and 3.1 to 16.6 for vertical cracks. This may also be attributed to the orbital inclination contribution to atomic oxygen undercutting. Undercut profiles of cracks in aluminized-Kapton MLI located on the leading edge of LDEF were found to be wider than predicted by current Monte Carlo models for pure fixed ram. This is probably because the Monte Carlo model did not take into consideration thermal velocity or orbital inclination contributions to atomic oxygen undercutting as well as a period of time when isotropic arrival of atomic oxygen possibly occurred during partial loss of the MLI cover layer.

REFERENCES

1. Gulino, D. A.: Space Station Solar Concentrator Materials Research. NASA TM 100862, 1988.
2. U.S. Standard Atmosphere, 1976, U.S. Govt. Printing Office, Washington, DC, 1976, p. 30.
3. Rutledge, S. K.; and Mihelcic, J. A.: Undercutting of Defects in Thin Film Protective Coatings on Polymer Surfaces Exposed to Atomic Oxygen. NASA TM 101986, 1989.
4. de Groh, K. K.; Terlep, J. A.; and Dever, T. M.: Atomic Oxygen Durability of Solar Concentrator Materials for Space Station Freedom. Proceedings from the 5th Annual Air Force Workshop on Surface Reactions in the Space Environment, Evanston Il, 1990.
5. Banks, B. A.; Auer, B. M.; Rutledge, S. K.; and Hill, C. M.: Atomic Oxygen Interaction with Solar Array Blankets at Protective Coating Defect Sites. Proceedings from the SOAR Symposium, Albuquerque, NM, June, 1990.
6. Banks, B. A.; Rutledge, S. K.; Auer, B. M.; and DiFilippo, F.: Atomic Oxygen Undercutting of Defects on SiO_2 Protected Polyimide Solar Array Blankets. Materials Degradation in Low Earth Orbit (LEO). The Minerals, Metals & Materials Society, 1990, pp. 15-33.
7. Bourassa, R. J.; and Gillis, J. R.: Data Summary - Atomic Oxygen Flux and Fluence Calculation for LDEF. Boeing Defense and Space Group, Seattle, WA, 1990.
8. Kinard, W. ed.: LDEF Spaceflight Environmental Effects Newsletter, Vol. II, No. 1, March 1991, pp. 3-4.
9. Grote, M. G.; Calhoun II, L. D.: Cascade Variable-Conductance Heat Pipe (A0076). The Long Duration Exposure Facility (LDEF) Mission 1 Experiments, NASA SP-473, 1984, pp. 66-69.
10. Leger, L. J.; and Visentine, J. T.: A Consideration of Atomic Oxygen Interactions with the Space Station. J. Spacecraft, Vol. 23, No. 5, Sept.-Oct. 1986, pp. 505-511.
11. Banks, B. A.; de Groh, K. K.; Rutledge, S. K.; Stueber, T. J.; Dever, T. M.; and Hotes, D.: Performance and Durability of Space Solar Dynamic Power System Optical Surfaces. Solar Engineering 1990, The American Society of Mechanical Engineers, NY, 1990.



- ≈14% reaction probability on first impact for Kapton in LEO
- Unreacted atomic oxygen scatter with a cosine distribution
- Scattered atomic oxygen cause undercutting in direct ram

Figure 1. Contribution to atomic oxygen undercutting due to unreacted atomic oxygen scattered with a cosine distribution.

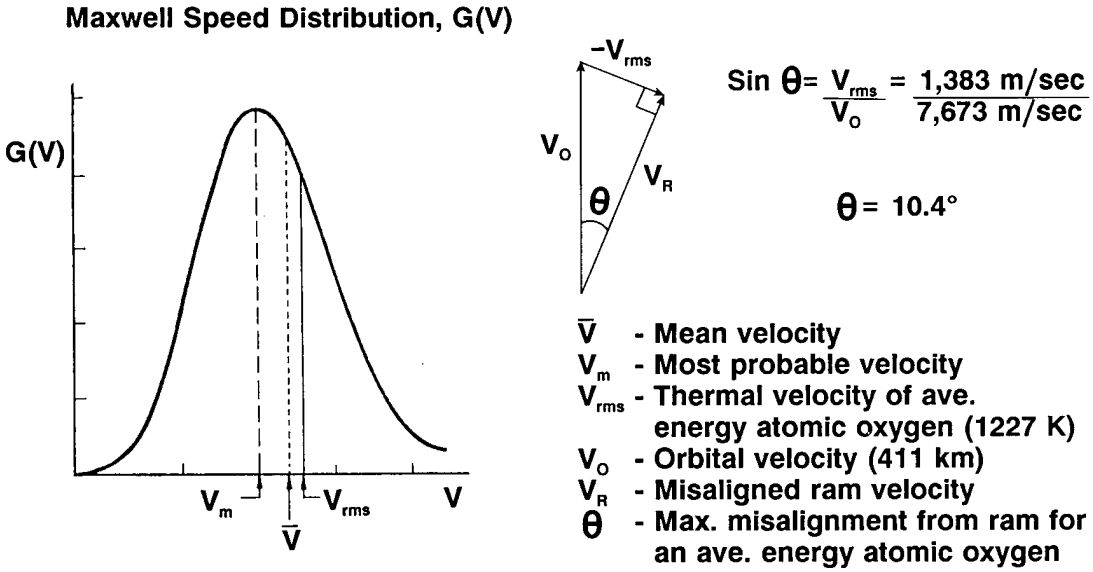


Figure 2. Misalignment of ram atomic oxygen impact due to thermal velocity contributions of randomly oriented hot thermosperic oxygen.

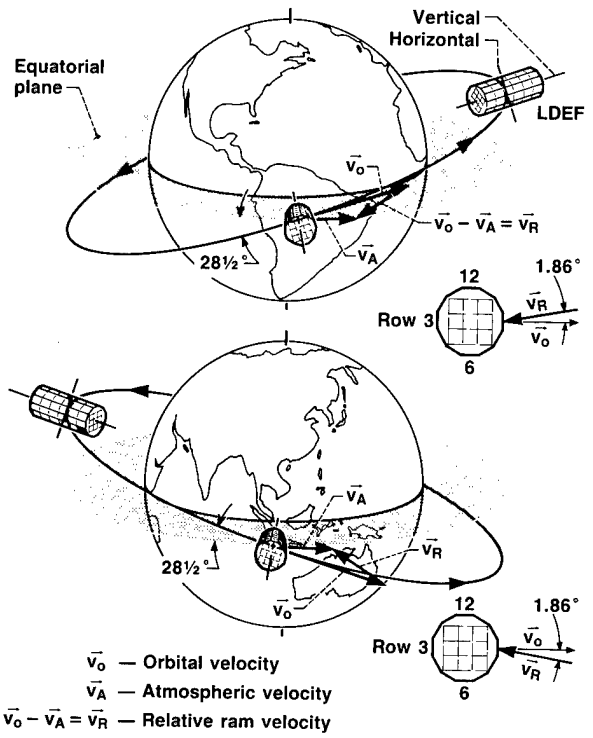


Figure 3. Earth's atmospheric contribution to misalignment of ram atomic oxygen impact on LDEF.

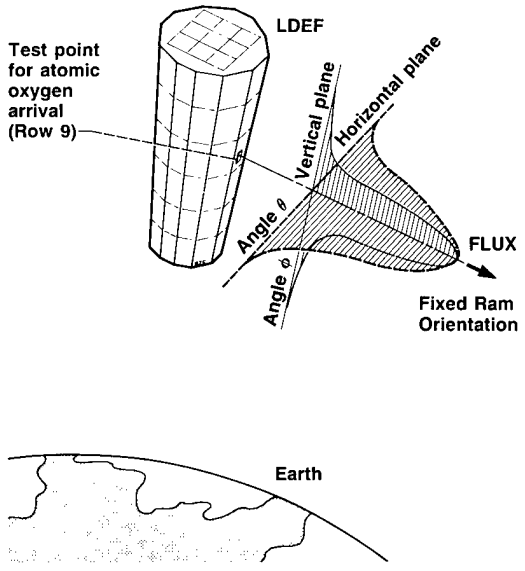


Figure 4. Angular variation in atomic oxygen flux on LDEF due to the thermal and orbital inclination velocity contributions.

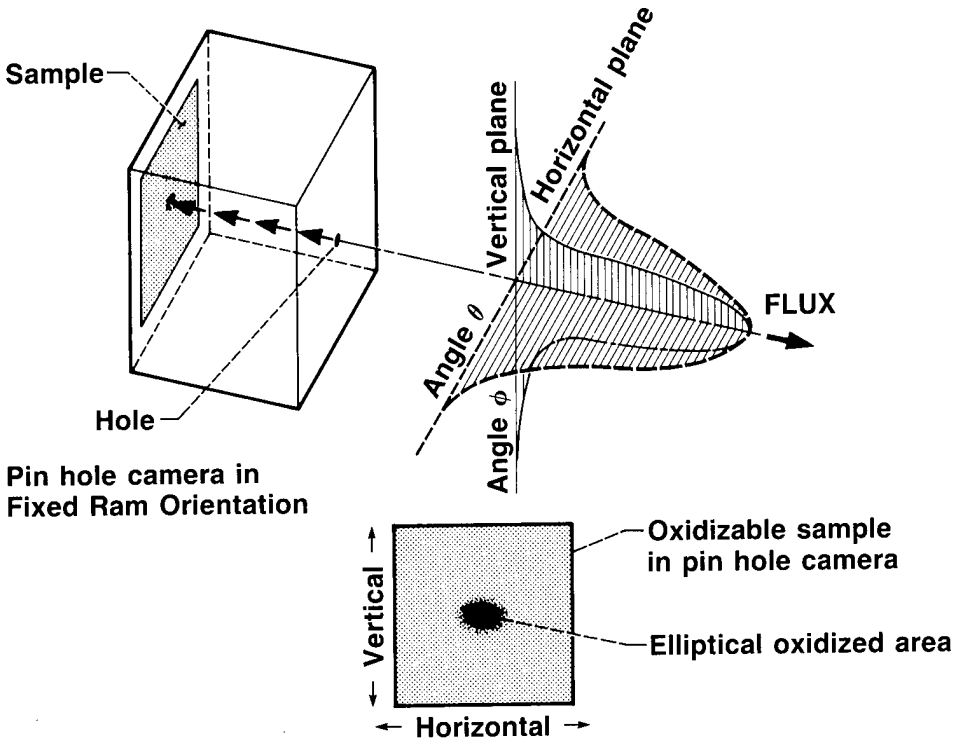
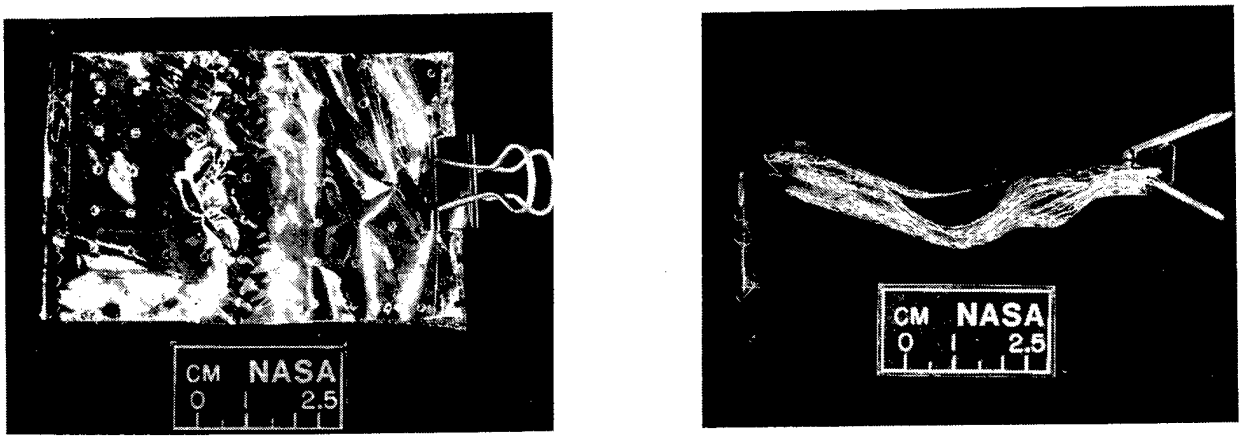
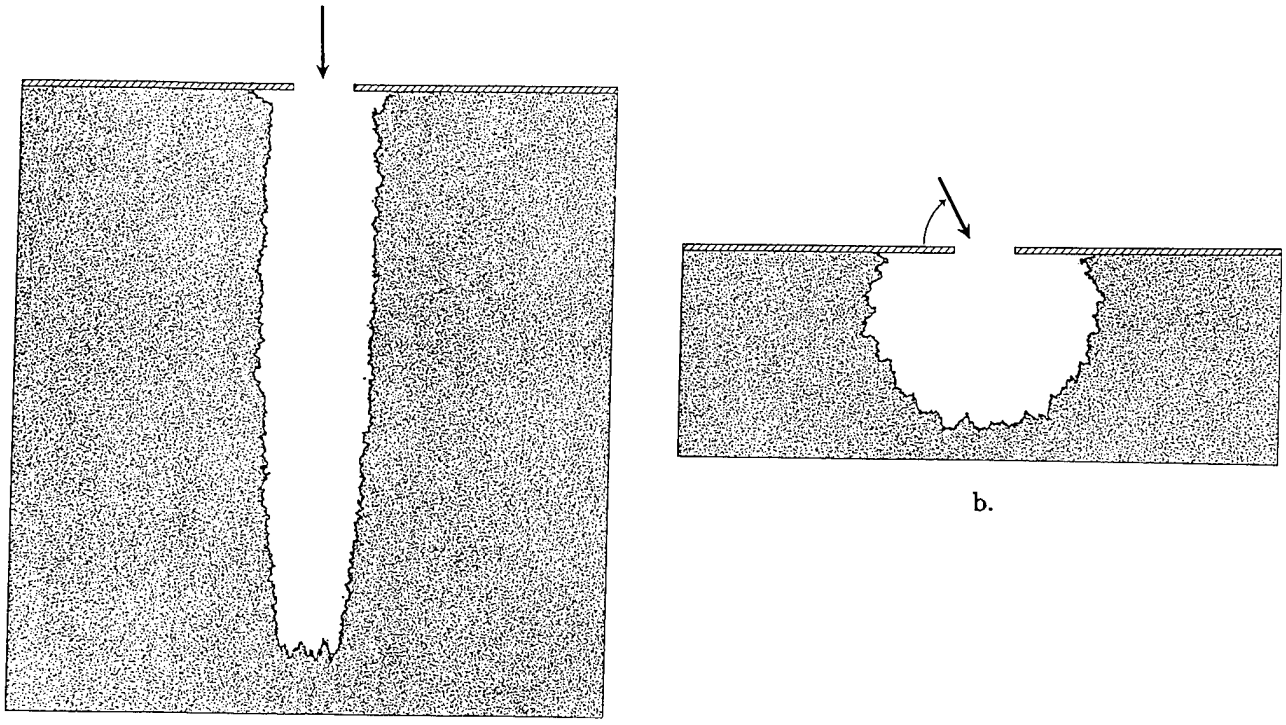


Figure 5. Effect of LDEF flux distribution variation in horizontal and vertical planes on pin hole camera samples.



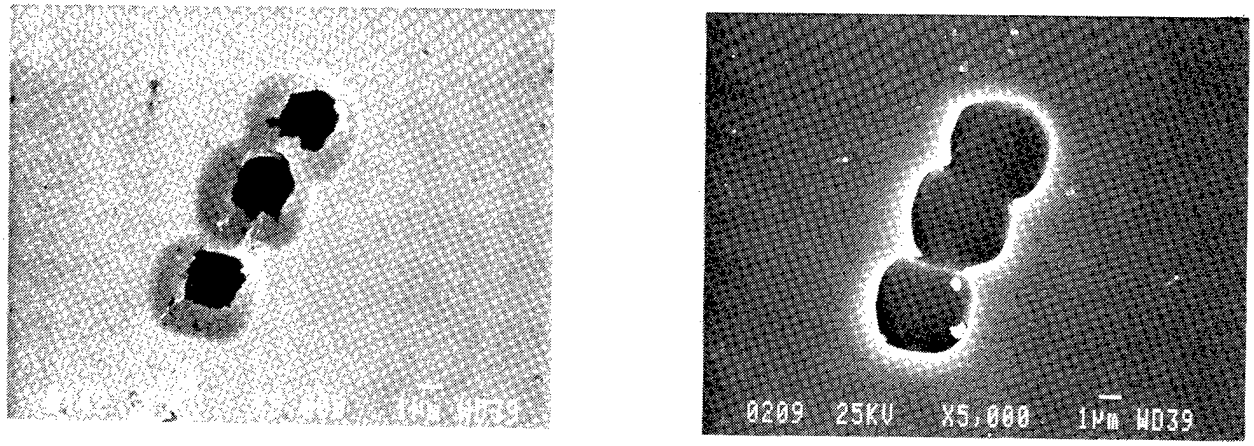
a. b.

Figure 6. Aluminized-Kapton multilayer insulation from the Cascaded Variable-Conductance Heat Pipe Experiment (A0076) located on row F-9: a. top view, b. side view.



a. b.

Figure 7. Monte Carlo model predictions for protected Kapton in: a. normal incident space ram, b. sweeping space ram.



a. b.

Figure 8. Atomic oxygen undercutting at pin holes defects on LDEF aluminized-Kapton MLI exposed to an atomic oxygen fluence of 5.77×10^{21} atoms/cm^2: a. with aluminum, b. aluminum chemically removed.

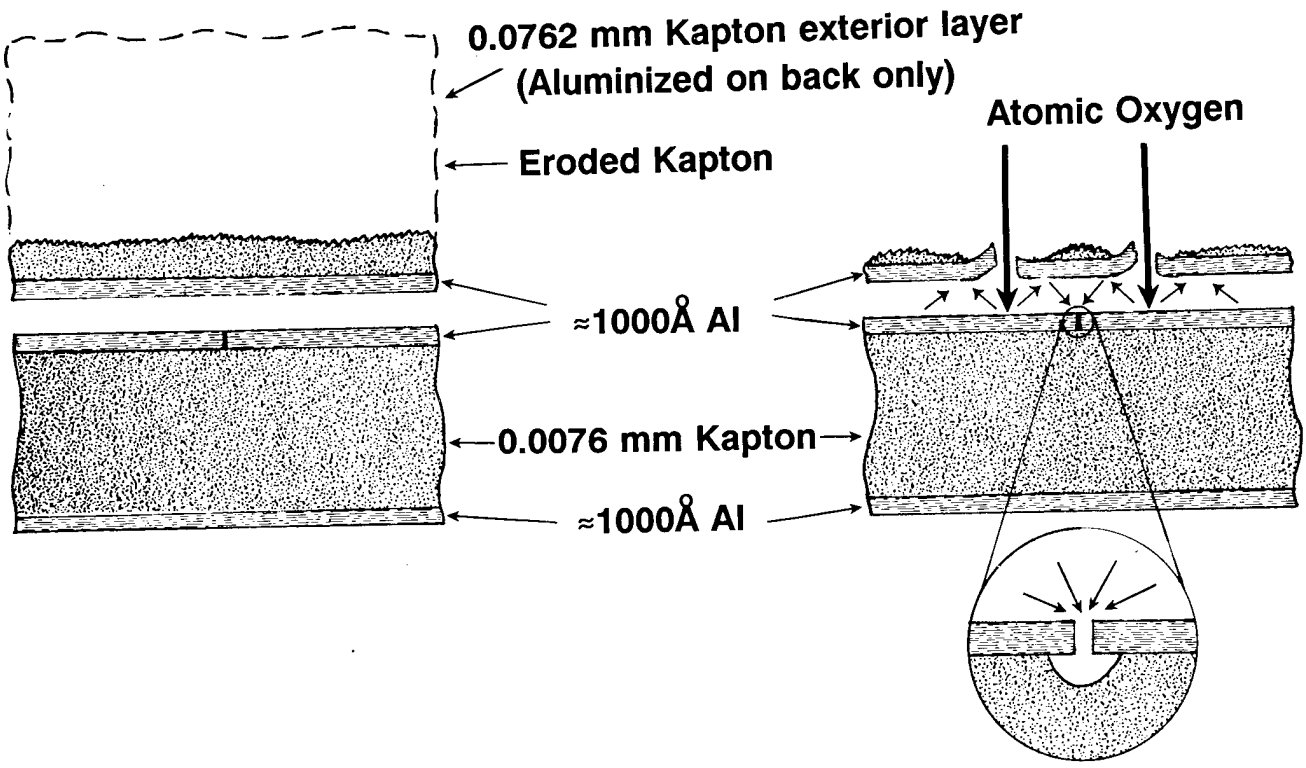
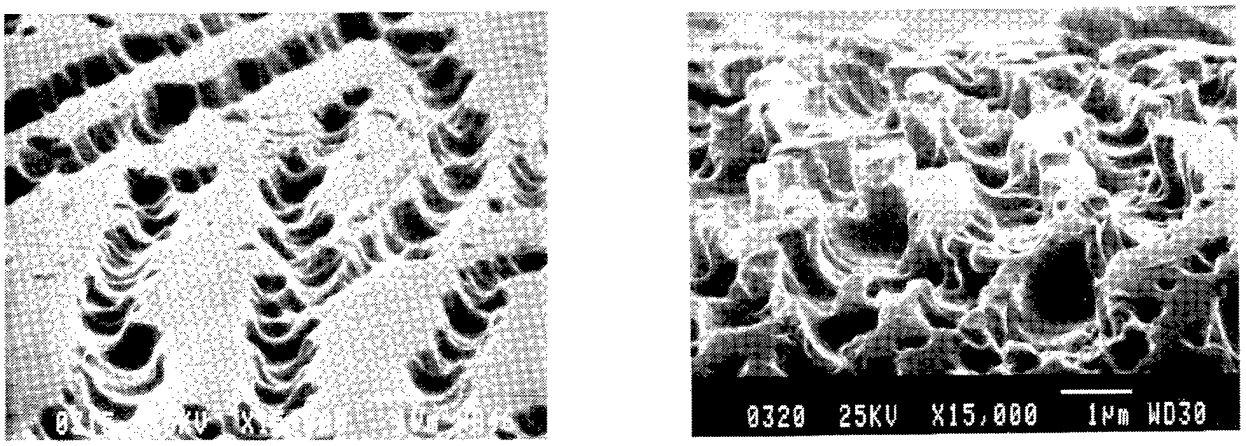


Figure 9. Scattering of atomic oxygen due to partial loss of the Kapton cover layer.



a. b.

Figure 10. Atomic oxygen undercut profiles for LDEF aluminized-Kapton: a. narrow cracks, b. wide cracks.

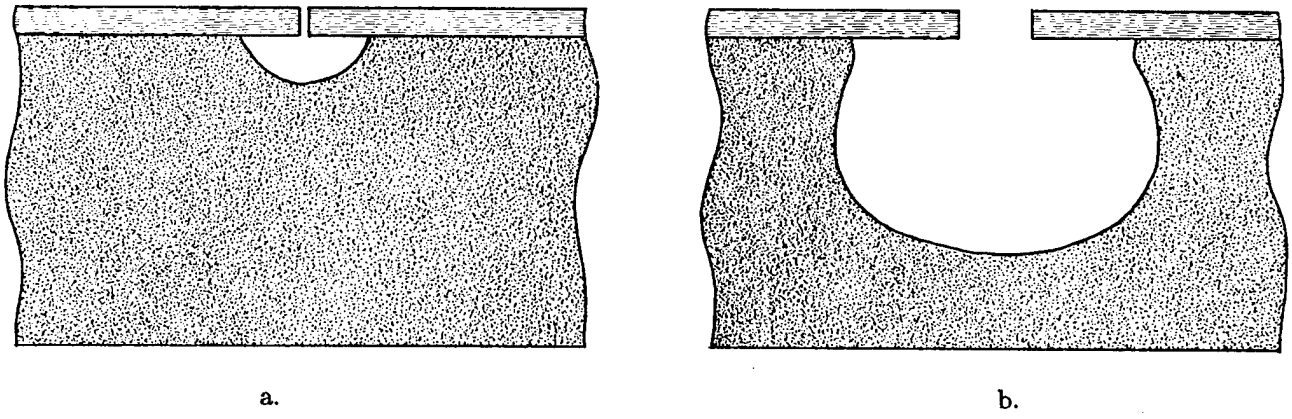


Figure 11. Atomic oxygen undercut profiles of LDEF aluminized-Kapton: a. narrow cracks (<0.1 μm), b. wide cracks (>0.1 μm).

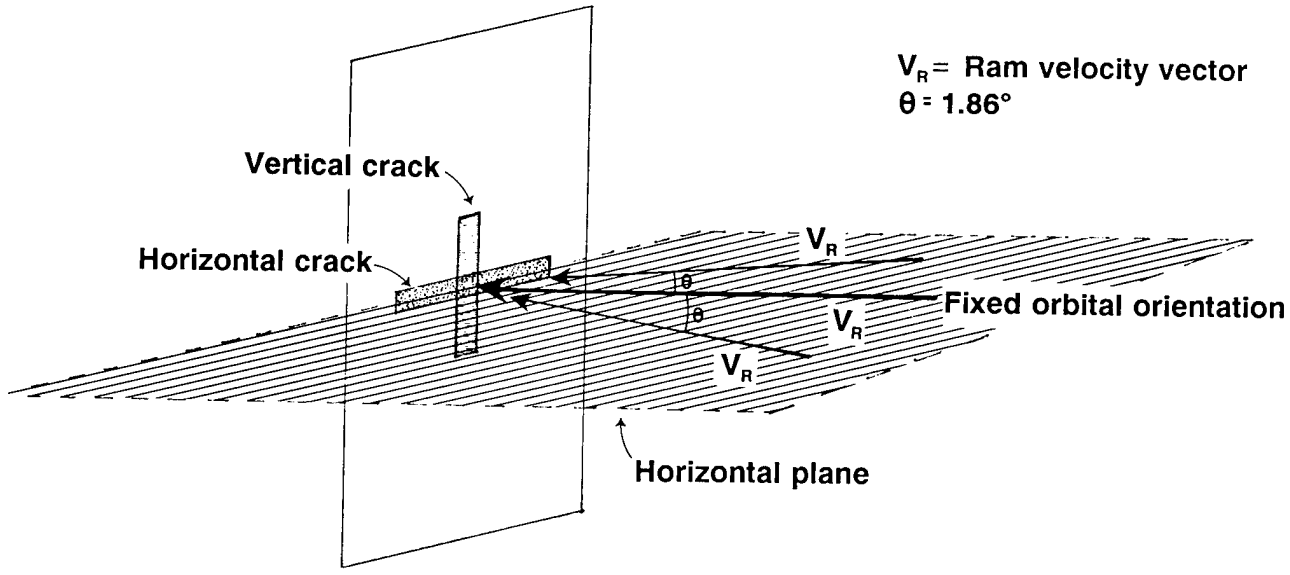
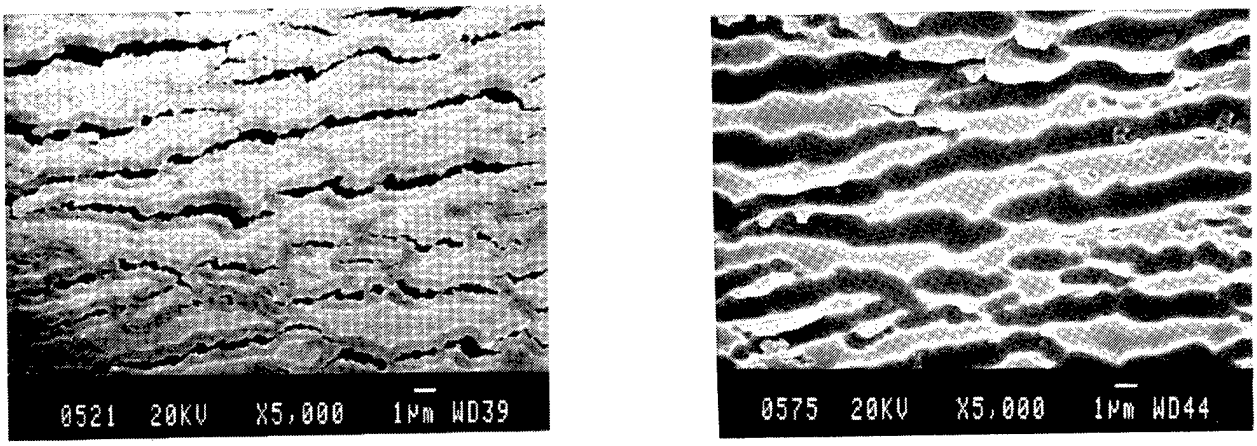
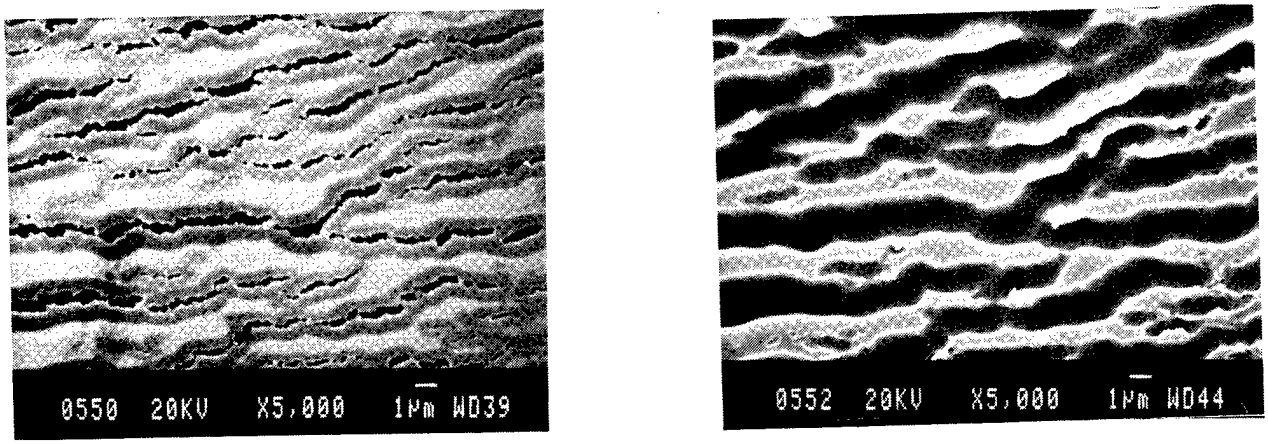


Figure 12. Effect of orbital inclination on ram atomic oxygen impact in LDEF's horizontal and vertical planes. Ram atomic oxygen swept parallel to horizontal cracks and perpendicular to vertical cracks.



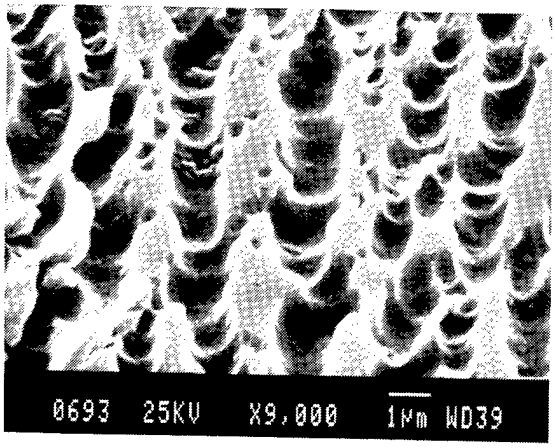
a. b.

Figure 13. Wide horizontal cracks in aluminized-Kapton MLI sample: a. with aluminum, b. aluminum chemically removed.

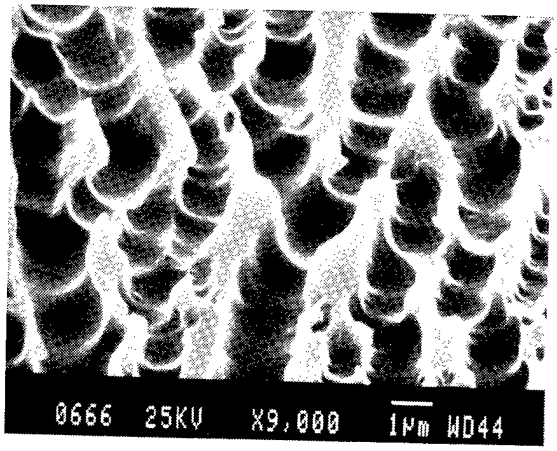


a. b.

Figure 14. Wide vertical cracks in aluminized-Kapton MLI sample: a. with aluminum, b. aluminum chemically removed.

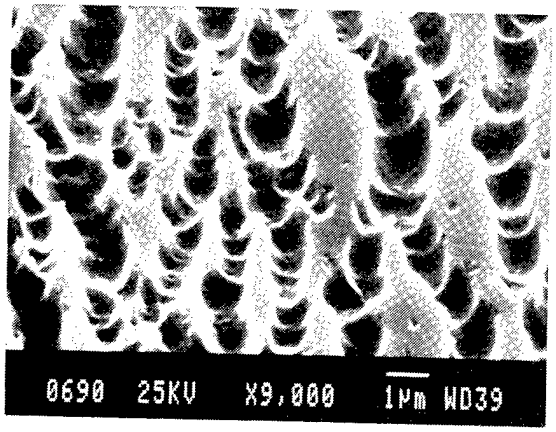


a.

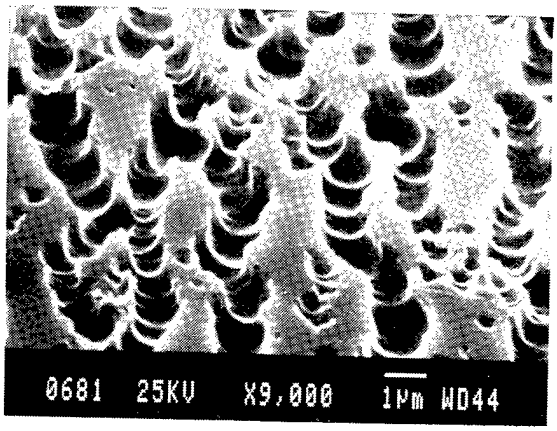


b.

Figure 15. Wide cracks in aluminized-Kapton MLI sample: a. horizontal undercut profiles, b. vertical undercut profiles.



a.



b.

Figure 16. Narrow cracks in aluminized-Kapton MLI sample: a. horizontal undercut profiles, b. vertical undercut profiles.

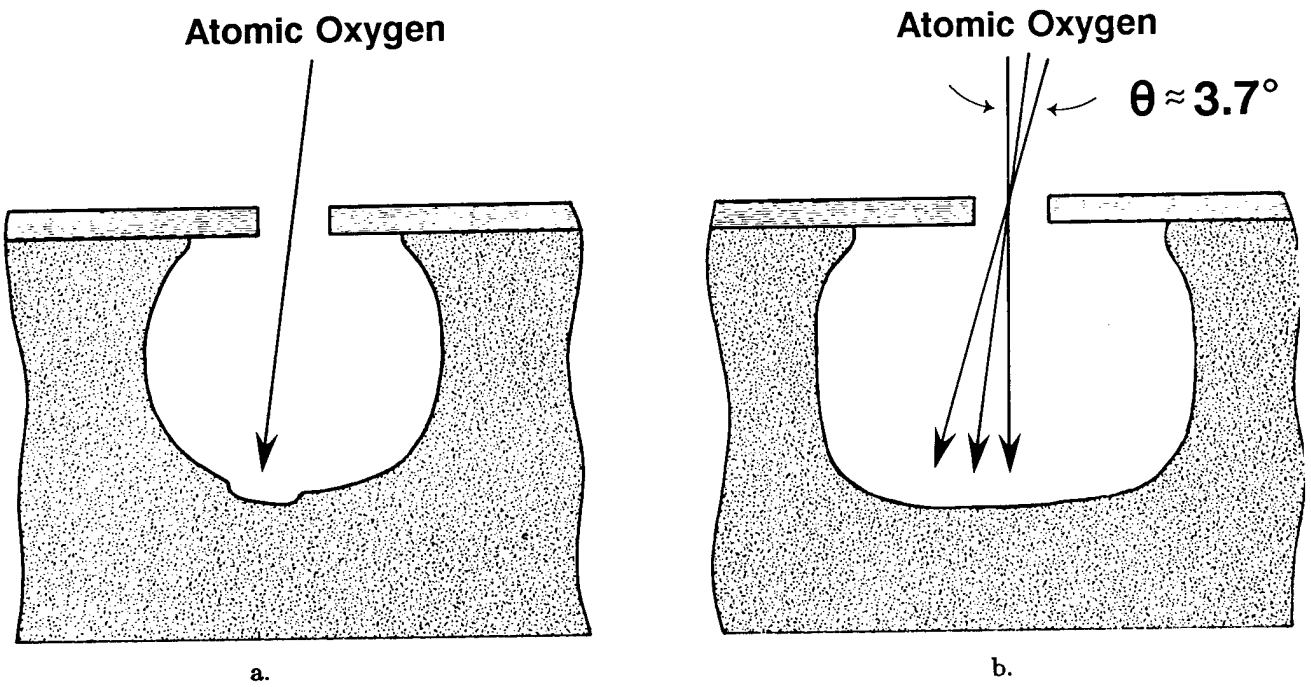


Figure 17. Variation in undercut profiles due to Earth's atmospheric contribution to ram impact misalignment: a. horizontal cracks (sweep was parallel to crack), b. vertical cracks (sweep was perpendicular to crack).

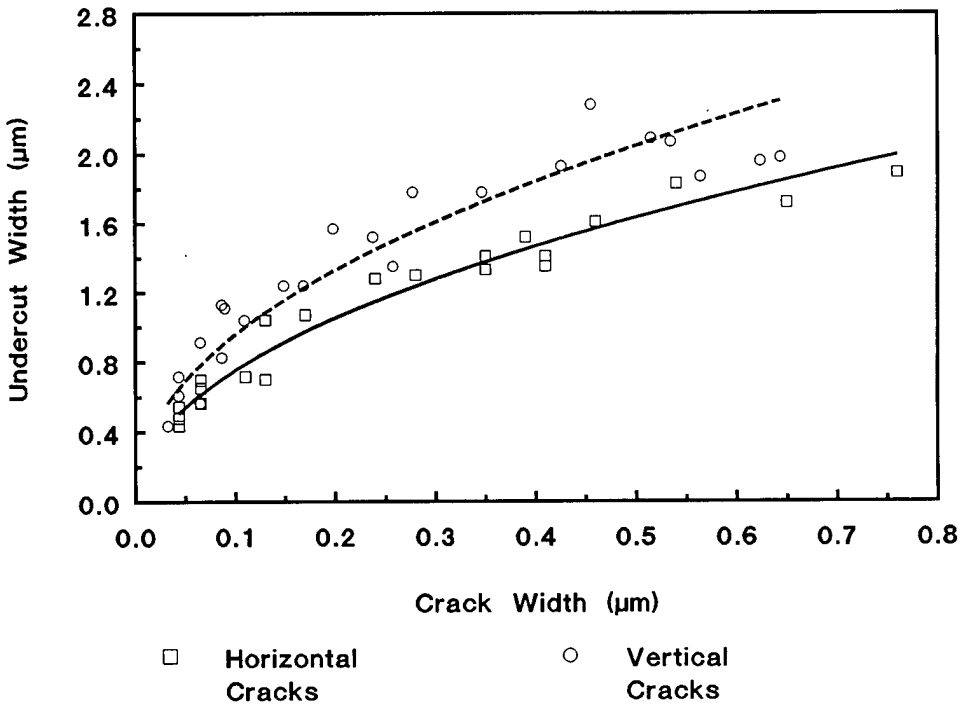


Figure 18. LDEF aluminized-Kapton MLI: undercut width verses crack width.

PRELIMINARY RESULTS FOR LDEF/HEPP THERMAL CONTROL SAMPLES

Lonny Kauder
NASA Goddard Space Flight Center
Greenbelt, MD 20771
Phone: 301/286-5309, Fax: 301/286-6916

SUMMARY

Specimens of Kapton coated with black paint, white paint and thin film oxides were flown at three locations aboard LDEF to evaluate their resistance to atomic oxygen erosion. Post flight emittance and solar absorptance measurements are compared with pre flight values.

INTRODUCTION

Among the numerous experiments flown aboard the Long Duration Exposure Facility (LDEF), the late Ben Siedenburg of the Goddard Space Flight Center's Thermal Engineering Branch, placed sixty five 1 inch by 12 inch strips of Kapton coated with various black paints, white paints, clear coatings, and thin film oxides at three locations on the LDEF. The purpose of this experiment was to evaluate atomic oxygen resistant protective coatings for Kapton. This paper summarizes the results of that experiment.

The sixty five coatings were divided into 5 sets. Two sets were flown in the ram direction on top of the MLI blanket of the Cascade Variable Conductance Heat Pipe Experiment (CVCHPI, tray F9). These thermal control samples saw UV and atomic oxygen. Two other sets were flown on top of the MLI blanket of the Low Temperature Heat Pipe Experiment (HEPP, tray F12) perpendicular to the ram direction and saw UV and much less atomic oxygen. The last 13 samples were taped to the perimeter of the HEPP power tray (H1) on the space end of the satellite. These samples also saw UV and some atomic oxygen. Of the 65 samples flown 52 were recovered with varying degrees of degradation. The remaining 13 samples (located on the CVCHPI experiment tray F9) were lost in space before retrieval due to atomic oxygen erosion of the Kapton tape which held the samples to the MLI blanket.

RESULTS AND DISCUSSION

From data recently provided at the LDEF Symposium it is known that the coatings flown aboard LDEF completed approximately 34,000 thermal cycles during the 5 years 10 months in orbit. Available estimates of the atomic oxygen exposure and equivalent sun hours (ESH) indicate that the samples on the ram side (tray F9) could have seen as much as 8.32x10^21 atoms/cm^2 and 11,100 ESH. The samples on row F12 saw only 1.2x10^21 atoms/cm^2 and 6,900 ESH. While the samples flown on the H1 tray saw 3.64x10^20 atoms/cm^2 and 14,500 ESH. In this environment, degradation of thermal control coatings was observed on each of our experiment trays. The exact cause of this degradation is not yet known but contamination from parts of the spacecraft is suspected to have played a major role in the observed degradation.

The accompanying table (table I) gives the solar absorptance and normal emittance data for the GSFC samples flown on the LDEF. With the exception of Teflon, the coatings were on 1/3, 1/2, 1 or 5 mil VDA Kapton substrates. The solar absorptance and normal emittance measurements can be compared to measurements of thermal control samples that were coated at the same time but were kept under variable laboratory conditions at the Goddard Space Flight Center (GSFC) over the 5 year 10 month flight of the LDEF. Currently many of these samples are awaiting analysis by the materials branch at GSFC to determine if the observed degradation is due to surface contamination or is an inherent property of the coatings themselves. Initial analysis by the Materials Branch at GSFC however, seems to indicate that much of the observed degradation was caused by outgassing of methyl silicon species from coatings, adhesives or rubber products aboard the spacecraft. These outgassing products were then turned brown by the action of UV and atomic oxygen near the end of the flight. A more detailed analysis is expected to be completed over the next few months. As the attached charts show the white paint samples appear to have suffered most from this degradation process and consequently showed the largest change in solar absorptance. Some contamination due to outgassing does appear to have originated from the acrylic adhesive backing used in the Kapton tape. This was evident by a thin dark line of degradation running along the tape sample border. The degree to which this source contributed to the overall contamination of the LDEF is not yet known.

The samples that appear to have suffered the least degradation and erosion are Kapton overcoated with silicon oxide. These did show some small change in solar absorptance but this was probably due to the general contamination experienced by all parts of the spacecraft. The Kapton samples overcoated with Indium Oxide and Indium Tin Oxide however did not fair as well as the silicon oxide coated samples. This fact may not be apparent from the absorptance and emittance data. It is apparent that these coatings did offer some protection to the kapton substrate but in some instances the Kapton had been eroded in two. It is not known at present whether this was due to erosion of the Indium Tin Oxide layers by atomic oxygen or whether it is related to erosion due to pre-flight handling. It should be pointed out however that although the

silicon oxide coated Kapton showed little signs of degradation or erosion, the samples that were recovered were from tray F12 (perpendicular to the ram direction) and consequently saw much less atomic oxygen than the samples of ITO Kapton and Indium oxide Kapton. The samples mounted in the ram direction on the F9 tray would have provided the definitive test for the Silicon Oxide overcoating; however these samples were among the samples lost in space.

As you might suspect the worst degradation was observed in the unprotected Kapton. In some instances 5 mil Kapton had patches which were completely eroded away. Urethane and silicone overcoating of some of the Kapton did little to prevent their eventual erosion by atomic oxygen.

Although the black paint samples (Z306 & RTV615 with carbon black) showed little change in absorptance or emittance they did show some signs of contamination and tended to curl as did the white paints. This curling was probably caused by shrinkage of the paints.

CONCLUSION

Although the true degradation of these coatings in low Earth orbit has been compromised by the molecular contamination from various sources on LDEF, it is clear that coatings like Silicon Oxide do provide a measure of protection for Kapton against atomic oxygen erosion. Still yet to be determined is the change in conductivity of the Indium Oxide and Indium Tin Oxide coated Kapton and VDA Teflon. In addition the analysis of the contaminate on each of the samples has yet to be accomplished. These tests are expected to be completed in the next few months.

TABLE I. COMPARISON OF PRE-FLIGHT AND POST FLIGHT SOLAR ABSORPTANCE AND EMITTANCE FOR SELECTED THERMAL CONTROL COATINGS

Sample	Substrate	Location on LDEF*	Absorptance	Emittance (normal)
Vapor Deposited Aluminum	Teflon 5mil	Control	0.09	0.02
		F9	0.14	0.12
		F12	0.13	0.09
		H1	0.15	0.05
S13GLO	Kapton 5mil	Control	0.16	0.90
		F9	0.42	0.88
		F12	0.41	0.89
		H1	0.47	0.89
RTV 615 white paint	Kapton 1/3mil	Control	0.23	0.87
		F9	0.47	0.85
		F12	0.33	0.86
		H1	0.40	0.86
Z306 Black paint	Kapton 1/3mil	Control	-	-
		F12	0.95	0.91
		H1	0.94	0.90
200Å SnO2/In2O3	Kapton 1/2mil	F9	0.35	0.59
		F12	0.31	0.60
		H1	0.35	0.64
200Å SiOx	Kapton 1/2mil	Control	0.34	0.56
		F12	0.36	0.57
		H1	0.36	0.58
500Å SiOx	Kapton 1/2mil	Control	0.33	0.57
		F12	0.34	0.57
		H1	0.37	0.60

TABLE I. CONTINUED

Sample	Substrate	Location on LDEF*	Absorptance	Emittance (normal)
700Å SiOx	Kapton 1/2mil	Control	0.32	0.57
		F12	0.32	0.56
		H1	0.36	0.60
1000Å SiOx	Kapton 1/2mil	Control	0.33	0.58
		F12	0.34	0.57
		H1	0.40	0.61
Vapor Deposited Aluminum	Kapton 1mil	Control	0.35	0.65
		F12	0.35	0.57
		H1	0.35	0.59
Acrylic/Urethane	Kapton 1/2mil	Control	0.36	0.87
		F12	0.40	0.85
DC Q9-6312 clear silicone	Kapton 1/2mil	Control	-	-
		F12	0.41	0.83
		H1	0.37	0.79

* The control samples were kept at the GSFC for the duration of the flight.

ATOMIC OXYGEN INTERACTIONS WITH FEP TEFLON AND SILICONES ON LDEF

Bruce A. Banks
Joyce A. Dever
NASA Lewis Research Center
Cleveland, Ohio 44135
Phone: 216/433-2308, Fax: 216/433-6106

Linda Gebauer
Cleveland State University
Cleveland, Ohio 44115
Phone: 216/433-2310, Fax: 216/433-6106

Carol M. Hill
University of Akron
Akron, Ohio 44304
Phone: 216/433-2308, Fax: 216/433-6106

SUMMARY

The LDEF spacecraft has enabled measurement of the effects of fixed orientation exposure of high fluence atomic oxygen on fluorinated ethylene propylene (FEP Teflon) and silicones. The atomic oxygen erosion yield for FEP Teflon was found to be 3.64×10^{-25} cm^3/atom. This erosion yield is significantly higher than that measured from previous low-fluence orbital data. The FEP Teflon erosion yield was found to have the same dependence on oxygen arrival angle as Kapton and Mylar.

Atomic oxygen interaction with silicone polymers results in crazing of the silicone. Released silicone contaminants were found to darken upon further atomic oxygen exposure.

INTRODUCTION

FEP Teflon

Prior low-earth-orbital flight data characterizing atomic oxygen interaction with FEP Teflon has resulted in highly uncertain atomic oxygen erosion yield data. This was due to either

low fluence exposures (3.5×10^{20} atoms/cm^2 on STS-8), or high fluence sweeping atomic oxygen exposure of material which had uncertain surface chemistry due to pre-flight cleaning procedures (solar max retrieval). The atomic oxygen erosion yield of FEP Teflon has generally been reported to be less than 1×10^{-25} cm^3/atom with the most accepted value being 3.7×10^{-26} cm^3/atom (ref. 1). Thus with polyimide Kapton H having an erosion yield of 3×10^{-24} cm^3/atom, FEP Teflon was believed to have an erosion yield of only 1.2% that of Kapton H.

Ground-based laboratory atomic oxygen exposure of FEP Teflon has generally produced erosion yields which have greatly exceeded those observed in low fluence flight tests. This may have been due in part to synergistic effects associated with significant vacuum UV exposure of the FEP Teflon in ground-based laboratory facilities. Vacuum UV is believed to accelerate the oxidation rate of FEP Teflon in low energy ground-based laboratory facilities (ref. 2).

Atomic oxygen erosion dependence upon angle-of-attack has been evaluated in low earth orbit for Kapton H and Mylar (ref. 3). This data has indicated that the atomic oxygen erosion yield for Kapton and Mylar is dependent on $(\cos \Theta)^{1/2}$, where Θ is the angle between the surface normal and atomic oxygen arrival direction. The high atomic oxygen fluence exposure of the LDEF spacecraft, combined with its three-axis stabilized orientation, and the preponderance of FEP samples around LDEF, allowed an ideal opportunity to more accurately measure the atomic oxygen erosion yield and its angle-of-attack dependence than previous flight experiments have allowed.

Silicones

Early space flight data for atomic oxygen exposure of silicones has indicated atomic oxygen erosion yields between 1 and 2 orders of magnitude lower than that for Kapton H polyimide (ref. 1). Because of the tendency for silicones to develop a glassy SiO_2 surface upon atomic oxygen attack, silicones have been widely used as a means of protecting underlying oxidizable organic materials. Ground-based laboratory exposure of silicones to atomic oxygen has indicated protection of underlying organic materials, but not without degradation of the silicone itself. The silicones typically tend to craze upon high fluence atomic oxygen exposure (ref. 4). Ground-based laboratory tests have also indicated that silicones exposed to atomic oxygen and vacuum ultraviolet radiation can release polymeric scission fragments which deposit on organic and inorganic surfaces. Upon further atomic oxygen attack, and vacuum ultraviolet illumination, these fragments form a glassy, dark contaminant layer. LDEF provided an ideal opportunity to determine whether this vacuum-condensible transport mechanism was unique to ground-based laboratory RF plasma ashers, or also occurs in space.

LDEF MATERIALS

FEP Teflon samples were available in abundance on LDEF because of their use as silvered Teflon thermal blankets associated with the High Resolution Study of Ultra-Heavy Cosmic Ray Nuclei Experiment (A0178) which involved 16 full trays. Figure 1 shows a typical photo at retrieval of a silvered Teflon thermal blanket. Figure 2 depicts a pre-flight section view of the silvered Teflon thermal control blankets. Samples of FEP Teflon were obtained from the silvered Teflon thermal control blankets at various locations around the yaw axis as shown in figure 3.

Silicones considered in this evaluation were the following: silicone-coated conventional bicycle reflectors (see figure 4), Owens Illinois 650 on Chemglaze A276 from the Thermal Control Surfaces Experiment located on row 9A, RTV 670 on Chemglaze Z302 from the same experiment, silicone adhesives under polyimide Kapton tape used in the multi-layer insulation of the Cascade Variable-Conductance Heat Pipe Experiment (A0076) located on row 9F, and white pigmented silicone rubber samples located on row 8A as part of the Solar-Array Materials Passive LDEF Experiment (A0171).

LOW-EARTH-ORBITAL ENVIRONMENTAL EXPOSURE

LDEF was launched on April 7, 1984. After 5 3/4 years in low earth orbit (2,106 days), the atomic oxygen flux grew from an initial value of 2.57×10^{13} atoms/(cm^2 sec) to 3.92×10^{14} atoms/(cm^2 sec) at the end of mission due to orbital decay and a gradual increase in solar activity over the mission life (ref. 5). The total fluence as a function of atomic oxygen arrival angle with respect to the surface normal is shown in figure 3. The atomic oxygen fluence calculations take into account the observed 8° yaw offset, as well as an estimate of the atomic oxygen exposure associated with a brief period of misorientation after the LDEF retrieval. In addition to atomic oxygen exposure, solar and albedo illumination accumulated between a maximum of 11,114 estimated sun hours on row 9, and a minimum of 6,531 estimated sun hours on row 6. The vacuum ultraviolet solar radiation exposure occurred with much less variation around LDEF than atomic oxygen exposure which was dominant in rows 6-12.

RESULTS AND DISCUSSION

FEP Teflon

Post-retrieval analysis of the silvered Teflon thermal control blanket material indicated that atomic oxygen had oxidized the FEP Teflon at higher rates than had been predicted on the basis of previous low fluence flight data. Figure 5 is a scanning electron photomicrograph of a

surface of the FEP Teflon from row 10, which received an atomic oxygen fluence of 7.78×10^{21} atoms/cm^2, arriving at an angle of 22° from the surface normal. As can be seen from the photomicrograph, the surface has a microscopic roughness as a result of the atomic oxygen attack typical of materials having a volatile oxidation product. It is also noted that a contaminant particle on the original surface produces a pillar which can be used to estimate the amount of FEP Teflon which has been removed. Both the microscopic surface texture and the left-standing pillars as a result of protective contaminant particles, point back into the direction of maximum atomic oxygen arrival flux. As can be seen in figure 6, samples located on rows of high atomic oxygen fluence had a significant increase in diffuse reflectance, compared to those which were unexposed, or exposed to minimal atomic oxygen fluence. The increase in diffuse reflectance, caused by the microscopic surface texture, produced a milky-appearing diffuse-reflecting surface, as opposed to the original normal specular reflecting surface. Unexposed silvered Teflon samples were obtained from the perimeter of the tray areas where material was wrapped around the edge of the trays and protected from external exposure. Figure 7 compares the total, diffuse, and specular components of reflectance for samples which had low atomic oxygen exposure with those which had high atomic oxygen exposure. As can be seen from figures 7a and 7b, there is little change in total reflectance between high and low fluence atomic oxygen exposure of the silvered Teflon samples. High fluence exposed samples are dominated by diffuse reflectance, whereas low fluence exposed samples are dominated by specular reflectance. The overall effects of high and low fluence atomic oxygen exposure on the solar absorptance and thermal emittance of the silvered Teflon thermal control blanket materials are shown in Table I. As can be seen from Table I, only small changes in solar absorptance have occurred as a result of atomic oxygen exposure, and a slight reduction in thermal emittance occurs for high fluence atomic oxygen exposure, mostly resulting from reduction in the emitting FEP Teflon thickness as a result of atomic oxygen oxidation.

Atomic oxygen reaction with FEP Teflon was measured by comparing mass per unit area of exposed and unexposed FEP Teflon that was delaminated from the underlying silver, Inconel (Alloy 600), and Chemglaze Z306 paint. The recession calculated was verified by means of scanning electron microscopy at sites of pillars in the FEP Teflon where protective contaminant particles produced left-standing structures. Figure 8 shows the mass loss per unit area as a function of atomic oxygen arrival direction relative to the surface normal. As can be seen in figure 8, the experimental data much more closely follows a $(\cos \Theta)^{1.5}$ fit rather than a $\cos \Theta$ fit. Thus it appears that FEP Teflon, similar to Kapton and Mylar, experiences mass loss per unit area dependence upon $(\cos \Theta)^{1.5}$. One is readily invited to wonder if the $(\cos \Theta)^{1.5}$ dependence is true for all materials with volatile oxidation products. To predict the atomic oxygen erosion yield, one must divide atomic oxygen recession measurements by the atomic oxygen fluence, which can be found in figure 3. The resulting erosion yield angular dependence is shown in figure 9. The erosion yield thus follows a $(\cos \Theta)^{½}$ because the fluence drops off approximately as the $\cos \Theta$ (except near 90° where significant differences occur). As can be seen from figure 9, the predicted FEP Teflon erosion yield for normal atomic oxygen incidence is 3.64×10^{-25} cm^3/atom with an uncertainty of approximately $\pm 0.5 \times 10^{-25}$ cm^3/atom. Thus the atomic oxygen erosion yield of FEP Teflon is approximately 12.1% that of Kapton H.

The effect of vacuum ultraviolet solar radiation exposure on the LDEF FEP Teflon samples was observed as an increase in the near-surface modulus of the FEP Teflon. Beam flexure tests of FEP Teflon samples peeled from the silvered inconel and painted backing revealed an 8% increase in the flexural modulus of FEP samples which were exposed to 8,186 equivalent sun hours, compared to samples which were unexposed and of the same thickness. Such increase in flexural modulus is thought to be caused by photo-induced cross-linking in the near-surface layers. Vickers microhardness indent tests similarly indicated slight increases in the surface hardness of the vacuum ultraviolet exposed FEP Teflon.

SILICONES

All atomic oxygen-exposed silicone samples examined after LDEF retrieval indicated microscopic crazing or cracking. Figure 10 is a scanning electron photomicrograph of the silicone-coated bicycle reflector shown in figure 4, showing evidence of crazing and attack of the underlying polymeric material due to significant atomic oxygen oxidation. It is clear upon inspection of figure 10, that regions of atomic oxygen protection where the silicone has converted to SiO_2, are separated by regions where cracking occurred, which allowed exposure of unprotected underlying oxidizable material. Figure 11 is a scanning electron photomicrograph of the silicone adhesive and Kapton tape samples from row 9 which were exposed to an atomic oxygen fluence of approximately $\approx 4.92 \times 10^{21}$ atoms/cm^2. The atomic oxygen exposure for the Kapton tape silicone adhesive was lower than that typical of other samples on LDEF for row 9 because of temporary protection by a cover layer of aluminized Kapton and the Kapton of the tape itself. Exposure of the adhesive occurred only after the overlying Kapton was oxidized away. As can be seen in figure 11, crazing of the silicone has occurred as a result of atomic oxygen attack. Similar crazing was experienced for RTV 670 and Owens Illinois 650 silicones on thermal control paint surfaces on row 9. Low-earth-orbital atomic oxygen attack of silicones appears to cause depletion of polymeric scission fragments of the silicone, which probably contain methyl groups as indicated in ground-based exposures. As a result of surface oxidation and loss of oxidizable molecular fragments, the surface is left in a tensile state, but comprised chiefly of silicon dioxide, thus the surface tends to crack or craze. Depending on the particular silicone composition and atomic oxygen fluence, such crazing can allow exposure of the underlying material to atomic oxygen attack as seen in figure 10. As the atomic oxygen fluence increases on silicones, branch cracking may also occur.

White silicone rubber exposed on row 8 received atomic oxygen attack at 38° from the surface normal. Figure 12a is a post-retrieval photograph showing the white silicone rectangular samples in the center of the photograph. As can be seen in figure 12a, dark deposits occur to the right of silicone samples; however, between the dark deposit and the silicone samples is a lighter colored region where atomic oxygen is shielded from bombarding any contamination arriving. Although the roles of synergistic vacuum ultraviolet solar radiation exposure, atomic oxygen exposure, and silicone outgassing are not fully clear, it is clear from figure 12a, and the section view explanation shown in figure 12b, that atomic oxygen arrival is necessary to produce the dark color on the contamination layer. The contamination may be arriving at all surfaces in

the vicinity of the silicone samples due to either atomic oxygen-initiated polymer degradation or vacuum outgassing. Both LDEF results and ground-based laboratory RF plasma asher atomic oxygen interactions with silicones have indicated that brown contamination deposits on adjoining surfaces can occur. The implications of this deserve further investigation because silicones are frequently used in the vicinity of photovoltaic devices which rely upon high solar transmittance cover glass surfaces to maintain efficient conversion of solar energy to electrical power.

CONCLUSION

The atomic oxygen erosion yield of FEP Teflon was determined to be $3.64 \pm 0.5 \times 10^{-25}$ cm^3/atom for normal incidence atomic oxygen. The atomic oxygen erosion yield of FEP Teflon was found to have the same general dependence upon angle of arrival of atomic oxygen as Kapton and Mylar, all of which have the $(\cos \Theta)^{1/2}$ angular dependence. FEP silvered Teflon thermal control blankets become diffuse reflectors upon high fluence atomic oxygen attack; however, only small changes in solar absorptance and thermal emittance properties occur as a result of this exposure. The surface of FEP Teflon becomes harder as a result of vacuum ultraviolet solar radiation exposure.

Silicones craze upon atomic oxygen exposure, potentially allowing exposure of underlying oxidizable polymers. Silicones can release vacuum condensible contaminants upon atomic oxygen exposure. Such released contaminants darken upon further atomic oxygen exposure and vacuum ultraviolet exposure.

REFERENCES

1. Banks, B.A.; Rutledge, S.K.; Paulsen, P.E.; and Stueber, T.J.: Simulation of the Low-Earth-Orbital Atomic Oxygen Interaction with Materials by Means of an Oxygen Ion Beam. NASA TM 101971, 1989.

2. Koontz, S.; Leger, L.; and Albyn, K.: Vacuum Ultraviolet Radiation/Atomic Oxygen Synergism in Materials Reactivity. J. Spacecraft, vol. 27, no. 3, June 1990, pp.346-348.

3. Visentine, J.T., et.al.: STS-8 Atomic Oxygen Effects Experiment. AIAA paper 85-0415, Jan. 1985.

4. Banks, B.A.; de Groh, K.K.; Rutledge, S.K.; Dever, T.M.; Stueber, T.J.; and Hotes, D.: Performance and Durability of Space Solar Dynamic Power System Optical Surfaces. Solar Engineering - 1990, ASME, April, 1990, pp. 303-314.

5. Bourassa, R.J.; and Gillis, J.R.: Atomic Oxygen Flux and Fluence Calculation for Long Duration Exposure Facility (LDEF) Data Summary. Boeing Defense and Space Group, Aug., 1990.

TABLE I. - SOLAR ABSORPTANCE AND THERMAL EMITTANCE OF LDEF SILVERED TEFLON THERMAL CONTROL BLANKET MATERIALS

SAMPLE	SOLAR ABSORPTANCE α	THERMAL EMITTANCE ϵ
UNEXPOSED, FEP/AG (SHELDAHL CORP., 1990)	0.075	0.810
LDEF, D-5	0.084	0.804
LDEF, E-10	0.117	0.772

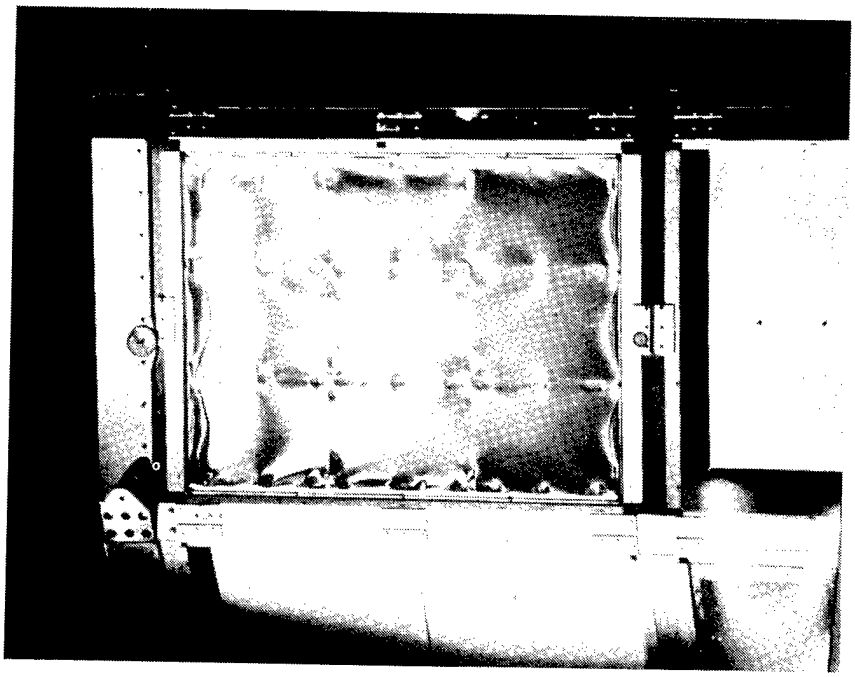


FIGURE 1. - SILVERED TEFLON THERMAL CONTROL BLANKET AT LDEF RETRIEVAL.

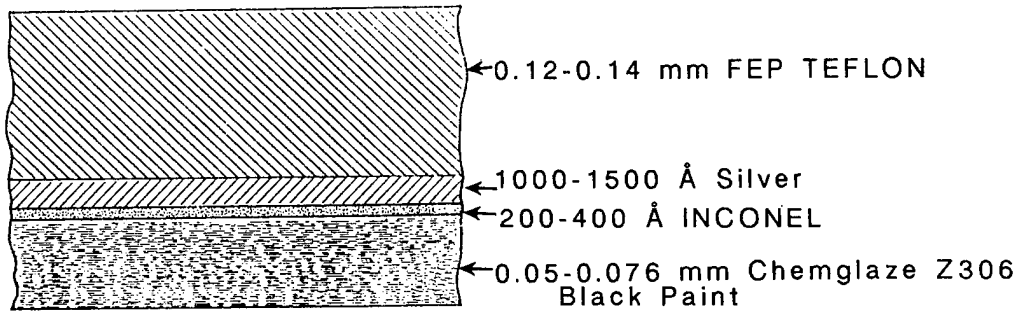
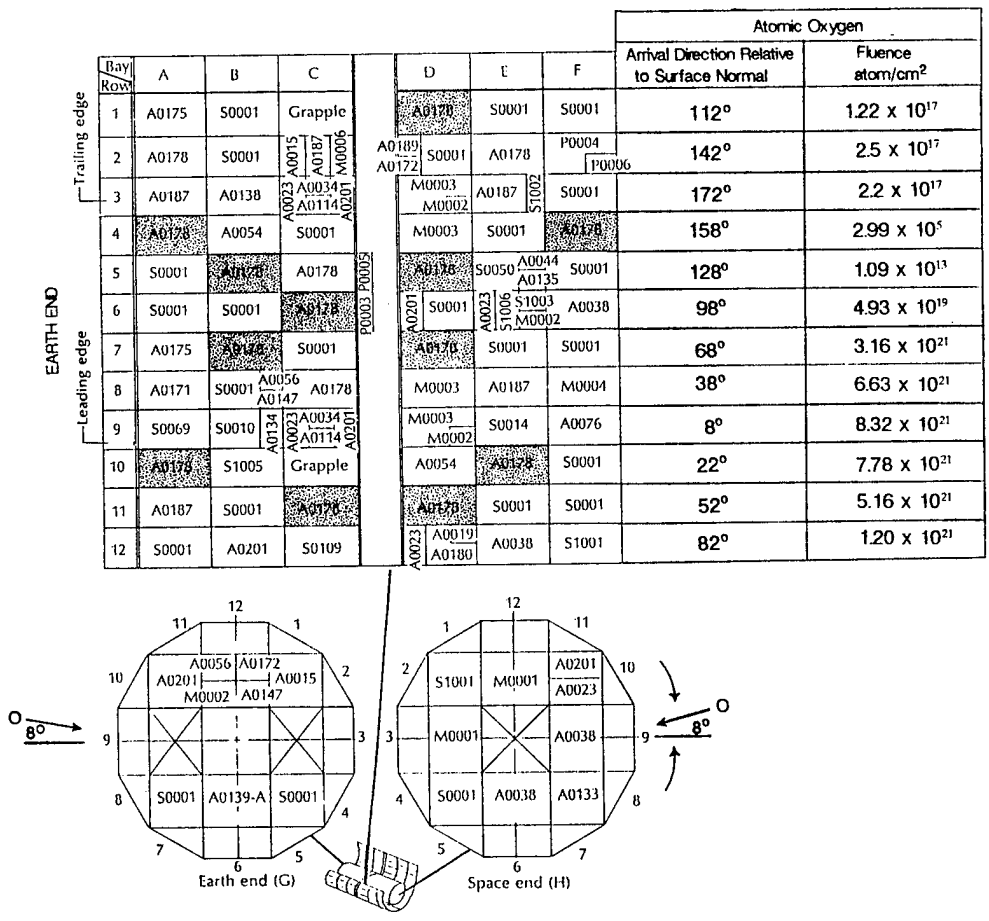


FIGURE 2. - PRE-FLIGHT SECTION VIEW OF SILVERED TEFLON THERMAL CONTROL BLANKETS.



Bay / Row	A	B	C	D	E	F	Atomic Oxygen: Arrival Direction Relative to Surface Normal	Atomic Oxygen: Fluence atom/cm²
1	A0175	S0001	Grapple	A0178	S0001	S0001	112°	1.22 x 10^{17}
2	A0178	S0001	A0015 A0187 M0006	A0189 A0172 S0001	A0178	P0004 P0006	142°	2.5 x 10^{17}
3	A0187	A0138	A0023 A0034 A0114 A0201	M0003 M0002	A0187 S1002	S0001	172°	2.2 x 10^{17}
4	A0178	A0054	S0001	M0003	S0001	A0178	158°	2.99 x 10^{5}
5	S0001	A0178	A0178	A0178	S0050 A0044 A0135	S0001	128°	1.09 x 10^{13}
6	S0001	S0001	A0178 P0003 P0005	A0201 S0001	A0023 S1006 S1003 M0002	A0038	98°	4.93 x 10^{19}
7	A0175	A0178	S0001	A0178	S0001	S0001	68°	3.16 x 10^{21}
8	A0171	S0001 A0056 A0147	A0178	M0003	A0187	M0004	38°	6.63 x 10^{21}
9	S0069	S0010 A0134	A0023 A0034 A0114 A0201	M0003 M0002	S0014	A0076	8°	8.32 x 10^{21}
10	A0178	S1005	Grapple	A0054	A0178	S0001	22°	7.78 x 10^{21}
11	A0187	S0001	A0178	A0178	S0001	S0001	52°	5.16 x 10^{21}
12	S0001	A0201	S0109	A0023 A0019 A0180	A0038	S1001	82°	1.20 x 10^{21}

FIGURE 3. - LOCATIONS OF FEP TEFLON SAMPLES (SHOWN AS DARK RECTANGLES) OBTAINED FOR ATOMIC OXYGEN INTERACTION EVALUATION. ALSO SHOWN ARE ATOMIC OXYGEN ARRIVAL ANGLES RELATIVE TO THE SURFACE NORMAL, AND ATOMIC OXYGEN FLUENCES FOR EACH LDEF ROW.

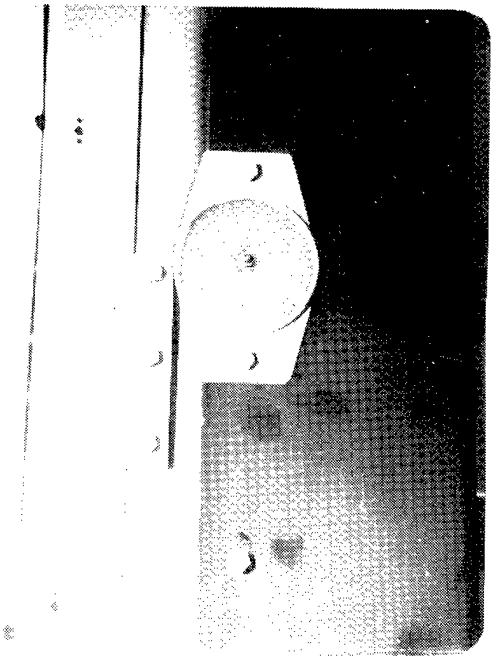


FIGURE 4. - SILICONE-COATED BICYCLE REFLECTOR AFTER RETRIEVAL.

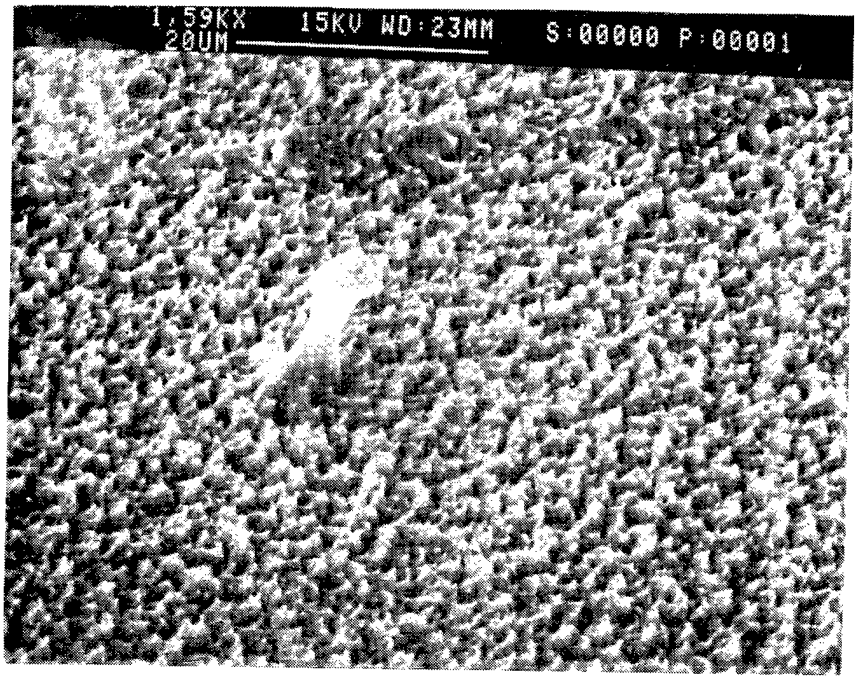


FIGURE 5. - FEP TEFLON FROM ROW 10, WHICH WAS EXPOSED TO AN ATOMIC OXYGEN FLUENCE OF 7.78 X 10^{21} ATOMS/CM^2, WHICH ARRIVED AT 22 DEGREES FROM THE SURFACE NORMAL.

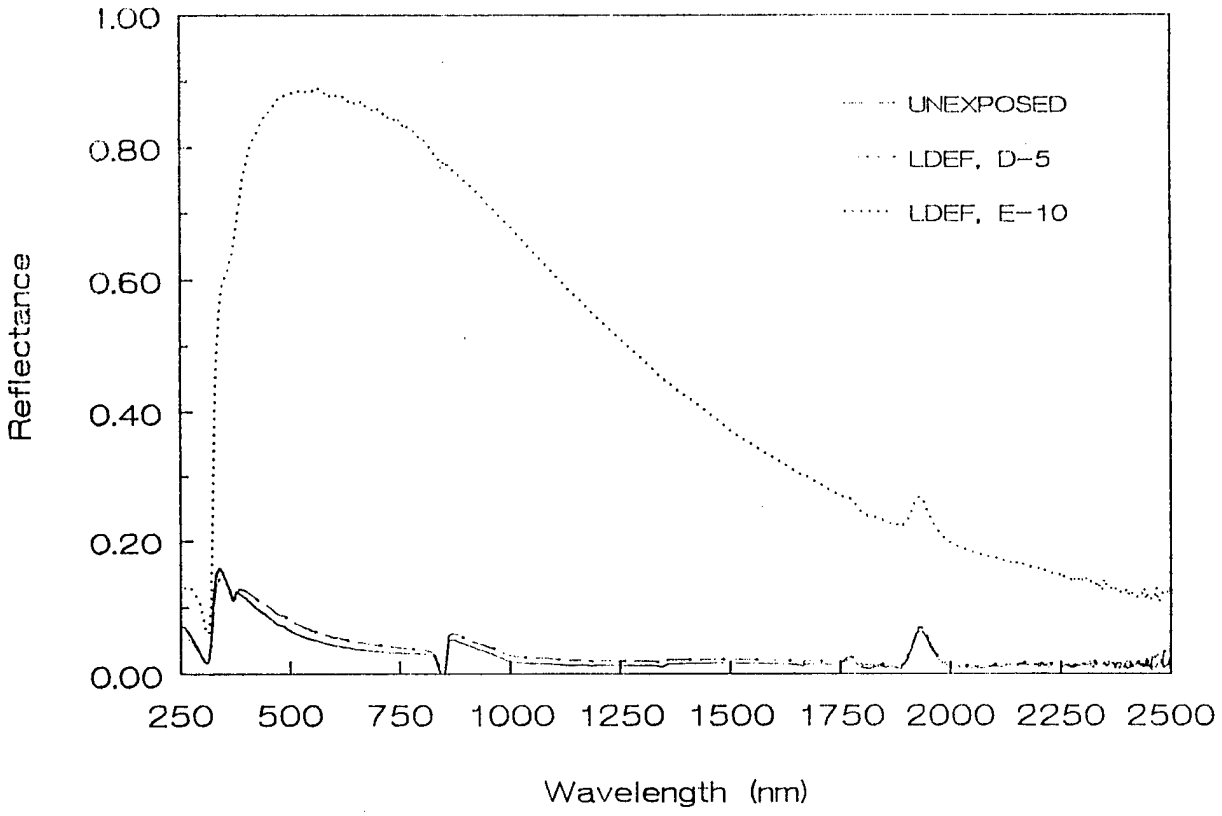
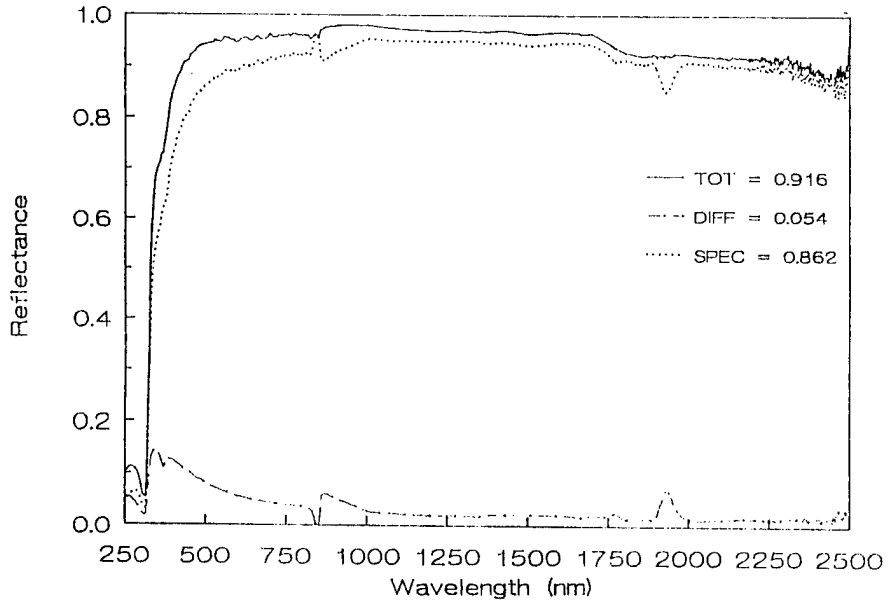
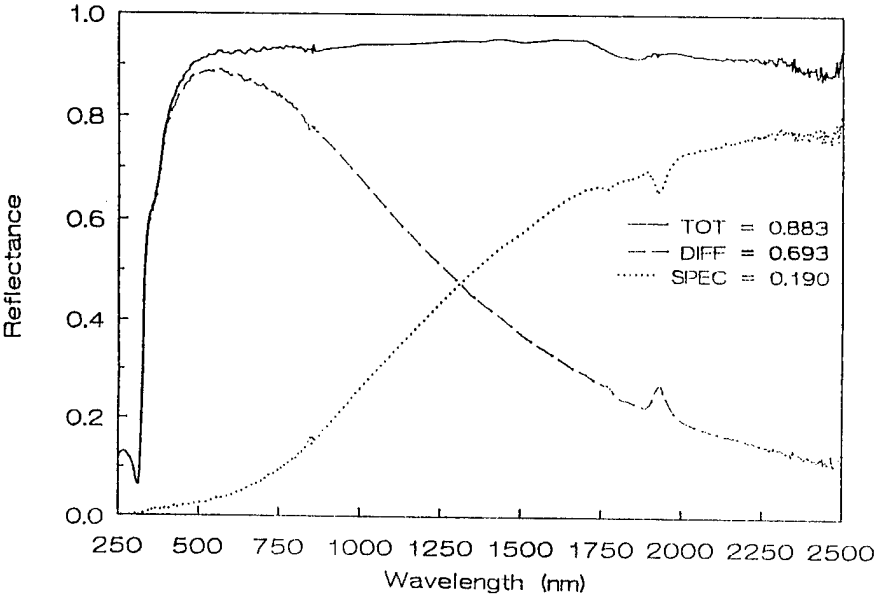


FIGURE 6. - DIFFUSE REFLECTANCE OF SILVERED TEFLON THERMAL CONTROL BLANKET MATERIALS AFTER LDEF RETRIEVAL.



(A) SAMPLE FROM D-5 EXPOSED TO A LOW ATOMIC OXYGEN FLUENCE (1.09×10^{13} ATOMS/CM^2).



(B) SAMPLE FROM E-10 EXPOSED TO A HIGH ATOMIC OXYGEN FLUENCE (7.78×10^{21} ATOMS/CM^2).

FIGURE 7. - TOTAL, SPECULAR, AND DIFFUSE SPECTRAL REFLECTANCE OF SILVERED TEFLON THERMAL CONTROL BLANKET MATERIALS AFTER LDEF RETRIEVAL.

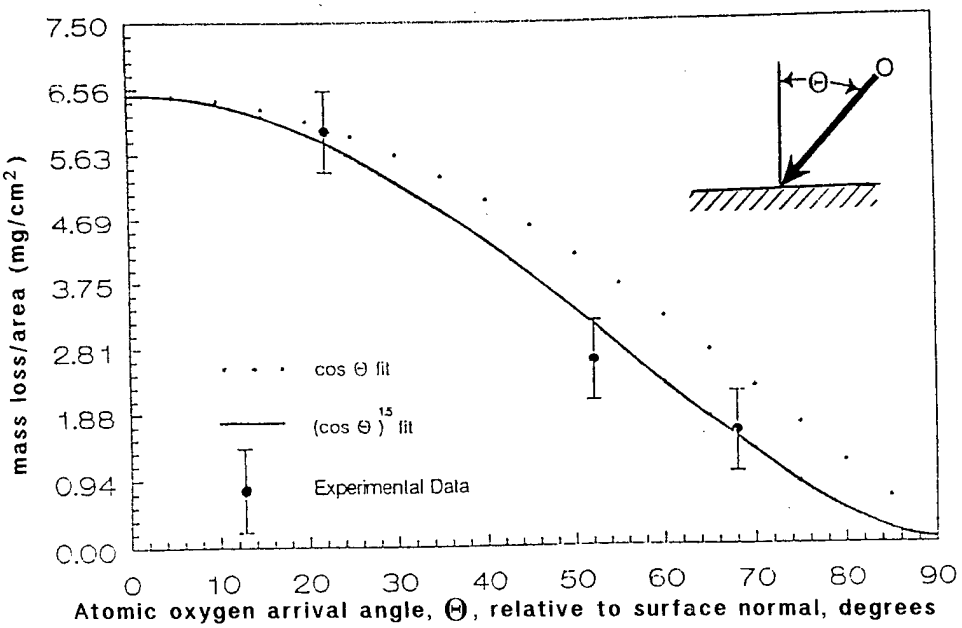


FIGURE 8. - FEP TEFLON MASS LOSS PER UNIT AREA AS A FUNCTION OF ATOMIC OXYGEN ARRIVAL DIRECTION.

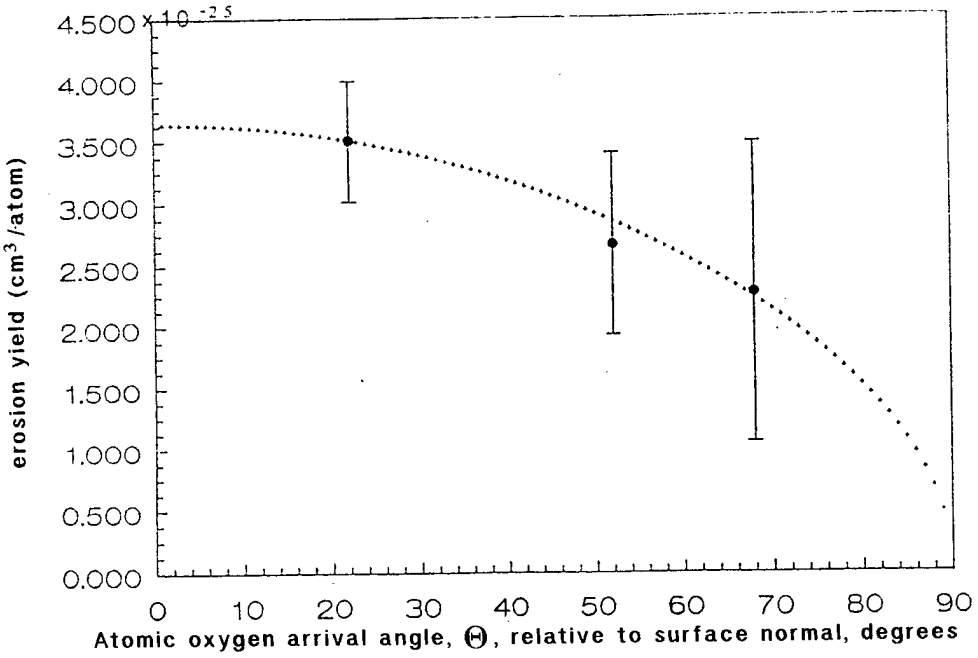


FIGURE 9. - ATOMIC OXYGEN EROSION YIELD ANGULAR DEPENDENCE FOR FEP TEFLON.

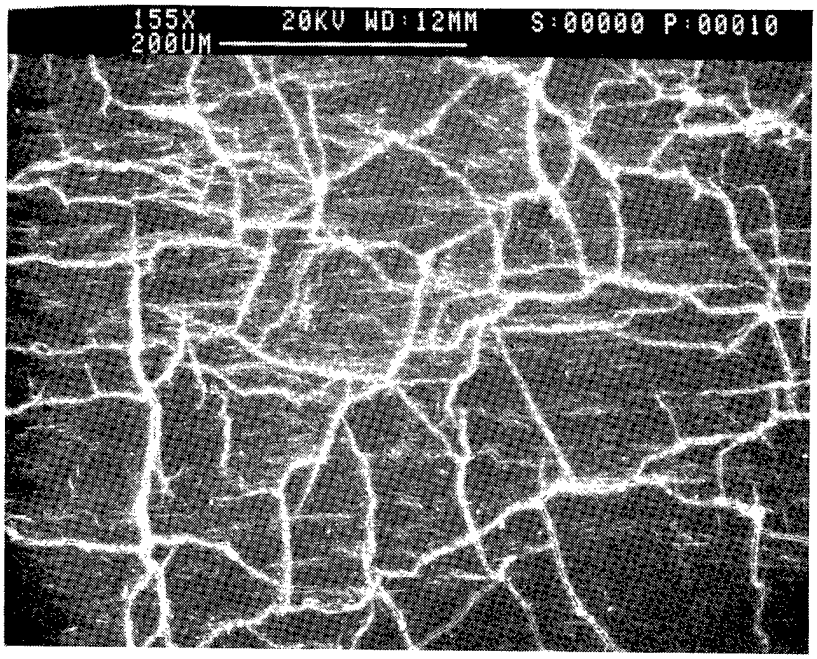


FIGURE 10. - SCANNING ELECTRON PHOTOMICROGRAPH OF THE SURFACE OF A SILICONE-COATED BICYCLE REFLECTOR AFTER SIGNIFICANT ATOMIC OXYGEN ATTACK.

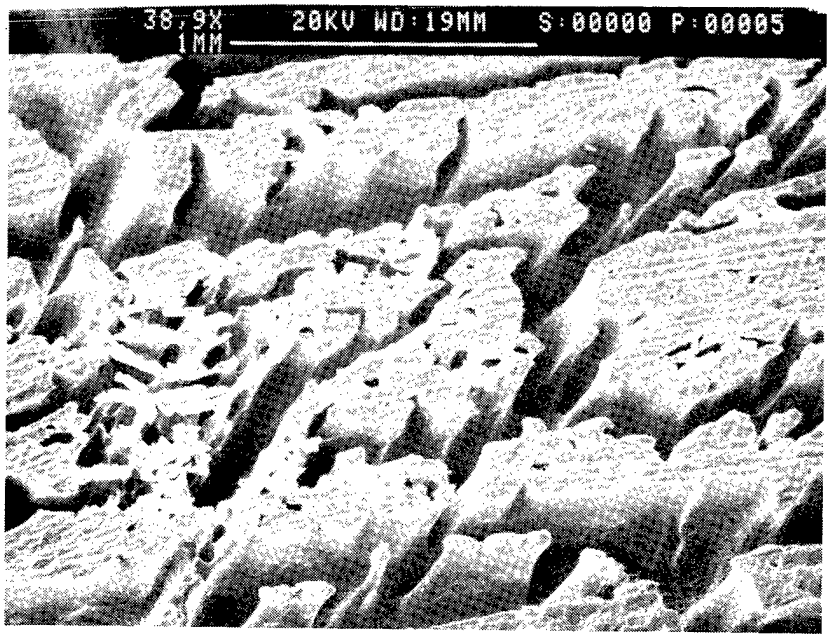
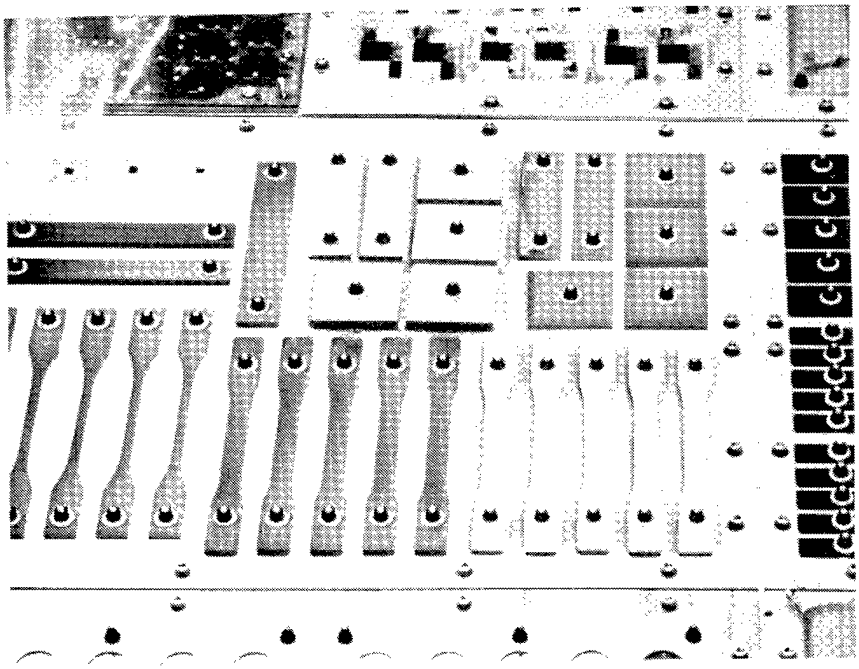
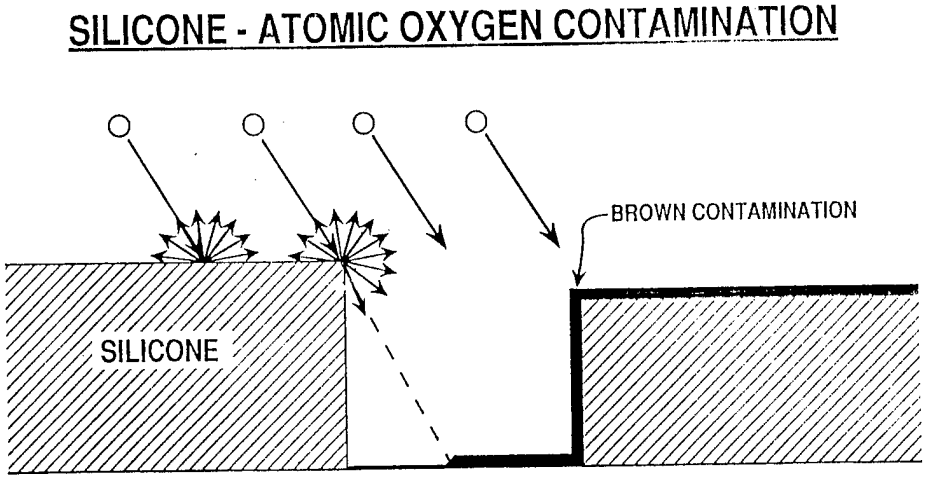


FIGURE 11. - SCANNING ELECTRON PHOTOMICROGRAPH OF SILICONE ADHESIVE FROM KAPTON TAPE AFTER EXPOSURE TO AN ATOMIC OXYGEN FLUENCE OF APPROXIMATELY 4.92 X 10^{21} ATOMS/CM^2.



(A) POST-RETRIEVAL PHOTOGRAPH SHOWING DARK CONTAMINATION TO THE RIGHT OF THE SILICONE SAMPLES, BUT SEPARATED FROM THEM BY A LIGHTER-COLORED REGION WHICH WAS SHIELDED FROM ATOMIC OXYGEN.



(B) SECTION VIEW SCHEMATIC DRAWING OF ATOMIC OXYGEN ATTACK AND RESULTING CONTAMINATION.

FIGURE 12. - ATOMIC OXYGEN INTERACTION WITH SILICONES PRODUCING A DARK, VACUUM-CONDENSIBLE CONTAMINANT ON ADJOINING SURFACES.

VACUUM ULTRAVIOLET (VUV) RADIATION - INDUCED DEGRADATION OF FLUORINATED ETHYLENE PROPYLENE (FEP) TEFLON ABOARD THE LONG DURATION EXPOSURE FACILITY (LDEF)

David E. Brinza, A. E. Stiegman, Paul R. Staszak,
Eric G. Laue and Ranty H. Liang
NASA/Jet Propulsion Laboratory

SUMMARY

Examination of fluorinated ethylene propylene (FEP) copolymer specimens recovered from the Long Duration Exposure Facility provides evidence for degradation attributed to extended solar vacuum ultraviolet (VUV) irradiation. Scanning electron microscopic (SEM) images of sheared FEP film edges reveal the presence of a highly embrittled layer on the exposed surface of specimens obtained from the trailing edge of LDEF. Similar images obtained for leading edge and control FEP films do not exhibit evidence for such an embrittled layer. Laboratory VUV irradiation of FEP films is found to produce a damage layer similar to that witnessed in the LDEF trailing edge films. Spectroscopic analyses of irradiated films provide data used to advance a photochemical mechanism for degradation.

INTRODUCTION

Fluorocarbon polymers have long been considered as physically and chemically stable materials suitable for spacecraft applications. Flexible second surface mirror radiators based on silver-coated FEP (Ag/FEP) are frequently employed in spacecraft thermal control. The Space-Exposed Experiment Developed for Students (SEEDS) tray (P0004) developed by Park Seed, Inc. located on the trailing edge as well as the Ultra-Heavy Cosmic Ray Experiment (A0178) developed by the University of Dublin utilized Ag/FEP blankets for thermal control on each of the sixteen experiment trays installed in various locations on LDEF. In addition to providing thermal control for the cosmic ray detection canisters, these Ag/FEP blankets have provided a wealth of micrometeoroid and debris environmental data. These blankets also provide a vast amount of exposed polymeric material for determining space environmental effects on chemical and mechanical properties.

Evidence for space environmental damage on the LDEF leading edge Ag/FEP blankets was apparent even during the orbital retrieval operations in January 1990. Many impact features and the

loss of specularity were noted during the photographic survey performed by the STS-32 crew. The effects of almost six years of space exposure on the trailing edge blankets were far less evident, even upon visual examination during de-integration activities at Kennedy Space Center. The LDEF Materials Special Investigation Group (MSIG)-initiated investigations into the property changes induced in the LDEF Ag/FEP blankets. The results presented here are an extension of the LDEF MSIG investigations and the ongoing studies at JPL into the fundamental aspects of polymer degradation in the space environment.

CHARACTERIZATION OF LDEF FEP FILMS

Samples for Scanning Electron Microscopy were prepared by cutting approximately 1 cm^2 specimens from leading edge, trailing edge and control materials, with care taken to avoid delamination of the films. The specimens were configured on a SEM mount in order to permit examination of the film surface and edges. The films were coated with a thin metal film ($\approx$200Å) to prevent charge-up distortion in the SEM images. Metallization was performed using a gold/palladium magnetron sputtering apparatus operating with 20-40 mtorr argon buffer gas to insure uniform coating with minimal damage to delicate surface features. SEM images were obtained at low electron energy using a video averaging system to provide high resolution images without inducing damage to the films.

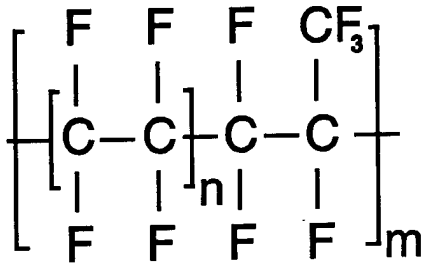
The SEM image shown in figure 1 depicts a cross-sectional view at x400 magnification of an LDEF Ag/FEP blanket control specimen. The control specimen was obtained from excess material trimmed from the flight blanket on the SEEDS (P0004) material during pre-flight assembly of the experiment. This view of the corner of the specimen clearly illustrates the multilayer construction of the LDEF Ag/FEP blanket material. The Chemglaze Z306 black paint coating ($\approx$45 micron thickness) applied to the silvered back surface of the blankets to provide radiative coupling to the experiment hardware is visible at the bottom of the image. The FEP film comprises the top 120 microns of the blanket. Note that the edge and upper surfaces of the FEP have smoothly deformed under the cutting operation.

An SEM image obtained at a x500 magnification of the sheared edge of the trailing edge exposed material from the P0004 experiment is presented in figure 2. In stark contrast to the control material, the trailing edge material shows evidence for a highly embrittled layer on outer surface of the FEP. The cutting operation has induced fracturing of this layer. As the underlying material deformed, the embrittled material separated into island-like fragments which appear to flow downward over the sheared edge. A more detailed view of the fragmented surface is shown in figure 3 at a magnification of x4000. From this view the thickness of the highly embrittled layer is estimated to be just over 1 micron. The distinct and sharply fractured features indicate the mechanical properties of the outermost surface have been dramatically altered as a result of almost six years exposure to the space environment.

LABORATORY STUDIES OF VUV-IRRADIATION OF FEP

Investigations into the mechanism and damage characteristics of VUV-induced degradation of FEP films have been initiated at JPL utilizing two light sources. A study was conducted to characterize the rate of bulk mass loss, as well as chemical, optical and surface morphological changes in FEP irradiated by a deuterium lamp. In another study, mass spectrometric analysis was used to detect molecular photodegradation products of FEP films exposed in an evacuated cell by broadband synchrotron radiation. Significant results from these and other laboratory studies and comparisons to observations for LDEF FEP films are summarized below.

Unravelling the photochemical and photophysical processes in FEP begins with an understanding of the wavelength dependent light absorption characteristics of the polymer. Based on the chemical structure of FEP illustrated below,



n~ 7

the absorption spectrum is expected to be dominated by the carbon-carbon and carbon-fluorine chromophores. The VUV absorption spectrum for FEP has not been reported due to the inability to produce sufficiently thin uniform films of the polymer. An absorption spectrum, however, has been reported (ref. 1) for a chemically similar polymer, polytetrafluoroethylene (PTFE). This spectrum shows an intense absorption at 160 nm which weakens at longer wavelengths (lower energies) and increases at higher energies. The absorption of light at these short wavelengths is expected to lead to direct bond dissociation and subsequent photochemical degradation. The overlap of the VUV absorption spectrum with solar VUV radiation, especially at the intense atomic hydrogen Lyman-alpha (121 nm) emission (ref. 2), will dominate the primary photodegradation processes within fluorocarbon polymers. Laboratory simulation studies of FEP photodegradation therefore required use of light sources which provide significant intensities of short wavelength radiation to duplicate processes anticipated in space exposure.

A long term exposure study of FEP exposed to a 25-watt deuterium lamp was performed to examine the loss of mass and changes of optical transmission as a function of exposure time. The lamp produced approximately a 4 solar equivalent hydrogen Lyman-alpha intensity ($\approx 2\ \mu W/cm^2$) of deuterium Lyman-alpha (124 nm) radiation at the sample location. DuPont FEP film (2 mil thickness) was exposed to the lamp under argon purge and was periodically weighed in order to determine exposure dependent mass loss. As witnessed in figure 4, the film experienced insignificant mass loss during the first 30 days of irradiation, followed by nearly linear mass loss over the remaining 60 days of exposure to the lamp. Figure 5 illustrates the change in optical transmission witnessed in the same irradiated FEP film. The growth of absorption in the short wavelength region is attributed to olefin formation within the film while the long wavelength

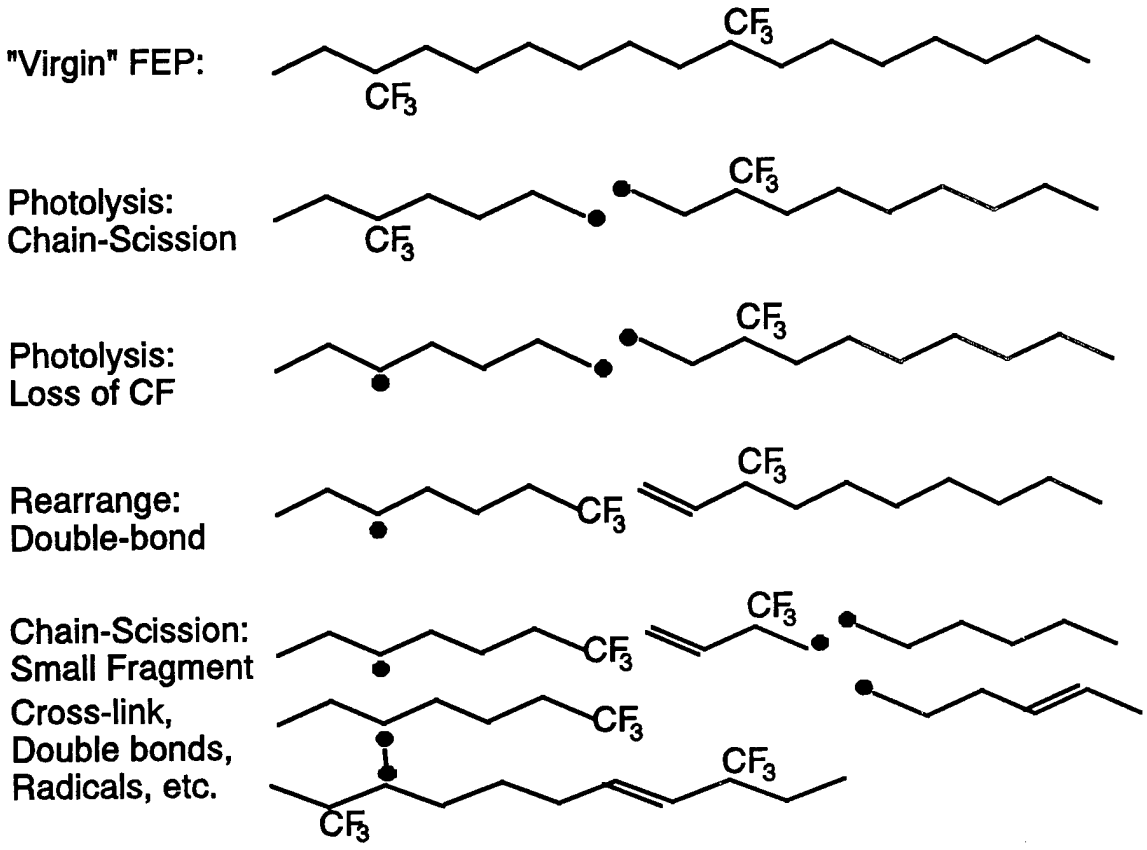
decrease in transmittance is attributed to an increase of light scattering by the film. After the 92-day exposure, the film was cut and the surface examined by SEM. As witnessed in figure 6, the exposed FEP developed an embrittled surface layer similar to that observed in the LDEF trailing edge material (see figure 3).

The composition of molecular products formed via VUV degradation of FEP was determined in a separate investigation. An FEP film was sealed in an evacuated cell fitted with a lithium fluoride window. The film was then exposed to broadband VUV synchrotron radiation (110 nm - 200 nm) from the white beam line at the University of Wisconsin Synchrotron Radiation Facility for 50 hours. Figure 7 presents the mass spectrometry trace of residual gas contained within a vacuum cell following the exposure. Although low molecular weight species appear abundant in the mass spectrum, a significant amount of higher molecular weight fragments are readily observed. Quantitative interpretation of the mass spectrum is complicated by fragmentation of high molecular weight species to produce the lower mass features. Direct inference of the primary products is not possible due to secondary chemistry of the products within the cell during and after irradiation.

Attempts to obtain infrared spectra of the damage layer in the laboratory-exposed resulted in rather poor quality spectra since the layer was very thin. However, the spectra did provide qualitative evidence for the presence of perfluorinated carbon-carbon double bonds (1375 cm^{-1}) and carbonyl groups (1730 cm^{-1}) within the exposed films. Infrared spectra of the LDEF trailing edge films similarly indicated the presence of olefinic (1379 cm^{-1}) and carbonyl functional (1736 cm^{-1}) groups. ESCA analysis of the LDEF film revealed the presence of 11% oxygen in the surface layer in the form of carbonyl, ether and ester groups. An electron spin resonance (ESR) study (ref. 3) performed on laboratory VUV-irradiated FEP revealed the formation of organic free-radicals ($\cdot CF_2-$ and $-CF_2 \cdot CFCF_2-$) within the film.

CONCLUSIONS AND IMPLICATIONS

The laboratory investigations to date indicate complex photochemical processes are involved in the VUV degradation of FEP. The primary processes involve direct photodissociation of carbon-carbon bonds (chain scission) and carbon-fluorine bonds. A schematic representation of the primary and secondary processes is presented below. These processes are deduced from the laboratory observations as follows. The apparent induction period in mass loss can be attributed to a random chain scission process in which a significant period of time is required to produce small molecule fragments in substantial quantity. The presence of higher molecular weight fragments in the residual gas analysis supports a random chain scission process also since an unzipping process should produce monomeric materials almost exclusively. The appearance of optical absorption in the 200 nm - 300 nm band and infrared spectra support the formation of carbon-carbon double bonds (olefins) in VUV irradiated FEP. Finally, the formation of the embrittled layer can be attributed to the formation of a highly cross-linked material near the surface. The similarity of the appearance of the laboratory and LDEF embrittled surface layers supports arguments for VUV radiation-induced degradation of FEP. Similarly embrittled layers have been found to form in PTFE and are also attributed to the formation of a highly cross-linked damage layer (ref. 4).



The absence of the embrittled layer on LDEF leading edge FEP films is readily accounted for due to atomic oxygen erosion which occurred during the course of the mission. In fact, there is considerable evidence for a strong synergistic effect between VUV and atomic oxygen in the erosion of FEP. Laboratory studies (ref. 5) have shown a considerable enhancement in reactivity of various materials to atomic oxygen in the presence of VUV. Morphological similarities of FEP films exposed to atomic oxygen and/or VUV in the laboratory and aboard LDEF have been observed and interpreted (ref. 6) via atomic force microscopy (AFM). The chemical alteration of the surface of LDEF FEP films is expected to lead to material which possesses higher reactivity to atomic oxygen. The upcoming Evaluation of Oxygen Interactions with Materials (EOIM-3) flight experiment scheduled for STS-46 in June 1992 presents a unique opportunity to assess this enhanced reactivity. Direct comparison of atomic oxygen erosion yields for "virgin" versus LDEF trailing-edge can readily be made with this flight experiment. The feasibility for utilizing LDEF FEP as a target material in the atomic oxygen reaction product detection portion of the EOIM-3 experiment is currently being examined.

Further laboratory studies are planned to perform *in situ* detection of VUV photolysis products from FEP. Direct mass spectrometry will be performed for FEP films irradiated at several wavelengths. The evolution of the product mass distributions as a function of irradiation time will

provide information on chain-scission and diffusion rates in the films. Measurement of the optical properties of irradiated FEP films are also planned and will be compared to the 10-year orbital flight data obtained from the SCATHA (P78-2) satellite (ref. 7).

Spacecraft engineers can readily account for changes in the optical absorption characteristics of external surfaces utilizing fluorocarbon-based thermal control materials. Concerns are raised for the mechanical integrity of such materials intended for extended use in the space environment. The baseline material for the exterior of the Space Station Freedom habitation modules is Beta-cloth. This material is a fluorocarbon impregnated woven glass fiber fabric. Based on the LDEF and laboratory investigations, the potential for Beta-cloth to become a significant source for particle contamination upon extended VUV exposure and thermal cycling should be assessed.

ACKNOWLEDGEMENTS

The research described in this publication was performed at the Jet Propulsion Laboratory, California Institute of Technology, under a contract with the National Aeronautics and Space Administration (NASA). The Long Duration Exposure Facility (LDEF) sample analysis was performed by the Materials Laboratory and the Center for Space Microelectronics of the Jet Propulsion Laboratory, California Institute of Technology, and was jointly sponsored by the Key Technologies Directorate of the Strategic Defense Initiative Organization (SDIO) through the Air Force Materials Laboratory of the Wright Research and Development Center and NASA. Laboratory vacuum-ultraviolet studies were performed by the Center for Space Microelectronics, Jet Propulsion Laboratory, California Institute of Technology, and were jointly sponsored by the Innovative Science and Technologies Directorate of SDIO and NASA.

REFERENCES

1. Seki, K., Tanaka, H., Ohta, T., Aoki, Y., Imamura, A., Fujimoto, H., Yamamoto, H., and Inokuchi, H., Physica Scripta, vol. 41, 1990, pp. 167-171.

2. Heath, D. Thekaekara, M., and White, O.R., ed., The Solar Output and Its Variation, Colorado Associated University Press, Boulder, CO, 1977, pp. 193-212.

3. Kim, S. S. and Liang, R. H., Polm. Prepr., Am. Chem. Soc., Div. Polm. Chem., vol. 31, no. 2, 1990, pp. 389-390.

4. a) Rye, R. R. and Shinn, N. D., Langmuir, vol. 6, no. 1, 1990, pp. 142-146;
b) Khrushch, B. I., Ershov, Y. A., Lyulichev, A. N., Udovenko, V. F., Pshishukha, A. M., Strizho, G. D., Khimiya Vysokikh Energii, vol. 15, no. 6, 1981, pp. 520-525.

5. Koontz, S., Leger, L., Albym, K., and Cross, J., J. Spacecraft and Rockets, vol. 27, 1990, pp. 346-348.

6. Stiegman, A. E., Brinza, D. E., Anderson, M. S., Minton, T. K., Laue, E. G., and Liang, R. H., An Investigation of the Degradation of Fluorinated Ethylene Propylene (FEP) Copolymer Thermal Blanketing Materials Aboard LDEF and in the Laboratory, JPL Publication 91-10, 1991.

7. Hall, D. F. and Fote, A. A., Ten Year Performance of Thermal Control Coatings at Geosynchronous Altitude, AIAA Paper 91-1325, 1991.



Figure 1. SEM cross-sectional image of LDEF Ag/FEP control specimen showing sheared edge (magnification: x400).

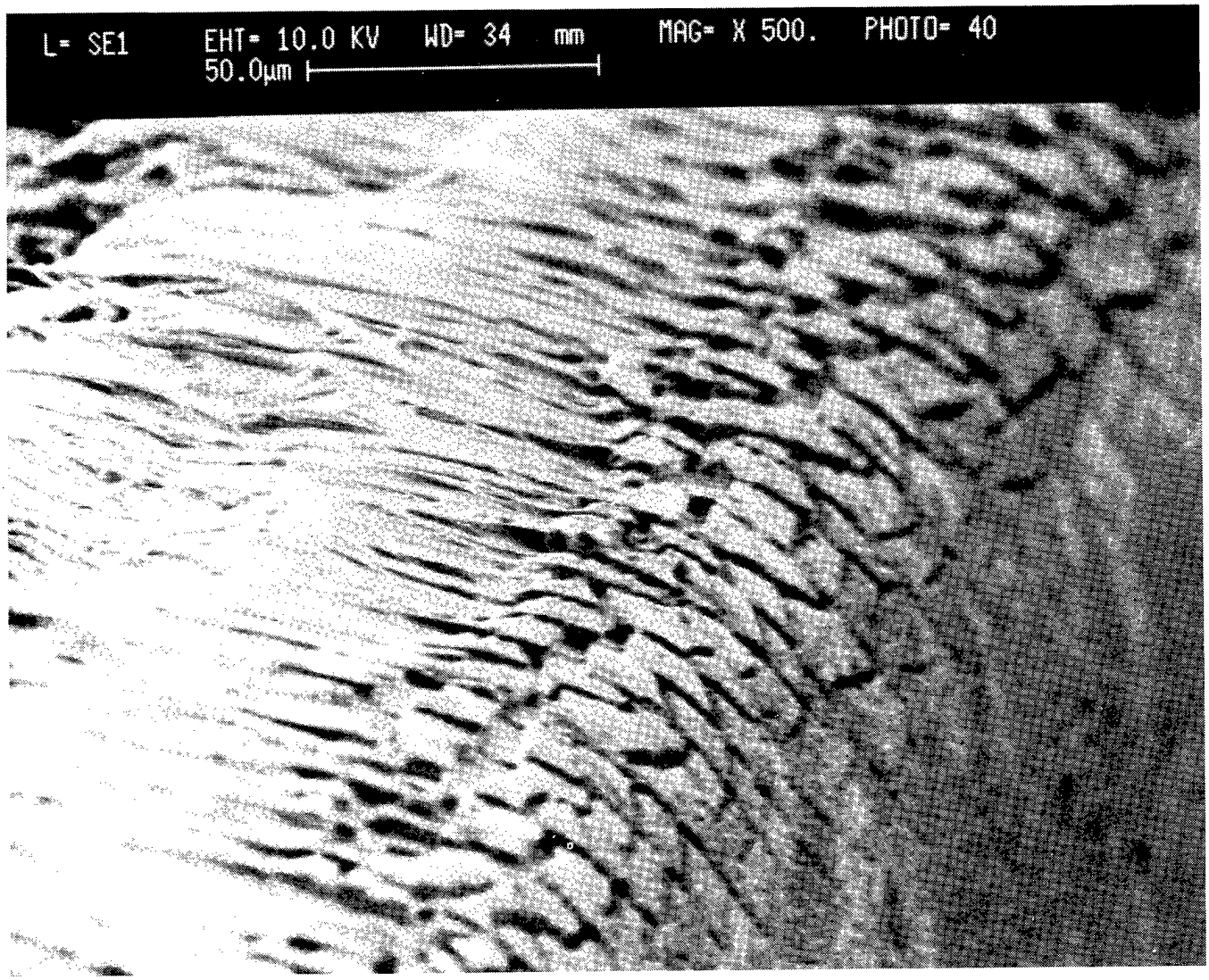


Figure 2. SEM image of sheared edge of trailing edge LDEF Ag/FEP specimen from showing embrittled surface layer (magnification: x500).

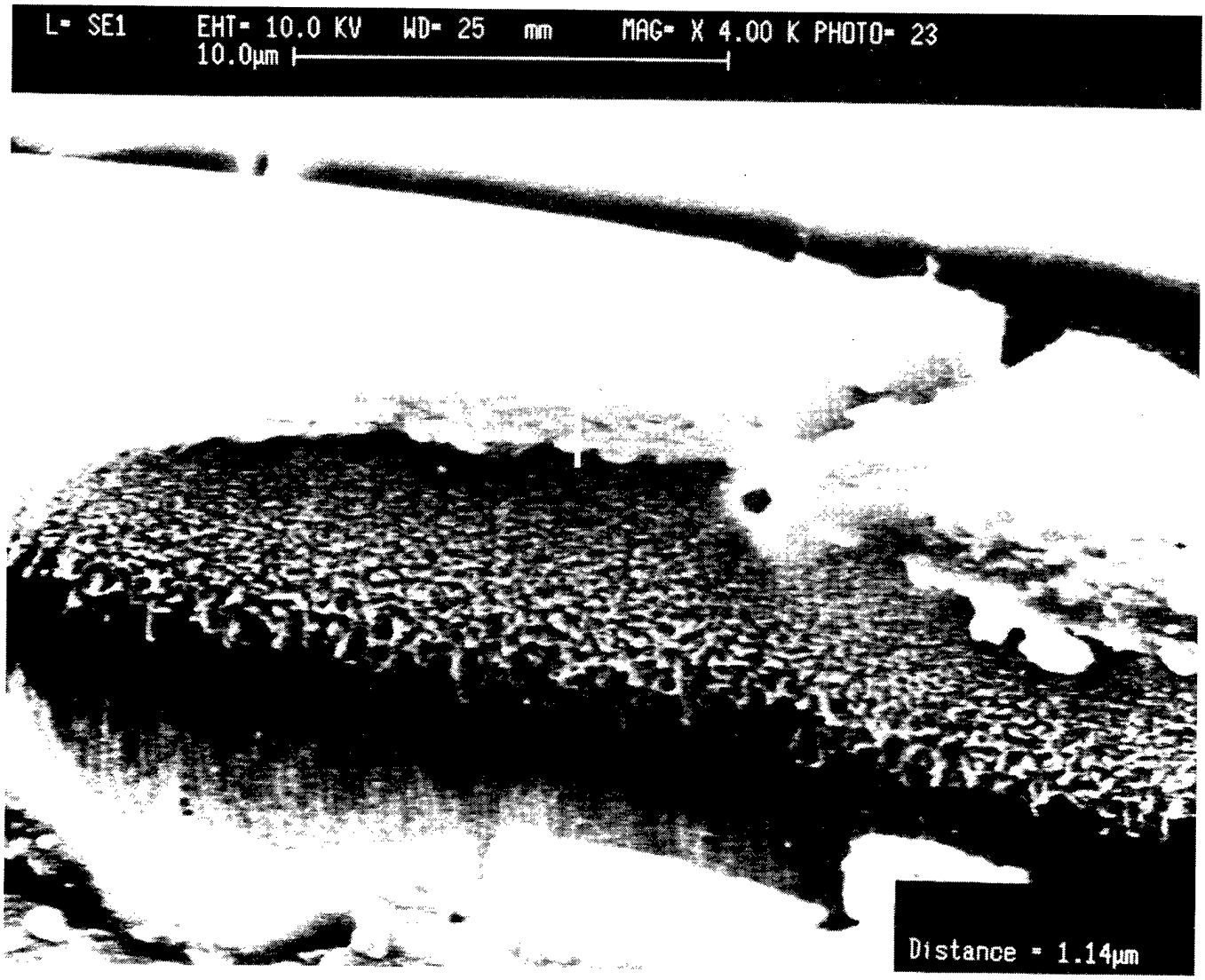


Figure 3. Detailed SEM image of trailing edge (P0004) LDEF Ag/FEP surface note the approximately 1 micron thick fragile layer.

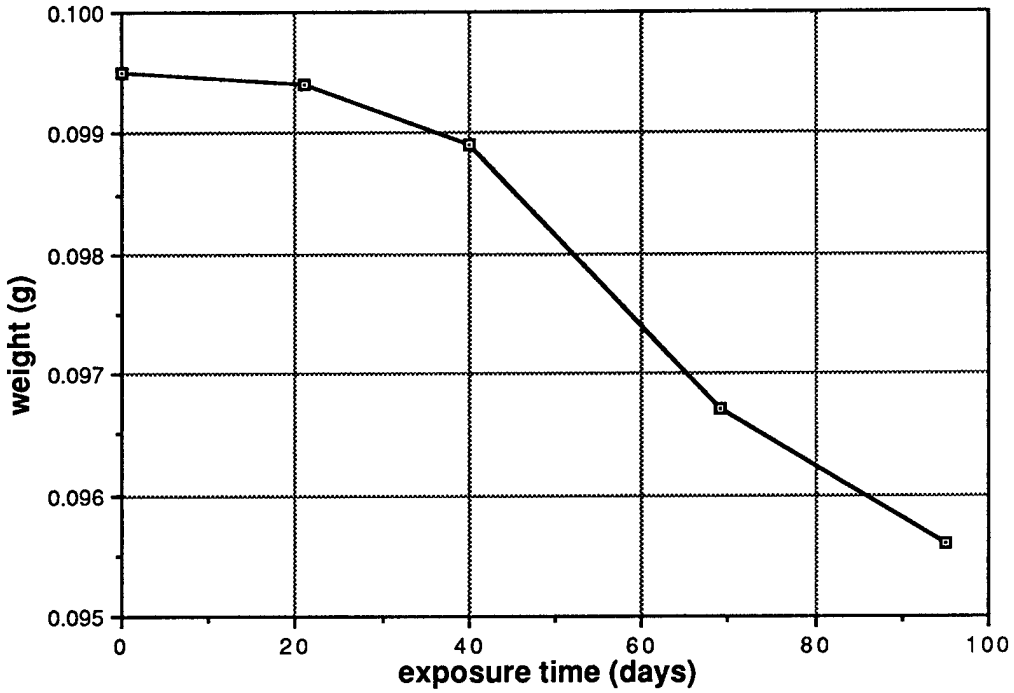


Figure 4. Mass loss as a function of exposure time for FEP irradiated with a deuterium lamp.

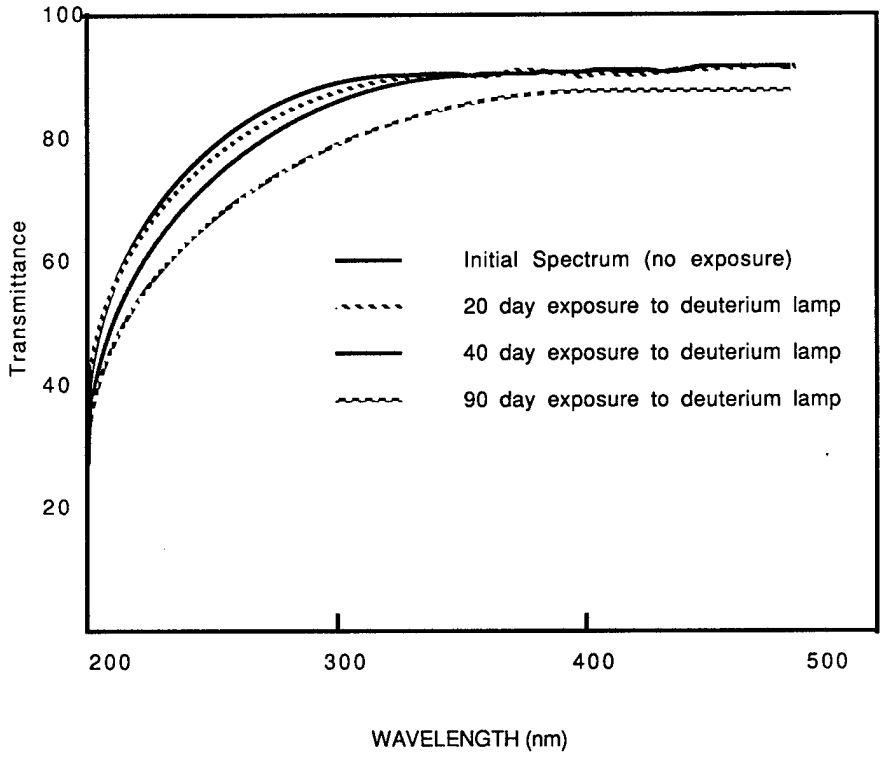


Figure 5. Optical transmission spectra for deuterium lamp irradiated FEP film at periodic exposure intervals.

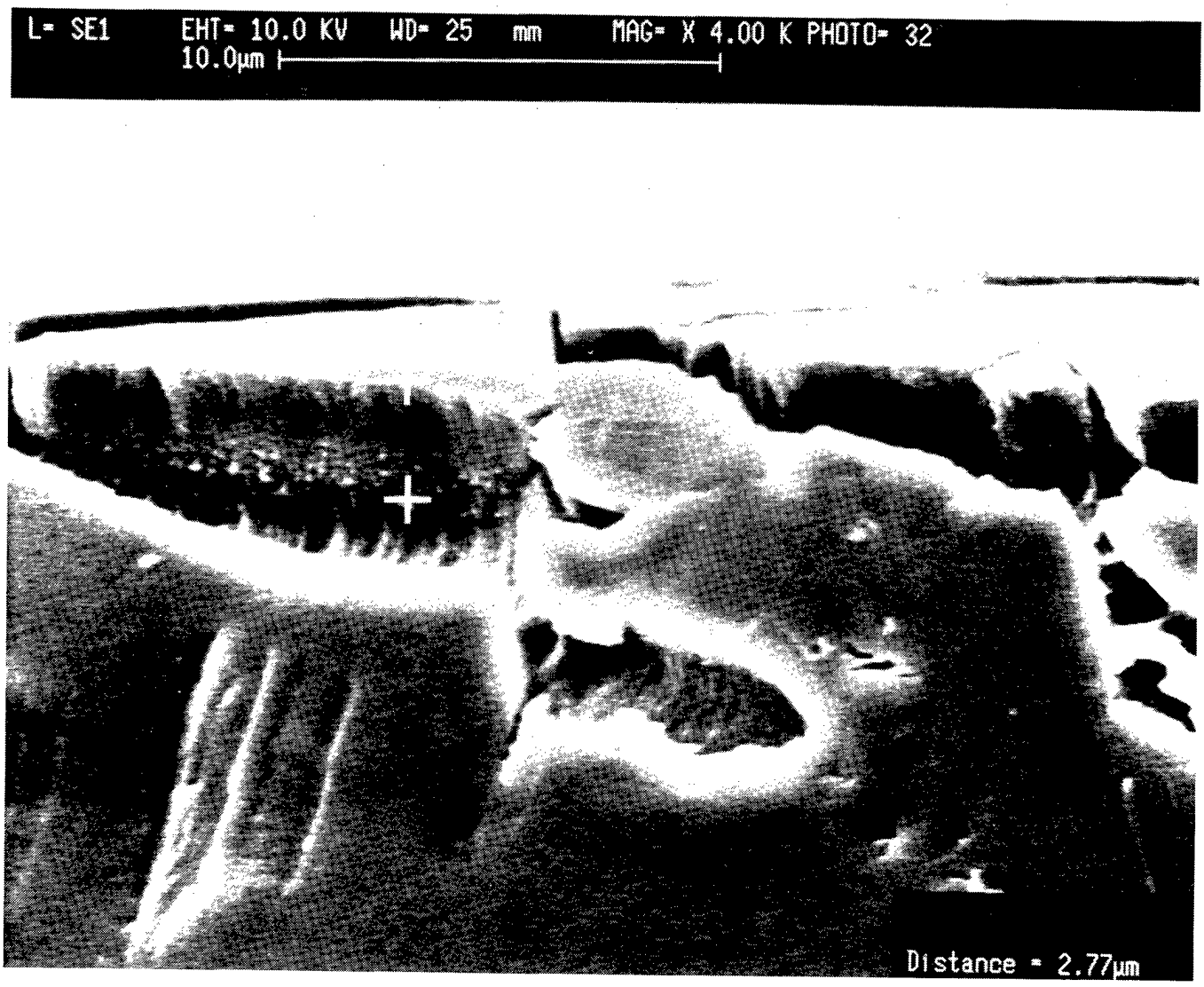


Figure 6. Detailed SEM image of the embrittled layer observed in sheared FEP exposed to a deuterium lamp for 92 days.

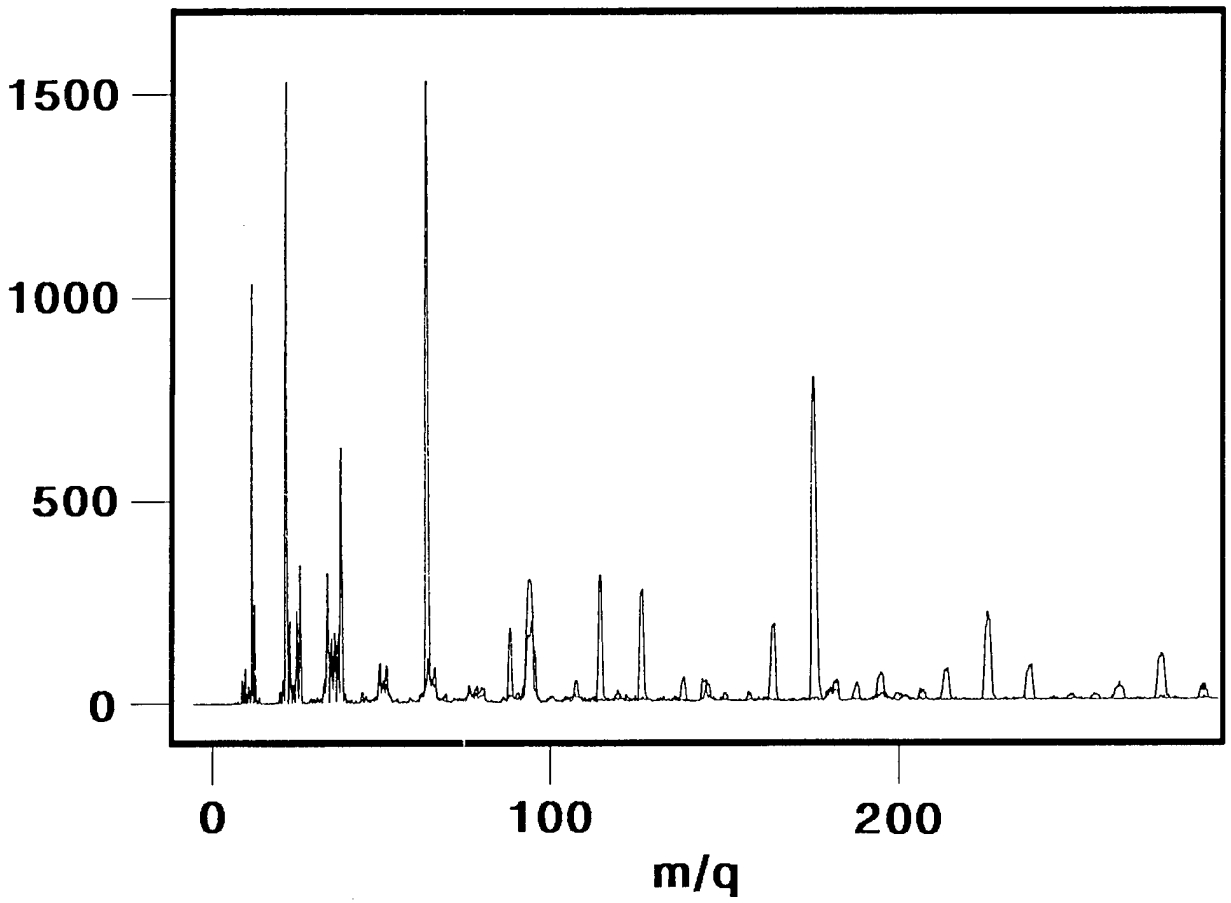


Figure 7. Mass spectroscopic analysis of residual gas from FEP exposed to VUV-radiation in a sealed, evacuated cell.

SPACE ENVIRONMENTAL EFFECTS ON SILVERED TEFLON THERMAL CONTROL SURFACES

C. S. Hemminger
W. K. Stuckey
J. C. Uht
The Aerospace Corporation
El Segundo, CA 90245
Phone: 310/336-1619, 310/336-7389; Fax: 310/336-1636

ABSTRACT

Cumulative space environmental effects on Ag/FEP were a function of exposure orientation. Samples from nineteen silvered Teflon (Ag/FEP) thermal control surfaces recovered from LDEF have been analyzed to determine changes in this material as a function of position on the spacecraft. Although solar absorptance and infrared emittance of measured thermal blanket specimens are relatively unchanged from control specimen values, significant changes in surface morphology, composition and chemistry were observed.

All Ag/FEP surfaces exposed to high atomic oxygen flux (rows 7-11), irrespective of exact angle, had a uniform cloudy appearance due to surface erosion. Scanning electron microscopy (SEM) showed a surface topography with sharp peaks and valleys, while x-ray photoelectron spectroscopy (XPS) detected a surface composition corresponding to contamination-free FEP, with less than 1 mole % oxygen.

Ag/FEP samples from rows 2 and 4, which flank the trailing edge row 3, had a nonuniform appearance, with alternating clear and cloudy bands. SEM imaging showed an intriguing variety of surface texturing in the cloudy areas, with surface wrinkling and puckering being most prevalent. XPS showed these surfaces to be contaminated nonuniformly with moderate to high concentrations of Si, O, C, N and S. Ultraviolet irradiation and thermal cycling ($< 0°C$) are presumed to be the dominant environmental factors.

The row 1, 5 and 6 samples, which are at larger angles to the trailing edge and exposed to low atomic oxygen flux, showed little or no texture development, and no surface contamination except low oxygen (which could be due to post-flight atmospheric exposure). XPS analysis does show significant degradation of the surface FEP on these rows, which we attribute primarily to UV radiation. The surface features are consistent with FEP molecular weight degradation, branching and crosslinking through free radical reactions, which can also be induced by x-ray or high energy electron irradiation.

We hypothesize that the FEP surfaces on LDEF are degraded by UV exposure at all orientations, but that the damaged material has been removed by erosion from the blankets exposed to atomic oxygen flux and that contamination is masking the damage in some areas on the trays flanking the trailing edge.

INTRODUCTION

Silvered Teflon (fluorinated ethylene propylene, FEP) is a light-weight thermal control material used extensively on satellite hardware. The thin silver film provides high solar reflectance while the transparent FEP Teflon overlayer gives high infrared emittance. Seventeen of the Long Duration Exposure Facility (LDEF) experiment trays were covered by Ag/FEP thermal blankets, and adhesively bonded Ag/FEP material protected a number of smaller components. Visible changes were noted on the Ag/FEP on both leading and trailing edges during the initial observations upon retrieval of LDEF: changes included surface cloudiness, discoloration and delamination at the metal/polymer interface. The leading edge blanket surfaces have become diffuse and appear uniformly cloudy. The trailing edge blankets exhibit clear areas that are visibly unaffected, and cloudy areas. Some of the adhesively bonded Ag/FEP surfaces are significantly discolored; discoloration was also observed on many blanket edges near vents.

Solar absorptance and infrared emittance measurements on samples from the thermal blankets with 5 mil FEP have determined that the space environment exposed material has values that are relatively unchanged from control specimen values (ref. 1). This includes samples with extensive visible change such as the diffuse leading edge blanket surfaces. Material with a thinner FEP layer, e.g. adhesively bonded Ag/2 mil FEP, did show significant infrared emittance change due to a higher percentage of the FEP layer lost to atomic oxygen erosion (ref. 2). Highly discolored areas of Ag/FEP also have measurably changed thermal control properties.

In this study samples of Ag/FEP have been analyzed from as many LDEF locations as available to determine surface changes in the material as a function of position on the spacecraft. Significant changes in surface morphology, composition and chemistry were observed.

EXPERIMENTAL

Samples

Ag/FEP samples were obtained from ten of the twelve rows of LDEF for this investigation. Exposed and protected edge samples from 14 of the 16 blankets from A0178, High-Resolution Study of Ultra-heavy Cosmic-Ray Nuclei (Dublin Institute for Advanced Studies and European Space Agency, ESTEC) were obtained through the Materials Special Investigation Group. Many of these pieces were cut from the ground strap section. A sample from the P0004-1 Seeds in Space Experiment (George W. Park Seed Company, Inc.) blanket was provided by NASA Langley. Adhesively bonded samples were obtained on row 9 from M0003, Space Environment Effects on Spacecraft Materials, of The Aerospace Corporation and from the A0076 Cascade Variable-Conductance Heat Pipe Experiment of McDonnell Douglas Astronautics Company. A map showing the areas in gray from which samples were obtained is shown in Figure 1. A schematic representation of the blankets is shown in Figure 2, indicating the Teflon, silver, Inconel, and paint which comprise the entire blanket structure as used on LDEF.

Scanning Electron Microscopy / Energy Dispersive X-ray Spectroscopy (SEM/EDS)

Ag/FEP samples from 9 of the 12 rows have been examined by SEM/EDS; their locations are indicated on the Figure 1 map. The FEP surfaces were coated by carbon evaporation to

minimize surface charging effects. A JEOL 840 SEM with an EDAX 9900 EDS system was used for this study. Electron micrographs were acquired using a 5 kV accelerating voltage.

X-Ray Photoelectron Spectroscopy (XPS)

One or more sections of each available Ag/FEP sample was analyzed by XPS using a VG Scientific LTD. ESCALAB MK II. Samples were mounted on standard sample stubs with double-sided tape. The Mg Kα source was chosen for x-ray irradiation. Survey scans from 0 to 1100 eV binding energy were acquired to qualitatively determine the sample surface composition; analysis depth is about 50 - 100 Å. High resolution elemental scans were subsequently run to obtain semi-quantitative elemental analyses from peak area measurements and chemical state information from the details of binding energy and shape. Surface charge corrections were made by setting the F1s peak binding energy to 289.0 eV. Measured peak areas for all detected elements were corrected by elemental sensitivity factors before normalization to give surface mole %. The quantitation error on a relative basis is ≤10% for components >1 mole %. Large uncertainties in the relative elemental sensitivity factors can introduce absolute errors of a factor of two or even greater. All elements of the periodic table except H and He can be detected by XPS with a Mg Kα source. The detection limit is about 0.1 surface mole %, but spectral overlaps between large peaks and small peaks can make it impossible to detect minor components.

RESULTS AND DISCUSSION

The leading edge samples were uniform in appearance from rows 7 through 11. Typical results of analyses with SEM and XPS are shown in Figure 3. The control surface, which is a non-flight FEP surface, is featureless in the SEM while the flight sample shows a typical erosion pattern in FEP for high velocity atomic oxygen erosion. The XPS data for the control surface shows carbon and fluorine only. The XPS analysis of the exposed surface shows that the surface composition of the FEP remaining after the erosion is indistinguishable in carbon and fluorine composition from the control, with trace amounts of some contaminants (Si, N, S, and Cl) and measurable oxygen present. This oxygen could be from the atomic oxygen interaction or from water adsorption from the atmosphere after retrieval. Water adsorption could be enhanced on the erosion-roughened surfaces which have much higher surface area than the control. Some variations in the erosion pattern on leading edges were observed as shown in Figure 4.

Exposed trailing edge samples were found to have developed a wide variety of surface morphologies, very distinct in appearance from the featureless control surface and the atomic oxygen eroded surfaces. The blanket surface areas which appear fogged or cloudy on the trailing edge have become sufficiently diffuse to change visibly. Many of the clear, visibly unaffected areas, however, also have morphology changes, as seen in Figure 5. Within short distances on some trailing edge samples both the surface morphology and surface contamination levels were observed to change dramatically. This is shown in Figure 6; silicon, detected as SiO_2, is one of the most significant contaminants on trailing edge Ag/FEP surfaces. It is currently not clear if any causal relationship exists between observed morphology type and surface contamination build-up. It is possible that some morphologies will have a higher probability of trapping or adsorbing outgassed or backscattered species, thereby leading to greater surface contamination buildup. Some additional morphology types observed on exposed trailing edge FEP surfaces are seen in Figures 7 and 8. Figure 7 shows a series of closely spaced bands on a section of the thermal blanket from bay A of row 2 (A2). Figure 8 shows that some trailing edge surfaces are still relatively smooth; this was most typical of samples at larger angles to the trailing edge, e.g. rows 1, 5 and 6. EDS analysis showed the bright spots to be relatively high in Si concentration.

A summary of the SEM and XPS results is shown in Table I. The leading edge samples, from row 7 to 11, all show the roughened surface typical of atomic oxygen erosion of FEP. The XPS results indicate a clean, relatively uncontaminated surface with only small increases in surface oxygen concentration. Because of low contamination and a carbon 1s (C1s) XPS spectrum indistinguishable from the control material, the leading edge surfaces are characterized as clean FEP. The C1s spectrum from the D7 blanket surface is shown in Figure 9a; curve-fitting reveals the major CF_2 peak at 292 eV and moderate CF and CF_3 peaks (approximately 10% each) at 289.5 eV and 294 eV respectively. This matches the spectrum predicted for FEP with an approximate ethylene/propylene comonomer blend of 90%/10%

On the trailing edge of LDEF changes are observed both by SEM and XPS. The surfaces have lost the smooth, featureless texture of the unexposed FEP, even when the amount of contamination remains low, as indicated by silicon concentration. XPS data divides the trailing edge surfaces into two categories. The first is characterized by low contamination levels (Si < 1%) and a C1s spectrum as in Figure 9b that differs significantly from that of clean FEP, but does not have a major peak at 285 eV. The second category is characterized by moderate to high levels of surface contamination (Si, O, C, N, and S) and a C1s spectrum dominated by a peak at 285 eV, as seen in Figure 9c and d. The C1s peak at 285 eV is predominantly due to C-C bonds, and is thought to build up on the trailing edge surfaces from decomposition products of outgassed hydrocarbons and silicones.

The C1s spectrum in Figure 9b arises from degradation of the FEP surface. Curve-fitting shows that the decrease in intensity of the CF_2 peak at 292 eV is accompanied by major increases in intensity at 294 eV, 289.5 eV and 287 eV, assigned to CF_3, CF and C-$(CF_n)4$ respectively. These changes are consistent with damage to the carbon backbone of the Teflon polymer resulting in molecular weight degradation, new chain terminations, branching and crosslinking through free radical reactions. The solar ultraviolet (UV) radiation exposure of the LDEF surfaces is thought to have caused this FEP surface degradation. The FEP surfaces were also exposed to the stress of about 34,000 thermal cycles, but the maximum temperatures calculated for Ag/FEP blankets on LDEF are less than 0°C (ref. 3) and not sufficient to break chemical bonds. Exposure of FEP to the XPS x-ray source for several hours induced similar shifts in the C1s spectrum; almost all of the FEP C1s spectra used for curve-fitting in this study were acquired during the first minute of sample exposure to the x-ray source to minimize surface degradation from the analysis itself. A recent study of the degradation of polytetrafluoroethylene (PTFE) Teflon by 3 keV electrons showed very similar XPS C1s spectra changes to those seen in Figure 9b as a function of electron irradiation and subsequent heating to drive off volatiles.(ref. 4). Degradation of the PTFE was attributed to the type of damage described above.

Future work with the LDEF AG/FEP thermal control material at this facility will address the problem of delamination at the metal/polymer interface. This interface strength degrades during earth storage of laboratory controls and deterioration is accelerated in the space environment. A delamination of the Ag/FEP has the potential for catastrophic failure of the material's thermal control properties; this was deterred on the LDEF blankets by the presence of the paint on the back surfaces. We are also interested in the effects of adhesive bonding on Ag/FEP performance. Discoloration and streaking was observed at the metal/polymer interface of adhesively bonded Ag/FEP on LDEF, with some degradation of thermal control properties.

SUMMARY

The cumulative space environmental effects on Ag/FEP were a function of location and exposure orientation. The leading edge of LDEF was dominated by the effect of the atomic oxygen resulting in erosion of the Teflon. The resulting surfaces were highly textured and not significantly contaminated; contaminants and UV-degraded FEP appear to have been removed by the surface erosion. The trailing edge samples had a wide variety of new surface morphologies in addition to the presence of more extensive contamination. On trailing edge surface areas where contamination was relatively low (particularly at larger angles to the trailing edge), XPS detected degraded FEP, most likely caused by UV exposure. This degradation appears to result from damage to the carbon backbone of the Teflon polymer resulting in molecular weight degradation, new chain terminations, branching and crosslinking through free radical reactions. The UV degradation could have occurred at a slow rate during the entire mission but the erosion of the Teflon would have occurred more rapidly near the end of the mission as the altitude dropped and the atomic oxygen flux rapidly increased.

ACKNOWLEDGEMENTS

The authors would like to acknowledge the many contributors to this work within The Aerospace Corporation, including T. Giants, S. Gyetvay, J. Mallon, N. Marquez, and C. Su. In addition we would like to thank H. G. Pippin of Boeing Aerospace & Electronics and W. Slemp of NASA Langley Research Center for making the samples available to us, and D. Wheeler of NASA Lewis Research Center for his helpful discussions on Teflon radiation damage.

REFERENCES

1. B. A. Stein and H. G. Pippin: Preliminary Findings of the LDEF Materials Special Investigation Group. First LDEF Post-Retrieval Symposium. NASA CP-3134, 1992.

2. D. R. Wilkes, L. M. Hummer, M. J. Brown, and J. M. Zwiener: Thermal Control Surfaces Experiment (S0069) Initial Materials Investigation. First LDEF Post-Retrieval Symposium. NASA CP-3134, 1992.

3. W. M. Berrios and T. R. Sampair: LDEF Post Flight Thermal Analysis. LDEF Science Office, NASA Langley Research Center.

4. D. R. Wheeler and S. V. Pepper: X-ray Photoelectron and Mass Spectroscopic Study of Electron Irradiation and Thermal Stability of Polytetrafluoroethylene. J. Vac. Sci. Technol. vol A8, no. 6, Nov/Dec 1990, pp. 4046-4056.

TABLE I. SUMMARY OF SEM AND XPS RESULTS

LDEF Row	SEM Morphology of Exposed FEP Surface	Bay	Surface Si%	Surface O%	C1s Envelope
1	Smooth; particulate contamination	D	0.2	2	Degraded FEP
2		A	0.7	6	Degraded FEP
2		F(Boeing)	2 - 8	11 - 32	Contamination
2	Puckered texture; more distinct in cloudy bands	F(NASA)	8 - 19	30 - 51	Contamination
3 (TE)					
4	Puckered and wrinkled textures in bands	F	0.2 - 7	4 - 31	Contamination
4		A	0.1	3	Degraded FEP
5	Slighty lumpy (B)	B, C, D	0.1	3 - 5	Degraded FEP
6	Some areas of puckered texture	C	<0.1	1 - 2	Degraded FEP
7	Eroded, sharp pinnacles (B)	B, D	<0.1	0.6	Clean FEP
8	Eroded, sharp pinnacles	C	<0.1	0.6	Clean FEP
9 (LE)		D, F	0.1 - 0.8	0.8	Clean FEP
10	Eroded, rounded peaks	A	0.1	0.6	Clean FEP
11	Eroded, sharp pinnacles (C)	C,D	<0.1	0.4	Clean FEP
12					
Control FEP	Smooth, featureless		<0.1	<0.1	Clean FEP

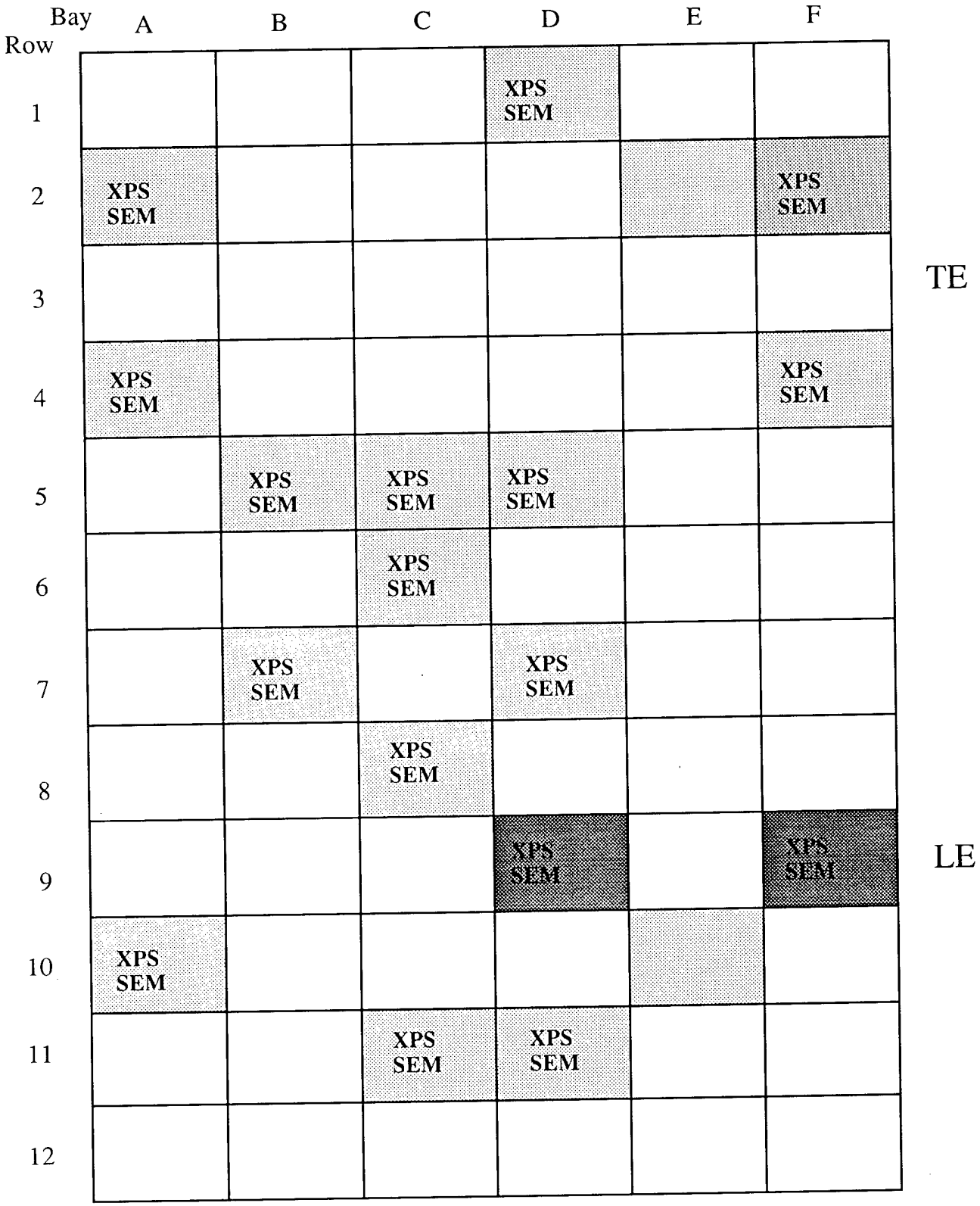


Figure 1. Silvered Teflon blanket locations on LDEF are indicated by areas in gray. Blankets used for SEM and XPS studies are also shown. Row 9 samples are adhesively bonded.

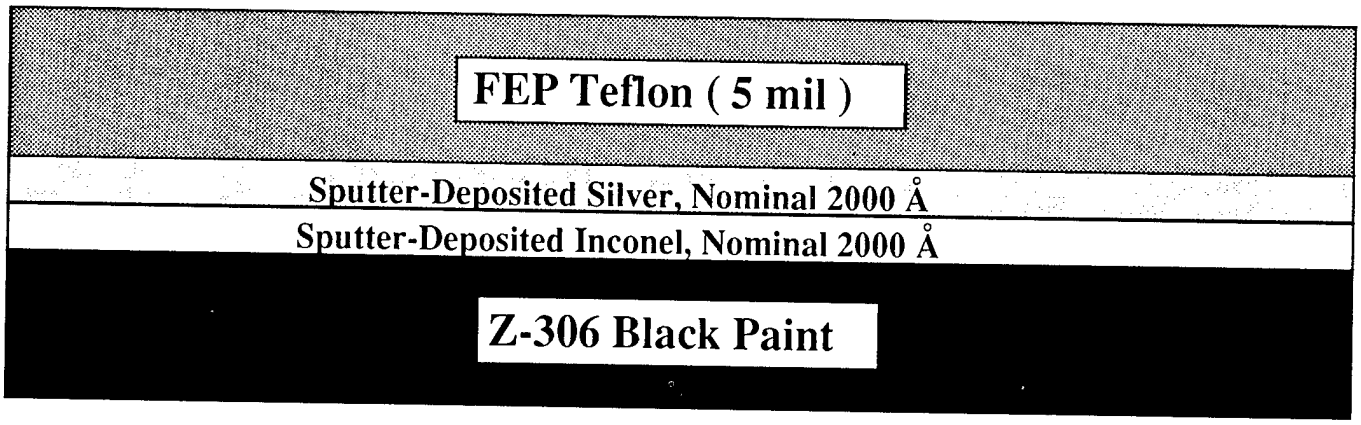
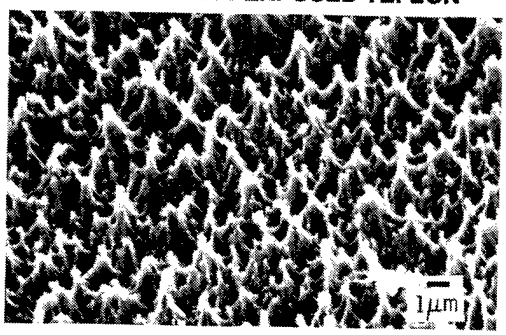


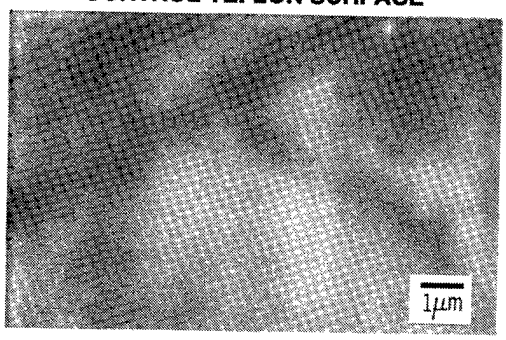
Figure 2. Schematic of 5 Mil Silvered Teflon Thermal Blankets

Scanning Electron Microscope Image

LDEF TRAY C11 EXPOSED TEFLON



CONTROL TEFLON SURFACE



Surface Composition Determined by X-Ray Photoelectron Spectroscopy

MOLE %

C	F	O	OTHER
27	72	0.4	TRACE Si, N, S, Cl
27	73	TRACE	NONE DETECTED

Figure 3. Leading edge sample of Ag/FEP compared to control sample. Typical results of analyses with SEM and XPS.

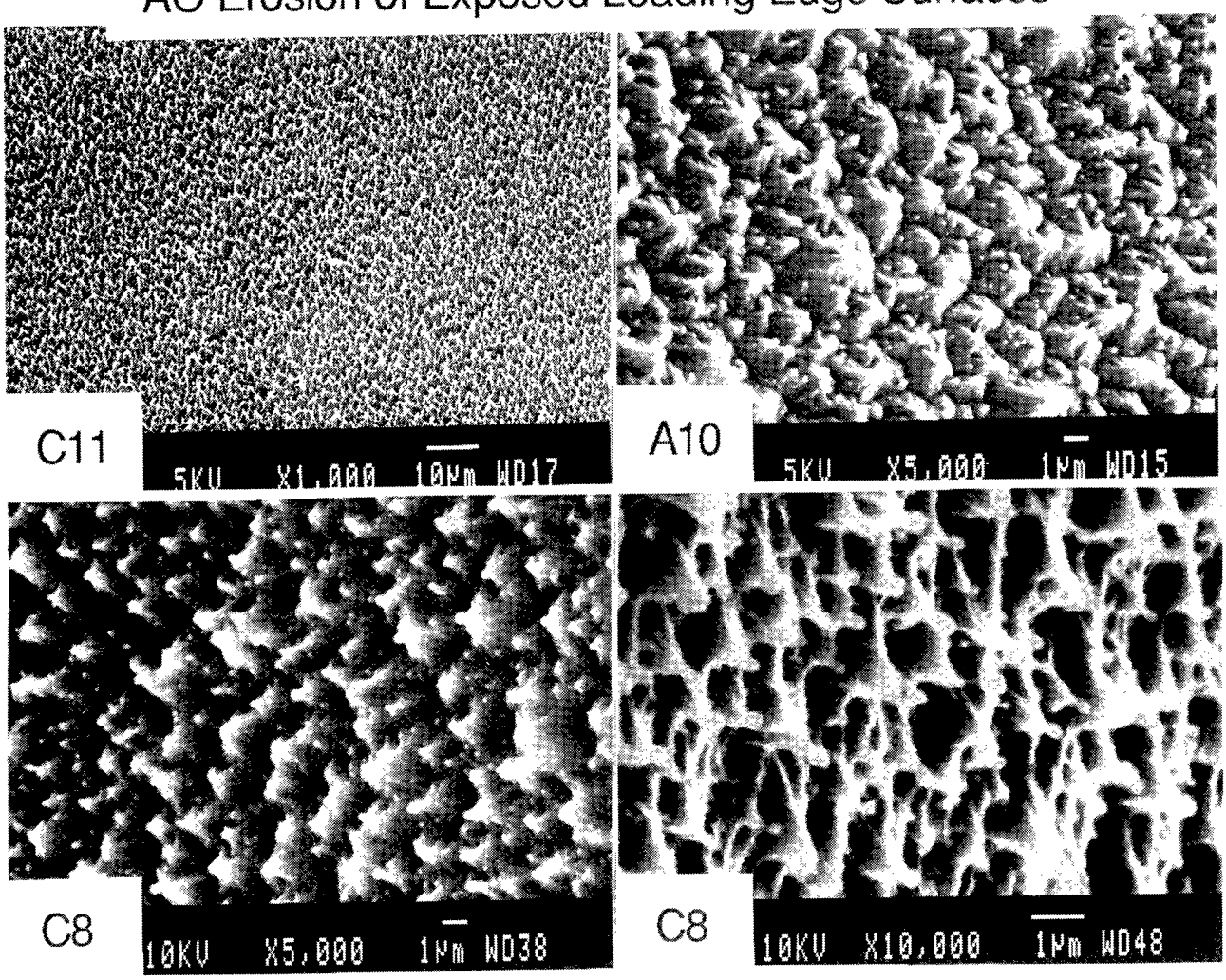


Figure 4. Some variations in the erosion pattern on leading edge samples of Ag/FEP.

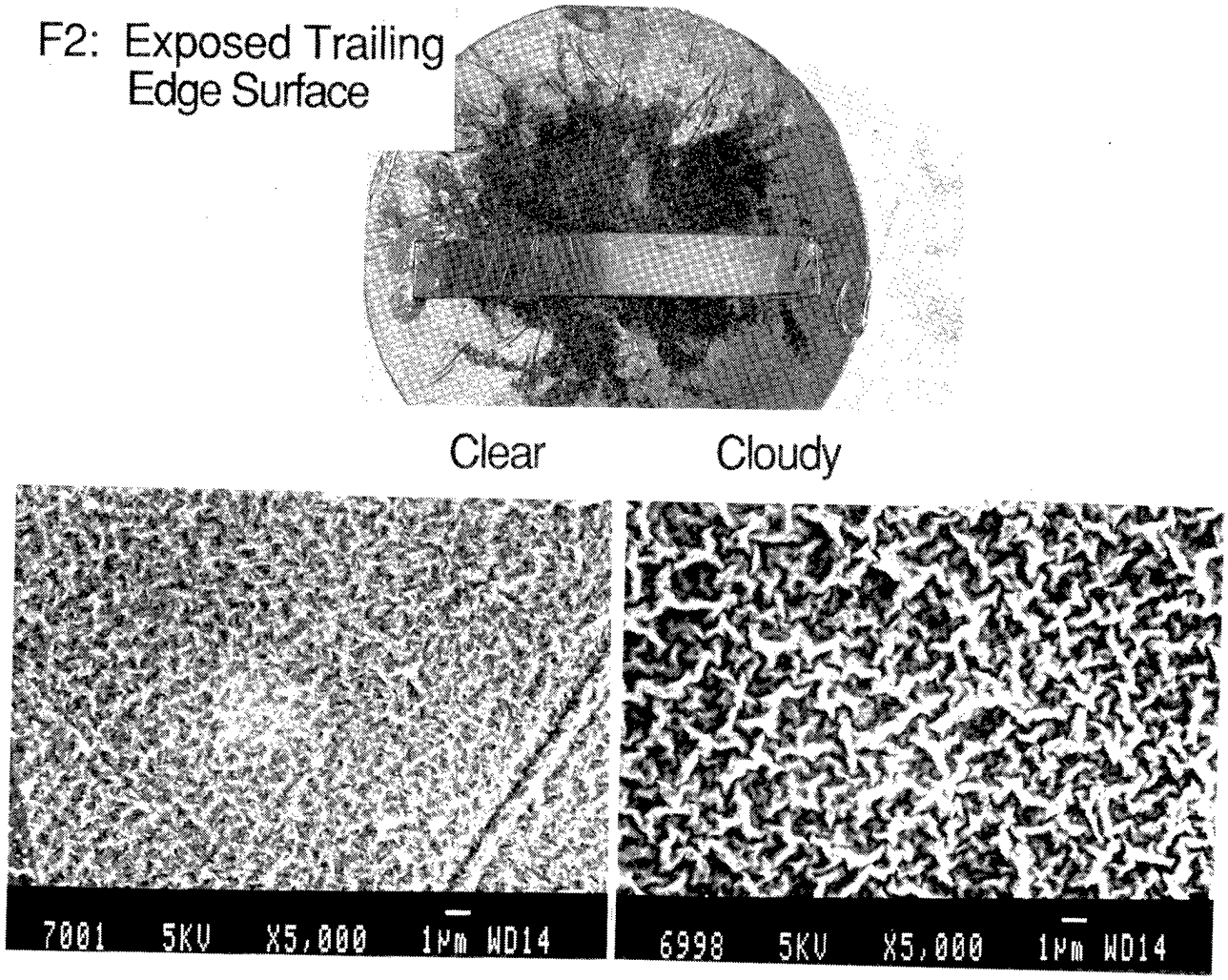


Figure 5. Exposed trailing edge surface from F2 showing morphology changes by SEM in adjacent clear and diffuse areas of Teflon.

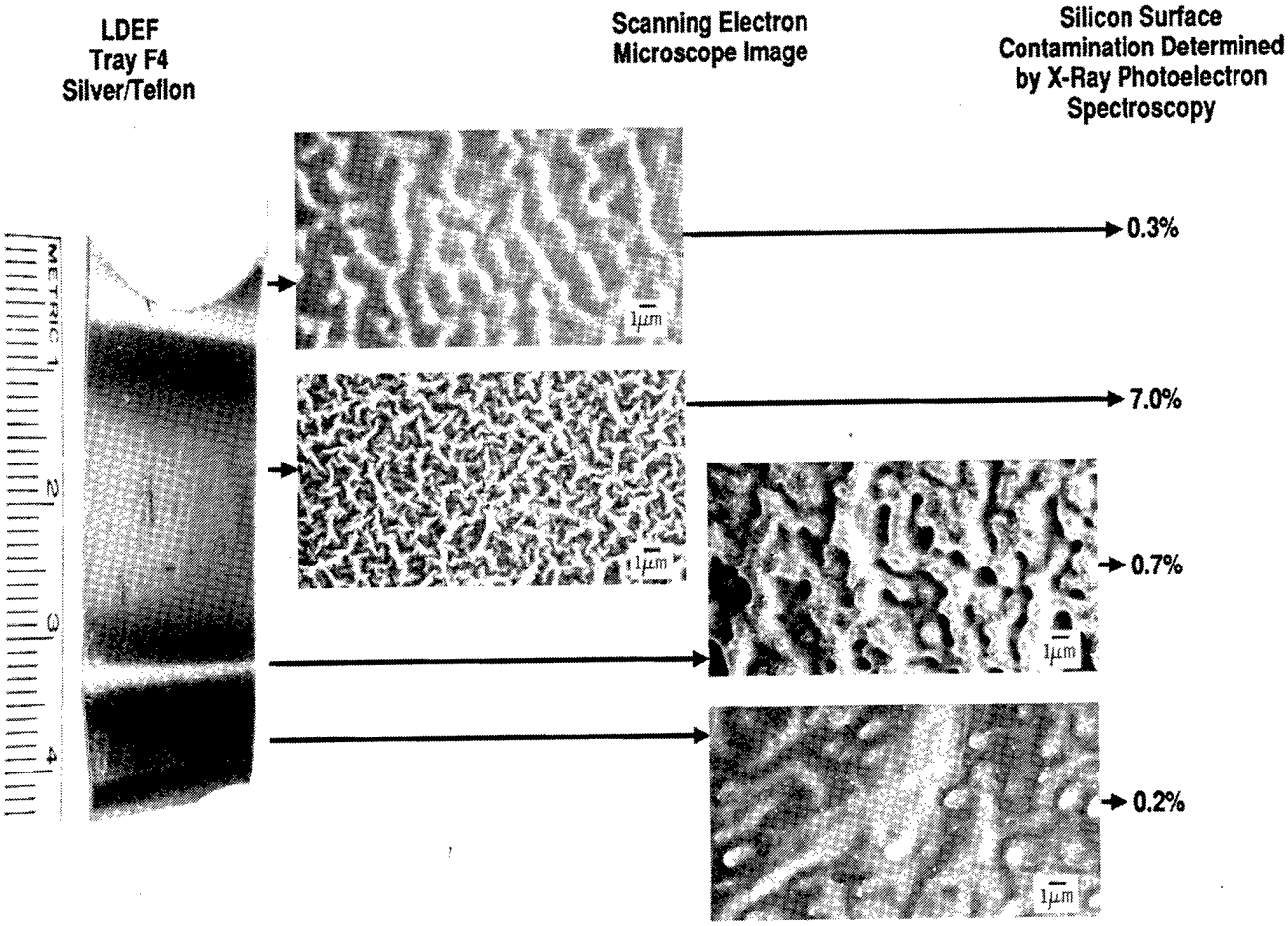


Figure 6. Changes in Teflon surface morphology and surface contamination level, as represented by Si concentration, for a series of adjacent bands on an exposed trailing edge surface from F4.

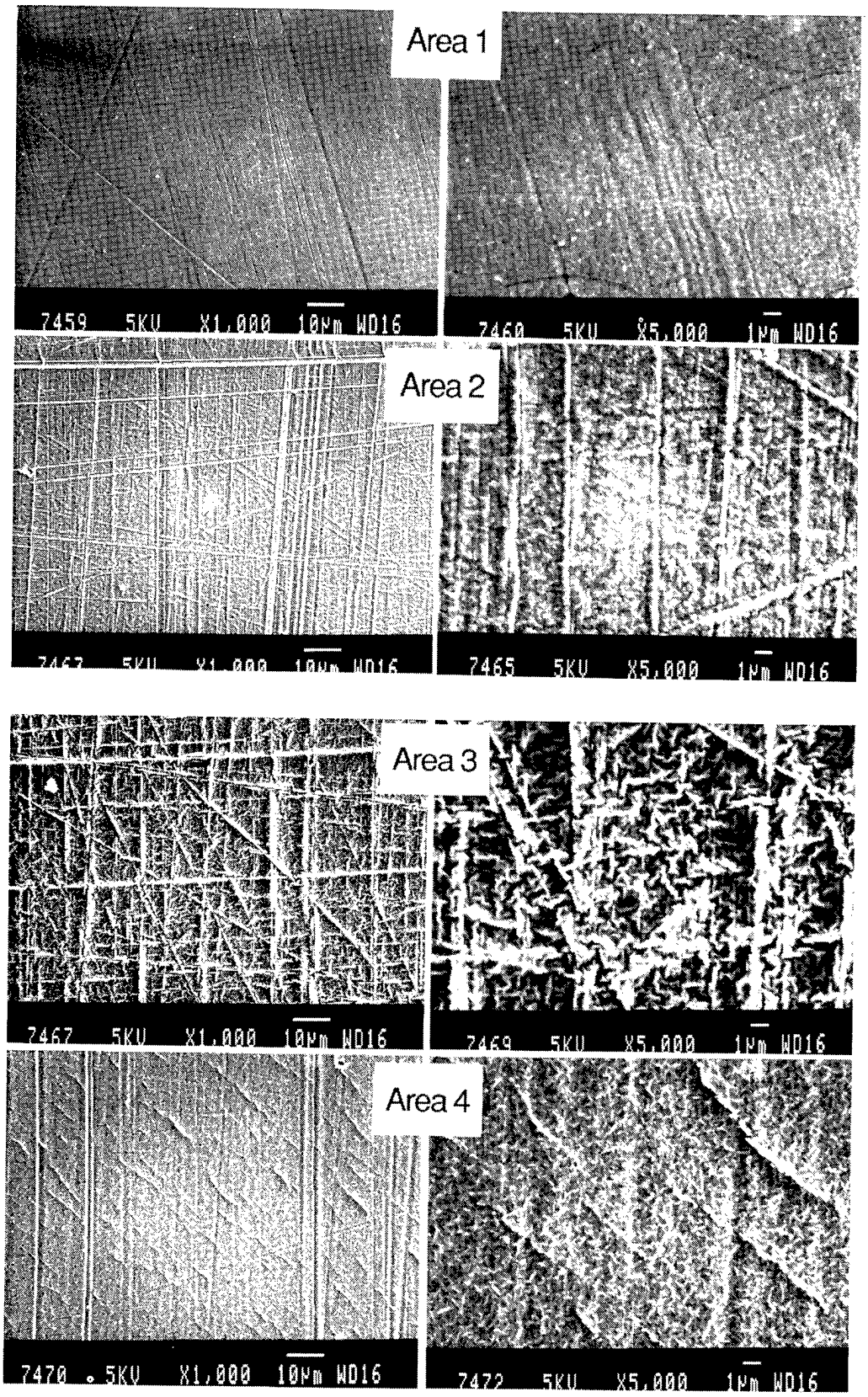


Figure 7. SEM images of morphologies in a series of 6 closely spaced bands on a section of exposed Teflon from trailing edge A2.

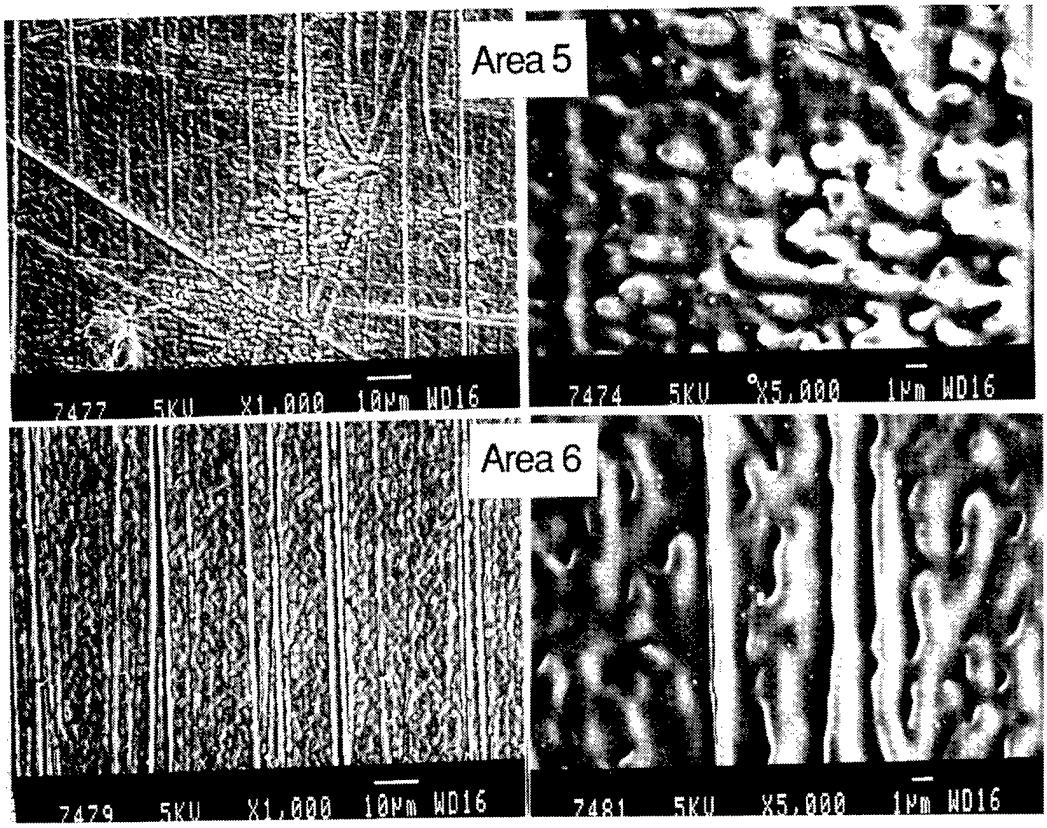


Figure 7. SEM images of morphologies in a series of 6 closely spaced bands on a section of exposed Teflon from trailing edge A2.

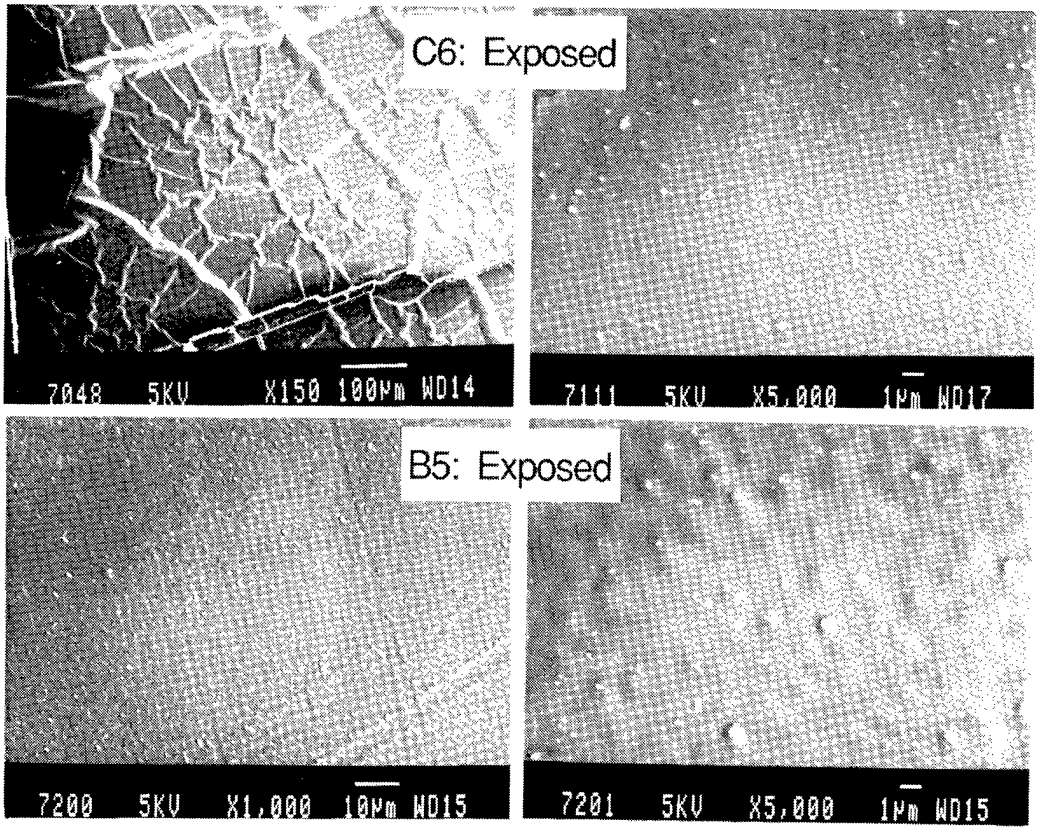


Figure 8. Exposed trailing edge surfaces that are still relatively smooth. Bright spots are relatively high in Si concentration.

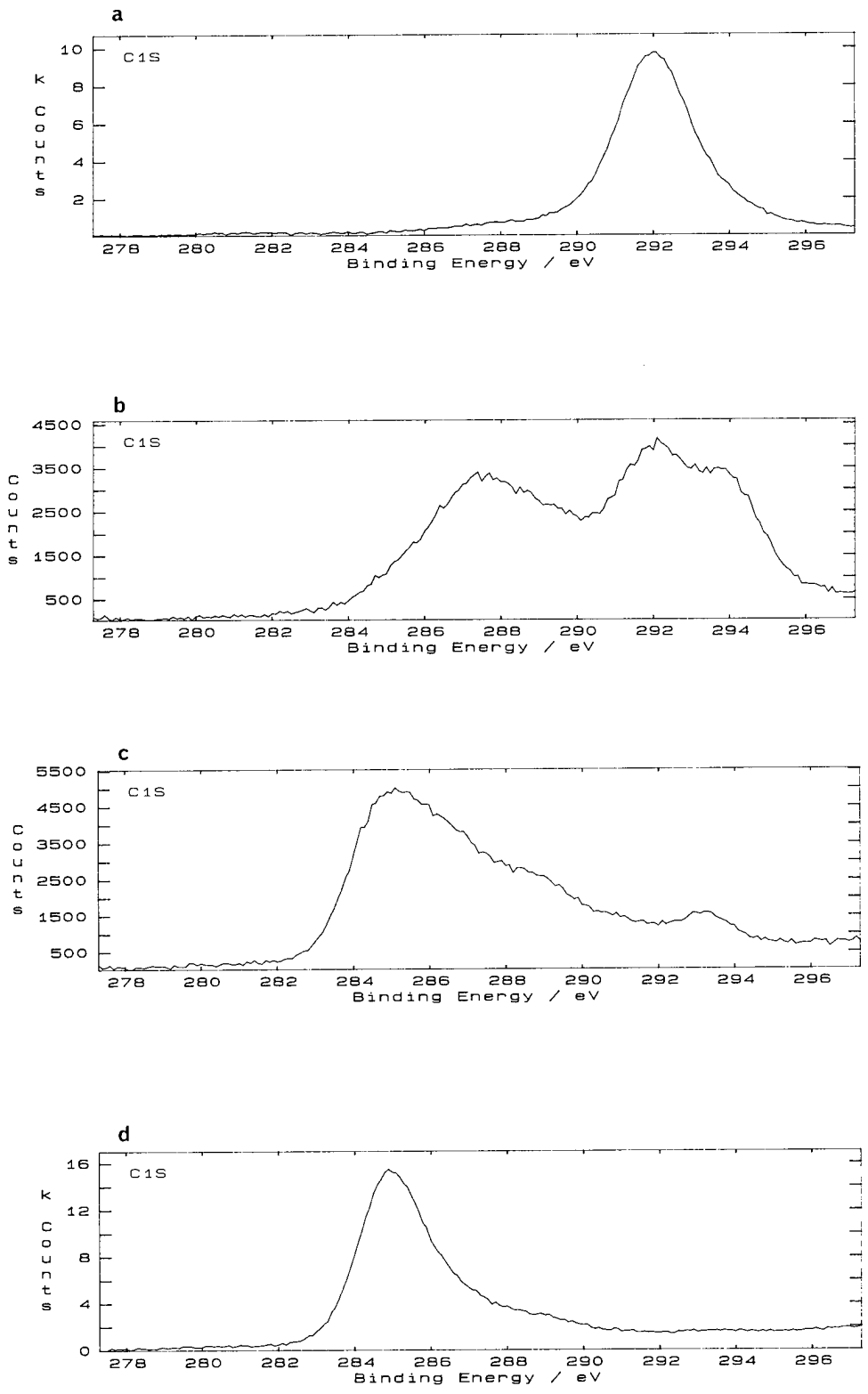


Figure 9. XPS spectra of the C1s region from Ag/FEP blanket surfaces.
a. D7 blanket surface. Characteristic of clean FEP.
b. B5 blanket surface. Characteristic of degraded FEP.
c. F4 blanket surface. Characteristic of contaminated, degraded FEP.
d. F2 blanket surface. Characteristic of heavily contaminated FEP.

RESULTS OF EXAMINATION OF SILVERED TEFLON FROM THE LONG DURATION EXPOSURE FACILITY

Ken Rousslang, Russ Crutcher, and Gary Pippin
Boeing Aerospace & Electronics Division
Seattle, WA 98124-2499
Phone: 206/773-2846, Fax: 206/773-4946

A significant effort to determine the effects of Low Earth Orbit (LEO) exposure on silver backed fluorinated ethylene-propylene (FEP) blankets from the Long Duration Exposure Facility (LDEF) has been carried out at Boeing under contract to NASA Langley Research Center. This paper describes the results of this investigation. Extensive measurements of surface, optical, chemical and mechanical properties have been conducted. Effects of contamination and erosion rates of the FEP layer have been determined. Specific results are reported on solar absorptance, thermal emittance, diffuse reflectance, cross sectional microphotography, secondary ion mass spectroscopy, electron scattering for chemical analysis, scanning electron microscopy, % elongation and tensile strength. These measurements show the effects of two distinctly different exposure environments, solar exposure and simultaneous atomic oxygen (AO) and solar exposure.

The data presented are from a first look survey. Recession of FEP occurs under combined exposure to atomic oxygen and solar ultraviolet radiation. Mechanical properties of FEP which was under combined exposure are not appreciably degraded relative to values from the original material. Under combined exposure, diffuse reflectance increased with increasing AO fluence but bulk optical properties remained unchanged. In contrast, material exposed only to solar radiation remained specular, did not lose mass, but did show significant decrease in ultimate tensile strength and % elongation to failure.

Measurements were made on samples taken from areas free from large visible impacts to assess the condition of the intact material. While properties are reported as a function of location, microenvironmental effects such as impact events, mechanical loads, shadowing by nearby structure, or contamination have not yet been quantified. Effects of thermal cycling have not been determined. Each blanket received the same number of thermal cycles and very little cracking is observed. The temperature extreme for each blanket is unknown.

The locations of the blanket pieces provided to Boeing to characterize are identified in figure 1. Most pieces are from near blanket edges and include a flat exposed area about 2" wide, a shielded area about 1" wide, perpendicular to the exposed surface of the blanket, and a transition area with about a one-half inch radius of curvature between the flat surfaces. Areas from around the copper grounding straps were provided from twelve of the blankets and six pieces were provided from the F-2 blanket. Table 1 shows that both solar absorptance and thermal emittance are essentially independent of location and showed virtually no change from preflight values, with the exception of visibly contaminated specimens, which showed large increases in absorptance. The diffuse reflectance is extremely low for trailing edge specimens and increases as a function of increased atomic oxygen exposure, until the diffuse component is the major portion of the total reflectance in the visible region of the spectrum. The % diffuse reflectance is reported at two wavelengths in table 2. These wavelengths bracket the region of the spectrum exhibiting the largest change in the diffuse reflectance and are representative of the amount of change in the visible region of the spectrum as specimens were exposed to significant amounts of

atomic oxygen. Diffuse reflectance measured in the IR region of the spectrum between 4000 and 500 wave numbers show only a slight increase for oxygen exposed specimens relative to solar exposed specimens. The trailing edge material exhibits a relatively flat profile at about 5% transmission. The slightly increased transmission of leading edge specimens may be due to small decreases in the thickness; however the curves are also essentially flat. Blanket A4 is a notable exception, exhibiting large increases between 4000 and 2500 wave numbers.

Bidirectional Reflectance Distribution Function (BRDF) measurements, shown in figure 2, also show increased diffuse reflectance for specimens exposed to AO. BRDF measurements on samples from C11 and A 10 are asymmetric due to the orientation of the sample with respect to the incident laser beam and the directionality of the roughened surfaces of these specimens. The surface texturing of blankets exposed to atomic oxygen causes the diffuse appearance of those blankets. SEM images in figure 3 show the classic pattern of surface texturing observed previously on specimens from shuttle flights and the Solar Max repair mission. The textured peaks point generally in the direction of the impinging oxygen (ram direction). This effect can be clearly seen in the transition region of blankets where a short distance provides about a 90 degree range of angles. The orientation and degree of texturing changes dramatically with the rapid change of angle.

ESCA data in table 3 for the % carbon, fluorine, and oxygen on the surfaces of the blankets show primarily the effects of contamination. Oxygen content on all unexposed surfaces and trailing edge exposed surfaces shows large variations. The oxygen content is correlated with observed silicone contamination content. For leading edge exposed surfaces, the elemental compositions by mole % are relatively constant. These surfaces do not have the silicon containing contaminant films due to the continual erosion by atomic oxygen. These observations are consistent with our SIMS data discussed below. The small % oxygen observed on leading edge exposed specimens is most likely due to partially oxidized species on the surface.

Secondary Ion Mass Spectroscopy (SIMS) was performed on the surface of a number of FEP blankets. Those surfaces which were exposed to substantial amounts of AO produced SIMS essentially identical to SIMS of a ground control specimen; the major peaks are all matched with easily identifiable fragments from FEP. SIMS on FEP from specimens toward the trailing edge, not exposed to atomic oxygen, exhibit complex SIMS spectra. The peaks clearly associated with FEP are present. Additional peaks appear at almost every mass between 25 and 250 amus. These peaks are attributed to deposited hydrocarbons and siloxane based materials which have outgassed onto the blankets. Figures 4 and 5 show representative examples of these two types of spectra. Spectra from both exposed and unexposed specimens from blankets toward the leading edge are similar to the spectra from the specimen from blanket A10, shown in figure 4. Spectra of both exposed and unexposed specimens from blankets toward the trailing edge are similar to the spectra from the specimen from blanket CO5, shown in figure 5. Exposure to solar ultraviolet and vacuum ultraviolet and vacuum ultraviolet radiation embrittle FEP, decreasing the % elongation to failure and the ultimate tensile strength. The graph of tensile strength vs solar exposure in figure 6 shows a decrease of about 30% for exposed specimens relative to unexposed specimens taken from the edge. For these same specimens, the % elongation decreased about 25%. Blankets exposed simultaneously to solar radiation and atomic oxygen lost mass and became thinner. These specimens show only small decreases in tensile strength, as shown in figure 7, and % elongation in comparison with unexposed specimens from the same blankets. Solar UV radiation of sufficiently short wavelengths has enough energy to break bonds in the FEP backbone and induce crosslinking in the polymer, making it more brittle. Under simultaneous exposure, UV induced bond breaking provides reaction sites for the atomic oxygen to attack the polymer backbone, producing volatile products which then leave, exposing new reaction sites. Similar processes occur with hydrocarbon and siloxane materials outgassed onto the FEP surface.

Individual % elongation measurements, plotted as a function of atomic oxygen fluence in figure 7, show essentially two populations. The implication is that for one group of blankets, oxygen exposure is sufficient to remove virtually all the material altered by the UV photons, while for the other group, the changes in the chemical structure and embrittlement due to crosslinking has occurred in the bulk of the FEP. The percent elongation versus atomic oxygen angle of incidence is shown in figure 8.

Blanket thicknesses were determined using cross section photomicrographs of specimens from exposed and unexposed areas from blankets located toward the trailing edge and unexposed areas from blankets located toward the ram direction. Attempts were also made to use areal weights to estimate recession. While this method confirmed that specimens exposed to atomic oxygen were generally thinner than specimens from toward the trailing edge, it was not as precise as using cross sections. The average thickness determined form the photomicrographs is about 5.2 mil. The results of our thickness determination and subsequent recession rate calculations are reported in table 4 and plotted in figure 9. Using calculated atomic oxygen fluences (ref 1) and measured thicknesses for exposed portions of blankets on rows 7, 8, 10, and 11, the recession rate was determined to be 0.35 $\pm$ 0.13 10E-24 cm3/atom. The actual ranges for each row are also listed in table 4. The values for each row are identical to within the uncertainty of the measurements of which the calculations are based.

There are "edge effects" which influence the degradation rate of the FEP. The stress on the material at the edge is different from that in the center of the blankets. Material being stretched around a radius is under tension. At the very least, this alters the structure of the near surface material, and possibly some of the chemical bond lengths in the polymer backbone. It is likely that these effects make the material more susceptible to degradation. A second effect, especially to transition regions from exposed to unexposed areas, is scattering of oxygen from the tray edge back onto the blanket. In each case, the curved transition region provides a continuous range of exposure angles over about 90 degrees. Both these effects should increase the erosion rate. However, the measured rate may still not be higher than for unstressed areas nearer the center. Depending on the mechanism of erosion and location of attack, the oxygen arrival rate may be the rate limiting step.

Surface particulate contamination protects material immediately beneath the particle. As material around the particle is eroded, the remaining structure provides an opportunity for enhanced scattering onto adjacent surfaces from the sides of the structure. An example showing the results of this process is shown in figure 10. The area of blanket D7 shown in this SEM is labeled shielded, but is actually in the transition region and was exposed to atomic oxygen. The areas to the lower right of each structure are slightly recessed and smoother textured relative to the remainder of the surface. Due to oxygen arriving from two different directions, scattering from the sides of the structures and direct impingement, the immediate areas to the lower right of each structure received greater oxygen fluence than the remainder of the surface. This lead to increased recession and suppressed the texturing associated with a well defined impingement angle.

The problem of determining recession rates at stress points remains. The materials were all thermally cycled but damage induced by this effect has not been quantified. Stresses induced by thermal lag in delaminated areas may have caused those areas to increase with each cycle. The visible damage from impacts in areas where velcro fasteners are attached to the blankets is much more extensive than for impacts which struck in blanket areas without support. The average properties over large areas still need to be estimated from measurements on individual specimens. Just under 2% of the area of each blanket from row 10 was blackened due to impacts. Both the averaged solar absorptance and the increased heat load over an entire blanket needs to be determined.

The FEP maintained its thermal control properties throughout the mission. The impacts did not compromise this function and the blankets each maintained mechanical integrity. Atomic oxygen induced roughening, which increased the diffuse reflectance, requires precautions be taken if this material is to be used near critical optical surfaces. The question remains whether the UV degradation had reached an end of life value or was continuing for trailing edge samples. The adhesion of the silver to the FEP was much better for trailing edge specimens than for leading edge specimens, which were separated with ease. Certain areas of the piece of blanket A4 provided to Boeing show surface texturing and shadowing around particulates which indicates exposure to atomic oxygen. Examination of on-orbit photographs show that a scuff plate extends past the end of row three and was exposed to atomic oxygen. The exposed surface of this scuff plate was in line of sight of the A4 surface area which shows texturing. The diffuse reflectance of this area of the blanket is typical of exposed surfaces from the leading edge of LDEF. The evidence indicates that atomic oxygen scattered from the scuff plate reaches the surface of blanket A4. Indirect scattering must be considered when critical surfaces are being designed and located on a spacecraft in LEO.

Predictions of material lifetime for recession of ram facing surfaces based on LDEF specimens only allows estimates of a lower bound of FEP thickness necessary for long term use. If the recession rate of FEP under combined exposure is controlled by the UV exposure rate, then <5 mil thickness loss could be expected over a thirty year period for a ram facing surface. This is based on the observed recession over the 5 year 10 month exposure and the fact that the solar UV exposure rate should be essentially constant over the 30 year period. If the recession rate is controlled by the atomic oxygen exposure rate, then ~16 mil thickness loss could be expected over thirty years. This prediction is based on Space Station Freedom receiving an estimated ram fluence of 1.5E+23 oxygen atoms/cm_2. To maintain constant absorptance and emittance values over this time period would require at least seven mils of FEP. These estimates assume constant rates of degradation. The rate may accelerate, and is at least higher than our reported average, given an induction period prior to the onset of the mass loss. The results demonstrate that UV alone does not cause recession of FEP. It has not yet been determined experimentally that oxygen alone is sufficient or if UV is necessary for erosion to occur. However, it is probable that UV is required, at least initially, to produce sites in the polymer susceptible to oxidation. Deposited molecular contamination films alter the recession rate by "consuming" oxygen or UV. There is more material with which to react, and formation of oxide films may block attack on the substrate. These effects probably slow the observed recession rate relative to clean material. In conclusion, the FEP blanket material was effective in protecting the silver second surface mirror for the entire mission. In general, end of life optical properties were unchanged from preflight values and the blankets maintained their mechanical integrity. Expected surface texturing was observed for areas exposed to atomic oxygen. The average recession rate was greater than values reported for experiments flown on shuttle flights. This work was carried out under contract NAS1-18224, Task 12. The support of NASA Langley Research Center through the LDEF Project Office and the LDEF Materials Special Investigation Group is gratefully acknowledged.

REFERENCE

1. Bourassa, P. J.; Gillis, J. R., and Rousslang, K. W.: Atomic Oxygen and Ultraviolet Radiation Mission Total Exposures for LDEF Experiments. First LDEF Post-Retrieval Symposium, NASA CP-3134, 1992.

Table 1: Solar Absorptance and Thermal Emittance as a Function of Location on LDEF

TRAY #	ABSORPTANCE EXPOSURE		EMITTANCE EXPOSURE	
	EXPOSED	UNEXPOSED	EXPOSED	UNEXPOSED
D1	0.04	0.07	0.80	
A2	0.06 0.15*	0.08	0.81	
F2	0.05	0.06	0.81	0.81
B5		0.04		0.80
C5	0.07	0.05	0.81	
C6	0.05	0.05	0.80	0.80
B7	0.04	0.04	0.81	
D7	0.06	0.04	0.80	0.80
C8	0.08		0.78	
C8	0.24*		0.84*	
A10	0.06	0.06		
C11	0.06	0.06	0.79	0.80
D11	0.04	0.06	0.78	0.78

* Visibly contaminated specimens

Table 2: Percent Diffuse Reflantance of FEP at 400 and 600nm

SPECIMEN LOCATION	EXPOSURE	% DIFFUSE REFLECTANCE	
		at 400 nm	at 600 nm
A2	Unexposed	16	7 1/2
C6	Unexposed	15 1/2	7 1/2
E10	Unexposed	27	13 1/2
E2	Exposed	19	10
B7	Exposed	28	14
F4	Exposed	18 1/2	8 1/2
C11	Exposed	82	67
D7	Exposed	29 1/2	15
D11	Exposed	59	39 1/2
D1	Exposed	13	4 1/2
A10	Exposed	85	94
C5	Exposed	13 1/2	5
Ground Reference		15	8
C8	Exposed	86	76
A4	Exposed	76	96 1/2

Table 3: Results of ESCA Measurements on FEP to Determine The Surface Elemental Composition

TRAY #	EXPOSED				UNEXPOSED			
	% FLUORINE	% OXYGEN	% CARBON	% SILICON	% FLUORINE	% OXYGEN	% CARBON	% SILICON
GND	65.7		34.3					
D1	57.3	2.9	39.4		12.1	31.0	44.9	9.5
A2	52.2	5.6	42.1	7.2	21.6	25.3	42.1	8.9
E2	45.0	13.6	38.6		8.6	43.3	25.8	
F2	45.5	13.1	37.6					
A4	21.1	23.3	46.5					
F4	51.8	6.0	42.1		5.0	47.2	23.8	
B5	52.1	4.8	43.1		11.2	31.0	46.1	8.7
C5	51.8	5.5	42.7					
D5	54.7	4.8	40.5		26.1	30.1	31.1	
C6	59.8	2.2	38.0		13.8	27.6	51.0	4.4
B7	65.2	1.4	42.7		41.0	28.7	30.3	
D7	64.6	1.2	34.2		9.5	45.0	19.0	26.5
C8	63.2	1.8	35.0					
A10	63.9	1.4	34.7		65.1	2.0	33.0	
E10	64.6	1.5	33.9		1.4	51.8	14.9	
C11	64.6	1.2	34.1		42.5	21.0	24.2	12.3
D11	63.5	0.8	35.7		15.4	42.6	22.5	19.5

Table 4: Average Recession Rates of Silver Backed FEP Blankets Exposed to Atomic Oxygen

LOCATION	RECESSION RATE (10E-24cm3/oxygen atom)
B7	0.26-0.47
D7	0.20.0.41
C8	0.28-0.38
A, E10	0.32-0.40
C11	0.28-0.41
D11	0.33-0.46
Average range	0.28-0.42
Average	0.35±0.13

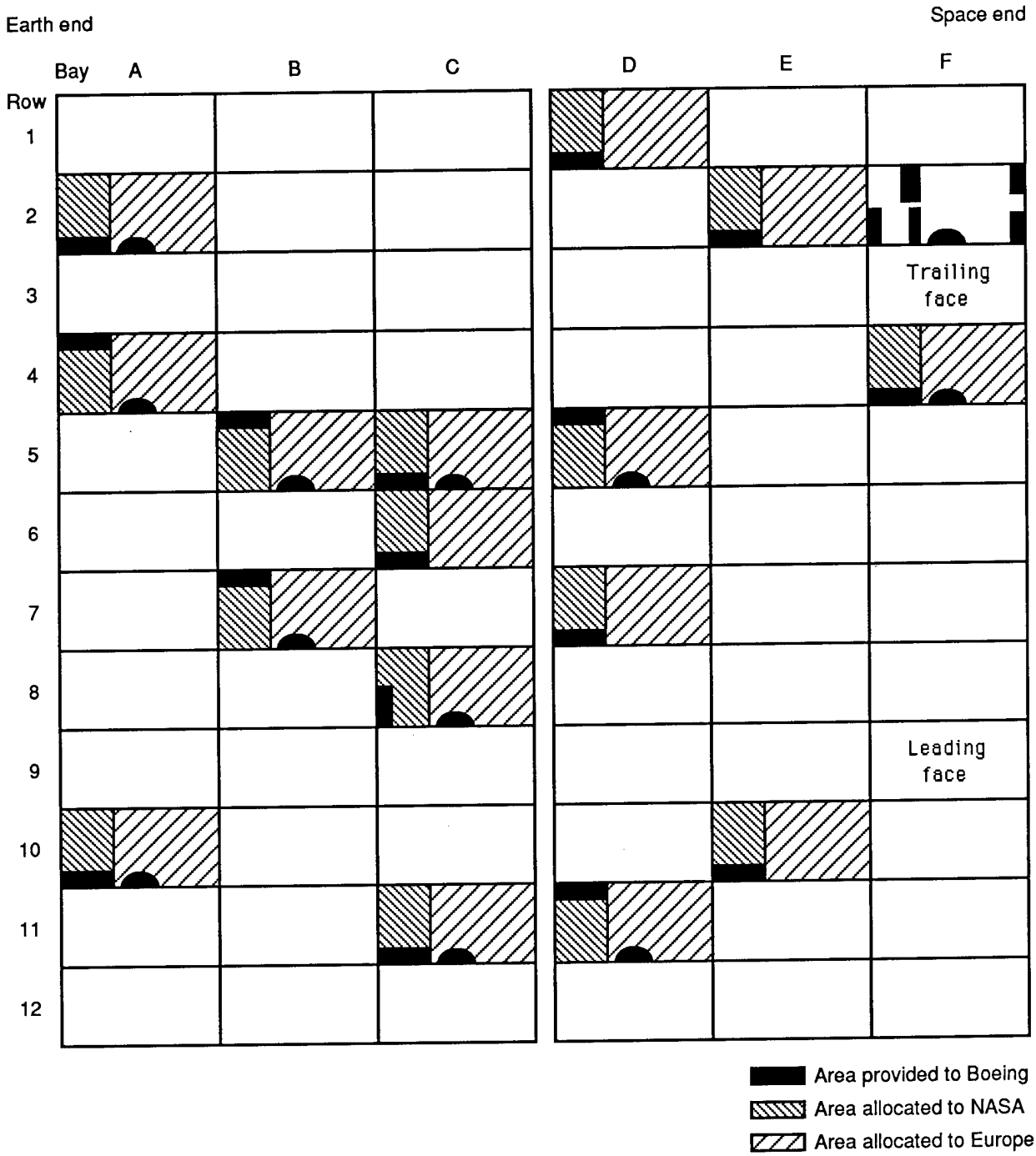


Figure 1. LDEF A0178 and P0004 thermal cover allocations

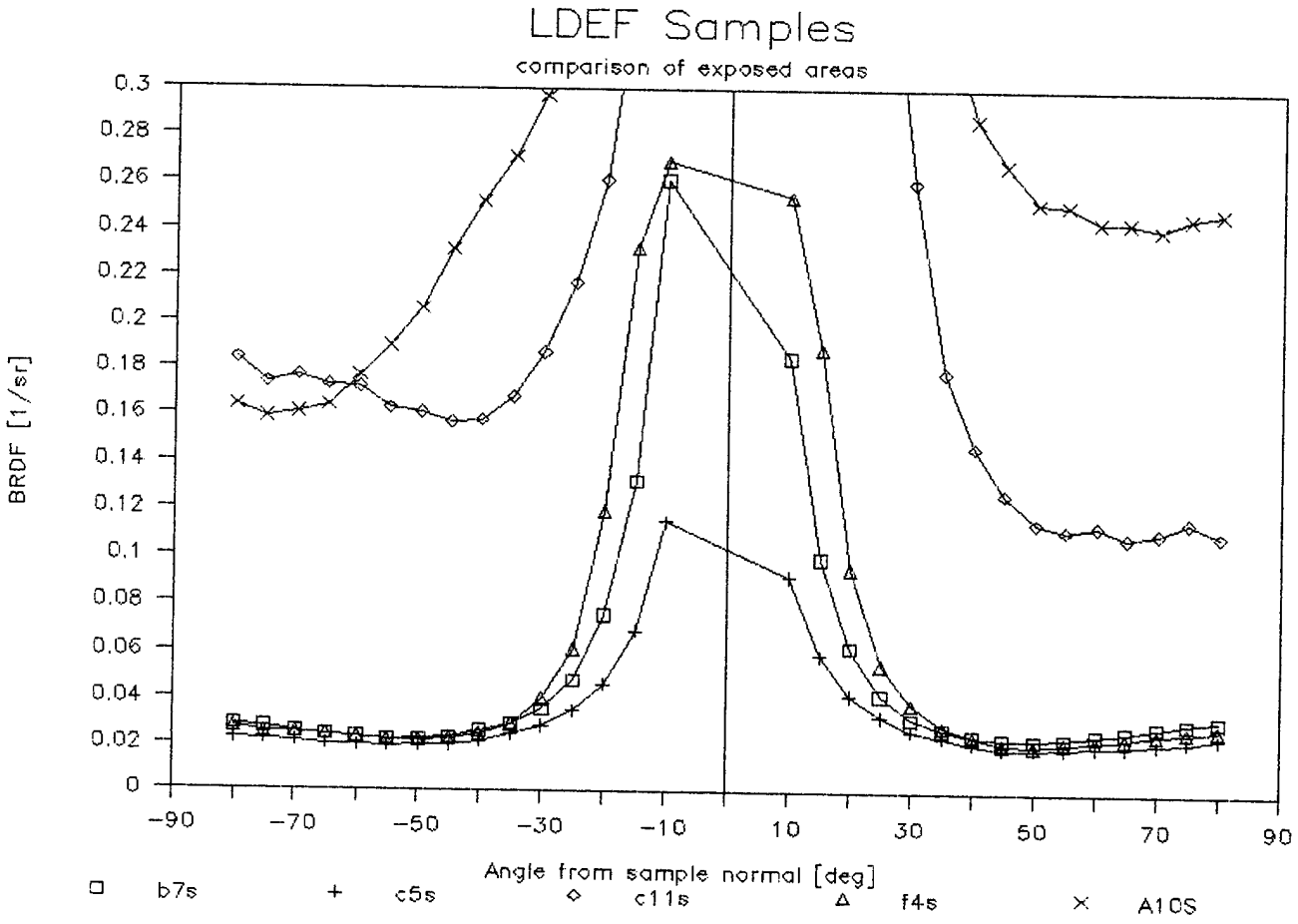


FIGURE 2 BRDF Measurements From Exposed Areas of Ag/FEP Specimens From Rows 4, 5, 7, 10 and 11

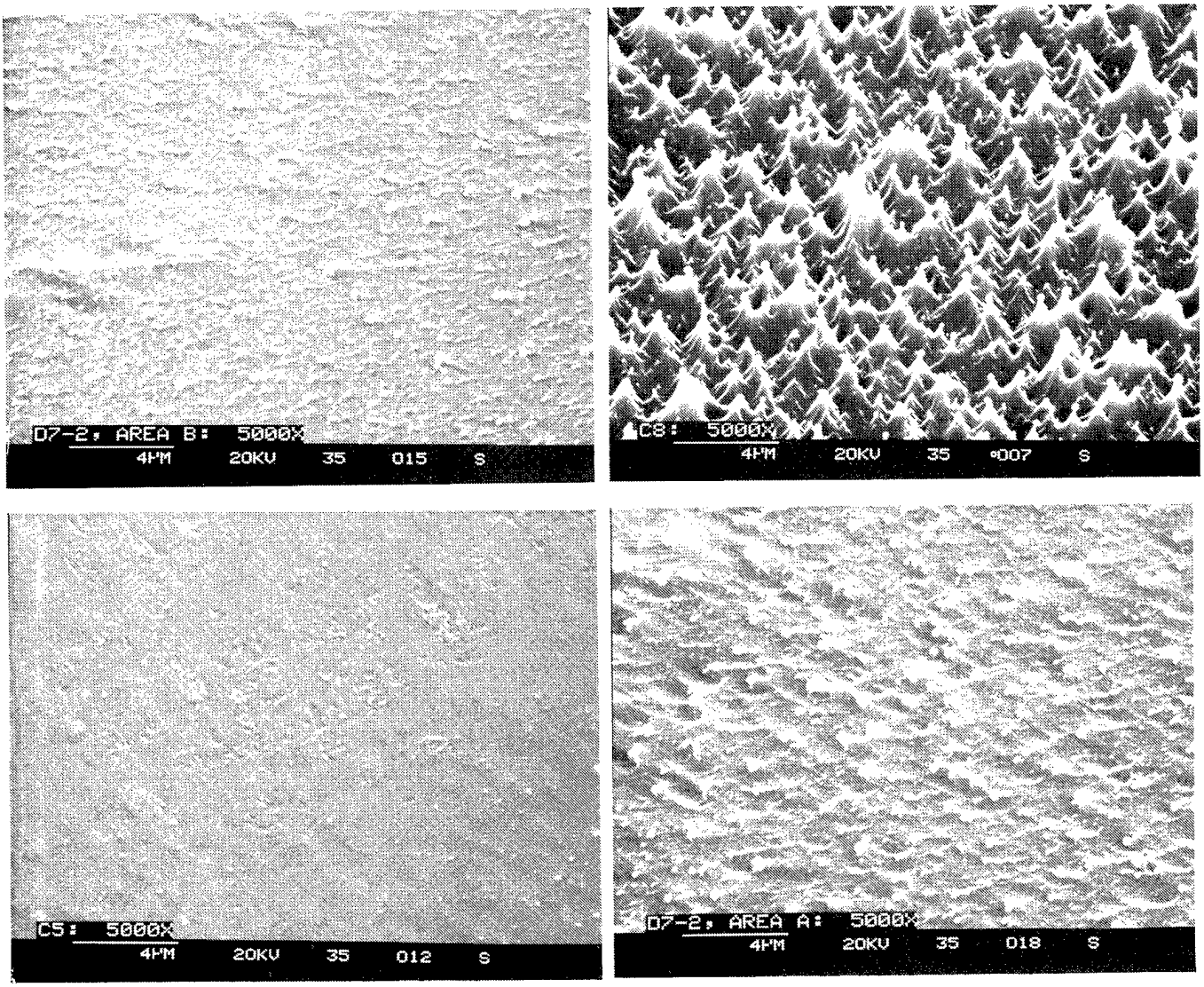


Figure 3. Images From Scanning Electron Microscopy of FEP Surfaces From Selected Thermal Control Blankets

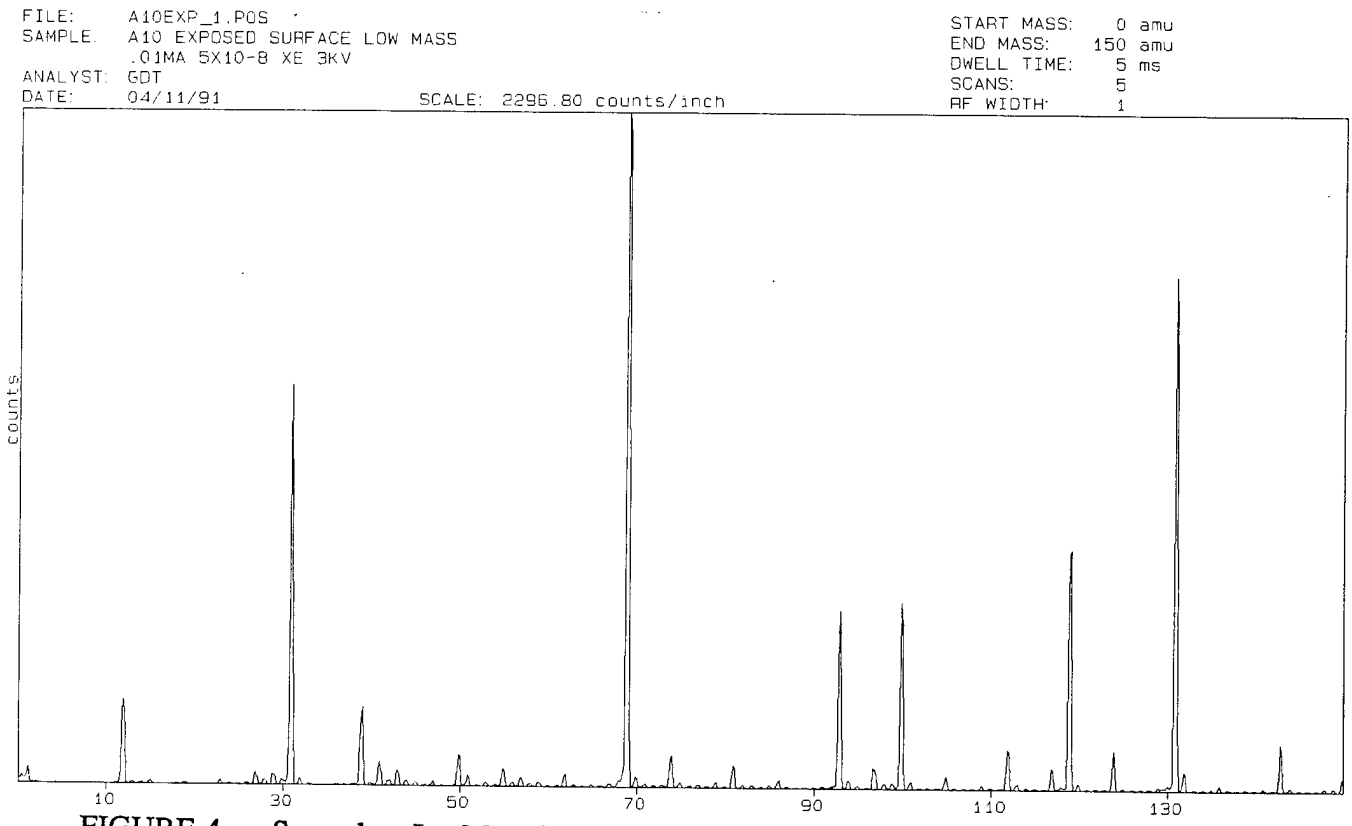


FIGURE 4 Secondary Ion Mass Spectrum From Exposed FEP Material From Blanket A10 on LDEF

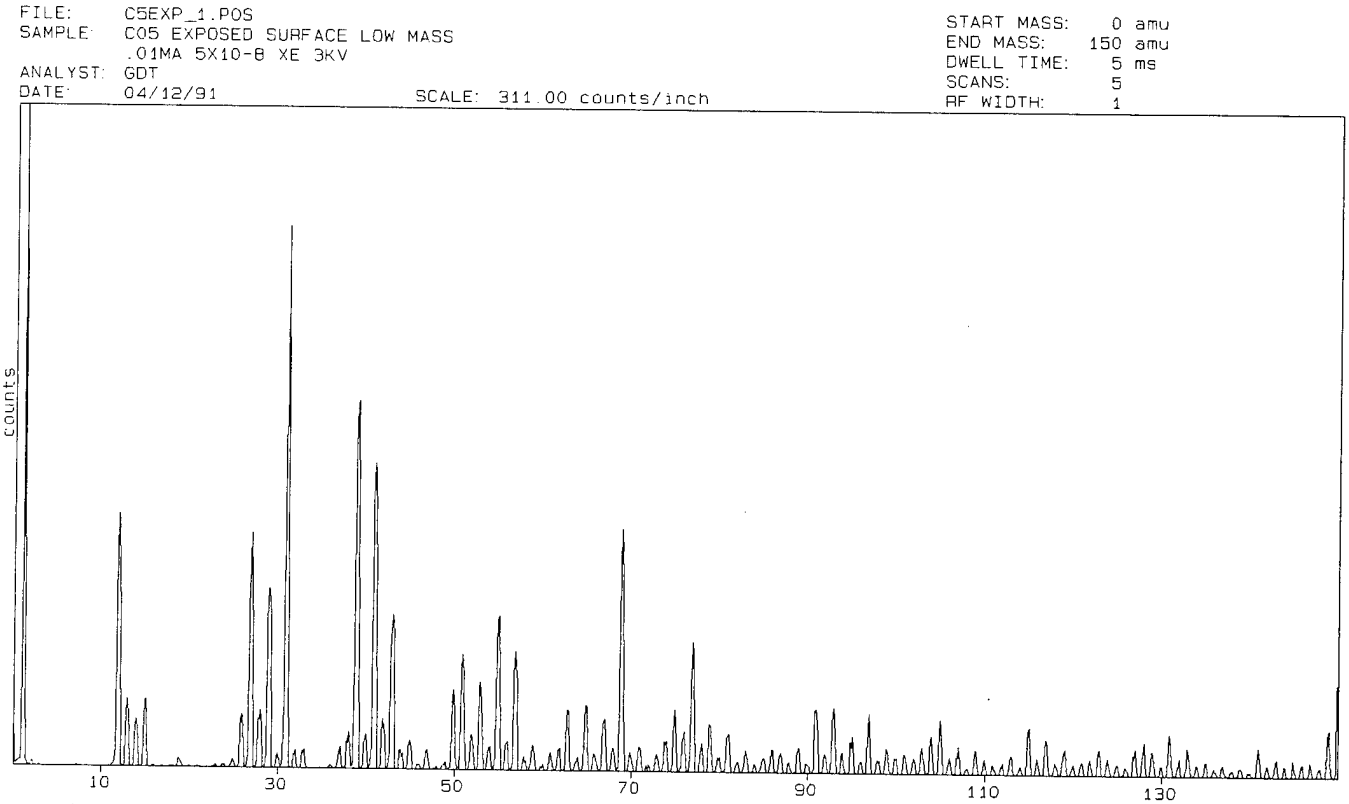


FIGURE 5 Secondary Ion Mass Spectrum From Exposed FEP Material From Blanket C05 on LDEF

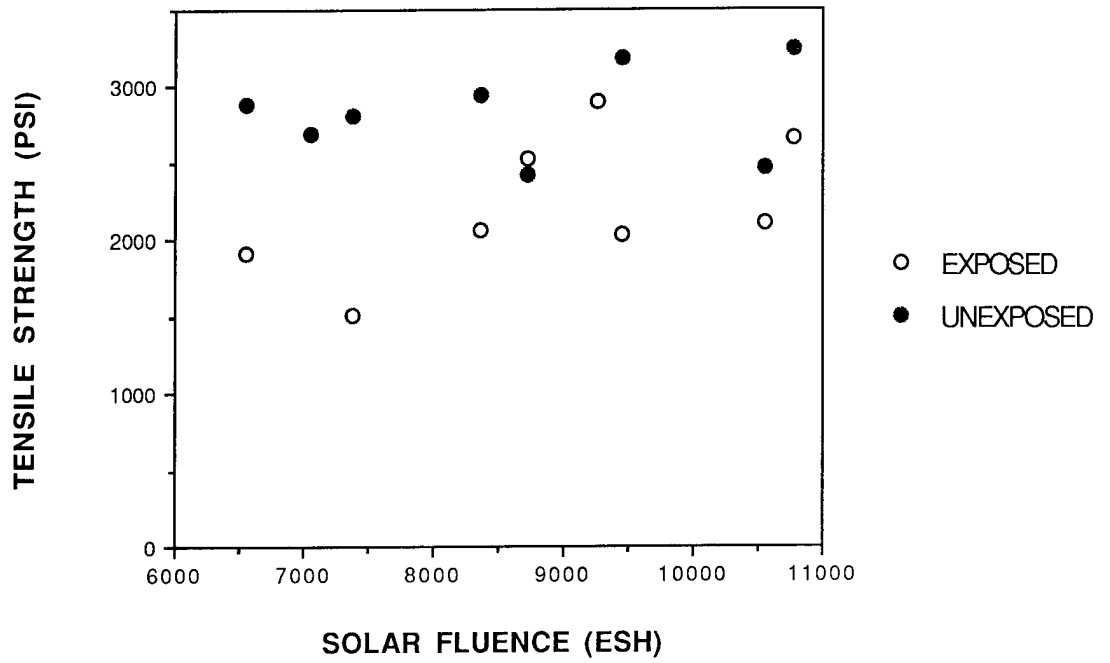


FIGURE 6 Tensile Strength of FEP Film From Ag/FEP Blankets on LDEF as a Function of Solar Fluence

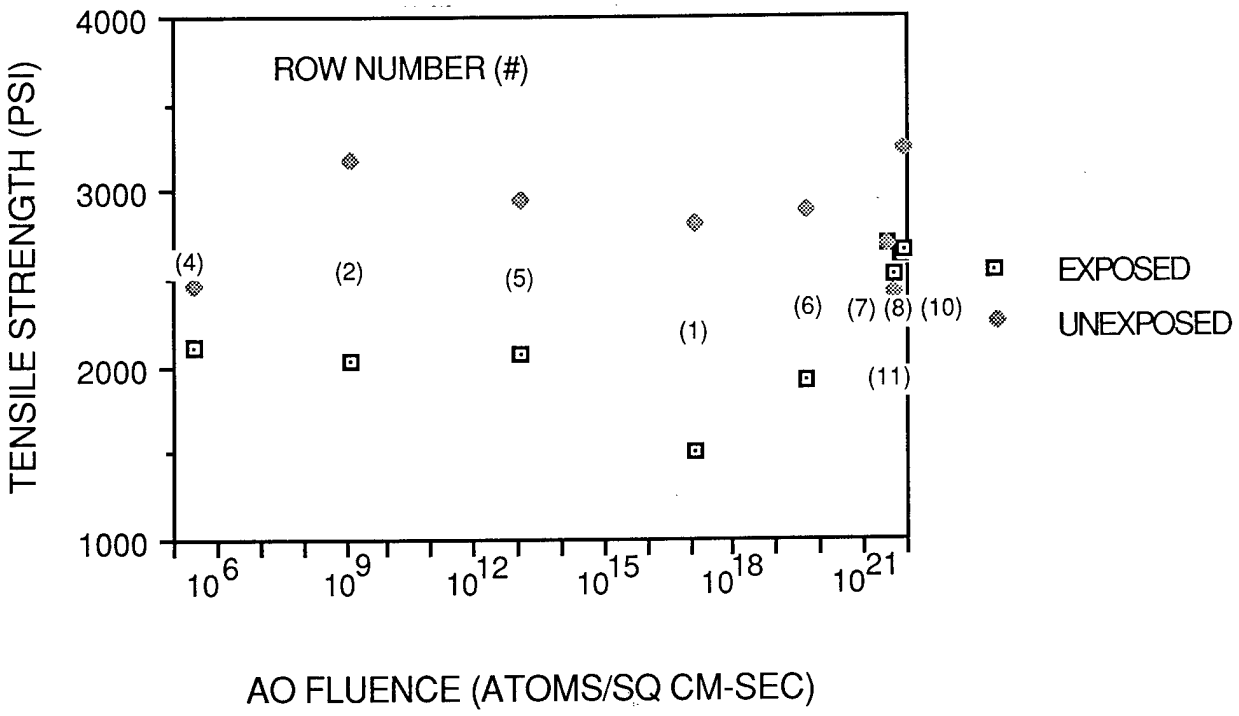


FIGURE 7 Tensile Strength of FEP Film From Ag/FEP Blankets on LDEF as a Function of Atomic Oxygen Fluence

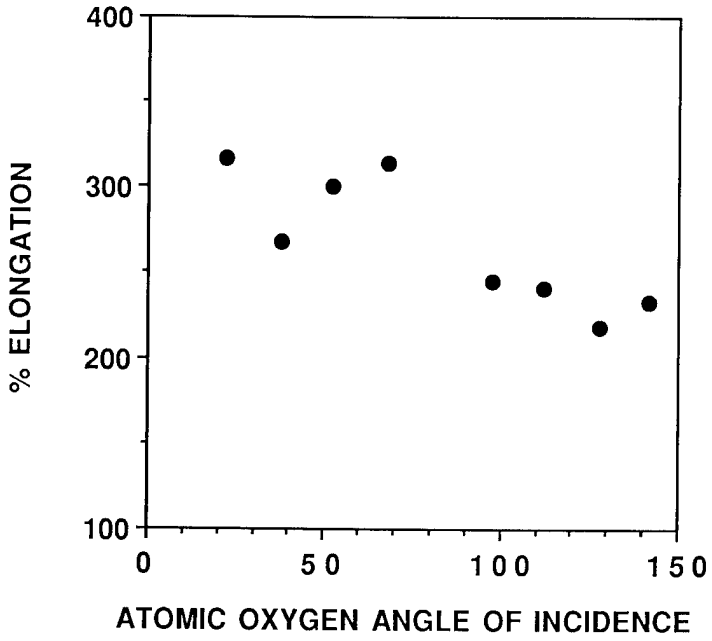


FIGURE 8 % Elongation vs Atomic Oxygen Angle of Incidence

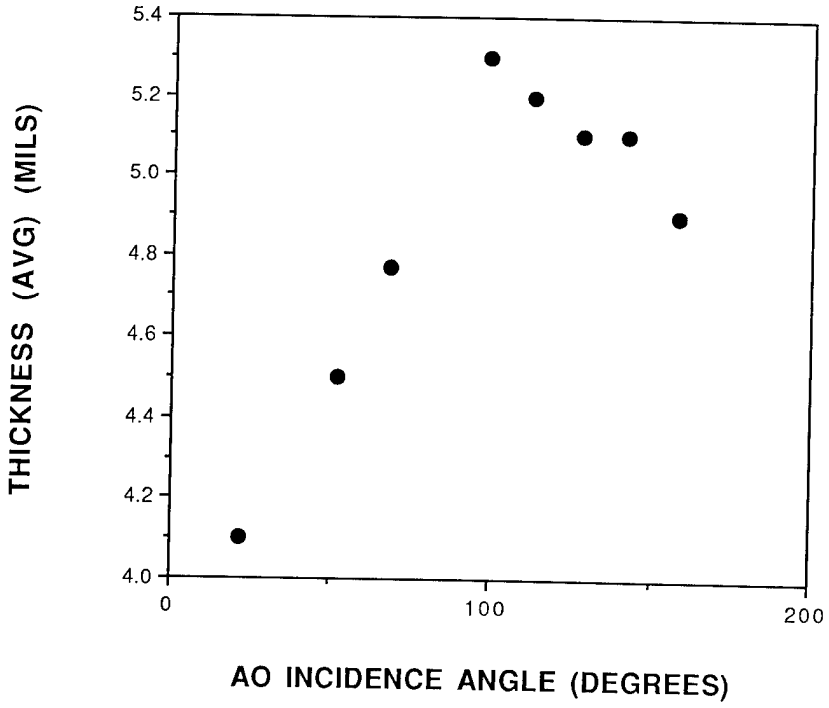


FIGURE 9 Thickness vs Atomic Oxygen Angle of Incidence

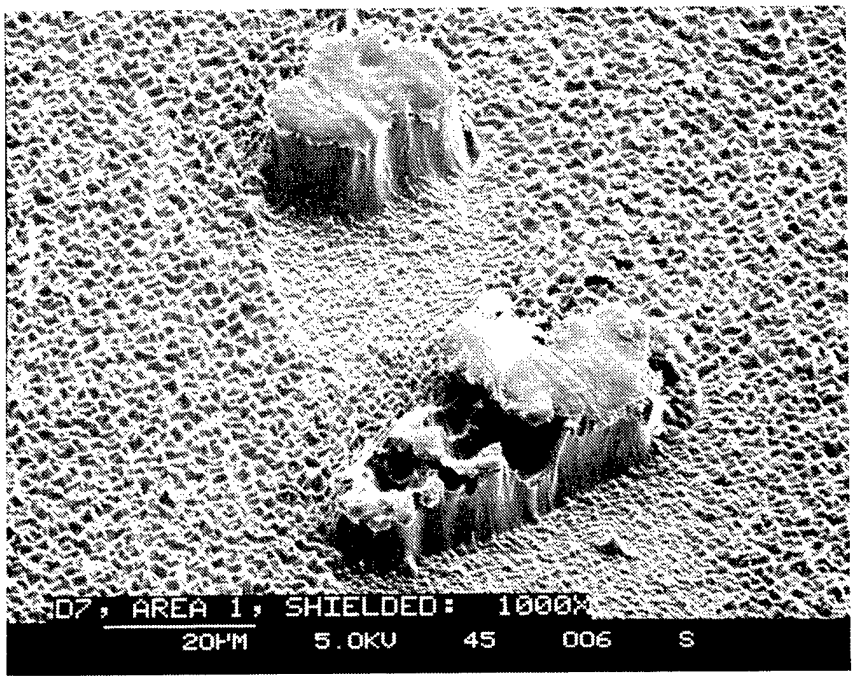


FIGURE 10 Image From Scanning Electron Microscopy of FEP Surface of Specimen From Blanket DO7

SILVER TEFLON BLANKET: LDEF TRAY C-08*

E. R. Crutcher, L. S. Nishimura, K. J. Warner, and W. W. Wascher
Boeing Defense and Space Group
Seattle, WA 98124-2499
Phone: 206/773-7002, Fax: 206/773-1473

SUMMARY

A study of the Teflon blanket surface at the edge of tray C-08 illustrates the complexity of the microenvironments on LDEF. The distribution of particulate contaminants varied dramatically over a distance of half a centimeter (quarter of an inch) near the edge of the blanket. The geometry and optical effects of the atomic oxygen erosion varied significantly over the few centimeters where the blanket folded over the edge of the tray resulting in a variety of orientations to the atomic oxygen flux. A very complex region of combined mechanical and atomic oxygen damage occurred where the blanket contacted the edge of the tray. A brown film deposit apparently fixed by ultraviolet light travelling by reflection through the Teflon film was conspicuous beyond the tray contract zone. Chemical and structural analysis of the surface of the brown film and beyond toward the protected edge of the blanket indicated some penetration of energetic atomic oxygen at least five millimeters past the blanket-tray contact interface.

INTRODUCTION

Many of the quantitative results for surface contamination are based on measurements made on the Silver/Teflon blanket material. This material was distributed over much of the surface of LDEF and faced nearly every direction. This wide distribution made the Silver/Teflon blanket a very desirable material for the study of the effects of orientation in orbit. This paper documents work in progress and will be brief though the figures and photographs do illustrate features of the distribution of contaminants that are relevant to other papers in this publication (Ref. 1, 2, and 3).

Figure 1 of this paper shows the location on LDEF of the A0178 experiment trays that were covered with Silver/Teflon material and the "Seeds" experiment, tray F-02, that was also protected with a covering of the same Silver/Teflon blanket insulation material. Figure 2 shows the location of tray C-08 with respect to its position in orbit and with respect to the experiments surrounding the location of the sample presented in this paper. Photographs 1, 2, and 3 are macrophotographs of the sample documented in this report. The sample is about 30 millimeters long and 5 millimeters wide. The Silver-Inconel-Z306 backing was removed to simplify the study of modifications in the Teflon. Photograph 1 was taken using transmitted light. The dark bands are regions where the visible light is scattered by the surface roughness resulting in little transmission of light. In orbit these regions would scatter light from the surface allowing little light to penetrate to the silver layer. Photograph 2 is an oblique toplighted view of the sample exhibiting the surface light scatter of the zones that appeared dark with transmitted light. Photograph 2 also illustrates the thin film interference colors associated with the brown deposit on the surface of the sample. This distribution indicates a slight fold in the blanket at the edge with an atomic oxygen attack zone and a second, thinner brown layer.

*Work done under NAS 1-18224, Task 12

The bottom panel of Figure 2 illustrates a variety of optical properties that relate to changes in the Teflon film. The retardation value is proportional to the thickness of the film and to local frozen stresses. The orientation of the high refractive index indicates the history of directional stresses. Teflon is optically a biaxial type orthorhombic film. This film appears to have become biaxially clinic as a result of its exposure or handling. It is interesting to note that the orientation of the high refractive index changes by 15 degrees from the edge of the blanket to the area on the face of the tray. Also of interest is that the change in retardation corresponds to a thickness change of 0.8 milli-inches. This agrees with the measured values of about 1 milli-inch for Teflon facing directly (90 degrees) into the ram direction when corrected by dividing 0.8 by the sine of the orientation of the tray, 52 degrees: $\{0.8/(\sin 52) = 1.0\}$

Figures 3 through 6 are a continuous collage of photographs illustrating the variations in surface modifications and surface coatings for the sample indicated in Figure 2. Figure 7 summarizes details of the atomic oxygen and ultraviolet light exposure at the edge of the tray and Figure 8 shows the results of a chemical analysis of the surface.

RESULTS

Tray C-08 faced at an angle of 52 degrees into the ram direction and illustrates the erosion typical of atomic oxygen exposure. Features of this erosion can be seen in Figure 3, a section of blanket approximately five millimeters long extending from the front facing section of the blanket to where the blanket began bending around the edge of the mounting frame. The magnification in the running sequence of photographs is about 60x. The lower sequence of photographs includes electron microscopy photomicrographs at about 1000x, a row of light microscopy photomicrographs at about 500x, and a final row of phase contrast light microscopy photomicrographs at about 250x. The left side of the figure illustrates the even erosion pattern seen in this front facing area of the blanket furthest from the fold at the edge of the tray. The blanket has a mild frosted appearance due to the even distribution of the small etch pattern. The pattern does exhibit an orientation effect seen in the general tendency for ridges and groves to align with the edge of the tray, at right angles to the incident atomic oxygen flux in the plane of the blanket. By the fourth frame from the left in this sequence protruding areas of particle protected Teflon become obvious features. This concentration of larger particles into a narrow band at the edge of the tray is seen in Figures 3 and 4. Its location with respect to the edge of the tray is shown in Figures 2 and 8. The right side photographs of Figure 3 show a metal particle that had protected a small area of the Teflon surface and the effects associated with that protection relative to the atomic oxygen eroded surface around it . Part of the metal particle (black crescent) can be seen in each photograph (see also Ref. 2, photo. 2 of Fig. 1). The first photograph shows the smooth surface of the Teflon protected by the metal from direct atomic oxygen and ultraviolet light. The second photograph, focused at about half way down to the fully eroded surface, shows the partially eroded edge that occurred only on one side of the feature. The third photograph is focused on the fully eroded surface and indicates a patterning effect in the erosion immediately around the feature effected by the presence of the feature (this photograph is shown better in Figure 4). The electron photomicrograph on Figure 3 shows a similar feature photographed from an adjacent piece of Teflon at this same distance from the edge of the blanket. The partial erosion along one edge of such a feature always occurred on the same side of the features in a given locality. For the features in this area of tray C-08 the partial erosion occurred on the earth facing side that was partially shielded from the ram normal direction. The other sides tended to be straight and smooth down to the local erosion depth.

Near the left side of Figure 4 there is a numbered marker, "25.0", indicating the number of millimeters from the edge of the blanket. The markers 23.4 and 21.9 delineate a highly eroded, highly light scattering region of the blanket. In this region etch pits become a dominant feature. With light microscopy the feathered edges prominent in the electron photomicrograph above disappear as the focus is adjusted into the pits themselves. What appears to be raised globular structures in the light photomicrograph below the

electron photomicrograph are actually the bottoms of the etch pits. In this area the appearance of the groves and ridges seen on the front of the blanket are seen as though in cross-section. Further to the left in Figure 4 the pits become smaller again though larger than those on the front face and more irregular in distribution.

In Figure 5 another band of highly scattering etch pits is encountered and is seen to have a structure similar to the highly scattering zone seen in Figure 4. The pits are large but not quite so deep as those seen in Figure 4. Beginning at 19.3 millimeters and continuing to the right to 18.4 millimeters from the edge of the blanket is a very rough region of eroded and mechanically damaged Teflon. The complex patterning evident here in both the electron and light microscope photomicrographs suggests preferential etching associated with surface damage and induced stress. At 18.4 a layer of brown molecular film begins. This position apparently marks the boundary of a significant reduction in the atomic oxygen fluence. The film has been exposed to some atomic oxygen as is indicated by the oxidation of the top layer of the film (see Figure 9) and by the fact that there is evidence of atomic oxygen erosion further along the blanket closer to the edge (see Figure 6).

Figure 6 illustrates the continuance of the film and, toward the right, the last evidence of atomic oxygen erosion. The erosion is so slight it only appears with electron photomicrography or phase contrast light photomicrography (lowest set of photographs on the right). The structure of a light scattering band at about 13 millimeters from the edge of the blanket is shown in the middle photograph of the three photographs along the bottom right of Figure 6.

Figure 7 consists of three illustrations. The uppermost indicates the orientation of tray C-08 with respect to the ram direction. The middle illustration is a closeup view of the edge of tray C-08 indicating the location of the concentration of large particles and the change in orientation with respect to the atomic oxygen flux as the blanket curved over the edge of the frame of the tray. The bottom illustration indicates the path of the polymerized ultraviolet light that fixed the brown film to the blanket beyond the contact point of the blanket to the metal tray.

Figure 8 illustrates the surface chemistry of the exposed and etched Teflon and the film covering the Teflon. The surface chemistry was determined by ESCA directly from the surface and by FTIR of successively removed layers of film.

Photographs 3, 4, and 5 are of impact sites and illustrate methods for extracting additional information from these locations. The timing of the impact is suggested by the amount of atomic oxygen erosion experienced by the ejecta. In Photograph 3 the ejecta is well eroded as is the interior of the crater (compare Ref. 2, photo. 3 of Fig. 3). When these features are viewed with crossed linear polarizing filters the stress distribution around the site becomes visible. Photograph 4 show the stress distribution and with the addition of a first order compensator plate indicates that the stress around the crater is compressive (blue quadrants are parallel to the compensator's high refractive index direction). Photograph 5 was taken using circular polarized light and by the color banding indicates significantly more stress than that shown by the impact documented in Photograph 4. Variation of erosion rates with stress may be evident at some of these sites but that has not been investigated at this time. The amount of residual frozen stress may be a very useful indicator of the kinetics of the impact.

Photographs 6 and 7 are provided as a comparison to Teflon seen on trailing tray surfaces. Ultraviolet light by itself degrades the surface of Teflon as seen on the surface of tray A-02 (photograph 6). The ultraviolet light degradation of Teflon may enhance atomic oxygen erosion of the surface. Photograph 7 illustrates a special microenvironment on tray A-02 where atomic oxygen apparently reflecting off a trunnion shield eroded a trailing tray surface.

Photograph 8 shows an area of C-08 protected by a particle during atomic oxygen exposure with undercutting due to the angle of exposure. The dark shadow-like line is the maximum extent of

undercutting from the thin sharp edge at the front of the bright zone in the photograph. Notice that the trailing edge of the particle protected area also has a sharp boundary.

CONCLUSION

The distribution of particulate contaminants varied dramatically with location near the edge of the tray.

The atomic oxygen erosion depth measured directly by the height of particle protected areas above the surrounding etched blanket is approximately 25 to 30 micrometers.

The atomic oxygen erosion depth measured by optical retardation is approximately 20 micrometers on the face of the blanket exposed at 52 degrees to the ram direction. Dividing by the sine of this angle indicates a projected erosion depth of 25 micrometers in the 90 degree orientation.

Brown film deposits seen on the "protected" parts of the blanket folded into the tray received ultraviolet polymerizing radiation by reflection through the Teflon from the front surface of the blanket at the edge of the tray.

Atomic oxygen penetrated through small gaps onto interior surfaces at detectable concentrations in some areas.

Optical properties of the Teflon film indicated significant differences in impact stresses and in mechanical stress as a result of orbital exposure.

REFERENCES

1. Crutcher, E. R. and K. J. Warner: Molecular Films Associated with LDEF. First LDEF Post-Retrieval Symposium, NASA CP-3134, 1992.

2. Crutcher, E. R. and W. W. Wascher: Particle Types and Sources Associated with LDEF. First LDEF Post-Retrieval Symposium, NASA CP- 3134, 1992.

3. Crutcher, E. R., L. S. Nishimura, K. J. Warner, and W. W. Wascher: Quantification of Contaminants Associated with LDEF. First LDEF Post-Retrieval Symposium, NASA CP-3134, 1992.

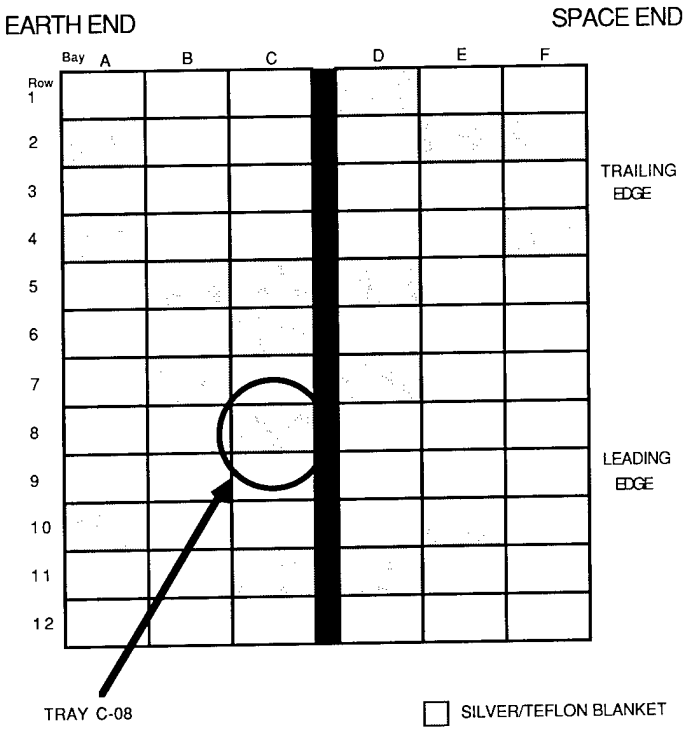


Figure 1: Distribution of Silver/Teflon Blanket Material.

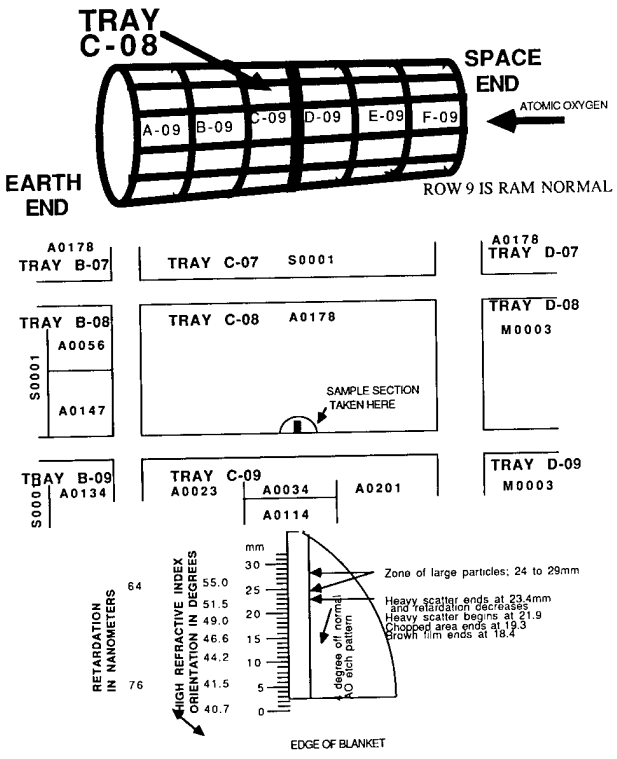


Figure 2: Orientation of Tray C-08 on LDEF, Location of Sample with Respect to Surrounding Experiments, and Zones of Interest on the Sample.

Figure 3: Photomicrographs of the Sample from 31.5 mm to 26 mm.

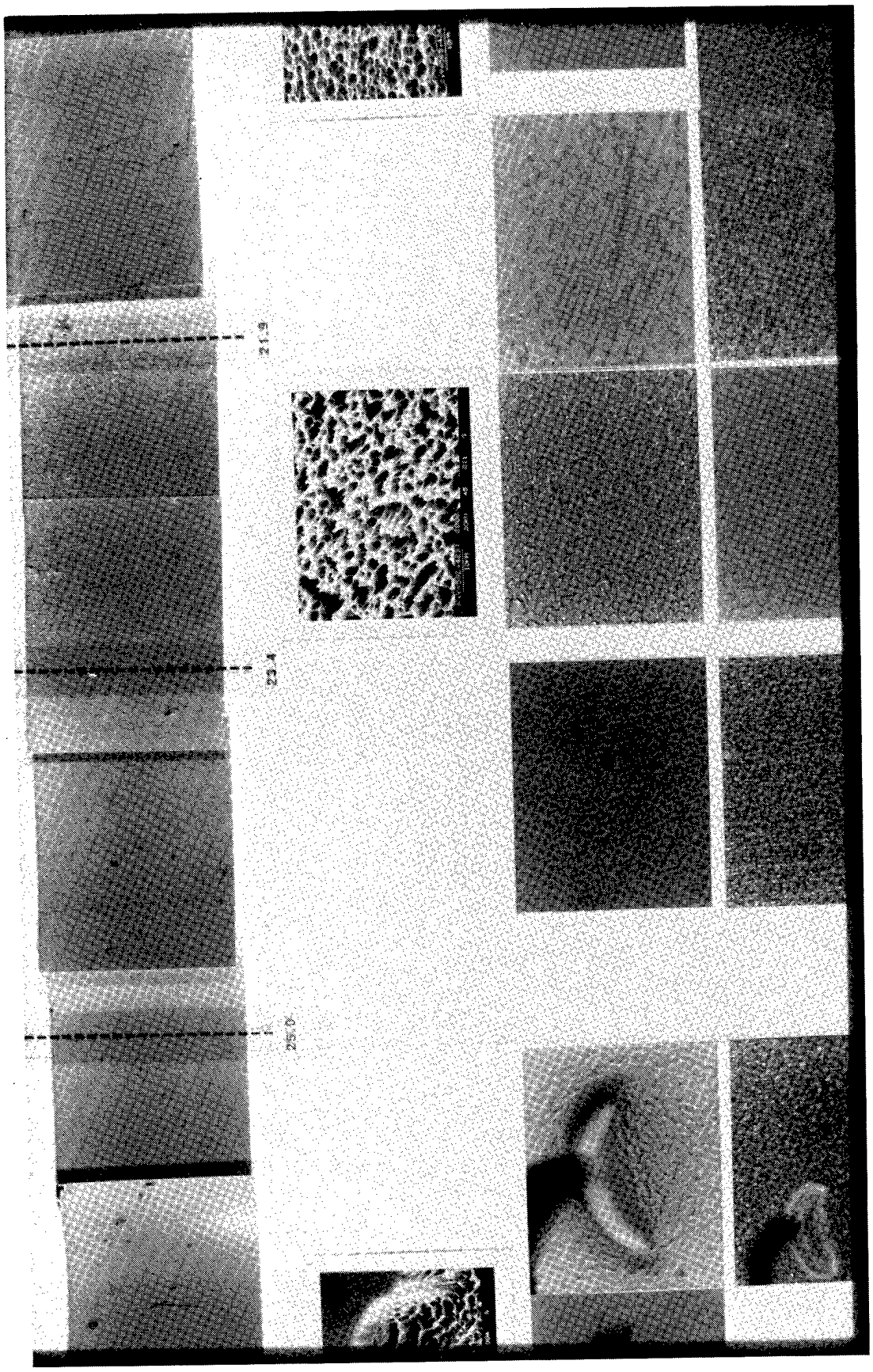


Figure 4: Photomicrographs of the Sample from 26.5 mm to 20 mm.

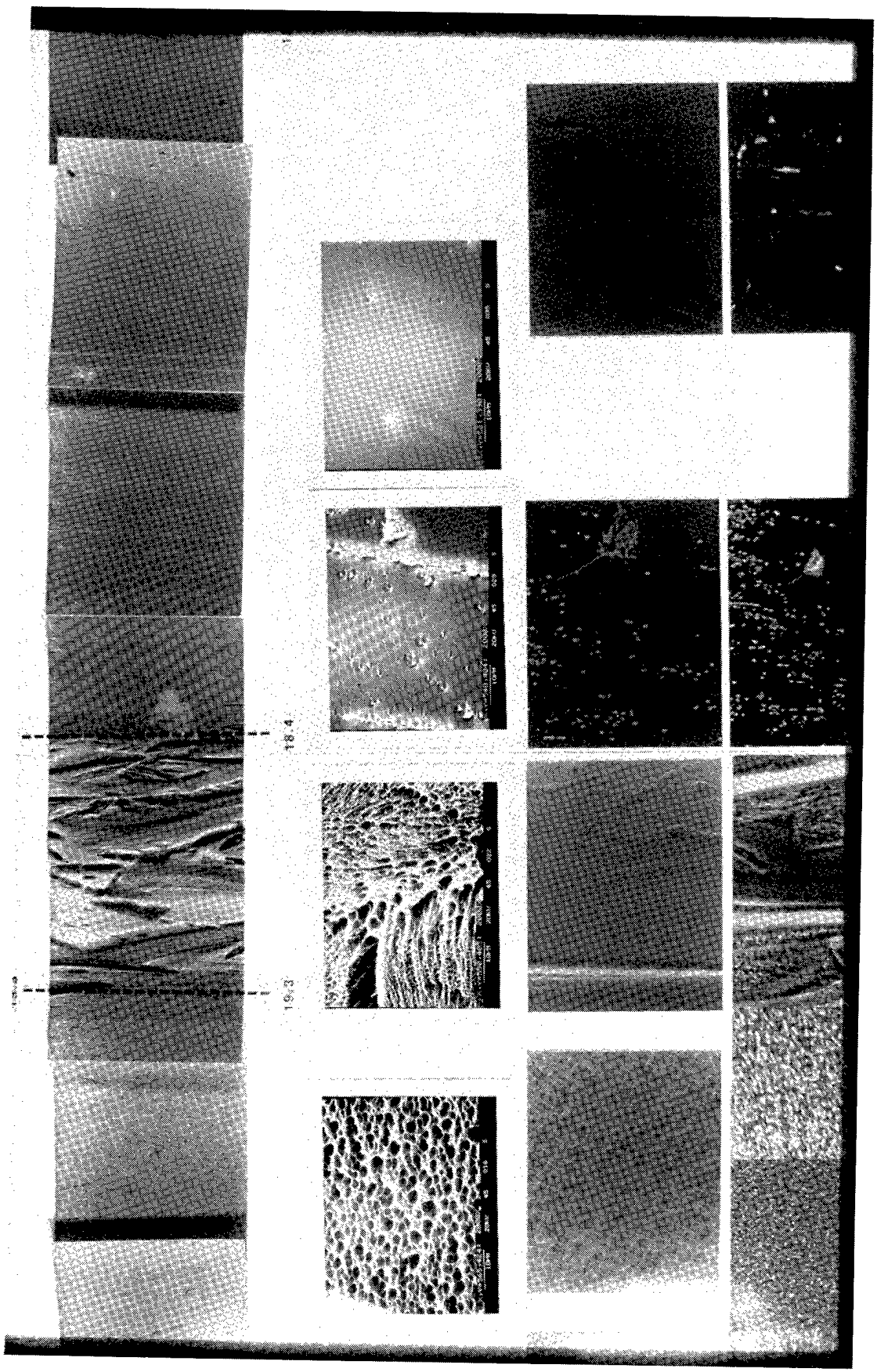


Figure 5: Photomicrographs of the Sample from 20.5 mm to 15 mm.

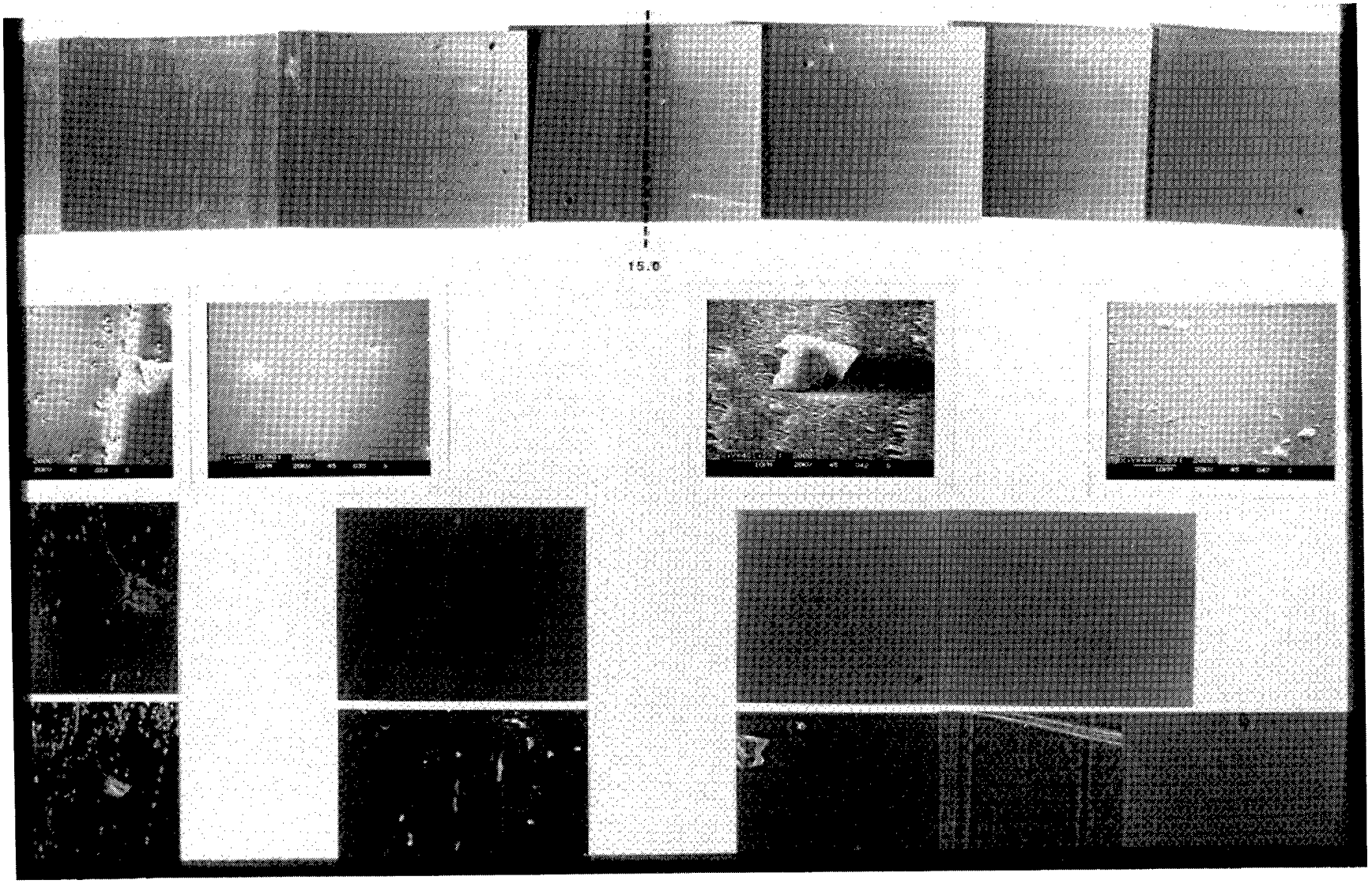


Figure 6: Photomicrographs of the Sample from 17 mm to 12 mm.

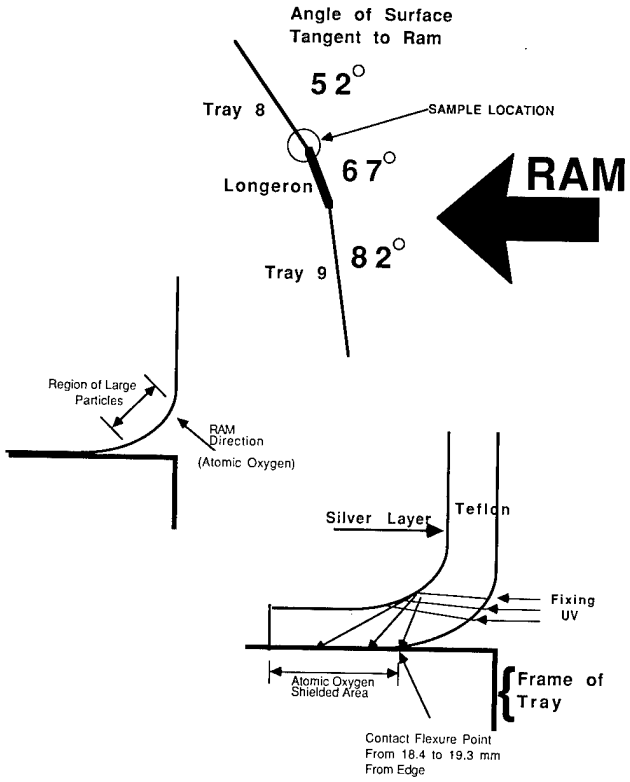


Figure 7: Orientation of the Tray to Ram Direction, Atomic Oxygen Direction at Curvature of the Blanket, and the Path of Ultraviolet Light Through the Teflon to Fix the Molecular Film.

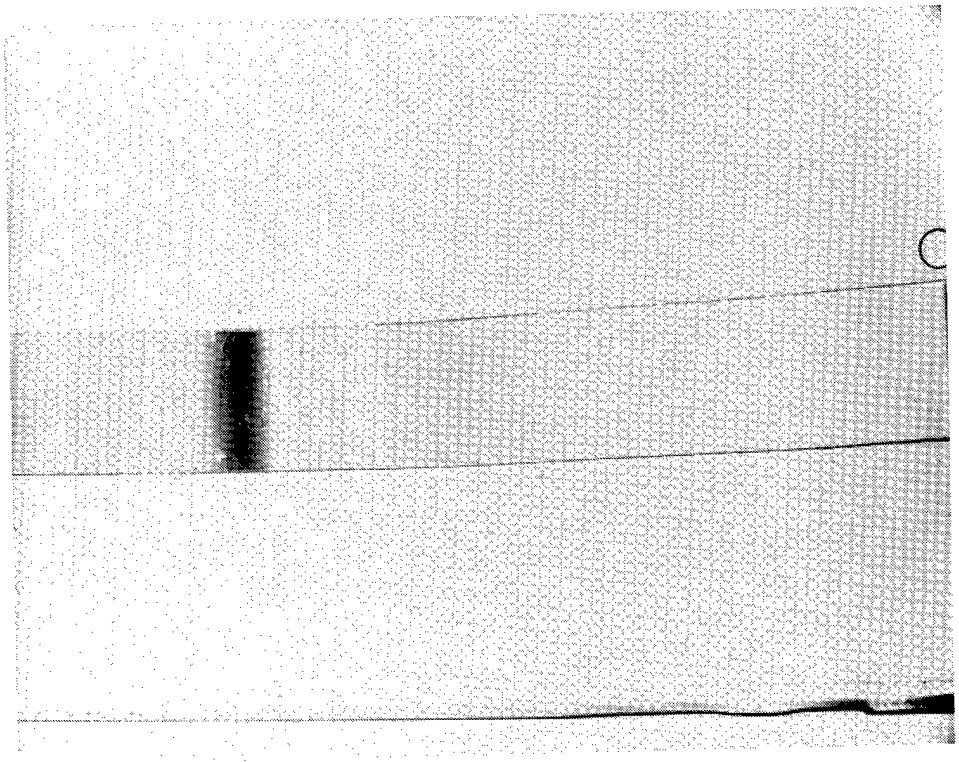
Brown Film Area

	F	O	C	Si	IR Spec
Layer 1	1	52	15	32	SiOx
Layer 2					Brown Film
Layer 3	66	-0-	34		FEP

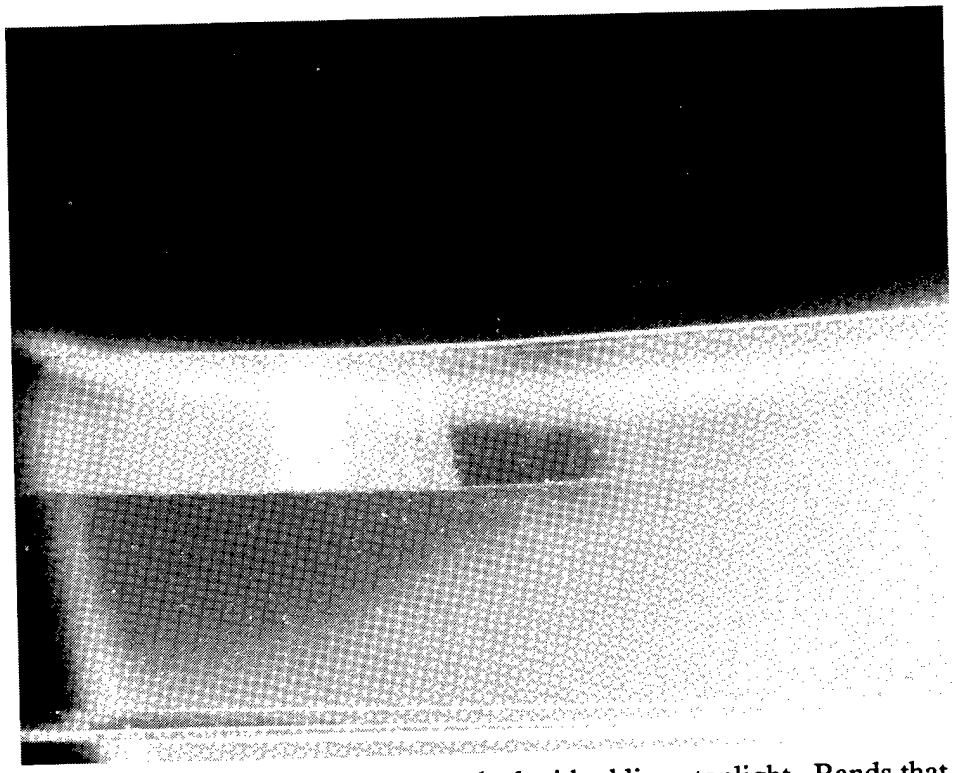
Atomic Oxygen Attacked Surface

F	O	C	Si	IR Spec
68%	2%	35%	-0-	FEP with a trace of Carbonyl

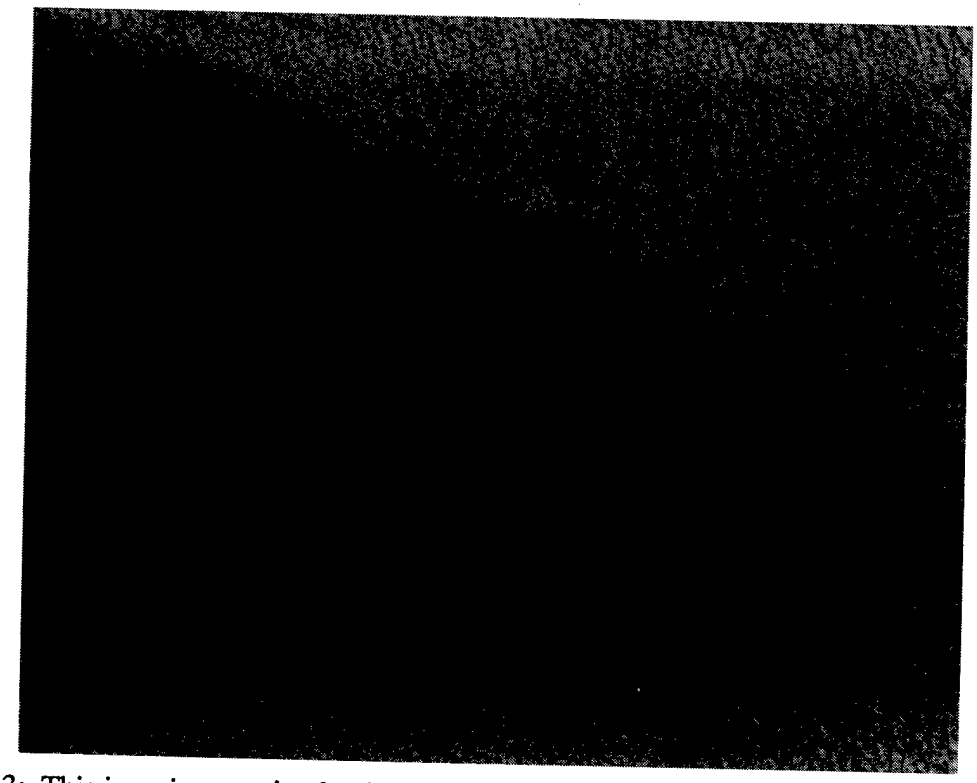
Figure 8: Surface Chemistry of Atomic Oxygen Attacked Teflon and Brown Film Area.



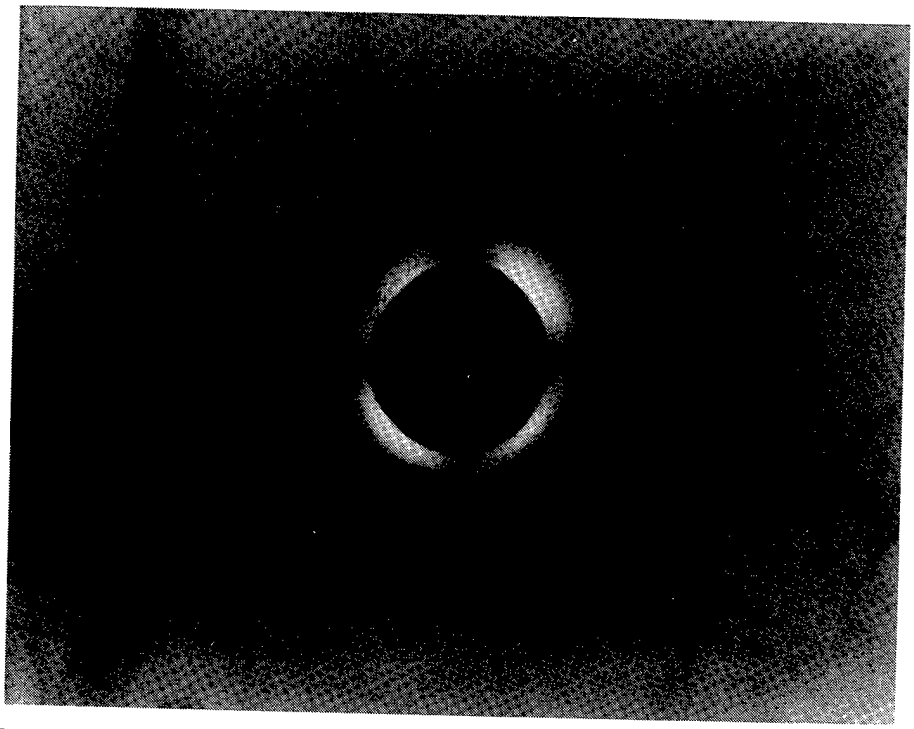
Photograph 1: Macrophotograph of the specimen studied in this article. The end with the circle was inside the tray. Transmitted illumination was used for this photograph.



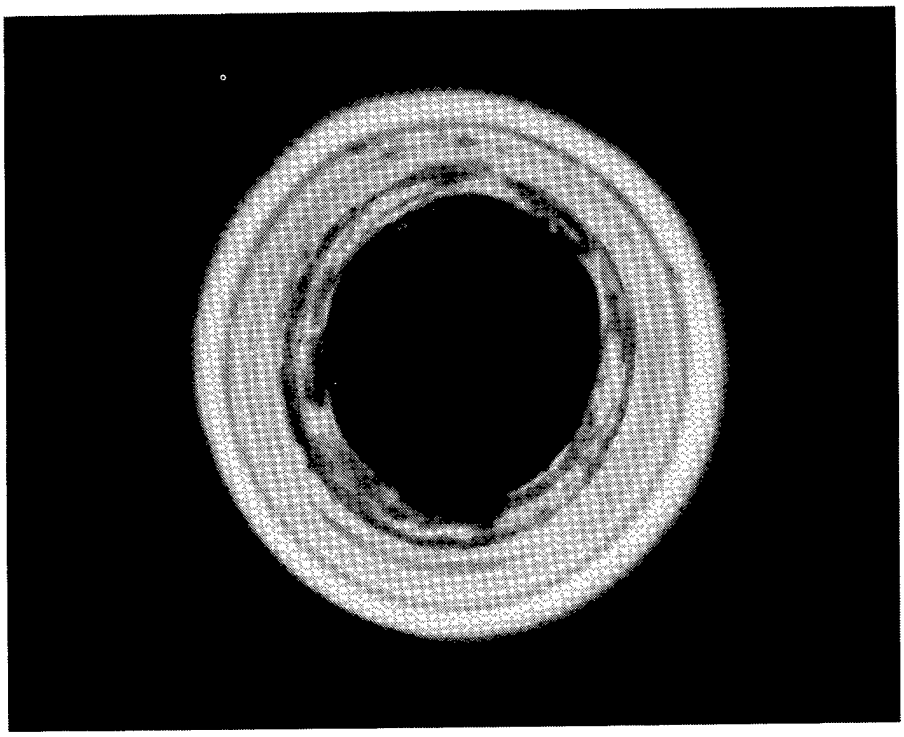
Photograph 2: This is the same sample photographed with oblique toplight. Bands that were dark in Photograph 1 are now bright due to light scatter. Along one edge interference colors can be seen. There are over ten orders of color indicating a thickness of over two micrometers.
(See color photograph, p. 1203.)



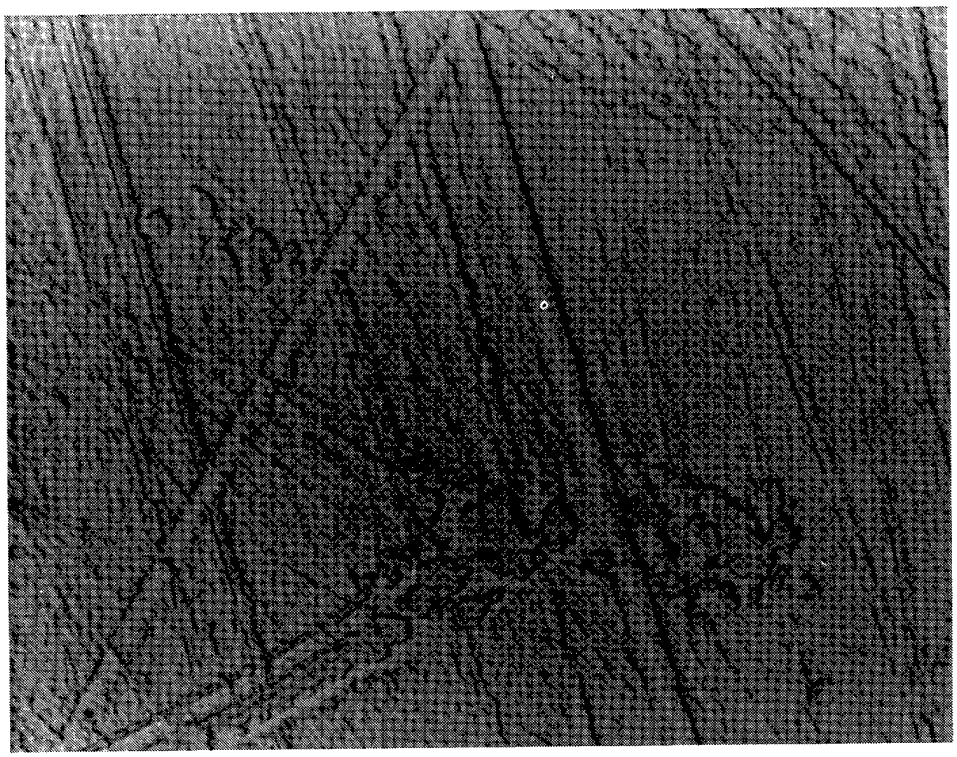
Photograph 3: This is an impact site that has undergone considerable atomic oxygen erosion since the impact. Transmitted illumination at a magnification approximately 500X.



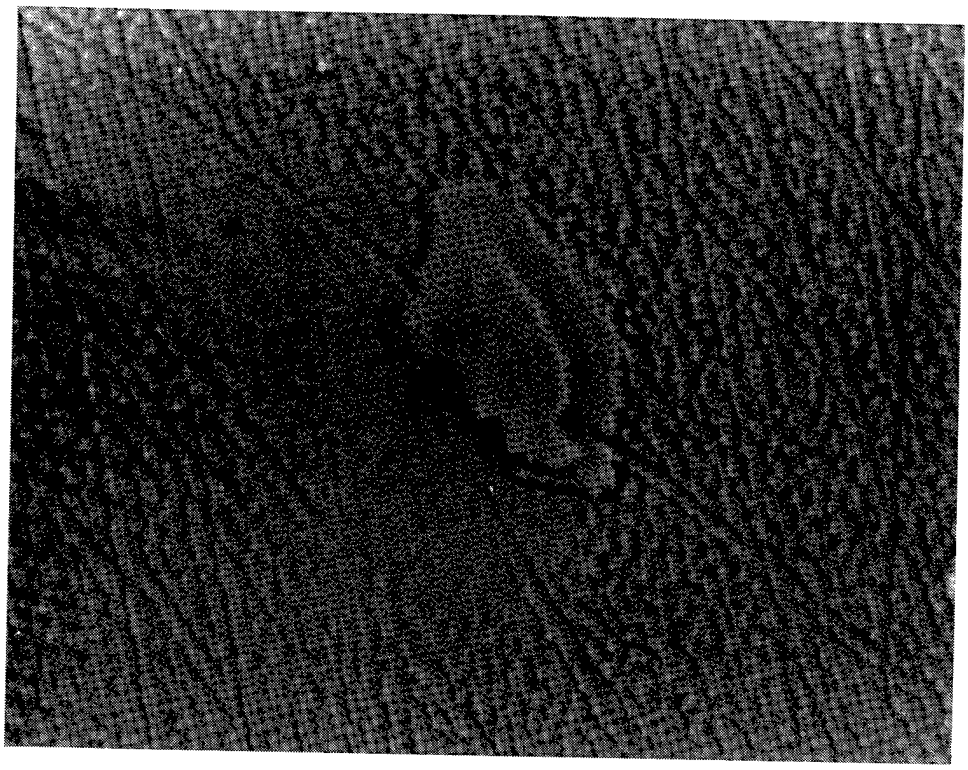
Photograph 4: Transmitted cross polarized light with a first order compensator plate was used to indicate the compressive stress frozen in the Teflon at this impact site. Transmitted illumination at a magnification approximately 300X. (See color photograph, p. 1204.)



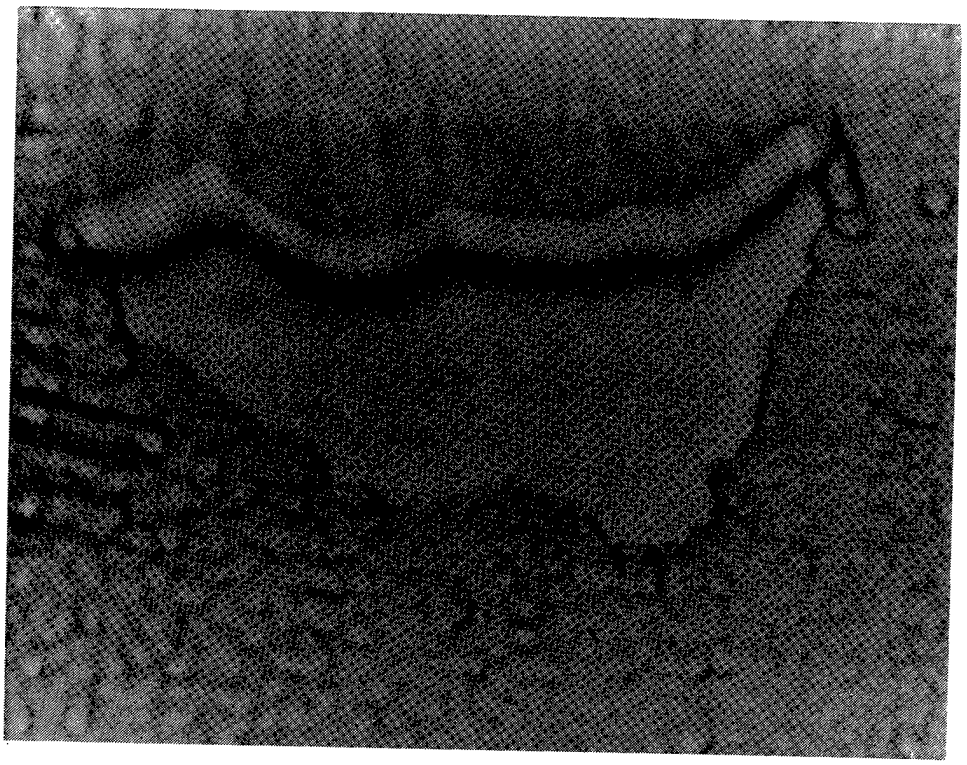
Photograph 5: Transmitted circular polarized light photograph of another impact site exhibiting very high residual stress. Transmitted illumination at a magnification approximately 125X.
(See color photograph, p. 1204.)



Photograph 6. Front surface of trailing tray A-04, Teflon surface exhibiting UV degradation. Transmitted illumination at a magnification approximately 550X.



Photograph 7: Microenvironmental effects of atomic oxygen reflected from a trunnion shield back onto the Teflon surface of tray A-04, a trailing tray. Transmitted illumination at a magnification approximately 1000X.



Photograph 8: Very shallow angle etch pattern area on tray C-08. Transmitted illumination at a magnification of approximately 250X.

PRELIMINARY INVESTIGATIONS INTO UHCRE THERMAL CONTROL MATERIALS

François Levadou and Mike Froggatt
European Space Research and Technology Centre
Noordwijk, The Netherlands
Phone: (31) 1719-83915, Fax: (31) 1719-84992

Martin Rott
Lehrstuhl für Raumfahrttechnik
TU München, Germany
Phone: (49) 89/2105-2578, Fax: (49) 89/2105-2468

Eberhard Schneider
Fraunhofer-Institut für Kurzzeitdynamik
Ernst-Mach Institut (EMI), Freiburg/Br., Germany
Phone: (49) 761/2714-326, Fax: (49) 761/2714-316

SUMMARY

This paper presents an overview of the initial work which has been done in the ESTEC Materials and Processes Division to evaluate the effect of space environment on the thermal blankets of the Ultra-Heavy Cosmic Ray Nuclei Experiment (UHCRE) :

1. Preliminary survey of the perforations of the two-thirds of the thermal blanket returned to ESTEC.
2. Thermo-optical properties and thickness recessions of three samples cut from each of the third centre parts of the 16 thermal blankets were measured and effects of environments, i.e.: sun illumination and atomic oxygen fluences, evaluated.
3. Contamination has been analysed on trays, external blanket and internal aluminized Kapton foil by IR technique and SEM/EDX examination.
4. The pattern of contamination on the Al Kapton foils has been observed, sketched and related to atomic oxygen flow.
5. LDEF yaw angle misorientation has been evaluated from the contaminated areas visible on some of the trays.

In addition, impacts of micrometeoroids and space debris have been experimentally simulated on spare flight thermal blankets by means of the plasma acceleration facility of the TU Müchen and the EMI light gas gun acceleration facilities. Glass, steel and aluminium projectiles with sizes between about 50 μm and 1 mm have been accelerated in a velocity range between 2 km/s and 10 km/s. Circular shock-induced delamination zones surrounding impact locations in the foil have been obtained.

Relations between penetration/perforation hole characteristics and projectile parameters have been established.

Experiment A0178

INTRODUCTION

The ULTRA-HEAVY COSMIC RAY EXPERIMENT [AO178], a joint ESA/DIAS (Dublin Institute of Advanced Studies) investigation, which flew on NASA's LONG DURATION EXPOSURE FACILITY was recovered in January 1990 after 5 years 8 months in space.

The main objective of the experiment is a detailed study of the charge spectra of ultraheavy cosmic-ray nuclei from zinc (Z=30) to uranium (Z=92) and beyond using solid-state track detectors. Among the 72 trays mounted around the periphery of the facility, 16 were devoted to UHCRE. Figure 1 shows the side experiment bays in an opened out configuration with the bays occupied by the UHCRE highlighted by cross-hatching.

INVESTIGATIONS PERFORMED

At ESTEC

Besides the support during the dis-assembly of the experiment at ESTEC, as part of these preliminary investigations, the following materials analyses were done :

- measurements of thermo-optical properties;
- determination of Atomic Oxygen effects on FEP thermal blanket;
- impact pattern analysis;
- contamination analysis on FEP and Kapton thermal blankets and trays;
- evaluation of LDEF yaw misorientation;

some other analyses will be performed in the near future, e. g., : effect of Atomic Oxygen on copper grounding straps, velcro-pull test, cylinders contamination and welds analysis, etc...

Outside ESTEC

Some tests have already been funded by ESTEC Materials and Processes Division particularly simulation tests of impacts to determine the relationship between projectile diameter and perforation diameter to try to explain the halo pattern formation.

Some other studies, funded by the ESA COLUMBUS programme are on-going:

- Scanning of the thermal blankets;
- Chemical composition analysis of dust residues at impact sites.

CONSTRUCTION OF UHCRE TRAY

A description of the materials of which the experiment is composed, is limited in this paper, to those used for the thermal control. Each tray consists of a NASA supplied tray in which 3 aluminium cylinders containing the detector stacks are installed. On the top of the tray is a black anodized aluminium frame carrying a single silver/FEP thermal blanket, and on the bottom an aluminium frame on which six aluminized Kapton foils are mounted. See figure 2.

The cylinders are painted with Astral Pyrolac 123 epoxy primer and Chemglaze Z306 polyurethane black paint. The external top thermal blanket is 5 mil (127 μm) Silvered FEP Teflon manufactured by Scheldahl. The inner surface of the blanket is painted black with Chemglaze Z306 (Figure 3). The internal thermal blankets are Scheldahl 5 mil aluminized Kapton, the aluminized side facing the interior of the tray. Both the top and the bottom blankets were attached to their frames using Astro Velcro; the Astro Velcro was bonded to the frames and blankets with Dow Corning DC 6-1104 silicone adhesive and DC1200 primer.

EFFECT OF THE SPACE ENVIRONMENT

Preparation of samples

To evaluate the effect of the space environment, particularly the effect of atomic oxygen on the top FEP thermal blanket, it was necessary to define an accurate method for the evaluation of erosion, i.e., the decrease in thickness of the FEP foil.

Using one of the seven flight spare blankets sealed in plastic bags and stored in a container at ESTEC since the integration of UHCRE, an investigation of the uniformity of the "as delivered" material was carried out. Fourteen samples were cut along one dimension of one of the spare blankets using a circular cutting tool of 2.47 cm in diameter. The black paint was removed from the metallized FEP by dipping the samples in a beaker of chloroform. After storing the samples for 48 hours in a temperature and humidity controlled room (20°C and 60% RH), the thickness and weight of each sample was measured. The weights ranged from 126 to 137 mg and the thicknesses from 121 to 132 μm. Graphs of thickness versus weight were plotted (Figure 4) and a very good correlation was found; the correlation straight line passing through the origin. Calculated thicknesses of samples from weight, diameter and using the density value of 2.15 g/cm^3 given by the manufacturer were also plotted on the same graph and show that weight measurement is more accurate than thickness measurement. The relation obtained between thickness and mass is :

$$e\ (\mu m) = 968.88 \times m\ (mg) \quad [1]$$

Plotting sample thickness against sample position along a one meter length of foil it was found that the thickness was not smooth but had a wavy form as shown in figure 5.

Having determined a suitable method of assessing erosion of the foils, samples were cut from the flight thermal blankets using the same technique. Three samples of 2.47 cm diameter were cut from the 1/3 centre part of each foil, one from the top, one from the centre and one from the bottom, care being taken to avoid taking pieces containing an impact. A total of 48 samples were cut. Also one sample from blankets E02 and one sample from blanket E10, of size approximately 6 x 6 cm were cut to perform total hemispherical emittance measurement.

Thermo-optical properties measurements.

Emittance

Normal emittance. The normal emittance was measured using Gier & Dunkle DB 100 equipment on all 50 flight samples and on the 14 flight spare samples. Figure 6 shows the result of all measurements versus the calculated thickness, using equation [1]. Figure 7 shows the results by LDEF rows (row 0 being the spare flight samples). The effect of atomic oxygen on the leading rows can clearly be seen.

Total hemispherical emittance. The total hemispherical emittance was measured on a spare flight sample and a sample from row E10 using a thermal dynamical technique developed at ESTEC. Table 1 gives the results obtained. The absolute accuracy of the method is 2%, but the reproducibility of the measurement is $\Delta\varepsilon_H = 0.003$; that is why the results are given with three digits. Surprisingly the ratio $\varepsilon_H/\varepsilon_N$ between spare and flight samples was different. The flight sample was then polished using optical paper until a shiny appearance similar to the flight spare foil was obtained. New measurements of normal and hemispherical emittance were performed and showed a marginal effect on normal emittance. Previous measurements performed in the past confirm that the ratio $\varepsilon_H/\varepsilon_N$ increases when thickness decreases.

Solar absorptance

The absolute solar absorptance of one sample (middle one) of each 1/3 part was measured using a Beckmann Spectrophotometer UV 5240 and an integrating sphere attachment for a centred sample. Figure 8 presents the results by LDEF row number (row 0 being the spare flight sample) and figure 9 presents the solar absorptance versus the UV irradiation time in space [Ref 1 and 2]. On this last graph samples from

rows 1 to 6 were differentiated from samples from rows 7 to 12. It seems there is a slight influence of UV irradiation on the solar absorptance which appears to be independent of atomic oxygen erosion.

Figure 10 shows also an influence of UV irradiation on the absorptance/emittance ratios

Recession due to Atomic Oxygen

After measurement of the thermo-optical properties, the paint layer was easily delaminated from the samples; slightly easier on those from the leading rows, i.e, samples exposed to atoms, rather than those on the trailing rows. The delamination took place at the silver/FEP interface; the metallic layers staying on the paint. The samples were weighed to evaluate the effect of atomic oxygen erosion. It should be emphasized that in view of the insufficient knowledge of the initial thickness of each sample,(an error in the order of 10 μm), the erosion should preferably be determined using the maximum number of samples possible from each foil, particularly for those rows which are near 90 degrees incidence. It is why in view of the small amount of samples, three for row 8 and 6 for rows 7, 10 and 11, the spread of the calculated recession of thickness is large. Mean values of the recession were calculated for each row. Figure 11 shows the recession versus the cosine of the atoms incident angle. The power function [2] determined using the mean calculated values gives for recession at normal incidence a value of $3.65\ 10^{-25}$ cm^3/atoms.

$$R = 3.65\ 10^{-25} \times \cos(\theta)^{0.32}\ (cm^3/atoms)\ [2]$$

This value is about 10 times higher than the recession expected for the LDEF flight based on previous measurements.

IMPACT HALO ANALYSIS

The UHCRE thermal control blankets are studded with many micrometeoroid and debris punctures, particularly those on the leading rows. Around the impact sites are strange halos initially consisting of several black rings followed by a quasi circular delamination zone, not always easily visible particularly for the blankets eroded by the atoms (see figure 12). The delamination zones have large diameters which are at least twenty times bigger than the impact hole. It seems that there are synergistic effects from other environments.

Thermal cycling due to the shadowing of the LDEF at each orbit may have weakened the adhesion of the silver layer with the FEP over time and therefore may explain why there are large differences in the size of the delamination zones; differences which could also be explained by the amount of energy delivered into the material on impact. After the impact, oxygen atoms have penetrated between the FEP and the silver inside the delamination zone and oxidized the silver. The question to be solved is, why are they rings and not a general blackening of the delamination zone.

To try to confirm some of these assumptions, the silver layer surrounding one impact halo, together with the paint film peeled from the FEP, was examined using a Cambridge Scanning Electron Microscope Type S360, equipped with a four element backscatter detector and a Link AN10000 energy dispersive analyser with a windowless X-ray detector. Secondary electron images as well as atomic number contrast imaging was performed on the area around the impact hole. The dark and shiny fringes were analysed using EDX. The EDX results show the presence of oxygen and the absence of fluorine in the dark fringes. The shiny fringes show the presence of fluorine and the absence of oxygen. In both cases high carbon and silver concentrations were found. Fluorine and oxygen linescans running over the dark and shiny fringes and over the impact hole confirm the alternate appearance of oxygen and fluorine for each circular ring (Figure 13). The dark fringes appear to be oxidized silver, while the shiny fringes appear to be fluoro-carbon coated silver. There is yet no explanation concerning the formation of such fluorocarbon deposition at time of impact.

CONTAMINATION ANALYSIS

Contamination on trays

The trays, situated on the leading face of LDEF, exhibit on the earth and space facing ends, contamination stains, sometimes called "nicotine stains", radiating from the corners of the trays and having the shape of a cone (figure 14).

Wipes of this contamination were taken from several positions, i.e., on the edge of the conical shape where the contamination is light colored, on the centre where the contamination is more brown and also on a rivet head where the contamination is really dark. It was not so easy to wipe, several rubs were necessary, showing a polymerization of the contamination.

Infrared analysis

Infrared analysis of the three wipes was performed. The spectrum obtained, figure 15, indicates a silicone contaminant. Although there are a lot of silicones used on LDEF, the most probable contaminant source inside the LDEF body itself and outside the trays, is the Chemglaze Z306 polyurethane black paint and Chemglaze 9924 primer used in a large amount on the LDEF structure and the experiment trays. The manufacturer has since confirmed that Chemglaze Z306 contains, as a wetting agent, Dow Corning DC230 silicone in the level of approximately 0.05% in the dried film and that 9924 does not.

The IR spectrum of DC 230 (figure 16) given by Sadtler shows some similarities with the one of LDEF tray contamination, but the alterations of the outgassed materials due to space environments make conclusive identification impossible.

Tests performed

A standard weightloss/VCM test (ASTM E595) was performed to verify the contamination due to Chemglaze Z306 and also the primer 9924. To increase the amount of contaminants the parameters of the test were changed. Instead of a run of 24 hours, the test duration was doubled and instead of a condenser plate temperature of 25°C, the temperature was 15°C.

After the test, wipes were taken from a small part of the condenser plate and infrared tests carried out. The spectra are more complex. The spectrum of Z306 (figure 17) shows the presence of iso-cyanate group which means that there is an incomplete cure of the paint. Earlier tests on Chemglaze 9924/Z306 have shown that after re-evaporation of the condensed materials during a VBQC test (principle of VBQC test described in reference 3), the component left on the quartz crystal was mainly siloxane (figure 18).

The condenser plates were then submitted to UV irradiation for 300 equivalent sun-hours and irradiated for 4 hours in a plasma asher with oxygen. Polymerization of the polyurethane occurred on the condenser plate, but it is still impossible to confirm the presence of silicone (figure 19). More investigations have to be done in this direction.

It can be concluded that the stains are a result of oxidisation of outgassed silicones by atomic oxygen. Synergetic effects with UV light may modify polymerization and colour, but in itself the UV does not fix and polymerize the contaminant. This fact will be confirmed later in the document.

Yaw angle misorientation

To illustrate further the fact that Atomic Oxygen can pass through gaps in the LDEF structure and experiment trays and oxidize outgassed silicone products, one should refer to figure 14. At each corner of the trays there is a gap of about 4 cm x 4 cm where atomic oxygen and UV can enter the LDEF structure. The contamination stains radiate in a conical shape out from the corner gaps, at various angles in relation to the top flange.

If one transposes the angle of these stain traces onto a sketch of the LDEF cross section one can see that the lines are practically parallel and in line with the direction of travel of LDEF and thus in line with the atomic oxygen flux. It can thus be concluded that these stains are a result of oxidization of outgassed silicones by atomic oxygen.

For all trays, the difference between the theoretical angle with the speed direction and the angle between the axis of the cone and the flange, gives the yaw misorientation angle. Table 2 gives the results obtained for some trays. As this estimation was done using pictures, the accuracy of the mean value obtained is unknown.

VISUAL INSPECTION OF ALUMINIZED KAPTON FOILS

The foils were laid out on a large table in a clean room and inspected visually on each side. The contamination patterns, suspected micrometeoroid impacts and any other points of interest were noted and sketched [Ref 4].

Observations

Aluminized side of foils

Contamination. Five of the foil sets exhibited contamination on the aluminized side. Table 3 shows in tabular form a visual assessment of the amount of contamination. The contamination on the foils concerned was situated directly below vent holes or gaps around the upper FEP/TEFLON foils.

Manufacturing faults. Many of the foils exhibited what was thought to be micrometeoroid impacts or ejecta after impacts. As many of these "impacts" were located in positions where it was not possible for a micrometeoroid to travel (under cross members and tubes) an investigation was instigated. It was concluded that these "impacts" were in fact manufacturing faults caused by spatter of aluminium containing tungsten from the vacuum deposition process.

Kapton side of foils

Contamination. Twelve foils were contaminated to a greater or lesser extent. Table 4 shows in tabular form the visual assessment of the amount of contamination. Those foils which were contaminated were not always covered by a continuous layer of contamination, the pattern of contamination was determined by the obstructions which may be in the vicinity of the foils. Any structural obstruction in the area would form a shadow effect in front of the foil. The foils on tray E02 are a good example of this (figure 20). A diagonal structural member inside LDEF, situated in close proximity to the foils, has shielded the foils from contamination or the "fixing" medium which would polymerize or oxidize it (atomic oxygen and UV).

Manufacturing faults. The manufacturing faults observed on the aluminized side were visible on the Kapton side as heat affected zones.

Analysis of contamination

Examination by Scanning Electron Microscope of samples of the contaminated foils concluded that the shading on the Kapton foils was not atomic oxygen erosion, which was a possibility, but was in fact contamination. This contamination, which contains silicone, is thought to have originated from polyurethane paints and silicone adhesives, in the vicinity of the foils.

If one indicates on a cross-sectional view of the LDEF (figure 21) which foils were contaminated, making the stripe proportional to the estimated amount of contamination, one can see that the foils in rows 8, 10 and 11 were contaminated on the aluminized side and that the foils in rows 1, 2, 4, 5, 6, 7 and 11 were contaminated on the Kapton side. The most heavily contaminated surfaces were the Kapton side of foils 2, 4 and 5 and the aluminized side of foils 8, 10 and 11.

As the contamination in the majority of cases is facing the RAM direction, and by analysis of the layer, is confirmed to contain silicon and oxygen, one can suppose that outgassed silicone products have been oxidized by atomic oxygen to form a silicon oxide layer on the foils. Silicon oxide being resistant to atomic oxygen erosion would not be removed by the cleaning action of atomic oxygen and thus form a protective layer for the Kapton. The possibility that the outgassed products could have been polymerized by ultra violet radiation can also be considered but as the LDEF structure was radiated symmetrically between leading and trailing sides by sun-light during its life time it would not explain why the contamination was orientated in the RAM direction.

IMPACTS TESTS

Impact experiments have been performed at the EMI-light gas gun facilities and TUM plasma accelerator in an effort to simulate impact features which have been identified on exposed UHCRE foils.

TUM plasma accelerator

The TUM plasma accelerator is currently able to accelerate particles in the mass range of 10^{-5} to 10^{-10} g. The velocity range is 2 km/s to 18 km/s respectively. The accelerated particles are glass spheres with a density of 2.5 g/cm^3. The facility is described in Ref 5.

In order to obtain a realistic survey of the impact characteristics on silvered Teflon thermal blankets, a test series has been performed within the size-velocity regime of the Munich particle accelerator. All impact craters have been examined under the optical microscope.

In table 6 the important data for all impacts are compiled. Size and velocity of the particles are listed as well as the major dimensions of the impact craters. From figure 22 it can be derived how the crater dimensions are defined. In one case, where there was a complete perforation of the test sample, the dimension d_5, denotes the output diameter on the rearside of the thermal blanket. Figure 23 shows the photograph of a 46 µm particle impacting at 7.2 km/s. The essential characteristics which were observed at most of the impacts can be seen clearly: a central crater surrounded by a halo-like pattern. A closer look at the halo shows that it consists of many small concentric cracks within the teflon films. There are also some optical effects, which are caused by a delamination of the target. A very sharp ring marks the borderline of the delamination zone. In addition to the concentric halo pattern, some radial structures can be seen on the photograph. These structures are on top of the teflon foil and could have been caused by target or projectile material ejected along the surface.

The structure of the crater is illustrated in the schematic cross-section of figure 22. In all cases, the diameter d_4, of the delamination zone is larger than the diameter d_3, of the area with the shock induced circular cracks. Especially for the slower impacts, the diameter d_4 is significantly larger than d_3.

Figure 24 shows the impact crater of a 97 µm particle at 2.3 km/s. The shock induced cracks around the central crater can be seen clearly. In this case, the delamination zone is very large. Its borderline is the faint light line at the top of the photograph.

Figure 25 shows the microscopic picture of a very fast impact. At 12.6 km/s, the 71 µm particle perforated the thermal blanket completely.

In conclusion it can be said that the experiments described here basically show the same crater characteristics which were observed on the original flight thermal blankets. Nevertheless, further experiments are necessary; especially impact tests on the original UHCRE flight thermal blankets are of great importance. The long exposure to the space environment might have changed the mechanical properties of the thermal blankets (e.g., adhesion between the single layers), leading to different crater characteristics. In this case it will be possible to distinguish between impacts which occurred at the beginning of the mission and those at the end of the mission.

EMI Light gas gun experiments

The light gas gun acceleration principle has been described by Crozier and Hume [Ref 6].

In a first series of experiments aluminium, glass, and steel spheres with diameters between 350 μm and 1000 μm have been used as projectiles; impact velocities range from 2.8 km/s up to 8.5 km/s at normal incidence.

In all cases perforation holes have been obtained with most of them being surrounded by a concentric halo zone (figure 26). The rims of the perforation holes show impact melt consisting of the foil material components, typical for hypervelocity impact. Further out the impact molten ring is surrounded by a system of radial cracks within the upper Teflon layer of foil, indicating that Teflon behaves brittle under extreme, high rate loading conditions. In all cases the extended halo zones have been found to be caused by delamination effects,which are very probably induced by shock waves. Thus, halo zones observed around craters and perforation holes in exposed UHCRE foils can be explained by shock wave delamination effects. Even slight colouring of these zones as it is frequently observed on exposed foils, may be due to impact plasma and/or atomic oxygen influences.

Detailed results of the impact simulation experiments are summarized in Table 6.

Figure 26 presents crater, respectively perforation hole diameters **D**, normalized by projectile diameters **d** versus impact velocity **v**. The data points can be approximated by a regression curve which yields a v exp 2/3 dependence. For hypervelocity impact craters such a dependence can be expected, since within the hydrodynamic regime of impact, crater volumes are proportional to the kinetic projectile energy. This holds for craters in semi-infinite targets. Data from perforations deviate from this v exp 2/3 curve more beyond the ballistic limit. There is additional scattering in the data due to relatively large local variations in the foil thickness. Figure 27 presents the results of tests performed by EMI and TUM.

Further experimental simulation of oblique impacts as well as of ricochet phenomena are planned.

ACKNOWLEDGEMENTS

We gratefully acknowledge the assistance of D. Collins, A. de Rooij, J-M. Saillier, M. van Eesbeek and G. Gourmelon from the ESTEC Materials & Processes Division in the work reported in this paper.

REFERENCES

[1] R.J. Bourassa, J.R. Gillis and K.W. Rousslang. Atomic Oxygen and Mission Total Solar Exposures for LDEF Experiments. First LDEF Post-Retrieval Symposium. NASA CP-3134, 1992.

[2] G. Drolshagen. Space Environment Analysis for LDEF. Internal ESTEC Working Paper no. 1588, July 1990.

[3] M. van Eesbeek & A. Zwaal. Outgassing and Contamination Model based on Residence Time. Proceedings of the Third European Symposium on Spacecraft Materials in Space Environments. (ESA SP-232, Nov 85).

[4] M. Froggatt. Inspection of the LDEF/UHCRE Aluminized Kapton Thermal Control Foils after Recovery from Space. Internal ESTEC Working Paper no. 1623, August 1991

[5] A. Hüdepohl, M. Rott, E. Igenbergs. Coaxial Plasma Accelerator with Compressor Coil and Radial Gas Injection. IEEE Transactions on magnetics, Vol. 25, No 1. pp. 232-237, 1989.

[6] W.D. Crozier & W. Hume. High velocity light gas gun. J. Appl. Phys. 28, 1957.

Table 1 : EMITTANCE

Sample	eH	eN	eH/eN
Spare	0.805	0.795	1.013
E10	0,795	0.770	1.033
E10 polished	0.792	0.763	1.038
1 mil FEP/Ag	0.547	0.487	1.128

Table 2. YAW ANGLE

Tray number	Yaw angle (degree)
C11 Earth side	10.41
C11 Space side	10.96
D11 Earth side	10.59
D11 Space side	11.17
C08 Earth side	10.99
C08 Space side	10.27
Mean value	10.7

Table 3. VISUAL INSPECTION OF ALUMINIZED SIDE OF FOILS

TRAY Nº	CONTAMINATION
D01	No contamination
A02	No contamination
E02	No contamination
A04	No contamination
F04	No contamination
B05	No contamination
C05	No contamination
D05	No contamination
C06	No contamination
B07	No contamination
D07	No contamination
C08	Contamination on left side of foils 1 & 4 and right side of foil 3
A10	Contamination on foils 1,2 ,3, 4 & 6. Contamination located below vent holes in and edge gaps around FEP/TEFLON upper foil.
E10	Contamination on foils 1, 2, 3 & 4. Contamination located below vent holes in and edges gaps around FEP/TEFLON upper foil.
C11	Contamination on right side of foils 3 & 6.
D11	Contamination on left side of foils 1 & 4.

Table 4. CONTAMINATION ON KAPTON SIDE OF FOILS

TRAY Nº	CONTAMINATION
D01	Possibly light contamination all over foils with some slightly heavier contaminated areas.
A02	Heavy contamination on all foils.
E02	Heavy contamination on all foils. Some areas possibly shaded by structures were not contaminated.
A04	Both heavy and light contamination.
F04	Heavy contamination.
B05	Three foils more contaminated than others.
C05	Heavy contamination.
D05	Both heavy and light contamination.
C06	Slight contamination.
B07	Slight contamination.
D07	Slight contamination.
C08	No contamination.
A10	No contamination.
E10	No contamination.
C11	No contamination.
D11	Slight contamination.

Table 5. IMPACTS PARAMETERS AND CRATER MEASUREMENTS

Particles		Crater Measurements				
v (km/s)	D (μm)	d1 (μm)	d2 (μm)	d3 (μm)	d4 (μm)	d5 (μm)
6.3	58	152	112	740	1340	
8.8	34	125	88	515	638	
7.2	46	162	108	740	1147	
5.4	61	192	197x118	895	1858	
5.9	48	102	84x58	490	560	
4.6	80	195	159x112	1337	2212	
2.3	97	136	115x89	789	1328	
5.0	80	210	142x180	968	1926x1835	
6.3	32	86	50	454	507	
2.2	69	85		315		
9.5	64	140	123	555	650	
1.9	180	201	143x176	1270	1566x1630	
12.6	71	335	106	672	692	56
7.5	35	102	64	382	473	

Table 6. MICROMETEOROID/DEBRIS SIMULATION ON UHCRE FOILS

Exp	Projectile				Hole diam	Halo diam
No	Mat	Diam (μm)	Mass (mg)	Speed(km/s)	(μm)	(mm)
1335	St	500	0.514	5.2	915	4.5
1336	St	350	0.176	4.9	724	3.9
1337	St	1000	4.11	5.4	1510	5.9
1344	Gl	1000	1.36	5.1	1560	6.1
1345	Al	900	1.03	5.4	1743	6.3
1346	Gl	500	0.17	4.6	984	4.7
1360	St	500	0.514	3.3	836	4.2
1361	St	1000	4.11	2.9	1335	5.2
1363	Al	900	1.03	2.8	1400	5.3
1364	St	350	0.176	3.2	541	3.6
1365	Gl	1000	1.36	2.9	1250	5.2
1366	Gl	500	0.17	2.9	748	4.0
1367	Gl	350	0.054	2.9	376	2.3
1372	St	1000	4.11	5.5	1614	6.2
1383	Gl	350	0.054	4.6	986	4.7
2510	Al	900	1.03	8.5	1940	6.5
2514	Gl	1000	1.36	7.8	1600	4.2
2515	Gl	500	0.17	7.0	1300	3.8
2516	St	350	0.176	7.9	660	1.4

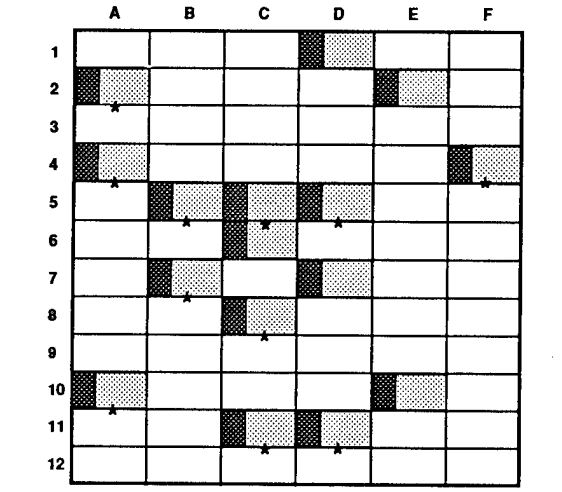


Figure 1. LDEF UHCRE [A0178]
Thermal blanket allocations

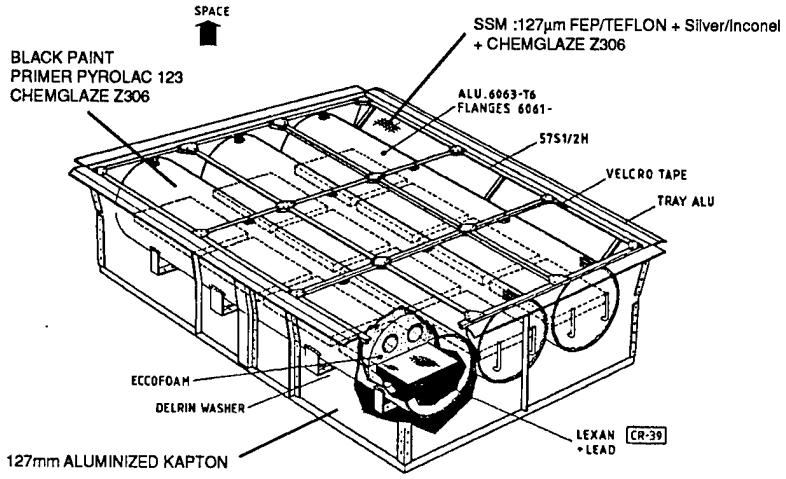


Figure 2. CONSTRUCTION OF UHCRE TRAY
The light top frame supports the thermal FEP cover

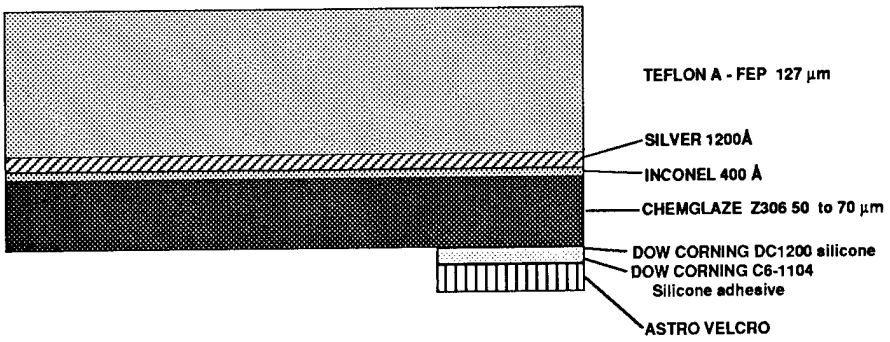


Figure 3. UHCRE THERMAL BLANKET
Scheldahl G401500 with Chemglaze Z306

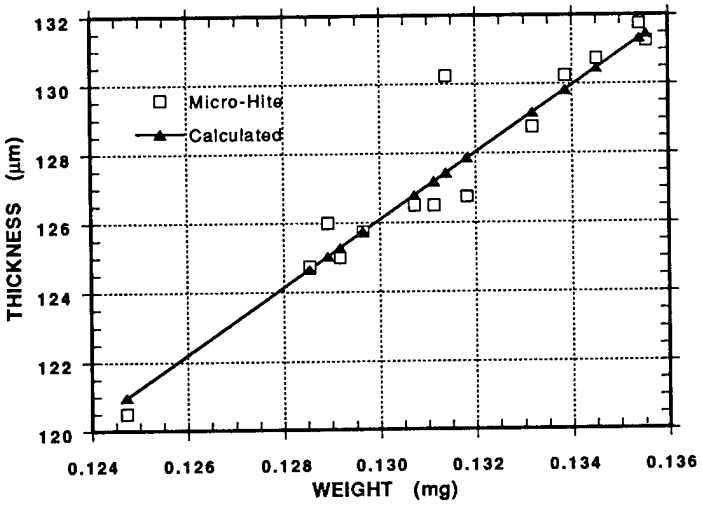


Figure 4. SAMPLE THICKNESS VS SAMPLE WEIGHT

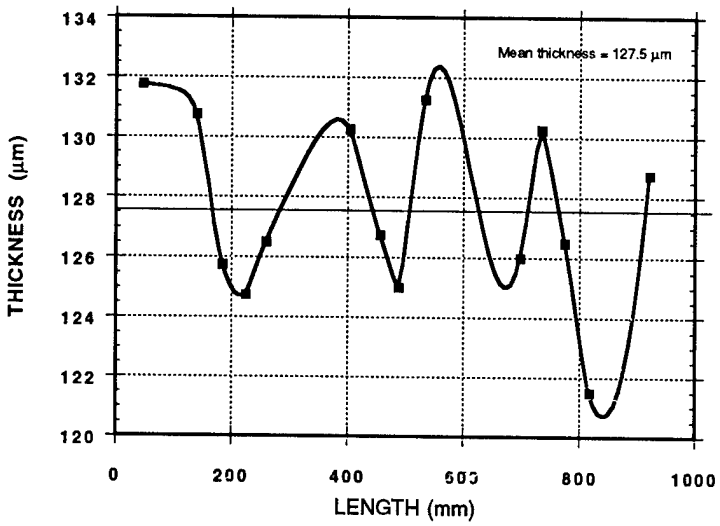


Figure 5. UHCRE SPARE BLANKET 9 THICKNESS PROFILE ALONG ONE SIDE

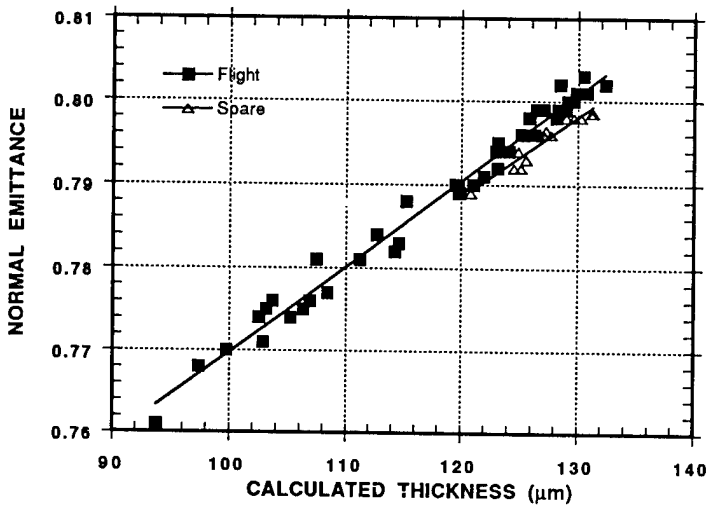


Figure 6. NORMAL EMITTANCE VS THICKNESS

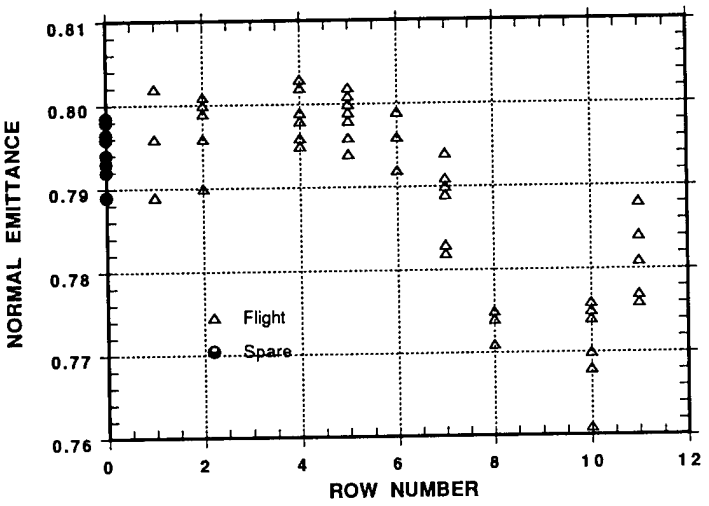


Figure 7. NORMAL EMITTANCE
VS
ROW NUMBER

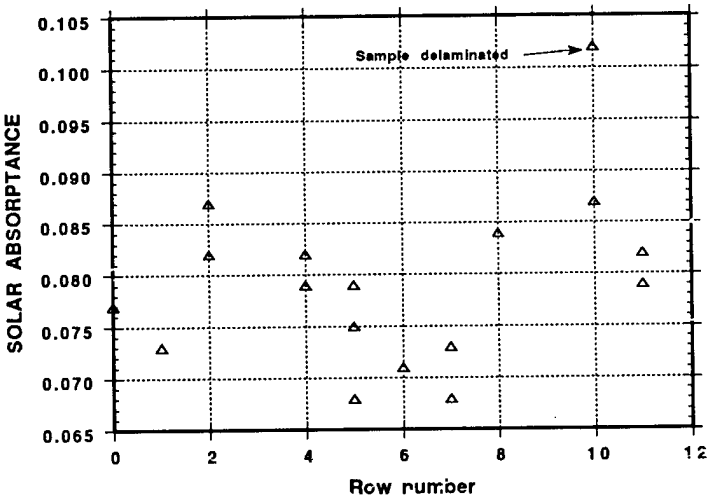


Figure 8. SOLAR ABSORPTANCE
VS
ROW NUMBER

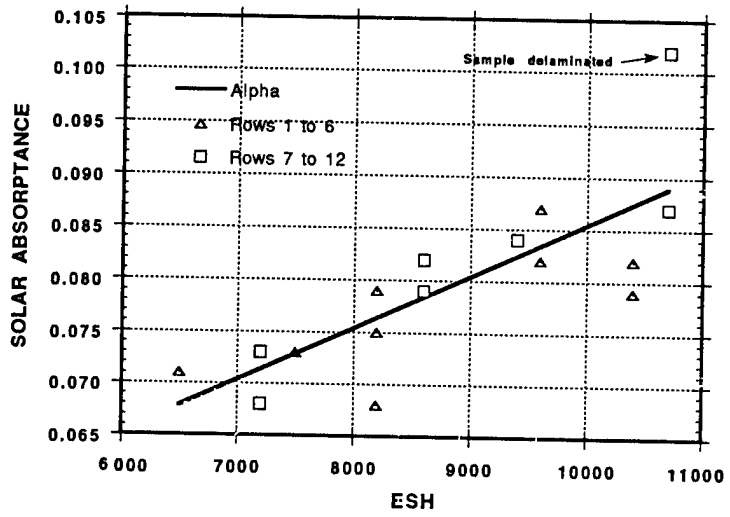


Figure 9. SOLAR ABSORPTANCE VS UV IRRADIATION

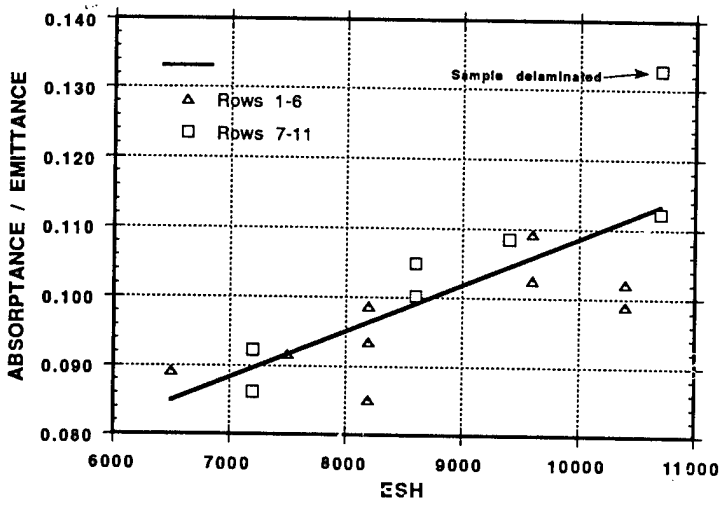


Figure 10. ABSORPTANCE/EMITTANCE RATIO VS UV IRRADIATION

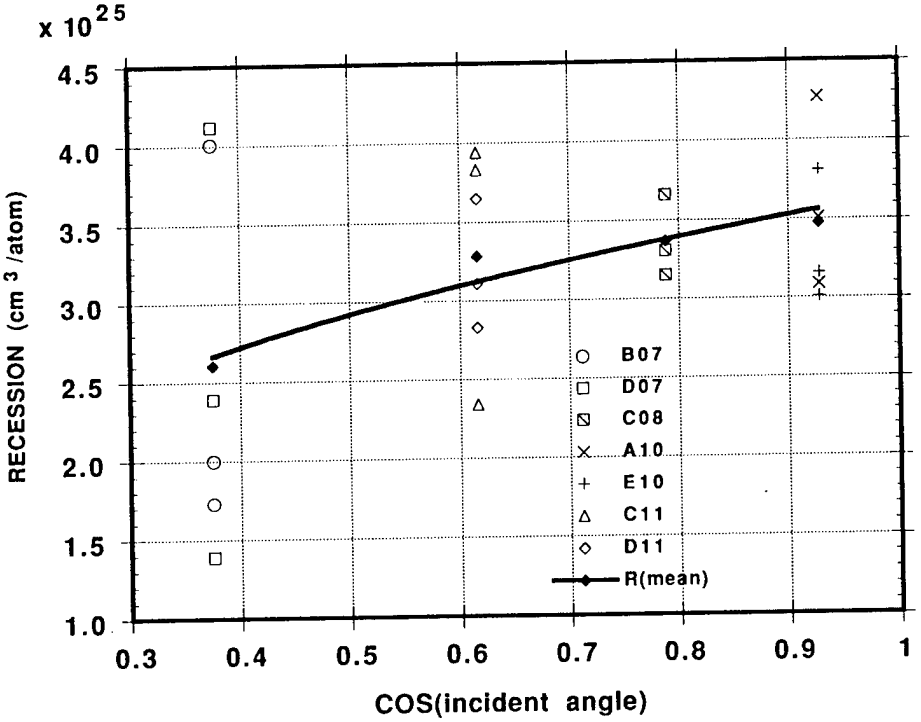


Figure 11. FEP RECESSION VS COS OF AO INCIDENT ANGLE

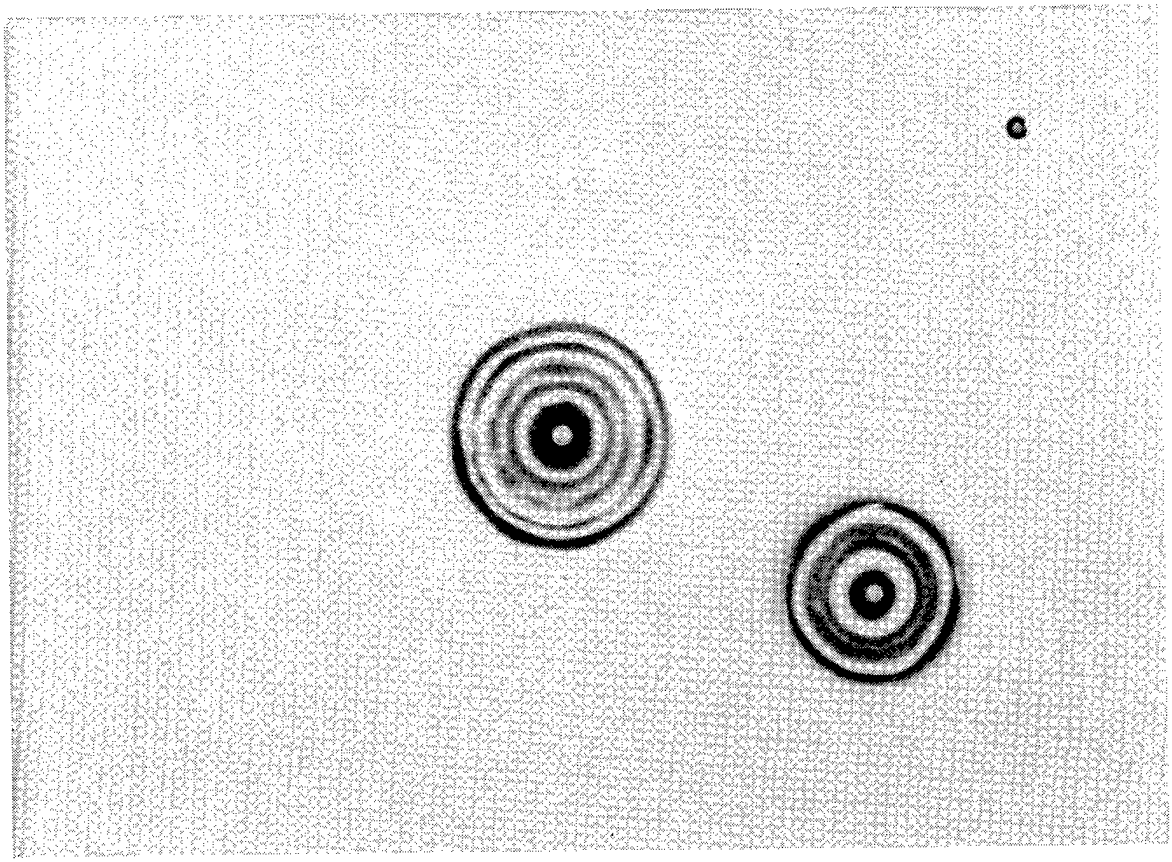
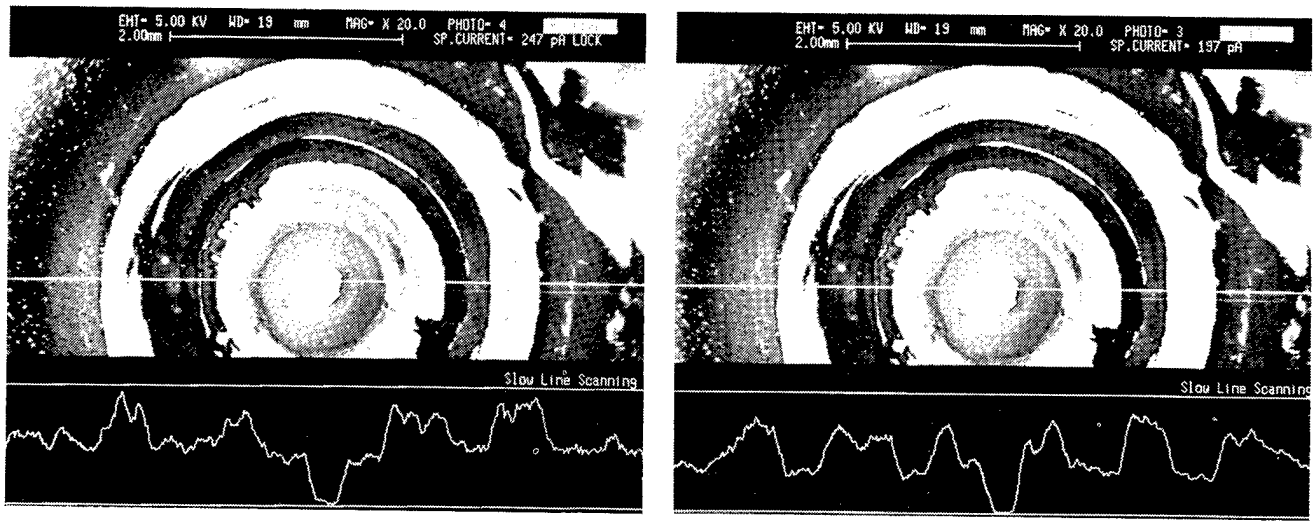


Figure 12. IMPACT HALO ON E10 FOIL



Fluor Linescan

Oxygen Linescan

Figure 13. IMPACT HALO EDX ANALYSIS

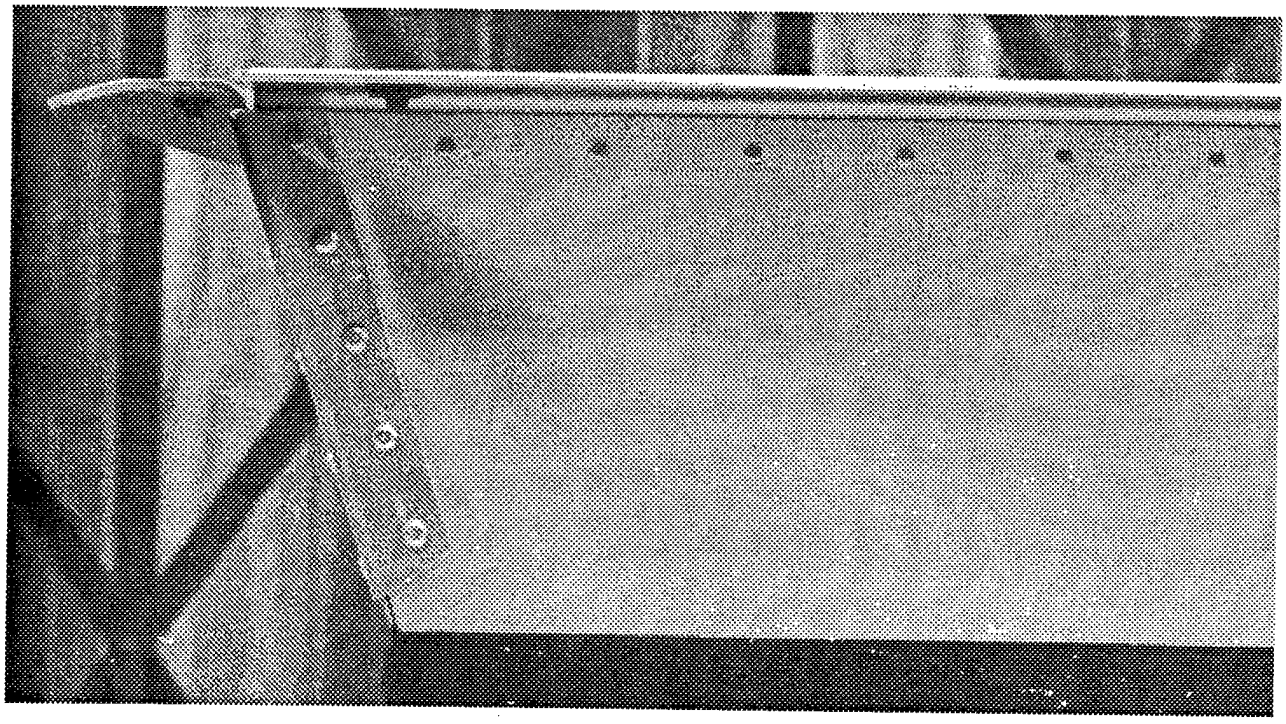


Figure 14. CONTAMINATION STAIN ON TRAY C11 EARTH SIDE

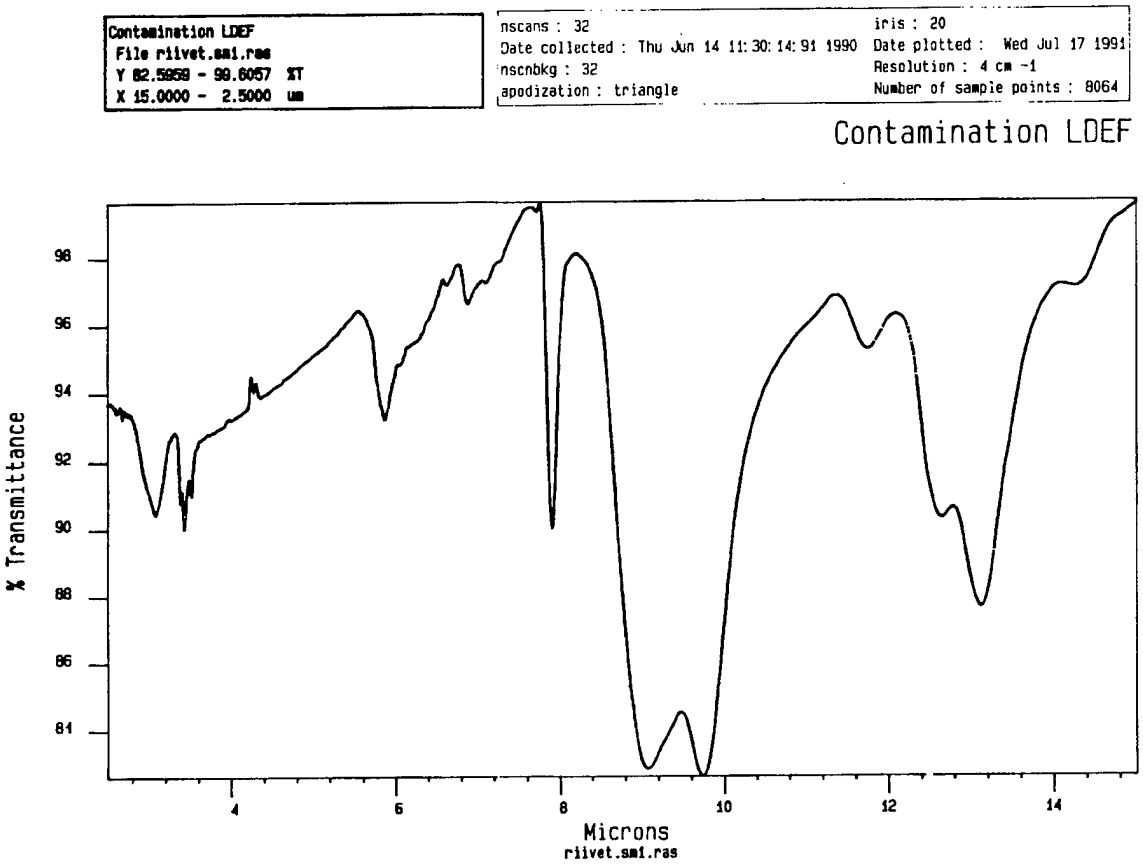


Figure 15

DOW CORNING 230 FLUID LUBRICANT

ALKYL-ARYL SILOXANE POLYMER

Sp. Gr. 1.009 Visc. 25°C 1400 cs
Pour Point -49°F
Source: Dow Corning Corp.
Film

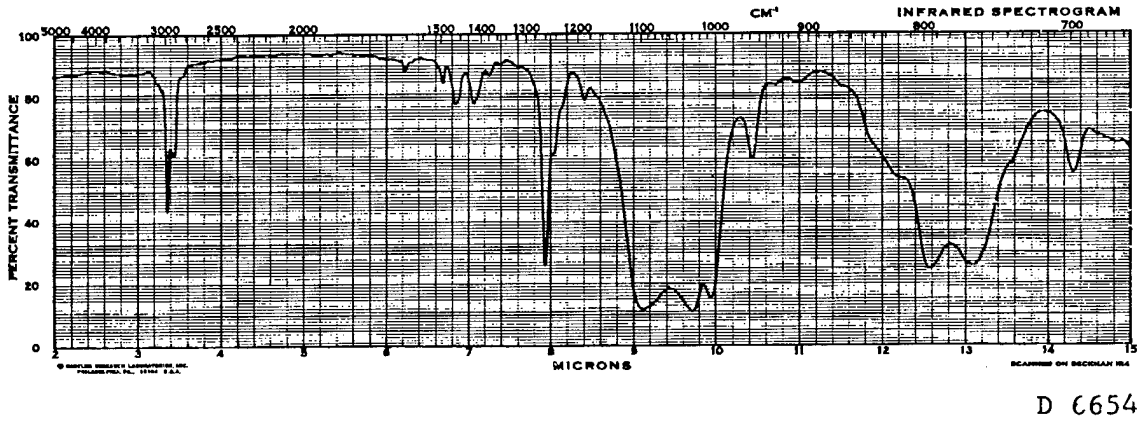


Figure 16

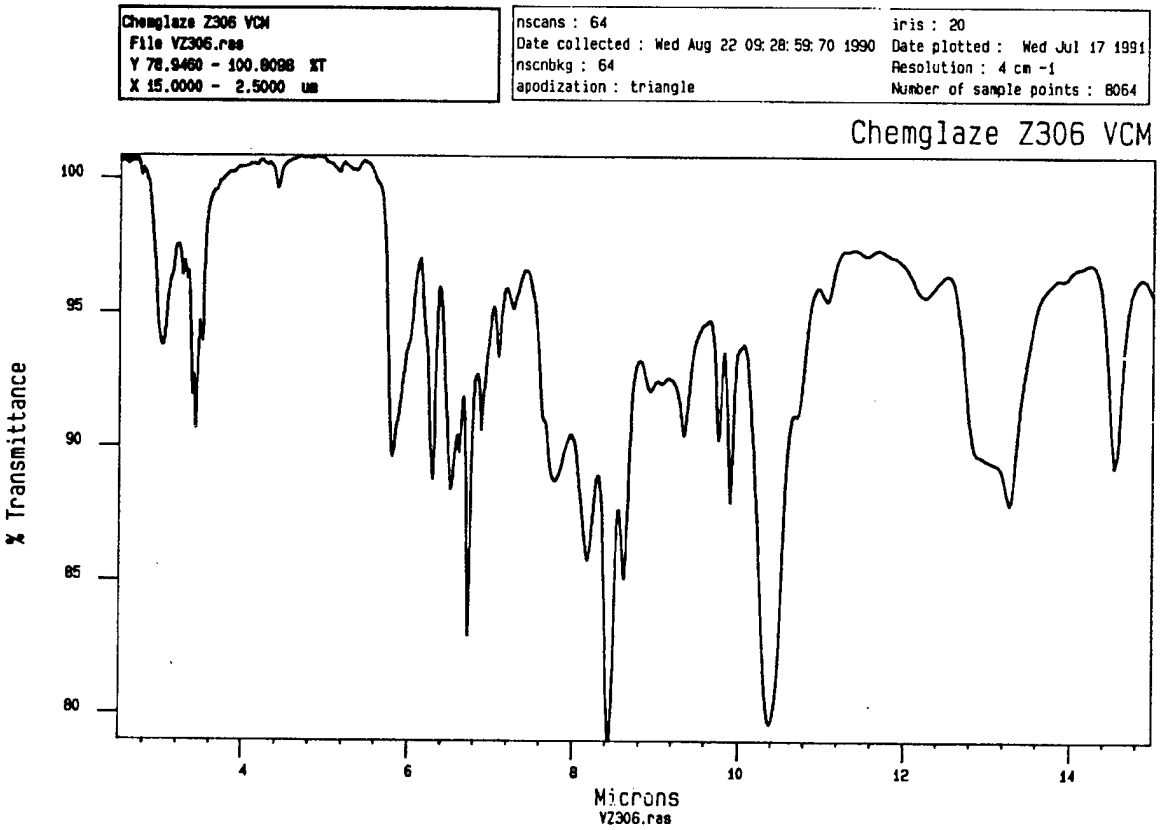


Figure 17

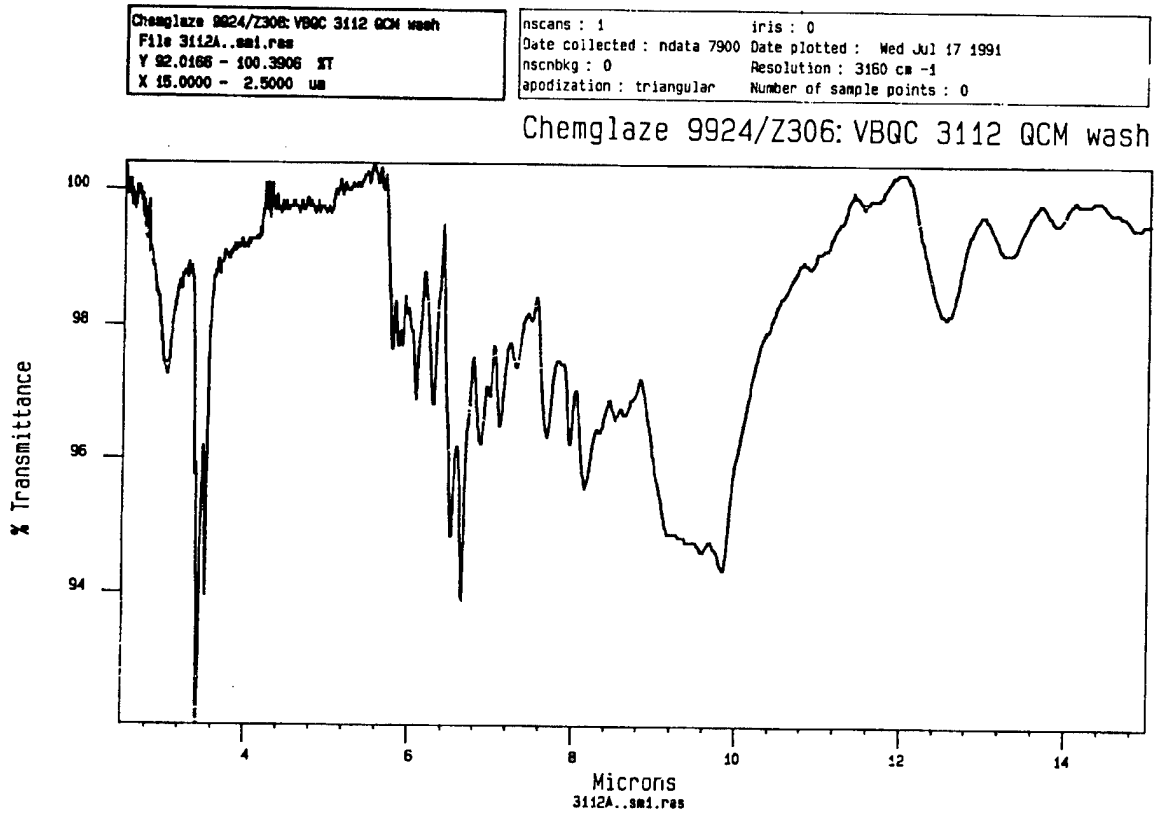


Figure 18

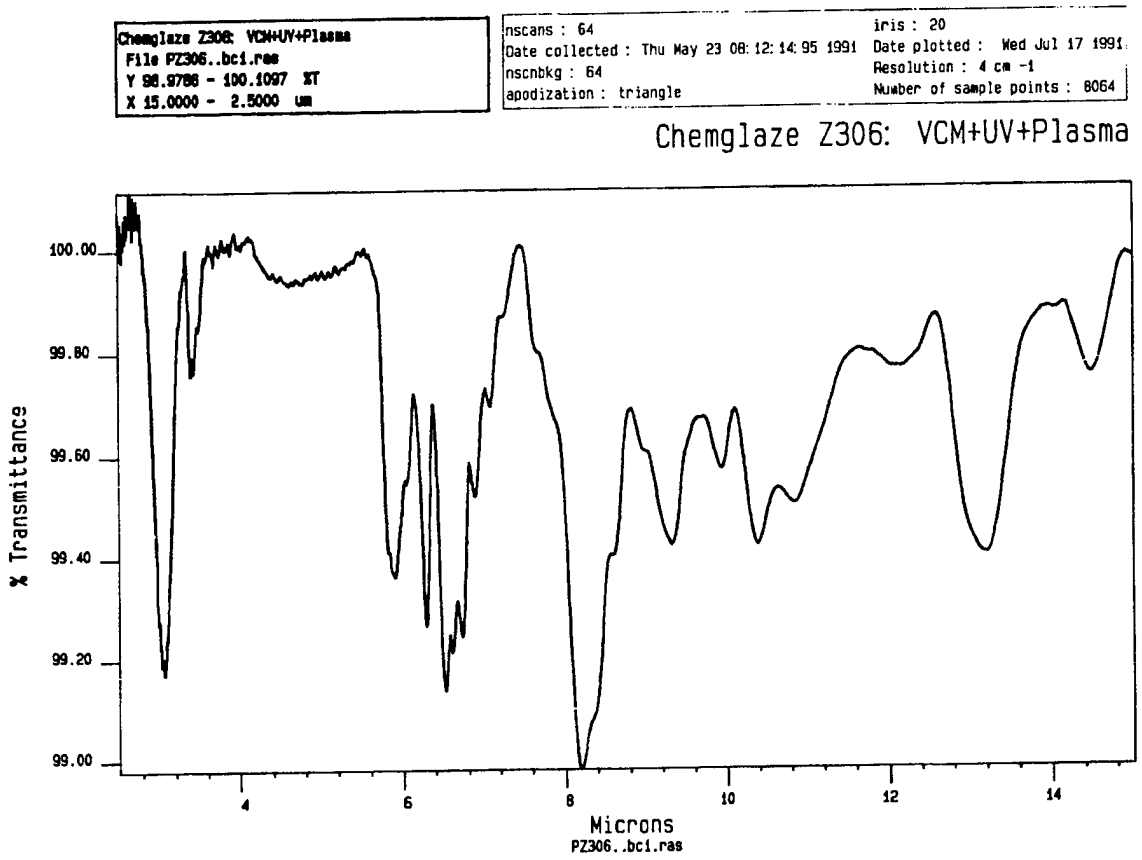


Figure 19

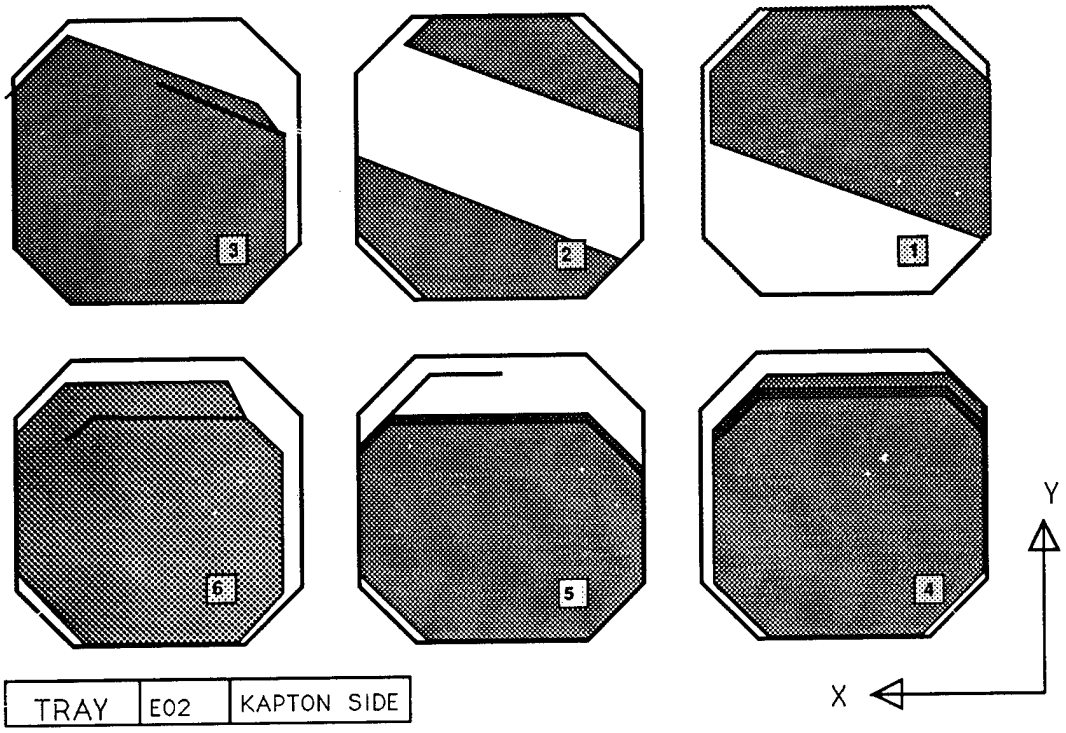


Figure 20. EXAMPLE OF CONTAMINATION ON KAPTON FOIL. SOME AREAS POSSIBLY SHADED BY STRUCTURE

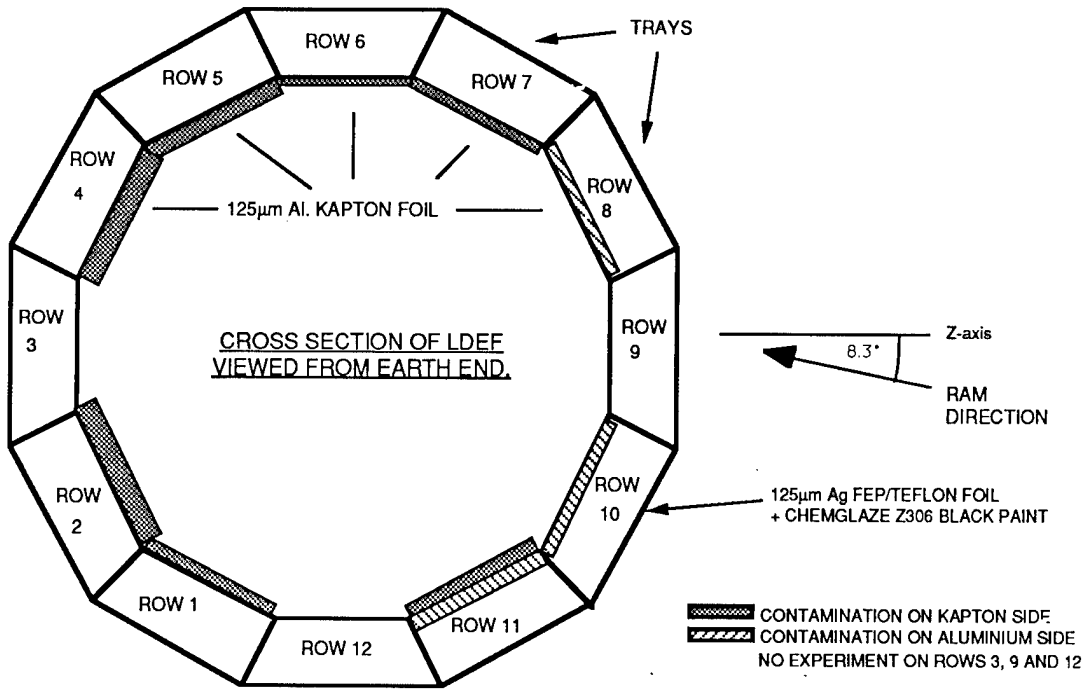


FIGURE 21. VIEW OF LDEF STRUCTURE WITH UHCRE AL KAPTON FOILS HIGHLIGHTED TO SHOW CONTAMINATION

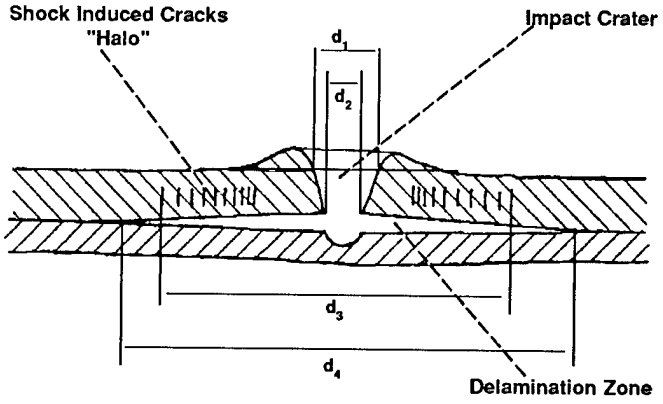


Figure 22. Schematic cross section of a typical impact crater and crater dimensions

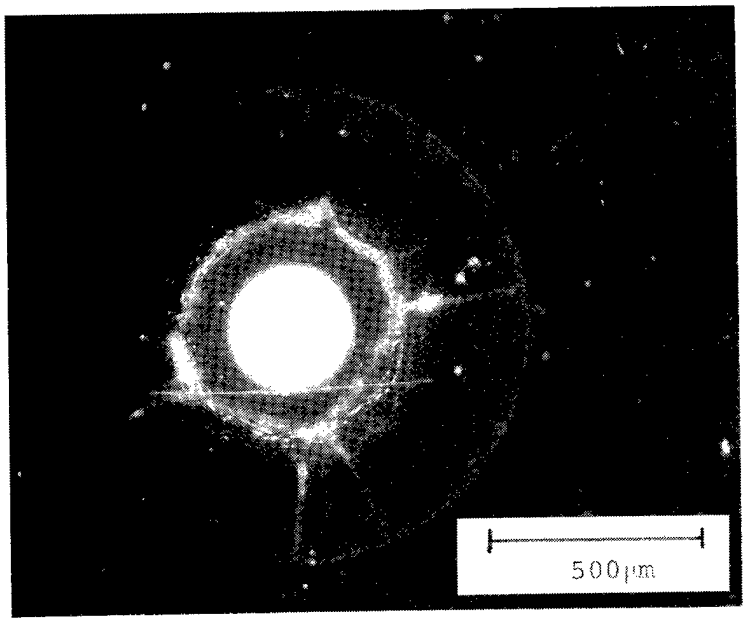


Figure 23. Impact crater.
46 µm glass particle, 7.2 km/s

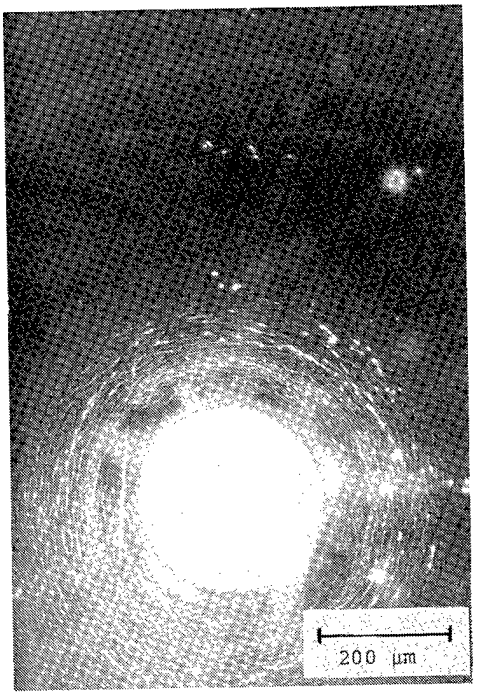


Figure 24. Impact crater.
97 µm glass particle, 2.3 km/s

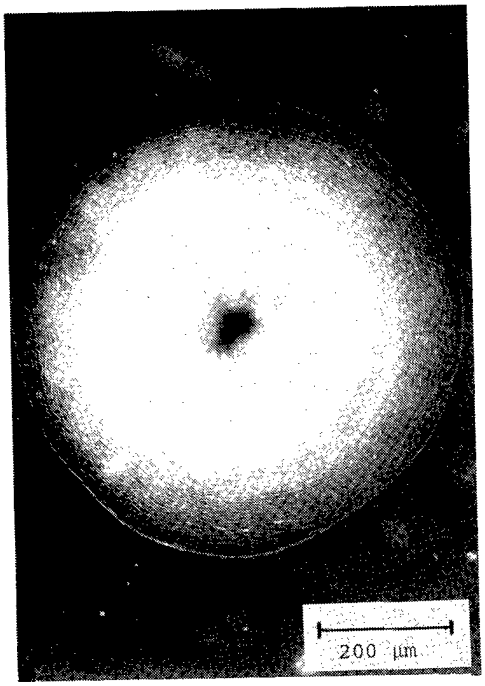


Figure 25. Impact crater.
71 µm glass particle, 12.6 km/s

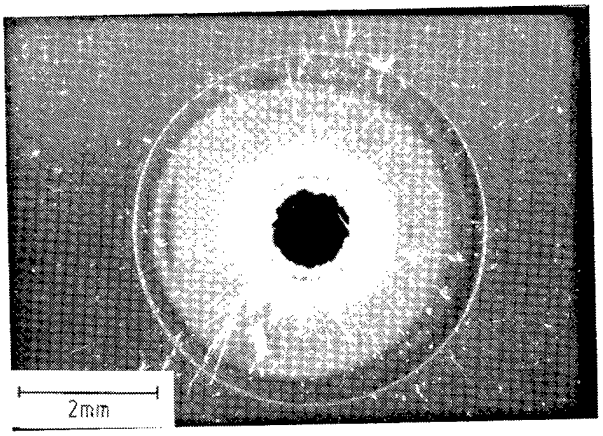


Figure 26. Perforation.
1 mm glass particle, 3 km/s

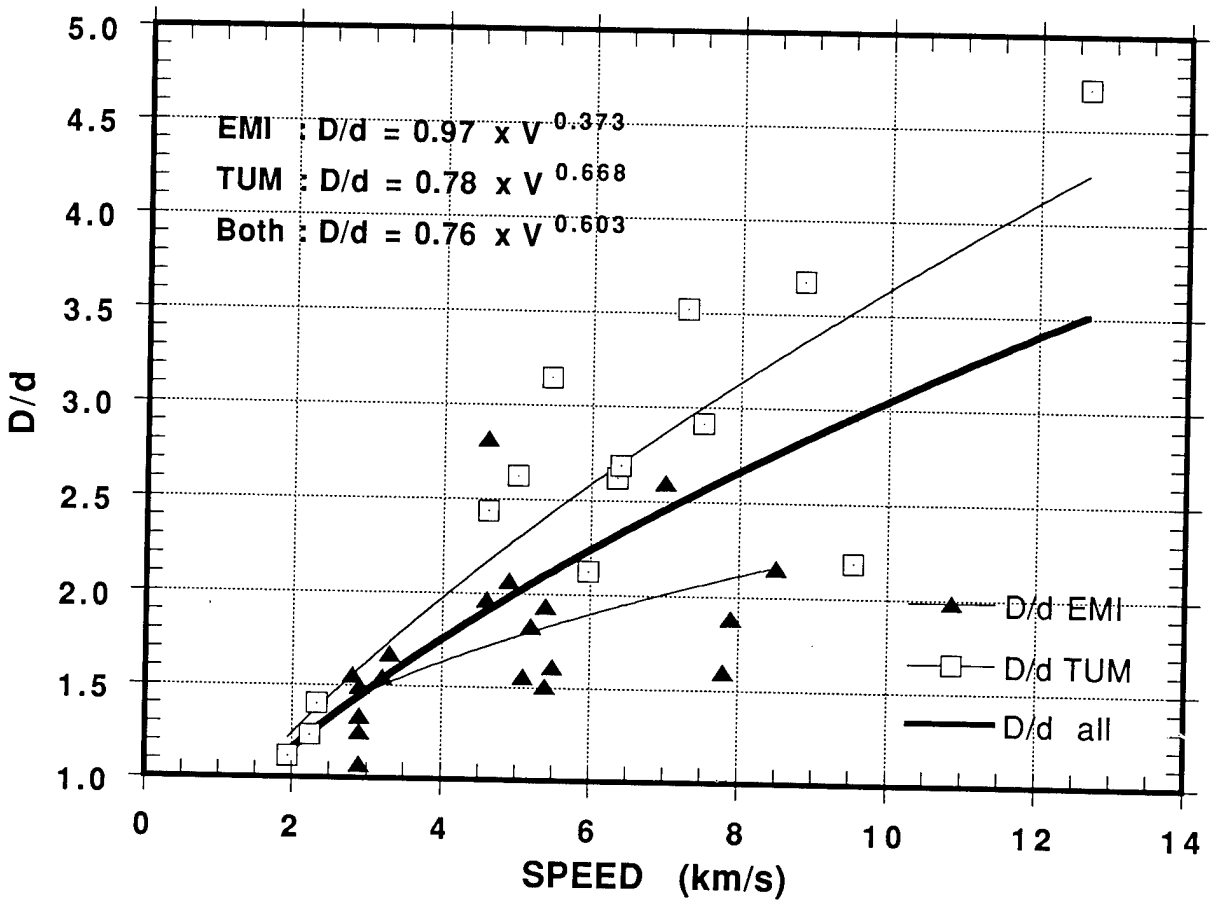


Figure 27. D/d RATIO
vs
PROJECTILE SPEED

INITIAL MATERIALS EVALUATION OF THE THERMAL CONTROL SURFACES EXPERIMENT (S0069)

Donald R. Wilkes
M. John Brown
Leigh L. Hummer

AZ Technology, Inc.
3322 Memorial Parkway SW, Suite 93
Huntsville, AL 35801
Phone: 205/880-7481, Fax: 205/880-7483

James M. Zwiener
NASA Marshall Space Flight Center
Marshall Space Flight Center, AL 35812
Phone: (205)544-2528, Fax: (205)544-0212

INTRODUCTION

The natural and induced long term effects of the space environment on spacecraft surfaces are critically important to many of NASA's future spacecraft--including the Space Station. The damaging constituents of this environment include thermal vacuum, solar ultraviolet radiation, atomic oxygen, particulate radiation, and the spacecraft induced environment. The inability to exactly simulate this complex combination of constituents results in a major difference in the stability of materials between laboratory testing and flight testing. The Thermal Control Surfaces Experiment (TCSE) was flown on the National Aeronautics and Space Administration (NASA) Long Duration Exposure Facility (LDEF) to study these environmental effects on surfaces--particularly on thermal control surfaces.

The TCSE was a comprehensive experiment that combined in-space measurements with extensive post-flight analyses of thermal control surfaces to determine the effects of exposure to the low earth orbit space environment. The TCSE is the first space experiment to measure the optical properties of thermal control surfaces the way they are routinely measured in the laboratory.

EXPERIMENT DESCRIPTION

The basic objective of the TCSE on the LDEF was to determine the effects of the near-Earth orbital environment and the LDEF induced environment on spacecraft thermal control surfaces. In summary, the specific mission objectives of TCSE were to:

- Determine the effects of the natural and induced space environment on thermal control surfaces
- Provide in-space performance data on thermal control surfaces

- Provide in-space comparison to ground-based environmental testing of materials

- Develop and prove instrumentation to perform in-space optical testing of materials.

To accomplish these objectives, the TCSE exposed selected material samples to the space environment and used in-flight and post-flight measurements of their thermo-optical properties to determine the effects of this exposure.[1] The TCSE hardware was designed to expose 25 "active" and 24 "passive" test samples to the LDEF orbital environment. The active and passive test samples differed in that the space effects on the passive test samples were determined only by pre- and post-flight evaluation. The optical properties of the 25 "active" samples were measured in-space as well as in pre- and post-flight analysis.

In-Space Measurements

The primary TCSE in-space measurement was hemispherical reflectance as a function of wavelength (100 wavelength steps from 250 to 2500 nm) using a scanning integrating sphere reflectometer. The measurements were repeated at preprogrammed intervals over the mission duration.

The secondary measurement used calorimetric methods to calculate solar absorptance and thermal emittance from temperature-versus-time measurements. The "active" sample surfaces were applied to thermally isolated (calorimeter) sample holders. To aid in the calorimetric calculations, three radiometers were used to measure the radiant energy (solar and Earth albedo, Earth albedo, and Earth infrared (IR) emitted) incident upon the samples. The radiometers also determined the total exposure of the samples to direct solar irradiance.

Flight Samples

The materials chosen for the TCSE mission comprised the thermal control surfaces of the greatest current interest (in 1983) to NASA, MSFC and the thermophysical community. The samples flown on the TCSE mission were:

- A276 White Paint
- A276/OI650 Clear Overcoat
- A276/RTV670 Clear Overcoat
- S13G/LO White Paint
- Z93 White Paint
- YB71 White Paint
- YB71 over Z93
- Chromic Acid Anodize
- Silver/FEP Teflon (2 mil)
- Silver/FEP Teflon (5 mil)
- Silver/FEP Teflon (5 mil Diffuse)
- White Tedlar
- D111 Black Paint
- Z302 Black Paint

- o Z302/OI650 Clear Overcoat
- o Z302/RTV670 Clear Overcoat
- o KRS-5 IR Crystal
- o Silver

Many of these materials were selected because they are good reflectors of solar energy while also being good emitters of thermal energy to the cold sink of space, i.e. they have a low solar absorptance (α_S) and a high room temperature emittance (ε_T). The range of low α_S/ε_T thermal control surfaces include materials that were expected to be very stable for the planned 9-12 month LDEF mission while others were chosen because they were expected to degrade significantly.

Another class of materials flown on the TCSE was black paints. These are important as solar energy absorbers and light absorbers for science instruments.

Some of the materials were expected to react with the residual atomic oxygen at the LDEF orbital altitude. Transparent coatings were applied over a few of these samples to protect the samples from AO.

TCSE Flight Hardware

The TCSE is a completely self-contained experiment package; providing its own power, data system, reflectometer, and pre-programmed controller for automatically exposing, monitoring, and measuring the sample materials. The TCSE was developed as a protoflight instrument where one instrument was built, made to work within required specifications, qualification tested, and flown.

The TCSE was built in a 305 mm (12 in.) deep LDEF tray (see Figure 1). The active and passive samples were mounted in a semicircular pattern on a circular carousel. The carousel is tilted at 11 degrees from the outer tray surface to allow a 115 mm (4.5 inch) diameter integrating sphere to fit between the deep end of the carousel and the outer shroud. This design satisfied the LDEF requirement to remain within the outer edges of the tray and also provided a field of view of space greater than 150 degrees for the samples. This design maintained mechanical simplicity and inherent reliability. Figure 2 shows the basic specifications for the TCSE flight hardware.

TCSE MISSION SUMMARY

The LDEF was placed in low earth orbit by the Shuttle Challenger on April 7, 1984. LDEF was retrieved by the Shuttle on January 12, 1990 after 5 years 10 months in space. The orbit had a 28.5^{O} inclination and an initial altitude of 463 km (250 N mi). The orbit degraded over the 5 year 10 month mission to an altitude of 330 km (178 N mi).

The LDEF was gravity-gradient stabilized and mass loaded so that one end of LDEF always pointed at the earth and one side pointed into the velocity vector or RAM direction. The LDEF was deployed with the TCSE located on the leading edge (row 9) of LDEF and at the earth end of this row (position A9). In this configuration, the TCSE was facing the RAM direction. The actual LDEF orientation

was slightly offset from this planned orientation. The LDEF was rotated about the long axis where row 9 was offset from the RAM direction by about 8°.[2] This LDEF/TCSE orientation and mission duration provided the following exposure environment for the TCSE:

Total space exposure	5 years 10 months
Atomic oxygen fluence[3]	8.0×10^{21} atoms/cm^2
Solar UV exposure[4]	1.0×10^4 ESH
Thermal cycles	3.3×10^4 cycles
Radiation (at surface)[5]	3.0×10^5 rads

The TCSE operated for 582 days before battery depletion.[6] The battery power was finally expended while the sample carousel was being rotated. This left the carousel in a partially closed position. Figure 3 is a photograph taken during the LDEF retrieval operations showing where the carousel rotation stopped. This carousel position caused 35 of the samples to be exposed for the complete LDEF mission (69.2 months), and 14 exposed for only 582 days (19.5 months) and therefore protected from the space environment for the subsequent four years.

FLIGHT MATERIALS ANALYSIS

Many different changes were observed in the TCSE samples due to their prolonged space exposure. These changes ranged from the obvious cracking and peeling of the overcoated samples to the subtle changes of UV fluorescence in some samples.[7] Some samples changed more than expected while others changed less than expected.

The primary measurements used for this analysis were total hemispherical reflectance from 250 to 2500 nm. Both in-space and laboratory reflectance measurements were performed on the test samples. Laboratory measurements of spectral reflectance were obtained using a computer controlled Beckman model DK-2A Spectrophotometer equipped with a Gier-Dunkle 203 mm (8 inch) integrating sphere. The flight reflectometer provides similar data to the laboratory instrument.[1]

Figures 4 and 5 are pre-flight and post-flight photographs of the TCSE sample carousel showing changes to many of the samples. Figure 6 summarizes the optical measurements on the TCSE flight samples.[1]

A276 White Paint

Chemglaze A276 polyurethane white paint has been used on many short term space missions including Spacelab. It was known to degrade moderately under long term UV exposure and to be susceptible to AO erosion.[8] To evaluate the effectiveness of AO protective coatings, A276 samples were flown with and without overcoatings. Two materials were used as protective coatings over A276--RTV670 and Owens Illinois OI650.

The post-flight condition of the A276 samples were somewhat surprising in that the unprotected TCSE A276 samples are very white. Previous flight and laboratory tests indicate that almost six years of solar UV exposure should have rendered the

A276 a medium brown color. The overcoated TCSE samples, however, do exhibit the characteristic UV darkening. Initial visual inspection at KSC of unprotected A276 samples on the trailing edge of LDEF (almost no AO exposure) showed that they also degraded as expected.

Apparently, as the unprotected A276 samples on the RAM side of LDEF degraded, their surfaces were eroded away leaving a fresh, undamaged surface. Pippin[9] reported that the A276 binder eroded away leaving the white pigment exposed. Some degradation of this TiO_2 pigment should have also been observed due to UV exposure (in the absence of AO). It is possible that there was sufficient oxygen on leading edge surfaces to inhibit oxygen based pigment damage.[10]

Figure 7 shows pre-flight, in-space, and post-flight measurement of solar absorptance (α_s) for the unprotected A276 and overcoated A276 samples along with the detailed reflectance curves. These data show that both protective coatings protected the A276 from AO erosion but allowed the A276 coating to degrade from solar UV exposure. The data for the unprotected A276 shows only a small amount of degradation early in the almost 6 year exposure. While most of the AO fluence occurred late in the LDEF mission, the TCSE in-space measurements show there was sufficient AO present early in the mission to inhibit UV degradation.

Figures 8 and 9 show physical damage on the overcoated A276 calorimeter samples. The unprotected A276 samples did not crack or peel. The passive samples with these same protective coatings also crazed and cracked but did not peel. Calorimeter samples were thermally isolated from the TCSE structure and therefore saw wider temperature excursions, possibly causing the peeling of the overcoated samples.

The extended space exposure also changed the UV fluorescence of both the A276 and overcoated A276 coatings. This fluorescence is easily seen using a short wavelength inspection black light. The RTV670 and OI650 coatings glow a bright yellow under this UV illumination. Preliminary measurements show both a change in the peak wavelength and an increase in the magnitude of the fluorescence.[7]

Z93 White Paint

The Z93 white thermal control coatings flown on the TCSE were almost impervious to the 69 month LDEF mission (see Figure 10). The Z93 samples showed an initial improvement in the solar absorptance, which is typical of silicate coatings in a thermal vacuum environment. The initial improvement is due to an increased reflectance above 1300 nm. This is offset by a very slow degradation below 1000 nm and results in only a 0.01 overall degradation in solar absorptance for the extended space exposure. Because of the excellent performance of the Z93, it is the leading candidate for the radiator coating on Space Station Freedom.

As with the A276 samples, the LDEF space exposure also changed the UV fluorescence in the Z93 samples.[7] The unexposed Z93 coatings fluoresce naturally but much of this fluorescence was reduced by the LDEF exposure. Fluorescence of the ZnO pigment in Z93 and its decrease under UV exposure has been previously reported.[11] This reduced fluorescence in Z93 samples is not confined to the leading edge samples, but is also found on LDEF trailing edge samples as was observed on LDEF experiment A0114 samples.[1]

YB71 White Paint

The YB71 coatings on the TCSE behaved similarly to the Z93 samples. A small increase in the infrared reflectance early in the mission caused a decrease in solar absorptance (see Figure 11). This was offset by a slow long term degradation resulting in a small overall increase in solar absorptance. The TCSE YB71 samples were made before the preparation and application parameters for this new coating were finalized. This resulted in a wide spread in the initial solar absorptance for the different samples. The samples with YB71 applied over a primer coat of Z93 had a somewhat lower α_s than the other YB71 samples. Current YB71 samples are consistently below 0.10 solar absorptance.

S13G/LO White Paint

The S13G/LO samples on the TCSE degraded significantly on the LDEF mission. Figure 12 shows the change in solar absorptance for the LDEF mission of the TCSE S13G/LO calorimeter sample along with the spectral reflectance. As with Z93, the UV fluorescence of the S13G/LO coatings decreased markedly due to the LDEF exposure.[7]

White Tedlar Film

White Tedlar is another material that was expected to degrade over the 5.8 year LDEF mission due to solar UV exposure. Instead, the optical properties of this material improved slightly, as shown in Figure 13. The surface remained diffuse and white, similar to pre-flight observations. As with A276, Tedlar has been shown to be susceptible to AO erosion. The erosion effect of AO is the apparent reason for the lack of surface degradation of these flight samples.

The TCSE in-flight data shows that only a small degradation in solar absorptance was seen early in the LDEF mission. This indicates that, as with the A276 samples, there was sufficient AO early in the mission to erode away damaged material or otherwise inhibit significant degradation. The subsequent high AO fluence then eroded away all the damaged surface materials and even provided a slight improvement in solar absorptance. Similarly with the other samples, additional analyses are planned to better define these effects.

Chromic Acid Anodize

There were two chromic acid anodize samples on the TCSE sample carousel. These two samples degraded significantly during the first 18 months of the LDEF/TCSE mission as shown by the TCSE in-space measurements (see Figure 14). When the TCSE batteries were depleted (19.5 months mission time), the carousel stopped where one of the two anodize samples was exposed for the remainder of the LDEF mission while the other was protected. The two samples show a significantly different appearance. The sample with 19.5 months exposure has an evenly colored appearance except for several small surface imperfections. The sample that was

exposed for the entire 69.2 month mission has a mottled, washed out appearance. The detailed pre- and post-flight reflectance curves for the two anodize samples are shown in Figure 14. Further study will be required to determine why the solar absorptance of the anodize sample exposed for the complete mission improved in the latter stages of the mission.

Silver Teflon Solar Reflector

There were three different silver Teflon materials on the TCSE. The front cover of the TCSE and one calorimeter sample were two mil thick silver FEP Teflon bonded to the substrate with Y966 acrylic adhesive. The other samples were five mil thick silver FEP Teflon (specular and diffuse) and were bonded to the substrate with P223 adhesive.

The silver Teflon surfaces on the TCSE underwent significant appearance changes where the surface color was changed to a diffuse, whitish appearance. This change is caused by the eroding effect of atomic oxygen and results in a rough, light scattering surface. Preliminary measurements indicate a loss of about one mil of Teflon for the TCSE mission in addition to the roughened surface. A one mil loss of Teflon from the two mil samples would cause a significant loss of emittance, as was measured.[7]

While the AO roughened silver Teflon surfaces underwent striking appearance changes, the reflectance and solar absorptance did not degrade significantly due to this effect. For the 5 mil coatings with P223 adhesive, only small changes in reflectance (see Figure 15) and solar absorptance were measured. In addition, there was very little change in emittance.

The two mil silver Teflon coatings, however, did degrade significantly as shown in Figure 15. These coatings had a brown discoloration. Laboratory evaluation of these coatings with Nomarski microscopes revealed the discoloration was under the Teflon surface. Further investigation determined that the brown discoloration is associated with cracks in the silver/inconel metalized layer. Laboratory tests show that the application of the pre-adhesive type silver Teflon can crack the metalized layers. Removal of the paper backing on the adhesive and removal of air bubbles from beneath the silver Teflon can over-stress the metal layers causing significant cracking. It appears that a component of the adhesive migrated through the cracks into the interface with the Teflon over the long exposure to thermal vacuum. Subsequently, this internal contaminant was degraded by solar UV exposure causing the brown appearance. As a result, the reflectance decreased (see Figure 15) and more than doubled the solar absorptance.

The reflectance of the 2 mil silver Teflon, and its resulting solar absorptance, did not change significantly early in the TCSE mission. Only a small increase in solar absorptance was measured through the first 16 months of exposure. This indicates that this internal contamination and subsequent optical degradation occurs slowly over long space exposure.

Black Paints

Two different black paints were flown on the TCSE - IITRI D111 and Chemglaze Z302. D111 is a diffuse black paint that performed very well with little change in either optical properties or appearance as a result of the TCSE mission.

Z302 gloss black was the other black coating flown on the TCSE. Z302 has been shown to be susceptible to AO exposure.[8] In anticipation of these erosion effects, protective OI650 and RTV670 coatings were applied over some of the Z302 samples to evaluate their effectiveness. As expected, unprotected Z302 was heavily eroded by the AO exposure. Two of the TCSE Z302 coatings were exposed to the environment for the total 5.8 year LDEF mission. These unprotected Z302 sample surfaces eroded down to the primer coat. Two other samples were exposed for only 19.5 months and, while they did erode, still had good reflectance properties.

The overcoatings for the Z302 behaved similarly to the overcoatings on the A276 samples. The Z302 appears to have been protected by the overcoatings but the overcoats cracked and crazed. The coatings that were applied to the calorimeter sample holders peeled away from the substrate because of the wider temperature excursions of these thermally isolated samples.

In addition, the fluorescence of the Z302 samples changed due to the LDEF exposure. Using a short wavelength UV black light, the unprotected Z302 exhibited a pale green fluorescence while the overcoated samples fluoresced bright yellow. Initial spectral analysis of the Z302 samples show that the control samples naturally fluoresce; however, the LDEF exposure caused a wavelength shift and an increase in the magnitude of the fluorescence.[7] Additional studies will be performed to fully characterize these effects.

SUMMARY

The TCSE has provided excellent data on the behavior of materials and systems in the space environment. Expected effects did happen, but in some cases the magnitude of these effects was more or less than expected or was offset by competing processes. A number of unexpected changes were also observed, such as the changes in the UV fluorescence of many materials.

The performance of the materials tested on the TCSE ranges from very small changes to very large changes in optical and mechanical properties. The stability of some of the materials such as Z93, YB71 and silver Teflon (with P223 adhesive) shows there are some thermal control surfaces that are candidates for long term space missions. The materials that significantly degraded offer the opportunity to study space environment/material interactions.

The TCSE is the most comprehensive thermal control surfaces experiment ever flown. The TCSE is also the most complex system, other than the LDEF with experiments, recovered from space after extended exposure. The serendipitous extended exposure of the prolonged LDEF mission only added to the significance of the data gathered by the TCSE. In all, the TCSE was an unqualified success. This analysis effort has only begun the process of deriving the greatest benefit from the TCSE.

REFERENCES

1. Wilkes, D.R. and Hummer, L.L.; "Thermal Control Surfaces Experiment Initial Flight Data Analysis", Final Report for Contract NAS8-36288; AZ Technology Report No.: 90-1-100-2, June 1991.

2. Banks, B.A.; "LDEF Yaw Estimated at Eight Degrees", LDEF Spaceflight Environmental Effects Newsletter, Vol. II, Number 1, March 15, 1991.

3. Bourassa, R.J. and Gillis, J.R.; "Atomic Oxygen Flux and Fluence Calculation for Long Duration Exposure Facility (LDEF) LDEF Supporting Data", Contract NAS1-18224, January 1991.

4. Berrios, W.M.; "Long Duration Exposure Facility Post-Flight Thermal Analysis, Orbital/Thermal Environment Data Package," NASA LaRC, Hampton, VA, October 3, 1990.

5. Benton, E.V. and Heinrich, W.; "Ionizing Radiation Exposure of LDEF", University of San Francisco Report USF-TR-77, August 1990.

6. Wilkes, D.R., Hummer, L.L., and Zwiener, J.M.; "Thermal Control Surfaces Experiment Flight System Performance"; 1st LDEF Data Conference, NASA CP-3134, 1992.

7. Zwiener, J.M., Wilkes, D.R., Hummer, L.L.; "Unusual Materials Effects Observed on the Thermal Control Surfaces Experiment (S0069)"; 1st LDEF Data Conference; NASA CP-3134, 1992.

8. Whitaker, A.F., Little, S.A., Harwell, R.J., Griner, D.B., DeHaye, R.F.; "Orbital Oxygen Effects on Thermal Control and Optical Materials, STS-8 Results", AIAA-85-0416, January 14, 1985.

9. Pippin, G.; "Materials SIG Summary Document Released", LDEF Spaceflight Environmental Effects Newsletter, Vol. I, Number 8, January 23, 1991.

10. Zerlaut, G.A., Gilligan, J.E.; "Study of In-situ Degradation of Thermal Control Surfaces", NASA Contract NAS8-21074 Final Report. IITRI Report U6061-29, Feb. 20, 1970.

11. Zerlaut, G.A. and Harada, Y., "Stable White Coatings", ITT Research Institute Report IITRI-C207-27, NASA Contract NAS7-100, January, 1964.

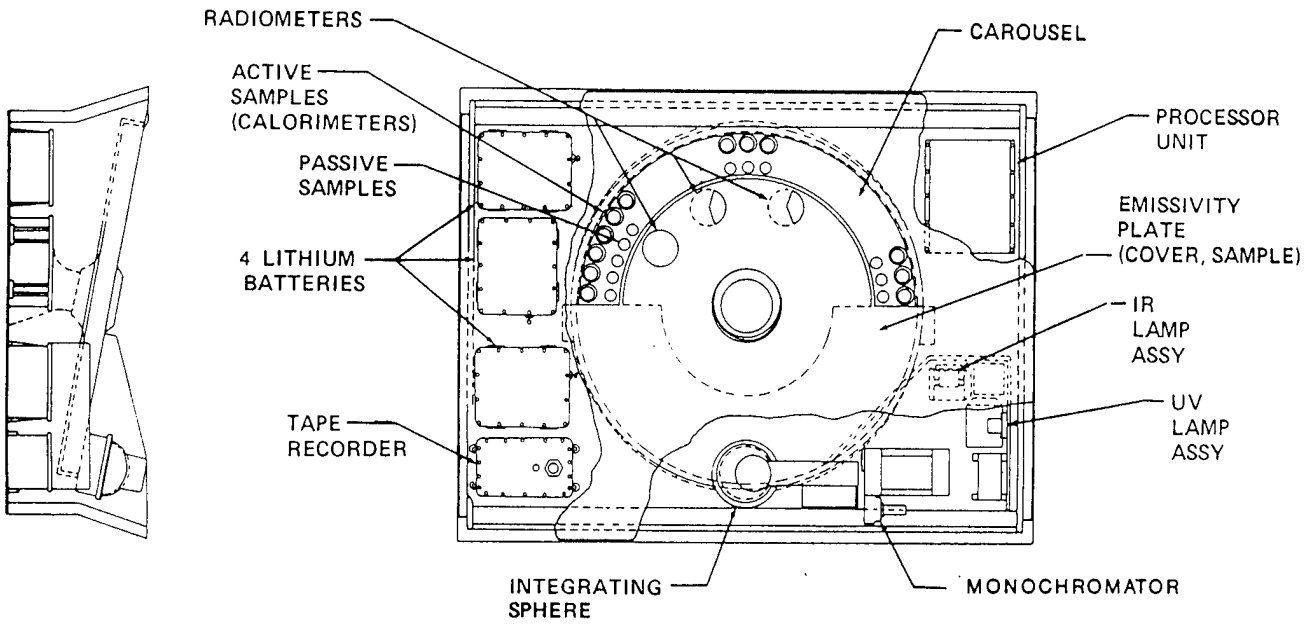


Figure 1 - TCSE Assembly

Size	1.24m x .84m x .30m (48.75 x 33 x 12 in.)
Weight	80.5kg (177 Pounds)
System Controller	1802 MicroProcessor
Battery Capacity	72 Amp Hours at 28 VDC
Data Recorder	Lockheed 4200
-Capacity	54 x 10^6 Bits
Reflectometer	
-Wavelength Range	250 to 2500 nm
-Wavelength Resolution ($\Delta\lambda/\lambda$)	$\leq$ 5%
-Reflectance Accuracy	2%
-Reflectance Repeatability	1%
Calorimetric Measurements	
-Solar Absorptance	Accuracy - 5%
-Total Emittance	Accuracy - 5%

Figure 2 - TCSE Flight Hardware Specifications

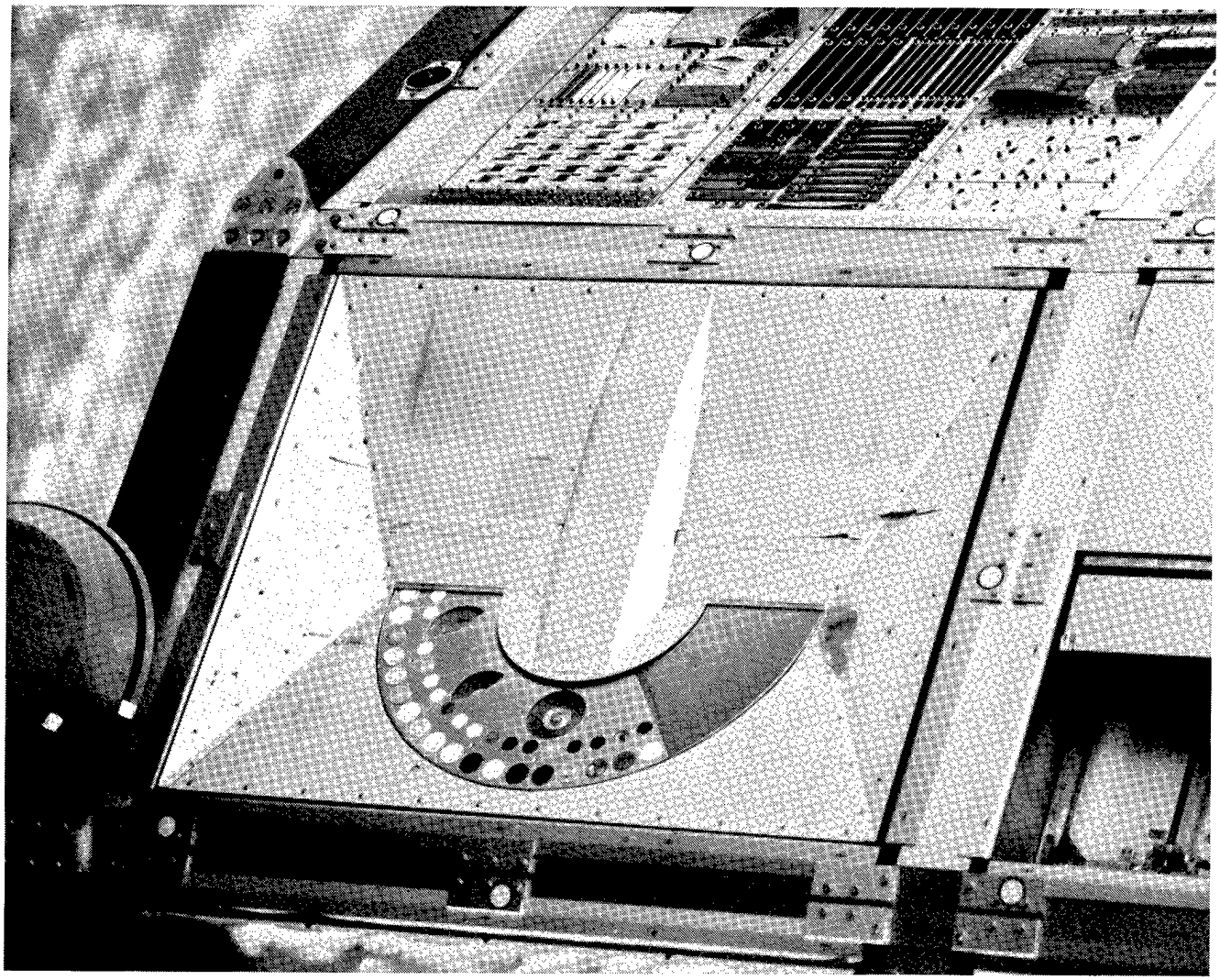


Figure 3 - TCSE Condition during LDEF Retrieval

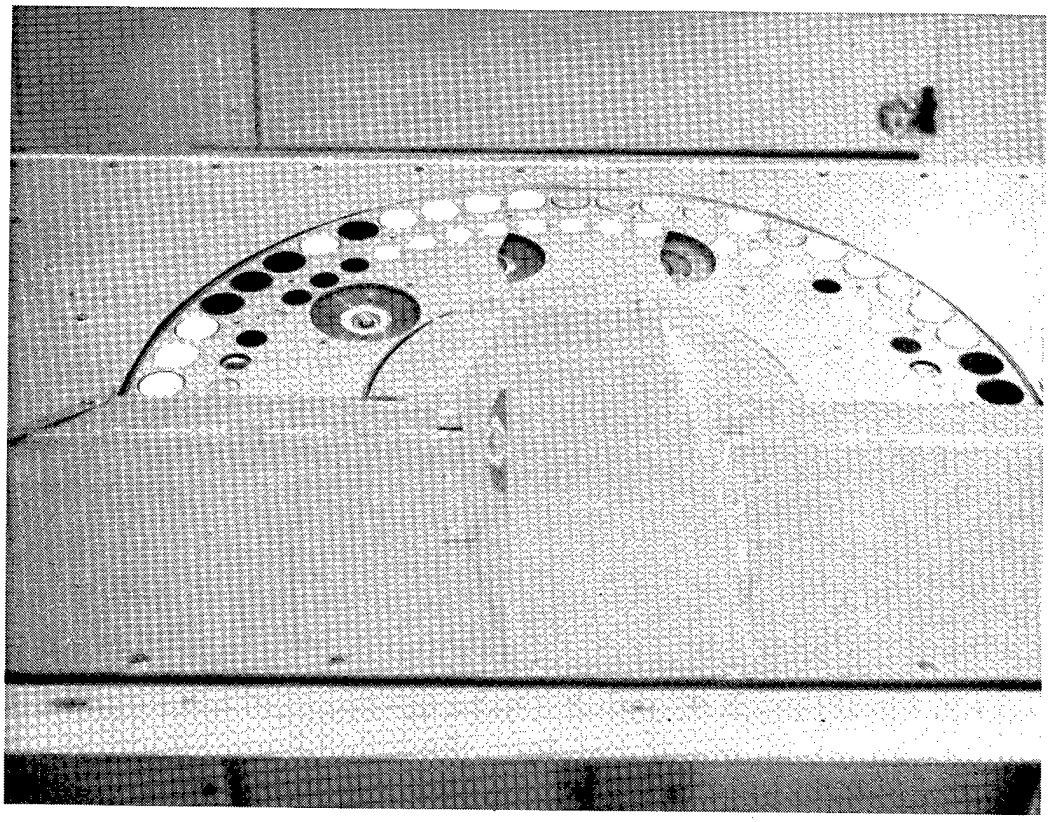


Figure 4 - Pre-flight Photograph of the TCSE Flight Samples

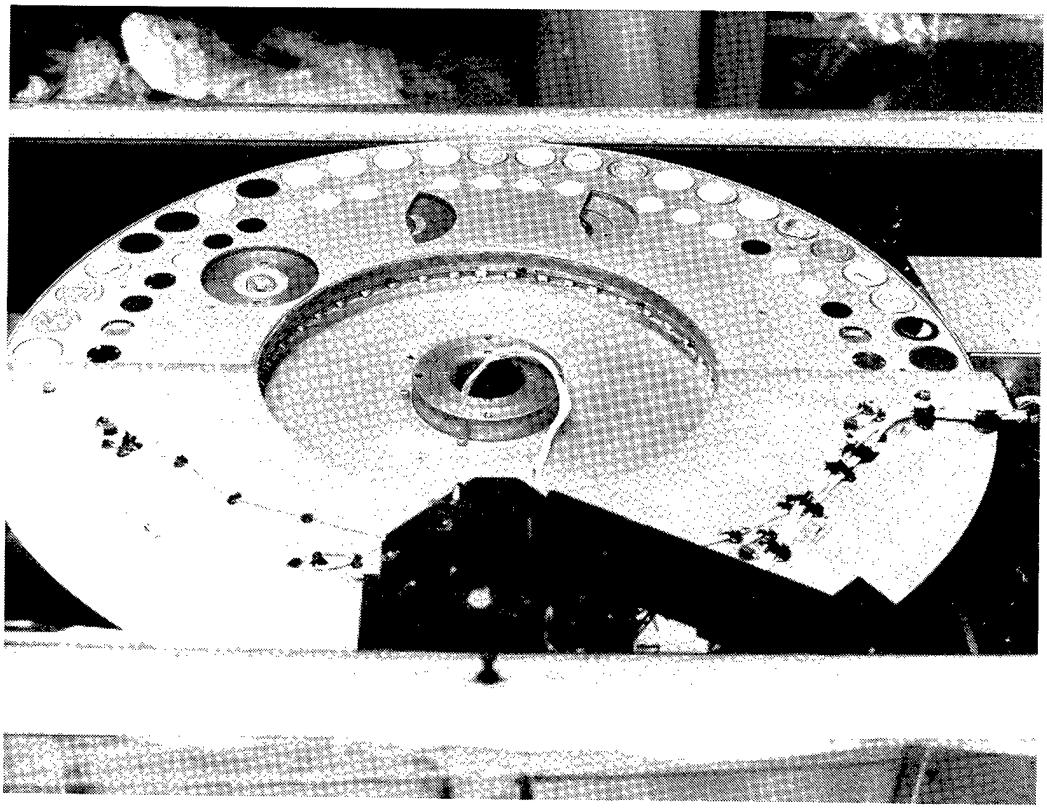


Figure 5 - Post-flight Photograph of the TCSE Flight Samples

Material	Source	Solar Absorbtance (α_s) Pre-flt	In-flt (15 Months)	Post-flt	$\Delta\alpha_s$	Emittance (ε_T) Pre-flt	Post-flt	$\Delta\varepsilon_T$
Tedlar	MSFC	.25	.26	.22	-.03			
A276	MSFC	.25	.30	.24	-.01	.90	.93	.03
A276 w/RTV670	MSFC	.27	.53	.62	.35	.91	.88	-.03
A276 w/OI650	MSFC	.25	.54	.59	.34	.90	.89	-.01
Z93	IITRI	.14	.13	.15	.01	.91	.92	.01
S13G-LO	IITRI	.18	.22	.37	.19	.90	.89	-.01
YB71	IITRI	.13	.12	.15	.02	.90	.89	-.01
YB71 over Z93	IITRI	.10	.11	.11	.01	.85	.87	.02
Silver Teflon (2 mil)	Sheldahl	.07	.08	.16	.09	.66	.46	20
Silver Teflon (5 mil)	LaRC	.06	.06	.08	.02	.81	.78	-.03
Silver Teflon (5 mil textured)	LaRC	.07	.08	.10	.03	.82	.79	-.03
Chromic Acid Anodize	LaRC	.40	.50	.47(.54*)	.07(.14*)	.84	.84	0
D111 Black	IITRI	.98	.99	.99	.01	.93	.90	-.03
Z302 Black	MSFC	.97	.98	.98*	.01	.91	.92	.01*
Z302/OI650	MSFC	.98	.99	.99	.01	.90	.90	0
Z302/RTV670	MSFC	.98	.99	.99	.01	.91	.90	-.01

*19.5 Months Exposure

Figure 6 - TCSE Optical Measurement Summary

LDEF Thermal Control Surfaces Experiment

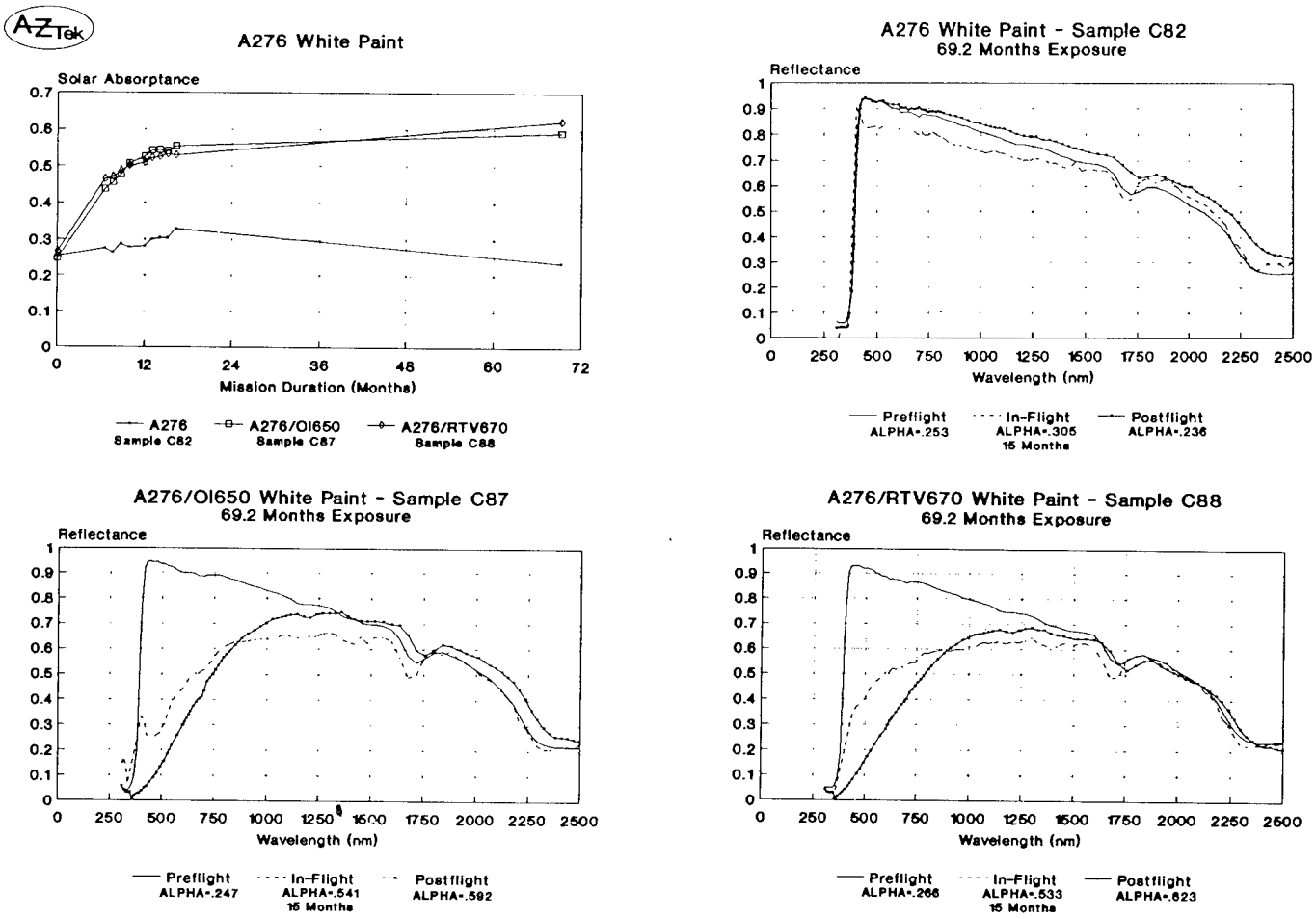


Figure 7 - Optical Properties of A276 White Paints

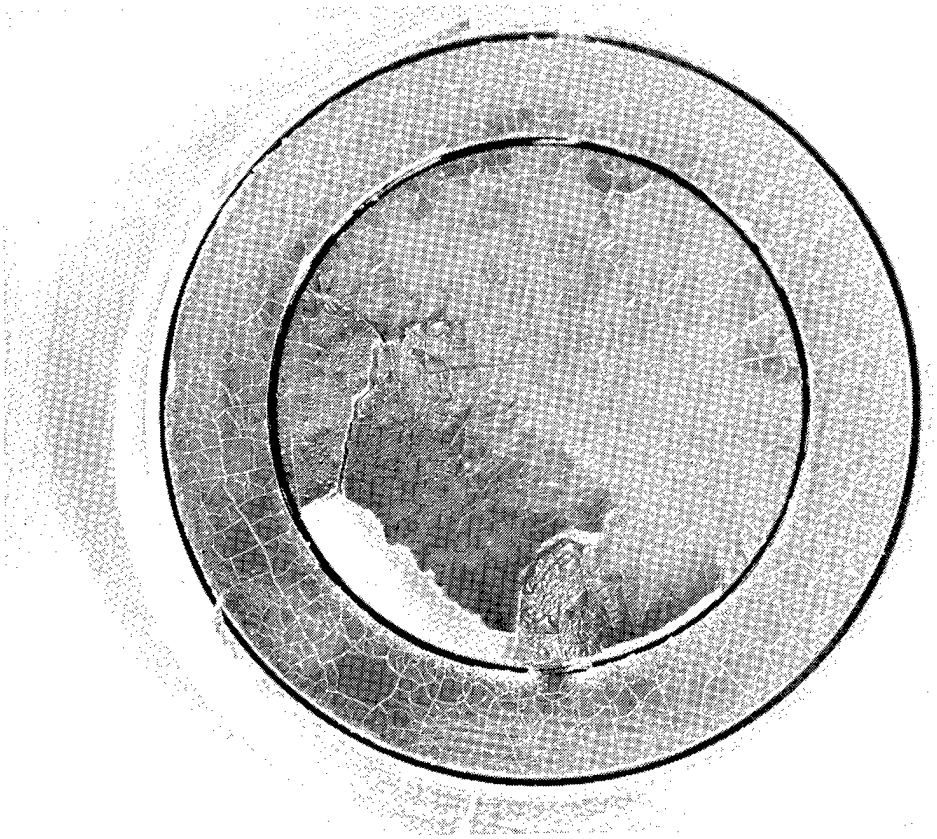


Figure 8 - Post-flight Condition of OI650 over A276

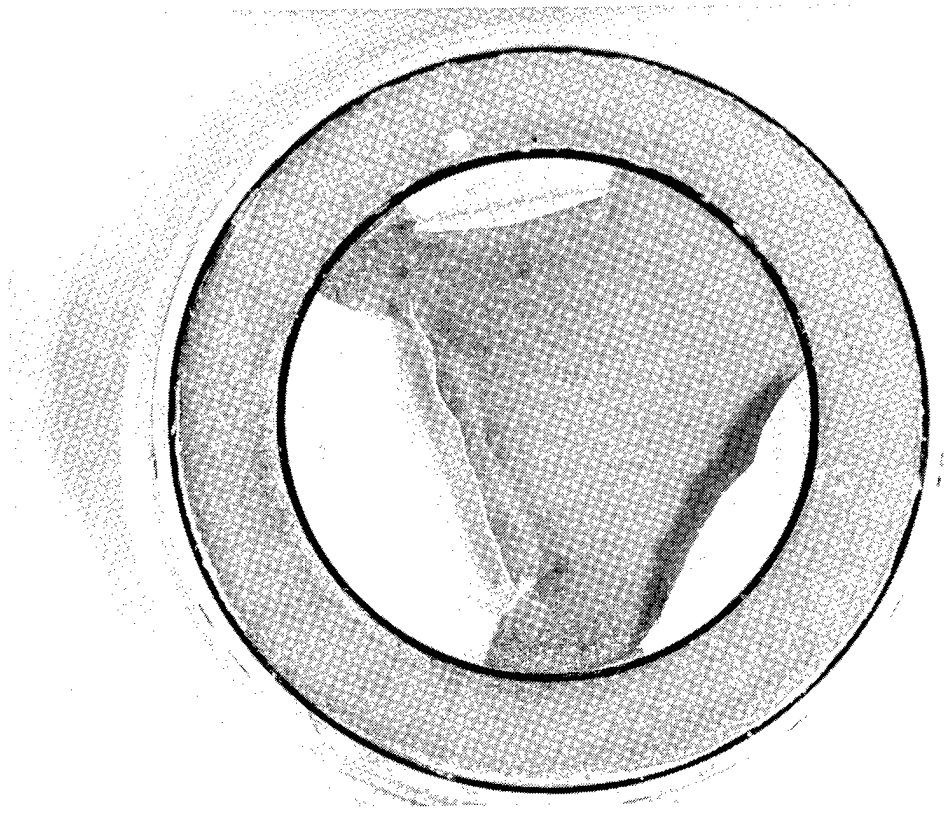


Figure 9 - Post-flight Condition of RTV670 over A276

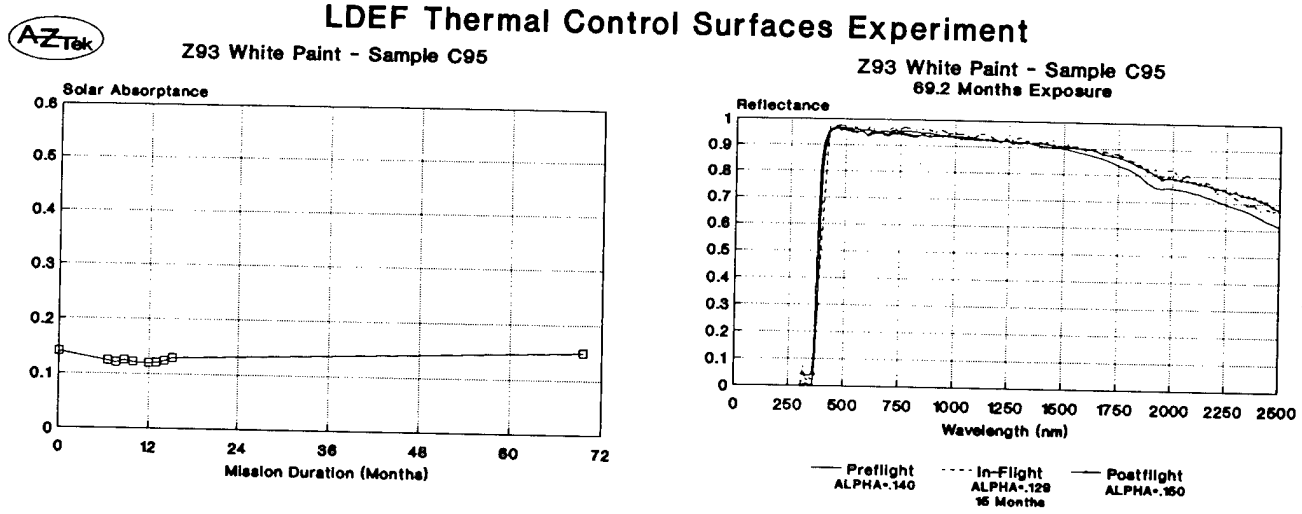


Figure 10 - Optical Properties of Z93 White Paint

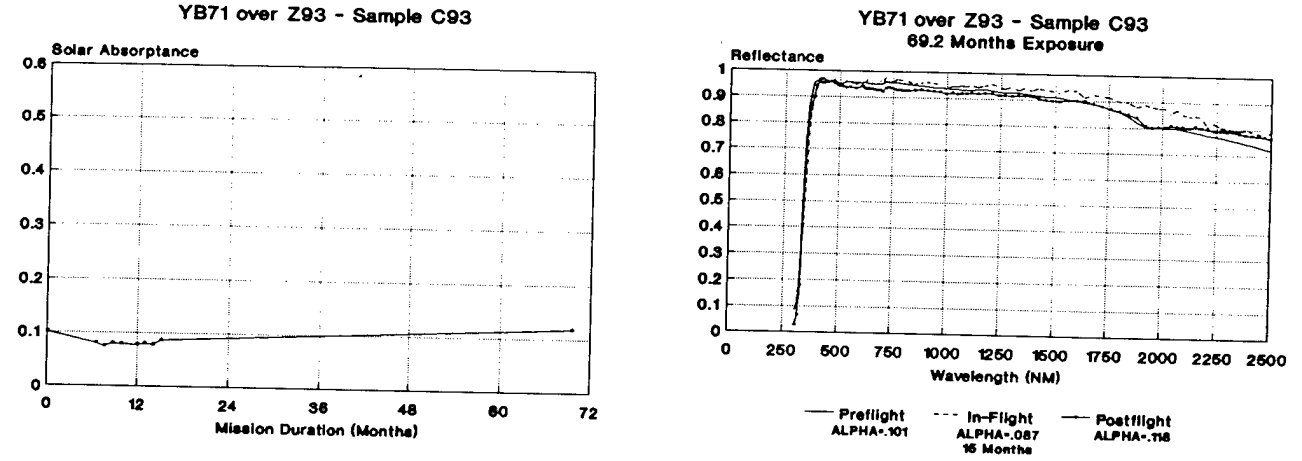


Figure 11 - Optical Properties of YB71 White Paint

LDEF Thermal Control Surfaces Experiment

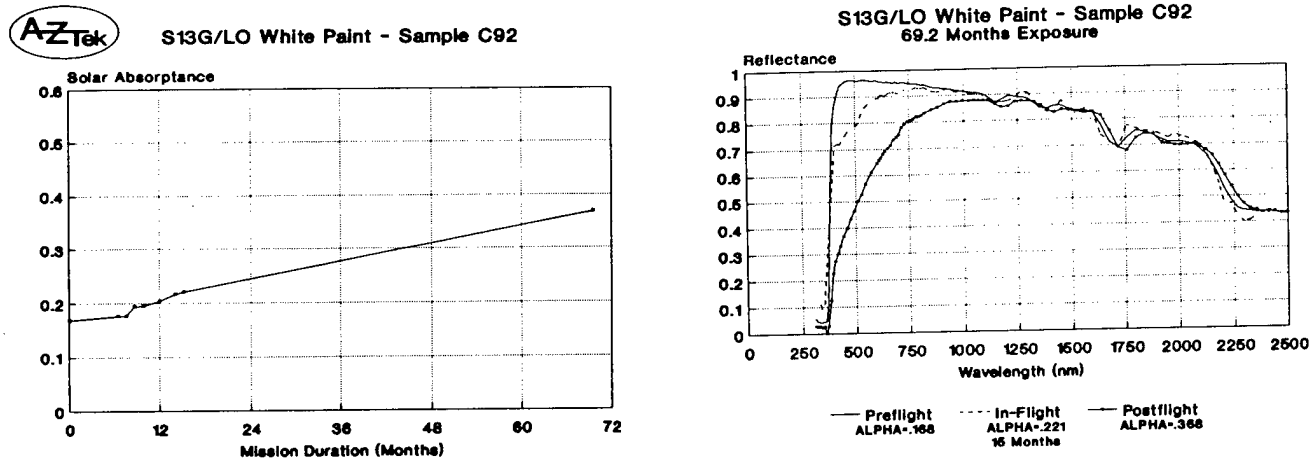


Figure 12 - Optical Properties of S13G/LO White Paint

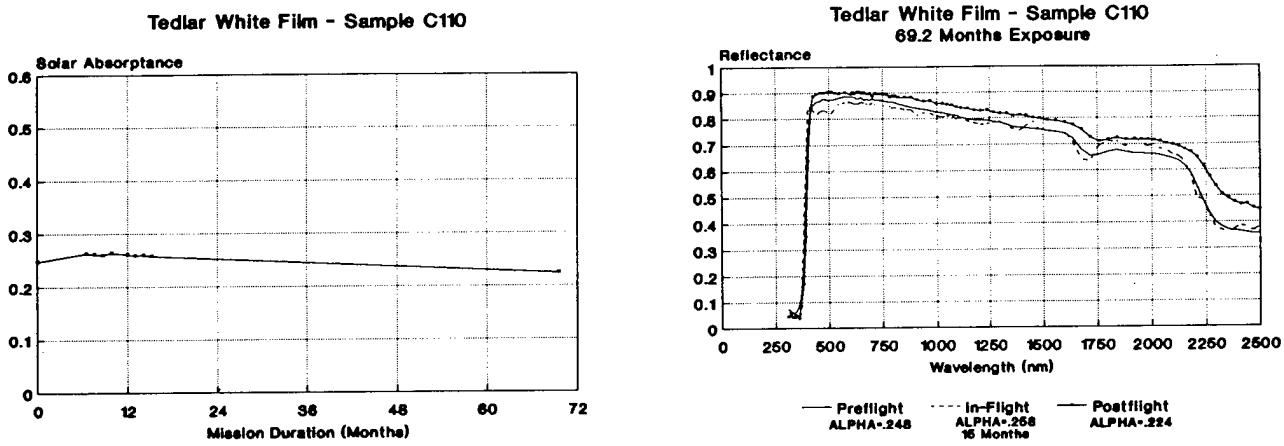


Figure 13 - Optical Properties of White Tedlar

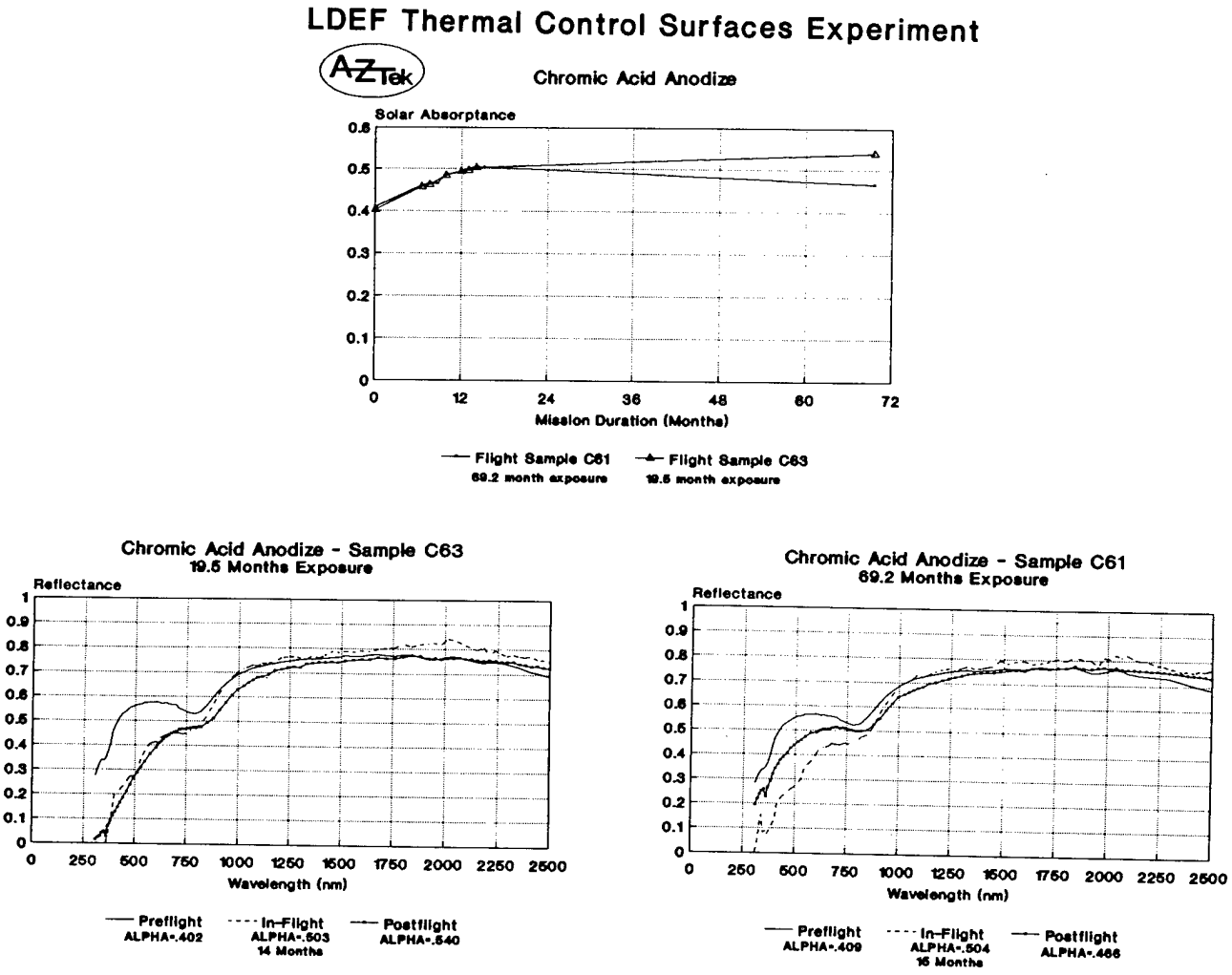


Figure 14 - Optical Properties of Chromic Acid Anodize

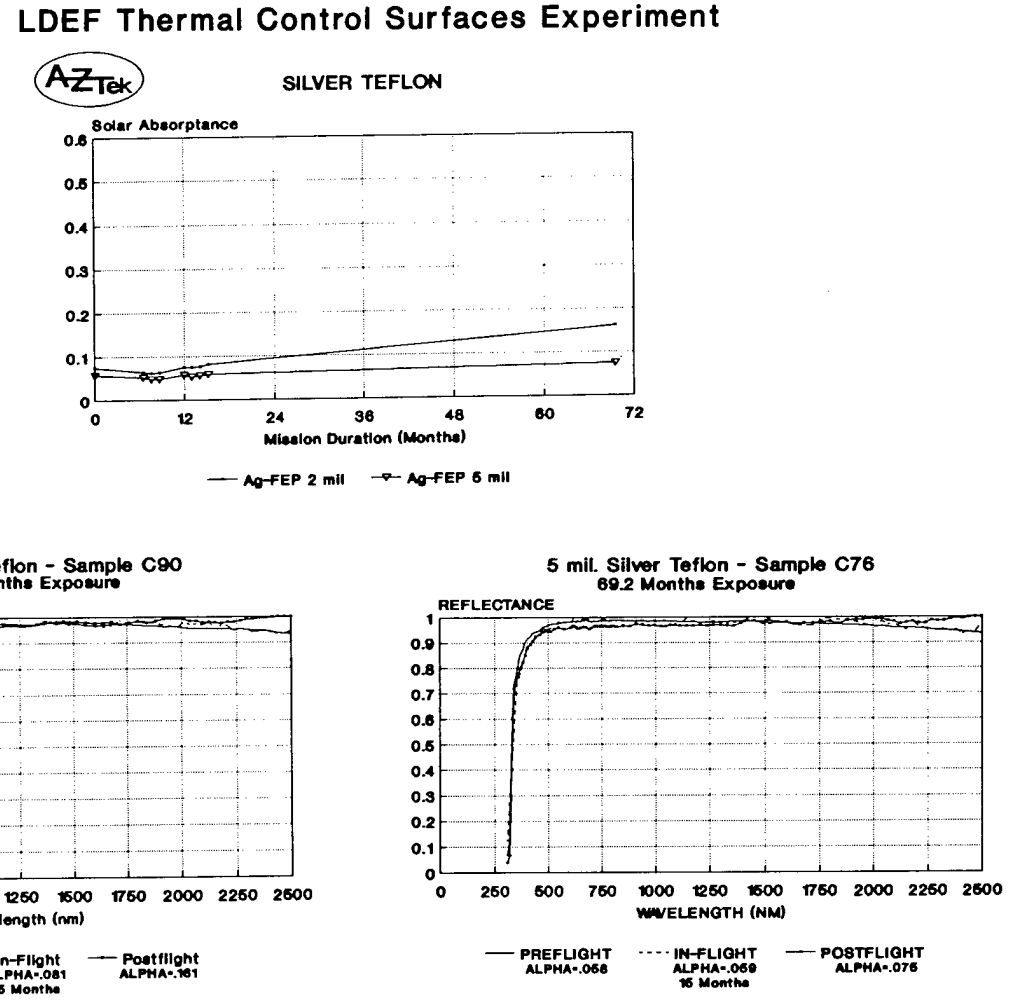


Figure 15 - Optical Properties of Silver Teflon

UNUSUAL MATERIALS EFFECTS OBSERVED ON THE THERMAL CONTROL SURFACES EXPERIMENT (S0069)

James M. Zwiener
Kenneth A. Herren
NASA Marshall Space Flight Center
Huntsville, Ala. 35812
Phone: 205/544-2528, Fax: 205/544-0212

Donald R. Wilkes
Leigh Hummer
Edgar R. Miller
AZ Technology
Huntsville, Ala. 35801
Phone: 205/880-7481, Fax: 205/880-7483

SUMMARY

A number of unusual effects were observed on the Thermal Control Surfaces Experiment (TCSE) test samples, front cover, and structural components. These effects include Atomic Oxygen (AO) texturing of the exposed surface of the silver Teflon (Ag/FEP) thermal control material, "brownish" discoloration of the Ag/FEP material, changes in fluorescence of thermal control paint samples, and meteoroid/debris impact effects on silver Teflon.

INTRODUCTION

The following paper provides an early assessment of the Thermal Control Surfaces Experiment (TCSE) in terms of what could be called "unusual" material effects that were caused by the 5.8 years exposure to the space environment. Unusual in the context of this discussion means effects on material or hardware that were either not expected or whose magnitude was more significant than anticipated. These effects are, in most cases, significant in that they may cause reconsideration of the utilization of some materials previously considered reasonably stable for long-term spacecraft applications. In addition, some of the detrimental effects can be avoided when the causes are understood, as in the case of the brownish discoloration of the silver Teflon (Ag/FEP) thermal control material. Information will be presented that details three of the many unusual effects found and investigated during the postflight analysis. These three effects are the changes to Ag/FEP, impact damage to TCSE front cover, and fluorescence changes of thermal control coatings.

SILVER TEFLON THERMAL CONTROL COATING

Overall Surface Observations

The inflight photograph in Figure 1 shows the TCSE location on row 9 and its orientation within approximately 8 degrees of the AO RAM vector. AO fluence in the RAM direction was 9.75×10^{21} atoms/cm^2.

An overall view of the front thermal cover is shown in Figure 2 after removal from the TCSE main structure during post flight disassembly. The front thermal cover has a Sheldahl 0.05 mm (2 mil) thick Ag/FEP thermal control material applied with Y966 acrylic adhesive. Covered areas have no apparent damage and are still highly specular. Areas exposed to the space environment are clearly delineated and have a diffuse, whitish appearance with brown discoloration. This brownish discoloration varies from light brown to dark brown. Changes in Ag/FEP visual appearance are the result of two damage mechanisms--AO erosion and internal damage associated with cracking of the silver/inconel layer.

Optical Property Measurements

Samples were cut from the TCSE front cover for optical property measurements. Total hemispherical reflectance measurements were made on samples from different locations on the front cover having varying degrees of damage. Figure 3A is a plot of this data showing the magnitude of reflectance loss in the brownish discolored regions. For those regions having a low degree of the brownish discoloration, it can be seen that the total reflectance values are basically unchanged with an solar absorptance (α_S) of 0.10 as compared to the ground reference sample (unexposed) with an α_S of ~0.08. The worse case brownish area had a solar absorptance as high as 0.49.

The emittance (ε_T) was also measured at several locations on the front panel and is plotted in Figure 3B. The protected areas were unchanged but exposed regions degraded from an emittance of 0.68 to 0.48. Comparison with measurements of ground control samples shows that approximately 25 microns (0.001 inch) to 33 microns (0.0013 inch) of Teflon was removed by AO. Eddy current thickness measurements confirm these numbers.

Atomic Oxygen Damage to the Surface of the Silver Teflon

AO erosion of the exposed Ag/FEP surface is typical of that observed on previous flight experiments. Erosion of the exposed Teflon surface creates a nonuniform etching pattern as shown in the Scanning Electron Microscope (SEM) photo in Figure 4. This results in a roughened surface with peaks ~1.5 microns apart which scatters incident light in a manner similar to a sand-blasted piece of glass.

Figure 5 shows a schematic cross section of the Ag/FEP as applied to the aluminum surface. The Ag/FEP is composed of an outer Teflon layer, a silver layer deposited on the Teflon, an inconel protective layer deposited on the silver, and

Y966 acrylic pressure sensitive adhesive. The silver layer provides the high reflectance (low absorptance) and the Teflon provides the high emittance for thermal control. As seen in the schematic for undamaged Teflon, the incident light (solar flux) transmits through the smooth clear Teflon and specularly reflects off the silver layer. AO damage to the Teflon creates a roughened surface which causes scattering of the incident light.

Optical measurements taken at position "1" in Figure 3, show that AO roughening alone produces less than a 0.03 increase in solar absorptance. Larger increases in solar absorptance were measured at positions "2" and "3" where the brownish discoloration occurs. Details of the brownish discoloration will be described in the following sections.

Silver Inconel Layer Cracking

A close up of the silver Teflon covered area is shown in Figure 6, showing that the silver/inconel layer is cracked. Location "1" is typical of most of the covered region having a regular, straight cracking pattern. Location "2" is where the two Ag/FEP layers meet and slightly overlap and is typical of areas that received excessive stress during application. When the Ag/FEP material is stressed, the silver/inconel layer cracks, even to the point of shattering as it is bent around protrusions.

Figure 7 shows a cross section of Ag/FEP during application. The silver/inconel layer undergoes severe stress during application as the Teflon layer is bent. The silver/inconel layer is on the outside of the bending radius and is stretched beyond its elastic limit and cracks. Ground tests were performed where new Ag/FEP was applied to aluminum plates identical to the TCSE front thermal cover. Results show that when Ag/FEP is applied to an aluminum substrate by the method shown in Figure 7, the silver/inconel layer cracks. Photomicrographs of Ag/FEP before and after application to the aluminum plates is presented in Figure 8. The induced cracking pattern is in the silver/inconel layer. Note that SEM inspection of new Ag/FEP applied to aluminum failed to find any cracks in the Teflon surface. Results for Ag/FEP with thicknesses from 0.25 mil to 5.0 mil show that cracking density decreases for increasing thickness of Teflon.

Silver Teflon Material Internal Damage

Silver Teflon on the TCSE that was exposed to AO and solar ultraviolet radiation has an overall whitish diffuse color. At specific locations (Figure 2 "C") a brownish streaking appearance is observed. Covered areas of Ag/FEP had neither the whitish diffuse color nor the brownish discoloration.

Figure 9A provides a close-up view of a sample (S-1) cut from the TCSE front thermal cover showing the typical brownish discoloration. The SEM image of this sample (Figure 4) shows that the Ag/FEP surface is not cracked nor is there any indication of a significant contaminant layer on the Ag/FEP that could cause the brownish appearance. The TCSE Ag/FEP was bonded to an aluminum substrate which prevented flexing of the material that might have caused cracks to show up in the top Teflon layer as has been observed on other experiments.

Visible microscopic examination also failed to find surface contamination in the brownish discolored areas. Internal damage to the Ag/FEP material in the form of a brownish streaking effect was observed along the silver/inconel cracks. This brownish color appears to have spread from silver/inconel cracks to the interface region between the Teflon and silver/inconel layer.

Referring to the view of sample S-1 in Figure 9A, area "1" has the typical AO damage but lacks the brownish discoloration, whereas area "2" has the typical brownish color. At area "3", in comparison, the surface diffuse layer of the Teflon was removed during the cutting operation returning the Ag/FEP to its original specular appearance. In general any contact including touching or wiping of the Teflon surface which has the whitish diffuse color returns it to its original specular appearance.

An enlargement of location "B" in Figure 9A is shown in Figure 9B. Note the brownish streaks/cracks going from area "1" to "2" were not disturbed by the removal of the surface diffuse layer on the Teflon.

Figure 9C, is an enlargement of area "C" of Figure 9B. The intensity of the brownish darkening can be seen to be a function of the closeness and degree of silver/inconel layer cracking. Areas "1" and "2" of Figure 9C have the diffuse Teflon surface which blurs the image of the cracks. When the diffuse layer is removed as in areas "3" and "4", a clearer image is seen of the silver/inconel cracks. These images demonstrate that the brownish streaking is not on the Teflon surface, and since the silver/inconel layer is opaque, the streaking must be located at the Teflon/silver interface. In addition it appears that the discoloration, which is probably a component of the adhesive, spreads outward from the cracks between the Teflon/silver interface.

Based on the postflight analysis the brownish streaking was the result of a series of events, starting with the initial cracking of the silver/inconel layer during application to the TCSE front thermal cover. Subsequent long-term exposure to thermal cycling and solar ultraviolet caused the brownish discoloration. The intensity of the brownish discoloration is a direct function of the crack density which appears to be caused by excessive handling or stretching.

METEOROID/DEBRIS IMPACT PENETRATION ON THE FRONT COVER

The front cover of the TCSE experiment had one penetration from a meteoroid/debris impact. Figure 10A provides a close-up view of the impact showing the crater and Ag/FEP layer "blown" back from the crater rim. At location "1" of figure 10A, the Teflon layer has radial cracks emanating from the crater impact center. Some of the silver/inconel layer is still attached to the Teflon. For the Ag/FEP closest to the impact area, the silver/inconel and adhesive layers are missing. The exit of the impact event is shown in Figure 10B, with the small region indicated at area "1".

FLUORESCENCE CHANGES OF THERMAL CONTROL COATINGS

Most of the thermal control paint coatings underwent changes in their ultraviolet fluorescence characteristics. This was discovered during post-flight inspection with a UV black light. As an example, Z302 black paint with the OI650 overcoat had a bright yellow fluorescence when exposed to UV black light.

Ambient temperature fluorescence spectra for the TCSE flight samples of Z93, YB71, and Z302 are presented in Figures 11 and 12. The spectral peak at ~280 nm is the reflection of the irradiance source consisting of a 1 kilowatt HgXe source filtered through an attached monochromator. A Bechman DK2A spectrometer operating in the energy mode, was utilized for measuring the fluorescence emission.

As seen in Figure 11A the fluorescence for Z93 white paint is reduced after exposure to the space environment and decreases with increasing exposure. In addition, samples of Z93 from the LDEF leading and trailing edge of experiments (A0114/Gregory/Peters) exhibited identical fluorescence spectra. These spectra were also identical to the TCSE Z93 samples. The changes in fluorescence for Z93 is therefore independent of AO but is a function of the solar irradiation exposure.

Previous work at IITRI showed that the ZnO pigment in Z93 fluoresced. In comparison, YB71 white paint which has the same silicate binder as Z93 doesn't fluoresce (see Figure 11B). Therefore the source of the Z93 fluorescence is the ZnO pigment and not the silicate binder.

Fluorescence spectra for Z302 black paint exhibited a different effect than Z93 as shown in Figure 12. The fluorescence shifted from the ultraviolet region into the visible. A276 white paint samples had the same shift in fluorescence spectra as the Z302 material. In addition, the silicone overcoat on Z302 enhances its fluorescence spectra as seen by comparing the Z302/OI650 spectral data in Figure 12B to the uncoated Z302 data in Figure 12A.

CONCLUDING REMARKS

Besides the unusual material effects briefly described here, many other intriguing effects were found. Some of these unusual effects include changes to coatings internal to the TCSE experiment related to indirect exposure to AO, plume shaped shadow images found on the side of the TCSE LDEF tray along with image reversals, and light diffraction by exposed Ag/FEP. Other unusual effects included fiberglass panels covered with Ag/FEP which degraded differently than Ag/FEP on aluminum, and contamination internal to TCSE that appears affected by indirect AO and solar ultraviolet exposure. Studies are continuing to understand and fully characterize these "unusual effects" and determine their mechanisms.

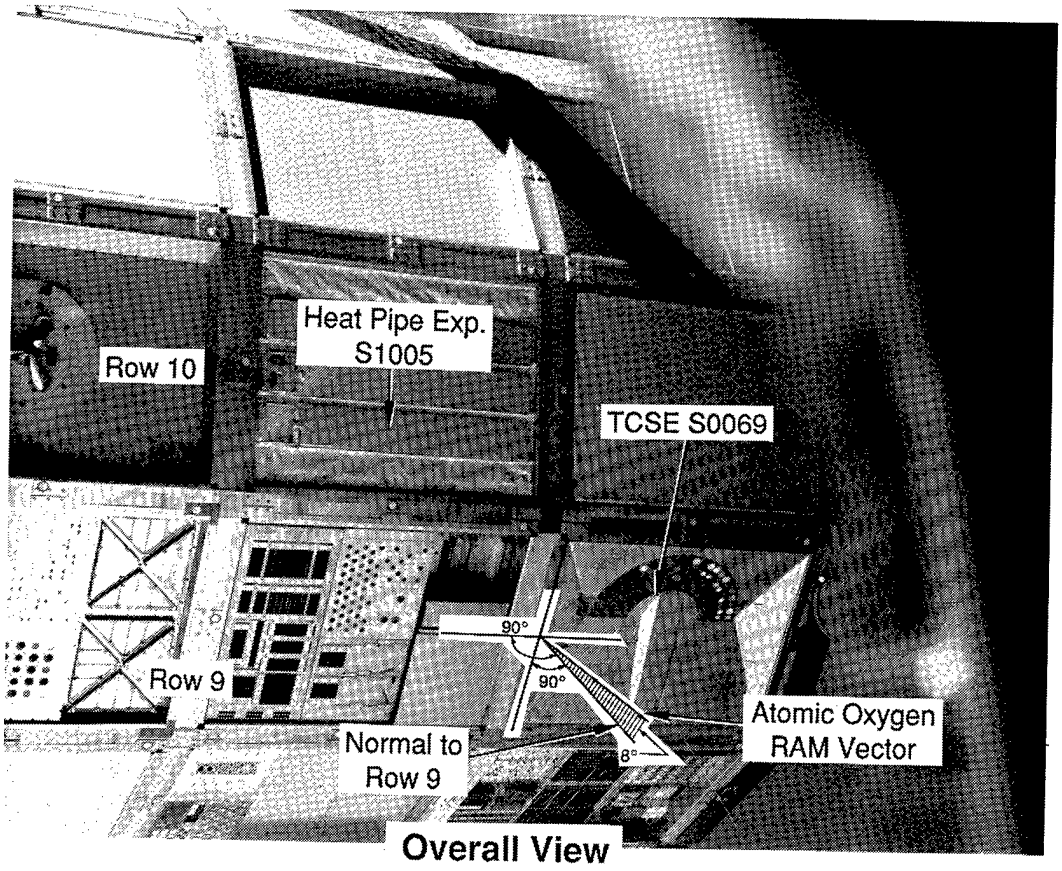

Heat Pipe Exp.
S1005
Row 10
TCSE S0069
90°
90°
Row 9
Atomic Oxygen
RAM Vector
Normal to
Row 9
8°
Overall View

Figure 1

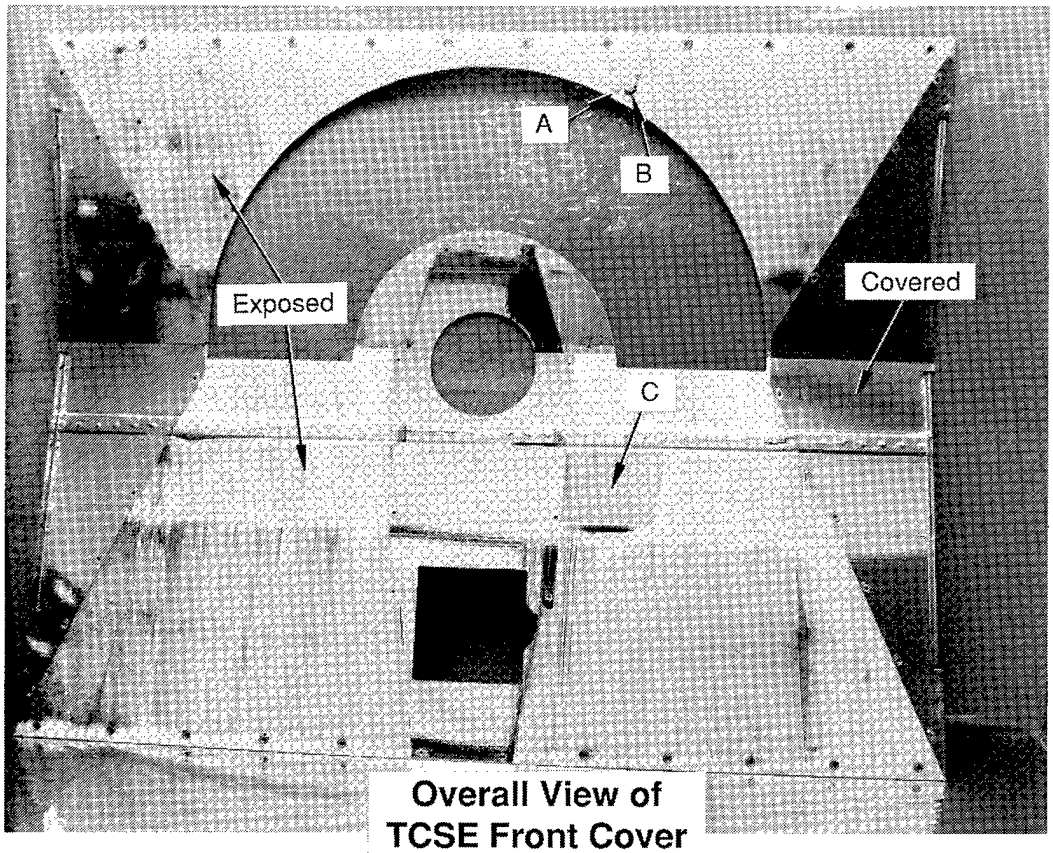
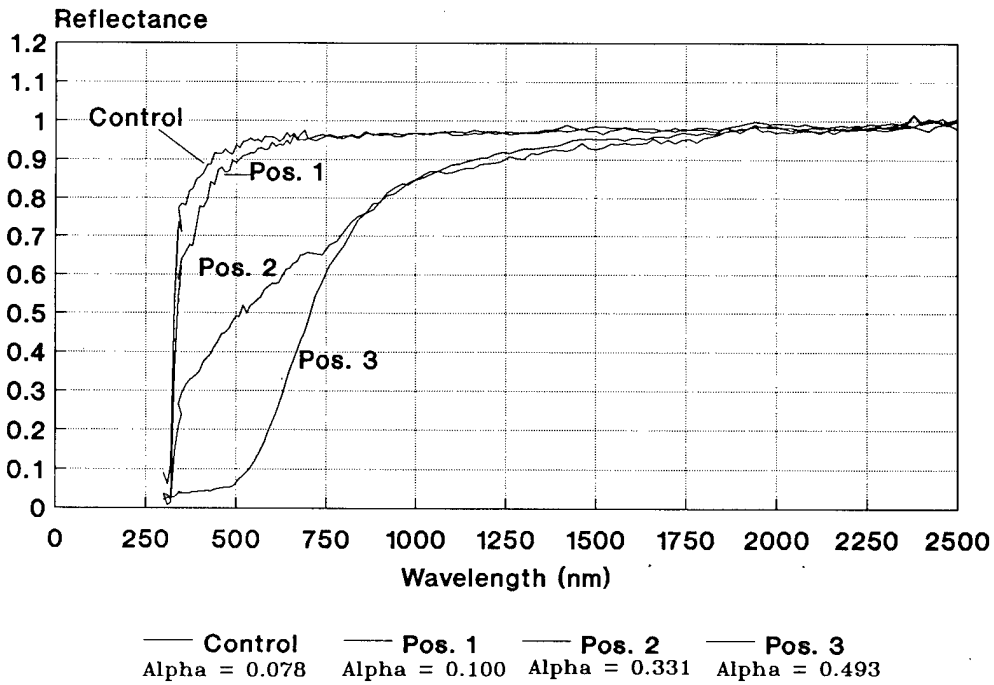


Figure 2

A. VARIATION IN REFLECTANCE PROPERTIES OF SILVER TEFLON



B. EMITTANCE OF SILVER TEFLON

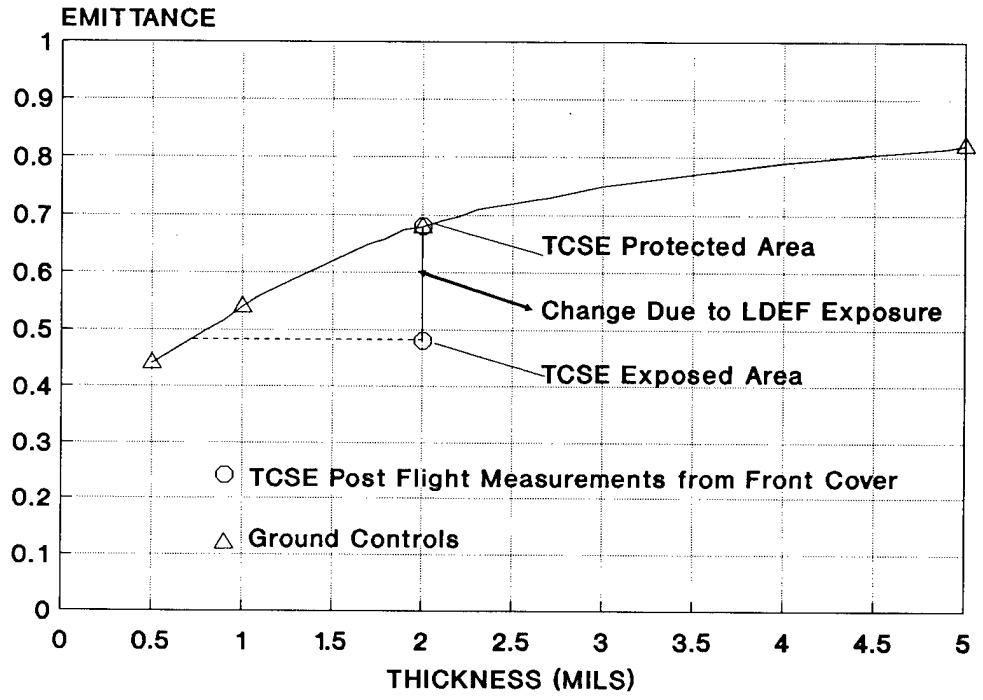
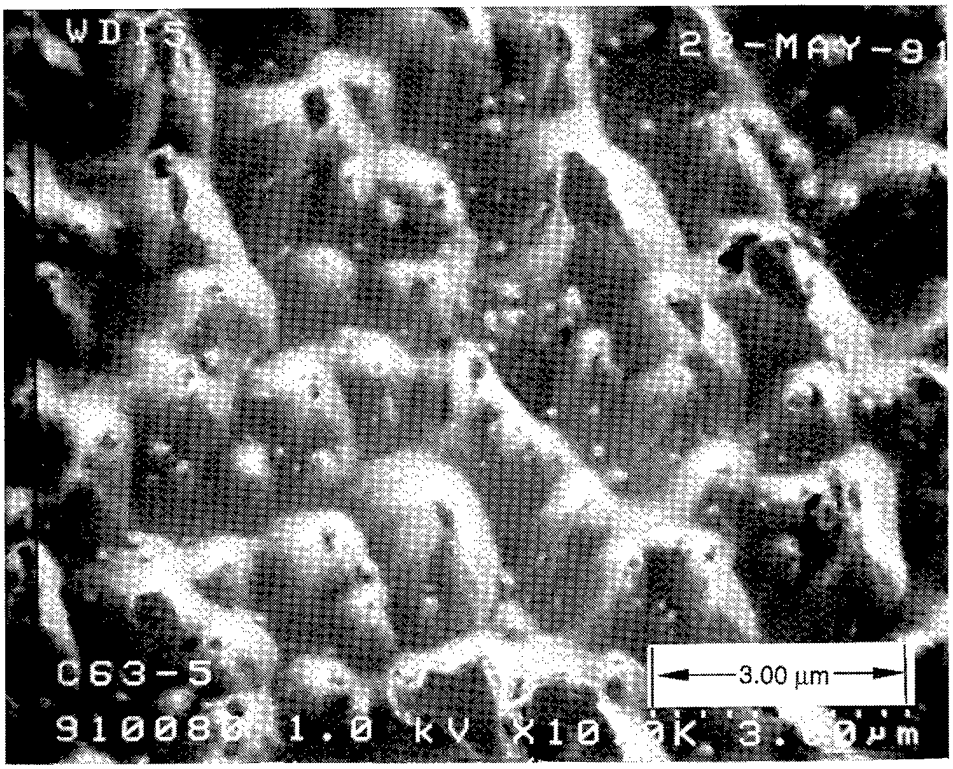


Figure 3. Optical Properties of TCSE Front Cover.



SEM of Exposed Teflon Surface
Sample #S-1

Figure 4

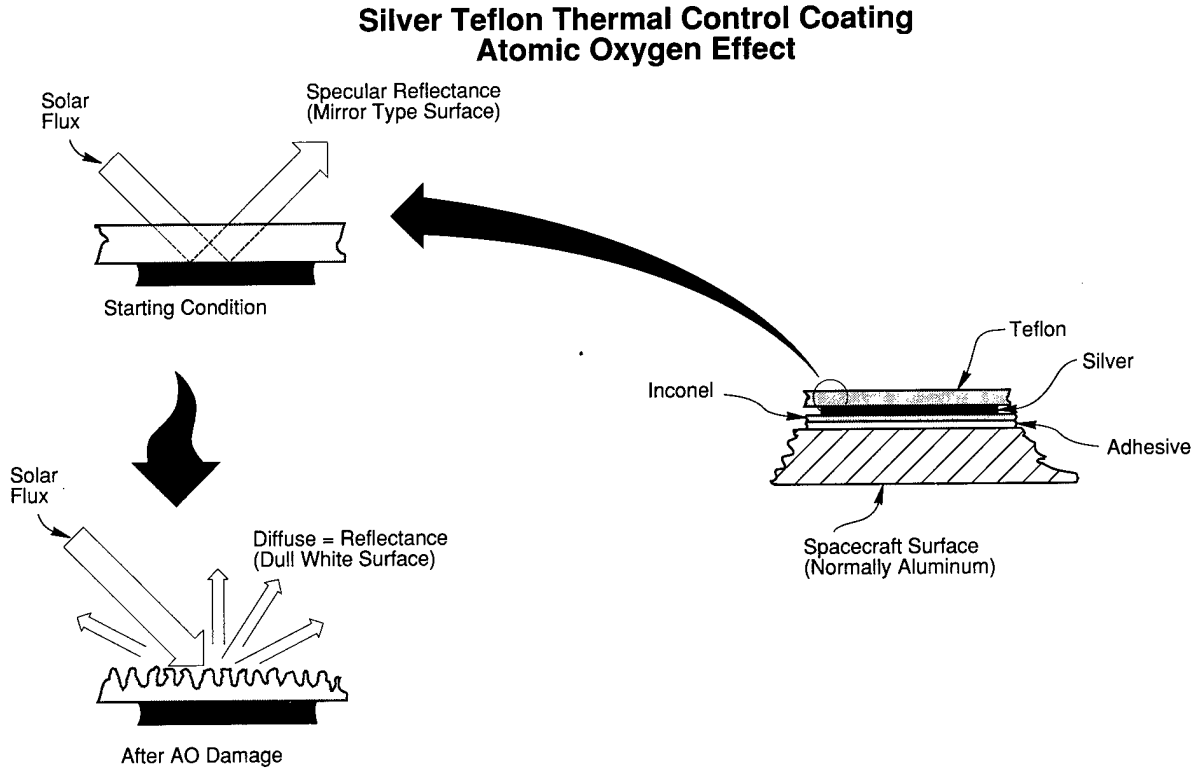
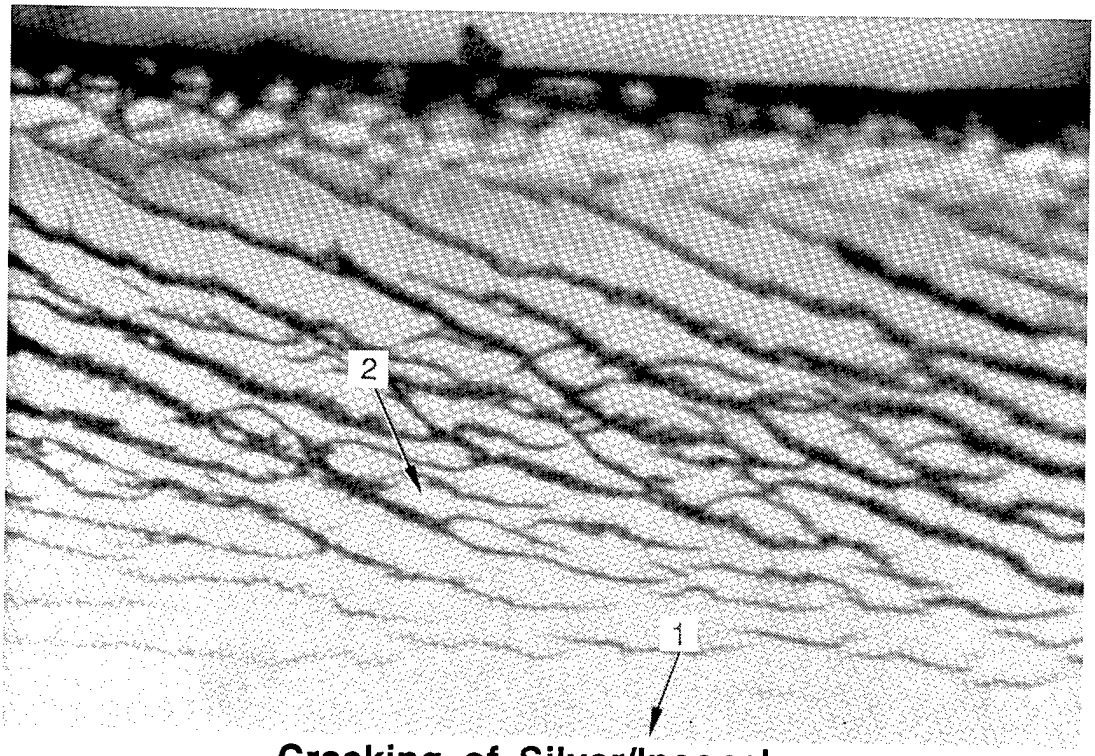
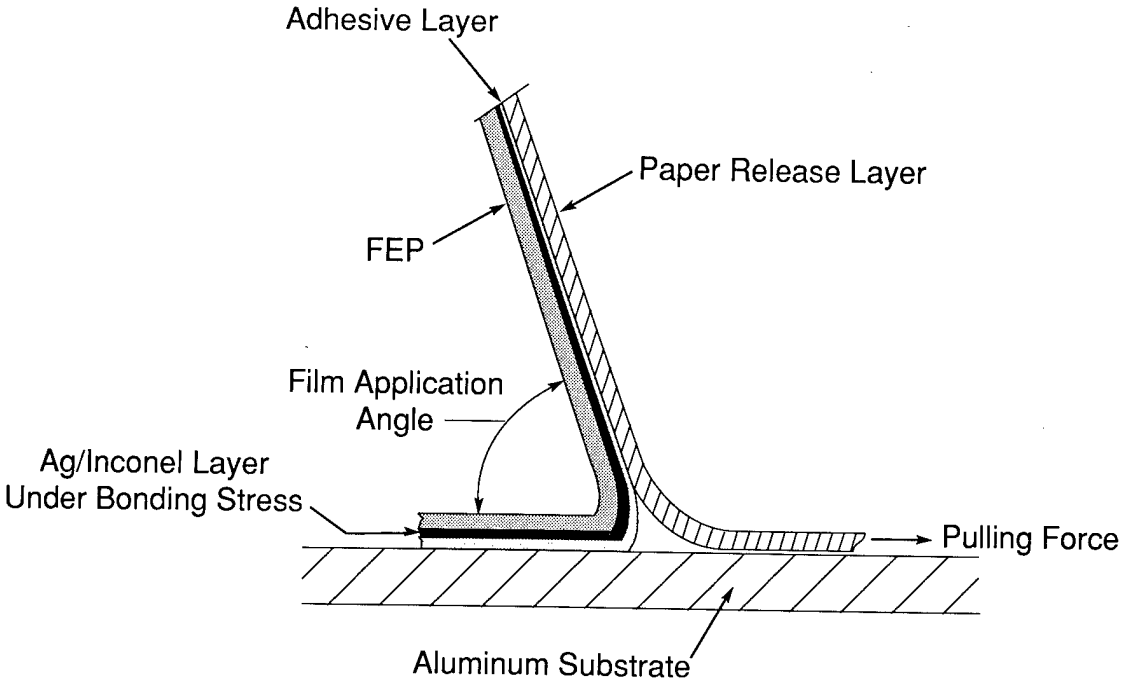


Figure 5



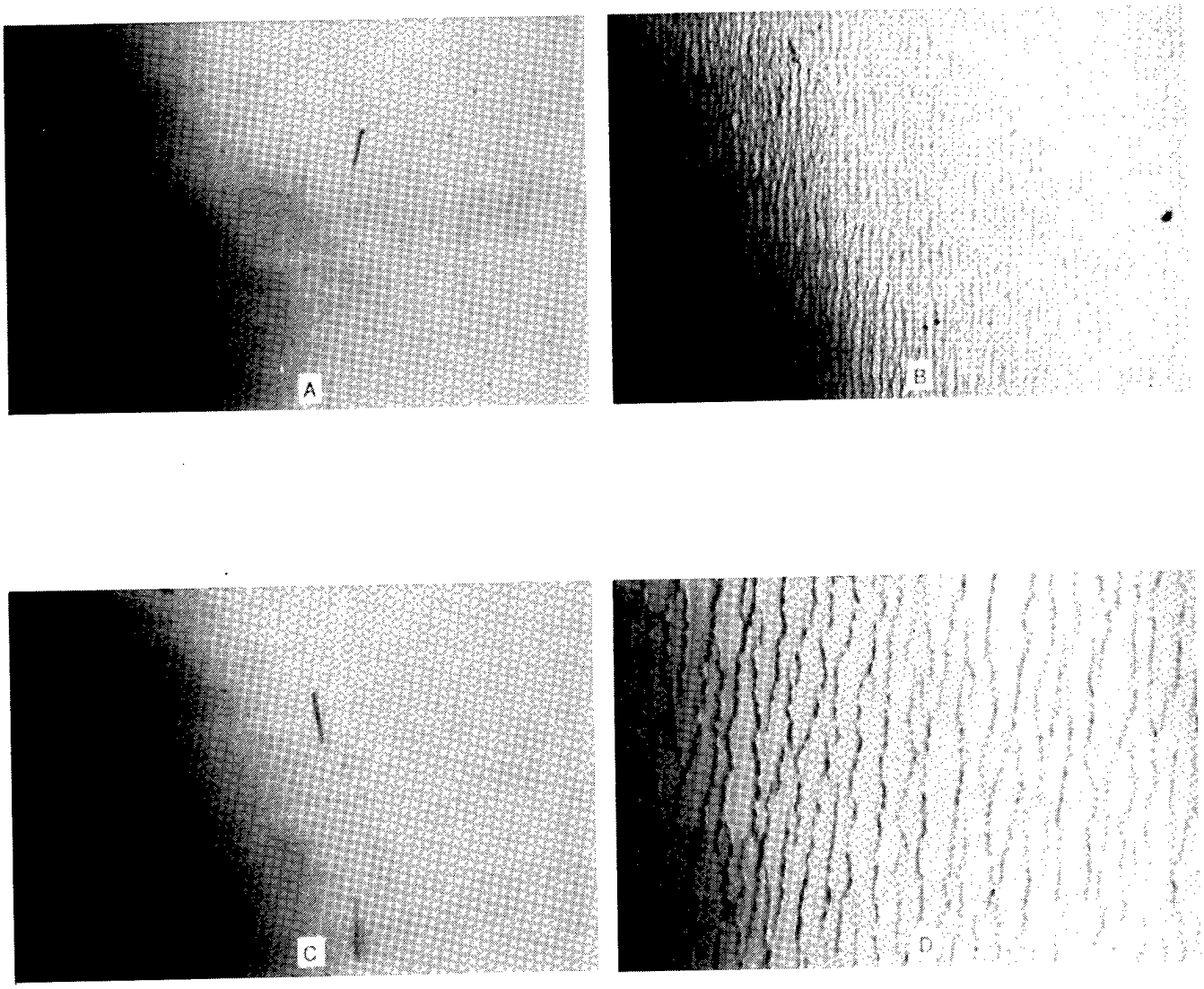
Cracking of Silver/Inconel Layer - Overlap Region

Figure 6



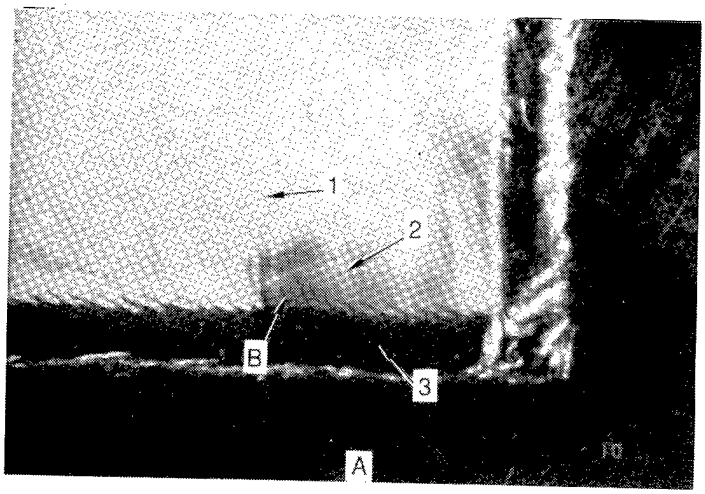
Schematic of Silver Teflon Application

Figure 7

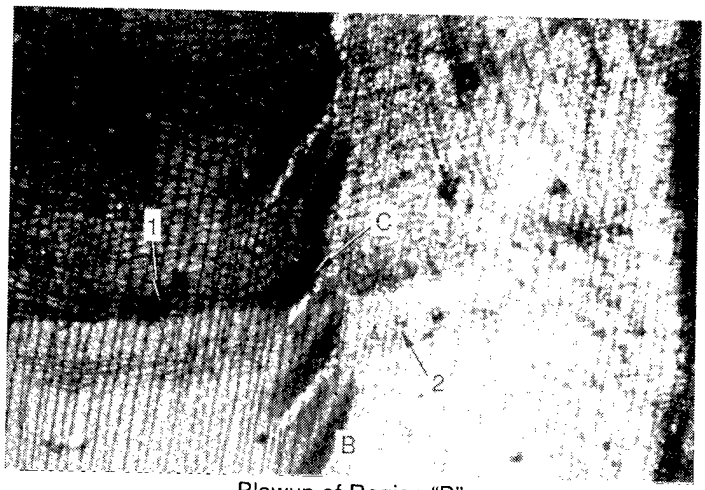


Silver Inconel Layer Cracking During Application of 2 MIL Silver Teflon

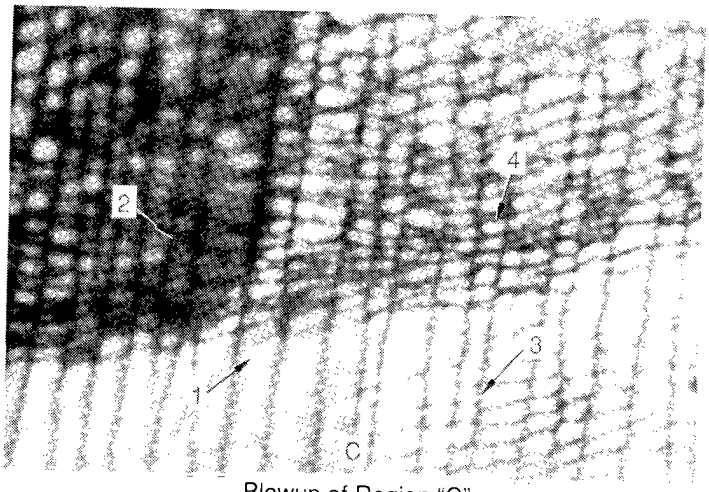
Figure 8



Corner of Sample "S-1"



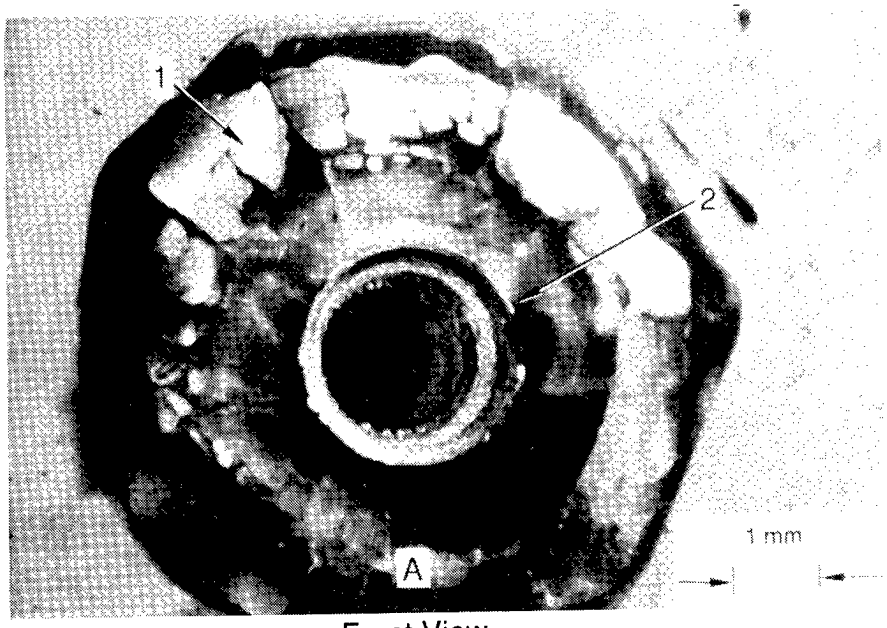
Blowup of Region "B"



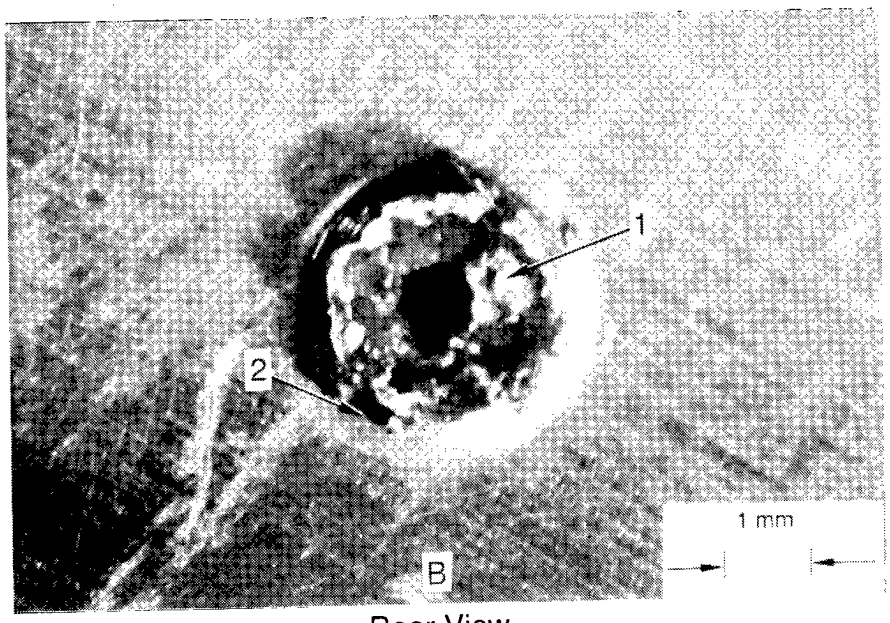
Blowup of Region "C"

Silver Teflon "Brownish" Discoloration and Silver/Inconel Layer "Crack" Association

Figure 9



Front View

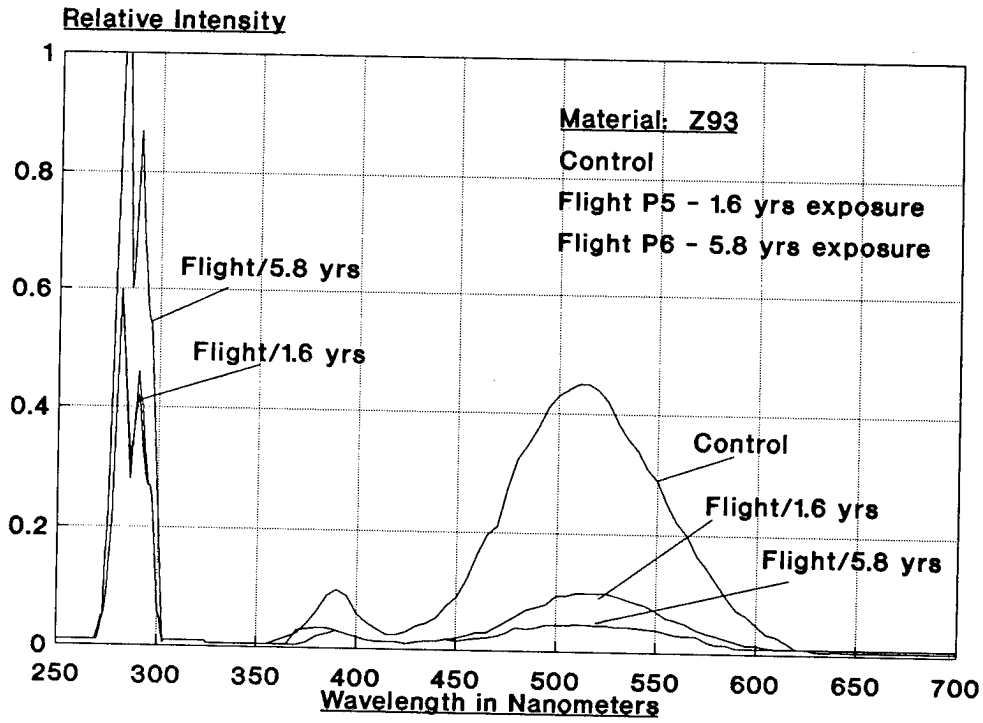


Rear View

Impact Penetration of Front Panel

(Panel: 6061AL; 0.063 MIL Thickness)

Figure 10



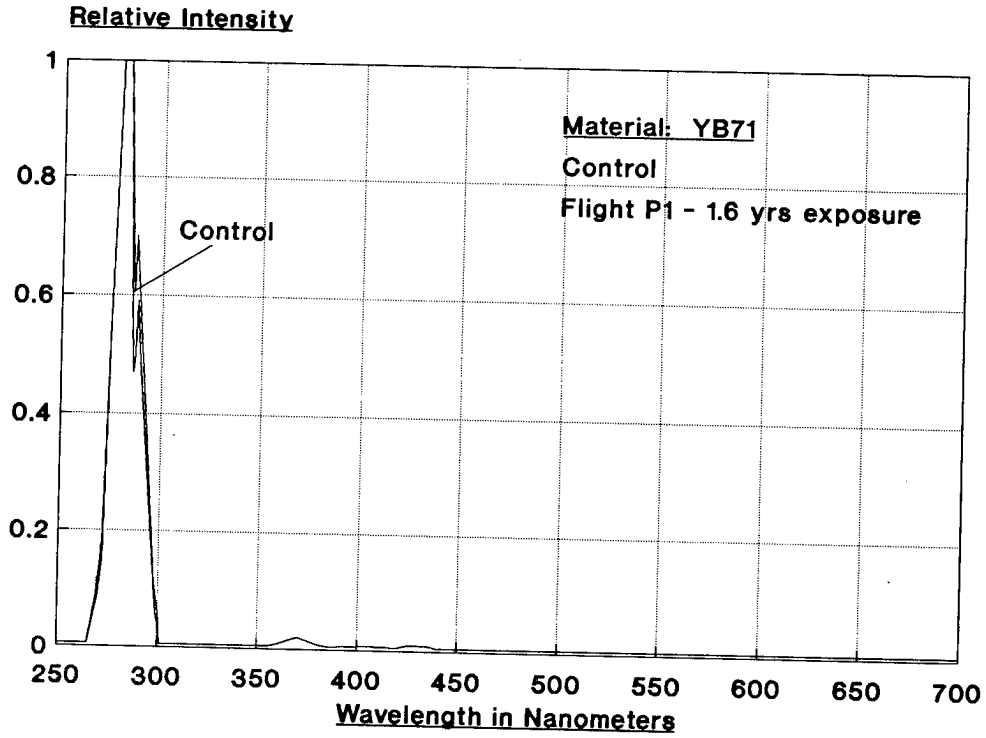


Figure 11. Fluorescence Spectra of Z93 and YB71.

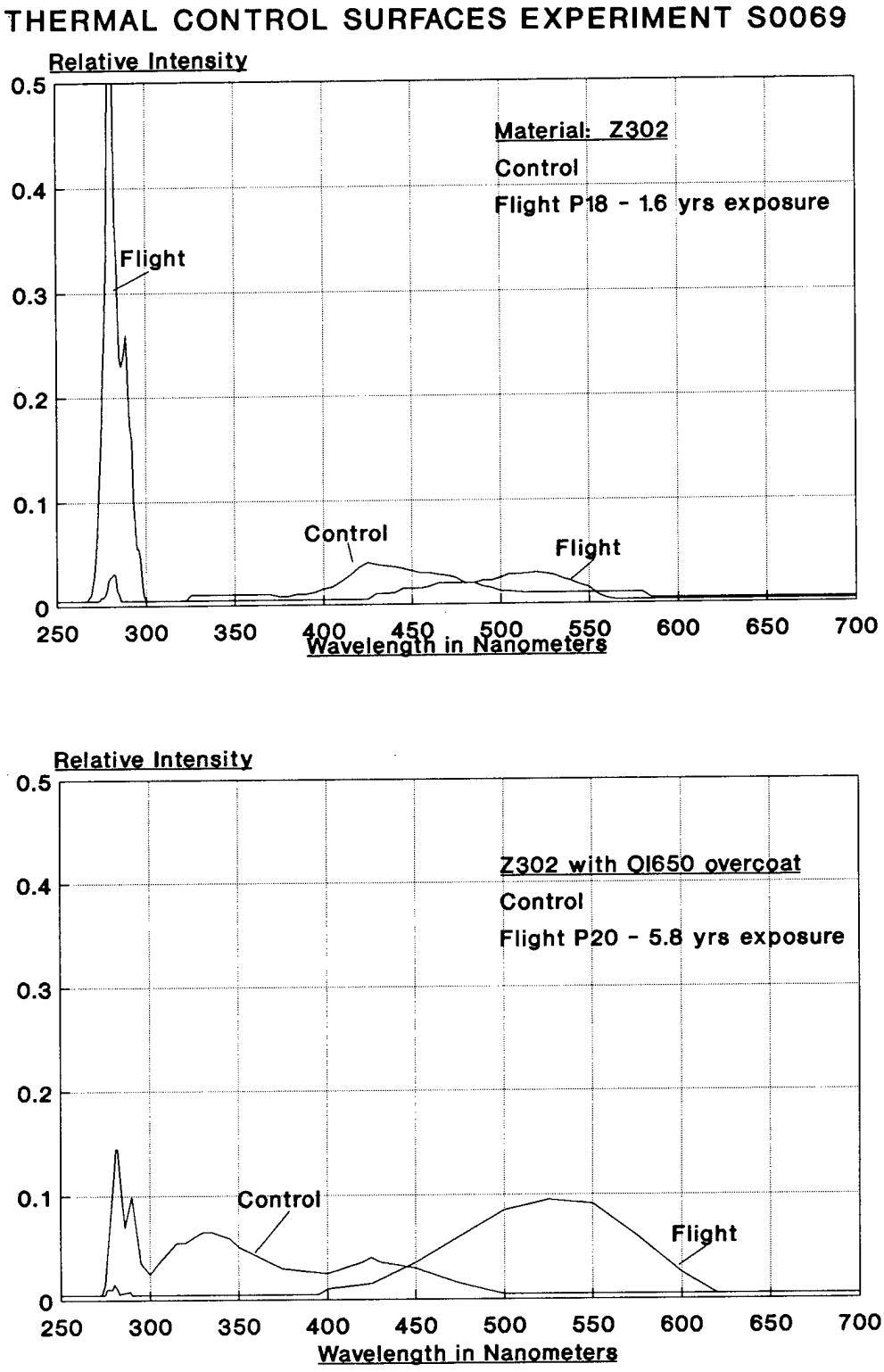


Figure 12. Fluorescence Spectra of Z302 and Z302 with OI650 Overcoat.

EFFECTS OF LOW EARTH ORBIT ENVIRONMENT ON THE LONG DURATION EXPOSURE FACILITY THERMAL CONTROL COATINGS

Thomas R. Sampair
Lockheed Engineering & Sciences Company
144 Research Dr.
Hampton Va. 23666
804 - 766 - 9633

William M. Berrios
NASA/LaRC
MS 434
Hampton Va. 23665-5225
804 - 864 - 7183

SUMMARY

The Long Duration Exposure Facility (LDEF) was brought back to Earth on January 20, 1990 after spending 5¾ years in low Earth orbit (~ 250 NM). One of the benefits of the facility was the opportunity to study the before and after effects of low Earth orbit space environment on the spacecraft thermal control coatings. Since the LDEF's thermal control was totally passive by design, the selection of the external surface absorptivity to emissivity ratio (α/ε) and the ability for the coating to retain the α/ε over time was an important consideration in the thermal design of the LDEF spacecraft. The primary surface coating chosen for the LDEF structure was clear chromic anodized aluminum with an average design α/ε of 0.32/0.16. External surface absorptivity (α) and emissivity (ε) were measured on all intercostals, longerons, tray mounting flanges, thermal control panels, and a limited number of experiment surface coatings after the experiment trays were removed from the LDEF structure.

All surface α/ε measurements were made using portable hand held infrared and solar spectrum reflectometers. The absorptivity measurements were taken with a Devices and Services SSR-ER version 5.0 solar spectra reflectometer which has a stated uncertainty of ± 0.01, and all normal emissivity measurements were made using the Gier Dunkle DB-100 infrared reflectometer also with a stated uncertainty of ± 0.01. Both instruments were calibrated in the laboratory by Langley Research Center (LaRC) instrumentation personnel before being used in the field at the Kennedy Space Center (KSC).

A combined total of 733 measurements were taken on the anodized aluminum hardware which included the structure (intercostals, longerons, and center ring), earth and space end thermal control panels, and experiment tray mounting flanges.

The facility thermal control coatings measured in this survey cover 33% of the total exposed LDEF surface area. To correlate low Earth orbit environmental effects on the anodized coatings, measurements were taken on both exposed and unexposed surfaces and compared to quality assurance (QA) measurements taken on the new surfaces at the time of hardware fabrication in 1978.

The results of this survey showed that anodized coatings on aluminum surfaces remain very stable under the harsh environment of low earth orbit. The anodized aluminum average absorptivity degradation of 0.05 was consistent with LaRC in house test which showed for the worst case no more than a 15% increase in absorptivity over 2000 hours of a one sun exposure in the vacuum test chamber. The study also revealed that the A276 and S13-GLO white paints displayed varying degrees of thermo-optical property degradation depending upon the location on LDEF relative to the AO flux and the amount of UV exposure received. The use of the A276 and S13-GLO white paints on spacecraft requiring precise thermal control on extended low earth orbit missions could produce unwanted thermal excursions as these coatings degrade over time. A 100% increase in absorptivity should be accounted for in the spacecraft thermal design if these paints are used. The Chemglaze Z306 black paint which was used on the interior of the LDEF had an average α/ε of 0.96/0.92 with a small variation of ± 0.01 for both α and ε.

INSTRUMENTATION

The LDEF spacecraft provided a unique opportunity to study the degradation effects from exposure to low Earth orbit on thermal control coatings. The LDEF used several types of coatings and thermal blankets to passively control the thermal environment to ensure experiment survivability. The primary exterior coatings utilized on LDEF were clear and black chrome anodized aluminum, A276/S13-GLO white paints, kapton/silver teflon thermal blankets and other materials (Figure 1). The clear anodizing was chosen for the main thermal control coating because of its durability and for the ease of varying the α/ε properties with the variable chromic anodizing process developed at Langley Research Center by R. J. Duckett & C. S. Gilliland (Ref 1). After the experiment trays were de-integrated from the LDEF structure, α/ε surface measurements were made on all intercostals, longerons, thermal control panels, tray mounting flanges and a limited number of experiment surfaces (Figure 2). All α/ε measurements were made using portable infrared and solar spectrum reflectometers. The solar spectrum reflectometer model SSR-ER version 5.0 was made by Devices and Services Co. of Dallas Texas. The model SSR-ER was designed to provide accurate measurements (repeatability ± 0.003) of total solar reflectance for the wavelength range from 330 to 2500 nanometers with a 0.001 resolution. The instrument unit consists of a measuring head, modular digital processing electronics, and a liquid crystal display which can show either total solar reflectance or solar absorptivity (1 - reflectance). The measuring head consists of a single tungsten-halogen light source and four filtered detectors all enclosed inside a light-weight aluminum housing in which the inside surface is coated with barium sulfate reflectance paint. The four detectors in the collimator measure the reflected energy in the infrared, red, blue, and ultra-violet wavelength ranges and are then integrated into a weighted sum to produce the solar spectrum measurement. The measurement head is designed to measure total solar reflectance for an incidence

angle of 20 degrees off normal and can display either reflectance or absorptivity data for the weighted sum or for any one of the four detectors for air masses of 0, 1, 1.5, or 2. All absorptivity values presented in this report are for an air mass of zero. All QA absorptivity measurements were made with the Gier Dunkle MS-251 solar reflectometer by Langley QA personnel during hardware fabrication in 1978.

The emissivity measurements were obtained using a Gier Dunkle DB-100 infrared reflectometer. The instrument is packaged in a single carrying case which includes the electronics, a digital readout, and the inspection head. The DB-100 has a measurement time of 3 seconds per sample with an accuracy of ±1 % of full scale for gray samples and ±3 % of full scale for non-gray samples. The device has a stated reproducibility of ±2 % of full scale. Another feature of this instrument is that the reading can be made independent of the sample temperature. The DB-100 measures reflectance directly and the normal emissivity reading is obtained by taking one minus the reflectance (1 - reflectance). The values presented in this report are normal emissivities.

RESULTS

Absorptivity and emissivity measurements were taken at 397 locations (exposed and unexposed) on the LDEF structure (intercostals, longerons, and center ring), 55 exposed locations on the space end thermal control panels, 60 exposed locations on the black chrome earth end panels, and 221 exposed and unexposed locations on the tray lip flanges. Unexposed surface measurements were taken on areas of the facility which were shadowed by tray flanges and mounting clamps and therefore were not directly exposed to AO and UV flux. The exposed anodized aluminum thermal control coatings measured in this survey represent 539 ft^2 (33%) out of the total exposed LDEF surface area. To correlate low Earth orbit environmental effects on the anodized coatings, measurements were taken on both exposed and unexposed surfaces and compared to QA measurements taken at the time of hardware fabrication in 1978.

Table 1 presents the average α/ε results obtained for all measurements taken from the QA log, the unexposed surfaces, and the exposed surfaces for LDEF's structural members, earth and space end thermal control panels, and experiment tray lip mounting flanges (3", 6", and 12" trays). Also shown in Table 1 are the design specifications for each type of hardware listed above. The average absorptivity of 246 exposed surface measurements taken around the LDEF periphery was 0.36 ± 0.05 which was an increase of 0.05 over the QA log average of 0.31 ± 0.02. The observed average 0.05 degradation (16%) is consistent with a LaRC solar stability test done at the time when the variable anodizing process was being developed. This test showed the solar degradation to be no more than 15% for over 2000 hours of a one sun exposure in a vacuum test chamber (Ref 1). The average absorptivity for the 125 unexposed structural surfaces was 0.33 ± 0.04, a 6.4% increase over the original 0.31. This small change in absorptivity most likely can be attributed to the different measuring instruments employed or the presence of contamination on the unexposed surfaces.

Presented in Figure 3 are the average row absorptivities versus LDEF row location for the QA log, unexposed, and exposed surface measurements. The figure shows almost no change in absorptivity on the leading edge row 9 to approximately a 24% increase on the trailing edge row 3. Figure 4 shows the average row emissivity for each category of measurement made versus LDEF row location. The average normal emissivity for exposed surfaces was 0.15 ± 0.03 which was the same as the QA log average of 0.15 ± 0.03. One consistent trend observed while surveying the structure was the 20.0% increase in unexposed surface average emissivity (0.18 ± 0.04) over the QA average emissivity values.

Figure 5 shows a plot of the average row α/ε versus row location on the spacecraft. From this figure one can notice that the leading edge rows are much closer to the QA log ratios than the trailing edge rows which were shielded from AO flux. The overall LDEF average structure α/ε's obtained from the QA log, unexposed, and exposed measurements were 2.07, 1.83, and 2.37 respectively. The unexposed α/ε showed a downward shift compared to the QA but this is due to the unexpected increase in unexposed emittance. The results indicate that the overall exposed and unexposed average α/ε values remained within the design range of 1.67 to 2.43 throughout the six year LDEF mission, even though locally the α/ε varied depending upon which row location was being examined on the LDEF.

The LDEF was designed to accommodate 3", 6", and 12" deep trays. The 3" trays flanges were designed with an α/ε range from 1.11 to 1.48 ($\alpha/\varepsilon = 0.32 \pm 0.02/0.25 \pm 0.02$) and the average α/ε ratio for new tray flanges was 1.32 compared to the EOM ratio of 1.56 which exceeded the α/ε design limit by 5.4%. The 3" tray QA log average absorptivity of 0.33 ± 0.02 was unchanged compared to the unexposed average of $.033 \pm 0.03$ except for measurement tolerances. The 3" tray exposed absorptivity showed a 9.1% increase of 0.03 to 0.36 ± 0.04. The average new QA log normal emissivity for these trays was 0.25 ± 0.01 compared to the exposed surface emissivity of 0.23 ± 0.04 which is an 8% decrease from new. The unexposed 3" tray emissivity showed a small decrease of 0.01 from QA values to 0.24 ± 0.04. Both the 6" and 12" trays were designed with an α/ε range of 1.68 to 2.43 with new 6" trays having a QA log α/ε of 1.84 which had degraded to 2.21 by the time the LDEF was retrieved. The absorptivity measurements show the anodized coating for these trays increased by 0.04 from 0.33 ± 0.01 to 0.37 ± 0.03 (12%) while the emissivity declined by 0.01 from 0.18 ± 0.03 to 0.17 ± 0.02 by the EOM. The α/ε for the 12" trays essentially remained unchanged (1.98 vs 2.03) from the QA log to the EOM with an average absorptivity rise of 0.03 coupled with an increase in emissivity of 0.01. The increase in exposed emissivity for the 12 inch trays cannot be explained at present but it is within the statistical variation of all measurements made.

The LDEF employed thin aluminum panels at each end of the facility to control heat flow in and out of the ends of the spacecraft. The space facing panels used a clear chromic anodized finish with a design α/ε range from 1.78 to 2.57. The QA log α/ε was 2.13 at the time of fabrication and had degraded to 2.42 for exposed surfaces by the EOM but was still within the required design limits. The average absorptivity increased 8.8% from 0.34 in 1978 to 0.37 by the end of the LDEF mission and the average emissivity for the panels showed no change except for tolerances from new to EOM (0.15 ± 0.01 vs 0.15 ± 0.02). The earth facing panels were black chrome anodized for an α/ε range from 7.75 to 10.88 and had a QA log average value of 10.0.

The 60 α/ε measurements made on the 12 panels reveal that the surface properties remained very stable over the LDEF mission with the average absorptivity increasing only 0.02 from the QA log of 0.90 to 0.92 for the EOM. The emissivity also showed very little change from the QA log measured value of 0.09 to the EOM value of 0.08 (11 %). Unexposed measurements were not available for either the space or the earth end thermal panels. Overall changes in the α/ε values for the anodized surfaces were small relative to the accuracies of the measurements taken, but the consistency in observed trends indicates that the results presented are valid.

Summarized in Table 2 are the exposed surface coating α/ε averages for the white and black paints, structural members, and some selected tray clamps along with the number of samples taken for each type of coating. A276 white thermal control paint was used on several experiments and on thermal control test disks which were located on selective tray clamps placed around the LDEF periphery. The specimens located on the leading edge (ram direction) of LDEF showed the organic binder of the A276 paint had been broken down by the attack from AO which left only a white chalky pigment. The specimens located on the trailing edge (shielded from AO) had developed a hardened dark brown finish while other specimens showed only patches of brown depending upon their orientation with respect to the AO flux (ram direction). An example would be two of the experiment trays coated with A276 paint: one located on row 6 and the other located on the opposite row 12. Both trays received the same intensity of UV flux during the mission, but because the LDEF was yawed 8° (Figure 6) the row 12 tray was exposed to a 2300% larger increase in AO flux than the row 6 tray (Ref 2). The result was that the row 6 tray remained brown in color while the row 12 tray was bleached white with brown spots. The dark brown areas were due to the UV polymerization of the A276 organic binder and had an average absorptivity approximately twice as high as the white control sample absorptivity of 0.29. The average absorptivity for the A276 ranged from 0.22 ± 0.02 for the white appearance to 0.45 ± 0.05 for the dark brown finish with the actual measurements ranging from 0.20 to 0.55. The typical new paint α/ε values for A276 are 0.20/0.80. The emissivity for the A276 showed no change from the control sample value of 0.88 even though there was severe color change. This can be attributed to the fact that the emissivity of painted coatings are more a function of the coating thickness and chemical matrix (i.e. material's infrared absorption band) than other factors such as color.

S13-GLO white paint was also used as a thermal control coating on a few experiment surfaces and cover shields. The absorptivity for the white S13-GLO was 0.20 ± 0.02 and had risen to 0.35 ± 0.05 for the yellow surfaces. The actual measurements ranged from 0.17 for the white surfaces to 0.43 for the darkest yellow surfaces. The typical new paint α/ε specification for S13-GLO is 0.17/0.90. The emissivity for the S13-GLO, like that of the A276, did not vary with color change and the average from all readings was 0.89 ± 0.01. There were not any control samples available for this coating nor were any measurements made prior to flight.

Chemglaze Z306 black paint was used as the primary thermal control coating on all LDEF interior structural members and experiment tray bottoms. The Z306 measurements taken from the LDEF interior gave an average α/ε of 0.96/0.92 with a small variation of ± 0.01 for both α and ε. The Z306 showed good durability on the interior surfaces of the LDEF but these surfaces were not subjected to direct AO and UV exposure.

Silver teflon thermal control blankets were also used extensively on some LDEF experiments (~ 17 trays). However, because the portable instruments employed require direct surface contact, none of the blankets were measured for fear of surface contamination from the measurement head. Therefore the LDEF Materials Special Investigation Group (MSIG) was given the responsibility for the α/ε analysis of these blankets.

CONCLUSION

From the results of the LDEF external α/ε surface survey, it can be concluded that the clear chromic acid anodizing process as developed by Duckett and Gilliland (Ref 1) has proven to be a stable spacecraft thermal control coating. Measurements have confirmed that the exposed surface (intercostals and longerons) average absorptivity degraded no more than 16% over the life of the LDEF mission. Furthermore the exposed surface average emissivity also showed very little degradation from new values. The study also revealed that the paints A276, S13-GLO, and Z306 suffered from long term exposure to the low Earth orbit space environment. The paint pigment binders were susceptible to both UV polymerization and AO erosion.

REFERENCES

1. Duckett R. J. & Gilliland C. S.: Variable Anodic Thermal Control Coating on Aluminum, AIAA 18th Thermophysics Conference, June 1-3, 1983, AIAA-83-1492

2. Bourassa R. J., Gillis J. R., Atomic Oxygen and Mission Total Solar Exposures for LDEF Experiments, First LDEF Post-Retrieval Symposium, NASA CP-3134, 1992.

TABLE 1 LDEF ANODIZED ALUMINUM COMPARISON OF RESULTS

HARDWARE	DESIGN		QA RECORD 1978			UNEXPOSED 1990			EXPOSED 1990		
	α	ε	α	ε	α/ε	α	ε	α/ε	α	ε	α/ε
INTERCOSTALS	.32±.02	.16±02	.30±.02	.16±.02	1.88	.31±.04	.18±.04	1.72	.34±.04	.16±.03	2.13
LONGERONS	.32±.02	.16±02	.32±.01	.14±.01	2.29	.34±.05	.17±.04	2.00	.37±.05	.15±.03	2.47
INTERC & LONG	.32±.02	.16±.02	.31±.02	.15±.03	2.07	.33±.04	.18±.04	1.83	.36±.05	.15±.03	2.37
3" TRAY LIPS	.32±.02	.25±.02	.33±.02	.25±.01	1.32	.33±.03	.24±.04	1.38	.36±.04	.23±.04	1.56
6" TRAY LIPS	.32±.02	.16±02	.33±.01	.18±.03	1.84	.35±.03	.17±.01	2.06	.37±.03	.17±.02	2.18
12" TRAY LIPS	.32±.02	.16±02	.33±.01	.17±.01	1.94	.34±.02	.18±.02	1.89	.36±.02	.18±.03	2.00
TRAY CLAMPS	.32±.02	.16±.02	.32	.16	2.00	.32±.01	.18±.01	1.78	.33±.03	.15±.01	2.20
SPACE THM PL	.34±.02	.16±.02	.34±.02	.15±.01	2.27	-	-	-	.37±.03	.15±.02	2.47
EARTH THM PL	.90±.03	.10±.02	.90	.09	10.0	-	-	-	.92±.03	.08±.01	11.5

TABLE 2 LDEF POST FLIGHT EXPOSED SURFACE COATINGS SUMMARY

LDEF MATERIAL	LOCATION ON LDEF	DESCRIPTION	NUMBER OF SAMPLES	α*	ε**	α/ε
AL 6061 - T6	INTERCOSTALS	ALL ROWS	98	.34 ± 04	.16 ± .03	2.13
AL 6061 - T6	LONGERONS	ALL ROWS	148	.37 ± .05	.15 ± .03	2.47
AL 6061 - T6	STURCTURE	INTERCOASTAL & LONGERONS	246	.36 ± .05	.15 ± .03	2.37
AL 6061 - T6	EARTH THERMAL PANELS	BLACK CHROMIC ANODIZED	60	.92 ± .03	.08 ± .01	11.08
AL 6061 - T6	SPACE THERMAL PANELS	CLEAR ANODIZED	55	.37 ± .03	.15 ± .02	2.47
AL 6061 - T6	CENTER RING	BARE ALUMINUM	26	.39 ± .06	.09 ± .02	4.45
AL 6061 - T6	TRAY CLAMPS	CONTROL SAMPLES - ANODIZED	8	.33 ± .01	.17 ± .01	1.94
AL 6061 - T6	TRAY CLAMP E - 3 # 8	BROWN TINT ON EXPOSED SIDE	1	.36	.16	2.26
AL 6061 - T6	TRAY CLAMP E - 6 # 8	EXPOSED IS DARKER THAN UNEXP	1	.30	.15	1.98
AL 6061 - T6	TRAY CLAMP E - 9 # 6	ALUMINUM IS CLEAR	1	.30	.15	2.09
AL 6061 - T6	TRAY CLAMP E-12 # 6	DARKER ON EXPOSED	1	.35	.15	2.31
AL 6061 - T6	TRAY CLAMPS	ALL SAMPLES	4	.33 ± .03	.15 ± .01	2.20
A276 WHITE PAINT	E-12, H-6, F-6	WHITE TO LIGHT TAN COLOR	6	.22 ± .02	.91 ± .01	.24
A276 WHITE PAINT	E-12, H-6, F-6	MEDIUM TAN IN COLOR	2	.36 ± .03	.88	.41
A276 WHITE PAINT	E-12, H-6, F-6	MEDIUM TAN TO DARK BROWN	4	.45 ± .05	.88 ± .01	.51
A276 WHITE PAINT	TRAY CLAMP E - 3 # 8	BROWN IN COLOR	1	.53	.88	.60
A276 WHITE PAINT	TRAY CLAMP E - 6 # 8	TAN NON-UNIFORM COLOR	1	.42	.87	.48
A276 WHITE PAINT	TRAY CLAMP E - 9 # 6	WHITE IN COLOR	1	.32	.90	.36
A276 WHITE PAINT	TRAY CLAMP E-12 # 6	DULL CREAM BEIGE COLOR	1	.36	.87	.41
A276 WHITE PAINT	TRAY CLAMP	CONTROL SAMPLE - WHITE	4	.29 ± .01	.88	.33
S13GLO WHITE PAINT	D - 9 LEADING EDGE	WHITE - BEIGE IN COLOR	3	.27 ± .05	.89 ± .01	.30
S13GLO WHITE PAINT	D - 3 TRAILING EDGE	YELLOW - TAN IN COLOR	4	.35 ± .05	.89 ± .01	.39
S13GLO WHITE PAINT	G - 6 EARTH END	WHITE TO TAN IN COLOR	8	.21 ± .02	.90	.23
S13GLO WHITE PAINT	C - 9 LEADING EDGE	WHITE W/BROWN SPOTS	5	.20 ± .02	.87 ± .01	.23
S13GLO WHITE PAINT	C - 3 TRAILING EDGE	DARK YELLOW TO BROWN	2	.39	.89	.44
Z-306 CHEMGLAZE	E - 9 LEADING EDGE	BLACK W/PRIMER VISIBLE	3	.91 ± .06	.93 ± .01	.98
Z-306 CHEMGLAZE	LDEF INTERIOR	BLACK	5	.96 ± .01	.92 ± .01	1.04

* - SOLAR REFLECTANCE : DEVICES & SERVICES SOLAR REFLECTOMETER SSR-ER, VER. 5.0
** - INFRARED REFLECTANCE: GIER DUNKLE INFRARED REFLECTOMETER DB-100, NORMAL EMITTANCE

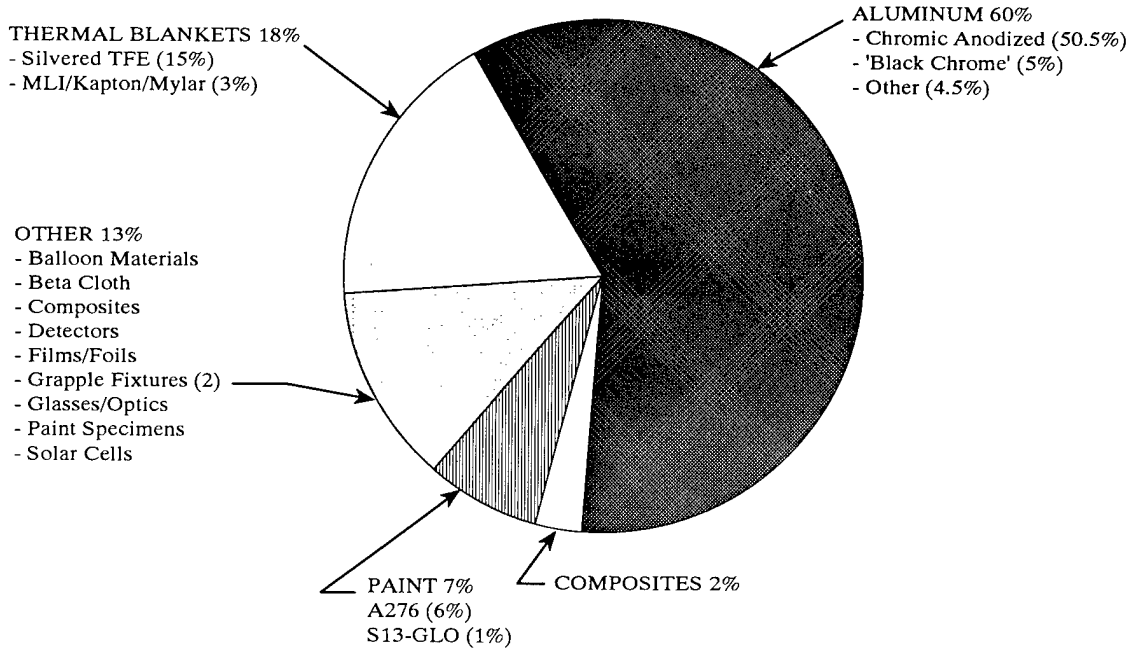


Figure 1. LDEF External Surface Coating Distribution.

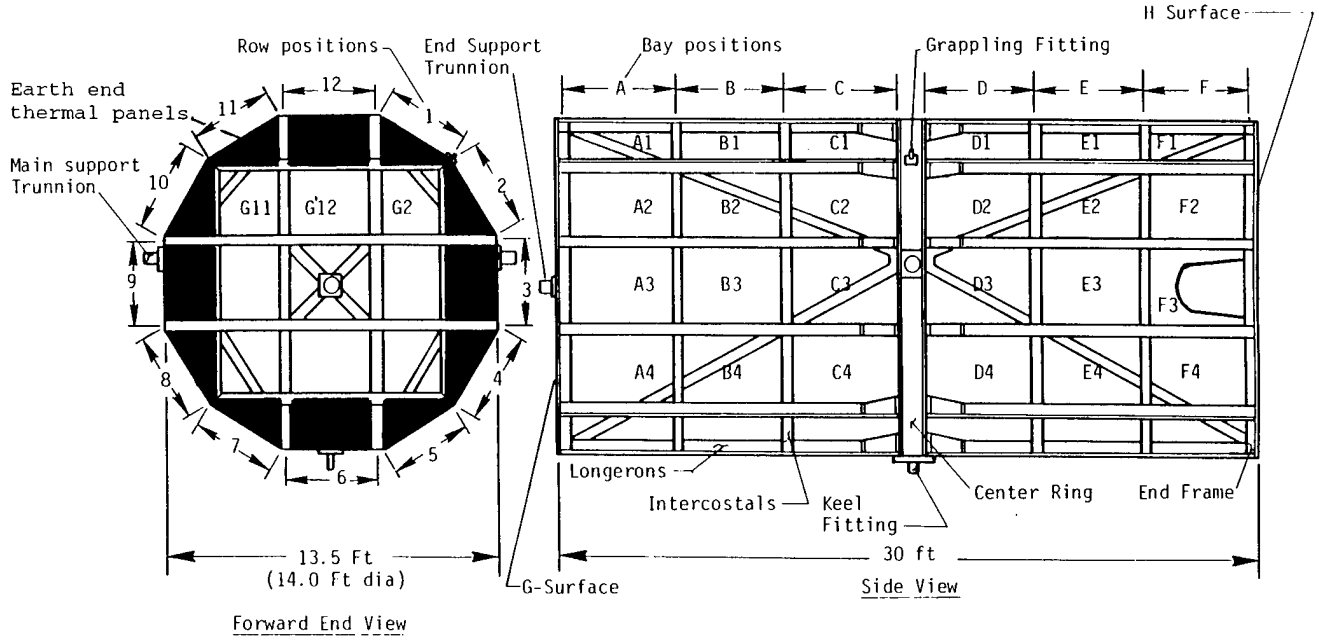


Figure 2. LDEF Description

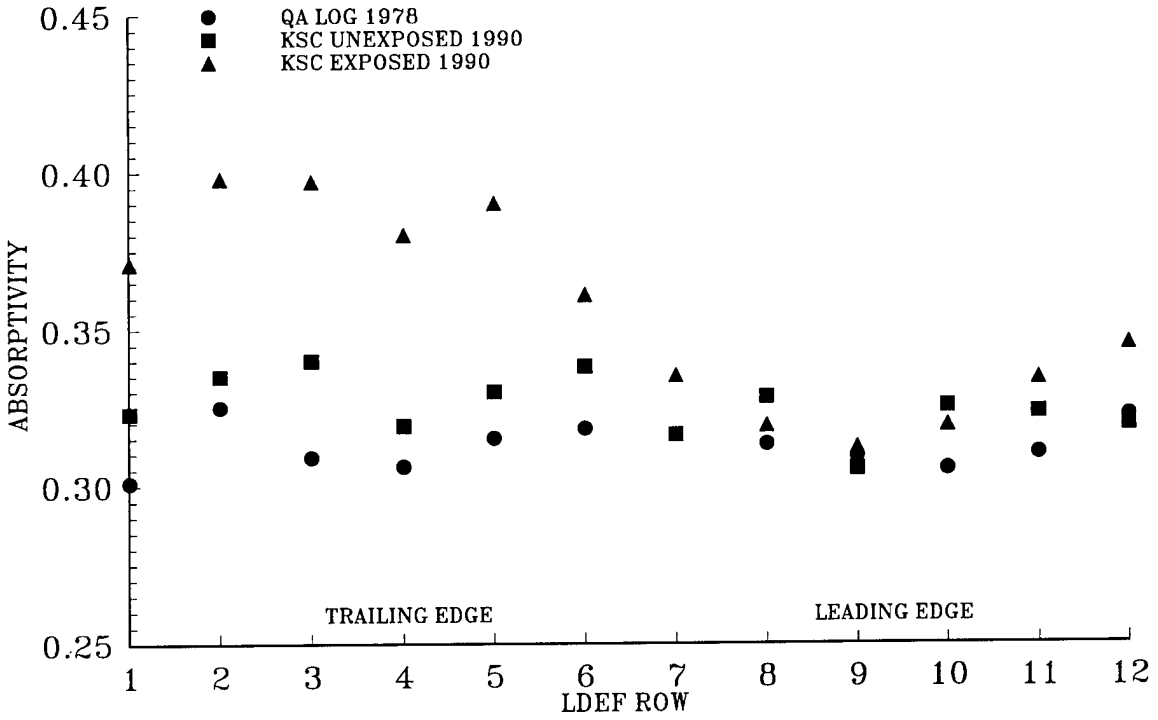


Figure 3. LDEF Structure: Average Absorptivity vs Row Location

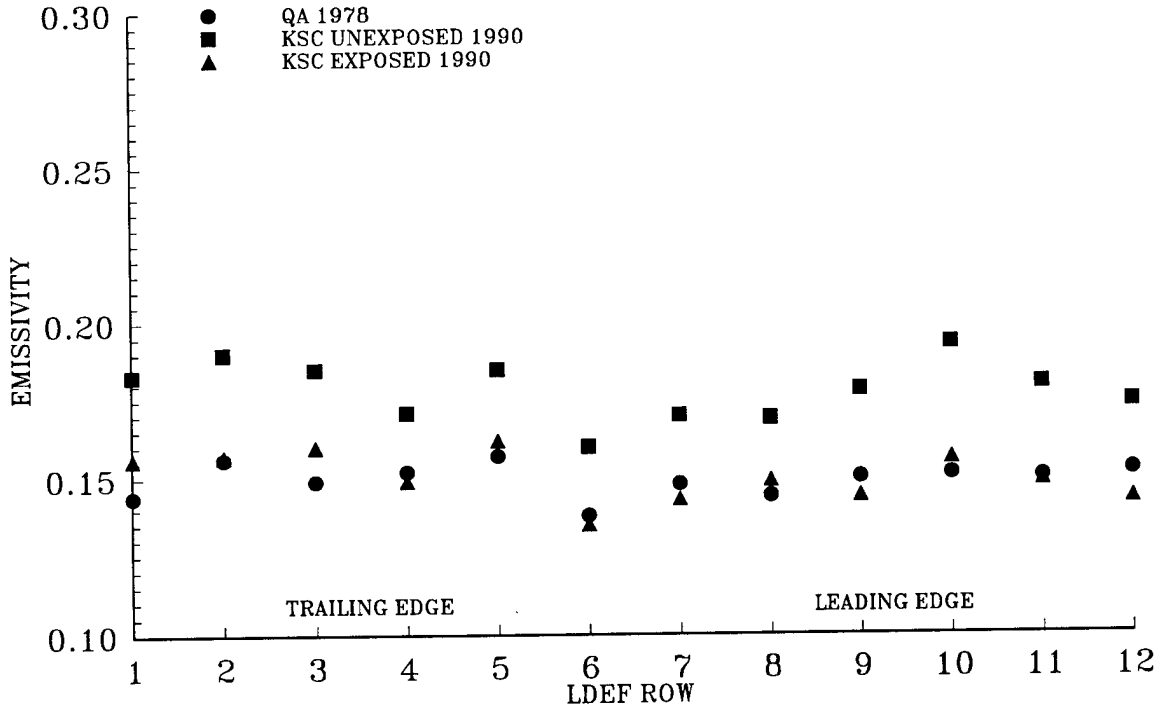


Figure 4. LDEF Structure: Average Emissivity Vs Row Location

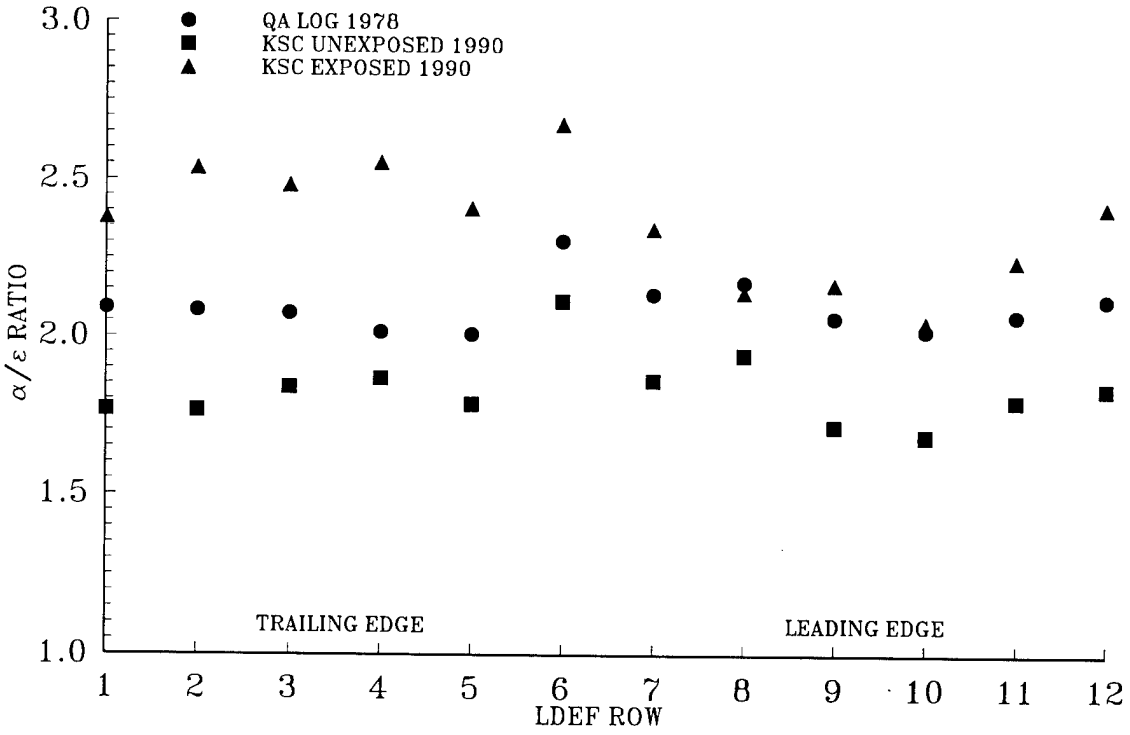


Figure 5. LDEF Structure: Average α/ε vs Row Location

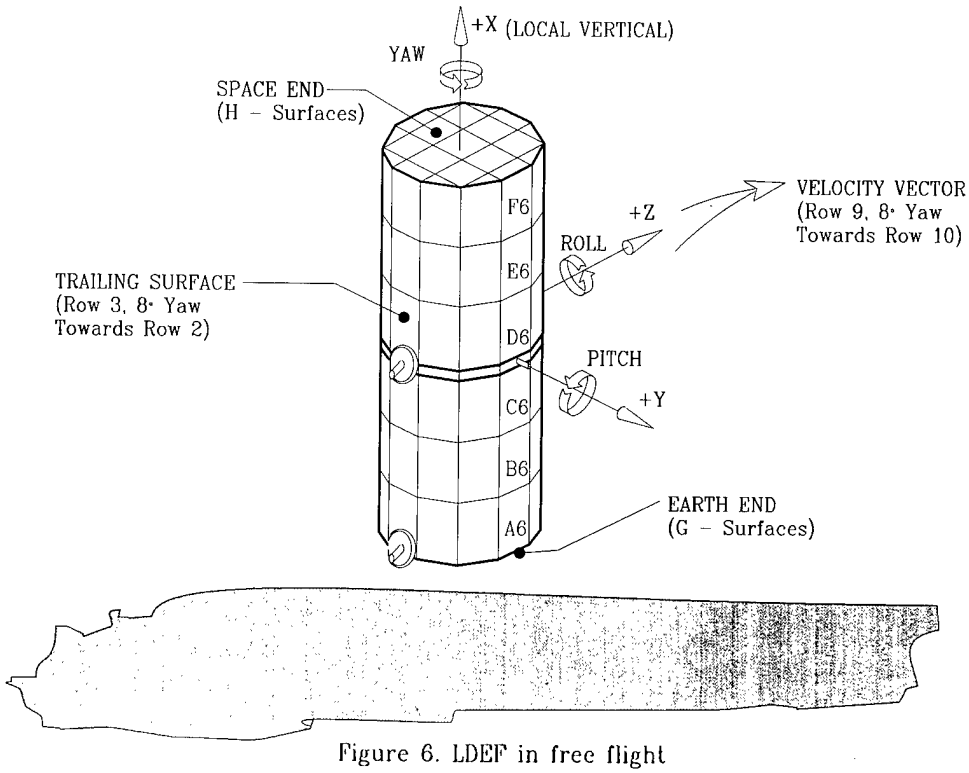


Figure 6. LDEF in free flight

SPACECRAFT THERMAL CONTROL COATINGS

Jean-Claude Guillaumon
CNES CT/TE/AE/MT/TH
18 Avenue E. Belin, 31055 Toulouse cedex (France)
Phone: (33) 61 55 71 19, Fax (33) 61 55 71 72

Alain Paillous
ONERA / CERT / DERTS
18 Avenue E. Belin, 31055 Toulouse cedex (France)
Phone: (33) 61 27 39 29, Fax (33) 61 27 40 99

SUMMARY

The Experiment AO 138-6 was located on the trailing edge of LDEF as part of the Experiment FRECOPA. It was purely passive in nature: material specimens 2 x 2 cm, independently mounted in sample-holders, with their surface in the same reference plane, were exposed to space. Thirty samples were set in a vacuum-tight canister which was opened in space a few days after LDEF deployment and closed still in orbit ten months later; twenty-four samples were directly exposed to space for the total flight duration (preflight handling, shuttle bay environment, separation from shuttle, shuttle environment, LEO environment, docking, descent, transfer to KSC). Materials included paints (conductive or not), SSMs, polymeric films, surface coatings, composite materials, metals. After sample retrieving, inspection and measurements were carried out in atmospheric laboratory conditions on each sample: observation with binocular lenses and SEM, spectral reflectance and transmittance using an integrating sphere in the wavelengthh range 280-2300 nm, emissivity by the means of a Gier & Dunkle portable reflectometer, ESCA-XPS and RBS measurements on some selected samples. The results obtained from flight have been compared to laboratory data obtained in UV-irradiation tests when these data were available. As a general statement a good spectral concordance is observed for all samples not in the canister so long as air recoveries are taken into account. For one material, the degradation is more important for the sample in the canister than for those of the same material mounted at the surface of the tray; for most samples in the canister the degradation is slightly higher than the one which can be predicted from laboratory standard irradiations. Contamination problems having been ruled out, the higher temperature experienced by the samples on the inside of canister probably explains these phenomena.

INTRODUCTION

Background

Spacecraft materials are exposed to the various components of the natural space environment: vacuum, atomic oxygen, UV sun radiation, ionizing particle fluxes, micrometeoroids. Other environment elements

which are due to spacecraft operations have also to be considered: thermal cycling on board, contamination by molecular products and dust, debris... All these components, acting alone or synergistically, are deleterious in their effects on materials; their exact mutual importance varies depending on the mission.

Therefore the degradation which will be experienced in space has to be predicted by space environment simulation tests to be carried out on ground. These tests must be simple (addressing only the most dangerous environment elements) and they must give reliable data in accelerated conditions.

Several facilities enabling one to perform combined environment tests (vacuum, UV, electrons, protons, thermal cycling) with *in situ* measure of material properties, have been widely used at the laboratories of DERTS in Toulouse for the last fifteen years. They have been improved over years and recently complemented with an equipment allowing material testing under atomic oxygen bombardment.

However, there are very few possibilities of comparison between actual degradation data obtained in space and space simulation test data obtained in laboratory.

The Experiment AO 138-6 "Spacecraft Thermal Control Coatings" was designed in order to meet this goal of comparison. This Experiment was a part of the FRECOPA project and was flown on LDEF[1].

Objectives

The purpose of AO 138-6 was:

- evaluate the degradation experienced in space by a number of materials on board spacecraft placed into Low Earth Orbit (LEO) by a Space Shuttle,

- validate simulation techniques used at DERTS, specially those employing UV-irradiations with *in situ* and *ex situ* measurements.

The exact objectives were:

a) expose material surfaces to

- either the whole environment for a satellite placed and retrieved in LEO by a Space Shuttle in all the mission phases (handling before launch, ascent, manœuvers in orbit, external Shuttle environment, docking, retrieving, descent, transportation to KSC...),

- or only the satellite environment during its autonomous free flight,

b) retrieve samples for laboratory analysis,

c) observe them; compare their thermo-optical properties after flight to the initial ones,

d) compare flight degradation data to laboratory degradation data obtained after UV-irradiation tests,

e) evaluate possible contamination effects due to the use of the Shuttle.

---

[1] NASA Long Duration Exposure Facility.

Most of these objectives have been reached in spite of a few programme modifications necessitated by the long delay of LDEF retrieval.

EXPERIMENT DESCRIPTION

The experiment was designed in order to allow exposure of a part of the samples to the whole spacecraft environment (in all mission phases); these samples were laid directly on the FRECOPA tray surface on two separate sample holders.

The other part of samples was protected from the external environment of LDEF for all mission phases, except free flight, by the means of a vacuum-tight FRECOPA canister in which they were stored. This canister was clock-operated; it was opened 10 days after separation from Shuttle and closed 10 months later, according to the initial operation schedule of LDEF. An O-ring butyl seal kept the samples under vacuum in the canister, after retrieval till laboratory analysis. Therefore initial plans called for spectral reflectance measurements to be performed at laboratory in a vacuum chamber after retrieving of the closed canister. For that purpose the FRECOPA canister had been designed[1] in order to be also opened and closed in the vacuum chamber, thus avoiding, at maximum, air recoveries[2].

Thirty samples were placed inside canister; twenty-four other were placed on the external tray. All (except one OSR) were 2 x 2 cm in size and their surface was in the same reference plane chosen for maximizing solar illumination; they were mounted independently in the sample-holders by spring system (see Figures 1 and 2). Irreversible maximum temperature sensors ("Temp-Plates®") were bonded to the sample substrates and sample-holders.

AO 138-6 was part of the FRECOPA experiment located on the trailing edge of LDEF.

MATERIALS

The Thermal Control Coatings (TCC) and materials tested are listed in Table 1. They belong to several categories: conductive or non-conductive paints (white, black, aluminized), SSMs[3] (silvered Teflon® FEP, aluminized Teflon® FEP, aluminized Kapton®), surface coatings (anodisations, MgF_2 layers, conductive ITO layers), organix-matrix composites (carbon/epoxy and Kevlar®/epoxy materials), OSRs[4]. The paints were applied onto aluminum or carbon/epoxy substrates.

---

1 C. Durin, Post-flight system analysis of FRECOPA (AO 138), Proceedings First LDEF Post-retrieval Symposium, Kissimee, FA, June 2-8, 1991.

2 The 4-year delay in LDEF retrieving have obliged to cancel the optical measure in vacuo planned for the canister samples, because the vacuum measurement chamber was part of a combined environment facility which was totally dismantled for complete transformation during this period of time.

3 Second Surface Mirrors.

4 Optical Solar Reflectors

OPERATIONS

Two complete AO 138-6 models have been integrated. One has been flown, the spare model has been stored in clean laboratory conditions for the complete LDEF mission duration and subsequently used as reference model during the post-flight analysis.

The delay of the LDEF retrieval (69 months in space instead of 10 months initially planned) has had two consequences :

a) The exposure of samples to space has not been equivalent for samples on the surface of the tray (69 months) and those inside the canister (10 months); this fact does not enable one to discriminate easily the features of an exposure of materials to the Shuttle-induced environment.

b) The *in vacuo* measure of spectral reflectance planned initially for the retrieved samples kept in the canister and still under vacuum has not been possible, because of the non-availability of the optical system (see foot-note at Section 2).

Visual inspection at KSC and at CNES/Toulouse revealed no trace of contamination on the tray surface. The canister was closed.

The pressure inside the canister was measured (after expansion of an external pressure loop connected to the canister); its value was 1.6 ± 0.06 mbar (N_2-equivalent). By GC/MS technique performed on the loop, the composition of residual gas was determined to be 79 % N_2, 13 % O_2 and 8% CO_2. After these measurements, the canister was connected to a vacuum line in order to get again high vacuum conditions in conformity with the Procedure of Operations. Unfortunately a leak happened when the valve was disconnected from the canister, and air was admitted to samples at atmospheric pressure.

In such conditions, no attempt was made for taking quick measurements of the solar reflectance of samples with a portable equipment under neutral Argon atmosphere. These measurements were thus only obtained in air for all samples using an Alphameter ELAN.

Detailed visual, photographic and microscopic inspections were performed. As for the samples at the surface of the FRECOPA tray, nothing unexpected was noted (no evidence of contamination). The maximum temperature sensors "Temp-Plates" were compared to those on the reference model; it was observed that the colour changes were similar on the flight model and on the reference model which had been kept in normal laboratory conditions. Thus no meaningful estimates of the maximum temperature actually experienced by the samples during flight are possible from the readings on the Temp-plates.

Spectral optical measurements of the reflectance and/or transmittance have been carried out with integrating spheres mounted on either a Beckman DK2A spectrophotometer (samples of canister) or a Beckman Acta M VII (samples of the tray). Solar absorptances and transmittances have been computed from the measurement values in the wavelength range 280 - 2300 nm.

Emissivities have been obtained with a Gier & Dunckle DB100 infrared reflectometer.

SUMMARY OF ENVIRONMENT CONDITIONS

Satellite: 3-axis, gravity gradient stabilized.

LDEF orbit: circular, 28°5 inclination, initial altitude 464 km (250 N. M.), altitude at capture 330 km.

Flight duration: 2105 days (69 months).

FRECOPA was on the trailing edge of LDEF. The samples were not receiving oxygen atoms during the mission (except for a very short period during capture : the corresponding fluence is estimated to be less than 5.7 10^{17} atoms cm^{-2}).

Sun illumination: 11100 equivalent sun hours (esh)[1] for samples at the surface of the tray, 1582 esh for those placed in the canister.

Albedo: 3981 esh for samples at the surface of the tray, 562 esh for those in the canister.

Particle irradiation: 3 10^5 rads, mainly due to electrons.

Thermal cycling: 34000 cycles. The temperature of samples can be estimated from the solar/vacuum tests performed on the Integration Model of FRECOPA, see Table 2.

RESULTS

The variations of solar reflectance and emissivity are given in Table 3. The variation is computed as the difference: final value - initial value.

COMPARISON BETWEEN FLIGHT AND LABORATORY DATA

For all the white paints, the spectral reflectance spectra recorded on the LDEF samples show a clear decrease of reflectance in the visible and ultraviolet part of spectrum and, simultaneously, a slight increase in the infrared. This increase in the infrared is weak for the white paints PSB, A276, PV100 and PCB-T; it is more obvious for S36, PSG 120 and PCB-Z (see Figures 3, 4 and 5 as examples).

This behaviour in the infrared was not foreseen. All the paints irradiated in a vacuum at laboratory with UV radiation and measured *in situ* had shown a reflectance decrease over the whole solar spectrum[2]. Post-irradiation exposures to air gave a recovery of degradation which was often partial in visible and ultraviolet

---

1 R. J. Bourassa, Post-flight system analysis of FRECOPA (AO 138), Proceedings First LDEF Post-retrieval Symposium, Kissimee, FA, June 2-8, 1991.

2 Except for A276 the reflectance spectrum of which is not modified in infrared.

and often nearly total in the infrared part of the spectrum; however a reflectance higher than the initial had only been observed in the case of the PSB paint.

Also the damage is often more pronounced in UV- visible on the paint samples of canister than on those irradiated in laboratory conditions.

Tables 4 and 5 give a comparison between degradation data from flight and from UV irradiations, previously performed at DERTS, for which *in situ* as well as *ex situ* measurements are available. Almost all degradation values measured after the flight for the samples in the canister are exceeding the ones predicted from *ex situ* measurements[1] at the same irradiation level (approximately 1500 esh). The discrepancies are maximum for PSB, S36, PSG 120 and aluminized Kapton.

However one must emphasize that these laboratory irradiation experiments were carried out seven years ago, in a facility equipped with a rather inaccurate optical reflectance measurement system: the uncertainty in the solar absorptance values was $\pm$ 0.01, but the uncertainty in spectral reflectance at wavelength above 1200 nm could reach $\pm$ 0.03. This feature should not obliterate the systematic tendency towards enhanced solar absorptance degradation observed in flight samples, but could explain that some increases of the infrared reflection have been ignored in laboratory experiments.

Several explanations of the too high degradation experienced by the materials in the canister can be given tentatively:

a) Contamination of samples: a contaminant layer when irradiated by solar UV radiation can lead to an enhanced solar absorptance. However the optical reflectance spectra measured on the OSRs, aluminum and FEP samples do not indicate the presence of contaminants. Moreover no evidence of Silicon or any other foreign element has been found by RBS or XPS methods on the aluminum and FEP samples of the Experiment AO 138-6 present in the canister or on the tray. These methods applied to other parts of the FRECOPA structure have shown Silicon in surface layers as thin as 50 to 75 Å; from the known sensitivity of these methods (approximately 10 Å for RBS) the contaminant thickness on the samples of Experiment AO 138-6 can be estimated to be definitely less than 50 Å. Some laboratory experiments at DERTS on OSR samples pre-contaminated with RTV silicones before their irradiation, indicate[2] that the solar reflectance increase ΔR_S due to a contaminant 50 Å thick (obtained from the VCM of a RTV 566 silicone, after combined irradiations simulating 7 years in GEO) is less than 0.01. Thus the high degradation which has been actually obtained in space is not fully explained by a silicone layer the thickness of which would be less than 50 Å.

b) Deficiency in the far UV of irradiations performed on ground: virtually no radiation with wavelength inferior to 185 nm is delivered by the UV sources used at DERTS. Far UV radiation at wavelength as low as that of Lyman-α ray is present in space on surfaces illuminated by the sun.

c) Depth of the thermal cycling: sample temperatures can have varied between -40 and + 85°C either during their exposure to space or after closure of the canister (see Section 5); all the standard UV irradiations have been performed at the laboratory at room temperature or at + 40°C. The radiation damage is probably enhanced at higher temperature; the binders of the white paints could be more altered which could cause the more pronounced changes observed in UV-visible.

---

1 The *ex situ* values should be comparable to the LDEF values since they have been obtained in air on specimens irradiated in vacuum. The *in situ* values should be comparable to those which would have been observed in orbit, without air recovery.

2 J. Marco, A. Paillous, Long-term tests of contaminated OSRs under combined environment. Proceedings Third European Symposium on Spacecraft Materials in Space Environment, p. 245, ESTEC, Noordwijk, The Netherlands, October 1-4, 1985.

LONG-TERM BEHAVIOUR

As a general statement it can be said that the degradation values obtained for the samples in the canister are smaller than those measured for those of same materials on tray, see Table 6. This is qualitatively in conformity with the illumination conditions: respectively 1582 and 11100 esh; however the difference is rather slight for the solar reflectance degradation values. This reduced gap could be explained by a higher temperature of the samples in the canister inducing exaggerated damage as compared to that of the samples on the tray (see Table 3). By the way, a deficiency in far UV of irradiation tests performed on ground (as mentionned at Section 7) can be ruled out because the degradation would have been far larger for the samples on the tray than for those in the canister.

The white silicate paint PSB constitutes a unique but major exception: Figures 6 and 7. The solar reflectance change is only $\Delta R_S = -0.01$ for the two samples on the tray but is far more important ($\Delta R_S = -0.05$) for the sample in the canister. Here also this difference could be explained by the higher temperature in canister; an other hypothesis could be a large recovery of the radiation damage of this paint during the short time exposure of the FRECOPA tray to oxygen atoms (see Section 5). This would require further investigation.

MATERIAL STABILITY

Forty five materials have been exposed to space environment in Experiment AO 138-6. The measured degradations of solar reflectance are given in Table 3. One must remember that:

a) all these results are related to samples irradiated with solar UV in high vacuum conditions in LEO, but returned to the earth atmosphere in which air recoveries have occurred on most material classes,

b) the samples have not received oxygen atoms in orbit (except the limited fluence during the capture) because FRECOPA was located on the trailing edge of LDEF.

The reflectance of most white paints and polymeric films has been probably severely degraded in space but a more or less important bleaching has been the consequence of the return to Earth and the degradations have been obliterated at least partly.

All black paints are more reflecting after flight.

The excellent behaviours of the OSR and the white conductive paint PCB-Z must be underlined.

The SSMs made of FEP Teflon show excellent clarity and specularity in contrast with the samples placed on other locations on LDEF and having received O-atoms. The stability of ITO layers depends largely on the manufacturing process which has been used; ITO has been proved quite effective in protecting Kapton from UV radiation.

CONCLUSION

The Experiment AO 138-6 has allowed retrieval of 45 material samples exposed on board the LDEF satellite to either the total mission flight or only the LEO environment. The samples have been retrieved in excellent conditions and their thermo-optical properties have been measured in laboratory.

The samples were located in the wake of LDEF during flight and have undergone only very high vacuum, solar UV irradiation and thermal cycling.

Contamination of the samples by the external and internal environments of the Space Shuttle seems to have been extremely weak, enabling us to obtain trustworthy data on space damage.

As a general statement a good spectral concordance between the flight results and laboratory UV-irradiation data is observed for all samples not in the canister, so long as air recoveries are taken into account. The degradation measured on the LDEF samples situated in the canister is slightly more important than the one which could be predicted from UV-irradiation tests performed at laboratory at room temperature (or at +40°C). The reason of this discrepancy is probably the large thermal cycling experienced by the samples in space; further experimental studies are required in order to elucidate this point

Table 1: List of materials tested in Experiment AO 138-6 on board LDEF.

BOX	PLATE	NUMBER	CLASS	CHEMICAL NATURE	REFERENCE	SUBSTRATE	MANUFACTURER	ORIGIN
X		D5	Aluminum paint	Aluminum / silicone	PSG 173	Aluminum	ASTRAL	CNES/TH
X		E6	Black Kapton	Black Kapton	G 113600	Bonded to AU4G with 3MY966	SHELDAL	Aérospatiale Cannes
X		E5	Black paint	Polyurethane	PU 1	AU4G	ASTRAL	Aérospatiale Cannes
X		A4	Black paint	Graphite / silicone	VHT SP 102	(0,05 mm)	SPEREX	Aérospatiale Cannes
X		A3	Black paint	Graphite / silicone	HT 650	TA6V (0,5 mm)	FIBA	Aérospatiale Cannes
X		B7	Black paint / Kapton	Polyurethane	Z 306	Kapton 100	Hughson Chemicals	Aérospatiale Cannes
	X	F4	Composite material	Carbon fibers / epoxy		Bonded to Ti with space adhes.	Aérospatiale Aqultaine	Aérospatiale Aquitaine
	X	F3	Composite material	Carbon fibers / epoxy		bonded to CFRP with space adhes.	Aérospatiale Aquitaine	Aérospatiale Aquitaine
	X	F2	Composite material	Carbon fibers / epoxy			Aérospatiale Aquitaine	Aérospatiale Aquitaine
	X	F1	Composite material	Kevlar Fibers / epoxy			Aérospatiale Aquitaine	Aérospatiale Aquitaine
	X	H3	Conductive black paint	Carbon / polyurethane	313-BCU (B-2)		GSFC & Hughson	NASA / GSFC
	X	H2	Conductive black paint	Carbon / silicone	313-BCS (A-2)		GSFC & GE	NASA /GSFC
X		D4	Conductive black paint	Polyurethane	Chemglaze L300 (80 microns)	Pyrolac P123 primer / alu	Hughson Chemicals	ESTEC
X		A7	Conductive black paint	Graphite / polyurethane	PNC	Aluminum	CNES/TH	CNES/TH
	X	G9	Conductive SSM	Silvered FEP + ITO	200 A° WRF 5.5.80 ITO		General Electric	DERTS (USAF/AFML)
	X	G8	Conductive SSM	Silvered FEP + ITO	8 ITO 200 RF 5.3.80		General Electric	DERTS (USAF/AFML)
	X	G5	Conductive SSM	Aluminized Kapton + ITO	838 K3		General Electric	DERTS (USAF/AFML)
	X	F12	Conductive SSM	Silvered FEP (125 microns) + ITO			SHELDAHL	DERTS
X		C6	Conductive SSM	Aluminized Kapton + ITO	838 K3		General Electric	DERTS (USAF/AFML)
X		C3	Conductive SSM	Silvered FEP (125 microns) + ITO	G 409 450		SHELDAL	DERTS
X		B4	Conductive SSM	Silvered FEP (125 microns) + ITO	8 ITO 200 RF (5.3.80)		General Electric	DERTS (USAF/AFML)
X		C4	Conductive white paint	Zinc orthostannate / silicone	PCB-Z	Aluminum	CNES/TH	CNES/TH
X		A2	Conductive white paint	Tin orthotitanate / silicone	PCB-T	Aluminum	CNES/TH	CNES/TH
	X	G4	Fabric	Teflon-impregnated glass fabric	Betacloth	Bonded to aluminum	Du Pont de Nemours	ESTEC
X		C7	Fabric	Teflon-impregnated glass fabric	Betacloth		Du Pont de Nemours	ESTEC
X		C2	OSR	Silvered silica			OCLI	Aérospatiale Cannes
X		C1	OSR	Silvered silica			OCLI	Aérospatiale Cannes
X		B2	OSR	Silvered silica			OCLI	Aérospatiale Cannes
X		B1	OSR	Silvered silica			OCLI	Aérospatiale Cannes
	X	G3	Polymeric film	Polyimide Kapton	Kapton H (12 microns)	Over AG5	Du Pont de Nemours	DERTS
	X	G2	Polymeric film	Polyimide Kapton	Kapton H (50 microns)	Over AG5	Du Pont de Nemours	DERTS
	X	G12	Polymeric film	FEP Teflon (125 microns)			Du Pont de Nemours	DERTS
	X	F10	Polymeric film	Polyimide Kapton	Kapton H (50 microns)	Over AG5	Du Pont de Nemours	DERTS
	X	G7	Silica fabric	Astroquartz / FEP / aluminum	581 Lot 98269		General Electric	DERTS (USAF/AFML)
	X	H1	SSM	Aluminized Kapton + silicone	Hirschfields Nr4		King-Seeley	NASA / GSFC
	X	F7	SSM	Silvered FEP (125 microns)	G 401500		SHELDAL	DERTS
	X	F5	SSM	Aluminized Kapton (25 microns)	39 116 (charge moyenne)		REXOR	CNES/BA
	X	F11	SSM	Aluminized Kapton (12 microns)	(charge max)		CAMVAC	CNES/BA
X		E2	SSM	Aluminized Kapton (25 microns)	(charge max)		CAMVAC	CNES/BA
X		D7	SSM	Aluminized Kapton (25 microns)	39 116 (charge moyenne)		REXOR	CNES/BA
X		D1	SSM	Silvered FEP (125 microns) + adhesive	G 401 901	AU4G1	SHELDAL	Aérospatiale Cannes
X		C5	SSM	Aluminized Kapton (25 microns)	G405150	Bonded to AU4G with 3MY966	SHELDAL	Aérospatiale Cannes
X		B3	SSM	Silvered FEP (125 microns)	G 401500		SHELDAL	DERTS
	X	G6	Surface coating	Vacuum deposited aluminum		Aluminum A5	DERTS	DERTS
	X	G11	Surface coating	Kapton H (25 microns) alum. both sides	703638		REXOR	CNES/TH
	X	F6	Surface coating	Vacuum deposited aluminum		Aluminum A5	DERTS	DERTS
X		E7	Surface coating	Chemical anodization		AU4G	Aérospatiale Cannes	Aérospatiale Cannes
X		E4	Surface coating	MgF2 / aluminum coating	Amplivex 90 IR métallique	Aluminum A5	MTO	DERTS
X		D2	Surface coating	Vacuum deposited aluminum		Aluminum A5	DERTS	DERTS
	X	G10	White paint	Zinc orthotitanate /silicone	S36	Aluminum	CNES/TH	CNES/TH
	X	G1	White paint	Zinc orthotitanate / silicate	PSB	Aluminum	CNES/TH	CNES/TH
	X	F9	White paint	Zinc orthotitanate /silicone	S36	Aluminum	CNES/TH	CNES/TH
	X	F8	White paint	Zinc orthotitanate / silicate	PSB	Aluminum	CNES/TH	CNES/TH
X		E3	White paint	ZnO / silicone	PSG 120 (Ref. 18)	Carbon fibers	ASTRAL	Aérospatiale Les Mureaux
X		D6	White paint	ZnO / silicone	PSG 120 (Ref. 17)	Carbon fibers	ASTRAL	Aérospatiale Les Mureaux
X		D3	White paint	Zinc orthotitanate / silicate	PSB	Aluminum	CNES/TH	CNES/TH
X		B6	White paint	ZnO / silicone	PSG 120 FD	Aluminum	ASTRAL	CNES/TH
X		B5	White paint	TiO2 / silicone	PV100	Carbon fibers	VITAVAR	Aérospatiale Les Mureaux
X		A6	White paint	Polyurethane	Chemglaze II A276 (70 microns)	Aluminum	Hughson Chemicals	ESTEC
X		A5	White paint	Zinc orthotitanate / silicone	S36	Aluminum	CNES/TH	CNES/TH

Table 2: Temperature of samples during flight.

Location	Conditions	Maximum temperature (°C)	Minimum temperature (°C)
Tray	opened	49 to 63	-43 to -52
Box	closed	67 to 85	-33 to -40
Box		65 to 82	-20 to -26

Table 3: Changes in thermo-optical properties of A0 138-6 samples.

BOX	PLATE	NUMBER	CLASS	CHEMICAL NATURE	REFERENCE	INIT. SOLAR REFL.	SOLAR REFL. CH.	INIT. TRANSM.	TRANSM. CH.	INIT. EMISSIV.	EMISSIV. CH.
X		D5	Aluminum paint	Aluminum / silicone	PSG 173	0,690	-0,080			0,317	-0,006
X		E6	Black Kapton	Black Kapton	G 113600	0,050	0,040			0,845	-0,012
X		E5	Black paint	Polyurethane	PU 1	0,030	0,040			0,885	-0,002
X		A4	Black paint	Graphite / silicone	VHT SP 102	0,050	0,013			0,860	0,001
X		A3	Black paint	Graphite / silicone	HT 650	0,030	0,010			0,873	-0,001
X		B7	Black paint / Kapton	Polyurethane	Z 306	0,040	0,035			0,906	-0,008
	X	F4	Composite material	Carbon fibers / epoxy		0,080	0,020			0,801	-0,012
	X	F3	Composite material	Carbon fibers / epoxy		0,090	0,010			0,778	0,051
	X	F2	Composite material	Carbon fibers / epoxy		0,080	0,030			0,836	-0,048
	X	F1	Composite material	Kevlar Fibers / epoxy		0,430	-0,090			0,896	-0,006
	X	H3	Conductive black paint	Carbon / polyurethane	313-BCU (B-2)	0,030	0,010				
	X	H2	Conductive black paint	Carbon / silicone	313-BCS (A-2)	0,030	0,010				
X		D4	Conductive black paint	Polyurethane	Chemglaze L300 (80 microns)	0,050	0,035			0,843	-0,013
X		A7	Conductive black paint	Graphite / polyurethane	PNC	0,080	0,020			0,796	-0,040
	X	G9	Conductive SSM	Silvered FEP + ITO	200 A° WRF 5.5.80 ITO	0,890	0,000			0,804	0,011
	X	G8	Conductive SSM	Silvered FEP + ITO	8 ITO 200 RF 5.3.80	0,910	-0,040			0,810	0,009
	X	G5	Conductive SSM	Aluminized Kapton + ITO	838 K3	0,610	-0,020			0,762	-0,013
	X	F12	Conductive SSM	Silvered FEP (125 microns) + ITO		0,910	-0,030			0,803	0,007
X		C6	Conductive SSM	Aluminized Kapton + ITO	838 K3	0,600	-0,020			0,762	-0,041
X		C3	Conductive SSM	Silvered FEP (125 microns) + ITO	G 409 450	0,900	0,000			0,804	0,002
X		B4	Conductive SSM	Silvered FEP (125 microns) + ITO	8 ITO 200 RF (5.3.80)	0,900	0,000			0,810	0,006
X		C4	Conductive white paint	Zinc orthostannate / silicone	PCB-Z	0,780	-0,040			0,872	0,000
X		A2	Conductive white paint	Tin orthotitanate / silicone	PCB-T	0,720	-0,100			0,815	0,000
	X	G4	Fabric	Teflon-impregnated glass fabric	Beta cloth	0,700	-0,140			0,895	0,001
X		C7	Fabric	Teflon-impregnated glass fabric	Beta cloth	0,680	-0,100			0,895	0,000
X		C2	OSR	Silvered silica		0,940	-0,010			0,798	0,000
X		C1	OSR	Silvered silica		0,940	-0,010			0,798	0,000
X		B2	OSR	Silvered silica		0,940	-0,010			0,798	0,000
X		B1	OSR	Silvered silica		0,940	-0,010			0,798	0,000
	X	G3	Polymeric film	Polyimide Kapton	Kapton H (12 microns)	0,210	0,000	0,550	-0,030	0,694	-0,015
	X	G2	Polymeric film	Polyimide Kapton	Kapton H (50 microns)	0,130	0,020	0,600	-0,030	0,778	-0,004
	X	G12	Polymeric film	FEP Teflon (125 microns)		0,060	0,010	0,920	-0,010	0,802	0,003
	X	F10	Polymeric film	Polyimide Kapton	Kapton H (50 microns)	0,130	0,010	0,600	-0,020	0,778	-0,004
	X	G7	Silica fabric	Astroquartz / FEP / aluminum	581 Lot 98269	0,830	-0,050			0,845	-0,760
	X	H1	SSM	Aluminized Kapton + silicone	Hirschfields Nr4	0,550	-0,010				
	X	F7	SSM	Silvered FEP (125 microns)	G 401500	0,930	-0,010			0,795	0,000
	X	F5	SSM	Aluminized Kapton (25 microns)	39 116 (charge moyenne)	0,650	-0,030			0,667	-0,003
	X	F11	SSM	Aluminized Kapton (12 microns)	(charge max)	0,670	-0,040			0,556	-0,014
X		E2	SSM	Aluminized Kapton (25 microns)	(charge max)	0,660	-0,020			0,551	-0,001
X		D7	SSM	Aluminized Kapton (25 microns)	39 116 (charge moyenne)	0,640	-0,020			0,667	-0,005
X		D1	SSM	Silvered FEP (125 microns) + adhesive	G 401 901	0,920	-0,010			0,795	0,000
X		C5	SSM	Aluminized Kapton (25 microns)	G405150	0,640	-0,030			0,650	-0,002
X		B3	SSM	Silvered FEP (125 microns)	G 401500	0,930	-0,020			0,795	0,001
	X	G6	Surface coating	Vacuum deposited aluminum		0,900	0,000			0,023	-0,001
	X	G11	Surface coating	Kapton H (25 microns) alum. both sides	703638	0,910	-0,010			0,027	-0,002
	X	F6	Surface coating	Vacuum deposited aluminum		0,910	0,000			0,023	-0,002
X		E7	Surface coating	Chemical anodization		0,520	-0,060			0,343	0,000
X		E4	Surface coating	MgF2 / aluminum coating	Amplivex 90 IR métallique	0,890	-0,030			0,025	-0,001
X		D2	Surface coating	Vacuum deposited aluminum		0,900	-0,010			0,023	-0,002
	X	G10	White paint	Zinc orthotitanate /silicone	S36	0,820	-0,080			0,854	0,001
	X	G1	White paint	Zinc orthotitanate / silicate	PSB	0,820	-0,010			0,895	-0,003
	X	F9	White paint	Zinc orthotitanate /silicone	S36	0,820	-0,080			0,856	-0,003
	X	F8	White paint	Zinc orthotitanate / silicate	PSB	0,820	-0,010			0,895	-0,003
X		E3	White paint	ZnO / silicone	PSG 120 (Ref. 18)	0,820	-0,070			0,880	-0,001
X		D6	White paint	ZnO / silicone	PSG 120 (Ref. 17)	0,780	-0,070			0,876	-0,002
X		D3	White paint	Zinc orthotitanate / silicate	PSB	0,850	-0,060			0,895	-0,001
X		B6	White paint	ZnO / silicone	PSG 120 FD	0,810	-0,060			0,872	-0,003
X		B5	White paint	TiO2 / silicone	PV100	0,780	-0,080			0,865	-0,001
X		A6	White paint	Polyurethane	Chemglaze II A276 (70 microns	0,750	-0,240			0,877	-0,005
X		A5	White paint	Zinc orthotitanate / silicone	S36	0,800	-0,040			0,856	-0,001

Table 4: Comparison between flight results and laboratory degradation predictions.

	UV simulation results[1]			Degradation predicted	Actual LDEF degradation	
Material nature	esh number	ΔR_S[2] *in situ*	ΔR_S *ex situ* (with air recovery)	Samples in canister for 1450 esh (1450 esh)	Samples in canister (11100 esh)	Samples on tray
PSB1000	-0.028	-0.019	≅-0.028	-0.050	-0.010	
S361000	-0.055	-.015	≅ -0.020	-0.040	-0.08	
PSG 120FD	600	-0.033	-0.022	≅-0.030	-0.075	-
A 276	1250	-0.307	-0.270	-0.270	-0.250	-
PCB-T	1500	-0.140	-0.085	-0.085	-0.100	-
PCB-Z	1500	-0.030	-0,020	-0.020	-0.030	-
FEP700	-0.007	-0.007	≅-0.012	-0.014	-0.010	
Kapton alu	1500	≅-0.012	≅-0.008	≅-0.008	-0.025	-0.035
Kapton alu (conductive)	1500	-0.035	-0.018	-0.018	-0.020	-0.020
Betacloth	1500	-0.11	-0.10	-0.100	-0.100	-0.130

1 UV irradiation performed under high vacuum at room temperature.

2 ΔRs = final solar reflectance - initial solar reflectance.

Table 5: Ratio between flight degradations and degradations predicted from UV irradiations at laboratory.

Material	Ratio between ΔR_S values measured in the FRECOPA box and those predicted
PSB	1.8
S36	2.0
PSG 120FD	2.5
A 276	0.9
PCB-T	1.2
PCB-Z	1.5
FEP	1.2
Aluminized Kapton	3.0
Conductive aluminized Kapton	1.1
Betacloth	1.0

Table 6: Solar reflectance changes measured for FRECOPA samples in canister and on the tray.

Material nature	Actual degradation on LDEF	
	Canister	Tray
PSB	-0.05	-0.01
S36	-0.04	-0.08
FEP/silver	-0.015	-0.010
Kapton/aluminum	-0.025	-0.035
ITO/FEP/silver	0	0 à -0.04
ITO/Kapton/aluminum	-0.02	-0.02
Betacloth	-0.10	-0.13

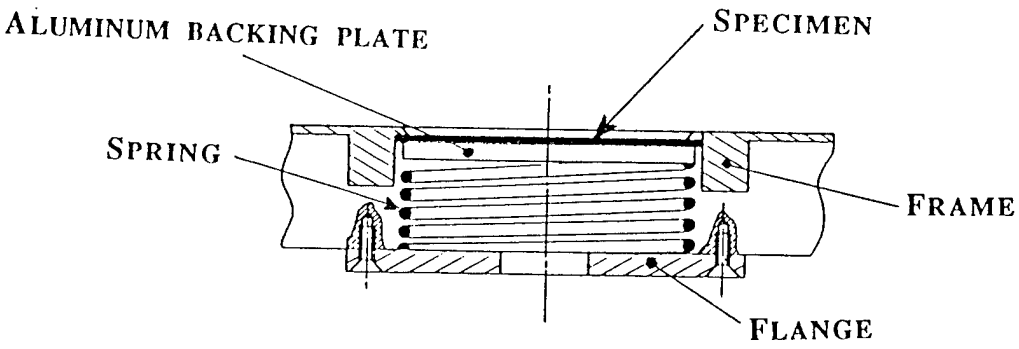


Figure 1: Mounting of specimens in the sample-holder.

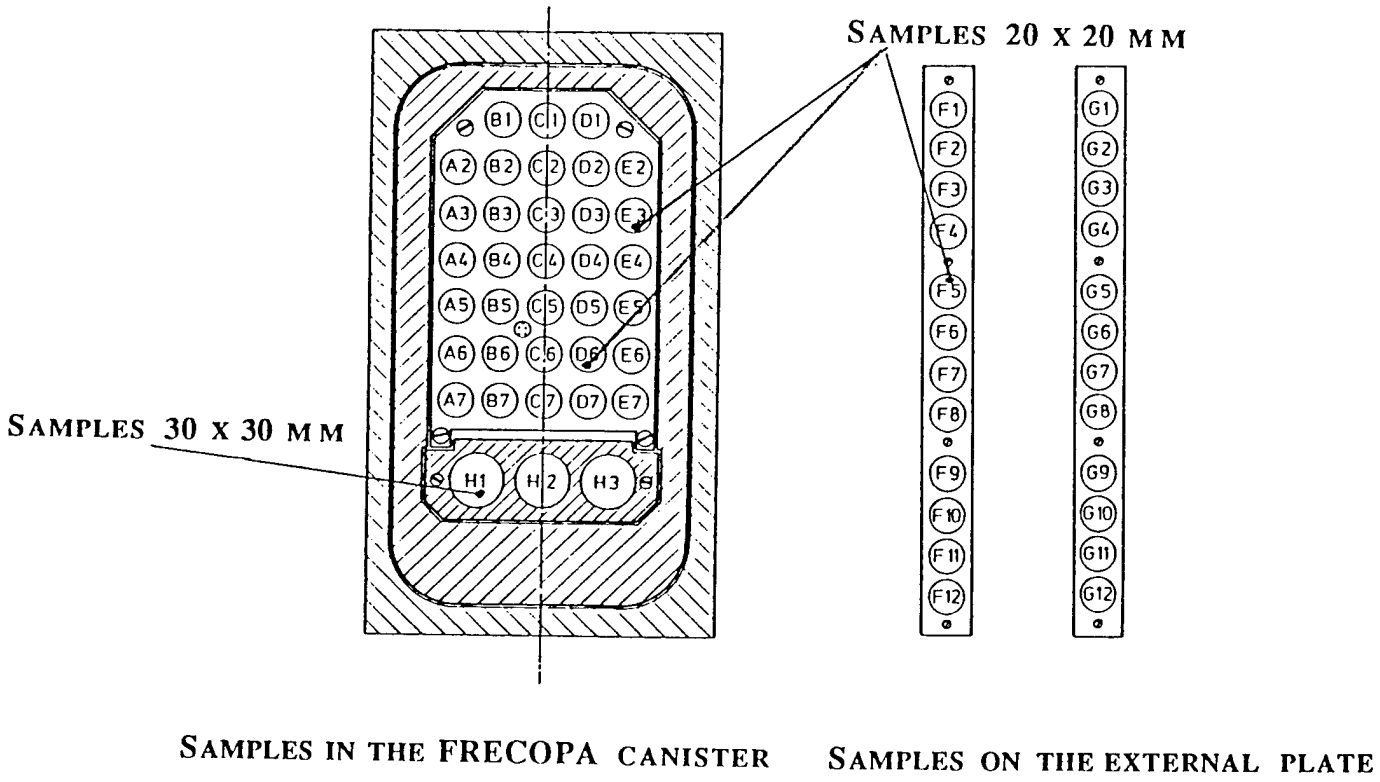


Figure 2: The sample-holders of Experiment AO 138-6.

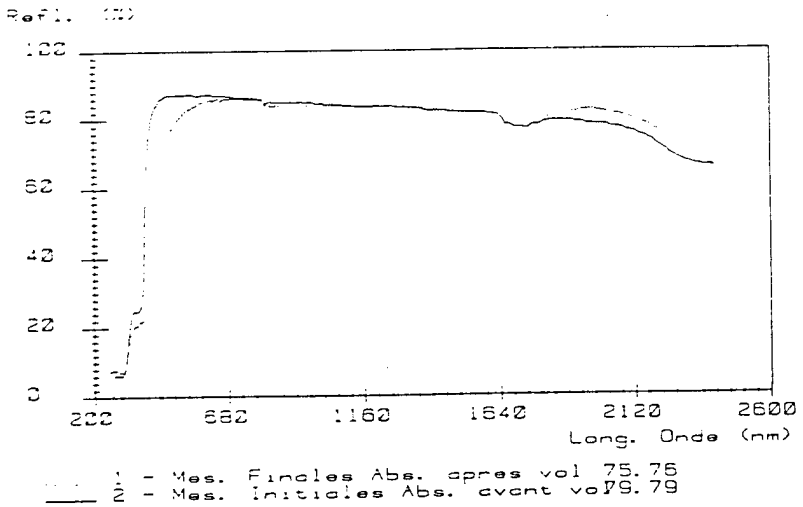


Figure 3: Reflectance spectra of the S36 white paint (sample in the canister).

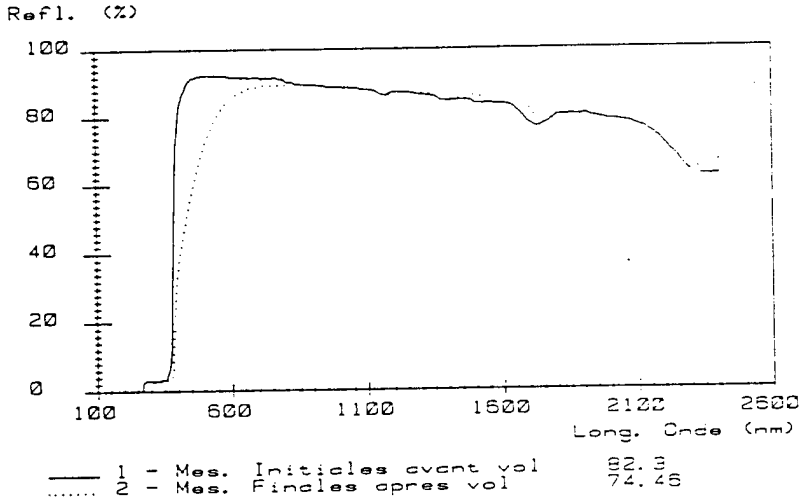


Figure 4: Reflectance spectra of the PSG120 white paint (sample in the canister).

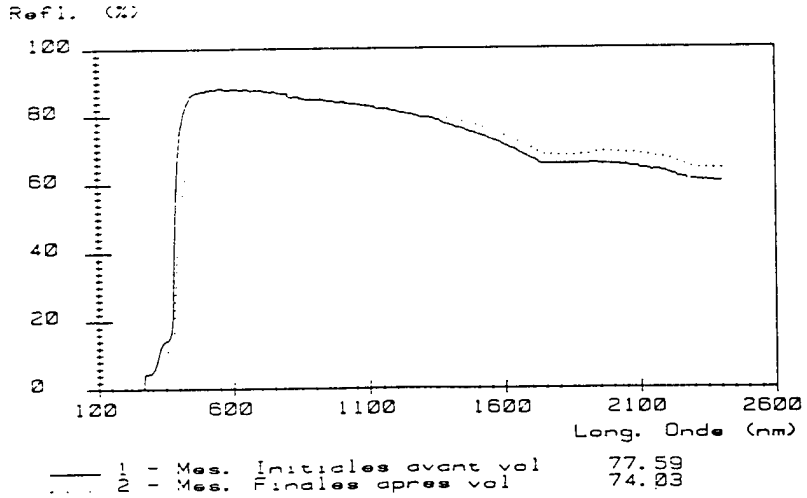


Figure 5: Reflectance spectra of the PCB-Z white paint (sample in the canister).

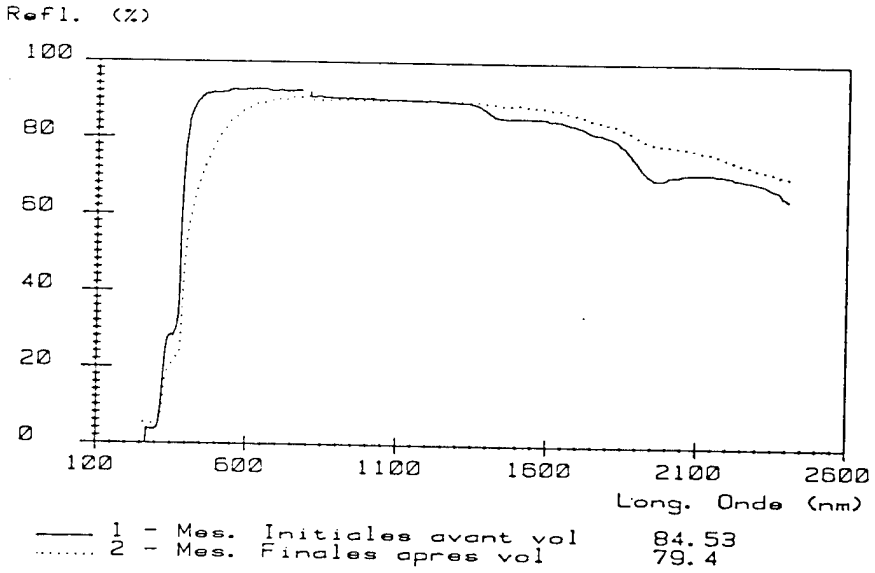


Figure 6: Reflectance spectra of the PSB white paint (sample in the canister).

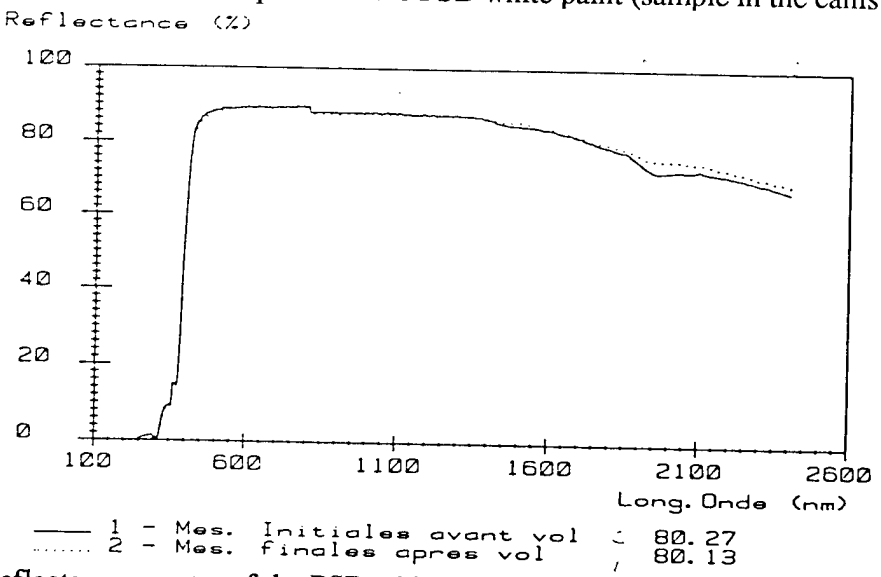


Figure 7: Reflectance spectra of the PSB white paint (sample on the external surface of tray).

LONG DURATION EXPOSURE FACILITY
EXPERIMENT M0003-5
THERMAL CONTROL MATERIALS

Charles J. Hurley
University of Dayton Research Institute
Dayton, OH 45469-0137
Phone: 513/255-3220, FAX: 513/258-8075

SUMMARY

The LDEF M0003-5 Thermal Control Materials Experiment contained numerous thermal control coatings, metallized and nonmetallized polymeric films, adhesives, optical solar reflectors and metallic foils. The materials were located on the leading and trailing edges of the satellite, therefore exposed to two different low earth orbital environments. Many specimens received total exposure periods of 0.9 years and 5.75 years respectively. This paper visually exhibits a small selection of the total number of flight specimens. This paper summarizes the material's physical and optical performance as a function of location and duration of exposure. Comments concerning specimen condition, degradation, contamination, optical reflectance and transmittance are provided.

INTRODUCTION

The experiment was sponsored by the Wright Laboratory Materials Directorate, Wright-Patterson Air Force Base, OH. The objective of the experiment was to understand the changes in the properties and structure of materials after exposure to the space environment and compare changes with predictions based on laboratory experiments. The approach taken was to measure the optical and physical properties of materials before and after long term space exposure to the low earth orbital environment (UV, electrons, protons, atomic oxygen, thermal cycling, vacuum, debris and micrometeoroids).

THERMAL CONTROL MATERIALS

A Series

Pigmented Coatings	44
Metallized Polymer Films	28
Quartz Fabrics	8

B Series

Optical Solar Reflectors (Second surface)	8
Gold Mirrors (First surface)	4
Silver Mirrors (First surface)	6
Aluminum Mirrors (First surface)	4

C Series

Metallized Polymeric Films	8
Metallized Bonded Films	14
Clear Films	10
Total	134

FLIGHT SPECIMEN LOCATIONS

Tray L3 - Location D9

Leading Edge -RAM Direction - Exposure 5 yr 10 mth

A Series (0.9375 in. dia. discs)	22
B Series (1.000 x 1.000 in. squares)	6
C Series (7.000 x 1.000 in. strips)	16

Tray L6 - Location D8

Leading Edge -RAM Direction - minus 30 degrees - Exposure 1 yr

A Series (0.9375 in. dia. discs)	22
B Series (1.000 x 1.000 in. squares)	5

Tray T3 - Location D3

Trailing Edge - Exposure 5 yr 10 mth

A Series (0.9375 in. dia. discs)	22
B Series (1.000 x 1.000 in. squares)	6
C Series (7.000 x 1.000 in. strips)	16

Tray T6 - Location D4

Trailing Edge - minus 30 degrees - Exposure 1 yr

A Series (0.9375 in. dia. discs)	14
B Series (1.000 x 1.000 in. squares)	5

PRELIMINARY RESULTS

A selection of thermal control coatings, mirrors and polymeric films are illustrated in the enclosed figures. The photographic records are annotated to describe visual observations and surface absorptance changes in the materials. Visual observations were performed with illuminated magnifiers. Absorptance measurements were performed with a Perkin-Elmer Lambda 9 spectrophotometer. Preliminary observations indicate the following conclusions:

Kapton/Al materials exhibited probable atomic oxygen erosion

Fabric materials were very stable

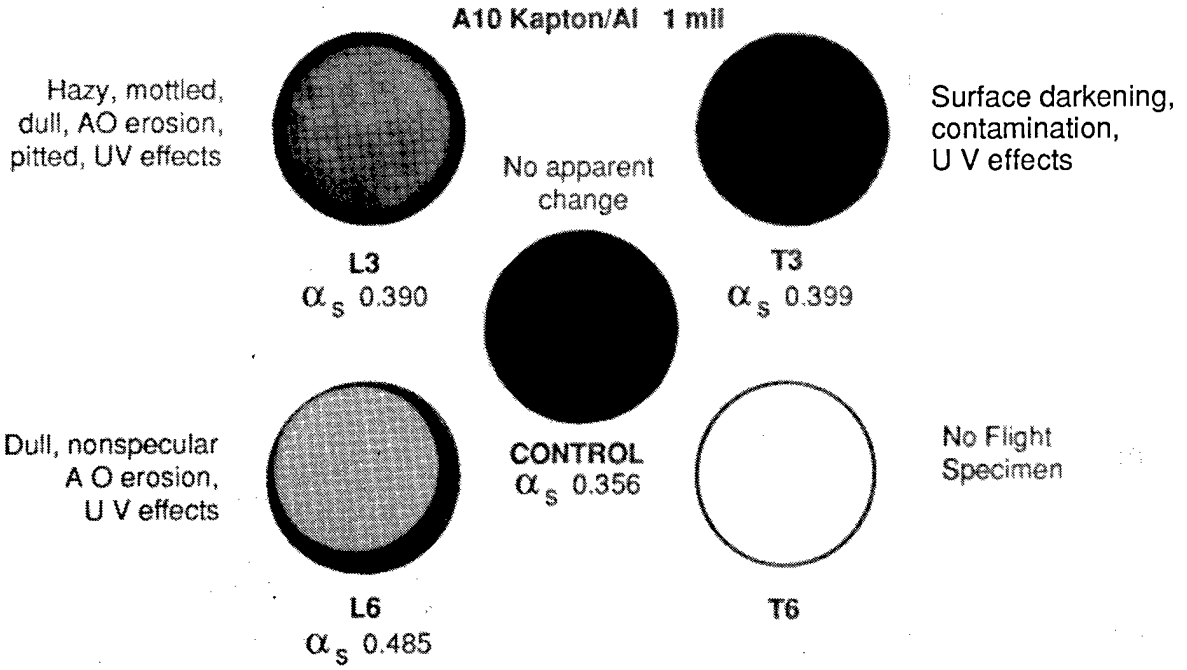
In_2O_3 coatings on Kapton and FEP appeared to provide protection from atomic oxygen erosion

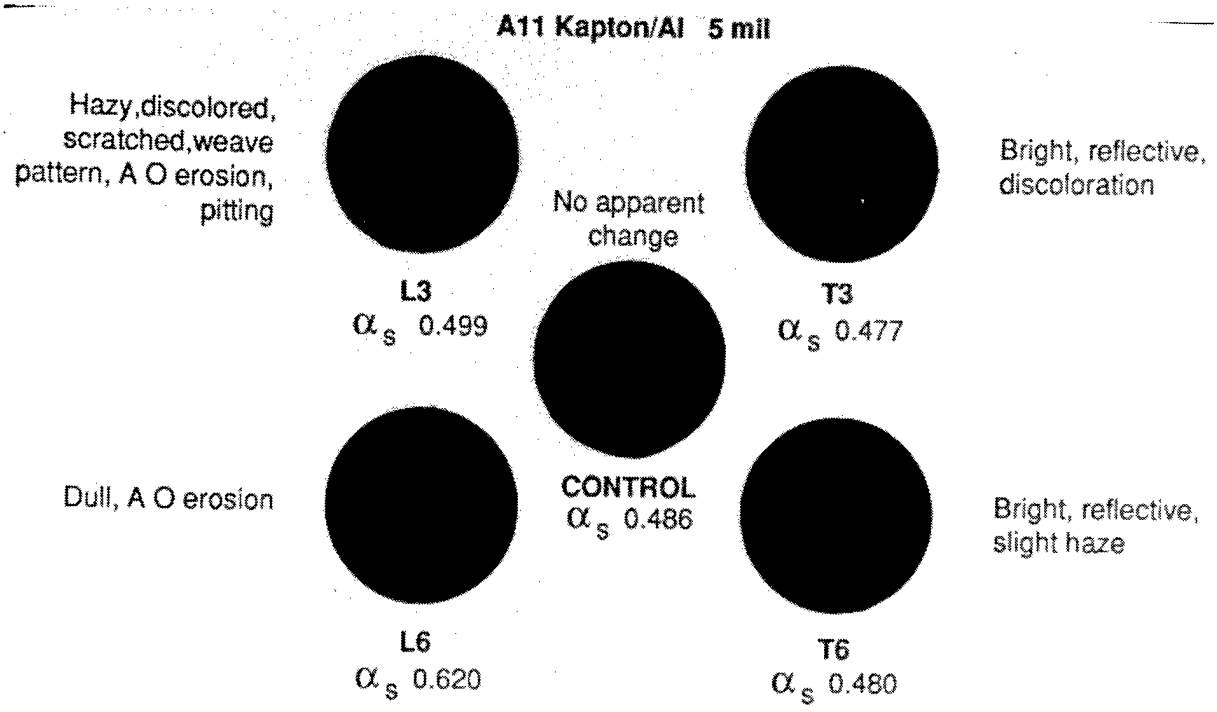
White inorganic coatings exhibited less damaging effects than white organic coatings

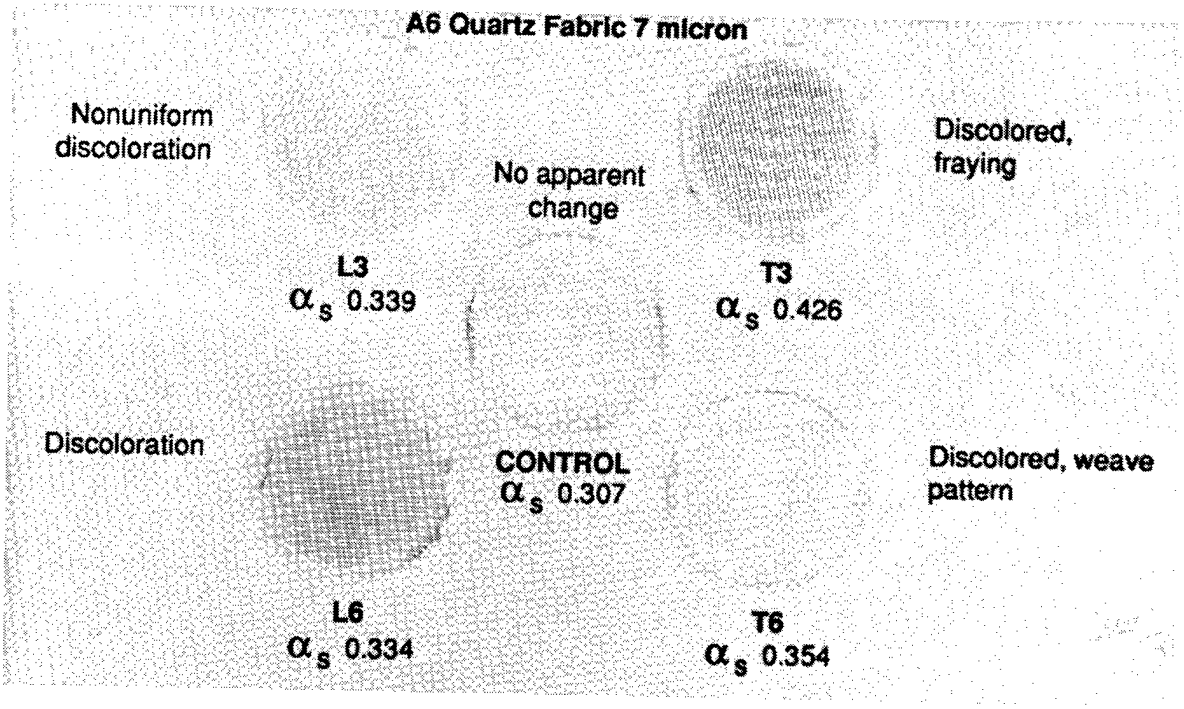
RTV 560 + 12% graphite adhesive bonds failed in all cases

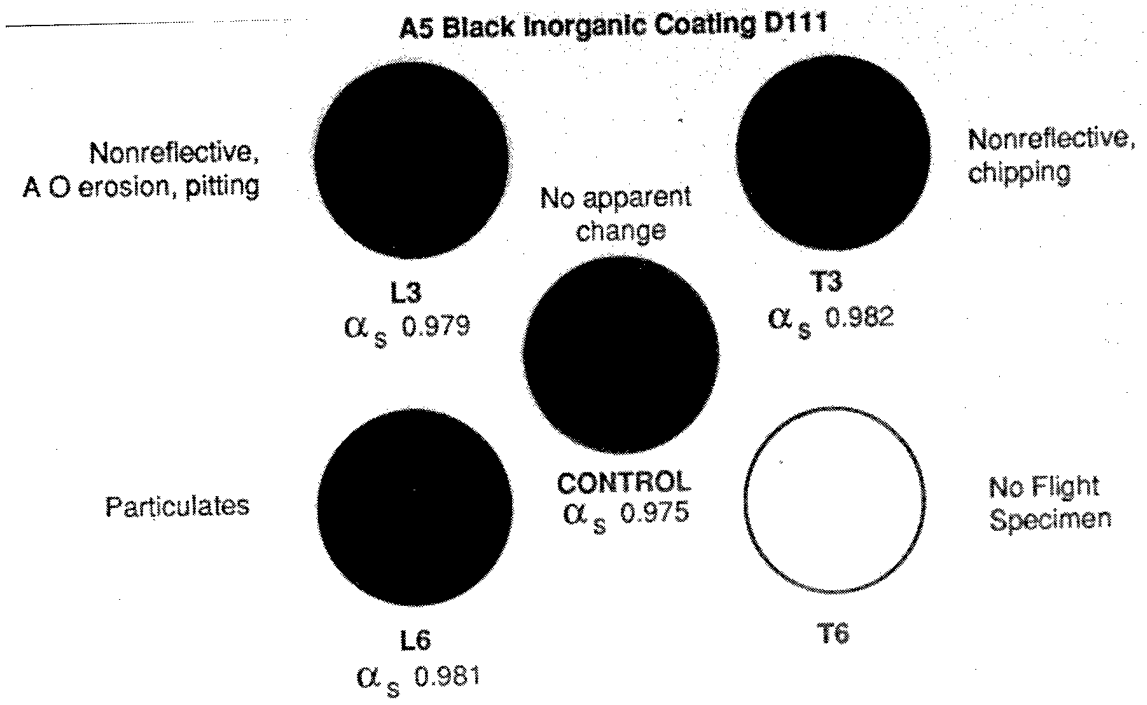
EC57 and Y966 adhesive bonds remained intact

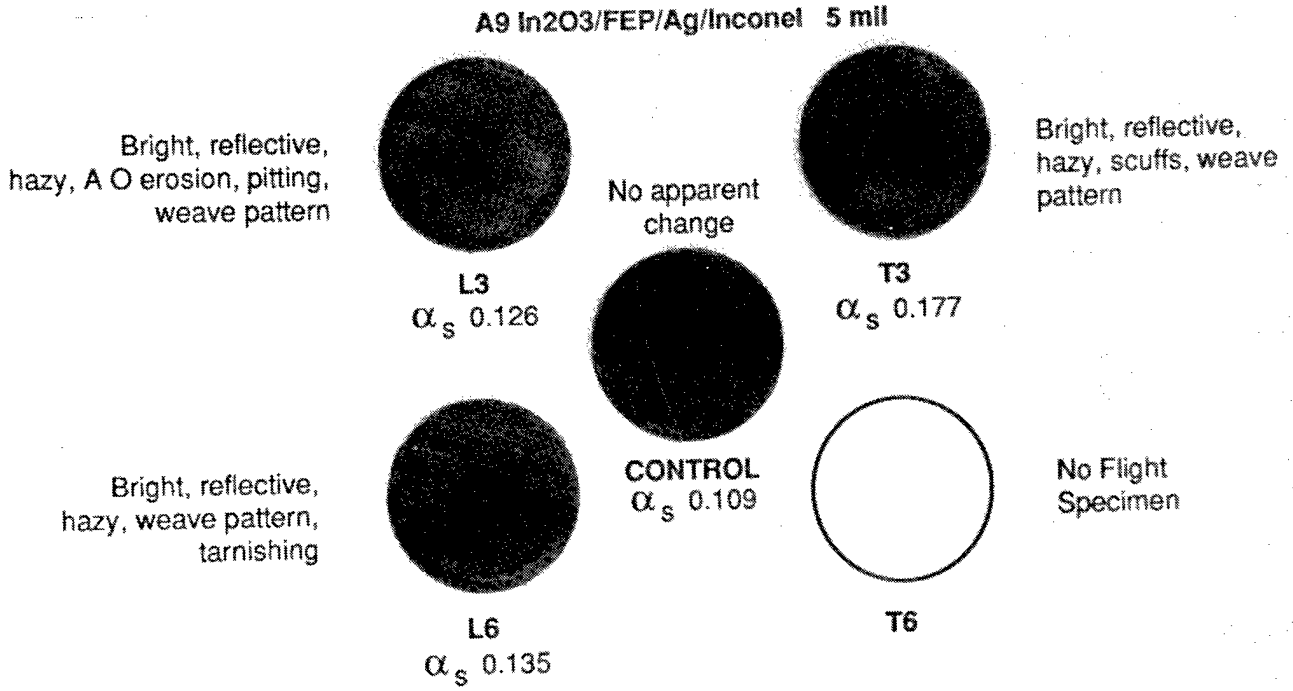
Fourteen of the thirty two polymer film strips exhibited separation and tearing due probably to thermal cycling

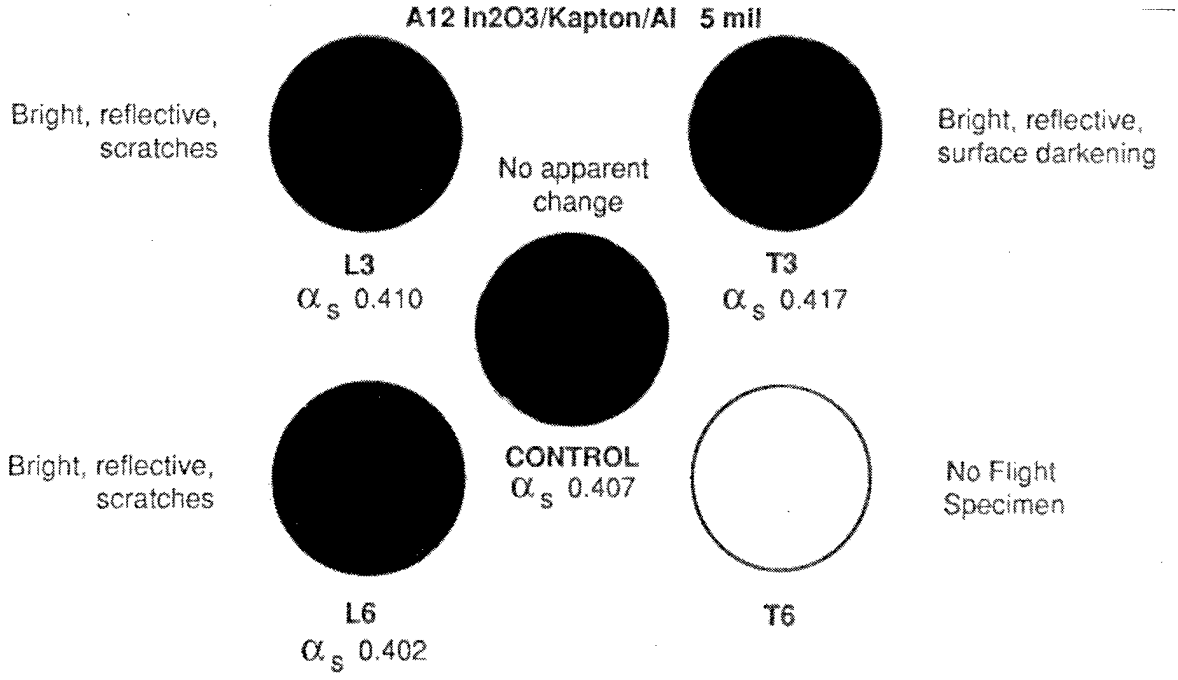


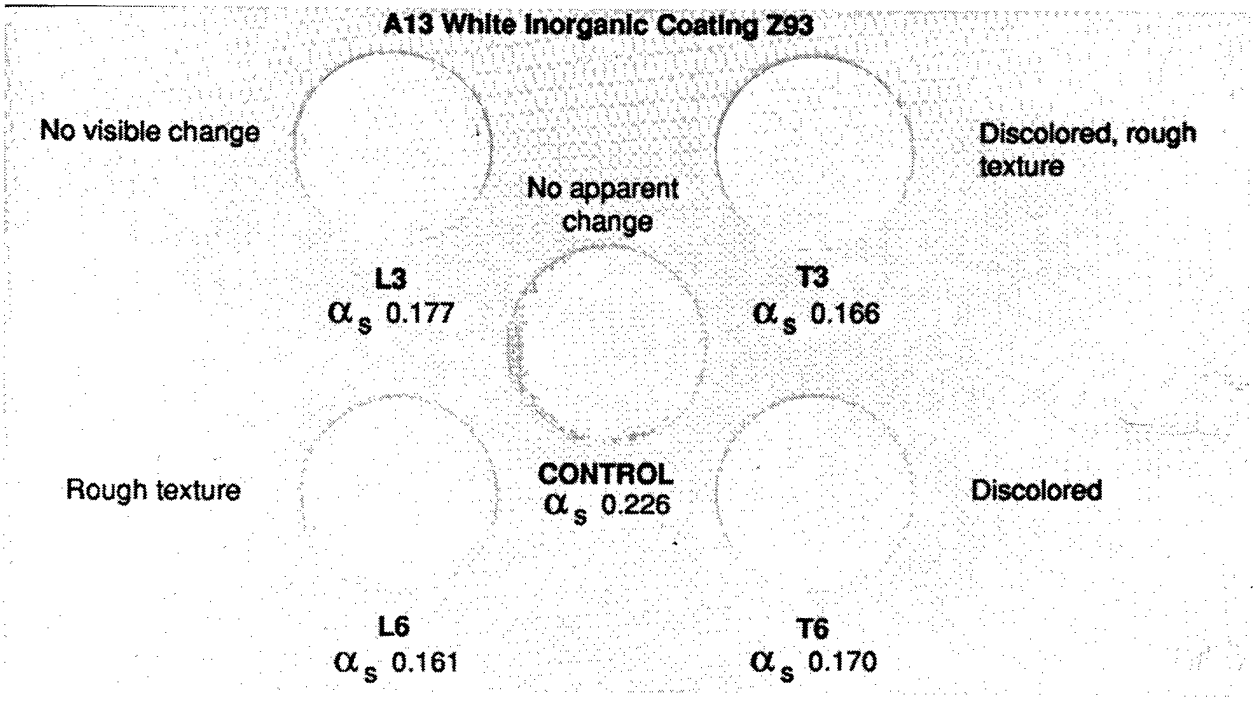

A11 Kapton/Al 5 mil
Hazy,discolored, scratched,weave pattern, A O erosion, pitting
L3
α_s 0.499
No apparent change
T3
α_s 0.477
Bright, reflective, discoloration
Dull, A O erosion
CONTROL
α_s 0.486
L6
α_s 0.620
T6
α_s 0.480
Bright, reflective, slight haze

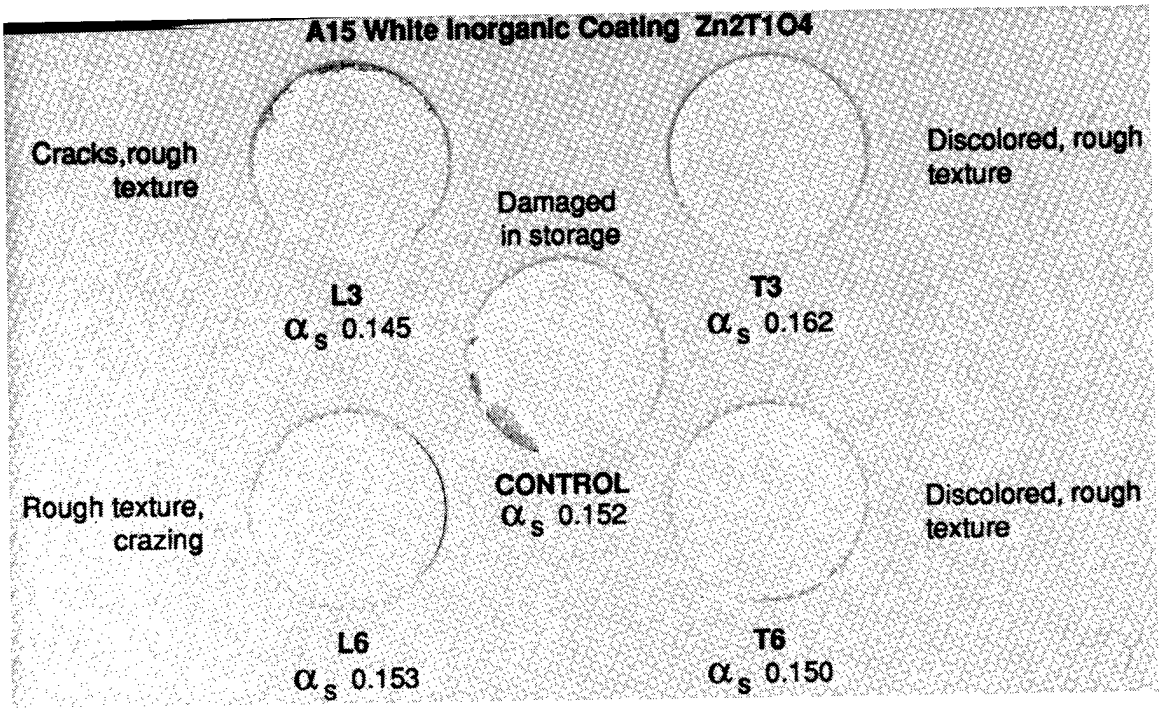

A6 Quartz Fabric 7 micron
Nonuniform discoloration
L3
α_s 0.339
No apparent change
T3
α_s 0.426
Discolored, fraying
Discoloration
CONTROL
α_s 0.307
L6
α_s 0.334
T6
α_s 0.354
Discolored, weave pattern

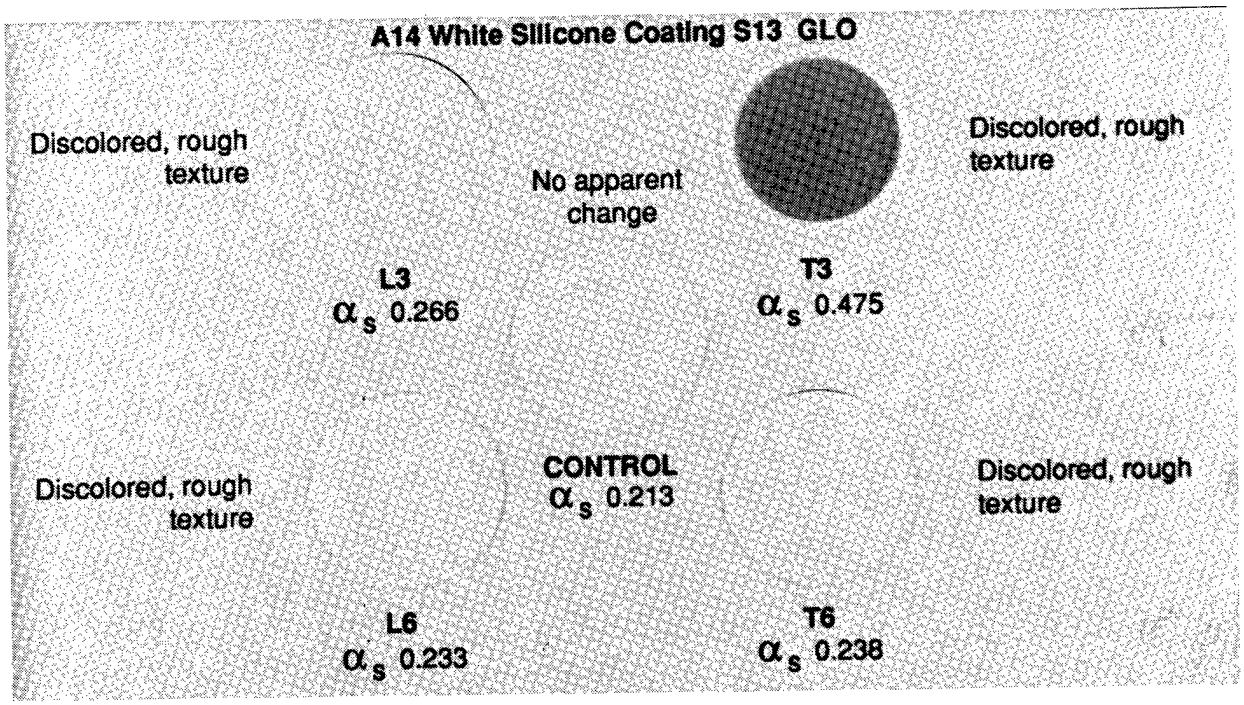

A5 Black Inorganic Coating D111
Nonreflective, A O erosion, pitting
L3
α_s 0.979
No apparent change
CONTROL
α_s 0.975
T3
α_s 0.982
Nonreflective, chipping
Particulates
L6
α_s 0.981
T6
No Flight Specimen

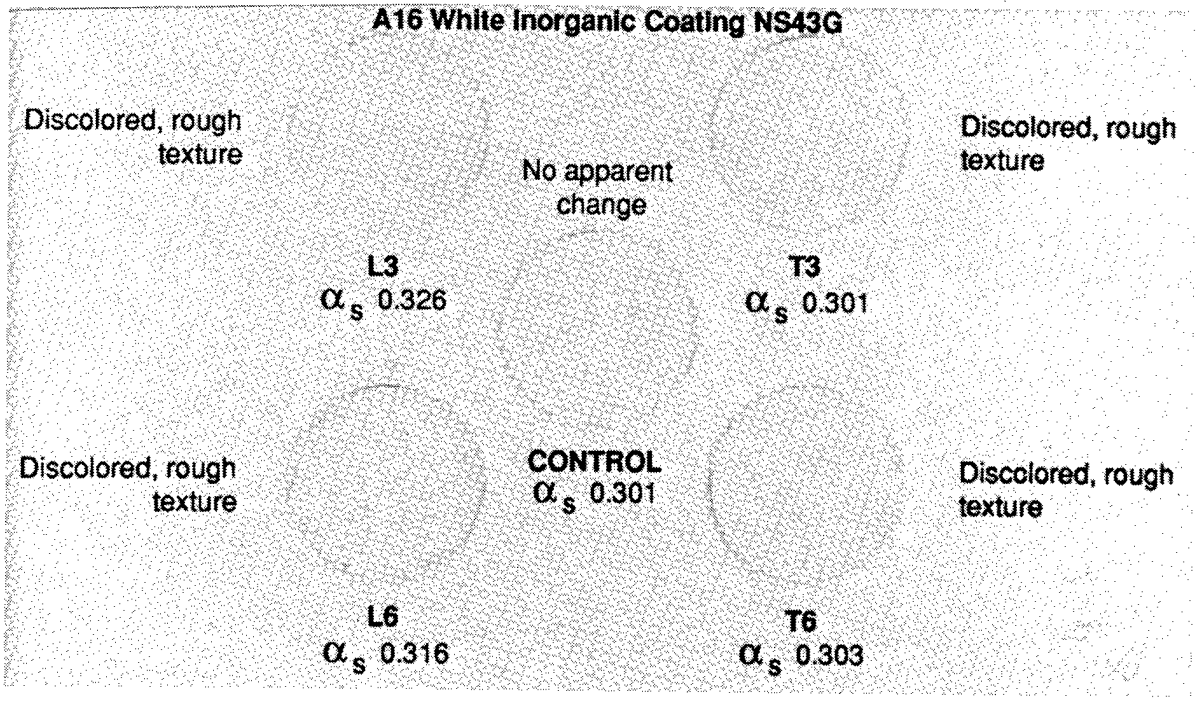

A9 In2O3/FEP/Ag/Inconel 5 mil
Bright, reflective, hazy, A O erosion, pitting, weave pattern
L3
α_s 0.126
No apparent change
CONTROL
α_s 0.109
T3
α_s 0.177
Bright, reflective, hazy, scuffs, weave pattern
Bright, reflective, hazy, weave pattern, tarnishing
L6
α_s 0.135
T6
No Flight Specimen

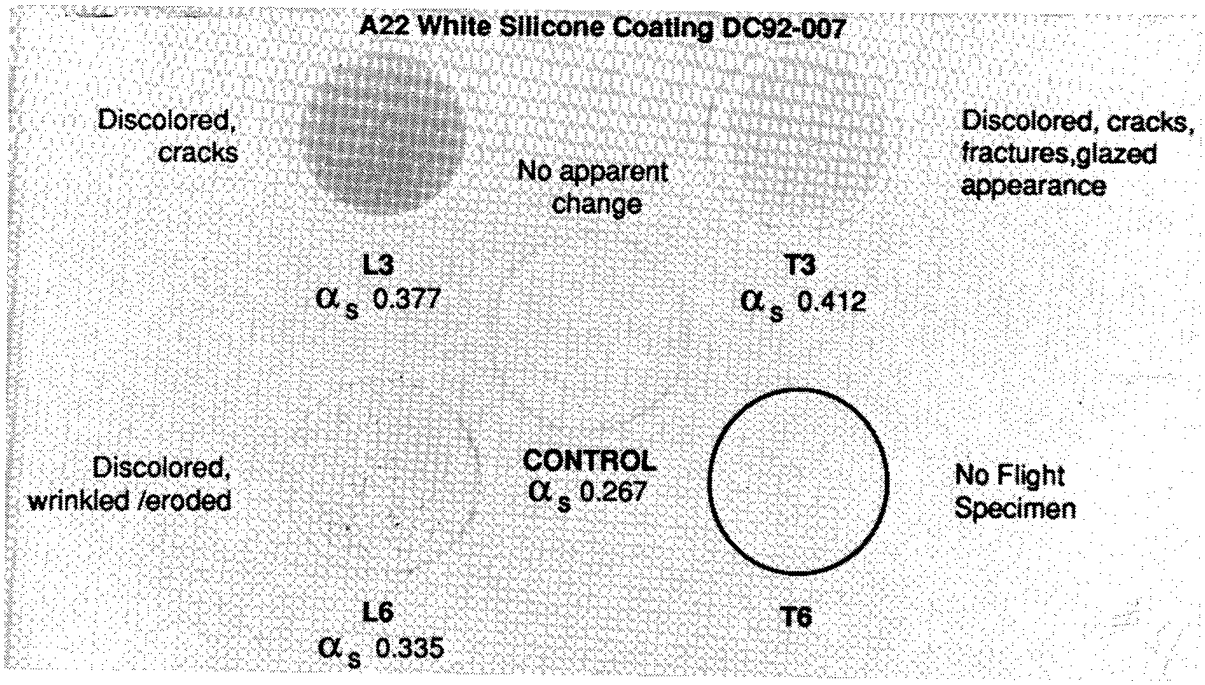

A12 In2O3/Kapton/Al 5 mil
Bright, reflective, scratches
Bright, reflective, surface darkening
No apparent change
L3
α_s 0.410
T3
α_s 0.417
CONTROL
α_s 0.407
Bright, reflective, scratches
No Flight Specimen
L6
α_s 0.402
T6


A13 White Inorganic Coating Z93
No visible change
Discolored, rough texture
No apparent change
L3
α_s 0.177
T3
α_s 0.166
Rough texture
CONTROL
α_s 0.226
Discolored
L6
α_s 0.161
T6
α_s 0.170

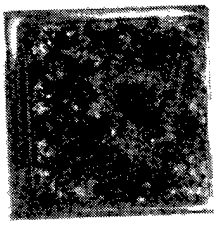

A15 White Inorganic Coating Zn2T1O4
Cracks,rough texture
Damaged in storage
Discolored, rough texture
L3
α_s 0.145
T3
α_s 0.162
Rough texture, crazing
CONTROL
α_s 0.152
Discolored, rough texture
L6
α_s 0.153
T6
α_s 0.150


A14 White Silicone Coating S13 GLO
Discolored, rough texture
No apparent change
Discolored, rough texture
L3
α_s 0.266
T3
α_s 0.475
Discolored, rough texture
CONTROL
α_s 0.213
Discolored, rough texture
L6
α_s 0.233
T6
α_s 0.238


A16 White Inorganic Coating NS43G
Discolored, rough texture
No apparent change
Discolored, rough texture
L3
α_s 0.326
T3
α_s 0.301
Discolored, rough texture
CONTROL
α_s 0.301
Discolored, rough texture
L6
α_s 0.316
T6
α_s 0.303


A22 White Silicone Coating DC92-007
Discolored, cracks
No apparent change
Discolored, cracks, fractures,glazed appearance
L3
α_s 0.377
T3
α_s 0.412
Discolored, wrinkled /eroded
CONTROL
α_s 0.267
No Flight Specimen
L6
α_s 0.335
T6

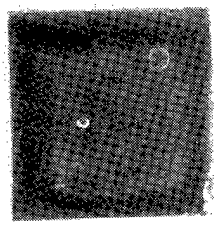
B5 OSR Ag Mirror



Severe A O erosion, black residue, rough texture

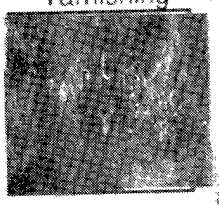
L3
α_s 0.864

Fingerprint Contamination, Tarnishing

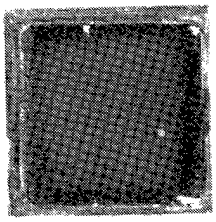


T3
α_s 0.270

Surface contamination, tarnishing, micrometeroid impact site

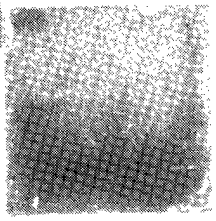


CONTROL
α_s 0.253



A O erosion, black residue, surface cracks, rough texture

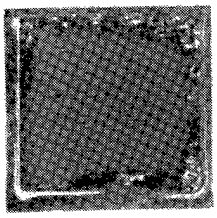
L6
α_s 0.861



T6
α_s 0.246

Surface contamination, tarnished

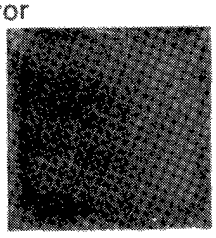
B6 OSR Ag Mirror



Severe A O erosion, black residue, probable crater site

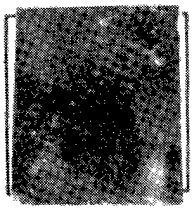
L3
α_s 0.930

Fingerprint Contamination Tarnishing



T3
α_s 0.384

Discolored, contamination, tarnished



CONTROL
α_s 0.206

No Flight Specimen

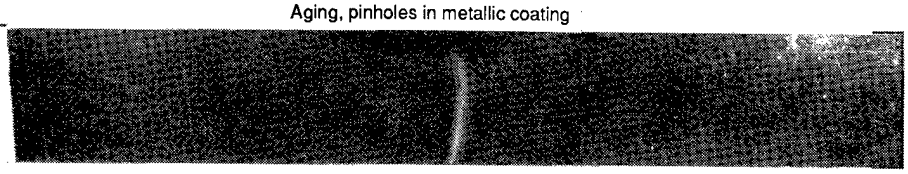
L6

No Flight Specimen

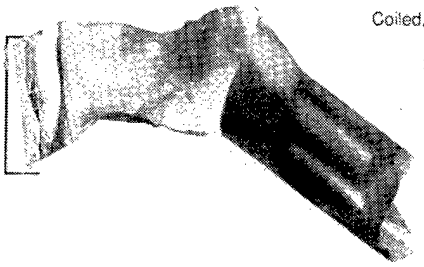
T6

C2 FEP/Ag/Inconel 5 mil

Aging, pinholes in metallic coating



CONTROL



Coiled, wrinkled, discolored

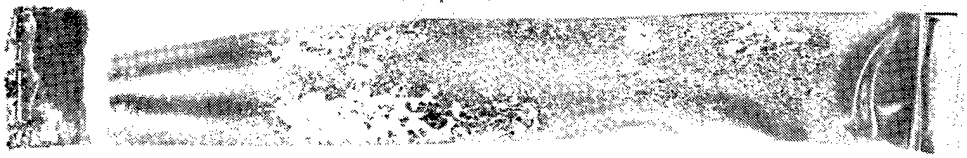
FEP surface: bright, reflective
semitransparent
Metal surface: cracked, crazed,
black powdery
appearance

L3

Edge torn



Edge torn FEP surface: stained, discolored, hazy



Metal surface: cracked, crazed, peeling

T3

C3 Kapton/Al 1 mil

Kapton surface: weave pattern from protective cloth visible



Metal surface: no apparent change

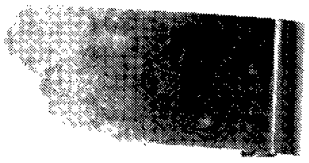
CONTROL

Edge torn



Kapton surface: discolored, eroded

50% of film missing
edge torn & ragged



Metal surface: shiny & reflective

L3

Kapton surface: bright, shiny, reflective

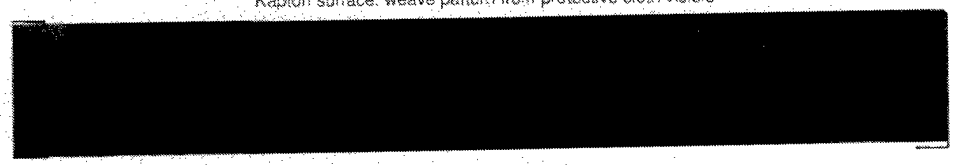


Metal surface: bright, shiny, reflective

T3

C4 Kapton/Al 5 mil

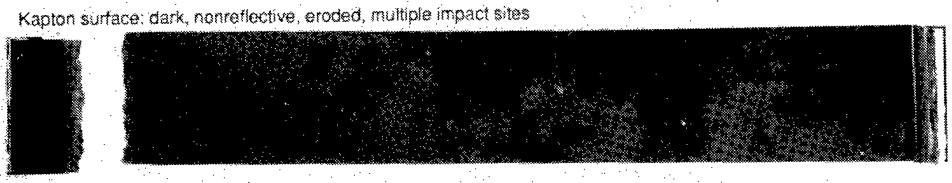
Kapton surface: weave pattern from protective cloth visible



Metal surface: no apparent change

CONTROL

Kapton surface: dark, nonreflective, eroded, multiple impact sites



Metal surface: no apparent change

L3

Kapton surface: no apparent change



Metal surface: no apparent change

T3

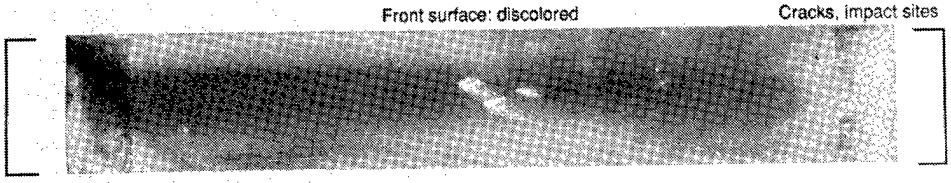
C16 Polyphenylsulfone 10 mil

No apparent change

CONTROL

Front surface: discolored

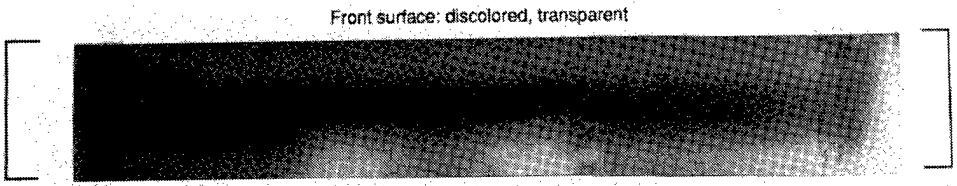
Cracks, impact sites



Reverse side: shiny, reflective

L3

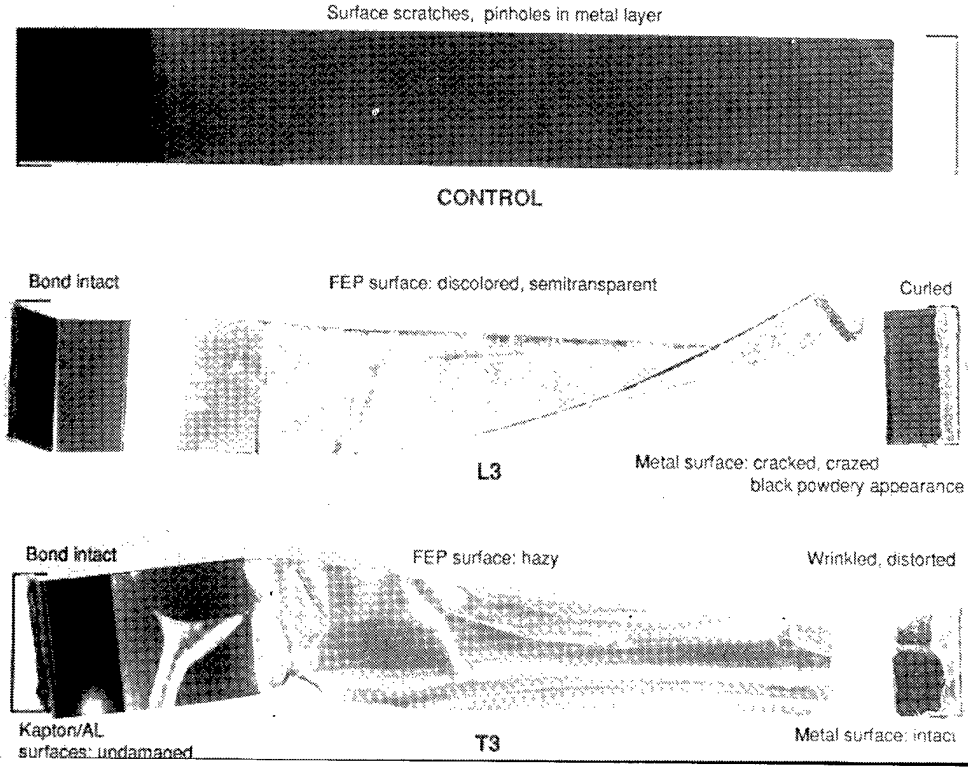
Front surface: discolored, transparent



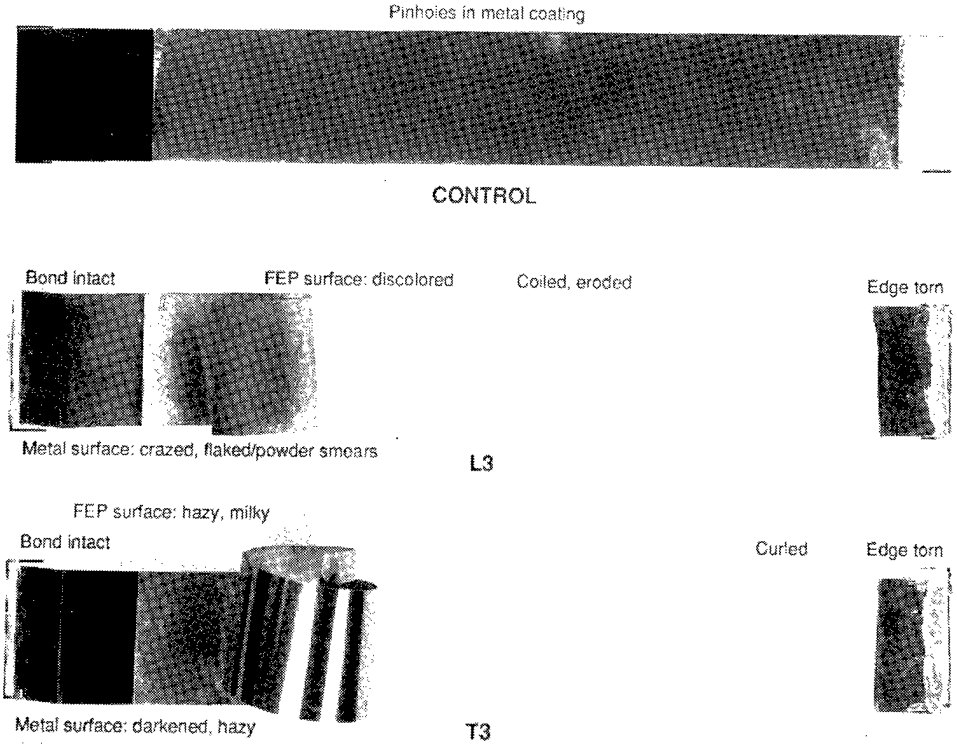
Reverse side: shiny, reflective

T3

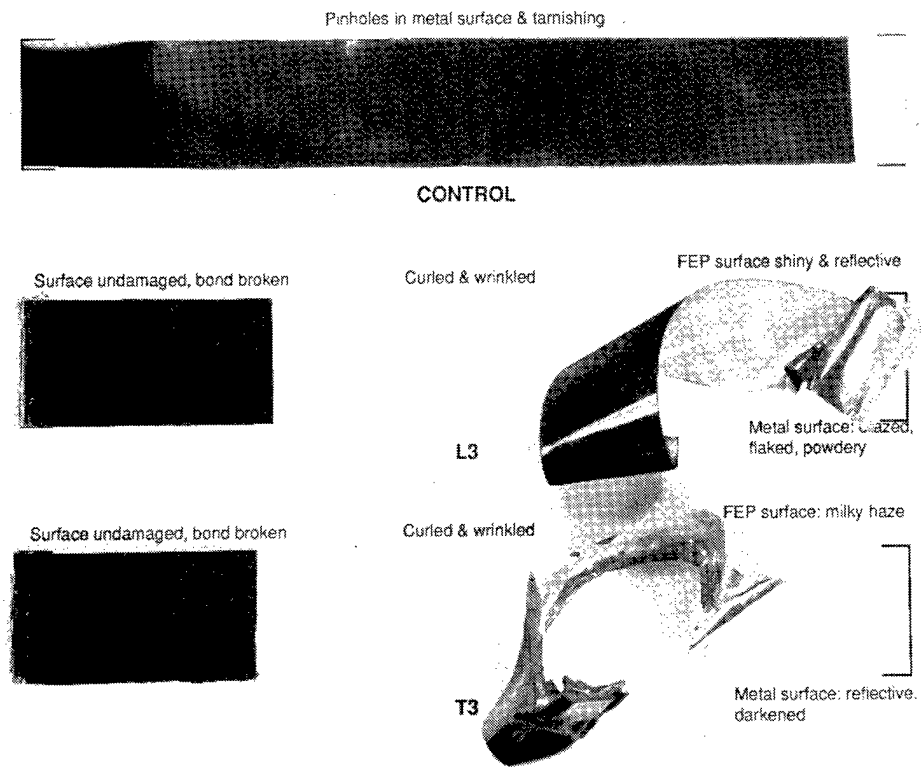
C11 FEP/Ag/Inconel/Y966/Kapton/Al 5 mil



C6 FEP/Ag/Inconel/EC57C/Kapton/Al 5 mil



C9 FEP/Ag/Inconel/RTV560 +12% graphite/Kapton/Al 5 mil



RESULTS OF EXAMINATION OF THE A276 WHITE AND Z306 BLACK THERMAL CONTROL PAINT DISKS FLOWN ON LDEF*

Johnny L. Golden
Boeing Defense and Space Group
POBox 3999 M/S 82-32
Seattle, WA 98214-2499
Phone: (206) 773-2055, FAX: (206) 773-4946

SUMMARY

Specimens of A276 white and Z306 black thermal control paints were analyzed for the effects of space environmental exposure as part of LDEF Materials Special Investigation Group activity. The specimens, actually disks or spots of paint on tray clamps, were located at regular intervals on all LDEF longerons and intercostals. The principle conclusions from the analysis are: UV exposure degraded the surface resin of A276 paint, with coating solar absorptance increasing with UV exposure; contamination, though detected, was not enough to have adversely affected optical properties; atomic oxygen eroded resin on specimens with incidence angles of up to 100 degrees; the erosion of Z306 paint on leading edge specimens removed a minimum of 10 microns of that coating; and the erosion of A276 paint at up to 80 degrees incidence angle resulted in near original condition solar absorptance readings.

INTRODUCTION

White-on-black disks of polyurethane thermal control paint were applied to over two hundred of the tray clamps on LDEF as part of a spacecraft stabilization experiment. These paint disks now exhibit varying degrees of discoloration and deterioration as a result of space environmental exposure. Since the specific thermal control paints are standard materials for spacecraft use, the extent and nature of the changes in these materials need to be determined for future design. In addition, these disks also provide a unique opportunity to characterize two common materials for all surface locations available on LDEF.

The thermal control coating disks are described as 4 cm diameter disks of Chemglaze Z306 black polyurethane thermal control paint applied to the approximate center of 38% of the anodized 6061-T6 aluminum alloy tray clamps. A 3 cm diameter aluminum foil disk, which had been coated with Chemglaze A276 white polyurethane thermal control paint, was adhesively bonded in the center of each black disk . Chemglaze 9924 primer was used prior to the application of Z306 on the tray clamps, and prior to the application of A276 to the adhesive backed aluminum foil.

The appearance of the thermal control coating paint disks at retrieval varied as a function of position on LDEF. The disks on leading edge rows were mottled but still white, with black paint occassionally eroded down to the red primer. The disks on trailing edge rows showed that the white paint had discolored to a brown, and that the black paint appeared unaffected. Disks on earth and space ends had varying degrees of discoloration, with some disks showing a partial discoloration of the white coating.

*Work done under NAS 1-18224, Task 12

These paint disks were not part of any specific materials experiment on LDEF. To take advantage of this opportunity, the analysis which follows was authorized and directed by the LDEF Materials Special Investigation Group. The objective of this analysis is to characterize the changes which have occurred with the thermal control coating disks on LDEF as a function of space environmental exposure.

RESULTS AND DISCUSSION

Optical Microscopy

Low magnification (16X) microscopy was used to observe contaminants and the general integrity of the paint disks. Contamination from numerous sources was observed on all specimens. Fibers and shop debris were seen imbedded in uneroded paint coatings. Yellow paint particles were observed on and around the black paint, apparently the result of overspray from when the tray clamp disks were originally painted. Uneroded white paint disks also exhibit solvent marks, where it appears that a solvent wiping operation wicked contaminants into the coating surfaces, resulting in a mottled discoloration pattern.

Cracking patterns were observed in the white paint disks from the leading edge. Cracking was sometimes localized to the edge region of these disks, but was also observed as a pattern of parallel cracks on large areas of the bulk white coating on other disks. Cross-sections, to be discussed later in this paper, showed that these cracks go completely through the coating to the substrate. It is surmised that these cracks are the result of atomic oxygen erosion of the white coating, coupled with residual stresses imparted to the white paint disks when they were originally punched out of the painted aluminum foil.

High magnification (1000X) optical microscopy was used to observe disk surfaces with both bright field and dark field illumination. Bright field illumination indicated that trailing edge white paint surfaces were still resin rich, whereas leading edge white paint surfaces were now pigment rich. Dark field illumination revealed that the pigment particles in trailing edge white paint disks were still very reflective, indicating that the pigment particles themselves had not discolored due to space environmental exposure.

Contamination Analysis

Contamination analysis was conducted to determine if the white coating discoloration was due, principally or in part, to the deposition of a contaminant. Initial analyses were conducted nondestructively. Twenty white paint specimens from various locations around LDEF were measured for diffuse and specular infrared reflectance. The total infrared reflectance spectra for leading and trailing edge specimens were nearly identical. There was no evidence of IR absorptions due to an unusual organic contaminant on trailing edge disks. The only real difference observed using IR reflectance spectroscopy was that the diffuse component for leading edge specimens was enhanced when compared to trailing edge specimen spectra.

Secondary analyses were conducted destructively. The discoloration of trailing edge white paints could not be removed with solvent wiping, using either methyl ethyl ketone or petroleum ether. Scrapings from control, leading edge, and trailing edge specimens were delicately taken with the aid of a microscope, in an attempt to remove the very surface

layers for transmission IR spectroscopy. Examples of these spectra are shown in figures 1- 3. The control spectrum in figure 1 indicates characteristic absorptions for the polyurethane resin and for the silicate binder in the paint pigment. The spectrum in figure 2 indicates that there was no detectable resin left on the surface of the leading edge white paint specimen, with the only absorption band attributable to the silicate binder. The spectrum in figure 3 for the trailing edge specimen, when compared directly with figure 1, indicates that the darkened paint surface is only slightly modified paint resin. If any organic contaminant contributes to the darkened surface of trailing edge white paint, it is not detectable or discernible by this technique.

Cross-Sectioning

Cross-sections were made of four specimens from different environments on the LDEF surface, after all nondestructive measurements for those specimens had been completed. The attempt to measure the depth of atomic oxygen driven resin recession on the leading edge white paint specimen was not successful. The surface of the eroded white paint specimens is essentially pigment particles, held in place by weak attractive forces due to the small size of the particles. When trying to mount the cross sections prior to polishing, those loosely attached pigment particles 'wash' off of the surface, making resin erosion measurements impossible. Current attempts, in progress, to measure resin erosion are making use of surface stabilization prior to encapsulation.

Cross sections were also used to measure the extent of erosion on leading edge black paint. The results are questionable due to observed variability in the black paint coating thickness. Measurements of black paint thickness on trailing edge specimens, which should be uneroded by atomic oxygen, typically had a 50% variation in thickness. In general, the black paint was observed to be thinner toward the outer (subsequently exposed) edge, probably as a consequence of the painting operation. The result of this variation is that the comparison of coating thicknesses in protected (under the white paint disk) and exposed areas to determine extent of coating erosion has a high degree of uncertainty. If the variability in black paint thickness is ignored, recession observed for the Z306 paint on leading edge specimens was approximately 10 microns (0.0004 inch).

The extent of black thermal control paint erosion can be approached qualitatively from another perspective. A number of paint disks from the leading edge area had the exposed black paint completely eroded away, leaving only the characteristic red of the underlying primer pigment. The primary surface on tray E9 had also been painted with Z306, and portions of this surface were eroded down to the primer as a result of atomic oxygen exposure. If one considers the minimum and typical thickness at which Z306 is applied, it can lead to at least a range of erosion that occurred for this material. The minimum thickness of paint measured on paint disk cross sections was 10 microns. Polyurethane paints are typically applied to a minimum thickness of 25 microns. These thicknesses provide a range of erosion that occurred on LDEF leading edge surfaces. This erosion range would indicate that the carbon black filled Z306 coating is much more resistant to atomic oxygen erosion than the graphite fiber reinforced composites, which exhibited complete erosion to a depth of 50 to 75 microns (ref. 1).

Cross-sectioning was also used to characterize the darkened surface of trailing edge white paint. The darkened, or discolored portion of the white paint was found to be extremely thin, approximately 0.2 microns in thickness. There also appeared to be titania pigment particles located in the discolored portion, indicating that the discoloration was due to darkening of the very surface layer of the paint resin.

Surface Analysis

A number of surface spectroscopy techniques were used to characterize the subject surfaces. SEM images of a leading edge white coating are shown in figures 4 and 5. Lower magnification (figure 4) shows the rough, porous character of the eroded surface. Higher magnification (figure 5) illustrates the total absence of resin on the paint surface. The submicron sized spherical particles are titania pigment. The larger plate-like particles have been identified through EDAX as a magnesium silicate, most likely talc, a common binder in white paint pigment packages.

ESCA was used to identify the chemical composition of the very surface (10Å depth) of the paint disks. Using ESCA, the presence of fluorine was detected on all specimen surfaces, with the exception of the control specimen and leading edge black paint surfaces. That the fluorine was not observed on the control specimen indicated that the fluorine was deposited as a result of environmental exposure. Since the leading edge black paint specimens were in a continual state of erosion during exposure, it is not surprising that fluorine was not found on these surfaces. The fluorine would most likely have come from the decomposition and erosion of nearby FEP thermal control blankets, with deposition not occurring through a typical line-of-sight mechanism.

Increased surface concentrations of silicon, as compared to the control specimen, were also observed using ESCA. The increased levels of silicon observed on leading edge white and black thermal control paints is expected. Both the black and white paints contain silicates as part of their pigment systems. However, the increased levels of silicon on trailing edge specimens are indicative of contaminant deposition.

Optical Properties Measurements

Solar absorptance and thermal emittance measurements were made for 100 of the white paint disks on LDEF. Optical property measurements for the Z306 black paint areas on the disks were not obtained due to their dimension and shape. Solar absorptance measurements were made in accordance with ASTM E424, thermal emittance in accordance with ASTM E408. These measurements were made without removing the disks from the tray clamps.

Measurements made for white paint disks from the earth and space ends of LDEF are shown in figure 6. Emittance measurements indicated no significant differences between disks on the earth or space ends. The absorptance readings were generally greater for the peripheral areas at either end. Further discussion of the earth and space end absorptance measurements will be made later with the correlations to environmental exposure.

The disks from the side trays which were analyzed for absorptance and emittance are shown in figure 7. The disks were selected to represent all available incidence angles, with additional specimens selected to test variability along the length of the spacecraft.

Absorptance measurements as a function of row position are shown in figure 8. Multiple specimens measured for a particular row position show the limited variability in absorptance for a particular row position. This variability was random, not indicating any trends in absorptance along the length of the spacecraft. The data do not form a symmetric

distribution due to the offset in yaw reported elsewhere (ref.2). Control specimen absorptance was comparable to that from specimens on rows 9 and 10.

Emittance measurements as a function of row position are shown in figure 9. Statistical analysis indicates a marginally significant increase in emittance for leading edge specimens (0.88 ± 0.02) as compared to trailing edge specimens (0.86 ± 0.02). The increase in emittance is consistent with the roughening of leading edge surfaces observed by microscopy, caused by atomic oxygen erosion of the paint resin.

The absorptance and emittance measurements are plotted versus angle of incidence in figure 10. The incidence angles are based on an assumed eight degree offset in yaw angle. Figure 10 shows that the erosion effect of atomic oxygen maintains low absorptance levels for the A276 paint for incidence angles up to 80 degrees, with an apparent atomic oxygen effect discernible to an incidence angle of 100 degrees. It is actually fortunate for the present analysis that LDEF was out of yaw. Due to the extremely steep solar absorptance change in the atomic oxygen transition region, the yaw offset provided two separate incidence angle environments in this area.

In an attempt to characterize the environmentally induced changes observed for A276 paint, figure 11 represents solar absorptance measurements as a function of atomic oxygen fluence. The atomic oxygen fluence levels used in figure 11 are predictions based on the LDEF AO fluence model developed by Boeing (ref.3). Atomic oxygen fluence is represented logarithmically. Absorptance data from earth and space end disks are not included in figure 11, due to a scatter in those data which will be discussed with the next figure. From figure 11, it appears that a fluence level of 10^{21} oxygen atoms per cm^2 is necessary to cause sufficient resin erosion in the A276 white thermal control paint to maintain coating optical performance, removing the darkened resin which degrades the coating's absorptance.

However, it must be recognized that coupled with the atomic oxygen effect is the effect of UV radiation. Figure 12 shows the absorptance of all disks measured, including earth and space end disks, as a function of predicted solar fluence in equivalent sun hours (ref. 3). Also included in figure 12 are data from LDEF Experiment S0069 for comparison (AZTEK, ref.4).

The scatter in data obtained for the earth and space ends disks of LDEF is shown in figure 12. Both earth and space end disks were predicted to receive approximately the same fluences of atomic oxygen, assuming no vehicle pitch offset or over-riding effects of local environments. However, it is apparent that there were some local differences in atomic oxygen fluence which resulted in the observed scatter. The trend of increased absorptance with increasing UV exposure is still intact with the earth and space end disk data. But the ends of LDEF were in the transition region with regards to atomic oxygen fluence, where slight differences in surface orientation and position could markedly affect atomic oxygen fluence. When compared to absorptance data from the disks on LDEF side trays, data from the space end disks indicate incidence angles ranging from 85 to 105 degrees.

Figure 12 suggests a gradual absorptance increase for A276 that accompanies increasing UV exposure in the absence of atomic oxygen. Part of the evidence for this trend is from the data provided by experiment S0069, which showed an increase in the absorptance of A276 occurring in the early, low atomic oxygen flux portion of the LDEF mission. Taken as a whole , the data in figure 12 suggest that all of the A276 paint disks were darkening according to this trend in the initial years of the LDEF mission. This was when LDEF was

still in a relatively high orbit. But as the orbital altitude began to decay, the atomic oxygen flux began to increase rapidly. The AO flux model has predicted that about 54% of the atomic oxygen fluence on LDEF occurred in the last six months of the mission (ref. 3). It was during this latter phase that the atomic oxygen erosion removed UV damaged paint resin where the total fluence was sufficient, and brought A276 absorptance readings back to nominal on leading edge specimens.

CONCLUSIONS

The first goal of the analysis of thermal control coating disks was to determine if the discoloration observed for A276 white paint was due to pigment discoloration, resin degradation, contaminant deposition, or a combination of all these mechanisms. Microscopy has shown that pigment discoloration did not occur. Surface spectroscopy has shown that there are contaminants detectable on stable surfaces. Fluorine and increased levels of silicon were detected on all flight specimens, with the exception of Z306 black paint on leading edge disks which were in a continual state of atomic oxygen erosion. However, the amount of these contaminants was quite low, much too low to cause the measured increases in solar absorptance for A276 white paint. IR spectra of surface scrapings from discolored A276 paint, as compared to control paint, tends to indicate that the discoloration is principally in the paint resin itself, induced by the thousands of hours of UV exposure attained by LDEF.

The second goal of the analysis was to quantify changes in design properties which resulted from space environmental exposure. Surfaces exposed to atomic oxygen up to an incidence angle of 100 degrees showed evidence of surface erosion. A276 paint surfaces at and near the leading edge did not have any visible resin remaining, and this erosion apparently led to cracking and crazing. The depth of erosion which occurred for A276 specimens was indeterminate. Measurements of erosion extent for Z306 black paint cross-sections have been questionable, due to the observed variability in coating thickness. Ignoring this thickness variability, the Z306 erosion was estimated at about 10 μm (0.0004 inch) minimum. Cross-sectioning also indicated that the A276 surface discoloration was limited to the upper 0.1-0.2 μm of the paint surface.

Optical property measurements have been compared to modelled predictions of atomic oxygen fluence and UV exposure. These comparisons have suggested a trend in the observed absorptance increases of A276 white paint with UV exposure. This trend helps to corroborate the spectroscopic evidence that the darkened A276 paint was caused by UV induced degradation of the paint resin system. Solar absorptance measurements also indicated that sufficient atomic oxygen fluences were received at incidence angles up to 100 degrees to observe paint resin erosion. This erosion significantly degraded the mechanical integrity of the paint coatings, but at incidence angles up to 80 degrees on the LDEF mission (and fluences of 10^{21} oxygen atoms per cm^2), this erosion was sufficient to bring the UV damaged white paint back to near-original absorptance levels.

REFERENCES

1. P. George: Results From Analysis of Boeing Composite Specimens Flown on LDEF Experiment M003. First LDEF Post-Retrieval Symposium, NASA CP-3134, 1992.

2. J. C. Gregory: LDEF Attitude Measurement Using A Pinhole Camera With A Silver/Oxygen Atom Detector. First LDEF Post-Retrieval Symposium, NASA CP-3134, 1992.

3. R. J. Bourassa: Atomic Oxygen And Ultraviolet Radiation Mission Total Exposures For LDEF Experiments. First LDEF Post-Retrieval Symposium, NASA CP-3134, 1992.

4. M. J. Brown, et al.: Measurement And Analysis of LDEF/TCSE Flight Samples. AZ Technology Report No. 90-2-107-1, February 1991.

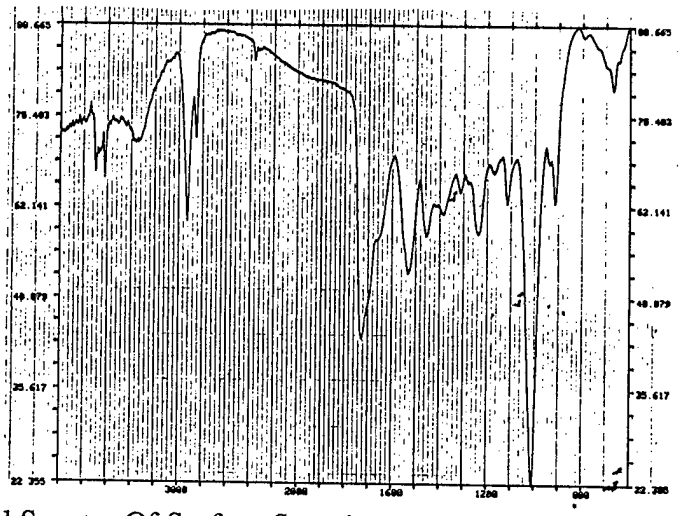


Figure 1. Infrared Spectra Of Surface Scraping From A276 White Thermal Control Paint On A Control Clamp.

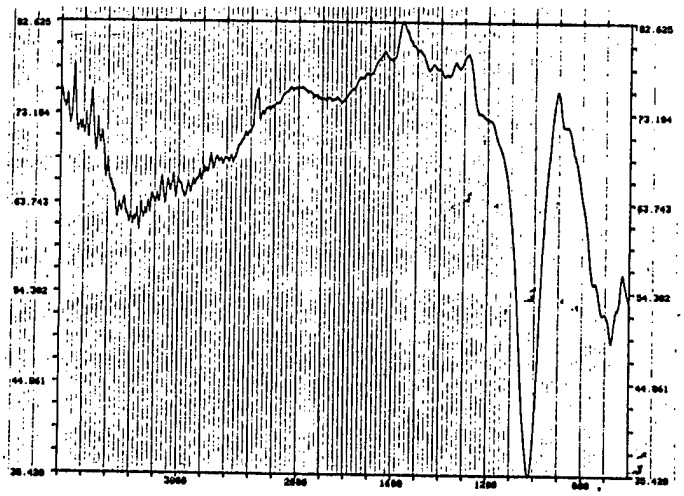


Figure 2. Infrared Spectra Of Surface Scraping From A276 White Thermal Control Paint On A Leading Edge Clamp B9-7.

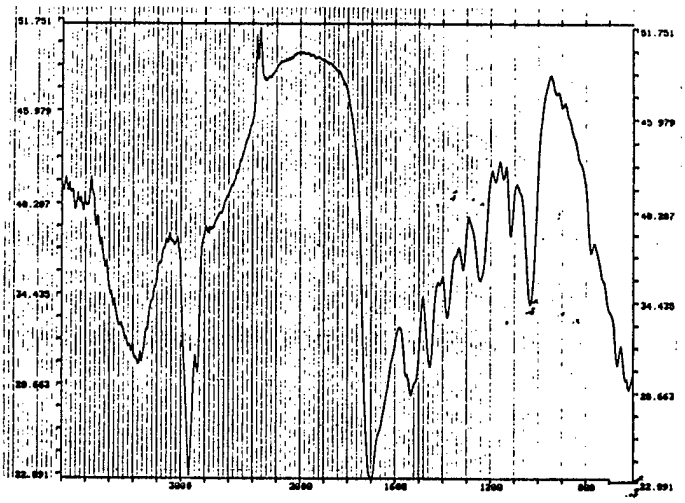


Figure 3. Infrared Spectra Of Surface Scraping From A276 White Thermal Control Paint On A Trailing Edge Clamp.A3-7.

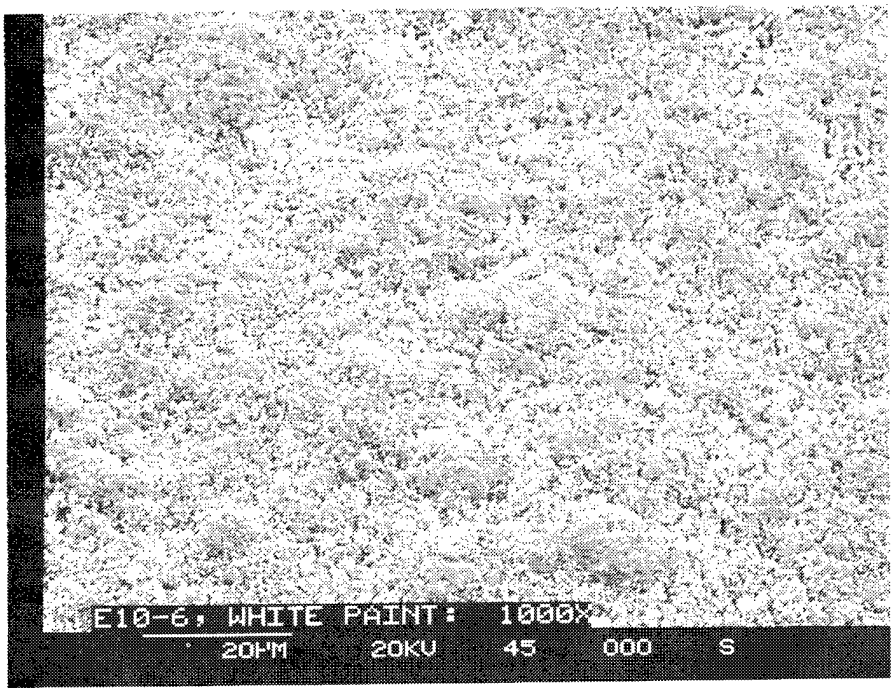


Figure 4. SEM (1000X) From A276 White Thermal Control Paint Located On Tray Clamp E10-6. Roughened surface is typical of leading edge white paint specimens, showing the loss of polyurethane resin from the surface.

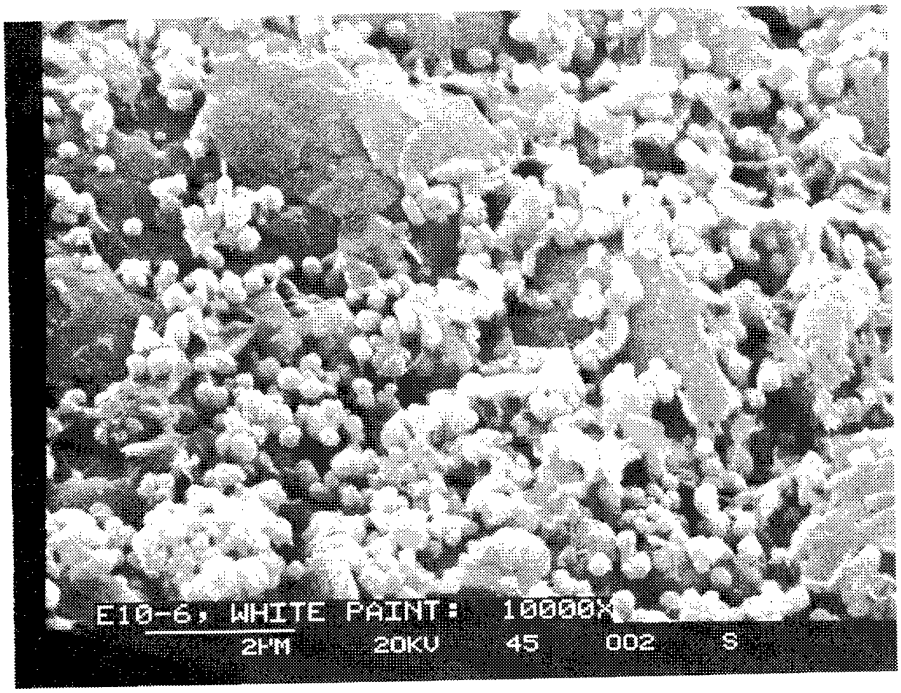


Figure 5. SEM (10,000X) From A276 White Thermal Control Paint Located On Tray Clamp E10-6. Small spherical particles are titania pigment, large plate-like crystals are magnesium silicate (talc).

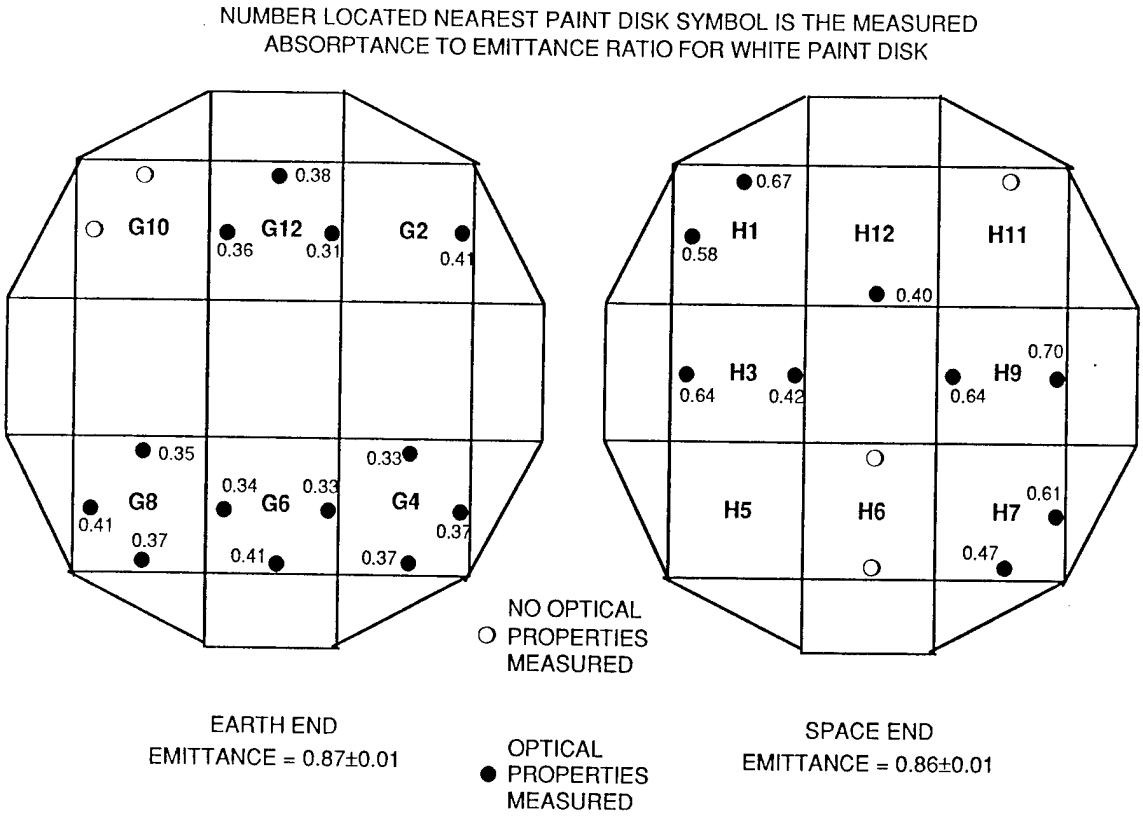


Figure 6. Optical Property Data For LDEF (MSIG) End Tray Clamps With Paint Disks

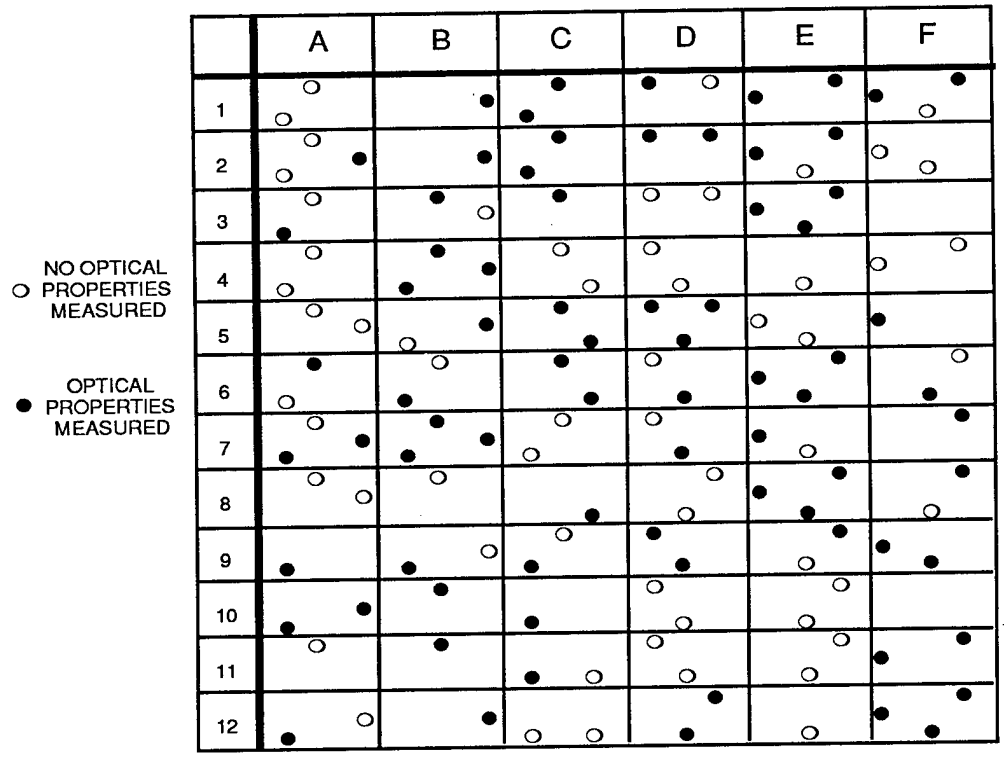


Figure 7. Map of Side Tray Clamps Available to LDEF MSIG

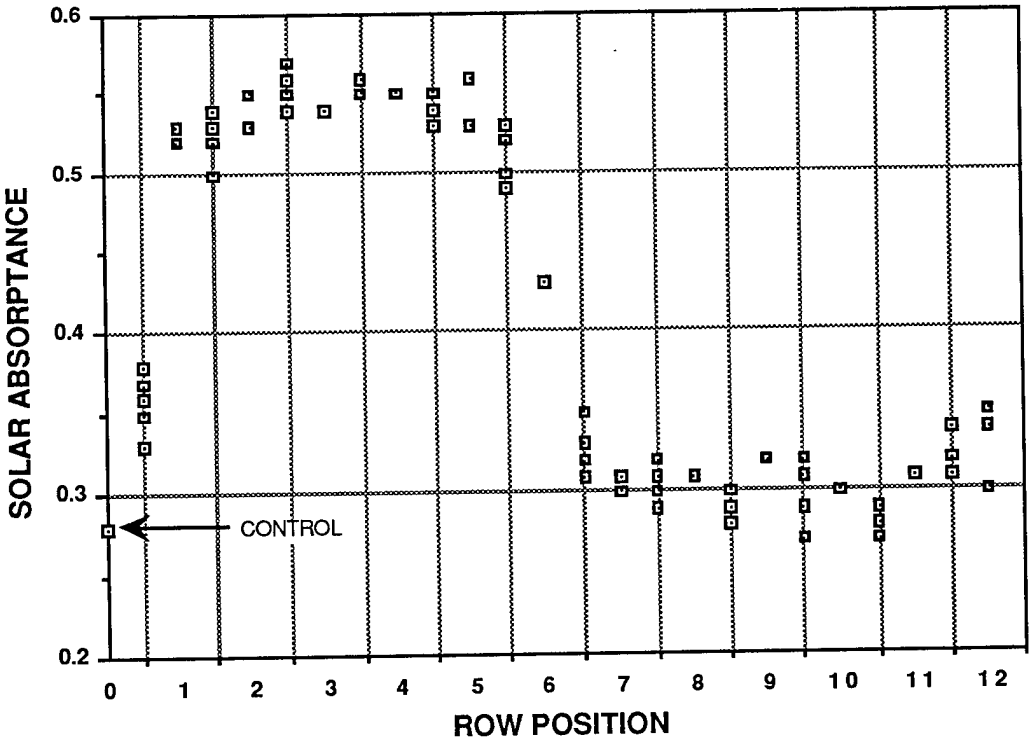


Figure 8. Absorptance Versus Side Tray Position For A276 White Paint Disks

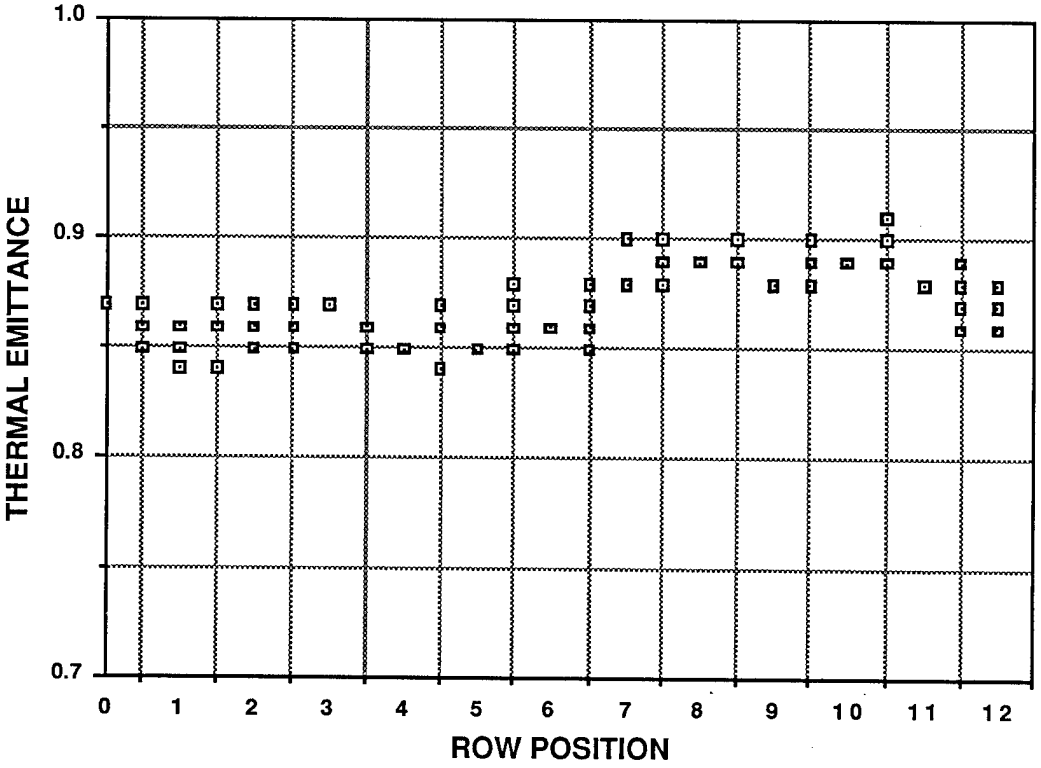


Figure 9. Emittance Versus Side Tray Position For A276 White Paint Disks

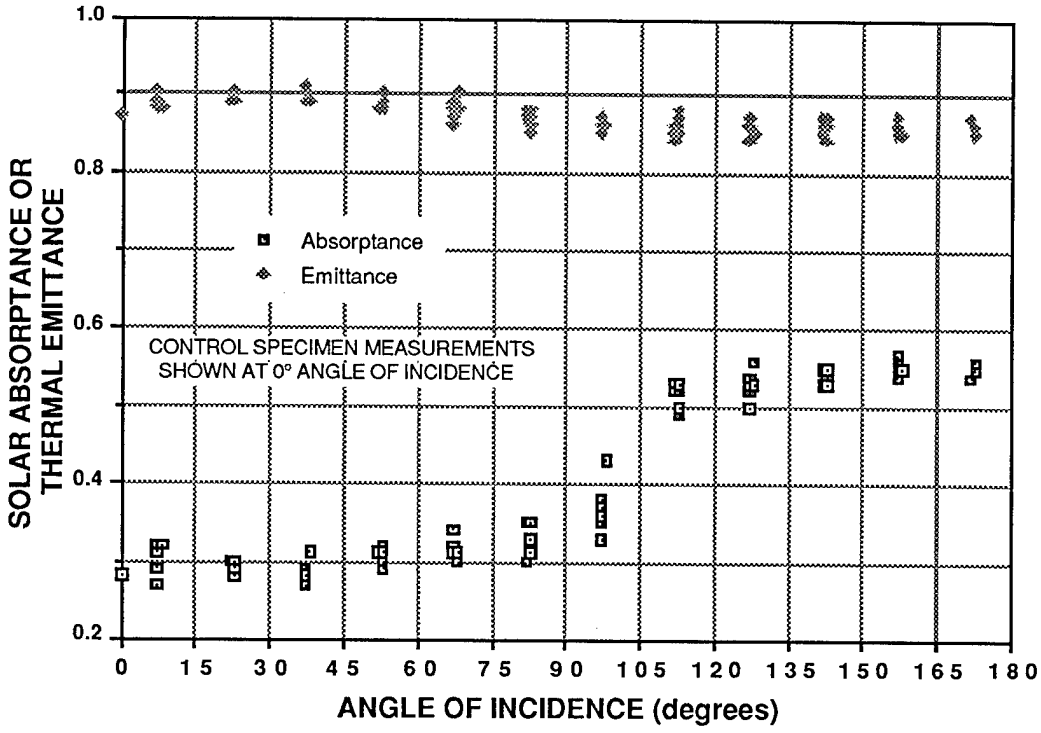


Figure 10. Optical Properties From Side Tray A276 White Thermal Control Paint Disks

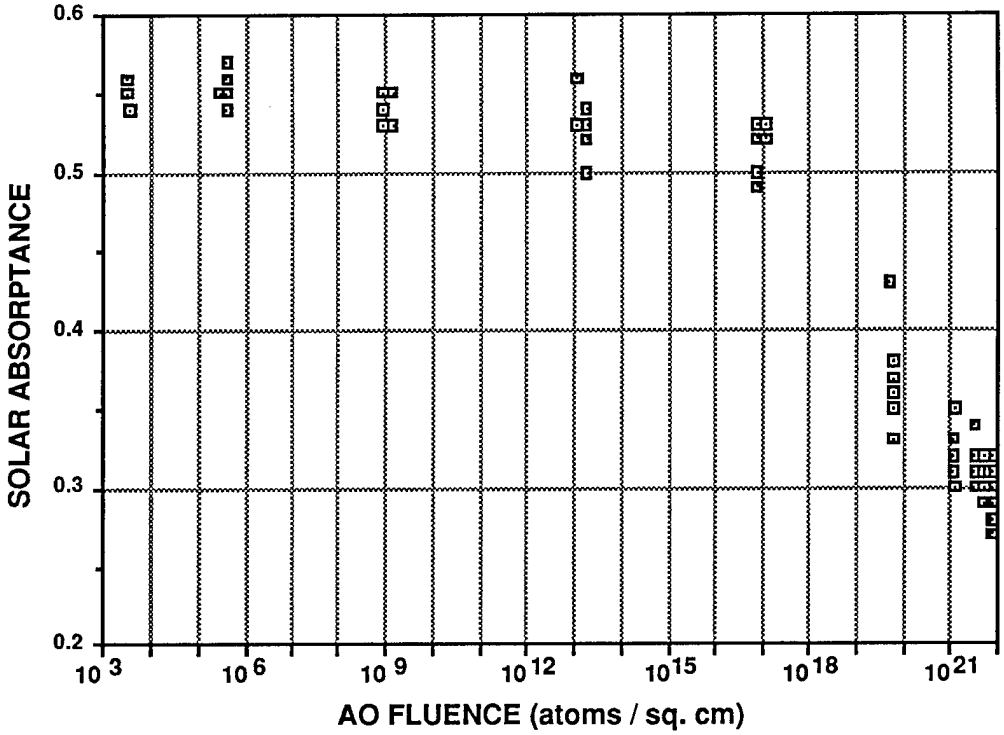


Figure 11. Absorptance Versus Atomic Oxygen Fluence For Side Tray A276 White Thermal Control Paint Disks

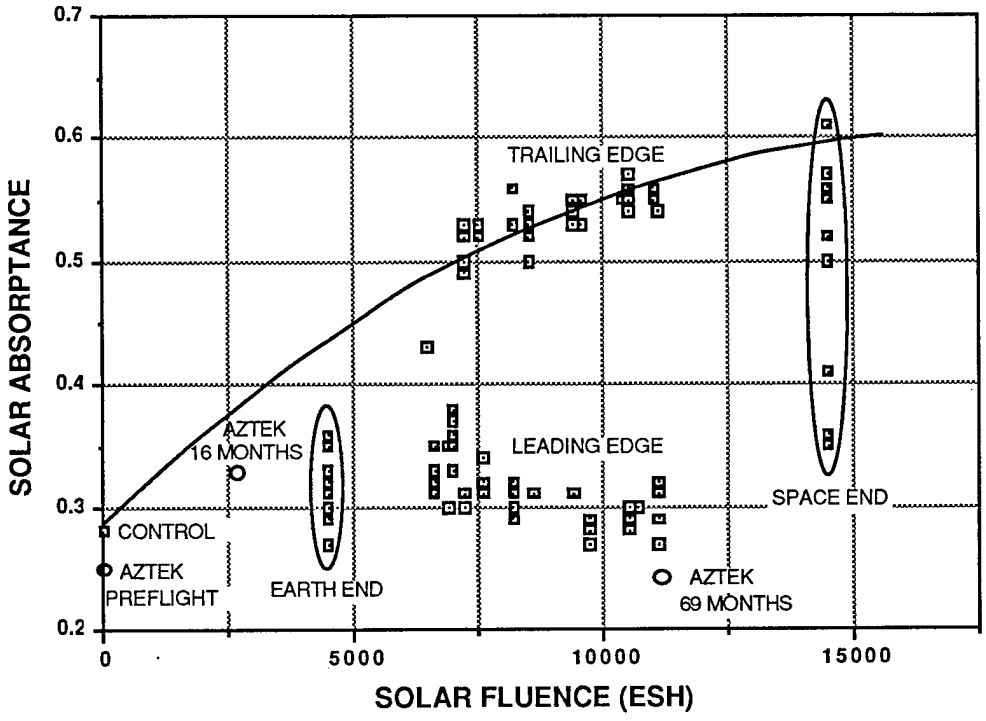


Figure 12. Absorptance Versus Solar Fluence For All A276 White Thermal Control Paint Disks

ION BEAM TEXTURED AND COATED SURFACES EXPERIMENT (IBEX)

Michael J. Mirtich and Sharon K. Rutledge
National Aeronautics and Space Administration
Lewis Research Center
Cleveland, Ohio

Nicholas Stevens
Ohio State University
Columbus, Ohio

and

Raymond Olle and James Merrow
Cleveland State University
Cleveland, Ohio

SUMMARY

Ion beam textured and commercial materials suitable for use in space power systems were flown in low Earth orbit on the Long Duration Exposure Facility (LDEF) for 5.8 years. Because of their location on LDEF (98° from the ram direction), the 36 materials were primarily exposed to vacuum ultraviolet radiation, thermal cycling, the vacuum of space, the micrometeoroid environment, and grazing incidence atomic oxygen. Measurements of solar absorptance and thermal emittance (pre- and post-flight) showed no changes for almost all of the materials, except for the S-13G and Kapton and coated Kapton samples. The optical property stability of ion beam textured surfaces and most other surfaces indicates that they are functionally durable to the synergistic rigors of the space environment.

INTRODUCTION

Future spacecraft relying on thermal control surfaces or solar thermal power generation will be subjected to the totality of the near-earth space environment. The combined effects of the near-earth environment may be synergistic and could cause degradation not observed in single exposure ground based simulation facilities. In situ exposure of various candidate materials to the space environment is required to evaluate material, optical, and electrical property durability, so that a choice of surface materials can be made with respect to optical and/or electrical performance, durability, and contamination protection requirements.

With this in mind, the IBEX, with 36 samples of various materials, was placed aboard the LDEF as a passive experiment. Twenty-seven of the samples had surfaces modified using ion beam technology, and nine were made up of commercially available materials. The materials are in some way useful in space power systems. The various types of materials tested include: ion beam

structured surfaces suitable for solar-thermal (concentrator) or space radiators, ion beam sputtered conductive coatings for thermal and space charge control, solar reflector surfaces, flexible thin film coatings and coatings for solar array blanket protection, painted and state-of-the-art solar thermal materials, and a micrometeoroid sensitive detector.

Data analysis to date and presented includes the optical properties of each surface before and after exposure to the space environment and the respective backup (not flown) surfaces, and scanning electron micrographs (SEM's) of ion beam textured surfaces.

IBEX SAMPLES AND LDEF LOCATION

Thirty-six (36) disks, each 2.4 cm in diameter, were placed in a tray whose dimensions were 42 X 48 cm. Twenty-seven (27) of the samples used an ion source to etch, sputter deposit a thin film coating, or texture a surface to obtain a desired optical property or surface conductivity.

The samples flown on IBEX are shown in Table I, where they have been arranged by category. There are six categories of surfaces. Category I includes ion beam textured surfaces suitable for space solar-thermal or space radiator applications. Materials such as copper, aluminum, inconel, stainless steel, and silicon were textured to give values of high absorptivity. Ion beam texturing can also be used to obtain high thermal emittance surfaces for these materials. Commercial paints (black chrome and nextel paint) and grafoil are also included in this category. The second category lists materials and surfaces suitable for use in thermal control. Some of these samples are standard commercial thermal control surfaces such as Kapton/Al, Teflon/Ag, S-13G, and embossed Teflon/Ag. Some of the Kapton/Al surfaces were textured to obtain sheet resistances of 10,000 ohms per square or less[1]. An overcoat of In_2O_3 was ion beam sputter deposited on Teflon/Ag to provide surface conductivity.

Categories III, IV, and V contain only one material per category. Category III is a potential solar sail (.1 μm Al/Textured Kapton). This surface has high solar reflectance, a high back side thermal emittance, and good electrical conductivity. Category IV is a micrometeoroid sensor surface of the type that has been flown on the OSO III and SERT II satellites (for 21.5 years on SERT II). Category V is an ion source beam shield made of a fiberglass composite coated with molybdenum to provide good surface conductivity and a low thermal emittance.

In category VI are solar array blanket materials. These include uncoated Kapton as well as Kapton coated with oxide-polymer films to minimize atomic oxygen degradation in low-earth orbit.

The 36 IBEX samples were placed in the tray shown in Figure I. Although it appears that there are 42 samples, 6 are actually screens over vent holes. This is a pre-flight photo of the tray with an anodized aluminum cover and an anodized coating of alumigold for thermal control. The IBEX tray measures 42 X 48 cm, and was placed on the LDEF in Row 6, Bay E[2]. It was designated experiment S1003 and took up one-sixth (1/6) of an LDEF tray.

The LDEF was launched and placed into LEO by the Challenger Shuttle in April, 1984. LDEF was retrieved in January, 1991, after 5.8 years in orbit, and taken to NASA Langley Research Center for viewing before disassembly. In this time, the IBEX samples were exposed to 6500 equivalent sun hours as well as 33,700 thermal cycles.

DATA ANALYSIS

The objective of this experiment was to measure the effects of exposure to the Shuttle launch and near-Earth space environments on the optical properties of the IBEX materials, and to obtain baseline data, not only for future performance of the materials in space, but also for ground simulation studies. It is well known that real time duplication of the totality of the space environment is almost impossible. However, some aspects of the environment are simulated quite well on the ground. Such simulations can be useful if a proper correlation is made to the real-time space environment. Materials flown in space in known environments and for extended periods of time can be used to make such correlations.

The IBEX approach, therefore, was to measure changes in optical properties by making spectral reflectance measurements between 0.25 and 2.5 μm using a Perkin-Elmer spectrophotometer, and between 1.5 and 15.5 μm using a Hohlraum reflectometer[3]. Both of these optical instruments are capable of making total and diffuse spectral reflectance measurements. These measurements give spectral absorptance and spectral reflectance values, from which the total reflectance, total absorptance, and emittance can be calculated. A Gier-Dunkle DB 100 was used to obtain total reflectance at 325 K.

Surface morphologies were documented using a scanning electron microscope. Electrical conductivity in the form of a sheet resistance measurement was determined for ion beam sputtered conductive surfaces. Weight loss measurements were made for the Kapton and the oxide-polymer coated Kapton samples. Measurement of surface chemistry changes will be done in the future using Rutherford backscattering (RBS) and electron spectroscopy for chemical analysis (ESCA). As part of the IBEX analysis, ground space-simulation studies will aid in identifying any synergistic effects of the total space environment.

POST FLIGHT RESULTS

Figure 2 shows the post-flight IBEX location relative to other experiments in LDEF tray E-6. Because of the location on LDEF, the IBEX samples were exposed primarily to thermal cycling, vacuum ultraviolet radiation, the vacuum of space, the micrometeoroid environment, and grazing incidence atomic oxygen (AO)[4]. The IBEX was also oriented at 98° relative to the peak direction of debris arrival. Initial viewing of the IBEX when mounted on the LDEF and the closeup of the IBEX shown in Figure 3 reveal no major surprises. There are a few visible impacts, and one of the textured silicon samples in position 4 was shattered; this may have been caused by mounting stress.

Category I

The samples in category I were either ion beam textured metals or commercial coatings that had a high solar absorptance. Shown in Figure 4 are photomicrographs of the surface morphologies of the various textured metals flown on LDEF. All the metals were textured using Ta as a seed material and an ion source with 1500 eV argon ions. An example of the spectral reflectance of such an ion beam textured IBEX metal is shown in Figure 5. Plotted is the

spectral reflectance (total, specular, and diffuse) between .25 and 2.5 μm for a fully textured silicon sample. A fully developed texture is usually a totally diffuse surface.

Results of optical property measurements are shown in Table II for some high absorptance materials. There were no changes in solar absorptance for all of the category I materials flown on LDEF. This is also true for the backup samples; no changes were measured in the visible and infrared over 13 years. Table II shows an increase in thermal emittance only for textured copper (from .50 to .69). This change was probably due to an oxide formation on the surface, which could cause an increase in thermal emittance. SEM's indicate no change in surface morphology for the ion beam textured materials flown on LDEF. Thus, the ion beam textured surfaces, which are delicate to the touch, were not affected by the experiment buildup, Shuttle launch, the Shuttle bay, or the space environment. Their stability should make them useful not only as optical absorbers, but also as space radiators.

Category II

Shown in Table III are the pre- and post-flight optical properties of some of the thermal control surfaces on the IBEX. The optical properties of silvered Teflon, aluminized Kapton, and embossed silvered Teflon (Wayne Slemp - NASA Langley) did not degrade after 5.8 years on LDEF. However, the S-13G sample flown in space had an increase in its solar absorptance from 0.15 to 0.40. Changes of this magnitude were observed by other LDEF experimenters and were probably due to exposure to the sun's ultraviolet radiation[5]. Most of the change in spectral absorptance took place in the visible and near UV wavelength regions. This can be seen the plot of spectral reflectance for the S-13G sample presented in Figure 6. The pre- and post-flight pictures of Figure 7 show the change in color of S-13G from white to brown.

IBEX samples 21 and 22 are silvered Teflon with an ion beam sputter deposited thin conductive coating of In_2O_3 on the Teflon side to provide a pre-flight sheet resistance of approximately 900 $\Omega/\square$. Sample 21 was flown with the In_2O_3 side exposed to space and sample 22 had the Ag side exposed to space. Figure 8 shows photomicrographs of pre- and post-flight sample 21. Although there were no measured changes in solar absorptance or thermal emittance, the photomicrograph shows cracking of the silver coating. The sheet resistance of sample 21 increased from 900 $\Omega/\square$ to 2000 $\Omega/\square$.

Presented in Figure 9 is a photomicrograph of sample 22 (Ag side up), and the back side of sample 21 (showing the silver side which was not exposed to space). Sample 22 looks like a dried up river bed, whereas sample 21 shows slight cracking, unlike the pattern in sample 22. Since the Ag side of sample 22 was exposed to the space environment, it could be that the silver oxidized. This warrants further investigation. Figure 10 shows the total reflectance of flight sample 22 and its backup. There is a large reduction in solar reflectance, which is a good indicator of oxidation of the Ag.

Category III

The solar sail (reflector) material (artist's concept shown in Figure 11), a coating of 0.1 μm Al on textured Kapton, normally has a coating of chromium (Cr) placed on the backside (Kapton) to obtain high emittance. The Cr was removed by ion beam sputtering, and the Kapton was given a surface

texture. Removal of the Cr allowed for a weight reduction, and texturing of the Kapton yielded a higher emittance than that provided by the Cr; this allowed the solar sail to operate at 0.2 A.U. (25 suns). There was no change in the value of solar reflectivity after exposure to space (ρ_s=.90), indicating that this type of solar sail material may be used in orbits where AO is not an environmental hazard.

Category IV

The micrometeoroid detector flown on IBEX was a 2000 Å layer of Al vapor deposited on stainless steel (by G. Hass of the Army Research and Development Center in 1963). This surface has a long history in space (Figure 12) and was ground calibrated in the 1960's when the majority of the micrometeoroid sensors (capacitor discharge or microplane sensors) had little or no such calibration[6].

Figure 12 shows satellites on which the aluminum sensor has flown, their orbits, and the duration of their time in space. Notice that data has been taken from SERT II for 21 years. The effects of the space environment (i.e. the debris/micrometeoroid environment) on the solar reflectance (or solar absorptance) of the sensors was negligible. The results are in agreement with the 1969 micrometeoroid flux model [7] and the 1987 Orbital Debris Model of Laurance and Brownlee[8].

From the accuracy of the sensor, these results indicate that a reflector surface (a highly polished metal or thin metal film deposit) should lose less than 1% of its specular reflectance in near-Earth orbit over 20 years. This is an important factor in the design of space solar dynamic/concentrator systems. No changes in solar reflectance were obtained on the LDEF for this surface as well.

Category V

Ion beam shields are used to protect solar cells and other surfaces from the efflux given off by an ion thruster during operation in space. A beam shield made of fiberglass composite was coated on both sides with a 0.1 μm ion beam sputter-deposited molybdenum (Mo) film. Because of the low emittance of Mo, this coating allows the beam shield to operate at a higher temperature, thus preventing mercury condensation during operation. The Mo also provides electrical conductivity to prevent plasma arcing. This surface returned unaltered after 5.8 years of exposure on LDEF.

Category VI

Kapton polyimide is the material considered for use in the Space Station Freedom solar array blanket. It has been shown on STS-8 that Kapton, which normally degrades in atomic oxygen, can be made more durable in the AO environment by coating with oxide-polymer films. Because of the promising results of the STS-8 flight[9], pristine Kapton and three different types of coated Kapton (Table IV) were substituted on IBEX just before launch of the LDEF.

At 98° to the ram direction the AO grazing incidence resulted in a fluence of only 4.93 X 10^{19} atoms/cm^2.[5] It is clear from scanning microscopy

inspection that the Al_2O_3, SiO_2, and 4% PTFE, 96% SiO_2 did protect the Kapton from AO. There was no evidence of spalling of the thin films after 33,700 cycles. However, there were changes in solar absorptance, probably due to UV darkening (a chemical change). This should not have a significant effect on a solar array blanket since the anti-solar side of the blanket would see only albedo illumination. The optical property of importance is the thermal emittance, which showed negligible change. Detailed results on the Kapton and coated Kapton materials are given in reference 4.

CONCLUDING REMARKS

Thirty-six materials with potential uses in spacecraft were flown on the IBEX/LDEF. One sample, textured Si, was returned from space shattered and this was believed to be due to mounting stress. Measurements of the optical properties of the remaining 35 samples indicated no change in either solar absorptance or thermal emittance, except for an increase in solar absorptance of S-13G and of the Kapton and coated Kapton samples. There was an increase in thermal emittance for the textured Cu. SEM's indicated no changes in surface morphology for the ion beam textured materials (potential absorbers or radiators) flown on LDEF. This stability showed that textured surfaces, delicate to the touch, could survive the rigors of the totality of space flight and the space environment.

The In_2O_3 coating on silvered Teflon showed cracking and a decrease in electrical conductivity. The mirrored surface (micrometeoroid detector) showed no change in solar reflectance and corroborated the results of this surface flown on SERT II and OSO III for as long as 21 years. Coated Kapton samples were not degraded by atomic oxygen attack. Thermal emittance changes were insignificant for the coated Kapton. There was no evidence of spalling of the coatings. There were absorptance changes, but they should not affect performance of solar array blankets.

REFERENCES

1. Mirtich, M.J.; Sovey, J.S.: Optical and Electrical Properties of Ion beam Textured Kapton and Teflon. J. Vac. Sci. Technol., March/April, 1978, pp. 697-701.

2. Clark, L.G.; Kinard, W.H.; Carter, D.J.; and Jones, J.L.: Long Duration Exposure Facility (LDEF) Mission I Experiments. NASA SP 473, 1984.

3. Mirtich, M.J.; and Kussmaul, M.K.: Enhanced Thermal Emittance of Space Radiators by Ion-Discharge Chamber Texturing. NASA TM 100137, 1987. Also in Surface and Coatings Tech., 33(1987), pp. 511-521.

4. Rutledge, S.K.; Olle, R.M.: Durability Evaluation of Photovoltaic Blanket Materials Exposed on LDEF Tray S1003. Proceedings of the 1st LDEF Meeting, Orlando, Florida, 1991.

5. Steube, K.E.; and Linford, R.M.F.: Long-Duration Exposure of Spacecraft Thermal Coatings to Simulated Near-Earth Orbital Conditions. AIAA 6th Thermoplastics Conference, Tulahoma, Tennessee, April, 1971.

6. Mirtich, M.J.; Mark, H.; Kerslake, B.: Effect of Eleven Years in Earth Orbit on a Mirror Surface. J. Spacecraft and Rockets, May-June, 1990, pp. 258-266.

7. Cour-Palais, B.G.: Meteoroid Environment Model, Near Earth to Lunar Surface. NASA SP 8013, 1969.

8. Laurance, M.R.; and Brownlee, D.E.: The Flux of Meteoroids and Orbital Space Debris Striking Satellites in Low Earth Orbit. Nature, Vol. 323, 1986, pp 136-138.

9. Banks, B.A.; Mirtich, M.J.; Rutledge, S.K.; and Swec, D.M.: Sputtered Coatings for Protection of Spacecraft Polymers. NASA TM 83706, 1984.

TABLE I

Ion Beam Textured and Coated Surfaces
LDEF Experiment

Category
I High Solar Absorptive Surfaces
II Thermal Control Surfaces
III Solar Reflector Surfaces
IV Micrometeoroid Sensitive Surface
V Conductive Ion Thruster Beam Shield
VI Solar Array Blanket Material

Sample Number	Sample Category	Sample Description*
3	I	Textured Si
4	I	Textured Si
5	I	Textured Ti (6% Al, 4% V)
8	I	Textured stainless steel (type 304)
10	I	Textured inconel
11	I	Textured copper coated with .1 μm Al)
13	I	Textured Cu
15	I	Textured pyrolytic graphite
27	I	Black chrome
28	I	Grafoil
31	I	Nextel paint
1	I	.1 μm Au/ textured FEP
2	I	.1 μm Au/ textured FEP
17	II	Textured Kapton/ .1 μm Al
18	II	Textured Kapton/ .1 μm Al
19	II	Textured Kapton/ textured Kapton/ .1 μm Al
20	II	Textured Kapton/ textured Kapton/ .1 μm Al
21	II	In_2O_3/Teflon/.15 μm Ag
22	II	.15 μm Ag/Teflon/ In_2O_3
23	II	Teflon/textured Teflon/.1 μm Ag
24	II	Teflon/textured Teflon/.1 μm Ag
29	II	5-mil Kapton/.1 μm Al
30	II	5-mil Teflon/.15 μm Ag
32	II	S-13 G
33	II	Embossed Teflon/ .15 μm Ag
25	III	.1 μm Al/textured Kapton
35	IV	1900 Å Al/stainless steel
36	V	.1 μm Mo/fiberglass composite/.1 μm Mo
6	VI	Kapton
34	VI	Kapton
7	VI	.065 μm (4% PTFE, 96% SiO_2)/Kapton
9	VI	.065 μm SiO_2/ Kapton
14	VI	.065 μm (4% PTFE, 96% SiO_2)/ Kapton
16	VI	.065 μm SiO_2/ Kapton
12	VI	.070 μm Al_2O_3/ Kapton
26	VI	.070 μm Al_2O_3/ Kapton

*Note: the first surface listed is the exposed surface.

TABLE II

ION BEAM TEXTURED HIGH ABSORPTANCE METALS AND COMMERCIALLY AVAILABLE COATINGS FLOWN ON LDEF

	SOLAR ABSORPTANCE		THERMAL EMITTANCE (325°K)	
SAMPLE	Pre-flight 1982	Post-flight 1990	Pre-flight 1982	Post-flight 1990
Si	.95	.96	.71	.68
Ti	.88	.88	.21	.18
Cu	.94	.94	.50	.69
Graphite	.96	.96	.78	.77
Inconel	.92	.92	.25	.25
Stainless Steel	.91	.93	.26	.28
Black Chrome	.90	.90	.18	.18
Nextal Paint	.97	.97	.91	.91

TABLE III

THERMAL CONTROL SURFACES FLOWN ON LDEF

	SOLAR ABSORPTANCE		THERMAL EMITTANCE (325°K)	
	Pre-flight 1982	Post-flight 1990	Pre-flight 1982	Post-flight 1990
S-13 G Backup	.15	.15	.89	.89
S-13 G Flight	.15	.40	.89	.89
Teflon/.15 μm Ag	.091	.092	.808	.807
Kapton/.1 μm Al	.48	.45	.86	.86
Embossed FEP/.15 μm Ag	.118	.125	.82	.82

Table IV. Changes in optical properties and mass for photovoltaic blanket samples on LDEF tray S1003.

MATERIAL AND SAMPLE DESIGNATION	TOTAL REFLECT-ANCE	TOTAL TRANSM-ITTANCE	SOLAR ABSORP-TANCE	THERMAL EMIT-TANCE	MASS LOSS (G)
UNCOATED KAPTON (NOT FLOWN)	0.135	0.576	0.289	0.70	-----
UNCOATED KAPTON (LDEF #6)	0.136	0.580	0.285	0.72	2.6E-4
UNCOATED KAPTON (LDEF #34)	0.130	0.583	0.286	0.71	2.4E-4
SiO_2 ON KAPTON (NOT FLOWN)	0.116	0.573	0.311	0.72	-----
SiO_2 ON KAPTON (LDEF #9)	0.105	0.561	0.334	0.72	8.3E-5
SiO_2 ON KAPTON (LDEF #16)*	---	---	---	---	7.2E-5
4% PTFE-96% SiO_2 ON KAPTON (NOT FLOWN)	0.109	0.584	0.307	0.72	-----
4% PTFE-96% SiO_2 ON KAPTON (LDEF #7)	0.103	0.578	0.319	0.72	8.1E-5
4% PTFE-96% SiO_2 ON KAPTON (LDEF #14)	0.103	0.576	0.321	0.71	7.4E-5
Al_2O_3 ON KAPTON (NOT FLOWN)	0.120	0.571	0.309	0.72	-----
Al_2O_3 ON KAPTON (LDEF #12)	0.118	0.545	0.337	0.71	9.0E-5
Al_2O_3 ON KAPTON (LDEF #26)	0.119	0.551	0.330	0.72	0

* SAMPLE SECTIONED FOR ANALYSIS PRIOR TO OPTICAL MEASUREMENTS

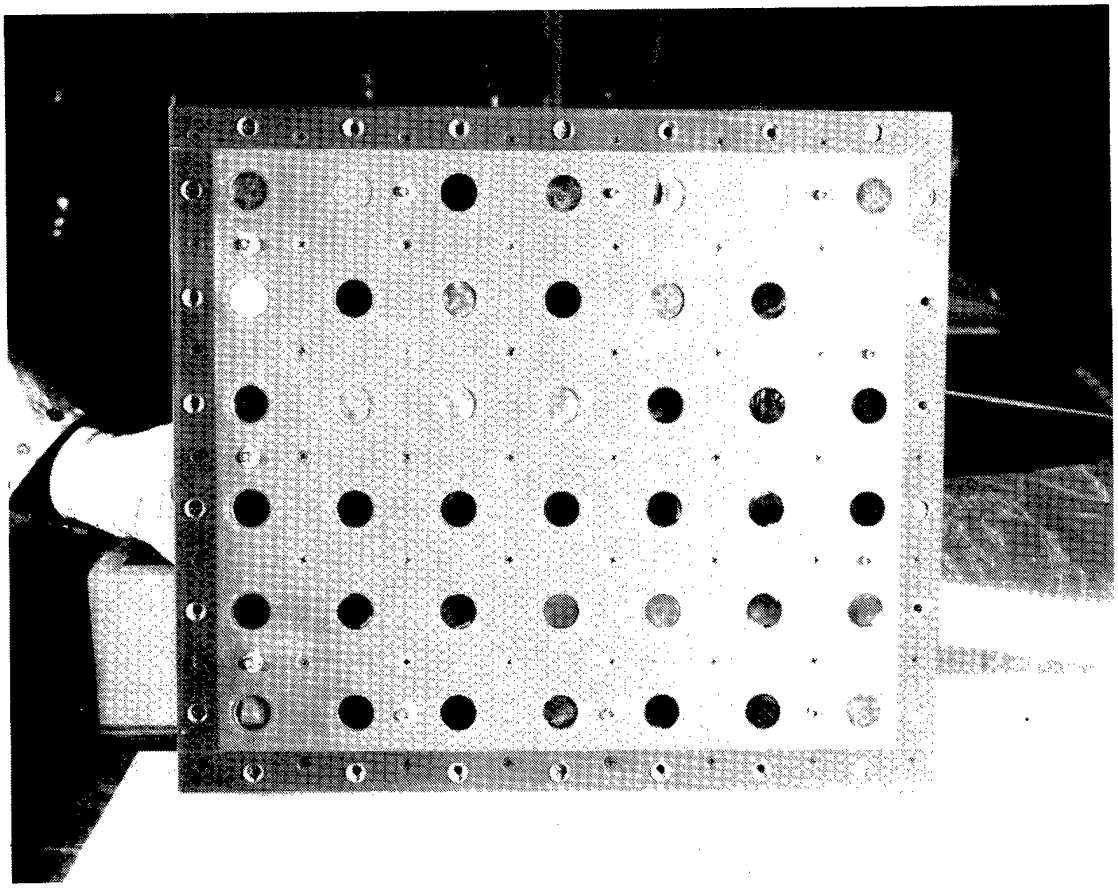


Figure 1. Pre-flight IBEX sample tray (42 X 48 cm).

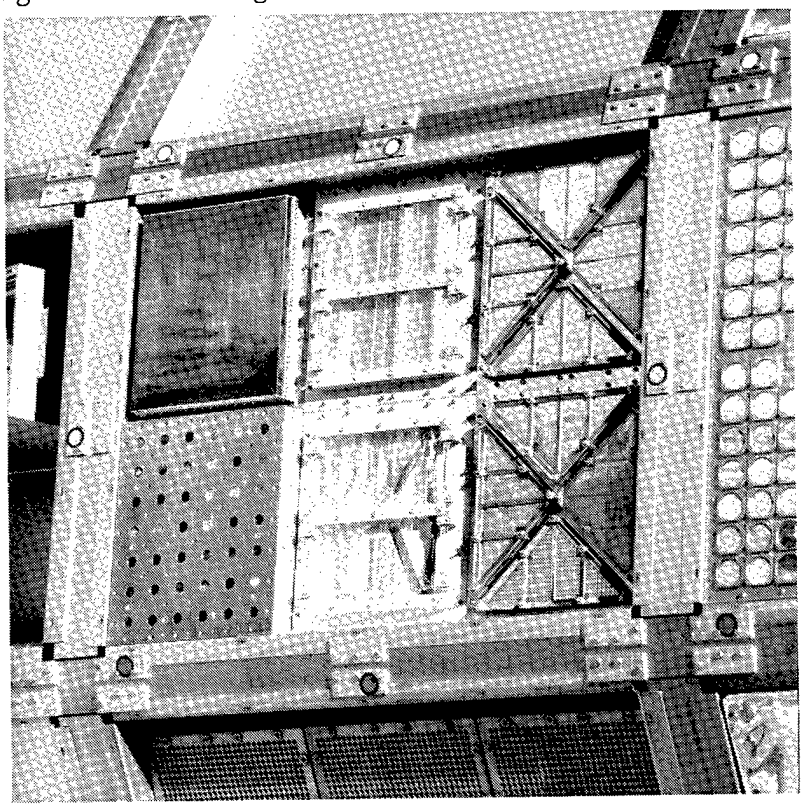


Figure 2. Post-flight photograph of IBEX location in tray E-6.

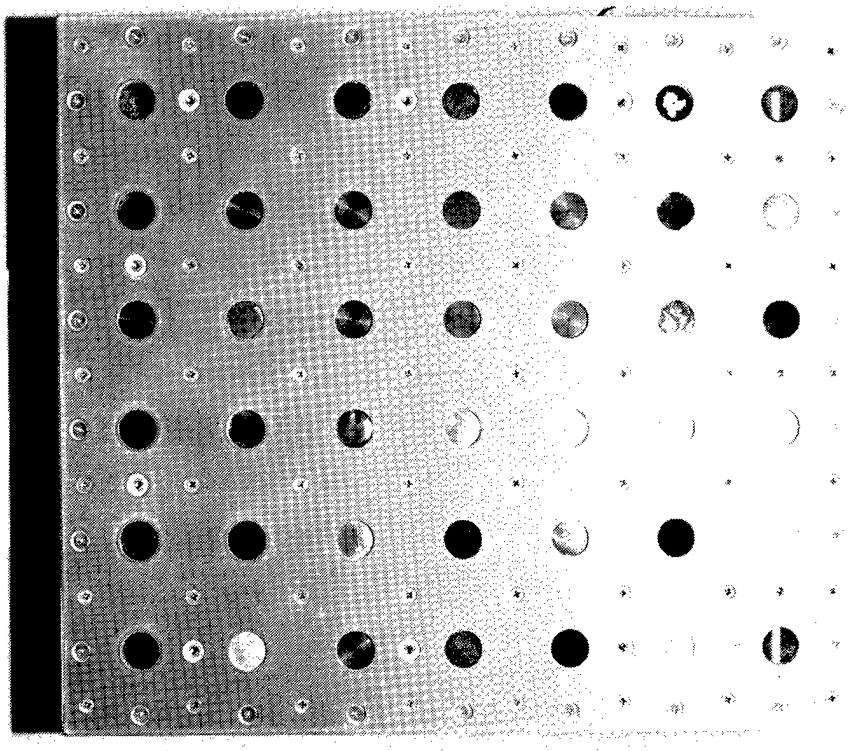
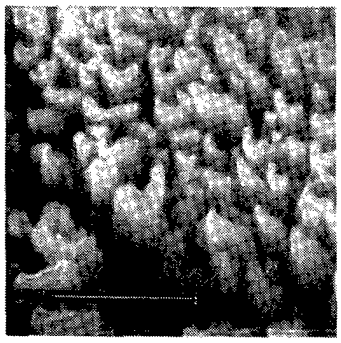
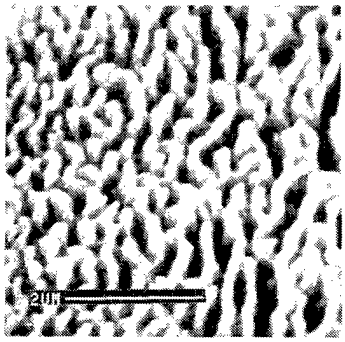


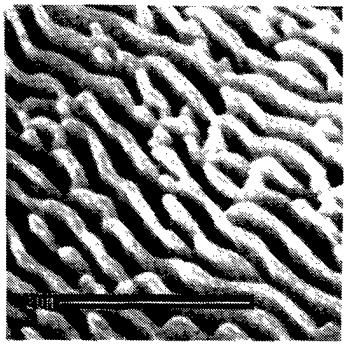
Figure 3. Photograph of post-flight IBEX tray.



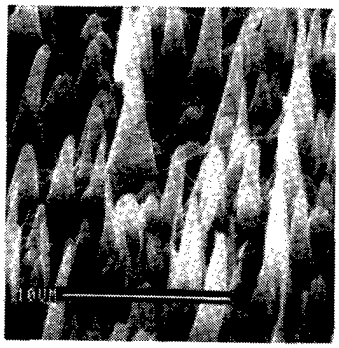
TEXTURED COPPER



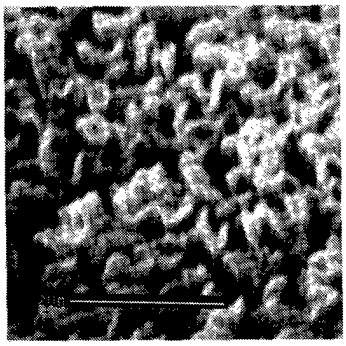
TEXTURED INCONEL



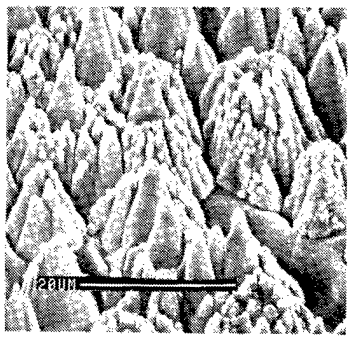
TEXTURED STAINLESS STEEL (304



TEXTURED PYROLYTIC GRAPHITE



TEXTURED SILICON



Al/Textured Cu

Figure 4. Scanning electron micrographs of textured metals flown on LDEF.

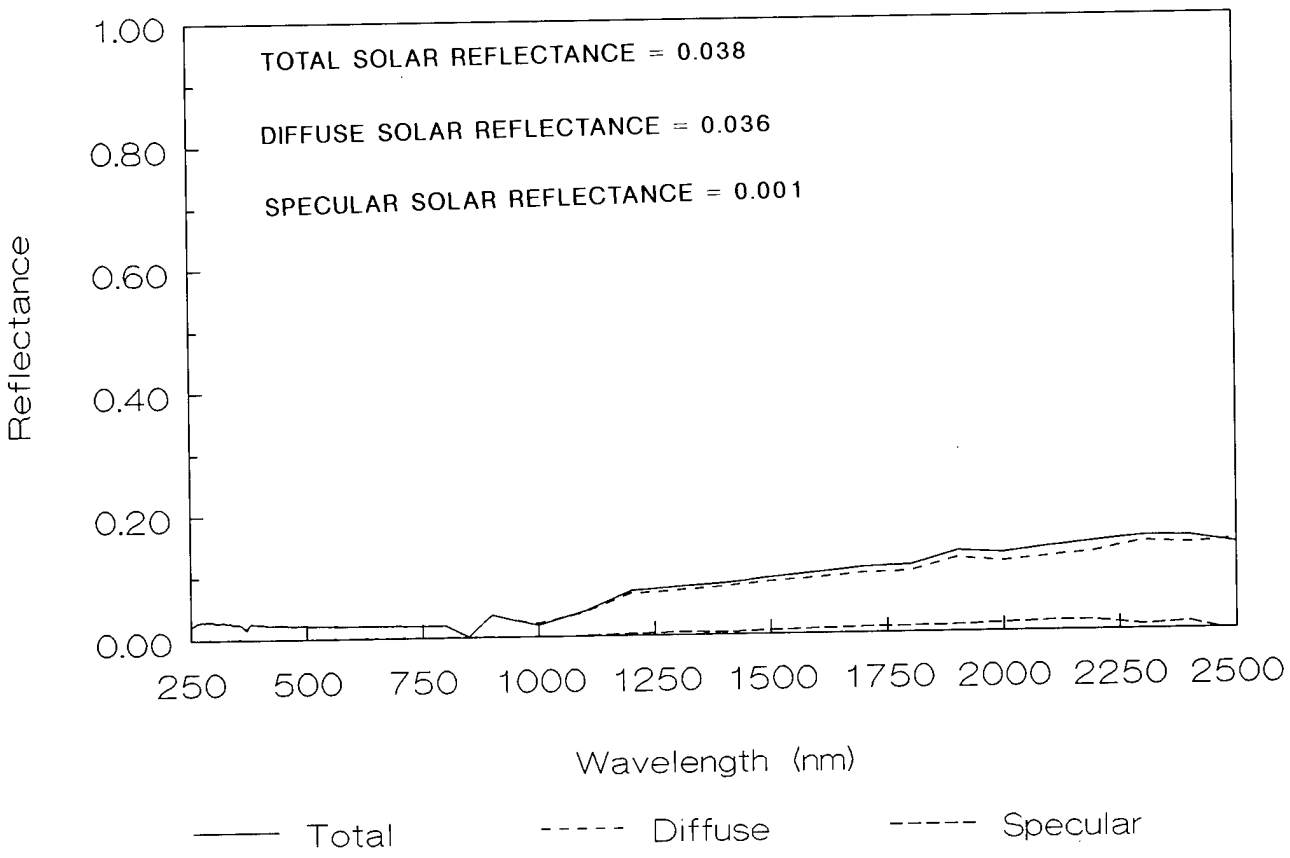


Figure 5. Spectral reflectance of post-flight textured Si (sample 3).

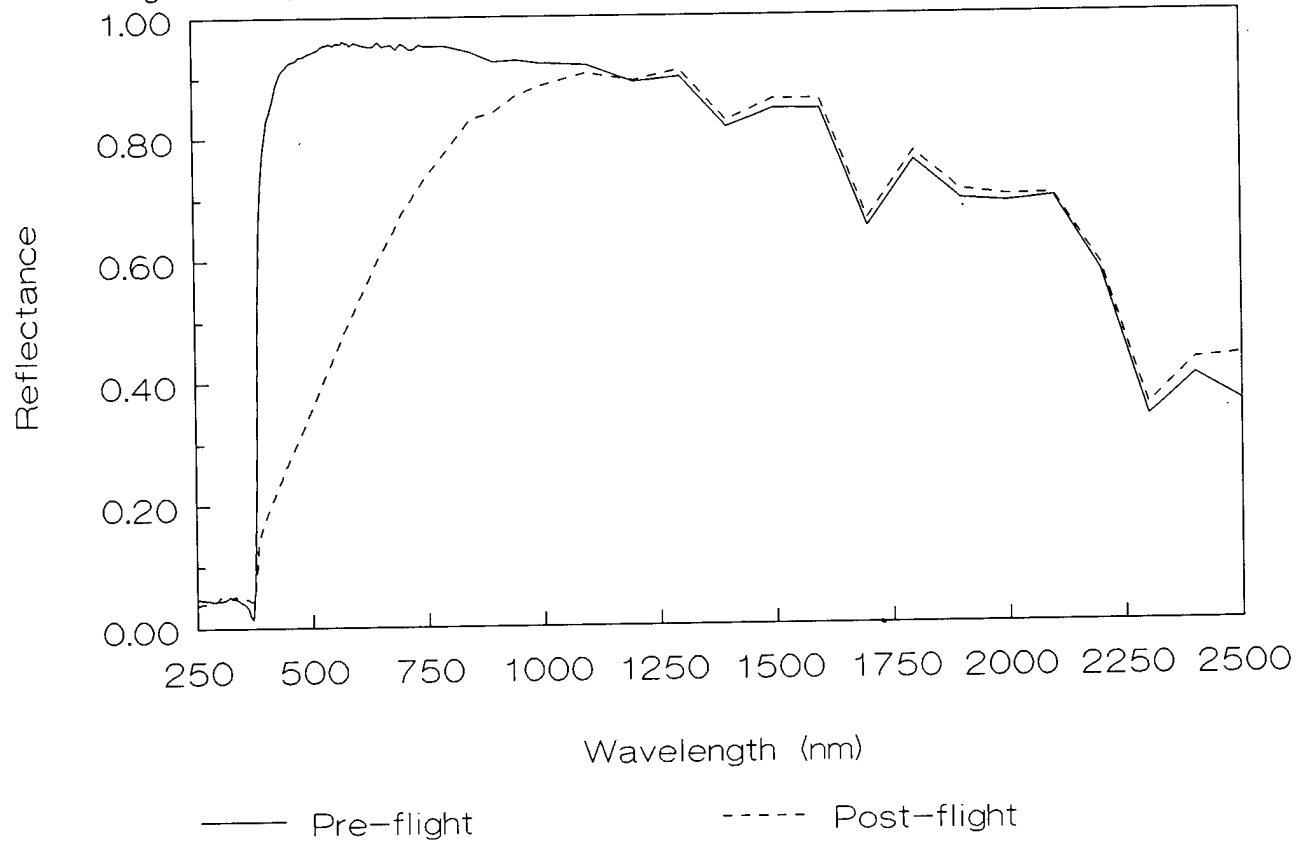


Figure 6. Pre- and post-flight total spectral reflectance of S-13G.

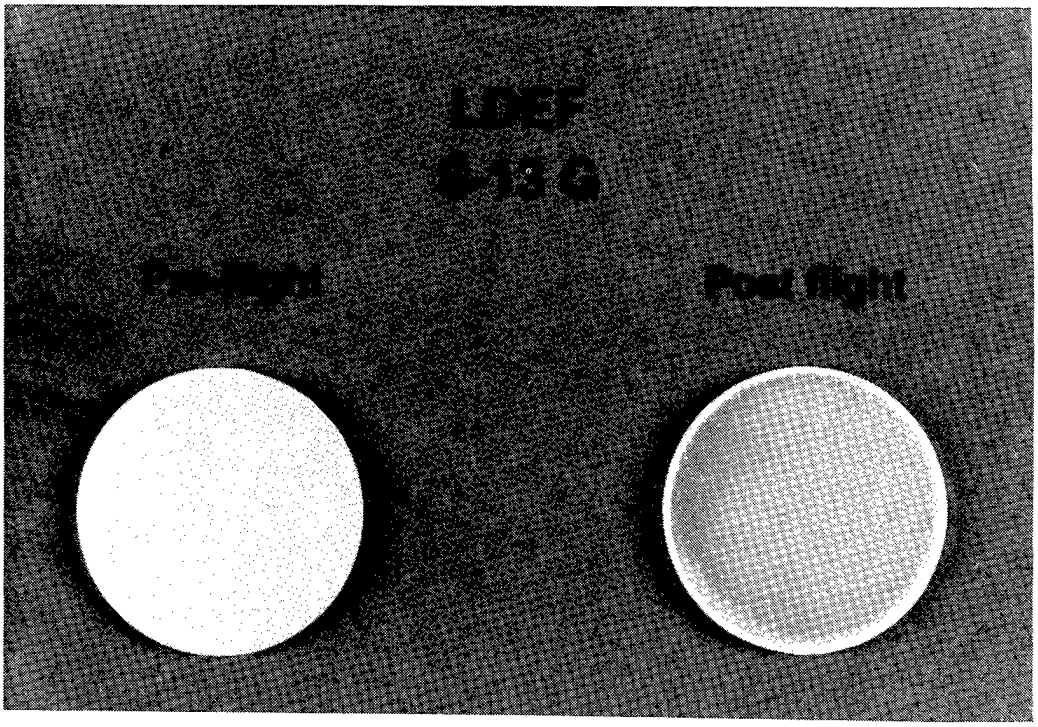


Figure 7. Photograph of pre- and post-flight S-13G.

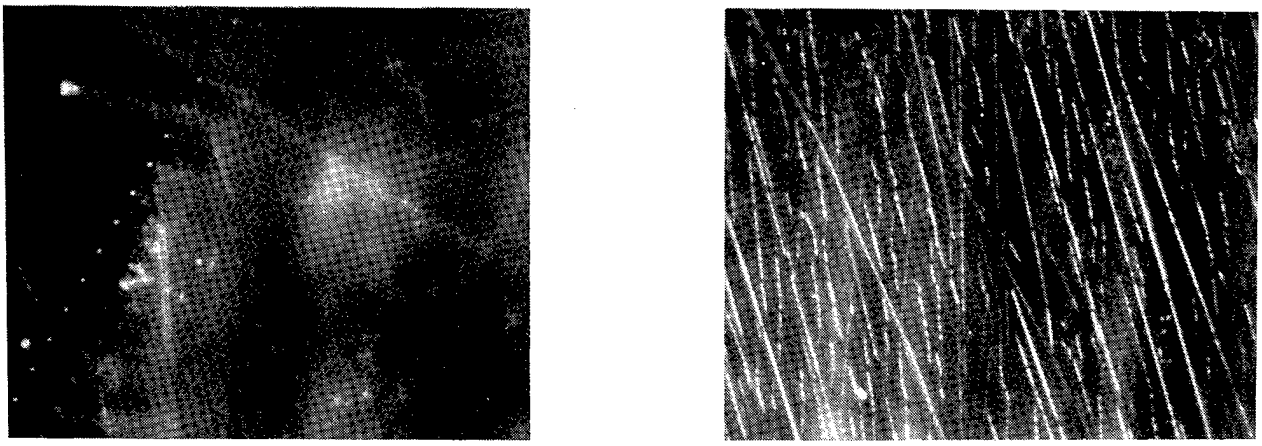
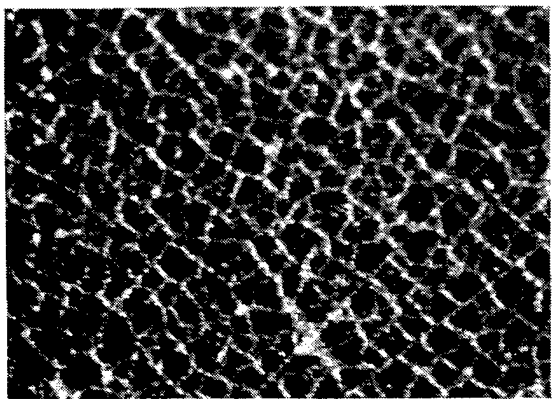
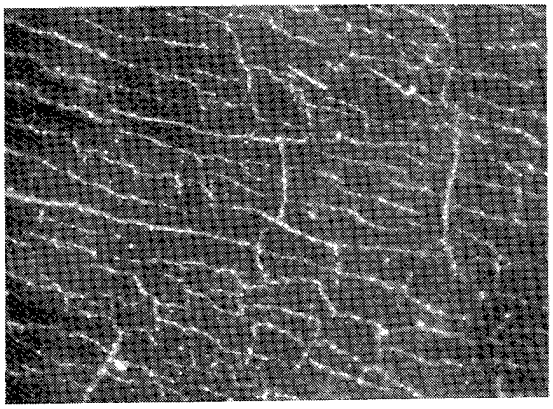


Figure 8. Photomicrograph (100X) of post-flight cracks in silver coating.



SAMPLE 22



BACK OF SAMPLE 21

Figure 9. Photomicrograph of sample 22 (Ag/Teflon/In_2O_3) and back of Sample 21 (Ag side not exposed to space).

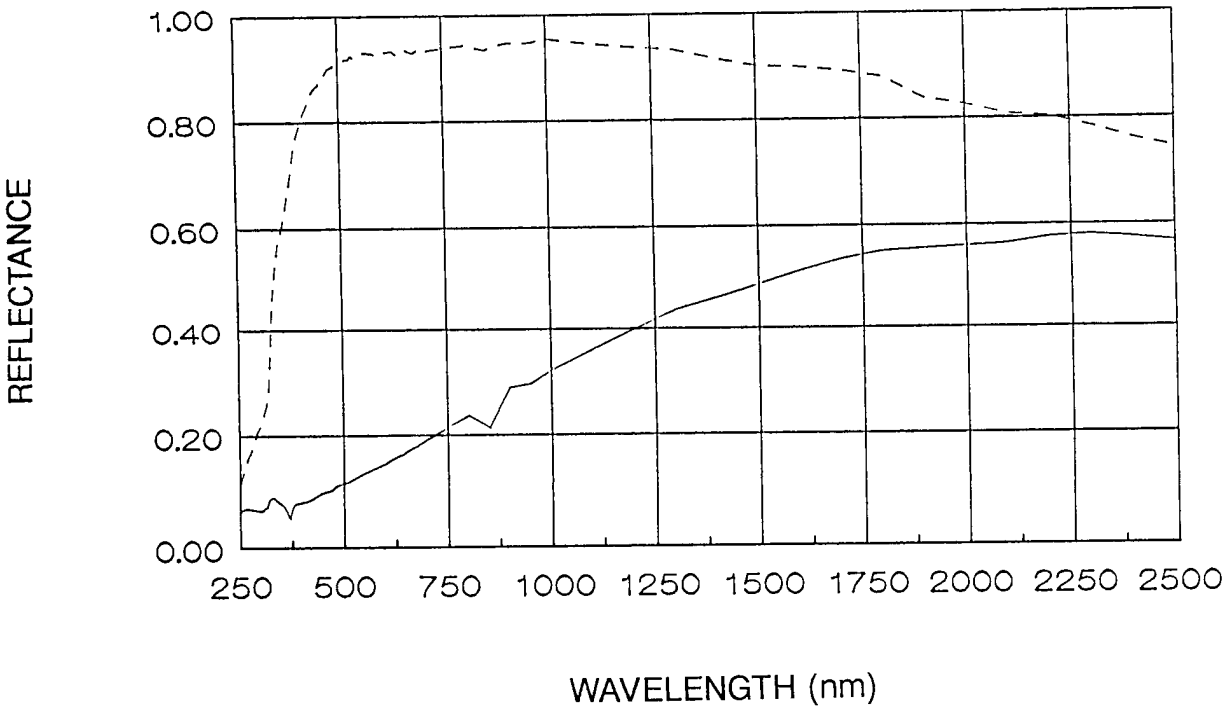


Figure 10. Total reflectance of sample 22 and its backup - Ag/Teflon/In_2O_3.

SOLAR SAIL

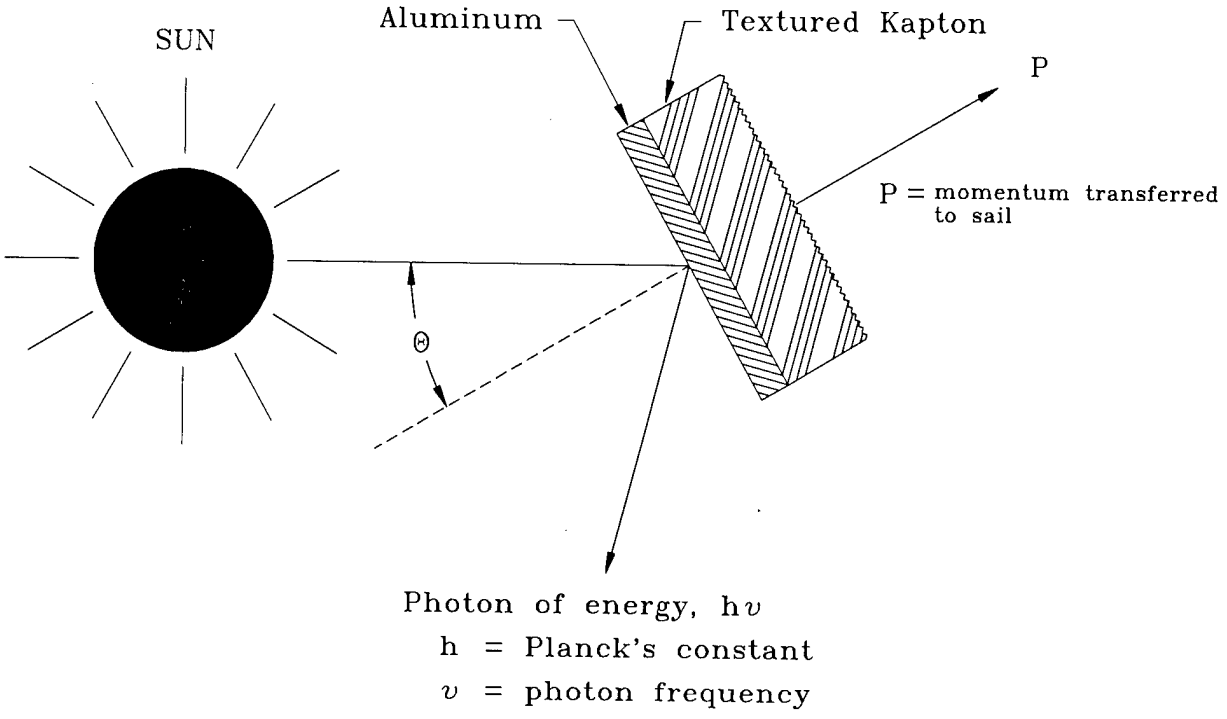


Figure 11. Artist's concept of solar sail using Al/Textured Kapton.

MICROMETEOROID/DEBRIS SENSITIVE MIRROR SURFACE 2000Å Al/STAINLESS STEEL

SATTELITE	ORBIT	TIME FRAME	COMMENT
SERT II	POLAR 1000 km	1970-1991	NO CHANGE IN α_{SUN} AFTER 21 YEARS
OSO II	EQUATORIAL 550 km, 33°	1967-1972	NO CHANGE IN α_{SUN} AFTER 5 YEARS
LDEF	EQUATORIAL 460 km, 28.5°	1984-1990	NO CHANGE IN α_{SUN} AFTER 5.5 YEARS

Figure 12. Micrometeoroid/debris sensitive mirror surface (2000Å Al/Stainless Steel) and satellites it has flown on.

ELLIPSOMETRIC STUDY OF OXIDE FILMS FORMED ON LDEF METAL SAMPLES

W. Franzen, J.S. Brodkin, L.C. Sengupta and P.L. Sagalyn
Army Materials Technology Laboratory

SUMMARY

The optical constants of samples of six different metals (Al, Cu, Ni, Ta, W and Zr) exposed to space on the LDEF have been studied by variable angle spectroscopic ellipsometry. Measurements were also carried out on portions of each sample which were shielded from direct exposure by a metal bar. A least-squares fit of the data using an effective medium approximation was then carried out, with thickness and composition of surface films formed on the metal substrates as variable parameters. The analysis revealed that exposed portions of the Cu, Ni, Ta and Zr samples are covered with porous oxide films ranging in thickness from 500 to 1000 Å. The 410 Å thick film of Al_2O_3 on the exposed Al sample is practically free of voids. Except for Cu, the shielded portions of these metals are covered by thin non-porous oxide films characteristic of exposure to air. The shielded part of the Cu sample has a much thicker porous coating of Cu_2O. The tungsten data could not be analyzed.

SYMBOLS

subscript p: polarization parallel to plane of incidence (horizontal plane)
subscript s: polarization perpendicular (senkrecht) relative to plane of incidence
subscript i: incident wave
subscript r: reflected wave

L = skin depth
E = oscillating electric vector (complex)
$r_p = E_{pr}/E_{pi}$
$r_s = E_{sr}/E_{si}$
n = index of refraction
k = extinction coefficient
$\tan \psi$ = amplitude ratio = $|r_p/r_s|$
Δ = phase difference between the p-polarized and s-polarized components of the reflected light
ϕ = angle of incidence
λ = wavelength in Angstroms
Å = Angstrom = 10^{-8} cm

INTRODUCTION

The technique of characterizing surface films and multilayer materials by spectroscopic ellipsometry has been greatly advanced in the last thirty years (refs. 1-6). In this technique, a plane-polarized monochromatic collimated light beam is reflected from the surface being analyzed. The reflected light will then be elliptically polarized, in general. In order to determine the parameters of the ellipse a Fourier analysis is performed of the time-varying intensity of the reflected beam after transmission through a rotating analyzer.

The important ellipsometric parameters ψ and Δ are derived from the real part $\tan\psi\cos\Delta$ and the imaginary part $\tan\psi\sin\Delta$ of the complex reflectivity ratio:

$$r_p/r_s = e^{i\Delta}\tan\psi\,. \qquad (1)$$

The optical constants n (index of refraction) and k (extinction coefficient) are computed from ψ and Δ. For a layered structure, the values of n and k so obtained are pseudo-optical constants, that is, not related to the optical properties of a single substance.

The values of ψ and Δ measured in this fashion reflect the composition of the surface to a depth on the order of the skin depth, L, a quantity that depends on the conductivity of the surface material at optical frequencies. For metals of high conductivity (e.g. aluminum) L is less than 200 Å for visible light; however, for metals of low conductivity like tungsten, L is substantially larger. For semiconductors like Cu_2O or CuO, L is still larger and for transparent insulators like Al_2O_3 or ZrO_2, L is effectively infinite.

EXPERIMENTAL

Square plates of dimensions 0.3 x 5 x 5 cm^3 of the six metals Al, Cu, Ni, Ta, W, and Zr were mounted on the LDEF in the locations indicated in Table I and then examined by ellipsometry after recovery. An aluminum bar 0.63 cm wide was affixed across the middle of each plate and shielded a portion of each sample from direct exposure to the space environment, as shown in Fig. 1.

A schematic diagram of the ellipsometer used to obtain the optical data is shown in Fig. 2. White light is generated from a high pressure xenon arc lamp and passes successively through a step-motor-controlled grating monochromator, an electronically controlled shutter, and a linear polarizer before reflection from the surface of the sample. The reflected light is directed through a rotating analyzer before falling on the photocathode of a photomultiplier.

During an experimental run at a fixed angle of incidence ϕ, data is obtained after executing a data acquisition program with input for ϕ, polarizer setting, wavelength range and sampling increment. For a given wavelength setting λ, the program subtracts the output of the multiplier for 150 revolutions of the analyzer with the shutter open from a similiar output obtained with the shutter closed. This effectively eliminates any contribution from background radiation. The step-motor is computer-driven to advance the wavelength setting of the monochromator to the next programmed sampling point, and the procedure just described is repeated. Most of the data reported herein was recorded over a wavelength range from 4000 to 8000 Å in 200 Å steps, and each set of data was obtained at three different angles of incidence for each specimen.

A computer program analyzes the output of the photomultiplier in terms of the Fourier coefficients of the time-varying optical signal and derives the corresponding values of the ellipsometric angles ψ and Δ for each wavelength setting. The measured values of ψ and Δ are functions of the change in the polarization of the reflected light from the sample and with mathematical manipulation can yield a great deal of information about surface structure and composition. For this purpose we employ a software package (VASE), written by the J.A. Woollam Company. VASE uses the Marquardt algorithm and a Bruggeman Effective Medium Approximation (ref.6) to make a least-squares fit of a model of the surface with variable parameters to the experimental data. For every material represented in our model, we must have available a table of optical constants in the same wavelength range as for the experimental data.

For the LDEF samples we chose a model consisting of a metal substrate covered by a porous oxide film. The porosity of the film was defined by the proportion of voids (air) present in it. That proportion and the thickness of the film were the two variable parameters in the least-squares fitting procedure. To fit the model we used published data obtained for each oxide-free metal substrate, bulk measurements for the appropriate metal oxide, and optical constants for air.

RESULTS

1. Aluminum

The Al_2O_3 film formed on aluminum when exposed to air is usually 20 to 55 Å thick (ref. 7). The difficulty of producing a smooth optically flat surface on metallic aluminum is well known (ref. 8). A critical selection from among the large number of studies of the optical constants of aluminum has been made by D.Y. Smith et al. (ref.9). For amorphous Al_2O_3 we used the data obtained by Hageman et al. (ref. 10).

For the exposed part of the sample a good fit was obtained for a 395 Å thick film of Al_2O_3 containing no voids which covers a metallic aluminum substrate. The shielded portion consists of a 68 Å thick layer of Al_2O_3 over metallic aluminum. The data obtained on the aluminum sample are shown in Figs. 3 and 4.

2. Copper

Many measurements of the optical constants of copper have been reported in the literature; we used the choice made by D.Y. Lynch and W.R. Hunter (ref.11). There are two stoichiometric copper oxides, cuprous oxide, Cu_2O (red) and cupric oxide, CuO (black). The copper-oxygen phase diagram shows a strong pressure dependence that causes CuO to be transformed into Cu_2O in a high vacuum (ref. 12), and therefore also presumably in space. A selection from among various values of the optical constants of both oxides has been made by C.G. Ribbing and A. Roos (ref.12).

The exposed portion of the copper sample fits a model consisting of a very thick (1039 Å) porous layer of Cu_2O containing 71% voids over metallic copper. The unexposed portion can be modelled by a 449 Å thick film of Cu_2O containing 69% voids over the metal. The optical constants for the exposed and shielded regions of the copper sample are shown in Figs. 5 and 6. The results of the least-squares best fit for the exposed portion of this sample are shown in Figs. 7 and 8.

3. Nickel

To construct models for the nickel sample, we relied on values of the optical constants reported by P. B. Johnson and R. W. Christy (ref. 13) for the metal, but for NiO we were able to find only a few scattered values in the literature (ref. 14). For that reason, we made our own measurements on a polished crystal of NiO provided by Prof. Clive Perry of Northeastern University. The results of this experiment are listed in Table II. For the exposed region on the nickel sample, the measured optical constants fit a model that consists of a porous 687 Å thick layer of NiO containing 65% voids over metallic nickel. The best fit for the shielded region converges to a value of 60 Å for the thickness of the oxide layer, with no voids present, over metallic nickel. Plots of the data for the Ni sample are shown in Figs. 9 and 10.

4. Tantalum

Tantalum forms a thin layer of Ta_2O_5 when exposed to the atmosphere. The formation of the oxide is diffusion-limited as in the case of aluminum. For tantalum metal we have used the data of Weaver et al. (ref.15). Tantalum pentoxide is an insulator whose index of refraction does not vary by more than 1% over the visible part of the spectrum (ref. 16). In our modelling program we have ignored these small variations and assumed instead constant values n=2.22 and k=0 for the wavelength range 4000 to 8000 Å. The data for the exposed metal fit best to a model consisting of a Ta substrate covered by a porous film of Ta_2O_5 which is 505 Å thick and contains 73% voids. The unexposed portion of the sample is covered by a 31.5 Å thick film of Ta_2O_5 free of voids. The measured optical constants of the sample are compared with the constants of the pure metal in Figs. 11 -12.

5. Tungsten

The optical constants of metallic tungsten in the visible part of the spectrum have been measured by Weaver et al. (ref. 17). Four different oxides of tungsten have been identified, which contain tungsten in different oxidation states and in varying stoichiometries. In each of these compounds a tungsten atom is surrounded by an octahedron of oxygen atoms, but the compounds differ in the extent to which oxygen atoms are shared by adjacent octahedra. In addition, a compound with composition W_3O (β-tungsten) is known. The compounds have different colors, which indicates a difference in their optical properties. We have been unable to find any reference in the literature to measurements of the optical constants of the different oxides. For that reason we have not been able to analyze the tungsten data shown in Figs. 13 and 14.

6. Zirconium

Ellipsometry carried out in our laboratory on a freshly polished zirconium metal sample, a duplicate of the LDEF sample, revealed substantially larger values for the extinction coefficient k over the visible spectrum than older values cited in the literature (ref. 18). For that reason, we decided to use our measured values (listed in Table III) in the analysis of the LDEF data.

ZrO_2 is an insulator transparent to visible light. A value of its index of refraction at a single wavelength (λ=5890 Å) is listed in Landoldt-Börnstein (ref. 19). On the assumption that ZrO_2 has negligible dispersion in the visible spectrum we have assumed constant values n=2.16 and k=0 in our fitting program.

The experimental data for the exposed part of the LDEF zirconium sample are best fit by a model consisting of Zr metal covered by a 688 Å thick porous film of ZrO_2 containing 81% voids. The unexposed part of the Zr sample is covered by a film of ZrO_2 42 Å thick without voids. The data are plotted in Figs. 15 and 16.

A summary of the results is presented in Table 4.

CONCLUDING REMARKS

The Ta, W and Zr plates were mounted on tray D9, the leading edge of the LDEF, and therefore exposed to an intense flux of atomic oxygen (8×10^{21} /cm^2 integrated over the flight duration). According to our ellipsometric analysis, the exposed portions of the Ta and Zr samples acquired rather thick porous oxide films as a result of this exposure. In this method, the porosity of the oxide film is obtained from a least-squares fit of the ellipsometric data and will be referred to in this section as the calculated proportion of

voids. All of the LDEF metal samples were also examined with an optical metallograph, which employs a different technique of determining film porosity and yields a value for the "measured porosity" of the metal samples. The latter technique relies upon the difference in contrast in the field of view at 500x whereby dark regions are interpreted as voids and light areas as those containing the metal substrate. A computer program is used to determine an average percentage of voids using at least ten different sampling spots on the specimen to ensure adequate representation of the whole surface.

The calculated proportion of voids in the Zr sample (0.81) corresponded well with the measured porosity (0.69) . However, for exposed Ta the calculated proportion of voids (0.73) was much larger than the measured porosity (0.10), possibly because the pores formed in the Ta_2O_5 film are too small to be resolved with an optical microscope.

The Al and Ni plates were mounted on tray D3, on the trailing edge of the LDEF and therefore exposed to an integrated oxygen flux (4×10^3 /cm^2) less than for any other placement on the satellite. Nevertheless, according to our ellipsometric analysis, thick oxide films were formed on the exposed portions of both metals, porous in the case of Ni (calculated void proportion, 0.65; measured porosity, 0.29), but practically free of voids for Al (for both calculated void proportion and measured porosity). Because the calculated number of oxygen atoms in such a film is much greater (on the order of 10^{17} atoms /cm^2) than the integrated flux of oxygen atoms, we suspect some other mechanism of oxide formation. For the Zr, Ta, Al and Ni samples, the shielded portions of the plates are covered by relatively thin non-porous oxide films typical of exposure to air at atmospheric pressure.

The most puzzling results were obtained for the Cu sample, mounted on the Earth end of the satellite (tray G12, oxygen flux 5×10^{19} /cm^2) because of very thick porous Cu_2O films on the exposed portion (0.71 calculated proportion of voids, 0.76 measured porosity) as well as on the shielded portion (0.69 calculated voids, 0.45 measured porosity). Micrographs of both regions show many scratches on the surface, probably as a result of careless handling, that might cause the ellipsometric analysis to be unreliable.

The extent to which our metal samples were subject to contamination from sources other than atomic oxygen (for example, due to ablation of paint and other materials from the LDEF structure) is a subject of speculation. There is some evidence of cross-contamination during flight that if extensive could affect the outcome of the ellipsometric analysis. However, the mean square error, which is a measure of goodness of fit between the model and the experimental data, is quite small for the analysis of the Al, Ni, and Zr samples (less than 5%). This is a strong indication that the model is correct in these cases. However, for the analysis of the Ta and Cu samples, the mean square error is rather high, which suggests that a different model might provide a more accurate representation of the surface layer. A discussion of the reasons for the high porosity of most of the oxide films, and an explanation of the absence of porosity in the case of the Al_2O_3 film is beyond the scope of the work reported here.

ACKNOWLEDGEMENTS

We would like to thank John A. Woollam of the University of Nebraska and Gerry Cooney of the J.A Woollam Company for their generous advice on many occasions, Jonathan Montgomery of our Physical Metallurgy group for his cooperation in preparing duplicate metal samples, A.R. Frederickson of Hanscom AFB for useful advice, and Clive Perry of Northeastern University for loan of a crystal of NiO.

REFERENCES

1. Budde, W.: Photoelectric Analysis of Polarized Light. Applied Optics, vol. 1, 1962, pp. 201-205.

2. Greef, R.: An Automatic Ellipsometer for Use in Electrochemical Investigations. Rev. Scient. Inst., vol. 41, 1970, pp. 532-538.

3. Suits, J.C.: Magneto-Optical Rotation and Ellipticity Measurements with a Spinning Analyzer. Rev. Scient. Inst., vol. 42, 1971, pp.19-22.

4. Aspnes, D.E.; and Studna, A.A.: High Precision Scanning Analyzer. Applied Optics, vol. 14, 1975, pp. 220-228.

5. Bu-Abbud, G.H.; Bashara, N.M.; and Woollam, J.A.: Variable Wavelength, Variable Angle Ellipsometry. Thin Solid Film, vol. 138, 1986, pp.27-41.

6. Woollam, J.A.; Snyder, PO.; and Rost, M.C.: Variable Angle Spectroscopic Ellipsometry: A Non-Destructive Characterization Technique for Ultra-Thin and Multilayer Materials. Thin Solid Films, vol. 166, 1988, pp. 317-323.

7. Halford, J.; Chin, F.K.; and Newman, J.E.: Effects of Vacuum Deposition Conditions on Ellipsometric Parameters, Optical Constants, and Reflectance of Ultrapure Aluminum Films. Journ. Opt. Soc. Am., vol. 63, 1973, pp. 786-792.

8. Natishan, P.M.; Peace, G.T.; and Slebodnik, P.F.: Surface Preparation of Aluminum for Ion Implantation. Metallography, vol. 23, 1989, pp. 21-26.

9. Smith, D.Y.; Shiles, E.; and Inokuti, M.: The Optical Properties of Metallic Aluminum. Handbook of Optical Constants Solids (E. Palik, editor), 1985, pp. 398-399.

10. Hageman, H.J.; Gudar, W.; and Kunz, C.: Optical Constants from the Far Infrared to the X-ray Region: Mg, Al, Cu, Ag, Au, Bi, C and Al_2O_3. Journ. Opt. Soc. Am., vol. 65, 1975, pp. 742-745.

11. Lynch, D.W.; Hunter, W.R.: Optical Constants of Metals. Handbook of Optical Constants of Solids (E. Palik, editor), 1985, pp. 280-285.

12. Ribbing, C.G.; and Roos, A.: Copper Oxides (Cu_2O, CuO). Handbook of Optical Constants of Solids II (E. Palik, editor), 1991, pp. 875-882.

13. Johnson, P.B.; and Christy, R.W.: Optical Constants of the Transition Metals: Ti, V, Cr, Mn, Fe, Co, Ni and Pd. Phys. Rev., vol. B9, 1974, pp. 5056-5070.

14. Landolt-Börnstein: Zahlenwerte und Funktionen, vol. II, part 8, 1962, pp. 2-198.

15. Weaver, J.H.; Lynch, D.W.; and Olson, C.G.: Optical Properties of V, Ta, and Mo from 0.1 to 35 ev. Phys. Rev., vol. B10, 1974, pp. 501-516.

16. Bombin, O.M.A.; and Neal, W.E.J.: Ellipsometric Measurements on Tantalum and Tantalum Oxide Films. Thin Solid Films, vol. 42, 1977, pp. 91-96.

17. Weaver, J.H.; Olson, C.G.; and Lynch, D.W.: Optical Properties of Crystalline Tungsten. Phys. Rev., vol. B12, 1975, pp. 1293-1297.

18. Optical Properties of Metals. Physik Daten, Fachinformationszentrum Karlsruhe, 1981, no. 18-1.

19. Landolt-Börnstein: Zahlenwerte und Funktionen, vol. II, part 8, 1962, pp. 2-151.

Table I. LOCATION OF SAMPLES ON SATELLITE

Sample	Tray	Location
Aluminum	D3	Trailing edge
Copper	G12	Earth end
Nickel	D3	Trailing edge
Tantalum	D9	Leading edge
Tungsten	D9	"
Zirconium	D9	"

Table II. MEASURED OPTICAL CONSTANTS OF NICKEL OXIDE

Wavelength (Å)	Index of Refraction	Extinction Coefficient
4000	1.929	0.483
4200	1.901	0.499
4400	1.888	0.520
4600	1.879	0.534
4800	1.882	0.550
5200	1.890	0.586
5400	1.901	0.604
5600	1.904	0.622
5800	1.919	0.642
6000	1.932	0.660
6200	1.938	0.676
6400	1.952	0.693
6600	1.965	0.709
6800	1.978	0.725
7000	1.987	0.740
7200	2.002	0.759
7400	2.026	0.777
7600	2.041	0.790
7800	2.048	0.801
8000	2.065	0.813

Table III. MEASURED OPTICAL CONSTANTS OF ZIRCONIUM METAL

Wavelength (Å)	Index of Refraction	Extinction Coefficient
4000	1.596	2.457
4200	1.666	2.558
4400	1.743	2.657
4600	1.827	2.748
4800	1.918	2.901
5200	2.104	2.969
5400	2.192	3.021
5600	2.284	3.075
5800	2.377	3.116
6000	2.470	3.154
6200	2.558	3.168
6400	2.639	3.195
6600	2.712	3.207
6800	2.778	3.235
7000	2.832	3.252
7200	2.882	3.274
7400	2.926	3.311
7600	2.962	3.336
7800	2.999	3.360
8000	3.033	3.392

Table IV. SUMMARY OF RESULTS

Sample	Exposed (E) or Shielded (S)	Oxide	Thickness of Oxide	Proportion of Voids
Al	E	Al_2O_3	395	0
Al	S	Al_2O_3	68	0
Cu	E	Cu_2O	1039	0.71
Cu	S	Cu_2O	449	0.69
Ni	E	NiO	687	0.65
Ni	S	NiO	60	0
Ta	E	Ta_2O_5	505	0.73
Ta	S	Ta_2O_5	31.5	0
W	E	?	not known	not known
W	S	?	not known	not known
Zr	E	ZrO_2	688	0.81
Zr	S	ZrO_2	42	0

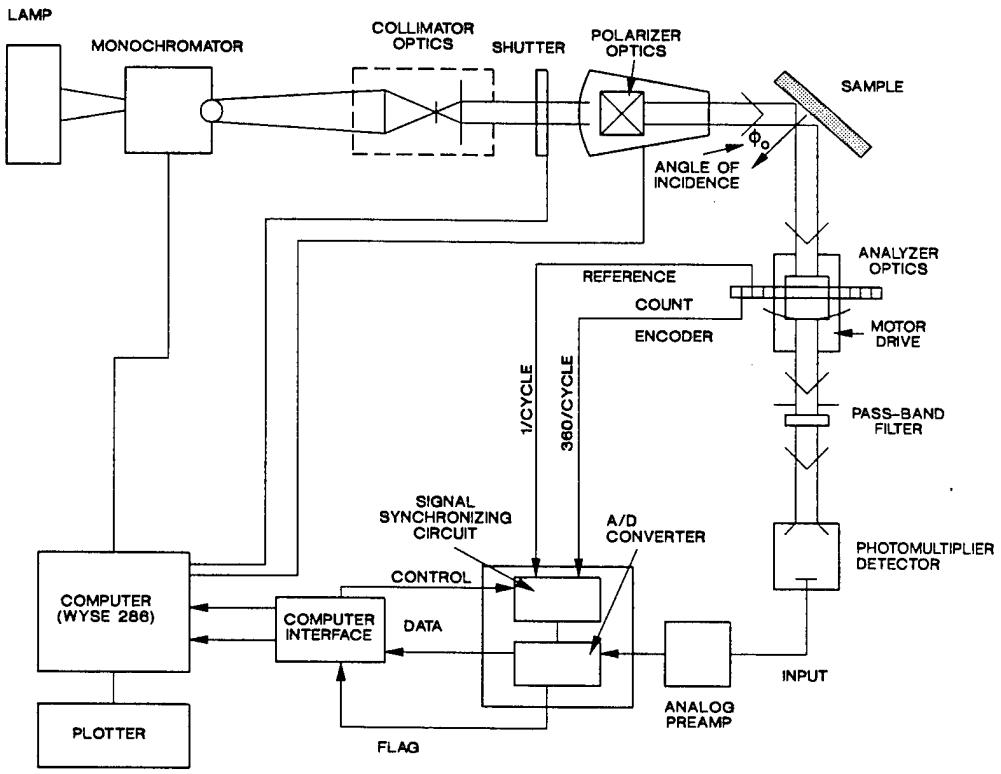


Figure 1. Diagram of metal plate with shielding strap.

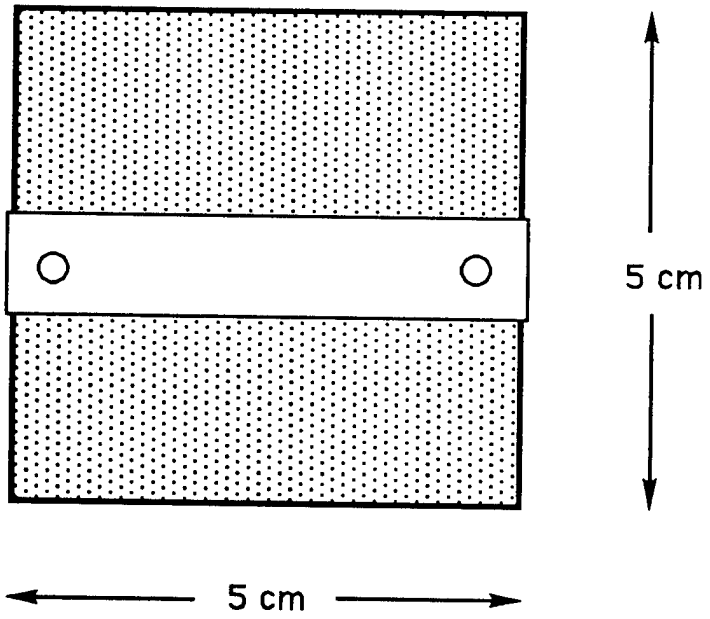


Figure 2. Schematic diagram of variable angle ellipsometer; designed and built by the J.A. Woolam Company, Lincoln, Nebraska.

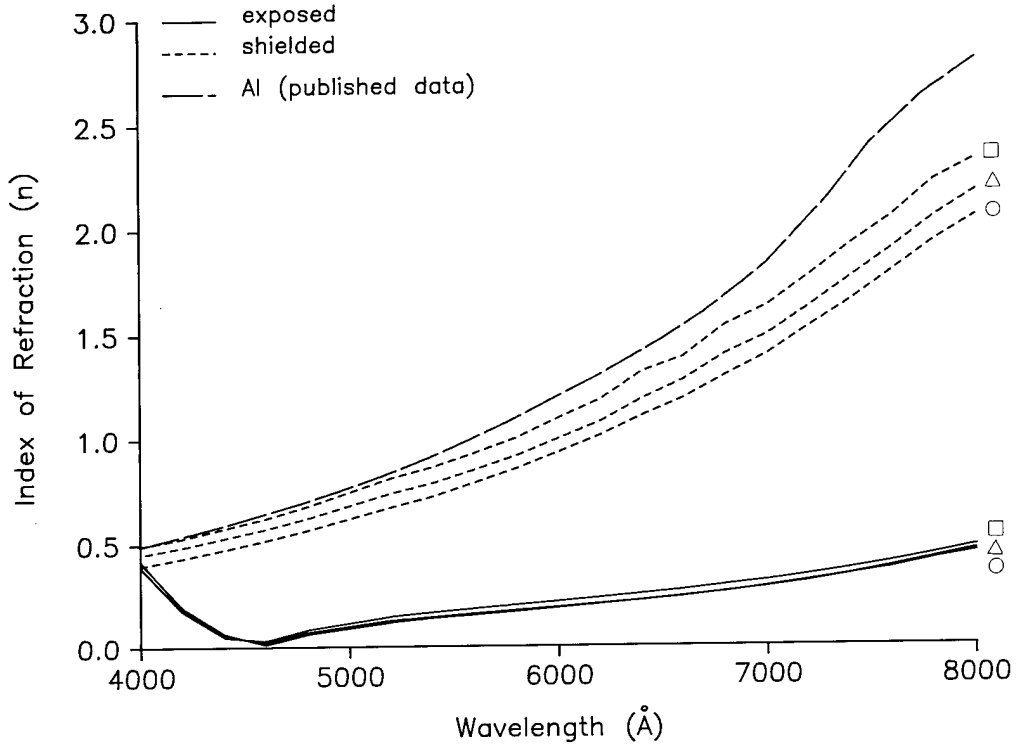


Figure 3. Index of refraction of LDEF aluminum sample for exposed region and shielded region. Index of refraction of aluminum (Ref. 9). ◘ ≡ angle of incidence = $\phi = 65°$; $\Delta \equiv \phi = 70°$; o ≡ $\phi = 75°$.

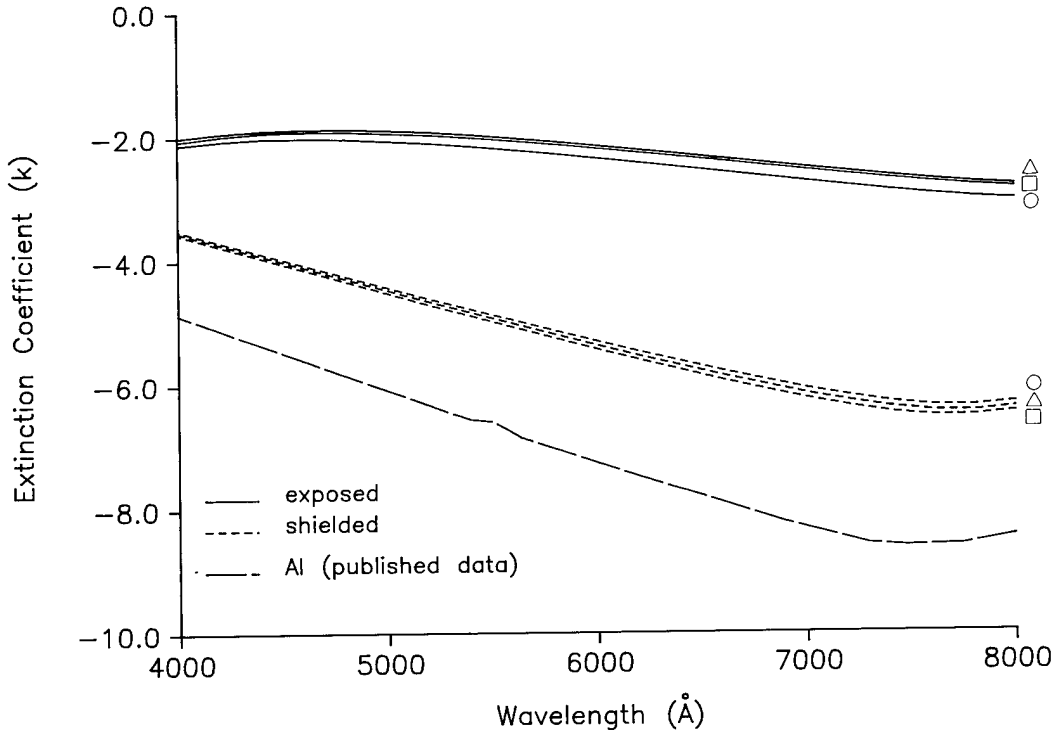


Figure 4. Extinction coefficient of LDEF aluminum sample for exposed region and shielded region. Extinction coefficient of aluminum (Ref. 9). ◘ ≡ angle of incidence = $\phi = 65°$; $\Delta \equiv \phi = 70°$; o ≡ $\phi = 75°$.

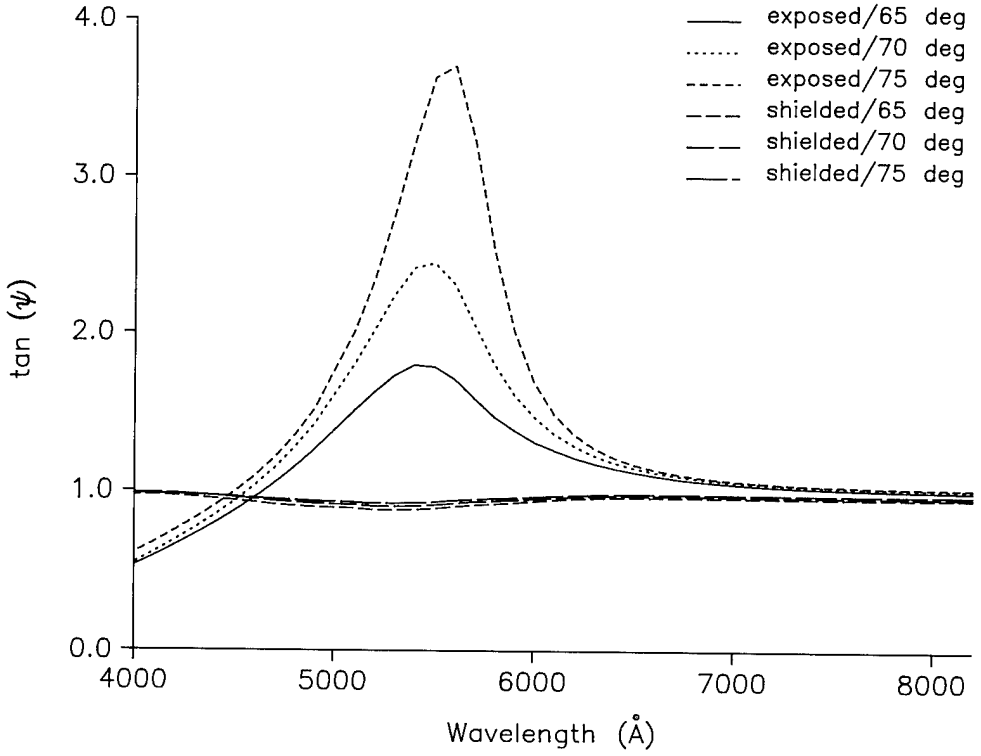


Figure 5. Tan ψ of LDEF copper sample for exposed region and shielded region.

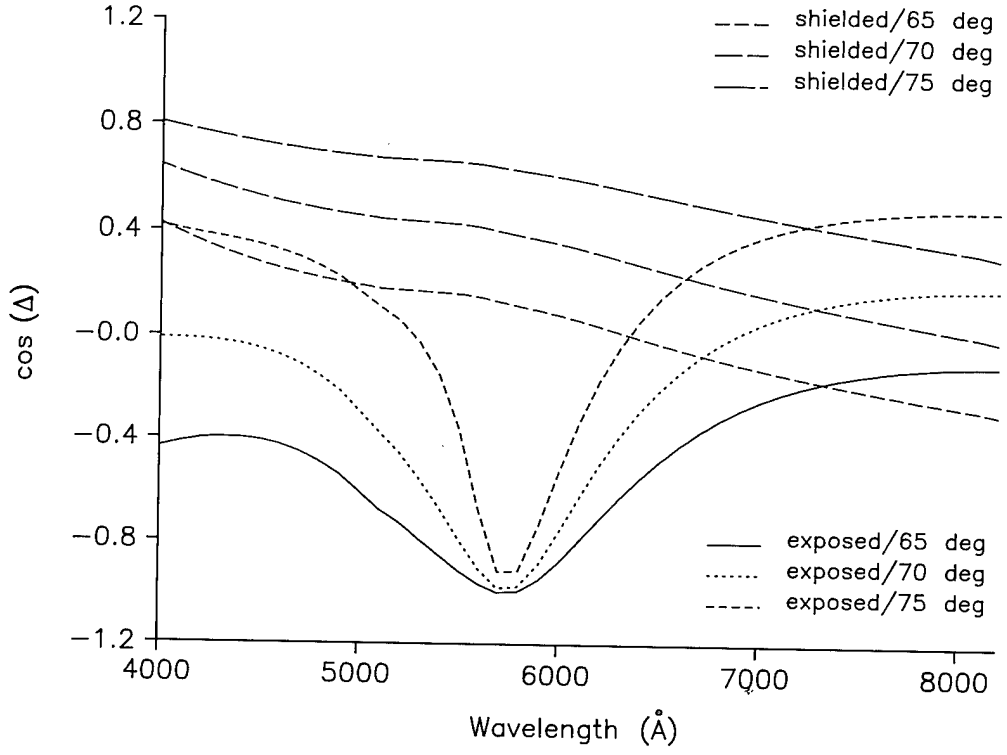


Figure 6. Cos Δ of LDEF copper sample for exposed region and shielded region.

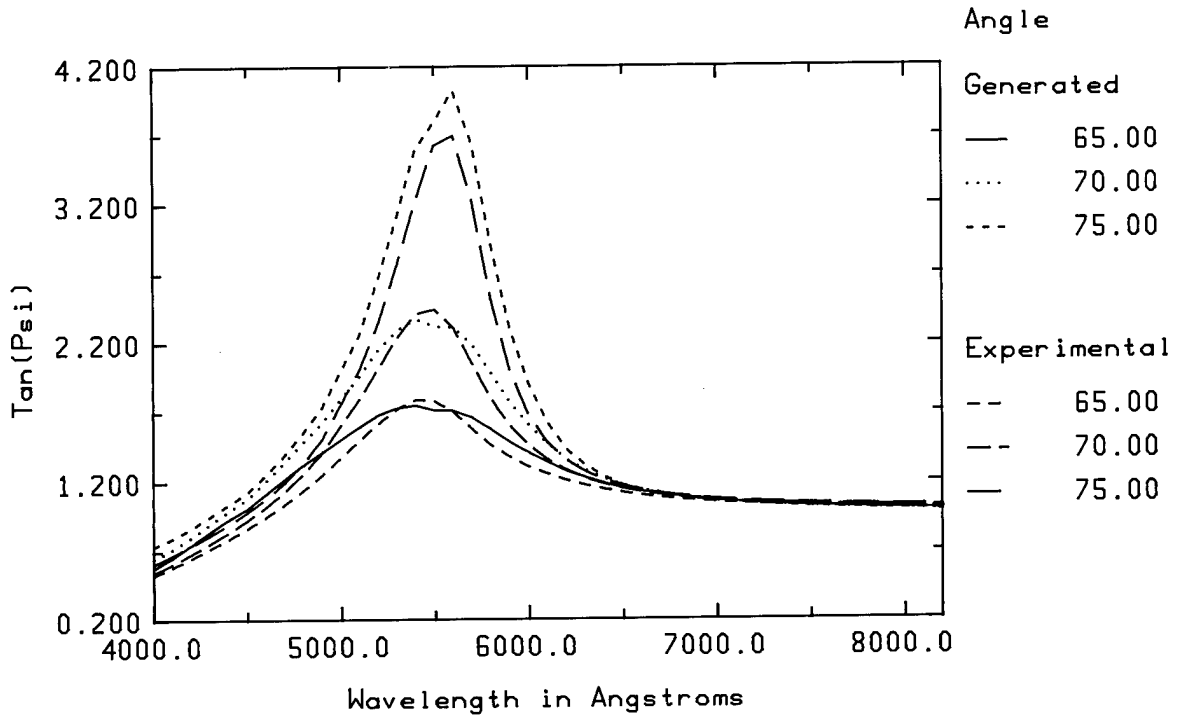


Figure 7. Experimental data shows tan ψ for the LDEF copper sample (exposed region); the generated data are obtained for the model of a 1039 Å thick film of Cu_2O containing 71% voids on metallic copper.

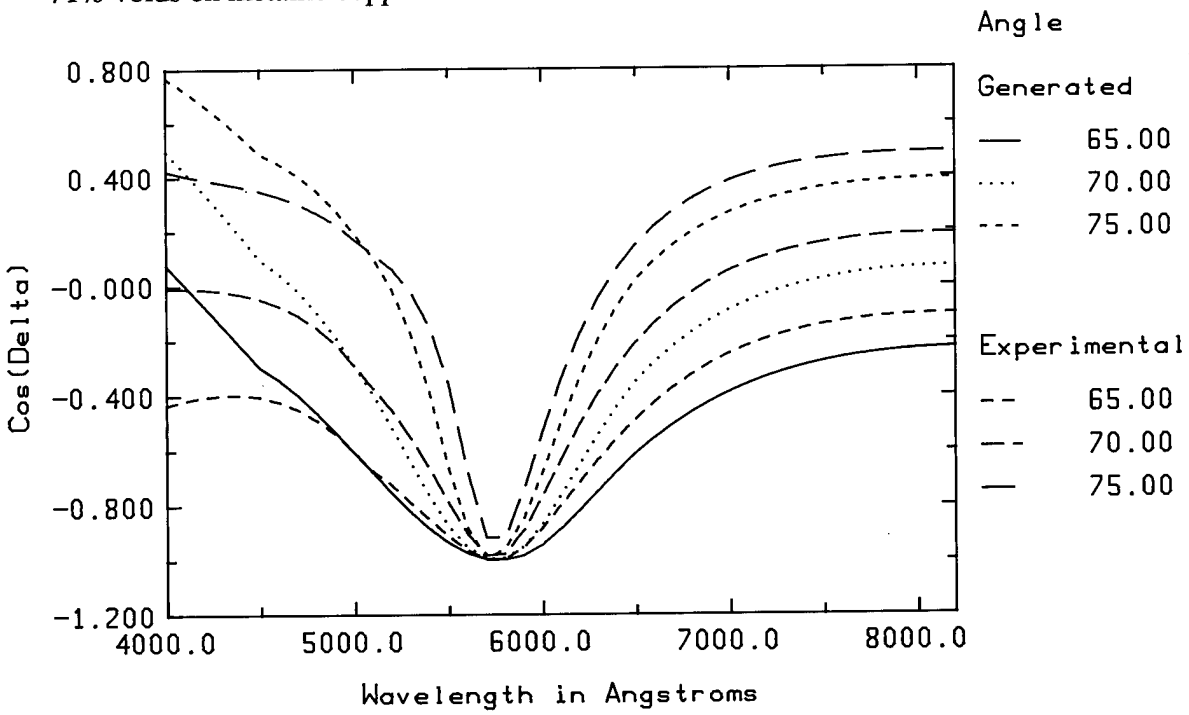


Figure 8. Experimental data shows cos Δ for the LDEF copper sample (exposed region); the generated data are obtained for the model of a 1039 Å thick film of Cu_2O containing 71% voids on metallic copper.

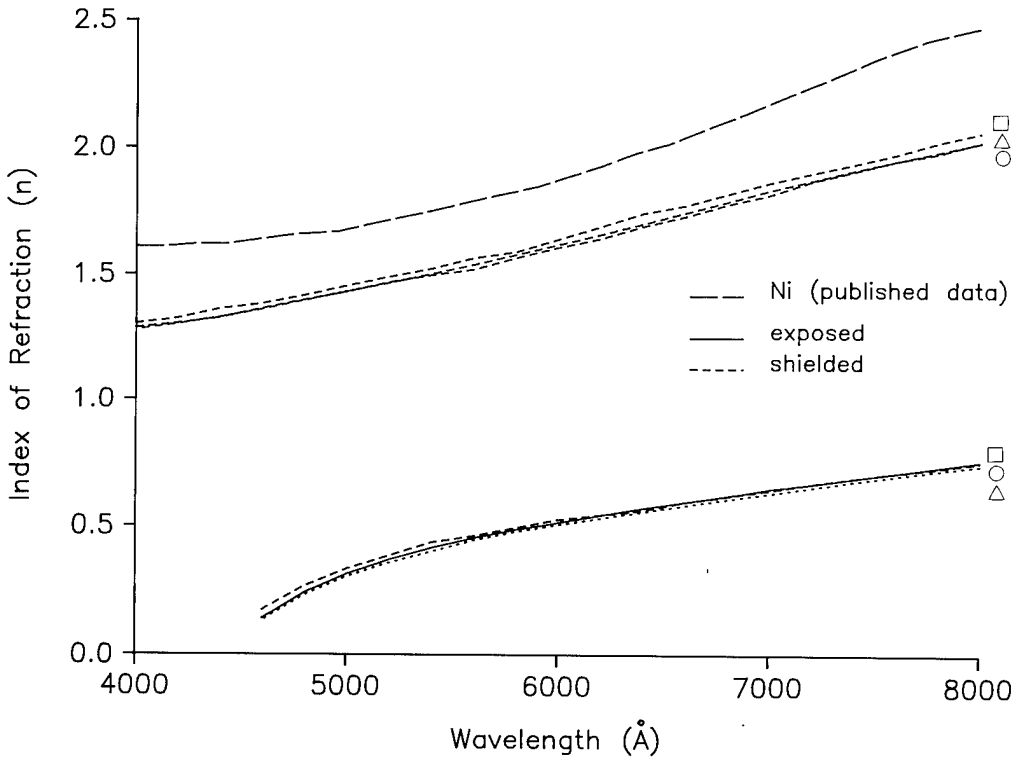


Figure 9. Index of refraction of LDEF nickel sample for exposed region and shielded region. Index of refraction of nickel (Ref. 13). □ ≡ angle of incidence = $\phi = 60°$; $\Delta \equiv \phi = 70°$; o ≡ $\phi = 80°$.

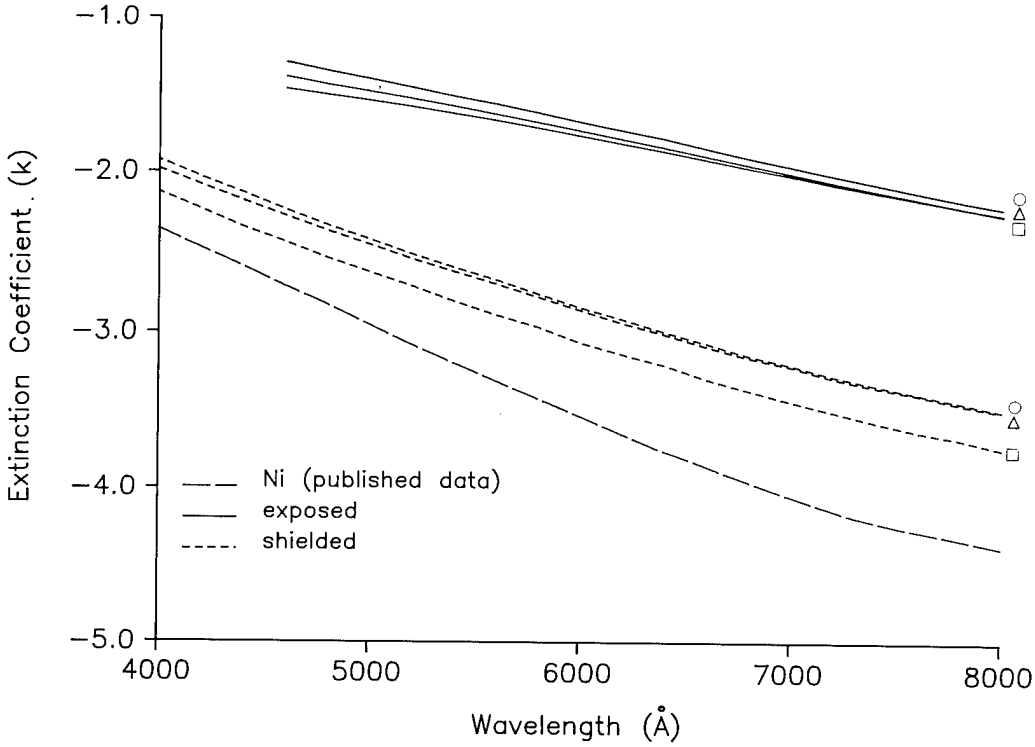


Figure 10. Extinction coefficient of LDEF nickel sample for exposed region and shielded region. Extinction coefficient of nickel (Ref. 13). □ ≡ angle of incidence = $\phi = 60°$; $\Delta \equiv \phi = 70°$; o ≡ $\phi = 80°$.

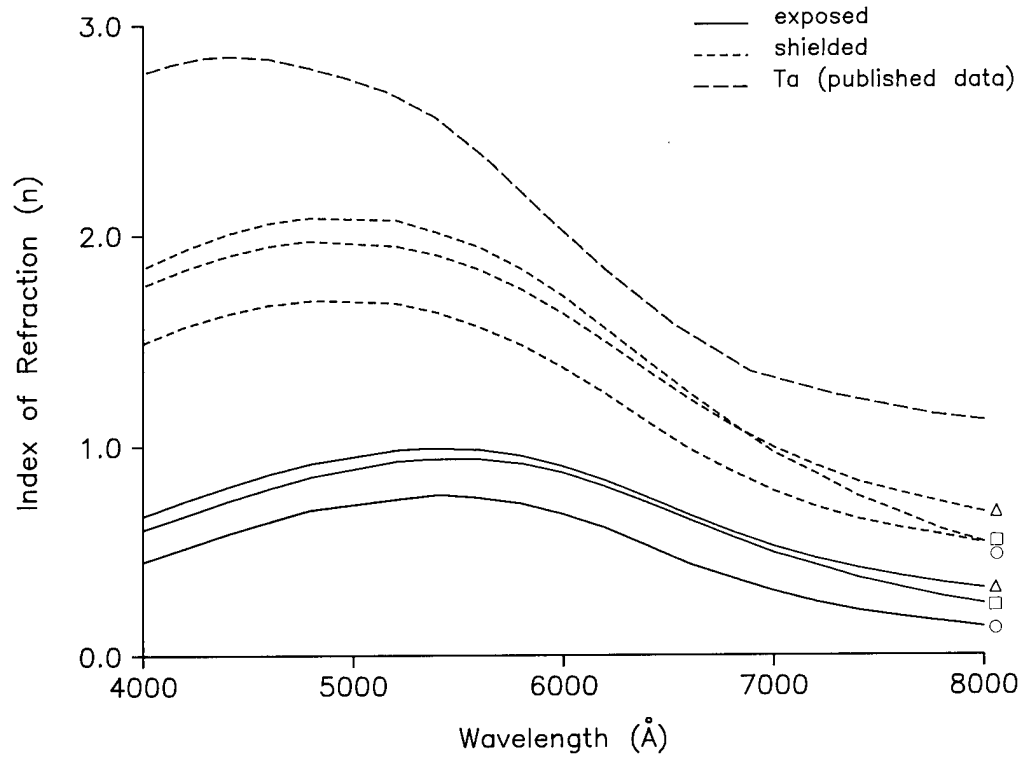


Figure 11. Index of refraction of LDEF tantalum sample for exposed region and shielded region. Index of refraction of tantalum (Ref. 15). □ ≡ angle of incidence = $\phi = 60°$; $\Delta \equiv \phi = 70°$; o ≡ $\phi = 80°$.

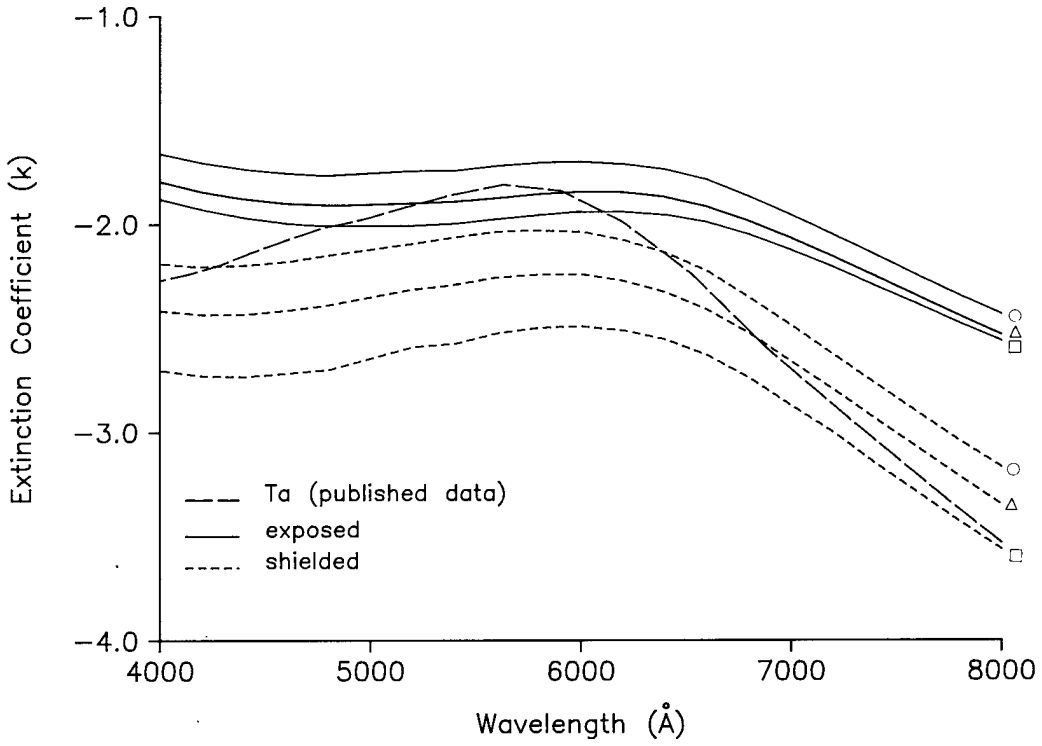


Figure 12. Extinction coefficient of LDEF tantalum sample for exposed region and shielded region. Extinction coefficient of tantalum (Ref. 15). □ ≡ angle of incidence = $\phi = 60°$; $\Delta \equiv \phi = 70°$; o ≡ $\phi = 80°$.

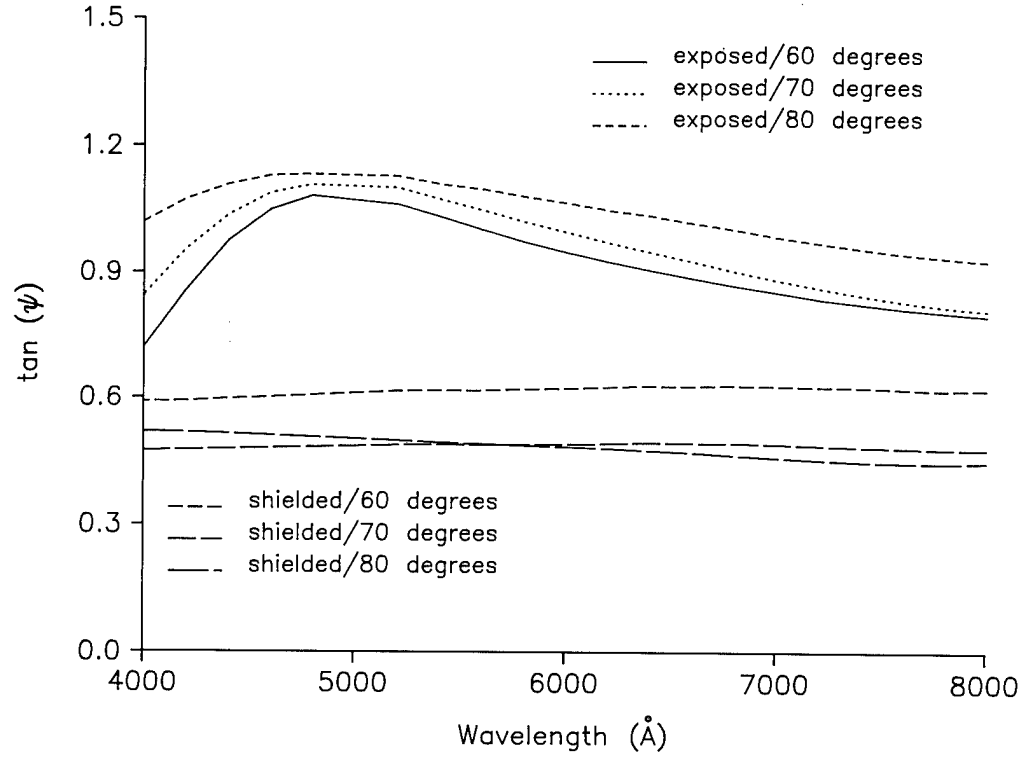


Figure 13. Tan ψ of LDEF tungsten sample for exposed region and shielded region.

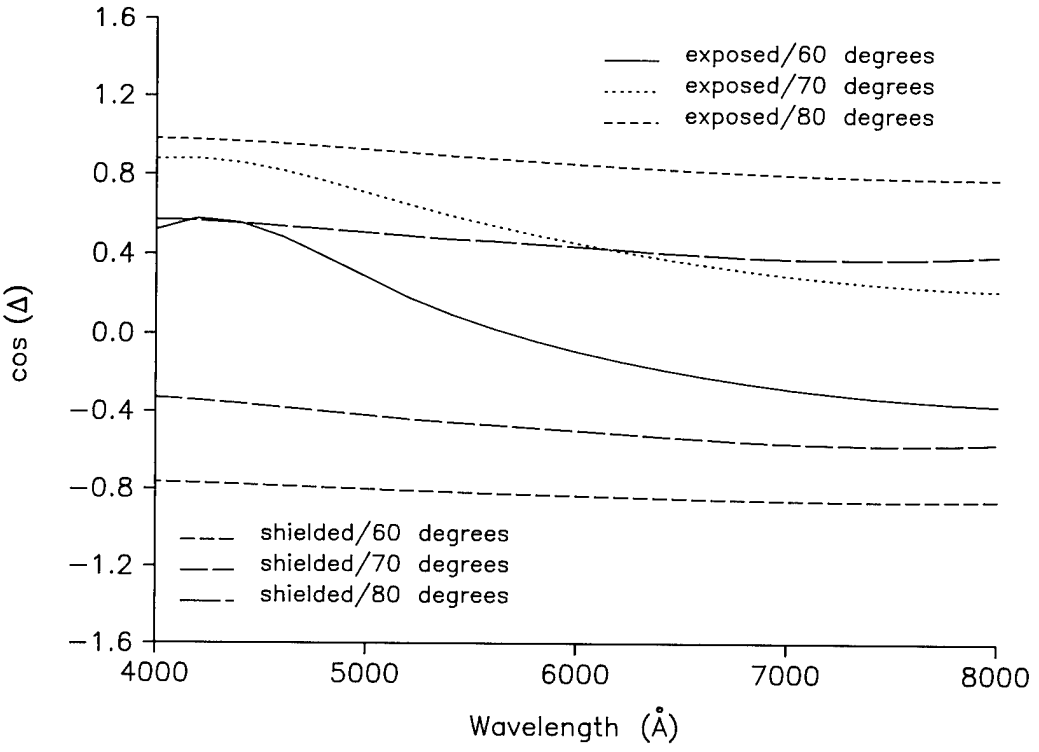


Figure 14. Cos Δ of LDEF tungsten sample for exposed region and shielded region.

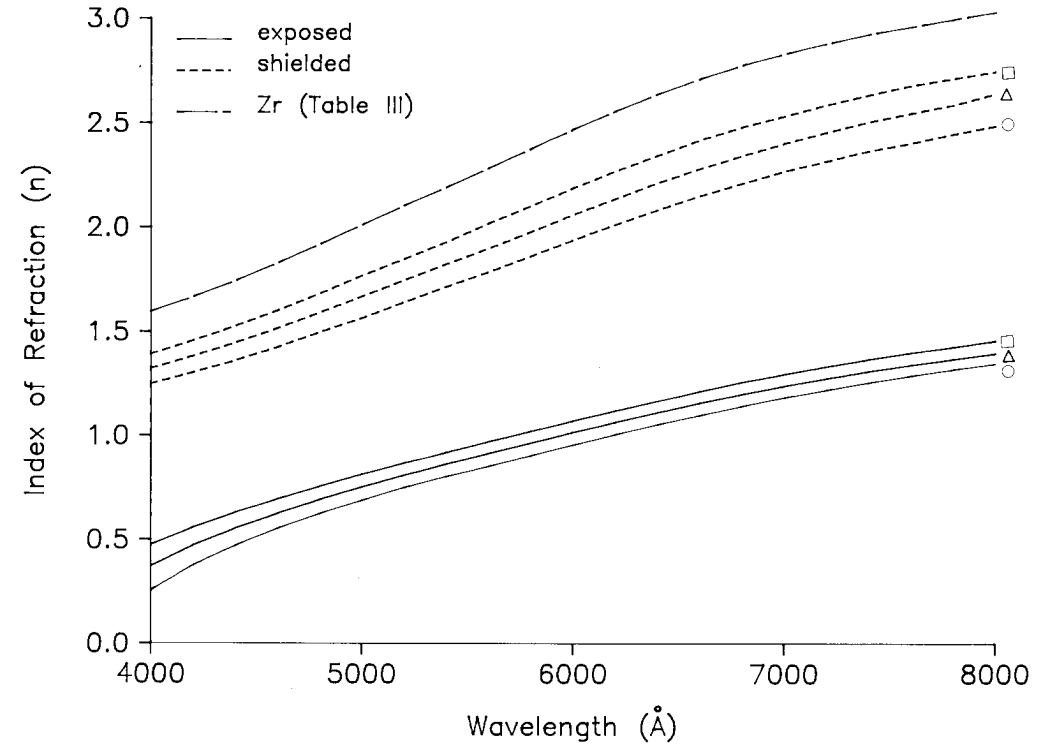


Figure 15. Index of refraction of LDEF zirconium sample for exposed region and shielded region. Index of refraction of zirconium (Table III). □ ≡ angle of incidence = $\phi = 65°$; $\Delta \equiv \phi = 70°$; o ≡ $\phi = 75°$.

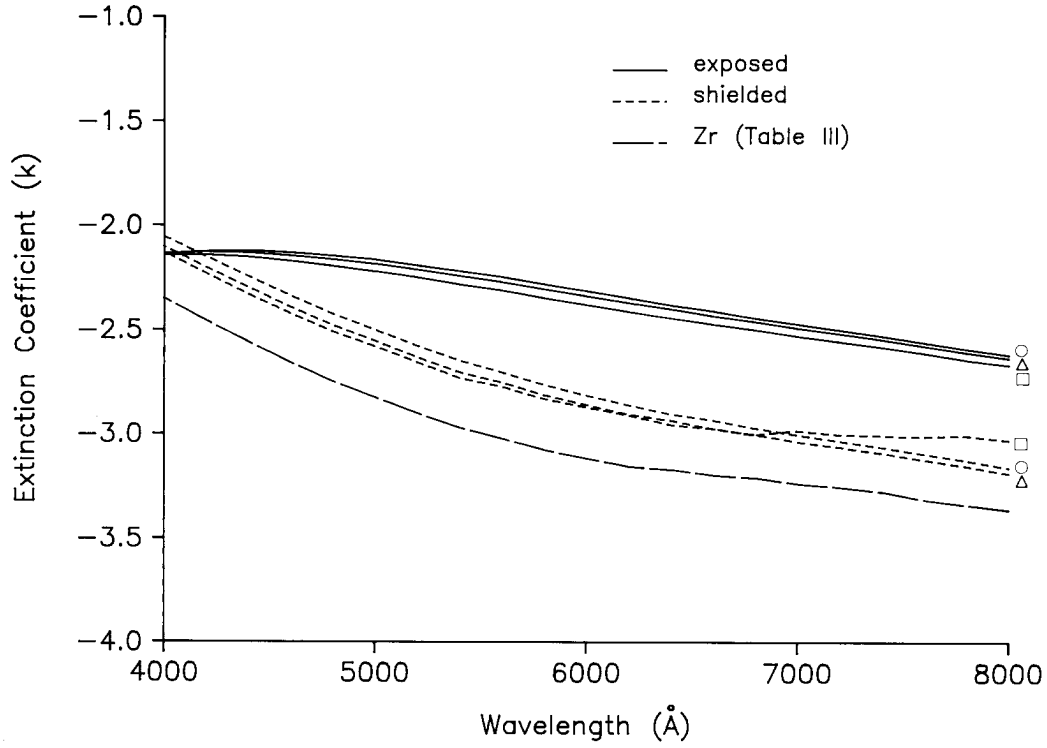


Figure 16. Extinction coefficient of LDEF zirconium sample for exposed region and shielded region. Extinction coefficient of zirconium (Table III). □ ≡ angle of incidence = $\phi = 65°$; $\Delta \equiv \phi = 70°$; o ≡ $\phi = 75°$.

SPACE ENVIRONMENTAL EFFECTS ON THE INTEGRITY OF CHROMIC ACID ANODIZED COATINGS*

Walter L. Plagemann
Boeing Defense & Space Group
Seattle, WA 98124-2499
Phone: 206 234-3025

SUMMARY

The LDEF tray clamps used to hold the experiment trays in place on the Long Duration Exposure Facility (LDEF) have been analyzed to determine the effects of long term space exposure on the performance of the chromic acid anodize coating. Spectroscopic anomalies observed appeared to be random and related to application techniques as opposed to exposure or position on LDEF. Thickness measurements indicated that the coating was less than 1u and was probably not degraded by space exposure. Metallurgical analysis revealed that leading edge exposure may have increased the porosity of the coating. Emittance values for the coating decreased uniformly by an average of 6.8% while solar absorptance values increased for trailing edge and decreased for leading edge specimens. The a/e ratio for the coating also increased as a result of long term space exposure.

INTRODUCTION

Chromic acid anodize finishing of aluminum is being considered as a candidate thermal control coating for use on Space Station and other spacecraft planned for use at low earth orbit (LEO). LDEF offers the unique opportunity to evaluate the performance of the chromic acid anodize after prolonged space exposure. The constant orientation of LDEF relative to the RAM direction throughout its entire mission has resulted in a unique distribution of exposure conditions. Since, as seen in Figure 1, the tray clamps were positioned uniformly around the satellite, they represent every possible environmental exposure condition to both atomic oxygen and ultraviolet flux. The condition of the clamps should provide a complete picture of the combined space effects on the performance and durability of the chromic acid anodize coating. The objective of this study was to characterize the performance of the anodize coating as a function of space environmental exposure. The analyses employed included; specular and diffuse reflectance, SEM and metallography, and solar absorptance and emittance measurements.

RESULTS

Specular and Diffuse Reflectance

Total, specular and diffuse reflectance spectra were obtained for each tray clamp analyzed to date. Data was obtained in the ultraviolet, visible, near infrared, and mid infrared regions of the spectrum. The individual spectra were examined for anomalies and particular changes in the various spectral signatures of the coating with respect to the type of exposure the clamps had seen on LDEF.

*Work done under NAS1-18224, Task 12

UV-Vis/NIR Region

There are large variations in the reflectance data obtained from different specimens, especially in the UV-Vis/NIR regions of the spectrum. Figure 2 presents two representative UV-Vis/NIR diffuse reflectance spectra. Note that there is nearly a 20% difference in the diffuse reflectance component between the two spectra. The total reflectance values, however, exhibited little variation in any of the clamps tested. There was also no apparent correlation between the differences observed and the position on LDEF. To date it appears that these spectral changes are probably related more to variations in application techniques than to space effects.

Mid Infrared Region

Figure 3 contains representative diffuse reflectance spectra obtained over the mid infrared region of the spectrum. The IR diffuse reflectance measurements yielded some interesting results. A typical IR spectrum from the reverse side of the clamp, which was shielded from any space effects, is presented in Figure 2B. As seen in this figure there is distinct evidence of organic contamination as evidenced by the CH2-CH3 absorptions around 2900 cm-1 and the carbonyl absorptions near 1640 cm-1. The exposed surfaces show significant reductions in the magnitude of the peaks in both of these regions indicating that space exposure may actually have "cleaned" some of the initial contamination from the LDEF surfaces. An additional absorption peak was observed on many of the exposed surfaces. This peak can be seen around 1070 cm-1 in the spectrum shown in Figure 2A. The presence of this peak has tentatively been attributed the formation of silicate compounds associated with the silicone contamination observed on many of the LDEF surfaces.

SEM and Metallography

Coating Thickness Measurements

SEM analysis was employed to measure the anodize coating thickness on the tray clamps. Small specimens cut from the clamps were fractured and photomicrographs were obtained of the fracture surfaces from both the front and back of the clamps. The coating thicknesses were then measured directly from the photomicrographs. The back side of each clamp acted as a control and the data was evaluated to determine if space exposure had any effect on the coating thickness. Typical photomicrographs showing the anodize coating are presented in Figure 4.

The data indicates no effect of space exposure on the thickness of the anodize coating. This conclusion is based on a limited number of observations, however, and more work is planned in this area. The SEM analysis did indicate that the coating was extremely thin averaging only between 4u and 6u.

Evaluation of Tray Clamps with Copper Grounding Straps

Several of the tray clamps on LDEF had copper grounding straps attached. One such clamp is pictured in Figure 5. These samples were intriguing because they had both exposed and protected areas on the same side of the clamp. Figure 6 contains photographs of the clamp from tray E02-6. The areas on the clamp which were protected by the shim and the ground strap can be easily detected as lighter regions on the clamp surface. Obviously contamination from external sources has contributed to some of the discoloration

on the exposed surfaces. The role of UV and atomic oxygen exposure in this discoloration is being investigated.

Figure 7 contains photomicrographs of cross sections obtained from exposed and protected areas of clamps subjected to leading (Figure 6 A&B) and trailing edge exposure (Figure 6 C&D). The most notable feature in these figures is what appears to be debris on the protected surfaces of the clamps. SEM photomicrographs (Figure 8) revealed that what appeared to be debris was actually a discrete layer on the surface of the clamp. EDX analysis of this layer indicated that it was comprised solely of aluminum, probably in the form of aluminum oxide. The exact source of this layer is unknown at the present time; however it is probably related to some smearing of the surface associated with the application of the anodize coating. Regardless of the source, Figure 7 indicates that it is absent from exposed areas on the surfaces of the clamps. This indicates that oxidation of the surface has probably occurred.

Coating Porosity

Figure 9 contains SEM photomicrographs of both exposed (Figure 9 A&C) and protected (Figure 9 B&D) areas from the surface of a trailing edge clamp. As seen in these figures, the surface of the clamp appears to be moderately pitted and there is no significant variation in the amount of pitting present on the exposed or protected surfaces. Figure 10 contains SEM photomicrographs of exposed (Figure 10 A&C) and protected (Figure 10 B&D) areas from a leading edge clamp. While pits are again present in both the exposed and protected areas of the coating, the number of pits on the exposed surface in this case is considerably greater than on the protected areas. Since the pits were observed on both the exposed and protected areas, coupled with the fact that their morphology was similar in both regions, it was concluded that their presence was probably the result of coating degradation as opposed to micrometeorite damage. This indicates that leading edge exposure may degrade the anodize coating. This observation is based on the examination of a limited number of samples, however, and more testing will be needed to verify the results.

SOLAR ABSORPTANCE AND EMITTANCE

The tray clamps were anodized prior to flight to achieve an a/e ratio of 2.1 +/- 0.2. The stability of this ratio is both a measurement of the durability of the coating and an indication of its effectiveness in thermally protecting the spacecraft. Since the effects of long term space exposure on the survivability of the anodize coating is an important parameter to be considered by designers of future low earth orbit spacecraft, considerable effort was expended in analyzing the absorptance and emittance of as many clamps as possible. To date 228 clamps have been analyzed. The data obtained from these clamps is summarized in Table I.

There was considerable variability observed in the optical property values obtained between tray clamps. Solar absorptance values ranged from 0.30 - 0.40; emittance values ranged from 0.12 - 0.20; and the calculated a/e ratio ranged from 1.60 - 2.80. Some of this variability was undoubtably due to inconsistencies in the application technique. In addition, there were only four ground control specimens available and any anomalies associated with the method of application of the coating would also be manifested in these specimens. Under normal circumstances this would make any meaningful statistical analysis of the results impossible. Fortunately, the reverse side of each clamp did not see the effects of space exposure. This affords a built in control for each clamp and allowed us to eliminate much of the variability expected between individual clamps. The fact that the optical values for the exposed and protected sides of the clamps could be compared allowed

us to conduct meaningful paired "t" analyses of the differences between the front and back of the clamps and determine the statistical significance of the results.

The most obvious conclusions which can be drawn from the data presented in Table I are that emittance values apparently decreased by an average of 5.6% as a result of space exposure and the a/e ratio increased by 5.6%. While these values are small, they are statistically significant at the 99% confidence level. The data in Table I also indicates that the clamps subjected to earth end exposure were the only ones which exhibited no change as a result of space exposure. This indicates that UV exposure may have had an adverse effect on the integrity of the anodize layer.

There were a number of subtle differences that were observed which are not apparent from the average values presented in Table I. These will be discussed in the subsequent sections.

Solar Absorptance

While the data in Table I indicates that the average solar absorptance values remained unchanged, closer scrutiny reveals some interesting trends. Figure 11 contains a graph of the average change in solar absorptance values between the front and back of the clamps as a function of position on LDEF. As seen in this figure, leading edge exposure has resulted in a slight decrease in solar absorptance values while trailing edge exposure has resulted in an increase. There also appears to be a transition zone in row 6 where little or no change occurred. Although these values are small, they are statistically significant at the 99% confidence level. Table II contains the results of a Duncan's New Multiple Range Test on the data from Figure 11.

Figure 12 is a plot of the change in solar absorptance values as a function of atomic oxygen flux. The data indicates that solar absorptance values generally decrease with increasing levels of atomic oxygen exposure. The relationship between the change in solar absorptance values and equivalent sun hours is presented in Figure 13. At first glance the data in Figure 12 appears to be quite scattered. A closer look, however, reveals that there are actually two distinct relationships indicated here. The first is for trailing edge specimens and it indicates a slight increase in solar absorptance with increasing sun hours. Leading edge specimens, however, actually show a decrease with increasing sun hours. The reasons for these trends as well as the ramifications of the interaction of atomic oxygen and UV exposure on the performance of the coating are being evaluated.

Thermal Emittance

The relationship between the change in emittance values and the position on LDEF is presented in Figure 14. As seen in this figure, the emittance values decreased relatively uniformly. This decrease is significant at the 99% confidence level and is apparently independent of the position of the clamps on the satellite. This would seem to indicate that the observed changes in emittance may be related to the silicon contamination which was generally present over the entire space craft. We will be investigating this possibility in future analyses. There were also no correlations observed when the change in emittance values were plotted against either the atomic oxygen flux or the equivalent sun hours.

The Ratio of Absorptance/Emittance

Figure 15 contains the relationship between the change in a/e and the position of the clamps on the satellite. The data indicates that space exposure increased the a/e ratio for the tray clamps. This relationship was again significant at the 99% confidence level. In

general, the observed change was more dramatic for trailing edge clamps than for those placed on the leading edge. There were no correlations when the changes in a/e were plotted against the atomic oxygen flux or the equivalent sun hours.

While the observed changes in the optical properties of the anodized coating were relatively small, they were statistically significant. It is unknown what effect longer exposure will have on the coating. Assuming that the observed changes were induced by space exposure, they could have already reached their maximum levels and will now be constant with time or they could be following an Arrhenius relationship and may increase with further exposure. This points out the need for future ground based simulation to attempt to duplicate these results and determine the effects of longer exposure on the performance of the coating.

TABLE I. Summary of Solar Absorptance and Emittance Measurements for Chromic Acid Anodize Coating on LDEF Tray Clamps

		Front			Back		
Row	n	α	ε	α/ε	α	ε	α/ε
1	16	.349	.153	2.28	.337	.164	2.06
2	21	.349	.152	2.30	.342	.157	2.18
3	15	.350	.149	2.35	.341	.156	2.19
4	9	.352	.151	2.33	.339	.161	2.11
5	13	.347	.151	2.30	.342	.161	2.12
6	17	.348	.155	2.25	.347	.161	2.16
7	17	.331	.151	2.19	.335	.163	2.06
8	9	.334	.150	2.27	.342	.160	2.14
9	15	.339	.145	2.33	.343	.155	2.21
10	12	.334	.149	2.24	.346	.163	2.12
11	13	.335	.151	2.22	.345	.167	2.07
12	17	.334	.142	2.35	.338	.155	2.18
SPACE	28	.348	.158	2.20	.350	.170	2.06
EARTH	24	.348	.168	2.07	.347	.169	2.05
AVG.	**228**	**.343**	**.153**	**2.24**	**.343**	**.162**	**2.12**

TABLE II. Statistical Evaluation of Solar Absorption Differences as a Function of Tray Position on LDEF

Statistical Evaluation of Solar Absorptance Differences

Row	10	11	8	7	12	9	6	5	2	3	1	4
$\overline{D}$	-1.17	-1.08	-0.78	-0.47	-0.35	-0.33	0.18	0.54	0.72	0.93	1.19	1.33

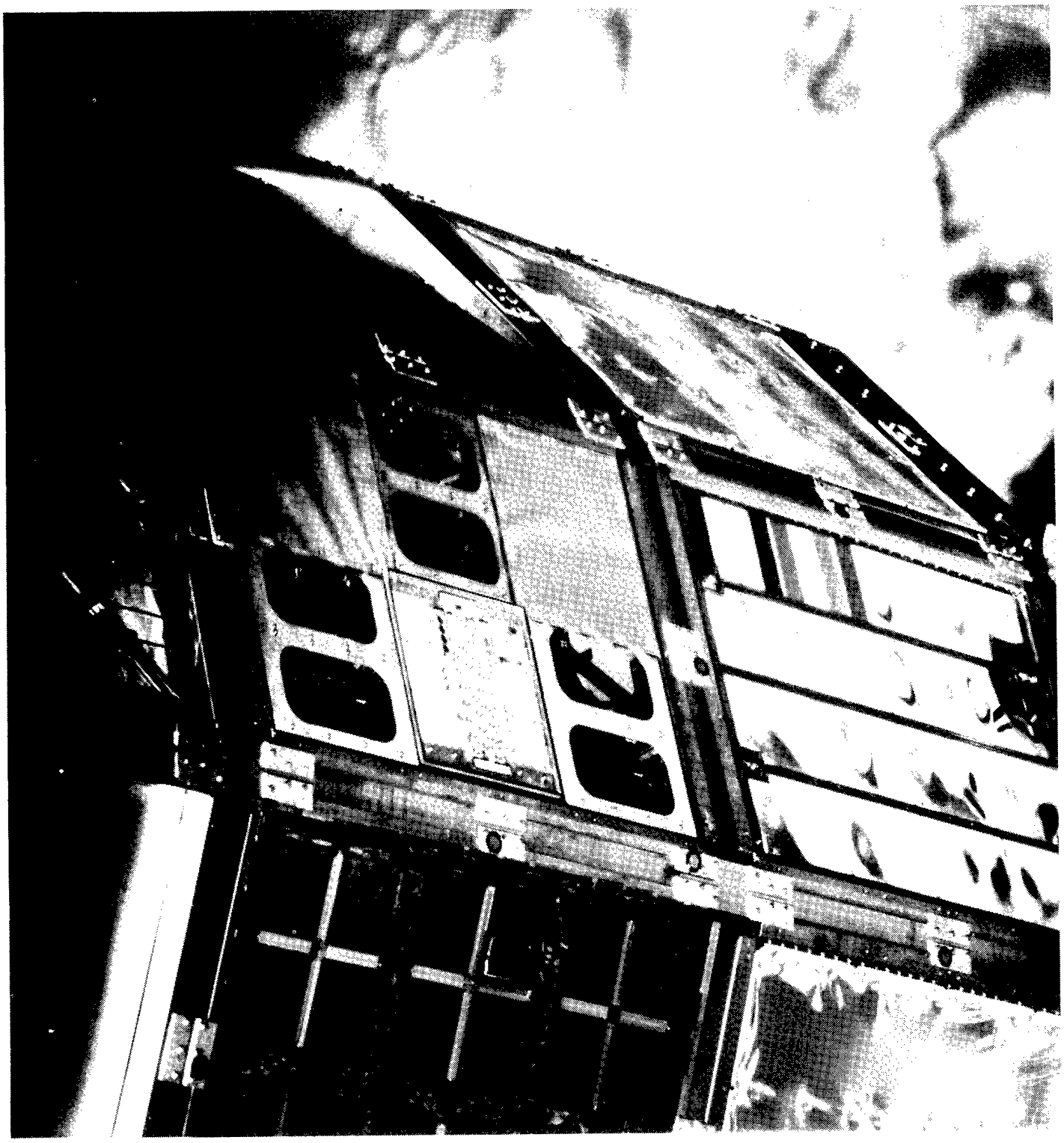


FIGURE 1. Photograph of LDEF showing the position of the tray clamps on the satellite.

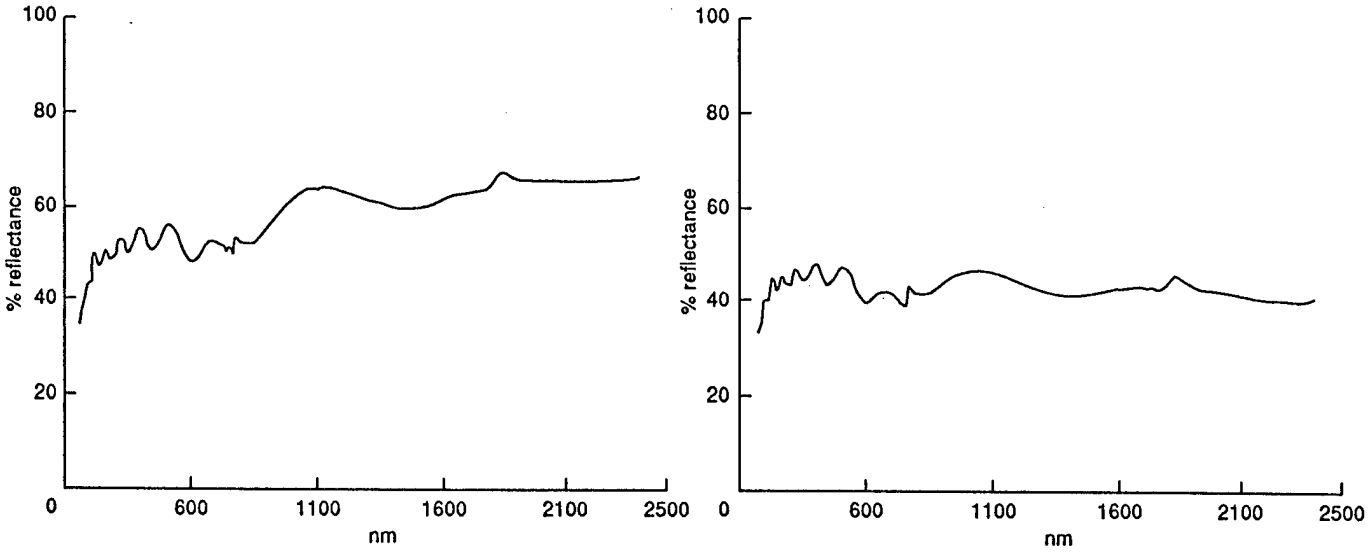


FIGURE 2. UV-Visible diffuse reflectance spectra from two tray clamps

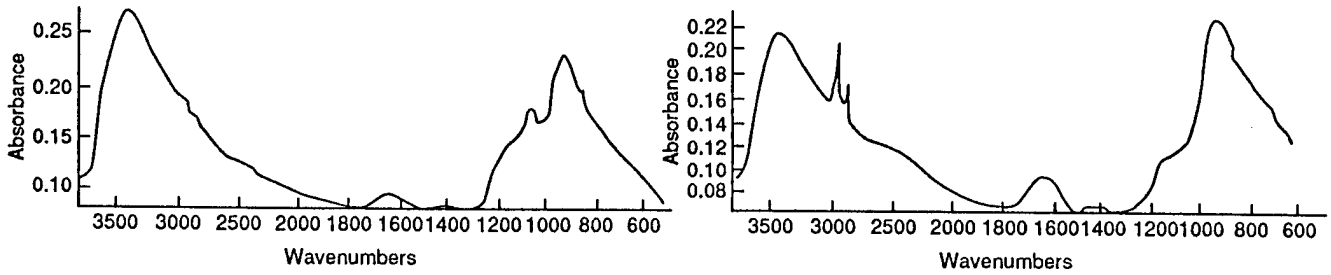


FIGURE 3. Typical infrared diffuse reflectance spectra from A) an exposed and B) a protected area of LDEF tray clamps

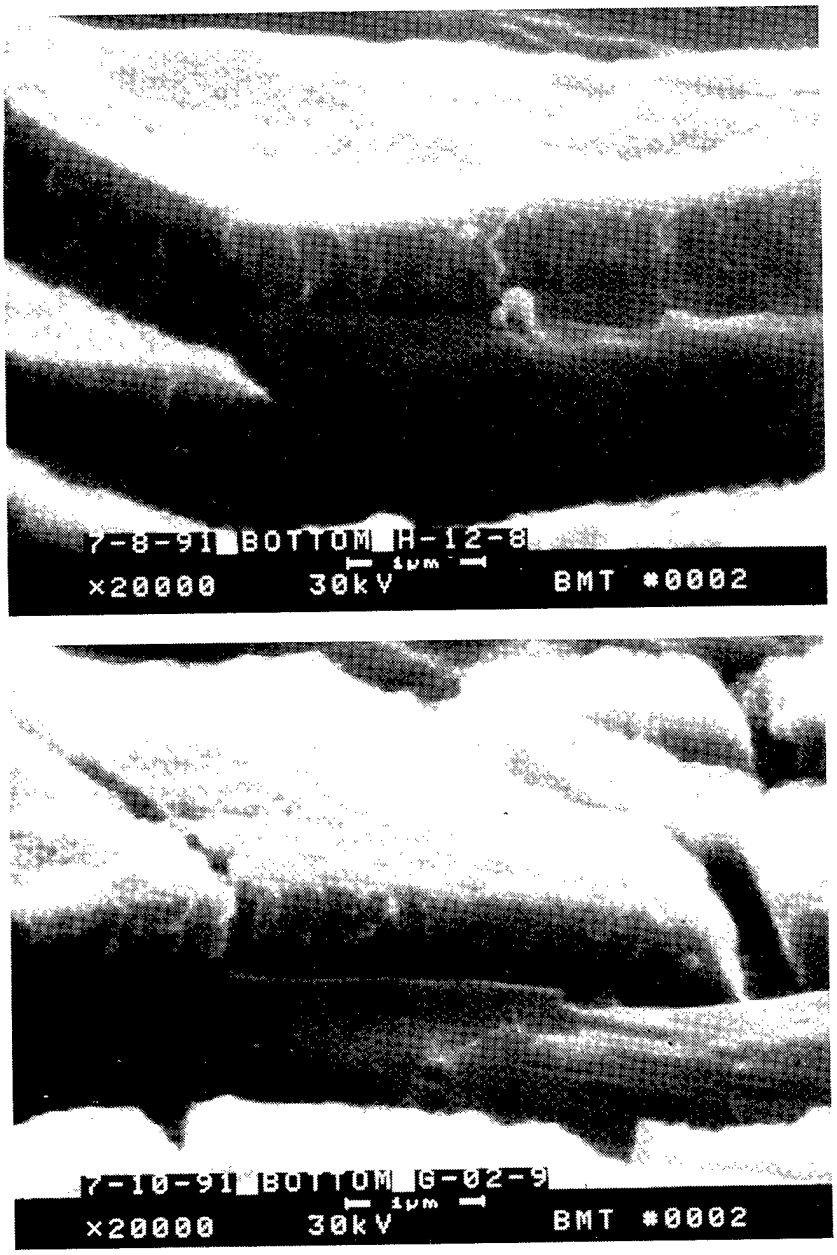


FIGURE 4. Typical SEM photomicrographs showing anodize coating thickness

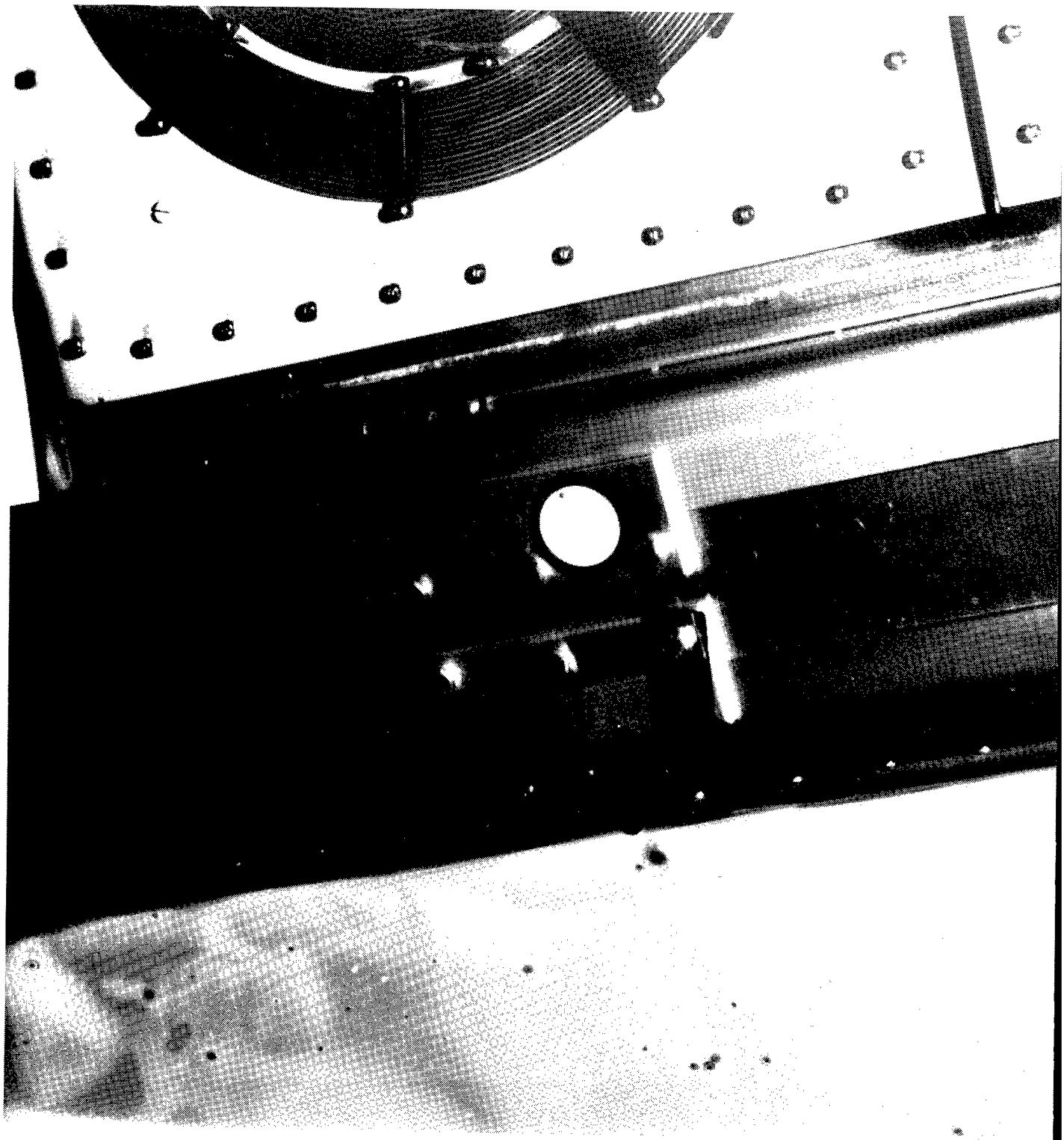


FIGURE 5. Photograph showing position of copper grounding strap on LDEF tray clamp.

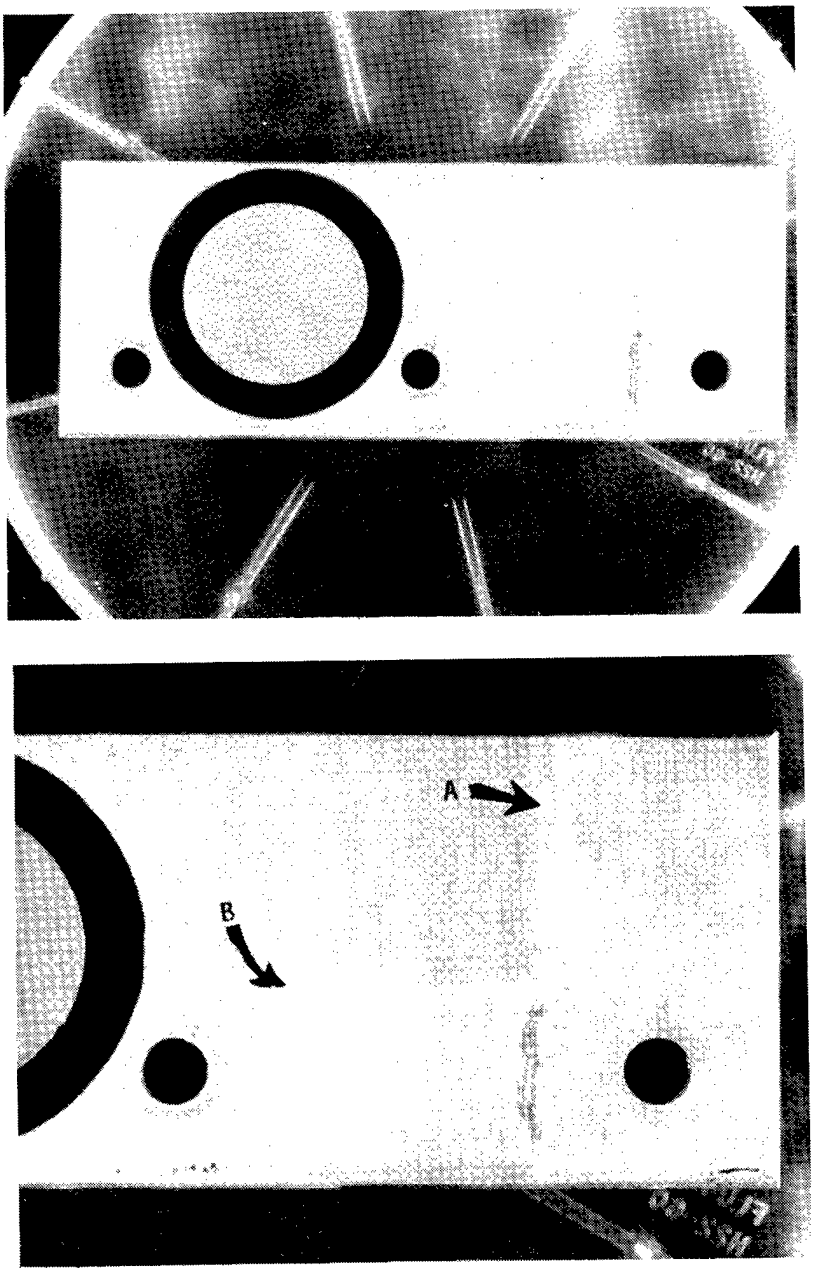


FIGURE 6 Photo macrographs of tray clamp E02-6 with arrows indicating boundaries between exposed regions and those protected by (A) the copper ground strap and (B) the aluminum shim.

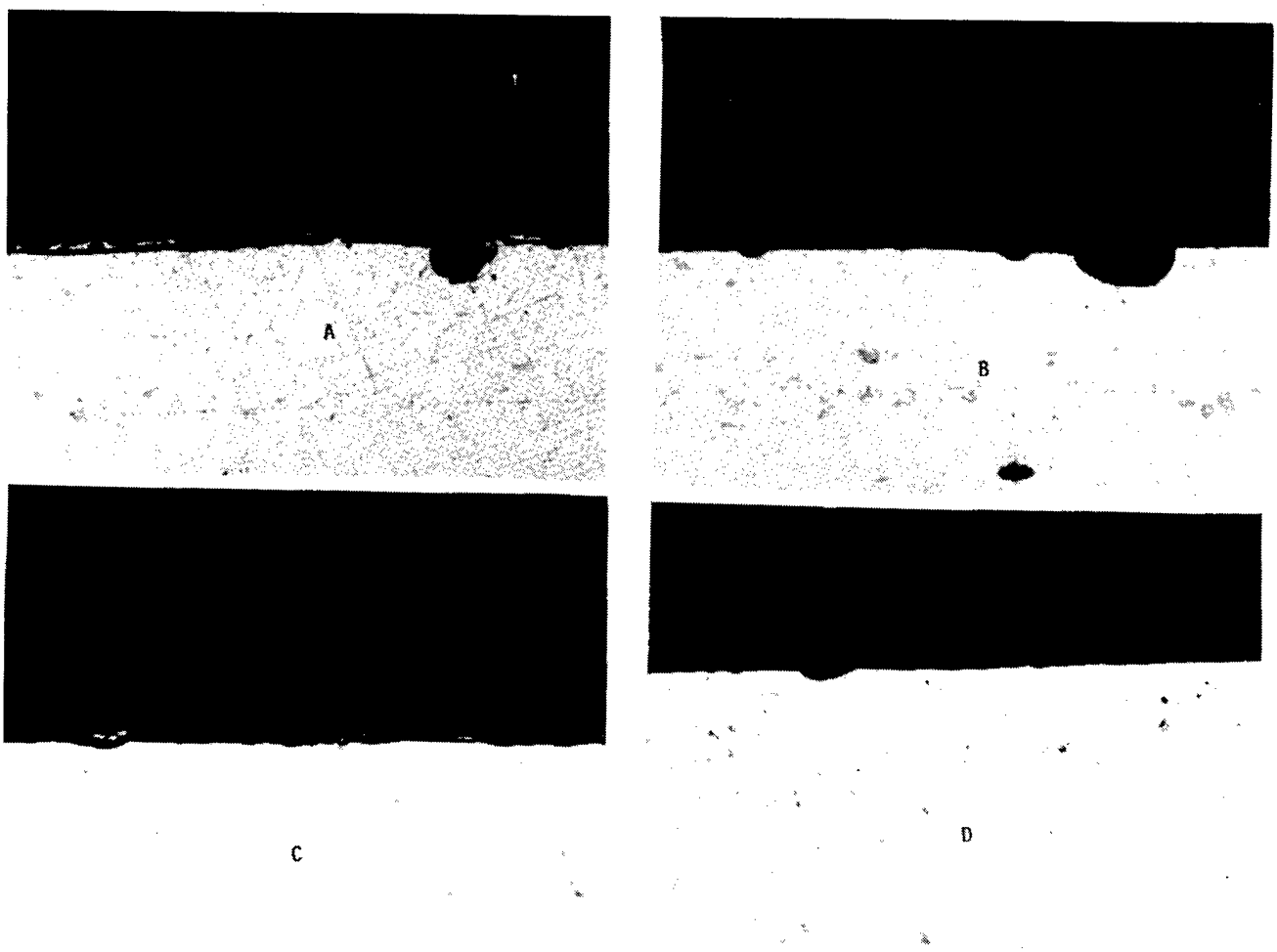


FIGURE 7 Optical photomicrographs at 1000X depicting (A) protected and (B) exposed regions from the surface of leading edge clamp E10-6 and from (C) protected and (D) exposed areas from trailing edge clamp E02-6.

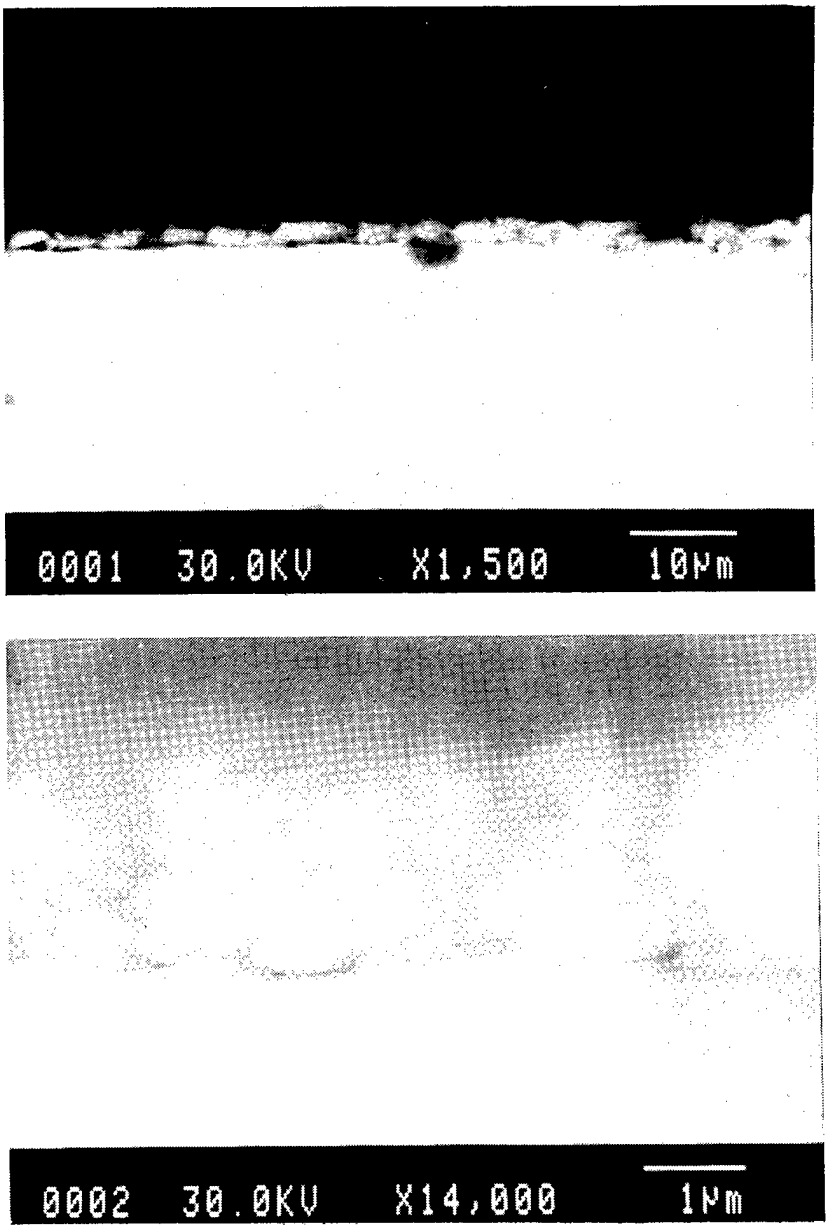


FIGURE 8 Higher magnification scanning electron photomicrographs depicting the observed surface layer on the protected surfaces of tray clamp E10-6.

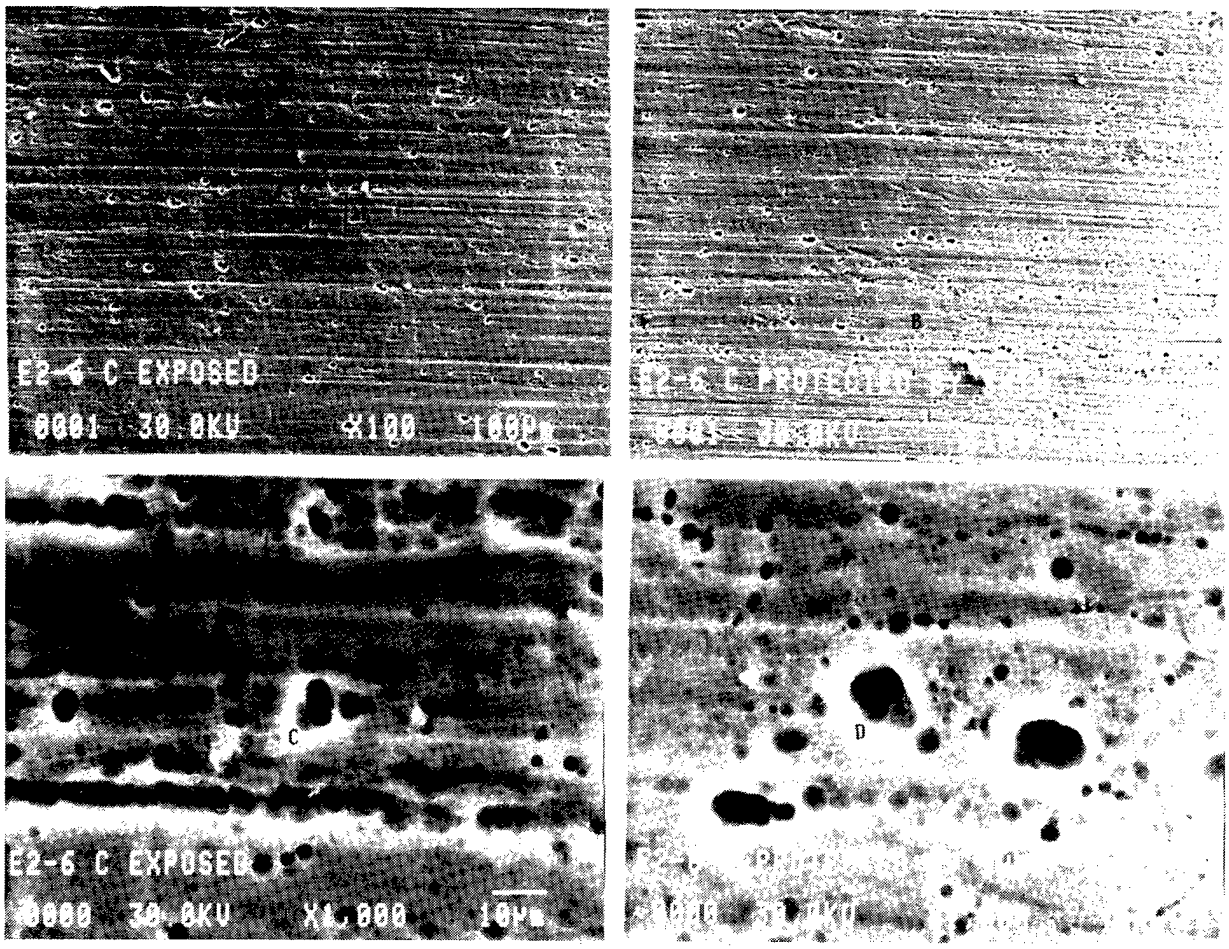


FIGURE 9. SEM photomicrographs depicting surface porosity on (A) exposed and (B) protected at 100X and (C) exposed and (D) protected at 1000X for trailing edge clamp E02-6.

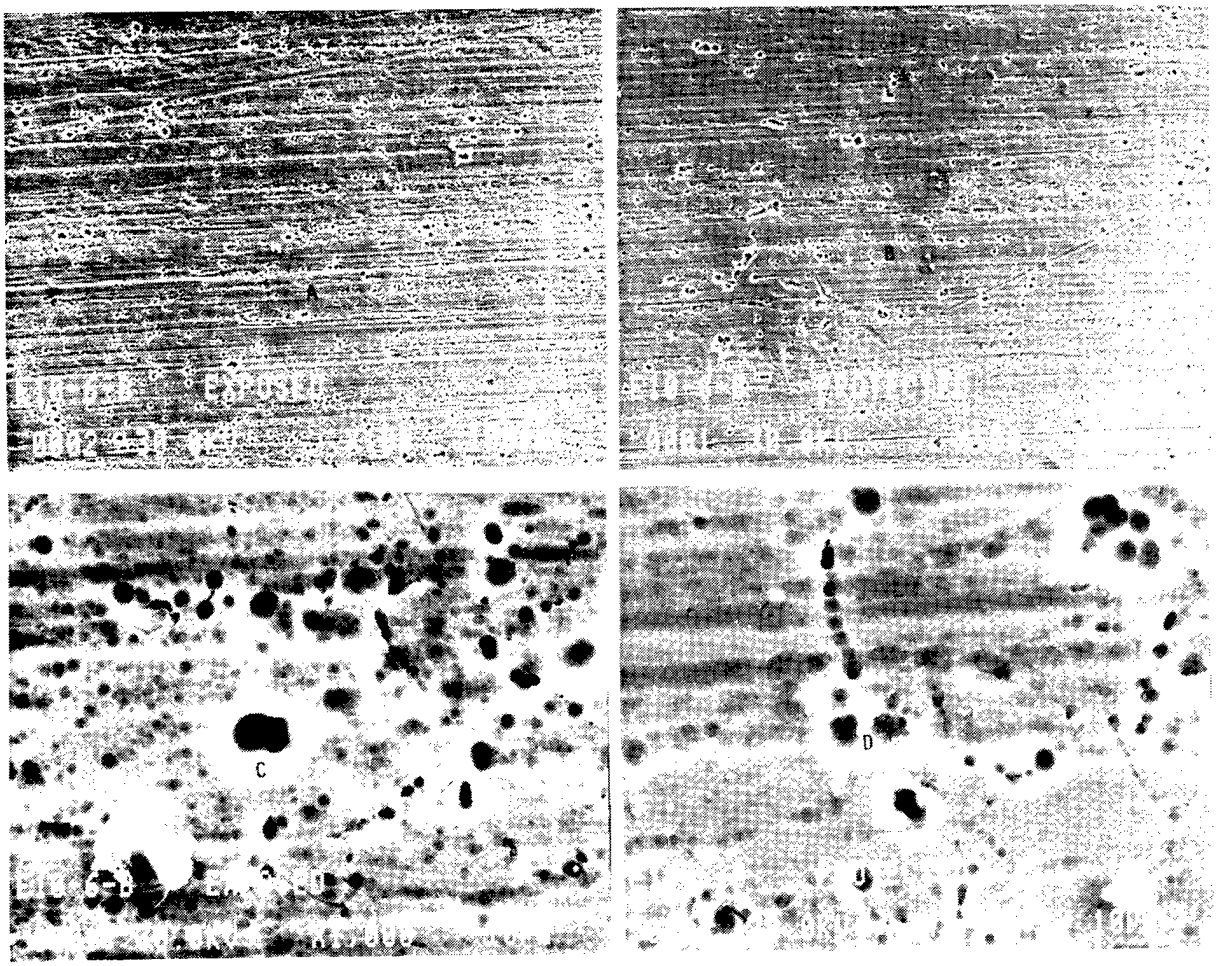


FIGURE 10. SEM photomicrographs depicting surface porosity on (A) exposed and (B) protected at 100X and (C) exposed and (D) protected at 1000X for leading edge clamp E10-6.

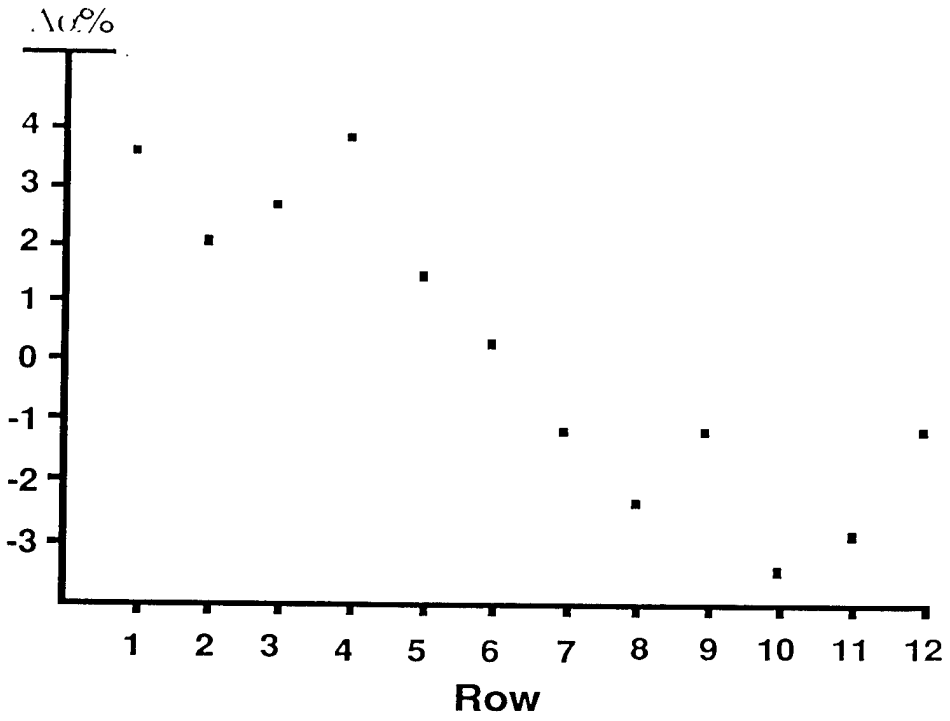


FIGURE 11. Percent change in solar absorptance as a function of position on LDEF

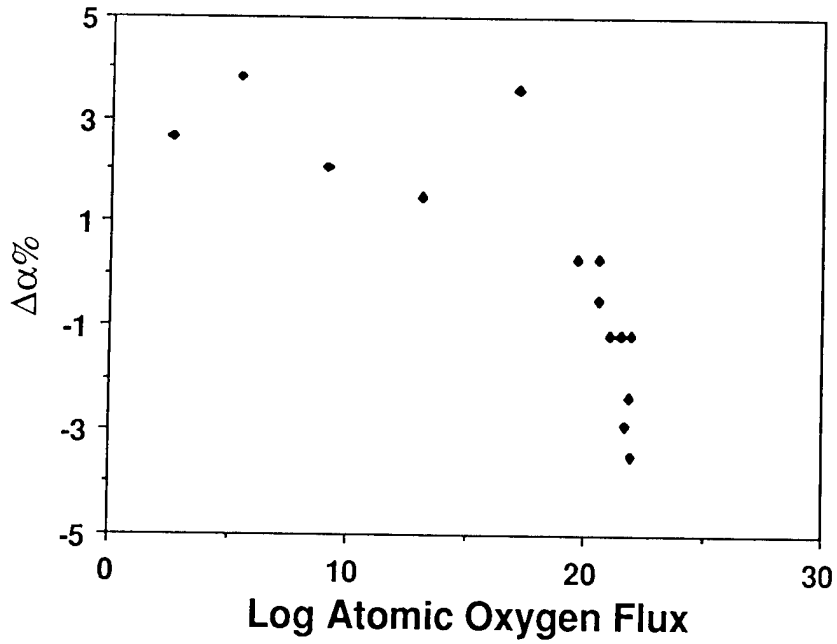


FIGURE 12. Percent change in solar absorptance as a function of atomic oxygen flux

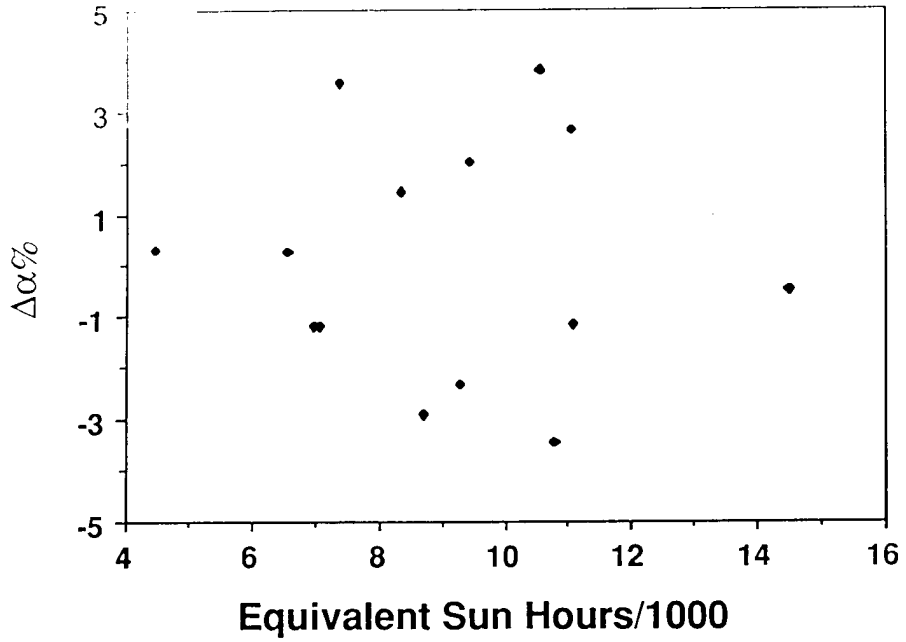


FIGURE 13. Percent change in solar absorptance as a function of equivalent sun hours.

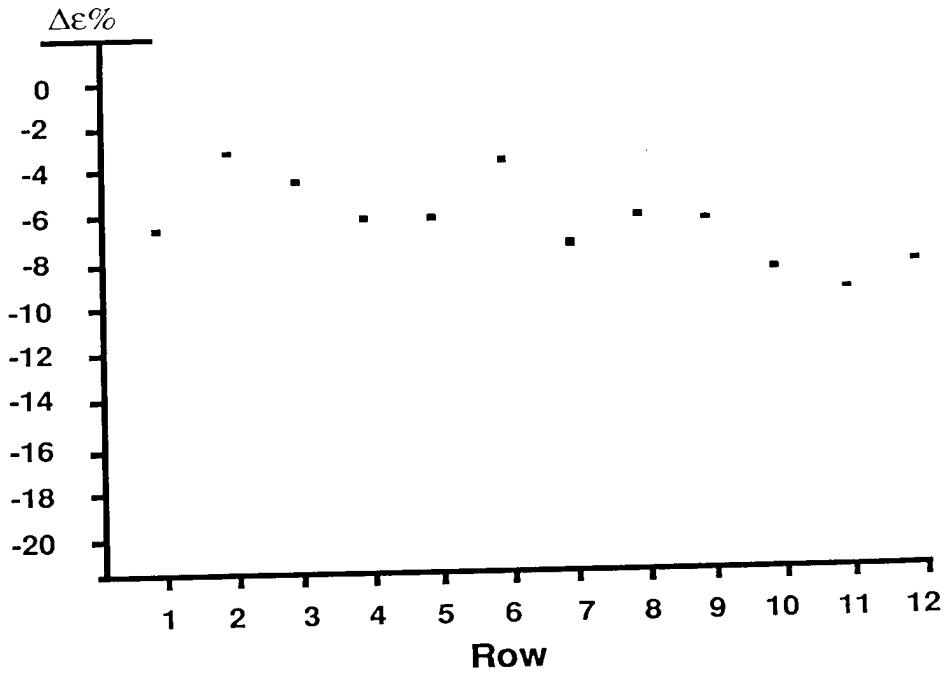


FIGURE 14. Percent change in emittance as a function of position on LDEF

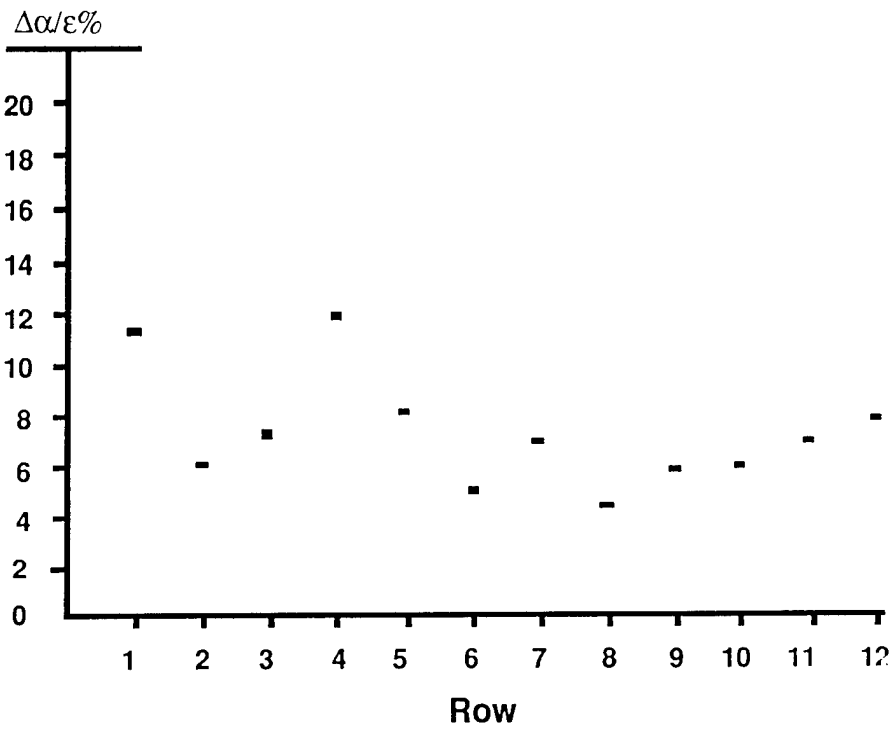


FIGURE 15. Percent change in the ratio of absorptance to emittance as a function of position on LDEF

M0003-10: LDEF ADVANCED COMPOSITES EXPERIMENT[1]

Gary L. Steckel
The Aerospace Corporation
El Segundo, CA 90245
Phone: 310/336-7116, Fax: 310/336-7055

Tuyen D. Le
The Aerospace Corporation
Phone: 310/336-7864, Fax: 310/336-7055

SUMMARY

The Advanced Composites Experiment includes nearly 500 samples of metal matrix, organic matrix, and glass matrix composites that were flown on the leading and trailing edges of LDEF. The experiment is a cooperative effort with participation by several aerospace companies. This paper is a review of the preliminary observations and test results that were made by The Aerospace Corporation. Estimated recession rates from atomic oxygen exposure for organic matrix composites are reported. Preliminary scanning electron microscopy observations for organic and metal matrix composites and microstructural analyses for metal matrix composites are presented.

EXPERIMENT DESCRIPTION

The Advanced Composites Experiment is a sub-experiment of LDEF Experiment M0003, "Space Environmental Effects on Spacecraft Materials". The sub-experiment is a joint effort between government and industry with Air Force Wright Laboratory, Flight Dynamics Laboratory, and The Aerospace Corporation, Mechanics and Materials Technology Center, serving as experimenters. The experiment includes numerous metal matrix composites, primarily graphite fiber-reinforced aluminum and magnesium, and several classes of graphite fiber-reinforced organic matrix composites. The latter includes graphite/epoxy, graphite/polysulfone, and graphite/polyimide composites with and/or without various thermal control or protective coatings. The metal matrix composites were supplied

[1]Funding for this effort was processed through Air Force Space Systems Division Contract F04701-88-C-0089 under an interagency agreement with Air Force Wright Laboratory.

by Aerospace and the organic matrix composites were supplied by General Dynamics Space Systems Division (GDSSD), Lockheed Missiles and Space Company (LMSC), Boeing Aerospace & Electronics, and McDonnell Douglas Space Systems Company (MDSSC). In addition, a number of graphite fiber-reinforced glass matrix composites were provided by United Technologies Research Center (UTRC). Each material supplier is responsible for performing postexposure tests and analyses on their flight articles and ground control samples. The test plans, analyses and results of the individual organizations are being closely coordinated in order to maximize the output of the experiment.

The experiment occupied approximately one-sixth of a 6 in.-deep peripheral tray on both the leading and trailing edges of LDEF. The trays were located on LDEF Bay D, Row 4 on the trailing edge and Bay D, Row 8 on the leading edge. The samples were mounted on both sides of cassettes with one side (Deck A) exposed to the space environment and the other side (Deck B) facing inward. The environments for the samples mounted on the leading and trailing A decks were similar except those on the leading edge were also exposed to relatively high fluxes of atmospheric constituents (primarily atomic oxygen). Although the samples on the B decks were not exposed to the radiation environment, the experiment design was such that they experienced thermal excursions similar to those of the exposure samples. The sample cassettes were decoupled from the LDEF in order to maximize the thermal excursions. For most materials, at least one sample was located on each deck and additional samples were maintained in a laboratory environment.

Although this was essentially a passive experiment, one or more samples of each class of composites was instrumented with thermistors and strain gages to monitor the thermal excursions on the leading and trailing edges and the resulting dimensional changes. The data acquisition system was set up to record temperatures and strains during the duration of an orbit once every 107 hours (approximately 78 orbits). Data were collected approximately every three minutes during the selected orbits. The data were recorded on magnetic tape until the tape was fully loaded, approximately fourteen months into the flight. No data were recorded during the unplanned final 4.5 years of the flight. The strain data are still being interpreted and will not be presented in this paper. The thermistor data indicated that the maximum and minimum temperatures for the uncoated graphite/epoxy composites were approximately +80°C and -45°C, respectively. The metal matrix composites tended to run a little hotter since they have a lower emittance. The maximum and minimum temperatures for graphite/magnesium, for example, were +110° and -40°C, respectively.

COMPOSITE MATERIALS

Most of the composite samples were 3.5 by 0.5 in. (8.9 by 1.3 cm) strips. There were also a limited number of 1 in. (2.5 cm) diameter mirror samples, a few 2.4 by 0.5 in. (6.1 by 1.3 cm) strips and several graphite/aluminum, graphite/magnesium and silicon carbide/aluminum wires. The latter were prepared by infiltrating the graphite or silicon

carbide fiber tow with molten aluminum or magnesium alloys. Most of the wires were approximately 0.025 in. (0.064 cm) in diameter.

The organic matrix composites in the experiment are listed in table I. Because of the cooperative effort, a very broad test matrix of graphite/epoxy composites having several different fiber-matrix combinations and lay ups were flown. Most of the graphite/epoxy composites were uncoated. With the exception of a T300/polyethersulfone composite, all of the graphite/thermoplastic composites had the P-1700 polysulfone matrix. Most of these composites had thermal control coatings. The remainder of the organic matrix composites had high-temperature polyimide or bismalimide matrices.

The metal and glass matrix composites included in the experiment are listed in table II. The graphite/aluminum strip and mirror samples included three different graphite fibers and two different alloy matrices. These composites also had four different lay ups. The graphite/magnesium strips and mirrors included P100/EZ33A/AZ31B and P100/AZ91C/AZ61A composites. The samples for LDEF were prepared during the early stages of the development of graphite/magnesium. At that time, P100/EZ33A/AZ31B was considered a leading candidate system for space applications. However, it was subsequently discovered that poor strength properties were inherent in this system and it was replaced by the P100/AZ91C/AZ61A system. Therefore, several P100/AZ91C/AZ61A samples were added to the test matrix shortly before the experiment trays were delivered to NASA. These samples are of great interest as they are representative of the current state-of-the-art for graphite/magnesium. The silicon carbide/aluminum composites included both discontinuous whisker-reinforced and continuous fiber-reinforced strips. The metal matrix wires included five fiber-matrix combinations for graphite/aluminum, three fiber-matrix combinations for graphite/magnesium, and Nicalon SiC fiber-reinforced 6061 aluminum. Most of the wires were prepared by infiltrating a single tow of fibers with the molten matrix alloy, but in some cases, several tows were infiltrated to form a larger diameter wire. The UTRC-supplied graphite/glass composites were uncoated and had either GY70 or Celion 6000 graphite fibers in a borosilicate glass matrix.

Each organization submitted a matrix of materials appropriate for studying specific phenomenon or for obtaining data on a certain composite system or set of systems. For example, the primary objective of the McDonnell Douglas experiment was to determine the effectiveness of various protective coatings for preventing property degradations in graphite/epoxy, graphite/polyimide and graphite/thermoplastic composites. Thus for each composite system, they flew uncoated control samples and those having up to three different coatings. Lockheed was interested in determining the effects of composite lay up and matrix cure temperature on the degree of thermal cycling induced microcracking. They submitted a test matrix consisting of unidirectional and cross-plied graphite/epoxy composites having three different fiber-matrix combinations in order to achieve these objectives. Thus, the different organizations submitted separate, independent experiments, but are working together to maximize the data output of the overall experiment.

Most of the composites in the experiment were developed for space structural applications. Thus, the primary properties of interest include the flexural or tensile properties, the coefficient of thermal expansion, solar emittance and absorptance, specific heat, thermal conductivity and physical properties such as fiber volume, void content and density. Post-exposure measurements vary for the different classes of composites, but include most of the above properties as well as surface analyses, macrophotography and microstructural analyses.

OBSERVATIONS AND PRELIMINARY RESULTS

Several observations were made from a visual inspection and by comparing preflight and post-flight photographs of the sample cassette assemblies (fig. 1). First, it was noted that all of the composites survived in excellent physical condition. Surface roughening due to atomic oxygen erosion for uncoated organic matrix composites mounted on the exposed leading edge was the only significant visible damage. However, the erosion depth appeared to be shallow relative to the overall thickness of the affected composites. Contamination was evident on both the leading and trailing edges. For example, a large contaminated area is apparent on seven samples in the lower left corner of the leading edge cassette in the post-flight photograph of figure 1. This contamination was from another experiment or from the LDEF structure. However, there were also rainbow outgassing stains on trailing edge samples adjacent to elastomeric samples, which were from a different subexperiment of M0003 but were mounted on the Advanced Composites Experiment cassette. The most dramatic change was a yellowing or browning of many of the thermal control coatings. This was only observed for the exposed samples on the trailing edge (fig. 1). The exposed leading edge paints and those on the Deck B samples remained white. The yellowed samples were McDonnell Douglas samples having a ZnO silicone coating and the brown samples included General Dynamics samples with ZnO and TiO_2 coatings and McDonnell Douglas samples with a leafing aluminum coating. Further discussion on the browning of thermal control coatings flown on the M0003 trays is given by Meshishnek and Gyetvay (refs. 1 & 2).

The only analyses performed on the organic matrix composites at The Aerospace Corporation were preflight and post-flight mass measurements and scanning electron microscopy (SEM) on some of the uncoated composites that were mounted on the leading edge. The mass measurements were made after the samples had equilibrated in a constant temperature, constant humidity laboratory. Thus, moisture variations were eliminated and the only significant mass changes were those that could be attributed to atomic oxygen erosion on the exposed leading edge. The erosion depth was calculated from the known composite density and exposure area and the measured mass loss. Since the fibers and matrix have different erosion rates and densities, this technique of determining the erosion depth is an approximation. The actual erosion depths are probably somewhat higher because the samples had resin-rich surfaces and the epoxy, which has a lower density than the

graphite fibers, erodes at a higher rate than the fibers. The most interesting results were for the General Dynamics composites. They flew several graphite/epoxy composites having several different fiber-matrix combinations and a wide range of fiber contents. The calculated erosion depths for these composites were inversely proportional to the fiber content (fig. 2). All of the composites provided by General Dynamics were fabricated following similar procedures. In particular, the same bleeder cloth was used so that the composites had similar surface conditions. Composites prepared by other experiment participants having significantly different surface conditions (either more matrix rich or less matrix rich) did not fall on the erosion depth versus fiber content curve established by the General Dynamics composites. Thus, it would appear that the fiber content and surface conditions are more important variables than the graphite fiber type or epoxy matrix type in determining the susceptibility of graphite/epoxy to atomic oxygen erosion. Perhaps the most important observation was that the erosion depths of the uncoated organic matrix composites were much less than for monolithic polymers. The estimated erosion depth for most of the graphite/epoxy composites was less than 0.007 cm, much less than the predicted erosion of 0.012 cm for monolithic epoxies (ref. 3) for the LDEF atomic oxygen fluence of approximately 7×10^{21} atoms/cm^2 for Row 8 (ref. 4).

Figure 3 shows SEM micrographs of the eroded surfaces of P75S/934 graphite/epoxy and T300/V378A graphite/bismalimide composites that were mounted on the leading edge. The "Christmas tree" or cone-like erosion fragments of the graphite/epoxy sample are typical of most of the uncoated organic matrix composites in the experiment. The rows of erosion fragments on these samples run parallel to the fiber direction with the apex of the cones or "Christmas trees" pointing in the direction of the LDEF velocity vector. The graphite/bismalimide composite formed deep erosion grooves between what appears in figure 3b to be relatively flat regions. When viewed from a different angle (fig. 3c), it is evident that the erosion fragments in these flat regions were finer with more of an acicular appearance and random arrangement as compared to the P75S/934 composite. The acicular erosion features, but without the deep erosion grooves, were also observed for three other composites: a T300/934 graphite/epoxy composite supplied by Boeing and T300/P-1700 graphite/polysulfone composites supplied by Boeing and McDonnell Douglas. It is not readily apparent whether these different erosion features are indicative of changes in the erosion characteristics, or are due to subtle variations in the initial surface conditions, fiber distribution, matrix chemistry, etc. of the composites. These preliminary observations indicate the need for more in-depth SEM studies by the organizations responsible for the organic matrix composites.

Numerous micrometeoroid or debris impact craters have been observed on the exposed samples. The diameter of most of the craters was less than 100 micrometers. A micrometeoroid/debris crater on a graphite/aluminum composite is shown in figure 4. Since the graphite/aluminum has an aluminum alloy surface foil, the crater has the same appearance as for monolithic aluminum. A cross section of this crater shows that it extended completely through the 0.004 in.(0.010 cm) 2024 aluminum surface foil, but did not extend into the underlying graphite fiber-reinforced interior. This may imply that penetration

through the foil is much easier than through the fiber-reinforced region of the composite, but may also be the characteristic depth of penetration into aluminum for this particular size of impact particle. More samples will need to be sectioned to make this determination. Perhaps the most significant observation in figure 4 is the presence of a delamination of the surface foil over an area approximately three times the crater diameter. It is not known whether the delamination occurred due to the impact energy or formed later due to thermal fatigue. Surface foil delaminations would affect important through-thickness properties, such as the thermal conductivity. In addition, the transverse strength of graphite/aluminum and graphite/magnesium is primarily provided by the surface foil. Large foil delaminations could therefore have serious consequences on the performance of these composites. Thus, if the delaminations propagate due to thermal fatigue, they could reach much larger sizes during extended missions and have adverse effects. Additional studies will be performed in an effort to determine whether the delaminations form due to the impact or if they develop and/or propagate during subsequent thermal cycling.

Etching of graphite/aluminum cross sections, such as in the cross section in figure 4, produced matrix darkening in the fiber-reinforced regions, which is an indication of plastic deformation. This is not surprising since the coefficient of thermal expansion mismatch between the graphite fibers and matrix induces high stresses in the matrix during thermal cycling. Nevertheless, there was no evidence of matrix microcracking in either graphite/aluminum or graphite/magnesium, the only materials that have been sectioned to date. Since the samples have seen over 33,000 thermal cycles, this indicates that these composites have excellent resistance to thermal fatigue for the LDEF thermal environment. Extensive thermal fatigue cracking was observed, however, on the surface foils of selected GY70/201/2024 graphite/aluminum samples (figure 5). This was surprising since the thermal stresses should be lower within the surface foils than within the fiber-reinforced regions of the composites. However, further inspection revealed that the cracks were always associated with a surface contaminant that was clearly visible on several trailing edge samples that had been mounted adjacent to one another. X-ray Photoelectron Spectroscopy (XPS)[2] showed the presence of silicon and oxygen, probably from on-orbit silicone contamination. The cracks probably initiated in a brittle oxide or aluminum silicate layer on the sample surface. Once the cracks were initiated, they propagated into the bulk of the foil. In some cases (fig. 5), the cracks propagated completely through the surface foil. However, there was no evidence of the cracks extending into the underlying Gr/Al region or along the interface between this region and the foil.

Less severe, isolated fatigue cracks were also observed on a few GY70/201/2024 graphite/aluminum composites. These cracks were always associated with surface defects such as surface foil blemishes, micrometeorite craters or engraved sample identification numbers (fig. 6). Apparently, these defects acted as stress concentrators and initiated

---

[2]C. S. Hemminger was responsible for the X-ray Photoelectron Spectroscopy and its interpretation.

thermal fatigue cracks. All of the graphite/aluminum composites that had surface foil cracks, due to either contamination or stress risers, had 2024 surface foils. No composites having 6061 surface foils showed any evidence of foil cracking. The composites having 6061 surface foils were heat treated to a T6 condition, whereas those having 2024 foils were in the as-fabricated condition. Thus, the 6061 foils probably had a higher yield strength, which would also tend to increase the fatigue life of the 6061 foils relative to the 2024 foils (ref. 5). These observations are consistent with post-flight microhardness measurements, which verified that the 6061 foils were significantly harder than the 2024 foils.

Surface foil cracks were also observed on several graphite/magnesium composites. In this case, all of the cracked samples had a very rough, mottled surface appearance (fig. 7), which XPS indicated was due to extensive surface oxidation. Several observations concerning the oxidation and foil cracking were made from an evaluation of all of the P100/AZ91C/AZ61A graphite/magnesium composites. These included samples from two panels, one having a single ply, unidirectional lay up and a second panel having 4 plies in a $(\pm 10^{\circ})_s$ lay up. The unidirectional panel had been stored in a laboratory for two years before it was decided to use it for LDEF. The surface of the panel was heavily oxidized and required abraiding to prepare samples having clean surfaces. The resulting rough surface was, however, susceptible to additonal oxidation, which was observed for all samples from this panel that were mounted on the A decks for both the leading and trailing edges. All of these samples also had extensive surface foil cracking. Samples mounted on the interior B decks showed much less oxidation and no foil cracking. Since the degree of oxidation was the same on the leading and trailing edges, we believe that these observations are indicative of prelaunch oxidation. The four ply panel was prepared for LDEF shortly before the experiment trays were delivered to NASA. This panel had very smooth surfaces that were not as prone to oxidation. As a result, the flight samples showed only light oxidation and no surface foil cracking. Thus, it is concluded that the surface foil cracking on graphite/magnesium is due to the formation of a brittle oxide layer that forms prior to launch, but can be eliminated by the application of suitable prelaunch handling and surface preparation procedures. It is further concluded that the thermal fatigue cracking observed for graphite/aluminum and graphite/magnesium was due to anomalous surface conditions.

It is too early in the evaluation process for the Advanced Composites Experiment to comment on the relative merits of the different classes of composites or to make comparisons between the different fiber-matrix combinations included in the experiment for a given composite class. However, since all of the composites in the experiment appear to have survived the extended space exposure in excellent physical condition, a full complement of tests will be performed to fully evaluate these critical spacecraft materials.

REFERENCES

1. Meshishnek, M. J.; Gyetvay, S. R.; and Jaggers, C. H.: Long Duration Exposure Experiment M0003 Deintegration/Findings & Impacts. First LDEF Post-Retrieval Symposium, NASA CP-3134, 1992.

2. Gyetvay, S. R.; Fishman, L.; and Meshishnek, M. J.: Long Duration Exposure Facility Experiment M0003 Deintegration Observations. First LDEF Post-Retrieval Symposium, NASA CP-3134, 1992.

3. Banks, B. A.: Atomic Oxygen Interaction with Materials on LDEF. LDEF Materials Data Analysis Workshop, NASA CP 10046, July 1990, pp. 191-216.

4. Bourassa, R. J.; Gillis, J. R.; and Rousslang, K. W.: Atomic Oxygen and Ultraviolet Radiation Mission Total Exposures For LDEF Experiments. First LDEF Post-Retrieval Symposium, NASA CP-3134, 1992.

5. Metals Handbook Ninth Edition, Volume 2, Properties and Selection: Nonferrous Alloys and Pure Metals. American Society For Metals, 1979.

TABLE I.- LIST OF ORGANIC MATRIX COMPOSITES

MATERIAL DESCRIPTION FIBER/MATRIX/COATING	LAY UP	SUPPLIER	NUMBER OF SAMPLES				
			LEADING		TRAILING		CONTROL
			A	B	A	B	
GRAPHITE/EPOXY STRIPS							
GY70/X-30/NONE, Sn-In	$(0/45/90/135)_{2S}$	GDSSD	4	4	3	3	5
GY70/X904B	$(0)_{16}$, $(0/90_2/0)_{2S}$	LMSC	3	3	3	3	0
GY70/934	$(0/45/90/135)_{2S}$	GDSSD	2	3	2	2	7
GY70/CE-339	$(0/45/90/135)_{2S}$	GDSSD	2	3	3	3	6
P75S/CE-339	$(0/45/90/135)_{2S}$	GDSSD	2	3	2	2	8
P75S/934	$(0/45/90/135)_{2S}$	GDSSD	2	2	2	2	8
T300/5208/NONE, Zn0, Al FLAKE		MDSSC	1	2	2	3	0
T300 TAPE/934	$(0)_{16}$	BOEING	3	3	3	3	4
AS/3501-6	$(0)_{16}$	BOEING	3	3	3	3	3
HMS/3501-5A	$(0)_{16}$, $(0/90_2/0)_{2S}$	LMSC	2	2	0	0	0
E-GLASS FABRIC/X904B	$(0)_{16}$	LMSC	1	1	1	1	0
GRAPHITE/THERMOPLASTIC STRIPS							
T300 FABRIC/P-1700 PS	$(0/90)_8$	BOEING	3	3	3	3	4
T300/P-1700 PS/NONE, TiO_2, ZnO, LEAFING Al		MDSSC	4	0	0	0	0
T300/PES/NONE, TiO_2, ZnO, LEAFING Al		MDSSC	1	0	5	2	0
W-722 FABRIC/P-1700 PS/NONE, TiO_2, ZnO	$(0/90)_8$	GDSSD	15	11	15	11	12
GRAPHITE/POLYIMIDE STRIPS							
GRAPHITE/LARC 160	$(0)_{16}$	BOEING	2	3	2	3	5
CELION 6000/PMR-15	$(0)_{16}$	BOEING	3	1	2	3	4
CELION 6000/PI/NONE, ZnO		MDSSC	1	0	1	0	0
T300/V378A (BISMALIMIDE)	$(0/45/90/135)_{2S}$	GDSSD	3	3	3	3	4

W-722 is a graphite/glass fabric.
The control samples listed were stored at The Aerospace Corporation. For those composites for which no control samples are listed, the controls were stored at the supplier's facility and were not included in The Aerospace Corporation records.

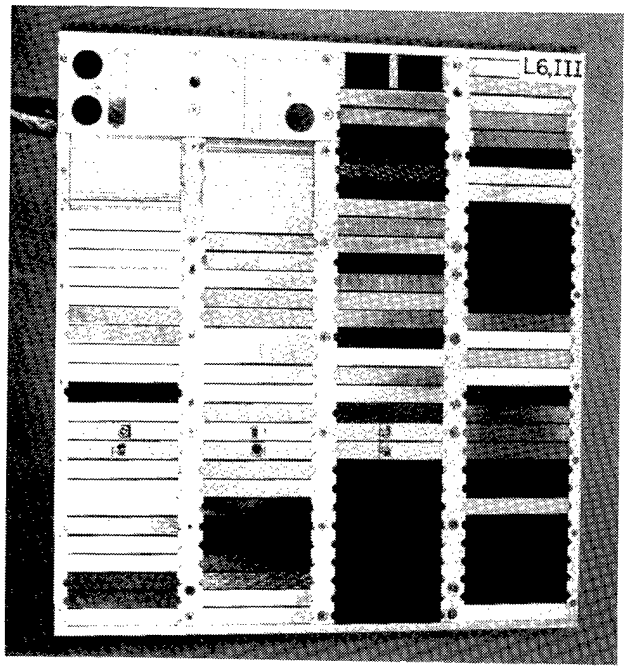
TABLE II.- LIST OF METAL AND GLASS MATRIX COMPOSITES

MATERIAL DESCRIPTION FIBER/MATRIX/SURFACE FOIL	LAY UP	NUMBER OF SAMPLES				
		LEADING		TRAILING		CONTROL
		A	B	A	B	
GRAPHITE/ALUMINUM						
GY70/201/2024 STRIPS	0, 90, OR $(0/\pm60)_S$	15	14	13	18	20
P55/6061/6061 STRIPS	0 OR 90	8	10	8	8	12
P100/201/2024 STRIPS	$(\pm20)_S$	2	2	2	2	2
P100/6061 WIRES	0	4	1	4	1	2
P55/6061 WIRES	0 OR $(0)_5$	8	3	8	3	6
GY70/201 WIRES	$(0)_8$	2	1	2	1	2
T300/6061 WIRES	0	2	1	2	1	2
GRAPHITE/MAGNESIUM						
P100/EZ33A/AZ31B STRIPS	0, 90, OR $(0/\pm60)_S$	9	11	7	8	33
P100/AZ91C/AZ61A STRIPS	0, 90 OR $(\pm10)_S$	6	4	6	6	3
P100/AZ31B WIRES	0	3	1	3	1	2
P100/AZ61A WIRES	0	4	1	4	1	2
P55/AZ91C WIRES	$(0)_5$	3	1	3	1	4
SILICON CARBIDE/ALUMINUM						
SiC_w/2124 STRIPS	DISCONTINUOUS	1	1	1	1	5
SiC_w/6061 STRIPS	DISCONTINUOUS	1	1	1	1	5
$SCS2_f$/Al STRIPS	$(0)_8$	2	2	2	2	6
NICALON SiC_f/6061 WIRES	0	18	5	18	5	5
GRAPHITE/GLASS						
GY70/GLASS STRIPS	(0/90)	1	0	1	0	1
CELION 6000/GLASS STRIP	2-D, DISCONTINUOUS	1	1	0	1	0
GY70/GLASS MIRRORS	(0/90)	1	0	1	0	0

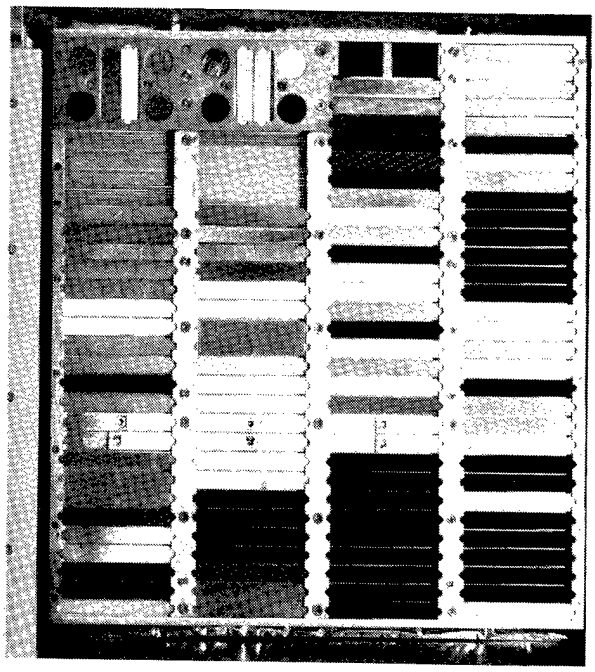
The discontinuous SiC/Al was supplied by AFWL/Flight Dynamics Laboratory. All other metal matrix composites were supplied by The Aerospace Corporation.
The graphite/glass composites supplied by UTRC had a borosilicate matrix.

LEADING EDGE EXPOSED

PREFLIGHT

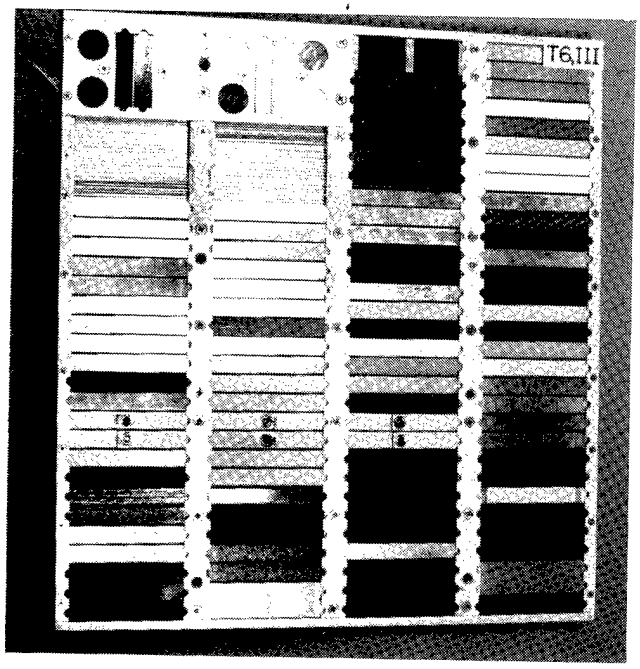


POSTFLIGHT



TRAILING EDGE EXPOSED

PREFLIGHT



POSTFLIGHT

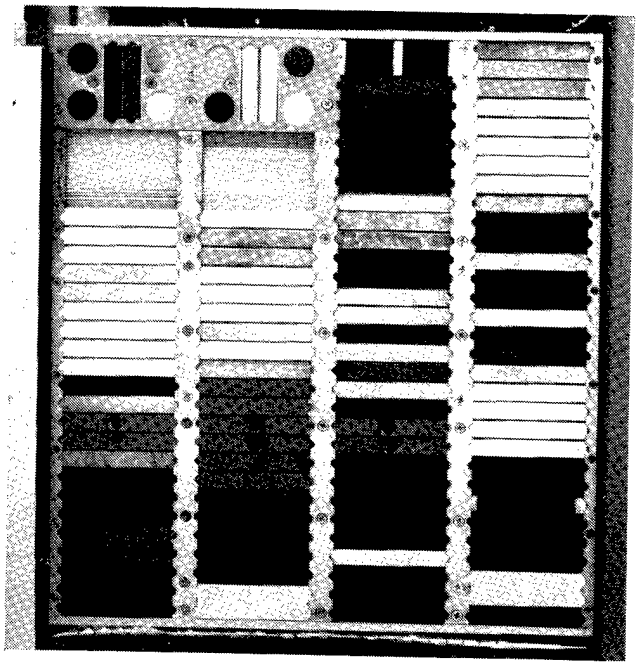


Figure 1. Preflight and Post-Flight Photographs of Exposed Side of Leading Edge and Trailing Edge Sample Cassettes.

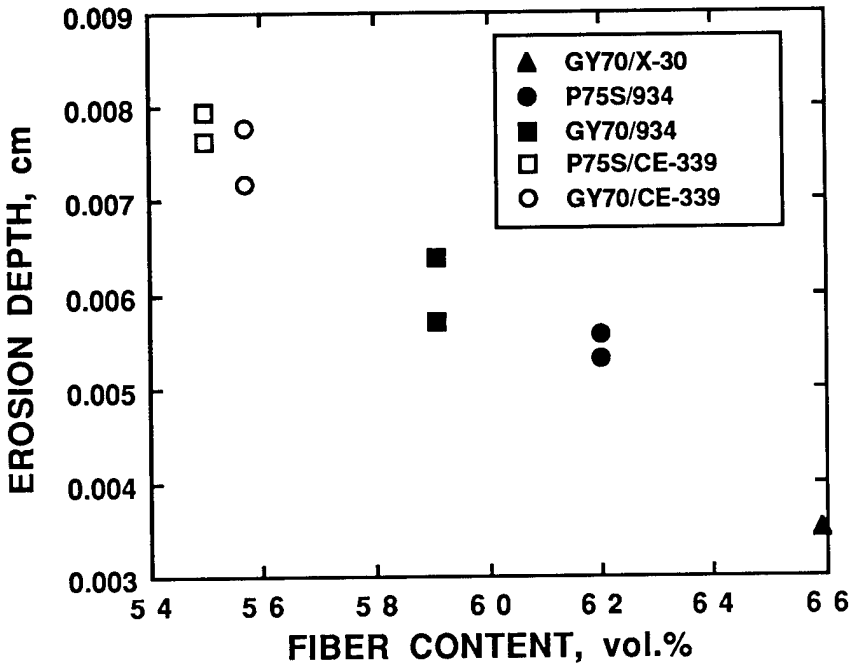
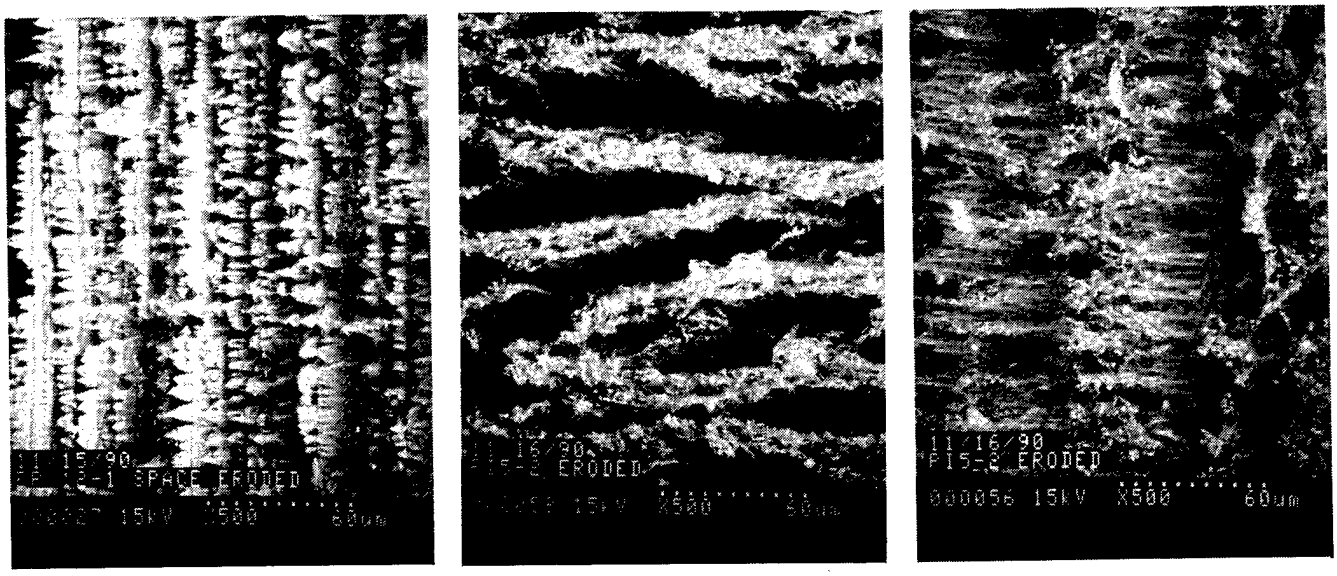


Figure 2. Estimated Atomic Oxygen Depth Versus Fiber Content for Several Graphite/Epoxy Composite Systems. All of the Composites Were Fabricated by General Dynamics, Space Systems Division and Had Similar Initial Surface Conditions.



(a) (b) (c)

Figure 3. Scanning Electron Micrographs of (a) P75S/934 Graphite/Epoxy and (b & c) T300/V378A Graphite/Bismalimide Exposed to Atomic Oxygen on the Leading Edge.

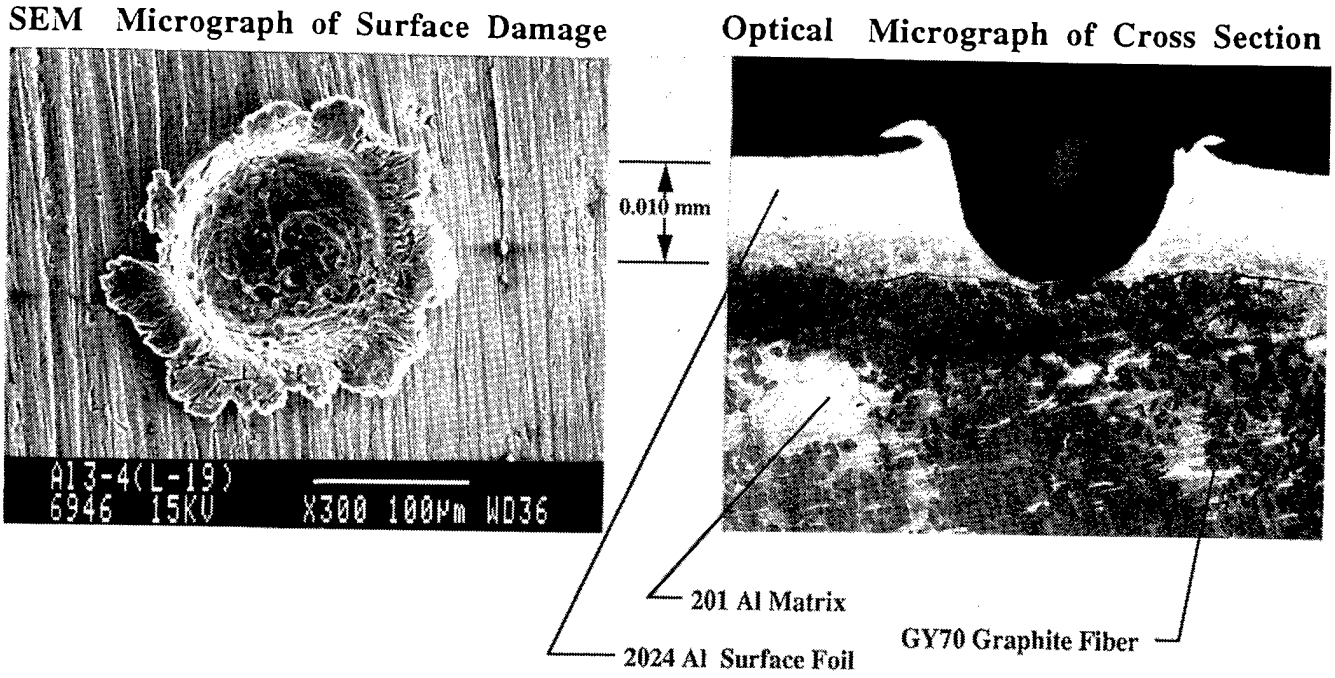


Figure 4. Micrometeoroid Damage to a GY70/201/2024 Graphite/Aluminum Composite.

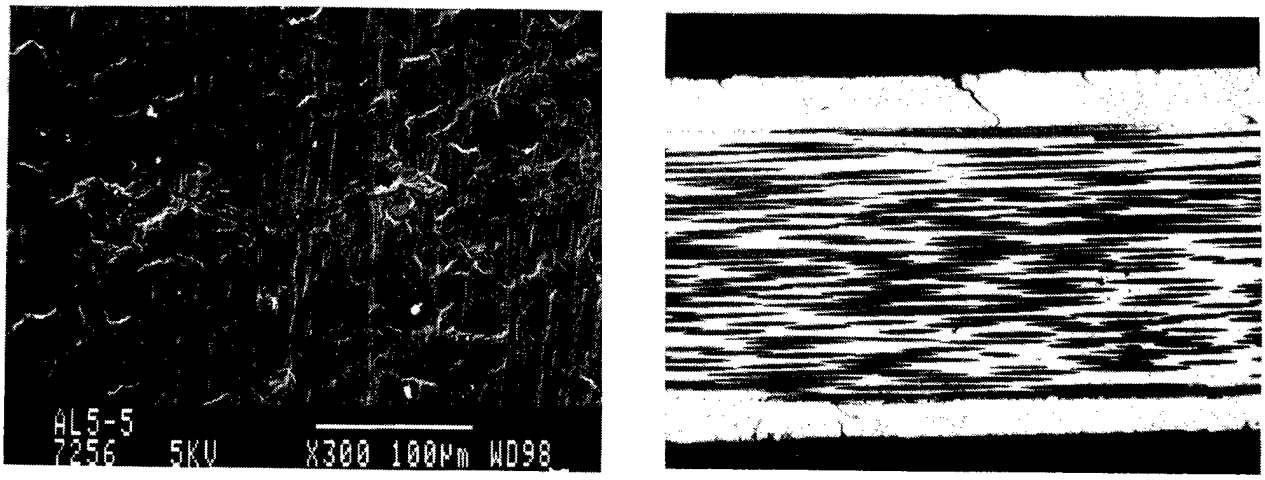
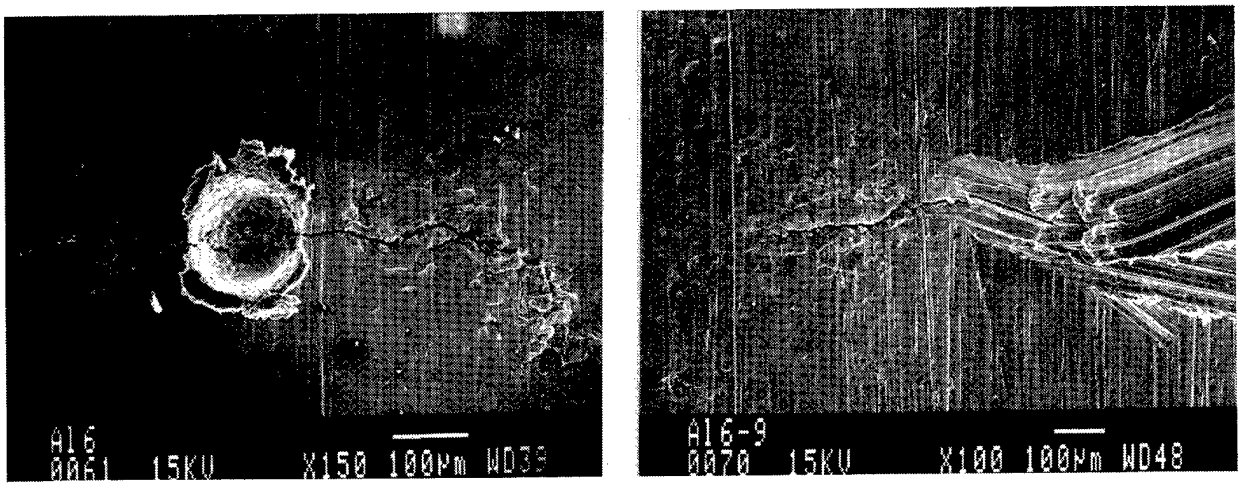


Figure 5. Surface Foil Cracking of a GY70/201/2024 Graphite/Aluminum Composite Resulting From Thermal Fatigue of a Brittle Contaminated Surface.



Micrometeorite Impact **Engraved Marks**

Figure 6. Isolated Fatigue Cracks That Initiated at Stress Risers on the Surface of GY70/201/2024 Graphite/Aluminum Composites.

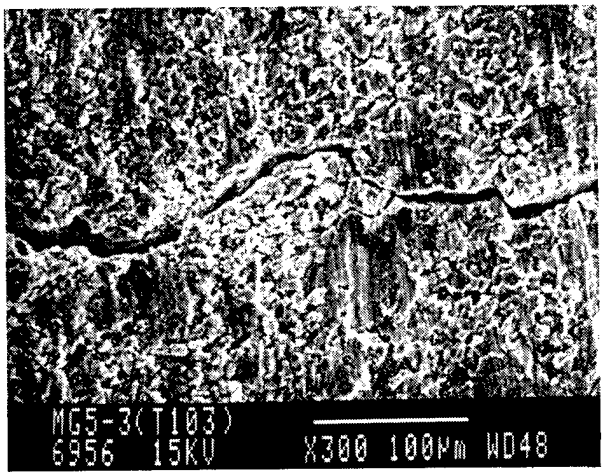


Figure 7. Scanning Electron Micrograph of a P100/EZ33A/AZ31B Graphite/Magnesium Composite Showing a Fatigue Crack That Formed Within a Brittle Oxide Layer.

LDEF - SPACE ENVIRONMENTAL EFFECTS ON MATERIALS: COMPOSITES AND SILICONE COATINGS

Brian C. Petrie
Lockheed Missiles and Space Company
Sunnyvale, CA 94088-3504

ABSTRACT

The objective of the Lockheed experiment is to evaluate the effects of long term low Earth orbit environments on thermal control coatings and organic matrix/fiber reinforced composites. Two diverse categories are reported here: silicone coatings and composites. For composites physical and structural properties have been analyzed; results are reported on mass/dimensional loss, microcracking, short beam shear, CTE, and flexural properties. The changes in thermal control properties, mass, and surface chemistry and morphology are reported and analyzed for the silicone coatings.

PRELIMINARY RESULTS FROM

THE LDEF/UTIAS COMPOSITE MATERIALS EXPERIMENT

R. C. Tennyson, G. E. Mabson, W. D. Morison and J. Kleiman
University of Toronto Institute for Aerospace Studies
4925 Dufferin Street
Downsview, Ontario, Canada
M3H 5T6

SUMMARY

A total of 107 epoxy matrix composite samples containing carbon, boron and aramid fiber reinforcements were flown on the LDEF satellite. For the first 371 days after deployment, strain and temperature data were recorded every 16 hours. Results were obtained on time to outgas, dimensional changes, coefficients of thermal expansion, atomic oxygen erosion and damage due to micrometeoroid/debris impacts.

INTRODUCTION

One of the composite materials experiments on-board LDEF was provided by the University of Toronto Institute for Aerospace Studies (UTIAS). The experiment included a stainless steel calibration tube, 62 composite tubes and 45 coupons. The samples were manufactured from different epoxy matrix composites containing carbon, boron and aramid (Kevlar®) reinforcements (see table 1). A data acquisition system was custom designed and constructed at UTIAS to record 16 thermal/strain gauges every 16 hours for a period of 371 days. The magnetic tape cassette-based unit functioned flawlessly and yielded 557 data points per sample. The experiment (AO180) was located at station D-12 on LDEF (fig. 1), 90° to the leading edge. LDEF was yawed 8° relative to the orbital velocity vector, according to NASA estimates, with a corresponding atomic oxygen fluence at station D-12 of about 1.2×10^{21} atoms/cm^2 (ref. 1). Photographs of the composite materials experiment are contained in fig. 2. The following report presents preliminary results from our LDEF experiment.

THERMAL RESPONSE, OUTGASSING AND DIMENSIONAL CHANGES OF LDEF SAMPLES

A listing of the composite materials that were monitored over the first 371 days after deployment of LDEF is given in table 2. Both temperature and strain (using conventional thermal foil gauges (MM-STG-50C) and strain gauges (MM-WK-13-250BG-350) were recorded to assess the thermal response changes due to space exposure. A stainless steel tube was employed as a means of calibrating the gauge system and determining if any deterioration occurred over the measurement lifetime. The predicted thermal/time response for the stainless steel tube based on a 16 hr. sampling rate is shown in fig. 3 (ref. 2). The higher frequency oscillations correspond to different locations on the orbit, with the lower frequency behaviour associated with orbital precession. These calculations take into account self-shadowing and seasonal variations in thermal flux.

Figure 4 presents the actual measured temperature-time (a) and strain-time (b) histories for the stainless steel tube over the first 371 days of exposure. It is interesting to note that there is no significant

strain change with time at a given temperature for the stainless steel. This demonstrates that no degradation in the gauge measuring system has occurred, and no significant outgassing or dimensional changes have taken place. Furthermore, the cyclic variations in the thermal/time response agree quite well with the predicted behaviour, although some discrepancy is evident beyond 300 days.

Using the same data, one can construct a thermal distortion vs. temperature curve, as shown in fig. 5a for stainless steel. One can see that in orbit (a), all the test data collapsed to a single straight line, yielding a slope [i.e., coefficient of thermal expansion (CTE)] of ~10×10^{-6}/°F which matches the ground-based value for this material (see table 3). In the lower figure (b), the same CTE was obtained in thermal-vacuum tests* after retrieval of LDEF, once again demonstrating that no deterioration of the measuring system took place throughout the six years of elapsed time.

Figure 6 presents the predicted thermal/time response of graphite/epoxy 934/T300 (ref. 3). The thermal/strain response curves are given in fig. 7 for 0° and 90° laminates. Note the larger amplitudes in the thermal response compared to those observed for stainless steel. This can be attributed to the much lower *thermal mass* and radiative properties of the composite samples relative to the stainless steel tube. Of particular importance is the *outgassing time* (t_o) and associated *dimensional change* ($\Delta\varepsilon$) summarized in table 2. Figure 8a contains a plot of the dimensional change (delta in microstrain) vs. time for the 90° laminate. The actual change in strain vs. temperature is given as well for both the 90° and 0° samples (figs. 8b and 8c, respectively). It is interesting to compare the *initial* and final *asymptotic* curves. For the 0° configuration, a slight shift in the CTE is evident. It is also clear that it took about 40 days for this material to outgas and asymptote to a constant CTE, as can be seen in the 90° sample curves. Note that a post-flight measurement of the 90° strain at ambient temperature showed a recovery in the dimensional change. This reflects re-absorption of moisture after retrieval of LDEF. Subsequent thermal-vacuum tests* also demonstrated these effects due to outgassing. A comparison of the CTE values measured in space (after 371 days) with those observed in simulator tests (after 2114 days in orbit and 184 days at ambient conditions) shows reasonable agreement. This indicates that no substantial degradation in material thermal response has occurred, other than that associated with outgassing.

Similar results were found for the other materials listed in table 1. Summaries of the outgassing times (t_o), dimensional changes ($\Delta\varepsilon$) and CTE values can be found in tables 2 and 3.

From a design viewpoint, these dimensional changes for the 0° and 90° laminates can be used to predict the $\Delta\varepsilon$ for an arbitrary laminate configuration. Clearly, the matrix-dominated properties are most affected by outgassing (i.e., see the 90° results) but it was also found that the angle ply laminate of boron/epoxy underwent a significant $\Delta\varepsilon$ change as well. Outgassing can lead to permanent dimensional changes of composite laminates in orbit and must be taken into account in the design of composite structures and joints where dimensional tolerances are critical (e.g., optical systems, truss joints, guidance systems and communication platforms).

ATOMIC OXYGEN EROSION

All UTIAS composite samples were mounted on the trays with aluminum end fixtures. Because of the location of our experiment and the yaw of LDEF in orbit, it is estimated by NASA that the angle of incidence of the atomic oxygen (AO) was 8°. Analysis of the flat laminates has shown that the end tabs provided a shadow region of approximately 5~6 mm (fig. 9a). It was further observed that AO

*These tests were conducted at the Canadian Communications Research Centre, David Florida Labs., Canadian Space Agency, Ottawa, Canada.

reflected off the cylindrical aluminum end fixtures located below the flat samples, resulting in circular erosion patterns on the bottom (unexposed region) face of the same flat samples (fig 9b).

Scanning Electron Microscope (SEM) analysis showed no erosion in the shadow region (fig. 10a) with triangular erosion patterns of the outer epoxy layer evident in the exposed region (fig. 10b). The triangular patterns result from low angle of incidence of AO, relative to the sample plane. Cross-sectional SEM photographs (figs. 11 and 12) clearly show the loss of the outer resin layer beyond the shadow region. Actual thickness loss measurements are given in fig. 13 where it is apparent that about 15 μm of epoxy was eroded. Neglecting any fiber loss, the erosion yield (i.e., cm^3/atom) for this epoxy is estimated at ~1.25×10^{-24} cm^3/atom. This compared favourably with previously published data (ref. 3) that quotes a value of ~1.7×10^{-24} cm^3/atom.

Atomic oxygen erosion of circular tubes was also studied. Because of the curvature, it is possible to investigate erosion loss and surface morphology changes as a function of angular position around the tube. Cross-sectional SEM photographs (fig. 14) clearly show erosion angle changes at different locations whose surface normals vary relative to the incident AO. Even at $\alpha = 90°$ one can see some erosion of the fibers. Thickness loss data are presented in fig. 15 and the maximum loss was estimated at ~160 μm; about one ply of material for near 'ram' conditions. The erosion yield for this material is estimated at ~1.9×10^{-24} cm^3/atom. Again, from ref. 3, the range of values reported for different graphite/epoxy materials is 2.1~2.6×10^{-24} cm^3/atom.

A design chart, fig. 16, has been compiled that permits a user to estimate material thickness loss as a function of satellite orbital altitude, time in orbit and AO angle of incidence relative to the surface normal. For reference purposes, data have been extracted from ref. 3 that provide the user with some information on erosion yields measured for a variety of materials (table 4).

MICROMETEOROID/DEBRIS IMPACTS

The UTIAS experiment suffered 74 impacts with craters <0.5 mm in diameter, and 10 impacts at ≥0.5 mm in size, randomly distributed over the surface area as shown in fig. 17. Figure 18 shows SEM photographs of the impact (a) and exit holes (b) observed on a 4 ply graphite/epoxy laminate of $(\pm45)_S$ construction. Of particular concern is the extensive spallation damage that occurred on the rear face (c) in which a rather large (5.7 mm) section of laminate was removed from the structure.

CONCLUSIONS

Based on the UTIAS/LDEF composite materials experiment, the following preliminary conclusions can be made:

(a) thermal model predictions are in excellent agreement with test data up to the first 300 days in orbit;

(b) outgassing of the polymer matrix composites occurred over periods ranging from 40 to 120 days, depending on the material system;

(c) significant dimensional changes occurred in the samples due to outgassing, which must be factored into the design of low distortion composite laminates;

(d) outgassing caused modest changes in CTE, leading to asymptotic values that should be used in the design of 'zero CTE' laminates for space applications;

(e) low angle of incidence atomic oxygen eroded the composite materials which were located approximately 82° off the ram direction;

(f) erosion by atomic oxygen of cylindrical tubes caused substantial thickness reductions amounting to about 160μ over the 70 months in low Earth orbit;

(g) micrometeoroid/debris impacts can penetrate four ply laminates with substantial rear face spallation damage.

REFERENCES

1. Bourassa, R. J.; and Gillis, J. R.: LDEF Atomic Oxygen Flux and Fluence Calculations. NASA LDEF MSIG Report NAS1-18224 Task 12, Jan. 1991.

2. Hughes, P. C.: LDEF Temperature Histories — A Simple Theory. UTIAS Report No. 340, July 1990.

3. Banks, B. A.: Atomic Oxygen Interaction with Materials on LDEF. Proc. LDEF Materials Data Analysis Workshop, NASA Conference Pubs. 10046, July 1990, pp. 191-216.

Table 1. Description of UTIAS/LDEF Composite Materials Experiment

Material	Geometry	Laminate	Number of Samples
Stainless Steel 304 (calibration tube)	tube*	—	1
G/E			
5208/T300	tube	$(90°)_4$	3
Narmco	tube	$(\pm 45)_{2s}$	3
G/E			
SP288/T300	tube	$(90)_4$	7
3M	tube	$(\pm 43)_{2s}$	6
	tube	$(\pm 43)_{4s}$	3
	tube	$(0)_4$	3
	tube	$(+60, -60, 0)_{2s}$	1
G/E	tube	$(90)_4$	3
934/T300	tube	$(\pm 45)_{2s}$	3
B/E	tube	$(\pm 45)_{2s}$	7
SP-290	tube	$(\pm 30)_{2s}$	6
3M	tube	$(+60, -60, 0)_{2s}$	1
A/E	tube	$(90)_4$	6
SP-328	tube	$(\pm 45)_{2s}$	6
3M	tube	$(\pm 30)_{2s}$	3
	tube	$(+60, -60, 0)_{2s}$	1
G/E			
5208/T300	flat*	$(\pm 45)_{2s}$	6
Narmco	flat	$(0)_4$	3
G/E	flat	$(\pm 43)_{2s}$	6
SP 288/T300	flat	$(0)_4$	3
3M	flat	$(90)_4$	3
G/E			
934/T300	flat	$(\pm 45)_{2s}$	6
Fiberite	flat	$(0)_4$	6
A/E	flat	$(\pm 43.5)_{2s}$	6
SP-328	flat	$(\pm 30)_{2s}$	3
3M	flat	$(90)_4$	3

* Tubes: 1.75 in. (4.45 cm) diameter
Flats: 3 in. (7.62 cm) width

Table 2. Dimensional Change ($\Delta\varepsilon$) and Time to Asymptote (t_o)

Material	Configuration	t_o (days)	Dimensional Change*				
			Initial			Final Asymptote	
			Lab. Calibration	First Deployed	$\Delta\varepsilon$ (10^{-6})	Strain	$\Delta\varepsilon$ (10^{-6})
Graphite/Epoxy 934/T300	$(90°)_4$	40	(@ -30°F) -1360	-1350	+10	-2550	-1200
Kevlar/Epoxy SP-328	$(90°)_4$	120	(@ 0°F) -2370	-1200	+1170	-4000	-2800
Graphite/Epoxy SP-288/T300	$(90°)_4$	40	(@ -15°F) -1200	-1200	0	-2100	-900
Graphite/Epoxy 5208/T300	$(90°)_4$	80	(@ -10°F) -1070	-550	+520	-2100	-1550
Boron/Epoxy SP-290	$(\pm 30°)_{2s}$	85	(@ -10°F) -800	-75	+725	+75	+150

* All values measured at temperature noted.

Table 3. Summary of LDEF Composite Materials Thermal Data — UTIAS Experiment

Material Type	Configuration	Strain Gauge No.	Thermal Gauge No.	Ambient* CTE α (10^{-6}/°F)	Space** CTE α (10^{-6}/°F)	Thermal-Vacuum Facility*** CTE α (10^{-6}/°F)
Stainless Steel (Calibration)	Tube	1	1	9.84	10.0	10.0
Graphite/Epoxy 934/T300	Flat $(0°)_4$	2 (0°) 3 (90°)	2	1.32 14.7	3.33 13.9 ~ 15	2.50 16.1
Kevlar/Epoxy SP-328	Tube $(90°)_4$	4 (90°) 5 (0°)	3	33.9 0.10	30 ~ 35 0.71	35.3 0.63
Graphite/Epoxy SP288/T300	Tube $(0°)_4$	6 (90°) 7 (0°)	4	14.6 0.97 ~ 1.57	13.6 ~ 14.3 -1.14 ~ 3.33	15.4 3.75
Graphite/Epoxy 5208/T300	Tube $(90°)_4$	8 (90°)	5	15.6	12.5 ~ 15.3	16.1
Boron/Epoxy SP-290	Tube $(\pm 30°)_{2s}$	9 (±30) 10 (±60)	6	1.57 11.7	1.67 ~ 2.22 7.5 ~ 11.1	0.44 ~ 2.0 12.7

* At atmospheric pressure prior to launch.

** Measured in space environment on LDEF during first 371 days in orbit.

***Measured in laboratory thermal-vacuum test facility (22 hrs. @ 10^{-5} torr, -40°F to 150°F) after 2,114 days in orbit and 184 days at ambient conditions.

Table 4

Classification of Erosion Yield Data

(Ref: "Atomic Oxygen" by B. Banks, Proc. LDEF Materials Data Analysis Workshop, NASA KSC Feb. 1990, NASA CP10046, July 1990)

Erosion Yield Range (10^{-24} cm^3/atom)

.01 — .09	.1 — .9	1.0 — 1.9	2 — 4	> 4
Al_2O_3	Polysiloxane/Kapton (ARO Kapton)	Various forms of Carbon	Kapton H Polymide	Silver
Al coated Kapton	Siloxane/Polymide	Epoxies	Polycarbonate Resin	
Diamond	Polysilane/Polymide	Polystyrene	Polyester	
ITO/Kapton	401-C10 (flat black)	Polybenzimidazole	Polysulphone	
Si Ox/Kapton (aluminized)	Z-306 (flat black)		PMMA	
Silicones	Urethane (black conductive)		Mylar	
RTV-615 (clear)	Apiezon Grease		Polyethylene	
Fluorpolymers	Tedlar (white)		Tedlar (clear)	
Teflon FEP	Osmium (bulk)		Z-302 (glossy black)	
Magnesium Fluoride on Glass			Various forms of Graphite/Epoxy	
Molybdenum			Kevlar/Epoxy	

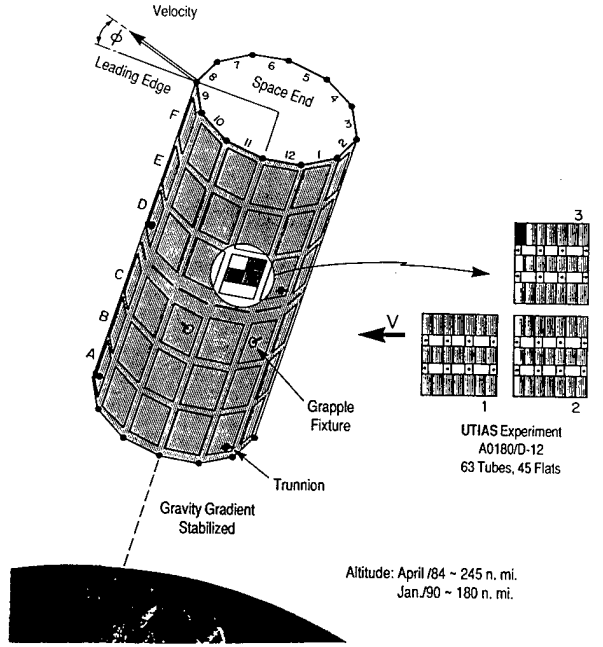


Fig. 1

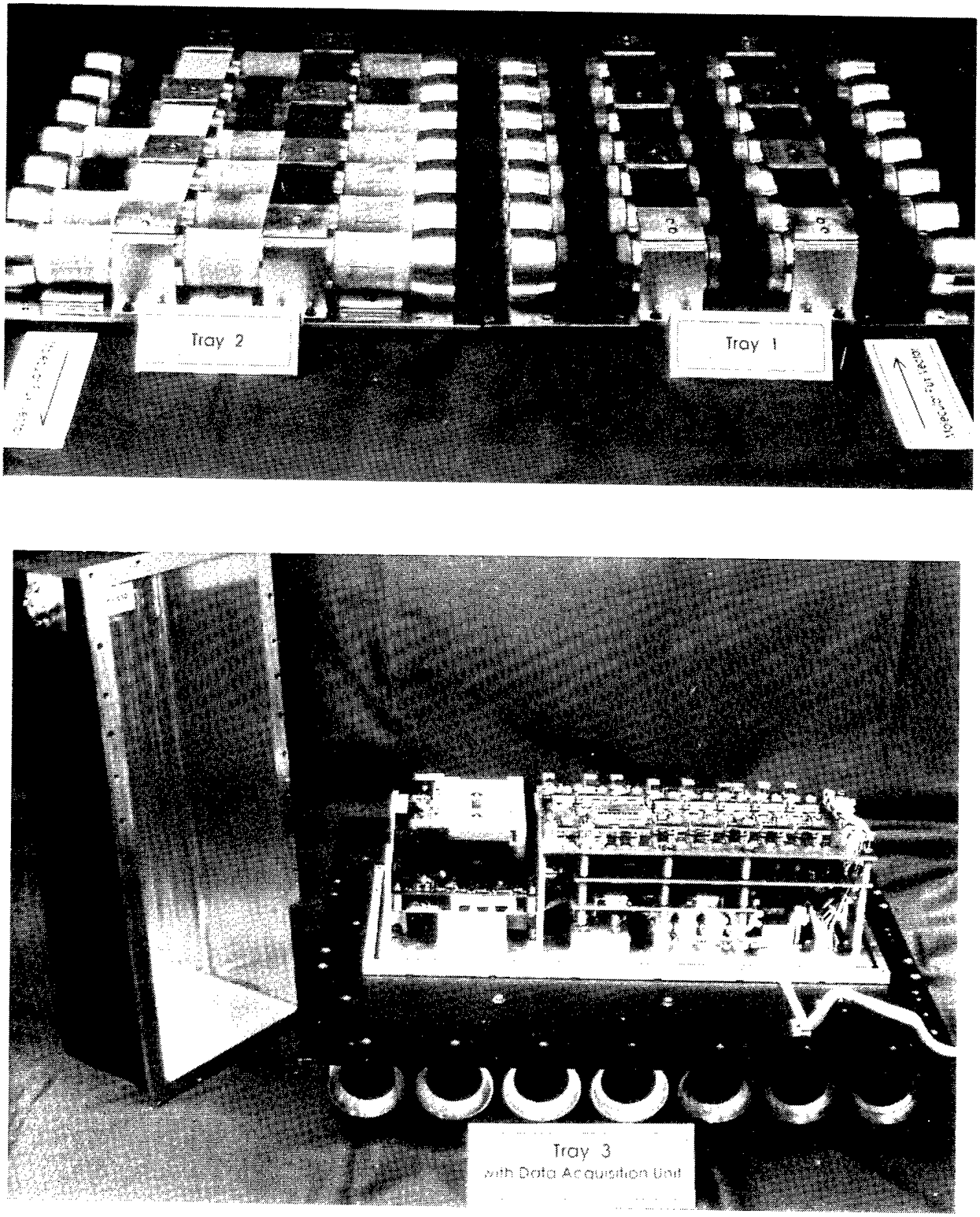


Fig. 2 **UTIAS** Composite Materials Experiment with Data Acquisition System

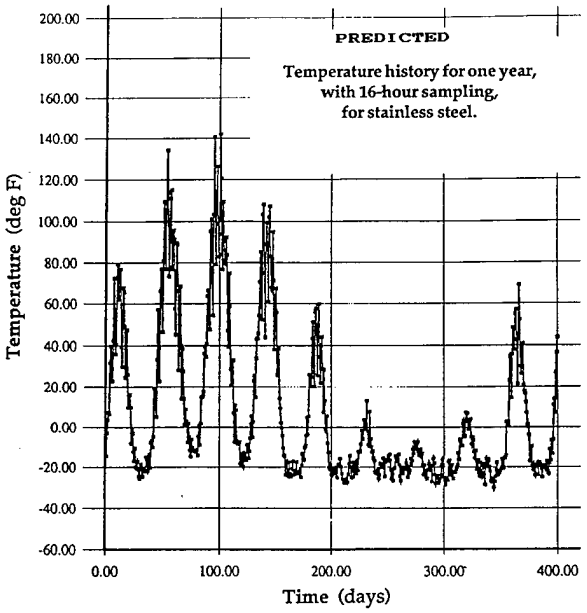


Fig. 3

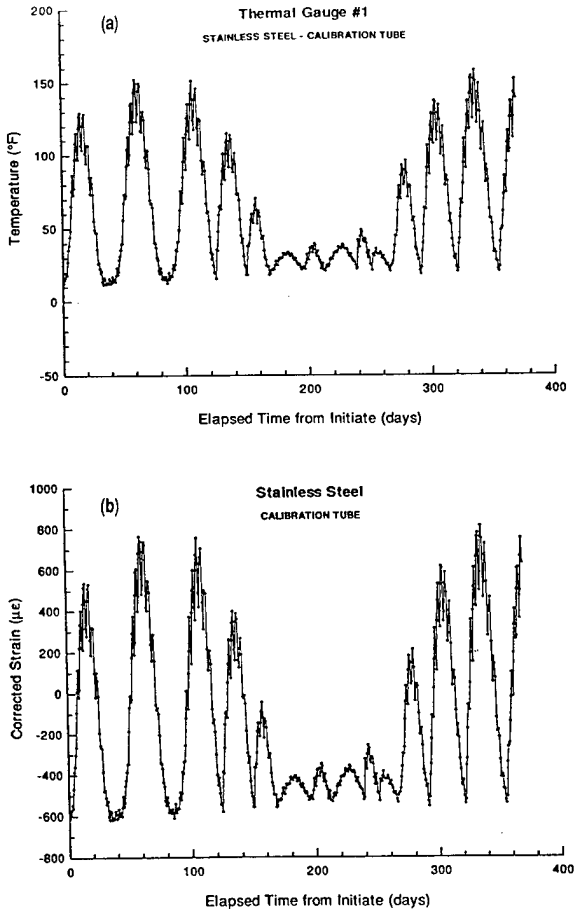
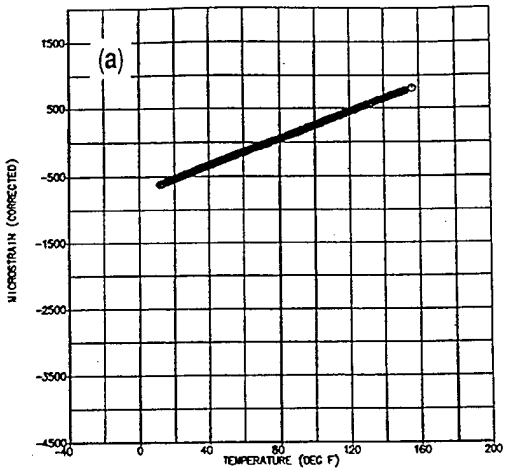


Fig. 4



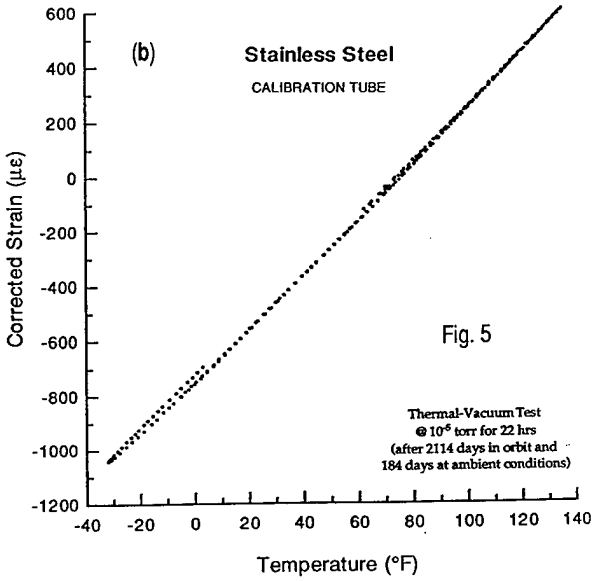


Fig. 5

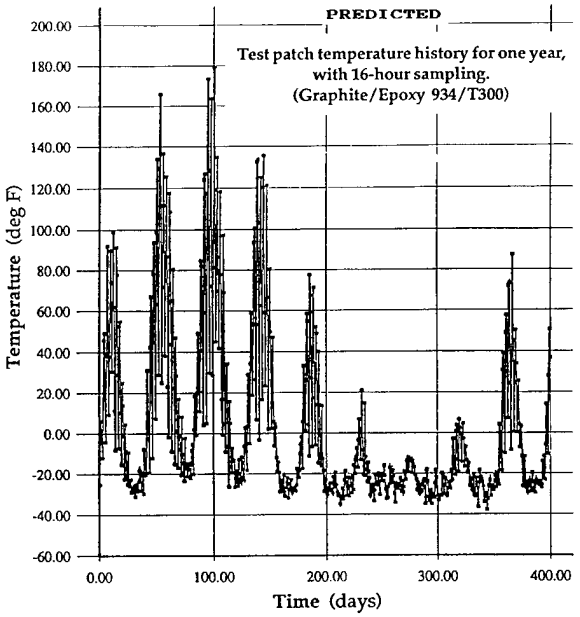
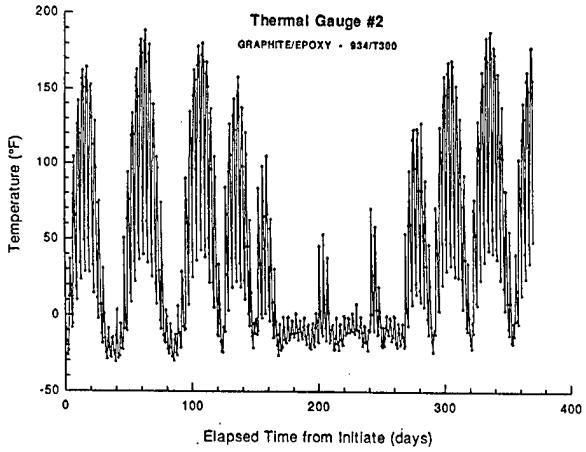
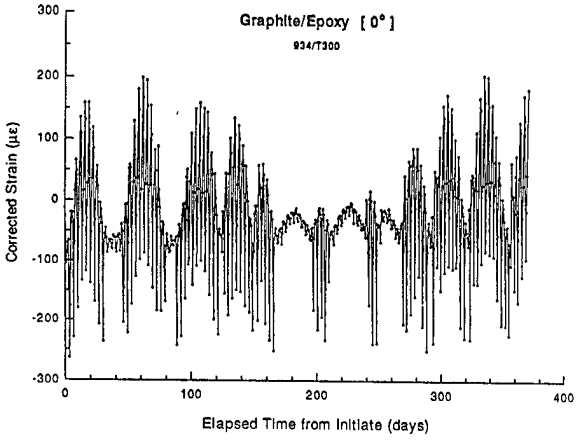


Fig. 6





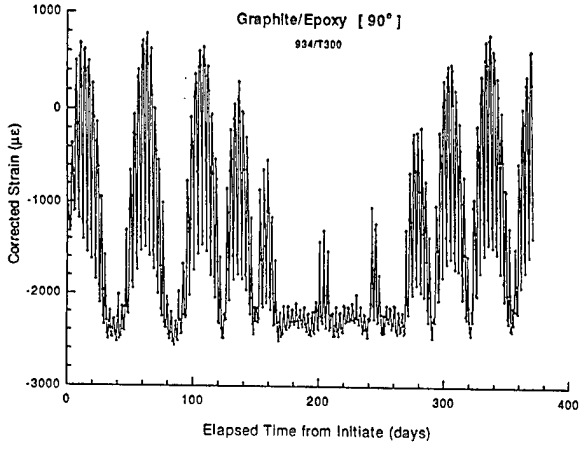
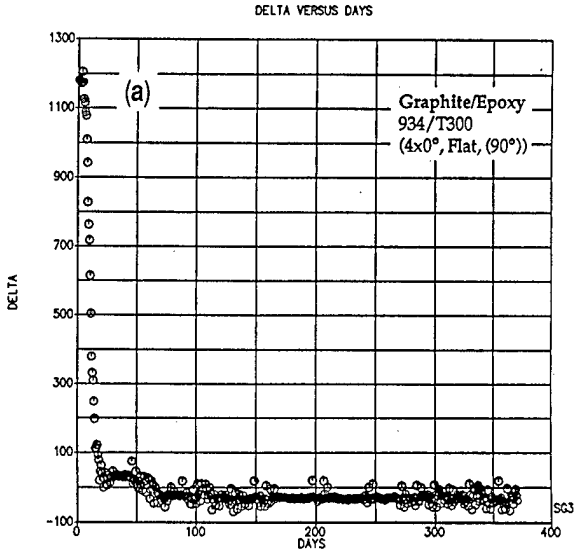
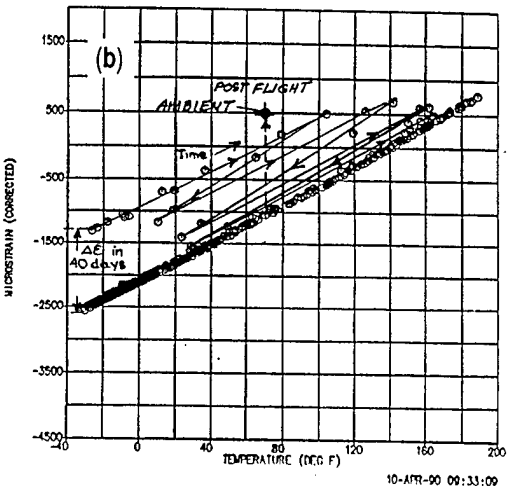


Fig. 7





GRAPHITE/EPOXY 934/T300 (90°)

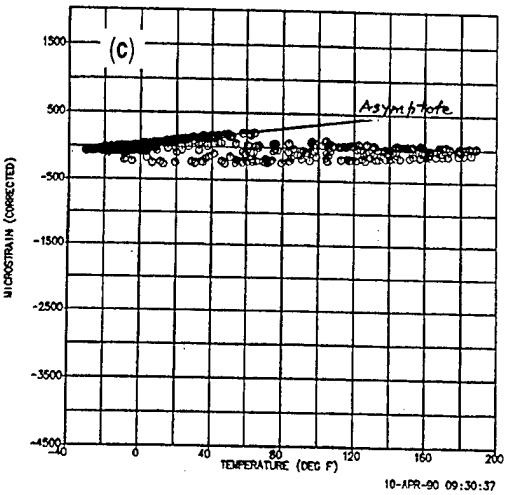
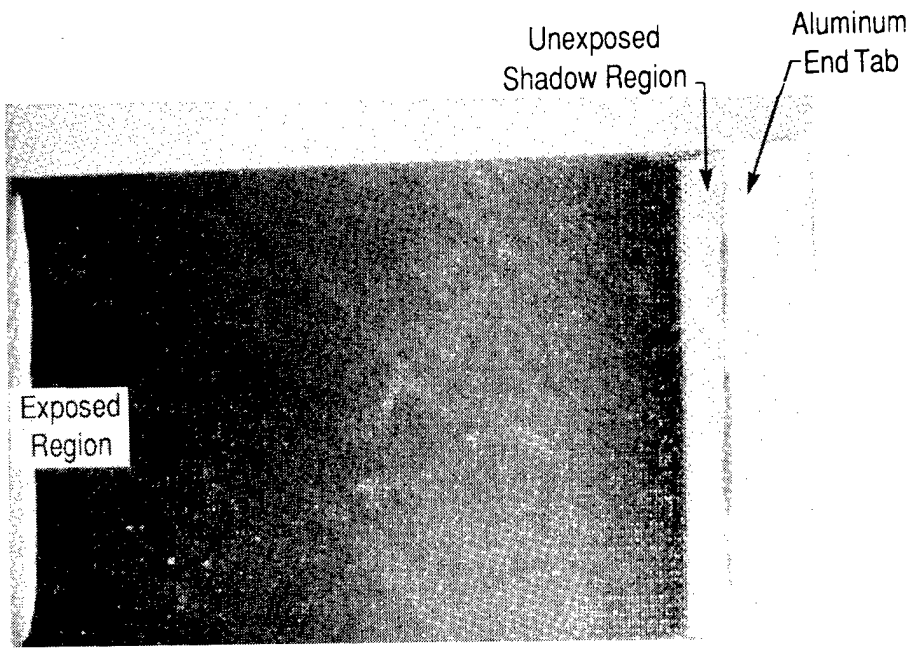
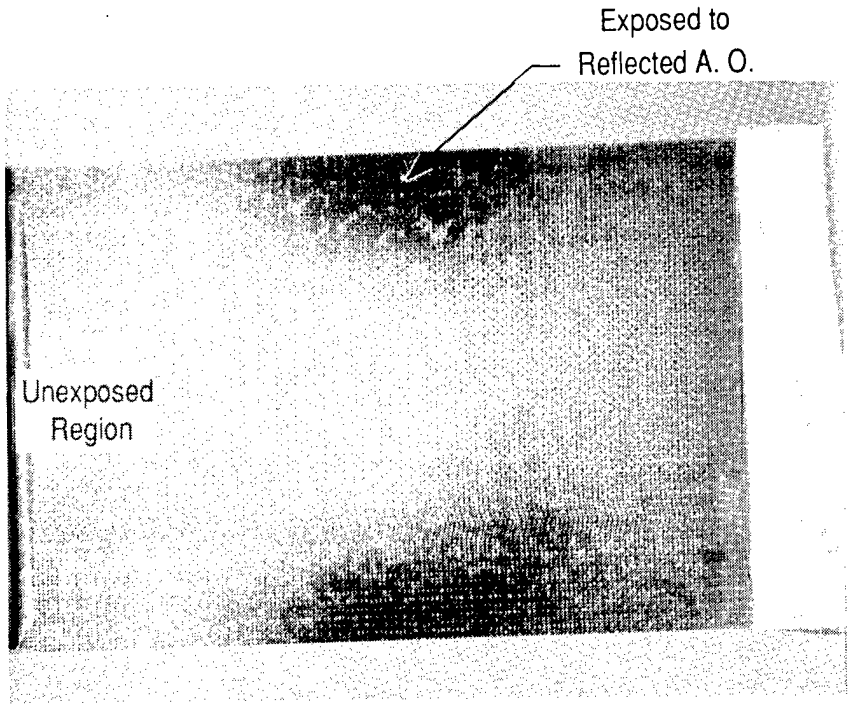


Fig. 8 GRAPHITE/EPOXY 934/T300 (0°)



(a) Exposed Face



(b) Bottom (Unexposed) Face

Fig. 9 Photographs of Top (a) and Bottom (b) Faces of Graphite/Epoxy **LDEF** Sample

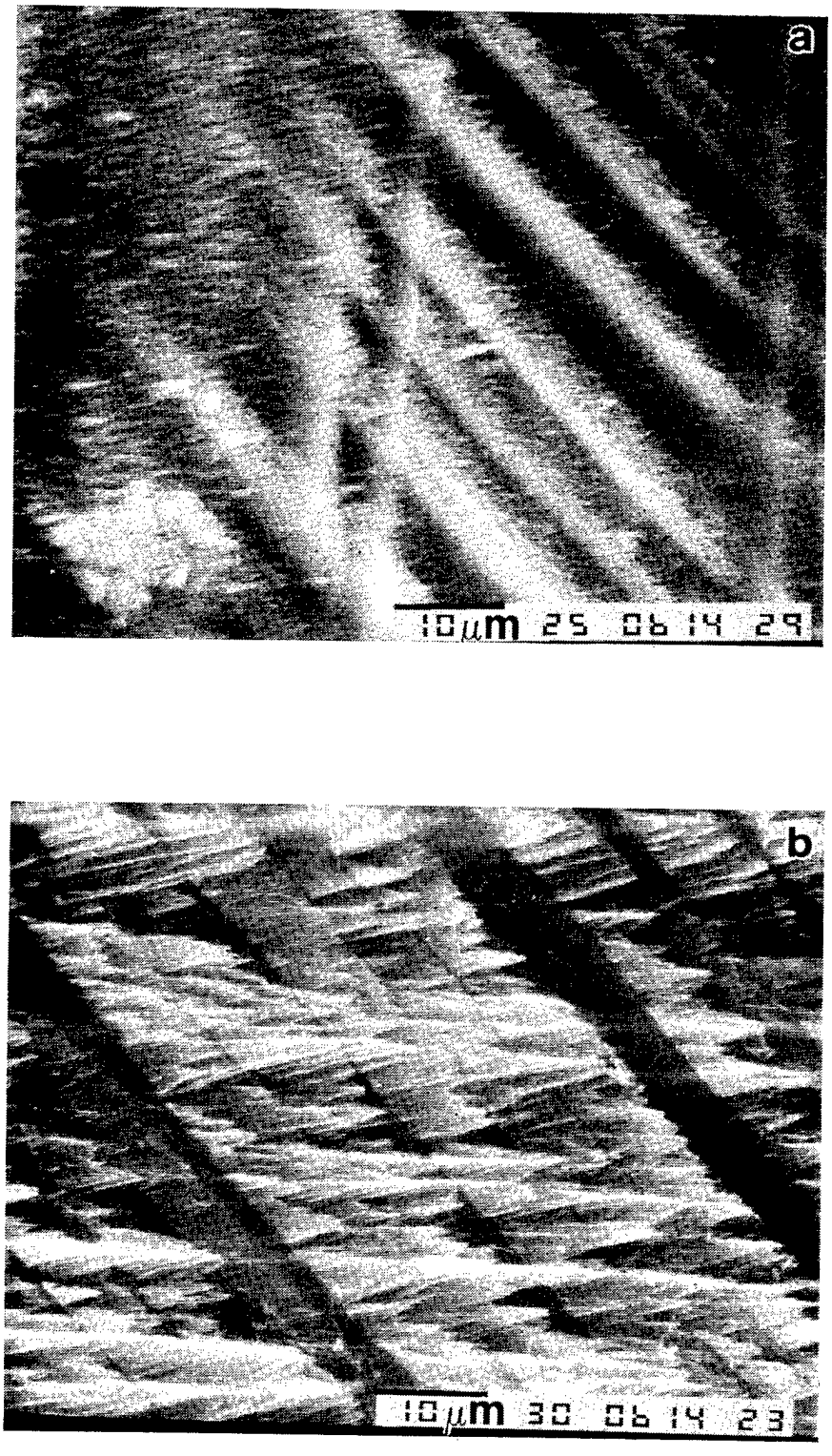
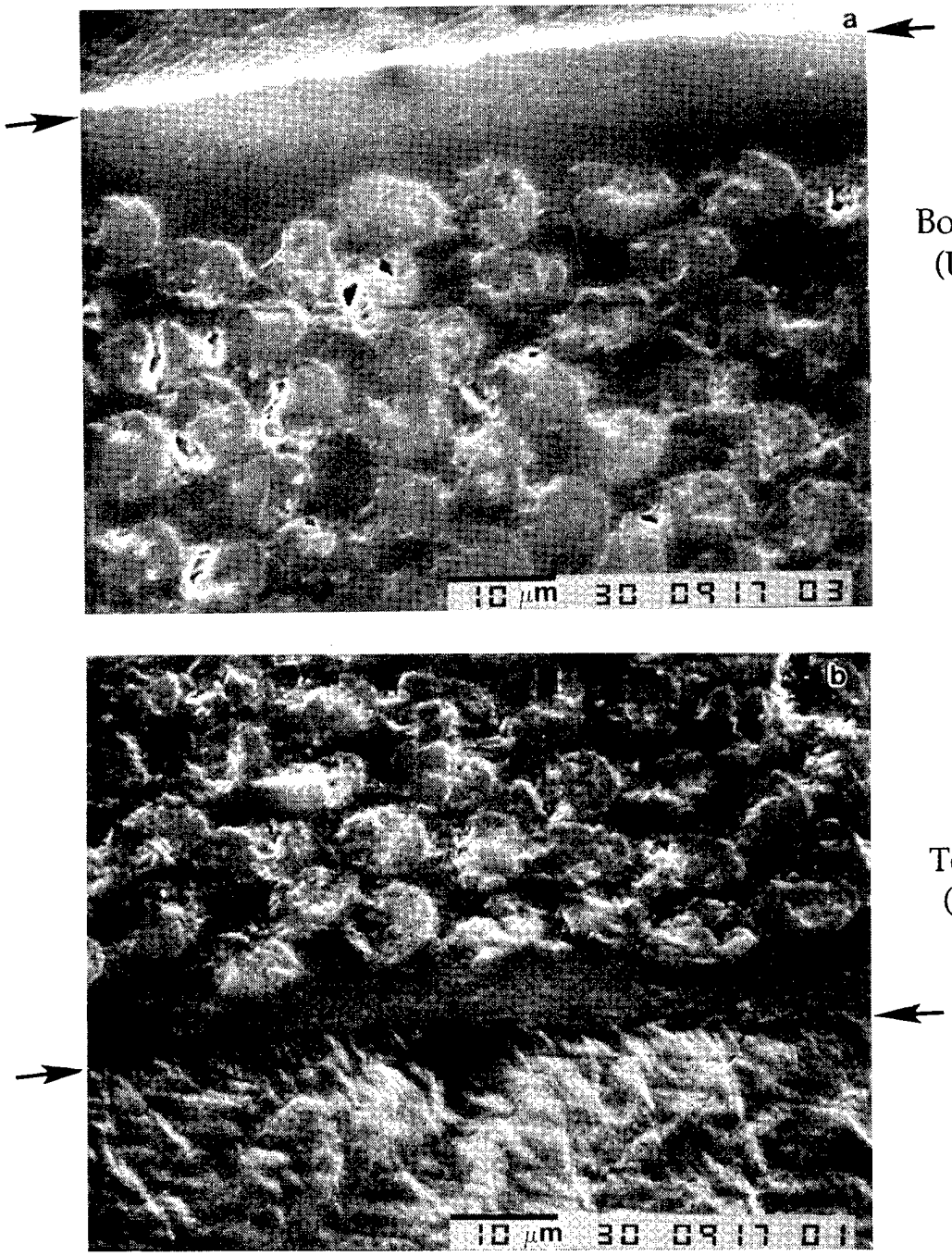


Fig. 10 SEM Photographs of Graphite/Epoxy **LDEF** Sample
a) 3 mm from end fixture (note boundary between unexposed/exposed regions)
b) 6 mm from end fixture-exposed region



Bottom Surface
(Unexposed)

Top Surface
(Exposed)

Fig. 11 Cross -Sectional SEM Micrographs of Graphite/Epoxy LDEF sample (F15)
(6 mm from end fixture in shadow region)
(Arrows indicate sample interface with potting compound)

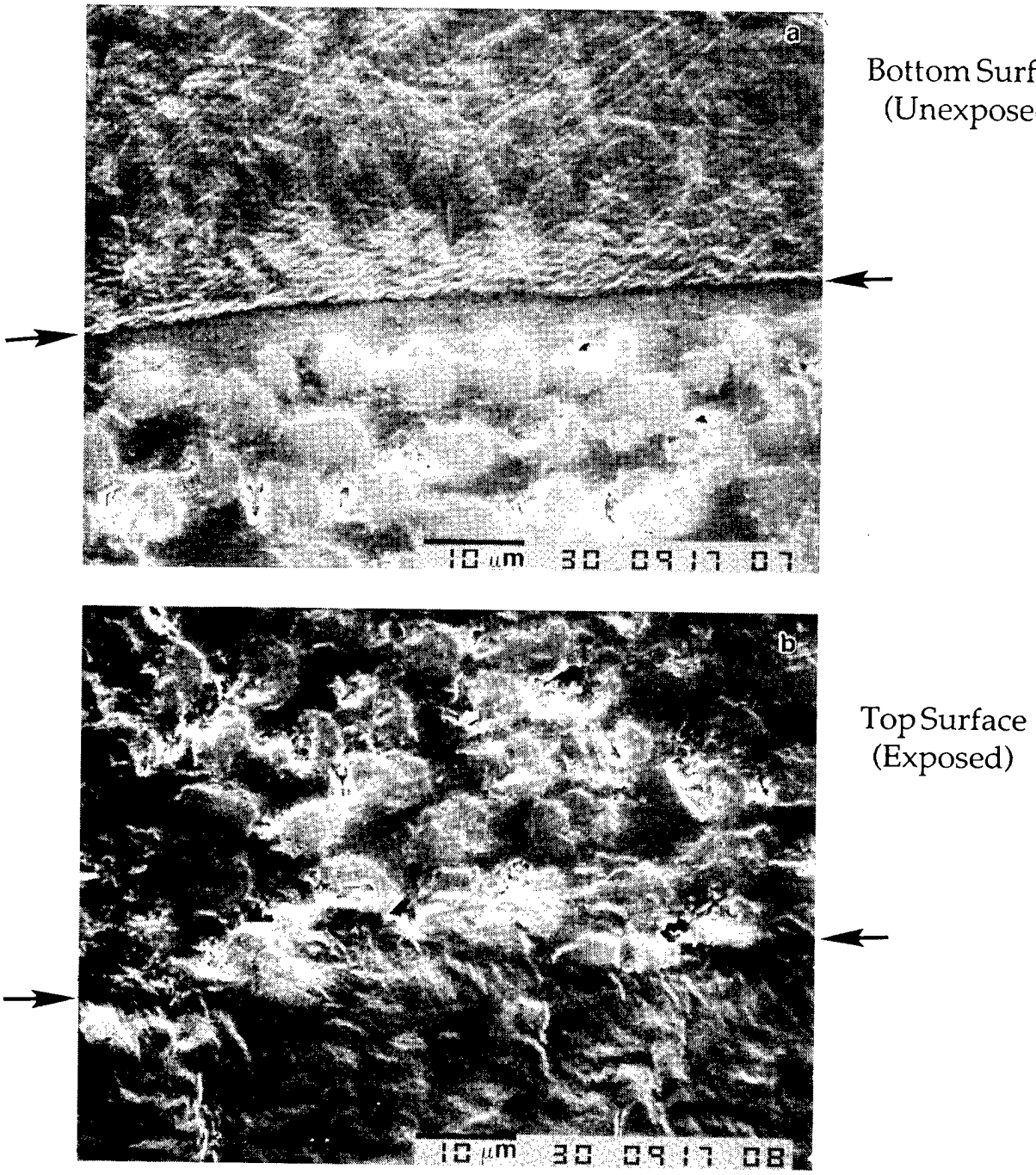


Fig. 12 Cross -Sectional SEM Micrographs of Graphite/Epoxy **LDEF** sample (F15)
(7 mm from end fixture, out of shadow region)
(Arrows indicate sample interface with potting compound)

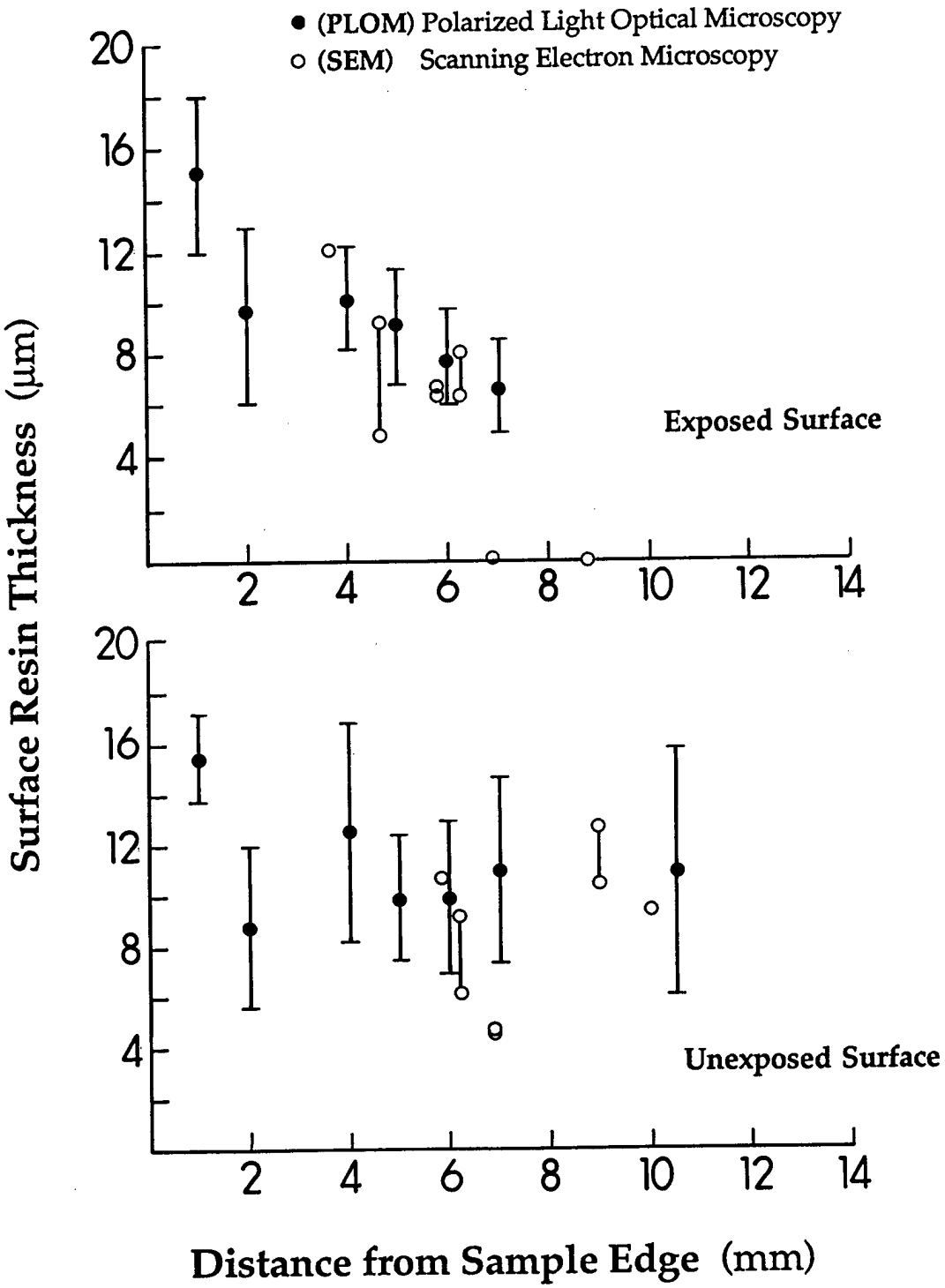


Fig. 13 Effect of Atomic Oxygen Erosion on Graphite/Epoxy **LDEF** Sample (F15)

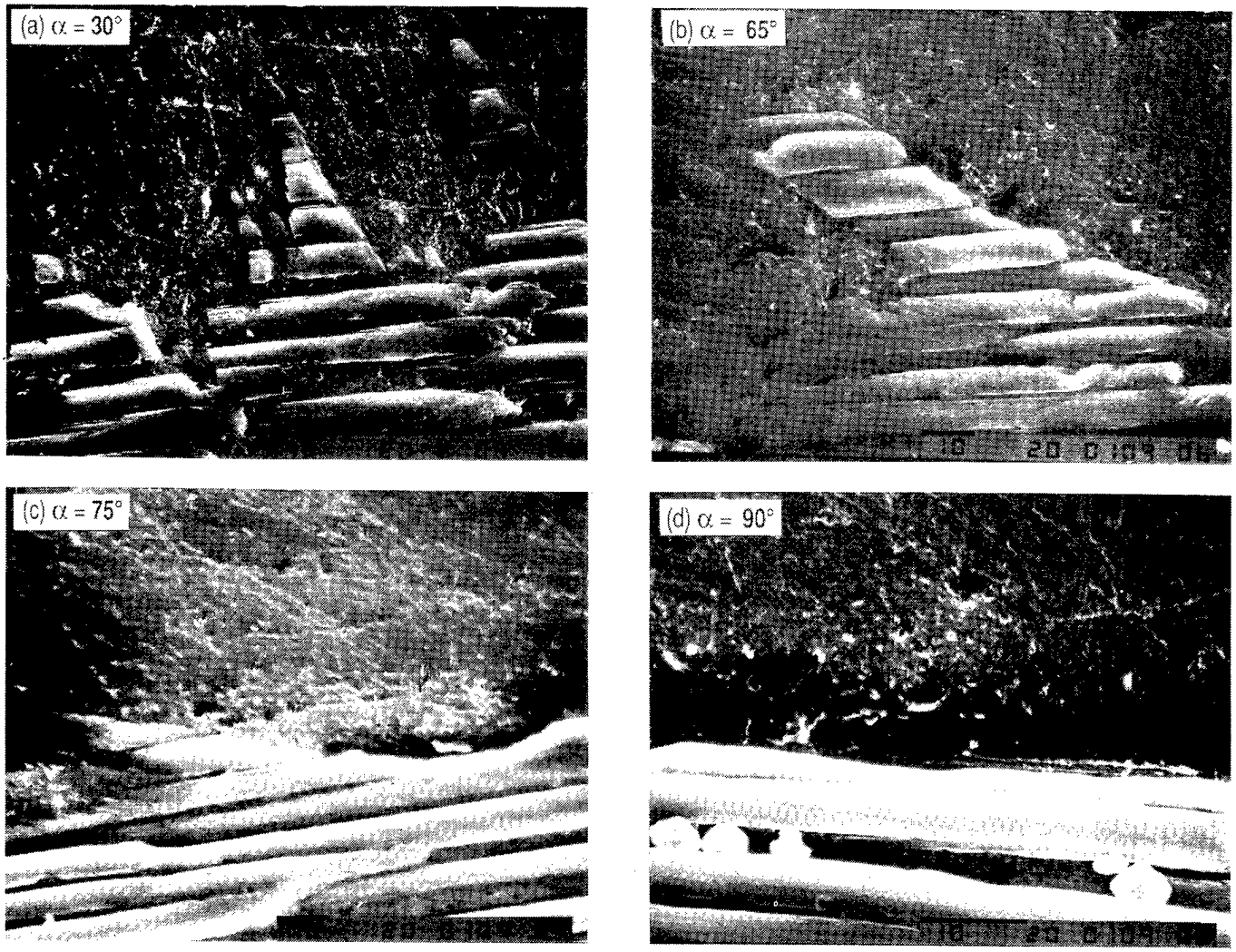


Fig. 14 Cross-Sectional SEM Photographs of Erosion Profile at Different Angular Positions (α) around Graphite/Epoxy Composite Tube

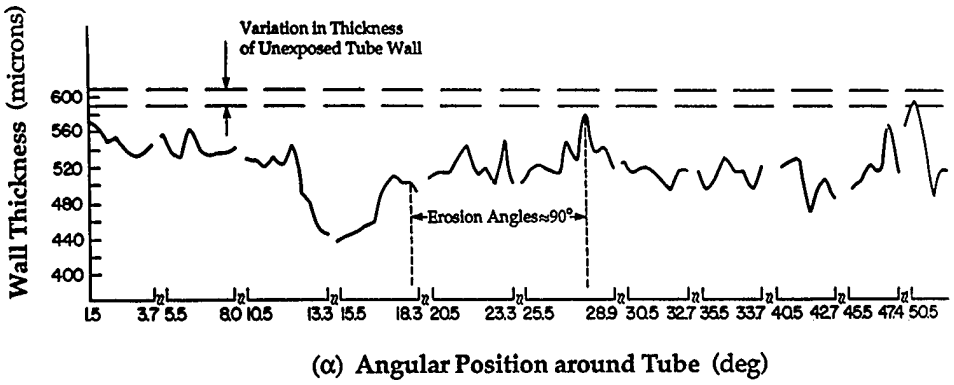
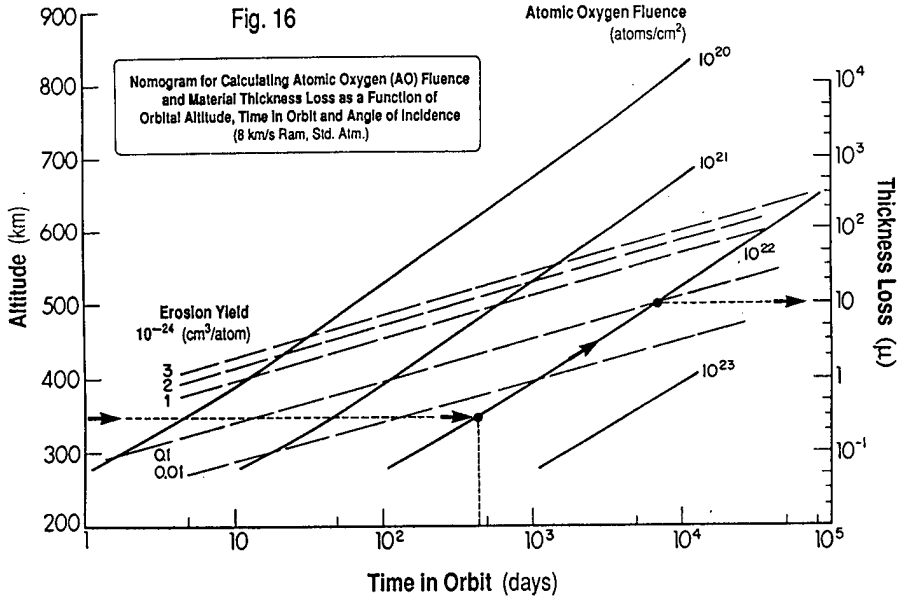
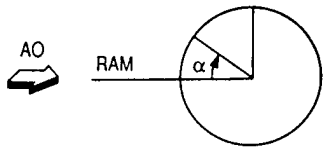


Fig. 15 Erosion Profile of Graphite/Epoxy Circular Tube due to Atomic Oxygen



Correction Factor* for Angle of Incidence (α) Relative to Surface Normal



For α =	*Multiply Thickness Loss by:*
0°	1
10	.985
20	.940
30	.866
40	.766
50	.643
60	.500
70	.342
80	.174
90	.044
100	.002
105	0

* Includes Thermal Velocity Effect

(Ref: LDEF Atomic Oxygen Flux and Fluence Calculations by R.J. Bourassa and J.R. Gillis, MSIG Rep't., Jan. 1991)

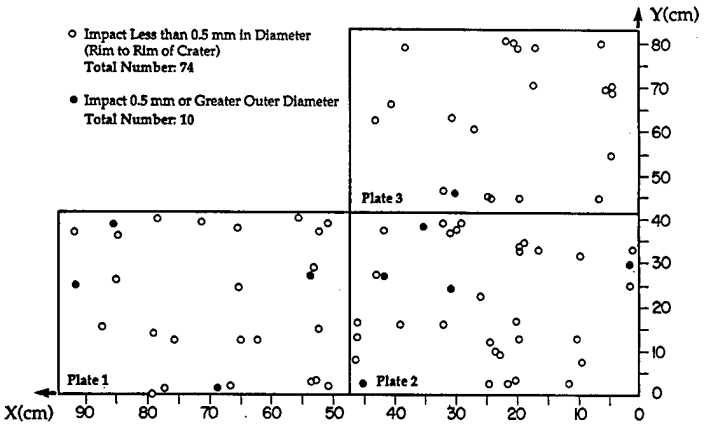


Fig. 17 Micrometeoroid/Debris Impacts on **UTIAS** Composite Materials
LDEF Experiment (A0180, Location D-12)

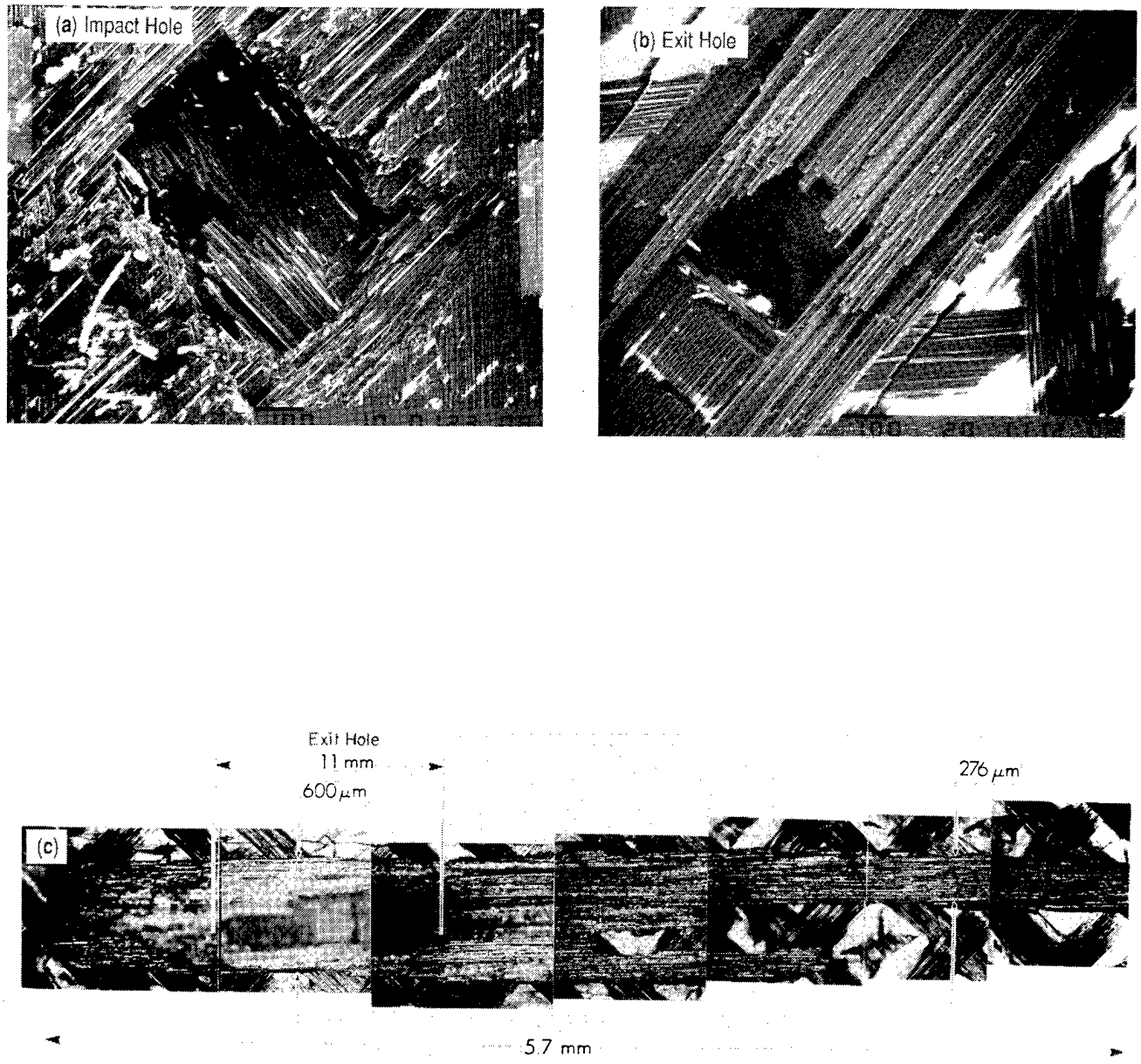


Fig. 18 View of Exit Damage from Micrometeoroid/Debris Impact on Graphite/Epoxy Laminate (5208/T300; $(\pm 45°)_s$)

LONG DURATION EXPOSURE FACILITY EXPERIMENT M0003 DEINTEGRATION/FINDINGS AND IMPACTS

M. J. Meshishnek
S. R. Gyetvay
C. H. Jaggers
The Aerospace Corporation
El Segundo, CA 90245

ABSTRACT

The Aerospace Corporation LDEF Experiment M0003 consists of 19 subexperiments from the Aerospace Laboratories, DoD Laboratories and contractor organizations and was designed to study the effects of the space environment on a large variety of spacecraft materials and components, both current and developmental. The experiment was housed in four LDEF trays and contained over 1250 specimens, two data systems, and two environment exposure control canisters. Nearly identical pairs of trays were located on the leading and trailing edges of LDEF. The materials in these trays span nearly all generic functions in spacecraft such as optics, thermal control, composites, solar power, and electronics. Effects of the space environment such as vacuum, ultraviolet, atomic oxygen, meteoroid and debris, thermal cycling and synergistic effects on various samples will be described. Summaries of the on board data will be presented.

INTRODUCTION

One of the most comprehensive materials experiments on board LDEF, M0003, was integrated by the Aerospace Corporation Materials Sciences Laboratory as principal investigator, and was designed to study the effects of the space environment on current and developmental spacecraft materials. Assembled on two leading edge (LE) and two trailing edge (TE) trays that contained over 1250 specimens, two active data systems, and two timed-exposure vacuum canisters, the experiment is a collection of 19 subexperiments from the Aerospace Corporation Laboratories, Air Force and Navy Laboratories, and Department of Defense (DoD) contractors. Many of these materials are currently in use on Space Systems Division (SSD) spacecraft.

An Industrial Advisory Group was formed to advise SSD (at that time SAMSO) on the selection of materials for this experiment. Funding was obtained from SSD, Aerospace Mission Oriented Investigation and Experimentation (MOIE) resources and from the DoD Space Test Program, managed by SSD/CLI. The integration of the experiment onto LDEF and subsequent deintegration and data retrieval after LDEF's recovery were funded by SSD/CLP. Analyses of the experiment were funded by the Strategic Defense Initiative Organization (SDIO) and the Wright Laboratory. The extended stay of LDEF in space provided a unique opportunity to study material issues such as longevity and space environmental stability which bear directly on mission performance of SSD programs.

The Aerospace Corporation as integrating agency was charged with documentation of the handling and disassembly of the M0003 experimental trays and providing support to the subexperimenters. This support included full photographic documentation of the trays, modules, and quarter-modules from the earliest stages of retrieval through the complete deintegration of the trays; photographic documentation of the condition of the individual test articles; packaging and return of the test articles; and providing flight data to the subexperimenters. Contamination of the M0003 trays was sampled and documented using non-volatile residue (NVR) solvent wipes and tape lifts. Special attention was given to documentation of meteoroid and debris (M+D) impact phenomenology.

The four M0003 trays were disassembled in a class 10,000 clean room facility at the Aerospace Corporation . As test articles were removed from the trays, they were individually examined, preserving the orientation of the test articles as mounted on the LDEF. They were photographed using Nomarski, bright field, and dark field optical microscopy techniques. Observations made of the condition of the M0003 test articles and of the underlying mounting hardware were compiled in an interactive data base. The data base can be sorted by subexperimenter, test article ID, material type, application, or observed damage effects. Micrometeoroid and debris damage was carefully photographed and optical microscope surveys were performed on selected M0003 hardware items.

EXPERIMENT OBJECTIVES AND DESCRIPTION

The immediate objectives of this experiment were to understand the changes in the structure and properties of materials resulting from exposure to the natural space environment and to compare them to predictions based on laboratory experiments. Ideally, correlation of changes in microstructure will be made with changes in physical properties. The longer term objectives were to improve the performance and usage of existing materials and to decrease the lead times for application of new materials on DoD space systems. An important outcome expected from this experiment is the understanding and modeling of material degradation.

This experiment was a cooperative effort and provided the first opportunity for DoD space programs and laboratories to evaluate materials and components after long exposures to the space environment. From the original recommendations of the Industrial Advisory Group, a mix of current and developmental spacecraft materials was selected for this experiment. An overview of the material categories, the originating agency and the principal investigator is given in Table I.

M0003 subexperimenters supplied the Aerospace principal investigator with post-flight analysis plans prior to return of their test article complements. In general, the experimental approach for most of the experimenters involved comparing preflight and postflight analyses of the specimens. Additionally, many experimenters were able to compare corresponding LE and TE test articles. For those experimenters who had test articles in the EECCs, and/or reverse-mounted or shielded test articles, additional comparisons were possible. Lastly, a few experimenters retained properly stored laboratory controls for analysis and comparisons. Thus, many types of test article comparisons are possible.

The M0003 hardware consisted of four peripheral trays, two experiment power and data systems (EPDS), two Environment Exposure Control Canisters (EECCs), and several Li/SO_2 batteries to satisfy power requirements. The experiment was equipped to record temperature, strain, quartz crystal

microbalance (QCM) frequency, solar cell output, fiber optics output, circuit interrogation and various data system parameters. One 6-inch deep and one 3-inch deep tray connected by a wiring harness, a data system (EPDS), and a canister (EECC) were located on Rows 8 and 9 of ring D on LDEF's leading edge. A similar configuration was located on Rows 3 and 4 of ring D on the trailing edge. The design of the trays was modular, allowing samples to be thermally coupled or decoupled from the tray and therefore, the LDEF structure. Over 1250 material test articles of more than 200 material types were mounted on these trays.

Figures 1 through 4 illustrate the layout of the trays with various sensors, primarily thermistors, also shown. Strain gauges that were used to measure the response of selected composite test articles are not shown, but were located on the reverse surface of test articles on Module III on trays D4 and D8. Twenty gauges per module were used, for a total of 40. Preflight photos of trays D8 and D9 are also shown in Figures 5 and 6. A preflight photo of the TE (D4) canister in the open position is shown in Figure 7. Trays D3 and D4 are not shown, but were similar.

Test articles were mounted on anodized black aluminum hardware modules within the trays. Many subexperiments contained duplicate sets of test articles mounted on both the leading and trailing edge trays; a few had sets in the EECCs as well. Some subexperiments also included a set of test articles that were mounted within the modules and were not directly exposed to the space environment. The test articles on the trays and EECCs included a variety of thermal control coatings, laser optics, composites, structural materials, laser communication components, dosimeters, antenna materials, contamination monitors, solar cells, fiber optics, and electronic piece parts.

The EECCs (on trays D4 and D8) were programmed to open in three stages allowing varying exposures of some materials. Two weeks after the initiate signal, the canisters opened to expose a large (~3/4 area) of specimens. The next canister stepped movement occurred approximately 23 weeks after deployment and exposed another row of samples (~1/8 additional area). The final canister stepped movement was at approximately 33 weeks and exposed the last row of samples (1/8 area) by opening to the canister's fullest extension. The canister drawer moved to the completely closed position at 42 weeks after initiate and remained closed during the remainder of the LDEF mission. The tape data which will be discussed later indicates that these programmed movements occurred properly. Thus, varying exposure times of 9, 19, and 40 weeks were accomplished for some samples in addition to the full mission exposure of 68 months for identical test articles in other M0003 trays.

Figures 8 and 9 are representative on-orbit photographs of the M0003 trays. Several points are evident in these photos. Debris from atomic oxygen-eroded metallized Kapton radar camouflage specimens is scattered about the D9 tray. Polymer film strips such as Kapton and silver Teflon (Ag/FEP) are broken and are projecting above the surface, on both the D9 and D3 trays. Solar cells are missing on both the D3 and D9 trays due to an adhesive failure. Typical atomic oxygen (AO) erosion phenomena are apparent on the D9 tray while UV degradation is more prevalent on the D3 tray. There is evidence of contamination due to outgassing on both trays. The painted sunshield on D4 has darkened due to UV damage while its counterpart on D8 has remained white.

Better illustrations of the damage to the specimens are shown in the photos taken at Aerospace Corp. before deintegration of the trays. These are shown in Figures 10 through 13. This damage will be discussed in some detail later.

The canisters were opened in the clean room roughly four months after arrival of the experiment at Aerospace. Special investigation group (SIG) personnel were present during this event and had sampled the canister gases and assisted in helium leak testing of the seals. The canisters were both essentially at atmospheric pressure and some leakage of the front seals was detected. Photos of the

opened D4 and D8 canisters are shown in Figures 14 and 15. Note the missing sample from canister D4 and erosion patterns on the stepped exposure samples on D8. Contamination patterns on the canister sides indicate the opening of the canisters by the degree of darkness of the deposits.

DATA SYSTEM

Table II shows in tabular form, the assignment of the various EPDS data channels on the LE (D8) and TE (D4) trays. The systems were set to run to end of tape and started scanning 2.33 hours after initiate. The scan time was set for 111.8 minute scans (1.25 orbits) every 93.16 hours. All channels were scanned five times at 3.49 minute intervals over the 111.8 minute period. An orbital scan consists of 32 points of averaged data from the five scans. Figure 16 shows, in graphic form, the scan format. A typical orbital plot from a solar cell string is shown in Figure 17. More informative are the minimum/maximum summary plots of the data channels. These plot the minimum and maximum values of each orbital scan for the 119 orbits for which data was collected. The corresponding min./max. plot for a solar cell channel is shown in Figure 18. The plot clearly shows the orbital precession of LDEF which directly affects the sun exposure. Other min./max. plots are given for other channels. Figure 19 depicts the thermal cycling of a graphite epoxy composite specimen. The same cyclic variance in the data due to the orbital precession of LDEF is seen. The data indicates that the thermal performance of LDEF and experiment M0003 were within design limits (ref. 1). For comparison, Figure 20 shows the same temperature data for a graphite aluminum composite specimen. Higher temperatures for both min./max. curves are seen due to the lower emissivity of the aluminum relative to the epoxy. Typical thermal cycling of corresponding leading edge and trailing edge modules are shown in Figures 21 and 22. Three thermistors were used per module and they tracked quite well.

EXPERIMENT OBSERVATIONS

Preliminary assessment of the M0003 experimental test articles was performed during the deintegration of the M0003 trays, using optical microscopy as the single examination tool. The objective of this nondestructive examination was to provide the subexperimenters with a quick-look summary of effects observed on their test articles that could assist them in planning their postflight investigations. The primary types of damage modes observed on the M0003 test articles were surface discolorations, atomic oxygen erosion, superficial corrosion, impact crater-formation, extraneous particulate matter adhesion to surfaces, coating microfracture-formation, and contamination residue and stain deposition. These damage modes were the result of combined effects from atomic oxygen impingement (LE only), UV radiation, thermal vacuum cycling, and outgassing contamination. Ion trails were observed on a few materials, but damage that could be attributed to proton or electron radiation was not observed on the M0003 test articles. In general, the material types on M0003 most adversely affected by the space exposure were thermal control materials, thin polymer sheets, optical mirrors, and thin film coatings. Some oxidation-sensitive metal films (notably silver) and thin polymer sheets which were vulnerable to embrittlement and AO erosion were almost destroyed. It should be noted that these observations are only qualitative and the in-depth investigation of the effects of the space exposure on the test articles was the prerogative of the subexperimenters, and was not the function of the deintegration team.

Many of the materials on M0003 are not considered advanced, but are in use on current satellite systems. Others are baseline materials against which performance improvements are measured. Thus, the response of these samples is important in updating the models for prediction of exposure effects and lifetime performance. A summary of performance of materials, by application follows:

Composite Materials

A large variety of structural composite materials was exposed on the M0003 leading and trailing edge trays. Cured and post-cured thermoplastic and thermoset resin matrices were used with low, medium, and high modulus mesophase pitch and polyacrylonitrile carbon fiber reinforcement. Some polyimide and carbon/polyimide fiber hybrid composites were also flown. Most composite constructions were either cloth laminates or varying-angle fiber wraps. The surfaces of composite specimens on the leading edge trays were superficially oxidized and had a matte black or light gray velvety appearance, depending on their susceptibility to atomic oxygen erosion. A light ashy residue was apparent on the exposed surface of these composites. The ashy residue, if sloughed from the surface on orbit, might become a source of serious contamination, especially to optical surfaces.

Most LE composites had TE counterparts which suffered little or no discernible damage from exposure. The most common effects noted with these materials were superficial darkening of the matrix due to UV exposure and/or discoloration of the surface due to photo-fixed contamination.

Many craters from micrometeoroid and space debris impacts were observed on these composites. The damage was confined to the immediate area of the crater on both leading and trailing edge specimens, but subsequent atomic oxygen erosion enlarged the affected area a slight amount on leading edge specimens. Figure 23 shows typical AO damage to a composite.

Solar Cells

Five different types of solar cell strings (Si and GaAs cells of conventional and high efficiency design) were flown on the leading and trailing edge of LDEF. These samples were instrumented and measurements were recorded for 14 months of exposure. The data system measured the voltage across a 0.05 Ω short circuit and the data reduction routine calculated the output current. Examination of the cell strings after retrieval showed the cover glasses over the cells were superficially contaminated. The silver welds on the interconnects appeared intact, but localized delamination of the cover glass was apparent on some cells around the welds. Since the current measurements did not show any significant change in the performance of these cells, this degradation probably occurred after the data recording period. The damage is illustrated in Figure 24.

Coated and uncoated solar cell cover glass specimens were exposed on LE and TE trays. In addition, there were reverse-mounted controls on a TE tray which experienced only the high vacuum and thermal conditions of the front face-mounted specimens. The cover glass coupons were mounted over Si wafers and held by Delrin retainers. The coatings included many of the UV-rejection coatings in use on present-day solar cell cover glasses. Many of the cover glasses were considerably stressed; these eventually cracked catastrophically, as did their duplicate laboratory controls. Others cracked only with exposure to the UV and atomic oxygen environments. The Delrin retainers were degraded on all of these specimens and flakes of Delrin contaminated the coating surfaces. Obviously, Delrin is not a material of choice for applications requiring endurance to AO or UV exposure on spacecraft.

Hypervelocity impacts on the cover glasses of the solar cell strings and the individual specimens resulted in craters surrounded by localized damage in the glass. The presence of the craters found on the M0003 test articles would likely impair solar cell performance only by the obscuration of the cell across the very small area of the crater. Typical damage in a solar cell is depicted in Figure 25.

Optical Samples

Optical specimens on the M0003 trays included metal mirrors, optical solar reflectors (OSRs), and dielectric-coated substrates. These materials were placed on LE and TE trays as well as in the leading and trailing edge canisters. The metallic mirrors became hazy on the leading edge trays due to corrosion of the surface. On the trailing edge, these materials were clouded by photo-fixed contamination stains. Uncoated optical substrates were also clouded by contamination on the trailing edge, but were relatively unaffected by exposure on the LE.

Most OSR specimens were relatively unaffected by exposure, but were susceptible to contamination-staining. The exceptions were silver OSRs; both coated and uncoated versions were oxidized on the leading edge. The uncoated OSRs were oxidized beyond usefulness.

The response of dielectric-coated optical specimens depended on the materials used in the coatings. Many specimens with highly-stressed coatings wrinkled and buckled with exposure. A MgF_2-coated fused silica substrate specimen exposed on all environments on the M0003 trays was crazed. Other specimen coatings suffered microcracks, but were not catastrophically damaged. The microcracking experienced by these coatings was probably due to the residual stress induced in their fabrication, as the laboratory control duplicates were also microcracked to some extent.

Hypervelocity impacts created craters surrounded by localized damage on many optical specimens. The greatest expanse of damage occurring due to impact was a 1-cm circle of blistered coating surrounding a 1-mm diameter crater on a mirror specimen, shown in Figure 26. Sensors or windows which are exposed to solar UV, atomic oxygen or micrometeoroids can experience significant optical performance degradation if the coatings are disrupted.

Thermal control materials

Polymeric films, such as silver Teflon (Ag/FEP) and aluminized and bare Kapton were eroded by atomic oxygen. Adhesive-backed Ag/FEP sheets, used as thermal protection covers over subexperiments on the M0003 trays, became milky white on both the leading and trailing edge trays. In space, the subsurface Ag reflective layer became gold-colored, perhaps due to UV-darkening of adhesive that was pressed through cracks in this layer during application of the sheets to the supporting hardware. Bare Kapton was embrittled and eroded on the LE surfaces, while Kapton coated with metal or silicone survived. The floating debris from the eroded metallized Kapton radar camouflage materials was prominent in the on-orbit photos of the M0003 LE trays (see Figure 8). Damage to the radar camouflage materials producing the Kapton debris is shown in Figure 27. Kapton was discolored on trailing edge surfaces, but remained intact. Aluminized Mylar used on adjacent LDEF trays was a serious source of extraneous debris when the Mylar was attacked by atomic oxygen, releasing very thin curls of aluminum film which were attracted to many surfaces on the M0003 trays. Thus, for long missions, or for extended exposure in LEO, the use of thin metallized polymer films is

risky. Kapton specimens in the leading edge canister showed signs of erosion by AO even with only 40 weeks exposure at 250 nmi. ITO-coated Kapton did not exhibit erosion under these conditions.

Many white and black thermal control paints and coatings were exposed on M0003. Some of them were developmental; others are the common materials used on spacecraft today. More than one subexperimenter flew the same paint in his test article complement, and many had both LE and TE exposure. Some coatings were also exposed in the canisters. Moreover, the EPDS sunshields and other M0003 data system sunshields were covered with white thermal control paints. These have provided large areas for M+D studies as well as thermal control material specimens.

Generally, all white paints susceptible to radiation damage causing color center formation were darkened by exposure to UV. These materials include those having TiO_2, Eu_2O_3, Al_2O_3, and ZnO pigments. This effect was prominent on the trailing edge. However, leading edge specimens were bleached or annealed due to the atomic oxygen exposure (especially those containing ZnO pigments). In some cases, erosion of the UV damaged layer restored whiteness. Aerospace Corporation subexperiment -18 exposed the white thermal control paints Chemglaze A276, S13GLO, YB-71 (ZOT) and the black paint D111, on both leading and trailing edge trays. Preliminary results on these materials are as follows:

Chemglaze A276 was used on the EPDS sunshield and is composed of TiO_2 pigment in a polyurethane binder. Table III summarizes the solar absorptance (α_s) values measured for both leading edge and trailing edge specimens compared to control specimens. Figure 28 shows the dramatic difference in response of the sunshields to the LDEF exposure from LE to TE. Close examination of the paint surface indicated that the TE specimen was glossy and specular while the LE was roughened, chalky, and full of numerous impact craters. These impact craters were surrounded by areas of blistered and peeling AO-eroded surface, pointing to preferential erosion of the organic polyurethane binder, leaving unsupported TiO_2 pigment as the surface. Figure 29 presents scanning electron microscope photos of the TE and LE specimens that show loss of binder from the LE specimen. Elemental analysis x-ray analysis indicates substantial loss of carbon signal from the surface of the LE specimen. As a final proof of concept, a specimen of LE EPDS sunshield paint was cut that contained a recessed bolt hole. The paint around the bolt hole had a glossy appearance where it was protected from AO on orbit, an indication that no erosion of the binder had occurred in that area. Figure 30 illustrates the response of the specimen to 500 hours of UV irradiation in a laboratory test. The darkening of the specimen only in the bolt-protected area where polyurethane binder was still present graphically reveals that the degradation is due to UV damage to the binder. The major whitening mechanism must be AO erosion of this damaged layer.

Comparison of the α_s values in Table III leads to two major points: the lower α_s of the LE specimen relative to the control indicates loss of binder has caused an index mismatch increase or that the α_s of TiO_2 is less than TiO_2 plus binder. Oxidation of the nonstoichiometric TiO_2 could also increase its reflectivity. Importantly, due to its severe susceptibility to UV degradation, Chemglaze A276 is not recommended as a white thermal control paint for spacecraft that require any significant mission lifetime.

The M0003 signal conditioning units (SCU) sunshields were painted with S13GLO and two each witness test articles were also flown on the D3 and D9 trays. S13GLO is a ZnO pigment encapsulated in K_2SiO_3 dispersed in a methyl silicone binder. Comparison of LE and TE specimens using either the test articles, shown in Figure 31, or specimens from the SCU covers, shown in Figure 32, dramatically shows the damage to the TE paints from UV. Reflectance curves of these two samples are given in Figure 33. Importantly, the roughly 300% increase in α_s from control to TE is

not in line with predictions from ground test results (ref. 2 and 3). These specimens are still under investigation, but microscopy and surface analysis have not indicated detectable erosion of the material. It is believed that the UV induced color centers formed by oxygen vacancies on the trailing edge are oxidized or annealed on the leading edge by AO. This mechanism is still under investigation. Response of S13GLO to AO and UV is important since this tends to be the paint of choice for many SSD programs because of its ease of application, low cost, low α/ε, and flexibility.

YB-71, which is Zn_2TiO_4 pigment in K_2SiO_3 binder commonly called "ZOT" demonstrated marked stability towards both AO and UV relative to the other white paints previously discussed. Table III shows a slight degradation of α_s identical for LE and TE specimens, presumably due to UV. Interestingly, some ZOT specimens formed crystalline whiskers in the K_2SiO_3 binder. Leading edge specimens are not whiter than the TE specimens indicating that bleaching or annealing of color centers is not a dominant mechanism in this material, for unknown reasons. Due to its UV stability, ZOT may be a good choice for LEO spacecraft. However, its stability towards electron/proton radiation is in doubt and renders it less effective at GEO or elliptical orbits.

D111 black thermal control paint which consists of bone black in K_2SiO_3 binder was essentially unaffected by AO, but some decrease in absorptance was measured relative to the TE specimen. Another black paint, Chemglaze Z306, which has a polyurethane binder sustained more severe degradation than D111. Most of the LDEF hardware was painted on the reverse surface with Chemglaze Z306. The properties of these paints are still under investigation. Other thermal control paints and coatings such as black anodized aluminum, used extensively on the M0003 test article mounting hardware, were bleached by UV exposure.

Tray Hardware

General observations and results of the examination M0003 hardware are as follows:

Extensive contamination deposits as a result of outgassing, contamination, and UV-photolyzed reaction are seen on the M0003 trays. The synergism between outgassing and UV is striking. This phenomenon of enhanced photodeposition needs to be taken into account in modeling, ground testing, and material qualification.

There were significant adhesive failures on M0003. Some adhesives (RTVs) which are commonly used to bond Kapton to Ag/FEP let go, as did acrylic adhesives bonding solar cells. The issue of adhesive performance as a function of thermal cycling and UV exposure poses a genuine concern for spacecraft in LEO and better (longer) testing and qualification is required.

Fasteners on LDEF and M0003 do not lend themselves to obvious interpretation of their performance. We have observed backed-out bolts, loose bolts, frozen bolts, broken bolts, on both the leading and trailing edges. Some bolts which were relatively loose, tightened or galled on removal. The some 1500 fasteners which were documented on M0003 during removal have been put into a data base for study. Clearly fastener performance will be a major issue for any system requiring longevity and/or maintenance in space.

For M0003, there is good news for electrical connectors, solder joints, wires, mechanisms, batteries, motors, tape recorders and computers. No significant anomalies were noted on orbit. Inspection also showed good performance and integrity after retrieval. No significant outgassing of electronic parts was observed. An early and perhaps risky conclusion is that all the costs and effort put

into reliability of electrical devices is overdone. There were devices on our experiment which were commercially-obtained and performed flawlessly.

MICROMETEROID AND DEBRIS

During the deintegration of the M0003 experiment, there was an opportunity to observe and photograph impacts in several types of materials. In addition, trays D4 and D8 contained sunshields and instrument covers which provide large areas (2/3 of trays D4 and D8) for debris studies. These were meticulously examined with all hypervelocity impacts 0.1 mm in diameter or larger charted. Figure 34 shows a computer-generated map of one of these surfaces. A histogram which summarizes the meteoroid and debris counts to date, is displayed in Figure 35. This data is currently being compared to existing meteoroid and debris models. Figures 36 through 38 are photographs illustrating typical impact phenomenology in various materials. While none of the damage should be considered as catastrophic, its affect on mission performance must be carefully evaluated. Interesting reaction zones are seen on some of these impact features, although they are not well understood at this time.

CONTAMINATION

Contamination from outgassing and particulates was legion on M0003. This was documented extensively through photography and sampled by means of solvent wipes and tape lifts. These were taken prior to and during disassembly. Optical and SEM photos were used to analyze the tape lifts while Fourier Transform Infrared (FTIR) spectroscopy was used to analyze the contamination films. This work is still in progress.

Heavy varnish-like deposits were found on the trays, the thickest being on D8 and D9. Flow patterns were observed which suggested that the origin of the outgassing was from within the LDEF structure. FTIR analysis of this residue is shown in Figure 39. Bands present in the spectrum suggest it is made up of hydrocarbons, urethanes, and silicones.

UV and AO altered the contamination on both leading and trailing edges. On the trailing edge, UV has darkened and photo-fixed the deposits. The same occurred on the leading edge; however, near the end of the LDEF mission, the higher AO concentration at lower altitude oxidatively removed some contamination. Silicone layers were oxidized to form a silicate or silica deposit. Thus, much of the contamination was covered with glassy-type coatings and could not be removed by solvent wipes. These synergistic effects of UV and contamination and AO and contamination (ref. 4 and 5) have been investigated previously . More work needs to be done in this area to quantify these effects. Chemglaze Z306 is a likely candidate for a source of much of this contamination.

Particulate contamination on individual test articles could be identified as originating from deteriorated nearby materials on M0003 and other LDEF trays. Debris found on test articles flown in the canisters, particularly fibrous debris (Figure 40), may have come from the shuttle payload bay.

SUMMARY

The most significant results from LDEF/M0003 and the resulting lessons learned or impacts are presented below, together with recommendations for future work.

Micrometeroid and debris impacts on M0003 were numerous; however, none caused catastrophic damage. Nevertheless, the size and number of such impacts raise serious concerns regarding the escalating amount of space debris. Damage to a system (especially optics) resulting in loss of mission performance needs to be carefully evaluated and modeled, not only with respect to collision probabilities, but also impact phenomenology.

Contamination on LDEF/M0003 was more pronounced and severe than expected and points to excessive outgassing from multiple sources. Examination of hardware surfaces indicates that outgassing occurred well into the LDEF mission and that venting from the interior of LDEF was a major source. Clearly, there is a need for cleaner spacecraft and better modeling of contamination transport. Contamination control should be made part of spacecraft design. Of particular note is the ubiquitous UV photolysis of contaminant deposits, as well as the alteration (oxidation) of such deposits by atomic oxygen. The synergistic effects of these three phenomena need to be better understood and modeled.

The degradation of some paints, coatings, and films was significantly greater than expected. The threefold increase in α_s of S13GLO, the crazing of MgF_2, and the erosion of Ag/FEP, all point to a need for better correlation of ground and flight test data, and better test methods. The significant number of adhesive failures raises the issue that longer testing is required to evaluate the effects of repeated thermal cycling on adhesive performance.

Synergistic effects are emerging as the most important and interesting phenomena, specifically the combined effects of AO and UV radiation on materials and contamination, reactions of AO and UV at debris impact sites, and the effects of UV and thermal cycling on materials, particularly polymers.

On the positive side, electrical and mechanical systems exhibited little or no anomalies. It would seem that much of the degradation of materials, especially from AO, is superficial and not a significant problem. This is especially true for structures and composites having any appreciable thickness.

ACKNOWLEDGEMENTS

The authors express their sincere appreciation to the Space Test Program (SSD/CLP), to the Strategic Defense Initiative Organization (SDIO/TNK), and to Air Force Wright Laboratory's Materials Directorate for sponsorship of this work. We would like to thank the NASA Langley LDEF Science Office for their unstinting support to our effort, and for the use of their photographs as a part of the documentation of the M0003 experiments. We also wish to acknowledge the contribution of the following individuals to this effort: Col. J. Armstrong, R. Bachus, D. H. Barker, G. W. Boyd, R. A. Brose, W. C. Burns, W. H. Childs, L. G. Clark, J. M. Coggi, A. F. DiGiacomo, L. Fishman, C. S. Hemminger, Capt. D. Johnson, J. L. Jones, 1st Lt. M. Jones, W. H. Kinard, C. Kiser, F. Knight, A. Levine, B. Lightner, N. Marquez, G. D. Martin, Lt. Col. M. Obal, L. A. Okada, R. O'Neal, K. W. Paschen, H. T. Sampson, T. A. Stoner, W. K. Stuckey, T. K. Tessensohn, G. A. To, H. E. Wang, W. Ward, D. B. Wisehart, J. C. Uht.

REFERENCES

1. Berrios, W. M.: "Long Duration Exposure Facility Post-Flight Thermal Analysis, Orbital/Thermal Environment Data Package," NASA Langley Research Center, Hampton VA, 3 October 1990.

2. Zerlaut, G. A.; Gilligan, J. E.; Ashford, N. A.: "Space Radiation Environmental Effects in Reactively Encapsulated Zinc Orthotitinates and Their Paints," AIAA paper No. 71-449, 24-28 April 1971.

3. Mell, R. J., and Harada, Y., "Space Stable Thermal Control Coatings," Wright Laboratories Materials Lab Report , AFWAL-TR-87-4010, May 1987.

4. Judeikis, H. S.; Arnold, G. S; Hill, M. M.; Young Owl, R. C.; and Hall, D. F.: "Design of a Laboratory Study of Contaminant Film Darkening in Space," SPIE Vol. 1165 , Scatter from Optical Components, 1989.

5. Meshishnek, M. J.; Stuckey, W. K.; Evangelides, J. S.; Feldman, L. A.; Peterson, R. V.; Arnold, G. S.; and Peplinski, D. R.: Effects on Advanced Materials: "Results of the STS 8 EOIM Experiment," Atomic Oxygen Effect Measurements for Shuttle Missions STS 8 and 41G Volume II NASA Technical Memorandum 100459, September 1988.

TABLE I. SUMMARY OF M0003 EXPERIMENTS

Sub-experiment number	Scope	Experimenter	Agency
-1	Radar camouflage materials and electro-optical signature coatings	Richard Porter	Wright Labs/SNA Wright Patterson AFB, OH 45433-6533
- 2	Laser optics	Linda De Hainaut	Phillips Lab/LTC Kirtland AFB, NM 87117-6008
- 3	Structural materials	Charles Miglionico	Phillips Lab/SUE Kirtland AFB, NM 87117-6008
-4	Solar power components	Terry Trumble	Wright Labs/POOC Wright Patterson AFB, OH 45433-6533
-5	Thermal control materials	Charles Hurley	Univ. of Dayton Research Inst. 300 College Park Dayton, OH 45469-0001
-6	Laser communication components	James N. Holsen	McDonnell Douglas Astronautics Corp. Dept. E465, Bldg. 287/3/309H P. O. Box 516 St. Louis, MO 63266
-7	Laser mirror coatings	Terry M. Donovan	Naval Weapons Center Thin Film Physics Div. Code 3818 China Lake, CA 93555
-8	Composite materials, electronic piece parts, fiber optics	Gary Pippin	Boeing Aerospace Co. Materials technology Dept., MS 2E-01 P. O. Box 3999 Seattle, WA 98124
-9	Thermal control materials, antenna materials, composite materials, and cold welding	Brian C. Petrie	Lockheed Missiles & Space Co. Dept. 62-92, Bldg. 564 P. O. Box J04 Sunnyvale, CA 94086
-10	Advanced composite materials	Gary L. Steckel	The Aerospace Corp. P. O. Box 92957, M2/321 Los Angeles, CA 90009
-11, -12	Contamination monitoring Radiation measurements	Eugene N. Borson	The Aerospace Corp. M2/250
-13	Laser hardened materials	James N. Holsen	McDonnell Douglas Astronautics Corp. Dept. E465, Bldg. 287/3/309H P. O. Box 516 St. Louis, MO 63266
-14	Quartz crystal microbalance	Donald A. Wallace	QCM Research 2825 Laguna Canyon Road P. O. Box 277 Laguna Beach, CA 92652
-15	Thermal control materials	Oscar Esquivel	The Aerospace Corp. M2/241
-16	Advanced composites	Joseph J. Mallon	The Aerospace Corp. M2/248
-17	Radiation dosimetry	Sam S. Imamoto, J. Bernard Blake	The Aerospace Corp. M2/260
-18	Thermal control paints	Christopher H. Jaggers	The Aerospace Corp. M2/241
-19	Electronic Piece Parts	Seymour Feuerstein	The Aerospace Corp. M2/244

TABLE II. DATA CHANNELS RECORDED BY DATA SYSTEM

	Leading Edge	Trailing Edge
Temperature	31	32
Strain	20	20
Solar Module Output	6	6
Quartz Crystal Microbalance	1	1
Fiber Optics	1	-
Circuit Interrogation	1	-
	Number of Instrumentation Monitor Channels	
DCPA/EPDS		
Voltage	2	2
Current	1	1
Temperature	1	1
Signal Conditioning Unit Temperature	2	2

TABLE III. SOLAR ABSORPTANCE OF THERMAL CONTROL PAINTS RETRIEVED FROM LDEF

		Solar Absorptance, α_s	
Material	Position	Test Article	Lab Control
A276	Leading Edge	0.228	0.282
	Trailing Edge	0.552	
YB-71 ZOT	Leading Edge	0.182	0.130
	Trailing Edge	0.182	
S13GLO	Leading Edge	0.232	0.147
	Leading Edge	0.228	
	Trailing Edge	0.458	
	Trailing Edge	0.473	
D-111	Leading Edge	0.933	0.971
	Trailing Edge	0.968	

Figure 1. Diagram of leading edge 3-in. tray, D9

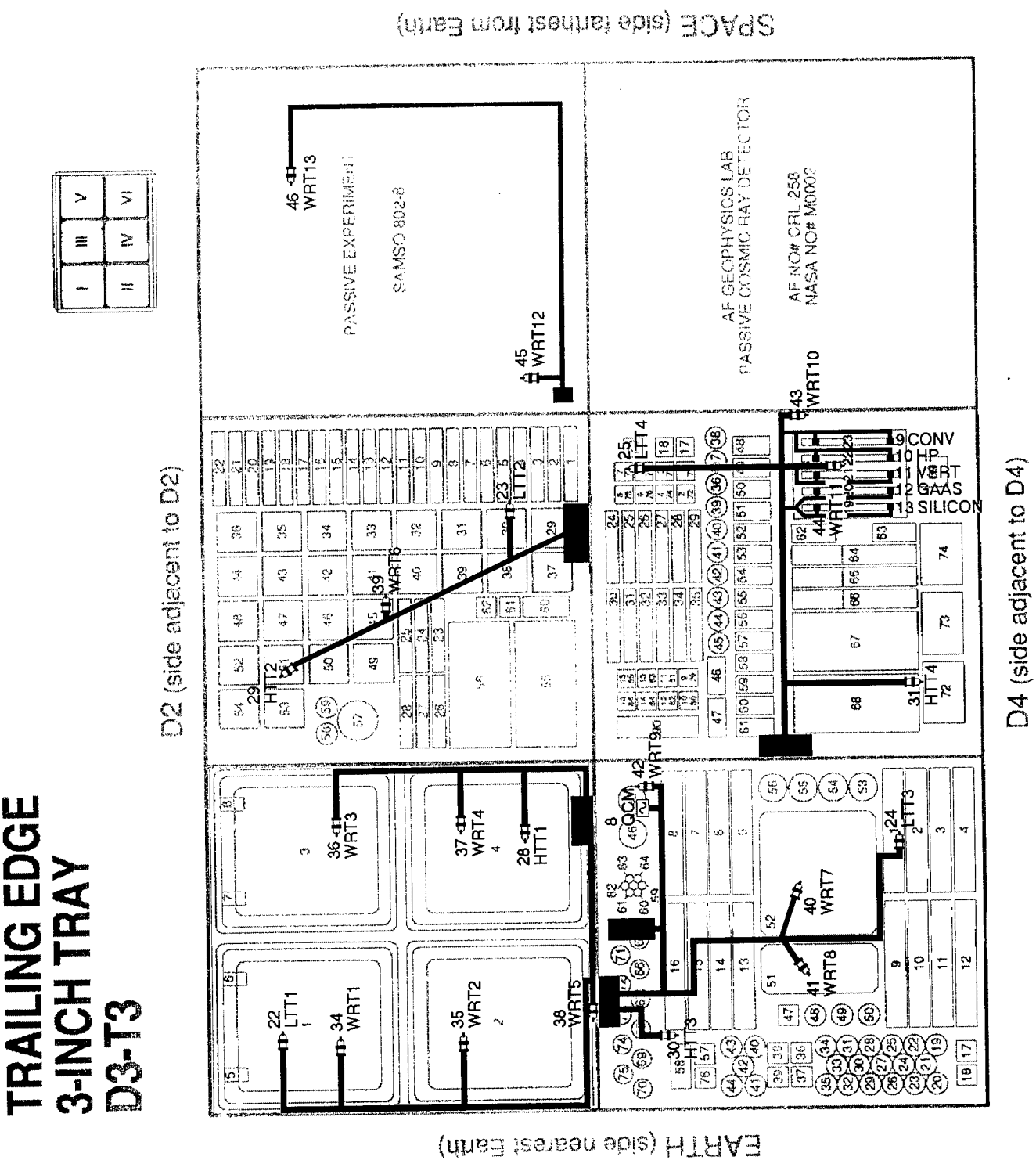


Figure 2. Diagram of trailing edge 3-in. tray, D3

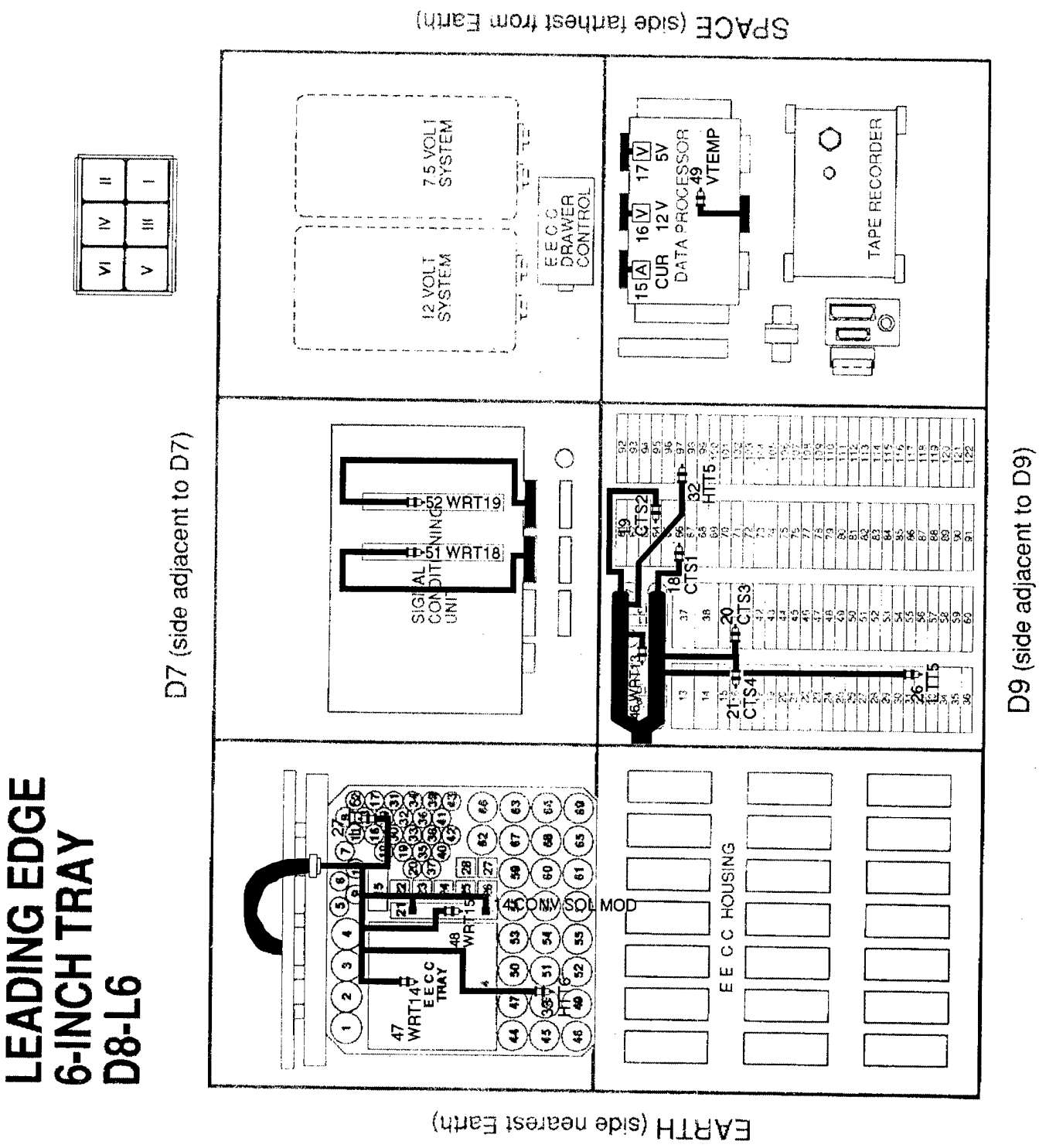


Figure 3. Diagram of leading edge 6-in. tray, D8

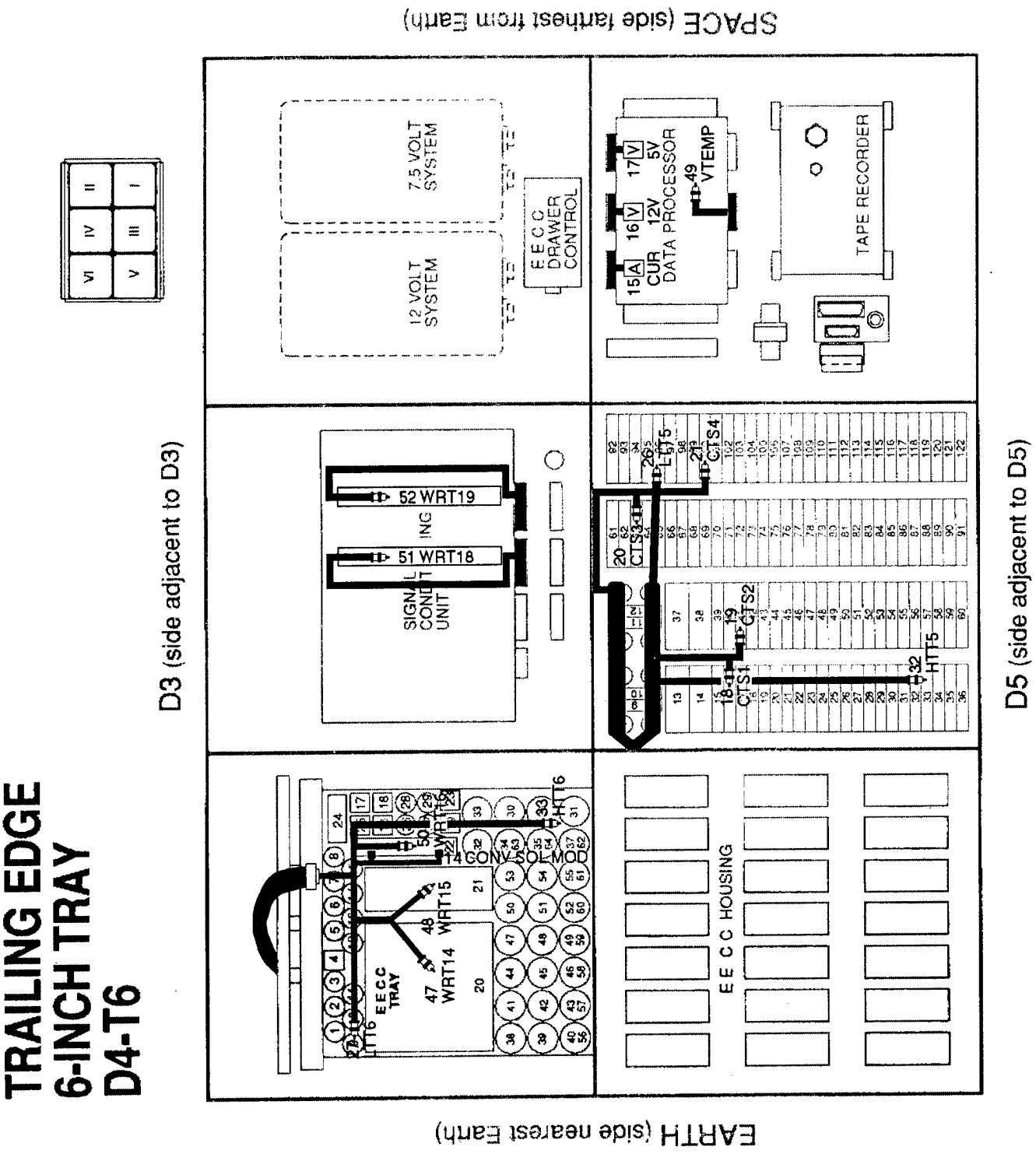


Figure 4. Diagram of trailing edge 6-in. tray, D4

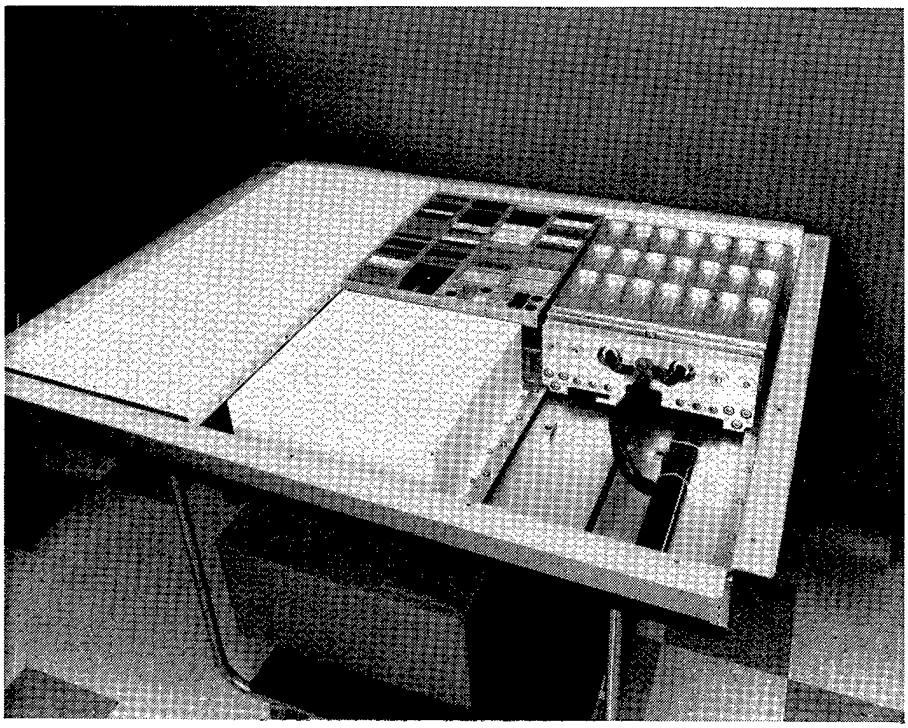


Figure 5. Preflight photograph of D8 tray

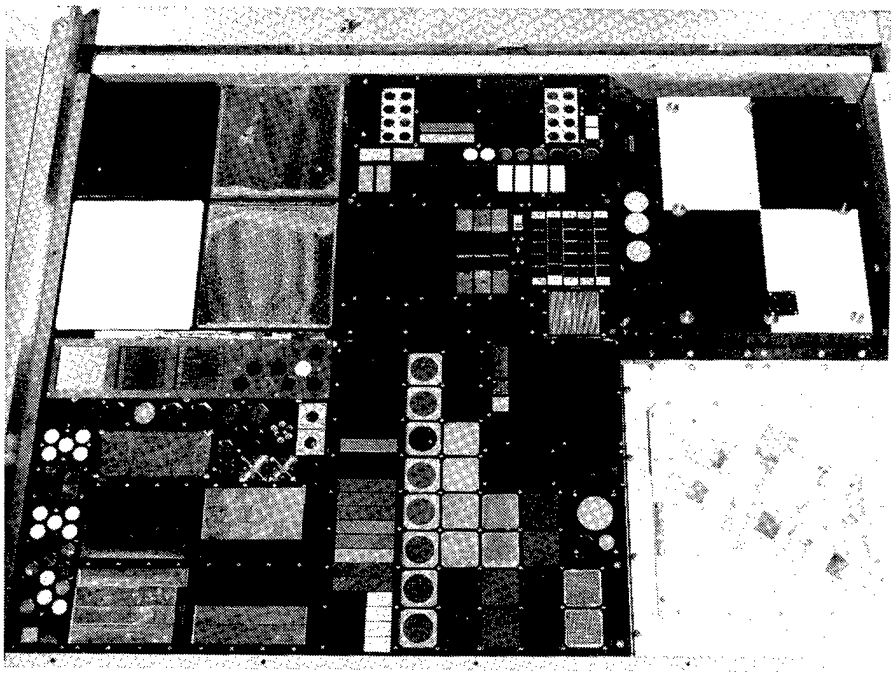


Figure 6. Preflight photograph of D9 tray

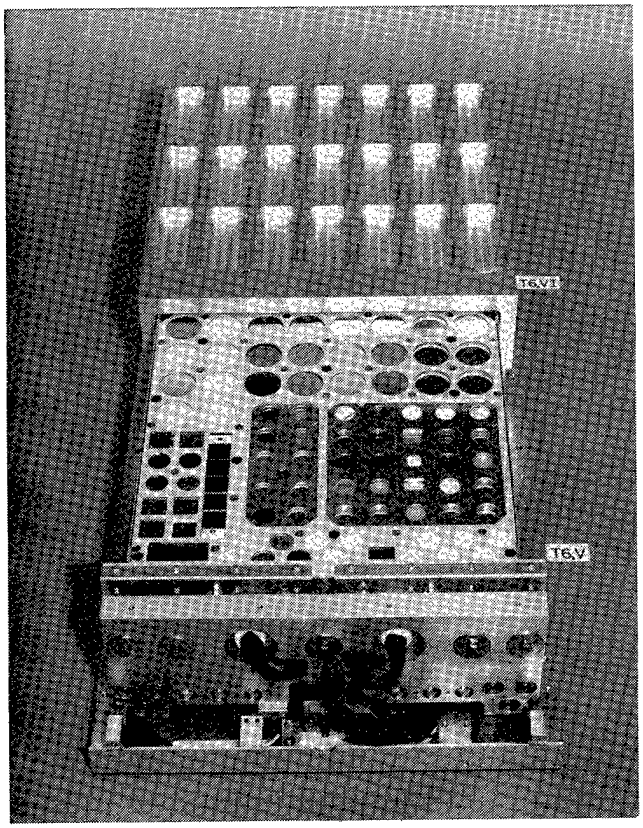


Figure 7. Preflight photograph of Environment Exposure Control Canister on D4, in open position

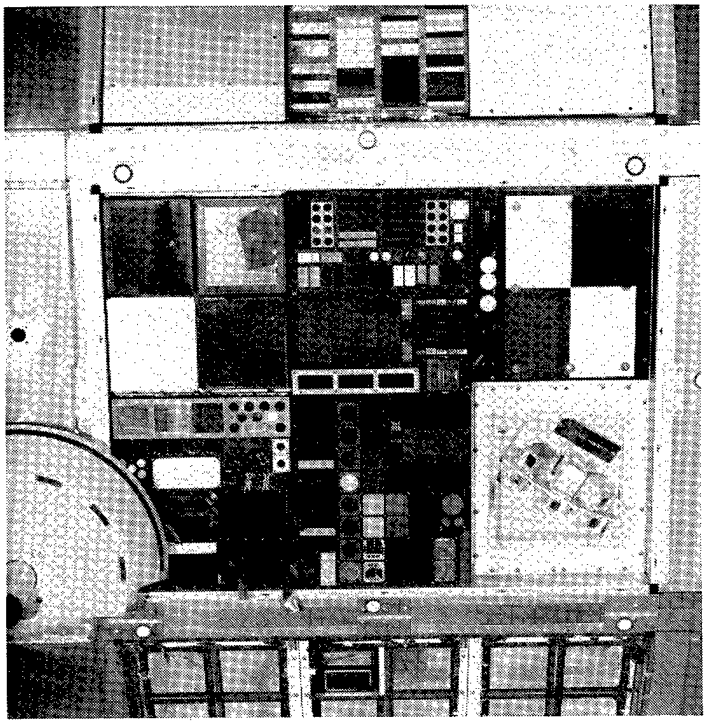


Figure 8. On-orbit photograph of D9 tray, leading edge. Note the debris above the surface from AO-deteriorated materials on the tray

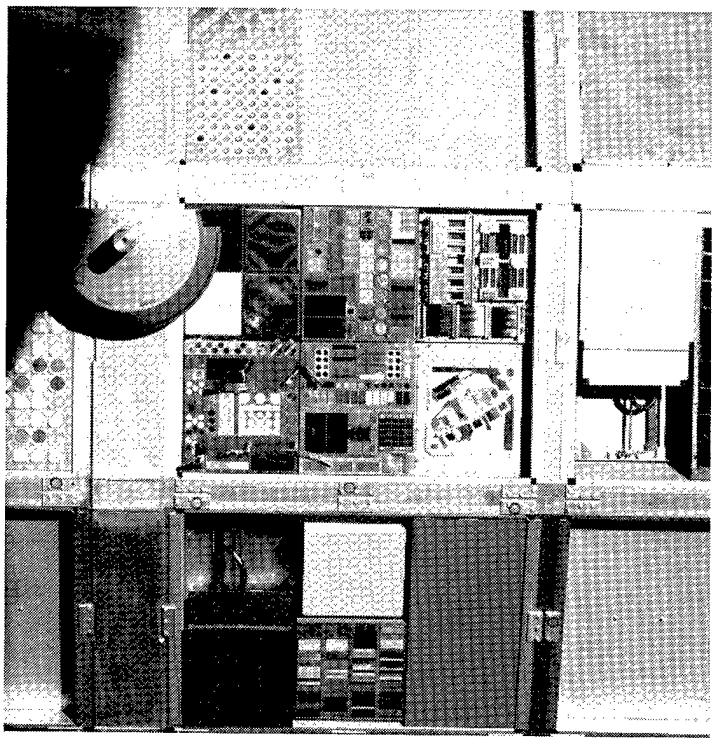


Figure 9. On-orbit photograph of D3 and D4 trailing edge trays.Most noticeable effects are contamination-staining and darkening of white paint coatings

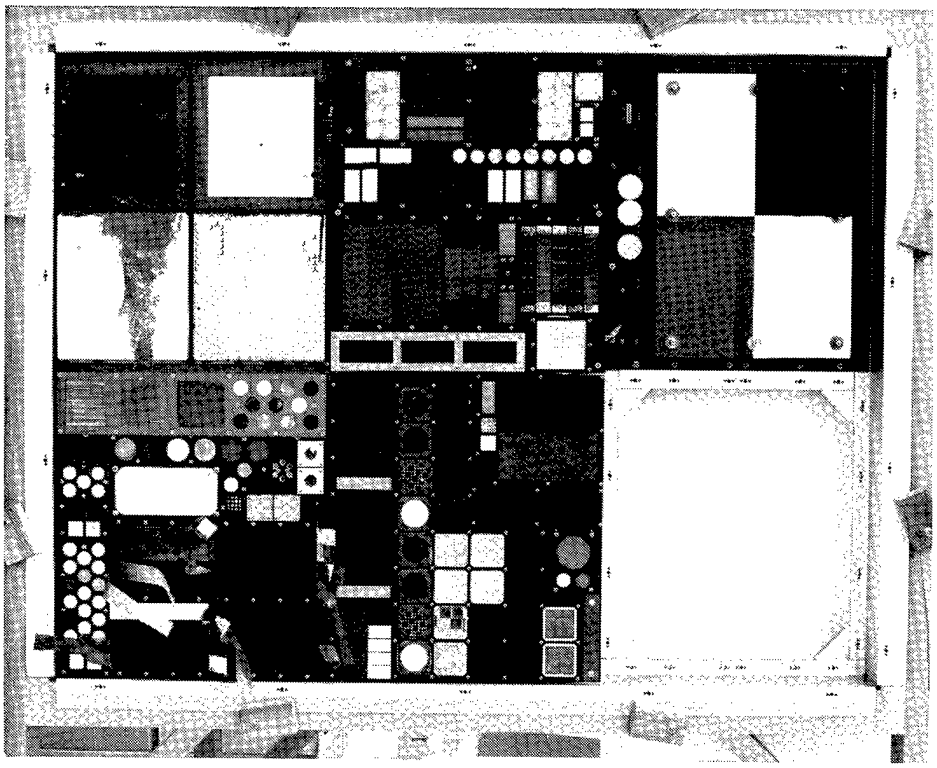


Figure 10. D9 tray postflight, before M0003 deintegration, in tray-holding fixture

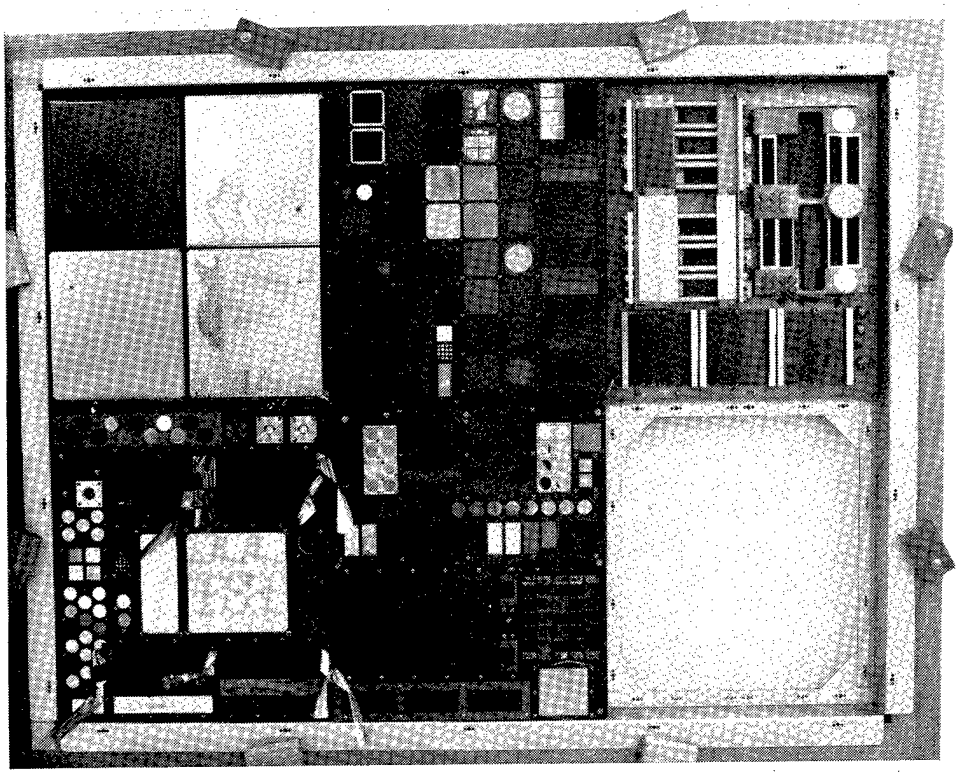


Figure 11. D3 tray postflight, before M0003 deintegration, in tray-holding fixture

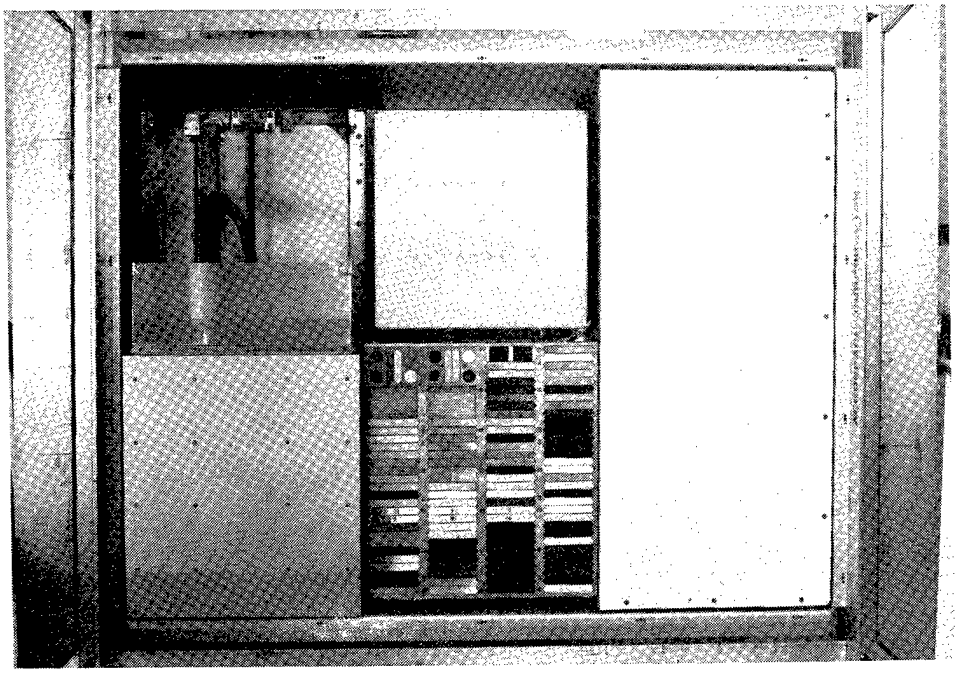


Figure 12. D8 tray postflight, before M0003 deintegration, in tray-holding fixture

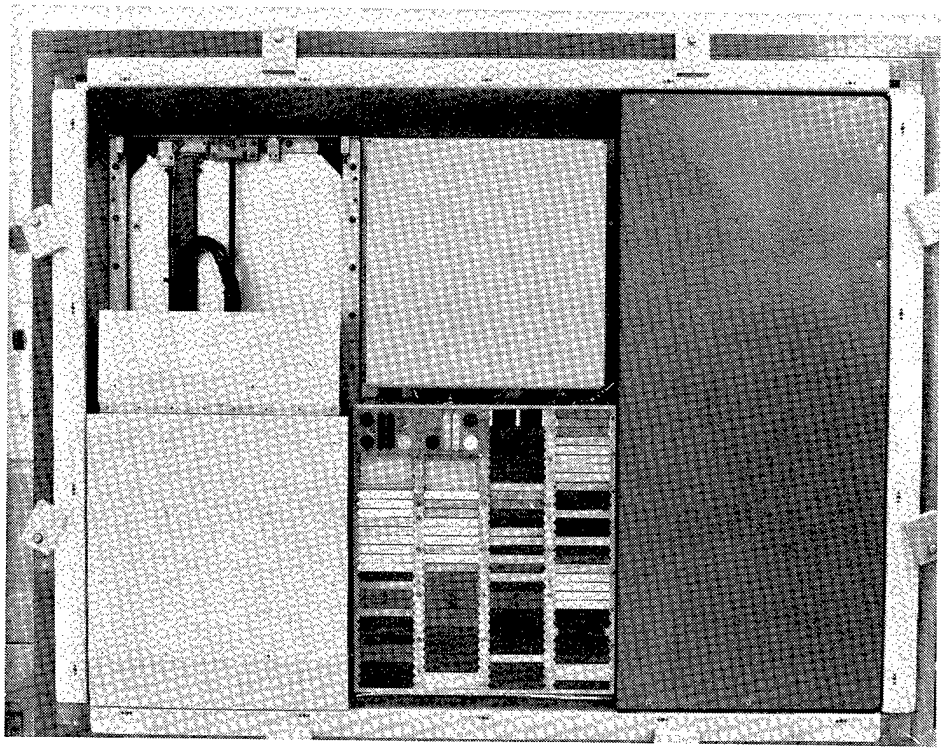


Figure 13. D4 tray postflight, before M0003 deintegration, in tray-holding fixture

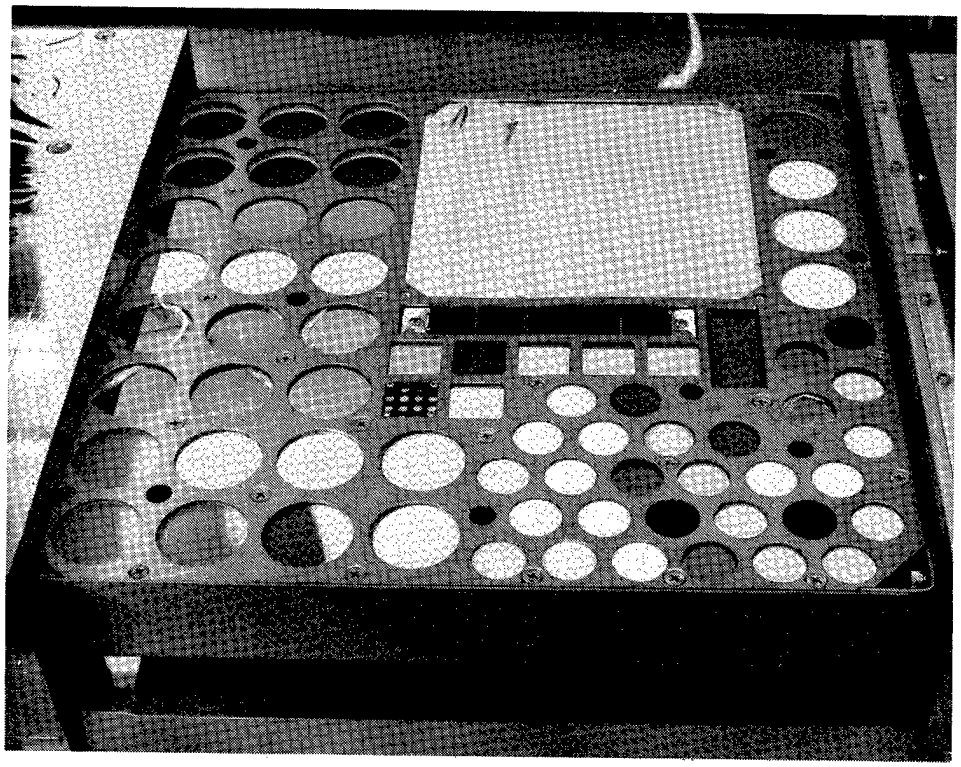


Figure 14. D8 (LE) canister in open position, postflight. The two rows to the left (top to bottom in photo) were exposed for 9 and 19 weeks, respectively. The remaining test articles were exposed for 40 weeks

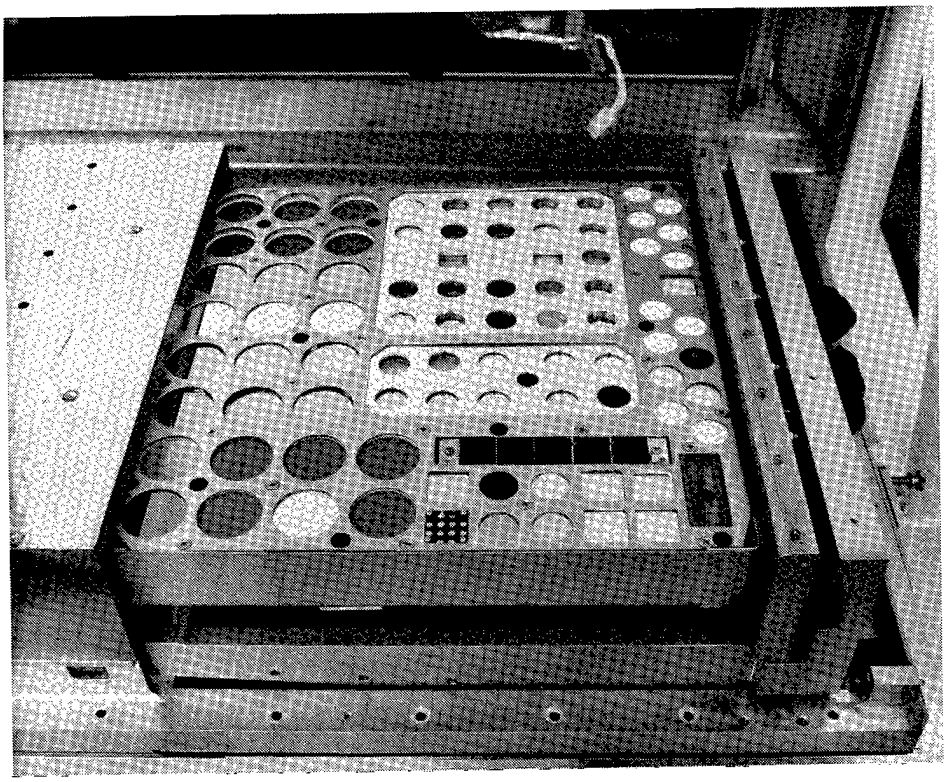


Figure 15. D4 (TE) canister in open position, postflight. Exposure was identical to that for D8 canister. Many, but not all test articles are duplicates of those flown on LE canister

Data Collection Timing

- **SCAN OFF period after initialization**
  - 2.333 hours
- **Data collection sequence**
  - 5 consecutive scans at 3.49 minute intervals
  - 32 intervals per sequence = 111.8 minutes
- **Time between sequences**
  - 93.16 hours
- **SCAN runs to end of tape**
  - approximately 429 days

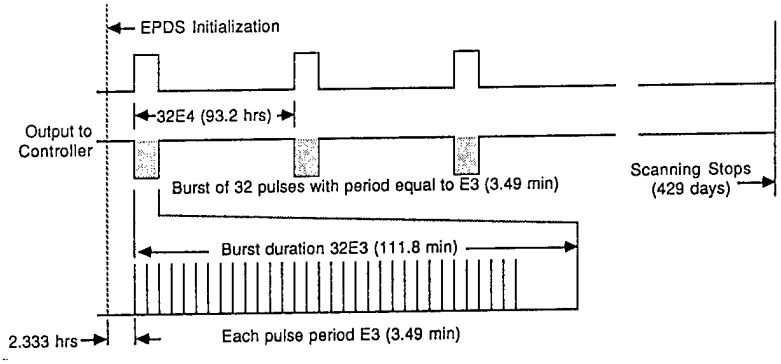


Figure 16. M0003 data collection sequence

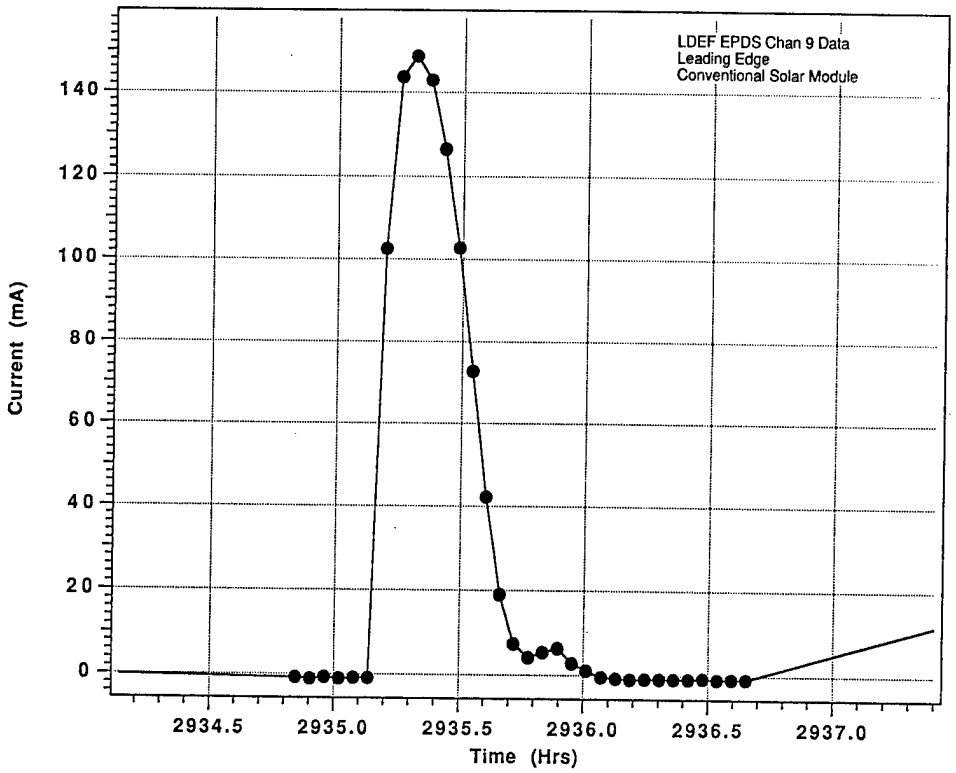


Figure 17. Typical orbital scan (111.8 min) data plot from conventional solar cell module

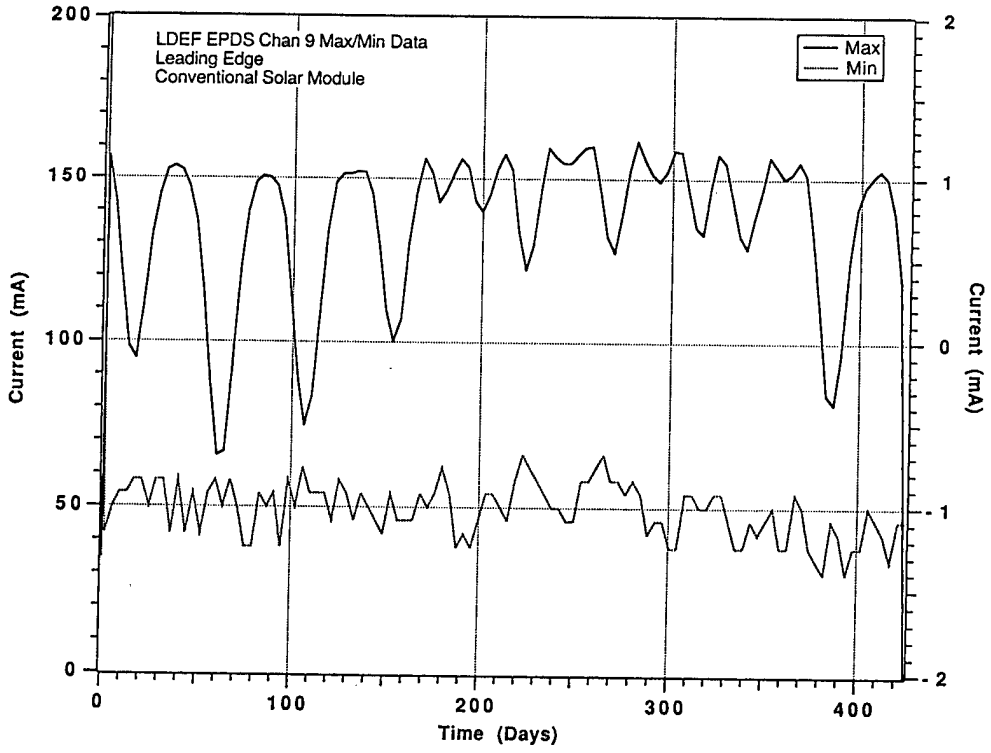


Figure 18. Min/max data plot for conventional solar cell data channel

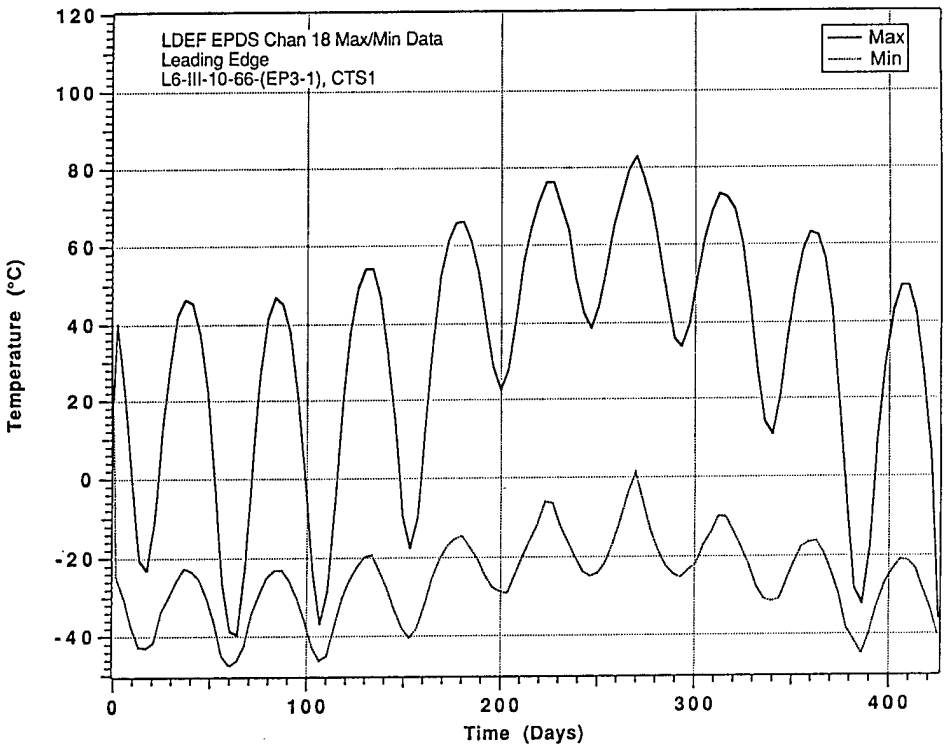


Figure 19. Min/max temperature plot for graphite-epoxy composite LE test article

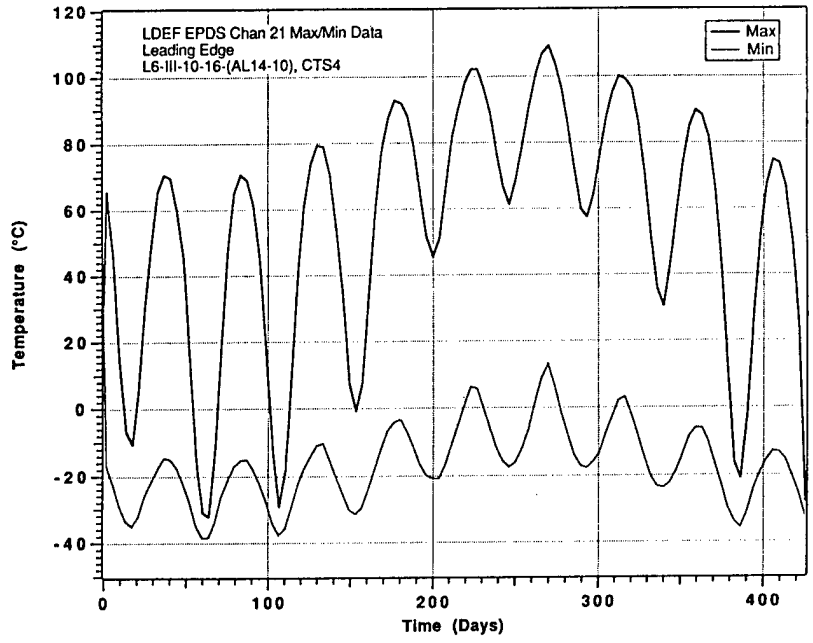


Figure 20. Min/max temperature plot for graphite aluminum composite LE test article

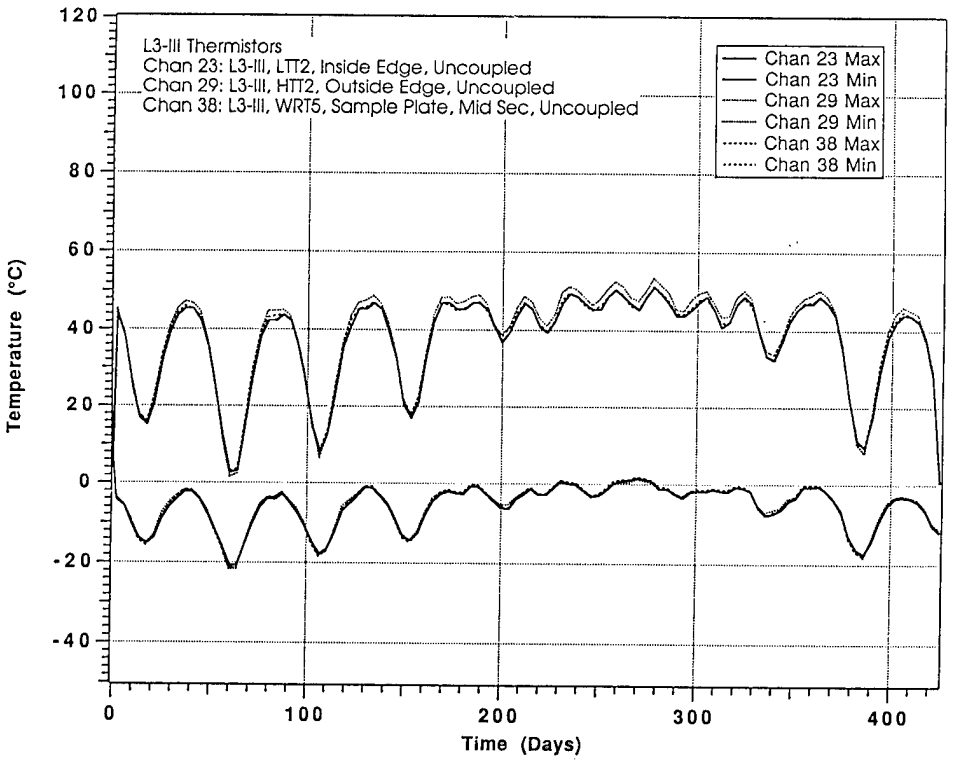


Figure 21. Thermal cycling plot for Module III on D9 (LE) tray

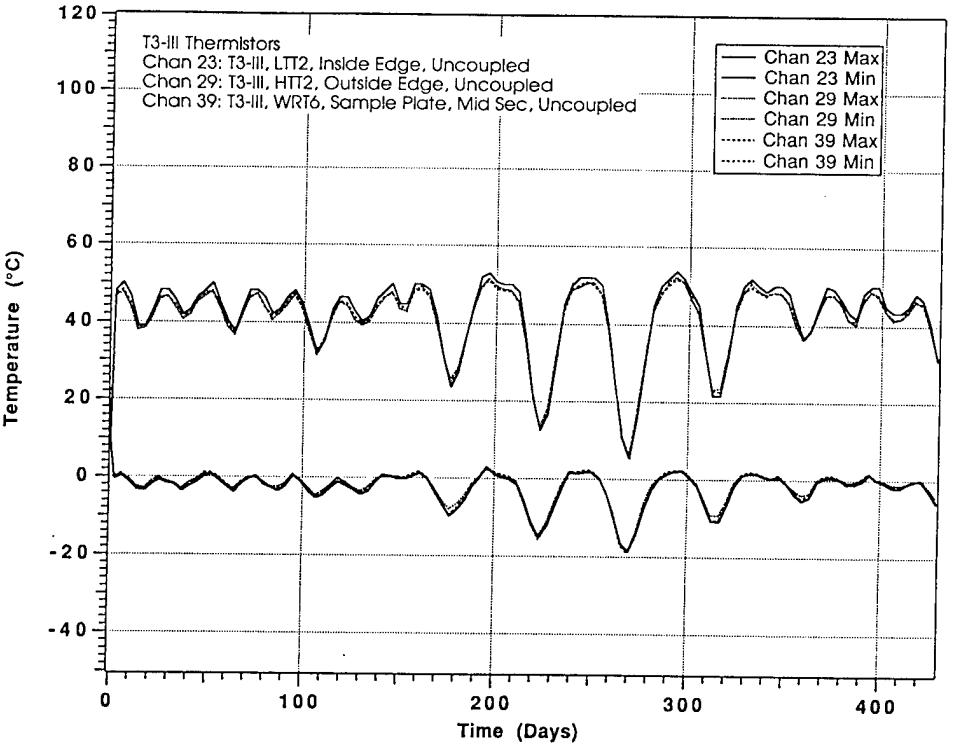


Figure 22. Thermal cycling plot for Module III on D3 (TE) tray

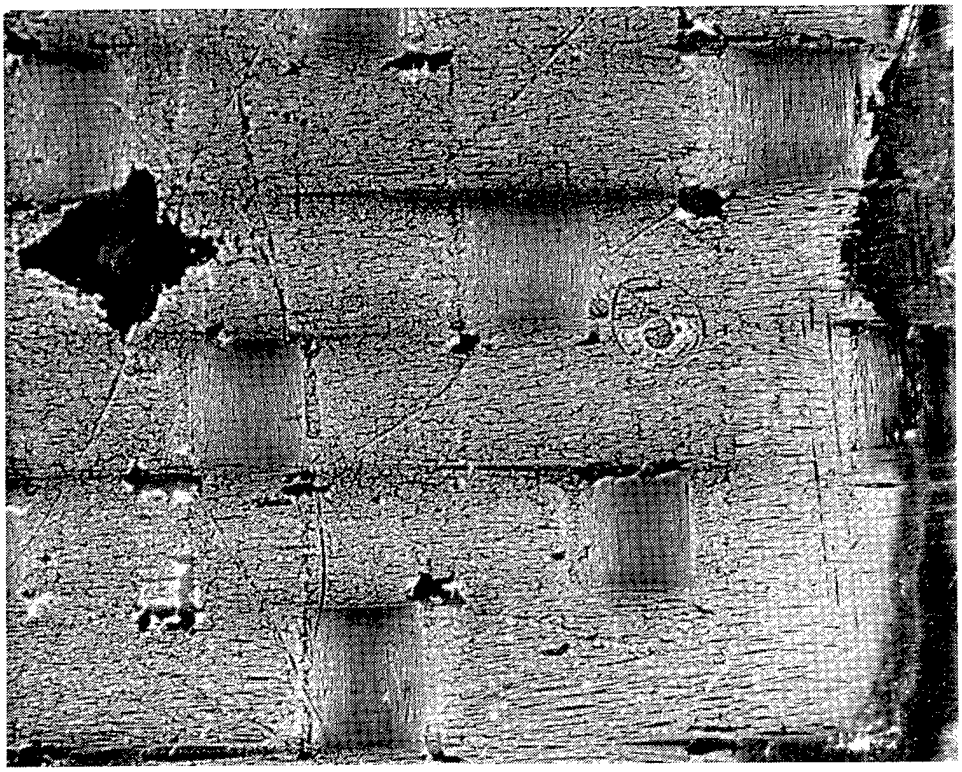


Figure 23. Atomic oxygen-eroded surface of graphite epoxy composite test article exposed on D9 (LE). Note enlargement of impact crater, upper left. Masked, unexposed surface is at right edge of photo

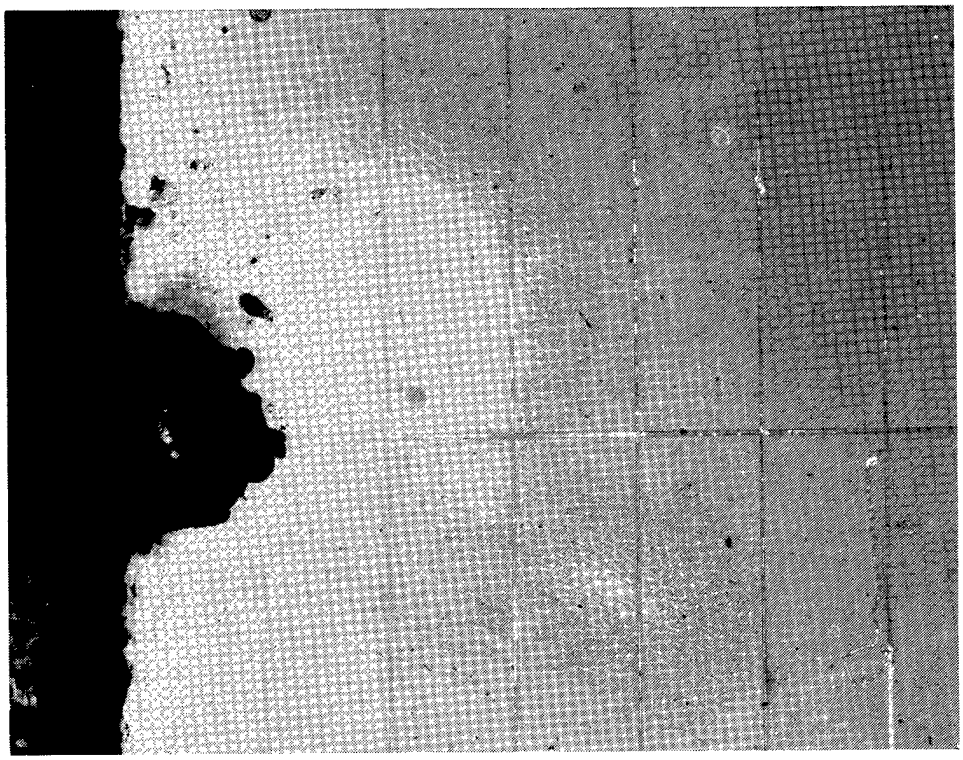


Figure 24. Localized delamination of cover glass near silver weld on LE solar cell

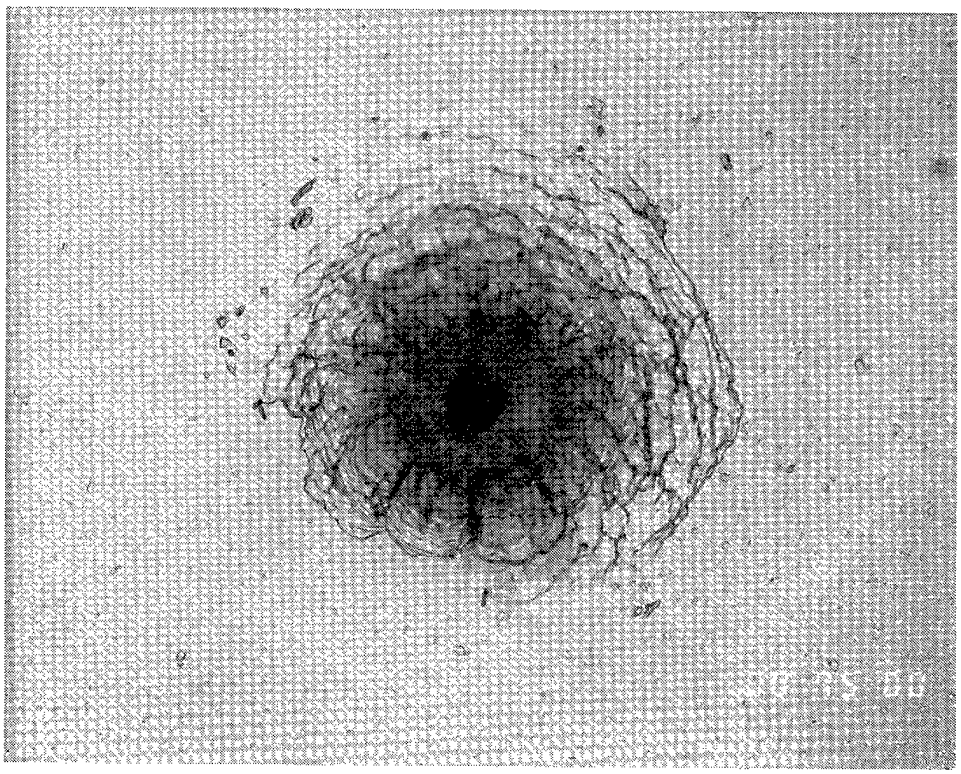


Figure 25. Typical micrometeoroid/debris damage in a solar cell cover glass

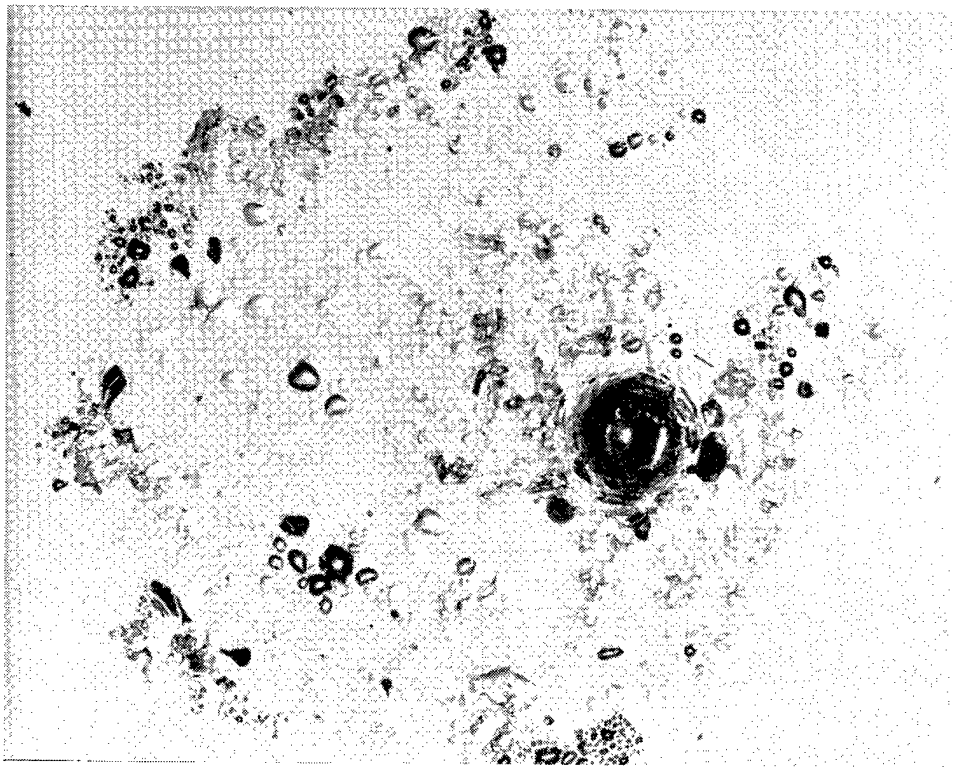


Figure 26. Blistered coating damage surrounding 1-mm dia. impact crater in LE ThF_4/Ag/Mo mirror test article

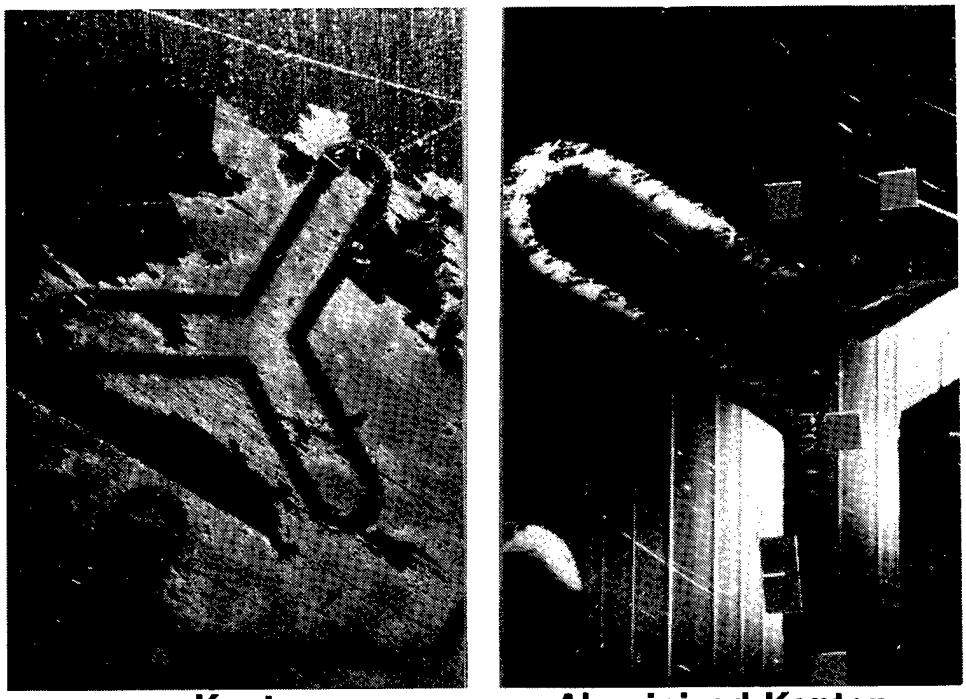


Figure 27. Atomic oxygen erosion of aluminized Kapton radar camouflage material. This produced significant debris which became scattered over many LDEF trays

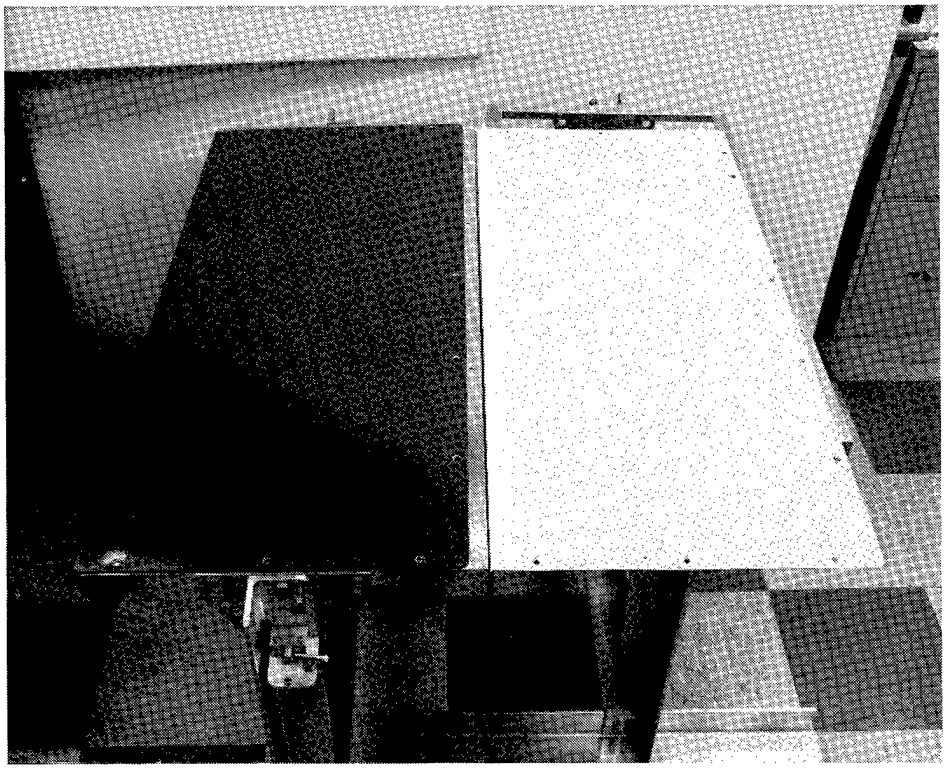


Figure 28. Chemglaze A276-painted sunshields flown on D4 (TE) on left and D8 (LE) on right

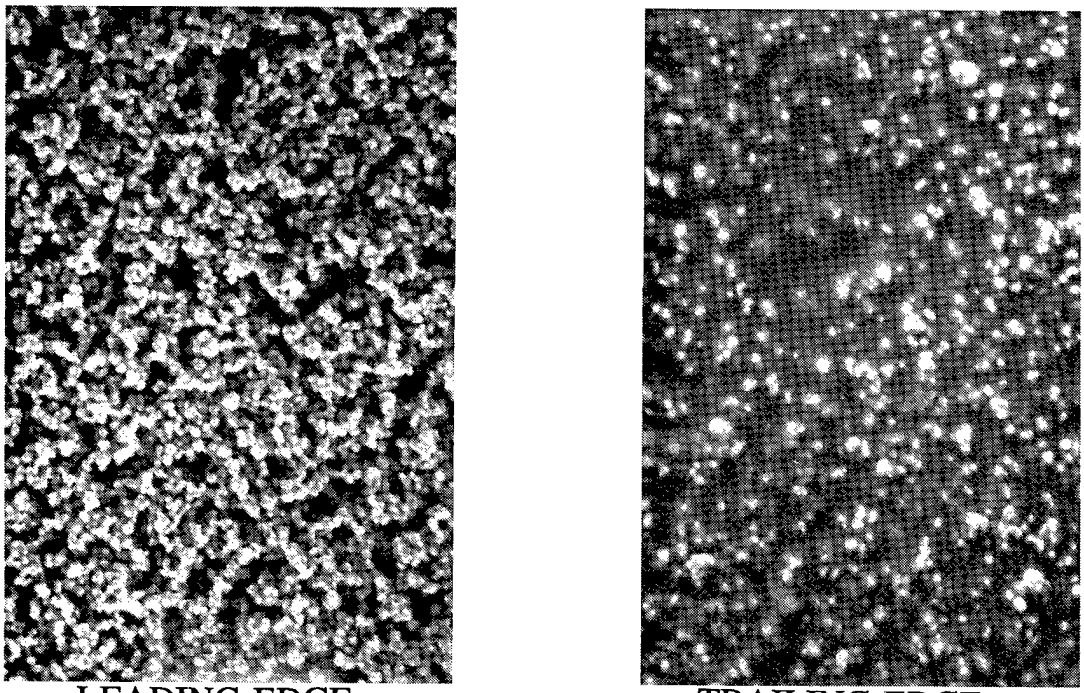


Figure 29. SEM micrographs of surface of Chemglaze A276 paint exposed on LE (left) and TE (right)

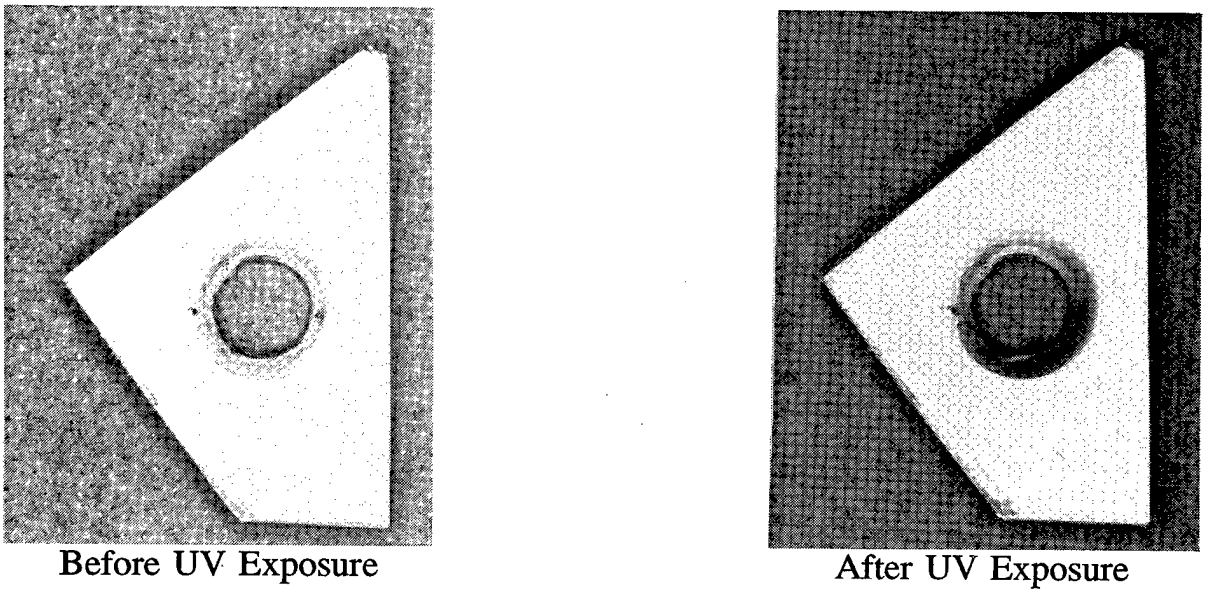


Figure 30. Response of protected Chemglaze A276 to UV radiation

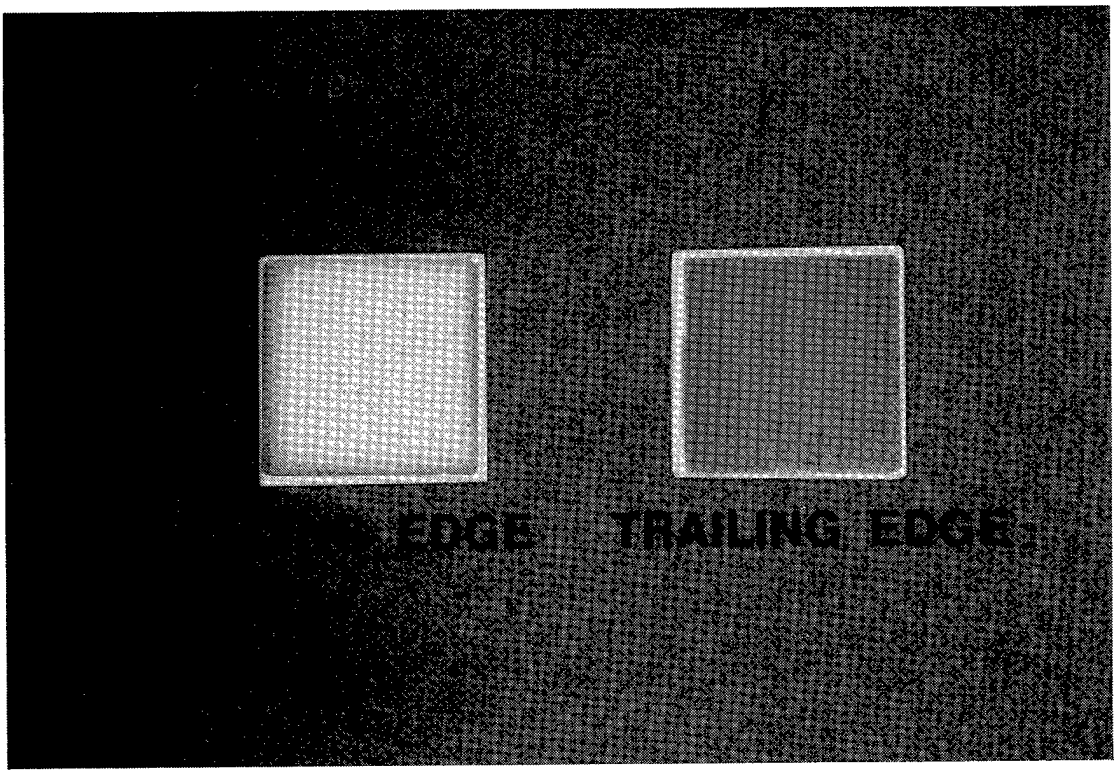


Figure 31. Side-by-side comparison of LE/TE S13GLO test articles

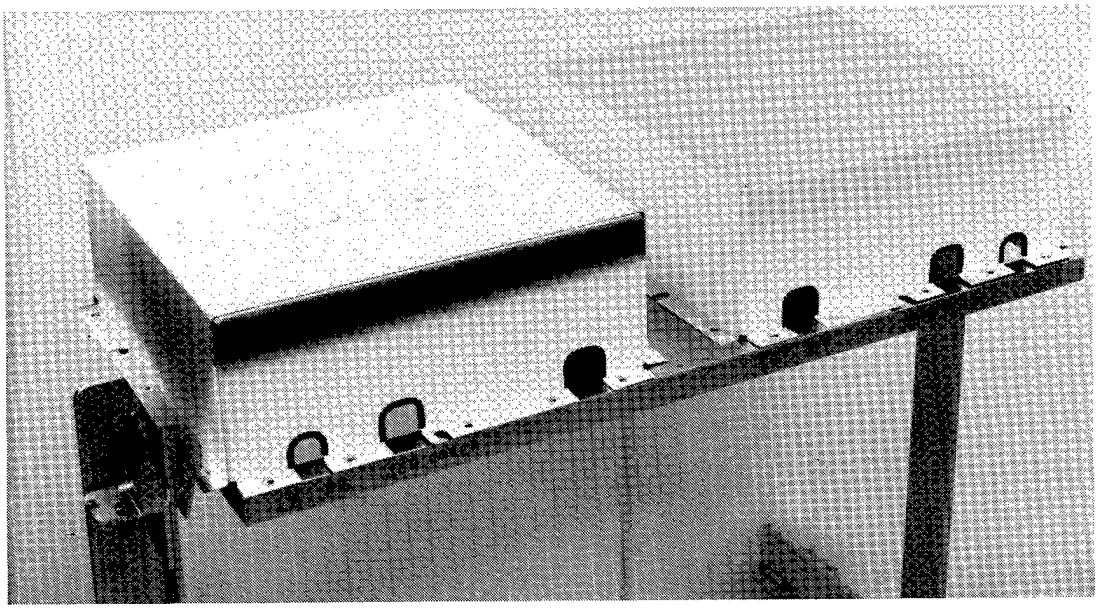


Figure 32. Signal conditioning unit (SCU) covers showing dramatic differences in damage from LE to TE. Note marked outgassing patterns on LE cover

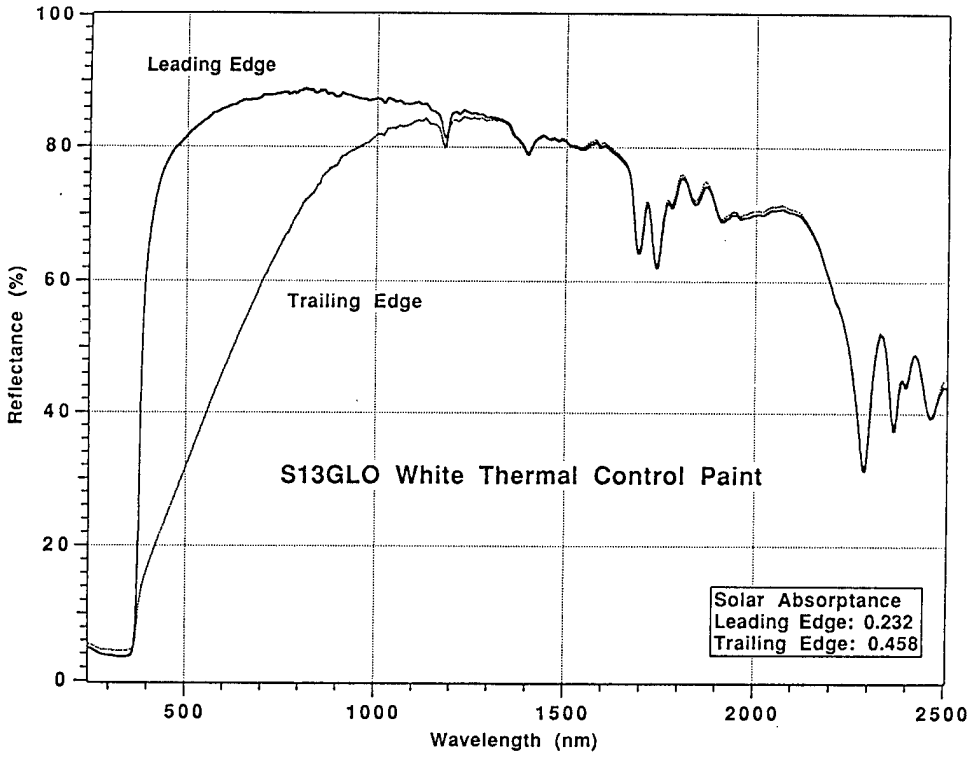


Figure 33. Reflectance curves for S13GLO

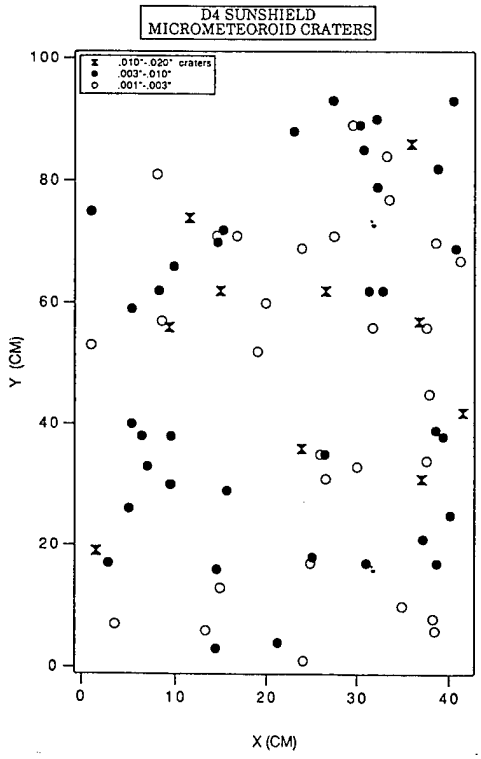


Figure 34. Micrometeroid/debris impacts on TE EPDS sunshield

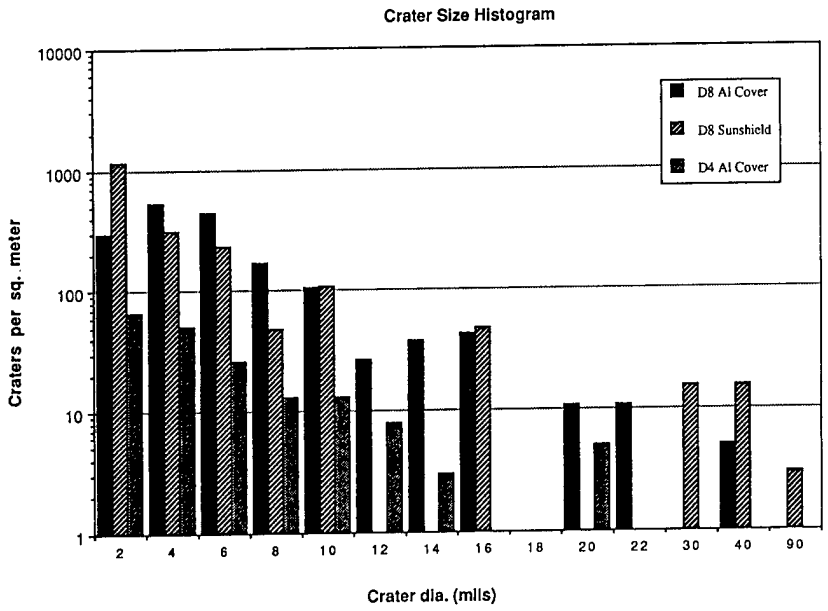


Figure 35. Histogram depicting micrometeroid/debris counts for various D4/D8 surfaces

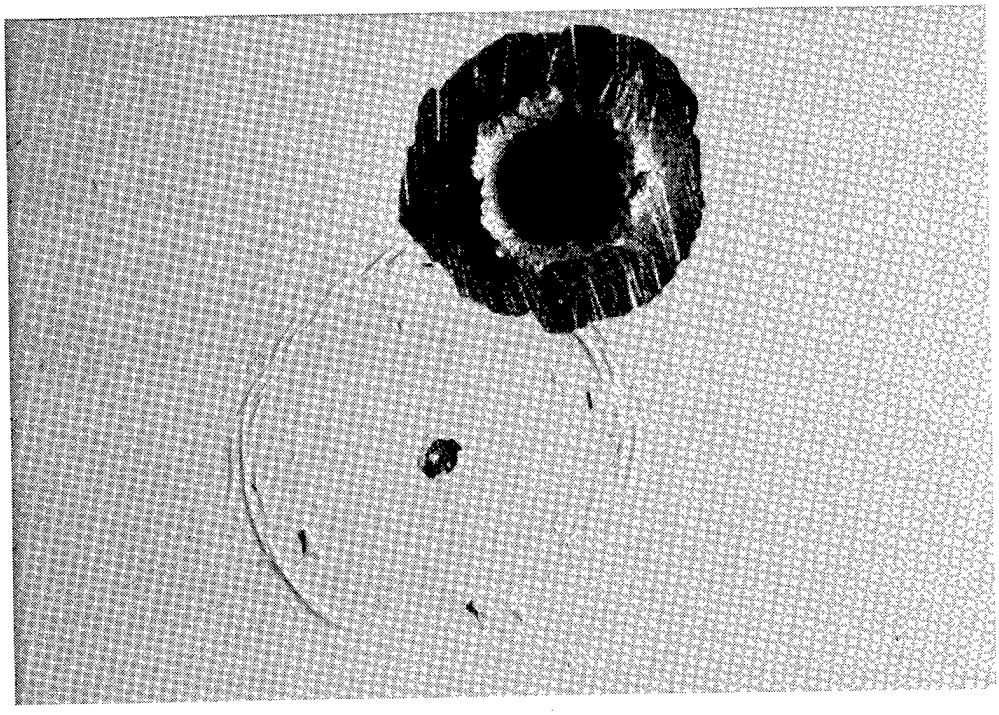


Figure 36. Puncture and impact crater in Chemglaze A276-painted EPDS sunshield on LE. The 2.5 mm dia. puncture is through 80 mil aluminum. Smaller impact is surrounded by zone of ruptured, eroded coating

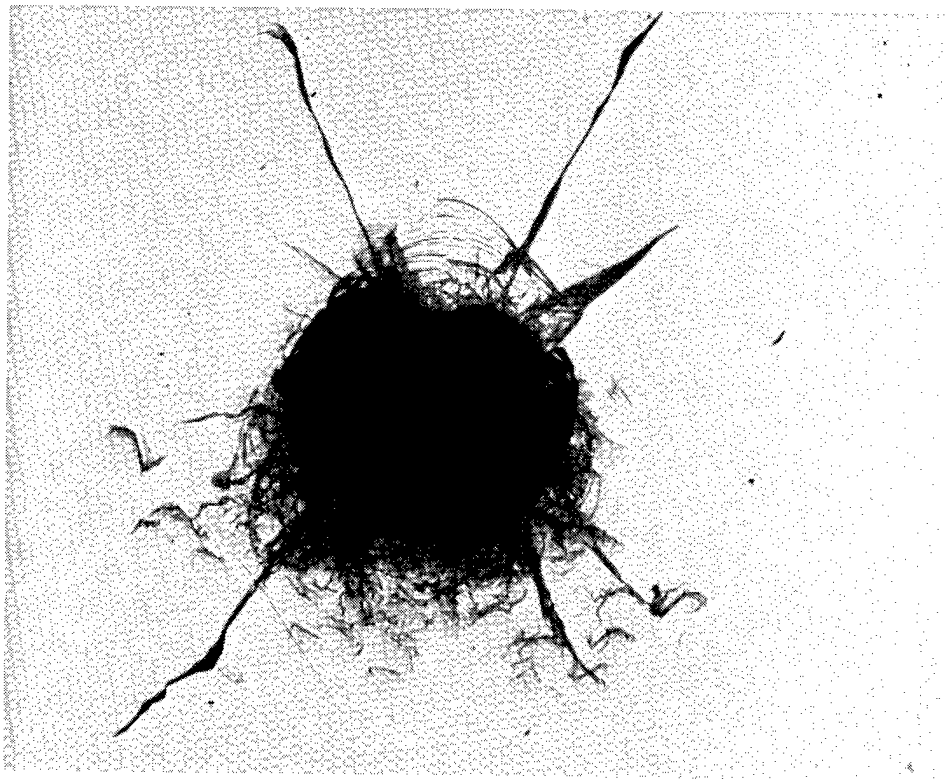


Figure 37. Impact crater (1.25 mm dia.) in glass test article

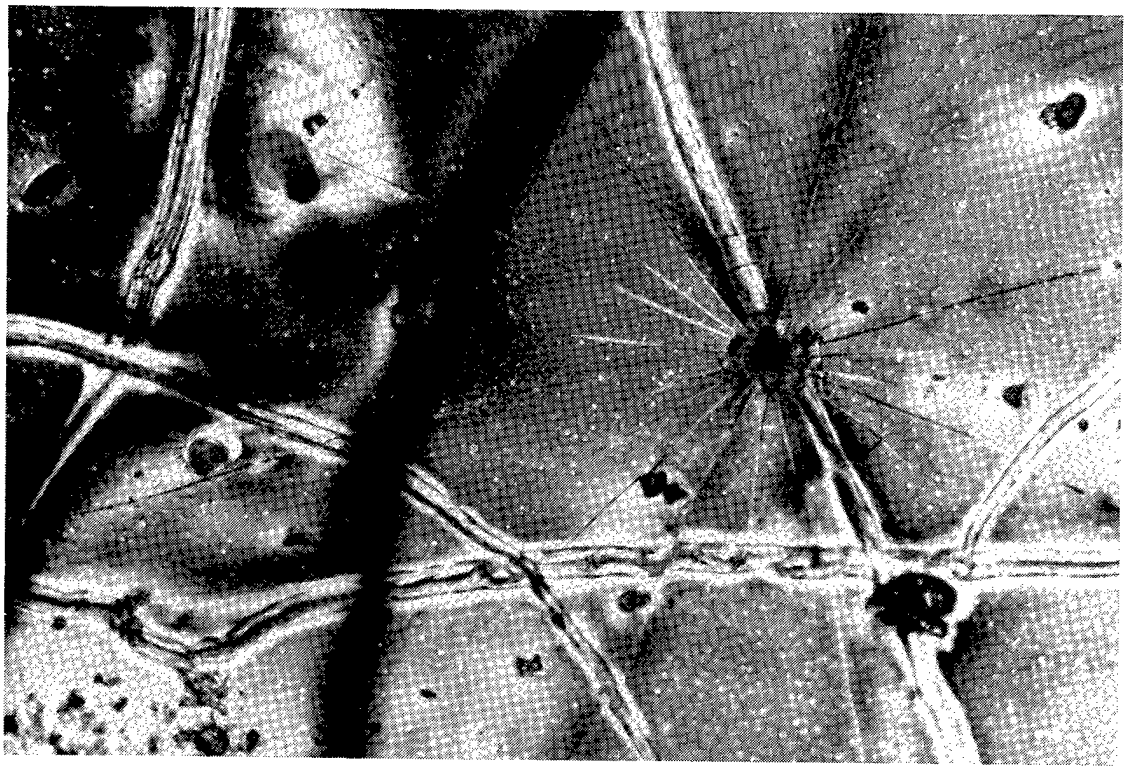


Figure 38. Hypervelocity impact on embrittled surface of vacuum-distilled black RTV 602

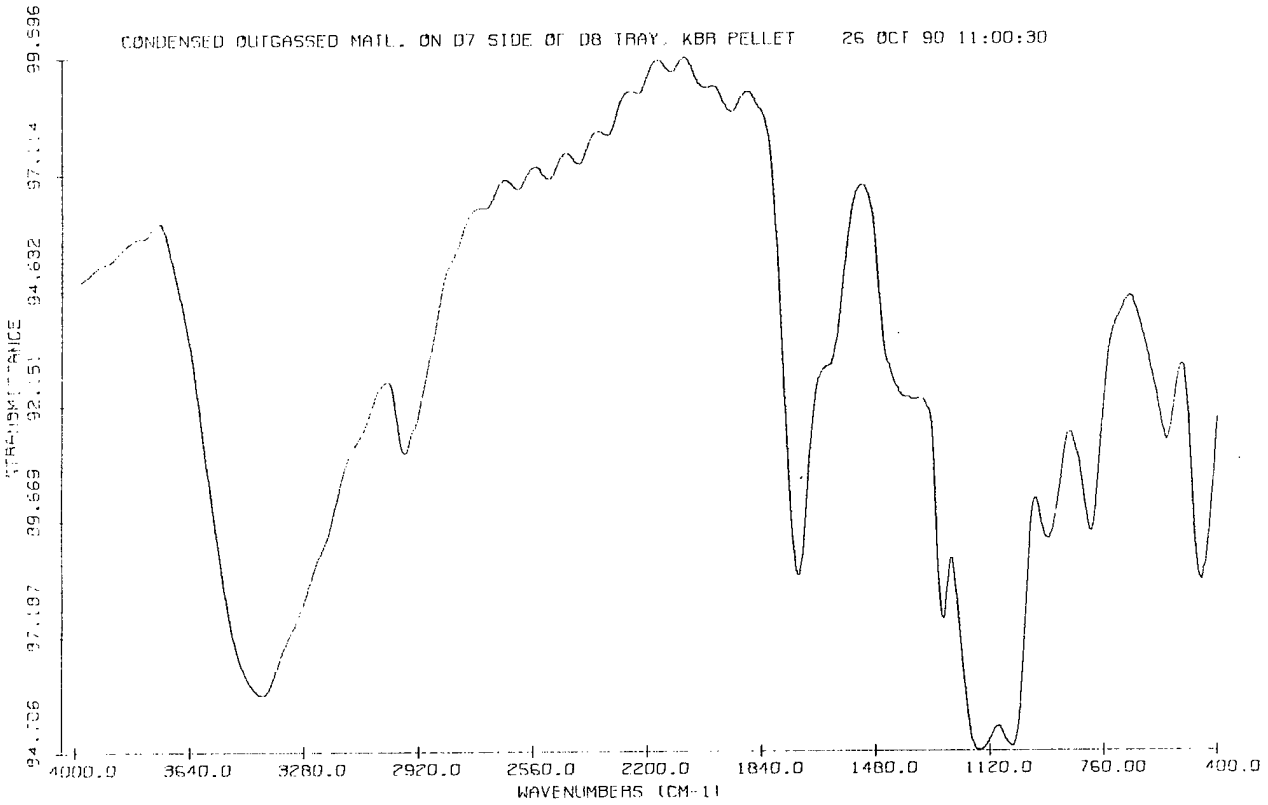


Figure 39. FTIR spectrum of varnish-like deposit on LE (D8) tray

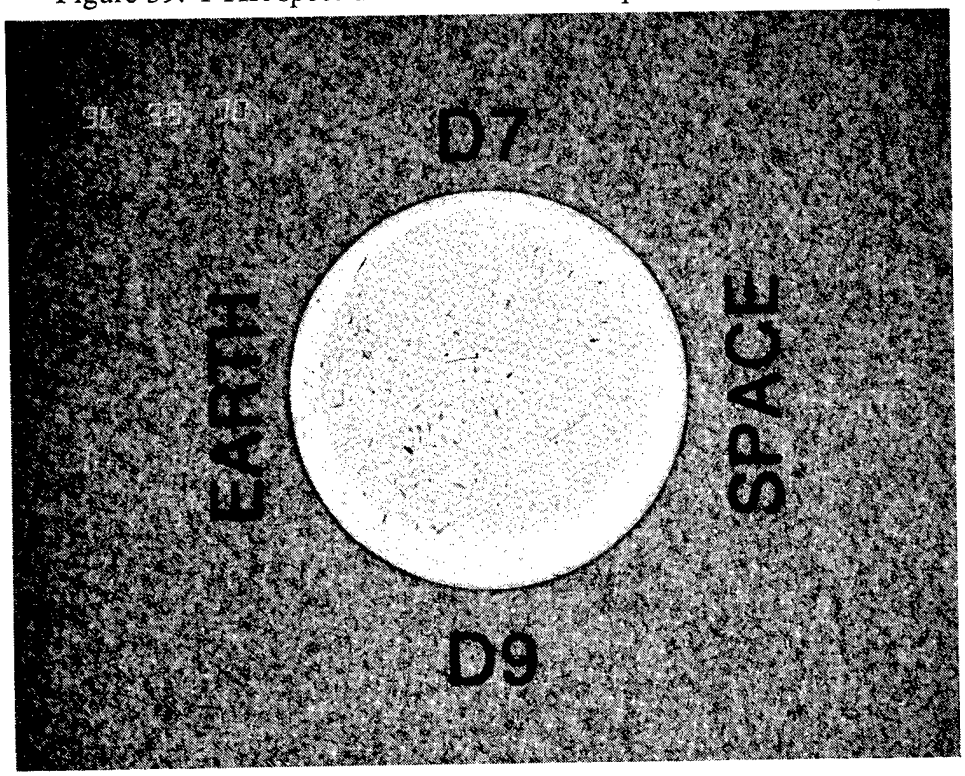


Figure 40. Debris contamination adhered to surface of 1.5 in. dia. silicone-based white paint test article exposed for 40 weeks in the TE (D8) canister

SURVEY OF RESULTS FROM THE BOEING MODULES ON THE M0003 EXPERIMENT ON LDEF

H. G. Pippin
Boeing Defense & Space Group
Seattle, WA 98124-2499
Phone: 206/773-2846, Fax: 206/773-4946

Owen Mulkey, Juris Verzemnieks, Emmett Miller,
Sylvester Hill and Harry Dursch
Boeing Defense and Space Group
Seattle, Washington 98124-2499
Phone: 206/773-0527, Fax: 206/773-4946

The Boeing Company provided specimens to be flown on the Long Duration Exposure Facility (LDEF) as part of the M0003 experiment. This hardware was for the M0003-8 and part of the M003-10 sub-experiments.

Our specimens were flown on the leading (tray D-9) and trailing (tray D3) edges, and on trays D-8 (38° from ram) and D-4. Some specimens were mounted in the Experiment Exposure Control Canisters.

Figure 1 shows a photo of tray D-9 taken on orbit. The failure of the hardware in one module and subsequent distribution of aluminum pieces onto adjacent hardware, including a number of our composite specimens, clearly is shown. It also shows that our solar cells had become detached during flight. The likely cause was failure of the adhesive, but the mechanism is not known. The effects of the aluminum flakes are to block the surface underneath from atomic oxygen and solar radiation, limiting recession of these materials. Since the absorptance/emissivity ratio for aluminum can easily range from 2.5 to 5, the potential exists for localized heating of small areas. However, the bulk temperature is probably little effected because the individual aluminum flakes are relatively small. The exposure time of the debris on our hardware is unknown. Figure 2 shows tray D-9 as it appeared subsequent to removal from LDEF in the SAEF-II building at KSC. The aluminum debris visible in the photo of figure 1 is not present in figure 2. This material was redistributed during the retrieval or re-entry operations.

Figure 3 is an on orbit photo of tray D3. Some Boeing composite specimens on tray D4 are also visible. The solar cells from this tray are also gone.

Composite hardware flown on our portion of the M0003 experiment include strips of five types of composites; LaRC 160 polyimide/graphite, 934/T300, 3501-6 epoxy/AS fibers, PMR15/C6000, and P1700/T300 composite specimens under compression, tensile, and flexure loads, lap shear specimens and a large T300/934 plate on the leading edge, one quarter coated with A-276 white polyurethane paint, one quarter coated with Z-306 black polyurethane paint, one quarter coated with Desoto white thermal control paint, and one quarter uncoated.

An active fiber optics experiment and a large quantity of electronic piece parts were flown on tray D-9. These items were inside an aluminum box and not directly exposed to the LEO environment. A thermocouple inside the fiber optics experiment compartment showed very benign thermal cycling. The results of our fiber optics experiment and analysis of the condition of our composite specimens are discussed in detail in separate papers.

Other hardware included anodized cadmium plated washers and fasteners, solid thin film lubricants, adhesive tape, three rod end bearings, several reaction bonded silicon nitride specimens, and one polished aluminum and one sulfuric acid anodized aluminum disc.

The fourteen solid thin film lubricant specimens include three types of material, Vespel SP1, Everlube 620C, and Lubribond A. These specimens flew on the trailing edge directly exposed to the incident solar radiation. A puck and plate friction and wear device is being reassembled to test these specimens.

Three rod end bearings, Astro P/N ADNE43J, were also flown on the trailing edge module. Two of these bearings have been examined and tested by the manufacturer, New Hampshire Ball Bearings, Inc. No changes were observed in the oscillating load performance, pre-load torque or the liner peel strength of the flight specimens

relative to ground control specimens. The only observed difference between flight and ground control specimens was a major loss of the chromate treatment applied to the cadmium plating on the flight hardware. No loss of cadmium was apparent; and the possibility exists that the chromate layer was damaged in post flight handling. Our conclusion is that passive exposure to solar UV and thermal cycling on LDEF did not degrade the performance of these bearings.

This finding is in contrast to the observations on the fasteners used to hold the T300/934 composite panel on tray D-9. These fasteners were standard aerospace grade, cadmium plated per QQ-P-416 Type 11, class 2. Coating thickness measurements were made on four individual fasteners in 13 specific locations on the fastener head, under the fastener head, and in the shank area. These measurements indicate that the cadmium thickness currently (post-flight) meets specification, and that evaporative loss of cadmium is not observed. These fasteners were anodized prior to use and the anodize coating was still intact subsequent to the flight.

These fasteners had an anodize coating over the cadmium plating. An examination of the fastener surfaces under an optical microscope did not reveal any unusual features when compared to control specimens.

Two 6061 aluminum discs were mounted on the trailing edge module, one disc was polished and the other disc was sulfuric acid anodized. Measurements of pre-flight and post flight solar absorptance and thermal emittance of these materials has been carried out. Post flight results are reported in table 1 and are average values of three measurements. The thermal emittance valves for the polished aluminum are so low that the differences are not meaningful. Significant increases are observed in solar absorptance of the polished aluminum and thermal emissivity of the anodized specimen.

Seven samples of reaction bonded silicon nitride were flown on LDEF, two on D3, two on D9 and 3 in an experiment exposure control canister on D8. These materials were made of a low density foam core with a very thin, higher density "skin." As a result of their individual exposures, the weight, dimensions, and optical properties of these materials were virtually unchanged. The common silicone/hydrocarbon based contaminants observed on many locations are present and are oxidized on the leading edge specimens. The damage caused by impact events is less severe than for "full density" glass or ceramics. The porous nature of the foam served to localize the impact damage and it is difficult to tell where the impacts occurred without careful examination. This material survived the LEO environments with negligible changes.

The examination of our fiber optics experiment, electrical piece parts, rod end bearings, and silicon nitride foam has been completed. Work is continuing on our composites, thermal control coatings, adhesives, solid thin film lubricants and fasteners. Results will be presented at the next LDEF post retrieval symposium.

The authors gratefully acknowledge the support of the Space Environment Effects Program through Wright Laboratories of Wright Patterson AFB and The Boeing Company for providing the resources and support to allow this work to be carried out.

Table 1. Optical Properties of Aluminum Discs From LDEF Tray D3.

SPECIMEN	PREFLIGHT		POSTFLIGHT	
	ABSORPTANCE	EMITTANCE	ABSORPTANCE	EMITTANCE
Sulfuric Acid Anodized BAC 5022, Grade B	0.40	0.75	0.42	0.84
Polished	0.15	0.06	0.25	0.03

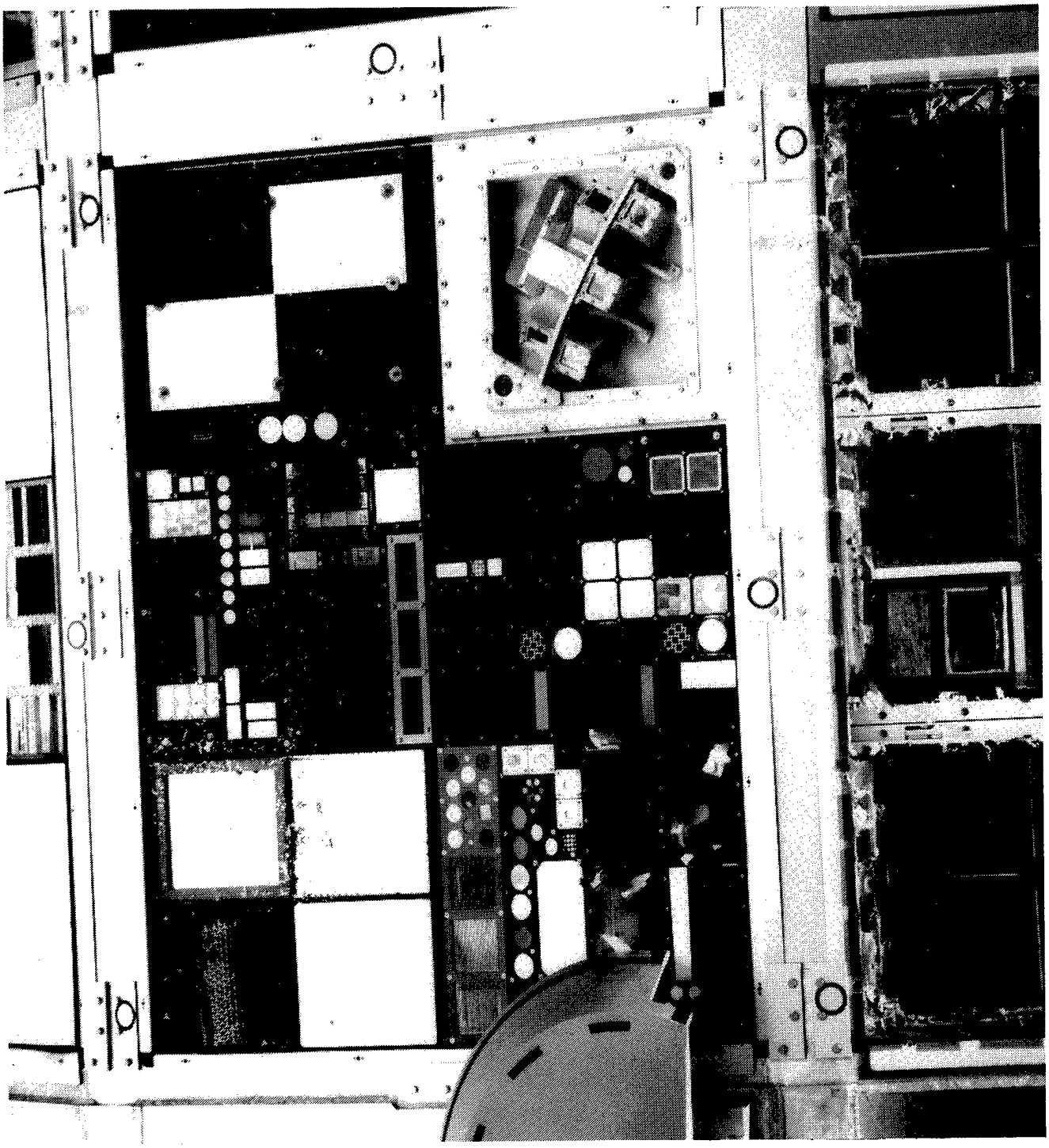


FIGURE 1 On-Orbit Photograph of Tray D-9 From The Leading Edge of LDEF

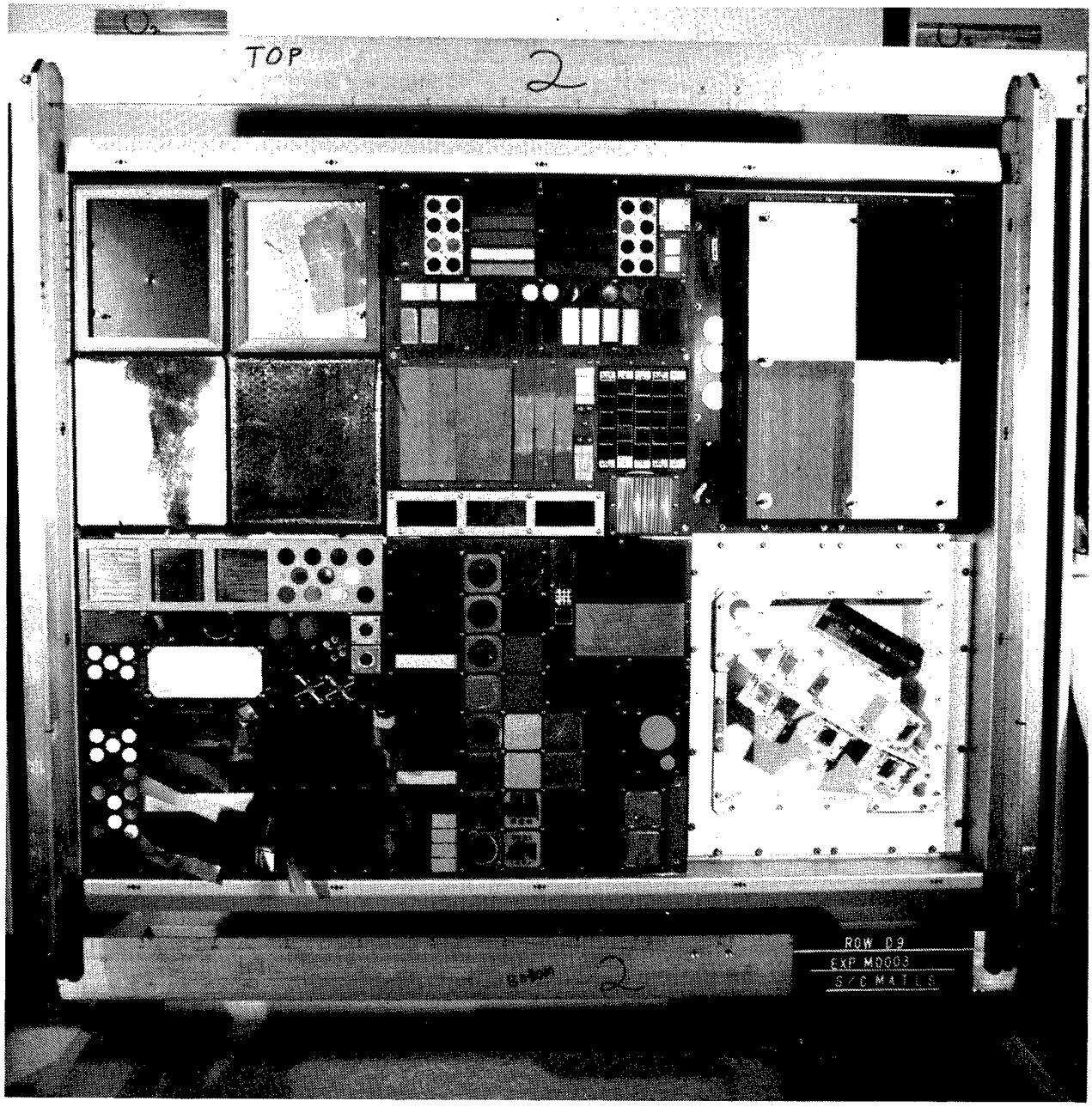


FIGURE 2 Photograph of Tray D-9 After Removal From LDEF at Kennedy Space Center

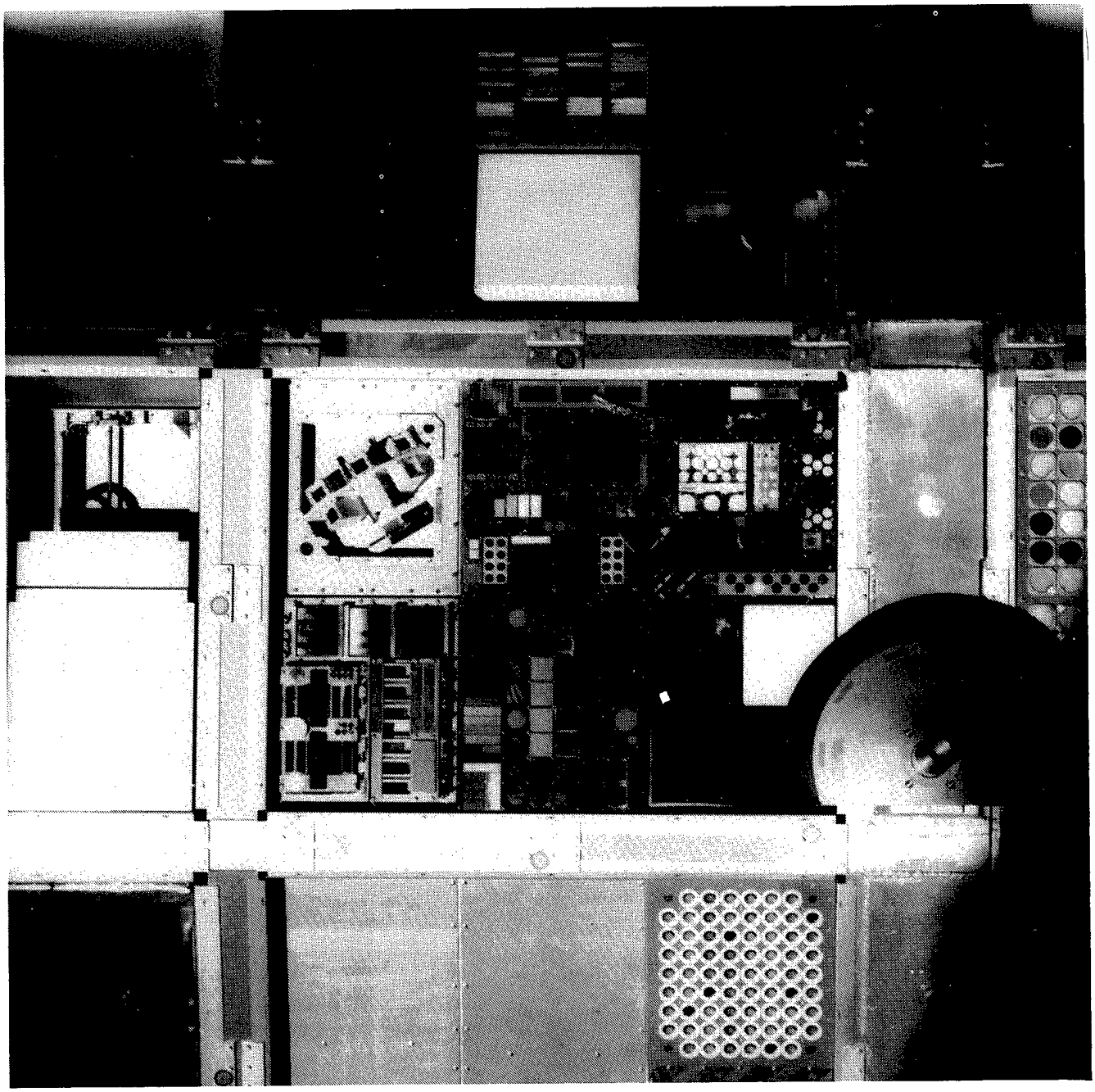


FIGURE 3 On-Orbit Photograph of Tray D-3 From the Trailing Edge of LDEF

RESULTS FROM ANALYSIS OF BOEING COMPOSITE SPECIMENS FLOWN ON LDEF EXPERIMENT M0003*

Pete E. George
Boeing Defense and Space Group
Seattle, Wa 98124-2499 M/S 73-09
Phone: 206/234-2679, Fax: 206/237-0052

Sylvester G. Hill
Boeing Defense and Space Group
Seattle, Wa 98124-2499 M/S 82-32
Phone: 206/773-2767, Fax: 206/773-4969

SUMMARY

Specimens of three organic matrix/ graphite fiber reinforced composites were flown at both the leading and trailing edge locations on the Long Duration Exposure Facility (LDEF). Selected specimens flown at the trailing edge position were held under tension, compression and flexure loads for the duration of the flight. Also, two epoxy adhesives with composite and metallic adherends were flown at the trailing edge position.

These specimens experienced 5.8 years of exposure to the low earth orbit (LEO) environment where they were subjected to atomic oxygen (AO), thermal cycling, ultraviolet (UV) light, and particulate radiation. Post flight mechanical, chemical, optical, and physical tests were performed and the results are compared here to preflight and published values.

AO erosion of the leading edge specimens resulted in a significant reduction of mechanical properties and a change in optical properties. Chemical changes occurred only on the surface.

INTRODUCTION

LDEF was deployed on April 7, 1984 and retrieved on January 12, 1990. The extended mission duration resulted in a higher fluence of AO along with an increased number of solar exposure hours relative to planned exposures. A summary of the exposure environment for experiment M0003-8 on board LDEF is given in Table I (ref. 1). The positions of our specimens relative to the velocity vector and earth are shown in Figure I. Due to M0003-8 positions on LDEF and the satellite's orbit , the leading and trailing edge specimens received essentially equivalent UV exposure. Leading edge specimens were also exposed to AO while trailing edge specimens were shielded by the satellite.

The intent of this paper is to report test results for the Boeing M0003-8 composite and adhesive specimens and discuss the implications for future earth and space based testing and space material selection.

*Work done under NAS 1-18224, Task 12

EXPERIMENT DESCRIPTION

The specimens flew on board LDEF at positions D9 (leading edge) and D3 (trailing edge) as shown in Figure I. 934 epoxy/T-300 graphite, P1700 polysulfone/T-300 graphite and PMR 15 polyimide/C6000 graphite were selected for exposure. The composite specimens were configured as 3"x6" flat panels located at positions D9 and D3. A set of preflight thermal cycled 934 epoxy/T-300 graphite panels were also flown at positions D3 and D9.

Additional composite specimens of the three material types mentioned above were flown at the trailing edge position D3. These specimens were configured as tensile, compression and flexure test coupons and were held in stress during the flight using preload fixtures adjusted to maintain a predetermined level of strain. Table II summarizes the composite materials flown on board LDEF M0003-8.

EC 2216 (BMS 5-92) and AF 143 (BMS 5-104) epoxy adhesive lap shear specimens were flown at the trailing edge D3 position. Both titanium-composite and composite-composite adherends were evaluated. The composite adherends were 934 epoxy/T-300 graphite.

The specimens described above were subjected to a series of chemical, physical, mechanical and optical tests. The results are compared to preflight values and/or values taken from LDEF specimen surfaces which were shielded from AO and UV exposure.

TEST METHODS

Optical Test Methods

Both exposed (facing away from satellite) and shielded (facing towards satellite) surfaces of the 3"x6" composite panels were tested for optical absorption and emissivity. Absorption testing was performed with a Perkin Elmer Lamda 9 UV/visible spectrometer with an integrating sphere per ASTM E424A. Emittance measurements were made with a Gier-Dunkle DB/100 infrared reflectometer per ASTM E-408A.

Chemical Test Methods

Infrared (IR) spectroscopy was performed for samples taken from both exposed (facing away from satellite) and shielded (facing towards satellite) surfaces of the 3" x6" composite panels. A Bio Rad Digilab FTS-60 Forier Transform IR spectrometer equipped with a UMA 300A IR microscope was used to make the measurements.

Elemental analysis of leading and trailing edge exposed and shielded surfaces was performed by X-ray photoelectron spectroscopy using a Surface Science Instruments M-probe model 2703.

Physical Tests

Glass transition temperatures were measured for leading and trailing edge 3"x6" panels by dynamic mechanical analysis (DMA). A Perkin Elmer DMA 7 system was used in three point bending mode at 1 Hz with a 3°C/min heating ramp rate. Storage modulus (G') transition temperature values are reported.

Thermal expansion coefficients were measured in the 0° direction using a Netzsch model 402 diletometer. Thermo mechanical analysis (TMA) was used for through thickness measurement of thermal expansion coefficients using a Perkin Elmer TMA 7 system.

Total mass loss (TML) and volatile condensible materials (VCM) measurements were made using the NASA-SP-R-0022A outgassing test. The test samples were held at 125°C and the collection plate at 25°C for 24 hours at 10^{-6} torr.

Surface recession due to AO erosion was measured by optical micrography of polished cross sections. Dye penetrant techniques were used with the same cross sections for microcrack investigation. Thin section microscopy using phase contrast (PC) and differential interference contrast (DIC) techniques was used to examine specimens for resin phase changes and resin degradation.

Mechanical Tests

Tensile and compression tests were performed per ASTM D695 and D638 respectively using an MTS 50KIPS servohydraulic test machine with a specimen mounted 1.00" extensometer. A crosshead speed of 0.05"/minute was maintained until failure. Modulus values were taken from the first linear portion of the curve. The tests were performed at room temperature.

Three point flexure testing was performed per ASTM D790 using an Instron model TT-D equipped with a deflectometer. A cross head speed of 0.1"/minute and a 21T span to depth ratio were used. Tests were performed at 600°F for the polyimide and 350°F for the epoxy and polysulfone as well as room temperature for all three.

Residual stress for the prestressed tension and compression specimens was measured with a 1.00" extensometer during relief of the load. For the prestressed flexure specimens, the amount of deflection at the center of the specimen was measured before and after removal from the mounting fixture.

TEST RESULTS

Optical Properties

Table III lists the pre and post flight optical absorption and emittance properties for the 3"x6" composite panels flown on M0003-8. Calculated absorption to emittance ratios are also presented in Table III. Significant increases in emittances were found for the leading edge exposed surfaces. Absorption values varied only a few hundredths compared to pre flight values with the exception of the PMR 15 polyimide leading edge exposed surface which displayed a very high 0.98 absorption value. The 934 epoxy and P1700 polysulfone leading edge exposed specimens both had a grey/white tint to their predominantly black surfaces while the PMR 15 polyimide leading edge exposed specimen was a very dark flat black color.

Chemical Properties

Infrared spectra for the leading edge exposed surfaces are presented in Figures II through IV along with IR spectra taken from the shielded backside surface of each panel. The data shows the lack of resin on the exposed surfaces of the 934 epoxy/T300 graphite and the P1700 polysulfone/T300 graphite specimens. This phenomenon has been observed by others for LDEF flown epoxy/graphite composites (ref. 2). The PMR 15 polyimide/C6000 graphite spectra for exposed vs unexposed does not show the same elimination of absorption peaks as the other two materials. The remaining absorption peak for the epoxy and polysulfone composites is around the 1100-1150 wave number region. This matches the spectra of sodium sulfate (Figure V) quite well (ref. 3). Although this has not been confirmed by other techniques, both materials contain sulfur, 934 epoxy in the curing agent and P1700 polysulfone in the polymer backbone. Sulfate salts may be enriched on the surface of these materials as AO erodes the surrounding organic material. Scanning electron microscopy reveals a "residue" among the peaks and troughs of the polysulfone and epoxy specimens which is not present for the polyimide specimens (See Figures XVI through XVIII). This "residue" may be AO resistant sulfur containing compounds.

Surface analysis by x-ray photoelectron spectroscopy (XPS) revealed an increase in oxygen percentage and a decrease in carbon percentage going from unexposed to leading edge exposed surfaces for epoxy, polysulfone and polyimide composite materials. There was also the appearance or increase in silicon percentage on the exposed surfaces. Low levels of sodium were found on all exposed surfaces as well as sulfur on exposed epoxy and polysulfone surfaces. The appearance of silicon is consistent with the outgassing of unbaked sealants and coatings which flew on LDEF (ref. 4).

Physical Properties

Glass Transition Temperatures as measured by dynamic mechanical analysis (DMA) for leading edge (Row D9) and trailing edge (Row D3) composite specimens are given in Table IV. A typical DMA trace for these measurements is shown in Figure VI. Comparison of post flight values with published data shows little change in glass transition temperatures. Also, leading and trailing edge test results were similar. The differences are within the error associated with determination of inflection points and different test methods. The leading edge polysulfone measurement was unsuccessful due to specimen mounting problems.

Both pre and post flight data for thermal expansion properties of the LDEF M0003-8 composites are listed in Table V. Test orientation relative to the specimens is shown in Figure VII. The coefficients of thermal expansion (CTE) for the post flight specimens are similar to preflight values where available. Also, leading edge data is similar to that taken from trailing edge specimens. CTE's in the x direction for the 934 epoxy/T300 graphite unidirectional composites displayed some variation. However these differences are most likely due to the low CTE values and experimental error.

Total mass loss (TML) and volatile condensible materials (VCM)test results are given in Table VI. The results show no significant change in TML or VCM levels when compared to preflight data. Also, test results for the leading edge and trailing edge samples are similar. The lack of any significant levels of VCM and the fact that pre and post flight TML values are so close indicates that the majority of the weight loss during these tests is most likely water.

Pre and post flight cross sectional micrographs of the LDEF M0003-8 3"x6" composite specimens are shown in figures VIII through XV. Figures VIII, X, and XII are preflight photomicrographs taken from the same panels as the M0003-8 composite specimens flown on LDEF. Figures IX, XI, and XIII were taken from post flight leading edge exposed composites. Figure XIV shows an area of the polysulfone/graphite leading edge specimen at higher magnification. Figure XV shows the trailing edge polyimide/graphite specimen.

The epoxy specimens did not display any microcracking in preflight observations. The polysulfone and polyimide photomicrographs do reveal postflight microcracking which was not apparent in preflight photomicrographs. Some microcracking of these materials may have occurred during flight. However, the post flight inspections were more detailed and may have uncovered microcracks which were beyond the resolution of the preflight inspection.

Figures XI, XII and XIII also reveal the dramatic loss of material due to atomic oxygen (AO) erosion of the leading edge specimens. On the left hand side of these photo micrographs is a region of material which has been shielded from AO attack by the clamping frames which secured the specimens to the experiment tray. Using these areas as a reference plane, the amount of AO recession was measured and is presented in Figure XV. The jagged features found on the surface of these materials has been typical of leading edge exposed organic materials on LDEF. However the size of the jagged features for these graphite reinforced composites is 50-75μm verses 1-2μm reported for FEP and kapton (ref. 5).

Figure XIV reveals two interesting AO erosion phenomena of graphite reinforced polymer matrix composites. Microcracks extend into the composite from the bottom of three of the AO erosion troughs. We do not know if these cracks are a cause or effect. Also on the right side of the photomicrograph a column of resin developed as it was shielded by slower eroding graphite reinforcement.

Thin section micrography using phase contrast and differential interference contrast techniques was used to detect changes in refractive index of the matrix polymers. Regions of different refractive index indicate a change in resin chemistry or phase. The exposed surfaces of the trailing edge specimens displayed changes in refractive index up to 10μm deep for the polysulfone and up to 30μm deep for the epoxy and polyimide specimens. With all the specimens the refractive index change did not proceed any deeper where graphite fibers were present.

We suspect the refractive index changes indicate polymer degradation due to ultraviolet radiation exposure. This change is not present where graphite fibers have prevented penetration of UV radiation into the material. Also, the refractive index change is not detected on the leading edge where AO erosion would have removed UV degraded material .

Scanning electron microscopy (SEM) was used to examine the AO exposed composite surfaces. Figures XVI through XVIII show the epoxy, polysulfone and polyimide composites at 1000X respectively. The same rugged features found with optical microscopy are evident here also. However, the less obtrusive higher resolution SEM technique reveals a stringy frayed appearance at the tops of the jagged features on the 934 epoxy/T300 graphite SEM photomicrograph. The P1700 polysulfone/T300 graphite also has a similar characteristic with 1-2μm clumps around the peaks. The same rugged appearance for the PMR-15 polyimide/C6000 graphite material is devoid of these "clumps" and "strings" and has a relatively clean appearance. These "clumps" and "strings" may be responsible for the grey/white tint of the epoxy and polysulfone specimens discussed earlier. Conversely the lack of these features along with the rugged surface for the polyimide material may explain its deep flat black appearance. This residual material may be the cause of differences in optical properties, surface chemistry and recession rates.

Mechanical Test Results

Tensile, compression and some of the flexure coupons were held under load for the duration of the flight. Additional flexure specimens were trimmed from the 3"x6" flat panels which flew at both leading (Row D9) and trailing (Row D3) edge positions.

The preloaded tensile specimens were removed from the preload fixtures with an extensometer in place to measure any remaining strain (see figures XIX and XX). Post flight removal of the compression

coupons was performed in a manner similar to the tensile specimens. The prestressed flexure coupons were held in 3 point bending load during the flight and the amount of deflection was measured before and after removal from the fixtures.

Preflight records indicate that the strain applied to the tensile and compression specimens in the preload fixtures was intended to load them to 25% of their ultimate strength based on control stress-strain curves. The amount of strain remaining on the specimens and the corresponding load based on subsequent mechanical testing of the coupons is presented in Table VII for tensile and compression coupons along with estimates of the original loads. Table VIII summarizes the results for removal of the prestressed flexure coupons.

The tensile and compression preload release data is inconclusive due to limited sample populations and wide scatter. However, significant levels of load were maintained on the specimens during the flight. Complexity of the preload fixtures and end crushing of the compression specimens may have prevented accurate application of preloads prior to flight. On the other hand, the data for residual warpage of the prestressed flexure coupons was very consistent (See Table VIII). This may have been due to the simplicity of the preloading device.

Upon removal from the three point flexure preload fixtures, which imparted a deflection of 200 mils, the 934 epoxy /T300 graphite specimens had an average of 1.5% residual deflection with very little difference between bag and tool side exposed specimens. Figure XXI shows the prestress flexure fixture and defines residual deflection. The P1700 polysulfone/T300 graphite flexure specimens which were also held with 200 mils of deflection displayed an average of 8.5% residual deflection. Tool verses bag surfaces were indistinguishable for the polysulfone specimens. The PMR-15 polyimide/C6000 graphite specimens, held with 240 mils of deflection during flight, displayed a residual deflection of 14 % for bag side exposed specimens and -6% for tool side exposed specimens. The negative value indicates residual deflection in the opposite direction of the preload fixture deflection. These results indicate the specimens were either warped prior to placement in the preload jigs or responded differently to LEO exposure based on which side was exposed. The former is the most likely possibility although confirming preflight observations are not available. The tool and bag side exposed polyimide specimens displayed different levels of residual deflection indicating some type of stress relief during exposure.

Table IX summarizes the mechanical test results for the M0003-8 composites. Also included are preflight values if available. Where preflight values are not available, published values are given as indicated. Published moduli values for the polyimide composites were not available due to their unique layup orientation.

The compression and tensile test results are inconclusive due to the spread of the data and the limited sample population. Pre and post flight strength values are very similar but all are well below anticipated levels for these material systems (except possibly for the polyimide). Most of the post flight test failures occurred outside of the gauge area or at locations with rough edges. The same problems may have existed for preflight testing, thus lowering the strength values. However, LEO exposure does not appear to have caused further strength reductions. Tensile moduli values compare favorably with preflight values for the epoxy and polysulfone system. Compression moduli data for the epoxy and polysulfone systems is questionable due to the severe end brooming which occurred during testing and may have been caused by damage to the specimen ends from the preload fixture.

The preflight flexural modulus value for the 934 epoxy/T300 graphite is about twice what one would expect for this system. We suspect that an incorrect chart speed was recorded on the data sheet and the real value is probably 16.2 Msi (one half of reported value). Using this as a preflight value, the test results reveal a slight increase for the trailing edge unstressed specimens and a definite decrease for the leading edge unstressed specimens. Trailing to leading edge specimen comparison shows a drop in modulus. Strength values varied greatly but the lowest values are associated with leading edge specimens.

The P1700 polysulfone/T300 graphite fabric moduli values decrease in the order: preflight , trailing edge, stressed trailing edge, leading edge. Strength values varied with the leading edge specimens being the lowest.

The PMR15-polyimide/C6000 graphite flexure specimens showed a decrease in moduli compared to preflight values. The most severe decrease is observed for the leading edge specimens which also displayed the lowest strength values.

The test results for the epoxy adhesive lap shear specimens are given in table IX. The shear stress values have increased 6.8 to 27.8 percent over preflight values. One possibility is that the cure reaction for the adhesives was not completely advanced prior to flight and reaction advancement may have occurred during LEO exposure. Due to the unavailability of preflight calorimetry data determination of cure advancement during LEO exposure is not possible.

DISCUSSION OF RESULTS

In this section we will attempt to relate our test results to specific elements of the LDEF environment and where reasonable offer an explanation for possible mechanisms associating causes and effects. The three environmental conditions discussed are thermal cycling, ultraviolet radiation, and atomic oxygen. Finally we will discuss the implications for future ground and space testing as well as space structure material selection.

Thermal Cycling

Thermal cycling of the M0003-8 composites is estimated to be between -20° F and 160° F for approximately 34,000 cycles. Qualitative photomicrographic analysis of polished cross sections did reveal a possible increase in microcracking over control photomicrographs for epoxy and polysulfone composites.

Extensive microcracking would have significantly impacted trailing edge mechanical properties which was not the case. However, the residual deflection for the prestressed flexure specimens does indicate some stress relief occurred for the polyimide and polysulfone composites. Residual stresses from the multidirectional reinforcement of the polysulfone and polyimide specimens (vs. unidirectional for the epoxy) combined with preload stresses and aggravated by thermal cycling may have caused stress relief by microcracking. The possibility of stress relief by microcracking (or perhaps thermoplastic creep in the case of the polysulfone) has serious implications for material selection for space applications.

Ultraviolet Radiation

The only observable effects of UV radiation were on the trailing edge 3"x6" flat composite specimens. The thin section microscopy observations show changes in the matrix resin up to 30μm deep. Any impact on mechanical or optical properties was not detected. Leading edge exposed composite materials did not display these changes as AO erosion removed any possible evidence. Synergistic AO and UV effects for leading edge composites may exist but no such evidence was found.

Optical coatings are typically used for thermal control of space exposed composite structures. These coatings also protect the underlying substrate from any UV degradation. Should this coating be removed (micrometeoroid impact, etc.) the effects on optical properties and AO erosion in the exposed areas would be of far greater concern than UV degradation of the substrate.

Atomic Oxygen

By far the most significant changes in organic composite properties were caused by atomic oxygen. The AO erosion of material from the leading edge exposed composites was responsible for reductions in mechanical properties and changes in optical properties. Undoubtedly leading edge exposed composites will require some type of AO protection for long term LEO exposure applications.

The IR spectra for the leading edge exposed epoxy and polysulfone specimens suggests the presence of sulfur containing compounds. We suspect that the residue observed by SEM among the jagged features of the leading edge exposed epoxy and polysulfone surfaces is this sulfur containing compound. If enrichment of this compound is occurring as the result of preferential erosion of surrounding hydrocarbon material in the matrix resin then the regions of exposed resin among the jagged surface features may be mostly this sulfur containing compound. This would explain the lack of IR absorption bands for the epoxy and polyimide surfaces.

The residual material discussed above may also explain the differences observed in optical properties for the leading edge exposed polyimide specimen vs. the epoxy and polysulfone. The polyimide specimen which did not display this residual material had a significantly higher optical absorption than the other two composites.

Finally, if indeed the observed "strings" and "clumps" are an AO resistant material then their presence may have provided AO shielding for the polysulfone and epoxy composites. These materials displayed lower recession rates than the polyimide specimens.

Ground based simulation testing of organic composites should address the vulnerability to atomic oxygen attack. Protective coatings can offer AO shielding for composites. However, should that coating be compromised by a micrometeoroid impact, the erosion of the composite substrate and undercutting of the coating could result in eventual failure of the structure. Coatings alone may not be adequate protection for long term LEO exposure applications.

ACKNOWLEDGEMENTS

The authors would like to acknowledge the following persons for their invaluable assistance: H.G. Pippin and H. W. Dursch of the Composites and Adhesives group of Boeing Defense and Space, W.L. Plagemann and D. B.Skoropinski of the Analytical Engineering Group of Boeing Defense and Space, and E.R. Crutcher of the Image and Particle Analysis Group of Boeing Defense and Space.

REFERENCES

1. Bourassa, R.J.; Atomic Oxygen and Ultra Violet Radiation Mission Total Exposures for LDEF Experiments. First LDEF Post-Retrieval Symposium, NASA CP-3134, 1992.

2. Young, P.R.; Slemp,W.S.; Witt, W.G. Jr; and Shen, J. Y.: Characterization of selected LDEF Polymer Matrix Resin Composite Materials, 36th International SAMPE Symposium, April, 1991.

3. Aldrich Library of Infrared Spectra. Edition III, Aldrich Chemical Co. Inc., 1981.

4. Crutcher, E. R.; Nishimura, L. S.; Warner, K.; and Washer, W. W.: Migration and Generation of Contaminants from Launch Through Recovery: LDEF Case History. First LDEF Post-Retrieval Symposium, NASA CP-3134, 1992.

5. Rousslang, K.; Crutcher, E.R.; and Pippen, H.G.; Results of Examination of Silvered Teflon from the Long Duration Exposure Facility. First LDEF Post-Retrieval Symposium, NASA CP- 3134, 1992.

TABLE I. - ATOMIC OXYGEN, SOLAR EXPOSURE AND THERMAL CYCLING

	LEADING EDGE TRAY POSITION D9	TRAILING EDGE TRAY POSITION D3
ATOMIC OXYGEN EXPOSURE (Impacts / cm^2)	8.32×10^{21}	3.71×10^3
INCIDENT SOLAR PLUS EARTH REFLECTED RADIATION (Equivalent solar hours)	11,076	11,045
THERMAL CYCLING (APPROXIMATE)	-20°F TO 160 °F 34,000 CYCLES	-20°F TO 160 °F 34,000 CYCLES

TABLE II. - M0003-8 SPACE EXPOSED COMPOSITES

Material andLayup Orientation	Leading Edge 3"x6" Panel	Trailing Edge 3"x6" Panel	Trailing Edge Stressed Mechanical Test Coupons
934 Epoxy/ T300 Graphite (0°)	X	X	X
934 Epoxy/ T300 Graphite (0°) Thermal Cycled Prior to Flight	X	X	
P1700 Polysulfone/ T300 Graphite Fabric (0°,90°)	X	X	X
PMR 15 Polyimide/ C6000 Graphite $(0/\pm45/0/\pm45)_S$	X	X	X

TABLE III. - PRE AND POST FLIGHT OPTICAL PROPERTIES

Material	Property	Preflight values	Post flight values			
			Unexposed side		Exposed side	
			Trailing	Leading	Trailing	Leading
934 Epoxy/ T300 Graphite	Absorption	0.90	0.90	0.90	0.87	0.93
	Emittance	0.73	0.83	0.79	0.82	0.93
	A/E	1.23	1.08	1.13	1.06	1.00
P1700 Polysulfone/ T300 Graphite	Absorption	0.92	0.90	0.92	0.88	0.93
	Emittance	0.73	0.81	0.83	0.82	0.93
	A/E	1.26	1.11	1.11	1.07	1.00
PMR-15 Polyimide/ C6000 Graphite	Absorption	0.91	0.88	0.91	0.90	0.98
	Emittance	0.77	0.83	0.79	0.79	0.93
	A/E	1.18	1.06	1.15	1.14	1.05

TABLE IV. - GLASS TRANSITION TEMPERATURES

MATERIAL	LEADING EDGE	TRAILING EDGE	PUBLISHED VALUES
934 EPOXY	192°C	193°C	204°C
P 1700 POLYSULFONE	-	184°C	190°C
PMR-15 POLYIMIDE	341°C	335°C	359°C

TABLE V. - CTE TEST RESULTS

Material	Measurement Orientation	Preflight Data	Leading Edge Test Results	Trailing Edge Test Results
		In. /In. C°	In. /In. C°	In. /In. C°
934 Epoxy/ T300 Graphite (0°)	Z-Y*	31.9×10^{-6}	31.2×10^{-6}	30.0×10^{-6}
	X	3.6×10^{-7}	6.1×10^{-7}	1.7×10^{-7}
P1700 Polysulfone/ T300 Graphite Fabric (0°,90°)	Z	N.T.	43.7×10^{-6}	42.5×10^{-6}
	X (Y - N.T.)	-1.8×10^{-6}	1.75×10^{-6}	1.58×10^{-6}
PMR 15 Polyimide/ C6000 Graphite $(0/\pm45/0/\pm45)_S$	Z	N.T.	39.5×10^{-6}	38.84×10^{-6}
	X,Y	N.T	N.T.	N.T.

TABLE VI. - TOTAL MASS TOSS (TML) AND VOLATILE COLECTABLE MATERIALS (VCM) TEST RESULTS

Material and Layup Orientation	Preflight		Post Flight Leadng Edge		Post Flight Trailing Edge	
	TML %	VCM%	TML %	VCM%	TML %	VCM%
934 Epoxy/ T300 Graphite	0.23	0.02	0.25	0.01	0.28	0.00
934 Epoxy/ T300 Graphite Thermal Cycled Prior to Flight	0.23	0.02	0.34	0.03	0.29	0.00
P1700 Polysulfone/ T300 Graphite	0.11	0.02	0.06	0.02	0.15	0.00
PMR 15 Polyimide/ C6000 Graphite	0.52	0.02	0.40	0.01	0.48	0.00

TABLE VII. - MEASURED RESIDUAL STRAINS AND ESTIMATED LOADS FOR PRESTRESSED TENSILE AND COMPRESSION SPECIMENS

MATERIALS	TENSION			COMPRESSION		
	Post Flight		Preflight	Post Flight		Preflight
	Strain In./In.	Est. load Ksi.	Est. load Ksi.	Strain In./In.	Est. load Ksi.	Est. load Ksi.
934 Epoxy/ T300 Graphite	0.00131	26	38	0.00098	8.9	29
P1700 Polysulfone/ T300 Graphite	0.00214	17	17	0.00112	7.8	14
PMR 15 Polyimide/ C6000 Graphite	0.00284	22	17	0.00109	8.0	16

TABLE VIII. - MEASURED RESIDUAL DEFLECTIONS FOR PRESTRESSED FLEXURE SPECIMENS

MATERIALS	Loaded Deflection Mils	Residual Deflection	
		Bag Side Exposed Mils	Tool Side Exposed Mils
934 Epoxy/ T300 Graphite	200	3	1
P1700 Polysulfone/ T300 Graphite	200	17*	
PMR 15 Polyimide/ C6000 Graphite	240	34	-14

* Bag and tool side indistinguishable

TABLE X. - ADHESIVE LAP SHEAR TEST RESULTS

ADHESIVE	ADHEREND	PREFLIGHT SHEAR STRESS Psi	POST FLIGHT SHEAR STRESS	
			Psi	# tested
AF 143 Epoxy	Ti - Composite	4515	4821	3
(BMS 5-104)	Composite-Composite	3640	4273	2
EC 2216 Epoxy	Ti - Composite	3750	4479	2
(BMS 5-92)	Composite-Composite	3145	4019	3

TABLE IX. - MECHANICAL TEST RESULTS
(75°F unless otherwise noted)

* Thermal Cycled Prior To Flight
** Tested At 350° F

(Strength) Ksi
(Modulus) Msi
(# Tested)

MATERIALS - TESTS	934 Epoxy/ T300 Graphite(0°)	P1700 Polysulfone/ T300 Graphite Fabric (0°,90°)	PMR 15 Polyimide/ C6000 Graphite $(0/\pm45/0/\pm45)_s$
PREFLIGHT FLEXURE-	220.5 Ksi 32.4 Msi 3	106.5 Ksi 12.7 Msi 3	118.9 Ksi 17.8 Msi 3
POSTFLIGHT FLEXURE-			
Leading edge unstressed	207.0 Ksi 13.6 Msi 4	97.3 Ksi 7.8 Msi 4	104.6 Ksi 6.3 Msi 4
Leading edge unstressed T.C.*	229.0Ksi 16.2 Msi 4	N.A.	N.A.
Trailing edge unstressed	238.0 Ksi 17.7 Msi 4	116.0 Ksi 10.4 Msi 4	137.0 Ksi 10.5 Msi 4
Trailing edge unstressed T.C.*	224.9 Ksi 16.1 Msi 4	N.A.	N.A.
Trailing edge prestressed	241.8 Ksi 16.3 Msi 5	118.8 Ksi 8.0 Msi 5	155.1 Ksi 11.4 Msi 5
Trailing edge prestressed (Elevated temperature)	119.7 Ksi 15.6 Msi 3	16.7 Ksi 4.5 Msi 3	81.1 Ksi 6.6 Msi 3
PREFLIGHT TENSION	152.7 Ksi est. 18-20 Msi 3	68.1 Ksi est 7-9 Msi 3	69.6 Ksi - 3
POST FLIGHT TENSION- Prestressed trailing edge	148.1 Ksi 21.0 Msi 2	66.2 Ksi 7.9 Msi 2	45.4 Ksi 8.0 Msi 2
PREFLIGHT COMPRESSION	118.1 Ksi est. 18-20 Msi 3	54.5 Ksi est 7-9Msi 3	64.5 Ksi - 3
POST FLIGHT COMPRESSION- Prestressed trailing edge	106.8 Ksi 8.3 Msi 3	50.8 Ksi 7.2 Msi 2	61.0 Ksi 6.9 Msi 2

*** Tested at 600° F

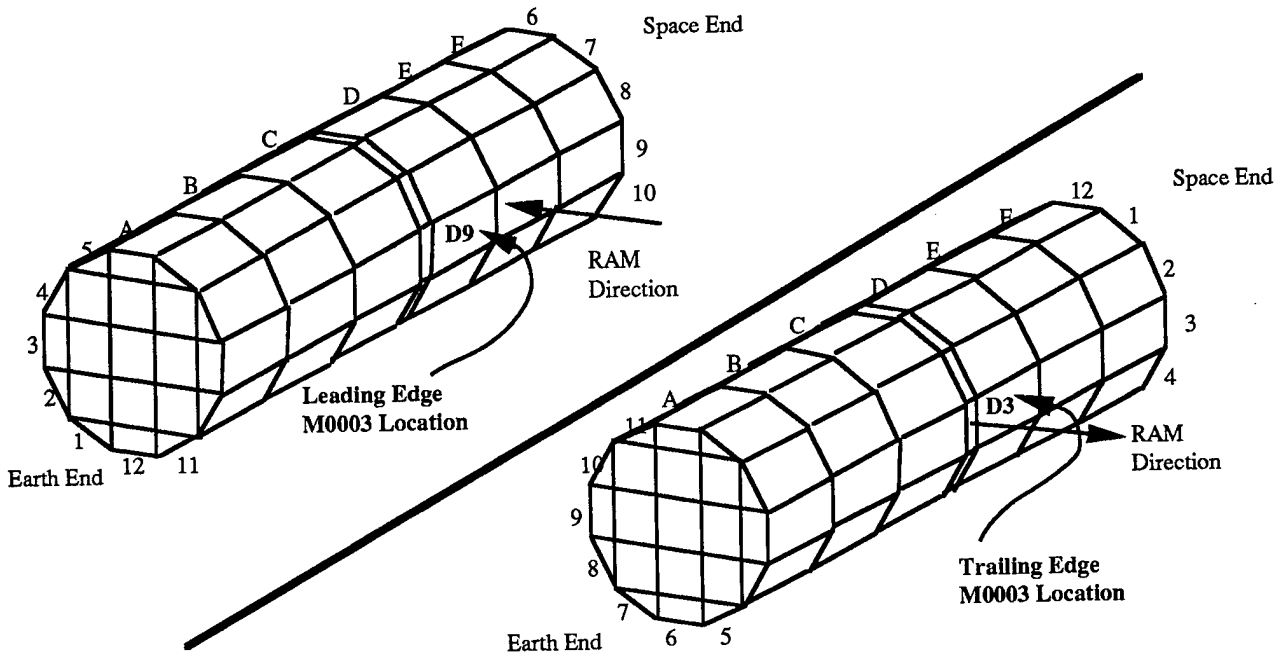


FIGURE I. - LOCATION AND ORIENTATION OF M0003-8 EXPERIMENT ON LDEF

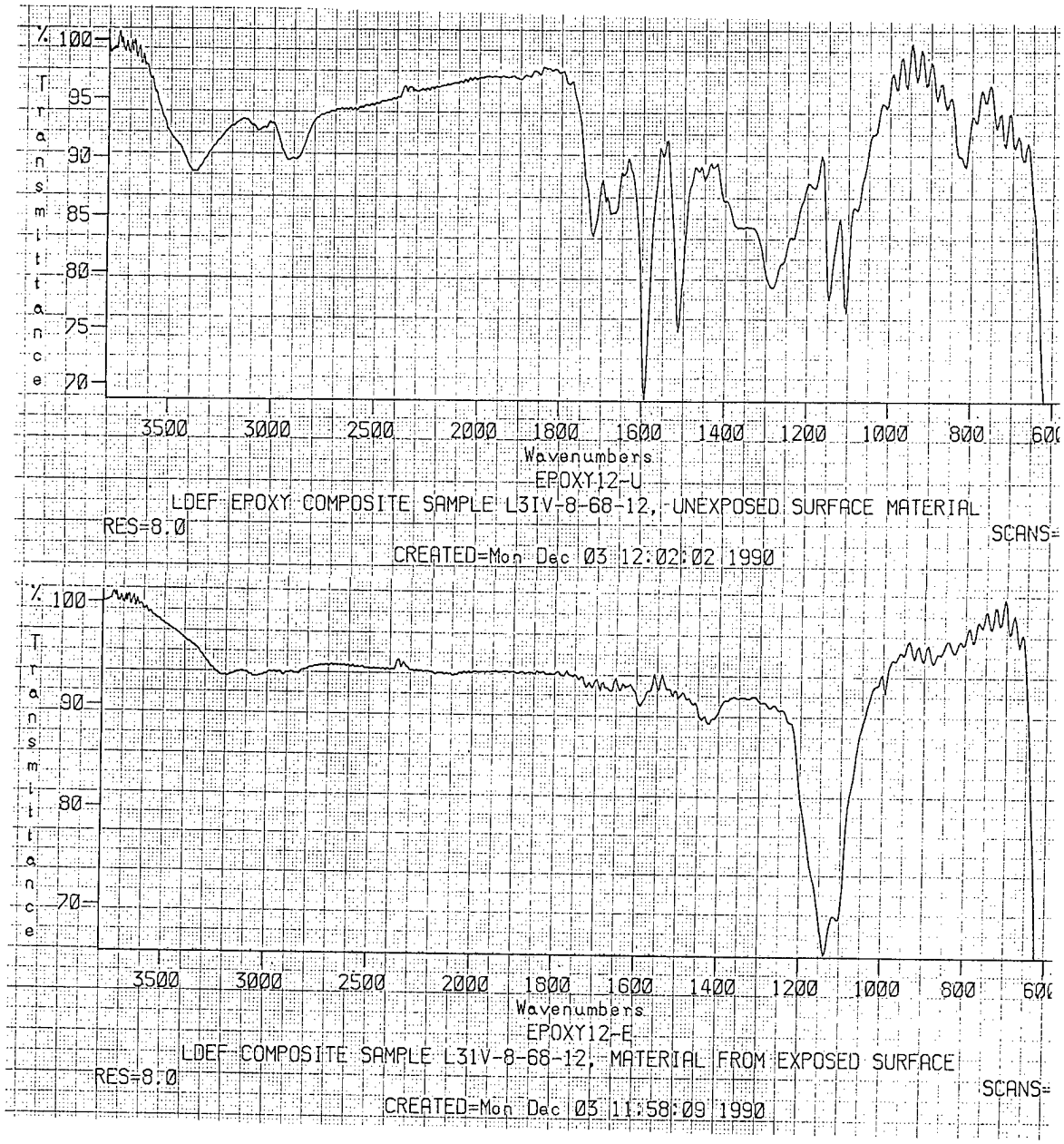


FIGURE II. - FTIR SPECTRA FOR SHIELDED AND LEADING EDGE EXPOSED 934 EPOXY/T300 GRAPHITE

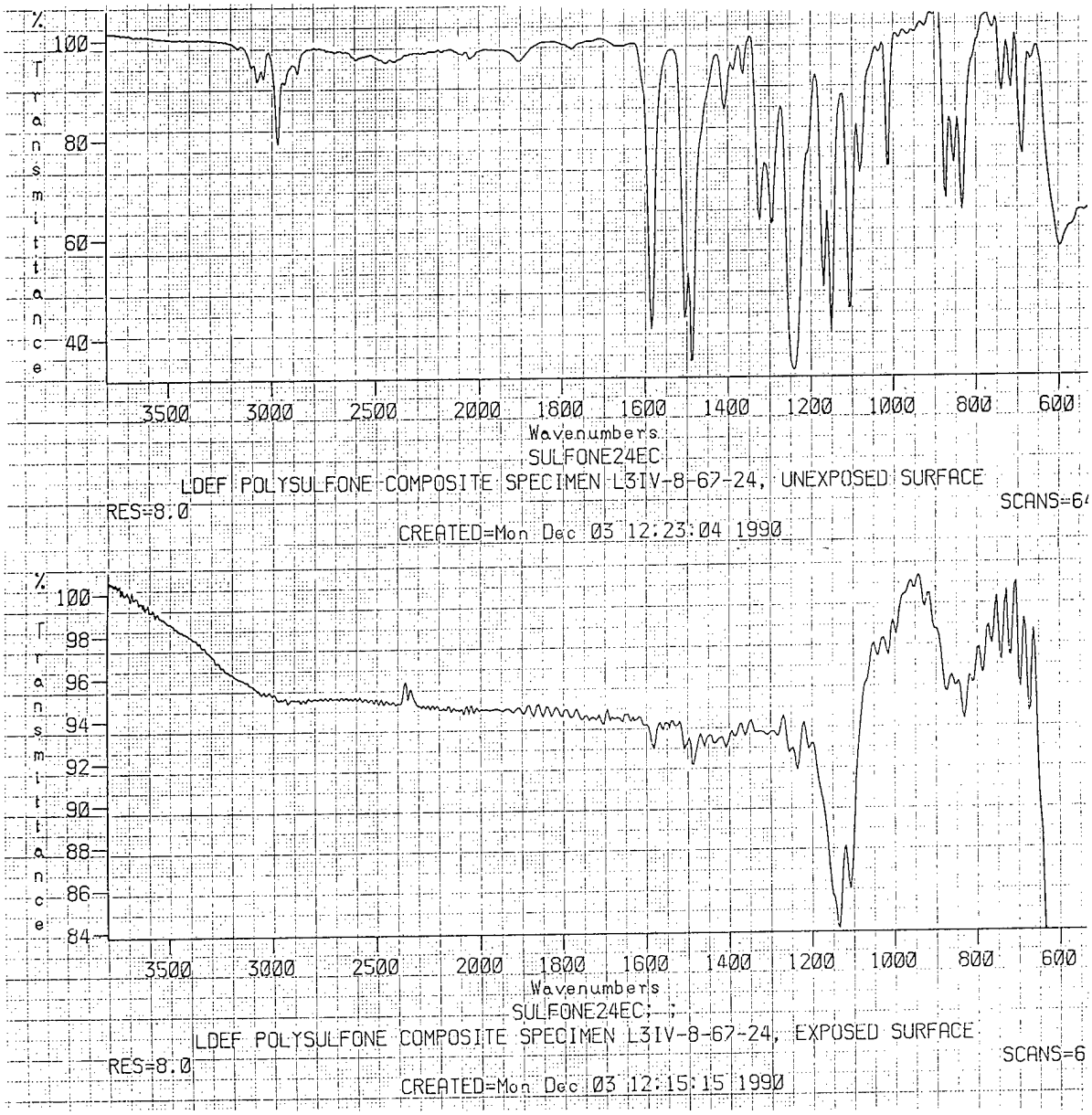


FIGURE III. - FTIR SPECTRA FOR SHIELDED AND LEADING EDGE EXPOSED P1700 POLYSULFONE/T300 GRAPHITE

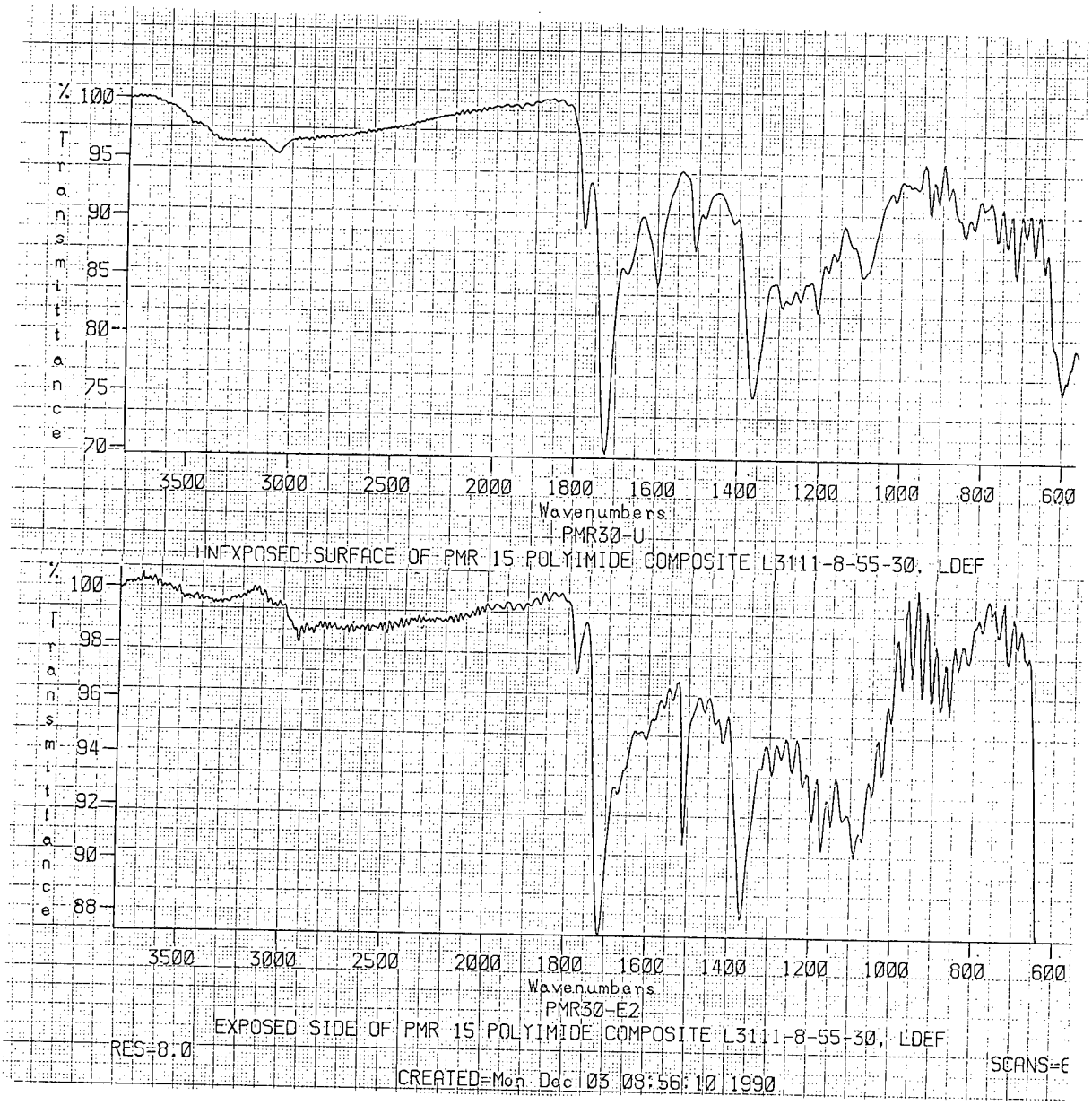


FIGURE IV. - FTIR SPECTRA FOR SHIELDED AND LEADING EDGE EXPOSED PMR-15 POLYIMIDE/C6000 GRAPHITE

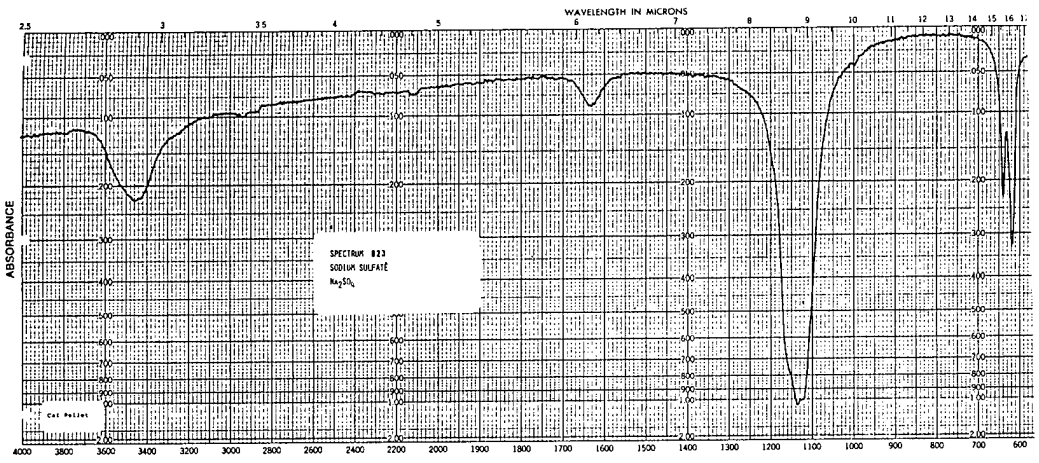


FIGURE V. - REFERENCE IR SPECTRA FOR SODIUM SULFATE ( )

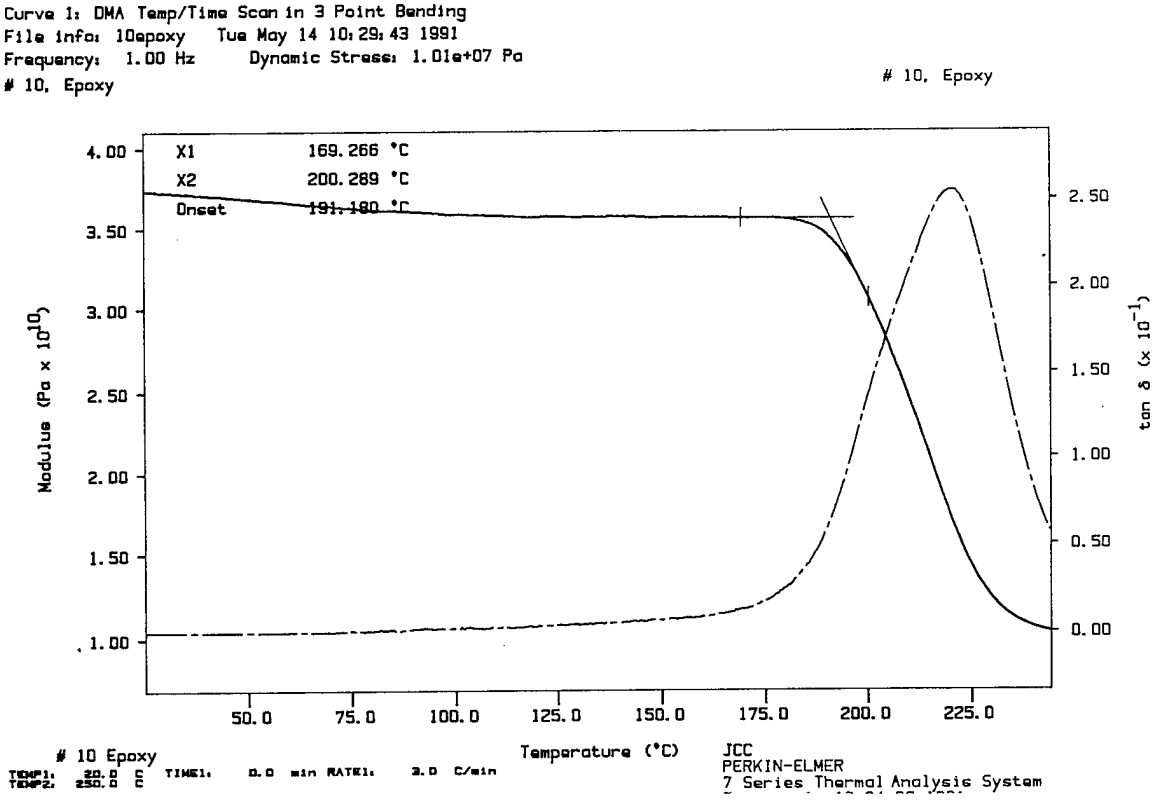


FIGURE VI. - DMA CURVE FOR LEADING EDGE EXPOSED 934 EPOXY/T300 GRAPHITE

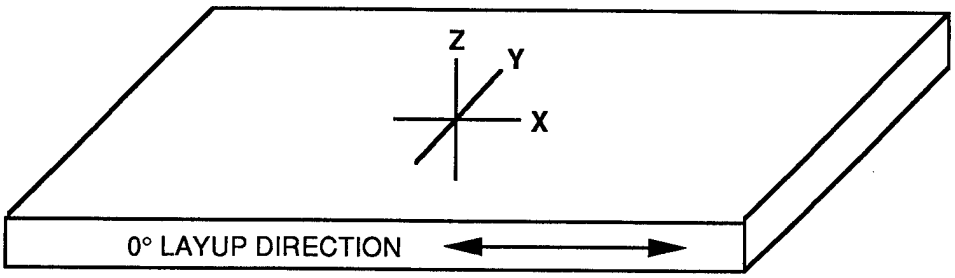


FIGURE VII. - TEST SPECIMEN ORIENTATION REFERENCE

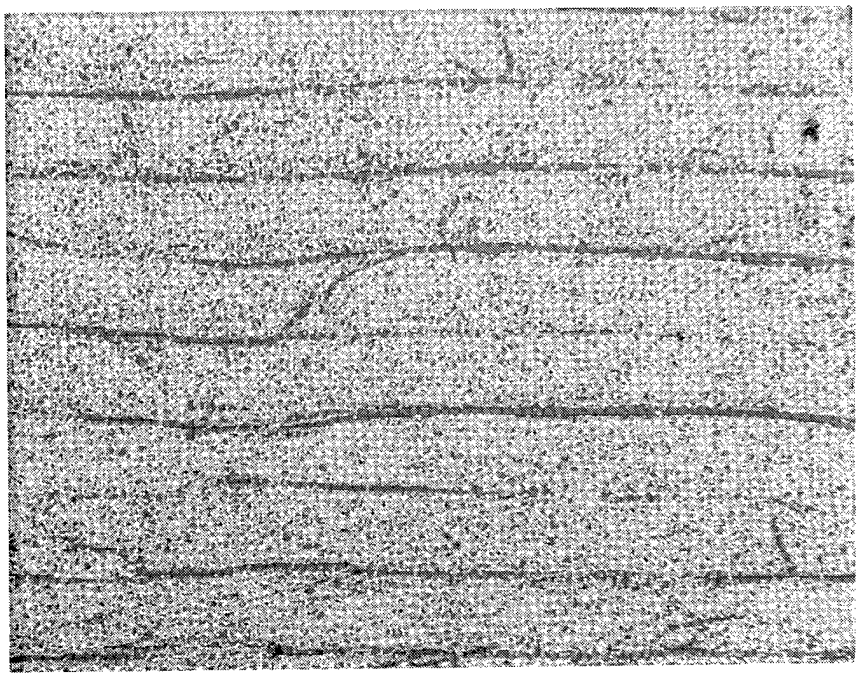


FIGURE VIII. - CROSS SECTION OF PREFLIGHT
934 EPOXY/T300 GRAPHITE (65X)

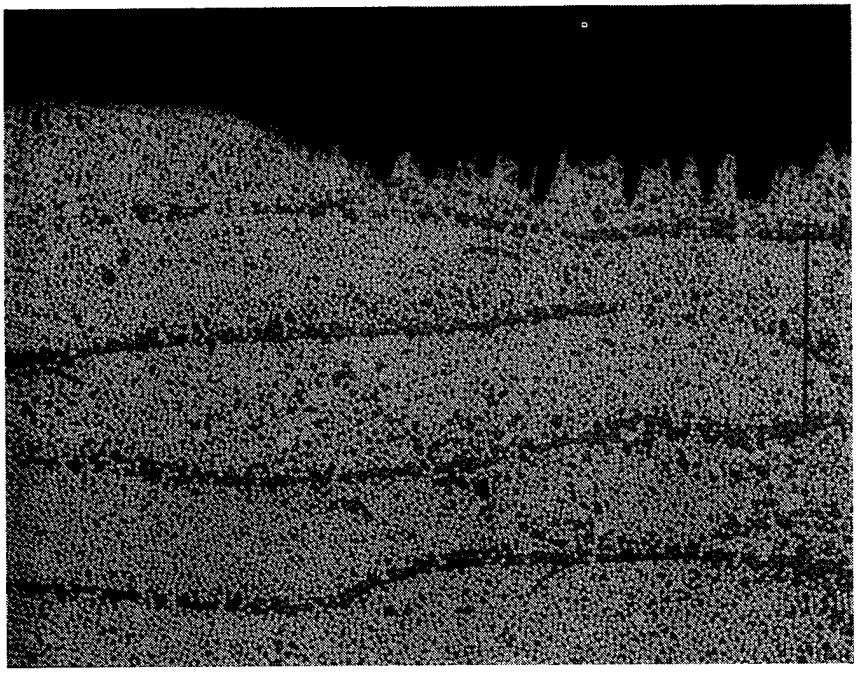


FIGURE IX. - CROSS SECTION OF POST FLIGHT LEADING EDGE EXPOSED
934 EPOXY/T300 GRAPHITE (100X)

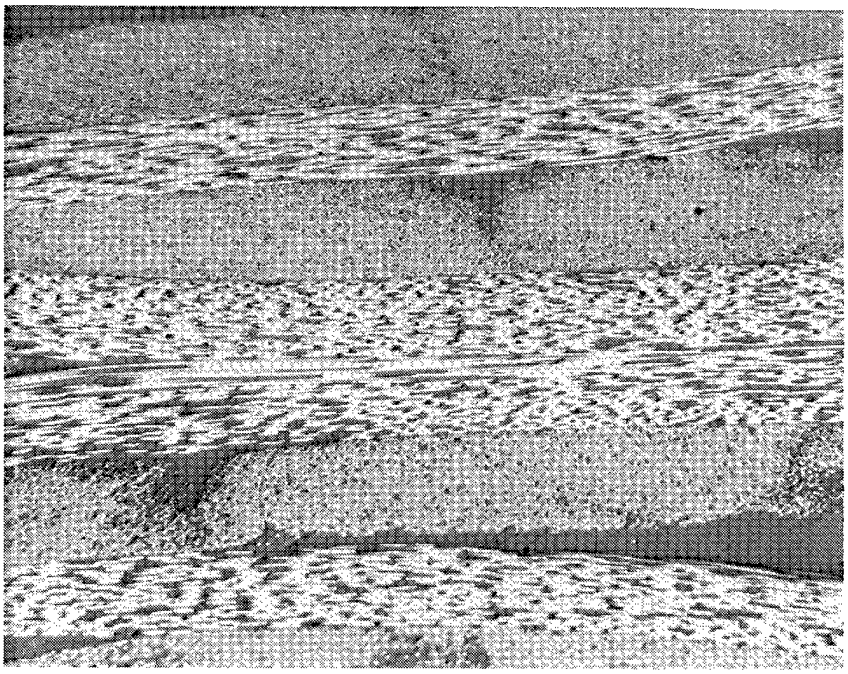


FIGURE X. - CROSS SECTION OF PREFLIGHT
P1700 POLYSULFONE/T300 GRAPHITE (65X)

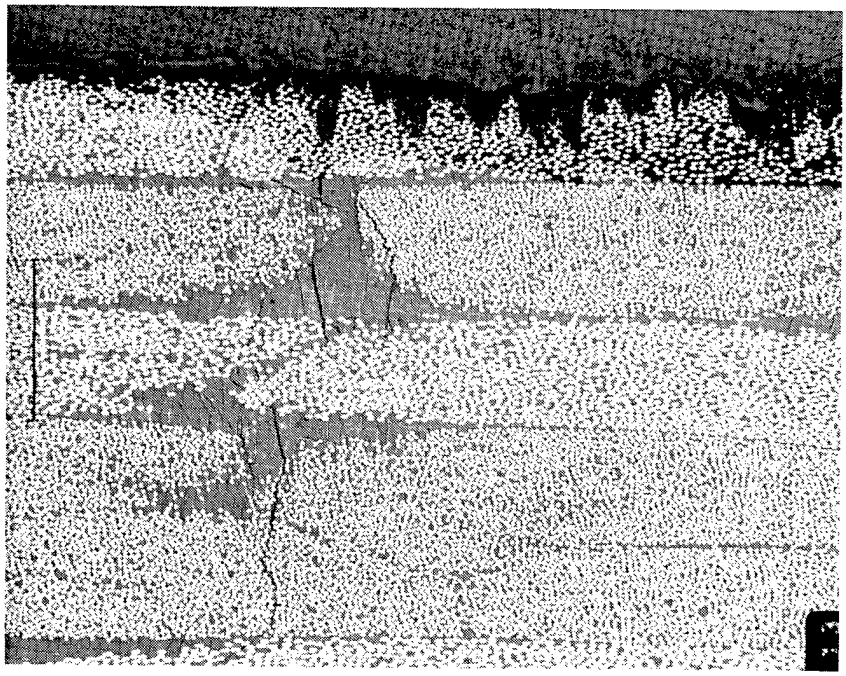


FIGURE XI. - CROSS SECTION OF POST FLIGHT LEADING EDGE EXPOSED
P1700 POLYSULFONE/T300 GRAPHITE (80X)

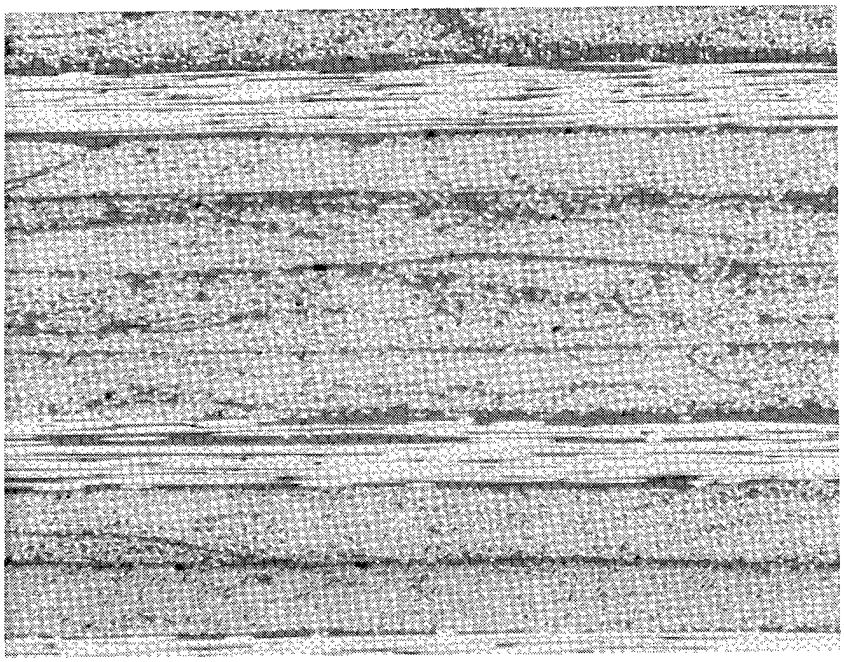


FIGURE XII. - CROSS SECTION OF PREFLIGHT
PMR-15 POLYIMIDE/C6000 GRAPHITE (65X)

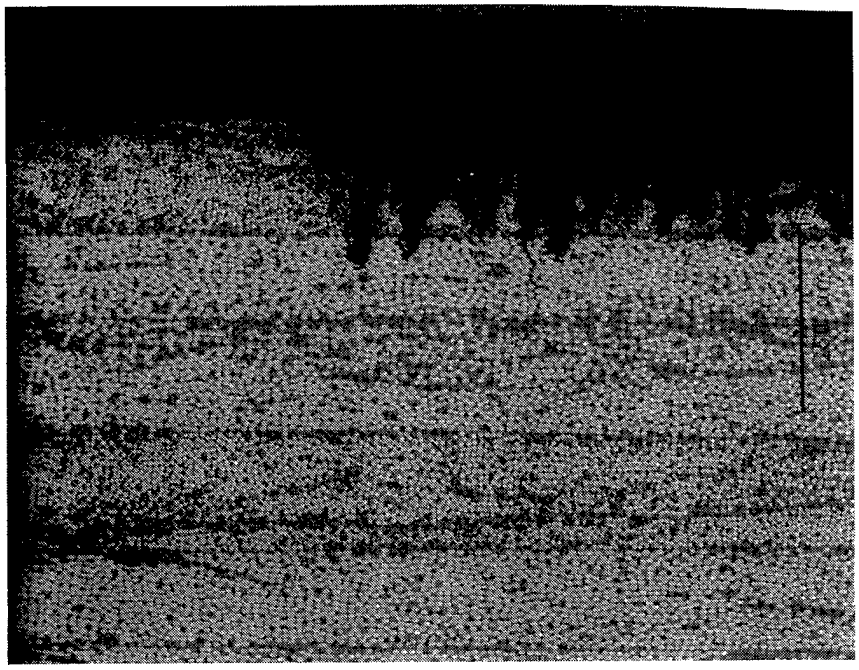


FIGURE XIII. - CROSS SECTION OF POST FLIGHT LEADING EDGE EXPOSED
PMR-15 POLYIMIDE/C6000 GRAPHITE (100X)

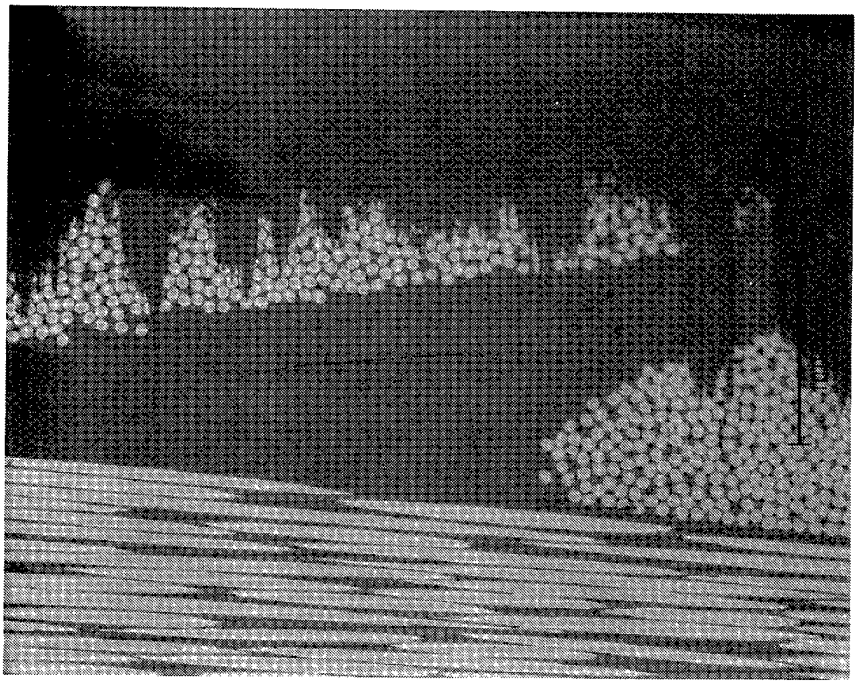


FIGURE XIV. - CROSS SECTION OF POST FLIGHT LEADING EDGE EXPOSED P1700 POLYSULFONE/T300 GRAPHITE (250X)

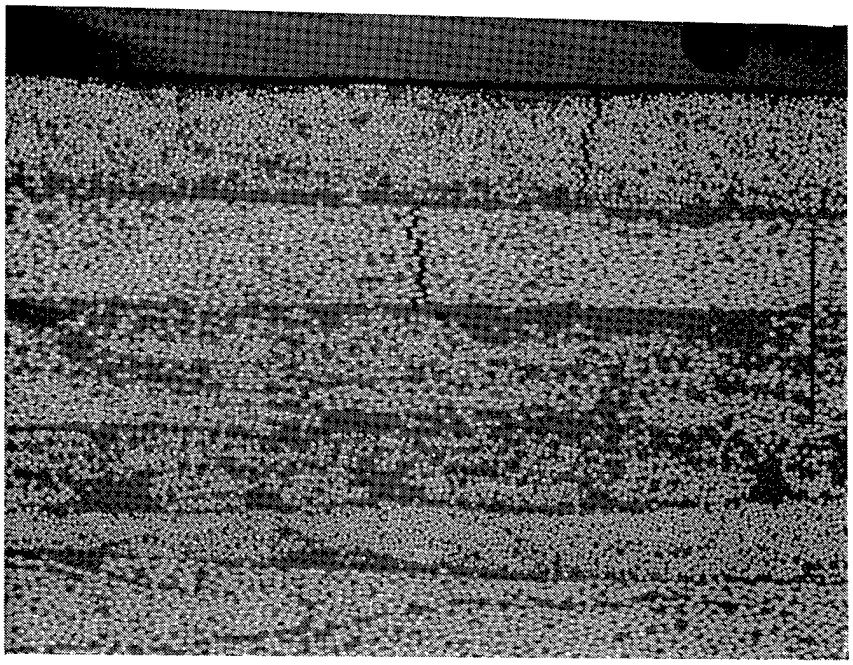
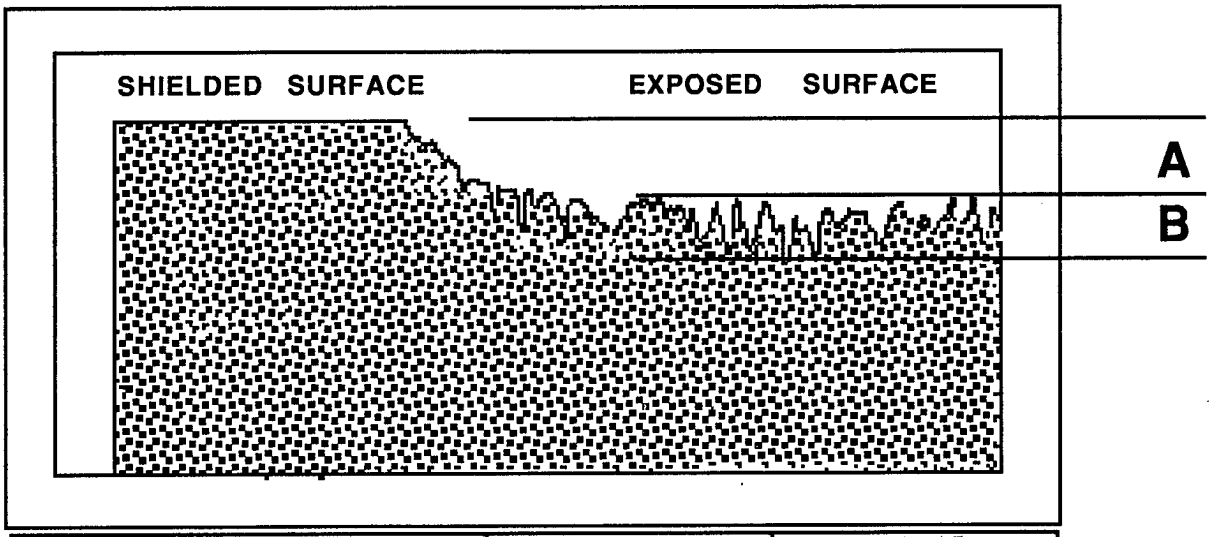


FIGURE XV. - CROSS SECTION OF POST FLIGHT TRAILING EDGE EXPOSED PMR-15 POLYIMIDE/C6000 GRAPHITE (100X)



	934 EPOXY /GRAPHITE	P1700 POLYSULFONE /GRAPHITE	PMR-15 POLYIMIDE /GRAPHITE
A	2.1 mils	2.1 mils	3.0 mils
B	3.1 mils	3.2 mils	4.8 mils
A+B	5.2 mils	5.3 mils	7.8 mils

FIGURE XVI. - RECESSION OF LEADING EDGE COMPOSITE SURFACES

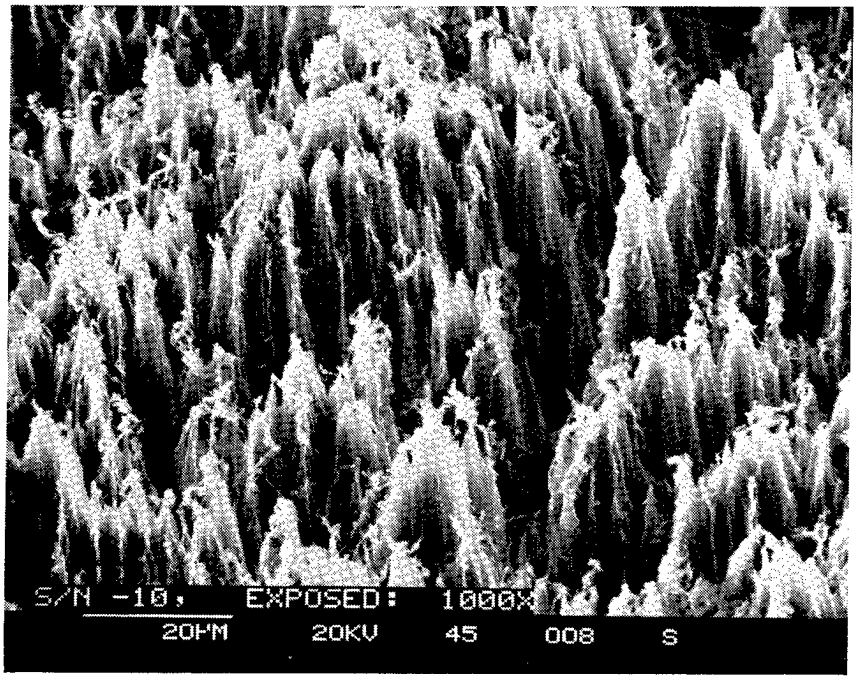


FIGURE XVII. - SEM PHOTOGRAPH OF LEADING EDGE EXPOSED 934 EPOXY/T300 GRATHITE SURFACE (1000X)

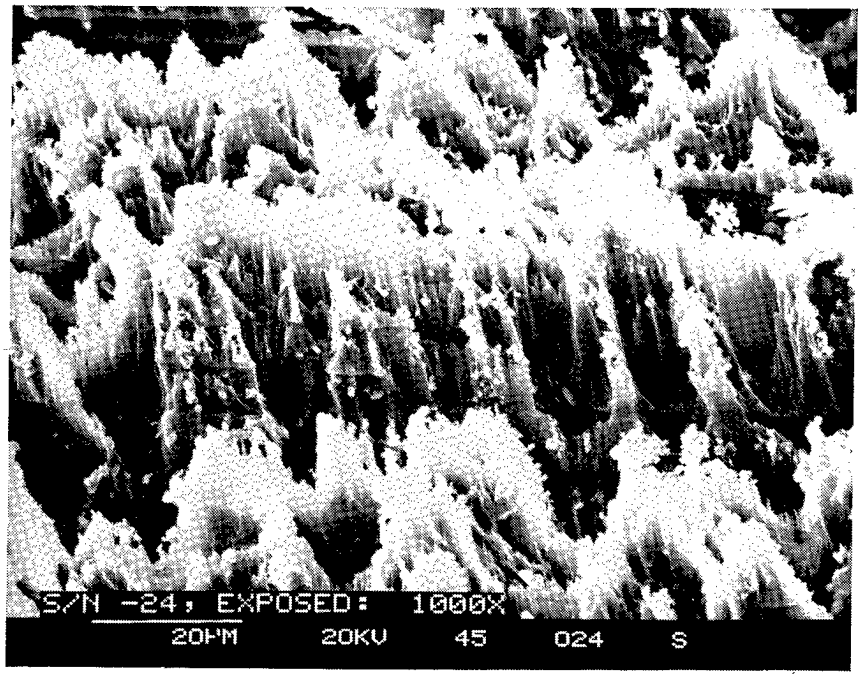


FIGURE XVIII. - SEM PHOTOGRAPH OF LEADING EDGE EXPOSED P1700 POLYSULFONE/T300 GRATHITE SURFACE (1000X)

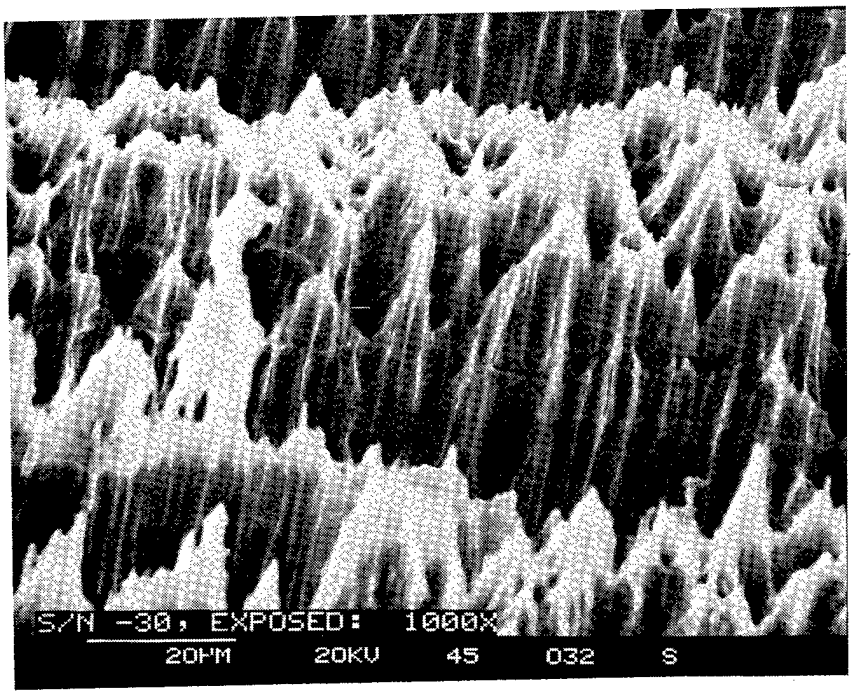


FIGURE XIX. - SEM PHOTOGRAPH OF LEADING EDGE EXPOSED PMR-15 POLYIMIDE/C6000 GRATHITE SURFACE (1000X)

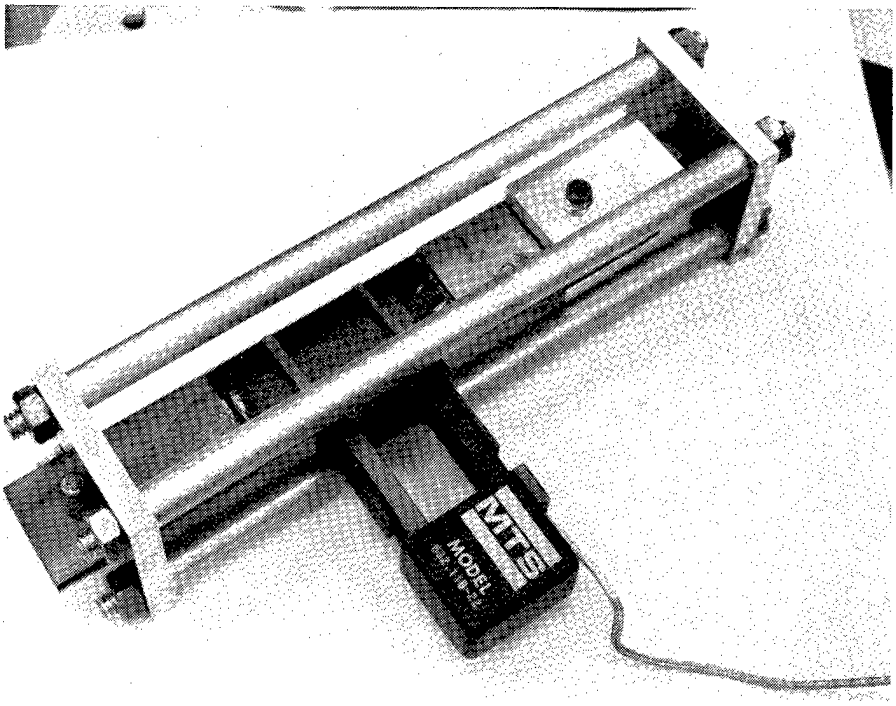


FIGURE XX. - EXTENSOMETER PLACEMENT FOR TENSILE PRELOAD REMOVAL

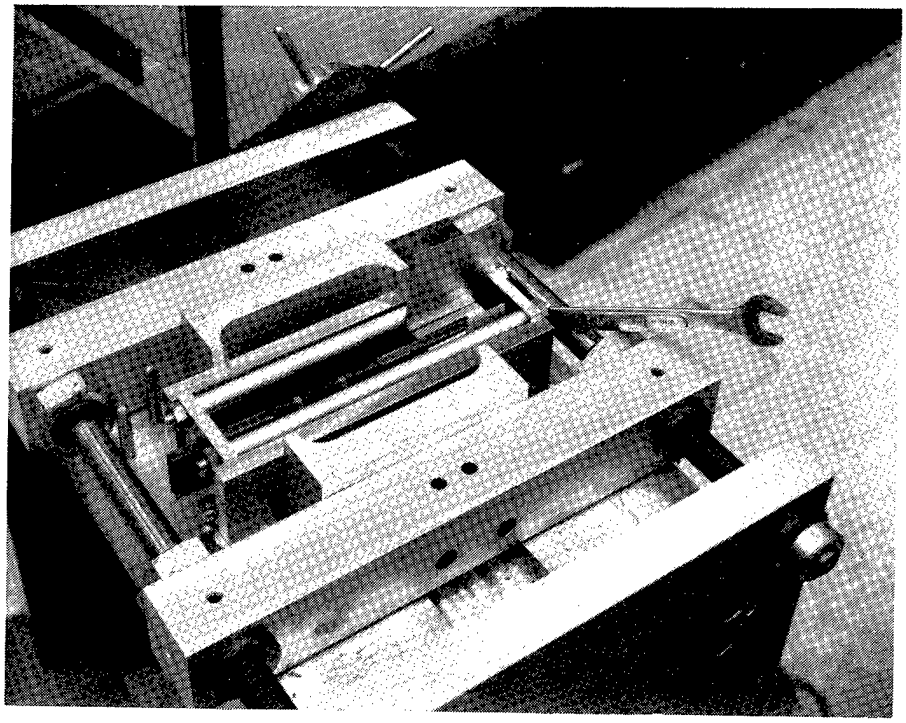
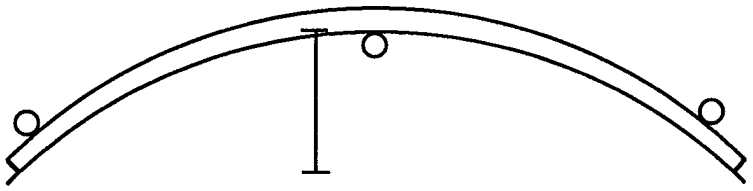
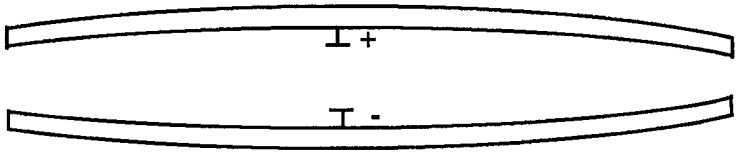


FIGURE XXI. - TENSILE PRELOAD REMOVAL



Prestressed Deflection as flown

Positive Residual Deflection after removal



Negative Residual Deflection after removal

FIGURE XXII. - PRESTRESSED AND RESIDUAL FLEXURE DEFLECTION DEFINITION

HIGH-TOUGHNESS GRAPHITE/EPOXY COMPOSITE MATERIAL EXPERIMENT

David K. Felbeck
University of Michigan
2250 G.G. Brown Laboratory
Ann Arbor, MI 48109-2125
Phone: 313-994-6662, Fax: 313-665-9370

SUMMARY

This experiment was designed to measure the effect of near-space exposure on three mechanical properties of specially toughened 5208/T300 graphite/epoxy composite materials. The properties measured are elastic modulus, strength, and fracture toughness. Six toughness specimens and nine tensile specimens were mounted on an external frame during the time of the LDEF mission. Three identical sets of specimens were manufactured at the outset: the flight set, a zero-time non-flight set, and a total-time non-flight set. To date, two toughness specimens and three strength and modulus specimens have been tested from each of the three groups.

INTRODUCTION

The then-recent development of procedures for improving the toughness of graphite/epoxy composites[1, 2] provided an appropriate material for near-earth space exposure testing when the Long Duration Exposure Facility (LDEF) was publicly proposed in the late 1970s. These procedures consist of introduction of a thin perforated layer of Mylar film between adjacent plies of a cross-ply composite so as to limit the area of inter-ply bonding. In this way, fracture of the composite is diverted when crossing the regions of no bonding between plies, with a consequent substantial increase in total area of fracture and an increase in fracture energy.

TEST PROCEDURE

The tensile/modulus dumbell-shaped specimens are each about 183 mm overall length with test section width about 19.5 mm. All specimens consist of eight layers of prepreg T300 graphite with 5208 epoxy, plus seven layers of Mylar, and are thus about 1.1 mm thick. Each specimen is tested initially for modulus, then fractured to determine strength.

The fracture toughness compact-tension specimens are about 190 mm long and about 70 mm wide overall. A narrow 27.5-mm transverse slot is machined on the initiation side, and a 22.5-mm 60° notch is cut out on the termination side to control out-of-plane buckling, with a net test section width of 20 mm. Each specimen consists of eight layers of prepreg plus seven layers of Mylar in the same manner as for the tensile/modulus specimens. Fracture toughness is measured using the Gurney method, in this case with the assumption that all work done following an 80% drop from the maximum load is neglected. The net work done divided by the *apparent* minimum fracture area is the fracture toughness R, where stress intensity factor $K_{Ic} = [ER]^{1/2}$.

For each of the two classes of specimens, tensile/modulus and fracture toughness, the cross-ply angle and the fraction (percent) of contact between adjacent plies are varied. The interlaminar contact fraction is controlled by the fraction of holes in the Mylar sheet.

EXPERIMENT LOCATION

Our experiment was located in tray D12, which was oriented so that the vector normal to the plane of the tray was 82° from the velocity vector; this panel was exposed to relatively low solar exposure. Other papers in this set will provide additional details regarding the nature of the exposure. Of particular importance here is that atomic oxygen produced erosion only in the surface epoxy but caused no loss of graphite filaments.

RESULTS TO DATE

All specimens were manufactured by us in December 1982, in preparation for delivery of the flight specimens to Langley the following spring. LDEF was launched approximately 16 months after manufacture of our specimens. The three sets of specimens were arbitrarily designated as:

Set A: flight specimens
Set B: zero time specimens
Set C: Total time, ground specimens

Six fracture toughness specimens, numbers 1-6, and nine tensile/modulus specimens, numbers 7-15, were manufactured for each of the three sets. Those specimens tested and reported here are as follows:

Group 2 Specimens : fracture toughness, ±20° layup, 18% contact
Group 5 Specimens : fracture toughness, ±45° layup, 36% contact
Group 8 Specimens : tensile/modulus, ±20° layup, 18% contact
Group 13 Specimens : tensile/modulus, ±45° layup, 36% contact
Group 15 Specimens : tensile/modulus, ±20° layup, 36% contact

Additional duplicates of the "zero-time" specimens were subjected to several modulus tests extending over approximately 18 months following manufacture, and the results are included in the summary of data below.

Toughness results for Groups 2 and 5 are shown in Fig. 1. Because of the unanticipated and substantial changes in the properties of the total time ground control specimens, we have elected to display all test results as a function of time since manufacture.

Modulus results for Group 8 are shown in Fig. 2, for Group 13 in Fig. 3, and for Group 15 in Fig. 4.

Strength results for Groups 8, 13, and 15 are shown in Fig. 5.

TENTATIVE CONCLUSIONS

Because our surface studies of the entire test panel have been given highest priority, we have not completed the mechanical property tests on the balance of the specimens. We are thus

reluctant yet to state any firm conclusions. Based on the very limited results, we observe the following:

- Marked degradation from exposure, of the order of a factor of at least two from the control specimens, is observed in the toughness specimens.
- Within the limits of rather large scatter, no significant net degradation in elastic modulus occurred from the 5.8-year exposure. Because of a trend toward increased modulus with time for the ground specimens, possible degradation effects from exposure may be masked.
- No significant degradation of strength of the flight specimens is observed.
- Substantial differences are observed in the behavior of specimens having different cross-ply angles and fraction of interlaminar contact, but a more definitive statement cannot be given until completion of the balance of testing, if then.

ACKNOWLEDGEMENT

This project was sponsored by National Aeronautics and Space Administration Langley Research Center Grant NAS1-17008.

REFERENCES

1. T.U. Marston, A.G. Atkins, and D.K. Felbeck, "Interfacial Fracture Energy and the Toughness of Composites," *Jour. of Materials Science*, v 9 (1974), p 447

2. L.-C. Jea and D.K. Felbeck, "Increased Fracture Toughness of Graphite-Epoxy Composites Through Intermittent Interlaminar Bonding," *Jour. of Composite Materials*, v 14 (July 1980), p 245

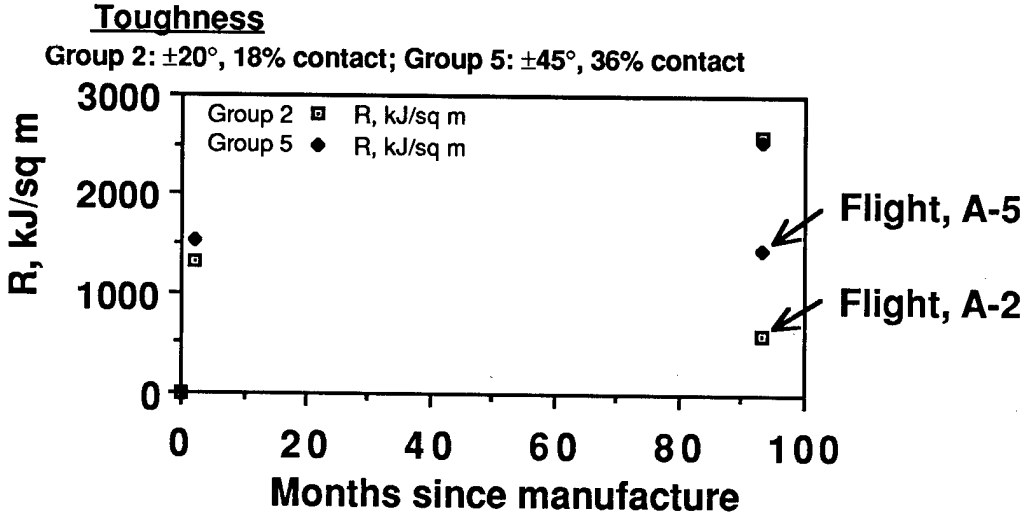


Fig. 1. Fracture toughness vs. time since manufacture of Group 2 and 5 specimens.

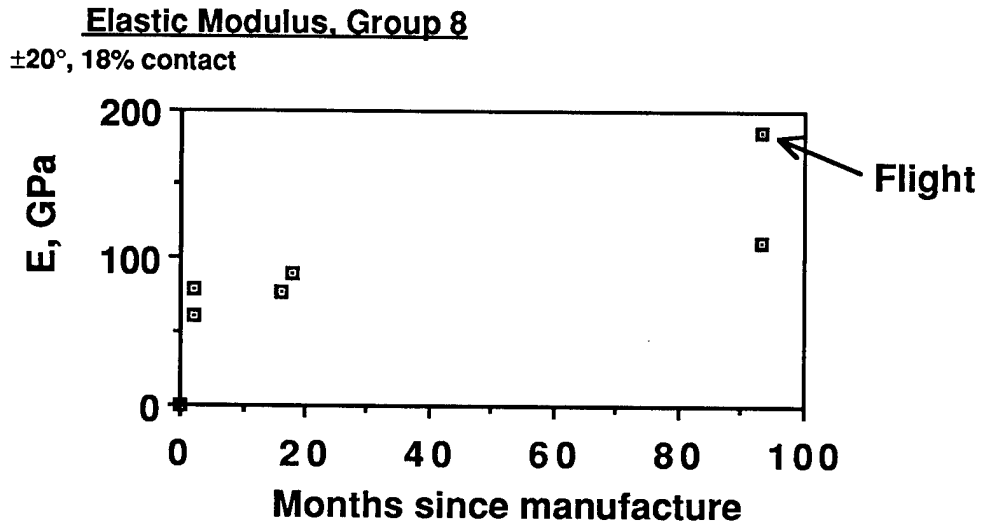


Fig. 2. Elastic modulus vs. time since manufacture of Group 8 specimens, ±20° layup, 18% interlaminar contact.

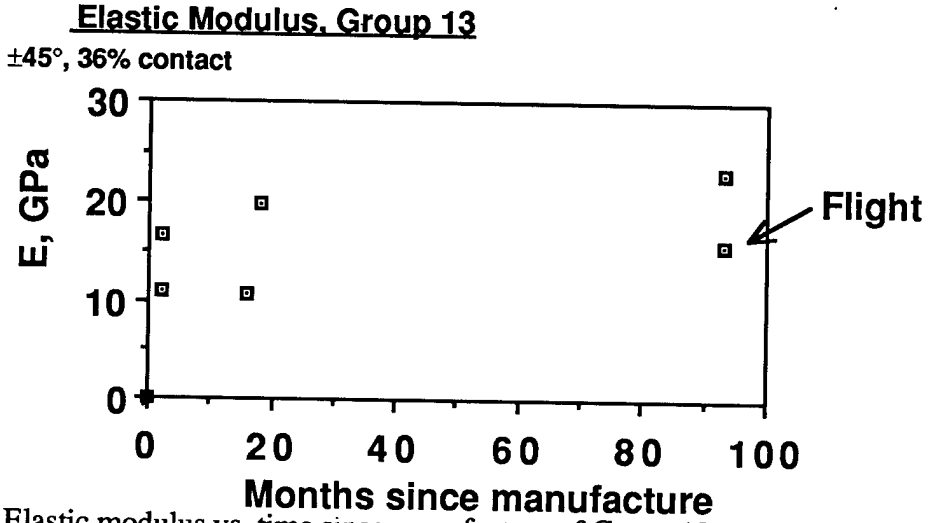


Fig. 3. Elastic modulus vs. time since manufacture of Group 13 specimens, ±45° layup, 36% interlaminar contact.

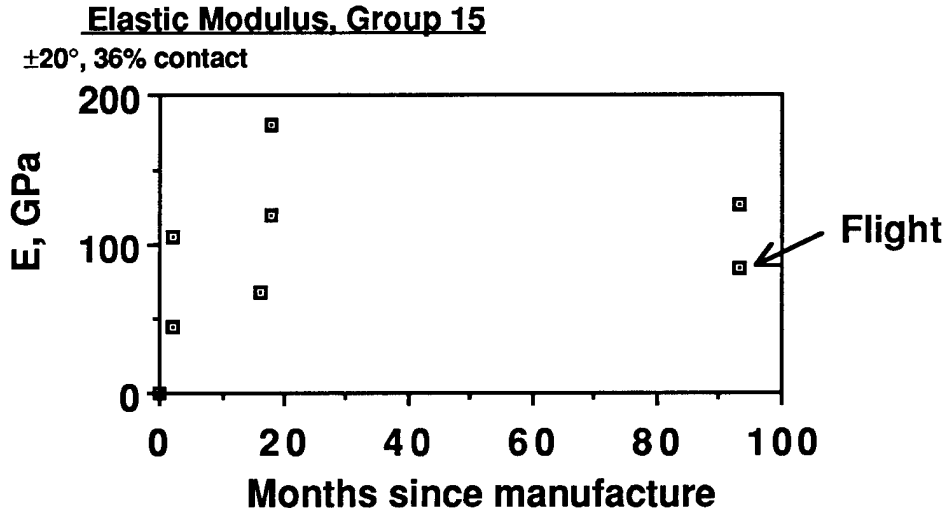


Fig. 4. Elastic modulus vs. time since manufacture of Group 15 specimens, ±20° layup, 36% interlaminar contact.

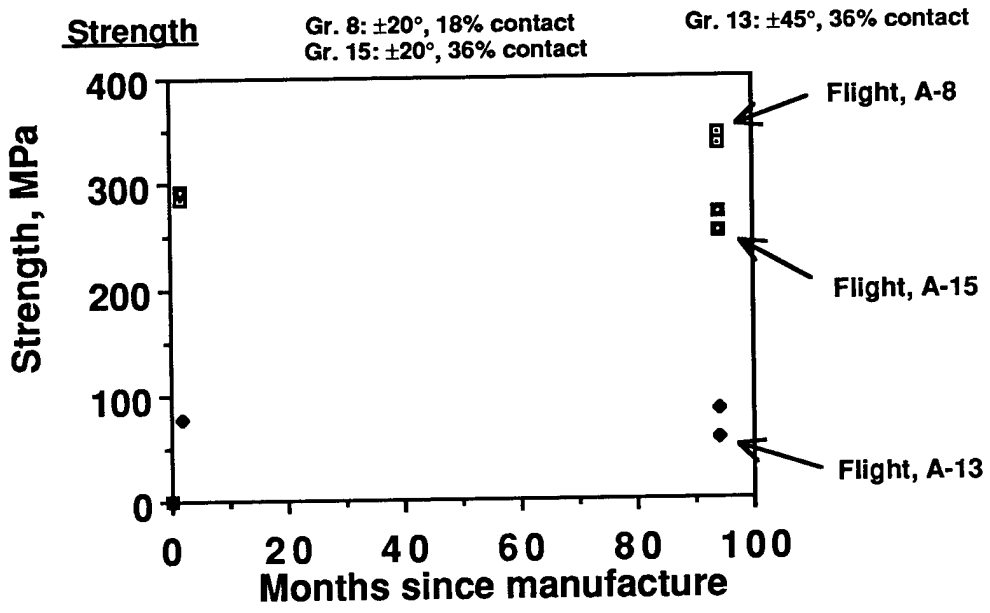


Fig. 5. Strength vs. time since manufacture of Group 8, 13, and 15 specimens.

EFFECTS OF LDEF FLIGHT EXPOSURE ON SELECTED POLYMER MATRIX RESIN COMPOSITE MATERIALS

Wayne S. Slemp, Philip R. Young, and William G. Witte, Jr.
NASA Langley Research Center
Hampton, Virginia 23665-5225

James Y. Shen
Lockheed Engineering and Science Company
Hampton, Virginia 23666

ABSTRACT

The characterization of selected graphite fiber reinforced epoxy (934 and 5208) and polysulfone (P1700) matrix resin composites materials which received over 5 years and 9 months of exposure to the LEO environment in experiment AO134 on the Long Duration Exposure Facility is reported. The changes in mechanical properties of ultimate tensile strength and tensile modulus for exposed flight specimens are compared to the three sets of control specimens. Marked changes in surface appearance are discussed, and resin loss is reported. The chemical characterization including infrared, thermal, and selected solution property measurements showed that the molecular structure of the polymeric matrix had not changed significantly in response to this exposure.

INTRODUCTION

The NASA Long Duration Exposure Facility (LDEF) provided a unique flight opportunity for conducting experiments in space and return of these experiments to Earth for laboratory evaluation. This paper reports the results of one of these experiments, AO134, Composite Materials for Large Space Structures(1), in which selected polymeric matrix composite materials were exposed to the low-Earth orbital (LEO) environment on LDEF. The materials were selected and fabricated at the Langley Research Center in 1982 and the final experiment assembly was conducted in 1983. The LDEF was deployed on April 7, 1984, and retrieved January 12, 1990, after over 5 years and 9 months in the LEO environment.

Figure 1 is a pre-flight photograph of the LDEF tray housing this and another experiment. Figure 2 shows the in-flight photograph of this experiment tray after LDEF recovery and the location of this experiment (in Tray B on Row 9 of LDEF). Row 9 was the leading edge of LDEF. A preliminary compilation of the exposure conditions experienced by specimens at this location during the 5-year 9-month orbital lifetime of the spacecraft is summarized in Table I. The objective of this experiment is to evaluate the response of resin matrix composite materials to extended LEO exposure which includes atomic oxygen, ultraviolet and particulate radiation, meteoroid and debris, vacuum and temperature cycling.

EXPERIMENTAL

Materials

The composite materials in this study are summarized in Table II. Two prepreg ply thicknesses of P1700 polysulfone thermoplastic and 934 epoxy thermoset were examined along with one ply thickness of 5208 epoxy thermoset. These composites were purchased as unidirectional prepreg material and fabricated at the Langley Research Center into a 4-ply $(\pm 45)_S$ lay-up so as to be matrix sensitive during tensile testing. The fabrication, quality control, processing, specimen preparation, and baseline testing were covered in previous reports (2,3). The flight specimens were cut from larger panels processed according to the prepreg manufacturer's specifications. The laminate thicknesses varied from 0.016-inch to 0.024-inch. The tensile specimens were 0.500-inch and 0.375-inch wide by 8-inches long with bonded, tapered fiberglass end tabs as illustrated in figures 3 and 4. One-inch-square specimens were also flown of the tensile test materials to more accurately evaluate mass change due to environmental exposure. Some square 934/T300 composites were coated with sputter-deposited metals to evaluated the metal's effectiveness for atomic oxygen protection of composites.

The exposed tensile specimens were mirrored by an identical set of specimens on the back side of the aluminum exposure plate, figure 5. This set of specimens was protected from direct environment exposure and experienced only vacuum and temperature cycling while in orbit. A matching set of specimens remained at Langley in a low humidity environment as controls.

Specimen Characterization and Testing

The chemical and physical characterization of retrieved specimens was conducted using a variety of techniques. Infrared spectra were recorded on a Nicolet 60SX Fourier Transform Infrared (FTIR) Spectrometer System using a diffuse reflectance technique (4). Glass transition temperature (Tg) determinations were made on a Perkin-Elmer Model 943 Thermomechanical Analyzer (TMA). Gel permeation chromatography (GPC) was performed on a Waters Associates system in chloroform using a $10^6/10^5/10^4/10^3$Å Ultrastyragel column bank. Scanning electron microscopy (SEM) and energy dispersive spectroscopy (EDAX) were performed either at Virginia Tech or Langley. The visual appearance of selected specimens was documented by various photographic techniques. Fiber/resin weight percents of the composites were determined by acid digestion according to ASTM D371. Mechanical property measurements on $(\pm 45°)_S$ tensile test specimens were performed at Langley according to ASTM D3039-76.

DISCUSSION

Visual examination of unprotected flight specimens revealed surface erosion from the extended exposure to atomic oxygen and also stripes of grey to black in some epoxy composites, figure 6. The center circular region received direct exposure for 5 years and 9 months; while the remaining outer-edge surface was protected by an aluminum template that held the specimen in place. The grey and black stripes in the photograph run in the

fiber direction of this $(\pm 45)_S$ specimen. The eroded appearance of these specimens was typical of all composite specimens in this experiment with 0.0055-inch ply thicknesses.

Samples from exposed and protected areas were cut from appropriate composites and analyzed by diffuse reflectance-FTIR. For this analysis, the sample was placed at the focal point of the diffuse reflectance optics and the spectrum of its surface recorded. Figure 7 shows spectra for a 5208/T300 specimen. A typical epoxy spectrum was obtained for the protected area. The absence of absorption bands in the spectrum for the exposed surface indicates a lack of matrix resin on that surface. The spectrum obtained by filing into the exposed surface and mixing the resulting powder with KBr essentially matched that of the protected side. Thus, DR-FTIR suggests substantial matrix resin loss due to exposure, but the molecular structure of the polymer which survived exposure was very similar to that of the unexposed polymer. The spectra in figure 8 for for the P1700/C6000 specimen shown in figure 9 indicates similar results.

The possibility that the Tg of the exposed side might be different from the protected side was examined by thermomechanical analysis. The TMA probe was carefully placed in contact with exposed and protected surfaces of several polysulfone specimens. Any movement in the probe as a function of temperature was recorded. Figure 10 summarizes the results of this evaluation. The Tg of a non-flight (control) specimen was essentially independent of the side examined. The slight variation in reported values can be explained by the discretionary judgement the analyst used in determining the inflection point in the TMA curve used to determine the glass transition. The Tg of flight samples with direct and protected exposure is also given in figure 10. A careful examination of all data suggests there is no significant difference in Tg for any of these samples.

Solution property data were obtained on selected polysulfone composites. Figure 11 shows GPC molecular weight distributions relative to a polystyrene standard for P1700 resin like that used to prepare prepreg, a control composite that remained at Langley, one which flew protected, and a composite which received direct exposure. The distributions are virtually superimposable and have been offset in figure 11 for clarity. There is also no discernable difference in various molecular weight averages for these four materials. These data support the general conclusion that there is no significant difference at the molecular level between polymer which survived exposure and the original polymer.

Figure 12 illustrates the erosion of the 5208/T300 graphite/epoxy flight exposed tensile specimens when compared to the virtually unaffected flight control specimen. The flight exposed specimens have the stripes typical to most of the specimens and the surface erosion caused these specimens to bow from unbalanced stress.

Figures 13 and 14 show ultimate tensile strength and tensile moduli for the five composite materials. No major differences are noted between baseline values obtained when the composites were tested in 1983, ground control composites which remained at Langley, and composites which flew protected. However, specimens which flew exposed experienced a deterioration in tensile strength and modulus. No doubt, more than a loss in matrix resin contributed to this phenomena since the thickness loss is not proportional to the loss in tensile properties by rule of mixtures. The P1700/C6000 specimens lost the least in thickness due to AO erosion and also retained more ultimate tensile strength than the other specimens. No explanation for this has been found.

Both 0.500-inch and 0.375-inch wide tensile specimens were included in this experiment to evaluate the influence of specimen edge effects on tensile test specimens exposed to atomic oxygen. A comparison of the results of tensile tests on these specimens

is shown in figure 15. The results indicate that reliable data can be obtained using the narrower 0.375-inch wide specimens. This will allow 25 percent more specimens to be exposed in a given area on future flight experiments.

Scanning electron microscope photographs, figure 16, illustrate the extent of erosion to these unprotected composites. An angled slice through a 4-ply lay-up is shown in the left photo. The enlarged area on the right shows that almost the total outer ply has been eroded away with only resin "fluff" and a thin layer of fiber remaining. The thickness loss for the graphite epoxy systems was 0.0045 inches of the 0.0055-inch thick outer ply.

The composite specimens which experienced vacuum and temperature cycling but were protected from ultraviolet and atomic oxygen exposure during flight exhibited less than a 10 percent change in ultimate tensile strength and modulus from the 5 years and 9 months in space. The results indicate that environmentally protected polymeric resin matrix composites should be capable of performing extended space missions.

Although substantial mass loss was typical of the uncoated polymeric resin matrix composites, the use of thin metallic sputter-deposited coatings protected the composite substrates from AO erosion. A coating of 1000 Angstroms of nickel with a 600 Angstrom overcoat of silicon dioxide, figure 17, exhibited no mass loss after 5 years and 9 months of LEO exposure. Aluminum coatings also provided similar protection.

CONCLUDING REMARKS

The uncoated resin matrix composites were severely degraded by atomic oxygen exposure, with thickness losses from 0.003 to 0.0045 inch. The molecular structure of surviving polymeric matrix resin after AO exposure appears unchanged; no chemical analysis techniques employed have been able to detect a chemical change in these resin matrices. These LDEF flight data indicate that atomic oxygen is the major LEO environmental factor leading to mechanical property changes in composite materials.

The P1700/C6000 polysulfone exhibited less thickness loss and degradation in tensile properties than the graphite/epoxy composites. Several thin metallic coatings which were sputter deposited onto the graphite/epoxy composite substrates protected the substrates from mass loss during the 5 years and 9 months of LEO exposure on LDEF. This illustrates that these composite materials can be safely used in space with thin metallic coatings to provide atomic oxygen protection. The flight composite specimens which experienced vacuum and temperature cycling but were protected from ultraviolet and atomic oxygen exposure exhibited minimal reductions in ultimate tensile strength and modulus. These results indicate that environmentally protected polymeric resin matrix composites should be capable of performing extended space missions

REFERENCES

1. Slemp, Wayne S.: Space Exposure of Composite Materials for Large Space Structures (AO134), NASA SP-473, pp. 24-26, 1984.

2. Witte, William G., Jr.: Manual for LDEF Tensile Tests, NASA TM-87624, Oct. 1985.

3. Witte, William G., Jr.: Baseline Tensile Tests of Composite Materials for LDEF Exposure, NASA TM-89069, Mar. 1987.

4. Young, P. R.; Stein, B. A.; and Chang, A. C.: Resin Characterization in Cured Graphite Fiber Reinforced Composites Using Diffuse Reflectance-FTIR, SAMPE, Vol. 28, pp. 824-837, 1983.

TABLES

- **Atomic oxygen**
  8.3×10^{21} atoms/cm^2
- **UV radiation**
  100-400 nm; 16,000 hrs
- **Particulate radiation**
  e^- and p^+: 2.5×10^5 rad surface fluence
  Cosmic: <10 rads
- **Micrometeoroid and debris**
  734 impact craters <0.5 mm
  74 impact craters <0.5 mm
- **Vacuum**
  1.33×10^{-4} - 1.33×10^{-5} N/m^2 (10^{-6} - 10^{-7} torr)
- **Thermal cycles**
  ~34,000 cycles: -29 to 71°C, ±11°
  (-20 to 160°F, ±20°)
- **Altitude**
  4.72×10^5 - 3.33×10^5 m (255-180 nautical miles)
- **Orbital inclination**
  28.5°

Table I. Preliminary environmental exposure conditions for row 9 of LDEF.

Sample	Type	Designation	Batch	Roll
1	Polysulfone/Graphite	P1700/C6000[a,d]	3W2407	1
2	Polysulfone/Graphite	P1700/C3000[a,d]	2W5272	1
3	Epoxy/Graphite	934/T300[b,d]	C2528	5
4	Epoxy/Graphite	934/T300[b,e]	C2627	2
5	Epoxy/Graphite	5208/T300[c,d]	1483	18

a Resin produced by Union Carbide Corp., fiber by Celanese Corp.
b Resin produced by Fiberite Corp., fiber by Union Carbide Corp.
c Resin produced by Narmco Materials Corp.
d 145 g/m^2 fiber areal weight.
e 95 g/m^2 fiber areal weight.

Table II. Composite materials in LDEF flight experiment.

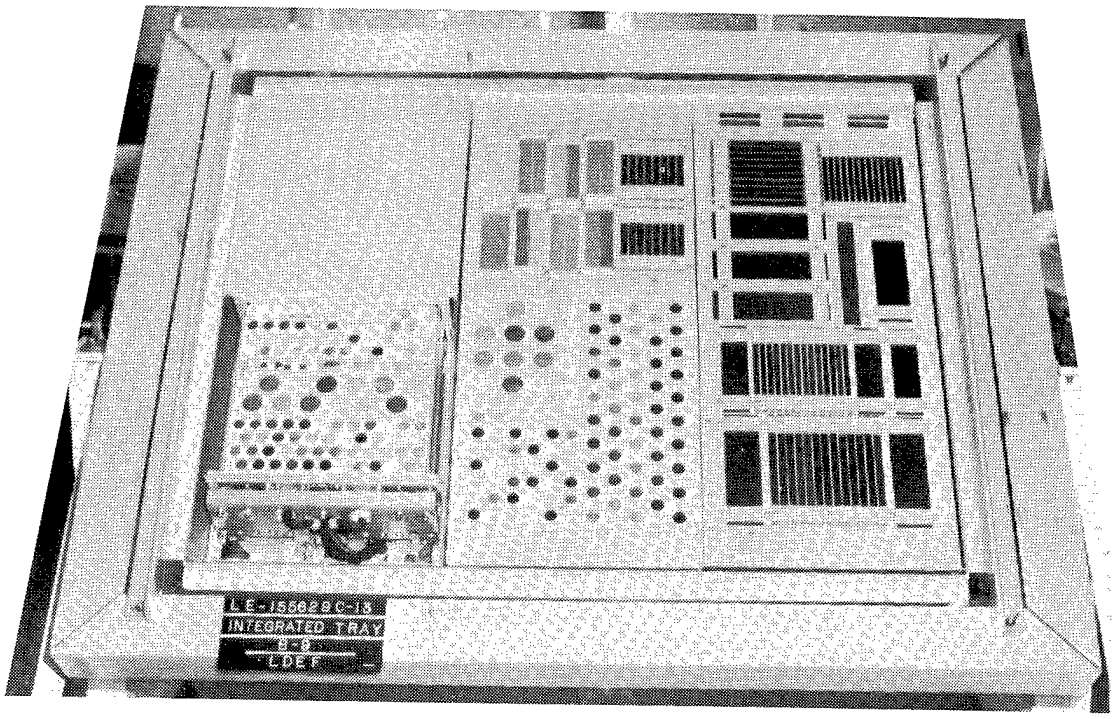


Figure 1. LDEF tray with Langley materials flight experiments.

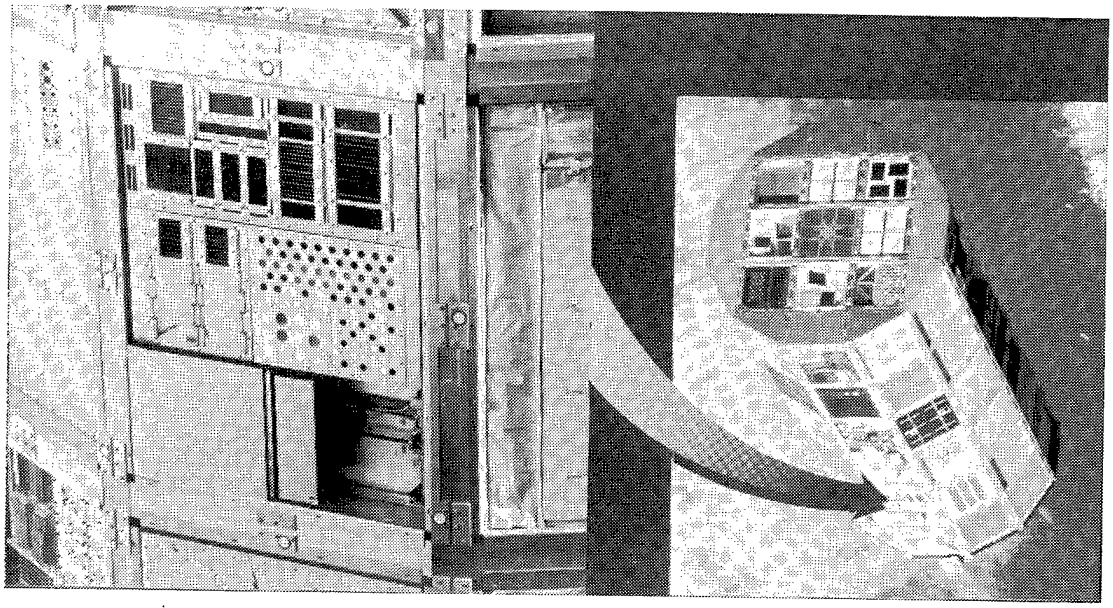


Figure 2. In-orbit photo of LDEF tray after recovery and tray location on leading edge of LDEF.

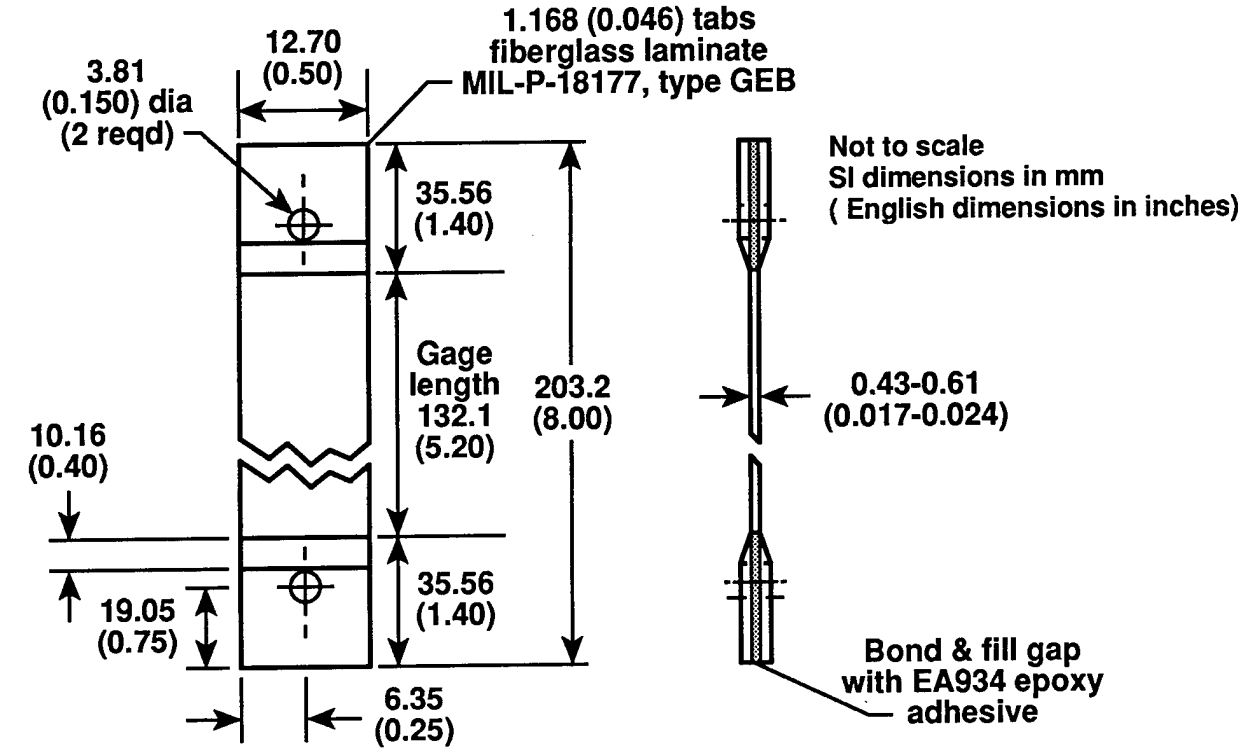


Figure 3. LDEF conposite tensile test specimen configuration for 0.500-inch wide specimens.

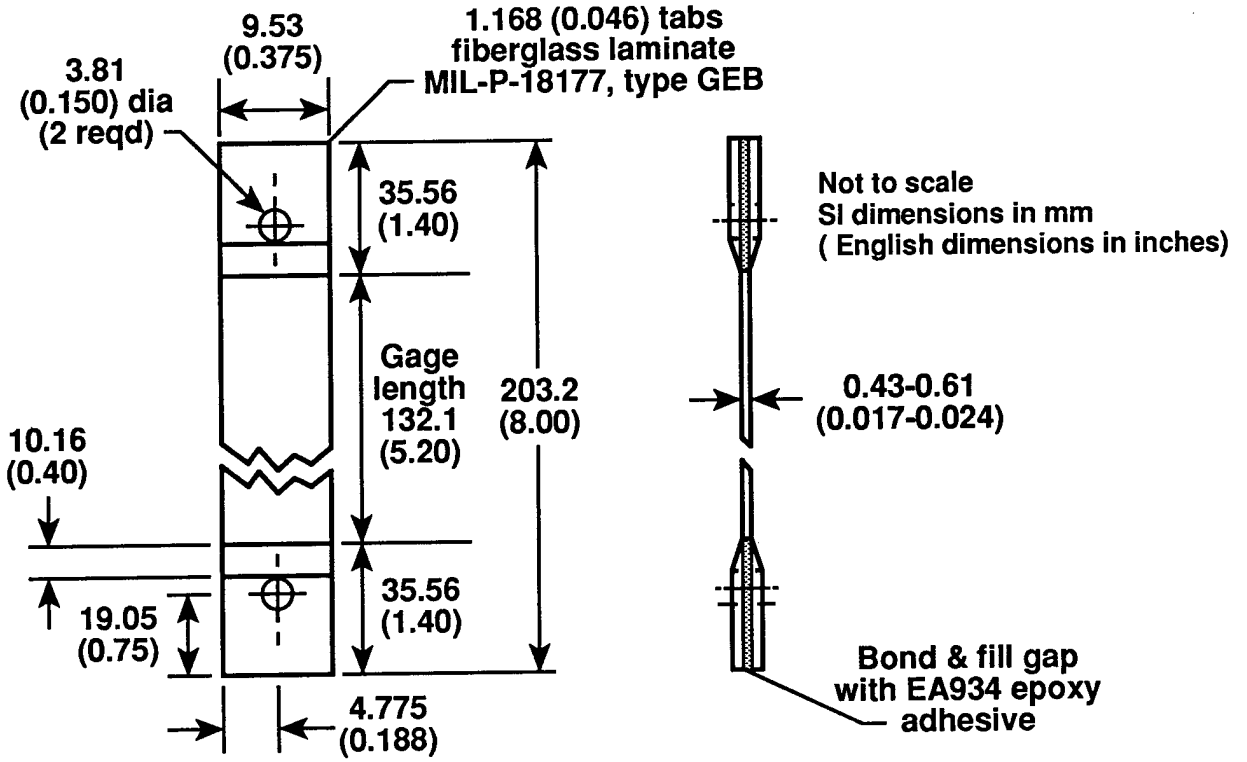


Figure 4. LDEF composite tensile test specimen configuration for 0.375-inch wide specimens.

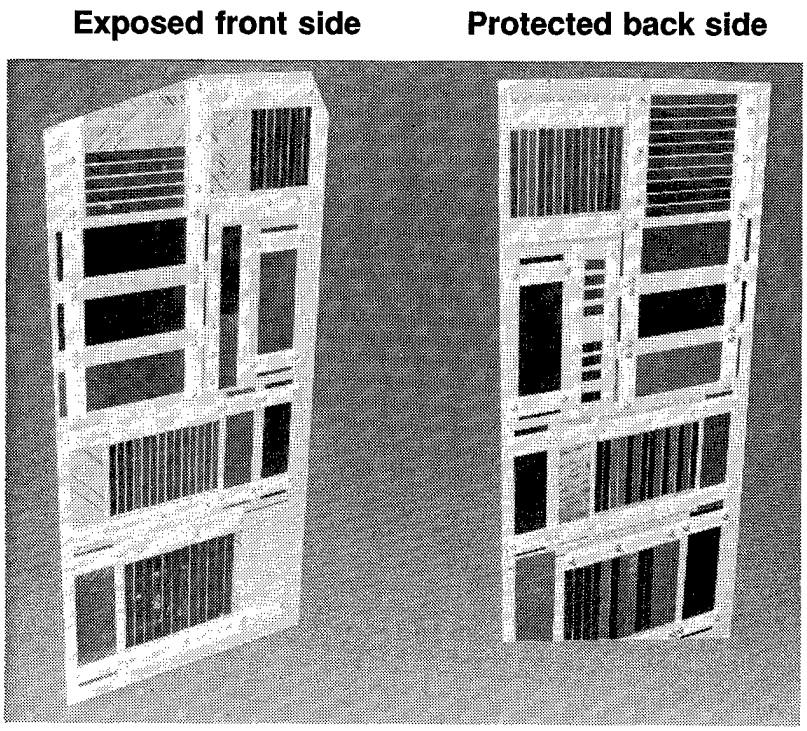


Figure 5. Tensile test specimens in LDEF experiment A0134.

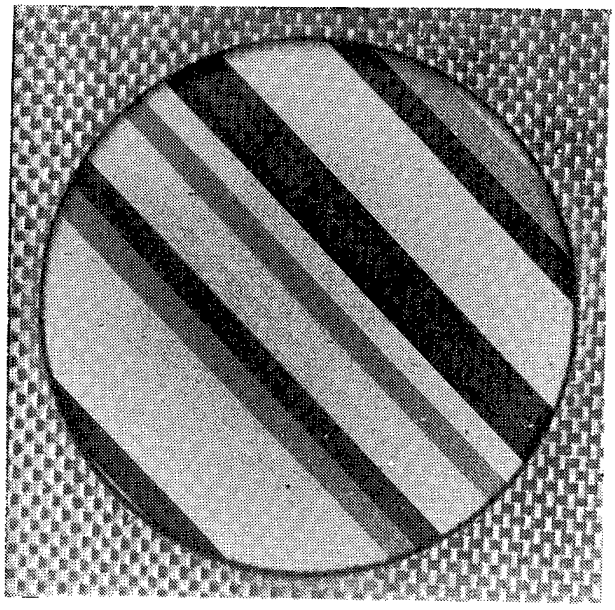


Figure 6. Uncoated 5208/T300 epoxy/graphite specimen with center area showing effects of 5.8 years of flight exposure.

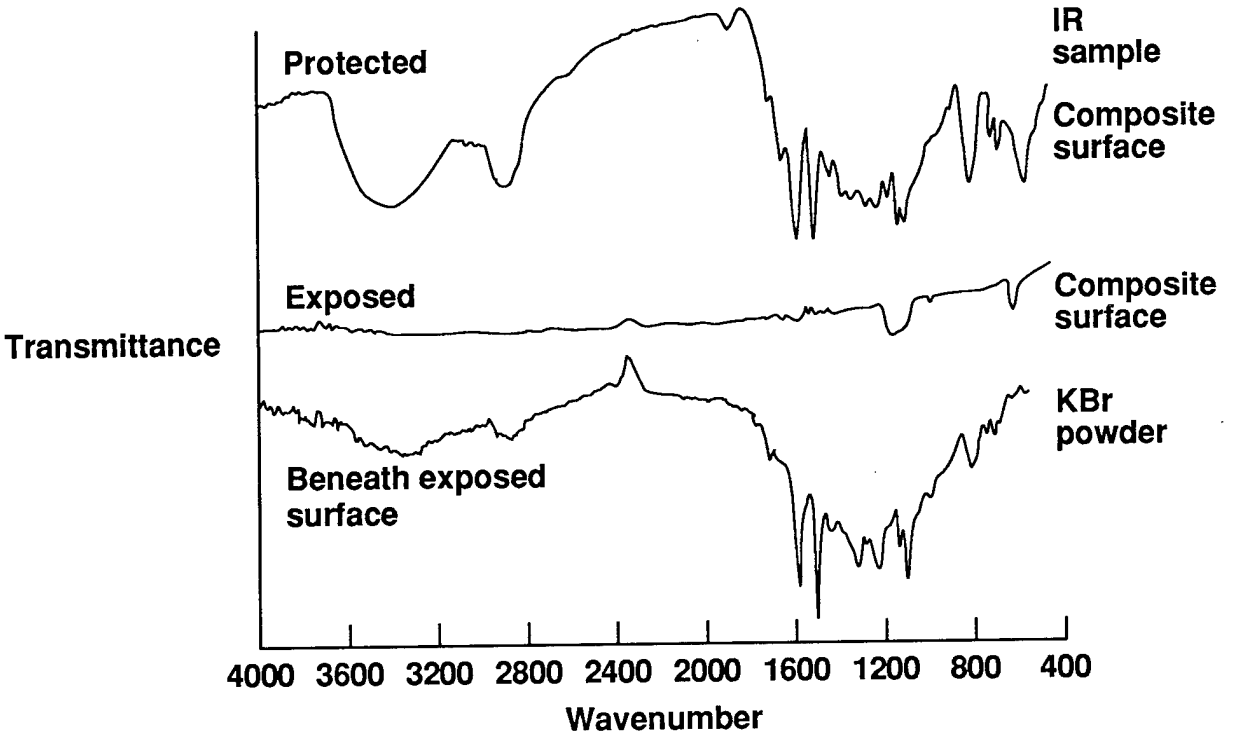


Figure 7. Direct reflectance FTIR spectra of LDEF exposed 5208/T300 epoxy/graphite composites.

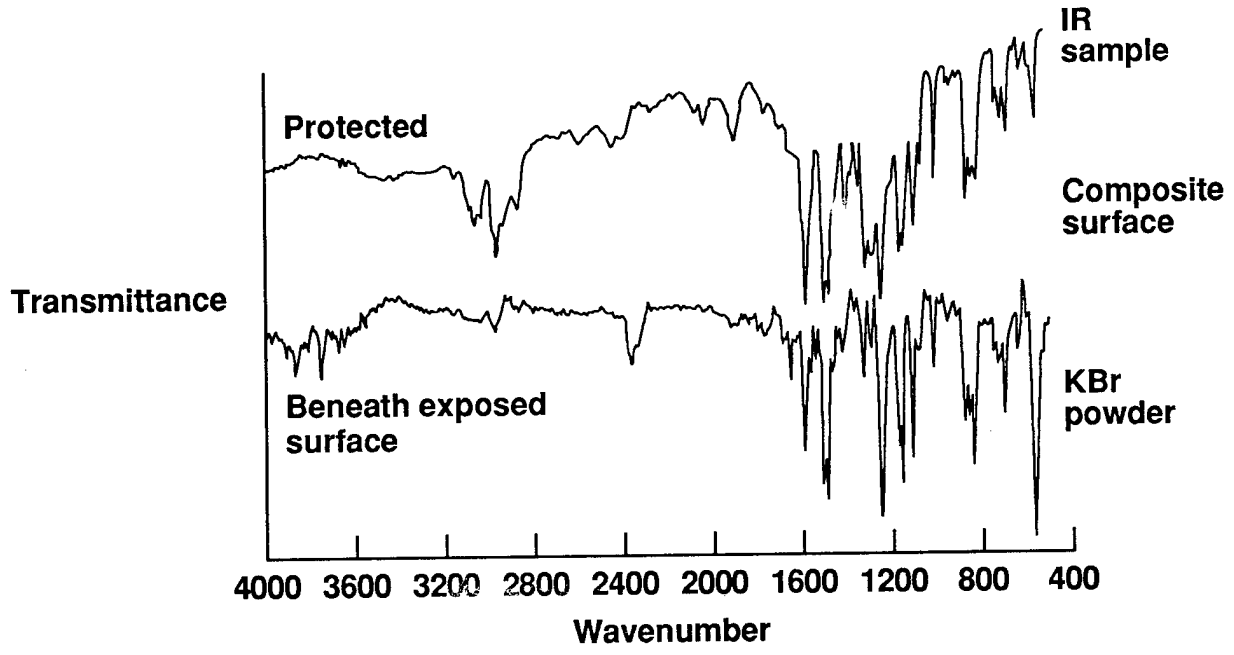


Figure 8. Direct reflectance FTIR spectra of LDEF exposed P1700/C6000 polysulfone/graphite composites.

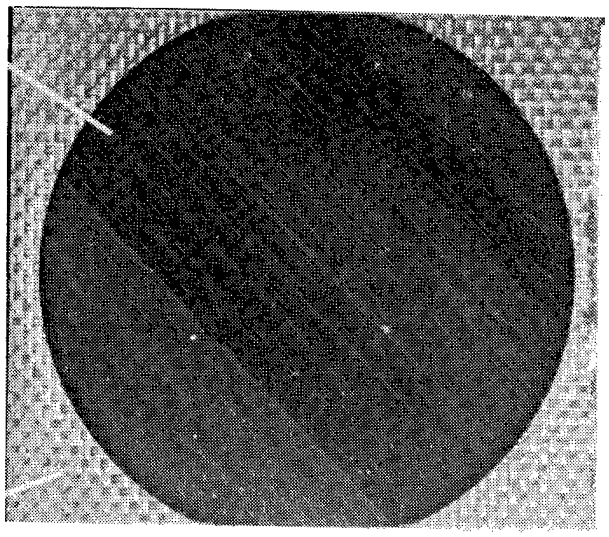


Figure 9. Effects of 5.8 years of LDEF flight exposure on uncoated P1700/C6000 polysulfone/graphite composites.

Sample	Tg (°C)	Contacted Side
Langley Control	167°	Random
	167°	
	170°	
	166°	
Flight Protected	164°	Side A
	166°	Side B
Flight Exposed	170°	Exposed side
	171°	
	169°	Nonexposed side
	171°	

Figure 10. Results of thermomechanical analysis of P1700/C6000 polysulfone composites.

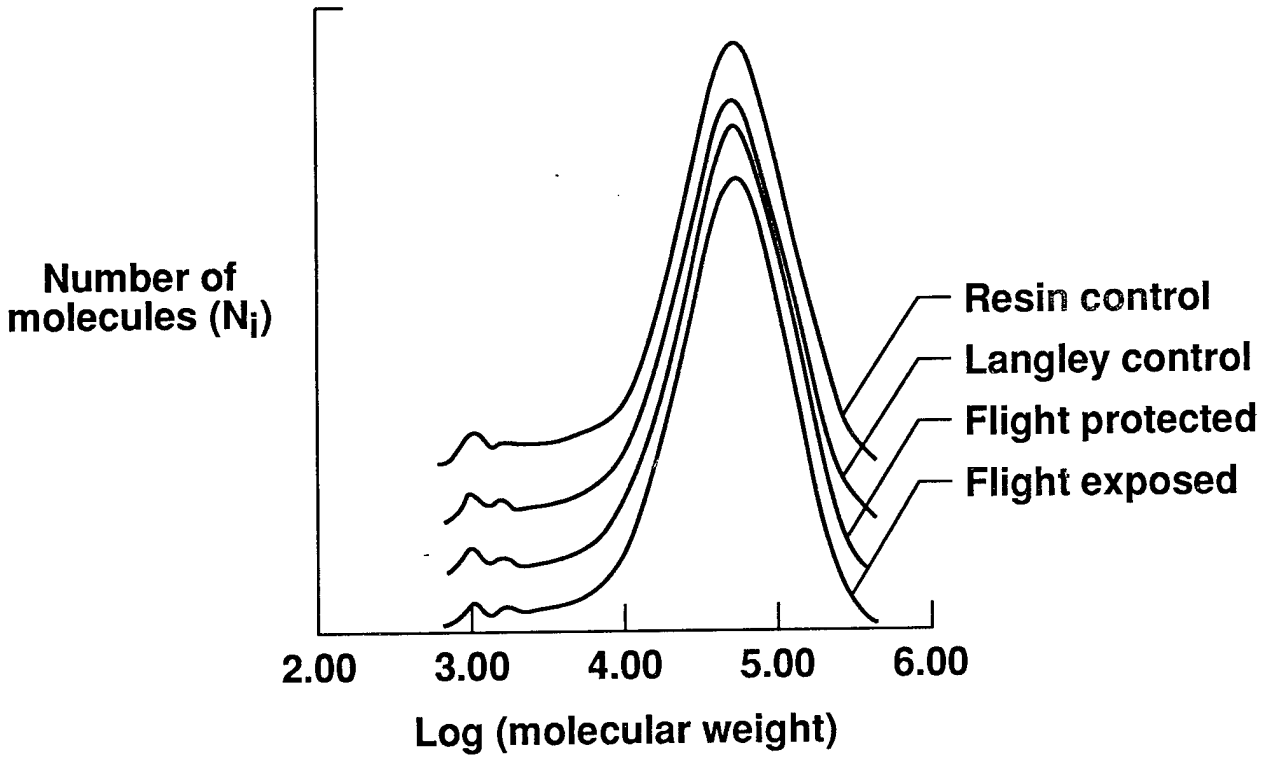


Figure 11. GPC molecular weight distribution of P1700 polysulfone composite matrix resin.

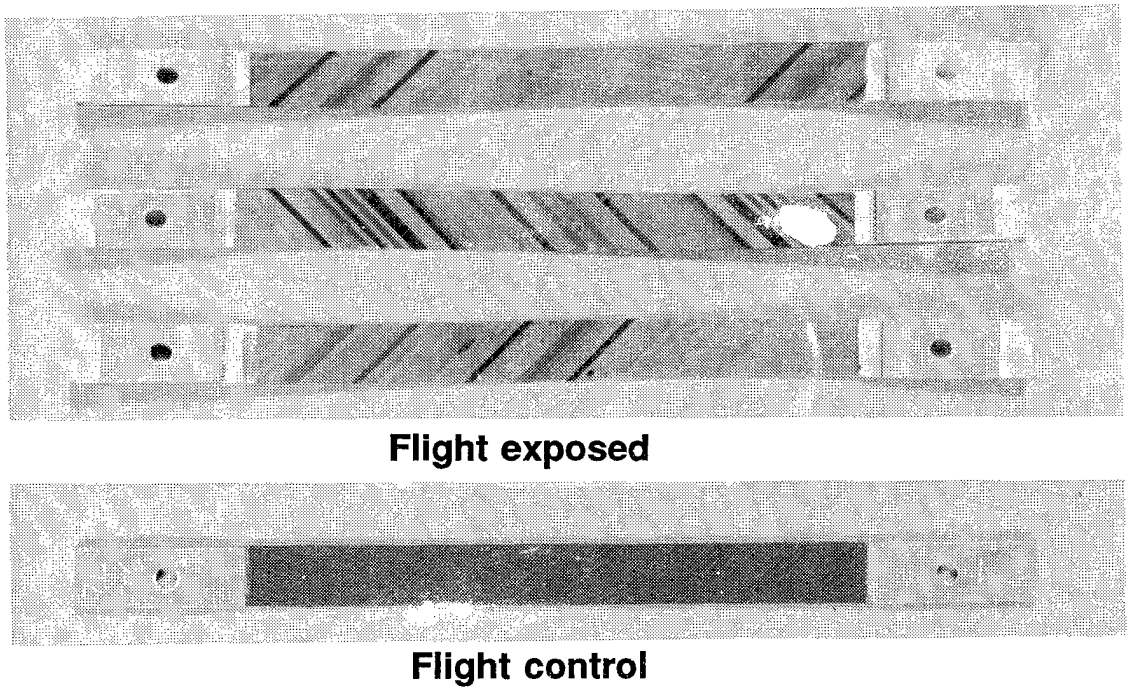


Figure 12. Epoxy/graphite composite 5208/T300 tensile specimens.

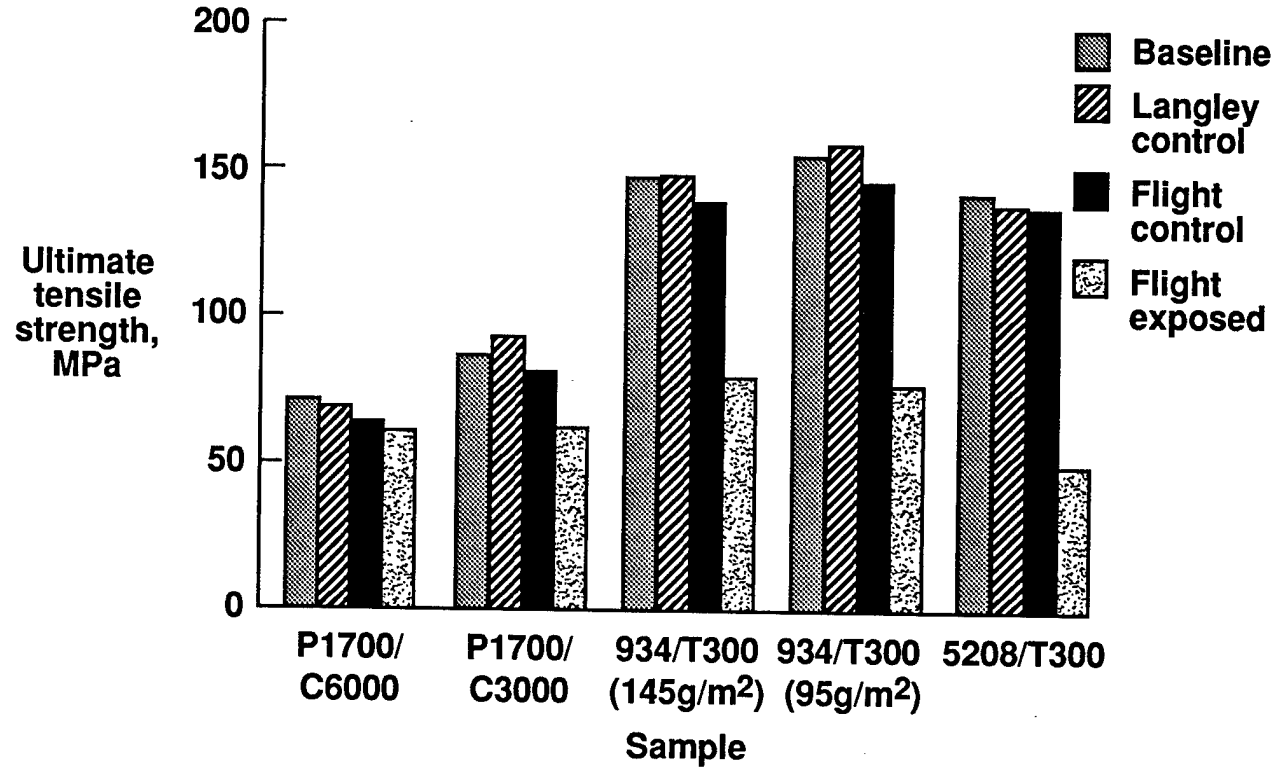


Figure 13. Effects of 5.8 years of LDEF flight exposure on ultimate tensile strength of composite materials.

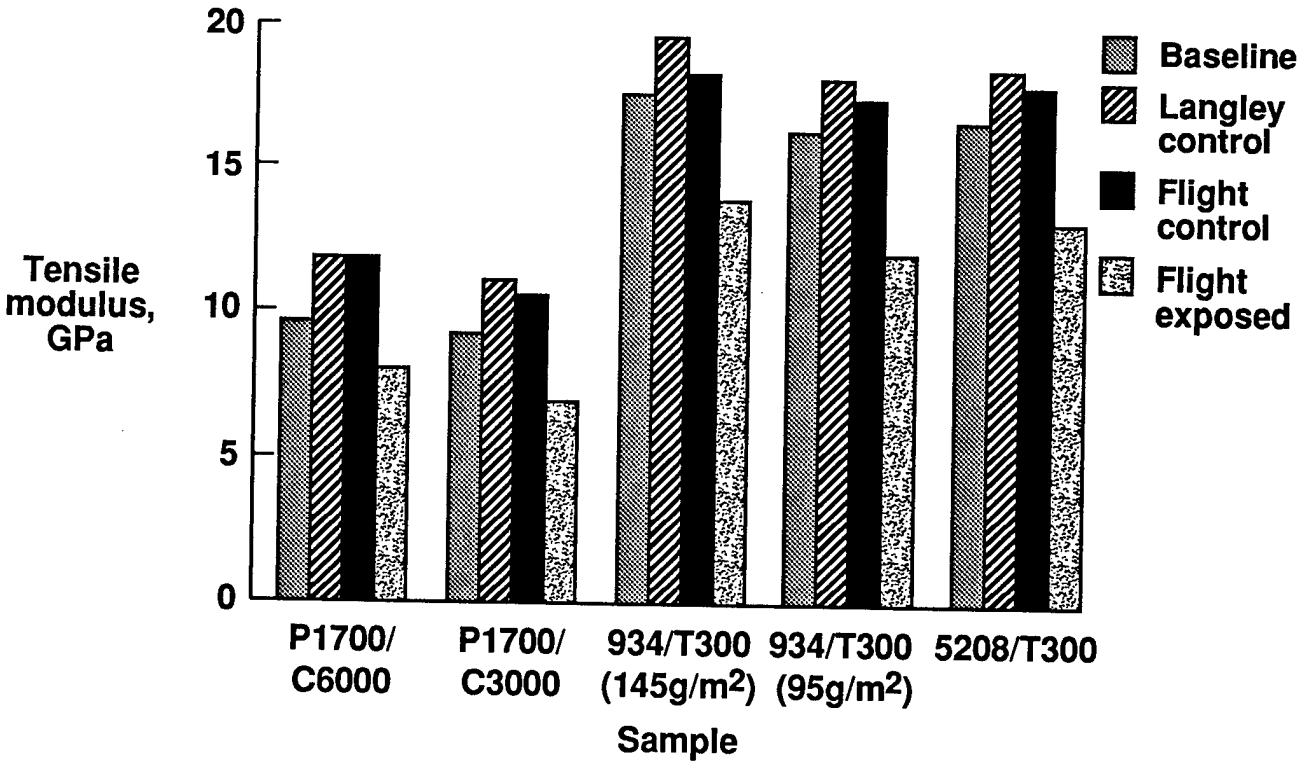


Figure 14. Effects of 5.8 years of LDEF flight exposure on tensile modulus of composite materials.

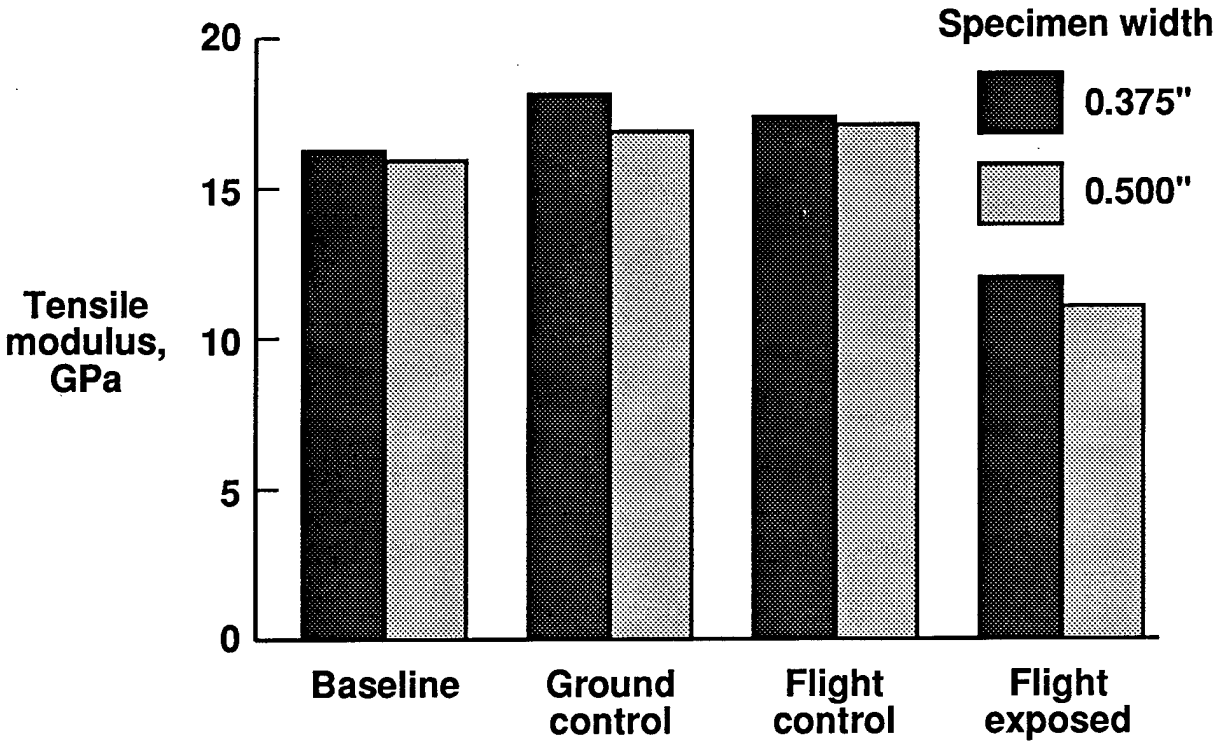


Figure 15. Comparison of tensile modulus of 0.500-inch and 0.375 inch width 934/T300 (95g/m^2) specimens.

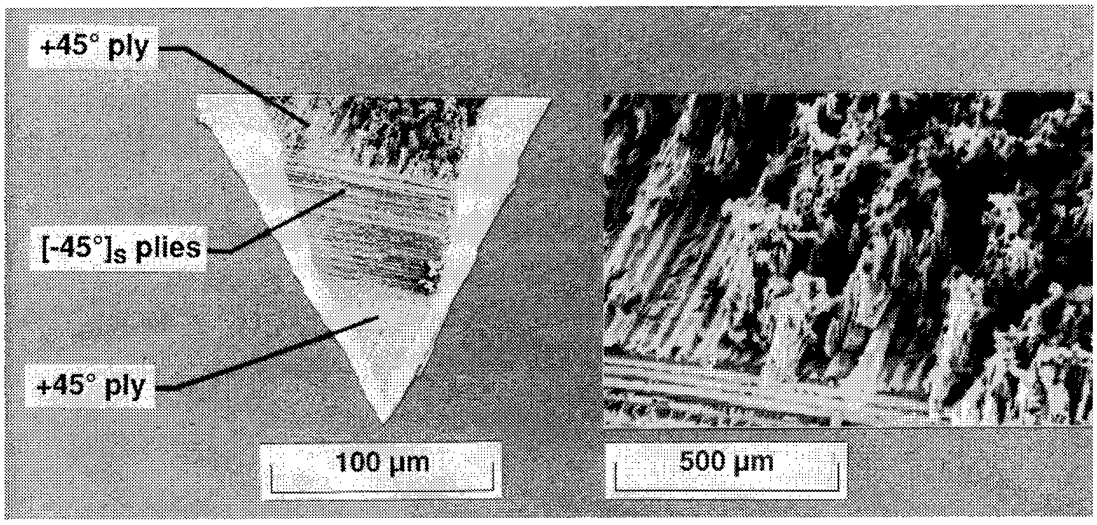


Figure 16. SEM of 5208/T300 epoxy/graphite $[\pm 45]_s$ composite after 5.8 years exposure.

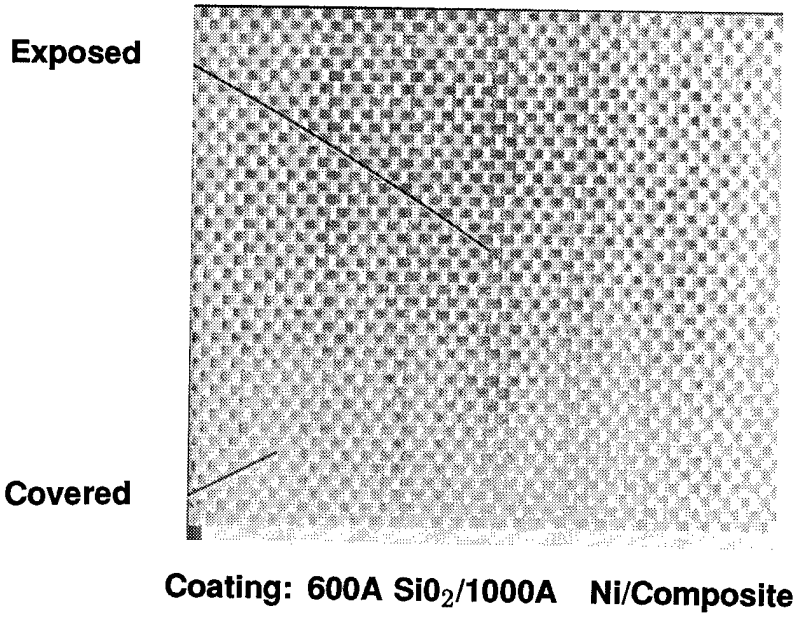


Figure 17. Effects of 5.8 years of LDEF exposure on coated 934/T300 epoxy/graphite composite.

EFFECT OF SPACE ENVIRONMENT ON COMPOSITE MATERIALS AND THERMAL COATINGS (A0 138-9)

Michel Parcelier
Aérospatiale
Space and Strategic Systems Division
78133 Les Mureaux-Cedex, France
Phone: (33) 1 34 92 36 78, Fax: (33) 1 34 92 10 97

Jean Pierre Assié
Aérospatiale
Space and Strategic Systems Division
06322 Cannes-la Bocca, France
Phone: (33) 92 92 72 49, Fax: (33) 92 92 71 90

SUMMARY

This paper presents an experiment within the FRECOPA project on composite materials, adhesives and thermal coatings. The aging of the specimens was limited because of the canister closing, the location on the trailing edge and the arrangement of the specimens inside the canister. The results show no evidence of change for several graphite fiber-reinforced epoxy matrix composite materials as well as for the 2 adhesives. Minor changes can be found on some second-surface mirrors. (See figures 1–16).

INTRODUCTION

This experiment was passive and was located in one of the three FRECOPA canisters in a 12-in.-deep peripheral tray that contained nine other experiments from France. The FRECOPA box provided protection for the specimens from contamination during launch and reentry phases of the LDEF mission.

Aérospatiale, as satellite manufacturer, designs and builds some parts and structures using different materials and technologies. The objective of this experiment was to assess the possible degradation of materials such as the following:

- graphite fiber-reinforced epoxy matrix composite materials: mechanical characteristics and dimensional stability,
- adhesives,
- thermal coatings.

GENERAL CONDITIONS OF THE EXPERIMENT

The arrangement of specimens chosen for this experiment has an influence on the data: due to the small surface area exposed to the direct space environment, and in order to have a greater number of specimens, 6 levels have been arranged as shown in Fig 1. The thermal coatings have been put in the

upper level in order to be directly exposed to space environment; in the lower levels, composite materials and adhesives were subjected to vacuum and thermal cycling.

For the choice of materials, instead of selecting a few materials to make the test data more reliable, we have chosen for a first approach to put more materials with a limited number of specimens on each test in order to have the tendencies on different materials. In addition, the requirement on weight for this experiment (≤ 1 Kg) led to minimizing the weight of the fixture: this is why we replaced pre-cut specimens by small panels that require a lighter fixture to meet LDEF vibration specification.

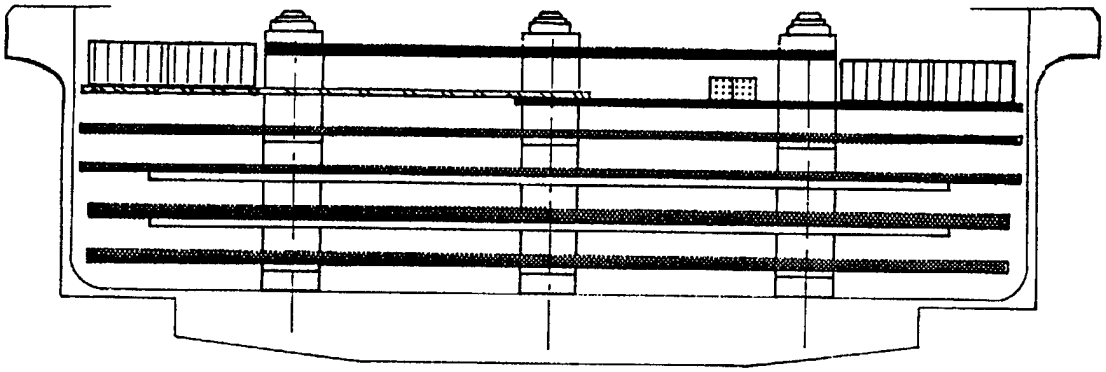


Fig.1 Cross-section showing the arrangement of specimens

The FRECOPA programmed timer made the box close just before the scheduled LDEF retrieval in 1985. From that time to the end of the mission, the specimens were not any longer subjected to direct space environment; in particular, the specimens were saved from the degradation due to a very low altitude of LDEF at the end of the mission. In addition, the specimens were located on the trailing edge.

COMPOSITE MATERIALS

Definition of materials

The laminates are based on a combination of the following constituents:

- 3 epoxy resin systems:
  - -code 87 (CyFo) — 120°C (250°F)
  - -BSL 914 (Ciba) — of which the service temperature is 150°C (300°F)
  - - Vx108 (Ciba-Brochier) — 180°C (350°F)
- 2 graphite fibers:
  - - T300 (high tensile strength)
  - - GY70 (ultra high modulus)

The list of materials as well as their location in the FRECOPA box are shown in table 1. Prior to testing, all flight and ground-based specimens had been dried to avoid the influence of moisture.

Appearance

A small part of GY70 / BSL 914 and one of T300 / Vx108 were exposed to direct space environment. A comparison with protected parts has been made by a scanning electronic microscope up to a magnification of 10000 times. No change has been revealed and fingerprints of peel plies used for manufacturing are still visible. Visual appearance only exhibits a slight change in color of the laminates similar to that observed on earth due to ultraviolet rays.

Levels	Materials
1A	sandwich (GY70 / code 87 + BSL 312 adhesive)
1B	sandwich (GY70 / BSL 914 + BSL 319 adhesive)
3A, 4A	unidirectional GY70 / code 87
3B, 4B	unidirectional GY70 / BSL 914
5A, 6A	unidirectional T300 / Vx108
5B	unidirectional GY70 / Vx108
6B	woven T300 fabric / Vx108

Table 1

Assessment of mechanical properties degradation

On unidirectional laminates, short beam shear, flexure and tensile tests have been carried out. Figures 1, 3 and 4 show the specimens used (dimensions in mm).

The results of these tests are reported in Fig 2 and 5 to 8. No change between flight and ground-based specimens have been exhibited within the temperature range used for satellite applications, but due to the normal scattering of data for such materials, minor changes may have not been revealed. For Vx108-based composite materials, short beam shear test has been carried out beyond 120°C (250°F) and up to service temperature (Fig 2): no degradation has been found on flight specimens.

Assessment of dimensional stability

Coefficient of thermal expansion (CTE) tests have been carried out between -40°C and 140°C on sandwich-construction specimens representative of antenna reflectors. The specimens were coated with PSG 120 FD white paint and located on top of the specimen arrangement in order to have a direct solar exposure.
The sandwich specimens consist of:

- GY70 / code 87 laminates (0°, 90°, 90°, 0°) + BSL 312L adhesive + aluminum honeycomb (two-step curing process)
- GY70 / BSL 914 laminates (0°, 90°, 90°, 0°) + BSL 319L adhesive + aluminum honeycomb (co-curing process).

In case of change in CTEs on flight specimens, it would have been necessary for computer modeling, to check whether input data had changed: so, CTEs of the constituents (unidirectional laminates and adhesive bars) have been carried out .

Length of specimens is 200 mm and the accuracy of the dilatometer is 1 μm. Curves for sandwich specimens are reported in Fig 11 and 12. For W and L directions, the curves show no change in thermal expansion within the range -40°C to 140°C. Curves for unidirectional laminates are shown in Fig 13 to 16. Except for a minor increase in CTE for BSL 914 laminates that has no influence on relevant sandwich specimens, no difference has been found between flight and ground-based specimens.

ADHESIVES

The shape of some composite material parts (i.e. small omega-style stiffeners) makes the surface treatment by sanding difficult to apply. A limited surface treatment by solvent cleaning may be an alternative for non-highly-stressed bonded joints but lack of data puts a brake on this possibility. Experiments within the LDEF project are an opportunity to test such bonded joints by tensile lap shear (Fig 9). The adhesives and adherents are representative of some bonded assemblies used for satellites (table 2):

Adhesive	Adherent
BSL 312 L (Ciba)	T300 / Vx 108 and 2024
Redux 408 (Ciba)	T300 / Vx 108

Table 2

Results are reported in Fig 10. As expected, adhesion failure has been found on each specimen; for each test, the low ultimate strengths are similar for the flight and ground-based specimens. Thermal cycling undergone by the flight specimens does not appear to affect these bonded joints.

THERMAL COATINGS

Good performances for thermal coatings are essential throughout the life cycle of spacecrafts. Our main interest is in the possible change of thermo-optical properties after an extended space exposure. Four types of second surface mirrors (SSM) were located on top of the arrangement of specimens to be exposed to direct solar and space environment for one year.

The SSM were bonded on both aluminum and graphite fiber / Vx108 epoxy system plates and are as follows:

- non-conductive standard OSR (OCLI)
- G408 831 Kapton (Sheldahl)
- G401 801 aluminized Teflon (Sheldahl)
- G401 901 silvered Teflon (Sheldahl)

Solar absorptance

Solar absorptance α_S is calculated by an integration of reflection spectrum between 0.25 and 2.5μm: data are given in table 3.

Support	SSM	Ground-based specimen	Flight specimen
aluminum	OSR	0.092 0.090 avg:0.093 0.096	0.118 0.114 avg:0.113 0.107
	Kapton	0.459	0.469
	Al Teflon	0.162	0.198
	Ag Teflon	0.116	0.139
composite material	OSR	0.120 0.094 avg:0.103 0.096	0.122 0.106 avg:0.111 0.104
	Kapton	0.467	0.472
	Al Teflon	0.165	0.195
	Ag Teflon	0.148	0.149

Table 3

Specular reflectance ratio

The specular reflectance ratio defines the capability for thermal coatings to be perfect mirrors: performing this test is a good way to assess whether the flight specimens show a milky aspect. The quantity of energy reflected outside a 2° angle from the normal direction of the reflected energy has been measured at 0.5 μm. Data reported in table 4 are expressed as the ratio of diffused reflection to total reflection.

Support	SSM	Ground-based specimen	Flight specimen
aluminum	OSR	2.7% 1.0% avg: 1.6% 1.1%	1.0% 1.0% avg: 1.0% 1.0%
	Kapton	22.2%	21.2%
	Al Teflon	21.8%	20.5%
	Ag Teflon	21.1%	22.7%
composite material	OSR	1.2% 1.2% avg: 1.2% 1.3%	1.7% 1.4% avg: 1.4% 1.3%
	Kapton	13.7%	15.0%
	Al Teflon	17.2%	21.2%
	Ag Teflon	18.4%	25.9%

Table 4

Infra-red emittance

The spectral emittance is given by comparison of emission between the specimen and a reference surface, both surfaces being heated at 100°C (240°F). The emission spectrum is collected by means of a Fourier transform spectrophotometer. Total emittance data (see table 5) are calculated by integration

of the spectrum.

Support	SSM	Ground-based specimen	Flight specimen
aluminum	OSR	0.745 0.715 avg: 0.739 0.757	0.752 0.729 avg: 0.738 0.733
	Kapton	0.646	0.695
	Al Teflon	0.653	0.723
	Ag Teflon	0.705	0.745
composite material	OSR	0.743 0.636 avg: 0.707 0.742	0.730 0.742 avg: 0.722 0.695
	Kapton	0.732	0.758
	Al Teflon	0.744	0.645
	Ag Teflon	0.714	0.729

Table 5

Results (for one-year direct solar exposure)

For Teflon and Kapton, data give tendencies on changes (only 2 specimens per material). OSRs appear to be more reliable (6 specimens). Solar absorptance data show a slight increase for each material (absolute increase is 0.03 maximum). Specular reflectance ratio is an important parameter for OSR: no change has been revealed. Due to the scattering of infra-red emittance data, no evidence of change has been found.

CONCLUSION

Compared with the materials of all LDEF experiments, the specimens of this experiment were relatively protected from direct space exposure (trailing edge and canister closed after one year-exposure): no evidence of change has been found on composite materials and adhesive specimens (subjected to only thermal cycles). Minor changes have been exhibited on thermal coatings (direct solar exposure for one year). These results show that we can rely on the materials already used.

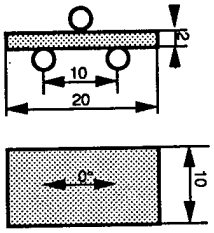
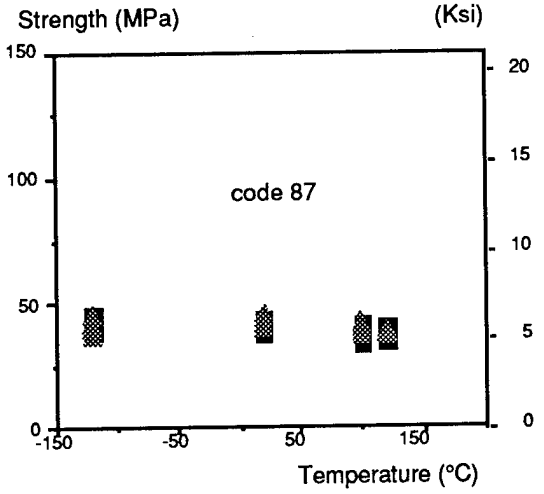
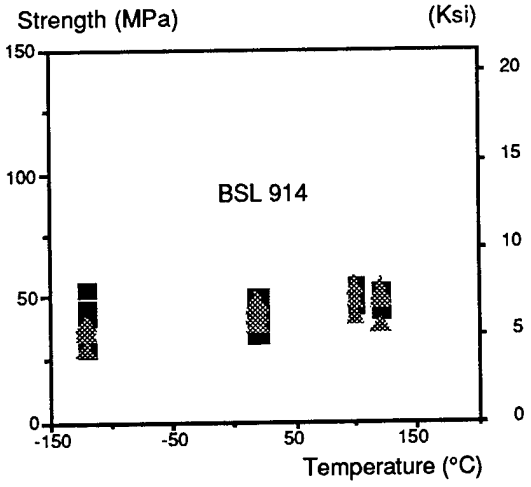


Fig 1 Short beam shear test specimen





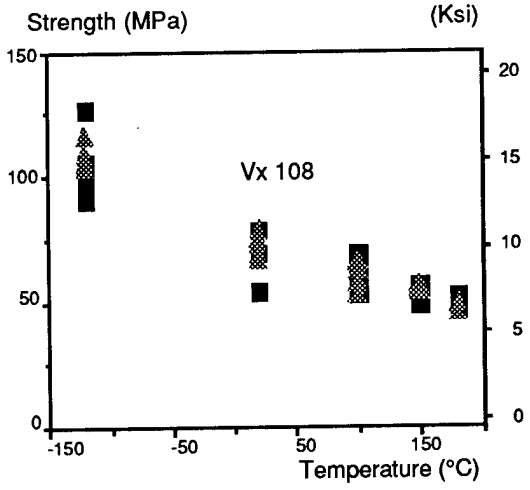


Fig 2 Short beam shear strength on unidirectional GY70 / epoxy systems

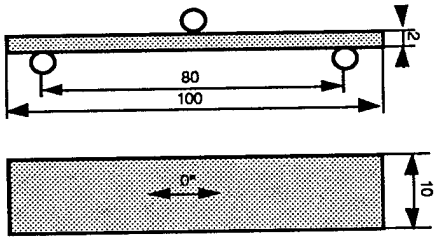


Fig 3 Flexure test specimen

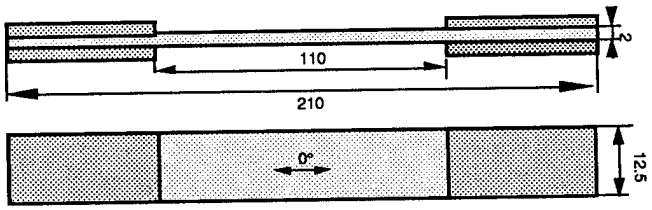


Fig 4 Tensile test specimen

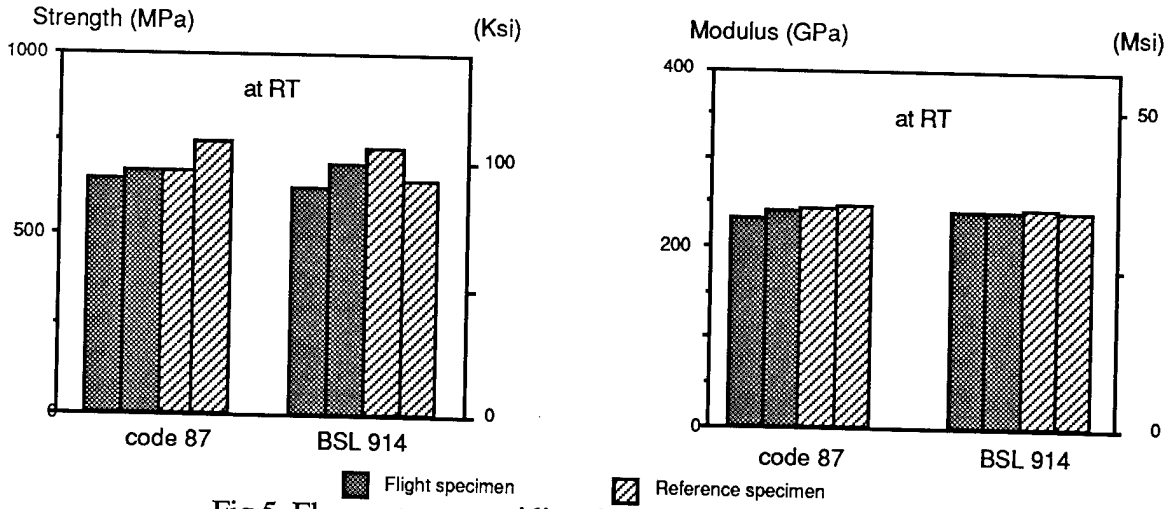


Fig 5 Flexure test on unidirectional GY70 / epoxy systems

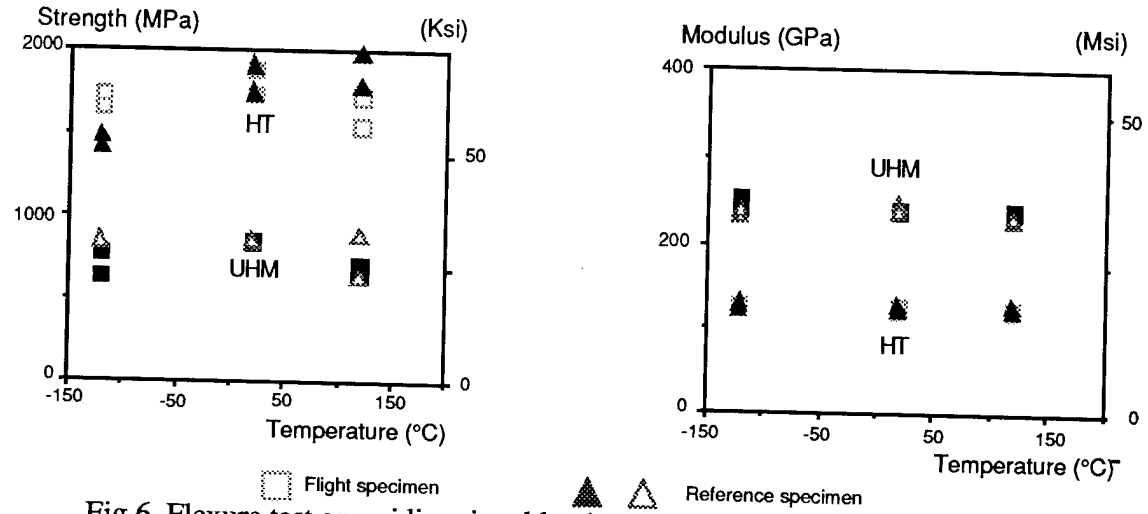


Fig 6 Flexure test on unidirectional laminates based on Vx 108 epoxy system

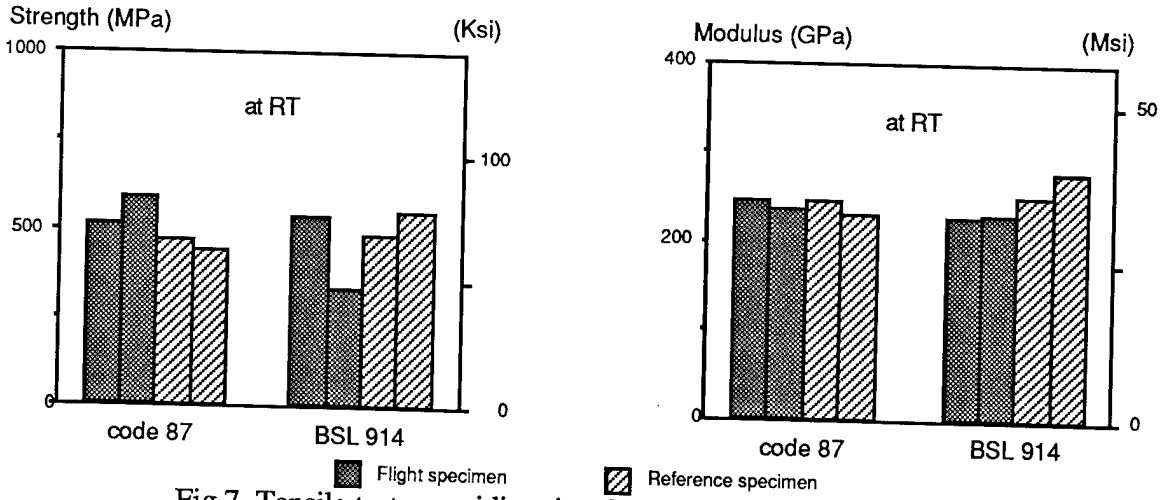


Fig 7 Tensile test on unidirectional UHM graphite fiber / epoxy

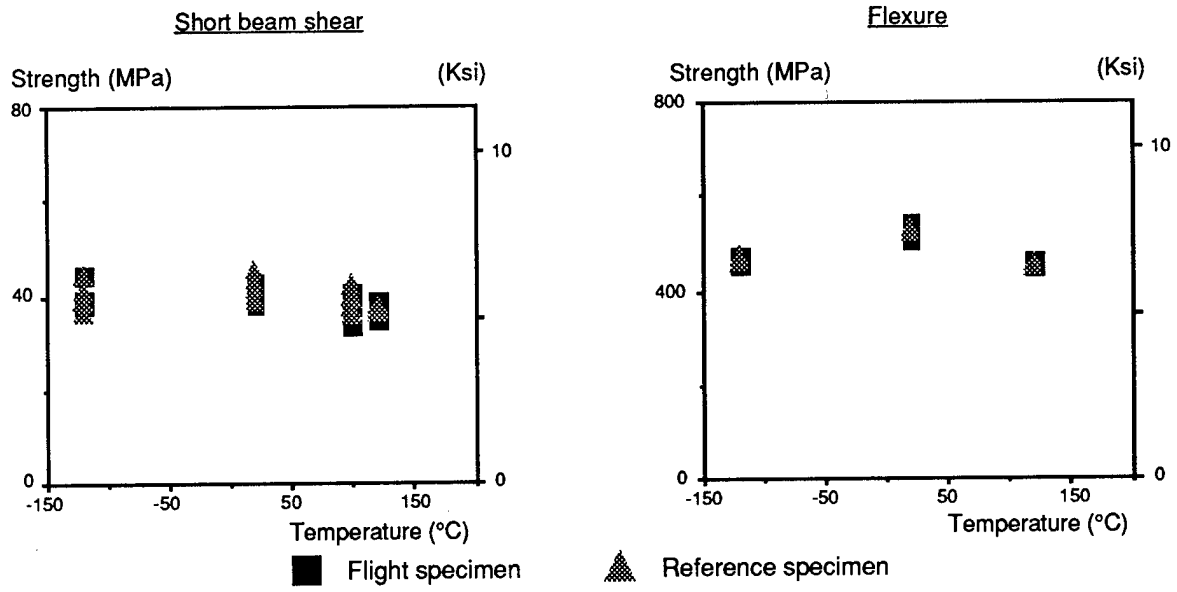


Fig 8 Tests on T300 fabric / Vx 108

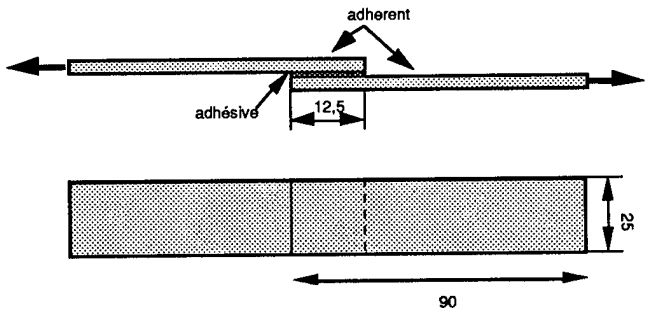


Fig 9 Tensile lap shear specimen

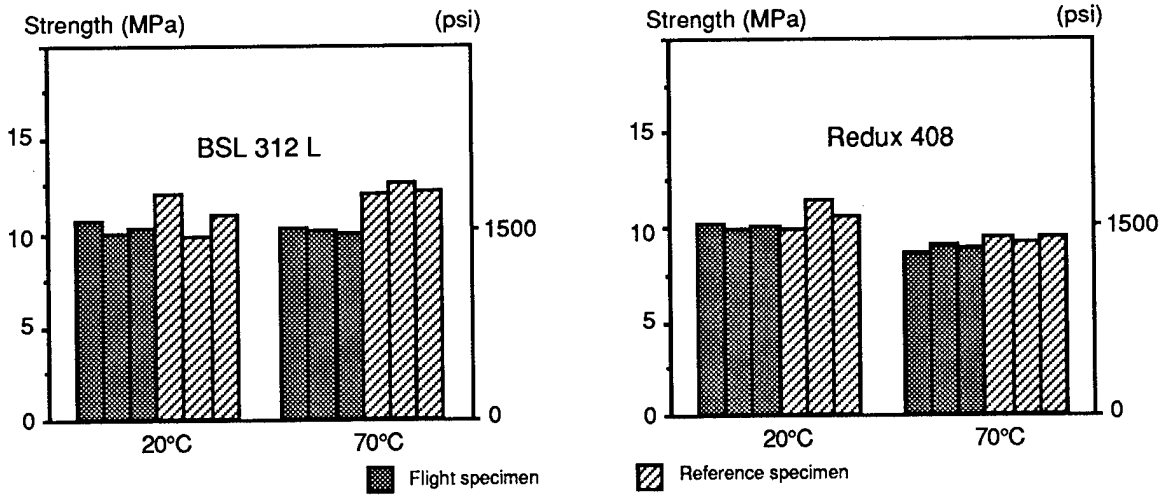


Fig 10 Tensile lap shear strength

COEFFICIENT OF THERMAL EXPANSION FOR HONEYCOMB SPECIMENS

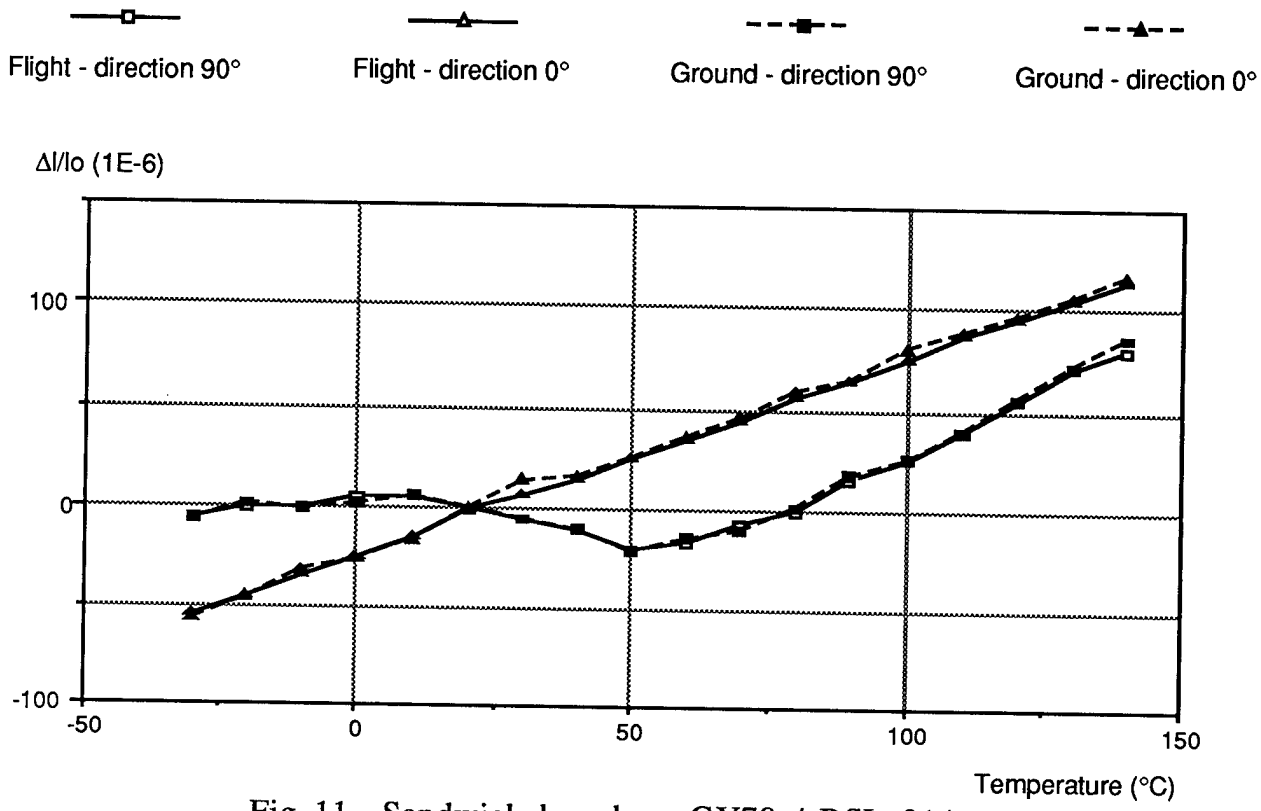


Fig 11 Sandwich based on GY70 / BSL 914

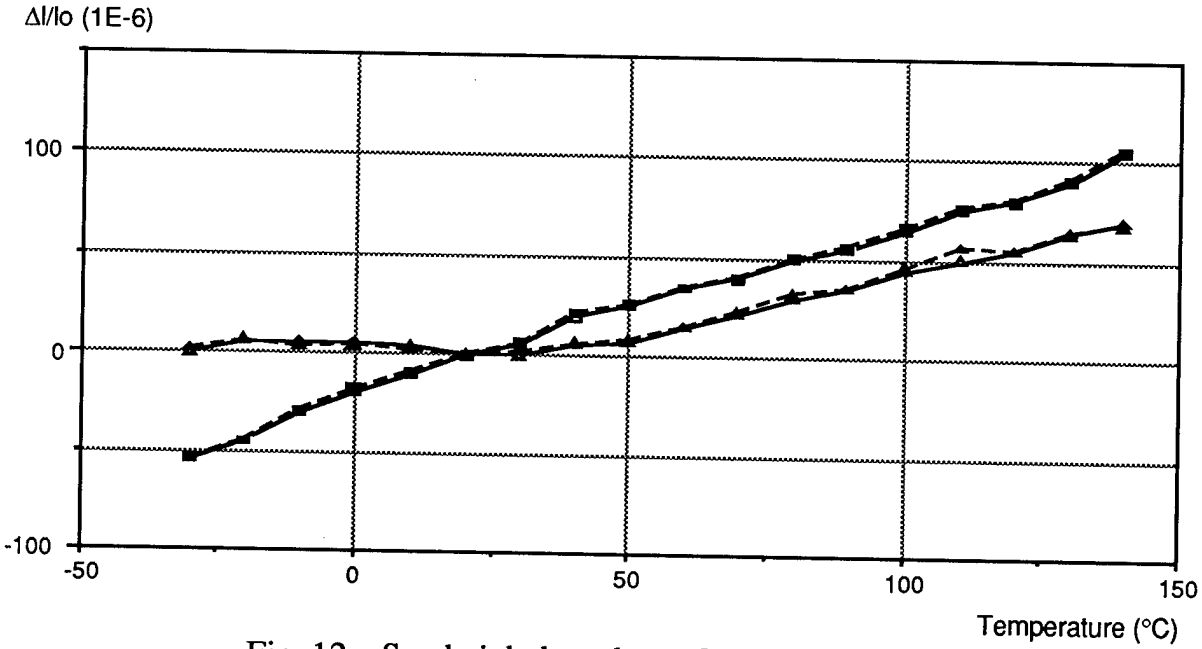


Fig 12 Sandwich based on GY70 / code 87

Caption:

——— Flight - - - - - Ground

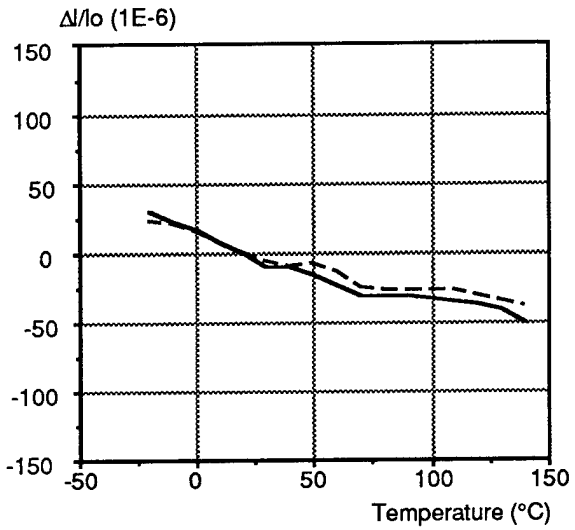


Fig 13 GY70 / BSL 914 - direction 0°

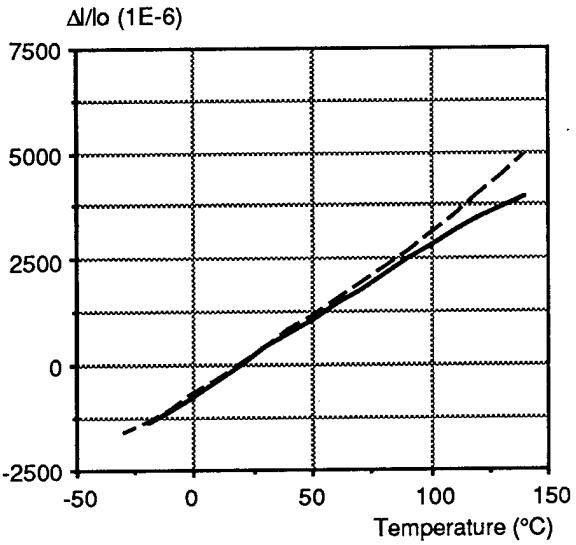


Fig 14 GY70 / BSL 914 - direction 90°

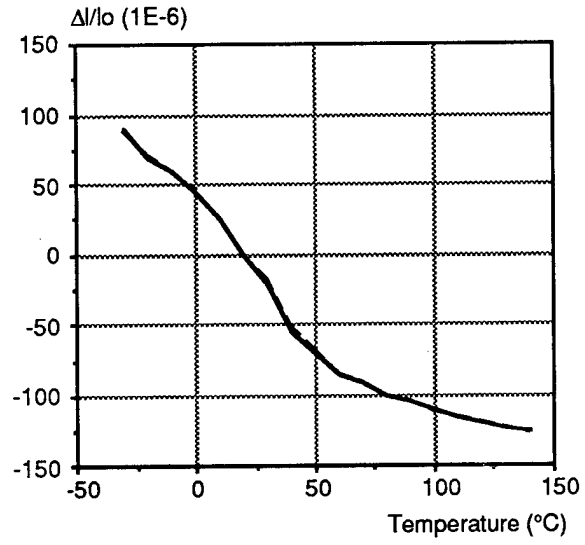


Fig 15 GY70 / code 87 - direction 0°

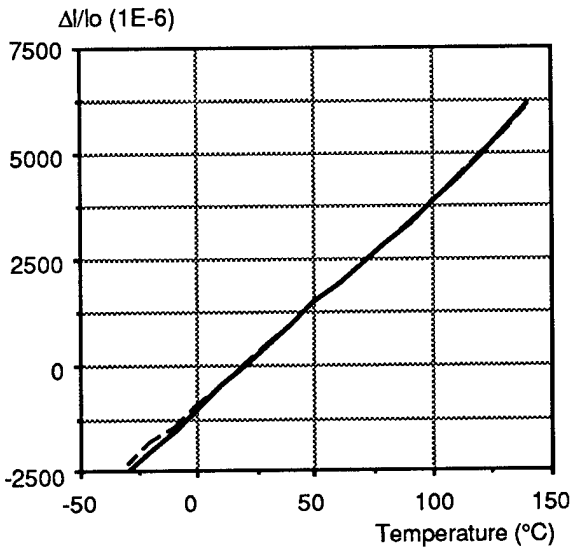


Fig 16 GY70 / code 87 - direction 90°

EFFECT OF SPACE EXPOSURE OF SOME EPOXY MATRIX COMPOSITES ON THEIR THERMAL EXPANSION AND MECHANICAL PROPERTIES (A0 138-8)

Heinrich JABS
Matra-Espace Toulouse FRANCE

FRECOPA

A0-138-8 Experience

1-Abstract

Assessment of the behaviour of the carbone/epoxy composites in space conditions. After an exposure of five years ,the mechanical characteristics and the coefficient of thermal expansion are measured and compared to reference values.

2-Experiment objectives

The experiment objectives are

-the first and main is to detect a possible variation of the coefficient of thermal expansion (CTE) of composite samples.

-the second is to detect a possible evolution of mechanical properties in simple elements and honeycomb sandwich assemblies.

-the third objective is to compare the behaviour of two epoxy resins which are commonly used in space structural production.

3-Tests

3-1:Samples

The various samples are listed and described in table 1; their shape being given in table 2.

3-2:CTE

The CTE is measured by the interferometric method in a vacuum chamber (P < 10-5 mmHg).
Two values are given:one for the rising temperature and one for the decreasing.
The mean step of temperature is 24 °C.

3-3:Mechanical tests

3-3-1:Micrography

Inspections on cuts for the various samples are made.

3-3-2:Mechanical tests

The mechanical tests below are achieved on the elements cut:

- -Interlaminar shear strength
- -flexural strength
- -flatwise tensile strength

4-Results

4-1:CTE

	CTE(t0) * 10E-6 °C-1		CTE(5years) * 10E-6 °C-1	
Reference	T ↗	T ↘	T ↗	T ↘
1	-1,6	-1,6	-1,6	-1,6
1b	-1,6	-1,6	-1,6	-1,5
2	1,2	1,2	-0,07	-0,2
2b	1,1	1,1	-0,3	-0,5
3	-0,2	-0,2	-0,3	-0,2
3b	-0,2	-0,2	-0,3	-0,15
4	-1,1	-1,1	-1,1	-1,1
4b	-1,1	-1,1	-2,5	-2,1
5	-1,1	-1,1	-1,1	-1,1
5b	-1,1	-1,1	-1,2	-1,3

4-2:Visual inspections

The surface inspection shows a surface state modification of the samples.(see pictures P1,P2,P3,P4).
We can see the cuts of the witness and flight samples on P5,P6,P7,P8,P9,P10.

4-3:Mechanical results

Table 3 gives all the mechanical resuts.
For reference : we put (UV) when the surface is the vaccum exposure side and (INF) for the other side,(VOL) is the flight sample and (SOL) the ground one.

5-Interpretation

5.1:Visual test

The visual test inspections don't show particular default. We can only see a color changing of the ink marking (white to brown).

Using the micrographic cut inspection we have :

- a surface modification : erosion
- some little cracks

5.2:Mechanical tests

5.2.1:Resin 934 (sample 2-3-4)

For the interlaminar shear strength, the observed margin is not representative (maximum variation : 19 %). We can note only an increase trend.
The interpretation of the flatwise tensile strength is difficult because of the scatter of the results. As a matter of fact the ground sample bonding has an adhesive break (fiber side), and for the light sample we have a delaminate skin composite.

5.2.2:Resin VICOTEX 108 (sample 5)

This resin seems more susceptible with the vacuum effects. We note an increase of the flexural module (+ 27%) and also for the interlaminar shear strength.
That should indicate a more significant reticulation for the V108 than the resin 934.

5.3:CTE

We have a very important change for the CTE value on sample 2 which is a sandwich aluminium honey comb with CFRP face sheets. And also we can see that the four CTE values are quite different for this sample. This has to be related with the scatter results of the flatwise strength.

6-Conclusion

There is no large variation of the CTE, except on sample 2, the sandwich aluminium honey comb CFRP sheets.
The resin V108 is more susceptible than the 934 in space conditions.

Table 1 : LIST AND COMPOSITION OF THE SAMPLES

REFERENCE NUMBER	SAMPLE TYPE (Shape reference)	FIBER/RESIN MATERIAL (supplier)	ADDITIONAL MATERIAL (supplier)	FIBER ARRANGEMENT
1 - 1'	Circular tube (A)	GY70 / 934 Unidirectional, e = 0,125mm (FIBERITE)	None	4 x (4.0°/±35°/4.0°)
2 - 2'	Sandwich Aluminium honeycomb CFRP face sheets (B)	GY70 / 934 Unidirectional, e = 0,125mm (FIBERITE)	- Alu honeycomb 4.40 AG5 (SNIAS) - Bond film : BSL 312 (CIBA)	$(0°/\pm 60°/0°/90°/\pm 42°)_S$
3 - 3'	Rectangular tube (C)	GY70 / 934 Unidirectional, e = 0,125mm (FIBERITE)	None	$(0°/\pm 60°/0°/90°/\pm 42°)_S$
4 - 4'	Rectangular tube (C)	GY70 / 934 Unidirectional, e = 0,125mm (FIBERITE)	None	0°
5 - 5'	Rectangular tube (C)	GY70 / V108 Unidirectional, e = 0,125mm (BROCHIER)	None	0°
6 - 6'	Sandwich Kevlar honeycomb Kevlar face sheets (D)	Kevlar / V108 Fabric e = 0,2 mm (BROCHIER)	Kevlar Honeycomb HRH 49-1/4 - 2.1 (HEXCELL)	2 x (0°, 90°)

Table 2

LDEF - A0 138 "FRECOPA"

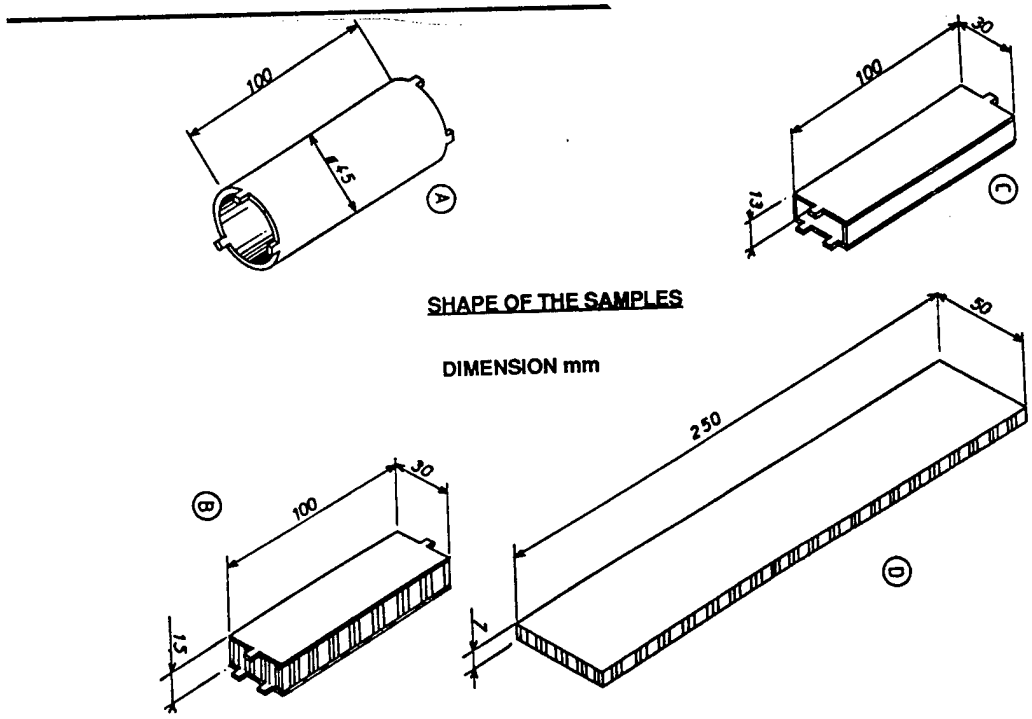


Table 3

LDEF - A0 138 "FRECOPA"

SAMPLE TYPE	REFERENCE	TEST	RESULT	(Reference %)	OBSERVATION
Rectangular tube GY70 / 934	3-F-D	ISS	32 MPa	0	Average 123 075 MPa + 19%
	3-F-U	ISS	32 MPa	0	
	3-F-D	FM	112 921 MPa	+ 9%	
	3-F-U	FM	133 229 MPa	+ 29%	
	3-G	ISS	32 MPa	0	
	3-G	FM	103 529 MPa	0	
Rectangular tube GY70 / 934	4-F-D	ISS	/		Average 245 705 MPa + 10%
	4-F-U	ISS	42 MPa	-10,6%	
	4-F-D	FM	246 119 MPa	+ 10,2%	
	4-F-U	FM	245 290 MPa	+ 9,8%	
	4-G	ISS	42 MPa	0	
	4-G	FM	223 291 MPa	0	
Rectangular tube GY70 / V108	5-F-D	ISS	53 MPa	+ 11,5%	Average 51 (+ 7,3%)
	5-F-U	ISS	49 MPa	+ 3,2%	
	5-F-D	FM	269 164 MPa	+ 26,6%	Average 270 255 MPa + 27,1%
	5-F-U	FM	271 344 MPa	+ 27,6%	
	5-G	ISS	47,5 MPa		
	5-G	FM	212 576 MPa		
Sandwich Aluminium honeycomb	2-F	FTS	187 daN		Delaminage
	2-G	FTS	11,4 daN		Adhesive fiber side
			3 daN		
			234,5 daN		

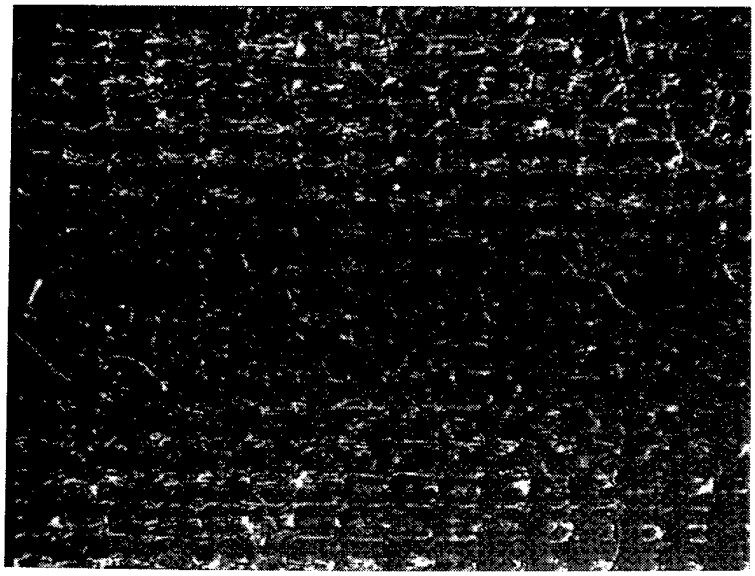
Legend:

F : Flight
D : Down face
U : Up face (direct space exposure)
G : Ground
ISS : Interlaminar shear strenght
FM : Flexural module
FTS : Flatwise tensile strength

WITNESS SAMPLE

Surface aspect
(Cell aspect)

G=6



Photograph 1

FLIGHT SAMPLE

Surface aspect
(Smooth aspect)

G=6

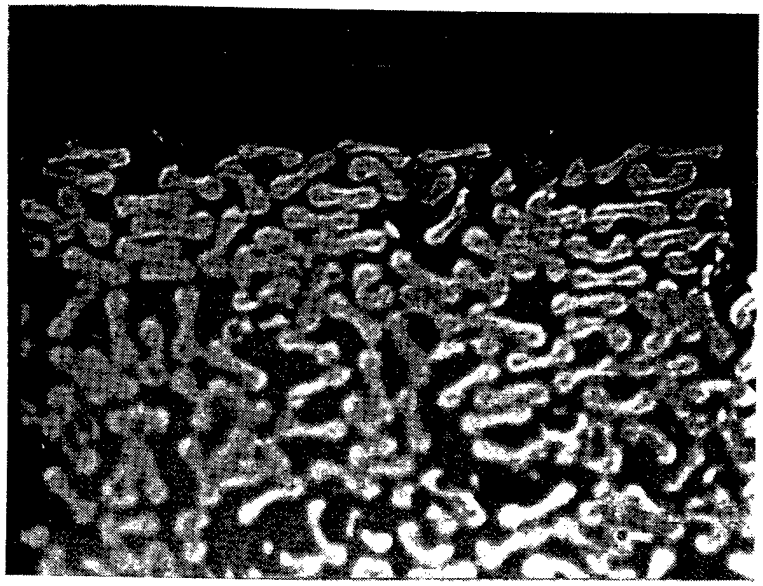


Photograph 2

WITNESS SAMPLE

Surface aspect

G = 500

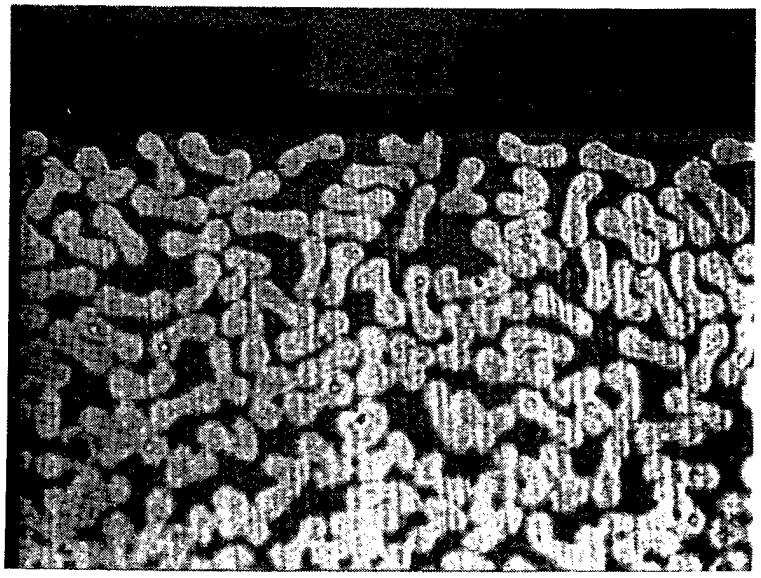


Photograph 3

FLIGHT SAMPLE

Surface aspect

G = 500

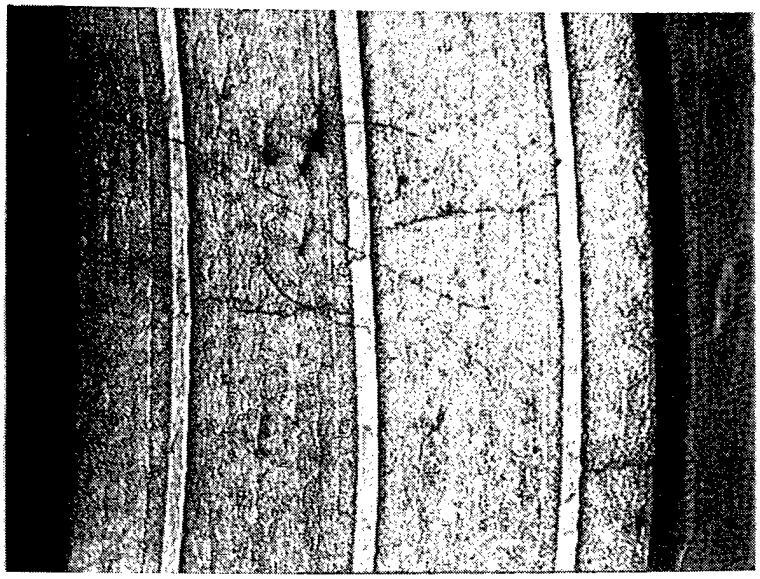


Photograph 4

WITNESS SAMPLE

General view

G=20

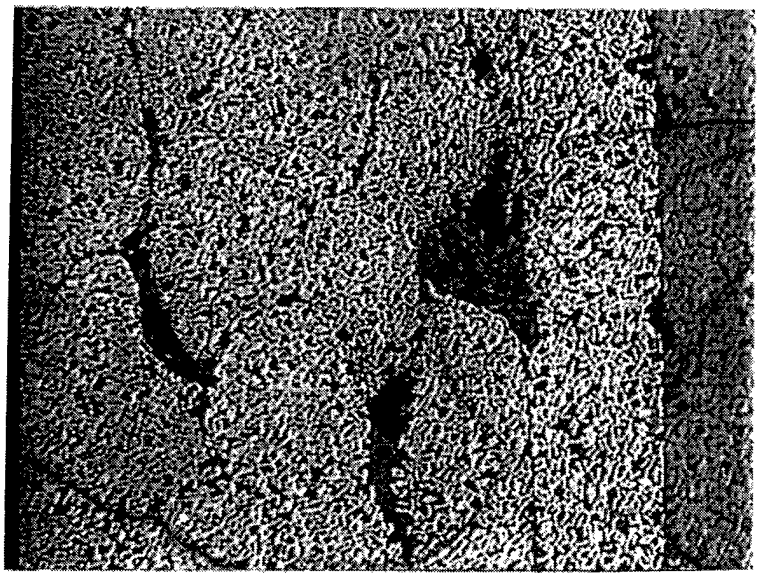


Photograph 5

WITNESS SAMPLE

Heap of resin

G=80

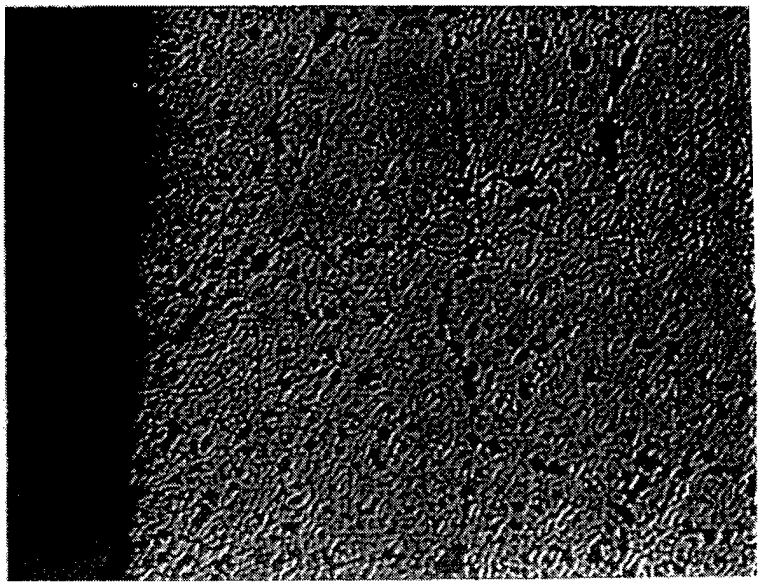


Photograph 6

WITNESS SAMPLE

Surface cracks
(Radial type)

G = 200

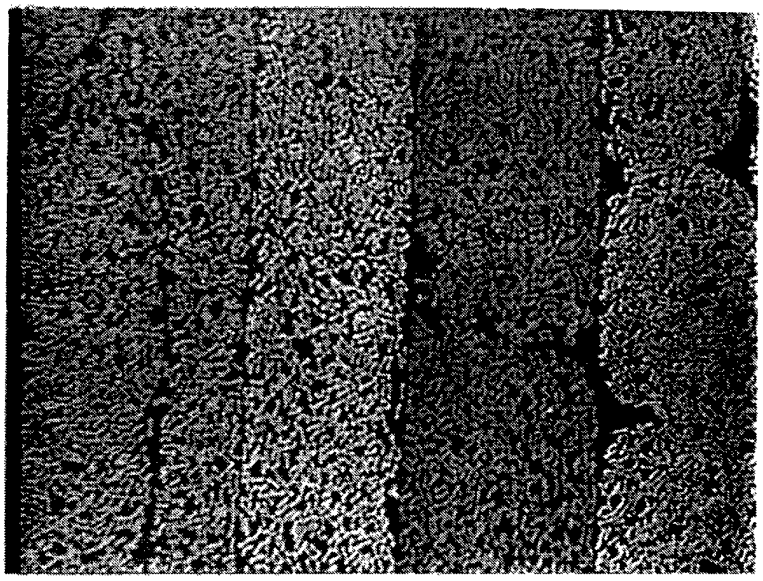


Photograph 7

WITNESS SAMPLE

Central cracks

G = 200

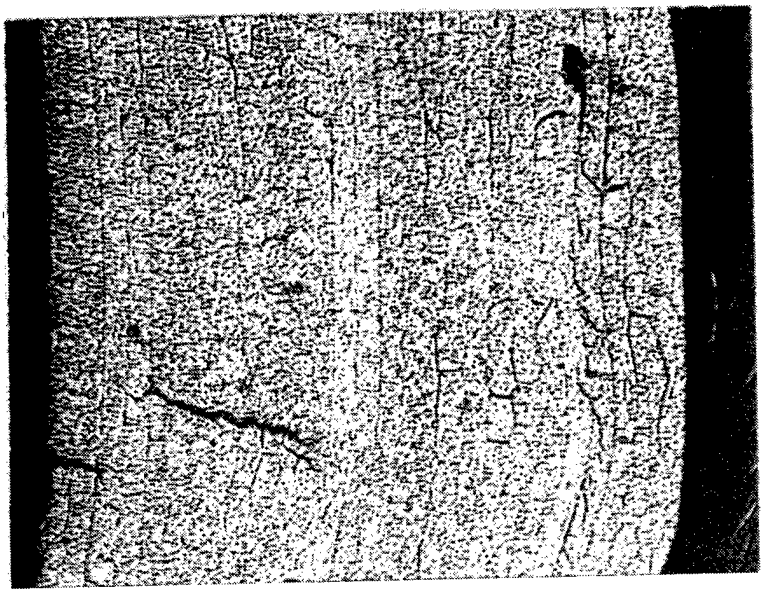


Photograph 8

FLIGHT SAMPLE

General view
(Sun exposed face)

G=20

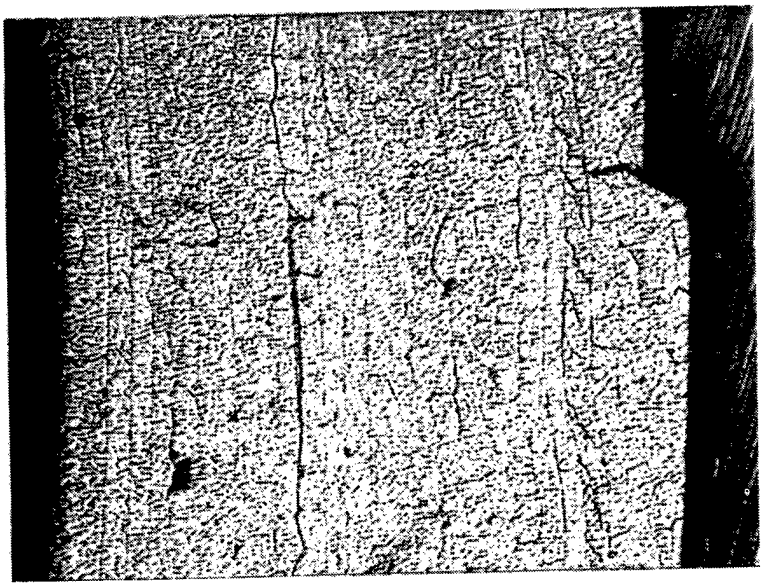


Photograph 9

FLIGHT SAMPLE

General view
(Sun exposed face)

G=20

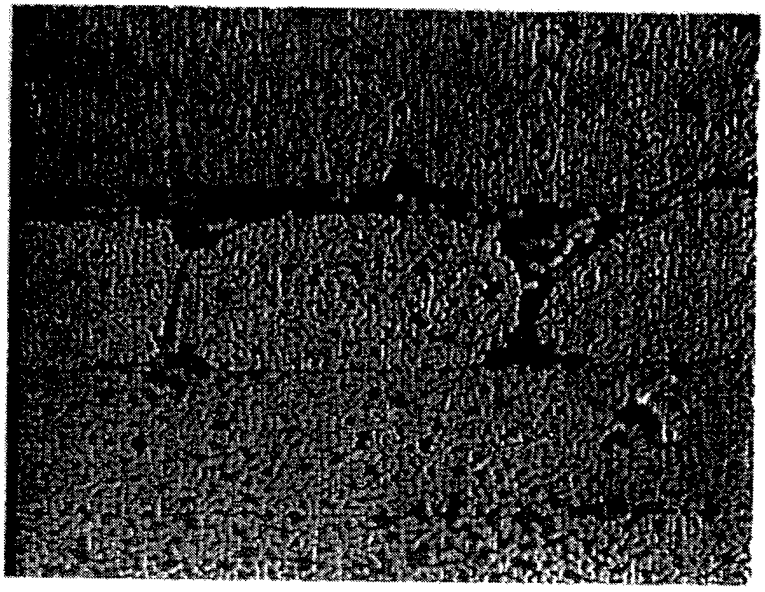


Photograph 10

FLIGHT SAMPLE

Heap of resin

G = 100

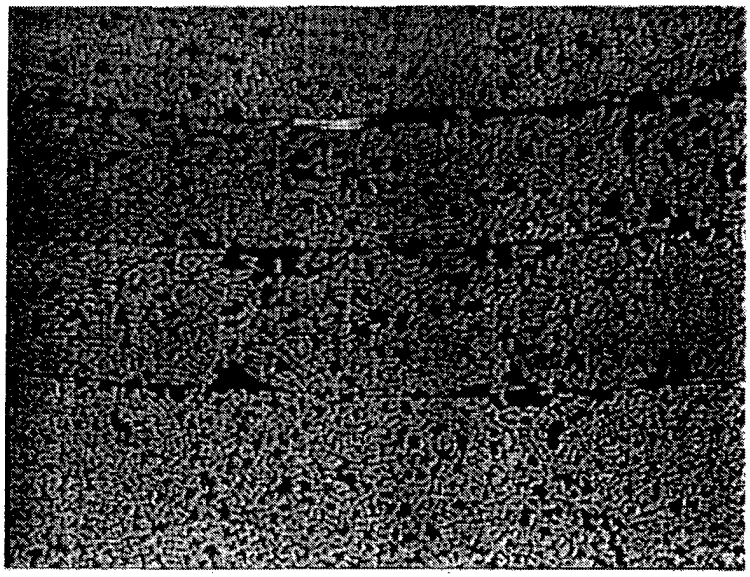


Photograph 11

FLIGHT SAMPLE

Concentrated cracks

G = 100



Photograph 12

MECHANICAL PROPERTIES OF SILICATE GLASSES EXPOSED TO A LOW-EARTH ORBIT

David E. Wiedlocher*, Dennis S. Tucker#, Ron Nichols# and Donald L. Kinser*
*Department of Materials Science and Engineering, Vanderbilt University, Nashville, TN 37235
#Marshall Space Flight Center, NASA, MSFC, AL 35812

EXTENDED ABSTRACT

The effects of a 5.8 year exposure to low-Earth orbit environment upon the mechanical properties of commercial optical fused silica, low iron soda-lime-silica, Pyrex 7740, Vycor 7913, BK-7, and the glass ceramic Zerodur were examined. Samples were 1" × 0.2" discs with grit-blasted surfaces in order to introduce sharply distributed surface flaw populations to enhance statistical reproducibility of data. Mechanical testing employed the ASTM-F-394 piston on 3-ball method in a liquid nitrogen environment.

Samples were exposed on LDEF in two locations corresponding to 1) the negative velocity vector, and 2) approximately perpendicular to the velocity vector facing Earth. Samples located in the tray affixed to the second row of the LDEF module, primarily receiving direct solar radiation, received seven micrometeorite impacts on glass samples and four impacts on the tray structure. Impacts were observed on all glass types with the exception of Vycor. Two Zerodur samples were affected with one suffering two impact events. Samples located in the tray on the Earth facing position received no observable impacts. The observed frequency of impact events averaged over the exposure time was 0.002 impacts/cm^2 year.

Weibull analysis as well as a standard statistical evaluation were conducted. The Weibull analysis revealed no differences between control samples and the two exposed groups. This was confirmed through optical microscopy evaluation of the fracture initiation origin. Statistical analysis including Student's t test for paired-mean values concluded strength measurements were within a 99 percent confidence interval. We thus concluded that radiation components of the Earth orbit environment did not degrade the mechanical strength of the samples examined within the limits of experimental error.

Statistical problems arising from the low frequency and location of micrometeorite or space debris impacts upon the samples precluded statistically valid measurement of impacted sample strengths. Upper bounds for the magnitude of the impact event damage upon the strengths for impacted samples were determined using calculated values of stress corresponding to the actual stress present at the impact site during testing. The upper bound of strength degradation for meteorite impacted samples based upon this analysis and the observations was 50 percent.

A paper describing this work is being submitted to the Journal of the American Ceramic Society and should appear in early 1992.

PATTERNS OF DISCOLORATION AND OXIDATION BY DIRECT AND SCATTERED FLUXES ON LDEF, INCLUDING OXYGEN ON SILICON

A. R. Frederickson, R. C. Filz and F. J. Rich
Space Physics Division
Air Force Geophysics Laboratory
Hanscom Air Force Base, MA 01731
Phone: 617/377-3211, Fax: 617/377-5571

P. Sagalyn
Army Materials Technology Lab
SCLMT-EMS
Watertown, MA 02172-0001
Phone: 617/923-5398

SUMMARY

A number of interesting discoloration patterns are clearly evident on MOOO2-1 which resides on three faces of LDEF: front face (ram), rear face (wake), and earth face. Most interesting is the pattern of blue oxidation on polished single crystal silicon apparently produced by scattered or direct ram oxygen atoms along the earth face. Perhaps normally incident atomic oxygen produces a thick oxide, while glancing incidence produces less oxide. Also, severe oxidation of CR-39 polycarbonate occurred on the ram face of LDEF, as expected. Most of the other patterns are seen in the NASA S13G/LO Thermal Control Paint. A complete explanation for the patterns has not yet been obtained. For example, all of the honeycomb outgassing holes have a small discoloration ring around them, but some of the rings are lighter, while most are darker, than the average paint color. The shadow cast by a suspended wire on the earth face surface is not easily explained by either solar photons or by ram flux. The shadow is a well defined white line and argues for a photon flux incident at 14 $\pm$ 2 degrees off the normal to the front face (#9) assuming that photons caused the darkening in the paint. But solar UV photon fluxes occurred over a wide range of angles and, thus, should not produce a sharply defined white shadow. Additionally, the ram flux was not expected to occur at a 14 degree angle, reports to date put it at 8 degrees. Ram flux would produce a dark shadow, not the actual white shadow. Thus, the shadows and the dark/light regions cannot be consistently explained by the process of solar UV paint-darkening modulated by ram flux oxygen bleaching of the paint.

INTRODUCTION

We present a series of observations which are important if one is to interpret the patterns of shadows on the surfaces of LDEF. These findings are serendipitous, the M0002-1 experiment was not designed for this purpose. The results are documented here so that those who do work on these

problems may use the peculiar results that we have found.

It is generally understood that ionizing radiation, including solar UV, will introduce color centers into many materials such as the paint binder in the NASA S13G/LO white thermal control paint. The color centers darken the paint to a brown color as seen with the naked eye. It is also known that attack by high energy oxygen atoms will oxidize and bleach the color centers. Therefore, painted surfaces on the front side of LDEF will be simultaneously darkened and bleached. Painted surfaces on the back side of LDEF will be darkened but not bleached. One would expect the paint on the back side of LDEF to be the darkest because it is not bleached. We found this to be true for most of the M0002-1 surfaces, but not for all of its surfaces.

The ram atomic oxygen in low orbit is known to readily oxidize materials [ref. 1*]. The CR39 track etch detector material was severely burned. This is to be expected based on existing knowledge. Most interesting is the pattern of blue silicon dioxide formed on the single crystal silicon by scattered ram atomic oxygen. The pattern implies that the angle of incidence might control the depth to which the silicon is oxidized. Silicon oxides are grown on the earth in the production of modern electronic devices. These oxides are grown at very high temperatures and their properties are known to depend on how they are grown. The oxides grow fast and thick in steam. In dry oxygen they grow thin and slowly, but with fewer charge trapping defects than in the steam-grown oxide. The LDEF sample is an oxide grown at low temperature by the ram oxygen. One might wonder if such an oxide has better properties than those produced on earth to date.

First, we present the results which are in agreement with the existing knowledge as we know it. The details which we do not understand, and which seem to have important implications, are presented subsequently. Photographs do not often reproduce well in documents such as this. Therefore, we offer to send photographs to those of you who have a need once you have read this report.

DARKENING AND BLEACHING OF PAINT

Since the LDEF was not launched in an orbit lying close to the ecliptic plane, and even though the LDEF was gravity-gradient stabilized, the LDEF surfaces experienced a large variety of solar insolation incidence angles with respect to the surface normal [refs. 2,3]. Only the earth-facing surface received a negligible solar insolation. Row 3 received a solar insolation similar to that received by row 9.

Figure 1 shows that row 3 is much darker than is row 9, presumably because row 3 has not been bleached by ram atomic oxygen. Figure 1 is a photograph purposely taken with both the D3 and D9 experiments, side by side, exposed to the same lighting and film development in order to minimize the effects of film color rendition on the photograph. If anything, the picture under-reports the difference in paint darkening between the two LDEF surfaces. Figure 1 does show that the dominant coloring processes are darkening by the space environment and bleaching by the ram environment.

*See top of pg. 214.

Variation of Darkening on Similar Surfaces

Also in reasonable facsimile to visual observation, figure 1 shows that the darkening varies strongly on the surface of each experiment. Most dramatic is the difference amongst surfaces that were painted at different times but are exposed to the same space fluxes. For example, referring to figures 1-3, we see that component C is always darker than component A. Component B should be the same as component D, but it is not. Instead, as seen in Fig. 3, component C darkened as D did, and component A darkened as B did. The substrate material of B and D are the same aluminum. This combination of events demonstrates that there is a significant difference among similar samples painted with, presumably, the same paint. We can only guess at the cause of the different darkening responses by the same paint. Perhaps it is the case that the paint with a higher percentage of binder will darken more, and therefore the stirring of paint during its application is critical. Or, perhaps, settling of the pigment below the surface of the binder during drying, leaving enhanced binder near the paint surface once dry, (or vice-versa) is a critical parameter. In any case, one application of S13G/LO is not the same as the next application of the same paint. Note that surfaces A, B, C, and D in Figs. 1-3 are all parallel to, and nearly coplanar with, the surface of row 3 on LDEF. Samples of these materials are available for those who would learn something useful by testing them; contact the authors.

Variation of Darkening on "Donuts" Around Out-gassing Holes

Everywhere on LDEF the outgassing holes showed contamination rings or donuts around the holes. M0002-1 was no exception. Figures 4 and 5 are included to show that the ring color can be EITHER darker OR lighter than the general surface color, for reasons unknown to us. Darker rings seemed to be the most common on LDEF as well as on M0002-1. We leave it for others to explain, but the explanation for the rings must include the fact that the rings are either darker than, or lighter than, the surrounding color.

RAM ETCHING OF CR39 POLYCARBONATE

One top layer of track detectors, exposed to the space environment, was 0.023 inch thick (0.058 cm) CR39 polycarbonate which was manufactured by PPG Industries. After exposure to the ram oxygen flux it was severely etched. In the corners where the ram oxygen flux was enhanced by reflection from the painted aluminum surface, which was at a right angle to the CR39 surface, the etching was exactly the thickness of the CR39. At the corner the CR39 was burned all the way through along about half of the line formed by the corner. Far from the corner where there was no enhancement the CR39 was only partially burned.

These samples are being held in storage. As one can see from the figures, there were a number of samples, each with corners at differing angles with respect to the ram flux. Careful inspection of figure 6 will show three sample corners, one fully burned through, one partially burned through, and one not burned through. The samples are available for measurement if someone is interested in measuring the burn rate as a function of the angle of the two corner surfaces with

respect to the ram flux direction. Contact the authors to obtain access to the samples.

A SHADOW, RAM FLUX, AND REVERSE VIDEO ??

Figure 7 is a view (from the earth) of the earth-facing surface. Carefully inspect the darkened paint on the "proton telescope" (there are six of the telescopes in this view, each at a different angle) which is in the lower right in the figure. This particular darkened paint is the darkest surface on the structure in figure 7.

For the most part, the earth facing end of the LDEF is not darkened because it does not directly face the sun at any time. However, the darkened regions shown in figure 7 are exposed directly to the sun when the satellite is passing from the night side to the day side, or vice versa. This is analogous to the rising or the setting sun shining directly on east and west-facing vertical surfaces here on earth. In particular, portions of each proton telescope extend beyond the earth-facing surface of LDEF and are exposed directly to the oxygen ram flux and to the rising or setting sun. For example, the dark brown region on the telescope in the lower right of figure 7 is directly impacted by ram oxygen flux.

There are three interesting phenomena exhibited by figure 7. The rest of this paper discusses these phenomena in order:

1) On the earth facing surface, paint exposed to ram flux was much darker than paint in the wake; this is in opposition to the results seen in figure 1.

2) There is a white line shadow in the otherwise darkened paint on the proton telescope mentioned above. This shadow seems to be in reverse video as discussed below.

3) The bright blue region is on a silicon sample which is not exposed to ram flux. Apparently the blue region is an oxide which formed from ram oxygen, perhaps from that which was scattered from the dark brown region which did extend out into the ram oxygen flux, below the earth-facing LDEF surface.

Phenomena 1. Another Discrepancy Concerning Paint Darkening in Ram and Wake

For the painted items which extended beyond the earth-facing surface, and which were exposed to direct solar uv irradiation, the ram surfaces were much darker than the wake surfaces. This is in contradiction to the result depicted in figure 1 and discussed in the associated text. Perhaps the LDEF was tilted slightly so that sunrise exposed these earth end ram surfaces to solar uv for a longer time than the earth end wake surfaces were exposed during sunset. Note that wake surfaces are exposed to uv during sunset and ram surfaces are exposed during sunrise for an eastwardly moving satellite. Understand that the earth end is exposed to direct solar uv for only a brief period each orbit; it is in shade from either the earth or the LDEF structure for most of the orbit. This particular experiment was located nearly midway between the ram edge and the wake edge of the earth face, but was slightly closer to the wake edge than the ram edge. Thus its position

along the earth face cannot explain the discrepancy that ram surfaces are much darker than wake surfaces. Could LDEF have been tilted?

Phenomena 2. A Reverse Video Shadow

In figure 7, carefully inspect the dark brown region on the lower-right telescope, and note the white shadow to the right of the suspended wire. Somehow the wire cast a white shadow by preventing the paint from being colored brown. Based on references 2 and 3 we know that the sun angle varied over a wide range and could not have cast such a well defined shadow behind the wire. We measured the position of the shadow relative to the LDEF to help us determine the cause of the shadow.

Figure 8 is a drawing of the measurement procedure. We sighted with a telescope from the ram direction. While remaining sighted on the wire and its shadow, we moved the telescope in the plane of the earth face of the LDEF. The shadow was found to be immediately behind the wire when the telescope was aimed exactly parallel to the line formed by the intersection of the plane, on which are mounted the six telescopes, with the earth face of LDEF. This line was constructed on LDEF to be at 14 degrees with respect to the surface normal of row 9 on LDEF. If the telescope was moved 2 degrees to either side, the shadow became visible behind the wire. Note that all previous reports of the ram direction indicate that the ram is at 8 to 10 degrees with respect to the surface normal of row 9. Why do we see a shadow at 14 degrees, and why is the shadow white, as if the white paint had not been colored behind the wire ??? If the ram flux were the cause of the shadow, then ram flux causes browning of the paint, AND, the ram flux is at 14 degrees, not 8 to 10 degrees. It is conceivable that at this telescope, the ram flow has become organized by interaction with the objects and subsequently flowed in a laminar fashion along the telescope mounting plane. Could it be possible that on row 9 of LDEF the ram flux bleached the uv browned paint, while on items protruding from the earth face the ram flux produced browning of the paint, not bleaching ?? How could one resolve this dilemma ? We don't know.

Phenomena 3. Formation of Silicon Dioxide

A very striking silicon dioxide is seen as a blue region on figure 7. The oxide is the thickest at the upper right corner of the silicon, and tapers smoothly to zero thickness at the lower and left sides of the silicon. (Note the aluminum strip across the center of the silicon sample. The strip holds the sample in place. The sample surface dimensions are 5 cm by 5 cm.) We feel that this oxide might have been formed by atomic oxygen flux scattered from the brown portion of the adjacent telescope.

This portion of the telescope extends out of the earth face of LDEF and is directly impacted by the ram flux. It is guessed that the pattern of oxide may have been produced by the following processes. The ram flux was diffusely scattered by the protruding telescope. Where the oxide is thickest, immediately adjacent to the telescope, the scattered oxygen atoms impacted the silicon surface in a

nearly normal direction. Where the oxide is thinner and not visible, the geometry was such that impacting atoms were incident at angles of 45 degrees or more. Perhaps the glancing atomic oxygen is often reflected and is less likely to penetrate to form an oxide. The geometry is such that the intensity of diffusely scattered oxygen could not have been substantially lower at the regions of the silicon far from the telescope, these regions were only twice as far from the source of scattered oxygen as were the nearest regions of the silicon. Thus, the far region of the silicon would experience a flux of roughly 1/4 that at the near regions of the silicon.

On the other hand, it could be that the intensity of direct ram flux varied across the sample in a manner appropriate to produce the blue pattern. It would be interesting if the sticking coefficient of oxygen is so strongly dependent on the incident angle around angles of 45 degrees.

It should be mentioned that thick silicon dioxide forms in atmospheric oxygen only at very high temperatures and is not easily grown to the greatest thickness that was seen here. We hope to further investigate the properties of this oxide.

REFERENCES

1. B. A. Banks, "Atomic Oxygen," in LDEF Materials Data Analysis Workshop, NASA Conference Pub. 10046, July 1990, 191-216.

2. W. M. Berrios and T. Sampair, "Long Duration Exposure Facility Solar Illumination Data Package," 1991. Available from W. M. Berrios, NASA LaRC, MS 434, Hampton, VA 23665-5225, telephone 804-864-7183.

3. R. Bourassa and G. Pippin, "Induced Environment Characterized, Effects Summarized," LDEF Spaceflight Environmental Effects Newsletter II, No. 3, pp 6-7, 15 June 1991. Copies available from LDEF Newsletter, PO Box 10518, Silver Spring, MD 20914, USA.

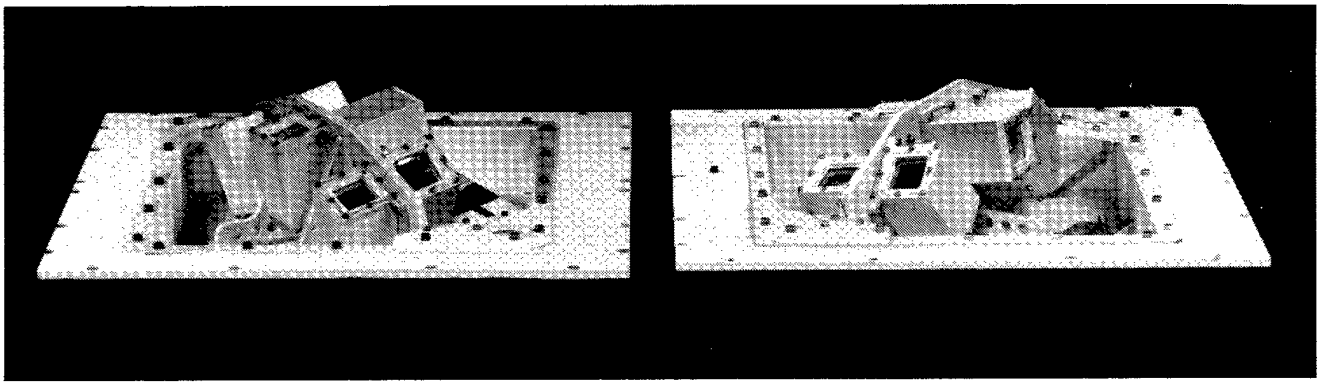


Figure 1. Side by Side Comparison of Wake Surface Paint Darkening (darker) and Ram Surface Paint Darkening (lighter).

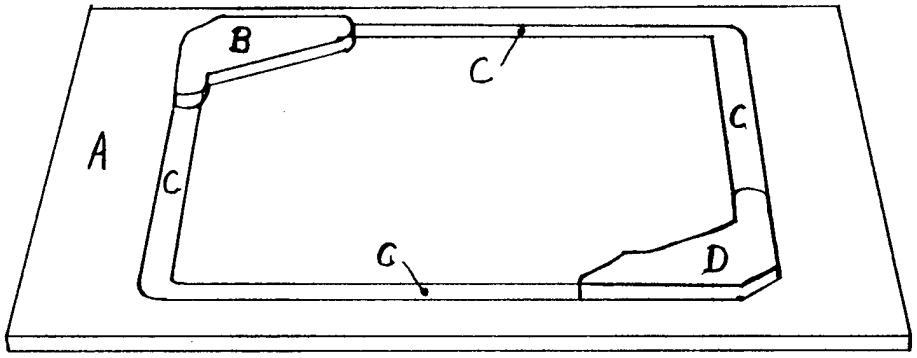


Figure 2. Definition of the Four Components of Note in figure 3.

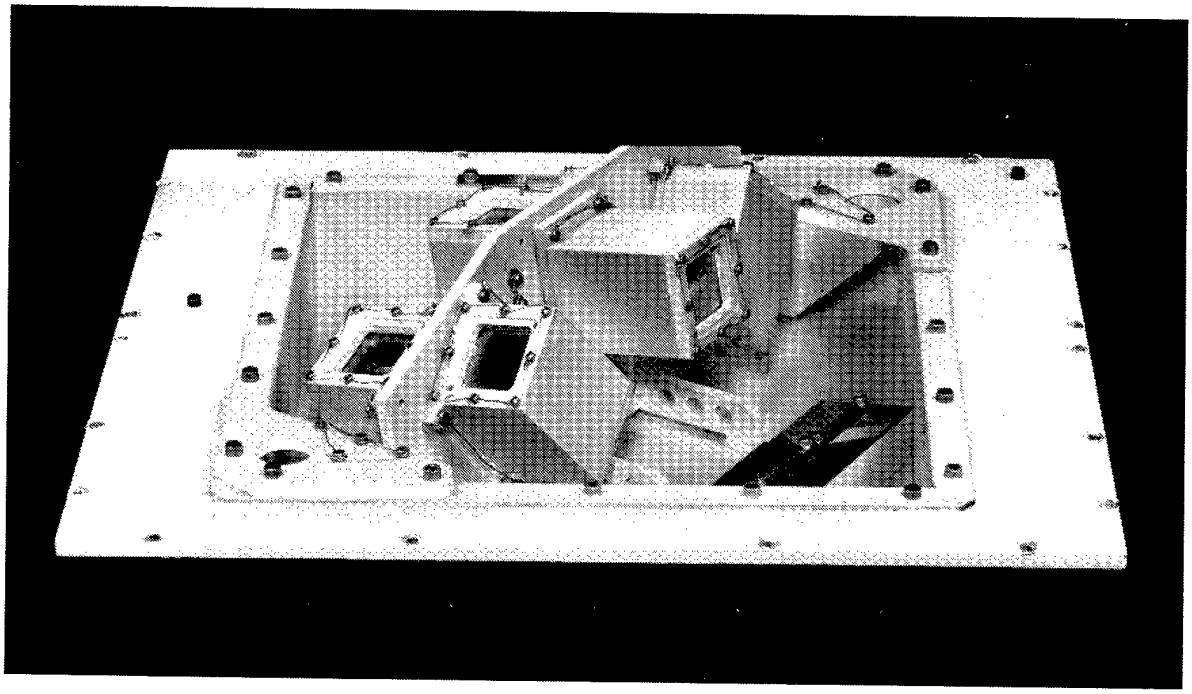


Figure 3. Variation of Darkening of the Same Paint on Different Coplanar Surfaces Exposed to Identical Darkening Agent Fluxes. Apparently, identical paint on identical surfaces will respond very differently, presumably due to different drying conditions or differences in paint preparation.

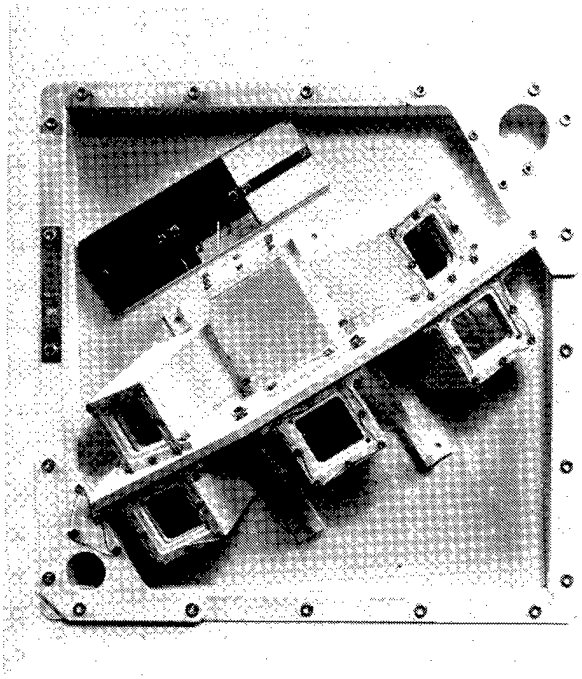


Figure 4. A View of the Variation of Paint Darkening Across a Surface on the Wake Side of LDEF.

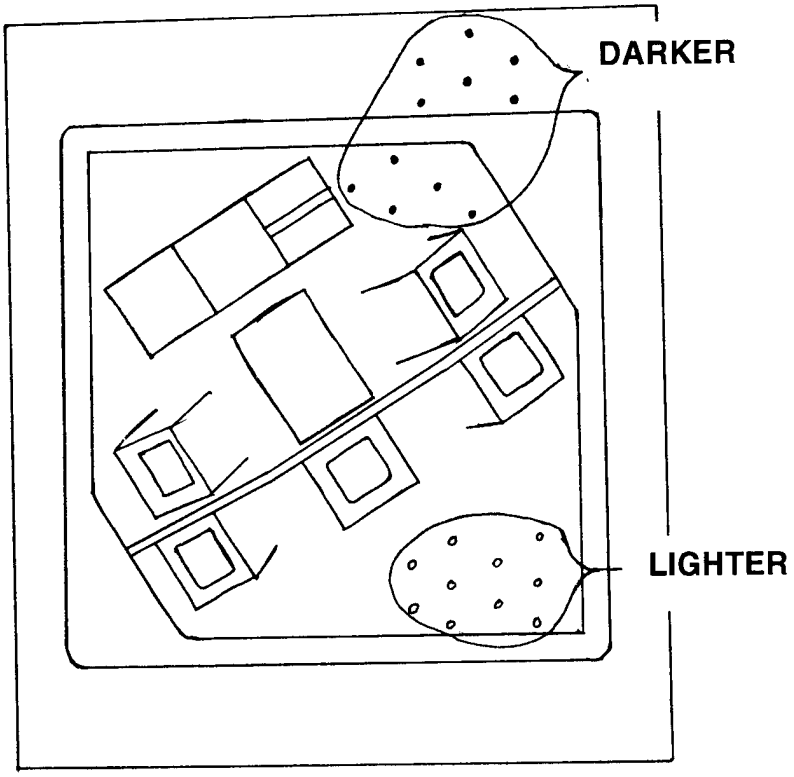


Figure 5. Note the Areas in Figure 4 Where the Outgassing Holes Have Reverse Video Rings.

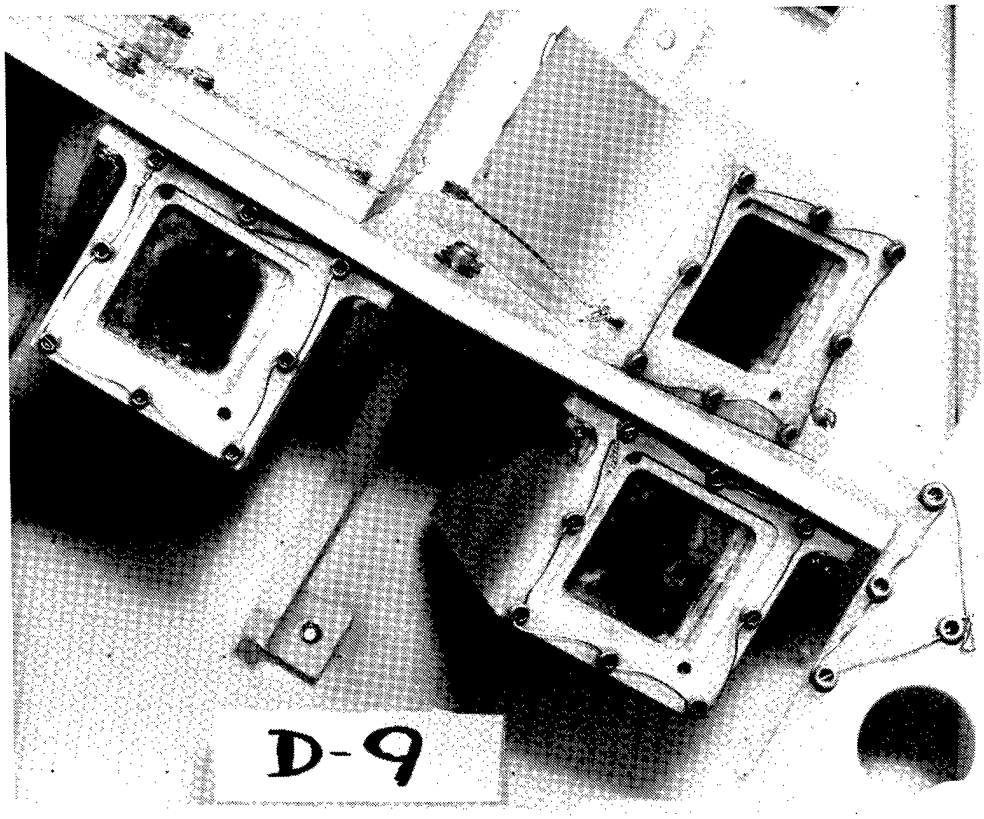


Figure 6. A Close View of the Enhanced Burning of CR39 Polycarbonate Near the Structural Corner Reflectors.

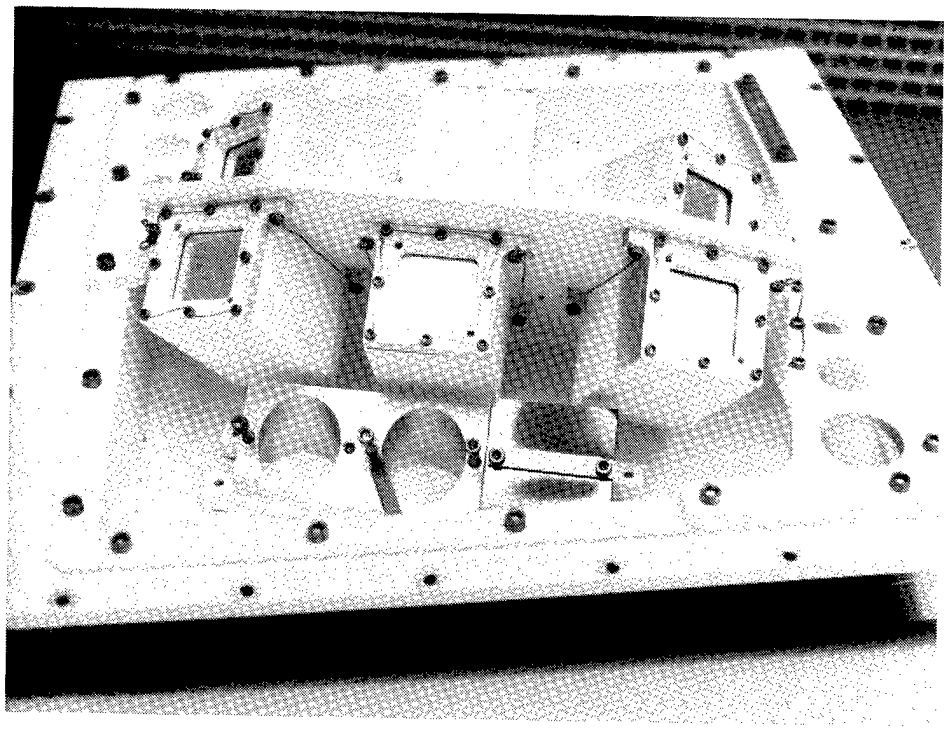


Figure 7. A View of the Earth-end Materials Showing the Blue Oxide on the Silicon, and the Adjacent Brown Region with the White Shadow of the Wire. The brown region extends out of the earth face of LDEF into the ram flux and the rising sun ultraviolet.

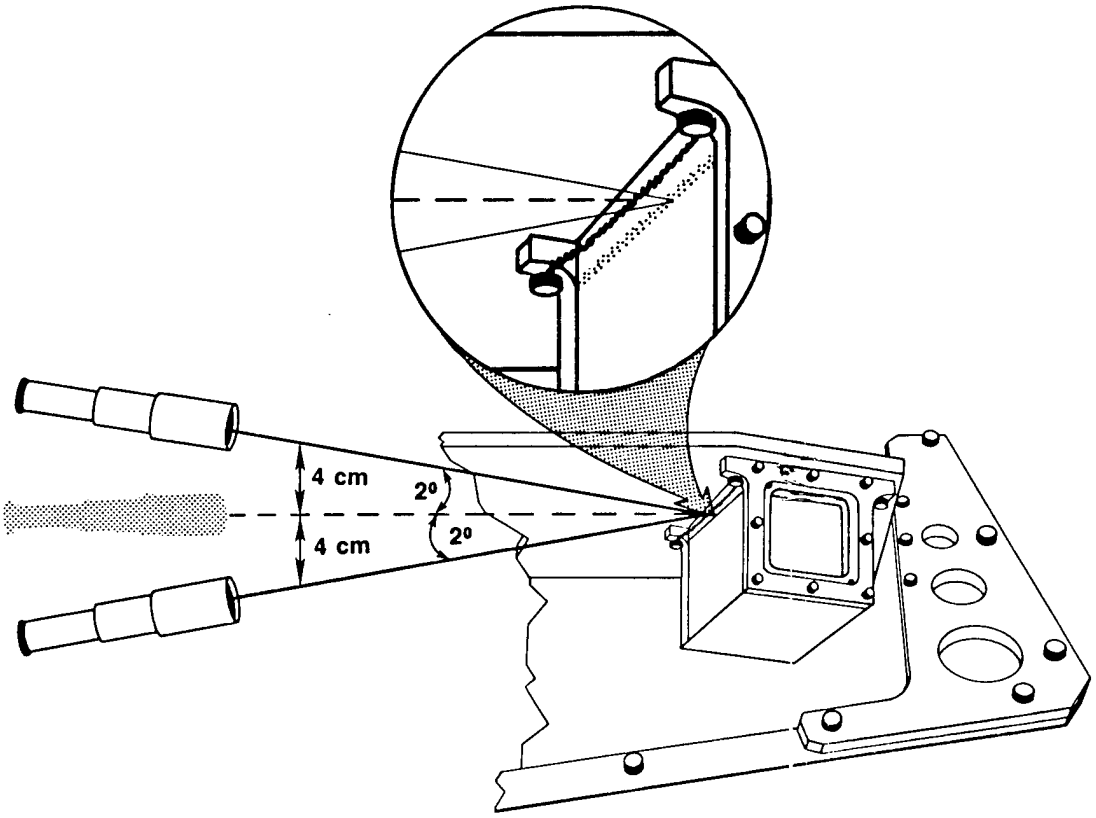
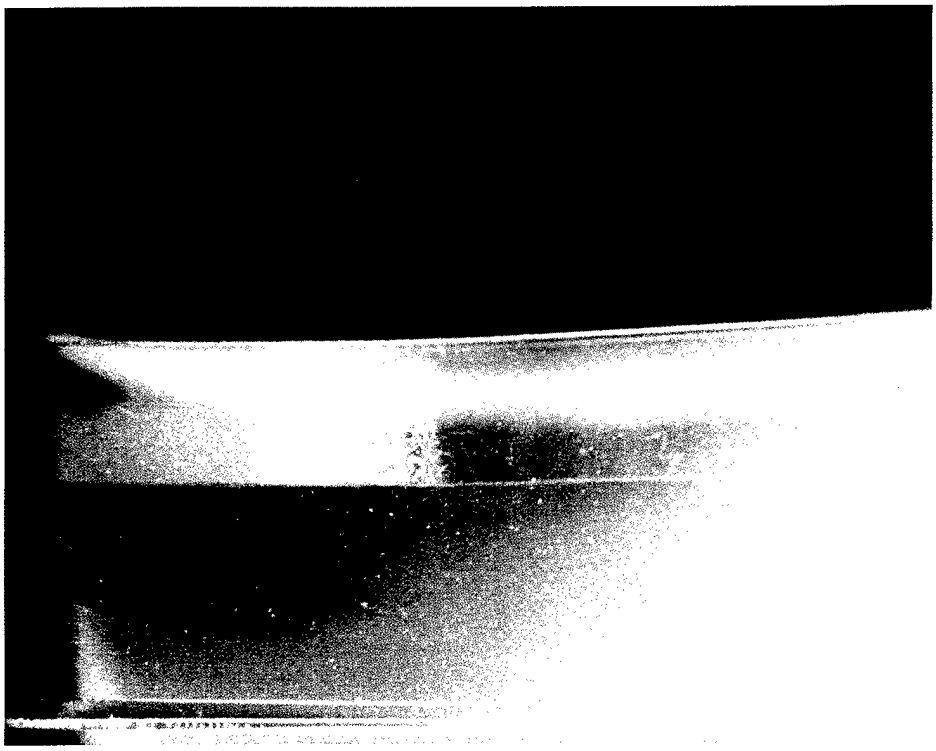


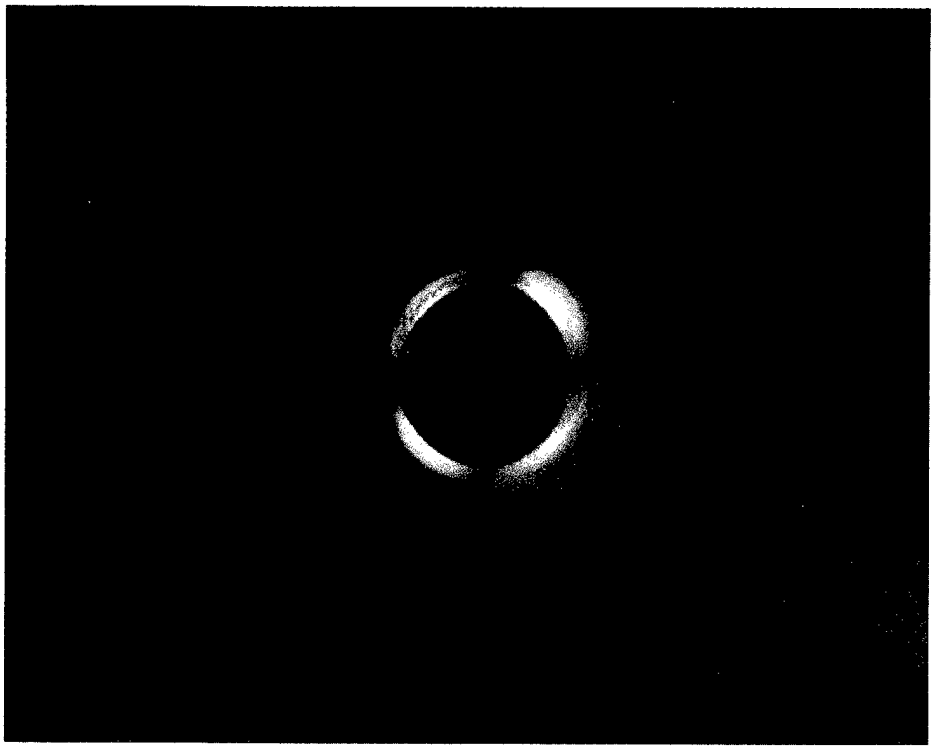
Figure 8. Detail Drawing of the Analysis of the Shadow's Direction on the Ram Wall of the Structure Shown in Fig. 7. The central viewing angle is displaced from the normal to face 9 of LDEF by 14 degrees. The shadow was definitely within 2 degrees of this direction, and this direction is parallel to the inclined planar surface which holds the six proton "telescopes."

COLOR PHOTOGRAPHS

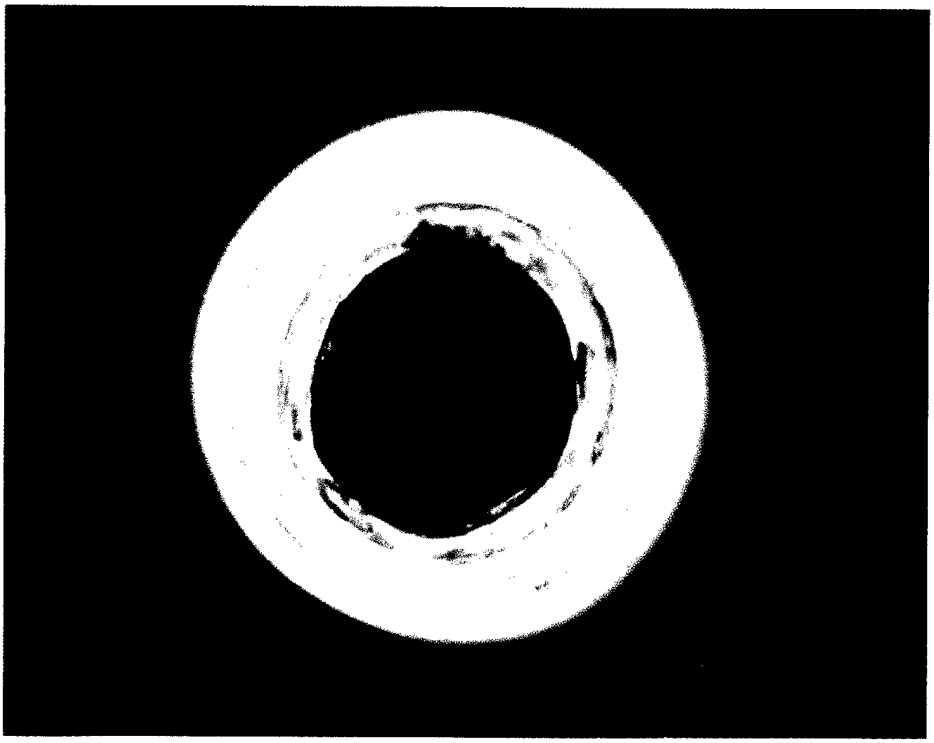


Photograph 2: This is the same sample photographed with oblique toplight. Bands that were dark in Photograph 1 are now bright due to light scatter. Along one edge interference colors can be seen. There are over ten orders of color indicating a thickness of over two micrometers.

(Color version of black and white photograph on p. 871.)

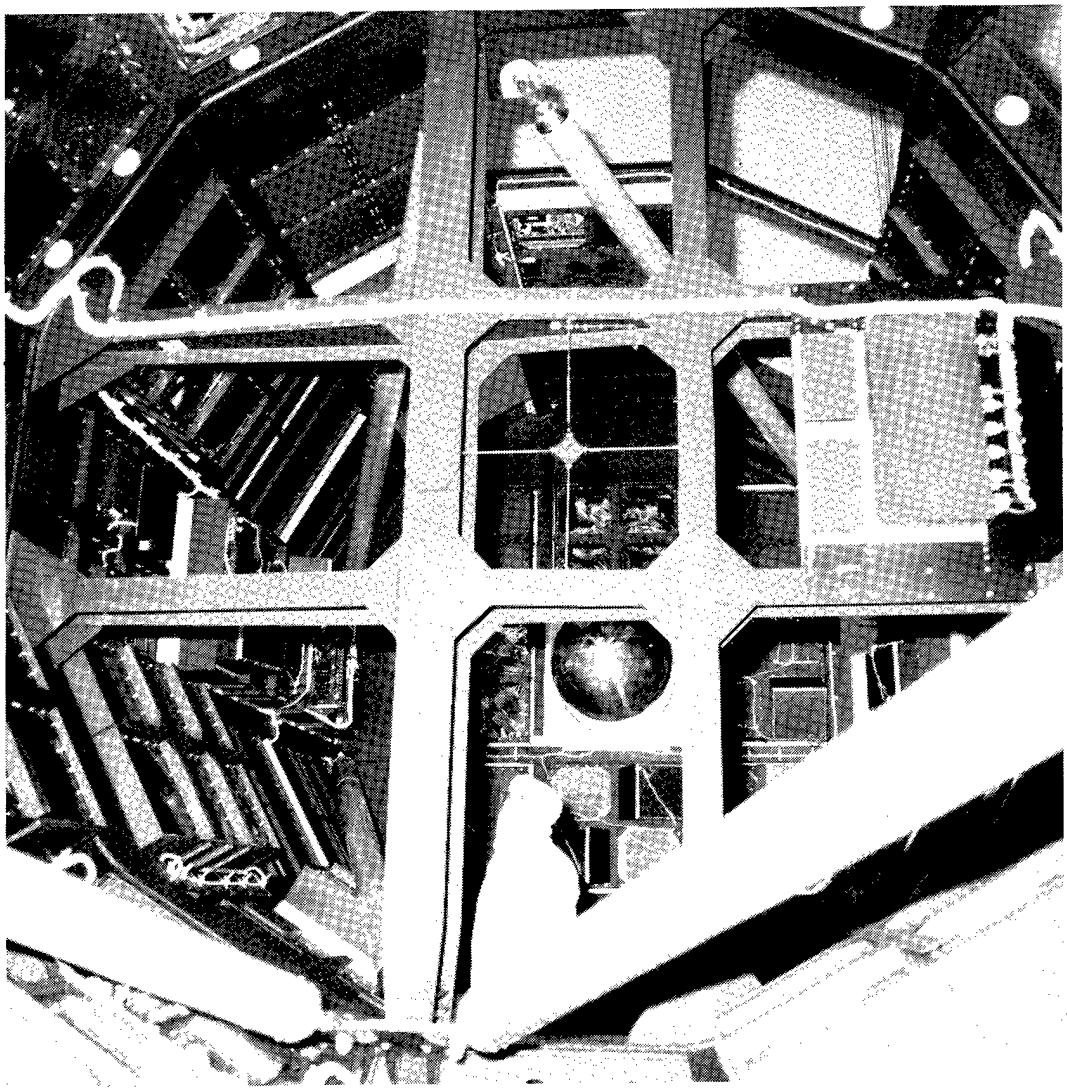


Photograph 4: Transmitted cross polarized light with a first order compensator plate was used to indicate the compressive stress frozen in the Teflon at this impact site. Transmitted illumination at a magnification approximately 300X. (Color version of black and white photograph on p. 872.)



Photograph 5: Transmitted circular polarized light photograph of another impact site exhibiting very high residual stress. Transmitted illumination at a magnification approximately 125X.
(Color version of black and white photograph on p. 873.)

AUTHOR INDEX



Adams, James H., 377

Ahearn, J. S., 1523

Allen, Thomas H., 1299

Amari, Sachiko, 503

Armstrong, T. W., 213, 347, 361

Assié, Jean Pierre, 1163, 1607, 1613

August, R. A., 225

Bayonove, J., 1639

Beaujean, R., 393, 1639

Benton, E. R., 325, 339

Bergman, L. A., 1283

Berrios, William M., 69, 935

Blakkolb, Brian K., 737, 1419

Bonnemason, Francis, 1301

Bosch, J., 367

Brennan, Patrick J., 1431

Brinza, David E., 817

Brooks, L. K., 1533

Brownlee, Donald E., 487, 549

Advani, A. H., 663

Allbrooks, Martha K., 459, 477, 567, 581, 583

Alston, Jim A., 1625

Angelo, Joseph A. Jr., 1637

Arrowood, R., 663

Atkinson, Dale R., 459, 477, 567, 581, 583

Banks, Bruce A., 781, 801

Beahm, Lorraine P., 377

Bennett, J. M., 1361

Benton, E. V., 213, 325, 339, 1639

Bernhard, Ronald P., 487, 581

Berry, J. N., 1257

Blue, M. D., 1317

Borg, Janet, 419

Bourassa, R. J., 643

Brinker, David J., 1395

Brodkin, J. S., 1005

Brown, M. John, 899

Bücker, H., 1639, 1667

Bühler, F., 585

Burge, D. K., 1361

Burris, Charles L., 763

Chapman, S. P., 1257

Chedotte, J. E., 1419

Colborn, B. L., 347, 361

Cooke, William J., 517

Csige, I., 325, 339

Dalbey, R. Z., 1361

Delpoux, M., 1639

Dever, Joyce A., 801

Dodds, Jerry, 1299

Donovan, T. M., 1361

Durin, Christian, 1593

Dybler, T., 225

Edelman, Joel, 1217

Ely, D. W., 225

Eugster, O., 585

Farrow, Allan, 705

Bunch, T. E., 549

Burns, Forrest, 255

Chang, J. Y., 313

Charlier, Jean, 1343

Christl, Ligia C., 723, 753, 755

Condé, Eric, 1613

Crutcher, E. R., 101, 121, 141, 155, 847, 861

Cutchin, J. H., 225

deGroh, Kim K., 781

Derrickson, James H., 213

di Brozolo, F. Radicati, 549

Domingo, C., 367

Drerup, Robert A., Jr., 1315

Dursch, Harry W., 1109, 1217, 1549, 1565

Dyer, C. S., 249

Ehrlich, Nelson J., 1635

Enge, W., 393

Facius, R., 1639

Felbeck, David K., 1143

Filz, R. C., 1189

Fisher, W. W., 663

Flatman, J. C., 249

Foote, John, 503

Franzen, W., 1005

Frigo, L. A., 339

Gartenbach, K. E., 1651

Gaubin, G., 1639

Geiss, J., 585

Giangano, D., 313, 1227

Golden, Johnny L., 975

Gregory, John C., 61, 237, 723, 753, 755

Grigsby, Doris K., 1635

Guillaumon, Jean-Claude, 945

Harmon, B. A., 237, 301

Hartmayer, R., 1283

Haskins, P. S., 225

Hawkins, Gary J., 1477

Heinrich, W., 1639

Finckenor, Miria, 435

Fishman, G. J., 237, 301

Fleming, Ronald H., 549

Frank, A. L., 325, 339

Frederickson, A. R., 1189

Froggatt, Mike, 875

Gasset, Y., 1639

Gebauer, Linda, 801

George, Pete E., 1115

Gillis, J. R., 643

Graul, E. H., 1639, 1661

Griffis, Dieter P., 529

Grote, Michael G., 1455

Gyetvay, S. R., 1073, 1361

Harris, David W., 549

Harvey, Gale A., 179, 1327

Havey, Keith, 1341

Heilmann, C., 1639

Hemminger, C. S., 831

Henderson, Kelly A., 737

Herren, Kenneth A., 919

Heuer, R. L., 1227

Hichwa, Bryant P., 1299

Hickey, John R., 1395, 1493

Hiendl, C. O., 1661

Hill, Sylvester G., 1109, 1115

Hill, Carol M., 801

Hodgson, Randall R., 1315

Holsen, James N., 1315

Horneck, G., 1639, 1667

Hörz, Friedrich, 477, 487, 581, 583

Humes, Donald H., 399

Hummer, Leigh L., 899, 919, 1577

Hunneman, Roger, 1477

Hunter, Jerry L., 529

Hurley, Donna L., 257

Hurley, Charles J., 961

Jabs, Heinrich, 1175

Jaggers, C. H., 1073

Jessberger, Elmar K., 503

Johnson, C. J., 1533

Johnston, A. R., 1283

Jonathal, D., 393

Jones, Leon L., 1225

Kamenetzky, Rachel R., 763

Kamykowski, E., 1227

Kantorcik, T., 313

Kassel, Philip J., 517

Kauder, Lonny, 797

Keegan, R., 367

Kesselman, M., 1227

Kinard, William H., 49, 517

King, S. E., 225

Kinser, Donald L., 1187, 1377

Kleiman, J., 1057

Kranz, A. R., 1639, 1651

Laird, C. E., 301

Lange, Gundolf, 503

Laue, Eric G., 817

Laurance, Mark R., 487

Le, Tuyen D., 1041

Lester, Dean M., 1225

Letton, Alan, 705

Levadou, François, 875

Levorsen, J. L., 1533

Liang, Ranty H., 817

Lightner, E. Burton, 3

Lind, D. L., 585

Lind, M. David, 1675

Linder, W. Kelly, 85

Linton, Roger C., 763

Little, Sally A., 1687

Long, Greg A., 1299

Maag, Carl R., 85

Mabson, G. E., 1057

Mandeville, J. C., 419

Marquez, B., 663

Martin, Glenna D., 49

Mason, James B., 1217

McCreight, Craig, 1431

McDonnell, J. A. M., 443, 565

McIntosh, Roy, 1431

McKisson, J. E., 225

Mendenhall, M. H., 1377

Merrow, James, 989

Meshishnek, M. J., 1073

Messenger, Scott, 487

Miglionico, C., 663

Miller, Edgar R., 919

Miller, Emmett A., 1109, 1533

Mirtich, Michael J., 989

Montague, Nancy L., 517

Mooney, Thomas A., 1511

Morison, W. D., 1057

Moss, C. E., 271

Mulholland, J. Derral, 517

Mulkey, Owen R., 1109, 1533

Murr, L. E., 663

Nichols, Ron, 1187, 1377

Nielsen, Kjeld Flemming, 1675

Nishimura, L. S., 121, 141, 861

Norman, Bret L. , 1637

O'Neal, Robert L., 3

O'Sullivan, D., 367

Oliver, John P., 517

Olle, Raymond M., 989, 1379

Olmez, Ilhan, 255

Ord, R. Neil, 1225

Padden, R. J., 1257

Paillous, Alain, 945

Parcelier, Michel, 1163

Parnell, T. A., 199, 213, 237, 301, 325, 339

Perotto, Alfred, 1607

Perry, Arthur T., 1691

Peters, Palmer N., 61, 723, 753, 755

Peterson, Robert B., 487

Petrie, Brian C., 1055

Phillips, G. W., 225

Pickert, M., 1651

Piercey, R. B., 225

Pippin, Gary, 617, 847, 1109

Plagemann, Walter L., 1023

Planel, H., 1639

Portal, G., 1639

Porter, D. C., 1533

Preuss, L., 1405

Quinones, S., 663

Raikar, Ganesh N., 753, 755

Reedy, R. C., 271

Reilly, Terrence W., 549

Reitz, G., 1639, 1643, 1667

Reynolds, John M., 763

Rich, F. J., 1189

Ritter, J. C., 225

Robertson, James B., 1547

Rock, Neil I., 705

Rott, Martin, 875

Roybal, R., 663

Rutledge, Sharon K., 989, 1379

Sagalyn, Paul L., 255, 679, 1005, 1189

Sanchez, A. D., 1257

Schäfer, M., 1639

Schneider, Eberhard, 875

Schott, J. U., 1639

Schulte, R., 1227

Seeley, John S., 1477

Sengupta, L. C., 1005

Shular, David, 1467

Singer, S. Fred, 517

Smajkiewicz, Ali, 1511

Smit, A., 367

Smith, D. W., 1533

Rivas, J., 663

Robertson, R., 663

Rooney, W. D., 1227

Rousslang, Ken, 643, 847

Rüther, W., 1639, 1661

Ryan, Lorraine E., 737, 1419

Sampair, Thomas R., 935

Sapp, Clyde, 459

Scheiman, David A., 1395

Schopper, E., 1639

Schuerger, Andrew C., 1637

See, Thomas H., 459, 477, 487, 581, 583

Selee, Steven R., 1299

Shen, James Y., 1149

Simon, Charles G., 459, 477, 503, 529

Slemp, Wayne S., 687, 1149

Smalley, R. B., Jr., 1225

Smith, Alan R., 257

Snead, L., 313

Spear, W. Steven, 1549, 1565

Stadermann, Frank, 503

Stadler, R., 1651

Staszak, Paul R., 817

Stauber, M., 313, 1227

Steckel, Gary L., 1041

Stein, Bland A., 617

Stein, C., 663

Stevens, Nicholas, 989

Stevenson, T. J., 443

Stiegman, Albert E., 817

Strganac, Thomas W., 705

Stuckey, W. K., 831

Sullivan, David, 1441

Sullivan, K., 565

Swan, Pat, 503

Taylor, E. W., 1257

Taylor, William W. L., 737, 1419

Tennyson, R. C., 1057

Thompson, A., 367

Tiller, Smith E., 1441

Tobias, C. A., 1639

Trumble, Terry M., 1255

Truscott, P. R., 249

Tucker, Dennis S., 1187, 1377

Tylka, Allan J., 377

Uht, J. C., 831

Vallimont, John, 1341

Venables, J. D., 1523

Verzemnieks, Juris, 1109

Walker, Robert M., 503

Warner, K. J., 121, 141, 155, 861

Warren, Jack, 487

Wascher, W. W., 101, 121, 141, 861

Watts, Alan J., 567

Watts, John W., 213, 325, 339, 347

Weimer, J. J., 753

Weinberg, Jerry L., 517

Weisenberger, A. G., 225

Wenzel, K.-P., 367

Whiteside, J. B., 1227

Wilkes, Donald R., 899, 919, 1577

Winn, Willard G., 287

Witte, William G., Jr., 1149

Wortman, Jim J., 517, 529

Yaung, James Y., 737, 1419

Young, Philip R., 687, 1149

Zinner, Ernst , 503

Zook, Herbert A., 569

Weller, Robert A., 1377

Whitaker, Ann F., 1241, 1377

Wiedlocher, David E., 1187, 1377

Williams, Kevin D., 705

Wiser, R., 753

Wong, W. C., 1419

Yang, T. C., 1639

Young, Leighton E., 1241

Zimmermann, M. W., 1651

Zolensky, Michael E., 459, 477

Zwiener, James M., 899, 919, 1577

REPORT DOCUMENTATION PAGE

Form Approved
OMB No. 0704-0188

Public reporting burden for this collection of information is estimated to average 1 hour per response, including the time for reviewing instructions, searching existing data sources, gathering and maintaining the data needed, and completing and reviewing the collection of information. Send comments regarding this burden estimate or any other aspect of this collection of information, including suggestions for reducing this burden, to Washington Headquarters Services, Directorate for Information Operations and Reports, 1215 Jefferson Davis Highway, Suite 1204, Arlington, VA 22202-4302, and to the Office of Management and Budget, Paperwork Reduction Project (0704-0188), Washington, DC 20503.

1. AGENCY USE ONLY *(Leave blank)*	2. REPORT DATE	3. REPORT TYPE AND DATES COVERED
	January 1992	Conference Publication

4. TITLE AND SUBTITLE
LDEF—69 Months in Space
First Post-Retrieval Symposium

5. FUNDING NUMBERS
WU 196-88-00-03

6. AUTHOR(S)
Arlene S. Levine, Editor

7. PERFORMING ORGANIZATION NAME(S) AND ADDRESS(ES)
NASA Langley Research Center
Hampton, VA 23665-5225

8. PERFORMING ORGANIZATION REPORT NUMBER
L-17042

9. SPONSORING/MONITORING AGENCY NAME(S) AND ADDRESS(ES)
National Aeronautics and Space Administration
Washington, DC 20546-0001

10. SPONSORING/MONITORING AGENCY REPORT NUMBER
NASA CP-3134, Part 2

11. SUPPLEMENTARY NOTES

12a. DISTRIBUTION/AVAILABILITY STATEMENT
Unclassified–Unlimited

Subject Category 99

12b. DISTRIBUTION CODE

13. ABSTRACT *(Maximum 200 words)*

This document is a compilation of papers presented at the First Long Duration Exposure Facility (LDEF) Post-Retrieval Symposium. The papers represent the preliminary data analysis of the 57 experiments flown on the LDEF. The experiments include materials, coatings, thermal systems, power and propulsion, science (cosmic ray, interstellar gas, heavy ions, and micrometeoroid), electronics, optics, and life science.

14. SUBJECT TERMS	15. NUMBER OF PAGES
Space experiment	612
	16. PRICE CODE: A99

17. SECURITY CLASSIFICATION OF REPORT	18. SECURITY CLASSIFICATION OF THIS PAGE	19. SECURITY CLASSIFICATION OF ABSTRACT	20. LIMITATION OF ABSTRACT
Unclassified	Unclassified	Unclassified	

NSN 7540-01-280-5500

Standard Form 298(Rev. 2-89)
Prescribed by ANSI Std. Z39-18
298-102

NASA-Langley, 1991

National Aeronautics and Space Administration
Code NTT-4

Washington, D.C.
20546-0001

Official Business
Penalty for Private Use, $300

Special Fouth-Class Ra'
Postage & Fees Pai
NASA
Permit Number G-27

Michael A. Rigdon
Institute for Defense Analyses 1801 N. Beauregard S

Alexandria VA 22311-1772

NASA

Postmaster: If Undeliverable (Section 158 Postal Manual) Do Not Return

